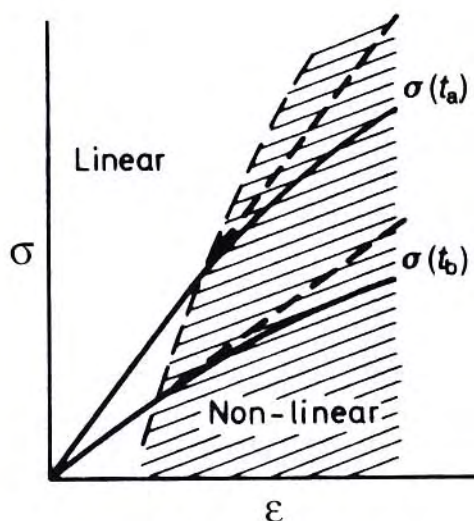


POLYMER VISCOELASTICITY

STRESS AND STRAIN IN PRACTICE



EVARISTO RIANDE
RICARDO DÍAZ-CALLEJA
MARGARITA G. PROLONGO
ROSA M. MASEGOSA
CATALINA SALOM

POLYMER VISCOELASTICITY

STRESS AND STRAIN IN PRACTICE

EVARISTO RIANDE

*Institute of Polymers of the Spanish Council
of Scientific Research
Madrid, Spain*

RICARDO DÍAZ-CALLEJA

*Polytechnic University of Valencia
Valencia, Spain*

MARGARITA G. PROLONGO

*Polytechnic University of Madrid
Madrid, Spain*

ROSA M. MASEGOSA

*Polytechnic University of Madrid
Madrid, Spain*

CATALINA SALOM

*Polytechnic University of Madrid
Madrid, Spain*



MARCEL DEKKER, INC.

NEW YORK • BASEL

Library of Congress Cataloging-in-Publication Data

Polymer viscoelasticity : stress and strain in practice / Evaristo Riande ... [et al.].

p. cm. — (Plastics engineering : 55)

Includes bibliographical references and index.

ISBN 0-8247-7904-5 (alk. paper)

1. Polymers—Viscosity. 2. Viscoelasticity. I. Riande, Evaristo. II. Series: Plastics engineering (Marcel Dekker, Inc.); 55.

TA455.P58P694 2000

620.1'9204232—dc21

99-40874
CIP

This book is printed on acid-free paper.

Headquarters

Marcel Dekker, Inc.

270 Madison Avenue, New York, NY 10016

tel: 212-696-9000; fax: 212-685-4540

Eastern Hemisphere Distribution

Marcel Dekker AG

Hutgasse 4, Postfach 812, Ch-4001 Basel, Switzerland

tel: 41-61-261-8482; fax: 41-61-261-8896

World Wide Web

<http://www.dekker.com>

The publisher offers discounts on this book when ordered in bulk quantities. For more information, write to Special Sales/Professional Marketing at the headquarters address above.

Copyright © 2000 by Marcel Dekker, Inc. All Rights Reserved.

Neither this book nor any part may be retrieved or transmitted in any form or by any means, electronic or mechanical, including photocopying, microfilming, and recording, or by any information storage and retrieval system, without permission in writing from the publisher.

Current printing (last digit):

10 9 8 7 6 5 4 3 2 1

PRINTED IN THE UNITED STATES OF AMERICA

Preface

This book is concerned mainly with the study of the viscoelastic response of isotropic macromolecular systems to mechanical force fields. Owing to diverse influences on the viscoelastic behavior in multiphase systems (e.g., changes in morphology and interfaces by action of the force fields, interactions between phases, etc.), it is difficult to relate the measured rheological functions to the intrinsic physical properties of the systems and, as a result, the viscoelastic behavior of polymer blends and liquid crystals is not addressed in this book.

We have approached the subject in such a way that the book will meet the requirements of the beginner in the study of viscoelastic properties of polymers as well as those of the experienced worker in other type of materials. With this in mind, Chapters 1 and 2 are introductory and discuss aspects related to chemical diversity, topology, molecular heterodispersity, and states of aggregation of polymers (glassy, crystalline, and rubbery states) to familiarize those who are not acquainted with polymers with molecular parameters that condition the marked viscoelastic behavior of these materials. Chapters 1 and 2 also discuss melting processes and glass transition, and factors affecting them.

Owing to the coil conformation of molecular chains, polymers above the glass-transition temperature exhibit high entropic elasticity. Chapter 3 discusses, using thermodynamic approaches, the relationship between stress and entropic elasticity in rubbery networks. The equation of state between stress and deformation in rubber elasticity is established through random-flight statistics. Swelling methods are described that enable information to be obtained on the topology of the networks. Vulcanizing systems, additives

(antioxidants, softeners and plasticizers, reinforcers), and applications are reviewed, as are elastomeric materials and thermoplastic elastomers commercially available. Chapter 3 also provides a summary of some aspects related to rubbers of interest in engineering.

Chapter 4 outlines operations of symmetry on ideal solids that show how the number of independent components of the modulus tensor diminishes as the number of symmetry elements in the solid increases. This analysis leads to the formulation of the generalized Hooke's law utilizing both elastic modulus and elastic compliances for amorphous solid materials. These relationships, conveniently modified, are further used in viscoelasticity. In this chapter the generalized law of Newton for ideal liquids is also stated.

Chapters 5 and 6 discuss how the mechanical characteristics of a material (solid, liquid, or viscoelastic) can be defined by comparing the mean relaxation time and the time scale of both creep and relaxation experiments, in which the transient creep compliance function and the transient relaxation modulus for viscoelastic materials can be determined. These chapters explain how the Boltzmann superposition principle can be applied to predict the evolution of either the deformation or the stress for continuous and discontinuous mechanical histories in linear viscoelasticity. Mathematical relationships between transient compliance functions and transient relaxation moduli are obtained, and interrelations between viscoelastic functions in the time and frequency domains are given.

Experimental methods to measure the viscoelastic functions in the time and frequency domain are described in Chapter 7.

In thermorheological simple systems, the time-temperature correspondence principle holds. Chapter 8 gives examples of isotherms for compliance functions and relaxation moduli. The shift factors are expressed in terms of terminal viscoelastic parameters, and the temperature dependence of the shift factors is interpreted in terms of the free volume and the WLF equation. The chapter outlines methods for determining the molecular weight between entanglements, and analyzes the influence of diluents and plasticizers on the viscoelastic functions.

Chapter 9 examines transient and nontransient viscoelastic functions in terms of the retardation times (compliance functions) and relaxation times (relaxation moduli) and compares retardation and relaxation times. Methods to determine retardation and relaxation spectra from compliance functions and relaxation spectra, respectively, are presented.

Mechanical models that represent the evolution of the viscoelastic functions in the time and frequency domain are described in Chapter 10. Chapter 11 discusses experimental scaling laws for viscosity, equilibrium recovery

compliance, and terminal relaxation times in terms of molecular models (spring-bead and reptation theories).

In the glassy state, long-range motions are frozen and only local motions are permitted. The viscoelastic behavior of polymers in the glassy state is discussed in Chapter 12, with emphasis on the mechanisms that could produce the sub-glass relaxations. The glass-rubber relaxation is discussed in terms of the KWW equation. Aging effects on the glass rubber relaxation are analyzed as well as the effect of crystalline entities on the relaxation viscoelastic behavior of semicrystalline polymers.

The stress in viscoelastic liquids at steady-state conditions is defined, in simple shear flow, by the shear rate and two normal stress differences. Chapter 13 reviews the evolution of both the normal stress differences and the viscosity with increasing shear rate for different geometries. Semiquantitative approaches are used in which the critical shear rate at which the viscosity starts to drop in non-Newtonian fluids is estimated. The effects of shear rate, concentration, and temperature on die swell are qualitatively analyzed, and some basic aspects of the elongational flow are discussed. This process is useful to understand, at least qualitatively, the rheological fundamentals of polymer processing.

As strain increases, the stress-strain isochrones deviate from linearity and some phenomena arise in polymeric materials in bulk. For an ideal plastic material, permanent or irreversible changes occur at a particular stress, defined as yield stress. Because thermoplastics and thermosets in engineering applications fail by yielding—that is, by the onset of plastic deformation—plastic deformation is closely associated with the technology of polymers. Chapter 14 presents an overview of yielding and deformation behavior in polymers. Theoretical approaches that have been developed to account for yield strength are outlined in this chapter. Polymers can fail in many other ways. Chapter 14 also discusses the analysis of the stress-strain curves of polymeric materials and enables their classification as brittle or ductile materials as well as establishing testing conditions for the ductile-brittle transition. The processes that take place when a polymer is fractured are described, as are crazing phenomena, characteristics of thermoplastic polymers. Crazing represents an intermediate state between microscopic fracture and yielding, and it is often a precursor to brittle fracture. Finally, the impact strength and fatigue are examined.

Among the main disadvantages of using polymers as structural components in engineering are their low stiffness and strength. To improve these properties, reinforced polymers or polymeric matrix composites are prepared. Chapter 15 provides an overview of these materials, mainly fiber-reinforced composites since they exhibit the best mechanical properties.

The methods utilized to measure the viscoelastic functions are often close to the stress patterns occurring in certain conditions of use of polymeric materials. Consequently, information of technological importance can be obtained from knowledge of these functions. Even the so-called ultimate properties imply molecular mechanisms that are closely related to those involved in viscoelastic behavior. Chapters 16 and 17 deal with the stress-strain multiaxial problems in viscoelasticity. Application of the boundary problems for engineering applications is made on the basis of the integral and differential constitutive stress-strain relationships. Several problems of the classical theory of elasticity are revisited as viscoelastic problems. Two special cases that are of special interest from the experimental point of view are studied: viscoelastic beams in flexion and viscoelastic rods in torsion.

Each chapter includes problem sets that we hope will facilitate the understanding of the subjects discussed in the book for those who are not familiar with the mechanical behavior of polymeric materials. This book should be used as a textbook in an undergraduate course of materials.

Evaristo Riande
Ricardo Díaz-Callejo
Margarita G. Prolongo
Rosa M. Masegosa
Catalina Salom

Contents

Preface

iii

1 Structure of Polymers	1
1.1 Introduction: Types of Polymers and Classification	1
1.2 Polymerization Processes	7
1.3 Molecular Weight and Molecular Weight Distribution	10
1.4 Configuration in Polymers	13
1.5 Conformational States in Polymers	16
1.6 Statistical Coil	18
Problem Sets	25
References	28
2 Crystalline and Amorphous States in Polymers	29
2.1 Introduction: Crystalline and Amorphous Regions in Polymers	29
2.2 Factors Determining the Crystallinity of Polymers	32
2.3 Crystal Structures of Polymers	33
2.4 Crystalline Morphology	37
2.5 Crystallization	43
2.6 Melting	46
2.7 Polymers in the Liquid Crystal State	51
2.8 Glassy State	57
2.9 Phenomenology of the Glass Transition	58

vii

2.10	Glass Transition and Free Volume	62
2.11	Factors Affecting the Glass Transition of Polymers	66
	Problem Sets	76
	References	83
3	Rubber Elasticity	85
3.1	Introduction	85
3.2	Thermodynamic Treatment	88
3.3	Statistical Treatment	93
3.4	Modifications to Simple Statistical Theory—Non-Gaussian Statistics	106
3.5	Swelling of Polymer Networks	109
3.6	Elastomers in Service	111
	Problem Sets	132
	References	139
4	Stress–Strain Relations for Ideal Solids and Ideal Liquids	140
4.1	Ideal Solids and Liquids: Constitutive Equations	140
4.2	Stress Tensor	143
4.3	The Second Law of Dynamics	146
4.4	Strain Tensor	147
4.5	Compatibility Equations	151
4.6	Effect of Symmetry on the Relationships Between the Stress and Strain Tensors in Ideal Elastic Systems	152
4.7	Generalized Stress–Strain Hooke’s Law for Isotropic Solids	162
4.8	Navier Equations	167
4.9	Generalized Strain–Stress Relationships for Ideal Elastic Systems	170
4.10	Thermoelastic Effects	172
4.11	Viscosity of Ideal Liquids	175
	Problem Sets	177
	References	195
5	Linear Viscoelasticity and Viscoelastic Functions	196
5.1	Viscoelasticity	196
5.2	Linear Viscoelasticity—Response of Materials to Transient Experiments	198
5.3	Boltzmann Superposition Principle in Creep Experiments	207
5.4	Memory Effects in Creep Experiments	212
5.5	Boltzmann Superposition Principle in Relaxation Experiments	214

5.6	Memory Function in Relaxation Experiments	216
5.7	Ramp Experiments	217
5.8	Laplace Transform Relationships Between Transient Relaxation Moduli and Transient Compliance Functions	218
5.9	Generalization of the Superposition Principle	221
5.10	Generalized Stress–Strain Relationships in the Frequency Domain	226
5.11	Generalized Stress–Strain Relationships for Viscoelastic Systems with Any Degree of Symmetry	227
	Problem Sets	228
	References	237
6	Dynamic Viscoelastic Functions	238
6.1	Introduction	238
6.2	Dynamic Relaxation Functions	239
6.3	Transformation of Relaxation Functions from the Frequency Domain to the Time Domain and Vice Versa	242
6.4	Complex Viscosity	242
6.5	Dissipated Energy in Dynamic Relaxation Experiments	243
6.6	Dynamic Creep Compliance Functions	244
6.7	Transformation of Compliance Functions from the Frequency Domain to the Time Domain and Vice Versa for Viscoelastic Solids	245
6.8	Dissipated Energy in Dynamic Creep Experiments	249
6.9	Analysis of Complex Creep Compliance Functions at Low Frequencies	250
6.10	Zero Shear Rate Viscosity and Steady-State Compliance Expressed in Terms of Viscoelastic Functions	252
6.11	Krönig–Kramers Relationships	253
6.12	Other Dynamic Viscoelastic Functions	255
	Problem Sets	257
	References	270
7	Experimental Determination of Viscoelastic Properties	271
7.1	Introduction	272
7.2	Experimental Determination of Dynamic Viscoelastic Properties	273
7.3	Torsion Pendulum	274
7.4	Corrections in the Determination of $G^*(\omega)$ from Free Oscillations in Shear	279
7.5	Forced Oscillations	280

7.6	Secondary Effects in Torsion	280
7.7	Effective Sample Length	283
7.8	Dynamic Mechanical Analysis by Transverse Flexion	285
7.9	Response of a Viscoelastic Rod to an Instantaneous Stimulus (Free Oscillations)	290
7.10	Determination of the Corrections in the Viscoelastic Functions Due to Clamping	292
7.11	Resonance Instruments	294
7.12	Wave Propagation	294
7.13	Experimental Determination of Static Viscoelastic Properties	296
7.14	Torsional Creep	296
7.15	Tensile Creep	298
7.16	Stress Relaxation	299
	Problem Sets	300
	References	304
8	Viscoelastic Behavior of Polymers Above T_g	306
8.1	Time-Temperature Correspondence Principle	306
8.2	Prediction of the Shift Factors for Viscoelastic Liquids	321
8.3	Prediction of the Shift Factors for Viscoelastic Solids	322
8.4	Influence of Temperature on Horizontal Shift Factors	323
8.5	Effect of Pressure on the Viscoelastic Response	327
8.6	Differentiation of Regions in the Master Curves of the Viscoelastic Functions	327
8.7	Influence of Diluents on the Viscoelastic Behavior of Polymers	339
8.8	Effects of Cross-Linking on the Viscoelastic Functions	343
	Problem Sets	348
	References	357
9	Retardation and Relaxation Spectra	359
9.1	Introduction	359
9.2	Formulation of Transient and Nontransient Relaxation Moduli in Terms of Retardation Spectra	360
9.3	Formulation of Transient and Nontransient Compliance Functions in Terms of Retardation Spectra	362
9.4	Important Inequalities Among Viscoelastic Functions	365
9.5	Determination of Viscosity and Steady-State (Equilibrium) Compliance from Relaxation and Retardation Spectra	366
9.6	Comparison of Retardation and Relaxation Times	368

9.7	Determination of Spectra from Viscoelastic Functions Using First-Order Approximations	371
9.8	Approximations of Higher Order	375
9.9	Experimental Retardation and Relaxation Spectra	378
9.10	Approximate Relationships Between Viscoelastic Functions	383
	Problem Sets	384
	References	393
10	Viscoelastic Models	394
10.1	Introduction	394
10.2	Maxwell's Model	395
10.3	The Kelvin-Voigt Model	398
10.4	Three-Element Standard Solid	400
10.5	Burgers Model	404
10.6	Maxwell and Kelvin-Voigt Generalized Models	406
10.7	Ladder Models	408
10.8	Distributed Constants Models	409
	Problem Sets	413
	References	422
11	Molecular Models of Viscoelastic Polymers	423
11.1	Concentration Regimes	423
11.2	Isolated Chains as Hookean Elements	425
11.3	Spring-Bead Model: Rouse Theory	425
11.4	Spring-Bead Model: Zimm Theory	428
11.5	Tube Model	430
11.6	Polydispersity and the Tube Model	434
11.7	Rouse Dynamics: Viscosity and Steady-State Compliance for Low Molecular Weight Chains in the Melt	434
11.8	Reptation Dynamics: Viscosity and Steady-State Compliance for High Molecular Weight Chains in the Melt	436
11.9	Comparison of Theoretical and Experimental Viscoelastic Results	439
11.10	Friction Coefficient	440
11.11	Concentration Dependence of Viscoelastic Functions in the Semidilute and Concentrated Regimes	443
11.12	Branched Polymers	446
	Problem Sets	447
	References	452

12 Viscoelasticity of Glassy and Semicrystalline Polymers	454
12.1 General Considerations	454
12.2 Relaxations in the Frequency Domain at Temperatures Slightly Higher than T_g	457
12.3 Topology of the Dynamics in the Vicinity of the Glass-Transition Temperature	460
12.4 Viscoelastic Functions for Glassy Systems in the Frequency Domain	463
12.5 Dispersions in the Glassy State and the Glass Transition	464
12.6 Molecular Cooperativity in the Glass Transition	468
12.7 Structural Recovery in the Glassy State: Aging	473
12.8 Memory Effects and Physical Aging	474
12.9 Influence of Physical Aging on the Viscoelastic Functions: Time-Aging Time Correspondence Principle	478
12.10 Nonlinear Behavior in Aging	482
12.11 Final Remarks on Aging Processes	483
12.12 Relaxation Behavior of Semicrystalline Polymers: General Considerations	485
12.13 General Features of Crystalline Polymers	494
12.14 Time-Temperature Correspondence Principle	496
12.15 Modeling the Viscoelastic Behavior of Crystalline Polymers	496
Problem Sets	498
References	507
13 Flow Behavior of Polymer Melts and Solutions	509
13.1 Introduction	510
13.2 Constitutive Equations	510
13.3 Second-Order Fluids in Simple Shearing Flow	515
13.4 Normal Stresses	517
13.5 Rheometry	518
13.6 Intrinsic Viscosity of Polymers	524
13.7 Flow Through a Slit	529
13.8 Sources of Error in Capillary and Slit Flows	531
13.9 Coaxial Cylinder: Couette Flow	536
13.10 Cone-Plate Viscometers	539
13.11 Plate-Plate Viscometers	541
13.12 Experimental Determination of Normal Stresses. Coaxial Cylinders	542
13.13 Factors Governing the Non-Newtonian Behavior of Polymers	546
13.14 Non-Newtonian Viscosity Models	550
13.15 Cox-Merz Rule	552

13.16	Influence of Diluents and Plasticizers, Blends, and Fillers on Flow	553
13.17	Parameters Influencing the First Normal Stress Difference	557
13.18	Die Swelling	558
13.19	Melt Index	560
13.20	Thixotropy and Rheopexy	562
13.21	Stretching Flow	563
	Problem Sets	568
	References	579
14	Yield Crazing and Fracture	582
14.1	Introduction: Ductile and Brittle Behavior	582
14.2	Shear Yield	584
14.3	Crazing	602
14.4	Fracture in Polymers	613
	Problem Sets	642
	References	651
15	Reinforced Polymers	653
15.1	Introduction	653
15.2	Polymer Matrices	655
15.3	Reinforcements: Fibers	664
15.4	Properties of Reinforced Polymers	670
15.5	Mechanical Properties of Unidirectional Composites	672
15.6	Laminates	681
15.7	Short Fiber Composites	684
	Problem Sets	690
	References	695
16	Multiaxial Analysis of Linear Viscoelastic Stress	696
16.1	Introduction	697
16.2	Integral Formulation of Viscoelastic Problems	697
16.3	Differential Form for the Constitutive Stress-Strain Relationship	701
16.4	Constitutive Equations in Differential Form for Multiaxial Tension States	703
16.5	Thermoviscoelasticity	706
16.6	Special Problems in Structural Linear Viscoelasticity	708
16.7	Formulation and Classification of the Boundary Problems in Viscoelasticity	708

16.8	Applicability of the Correspondence Principle. Quasi-Static and Dynamic Problems	709
16.9	Superposition and Saint Venant Principles	710
16.10	Problems with Special Symmetries	710
16.11	The Dynamic Problem	716
16.12	Plane Strain Problems	721
16.13	Plane Stress Problems	727
16.14	Indentation and Impact Problems	735
16.15	Roller Ball Indentation	740
16.16	Wave Propagation in Viscoelastic Materials	748
	Problem Sets	754
	References	767
17	Flexion and Torsion of Viscoelastic Beams and Rods	769
17.1	Introduction	770
17.2	Beam Bending: Preliminary Hypotheses and Stress Tensor	770
17.3	Bending Moment	772
17.4	Radius of Curvature	772
17.5	Momentum and Force Balances in Beams	775
17.6	Indentation of a Clamped Beam	776
17.7	Shear Stress Analysis in Elastic Beams	779
17.8	Shear Strain Analysis	783
17.9	Viscoelastic Beams	788
17.10	Transverse Vibrations in Viscoelastic Beams	789
17.11	Thermal Effects on Transverse Vibrations	808
17.12	Torsion of Viscoelastic Rods	816
17.13	Displacement and Strain Tensor in Torsion	816
17.14	Stress Tensor in Torsion	818
17.15	Equilibrium Equations for Torsion	819
17.16	Boundary Conditions	820
17.17	Torsion Function Found by Separation of Variables	821
17.18	Moment of Torque	822
17.19	Motion and Boundary Condition Equations	824
17.20	Analysis of Torsional Oscillations Using an Elastic Auxiliary Element	832
	Problem Sets	836
	References	864
Appendix		866
A.1	Laplace Transformation	866
A.2	Properties of the Laplace Transformation	867

A.3	Inverse of the Laplace Transformation	867
A.4	Carson Transformation	868
A.5	Fourier Transformation	868
A.6	Stieltjes Transformation	869
A.7	Table of Laplace Transformations	869
A.8	Reference	869
 <i>Index</i>		 871

POLYMER VISCOELASTICITY

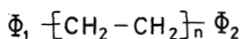
1

Structure of Polymers

1.1 Introduction: Types of Polymers and Classification	1
1.2 Polymerization Processes	7
1.3 Molecular Weight and Molecular Weight Distribution	10
1.4 Configuration in Polymers	13
1.5 Conformational States in Polymers	16
1.6 Statistical Coil	18
Problem Sets	25
References	28

1.1 INTRODUCTION: TYPES OF POLYMERS AND CLASSIFICATION

The word *polymer* literally means “many parts.” A polymer is a macromolecule that contains many groups of atoms, called monomeric units, that are covalently bonded. The simplest hydrocarbon chain polymer is polyethylene, with the general formula:



obtained from the monomer ethylene, $\text{H}_2\text{C}=\text{CH}_2$.

The number of ethylene monomeric units, n , can reach values between 10^3 and 10^6 . For high molecular weight chains, terminal groups ϕ_1 and ϕ_2 are present in low concentrations and will therefore have no effect on the

mechanical properties of the polymer. Terminal groups influence mainly the chemical stability of the polymer. Heating or irradiation can provoke the degradation of polymers with unstable terminal groups.

The polymer indicated above has a linear skeletal structure that can be represented by a chain with two ends. There are also polymers with nonlinear skeletal structures of the type shown in Figures 1.1 and 1.2. Nonlinear polymers are called branched polymers when they have side chains or branches of significant length covalently linked to the main chain. These polymers are characterized according to the number and size of the branches. There are also nonlinear polymers, known as cross-linked polymers or polymer networks, that have three-dimensional structures in which each chain is linked to the others via a sequence of chemical bonds.

The term *homopolymer* is generally used to describe the polymers whose chemical structure can be represented by the multiple repetition of a single type of repeating unit, which can contain one or more kinds of monomeric units. The chemical structure of a polymer is normally represented by placing the repeating unit between square brackets. For example, the homopolymer $A-A-A-A-A-A-$ would be represented by $[A]_n$, when n is the number of repeating units joined together to form the macromolecule. Tables 1.1a, 1.1b show the chemical structures of some common homopolymers, together with the monomers from which they derive.

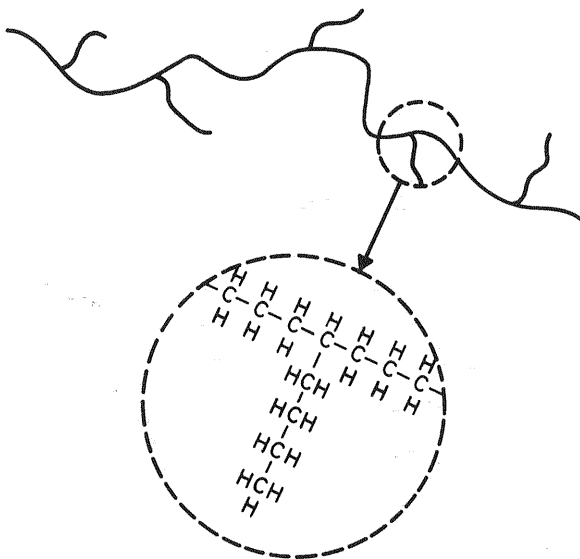


Figure 1.1 Side-branched polyethylene.

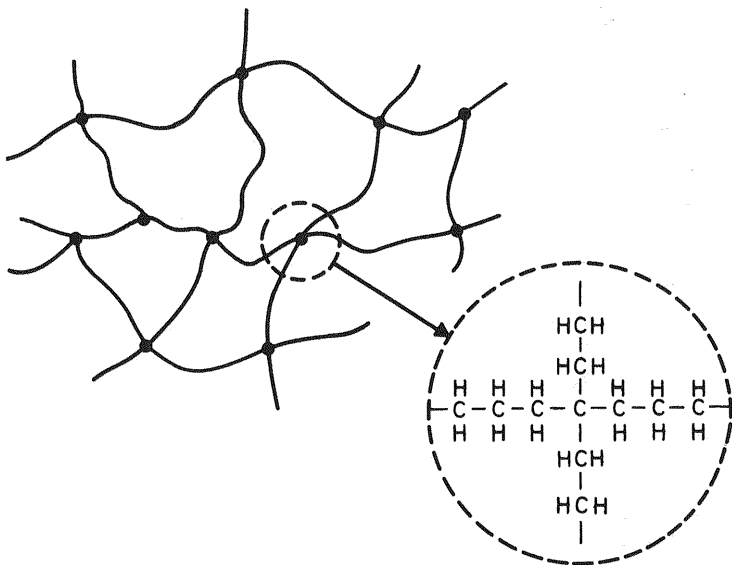


Figure 1.2 Cross-linked polyethylene.

The nomenclature of polymers is somewhat complex, due in part to the fact that the majority of polymers have more than one correct name; moreover, in some cases the registered trade names are also used to denote some polymers. The criterion adopted here is to use names that most clearly and simply state the chemical structures of the polymers. The polymers in Tables 1.1a and 1.1b have been named following the basic rules of nomenclature. Thus, the prefix “poly” is placed before the name of the monomer, and the name of the monomer is set within parentheses unless it is a simple word. In the case of repeating units containing more than one monomer (examples in Table 1.1b), the words contained in parentheses after the prefix “poly” must describe the chemical structure of the repeating unit.

The term *copolymer* is used to describe polymers whose molecules contain two or more different types of repeating units. There are various types of copolymers depending on how the repeating units are organized along the polymer chain. For simplicity, we will consider copolymers consisting of just two repeating units A and B. *Statistical copolymers* are copolymers in which the distribution sequence of the repeating units A, B obey statistical laws. *Random copolymers* are a special type of statistical copolymer in which the distribution of the repeating units is random:

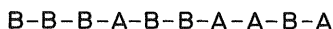


Table 1.1a Addition Polymers

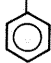
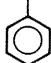
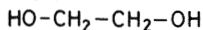
Ethylene	$\text{CH}_2=\text{CH}_2$	Polyethylene	$-(\text{CH}_2-\text{CH}_2)_n-$
Propylene	$\text{CH}_2=\text{CH}-\text{CH}_3$	Polypropylene	$-(\text{CH}_2-\underset{\text{CH}_3}{\text{CH}})_n-$
Styrene	$\text{CH}_2=\text{CH}$ 	Polystyrene	$-(\text{CH}_2-\underset{\text{C}_6\text{H}_5}{\text{CH}})_n-$ 
Vinyl chloride	$\text{CH}_2=\underset{\text{Cl}}{\text{CH}}$	Poly (vinyl chloride)	$-(\text{CH}_2-\underset{\text{Cl}}{\text{CH}})_n-$
Tetrafluoroethylene	$\text{CF}_2=\text{CF}_2$	Poly (tetrafluoroethylene)	$-(\text{CF}_2-\text{CF}_2)_n-$
Acrylonitrile	$\text{CH}_2=\underset{\text{CN}}{\text{CH}}$	Polyacrylonitrile	$-(\text{CH}_2-\underset{\text{CN}}{\text{CH}})_n-$
Methyl acrylate	$\text{CH}_2=\underset{\text{COOCH}_3}{\text{CH}}$	Poly (methyl acrylate)	$-(\text{CH}_2-\underset{\text{COOCH}_3}{\text{CH}})_n-$
Methyl methacrylate	$\text{CH}_2=\underset{\text{COOCH}_3}{\overset{\text{CH}_3}{\text{C}}}$	Poly (methyl methacrylate)	$-(\text{CH}_2-\underset{\text{COOCH}_3}{\overset{\text{CH}_3}{\text{C}}})_n-$
Dienes :	$\text{CH}_2=\underset{\text{R}}{\text{C}}-\text{CH}=\text{CH}_2$		$-(\text{CH}_2-\underset{\text{R}}{\text{C}}=\text{CH}-\text{CH}_2)_n-$
	$\text{R} \equiv -\text{H}$		Polybutadiene
	$\text{R} \equiv -\text{CH}_3$		Polyisoprene
	$\text{R} \equiv -\text{Cl}$		Polychloroprene

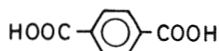
Table 1.1b Step Polymers

Ethylene glycol

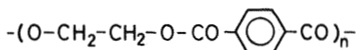


and

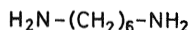
Terephthalic acid



Poly(ethylene terephthalate) (PET)

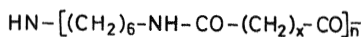
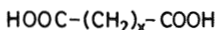


Hexamethylene diamine



and

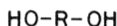
Dicarboxylic acids



X = 8 nylon 6.10

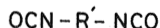
X = 4 nylon 6.6

Diol



and

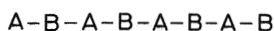
Diisocyanate



Polyurethane

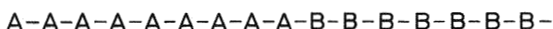


Alternating copolymers are those consisting of just two types of repeating units arranged alternately along the polymer chain:

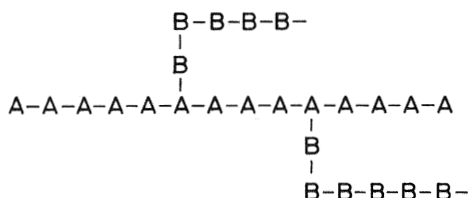


The properties of statistical, random, and alternating copolymers generally are intermediate to those of the parent homopolymers.

Block copolymers are linear copolymers in which the repeating units appear in groups or blocks of the same type, thus:



Graft copolymers are branched copolymers in which the chemical structure of the branches differs from that of the main chain. In their simplest form, they consist of long side chains of a second polymer chemically attached to the base polymer:



Unlike the copolymers described earlier, block and graft copolymers display characteristic properties of the constituent homopolymers though they also display certain unique properties that depend on the compatibility of the components and their respective glass transition temperatures.

The principles of nomenclature for copolymers are based on their structure and are given in Table 1.2, where A and B represent the names of repeating units. For example, a statistical copolymer of ethylene and propylene would be called poly(ethylene-stat-propylene), and a triblock copolymer of styrene (A) and isoprene (B) would be called polystyrene-*block*-polyisoprene-*block*-polystyrene. In some cases it is necessary to introduce square brackets in the nomenclature to clarify the notation. Let us see an example: An alternating copolymer of styrene and maleic anhydride would be called poly[styrene-*alt*(maleic anhydride)].

Polymers are commonly classified into three groups: thermoplastics, elastomers, and thermosets. This method of classification is based on the thermomechanical properties of the polymers as a consequence of their molecular structure. *Thermoplastics* are linear or branched polymers that become fluid when heat is applied. They can be molded and transformed using processing techniques such as injection molding and extrusion. Thermoplastics currently form the major proportion of polymers used in industry. Thermoplastics can be classified into crystalline and amorphous. *Elastomers* are cross-linked polymers with a low density of cross-linking points that can be easily deformed, reaching extensions of up to ten times their original dimensions and rapidly recovering their original size when the applied tension is released. It is precisely because of their network condition that they cannot flow, though they can recover their original dimension by the action of a recovering force of entropic origin when the applied tension is released. Thermosettable polymers or *thermosets* are rigid materials; their structure is that of polymer networks or meshes in which the chain movements are severely restricted due to the high density of the cross-linking

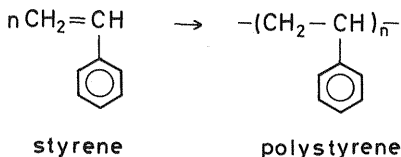
Table 1.2 Nomenclature for Copolymers

Type of copolymer	Nomenclature
Unspecified	Poly(A- <i>co</i> -B)
Statistical	Poly(A- <i>stat</i> -B)
Random	Poly(A- <i>ran</i> -B)
Alternating	Poly(A- <i>alt</i> -B)
Block	PolyA- <i>block</i> -polyB
Block-poly A	PolyA- <i>block</i> -polyB
Graft ^a	PolyA- <i>graft</i> -polyB

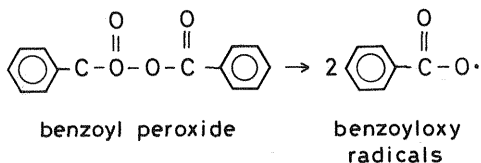
points (see Fig. 1.2). As occurs with elastomers, thermosets cannot be transformed once obtained, nor do they flow under the action of heat; instead they undergo degradation at high temperatures.

1.2 POLYMERIZATION PROCESSES

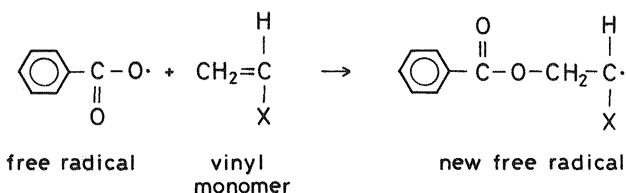
The requirement for monomer polymerization is that each monomer has to be left linked to at least two other monomers, and consequently, the monomer functionality has to be 2 or higher. Polymerization processes can be broadly divided into chain or addition polymerization and step polymerization (1–3). Chain polymerization involves the opening of double bonds of low molecular weight molecules (monomers) to form a polymer chain. For example, styrene polymerizes to polystyrene.



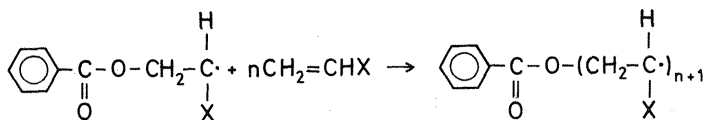
Chain polymerization involves three stages: initiation, propagation, and termination. The most important of the chain polymerization methods is free radical polymerization, in which the initiation step occurs by an attack on the monomer molecule by a free radical. A free radical is a reactive molecule possessing an unpaired electron and is usually formed by the decomposition of a relatively unstable molecule referred to as an initiator. In particular, those compounds containing peroxide bonds, ($-\text{O}-\text{O}-$), can produce free radicals by thermal decomposition, for example,



The free radical species react to open the double bond of the monomer and add to it:

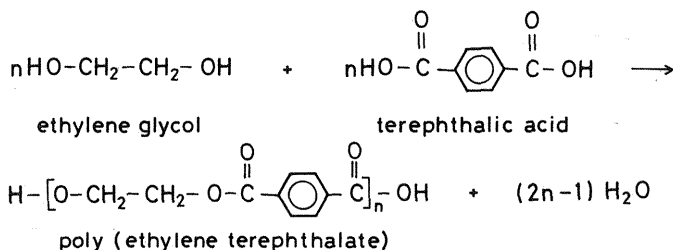


Following the initiation reaction a large number of monomers are rapidly added to the growing species:



This process of propagation continues until the reactive center is destroyed in what is called the termination stage. Termination occurs either by the combination of two growing radicals or by disproportionation, in which a hydrogen is transferred from one chain to the other, forming inactive polymer chains. Free radical polymerization is the most widely used process for the preparation of polymers from monomers having the general structure $\text{CH}_2=\text{CR}_1\text{R}_2$, such as vinyl polymers, acrylic polymers, and methacrylic polymers (see Table 1.1a).

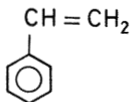
Step polymerization occurs by successive reactions between functional groups of reactants. A typical example is the synthesis of a polyester, where each of the two reactants possesses two reactive end groups (difunctional monomers):



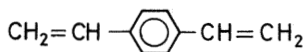
This polymerization process is a polycondensation in which the molecular weight builds up slowly as the small molecules of water are eliminated. Most step polymerization processes are polycondensations; thus the terms "step polymerization" and "condensation polymerization" are often used synonymously. The stepwise reaction leads successively from monomers to dimers, trimers, and so on, until finally polymer molecules are formed. The polymers obtained are classified by taking into account the functional group of the repeating unit, for example, polyesters ($-\text{CO}-\text{O}-$), polyamides ($-\text{CO}-\text{NH}-$), polyurethanes ($-\text{O}-\text{CO}-\text{NH}-$), polyethers ($-\text{O}-$), and polycarbonates ($-\text{O}-\text{CO}-\text{O}-$).

While linear polymers are synthesized from monomeric units with functionality 2, polymerization reaction of a mixture of monomers with functionality 2 and higher than 2 gives rise to cross-linked polymers. For example, let us consider the case of a polymerization reaction of polystyrene

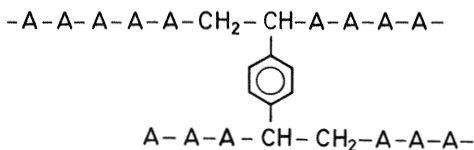
to which has been added a small percentage of divinylbenzene. Styrene is a monomer with functionality 2.



However, divinylbenzene is a monomer with functionality 4.



During the course of the reaction, the divinylbenzene will act as a cross-linking agent, and in the structure of the polymer obtained we will find cross-linking points (cross-links) of the type



where A represents the styrene monomer unit. As can be seen from the above scheme, the divinylbenzene acts as a union bridge between the polystyrene chains, obtaining a cross-linked structure similar to that shown in Figure 1.2. Once the polymer network has been obtained, the number of chains starting from a monomer unit is the same as the functionality of the starting monomer. The properties of the cross-linked polymer depend on the number of cross-links existing in the network and on the length of the chains between cross-links. Thus, if there are many cross-links, the chains between nodes are short, and consequently the mobility of the chains between cross-links will be strongly reduced. The product obtained in these circumstances is known as a thermoset. A typical example of a thermoset is the phenolic resin shown in Figure 1.3. This resin is obtained by reacting phenol (a trifunctional monomer) with formaldehyde (a bifunctional monomer).

On the other hand, if the cross-link density is low (the length of the chains between cross-links is large) and the mobility of the chains is high, the cross-linked material is called an elastomer. An example of a typical elastomer is *cis*-1,4-polyisoprene (natural rubber), which, by means of a cross-linking reaction with sulfur (vulcanization), gives rise to a network structure (see Fig. 1.4).

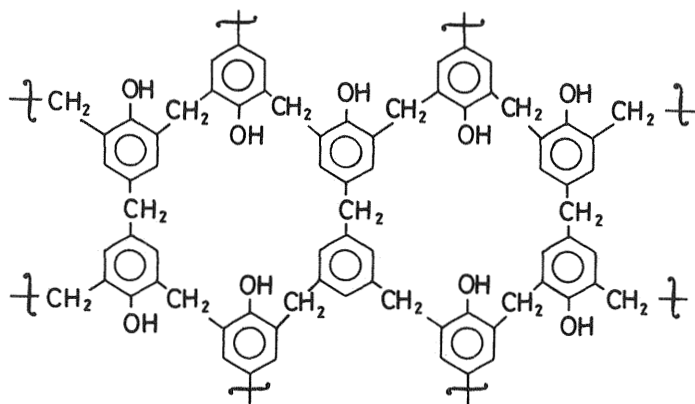


Figure 1.3 Structure of a phenolic resin.

1.3 MOLECULAR WEIGHT AND MOLECULAR WEIGHT DISTRIBUTION

Many properties of polymers depend on their size, which is expressed in terms of their molecular weight, M . For cross-linked polymers (polymer networks), the only significant molecular weight is that corresponding to the fragments of the polymer chains existing between the cross-linking points, since the molecular weight of the network itself is essentially infinite. The molecular weight of a homopolymer is related to the degree of polymerization, α , which is defined as the number of repeating units making up the polymer chain. Consequently, $M = \alpha M_0$, where M_0 is the molecular

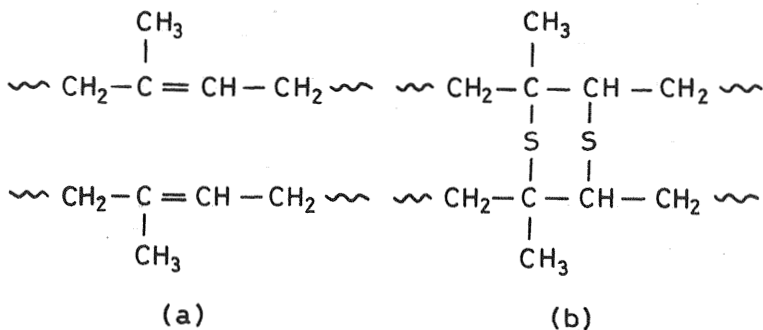


Figure 1.4 (a) *cis*-1,4-Polyisoprene (natural rubber). (b) Cross-linking reaction with sulfur (vulcanization).

weight of the repeating unit. To define the molecular weight of a copolymer, it is necessary to know the sum of the product αM_0 for each type of repeating unit.

In general, polymers do not have a unique molecular weight (in contrast with nonpolymeric substances). Instead, they have a distribution of molecular weights and therefore different intervals of αM_0 , which are known as fractions. Consequently, the distribution of molecular weights will be discontinuous. Nevertheless, since, for most polymers the changes in the intervals corresponding to each fraction are very small in comparison to the total interval of molecular weights, the distribution can be regarded as continuous, as shown in Figure 1.5. The ordinate is generally the weight fraction, w_i , of molecules of molecular weight M_i , but it is apparent that it might be appropriate occasionally to plot the molar fraction. The distribution of molecular weights can be characterized in terms of different molecular weight averages; these are defined taking into account the discontinuous nature of the distribution in which the macromolecular fractions contain N_i molecules of molecular weight $M_i = \alpha_i M_0$.

The two most important molecular weight averages are the number-average molecular weight, M_n ,

$$M_n = \frac{\sum N_i M_i}{\sum N_i} = \sum x_i M_i \quad (1.1)$$

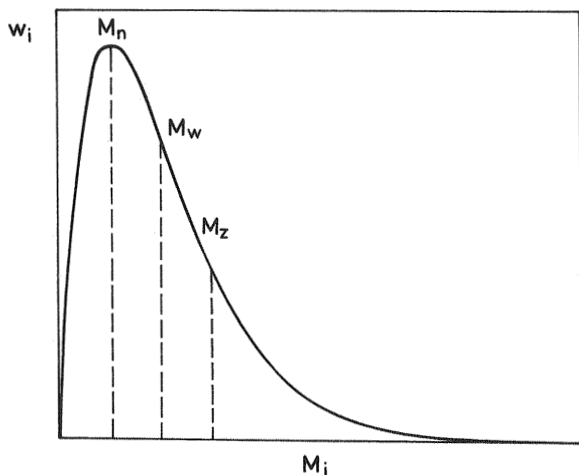


Figure 1.5 Typical molecular weight distribution of a polydisperse polymer sample.

and the weight-average molecular weight, M_w ,

$$M_w = \frac{\sum N_i M_i^2}{\sum N_i M_i} = \sum w_i M_i \quad (1.2)$$

where N_i is the number of molecules of molecular weight M_i and x_i and w_i are the molar fraction and weight fraction, respectively, of molecules of molecular weight M_i . Other averages are M_z and M_{z+1} given by

$$M_z = \frac{\sum N_i M_i^3}{\sum N_i M_i^2} = \frac{\sum w_i M_i^2}{M_w} \quad (1.3)$$

$$M_{z+1} = \frac{\sum N_i M_i^4}{\sum N_i M_i^3} = \frac{\sum w_i M_i^3}{M_w M_z} \quad (1.4)$$

For distributions with a single maximum, M_n is normally close to the maximum. M_w is always greater than M_n , except for monodisperse samples where all molecules have the same molecular weight and $M_w = M_n$. For simple distributions, M_w is typically 1.5 or 2 times M_n . The relative locations of the different weight averages are given in Figure 1.5. The ratio M_w/M_n is known as the polydispersity index and must, by definition, be greater than 1 for a polydisperse polymer; it provides a measure of the width of the distribution. It can be shown that the width of the number-average molecular weight distribution, expressed as its standard deviation, σ_n , is related to the ratio M_w/M_n as follows (see Problem 1.2):

$$\frac{\sigma_n}{M_n} = \sqrt{\frac{M_w}{M_n} - 1} \quad (1.5)$$

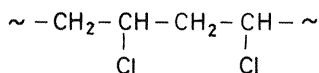
The standard deviation of a weight-average molecular weight distribution can be written as (see Problem 1.2):

$$\frac{\sigma_w}{M_w} = \sqrt{\frac{M_z}{M_w} - 1} \quad (1.6)$$

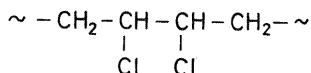
For many polymers, a narrow distribution of molecular weight leads to better properties than a wide distribution.

1.4 CONFIGURATION IN POLYMERS

The properties of polymer materials do not just depend on their chemical composition and molecular weight. Their molecular structure also has a marked influence on their physical properties. "Molecular structure" is understood to mean the arrangement of the atoms in the molecule. The term "configuration" refers to the organization of the atoms along the chain; to change a polymer configuration it is necessary to break and reform chemical or primary bond (3). On the other hand, the term "conformation" refers to the spatial arrangement of the atoms and substituents of a polymer chain; different conformations are obtained simply by rotation around the single primary bonds. Conformational isomers can therefore be interconverted without having to break any chemical bond in the chain. A polymer configuration is defined by the polymerization method, and a polymer preserves its configuration until it reacts chemically. The polymerization of asymmetrical monomers can give rise to head-to-tail, head-to-head, and tail-to-tail configurations along the chains. For poly(vinyl chloride), for example, the head-to-tail union leads to the structure

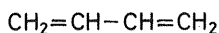


while the head-to-head union would give

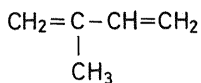


Due to energetic and steric reasons, the head-to-tail union is the preferred structure. In spite of this, radical addition polymers always contain a small proportion of head-to-head unions. The properties of these isomers are considerably different; in particular, the presence of head-to-head unions gives rise to irregularities that make it difficult for polymer chains to crystallize.

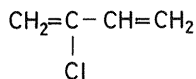
A wide range of polymers are obtained from the addition of conjugate diene monomers, notably 1,3-butadiene, isoprene, and chloroprene:



1,3-butadiene

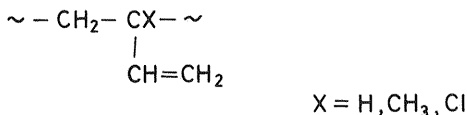


isoprene

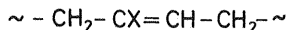


chloroprene

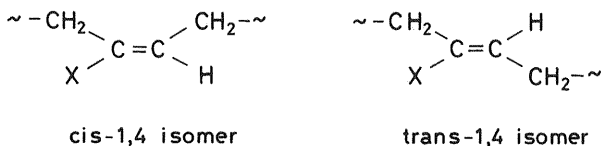
The addition of successive monomers can be made to the 1-2 bond; the polymerization is then called 1-2 addition and forms chains with the configuration



In the case of 1,3-butadiene, 1-2 addition and 3-4 addition are equivalent, but for isoprene and chloroprene, as is evident, 1-2 and 3-4 additions give different products. The third possibility is referred to as 1-4 addition and produces chains with the configuration



The 1-4 addition can take the *cis* orientation, leaving the substituents on the same side of the double bond, or the *trans* orientation, leaving them on opposite sides. These isomers are known as geometric isomers



In radical polymerizations the 1-4 *trans* addition usually predominates. This is thought to be due to the fact that the monomers are generally used in the *trans* form and they maintain their configuration during polymerization. It is possible to favor 1-4 *cis* addition by using ionic initiators. In general, 1-4 *cis* and 1-4 *trans* addition polymers can be crystallized when they are in the pure state, differing from each other in having very different melting points. But if the macromolecule contains both forms (randomly alternating *cis*, *trans*), then crystallinity is inhibited.

Polymerization of monomers with the chemical structure $\text{CH}_2 = \text{CXY}$, in which one of the carbon atoms carries two different substituents (X, Y), can give rise to three basic types of steric or spatial configurations known as isotactic, syndiotactic, and atactic. Let us consider two consecutive monomer units (a dyad) of a polymer chain, as shown in Figure 1.6a. Depending on the relative positions of the substituents X and Y, two stereochemical configurations can be defined: meso dyads (m) when equal substituents are located on the same side and therefore closest in space, and racemic dyads (r) if they are located on opposite sides as far away from each other as possible. Figure 1.6b shows the projections of these configurations on a plane. Triads (three consecutive monomer units) could be in the configurations mm, rr, or mr, as shown in Figure 1.6c. These triads are known as isotactic, syndiotactic, and heterotactic, respectively. In the illustration of Figure 1.6, the fully extended conformation has been chosen. Rotation around the C—C bonds of the

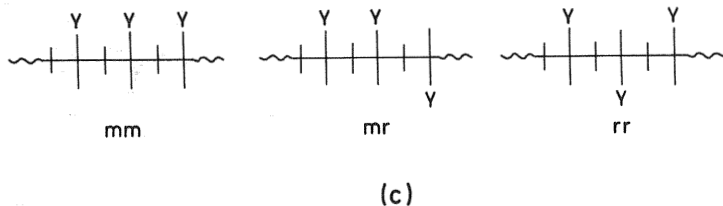
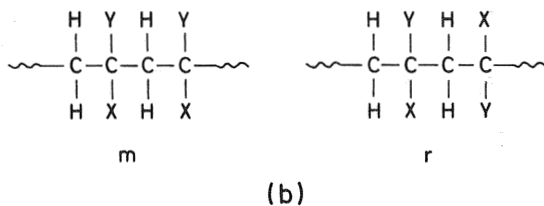
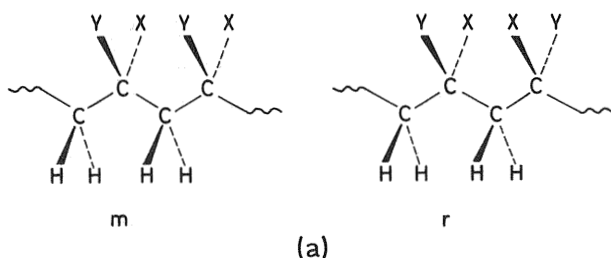


Figure 1.6 Configurational sequences. (a) Spatial representations of meso (m) and racemic (r) configurations. (b) Planar projections of m and r configurations, (c) Isotactic (mm), heterotactic (mr), and syndiotactic (rr) triads.

chain gives rise to other conformations, without modifying the steric configuration—isotactic, syndiotactic, or heterotactic. When meso configurations predominate, a polymer is said to be isotactic, whereas if racemic configurations are dominant, it is called syndiotactic. Real synthetic polymers are not obtained in either wholly isotactic (mmmmm...) or wholly syndiotactic (rrrrr...) configurations, so their degree of stereoregularity is defined by giving the proportion of triads or dyads. The stereochemical sequences are determined by the use of nuclear magnetic resonance (NMR).

Polymers in which the chains show meso and racemic dyads at random are not stereoregular and are known as atactic. In terms of the nomenclature, to specify whether it is predominantly isotactic or syndiotactic, the prefix *it-* or *st-*, respectively, is placed before the name of the polymer. The absence of a prefix indicates an atactic polymer. Stereoregular polymers can be obtained via special methods such as anionic and coordination polymerization. The properties of these polymers are going to vary dramatically depending on the degree of stereoregularity; in general it can be stated that the more regular a sample is, the greater will be its crystallinity and the lower its solubility.

1.5 CONFORMATIONAL STATES IN POLYMERS

As we have already mentioned, the conformation of a polymer chain is determined by the position taken in space by their atoms that can be interchanged by simple rotation about single bonds (4). There are flexible polymers that can adopt a large number of conformations, and rigid chains for which only a limited number of conformations are accessible. On the other hand, flexible polymers in the crystalline state adopt fixed conformations, whereas in solution or in the molten state they adopt a wide range of conformations. To illustrate what the conformational change consists of, we refer to the molecule of *n*-butane, shown in Figure 1.7. It can be seen that two extreme conformations can occur: the one known as *cis*, in which

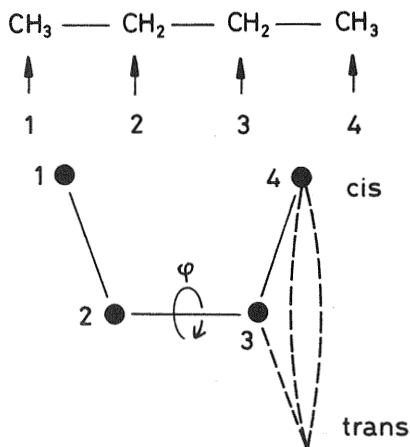


Figure 1.7 Conformation of *n*-butane.

carbons 1 and 4 are located as close as possible in space, and the one known as trans, in which they are located in opposite positions. The passage from one to the other is achieved by simple rotation around the $C_2 - C_3$ bond. As the terminal CH_3 groups are bulky, the cis conformation produces steric hindrances; accordingly the trans conformation is the most stable. To characterize the different conformations that occur in n -butane, the angle of rotation around the bond $C_2 - C_3$ is taken, with the convention of $\varphi = 180^\circ$ for the trans conformation and $\varphi = 0^\circ$ for the cis conformation. The lowest energy corresponds to trans; those known as gauche, $g'(\varphi = 300^\circ)$ and $g(\varphi = 60^\circ)$, are conformations with minimum energy though greater than trans; and cis is the least favorable. The interactions between the C_1 and C_4 groups are known as first-order interactions and are responsible for the energies of the gauche and trans states. The potential energy of interaction can be represented as a function of the angle φ as shown in Figure 1.8. The energy barriers between the three most stable conformations are of the order of thermal energy, RT . In the case of chains longer than n -butane, second-order interactions must also be borne in mind. These interactions are those that occur when groups joined via four bonds approach each other in space. The distance between these groups, and therefore their interaction potential energy, depends on two consecutive angles, as is the case of n -pentane. Considering only the minimum energy positions, t, g' , g, the conformations illustrated in Figure 1.9 can be identified. The lowest energy conformation is tt, while those with highest energy correspond to the combination $g'g' \equiv gg'$; the conformations with intermediate energies are $tg' = gt$, $tg \equiv g't$, and $g'g \equiv gg$. For n -hexane, it is necessary to consider three angles, the interactions being the same type as in n -pentane, first-order and second-order. In the case of a macromolecular chain of n atoms, $n - 3$

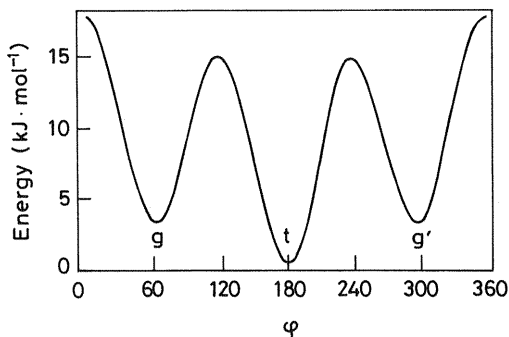


Figure 1.8 Conformational energy of n -butane as a function of the angle of rotation φ .

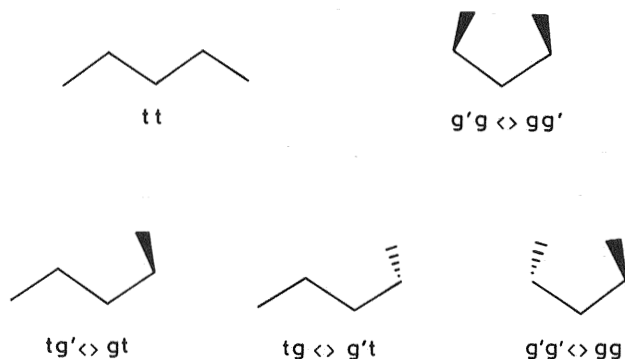


Figure 1.9 Conformations of *n*-pentane.

angles have to be considered, which in a strict sense will be able to take values between 0 and 2π , not just the minimum energy positions. Consequently, the rotation of the bonds of a polymer chain would lead to many different conformations, i.e., to different energy states, and not all the conformations of a chain would be equally stable. Taking into account values of n in the usual range 1000–10,000, the number of molecular conformations will be enormous, increasing as an exponential function of n . In some cases one of the possible conformations is much more stable than the others, and the macromolecule adopts this one exclusively; this is the case of polymers in the crystalline state. If the energy difference between conformational states is of the same order of magnitude as the thermal energy, macromolecule would adopt the entire set of possible conformations over time. This state of the macromolecule, in which the chain adopts any of the possible conformations, is known as a statistical coil. In it, each conformation ceases to be individually discernible and the only thing that matters is the set of all of them. It is impossible to determine the exact conformation of any macromolecular chain at any particular instant. However, despite the complexity of the conformational problem, the required information can be obtained statistically.

1.6 STATISTICAL COIL

The disordered state of a statistical coil is what is displayed by polymers in the molten and amorphous states and also in solution. To describe the conformation of a macromolecule consisting of a main chain $N + 1$ atoms, the positions of all them have to be determined. Using vectorial

notation in accordance with the diagram in Figure 1.10, this would be carried out knowing the vectors $\mathbf{l}_1, \mathbf{l}_2, \dots, \mathbf{l}_N$ making up the chain. These are inaccessible in many cases; therefore the tendency is to represent a conformation by a more global parameter such as the end-to-end distance of the chain \mathbf{r} , which is defined as

$$\mathbf{r} = \sum_{i=1}^N \mathbf{l}_i \quad (1.7)$$

The objective is to obtain the mean value of the end-to-end distance corresponding to the set of conformations that define the statistical coil state. For this, it is possible to think physically in two ways that might seem different at first sight but are in fact the same (ergodic hypothesis):

1. Determine the values that \mathbf{r} adopts with time for a particular macromolecule and then calculate a time average.
2. Determine the values of \mathbf{r} at a particular instant for N macromolecules of the sample, and thus calculate the instantaneous mean value of \mathbf{r} for the set of macromolecules. In this way, the mean square value of the end-to-end distance of the chain is defined as

$$\langle r^2 \rangle = \frac{1}{N} \sum_{i=1}^N \sum_{j=1}^N \mathbf{l}_i \cdot \mathbf{l}_j \quad (1.8)$$

The result of the two methods is the same for a polymer in the liquid state, because a macromolecule statistically takes all the possible conformations with time, which is equivalent to observing a large number of macromolecules at a particular instant. In the glassy state, each molecule adopts one specific conformation, and therefore the value of \mathbf{r} does not change with

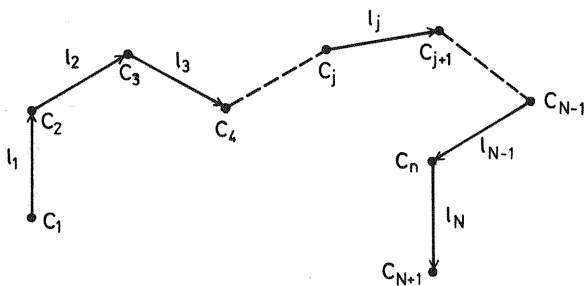


Figure 1.10 Position vectors of a macromolecular chain with $n + 1$ atoms.

time. In this case the only average that can be obtained is the instantaneous average considering the set of macromolecules in the glass.

To obtain the statistical properties of a chain, we consider a chain OP (Fig. 1.11) with a coordinate axis system established at one end. Let \mathbf{r} be the end-to-end vector of the macromolecule whose origin coincides with that of the coordinates and whose tip corresponds to the coordinate point (x, y, z) ,

$$\mathbf{r} = ix + jy + kz \quad (1.9)$$

The chain OP can adopt an enormous number of different conformations, each of which is characterized by a value of \mathbf{r} . Each value of \mathbf{r} will have a specific probability. The greater the number of conformations corresponding to a particular value of \mathbf{r} , the greater will be the probability. Consider first an artificially restricted chain with the ends O and P remaining on the x axis (see Fig. 1.12). When the separation between O and P is equal to the contour length, x_l , the chain is straight, i.e., a fully extended macromolecule. This conformation is achieved by a single path; consequently, the probability of acquiring this conformation is insignificant. However, when the end-to-end distance, x' , is much less than the contour length, the chain can adopt a large number of conformations while x' remains constant. When O and P coincide, the number of possible conformations is greatest, and the probability that x' is equal to zero is greater than for any other value of x' . Equating the number of possible conformations with the probability is

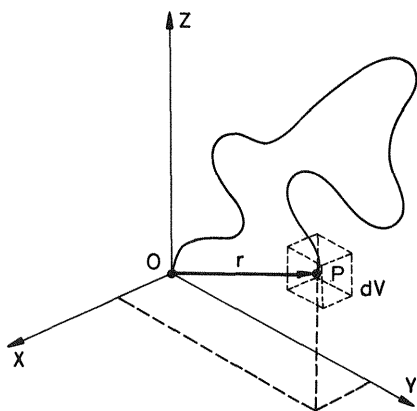


Figure 1.11 Schematic representation of a macromolecule with end-to-end distance \mathbf{r} .

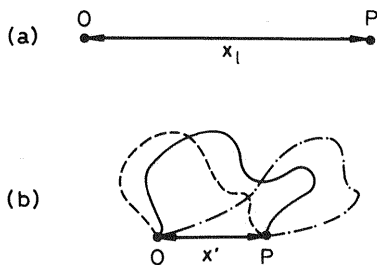


Figure 1.12 Schematic representation of a macromolecule with its ends in the x axis. (a) Fully extended conformation; (b) three of many conformations with end-to-end distance x' .

based on the consideration that each conformation is a priori equally probable. The function that models this behavior is the Gaussian function (5)

$$p(x) = \frac{\exp[-(x/\rho)^2]}{\sqrt{\pi\rho}} \quad (1.10)$$

where ρ is a representative length, i.e., a parameter of the model. The probability of the end-to-end distance being between x and $x + dx$ is linearly proportional to dx . Therefore, the probability that the end-to-end distance is between x and $x + dx$ is defined as the product of $p(x)$ and dx :

$$p(x)dx = \frac{\exp[-(x/\rho)^2]}{\sqrt{\pi\rho}} dx \quad (1.11)$$

The Gaussian function is shown in Figure 1.13, with a maximum at $x = 0$. In relation to the three-dimensional problem, the probability that the tip P of the vector \mathbf{r} is contained in a volume element dV (see Fig. 1.11) is, according to the Gaussian model,

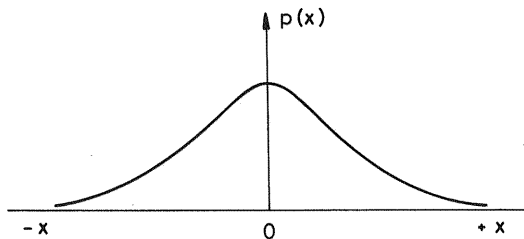


Figure 1.13 The Gaussian function $P(x)$ as a function of x .

$$\begin{aligned}
 P(x, y, z)dx dy dz &= p(x) p(y) p(z) dx dy dz \\
 &= \frac{\exp[-(x^2 + y^2 + z^2)/\rho^2]}{(\sqrt{\pi}\rho)^3} dx dy dz \\
 &= \frac{\exp[-(r^2/\rho^2)]}{(\sqrt{\pi}\rho)^3} dx dy dz
 \end{aligned}
 \tag{1.12}$$

The function of $P(x, y, z)$ is spherically symmetrical; it is a unique function of r . This result is obviously the expected one and implies that all directions of the vector OP are equally probable. In addition, the function $P(x, y, z)$ has a maximum when $r=0$, which corresponds to the case in which the two ends of the chain coincide, and it decreases as r increases (see Fig. 1.14). Equation (1.12) supplies information in only one direction of the space; to know the most probable value for the end-to-end distance, all directions of space have to be taken into account equally. Consequently, the probability of finding the end P of the chain at a distance r from the origin O in a spherical shell of thickness dr has to be calculated. The volume element in this case is $dV = 4\pi r^2 dr$ (see Fig. 1.15), and the probability is obtained as

$$P(r)dV = \frac{\exp-(r^2/\rho^2)}{(\sqrt{\pi}\rho)^3} 4\pi r^2 dr = \frac{4}{\sqrt{\pi}\rho^3} r^2 \exp\left[-\frac{r^2}{\rho^2}\right] dr
 \tag{1.13}$$

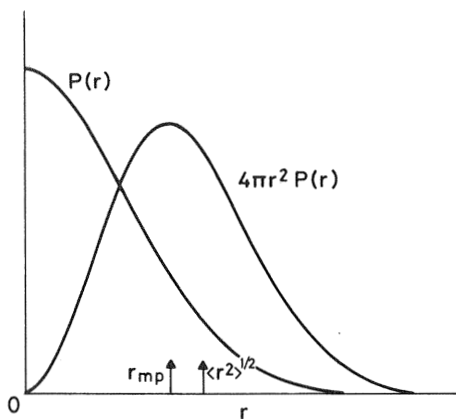


Figure 1.14 The Gaussian functions $P(r)$, $4\pi r^2 P(r)$.

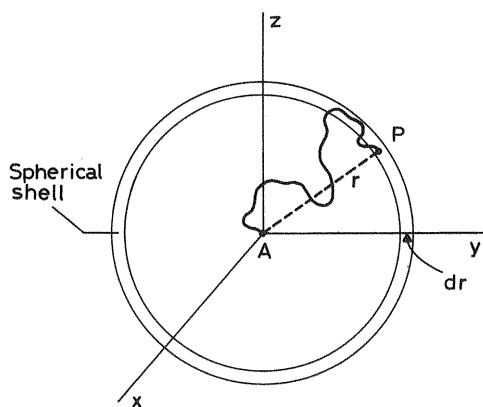


Figure 1.15 A spherical shell at a distance r that determines the distribution of r values regardless of direction in space.

The function $4\pi r^2 P(r)$ is represented in Figure 1.14. This function has a maximum at a value of $r \neq 0$ and takes on the value zero for $r = 0$, unlike the function $P(x, y, z)$ [Eq. (1.12)].

The most probable value for r , r_{mp} , corresponding to the maximum of the curve, is obtained by differentiating Eq. (1.3) and is $r_{mp} = \rho$. Another important mean quantity is the mean square end-to-end distance $\langle r^2 \rangle$:

$$\langle r^2 \rangle = \frac{\int_0^\infty r^2 4\pi r^2 P(r) dr}{\int_0^\infty 4\pi r^2 P(r) dr} = \frac{3}{2} \rho^2 \quad (1.14)$$

To calculate $\langle r^2 \rangle$, a model for the polymer molecule must be assumed. The simplest one is the freely jointed chain model. This model consists of a hypothetical chain with N links of length l , in which any link can adopt a random direction in space. Such a model excludes the restrictions imposed by bond angles of any structural restriction of the real chain. The calculation using Eq. (1.8) leads to

$$\langle r^2 \rangle = Nl^2 \quad (1.15)$$

given that the cosine of the angle formed by two vectors \mathbf{l}_i and \mathbf{l}_j takes values 0, +1, and -1 with equal probability and in average cancels out, giving the result $\langle \mathbf{l}_i \cdot \mathbf{l}_j \rangle = 0$ except when $i = j$; In that case the scalar product is equal to $\mathbf{l}_i \cdot \mathbf{l}_j = l^2$.

In general, it can be shown that the statistical distribution of end-to-end distances of a chain, independently of what its geometry might be, can be

represented by a Gaussian distribution function if the number of segments of the chain is sufficiently large, in order to guarantee that the correlation between bonds is totally lost over the length of the chain. The length of chain or the molecular weight necessary for this correlation to be lost, and for the Gaussian distribution of distances to be valid, depends on the chemical structure of the polymer and on the intramolecular interactions. In flexible polymer chains, just a small number of bonds ($N \simeq 20-50$) are enough for achieving this loss of correlation. For this reason the Gaussian function is applicable to flexible polymers in general unless their molecular weight is exceptionally low. In other, less flexible chain polymers, the number of bonds required for losing the correlation is greater, and the Gaussian function is applicable to them only from a particular molecular weight upward. In polymers with a more rigid structure, the correlation persists over a great number of bonds, and the Gaussian function is suitable only for very high molecular weights.

Equating (1.14) and (1.15), the parameter ρ is obtained:

$$\rho = \left(\frac{2}{3} Nl^2 \right)^{1/2} \quad (1.16)$$

The structural parameters of the freely jointed chain that can represent the real polymer chain and therefore fits a Gaussian function of end-to-end distances can be calculated. The first requirement that is going to be imposed is that the real chain and the model chain have the same value of mean square end-to-end distance; therefore the product Nl^2 is determined, but it does not permit N and l to be known independently. Consequently it will be necessary to add a further condition, which is that the two chains (the real one and the model) have the same length corresponding to that of the fully extended chain:

$$\langle r_r^2 \rangle = \langle r_m^2 \rangle = N_m l_m^2 \quad (1.17)$$

$$L_r = L_m = N_m b \quad (1.18)$$

Knowing the values of $\langle r_r^2 \rangle$ and L_r corresponding to the real chain, the values of N_m and b can be calculated. N_m and b define a model chain (see Fig. 1.16) that has the same Gaussian statistical length and the same extended length as the real chain and can be considered equivalent to the real chain.

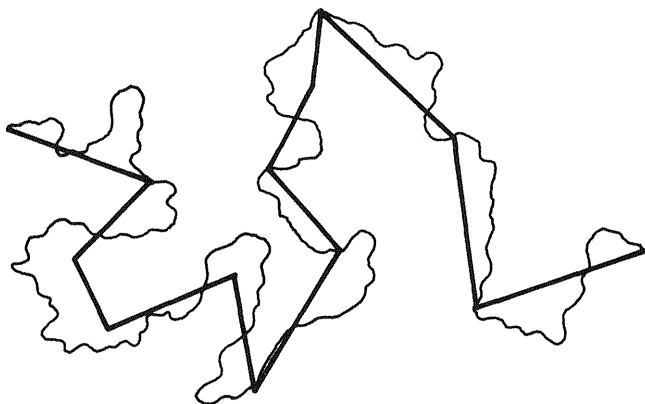


Figure 1.16 Schematic representation of the equivalent chain comprising N_m hypothetical bonds of length b connected by free joint.

PROBLEM SETS

Problem 1.1

From monodisperse samples of polystyrene of molecular weights, sample A, 10^3 g/mol; sample B, 5×10^4 g/mol; sample C, 2×10^5 g/mol; sample D, 10^6 g/mol, three blends were prepared by mixing them in the following mass ratios: (a) 0 : 1 : 1 : 0; (b) 1 : 1 : 1 : 0; (c) 0 : 1 : 1 : 1.

Calculate both the number-average and weight-average molecular weights.

Solution 1.1

(a) The numbers of moles in 2 g of the 0 : 1 : 1 : 0 blend are

$$N_A = N_D = 0 \quad (\text{P1.1.1})$$

$$N_B = \frac{1}{5 \times 10^4} = 2 \times 10^{-5} \text{ mol} \quad (\text{P1.1.2})$$

$$N_C = \frac{1}{2 \times 10^5} = 5 \times 10^{-6} \text{ mol} \quad (\text{P1.1.3})$$

From Eqs. (P1.1.2) and (P1.1.3) the number- and weight-average molecular weights are

$$\begin{aligned}
 M_n &= \frac{\sum N_i M_i}{\sum N_i} \\
 &= \frac{2 \times 10^{-5} \times 5 \times 10^4 + 5 \times 10^{-6} \times 2 \times 10^5}{2 \times 10^{-5} + 5 \times 10^{-6}} = \frac{2}{2.5 \times 10^{-5}} = 8.0 \times 10^4 \text{ g/mol}
 \end{aligned}
 \tag{P1.1.4}$$

and

$$\begin{aligned}
 M_w &= \frac{\sum N_i M_i^2}{\sum N_i M_i} \\
 &= \frac{2 \times 10^{-5} \times (5 \times 10^4)^2 + 5 \times 10^{-6} \times (2 \times 10^5)^2}{2} = 12.5 \times 10^4 \text{ g/mol}
 \end{aligned}
 \tag{P1.1.5}$$

(b) The number of moles in 3 g of the 1 : 1 : 1 : 0 blend are:

$$\begin{aligned}
 N_A &= \frac{1}{10^3} = 10^{-3} \text{ mol}; & N_B &= 2 \times 10^{-5} \text{ mol} \\
 N_C &= 5 \times 10^{-6} \text{ mol}; & N_D &= 0
 \end{aligned}
 \tag{P1.1.6}$$

The number-average molecular weight is

$$\begin{aligned}
 M_n &= \frac{10^{-3} \times 10^3 + 2 \times 10^{-5} \times 5 \times 10^4 + 5 \times 10^{-6} \times 2 \times 10^5}{10^{-3} + 2 \times 10^{-5} + 5 \times 10^{-6}} \\
 &= \frac{3}{1.025 \times 10^{-3}} = 2.9 \times 10^3 \text{ g/mol}
 \end{aligned}
 \tag{P1.1.7}$$

and the weight-average molecular weight is

$$\begin{aligned}
 M_w &= [10^{-3} \times (10^3)^2 + 2 \times 10^{-5} \times (5 \times 10^4)^2 + 5 \times 10^{-6} \times (2 \times 10^5)^2] \\
 &= 8.4 \times 10^4 \text{ g/mol}
 \end{aligned}
 \tag{P1.1.8}$$

(c) For the 0 : 1 : 1 : 1 blend,

$$M_n = 11.5 \times 10^4 \text{ g/mol} \quad M_w = 41.7 \times 10^4 \text{ g/mol}$$

Comparison of the results of (a) with those of (b) and of the results of (a) with (c) lead us to conclude that M_n is sensitive to the presence of low molecular weight molecules, whereas M_w is sensitive to the presence of high molecular weight chains.

Problem 1.2

Find the relationships between the average molecular weights and the standard deviations of the number- and weight-average molecular weight distributions σ_n and σ_w , respectively.

Solution 1.2

Let us assume the following distribution:

Number distribution

Moles	Mol w
n_1	M_1
n_2	M_2
\vdots	\vdots
n_n	M_n

The first moment of the distribution, or number-average molecular weight, is given by

$$M_n = \frac{\sum n_i M_i}{\sum n_i} = \frac{\sum w_i}{\sum w_i / M_i} \quad (\text{P1.2.1})$$

where w_i is the weight fraction of the species with molecular weight M_i . The variation of the distribution can be written as

$$\begin{aligned} \sigma_n^2 &= \frac{\sum n_i (M_i - M_n)^2}{\sum n_i} = \frac{\sum n_i M_i^2 - 2M_n \sum n_i M_i + M_n^2 \sum n_i}{\sum n_i} \\ &= \frac{\sum n_i M_i^2}{\sum n_i} - M_n^2 = \frac{\sum n_i M_i^2}{\sum n_i M_i} \left(\frac{\sum n_i M_i}{\sum n_i} \right) - M_n^2 \\ &= M_n M_w - M_n^2 = M_n^2 (M_w / M_n - 1) \end{aligned} \quad (\text{P1.2.2})$$

because, as will be shown below,

$$M_w = \frac{\sum n_i M_i^2}{\sum n_i M_i} \quad (\text{P1.2.3})$$

Mass distribution

Mass (g)	Mol w
m_1	M_1
m_2	M_2
\vdots	\vdots
m_n	M_n

The first moment of the distribution is the weight-average molecular weight given by

$$\begin{aligned}
 M_w &= \frac{\sum m_i M_i}{\sum m_i} = \sum w_i M_i \\
 &= \frac{\sum n_i M_i M_i}{\sum n_i M_i} = \frac{\sum n_i M_i^2}{\sum n_i M_i}; \quad w_i = \frac{m_i}{\sum m_i}
 \end{aligned}
 \tag{P1.2.4}$$

The variation of the distribution can be written as

$$\begin{aligned}
 \sigma_w^2 &= \frac{\sum m_i (M_i - M_w)^2}{\sum m_i} = \frac{\sum m_i M_i^2 + M_w^2 \sum m_i - 2M_w \sum m_i M_i}{\sum m_i} \\
 &= \frac{\sum m_i M_i^2}{\sum m_i} - M_w^2 = \frac{\sum m_i M_i^2}{\sum m_i M_i} \left(\frac{\sum m_i M_i}{\sum m_i} \right) - M_w^2 \\
 &= M_w M_z - M_w^2 = M_w^2 (M_z / M_w - 1)
 \end{aligned}
 \tag{P1.2.5}$$

where

$$\frac{\sum m_i M_i^2}{\sum m_i M_i} = \frac{\sum n_i M_i^3}{\sum n_i M_i^2}
 \tag{P1.2.6}$$

is the z -average molecular weight, M_z .

REFERENCES

1. HG Elias. *Macromolecules*, Vol 1 and 2. New York: Plenum, 1984.
2. RB Seymour, CE Carraher. *Polymer Chemistry: An Introduction*, 2nd ed., New York: Marcel Dekker 1988.
3. RJ Young, PA Lovell. *Introduction to Polymers*. New York: Chapman & Hall, 1991.
4. UW Gedde. *Polymer Physics*. London: Chapman & Hall, 1995.
5. PJ Flory. *Principles of Polymer Chemistry*. New York: Cornell University Press, 1953

2

Crystalline and Amorphous States in Polymers

2.1	Introduction: Crystalline and Amorphous Regions in Polymers	29
2.2	Factors Determining the Crystallinity of Polymers	32
2.3	Crystal Structures of Polymers	33
2.4	Crystalline Morphology	37
2.5	Crystallization	43
2.6	Melting	46
2.7	Polymers in the Liquid Crystal State	51
2.8	Glassy State	57
2.9	Phenomenology of the Glass Transition	58
2.10	Glass Transition and Free Volume	62
2.11	Factors Affecting the Glass Transition of Polymers	66
	Problem Sets	76
	References	83

2.1 INTRODUCTION: CRYSTALLINE AND AMORPHOUS REGIONS IN POLYMERS

Solid polymers can occur in the amorphous or crystalline state. Polymers in the amorphous state are characterized by a disordered arrangement of the macromolecular chains, which adopt conformations corresponding to statistical coils. The crystalline state is characterized by a long-range three-dimensional order (order extending to distances of hundreds or thousands

of times the molecular size of the repeating unit). The macromolecular chains in this state adopt fixed conformations such as planar zigzag, or helical. These chains are aligned parallel to each other, forming a compact packing that gives rise to a three-dimensional order. The differences in arrangement of polymer chains in the crystalline and amorphous states are schematically illustrated in Figure 2.1.

Depending on structure and temperature, amorphous polymers (which do not contain any crystalline region) show different physical properties. They are hard and brittle at low temperatures, when polymers are in the glassy state. A glass can be viewed as a solid that has frozen-in liquid-like disorder. As the temperature is raised, glasses exhibit glass transition, and they go over to the liquid viscoelastic state. Glassy polymers are prepared by rapid cooling of molten polymers. Polymers that easily form glasses have some irregularity in their structure. Examples include atactic vinyl polymers and random copolymers.

Many polymers have the capability to crystallize. This capability basically depends on the structure and regularity of the chains and on the interactions between them. The term "semicrystalline state" should be used rather than crystalline state, because regions in which the chains or part of them have an ordered and regular spatial arrangement coexist with disordered regions typical of the amorphous state. X-ray diffraction studies of samples of polymers crystallized from the melt reveal diffuse zones, char-

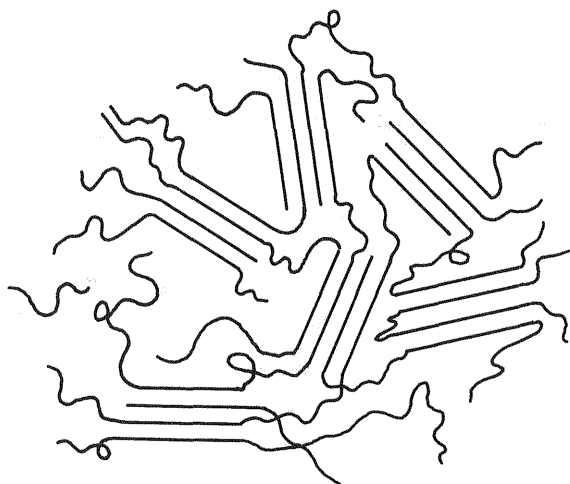


Figure 2.1 Conformational differences of polymer chains in the amorphous and crystalline states. Fringed micelle model. Parallel and coiled lines represent, respectively, portions of chains in the crystalline and the amorphous regions.

acteristic of disordered substances such as liquids, and clearly defined rings indicating the presence of the crystalline phase. In addition, the densities of crystalline polymers adopt intermediate values between those of totally amorphous samples and those theoretically calculated for 100% crystalline samples. Even the most perfect single crystals, obtained by crystallization from dilute solutions, can be regarded as partially crystalline. Figure 2.1 shows a schematic representation of the “fringed micelle” model (1), which represents the crystalline and amorphous regions of a polymer crystallized from the melt. In this model, the chains pass from amorphous to crystalline regions and vice versa, and they are sufficiently large to cross various crystalline regions, keeping them linked together. The supramolecular structures in crystalline polymers (see Sect. 2.4) are nowadays well known, and this model is strictly accepted only for polymers of very low crystallinity. Nevertheless, the basic idea of chains passing from crystalline to amorphous regions remains valid and has been successfully used to explain the properties of many semicrystalline polymers and fibres. The crystallinity of a sample depends not only on its molecular structure but also on the conditions under which the crystallization process took place and the thermal treatments applied to the sample after crystallization.

The physical and mechanical properties of polymer materials depend on the degree of crystallinity as well as on the crystalline structure and morphology (2–4). “Crystalline structure” refers to the way in which the chains, in a particular conformation, are packed, giving rise to the regular three-dimensional structure, while “crystalline morphology” refers to the size and shape of the crystallites, their arrangement, and their interconnection with the amorphous phase. Crystallinity confers on polymers certain characteristic properties, particularly with regard to the mechanical strength and resistance to solvents, that determine their selection for certain applications in preference to amorphous polymers. With crystalline polymers it is possible to manufacture textile fibers such as polyester and aliphatic polyamides (nylon), high resistance fibers such as polyaramides (e.g. Kevlar), and polyethylene (e.g., Spectra), gears and machinery parts with polyamides and flexible containers such as those made of polyethylene. Nevertheless, given the biphasic nature of semicrystalline polymers, a general characteristic is that they usually lack the transparency of amorphous polymers; hence the ideal transparent organic glass is atactic poly(methyl methacrylate).

In this chapter we study the characteristics that determine the crystallinity of polymers, crystalline morphology, and the factors affecting the crystallization and melting of polymers. We describe the amorphous state, focusing on the glass transition, a fundamental property for defining the mechanical behavior of polymers. The entire description refers exclusively to synthetic polymers.

2.2 FACTORS DETERMINING THE CRYSTALLINITY OF POLYMERS

Crystallization is the process of formation of a phase with long-range three-dimensional order from a disordered phase or from one that displays only local order. The crystallization provokes a discontinuous change in the enthalpy, volume, etc.; it is thus a first-order thermodynamic transition. Crystallization occurs at a particular temperature below which the state of equilibrium is the crystalline state. Nevertheless, below this crystallization temperature it is also possible to obtain a substance in a supercooled liquid state, i.e., a metastable state. When a liquid is cooled, its viscosity increases, and if the cooling is very fast, arrangement of the molecules into a crystal lattice can be prevented, giving rise to an amorphous solid. In the case of small molecules in this metastable state, insignificant changes in the external conditions generally produce crystallization. However, owing to their high molecular length, polymers can easily be obtained as amorphous solids by quickly cooling the melt. If, during the cooling, the loss of chain mobility is such that the chains cannot explore the entire conformational space, the most stable stretched conformation will not be adopted and the crystalline state will not be achieved. Moreover, many polymers remain in the amorphous state indefinitely. Even though from a thermodynamic point of view they ought to reach the equilibrium crystalline state, this process does not occur on the time scale of the laboratory (the time needed for reaching the crystalline state exceeds observable times).

On the other hand, since the crystalline state requires long-range order, only regular chains permitting such ordering will produce crystalline phases. The crystallizability of polymers is governed by the same structural factors as that of small molecules, such as interaction energy and geometry, and by specific factors of the polymer chains, i.e., chain regularity. Typical crystalline polymers are those in which the chains exhibit regular chemical structure and a regular geometry. Consequently, although linear molecular structures such as those of polyethylene are highly crystalline, branches decrease polymer crystallinity. In the same way, copolymerization limits crystallinity, up to the point that development of three-dimensional order is prevented in the case of random copolymers with a significant proportion of both comonomers. One of the factors most clearly determining the crystallizability of vinyl polymers, $(-\text{CH}_2-\text{CHR}-)_n$, is stereoregularity. In general, isotactic and syndiotactic polymers can crystallize, while atactic polymers with bulky side groups occur in the amorphous state. This is the case of polystyrene ($\text{R} \equiv \text{C}_6\text{H}_5$), poly(vinyl acetate) ($\text{R} \equiv -\text{O}-\text{CO}-\text{CH}_3$), and poly(methyl acrylate) ($\text{R} \equiv -\text{CO}-\text{OCH}_3$). But this situation is not general for all atactic polymers because the size of the side group and

the intermolecular interactions influence the development of crystallinity. Thus the crystallinity of atactic poly(vinyl alcohol) ($R \equiv OH$) and atactic poly(vinyl fluoride ($R \equiv F$)) can be justified on grounds of the small size of the side groups. Even polymers with atactic structure and bulky side groups crystallize if strong intermolecular interactions are present, as occurs in the case of polyacrylonitrile ($R \equiv -CN$). Finally, hydrogen bonding in polyamides determines their crystallinity.

Table 2.1 gives examples of the effect of regularity on the crystallinity of polymer chains.

2.3 CRYSTAL STRUCTURES OF POLYMERS

Experimental methods such as X-ray, electron, and neutron diffraction are used to determine the crystalline structure of many polymers (2). As in the case of small molecules, chain packing can be described via the corresponding unit cell of the seven crystal systems. The unit cell is formed by the arrangement of the monomers of the chains, and, depending on the complexity of the polymer, tens or hundreds of atoms can be found in the cell. As has already been mentioned, the chains adopt extended conformations of minimum energy, such as planar zigzag or helical forms. The conformation of an isolated chain is determined by intramolecular interactions, but in the crystal lattice strong intermolecular interactions, such as hydrogen bonding, can confer stability to a specific conformation. In all

Table 2.1 Effect of Regularity on the Crystallinity of Polymers

Source of the irregularity	Polymer	Degree of crystallinity (%) (typical)
Copolymerization	Linear polyethylene	70
	Isotactic polypropylene	70
	Random linear copolymer, ethylene-propylene	None
Branching	Linear polyethylene	70
	Branched polyethylene	40
No tacticity	Isotactic polypropylene	70
	Atactic polypropylene	None
Random <i>cis-trans</i> isomerism	Poly(<i>trans</i> -1,4-butadiene)	40
	Poly(<i>cis</i> -1,4-butadiene)	30
	Poly(1,4-butadiene), random <i>cis-trans</i>	None

Source: From Ref. 5.

cases, the polymer molecules traverse many unit cells. In the longitudinal direction the atoms are covalently bonded, but in transverse directions the interactions are relatively weak (van der Waals, hydrogen bonding); consequently the crystal units have anisotropic properties. The transverse organization is different from the longitudinal one, which leads to an anisotropy that prevents the appearance of cubic lattices. This anisotropic character is reflected in the mechanical properties, with moduli depending dramatically on the direction. It can be estimated that the modulus is about two orders of magnitude higher in the direction of the chains than in the transverse directions.

Below, a brief description is given of the conformations and crystalline structures of the most representative polymers. The most studied polymer is polyethylene. In this polymer, the lowest energy conformation has all the bonds in trans, i.e., the planar zigzag as shown in Figure 2.2. The chains are packed in orthorhombic cells bonded by van der Waals interactions giving rise to a unit cell of dimensions $a = 0.742$, $b = 0.493$, and $c = 0.253$ nm that contains two monomer units. Although the orthorhombic crystal structure is the most stable one, mechanical deformations can give rise to a monoclinic structure. The existence of more than one crystal structure is known as polymorphism. Polymorphism is relatively common in polymers for which various isoenergetic conformations can exist. Poly(tetrafluoroethylene) ($-\text{CF}_2-\text{CF}_2-$), displays triclinic crystallization at low temperatures and hexagonal at temperatures above 19°C . In this polymer, the lowest energy conformation departs from the conventional planar zigzag (all trans), due to the bulkiness of the fluorine atoms. Poly(tetrafluoroethylene)

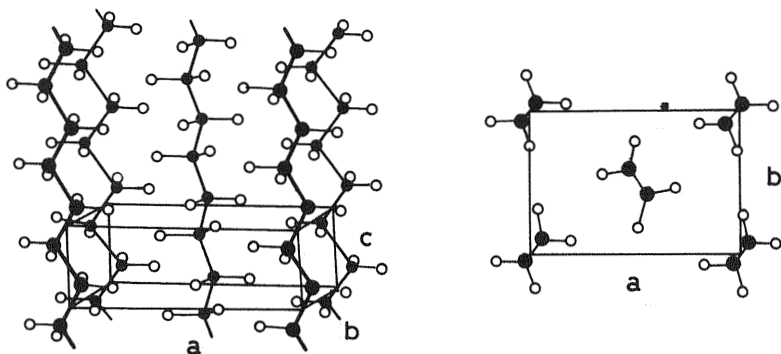


Figure 2.2 Orthorhombic crystalline structure of polyethylene: perspective view of the unit cell and view along chain axis.

adopts helical conformations in the crystalline state, as shown in Figure 2.3. The helices formed are 13/1 (13 repeat units per rotation of the helix) and 15/1 at low and high temperature, respectively. The transformation from one to the other involves volume changes of 1%. This volume change at room temperature makes it inadvisable to use this polymer in the manufacture of parts requiring dimensional stability. Vinyl polymers such as poly(vinyl fluoride) and poly(vinyl alcohol), with side groups relatively small, crystallize in extended zigzag conformations, forming structures similar to that of polyethylene.

Isotactic polymers always crystallize in helical conformations that facilitate the arrangement of the side groups. Figure 2.4 shows the 3/1 helix of isotactic polypropylene and isotactic polystyrene, originated by the alternation of trans and gauche bonds along the chain. If the side groups are bulkier, complex helices are formed such as those of isotactic poly(methyl methacrylate), which crystallizes in 5/2 helices. In syndiotactic polymers the conformation is again controlled by the size of the side group.

Polyamides are a typical example of chains whose conformation and chain packing in the crystalline state are determined by intermolecular interactions, i.e., the hydrogen bonding between the groups —NH and —CO of neighboring molecules. The chains adopt the all-trans conformation, facilitating the intermolecular hydrogen bond interactions. They become packed, forming laminae as shown in Figure 2.5 for nylon 6.6.

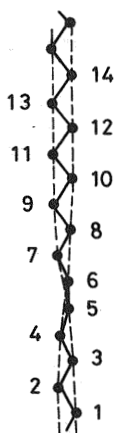


Figure 2.3 Crystalline conformation of polytetrafluoroethylene, 13/1 helix (13 CF_2 units per turn of the helix).

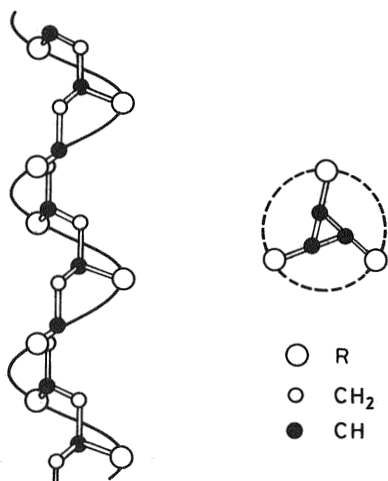


Figure 2.4 Isotactic 3/1 helix of polypropylene ($R \equiv \text{CH}_3$) and polystyrene ($R \equiv \text{C}_6\text{H}_5$).

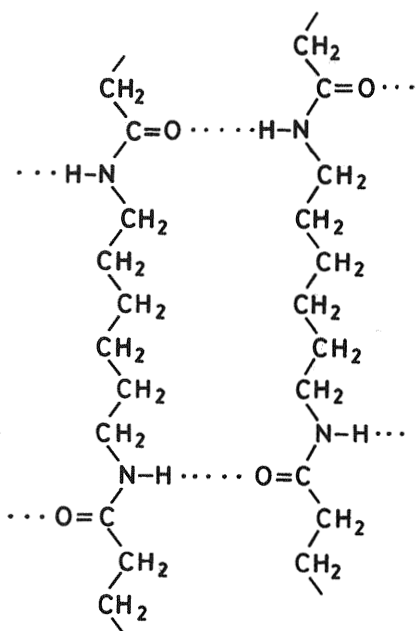


Figure 2.5 Crystalline conformation of polyamides: nylon 6.6.

2.4 CRYSTALLINE MORPHOLOGY

Crystallization of polymers can be carried out from the molten state or from solutions. These procedures lead to different morphologies. Starting from solution, single crystals are obtained with the shape of lamella (plates). Starting from the melt, small crystalline lamellae or crystallites are formed that are organized into complex structures known as spherulites.

2.4.1 Crystals Obtained from Solution

(a) Single Crystals: Shape and Structure

Although single crystals have no technological application, their study is essential for the understanding of the morphology and behavior of crystalline polymers. In the crystallization of polymers starting from very dilute solutions (concentrations less than 1%), polymer single crystals are generated by cooling or by addition of a precipitant. Single crystals have the shape of lamellae about 100 \AA thick and several micrometers in length (see Fig. 2.6) (6). The general characteristic of single crystals is their small size in comparison with the crystal size of small molecules, which limits their study by X-rays. The orientation of the chains in the lamellae, determined by electron diffraction, shows that the chains are nearly normal to the lamellar surface. Since polymer chains have dimensions of thousands of angstroms and the single crystals are about 100 \AA thick, the chains must be folded, entering and exiting via the upper and lower faces of the lamellae as shown in Figure 2.7. In this figure each of the straight lines represents the chain in its most stable extended conformation, while in the loops or folds the chain abandons the minimum energy conformation. In the case of

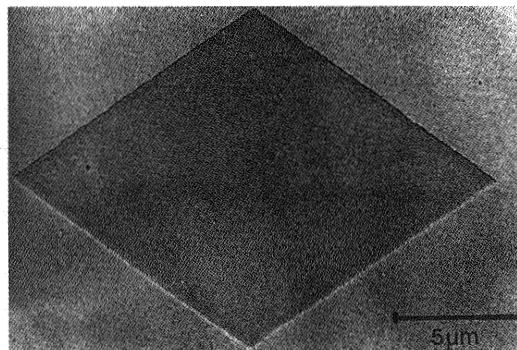


Figure 2.6 Electron micrograph of a single crystal of polyethylene. (From Ref. 6.)

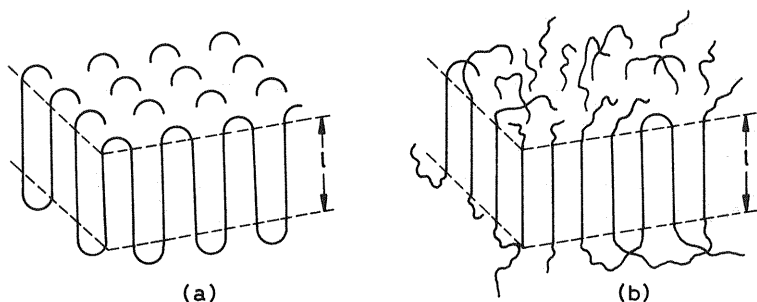


Figure 2.7 Folded-chain models for single crystals. (a) Regular adjacent reentry; (b) nonregular random reentry.

polyethylene, five C—C bonds, three of them in gauche conformation, are sufficient to form a loop.

Measurements of the density of single crystals give values lower than those calculated theoretically according to crystallographic data. They are not perfect crystals, having a degree of crystallinity less than 100%. The noncrystalline proportion is too large to be attributed to intercrystalline defects, and it is assumed that noncrystalline (amorphous) regions are formed on the surfaces. Although it is evident that the packing of folded chains is less compact than that of fully extended chains, the model of a totally regular adjacent folding (Fig. 2.7a) does not justify the results. On the other hand, nonregular folding (Fig. 2.7b) with entries in the surface at random would not correspond to single crystals of flat surfaces with perfectly demarcated edges. Therefore, an intermediate model is accepted.

Polymers crystallized from concentrated solutions exhibit more complex crystalline morphology (7). In dilute solutions, polymer coils are isolated from each other, but if the concentration increases, association and entanglement among the chains are favored. Therefore, there is a greater probability that a chain forms part of various crystallites, thus producing aggregated lamellae in multilayer morphologies.

(b) Thickness of the Crystalline Lamella

The most important dimension of the crystalline lamella is its thickness, since thickness is a measure of the period l , or length of chain in the fully extended conformation. The period of the single crystals depends on the crystallization temperature T_c and on further heat treatments e.g. annealing. The period always increases as the crystallization temperature increases. Experimentally, it is obtained that $l \sim (T_m - T_c)^{-1}$, where T_m is the melting

temperature of the polymer and T_c the crystallization temperature. The difference $T_m - T_c$ is called undercooling; the smaller the undercooling, the greater is l . If the crystals are annealed at a temperature T_a (maintained at a temperature T_a close to T_m), an increase in the period takes place. The increase in l is greater the closer T_a is to T_m . This increase in thickness is irreversible, and no decrease in l occurs when the annealed sample is cooled again.

2.4.2 Polymers Crystallized from the Melt

When polymers are crystallized from the melt, spherulite morphology is the most frequently observed. This morphology, as its name indicates, has a spherical shape consisting of aggregates of crystalline lamellae. Its diameter varies from micrometers up to millimeters in extreme cases. The spherulite morphology is usually obtained in the production processes, under quiescent conditions, for the majority of crystalline polymers. Spherulites are easily observed in an optical microscopy with polarized light and with the polarizer and analyzer crossed. They are recognized as birefringent circular areas with a dark cross, like a Maltese cross, having arms parallel to the polarizer and analyzer, respectively (see Fig. 2.8) (8). Observation of the spherulites in an electron microscope shows that they are made up of crystalline lamellae,

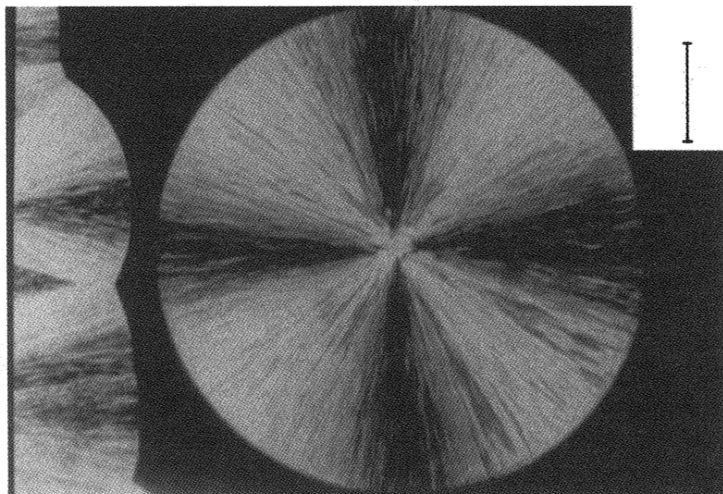


Figure 2.8 Spherulite of isotactic polystyrene crystallized from the melt. (From Ref. 8.)

like fibrils opening out into a fan from the center to the periphery following the radial direction. Studies with X-ray diffraction and electron diffraction show that these lamellae are similar to single crystals. The chains are located normal to the faces of the lamella and are folded in the same way as in single crystals. Figure 2.9 shows a representation of this morphology. The longitudinal and transverse refractive indices of the radial lamellae are different, and spherulites are therefore birefringent. The lamellae of spherulites nevertheless display a more irregular folding of chains than in single crystals. The different lamellae are not independent, and some polymer chains pass from one to another, giving rise to intercrystalline links. The material remaining between the lamellae is found to be disordered and therefore is amorphous. In addition, different spherulites are joined by chains that crystallize, forming part of more than one spherulite. This is possible because of the low correlation of movements of parts of the chain (segments) that are located far from each other. Long chains can crystallize simultaneously in various parts, forming crystallites belonging to the same or even different spherulites. The morphology of interlinked spherulites is justified by considering that polymer chains in the melt are meshed together, and when they crystallize the high viscosity of the medium makes it difficult to order themselves to form isolated crystals. This crystalline morphology explains the characteristic toughness of semicrystalline polymers. In some cases, the crystalline lamellae forming spherulites do not maintain any fixed orientation and are twisted into a spiral in the radial direction. The orientation is repeated at regular intervals along the radius, giving rise to the appearance of concentric rings when observed in a polarized light microscope (8), as shown in Figure 2.10. A single polymer can develop different types of spherulites depending on the crystallization conditions. Spherulites display a perfect spherical shape only at the start of crystallization; as the crystallization proceeds,

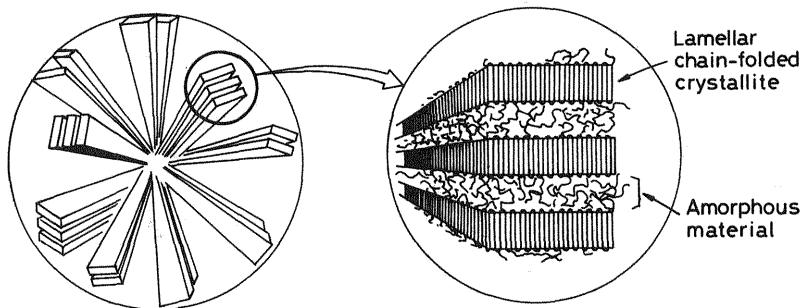


Figure 2.9 Model of spherulite morphology.

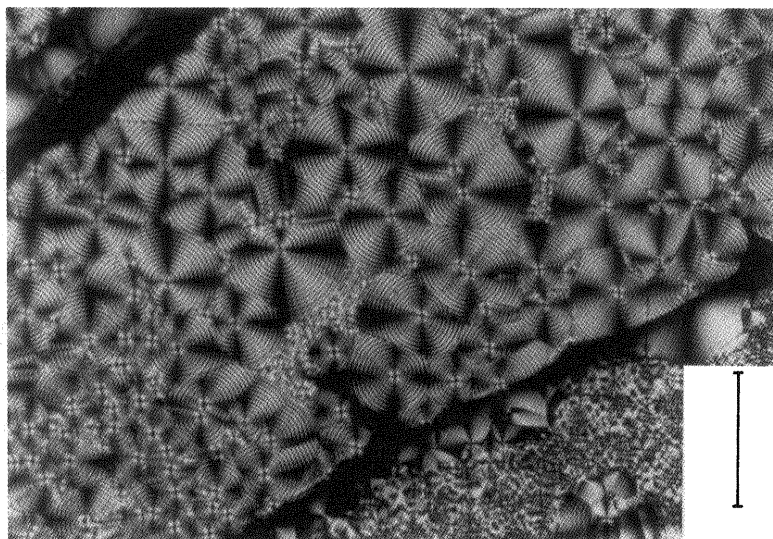


Figure 2.10 Ringed spherulites of polyethylene. (From Ref. 8.)

these spherulites collide with each other, giving rise to polyhedral or ovoid shapes (see Fig. 2.10). The number and size of the spherulites depend on the crystallization temperature, thus, when the undercooling increases, the number of nucleating spherulites increases, and therefore the size that they can reach decreases. Under normal crystallization conditions used in manufacturing processes, the size reached by the spherulites is usually of the order of magnitude of the wavelength of visible light. This is why crystalline polymers have turbid appearance while amorphous polymers are transparent (the light is scattered by spherulites but not by the crystalline lamellae, which are very much smaller than the wavelength of visible light).

2.4.3 Polymers Crystallized Under Stress

Polymers crystallized under stress develop morphologies different from those created under quiescent conditions. This fact has considerable technological repercussions, since many polymers are processed in the form of fibers or extruded through nozzles, and in these processes the crystallization takes place under stress. Synthetic polymer fibers, such as nylon, polyester, and acrylics, are manufactured by means of a spinning process, involving the extrusion of the polymer, either molten or in solution, through fine holes, followed by unidirectional drawing. This method creates a change

from an isotropic state (molten or solution) to a crystalline state in which the chains show a preferential orientation in the stretching direction. The crystallinity increase and the mechanical properties improve—particularly the longitudinal Young's modulus (9). In the transverse direction of the fiber the modulus is much lower than in the longitudinal direction. For example, isotropic poly(ethylene terephthalate) has a Young's modulus of 2.5 GPa and tensile strength of 70 MPa, while oriented fibers attain values of 14 GPa and 840 MPa, respectively. Nylon 6.6 increases in crystallinity up to 96%, and its tensile strength is increased by a factor of 4, reaching 340 MPa.

X-ray and electron microscopic studies have revealed a characteristic morphology in crystalline polymer fibers. The crystalline lamellae are not organized radially, instead forming elongated units oriented in the direction of the fiber. For flexible chain polymers the morphology of the fiber is well illustrated in the schematic model shown in Figure 2.11, in which fibrils oriented parallel to the direction of extension can be distinguished (10). The chains in the fibrils still partly maintain the folded conformation, and some of them pass from one crystal to another, acting as a link between them. The fibrils are only weakly bonded together. Crystalline and amor-

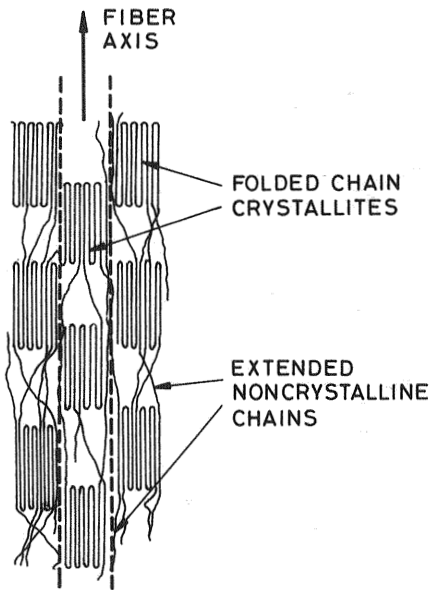


Figure 2.11 Fibrillar structure of oriented flexible crystalline polymers. The fibrils are demarcated by discontinuous lines.

phous regions each possess molecular orientation. Stretching of the fiber favors the arrangement of chains parallel to the axis of the fiber.

2.5 CRYSTALLIZATION

The importance of studying the crystallization process in technical and engineering applications derives from the need to know the rate and range of temperatures at which crystallization is produced and the degree of crystallinity attained.

2.5.1 Degree of Crystallinity

The degree of crystallinity, x_c , indicates the proportion of solid that is crystalline. This magnitude has great practical importance, as the mechanical properties of the material, and most of its properties in general, depend on the crystallinity. The simplest method to determine the degree of crystallinity of a polymer is based on the measurement of the specific volume, v . Crystallization implies a compaction of polymer chains, i.e., a decrease in the volume (increase in density) with respect to the amorphous material. If the biphasic model (amorphous phase + crystalline phase) is accepted for the semicrystalline sample, the specific volume can be written as

$$v = x_c v_c + (1 - x_c) v_a \quad (2.1)$$

where v , v_c and v_a are the specific volumes of the semicrystalline sample, the hypothetical 100% crystalline polymer, and amorphous polymer, respectively, at the measurement temperature T and x_c is the degree of crystallinity of the sample. The value of v_a can be determined experimentally if amorphous samples can be prepared at temperature T . The value of this parameter can alternatively be estimated by extrapolating the specific volumes of the liquid polymer to temperature T . Figure 2.12 represents the typical variation of the specific volume of a semicrystalline polymer with temperature up to and beyond the melting point. The value of v_c can be calculated from crystallographic data. According to Eq. (2.1), the degree of crystallinity of a polymer can easily be determined from the measurement of the specific volume. This method would be valid for all crystalline polymers when there is a significant difference between v_a and v_c . However, for some polymers, such as polytetrafluoroethylene, which is manufactured by a sintering process, the method breaks down, because the polymer contains a percentage of voids (1%) that falsifies the results. Other experimental techniques such as X-ray scattering, calorimetric thermal analysis, infrared

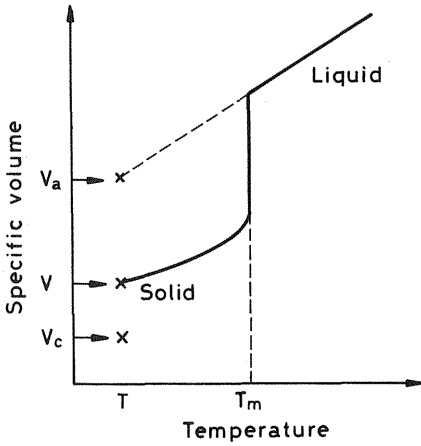


Figure 2.12 Variation of the specific volume of a semicrystalline polymer with temperature.

spectroscopy, and nuclear magnetic resonance also allow the determination of the crystallinity of polymers. In general, the values given by the different techniques can be correlated, though they do not entirely agree.

2.5.2 Kinetics of Crystallization

Crystallization is not an instantaneous process; it progresses with time. When a polymer crystallizes at constant temperature, lamellae are formed to which the polymer chains become incorporated. The chains fold with a certain period, and the lamellae grow longitudinally. In the case of crystallization from the melt, the longitudinal growth of the lamellae leads to an increase in the radius of the spherulites. The mechanism is similar to that of the crystallization of small molecules and consist of a first stage, called nucleation, in which nuclei are formed in the melt and a second stage of growth. This crystallization step is known as primary crystallization. A further stage, secondary crystallization, can occur; once the spherulites have made contact, the amorphous material remaining between the lamellae crystallizes.

The nucleation can be homogeneous or heterogeneous. Heterogeneous nucleation is caused by impurities, while homogeneous nucleation consists of the spontaneous aggregation of polymer chains at a temperature below the melting temperature in order to form a nucleus. The ordered regions that can persist in the molten polymer have great importance in homogeneous

nucleation. It is said that polymers have “structural memory,” because when the crystallization process is repeated several times, the crystals grow in exactly the same place in which they were located before being melted. The crystallization rate can be determined by dilatometric techniques, measuring the change of volume with time at a given crystallization temperature, or by means of microscopy, observing how the radius of the spherulites grows with time. At each temperature the radial growth occurs at a constant rate. When the rate of growth is plotted against the crystallization temperature, curves are obtained that display a maximum, as shown in Figure 2.13 (11). At temperatures close to melting, the rate of crystallization becomes zero. The Gibbs free energy of nucleation is proportional to the reciprocal of the undercooling [$G^* \sim 1/(T_m - T_c)$]. The crystallization is a nucleation-controlled process, as the crystallization rate is proportional to $\exp(-G^*/RT)$ so it tends to zero when T_c approach T_m . As the temperature is lowered there is an increase in the thermodynamic tendency toward crystallization that leads to an increase in the growth rate, but the system simultaneously becomes more viscous. This increase in viscosity decreases the molecular mobility, hindering the incorporation of the chains into the crystalline phase, and consequently the rate of crystallization again decreases. The

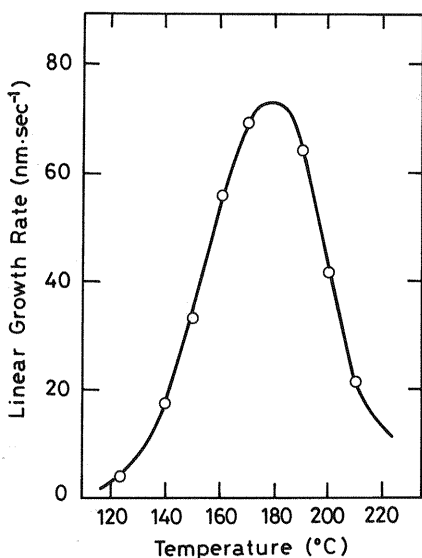


Figure 2.13 Variation of the crystal growth rate with temperature for poly(ethylene terephthalate), $T_m = 280^\circ\text{C}$. (From Ref. 11.)

temperature at which the maximum rate of crystallization is reached is about $0.8 T_m$ for most polymers.

The time dependence of the overall crystallization process is governed by Avrami's equation (12),

$$x_c = 1 - \exp(-Zt^n) \quad (2.2)$$

where x_c is the degree of crystallinity achieved in a time t , and Z and n are characteristic constants of the crystallization mechanism. The values of the exponential term lie in the range 2–4. Equation (2.2) is not suitable for describing the final stage of the crystallization process, when secondary crystallization occurs.

2.6 MELTING

Melting is the process opposite to crystallization. Crystalline order is destroyed in the melting process, and the material becomes a viscoelastic liquid above the melting temperature. The disappearance of the crystalline morphology and structure during melting is demonstrated through characteristic changes in the physical, mechanical, and thermodynamic properties of the material. X-ray diffraction patterns of molten flexible chain polymers merely show diffuse rings, indicating that the long-range order has disappeared. Discontinuous changes are produced in the volume, enthalpy, and entropy during melting and consequently this process is a first-order transition. Nevertheless, the melting of polymers shows certain peculiar characteristics that distinguish them from the melting of low molecular weight crystalline solids. First, melting of polymers does not occur at a unique temperature; instead it occurs over a temperature range that depends on the type of sample (molecular weight, polydispersity, branchings, etc.). The variation of the melting temperature with molecular weight is illustrated in Figure 2.14. The melting temperature of polymers with molecular weight lower than 10^3 g/mol strongly decreases as the length of the chain decreases. However, as the molecular weight increases, the melting temperature dependence on molecular weight becomes weaker. For high molecular weights there is a band of melting temperatures that is due to the presence of crystals of different thicknesses. Figure 2.15 shows the volume changes that occur during the melting of linear and branched polyethylene (13). In both cases the volume of the solid increases with temperature, and as melting is approached an abrupt change in volume occurs. For $T > T_m$, the volume of the liquid increases linearly with temperature. The sample of linear polyethylene (highly crystalline) has a narrow melting range; 70% of the crystal-

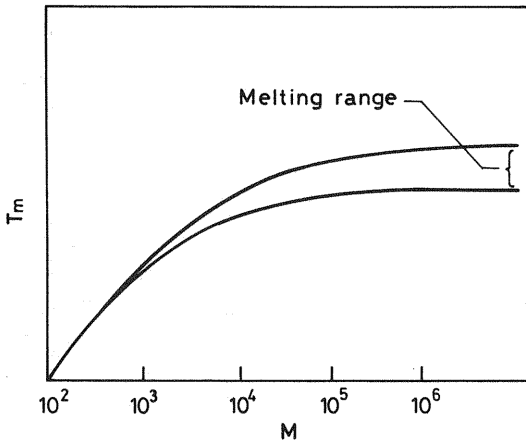


Figure 2.14 Dependence of the melting temperature on the molecular weight.

linity disappears within 3–4°C, while branched polyethylene (low crystallinity) displays a very broad melting range, about 40°C.

The second characteristic of the melting of polymers is that the melting temperature of a particular sample depends strongly on its thermal history and more particularly, on its crystallization temperature. The closer the

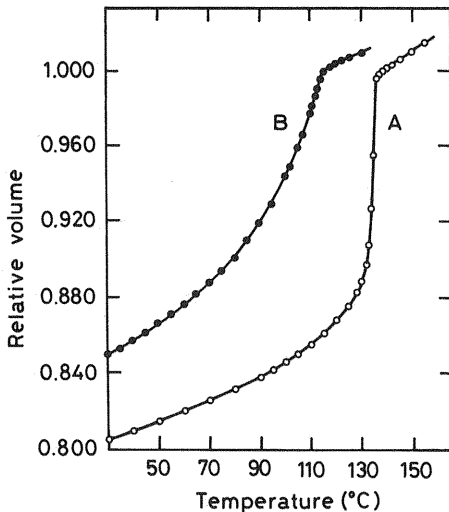


Figure 2.15 Variation of the relative volume with temperature for linear (A) and branched (B) polyethylene. (From Ref. 13.)

crystallization temperature is to the melting temperature, the higher will be the melting temperature. This behavior is a consequence of the decrease in the size and perfection of the crystalline lamellae when the undercooling ($T_m - T_c$) increases. Hence, for each sample the melting temperature is usually taken at the end of the melting, i.e., the temperature at which the final traces of crystallinity disappear, which corresponds to the melting of the most perfect crystals in the sample.

True thermodynamic equilibrium refers to the phase in their most stable state, and for the crystalline polymer phase the most stable conformation is the fully extended one. The equilibrium melting temperature, T_m^0 , corresponds to the melting of perfect crystals of infinite size with fully extended chains. The value of T_m^0 for a polymer is unique. Since the crystalline samples of polymers are made up of crystals of finite size in which the chains are folded and not fully extended, the experimentally determined melting temperature, T_m is always lower than T_m^0 . There is a strong dependence of T_m on the thickness of the crystalline lamella, l ; T_m always increases with l .

Surface effects can be disregarded in crystals of infinite size, and consequently the change in the Gibbs free energy in the crystal-liquid transition, ΔG_c (per unit volume of crystalline phase), is due solely to the melting of the crystalline phase. Melting of finite crystals also involves the destruction of the upper and lower surface faces, a contribution that is negative and is represented as $2\sigma_a/l$ (per unit volume), where σ_a is the surface free energy. The Gibbs energy of the phase change is canceled in the crystal-liquid equilibrium. Thus, for the infinite crystal at T_m^0 we can write

$$\Delta G_c = 0 = \Delta H_m - T_m^0 \Delta S_m \quad (2.3)$$

and

$$T_m^0 = \frac{\Delta H_m}{\Delta S_m} \quad (2.4)$$

ΔH_m and ΔS_m are the enthalpy and entropy of melting per unit volume, respectively.

For a crystal of thickness l at T_m the free energy change can be written as

$$\Delta G_c - 2\sigma_a/l = \Delta H_m - T_m \Delta S_m - 2\sigma_a/l = 0 \quad (2.5)$$

and the melting temperature becomes

$$T_m = (\Delta H_m - 2\sigma_a/l) \Delta S_m \quad (2.6)$$

Combining Eqs. (2.4) and (2.6), the following relationship between T_m and T_m^0 is obtained:

$$T_m = T_m^0 \left(1 - \frac{2\sigma_a}{\Delta H_m l} \right) \quad (2.7)$$

Equation (2.7) predicts that T_m for a finite crystal is always lower than T_m^0 . Equation (2.7) allows the determination of T_m^0 from the measurement of the melting temperature of crystals of different thicknesses. Actually, the plot of T_m vs $1/l$ gives a straight line whose intercept with the ordinate axis gives T_m^0 .

A simple method to determine T_m^0 is based on the dependence of the melting temperature on the crystallization temperature, T_c (14). T_m increases linearly with T_c as Figure 2.16 shows (15). Since T_m can never be lower than T_c , the line $T_m = T_c$ represents the limit, i.e., the situation of perfect reversibility in which melting and crystallization occur at the same temperature. The extrapolation of T_m to $T_m = T_c$ provides T_m^0 . This procedure is the one most widely used because it is applicable to all samples, not just to single crystals. Table 2.2 shows the values of T_m^0 , melting enthalpy, and melting entropy of some polymers (16). The values of ΔH_m , which

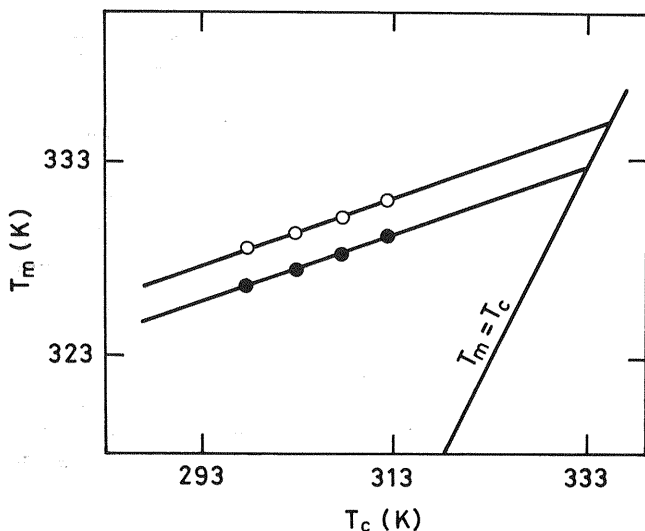


Figure 2.16 Variation of melting temperature with crystallization temperature for (○) poly(ϵ -caprolactone) and (●) poly(ϵ -caprolactone) in a blend with poly(4-hydroxystyrene) (85% weight fraction of PCL). (From Ref. 15.)

Table 2.2 Equilibrium Melting Temperatures T_m^0 Enthalpies ΔH_m and Entropies ΔS_m of Melting for Some Polymers

Polymer	T_m^0 ($^{\circ}\text{C}$)	ΔH_m (cal/mol) ^a	ΔS_m (cal/ $^{\circ}\text{C}\cdot\text{mol}$) ^a
Polyethylene	146	960	2.3
Polypropylene	200	1,386	2.9
Poly(<i>cis</i> -1,4-isoprene)	28	1,050	3.46
Poly(<i>trans</i> -1,4-isoprene)	74	3,040	8.75
it-Polystyrene	243	2,000	3.9
Poly(tetramethylene terephthalate)	230	7,600	15.1
Poly(decamethylene terephthalate)	138	11,000	27
Poly(decamethylene sebacamide)	216	8,300	17

^aExpressed per repeating unit.

Source: Ref. 16.

reflect the intermolecular interactions, lie in the interval 1000–10,000 cal/mol. As could be expected, the melting temperature values are not exclusively dependent on the melting enthalpy [see Eq. (2.4)]. The thermodynamic melting temperature, T_m^0 , is related to the flexibility of the polymer chains. The higher the flexibility, the larger the conformational entropy and hence the lower the value of T_m^0 . Rubbers have low melting temperatures due to the relatively high melting entropies reflecting the flexibility of their chains. At the other extreme, the engineering plastics such as aromatic polyamides, with very rigid chains and strong interactions among them, present high values of melting temperature that are characteristic of these materials. The presence of aromatic rings in the main chain increases the melting temperature with respect to aliphatic chains because it decreases the conformational entropy of the melt (less flexibility). In Section 2.11 the influence of the molecular structure of T_m is discussed in further detail for each type of polymer.

As occurs with other crystalline substances, the melting temperature of polymers decreases in the presence of solvents (melting point depression). Thermodynamic arguments lead to expressions that relate the depression of the melting point to the solution concentration. The equation that gives the melting temperature of a polymer solution as a function of the concentration (17) can be written as

$$\frac{1}{T_m} - \frac{1}{T_m^0} = \frac{R}{\Delta H_{2u}} \left(\frac{V_{2u}}{V_1} \right) (v_1 - \chi_{12} v_1^2) \quad (2.8)$$

where T_m^0 and T_m are, respectively, the melting temperatures of the pure polymer and of the polymer in a solution of composition v_1 (volume fraction of solvent), V_1 and V_{2u} are, respectively, the molar volumes of the solvent and the monomeric unit of the polymer, R is the universal constant, ΔH_{2u} is the melting enthalpy per monomeric unit, and χ_{12} is the polymer-solvent interaction parameter; the lower the value of χ_{12} , the stronger the interaction between the two components of the solution.

In the case of mixtures of a crystalline polymer and an amorphous polymer, a drop in the melting temperature of the crystalline polymer also occurs whenever the two polymers are miscible in the liquid state. In this case, the equation correlating the melting temperature with the composition is different from Eq. (2.8) because the large molecular size of the components causes the entropy of mixing to be considerably lower. The equation that gives the drop of the melting temperature for mixtures of crystalline polymer (2) + amorphous polymer (3) of similar size (18) is given by

$$\frac{1}{T_m} - \frac{1}{T_m^0} = -\frac{R}{\Delta H_{2u}} \left(\frac{V_{2u}}{V_{3u}} \right) v_3^2 \chi_{32} \quad (2.9)$$

where χ_{32} is the polymer-polymer interaction parameter.

The dependence of T_m on the molecular mass of the polymer has been interpreted as a melting point depression caused by the chain ends, which act as if they were a low molecular weight impurity (solvent). The lower the molecular weight, the larger the proportion of terminal groups and consequently the lower the melting temperature, T_m .

2.7 POLYMERS IN THE LIQUID CRYSTAL STATE

2.7.1 Liquid Crystal State

The liquid crystal state (LCS) shows order in one or two dimensions; it lacks the three-dimensional long-range order of the crystalline state. LCS has characteristics intermediate between those of the crystalline and the disordered amorphous states. These phases are called liquid crystals because many of them can flow like ordinary liquids but they display-birefringence and other properties characteristic of crystalline solids. In liquid crystal phases the molecules can move but the orientational order is conserved in at least one direction. The LCS can be displayed by small molecules and by polymers, but in both cases a characteristic chemical structure is needed. The existence of the liquid crystal state is related to the molecular asymmetry and the presence of strong anisotropic intermolecular interactions (19-21). Thus, molecules with a rigid rod structure can form highly ordered

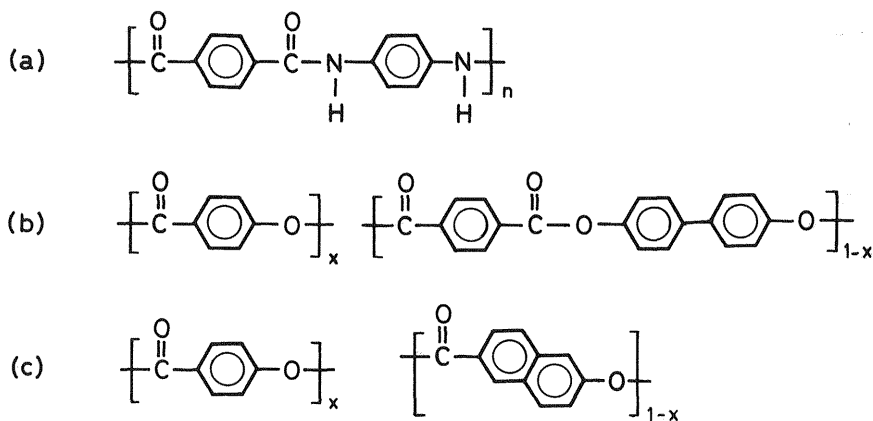


Figure 2.17 Repeating units of some main-chain liquid crystals. (a) Poly(*p*-phenylene terephthalamide (Kevlar); (b) copolyester of *p*-hydroxybenzoic acid and biphenylene terephthalate (Xydar); (c) copolyester of *p*-hydroxybenzoic acid and 2,6-dihydroxynaphthoic acid (Vectra).

states in concentrated solutions or in the molten state. Polymers with aromatic rings in the main chain connected by ester or amide groups take on the conformation of a rigid linear chain, giving rise to highly crystalline solids. When they are melted or dissolved, they partly maintain their order, passing through liquid crystal states before reaching the isotropic disordered liquid state. Typical examples of polymers with a rigid chain structure (main-chain LC polymers) are shown in Figure 2.17.

Liquid crystals are classified into two groups known as thermotropics and lyotropics. Thermotropics are those that are formed in the melting of crystalline solids, and they can remain in the liquid crystal mesophase without decomposition, passing to the isotropic liquid state when subsequently heated. As their mesophases are turbid, the temperature at which the transition to the isotropic liquid phase takes place is called the clearing temperature. Lyotropic LCs form mesophases in concentrated solution when the concentration exceeds a critical value.

Not all crystalline polymers pass through liquid crystal states. Flexible polymers, which adopt statistical coil conformations in the dissolved and molten states, pass directly to the isotropic liquid when dissolved or melted. Only if they are modified by introducing side mesogen groups could they form liquid crystal phases (side-chain LC polymers). The mesogen groups confer the liquid crystal characteristic; they have the form of rigid rods or discs, like those illustrated in Figure 2.18a. Figure 2.18b shows the possible

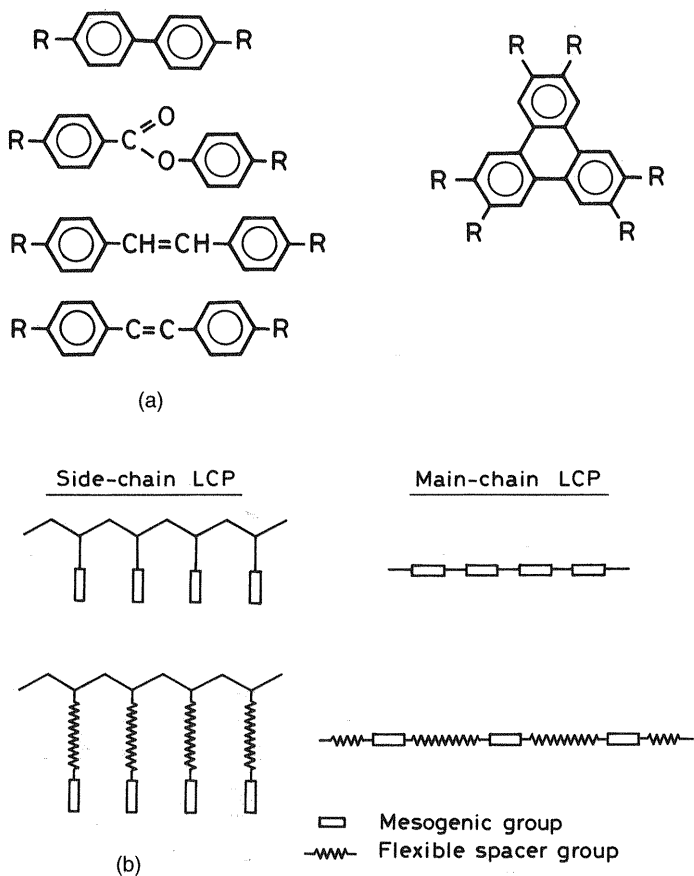


Figure 2.18 (a) Some typical mesogen groups. (b) Schematic representation of types of liquid crystal polymers according to the location of the mesogen groups: in the main chain (right) or as side substituents (left).

locations of mesogen groups giving rise to what are called main-chain LCPs and side-chain LCPs (5,19–22).

2.7.2 LC Mesophases

The liquid crystal state can be ordered in different forms known as mesophases (phases intermediate between the solid and liquid states). Figure 2.19 illustrates the possible orderings of the molecules in mesophases (5, 19–22). In the mesophases known as smectic, the molecules are oriented in one

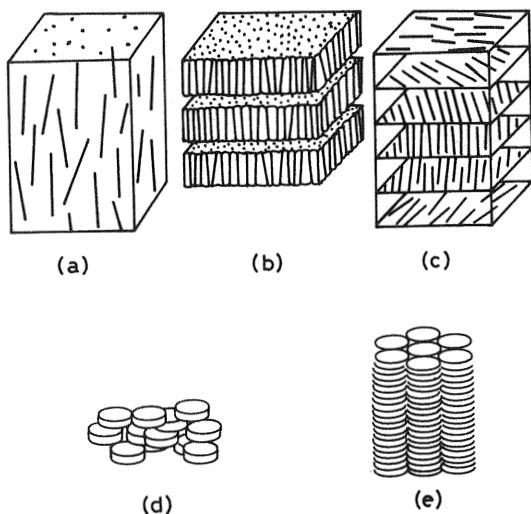


Figure 2.19 Orderings in LC mesophases. (a) nematic; (b) smectic; (c) cholesteric; (d) discotic-nematic; (e) discotic-columnar.

direction and ordered in parallel layers. Nematic mesophases lack ordering in layers and conserve only the orientation order. The optical anisotropy and the response to electric fields of nematic phases are the basis of their use in screens for calculators, watches, and electronic devices. In cholesteric mesophases the molecules are ordered in layers, with the direction of orientation slightly changing in consecutive layers, giving rise to helical structures. The periodicity of the helical layers depends on the temperature; as a result they display different colors depending on the temperature and can be used as temperature sensors. Finally, discotic mesophases are typical of disc-shaped molecules and can display nematic or columnar mesophases.

Liquid crystal polymers can occur in different mesophases depending on temperature and pressure. When the temperature rises, they can pass from one mesophase to another, from the more ordered to the less ordered state, until they reach the isotropic liquid state. The transitions solid-LC mesophase, LC mesophase-LC mesophase, and LC mesophase-isotropic liquid are first-order thermodynamic transitions. In them the volume and enthalpy show discontinuous changes (23). This means that they can be detected by dilatometry or by differential scanning calorimetry, as shown in Figure 2.20. The crystalline polymer melts, turning first into a smectic and then a nematic mesophase and finally reaching the isotropic liquid state. All the changes of volume and enthalpy undergone are additive.

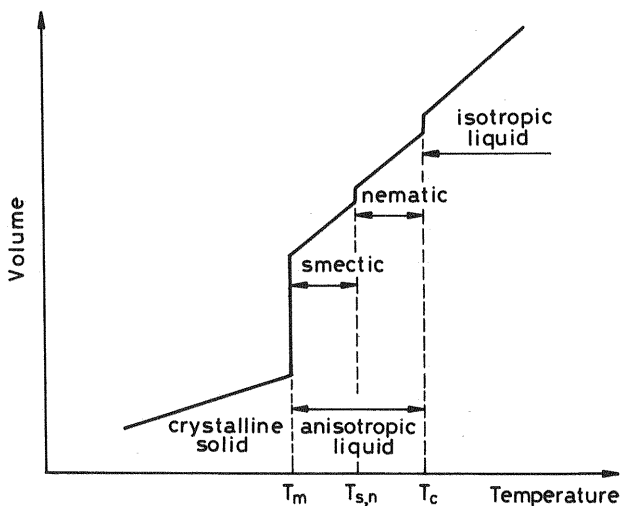


Figure 2.20 Transitions that an LCP can undergo with increasing temperature: melting to a smectic mesophase, T_m ; passage to a nematic mesophase, $T_{s,n}$, and passage to an isotropic liquid T_c .

2.7.3 Main-Chain LC Polymers

Main-chain LC polymers are characterized by their low solubility and by extremely high melting temperatures, in many cases decomposing before reaching the molten state. These characteristics are a consequence of their rigid chain structure with strong intermolecular interactions. The melting or dissolving of the crystals requires the breaking of many interactions and is therefore highly endothermic. On the other hand, in the solid-liquid transition very little entropy is originated, since the chains continue to maintain their stretched conformation. This is in contrast to the behavior of flexible macromolecules, which have higher melting entropy as they have much lower melting points. Main-chain LC polymers, such as aromatic polyamides, usually form lyotropic LCs with nematic mesophases. Lyotropic main-chain LC polymers are not used in the liquid crystalline state. Nevertheless, this is the state in which they are processed and once the solvent is eliminated, they possess excellent mechanical properties such as rigidity, tensile strength, and extraordinary chemical resistance. For this reason, they are used in advanced applications in the aerospace, telecommunication, and electrical industries. For example, Kevlar is processed dissolved in sulfuric acid to form high resistance fibers. A favorable characteristic for the processing is that the increase in the viscosity of the

solution with the concentration ceases when the critical concentration is reached and the mesophase is formed. The ordering of the chains in the direction of flow reduces the viscosity, which facilitates the processing of the fibers.

Thermotropic main-chain LC polymers are copolymers or terpolymers, generally polyesters and polyamides. Homopolymers have such high melting temperatures that they decompose before melting. There are several ways to lower their melting temperatures and be able to use them as thermotropics.

1. Copolymerize mesogenic monomers to form random copolymers with lower melting temperatures.
2. Incorporate bulky side groups that make packing difficult.
3. Attach flexible side chains onto the stiff main chain which decreases the interactions between the main chains.
4. Insert flexible chain portions (spacers) into the main chain to aid the solubility and decrease the transition temperature (see Fig. 2.18b).

2.7.4 Side-Chain LC Polymers

Side-chain liquid crystal polymers are obtained by fixing mesogenic units as side substituents of flexible polymer chains, commonly polyacrylates and polysiloxanes. The bonding of rigid rod type mesogenic groups directly onto the flexible main chain does not lead to LC mesophases, because, due to steric impediments, the arrangement of mesogenic moieties does not take place. Nevertheless, the attachment of mesogens to the main chain via flexible spacers stabilizes the ordered mesophase (5) (see Fig. 2.21). When alkyl chain spacers are used and the main chain is sufficiently long, smectic mesophases can be observed that, when the temperature is increased, can pass through a nematic mesophase to the isotropic liquid state. In side-chain LCs, the order of the mesophase can persist when the mesophase is cooled quickly to below the glass transition temperature; thereby it is possible to obtain a nematic (or smectic) glass, i.e., a rigid phase displaying the order and anisotropic properties of the LC phase. This characteristic makes them useful as materials for storing information. Unlike main-chain LC polymers, side-chain LCs do not possess such good mechanical properties, but their optical behavior—particularly their response to electric and magnetic fields—makes them useful as materials for nonlinear optics (mixers, amplifiers, and frequency modulators).

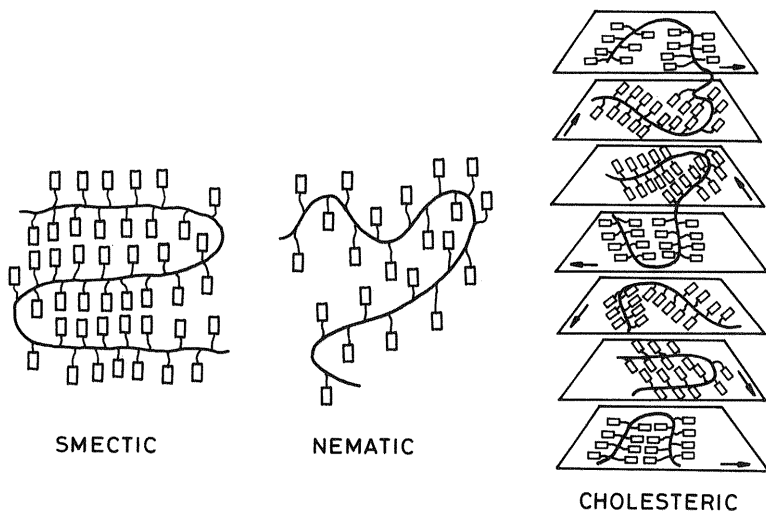


Figure 2.21 Side-chain LCPs organized in different mesophases.

2.8 GLASSY STATE

The introduction to this chapter made reference to the absence of long-range molecular order in amorphous polymers as being the characteristic differentiating them from crystalline polymers. Depending on the temperature and structure, amorphous polymers exhibit different types of physical and mechanical behavior. In a molten polymer the molecular segments interchange places because of the high possibility of conformational changes caused by thermal excitation. In a solid amorphous polymer, the movements of the chain segments are vibrations around fixed positions. When the temperature increases, the amplitude of the vibrations increases, transmitting a rise in tension to the intermolecular interactions. If the temperature continues to increase, a growing fraction of chain segments acquire enough energy to overcome these intermolecular interactions. Stronger modes of movement appear that involve the rotation and translation of chain terminals and chain segments or loops incorporating about 10 bonds (Fig. 2.22). These movements are an important mechanism for energy absorption, thereby imparting toughness to the material. A temperature can be assigned to each polymer at which, during the observation time of the experiment, these movements start to be detected. This temperature is the glass transition temperature, T_g (7,24,25). At temperatures below T_g , the polymer maintains the disordered nature of the melt but lacks molecular mobility;

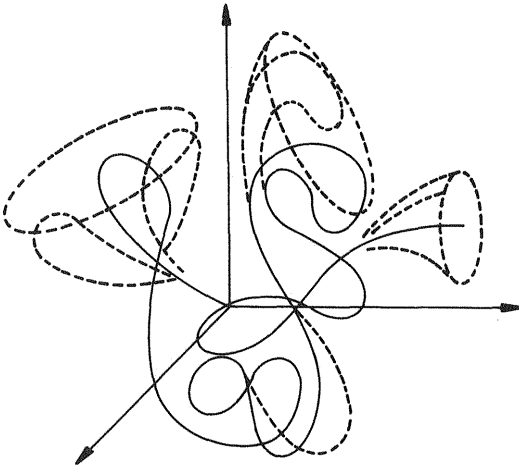


Figure 2.22 Movements of chain terminals, loops, and segments in the glass transition temperature range. (From Ref. 24.)

it is in the “glassy” state. This state is distinguished from the molten state in one aspect only: immobility of the molecular chains, which are frozen into nonextended conformations in contrast to the crystalline state. At temperatures above T_g the polymer is easily deformed due to the partial flexibility of the chains. There is therefore a drastic change in the rigidity and, in general, in the mechanical properties of polymers at T_g . The ability to adopt the glassy state is not confined to amorphous polymers. Any polymer, if it is cooled sufficiently below the melting temperature T_m without crystallizing, will undergo a glass transition. Semicrystalline polymers display a glass transition, but the changes in properties at T_g are normally less pronounced than in fully amorphous polymers. At temperatures between T_m and T_g the solid consists of rigid crystallites and an amorphous fraction of low modulus, so it will be both flexible and tough. Below T_g the solid comprises crystalline and glassy regions.

2.9 PHENOMENOLOGY OF THE GLASS TRANSITION

Let us assume an experiment consisting in cooling a liquid polymer until it solidifies. Figure 2.23 shows the evolution of the process in a V/T diagram. In some polymers, such as highly crystalline polyethylene, crystallization cannot be prevented and the path followed in the solidification is that

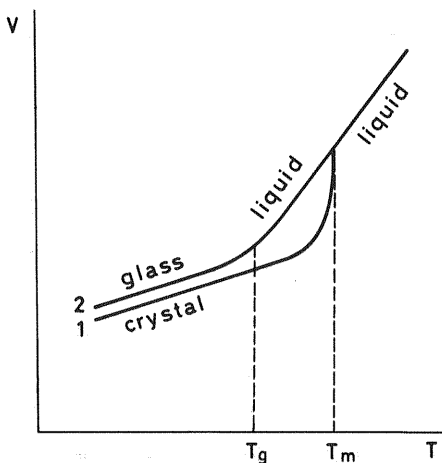


Figure 2.23 Volume–temperature dependence for glassy and highly crystalline polymers.

included by curve 1 in the figure. Amorphous polymers and even some crystalline polymers, when cooled quickly, follow path 2, in which the liquid phase persists until the liquid–glass transition occurs (25). In the vicinity of the glass transition, the slope of the V – T curve changes toward lower values than those corresponding to the liquid. The glass transition temperature is normally considered to be the temperature defined by the intersection of the straight lines corresponding to the liquid and glassy states. Similar behavior can be observed in the plots of enthalpy as a function of temperature.

In semicrystalline polymers (see Fig. 2.24) the change in the slope of the V – T curve in the region of T_g is mainly due to large-scale structural rearrangements in the amorphous zone, while the crystalline regions remain relatively unchanged. The higher the degree of crystallinity, the less pronounced will be the effect of the glass transition temperature on the properties of the material. In highly crystalline polymers, the glass transition temperature can be expected to be hardly detectable. Path 1 in Figure 2.24, which shows how the volume of a semicrystalline polymer behaves as the polymer expands, exhibits both melting and glass transition. Path 2 represents the volume expansion curves for glassy polymers. In this case, it can be seen that the polymer exhibits just a glass transition temperature. Many authors have suggested that the glass transition is simply a relaxation phenomenon where slow kinetics does not allow the structural relaxation to thermodynamic equilibrium within the experimental time scale.

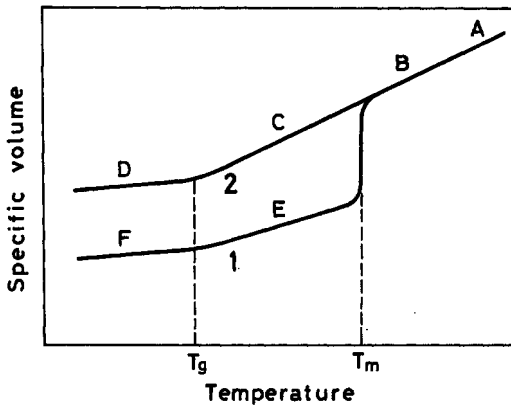


Figure 2.24 Specific volume–temperature dependence for semicrystalline polymers.

Glass transition has kinetic characteristic. As illustrated by Figure 2.25, the polymer cooled from the liquid to the glassy state follows the path ABC ; if it is cooled at a slower rate, the polymer will follow the path $AB'C'$, in such a way that T_g is lower when the rate of cooling decreases (26). The kinetic nature of the glass transition can also be revealed by analyzing Figure 2.26, which shows the variation of volume with time (27). The curves correspond to the following sequence of experiments. The polymer initially at one temperature T' ($T' > T_g$), is cooled to another temperature, T'' around T_g . At T'' the volume is not constant with time, as shown by the various curves of Figure 2.26. In the glassy state the polymer continues to shrink with time, and the magnitude of that shrinkage depends on how far the temperature T'' is from T_g . Therefore, the volume that is determined in the glassy state at each temperature depends on the time elapsed from the moment when the polymer was cooled until T'' was measured.

The decrease in volume with time in the glassy state indicates that, though slowly, conformational changes do take place over time, leading to greater density and an increase in brittleness. The changes in physical properties of glassy polymers when they are held at temperatures below their T_g is known as physical aging. In relation to physical aging, two aspects have to be taken into account. On the one hand, to obtain reproducible T_g data it is necessary to maintain the polymer sample at the measuring temperature for the same time. On the other hand, physical aging provides changes in mechanical properties (slow stiffening) that have to be considered in design.

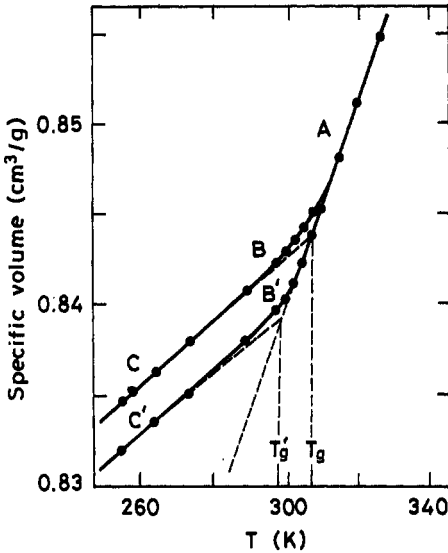


Figure 2.25 Specific volume–temperature dependence for poly(vinyl acetate) as a function of cooling rate.

It is worthwhile to comment on the temperature dependence of the first derivatives of volume and enthalpy. The first derivative of volume is the thermal expansion coefficient, α .

$$\alpha = \left[\frac{1}{V} \frac{\delta V}{\delta T} \right]_p \quad (2.10)$$

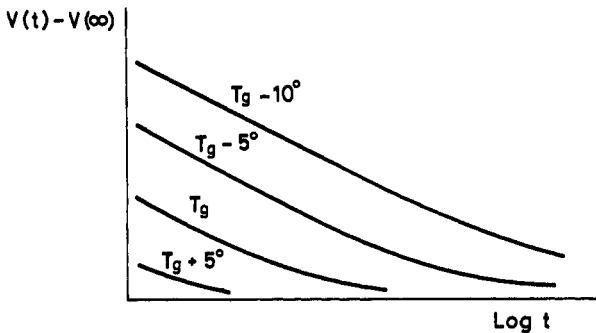


Figure 2.26 Volume–time dependence at different temperatures near the glass transition temperature.

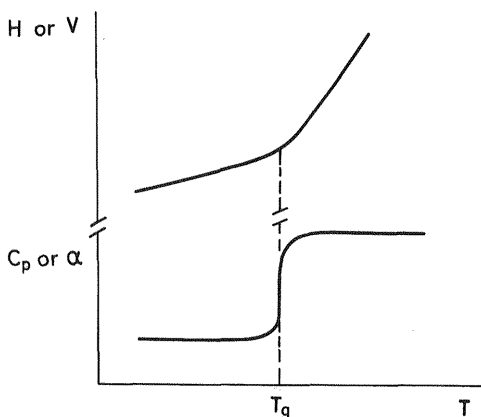


Figure 2.27 Volume (V), enthalpy (H), expansion coefficient (α), and heat capacity (C_p) as a function of temperature near T_g .

Figure 2.27 shows both the $V-T$ and $\alpha-T$ curves. It can be seen that at T_g there is a discontinuous change in the thermal expansion coefficient. Thus, for atactic polypropylene ($T_g = -19^\circ\text{C}$), the thermal expansion coefficient α for the glass (just below T_g) is $2.2 \times 10^{-4} \text{ K}^{-1}$, and for the liquid it is $8.1 \times 10^{-4} \text{ K}^{-1}$. The coefficient α for the glassy polymer is similar to α for the isotactic crystalline polymer at the same temperature (9). An analogous change is observed for the first derivative of H with respect to T , C_p , as a function of temperature. These changes in C_p and α at T_g provide the usual methods to determine T_g . The C_p-T or $\alpha-T$ curves shown in Figure 2.27 correspond to the cooling process; if a heating process follows, different curves of C_p or α vs. T would be obtained, due to the kinetic nature of the glass transition. The values of T_g reported in the literature for any polymer can vary around an interval of $10\text{--}15^\circ\text{C}$; this is a consequence of the dependence of T_g on the time scale of the experiment and on the measurement technique.

Figure 2.28 shows the variation of viscosity η with temperature for a polymer (28). In spite of the enormous change in η in passing through the glass transition, the behavior is qualitatively analogous to that seen for H or V .

2.10 GLASS TRANSITION AND FREE VOLUME

One of the most suitable approximations for analyzing the glass transition concerns the free volume. The free volume is the space in a solid or liquid

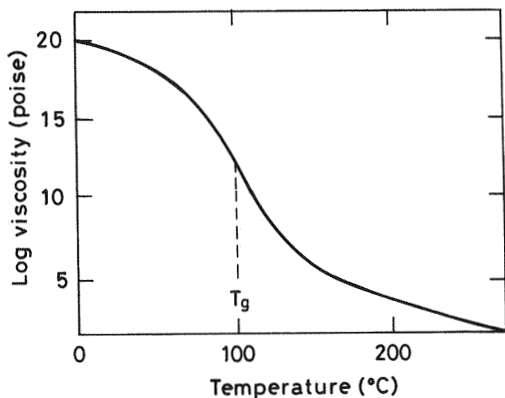


Figure 2.28 Viscosity–temperature dependence for an amorphous polymer.

not occupied by molecules; i.e., it is the empty space existing between molecules. In the liquid state the free volume is large, so molecular movements occur easily (the unoccupied volume facilitates the mobility of the molecules), and the molecules are therefore able to change their conformation freely. A drop in temperature reduces the thermal energy available for molecular motions. The free volume is sensitive to changes in temperature; thus the thermal expansion of the solid or molten polymer can be explained by a change in free volume. When the temperature of a molten polymer falls, the free volume shrinks until it is too small to allow long-range cooperative (micro Brownian) motions. The temperature at which this occurs is T_g ; below T_g only local conformational changes are permitted, and consequently the free volume shows a negligible temperature dependence.

The situation discussed above is shown schematically in Figure 2.29. The free volume, V_f , is represented by the shaded area; it can be seen that V_f remains constant below T_g (it is denoted V_f^*) and increases with temperature above T_g . The total volume of the sample, V , is the volume occupied by the molecules, V_0 , and the free volume V_f ; $V = V_0 + V_f$. The free volume fraction, f , is defined as V_f/V . Above T_g there will be a considerable contribution of V_f due to the expansion of the melt. The free volume at temperatures greater than T_g will be given by

$$V_f = V_f^* + (T - T_g) \frac{\delta V_f}{\delta T} \quad (2.11)$$

and dividing by V ,

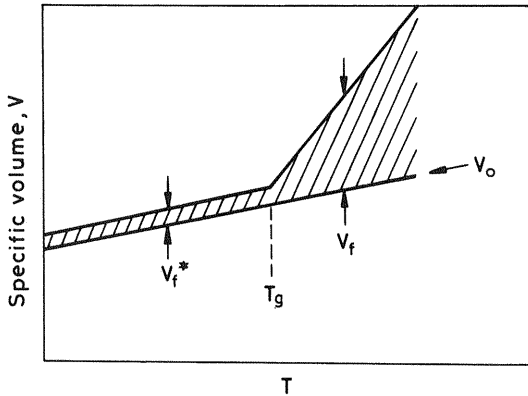


Figure 2.29 Scheme of the variation of the specific volume of a polymer with temperature. The free volume is represented by the shaded area.

$$f_i = f_g + (T - T_g)\alpha_f \quad (2.12)$$

where f_i and f_g represent the free volume fraction at any temperature above T_g and at T_g , respectively; α_f is the thermal expansion coefficient of the free volume, which can be assumed constant for temperatures slightly above T_g ; i.e., the increase of f with T is assumed to be linear and consequently $\Delta f / \Delta T = \text{constant} = \alpha_f$.

The free volume has been introduced intuitively, relating it to the gaps that allow conformational changes in the solid. It would therefore be possible to obtain f from the difference between the geometric volume of the segments and the total volume. Nevertheless, this type of calculation is not useful, as the free volume for molecular movement does not exactly coincide with the empty space in the solid. The concept of free volume is related to the occurrence of macromolecular motion rather than to the existence of gaps. For this reason, the free volume fraction is an empirical parameter whose value is determined on the basis of experimental results.

The free volume theory of glass transition is based on Doolittle's empirical assumption (29), which states that the viscosity, η , at $T > T_g$ is related to the free volume fraction by the equation

$$\eta = A \exp \left[B \frac{V_0}{V_f} \right] \quad (2.13)$$

where A and B are constants.

From Eq. (2.13),

$$\ln \eta = \ln A + B \frac{1}{f} \quad (2.14)$$

where $f \simeq V_f/V_0$, given that $V_0 \gg V_f$

If η_T corresponds to the viscosity at any temperature T , and η_{T_g} to the viscosity at T_g , then Eq. (2.14) leads to

$$\ln \left[\frac{\eta_T}{\eta_{T_g}} \right] = \ln a_T = B \left[\frac{1}{f_T} - \frac{1}{f_g} \right] \quad (2.15)$$

By substituting f_T by $f_g + \alpha_f(T - T_g)$ in Eq. (2.15), one obtains

$$\ln a_T = B \left[\frac{1}{f_g + \alpha_f(T - T_g)} - \frac{1}{f_g} \right] \quad (2.16)$$

Rearrangement of this equation gives

$$\log a_T = - \frac{B}{2.3f_g} \left[\frac{T - T_g}{f_g/\alpha_f + (T - T_g)} \right] \quad (2.17)$$

where the constant B is close to unity. Equation (2.17) is one form of the Williams–Landel–Ferry (WLF) empirical correlation (30) and can be stated as a function of universal parameters, giving

$$\log a_T = C_1 \frac{T - T_g}{C_2 + T - T_g} \quad (2.18)$$

The constants C_1 and C_2 are nearly universal and, within a reasonable degree of approximation, are valid for many polymers, taking the values -17.4 and 51.6 K, respectively. From the value of C_1 it can be deduced that the free volume fraction, f_g , at the glass transition is approximately 0.025. When the free volume fraction falls to this low value it seems that the conformational changes in the solid cease to occur. The value of C_2 , together with $f_g = 0.025$, allows the thermal expansion coefficient of the free volume to be known, which turns out to be $\alpha_f \simeq 4.8 \times 10^{-4} \text{ K}^{-1}$, valid for the great majority of polymers.

2.11 FACTORS AFFECTING THE GLASS TRANSITION OF POLYMERS

The influence of factors such as chemical structure, molecular weight, cross-linking and plasticizers in the glass transition of polymers can be related to the changes that they provoke on the free volume fraction, which, as we already know, reaches a critical value at the glass transition temperature. The factors affecting the glass transition can be classified into two types: (1) molecular factors, i.e., those related to the chemical structure of the polymer chain, and (2) external or controllable factors.

2.11.1 Factors Related to the Chemical Structure

(a) Main Chain

The effect of the chemical nature of the main chain of the polymer on the glass transition temperature is similar to the effect that it has on the melting temperature, T_m . The chemical structure has a determining influence on the flexibility of the chain. For example, polymers such as polyethylene, $(-\text{CH}_2-\text{CH}_2-)_n$, and polyoxyethylene, $(-\text{CH}_2-\text{CH}_2-\text{O}-)_n$, have relatively flexible chains as a result of the ease of rotation around their chain bonds. Thus they have low values of T_g and T_m , as can be seen in Table 2.3. The incorporation into the main chain of units that hinder rotation and consequently increase the rigidity of the chain clearly causes a large increase in T_g . For example, the incorporation of a *p*-phenylene ring (Ph) into the monomeric unit of polyethylene gives poly(*p*-xylylene), which has a T_g of around 353 K (see Table 2.3).

(b) Side Groups

In vinyl polymers, $(-\text{CH}_2-\text{CHR}-)_n$, the nature of the side group R has a pronounced effect on T_g as a result of restrictions on the rotation of the macromolecule. Large, inflexible, and bulky side groups cause an increase in rigidity, while flexible side groups have not marked effect. Table 2.4 presents

Table 2.3 Values of T_g and T_m for Various Polymers

Repeating unit	T_g (K)	T_m (K)
$-\text{CH}_2-\text{CH}_2-$	140–270	410–419
$-\text{CH}_2-\text{CH}_2-\text{O}-$	206	340
$-\text{CH}_2-\text{Ph}-\text{CH}_2-$	353	670

Table 2.4 Values of T_g for Various Polymers $(-\text{CH}_2-\text{CHR}-)_m$

Side group R	T_g (K)
$-\text{CH}_3$	250
$-\text{Ph}$	373
$-\text{Cl}$	354
$-\text{OH}$	358
$-\text{CN}$	370
$-\text{O}-\text{CH}_2-\text{CH}_2-\text{CH}_2-\text{CH}_3$	241
$-\text{O}-\text{CH}_2-\text{CH}-(\text{CH}_3)_2$	272
$-\text{O}-\text{C}-(\text{CH}_3)_3$	356

the values of T_g for several polymers of the general formula $(-\text{CH}_2-\text{CHR}-)_n$, with different types of substituents R (7). The last three examples show how the flexibility of the molecule varies according to the degree of compactness of the different isomers of the butyl radical, leading in the case of poly(vinyl *tert* butyl ether) to a considerable increase in T_g .

The T_g for some *n*-alkyl ethers of the general formula $(-\text{CH}_2-\text{CH}-(\text{OR}')-)_n$ where R' represents an *n*-alkyl group (24), are given in Table 2.5. Lower values of T_g are observed as the length of R' increase. The rise in the length of R' is associated with an increase in free volume at a given temperature.

Symmetry also affects T_g . It might be expected that polyisobutylene, $(-\text{CH}_2-\text{C}(\text{CH}_3)_2-)_n$, would have a T_g greater than polypropylene, $(-\text{CH}_2-\text{CH}(\text{CH}_3)-)_n$, as a consequence of the two $-\text{CH}_3$ groups bonded to the backbone, which would tend to increase the chain rigidity. But this is not the case; polyisobutylene is a rubber that has a T_g of -71°C , while polypropylene presents $T_g = -23^\circ\text{C}$. Another example of how symmetry plays an important role in the T_g is seen if we compare poly(vinyl chloride) ($T_g = 81^\circ\text{C}$) and poly(vinylidene chloride) ($T_g = -19^\circ\text{C}$) (31). As a general rule, it can be said that an increase in symmetry produces a decrease in the glass transition temperature.

Table 2.5 T_g of Some Poly(vinyl *n*-alkyl ether)s

Polymer	R'	T_g ($^\circ\text{C}$) at 1 Hz
Poly(vinyl methyl ether)	CH_3	-10
Poly(vinyl ethyl ether)	CH_2CH_3	-17
Poly(vinyl <i>n</i> -propyl ether)	$\text{CH}_2\text{CH}_2\text{CH}_3$	-27
Poly(vinyl <i>n</i> -butyl ether)	$\text{CH}_2\text{CH}_2\text{CH}_2\text{CH}_3$	-32

If the different tactic configurations of a single polymer, for example, poly(methyl methacrylate), are considered the lowest value of T_g corresponds to the isotactic polymer. At $T < T_g$ the specific volume of the isotactic polymer is lower than that of the atactic one, and the free volume fraction is the same for both polymers; therefore the volume occupied will be less in the isotactic polymer. Nevertheless, at $T > T_g$, both tactic configurations have similar specific volume; consequently the temperature at which the free volume is equal to 0.025 of the total volume is lower in the isotactic form than in the atactic one.

(c) Polarity of the Chain

The glass transition temperature rises with the polarity of the polymer chain. It is assumed that the decrease in the mobility of the chain in this case is due to an increase in intermolecular forces. Table 2.4 shows how the presence of polar groups such as $-\text{Cl}$, $-\text{OH}$, or $-\text{CN}$ tends to increase T_g more than do nonpolar groups of equivalent size. Polar interactions considerably restrict rotation; hence poly(vinyl chloride), $(-\text{CH}_2-\text{CHCl}-)_n$, has a T_g higher than that of polypropylene, $(-\text{CH}_2-\text{CH}(\text{CH}_3)-)_n$.

The chemical factors controlling T_g that have just been discussed will also have an effect on T_m , given that both temperatures are controlled by the rigidity of the main chain. It is not surprising, therefore, that a correlation is found between T_g and T_m in semicrystalline polymers. In these cases, when the temperatures are stated in kelvins, the value of T_g generally falls between 0.5 and $0.8T_m$ (32). Figure 2.30 shows T_m vs. T_g for various polymers such as polyethylene, polypropylene, polystyrene, and poly(ethylene oxide), illustrating this behavior. This demonstrates that in homopolymers it is not possible to independently control T_g and T_m . Nevertheless, this is indeed possible in copolymers. For example, in random copolymers of nylon 6.6 and nylon 6.10, T_g varies very little with respect to the T_g of the two homopolymers, since the rigidity of the main chain hardly changes. However, the irregularity introduced into the main chain in copolymerization will reduce the ability of the chains to crystallize, and as a consequence the melting temperature T_m of the copolymer will be lower than that of the homopolymers.

2.11.2 Controllable Factors Affecting the Glass Transition Temperature

(a) Effect of Pressure

When a polymer is at a temperature above its glass transition temperature and it is subjected to a compression, the free volume decreases. T_g therefore

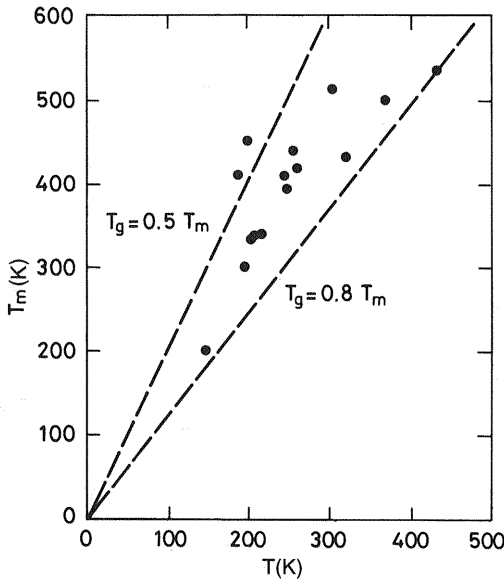


Figure 2.30 T_m vs. T_g for various polymers. (From Ref. 32.)

risers, and the polymer will thus be closer to its glass transition temperature. In general, T_g of polymers increases by around 20°C per 1000 atm of pressure. For small pressure changes, the effects are clearly negligible. So the effect of pressure of T_g becomes important only in the case of applications at very high pressure. Glass transition can also be observed as a function of pressure at constant temperature. Experiments could therefore be performed to measure, for example, the specific volume as a function of pressure in order to obtain the glass transition pressure.

(b) Effect of Molecular Weight

The dependence of T_g on molecular weight can be expressed according to the equation (33)

$$T_g^\infty = T_g + \frac{K}{M_n} \quad (2.19)$$

where K is a constant and T_g^∞ is the limit value of T_g for $M_n^{-1} \rightarrow 0$ ($M_n \rightarrow \infty$). This limit value is normally reached for values of M_n on the order of 10^5 . This equation can be deduced from the free volume theory,

taking into account that terminal bonds are associated with more free volume than the intermediate ones. This can be explained by considering that terminal bonds have greater mobility and each chain termination is the cause of an imperfection in the packing of the solid.

Let us consider a polymer of density ρ and molecular weight M_n . In this case, the number of chains per unit volume is $\rho(N_A/M_n)$; thus the number of chain terminals per unit volume is $2\rho(N_A/M_n)$, where N_A is Avogadro's number. If the contribution of one chain terminal to the free volume is represented by θ , the total free volume fraction due to the chain terminals, f_c , is given by

$$f_c = \frac{2\rho N_A \theta}{M_n} \quad (2.20)$$

If a polymer with this value of f_c has a glass transition temperature T_g , then f_c will be equivalent to the increase in the free volume that occurs when the polymer is thermally expanded between T_g and T_g^∞ . This means that

$$f_c = \alpha_f(T_g^\infty - T_g) \quad (2.21)$$

where α_f is the thermal expansion coefficient of the free volume. Combining Eqs. (2.20) and (2.21) gives the expression

$$T_g = T_g^\infty - \frac{2\rho N_A \theta}{\alpha_f M_n} \quad (2.22)$$

This equation has the same form as (2.19) with $K = 2\rho N_A/\alpha_f$.

Figure 2.31a represents the variation of T_g vs. M_n^{-1} for polystyrene. The slope of this straight line can be used to deduce the value of θ , since N_A , α , and ρ are known. It is obtained that $\theta = 80 \text{ \AA}^3$, a value approximately equal to half the size of the styrene monomer unit. Figure 2.31b shows a plot of T_g vs. M_n ; as can be seen, the effect of the molecular weight on T_g has very little importance when the molecular weight is high ($M > 10^5$).

Branching has a significant influence on the glass transition temperature. A small number of branchings in a polymer reduces the value of T_g . This fact is analyzed again based on the free volume theory; therefore, according to earlier statements a branched chain of a polymer with a number y of chain terminals will have a glass transition temperature given by

$$T_g = T_g^\infty - \frac{\rho y N_A \theta}{\alpha_f M_n} \quad (2.23)$$

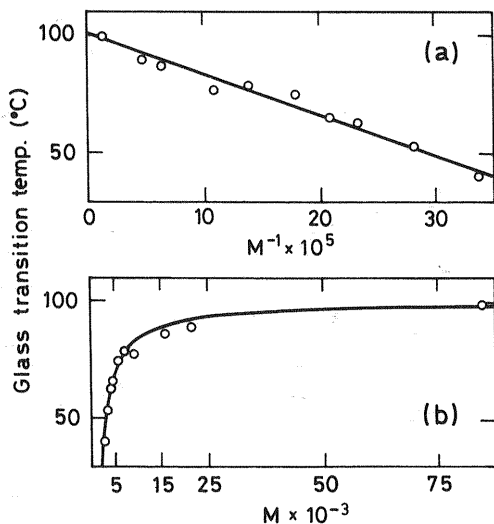


Figure 2.31 Dependence of the glass transition temperature as a function of the molecular weight (b) and its inverse (a). (From Ref. 33.)

where T_g^∞ is the glass transition temperature of a linear chain of infinite molecular mass. The linear chain has two terminals, so the number of branchings per chain will be $y - 2$. Equation (2.23) is valid only when the number of branchings is low. A high branching density will have the same effect as side groups; i.e., it will restrict the mobility of the chain and therefore increase T_g .

(c) Effect of Cross-Linking on T_g

Polymers with strong intermolecular interactions present high glass transition temperatures, because great energy is required to separate their chains. Cross-linkings constitute the strongest intermolecular interactions; they form real chemical bonds. As the cross-link density increases, the free volume decreases, and T_g consequently rises because the molecular mobility is more hindered. Figure 2.32 shows the variation of the specific volume with temperature for a series of styrene polymers cross-linked with different amounts of divinylbenzene (see Sect. 1.2). It can be seen that the transition temperatures are shifted toward higher values and the transition zone broadens as the divinylbenzene content increases (34). The effect of cross-linking on T_g is the inverse to that implied by a decrease in molecular weight. Normally, the introduction of cross-links into a polymer is accom-

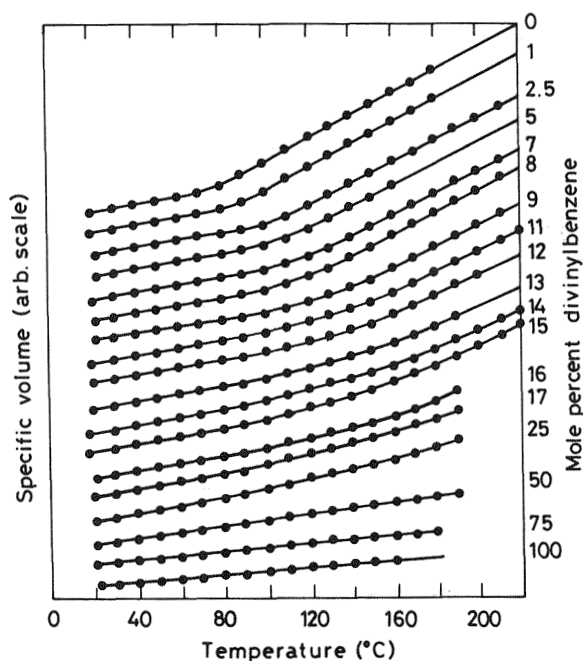


Figure 2.32 Effect of cross-linking on the glass transition temperature of the system styrene with divinylbenzene. (From Ref. 34.)

plished by the addition of a specific cross-linking agent that can be regarded as a comonomer. Consequently, two effects have to be considered: on the one hand, the copolymer effect (as a result of the incorporation of a second unit), and on the other hand, the cross-linking effect. Both are considered in the equation

$$T_g = T_g^\infty - \frac{K}{M} + K_x \rho \quad (2.24)$$

where M is the molecular weight between cross-links, K_x is a constant, and ρ is the number of cross-links per gram. This equation is analogous to that obtained for the relation between T_g and molecular weight [Eq. (2.19)], but it includes a further term, $K_x \rho$.

(d) Homogeneous Copolymer Systems and Miscible Mixtures

The introduction of a comonomer into a polymer influences the glass transition temperature. In general, a random copolymer of two monomers with

different T_g values has a glass transition temperature intermediate between those of the homopolymers. These random copolymers behave as regular polymers, showing a single glass transition temperature. Such is the case also for miscible mixtures of polymers or polymer blends. The dependence of T_g of a random copolymer, or of a miscible polymer mixture, on the composition can be predicted. Various equations have been proposed for expressing this dependence based on the assumption of additivity of free volume. One of the simplest is the classic rule of mixtures of Di Marzio and Gibbs (35), whose expression has the form

$$T_g = w_1 T_{g_1} + w_2 T_{g_2} \quad (2.25)$$

where w_i represents the weight fraction of the comonomers in the copolymer or the weight fraction of homopolymers in the mixture, and T_{g_i} represents the glass transition temperature of the homopolymers.

Another simple equation frequently used is that proposed by Fox (36):

$$\frac{1}{T_g} = \frac{w_1}{T_{g_1}} + \frac{w_2}{T_{g_2}} \quad (2.26)$$

This model presupposes homogeneity in the case of copolymers and in polymer mixtures, that is, random distribution at the segmental level. It has been considered that it represents the ideal behavior of miscible polymer mixtures, on account of which deviations of experimental data from this prediction have been used as a criterion to indicate the strength of interaction among the components in the amorphous phase of the mixture. This equation is nevertheless not applicable to block or graft copolymers. In their case a T_g value is obtained for each component if the blocks or graft branchings are sufficiently large, allowing each type of homopolymer to segregate into its own region.

(e) Plasticizers

The glass transition temperature of polymers decreases when a liquid such as an organic solvent or water is mixed with them. Liquids added to polymers to make them suitable for practical purposes, e.g., softer and more flexible at ambient temperature, are known as plasticizers. These substances are generally low molecular weight organic compounds, weakly polar, with glass transition temperatures in the range of -50 to -150°C and high boiling points, on the order of 300°C , to prevent evaporation losses. Weakly polar esters are good plasticizers because they tend to be miscible with many polar and nonpolar polymers. The most commonly used plasticizers are

obtained from phthalic acid and include diethyl, dibutyl, and *n*-dioctyl phthalates. These compounds act by weakening the intermolecular interactions by means of a solvating action. Plasticizers reduce the T_g and T_m of polymers, making them softer and more flexible, by distributing their molecules through the polymer and separating the chains. In addition to this physical action, the intermolecular interactions among the chains are weakened, because interactions are hindered at the points where the plasticizer is located.

Figure 2.33 illustrates how the T_g and T_m of poly(vinyl chloride) vary with the plasticizer content (37). Note how T_g falls faster than T_m . In this case miscibility limits the plasticizer content to approximately 40%. The effect of plasticizers in reducing the T_g is interpreted as being due to the increase of free volume of the system. By assuming that the free volume of a plasticizer system is the average of the free volumes of the components, one can write

$$f = f_g + \alpha_f(T - T_g)(1 - v_p) + \alpha_p(T - T_p)v_p \quad (2.27)$$

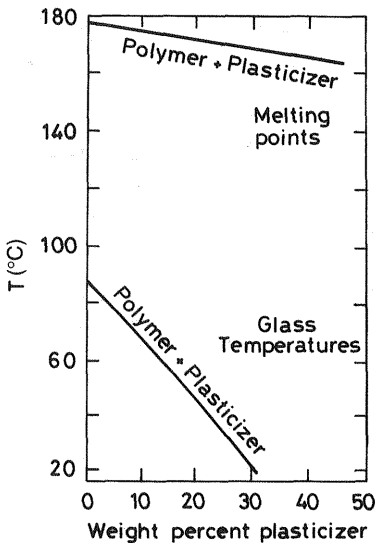


Figure 2.33 Variation of thermal transition temperatures of poly(vinyl chloride) with plasticizer content.

where f_g is the fraction free volume (0.025) at the glass transition temperature, α_f and α_p and T_g and T_p are, respectively, the expansion coefficients of the free volume and the glass transition temperature of the polymer and plasticizer, respectively, v_p and f are respectively the volume fraction of the plasticizer and the fractional free volume of the plasticizer system at temperature T . According to the free volume theory, the fractional free volume of the plasticized system at its glass transition temperature T'_g is f_g . Substituting T for T'_g and f for f_g in Eq. (2.27), the following expression is obtained, which relates the glass transition temperature to the plasticizer content:

$$T_g - T'_g = \frac{\alpha_p(T'_g - T_p)v_p}{\alpha_f(1 - v_p)} \quad (2.28)$$

Plasticizers of low molecular weight have a disadvantage due to their volatility and the facility with which they diffuse. This fact has provoked the development of polymeric plasticizers, formed by polymers of low T_g and miscible with the base polymer, which provide flexibility, facilitate the processing, and give the material longer service. Because of their longer predurability in relation to plasticizers of low molecular weight, polymer plasticizers are specially useful for food, electrical, and medical applications. A typical example of polymer plasticized with these materials is poly(vinyl chloride) (PVC) with copolymers of ethylene vinyl acetate (EVA).

(f) Crystallinity

Crystallinity also affects the glass transition temperature. The T_g of the amorphous phase in a polymer depends on the degree of crystallinity. In some cases, for example, in poly(ethyleneterephthalate), when the degree of crystallinity increases from 2% to 65%, T_g rises from 80°C to 125°C. On the other hand, in the case of poly(4-methylpentene), when the degree of crystallinity increases from 0% to 76%, T_g drops from 29°C to 18°C. T_g can increase or decrease with the degree of crystallinity; there is no universally accepted explanation for it. It has been suggested that it could depend on the relative densities of the amorphous and crystalline phases (38). Generally the crystalline phase has the higher density at T_g , the molecular chains that belong to the amorphous phase are restricted by the immobile crystalline phase, and T_g increases. When the crystalline phase has a lower density (rare occasions) than the amorphous phase, the entropy increases and T_g decreases.

PROBLEM SETS**Problem 2.1**

Demonstrate that the extended planar zigzag conformation of crystalline polyethylene is not permitted in crystalline polytetrafluoroethylene.

Data: C—C—C angle 112°C , C—C length 0.154 nm; atomic radius of H = 0.075 nm; atomic radius of F = 0.135 nm.

Solution 2.1

In the planar zigzag conformation of polyethylene (see Fig. 2.2) the centers of the substituents (hydrogen atoms) of alternate carbons will be separated by a distance

$$2 \times 0.154 \times \sin(112/2) = 0.255 \text{ nm} \quad (\text{P2.1.1})$$

The radius of a hydrogen atom is just 0.075 nm, which permits this configuration in polyethylene ($2 \times 0.075 = 0.15 \text{ nm} < 0.254 \text{ nm}$). Fluorine atoms are bigger and take up more space than that available ($2 \times 0.135 = 0.27 \text{ nm} > 0.254 \text{ nm}$). Then the most stable conformation is achieved by means of a small distortion of the C—C—C bond angle (116°C), giving rise to 13/1 helices as illustrated in Figure 2.3.

Problem 2.2

For a single crystal of polyethylene of thickness 12 nm, estimate the number of monomer units in each section of chain in the extended zigzag conformation as well as the number of folds of a chain of molecular weight $M = 10^5$ g/mol.

Data: C—C length = 0.154 nm; C—C—C bond angle = 112° .

Solution 2.2

Each monomer unit, $-\text{CH}_2-\text{CH}_2-$, occupies a length of extended chain given by

$$l = 2 \times 0.154 \times \sin(112/2) = 0.255 \text{ nm} \quad (\text{P2.2.1})$$

Therefore, there are $12/0.255 = 47$ monomer units in each section.

Since the $-\text{CH}_2-\text{CH}_2-$ unit possesses a mass of 28 g/mol, there will be $105,000/28 \approx 3571$ ethylene units in the chain.

Assuming that in each chain there are the same number of extended sections, x , as bends or folds,

$$3571 = 47x + x \quad (\text{P2.2.2})$$

so there are $x \sim 74$ folds in each chain.

Problem 2.3

Calculate the density of syndiotactic poly(vinyl chloride), PVC, knowing that it crystallizes in the orthorhombic system, $\alpha = \beta = \gamma = 90^\circ$, $a = 1.040$ nm, $b = 0.530$ nm, $c = 0.510$ nm, and that in each cell there are four monomer units ($-\text{CH}_2-\text{CHCl}-$).

Data: Atomic masses: C = 12, H = 1, Cl = 35.5 amu; Avogadro's constant = $6.023 \times 10^{23} \text{ mol}^{-1}$.

Solution 2.3

Mass of one monomer unit = 62.5 g/mol

Mass of the unit cell = $(4 \times 62.5)/(6.023 \times 10^{23}) = 4.15 \times 10^{-22}$ g

Density = $M/V = 4.15 \times 10^{-22}/(1.04 \times 10^{-7} \times 0.53 \times 10^{-7} \times 0.51 \times 10^{-7})$
 = 1.47 g/cm^3 .

Problem 2.4

The theoretical density of 100% crystalline polyethylene is 1 g/cm^{-3} , and that of amorphous polyethylene is 0.865 g/cm^{-3} . Calculate the crystallinity of a sample of density 0.97 g/cm^{-3} .

Solution 2.4

From Eq. (2.1),

$$(0.97)^{-1} = x_c \times 1 + (1 - x_c)/0.865 \quad (\text{P2.4.1})$$

Then $x_c = 0.80$, and the polymer is 80% crystalline.

Problem 2.5

The lattice constants for orthorhombic polyethylene have been determined as a function of temperature:

Lattice constants (nm)			
$T(\text{K})$	a	b	c
4	0.712	0.485	0.255
77	0.715	0.490	0.255
293	0.740	0.495	0.254
303	0.741	0.494	0.255

- (a) Calculate the coefficient of thermal expansion at 293 K.
 (b) Why is the constant c virtually independent of temperature?

Solution 2.5

(a) The volume of the unit cell for the orthorhombic crystallization system is $V = abc$. Figure P2.5.1 shows a plot of V versus T . From the slope of the straight line; $dV/dT = 1.74 \times 10^{-5} \text{ nm}^3/\text{K}$; therefore the thermal expansion coefficient, α , at 293 K will be

$$\alpha = \frac{1}{V} \frac{dV}{dT} = 1.87 \times 10^{-4} \text{ K}^{-1} \quad (\text{P2.5.1})$$

(b) The constant c is the length of the orthorhombic cell in the direction of the chain. Therefore it will depend on the C—C—C bond angle, so it is independent of temperature

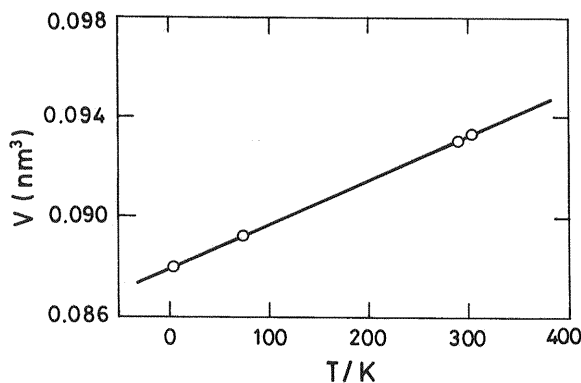


Figure P2.5.1

Problem 2.6

Poly- ϵ -caprolactone ($-\text{O}-(\text{CH}_2)_4-\text{CO}-$) $_n$, PCL, is a crystalline polymer of density 1.1 g/cm^{-3} . When a sample of molecular weight $M = 50,000 \text{ g/mol}$ is blended with amorphous poly(vinyl phenol), PVPH, of molecular weight 1500 g/mol and density 1.2 g/cm , homogeneous mixtures are formed. The table below gives the values determined for the melting point of PCL as a function of the volume fraction poly(vinyl phenol), v_3 .

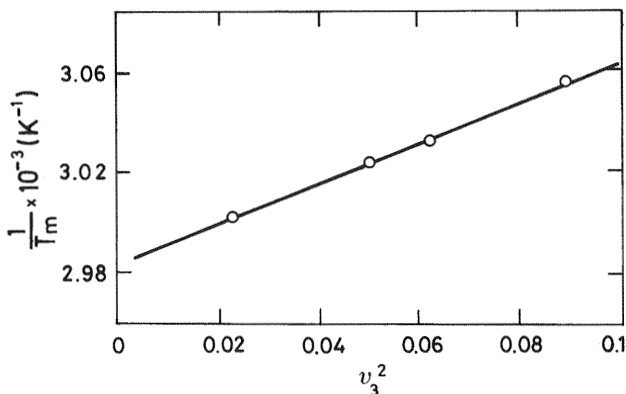
v_3	T_m (K)
0.3	327.0
0.25	329.7
0.225	330.6
0.15	333.0

Calculate the melting point of pure PCL and the value of the polymer-polymer interaction parameter, knowing that $\Delta H_{2u} = 3690 \text{ cal/mol}$.

Solution 2.6

Figure P2.6.1 shows the plot of $1/T_m$ versus v_3^2 . According to Eq. (2.9), the value of the intercept gives the melting point of pure PCL. $T_m^\circ = 335 \text{ K}$. The slope is $7.7 \times 10^{-4} \text{ K}^{-1}$, which allows the evaluation of χ_{32} . From the molecular weights of the monomer units and the corresponding densities, one obtains $V_{2u} = 102 \text{ cm}^3/\text{mol}$ and $V_{3u} = 100 \text{ cm}^3/\text{mol}$. Then from Eq. (2.9),

$$\chi_{32} = -1.4$$

**Figure P2.6.1**

This negative value indicates a strong polymer–polymer interaction that occurs via hydrogen bonding among the hydroxyl groups of poly(vinyl phenol) and the carbonyl groups of PCL. Polymers are miscible only when strong interactions are established among them, since the mixing entropy is very small due to their large size.

Problem 2.7

The glass transition temperature, T_g , of a linear polymer with number-average molecular weight $M_n = 3000$ is 100°C . The value of T_g increases to 130°C for a sample of the same linear polymer with $M_n = 10,000$. A branched sample of this polymer with $M_n = 6000$ has a T_g of 90°C . Determine the average number of branchings on the branched polymer.

Solution 2.7

If we apply the relationship between T_g and molecular weight, Eq. (2.22), to both linear polymer samples of number-average molecular weights 3000 and 10,000, then we have

$$373 = T_g^\infty - \frac{2\rho N_A \theta}{\alpha_f \times 3000} \quad (\text{P2.7.1})$$

$$403 = T_g^\infty - \frac{2\rho N_A \theta}{\alpha_f \times 10,000} \quad (\text{P2.7.2})$$

which leads to

$$\frac{2\rho N_A \theta}{\alpha_f} = 128,573; \quad T_g^\infty = 415.9 \text{ K}$$

By substituting the data obtained above into Eq. (2.23) and taking into account that T_g for the branched polymer is 90°C and $M_n = 6000$, we obtain a number y of chain terminals equal to 5. As a linear chain has two terminals, the number of branchings per chain, $y - 2$, will be 3.

Problem 2.8

Calculate the glass transition temperature, T_g for a noncrystalline ethylene-propylene random copolymer that contains 20 $-\text{CH}_3$ groups per 100 main-chain carbons, knowing that it reduces the degree of crystallinity of the copolymer to 0%.

Data: T_g for PE = -120°C ; T_g for PP = -19°C ; molecular weight of monomeric units: 42 (PP) and 28 (PE).

Solution 2.8

The T_g of a random copolymer is expressed by Eq. (2.28) (Fox equation). First we need to calculate the weight fractions of the comonomers in the copolymer. The copolymer has 20 $-\text{CH}_3$ groups per 100 main-chain carbons, which means that its content is 40% propylene comonomer, and as a consequence the weight fractions of the comonomers will be

$$w_{\text{PP}} = \frac{0.4 \times 42}{0.4 \times 42 + 0.6 \times 28} = 0.5 \quad (\text{P2.8.1})$$

and

$$w_{\text{PE}} = \frac{0.6 \times 28}{0.4 \times 42 + 0.6 \times 28} = 0.5 \quad (\text{P2.8.2})$$

Then

$$\frac{1}{T_g} = \frac{w_{\text{PP}}}{T_{g,\text{PP}}} + \frac{w_{\text{PE}}}{T_{g,\text{PE}}} = \frac{0.5}{153} + \frac{0.5}{254} \quad (\text{P2.8.3})$$

As a result the T_g of the copolymer is 191.2 K, or -82°C .

Problem 2.9

The refractive index, n , of a polymer was determined as a function of temperature. The results obtained were as follows.

T ($^\circ\text{C}$)	n
20	1.5913
30	1.5898
40	1.5883
50	1.5868
60	1.5853
70	1.5838
80	1.5822
90	1.5801
100	1.5766
110	1.5725
120	1.5684
130	1.5643

Determine the glass transition temperature of the polymer. Notice that $n \sim \rho^{-1}$ where ρ is the density.

Solution 2.9

If we plot the graph of n against T , we obtain Figure P2.9.1. The equations corresponding to straight lines 1 and 2 are, respectively,

$$y = 1.595 - 1.564 \times 10^{-4}x \quad \text{and} \quad y = 1.618 - 4.10 \times 10^{-4}x$$

The intersection of the two lines gives a value of 90.7°C , which corresponds to the glass transition temperature.

Problem 2.10

The plasticizer tri-*m*-tolyl phosphate is added to polystyrene to make it more flexible at ambient temperature. Determine the glass transition temperature of the polymer when the plasticizer content is 30% v/v.

Data: Expansion coefficient of polystyrene (PS), α_f : $5.1 \times 10^{-4} \text{ }^\circ\text{C}^{-1}$. Expansion coefficient of tri-*m*-tolyl, α_p : $8.5 \times 10^{-4} \text{ }^\circ\text{C}^{-1}$. Density of PS, 1.04 g/cm^3 at 25°C . Density of tri-*m*-tolyl phosphate, $\rho = 1.189 - 8.274 \times 10^{-4}(T - 273)$.

Solution 2.10

The effect of plasticizer in reducing T_g is interpreted as the increase in the free volume of the system. According to the free volume theory, we apply Eq. (2.28),

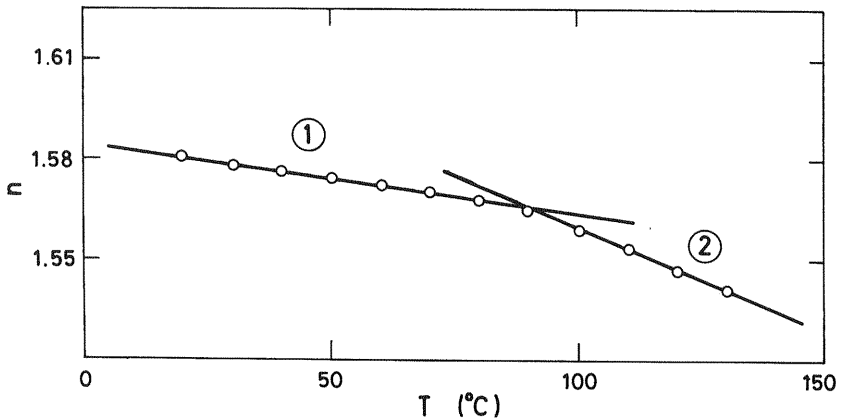


Figure P2.9.1

$$373 - T'_g = \frac{(8.5 \times 10^{-4})(T'_g - 203)(0.3)}{(5.1 \times 10^{-4})(1 - 0.3)} \quad (\text{P2.10.1})$$

Resolving the equation we obtain $T'_g = 302 \text{ K}$.

This result can be compared with the one obtained considering that the polymer-plasticizer system follows the Fox equation [Eq. (2.28)]. To apply this equation we must calculate the weight fractions of the components,

$$w_1 = \frac{\rho_1 v_1}{\rho_2 v_2 + \rho_1 v_1} \quad (\text{P2.10.2})$$

where v_1, v_2 are the volume fractions of the components and ρ_1, ρ_2 are the densities of the components. The calculation of the weight fractions gives the result

$$w \text{ plasticizer } (w_1) = 0.33; \quad w \text{ polymer } (w_2) = 0.67$$

Applying the Fox equation,

$$\frac{1}{T_g} = \frac{0.33}{203} + \frac{0.67}{373} \quad (\text{P2.10.3})$$

The value for T_g obtained from this expression is 292.2 K. As can be observed, there is a significant difference between the two results (around 10°C).

REFERENCES

1. CW Bunn. In: R Hill, ed. *Fibres from Synthetic Polymers*, pp 240–300. Amsterdam: Elsevier, 1953.
2. B Wunderlich. *Macromolecular Physics, Vol 1, Crystal Structure, Morphology, Defects*. London: Academic, 1973.
3. B Wunderlich. *Macromolecular Physics, Vol 2, Crystal Nucleation, Growth and Annealing*. London: Academic, 1976.
4. DC Basset. *Principles of Polymer Morphology*. Cambridge, UK: Cambridge Univ. Press, 1981.
5. F Rodriguez. *Principles of Polymer Systems*. McGraw Hill, 1982.
6. LH Sperling. *Introduction to Physical Polymer Science*. New York: Wiley, 1992.
7. RJ Young, PA Lovell. *Introduction to Polymers*. New York: Chapman & Hall, 1991.
8. C. Gonzalez, A Bello, JM Perea, E Perez. *Brit Polym. J.* **23**: 111, 1990.

9. NG McCrum, CP Buckley, CB Bucknall. Principles of Polymer Engineering. Oxford, UK: Oxford Univ Press, 1997.
10. (a) A Peterlin. *Textile Res J* **42**: 20 (1972). (b) WG Perkins, PS Porter. *J Mater Sci* **12**: 2355, 1977.
11. LH Palys, PJ Phyllips. *J Polym Sci Polym Phys Ed* **18**: 829, 1980.
12. M Avrami. *J Chem Phys* **7**: 1103, 1939; **8**: 212, 1940.
13. L Mandelkern, M Hellman, DW Brown, DE Roberts, FA Quinn Jr. *J Am Chem Soc* **75**: 4093, 1953.
14. L Mandelkern. *Crystallization of Polymers*. New York: McGraw-Hill, 1964.
15. EG Lezcano, C Salom, MG Prolongo. *Polymer* **37**: 3603, 1996.
16. L Mandelkern. The crystalline state, pp 145–200. In *Physical Properties of Polymers*. JE Mark, A Eisenberg, WW Graessley, L Mandelkern, SJL Koenig. Washington DC: AM Chem Soc, 1993.
17. PJ Flory. *Principles of Polymer Chemistry*. Ithaca NY: Cornell Univ Press, 1953.
18. T Nishi, TT Wang. *Macromolecules* **8**: 909, 1975.
19. M Ballauff. Structure of liquid crystalline polymers. In RW Cahn, P Haasen, EJ Kramer, eds. *Materials Science and Technology*, Vol 12. New York: VCH, 1993.
20. ET Samulski. The mesomorphic state. In *Physical Properties of Polymers*, pp 201–262, JE Mark, A Eisenberg, WW Graesley, L Mandelkern, SJL Koenig. Washington DC: Am Chem Soc, 1993.
21. UW Gedde. *Polymer Physics*. London: Chapman & Hall, 1995.
22. CK Ober, JI Jin, RW Lenz. In NA Plate, ed. *Liquid Crystal Polymers I*. *Adv Polym Sci Vol 59*. Berlin: Springer-Verlag, 1984.
23. H Finkelmann, G Rehage. *Adv Polym Sci*. **60**: 99, 1984.
24. DJ Williams. *Polymer Science and Engineering*. Englewood Cliffs, NJ: Prentice-Hall, 1971.
25. A Eisenberg. The glassy state. In *Physical Properties of Polymers*, pp 61–96. Washington DC: Am Chem Soc, 1984.
26. A Horta. *Unidades Didácticas*, Madrid: Ed. Universidad Nacional de Education a Distancia, 1982.
27. AJ Kovacs. *Fortschr Hochpolym Forsch* **3**: 394, 1963.
28. GO Jones. *Glass*. Mcthen, 1956.
29. AK Doolittle. *J Appl Phys*. **22**: 1471, 1951.
30. ML Williams, RF Landel, JD Ferry. *J Am Chem Soc* **77**: 3701, 1955.
31. J Brandrup, EM Immergut, eds. *Polymer Handbook*. New York: Wiley, 1975.
32. RF Boyer. *J Appl Phys* **25**: 585, 1954.
33. TG Fox, PJ Flory. *J Appl Phys* **21**: 581, 1950.
34. K Ueberreiter, G Kanig. *J Chem Phys* **18**: 399, 1950.
35. EA Di Marzio, JH Gibbs. *J Polym Sci* **40**: 121, 1958.
36. TG Fox. *Proc Am Phys Soc* **1**: 123, 1956.
37. LE Nielsen ed. *Mechanical Properties of Polymers*. New York: Van Nostrand Reinhold, 1962.
38. DJ Plazek, KL Ngai. The glass temperature (page 139). In: JE Mark ed. *Physical Properties of Polymers Handbook*. Woodbury NY: AIP Press, 1996.

3

Rubber Elasticity

3.1 Introduction	85
3.2 Thermodynamic Treatment	88
3.3 Statistical Treatment	93
3.4 Modifications to Simple Statistical Theory—Non-Gaussian Statistics	106
3.5 Swelling of Polymer Networks	109
3.6 Elastomers in Service	111
Problem Sets	132
References	139

3.1 INTRODUCTION

The term “elastomer” is currently applied to a set of polymeric materials that possess exceptional elastic properties similar to those of natural rubber. These properties can be summarized as (1–3)

1. Capability for instantaneous and extremely high extensibility under low mechanical stresses.
2. Elastic reversibility, i.e., the capability to recover the initial length when the deforming force is removed.

In theory, it is not difficult to associate this elastic behavior with the molecular structure of polymers. The coiled conformation of polymers is responsible for the anomalous macroscopic deformation observed in

rubbers. However, to meet the conditions of instantaneous and reversible deformation, two related aspects have to be considered. On the one hand, instantaneous deformation implies that the chain has great mobility for reacting to external stimulus (mechanical stress). This situation is achieved only when the glass transition temperature of the polymer considered is lower than the temperature of the experiment. On the other hand, during the deformation process the intermolecular forces between the polymer chains are broken. These intermolecular interactions are of a strength similar to those corresponding to the liquid state. Breaking the intermolecular force would lead to permanent macroscopic deformation. Reversibility during the deformation process is guaranteed by the presence of cross-links between chains that prevent one chain from slipping with respect to the others. The structure of an elastomeric material is a three-dimensional network of interlinked polymer chains.

The sequence of steps leading the preparation of polymer networks is shown in Figure 3.1. Figure 3.1a shows two linear polymer chains that by means of a cross-linking chemical reaction, become joined together by the formation of a covalent bond. The chemical reaction gives a tetrafunctional cross-link, since there are four chains departing from it. Figure 3.2b illustrates the process shown in Figure 3.1a as a global process affecting all the linear polymer chains that are going to form the network. The appearance of cross-links in the network changes the significance of the individual chains; therefore, when referring to a polymer chain in an elastomer network, the number of monomer units between two consecutive cross-links must be considered. The cross-link density has a decisive influence on the

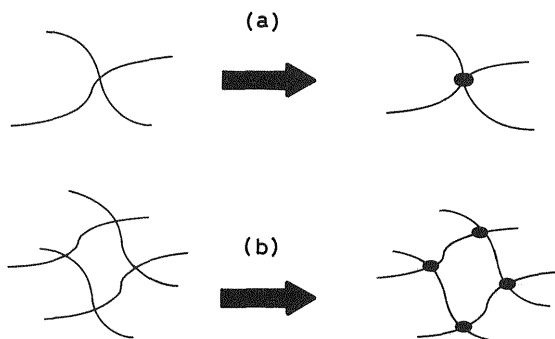


Figure 3.1 Covalent cross-linking reaction. (a) Cross-linking point between two macromolecules. (b) Several tetrafunctional cross-linking points between macromolecular chains, which form a polymer network.

elastic behavior of the network, as demonstrated further below. During the formation of the network, imperfections or defects occur that influence its mechanical behavior. The most common defects are illustrated in Figure 3.2. The first of these defects consists of the formation of physical entanglements (interlooping) (Fig. 3.2a). This defect contributes to the mechanical behavior in the same way as chemical cross-links do. The second defect is the appearance of a cross-link joining the beginning and end of the same chain, forming a loop (Fig. 3.2b). A cross-link of this kind makes no contribution to the elastic behavior of the network. Nor does the third type of defect, which consists of the formation of cross-links connecting chains to the network by just one of their ends. These chains (Fig. 3.2c) are called dangling chains. For the purpose of the theoretical treatments presented here, the elastomer network is assumed to be structurally ideal, i.e., all network chains start and end at a cross-link of the network.

The molecular mechanism causing elasticity in elastomers differs significantly from that found in other materials such as metals or ceramics. A typical tensile force–extension curve for an elastomer is shown in Figure 3.3. The curve displays three different regions; in the low deformation region there is a linear relation between the tensile force and the strain, i.e., the behavior is Hookean; this region extends up to a deformation of approximately 1%. In the high deformation region (up to 600%), the elastic behavior is markedly nonlinear and is related to the conformational entropy produced during the deformation process. Finally, the abrupt increase in the strength for deformation above 600% is due to the extensibility limit of the network and to a strain-induced crystallization process. The highly oriented polymer chains of the network under high deformation facilitate the formation of crystals, which increase the strength of the elastomer.

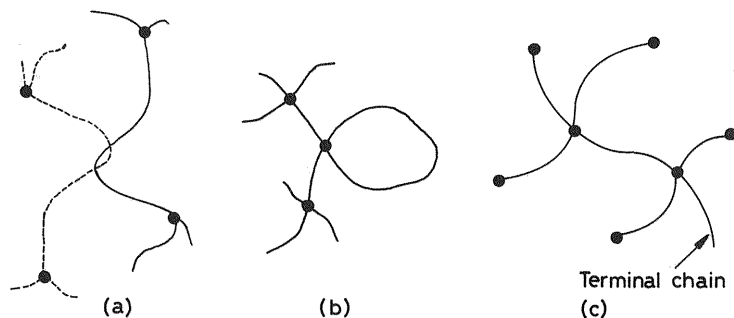


Figure 3.2 Types of network defects. (a) Physical entanglement; (b) looping; (c) terminal chains.

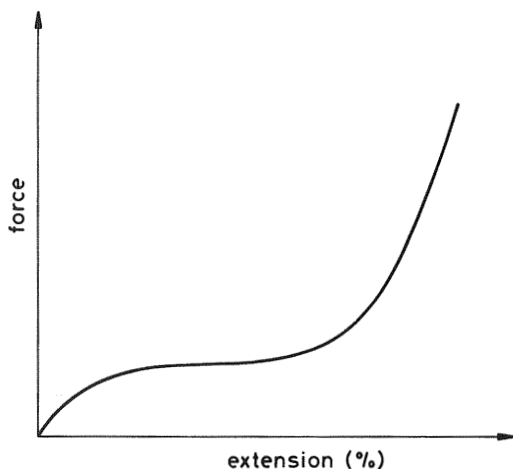


Figure 3.3 Force–extension curve of a typical lightly cross-linked rubber.

This chapter is divided into two parts. Throughout Secs 3.2–3.5, the fundamental concepts of rubber elasticity are reviewed in order to understand elastomeric behavior. The deformation process observed at the macroscopic level is connected with the changes in the thermodynamic quantities internal energy and entropy in Sect. 3.2. Also, the relation between the imposed stress and conformational changes undergone by the network chains is analyzed in Secs 3.3 and 3.4. The swelling equilibrium of elastomeric networks is reviewed in Sect. 3.5. Scientific interest in these materials arises from their great applicability as a result of their mechanical properties, which are unique and characteristic; therefore, different aspects in relation to engineering applications of rubbers are dealt with in Sect. 3.6.

3.2 THERMODYNAMIC TREATMENT

3.2.1 Changes in Internal Energy and Entropy in Deformation

The aim of the thermodynamic treatment is to relate the elastic force opposing the deformation of the elastomer to changes in energy and entropy occurring during the process.

Let us consider an elastic solid of initial length l_0 under a uniaxial tensile force f that causes an infinitesimal deformation dl . The work done on the solid is

$$dw = f dl \quad (3.1)$$

Equation (3.1) has been simplified by omitting the contribution to the work from the change in volume, dV , accompanying the extension dl . This simplification is justified because the work of expansion $-P dV$ (P =atmospheric pressure) is three or four orders of magnitude smaller than the term $f dl$ being considered. Equation (3.1) would be totally exact if the process were carried out under constant-volume conditions.

For a reversible change at constant volume, the work done is equal to the change in the Helmholtz function, F :

$$dw = dF = dU - T dS - S dT \quad (3.2)$$

where U is the internal energy and S the entropy. Under isothermal conditions, Eqs. (3.1) and (3.2) give the expression

$$f = \left(\frac{\partial F}{\partial l} \right)_T = \left(\frac{\partial U}{\partial l} \right)_T - T \left(\frac{\partial S}{\partial l} \right)_T \quad (3.3)$$

which relates the tensile force to changes in both internal and entropy per unit increase in length in the deformation process. The uniaxial tensile force f applied under equilibrium conditions will be equal to the recovering or elastic force that the solid experiences when it opposes the deformation.

With the aim of evaluating the change in internal energy accompanying the deformation process, the entropy term in Eq. (3.3) needs to be stated as a function of properties that can be determined experimentally. For this, we will make a simple thermodynamic deduction. According to the first law of thermodynamics,

$$dU = T dS + dw = T dS + f dl \quad (3.4)$$

By substituting Eq. (3.4) into Eq. (3.2) we obtain

$$dF = f dl - S dT \quad (3.5)$$

Therefore,

$$\left(\frac{\partial F}{\partial l} \right)_T = f \quad \text{and} \quad \left(\frac{\partial F}{\partial T} \right)_l = -S \quad (3.6)$$

Since F is a function of state:

$$\frac{\partial}{\partial l} \left(\frac{\partial F}{\partial T} \right)_l = \frac{\partial}{\partial T} \left(\frac{\partial F}{\partial l} \right)_T \quad (3.7)$$

and considering Eqs. (3.6) and (3.7), the important relationship

$$-\left(\frac{\partial S}{\partial l}\right)_T = \left(\frac{\partial f}{\partial T}\right)_l \quad (3.8)$$

is obtained, which is substituted into Eq. (3.3) to give

$$f = \left(\frac{\partial U}{\partial l}\right)_T + T\left(\frac{\partial f}{\partial T}\right)_l \quad (3.9)$$

Equation (3.9) allows the experimental determination of the two contributions to the elastic force. The entropic contribution, f_S ,

$$f_S = T\left(\frac{\partial f}{\partial T}\right)_l \quad (3.10)$$

can be obtained by determining how the elastic force varies with temperature at constant elongation. Once the entropic contribution has been determined, the energy contribution, f_U , is immediately obtained from Gibbs-Helmholtz equation as

$$f_U = \left(\frac{\partial U}{\partial l}\right)_T = f - T\left(\frac{\partial f}{\partial T}\right)_l \quad (3.11)$$

The application of Eqs. (3.10) and (3.11) requires the determination of the temperature coefficient of the elastic force, keeping the volume, V , and length, l , constant during the experiment. In practice, it is simpler to conduct this experiment under constant pressure (usually atmospheric pressure). In this case, instead of using the exact equations, (3.10) and (3.11), the following approximate expressions are used (2,4):

$$\left(\frac{\partial S}{\partial l}\right)_{T,V} \simeq \left(\frac{\partial f}{\partial T}\right)_{P,\lambda} \quad (3.10a)$$

$$\left(\frac{\partial U}{\partial l}\right)_{T,V} \simeq f - T\left(\frac{\partial f}{\partial T}\right)_{P,\lambda} \quad (3.11a)$$

where $\lambda = l/l_0$ is the elongation ratio.

3.2.2 Comparison with Experimental Data

Let us consider the tensile force necessary to deform vulcanized rubber in the temperature range 15–90°C and deformation interval 1–390% (5,6).

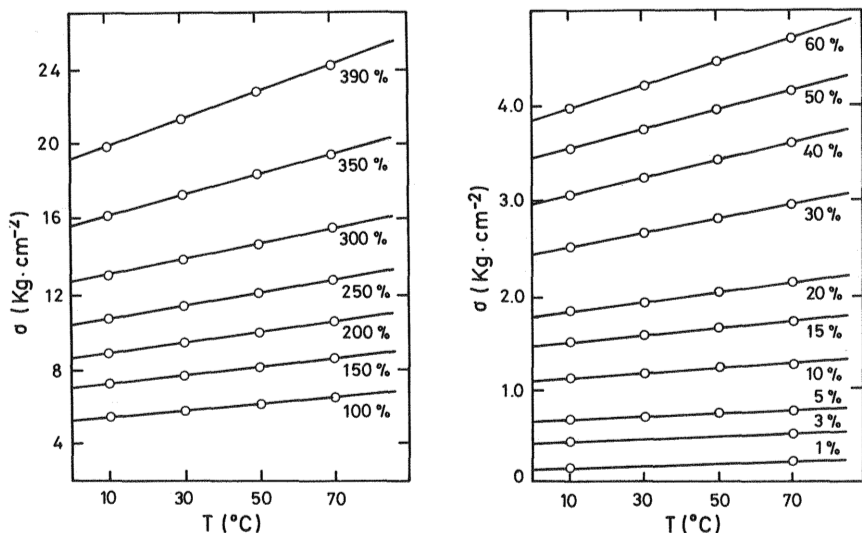


Figure 3.4 Stress at constant length as a function of temperature. Elongations as indicated (5,6). (From Ref 5.)

The experiment is conducted under conditions of thermodynamic equilibrium, ensuring that the changes in the elastic force with temperature are always reversible. Figure 3.4 represents the results obtained for the experiment described above. The force per unit cross-sectional area of the original sample ($\sigma = f/A$) is represented versus temperature. The strain is calculated by taking into account the increase in volume undergone by the network due to the increase in temperature. It can be seen that all the curves are straight lines, corresponding to the behavior indicated by Eq. (3.9). On the basis of the data shown in Figure 3.4 and according to Eqs. (3.10a) and (3.11a), the energy and entropy contributions to the elastic force represented in Figure 3.5 are obtained. It can be seen that up to deformation values corresponding to 350%, the entropic contribution is uniquely responsible for the recovering force experienced by the vulcanized rubber. The energy contribution remains virtually zero in this elongation range. Accordingly, Eq. (3.9) can be rewritten as

$$f = -T \left(\frac{\partial S}{\partial l} \right)_{T,V} \simeq T \left(\frac{\partial f}{\partial T} \right)_{P,\lambda} \quad (3.9a)$$

This means that f is proportional to the temperature and is determined exclusively by the entropy changes taking place during the deformation

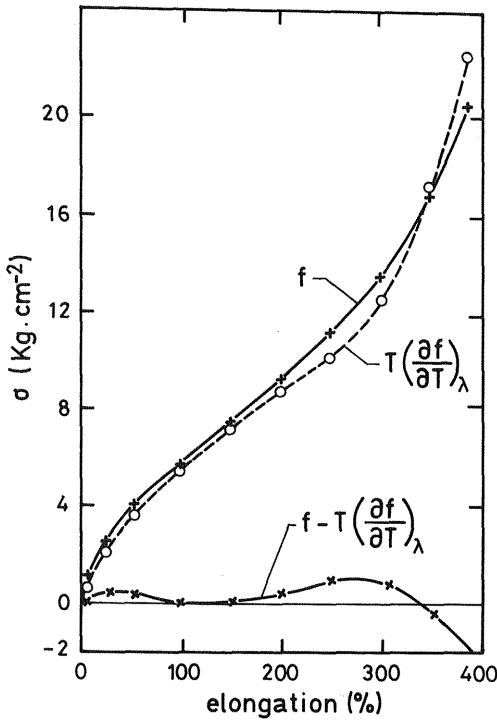


Figure 3.5 Internal energy and entropy contributions of tensile force, as functions of extension (5,6). (From Ref. 5.)

process. It can be confirmed that Eq. (3.9a) is an acceptable simplification of Eq. (3.9) in the region of intermediate elongations. For elongations higher than 350% it is not possible to ignore the energy component of f in Eq. (3.11a) in natural rubber since the phenomenon of strain-induced crystallization takes place. In this case the energy contribution to f may be larger than the entropic one, and therefore it cannot be neglected. An elastomer whose physical behavior is described by Eq. (3.9a) is termed an "ideal elastomer." This implies that the term $(\partial U/\partial l)_{T,V}$ is zero and therefore the elastomer is composed of ideal freely rotating chains. The small variation in internal energy undergone by elastomers in the range of moderate elongations is reminiscent of the behavior observed for ideal gases in which there are no intermolecular forces and consequently the internal energy is not a function of the distance between molecules or, therefore, of the volume.

3.3 STATISTICAL TREATMENT

The thermodynamic treatment of deformation made in the preceding section establishes the entropic nature of the recovering force. Nevertheless, this treatment does not provide direct information on the reorganization taking place at the molecular level during the process of elongation in elastomer networks. The interpretation of the process at the molecular level permits us to establish relations between the elastic force and the different molecular parameters involved. The statistical theory of rubber elasticity assumes that a large polymer chain can adopt a great number of conformations as a consequence of the thermal vibration of the atoms. It is further assumed that the chains between cross-linking points behave like isolated chains. The number of conformations that each chain can adopt is connected to the entropy content of the chain by means of the Boltzmann equation. The fundamental ideas on which the theory rests are due to the work of Meyer et al. and Karrer in the early 1900s. The statistical theory of elasticity was developed in 1934 by Guth and Mark.

This section seeks to make a quantitative evaluation of the relation between the elastic force and elongation. The calculation requires determining the total entropy of the elastomer network as a function of strain. The procedure is divided into two stages: first, the calculation of the entropy of a single chain, and second, the change in entropy of a network as a function of strain.

3.3.1 Elasticity of a Polymer Chain

In a polymer network the chains are connected through cross-links that restrict the motion of the chain ends. Consequently a polymer chain belonging to an elastomeric network can be represented as in Figure 3.6, i.e., with one end fixed at the origin O while the other is confined to a small volume $dV = dx dy dz$.

Boltzmann's equation, $S = k_B \ln \Omega$, relates the entropy to the number of conformations of the chain Ω . Considering an element of constant volume dV , the number of conformations available to the chain is proportional to the probability per unit volume, $p(x, y, z)$, multiplied by the size of the volume element, dV , Eq. (1.12); therefore, the entropy of the chain is given by the expression

$$S = k_B (\ln p(x, y, z) dV) \quad (3.12)$$

Substituting Eq (1.12) into Eq. (3.12) gives

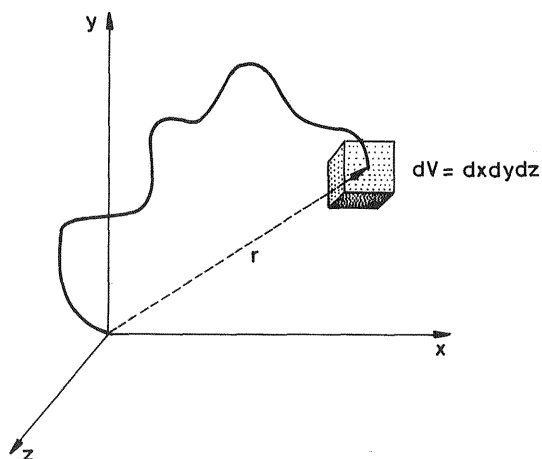


Figure 3.6 Polymer chain detached from a network with a coordinate system at one end.

$$S = C - k_B \frac{r^2}{\rho^2} = C - k_B \frac{3}{2} \frac{r^2}{\langle r^2 \rangle_0} \quad (3.13)$$

where $\langle r^2 \rangle_0$ represents the mean square end-to-end distance of the chain (see Sect. 1.6) and C is an arbitrary constant.

Equation (3.13) provides the value of the entropy of a chain whose ends are located at specified points separated by a distance r . This expression indicates that the entropy decreases as the end-to-end distance increases. If the chain is subjected to the action of an external force causing a macroscopic elongation, the chain end-to-end distance r will be greater than that corresponding to the undeformed state. Therefore, there will be a decrease in the number of conformations available to the chain and therefore a decrease in the conformational entropy. The chain will exercise a recovering force that opposes the external force. The recovering force tends to reduce the value of the end-to-end distance to that corresponding to the undeformed state. It can be asserted that the recovering or elastic force arises from the need to recover the state of maximum entropy, which corresponds to the undeformed state.

The work required to move the end of the chain from a distance r to another distance $r + dr$ is equal to the change in Helmholtz energy and is given by

$$\frac{dw}{dr} = \frac{dF}{dr} = -T \frac{dS}{dr} \quad (3.14)$$

where internal energy is assumed to be constant.

From Eqs. (3.13) and (3.14) we obtain

$$\frac{dw}{dr} = \frac{3kT}{\langle r^2 \rangle_0} r \quad (3.15)$$

Equation (3.15) provides the force \mathbf{f} necessary to keep the chain with an end-to-end distance equal to r :

$$\mathbf{f} = \frac{3k_B T}{\langle r^2 \rangle_0} \mathbf{r} \quad (3.16)$$

Under equilibrium conditions, this force is equalled by the equivalent recovering force. When the external force is removed, the recovering force causes r to decrease spontaneously. From Eq. (3.16) it can be concluded that (1) \mathbf{f} is proportional to the temperature, so that as T increases the force needed to keep the chain with a certain value of r increases, and (2) the force is linearly elastic, i.e., proportional to r .

3.3.2 Elasticity of a Network

The aim of this section is to find the relation between the elastic force and the deformation for a polymer network. For that purpose the change in entropy associated with deformation of the chains in the network must be evaluated. Figure 3.7 shows the distribution of the chain end-to-end vectors in the deformed (stretched) and undeformed (unstrained) states. The distribution has spherical symmetry in the undeformed state, and when the

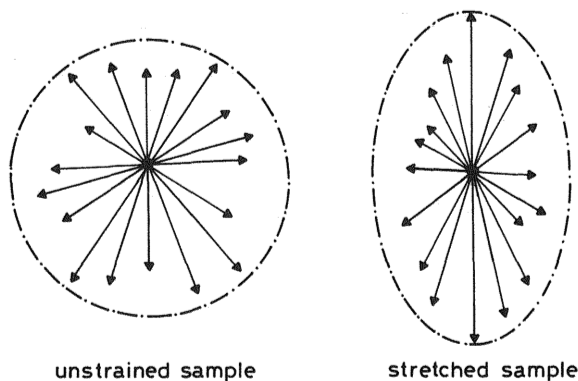


Figure 3.7 Schematic representation of chain end-to-end vectors for an unstrained sample and for a stretched sample.

sample is subjected to a uniaxial extension, the distribution is ellipsoidal. The change of distribution is associated with the change of entropy, related to the force causing the deformation.

Before undertaking the calculation of the change in entropy, a series of assumptions need to be made:

1. The network is made up of N chains per unit volume.
2. The network has no defects (see Sect. 3.1), that is, all the chains are joined by both ends to different cross-links.
3. The network is considered to be made up of freely jointed chains, which obey Gaussian statistics (see Chap. 1).
4. In the deformed and undeformed states, each cross-link is located at a fixed mean position.
5. The components of the end-to-end distance vector of each chain change in the same ratio as the corresponding dimensions of the bulk network. This means that the network undergoes an affine deformation.

Figure 3.8 shows a diagram of the deformation. The sample initially possesses dimensions x_0, y_0, z_0 , and when deformed it takes on dimensions x, y, z . According to the affine deformation model, the end-to-end distance vector of the chains of the strained network will change its components in

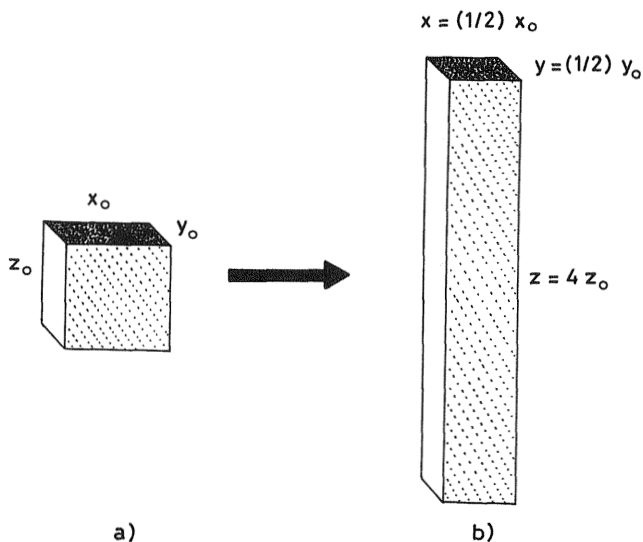


Figure 3.8 Model of deformation. (a) The unstrained state; (b) the strained state.

exactly the same proportion as the macroscopic dimensions (see Fig. 3.9), so that the extension ratios for the three coordinate axes are

$$\lambda_x = \frac{x}{x_0}, \quad \lambda_y = \frac{y}{y_0}, \quad \lambda_z = \frac{z}{z_0} \quad (3.17)$$

The volume of the network is assumed to remain constant during the deformation process, so

$$\lambda_x \lambda_y \lambda_z = 1 \quad (3.18)$$

Therefore only two extension ratios can vary independently, leaving the third one determined by Eq. (3.18)

According to Eq. (3.13), the entropy of an undeformed chain is given by

$$S = C - k_B \frac{r^2}{\rho^2} = C - \frac{k_B}{\rho^2} (x_0^2 + y_0^2 + z_0^2) \quad (3.19)$$

while the entropy of the deformed chains can be written as

$$S' = C - \frac{k_B}{\rho^2} (\lambda_x^2 x_0^2 + \lambda_y^2 y_0^2 + \lambda_z^2 z_0^2) \quad (3.20)$$

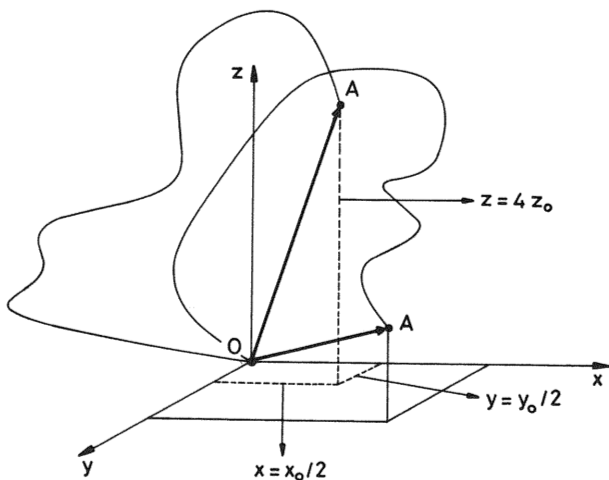


Figure 3.9 The affine deformation of chains.

Since C is a constant independent of r , the variation in entropy associated with the deformation for a single chain is

$$\Delta S = S' - S = -\frac{k_B}{\rho^2} [(\lambda_x^2 - 1)x_0^2 + (\lambda_y^2 - 1)y_0^2 + (\lambda_z^2 - 1)z_0^2] \quad (3.21)$$

The total change in entropy per unit volume for the N chains constituting the network is obtained by addition of the N contributions represented by Eq. (3.21).

$$\Delta S = \sum_1^N \Delta S_i = -\frac{k_B}{\rho^2} \left((\lambda_x^2 - 1) \sum_1^N x_{0i}^2 + (\lambda_y^2 - 1) \sum_1^N y_{0i}^2 + (\lambda_z^2 - 1) \sum_1^N z_{0i}^2 \right) \quad (3.22)$$

By definition,

$$\sum_1^N x_{0i}^2 = N \langle x_0^2 \rangle \quad (3.23)$$

where $\langle x_0^2 \rangle$ is the mean square value of the x components in the undeformed state. Given that there is no preference among the x , y , z directions because the directions of the end-to-end chain vectors, \mathbf{r}_0 , in the unstrained state are entirely random (isotropic state), we obtain

$$\langle x_0^2 \rangle = \langle y_0^2 \rangle = \langle z_0^2 \rangle = \frac{\langle r^2 \rangle_0}{3} \quad (3.24)$$

Substituting these equations into Eq. (3.22) gives

$$\Delta S = -\frac{k_B N}{\rho^2} \left(\frac{\langle r^2 \rangle_0}{3} \right) (\lambda_x^2 + \lambda_y^2 + \lambda_z^2 - 3) \quad (3.25)$$

Remembering that $\rho^2 = (2/3)\langle r^2 \rangle_0$ [see Eq. (1.14)], Eq. (3.25) can be simplified to

$$\Delta S = -\frac{k_B N}{2} (\lambda_x^2 + \lambda_y^2 + \lambda_z^2 - 3) \quad (3.26)$$

Equation (3.26) provides the change in entropy of the network subjected to a deformation represented by the extension ratios λ_x , λ_y , λ_z .

Considering that there is no change in internal energy associated with the isothermal deformation, Eq. (3.2) indicates that $w = -T\Delta S$, where w

represents the work done in the deformation process or elastically stored free energy per unit volume of the network. According to Eq. (3.26),

$$w = \frac{1}{2} Nk_B T (\lambda_x^2 + \lambda_y^2 + \lambda_z^2 - 3) \tag{3.27}$$

Particularizing Eq. (3.27) for the case of a simple elongation ratio λ along the z axis (see Fig. 3.10), Eq. (3.27) becomes

$$w = \frac{1}{2} Nk_B T \left(\lambda^2 + \frac{2}{\lambda} - 3 \right) \tag{3.28}$$

where use was made of the expression

$$\lambda_x = \lambda_y = \lambda^{1/2} \tag{3.29}$$

obtained from Eq. (3.18).

The total work is given by

$$W = \frac{1}{2} Nk_B TV \left(\lambda^2 + \frac{2}{\lambda} - 3 \right) \tag{3.30}$$

where it was considered that $W = wV$.

The elastic force associated with the deformation is obtained from Eq. (3.30) as

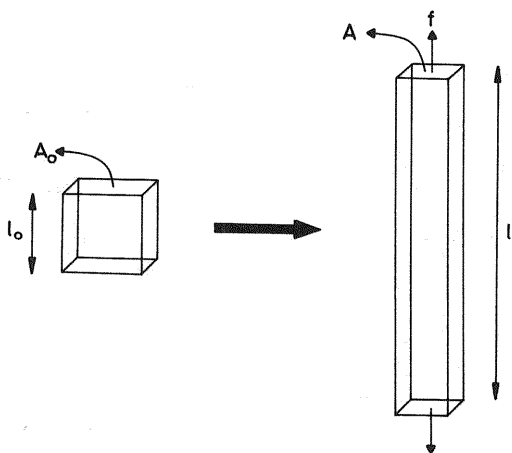


Figure 3.10 One-dimensional extension under the action of force f .

$$f = \frac{dW}{dl} = \frac{dW}{d\lambda} \frac{d\lambda}{dl} \quad (3.31)$$

Therefore, from Eqs. (3.30) and (3.31) one obtains

$$f = \frac{V}{l_0} Nk_B T \left(\lambda - \frac{1}{\lambda^2} \right) \quad (3.32)$$

The quotient V/l_0 is A_0 , the cross-sectional area of the sample in the unstrained state. If the force per unit area is expressed as $\sigma = f/A_0$, then Eq. (3.32) becomes

$$\sigma = G \left(\lambda - \frac{1}{\lambda^2} \right) \quad (3.33)$$

In this equation $G = Nk_B T$ represents the shear modulus of the elastomer, as will be confirmed in Problem 3.1 solved at the end of this chapter.

When a material is subjected to small deformations, the cross-sectional area of the unstrained sample, A_0 , coincides with the cross-sectional area of the strained sample, A . However, in the case of elastomers, in which the deformations can be extremely high, account has to be taken of the change in the cross section of the sample. Consequently, the value of the stress σ , calculated by using Eq. (3.33) and called nominal stress, does not coincide with the true tensile stress $\sigma_t = f/A$ (Fig. 3.10).

Since

$$\sigma_t = \frac{f}{A} = \frac{l}{V} f \quad (3.34)$$

Eq. (3.32) becomes

$$\sigma_t = \frac{l}{l_0} Nk_B T \left(\lambda - \frac{1}{\lambda^2} \right) = G \left(\lambda^2 - \frac{1}{\lambda} \right) \quad (3.35)$$

Equation (3.33) is suitable to study the experimental behavior in the interval of moderate deformations. For higher deformations the value of the shear modulus, $G = Nk_B T$, has to be decreased in order to achieve a better fit between experiment and theoretical treatment.

It is actually possible within the framework of the statistical theory of elasticity to deduce an expression similar to Eq. (3.33) that considers the experimentally observed decrease in modulus. This is done by using a model different from the affine deformation model, known as the phantom network model. In the phantom network the nodes fluctuate around mean

positions. When the elastomer is deformed, the fluctuation occurs in an asymmetrical manner. The fluctuations of a chain of the network are independent of the presence of neighboring chains. With these assumptions, an expression for the phantom network (2), equivalent to Eq. (3.33), is obtained:

$$\sigma = A_\phi N k_B T (\lambda - \lambda^{-2}) \quad (3.36)$$

where $A_\phi < 1$ is a parameter that reduces the value of $G = N k_B T$.

$$A_\phi = 1 - \frac{2}{\phi} \quad (3.37)$$

where ϕ is the functionality. In the case of functionality equal to 4.

$$A_\phi = \frac{1}{2}$$

and

$$\sigma = \frac{N k_B T}{2} (\lambda - \lambda^{-2}) \quad (3.36a)$$

Comparison of Eqs. (3.36a) and (3.33) indicates that the value of modulus G obtained from the affine deformation model is two times the value corresponding to the phantom network. This would mean that the latter model is more applicable in the region of moderate deformations and the affine model is more suitable in the region of low deformations.

3.3.3 Comparison with Experiment

(a) Stress–Strain Curves

A typical isothermal stress–strain curve is shown in Figure 3.11. The experimental behavior is represented by points, and the dashed line corresponds to Eq. (3.33). The experiment consists in a uniaxial tension on vulcanized rubber (2,7). The theoretical and experimental results agree only in the region of small elongations ($1 < \lambda < 1.3$). In the experimental curve two regions are distinguished where the experimental results diverge from the theoretical predictions in opposite directions: (1) the region of intermediate elongations, $1.3 < \lambda < 5.5$, in which the experimental curve lies below the theoretical prediction and exhibits an elastic behavior that would be described by the phantom network model; (2) the region of large elongations ($\lambda > 5.5$) in which the experimental curve displays a notable increase in

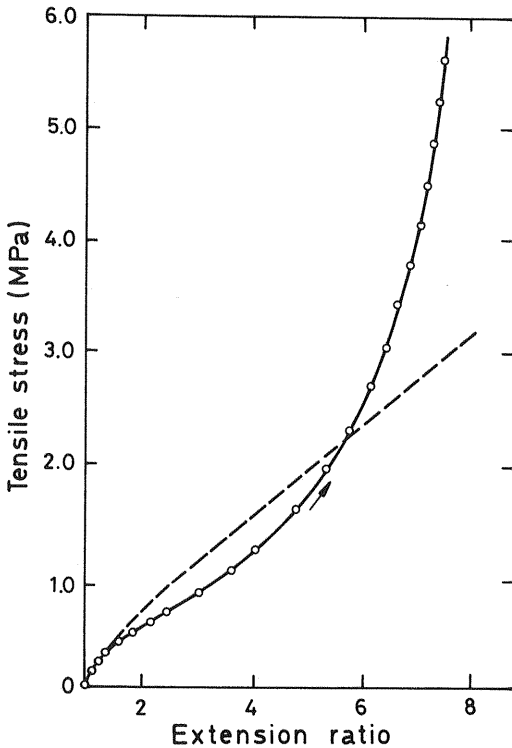


Figure 3.11 Isothermal stress-strain curve (2,7). (○) Experimental results. (---) Gaussian curve [Eq. (3.33), $G = 0.39$ MPa]. (From Ref. 2.)

stress, not shown by the theoretical curve. There are two aspects to bear in mind to explain the experimental behavior at large elongations. On the one hand, strain-induced crystallization can occur in rubber. The melting temperature of a polymer is inversely proportional to the melting entropy, which decreases when the polymer chains of a network are kept subjected to a stress. Consequently, in the deformed state the melting temperature increases, leading to crystallization of some of the chains of the network. The crystals formed act as extra cross-linking points, causing a notable increase in the modulus. On the other hand, the extensibility limit of the chains has to be considered at large deformations. The theoretical models explained in the preceding sections use Gaussian statistics, and this requires the extensibility of the chains not to be very large ($r \ll nl$). As will be demonstrated further below, an important point to obtain a better fit between the theoretical and experimental results is to consider the effects

of the extensibility of the polymer chains constituting the network (non-Gaussian effects) in the development of the theoretical model.

One way of checking the validity of Eqs. (3.33) and (3.36) is to resort to the Mooney–Rivlin semiempirical equation (2,3),

$$[\sigma] = \frac{\sigma}{\lambda - 1/\lambda^2} = 2C_1 + \frac{2C_2}{\lambda} \quad (3.38)$$

where $[\sigma]$ is called the reduced stress and $2C_1$ and $2C_2$ are the so-called Mooney–Rivlin constants. According to Eq. (3.33), the value of the reduced stress $[\sigma]$ is independent of λ in such a way that for the affine network model

$$2C_1 = k_B TN, \quad 2C_2 = 0 \quad (3.39)$$

while for the phantom network model with $\phi = 4$ [Eq. (3.36a)],

$$2C_1 = (1/2)k_B TN, \quad 2C_2 = 0 \quad (3.40)$$

Mooney–Rivlin plots for different types of vulcanized rubber are shown in Figure 3.12 (2,8). It can be seen that the constant C_1 shows a significant dependence on the type of rubber, while the constant C_2 adopts a value that is nearly constant but different from zero. The variation of C_1 with the degree of vulcanization of the rubber suggests that C_1 is a parameter related to the structure of the network and, in this regard, is connected to the parameter $G = Nk_B T$. However, C_2 is taken as a measure of the goodness of the fit between experimental and theoretical results. The lower the value of C_2 is, the better the theory fits the experimental results. In any case, the ratio $2C_2/2C_1$ is usually taken as a measure of the nonaffine character of the deformation so that a decrease in $2C_2/2C_1$ implies that the deformation approaches that of the affine model. The decrease in the reduced stress $[\sigma]$ with increasing deformation can be explained if account is taken of the transformation undergone by the network when it is deformed. In the region of low deformations, the polymer chains constituting the network form entanglements that embed the cross-links, and it is therefore appropriate to consider an affine deformation model to describe this situation. Nevertheless, as the elongation increases, the chains become extended, and the average density of entanglement points decreases. Consequently, the cross-links will fluctuate more freely around their equilibrium positions, and the network model that represents this situation is closer to the phantom model.

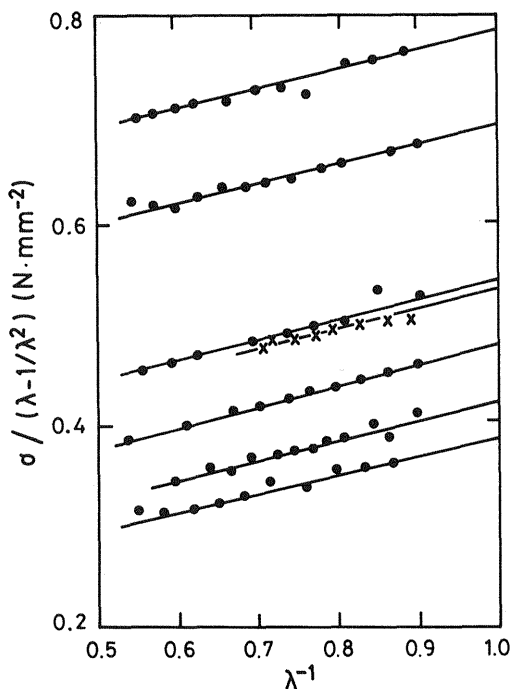


Figure 3.12 Mooney–Rivlin plots for various rubbers in uniaxial extension (8). (From Ref. 2.)

(b) Relation Between Stress and the Network Structure

There are two parameters used as a measure of cross-link density: the number of network chains, ν , usually expressed as ν/V , where V is the volume of the unstrained network; and the number of cross-links (μ) per unit volume, μ/V . The relationship between μ and ν is established by knowing the number of chains starting from a particular cross-linking point, ϕ (functionality). The two most important types of network are the tetrafunctional ($\phi = 4$) and the trifunctional ($\phi = 3$). Another characteristic parameter of a network is the number-average molecular weight between cross-links, M_c . The relation between the characteristic parameters is established in Problem 3.4

When elastomer networks are formed, the segments of chains that are close to each other in space may be crosslinked, independently of their locations along the chain. Therefore, the network has a totally random structure in which the number of cross-linking points and their locations

are unknown. Under these conditions, it is difficult to establish a relation between the stress and the structure of the network. Nevertheless, new synthesis techniques have permitted the preparation of model networks of known structure. One example of such a network is that obtained from hydroxyl-terminated linear chains of polydimethylsiloxane (PDMS) (9), using tetraethyl orthosilicate as a cross-linking agent. A diagram of the reaction is shown in Figure 3.13. If the number-average molecular weight, M_n and the molecular weight distribution of the linear chains of PDMS are previously known, a network is obtained with M_c equal to M_n and with the same distribution. Moreover, the functionality of the network is determined by the cross-linking agent, and in the above example $\phi = 4$. Model networks have been efficiently used to check the theories. By using model networks of PDMS with functionality $\phi = 4$ and $\phi = 3$, it has been possible to demonstrate that for the same value of M_c the deformation of the network is closer to the affine model when the functionality is high. Similarly, networks with the same functionality behave more like the affine deformation model when the value of M_c is lower (10–12).

A structural factor that has not been considered so far and that has a decisive influence on the elastic behavior of the network is the presence of physical cross-links or entanglements (see Fig. 3.3c), which, as mentioned in Sect. 3.1, are network defects that increase the modulus of the elastomer. When it comes to checking the validity of the theories, it is desirable to reduce this type of defect as far as possible because it complicates in an uncontrollable way the topology of the model network. To prevent the presence of physical cross-links, two different synthesis techniques have been resorted to (13,14). Both methods are based on trying to separate the linear chains of polymers as far as possible before producing the cross-linking reaction. The first technique consists of dissolving the linear chains and carrying out a cross-linking process in solution in such a way that the solvent solvates the linear chains and prevents intermolecular and intramolecular entanglements (see Fig. 3.14a). Once the network has been obtained, the solvent is extracted. The second technique consists of obtaining the network starting from linear chains oriented by the action of a stress (see Fig. 3.14b). Once the network is obtained, the orienting force is

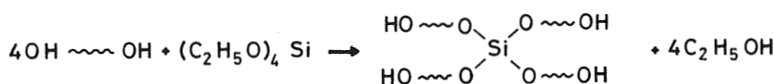


Figure 3.13 Synthetic procedure for preparing PDMS network of known structure [HO ~~~~ OH] represents a hydroxyl-terminated PDMS chain (9). (From Ref. 4.)

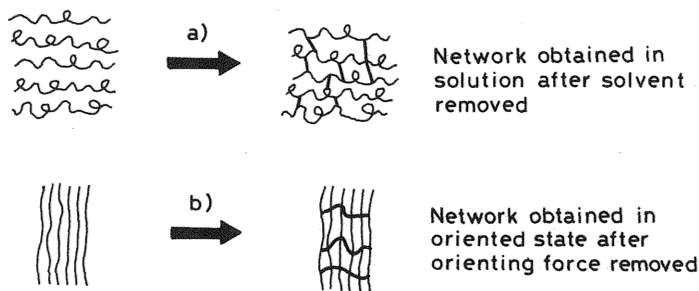


Figure 3.14 Methods to obtain elastomeric networks with a reduced number of entanglements. (a) Cross-linking reaction in the presence of a solvent. (b) Cross-linking reaction in the oriented state.

removed. In both cases the absence of defects in the network structure is achieved.

3.4 MODIFICATIONS TO SIMPLE STATISTICAL THEORY—NON-GAUSSIAN STATISTICS

In this section some general considerations of interest regarding non-Gaussian statistical theory are made with the aim of bringing the simple network model discussed in Section 3.2 closer to a real network (2,4).

Gaussian statistics can be applied to polymer chains whose extension is restricted in such a way that the end-to-end vector distance reaches a value less than 30% the length of the fully extended chain. For greater elongations, deviations from the Gaussian model start to become considerable. Unlike Gaussian statistics, non-Gaussian statistics consider that the polymer chain can reach a maximum elongation and provide an end-to-end distribution function that is valid for the entire range of values of r accessible to the chain.

The expression of the probability density function, $P(r)$, in logarithmic form corresponding to non-Gaussian statistics furnished by Kuhn and Gr \ddot{u} n in 1942 for a chain with n links of length l is given by

$$\ln P(r) = cte - n \left[\frac{r}{nl} \beta + \ln \left(\frac{\beta}{(\sin/h) \beta} \right) \right] \quad (3.41)$$

where β is defined by

$$\frac{r}{nl} = (\coth \beta) \beta - \frac{1}{\beta} = \mathcal{L}(\beta) \quad (3.42)$$

$\mathcal{L}(\beta)$ is the Langevin function, and $\beta = \mathcal{L}^{-1}(r/nl)$ is the inverse of the Langevin function.

By expanding Eq. (3.41) in series, one obtains

$$\ln P(r) = cte - n \left[\frac{3}{2} \left(\frac{r}{nl} \right)^2 + \frac{9}{20} \left(\frac{r}{nl} \right)^4 + \frac{99}{350} \left(\frac{r}{nl} \right)^6 + \dots \right] \quad (3.43)$$

If we truncate the series at the first term, which would be a good approximation for $r \ll nl$, Eq. (3.43) corresponds to the Gaussian distribution function. The theoretical treatment using Eq. (3.43) is similar to that carried out for Gaussian statistics: First the entropy is calculated for one chain, and then the change in entropy associated with the deformation process of the network is obtained. The final result gives the elastic force for a network of non-Gaussian chains. The rigorous treatment of the problem by non-Gaussian statistics is extremely complicated from a mathematical point of view; therefore, some assumptions are made in order to simplify the mathematical calculation. The simplest method is based on a network formed by three independent sets of non-Gaussian chains parallel to the axes of a rectangular coordinate system, which undergo affine deformation. With these simplifications, the force per undeformed unit of cross-sectional area for a network under uniaxial stress is given by (Fig. 3.10)

$$\sigma = \frac{G}{3} n^{1/2} \left(\mathcal{L}^{-1} \left(\frac{\lambda}{n^{1/2}} \right) - \lambda^{3/2} \mathcal{L}^{-1} \left(\frac{1}{\lambda^{1/2} n^{1/2}} \right) \right) \quad (3.44)$$

where n and l have the same meaning as before; n is the number of segments of length l belonging to a hypothetical freely jointed chain in which the end-to-end distance corresponding to the fully extended length chain is nl .

Experimental results are compared in Figure 3.15 with those obtained for Gaussian and non-Gaussian networks with $n = 75$ and $G = 0.273$ MPa, these values being used as adjustable parameters. From this comparison one can conclude that the consideration of the limited extensibility of the chains (non-Gaussian statistics) notably improves the agreement between theory and experiment at high elongations.

It is worthwhile to note that the equations describing the behavior of a Gaussian network [Eqs. (3.33) and (3.36)] depend on the structure of the network via a single parameter N , while the descriptions of non-Gaussian networks [Eq. (3.44)] include a second structural parameter, n . Therefore the number of chains, N , of the network determines the behavior observed in

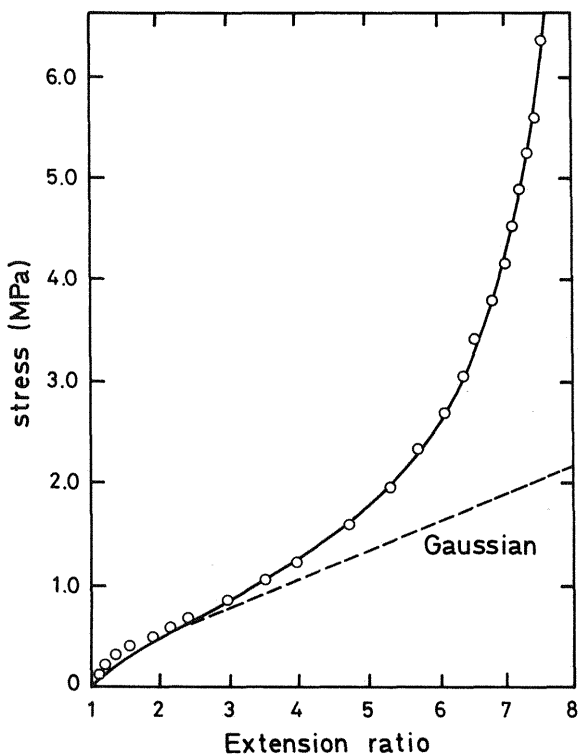


Figure 3.15 Isothermal stress-strain curve. Continuous line, non-Gaussian curve [Eq. (3.44) with $G = Nk_B T = 0.273$ MPa and $n = 75$]. (From Ref. 2.)

the region of low elongations in which Gaussian statistics are applicable. However, the elastic behavior at high elongations is controlled by the number of segments, n , of each chain. In reality, both n and N are usually used as adjustable parameters. The value of n is determined from the best fit between theoretical and experimental data at high elongations, while N is obtained from comparison between theory and experiment at moderate elongations. In spite of the fact that both parameters are fitted separately, they cannot in reality be regarded as independent, since n is inversely proportional to N .

The non-Gaussian model justifies the increase in modulus and therefore the strengthening of the elastomer network at high elongations, considering the limited extensibility of the chains forming the network. Nevertheless, taking into account that the increase in modulus at high elongations is shown mainly for networks that could undergo strain-induced crystalliza-

tion, it seems appropriate to evaluate the two effects separately. A comparison of the two effects appears in Figures 3.16 and 3.17, which show Mooney–Rivlin isotherms for model networks of polydimethylsiloxane (PDMS) with a high elongation capability and networks of poly(*cis*-1,4-butadiene) (PBD) with a high tendency toward crystallization. In noncrystallizable model networks of PDMS, the increase in modulus at high deformations occurs for all isotherms and does not disappear at high temperature as would be expected for limited chain extensibility (15,16). For PBD networks with a high tendency to crystallize the increase in the modulus is more pronounced than in the case of PDMS (the appearance of crystalline zones in the network strengthens its structure), but this effect decreases and even disappears with increasing temperature (17,18). These experimental results confirm that both effects have to be considered to explain the significant strengthening of elastomer networks at high elongation.

3.5 SWELLING OF POLYMER NETWORKS

Another way to deform an elastomer network is to put it in contact with a solvent. In this case molecules of solvent are absorbed in the network, giving rise to a phenomenon known as swelling. Swelling of a network by the

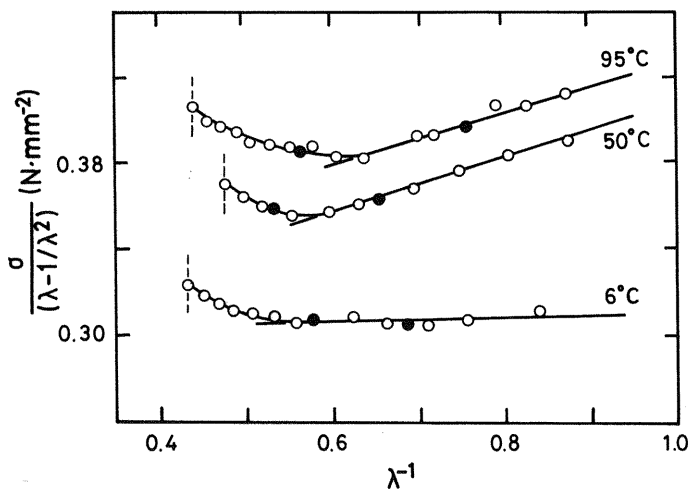


Figure 3.16 Mooney–Rivlin plots [Eq. (3.38)] showing the effect of the temperature on stress–strain isotherms for model PDMS networks (15,16). The filled circles represent the reversibility of the elastic measurements, and the vertical lines locate the fracture points. (From Ref. 15.)

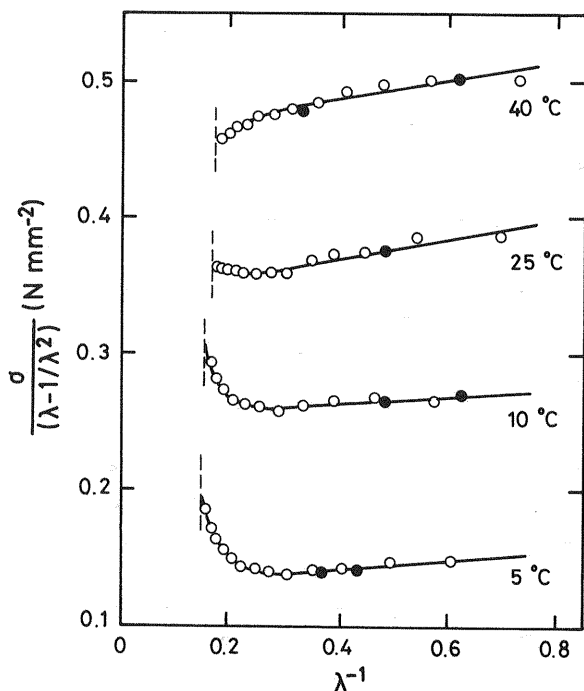


Figure 3.17 Mooney–Rivlin plots [Eq. (3.38)] showing the effect of strain-induced crystallization on the elastic behavior of highly crystallizable poly(*cis*-1,4-butadiene) networks at selected temperatures (17,18). The filled circles and the vertical lines have the same meaning as in Fig. 3.16. (From Ref. 15.)

action of a solvent constitutes a three-dimensional deformation. From the thermodynamic point of view, the network absorbs solvent until the swelling equilibrium is reached. In this situation,

$$\Delta\mu_1 + \Delta\mu_1 (\text{elastic}) = 0 \quad (3.45)$$

In other words, swelling equilibrium is reached when the drop in the chemical potential of the solvent in contact with the polymer is compensated for the rise in chemical potential undergone by the solvent due to the elastic pressure of the network.

The classical theory of swelling developed by Flory and Rehner in 1953 (1) provides the following expression for swelling equilibrium:

$$\frac{\rho A_\phi V_1 v_2^{2/3} (v_2^{1/3} - \omega v_2)}{M_c} = -[\ln(1 - v_2) + v_2 + v_2^2 \chi_{12}] \quad (3.46)$$

where ρ is the density of the network, M_c the average molecular weight between cross-links, v_2 the volume fraction of polymer at swelling equilibrium, χ_{12} the polymer-solvent interaction parameter, $A'_\phi = 1$ in the affine limit, V_1 the molar volume of the solvent, v_{2s} the volume fraction of polymer present during the cross-linking reaction of the network, and ω an entropic volume factor equal to $2/\phi$.

In a more recent theory of swelling equilibrium developed by Flory in 1979 (19), the extent to which the swelling equilibrium deformation is non-affine is taken into account. The nonaffine behavior depends on the looseness with which the cross-links are embedded in the network and consequently is related to the network structure and the degree of swelling at equilibrium. The final expression is

$$\frac{\rho F_\phi V_1 v_{2s}^{2/3} v_2^{1/3}}{M_c} = -[\ln(1 - v_2) + v_2 + v_x^2 \chi_{12}] \quad (3.47)$$

The factor F_ϕ characterizes the extension by which the deformation approaches the affine limit. This theory is more difficult to apply than that corresponding to Eq. (3.46) because the factor F_ϕ contains some parameters that are not present in the classical theory of swelling.

Equations (3.46) and (3.47) can be used in two different ways. First, if the polymer-solvent interaction parameter, χ_{12} , is known and the value of v_2 at swelling equilibrium is measured, then the molecular weight between cross-links, M_c , can be calculated using Eq. (3.46). Second, if the value of M_c is known and v_2 is measured at equilibrium, the polymer-solvent interaction parameter χ_{12} at polymer concentration v_2 can be determined.

Figure 3.18 shows an example of the variation with temperature of v_2 for a network of poly(methyl trifluoropropylsiloxane) (PMTFPS) in different solvents (20). Some aspects merit additional comments. The low values of v_2 , around 15%, suggest a good polymer-solvent interaction (low values of χ_{12}); therefore, acetates and tetrahydrofuran can be considered good solvents for PMTFPS. The opposite behavior (high values of v_2) is shown for PMTFPS networks swollen in *n*-chlorobutane.

3.6 ELASTOMERS IN SERVICE

As occurs with other plastic materials, elastomers, undergo certain processes before being used, such as cross-linking reactions, that lead to the formation of three-dimensional networks. Also it is necessary to incorporate certain chemical substances such as antioxidant agents, fillers, or plasticizers during their manufacture. These operations are aimed at improving the properties

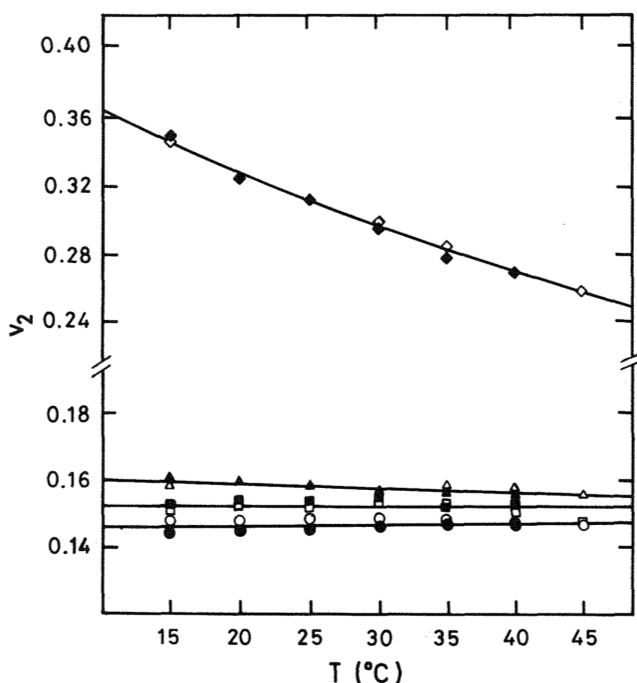


Figure 3.18 Polymer volume fraction (v_2) at swelling equilibrium for poly(methyl trifluoropropylsiloxane) (PMTFPS) networks as a function of the temperature in selected solvents (20). (\circ , \bullet) Butyl acetate; (\square , \blacksquare) tetrahydrofuran; (\triangle , \blacktriangle) ethyl acetate; (\diamond , \blacklozenge) *n*-chlorobutane. Empty and filled symbols represent values of v_2 obtained by increasing and decreasing the temperature, respectively. (From Ref. 20.)

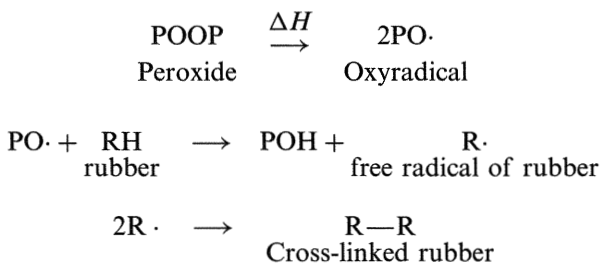
of the final products in order to optimize their utilization time under the best possible conditions and at a competitive cost on the market. Below are described the most usual processes to which these materials are subjected, along with the problems that can arise in service (21–23).

3.6.1 Vulcanization Process

Vulcanization of a rubber or an elastomer consists in creating chemical cross-links among the polymer chains in order to form a three-dimensional network. There are various types of cross-linking agents, and the most commonly used are described below. The process of vulcanization with sulfur is the most widely used. It is easy to obtain a broad variety of

cross-linked structures by varying the sulfur content in the vulcanization and also the time and temperature. Sulfur acts on the double bonds of the main chain, creating bridges of sulfur atoms that link the polymer chains through covalent bonds. Figure 3.19 shows different types of cross-linking unions that can be obtained in the vulcanization of natural rubber poly(*cis*-1,4-isoprene) (NR). The predominance of one type of specific union in NR networks can alter the properties of the rubber. For example, cross-links formed by a single atom of sulfur confers to natural rubber a relatively high thermal stability. Nevertheless, polysulfide cross-linking produces vulcanized rubbers with improved strength and fatigue properties.

Organic peroxides are another type of cross-linking agents. Vulcanization by means of peroxides is a free radical process that leads to the formation of carbon-carbon covalent bonds between chains. Below we show a diagram of the process:



The networks obtained through vulcanization by peroxides display high thermal stability. Nevertheless, the peroxide vulcanization process allows less control of the vulcanization than the sulfur process. Consequently it

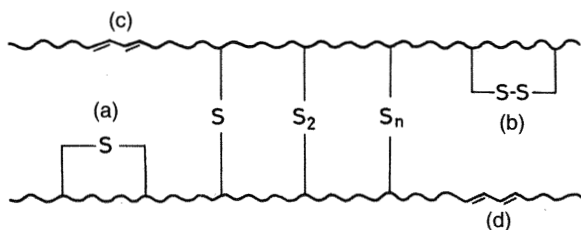
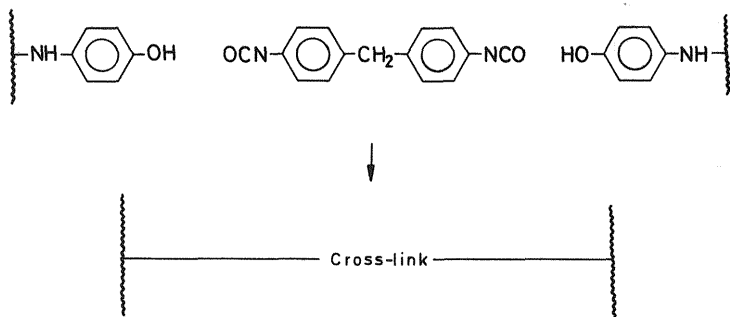


Figure 3.19 Sulfur cross-links obtained in vulcanization processes. S (C—S—C), monosulfur cross-link. S₂ (C—S—S—C), disulfur cross-link. S_n [(C—S—C), n = 3–6] polysulfur cross-link. (a, b) Intrachain cyclic. (c,d) Double-bond conjugated.

is more difficult to obtain a final product with well-defined properties. For example, uncontrolled increase of the cross-link density can occur due to reactions competitive with those shown above. Moreover, the oxy radicals react with the antioxidants present in the reaction medium, reducing the cross-link density of the vulcanized rubber. In spite of the drawbacks mentioned, the use of organic peroxides is necessary when it is impossible to carry out vulcanization with sulfur due to a lack of unsaturation in the rubber, as occurs in the case of silicones and ethylene-propylene rubber.

Currently, vulcanization processes for natural rubber and other diene rubbers are being carried out by reacting nitrophenols with diisocyanates. In this way, cross-links of the urea type are produced, as shown in the following diagram:



Vulcanized rubbers obtained by this method have a good balance of physical properties, though their cost is higher than that of any of the vulcanized rubbers mentioned earlier.

3.6.2 Degradation

When an elastomer is placed in service, some factors have to be taken into account. These factors reduce the service life of the elastomer and are related to the service temperature, service time, thickness of the elastomer, and the presence of oxygen.

The main problem is related to exposure of these materials to high temperatures in the presence of oxygen. These conditions favor the oxidative degradation of the elastomer, which leads to opposing changes in its structure. On the one hand, chain scission can occur, and on the other hand, cross-links can be generated. If chain scission dominates, the hardness and modulus of the elastomer will decrease. If, however, cross-links are generated, both the hardness and the modulus increase and the strain at fracture will decrease. Other mechanical properties are altered by an increase in

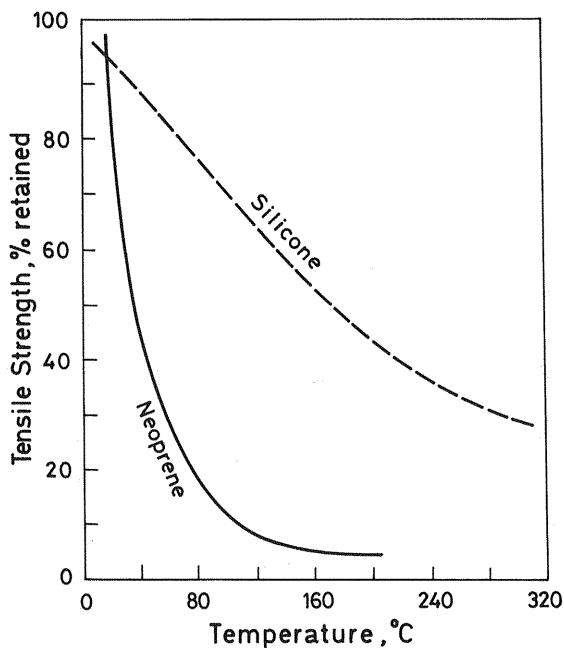


Figure 3.20 Tensile strength as a function of temperature for rubbers. (From Ref. 23.)

temperature. For example, the resilience of vulcanized rubber increases and its tensile strength decreases when the temperature rises, as the examples shown in Figure 3.20 reveal. For this reason, although rubber can be very resistant to the effects of aging at high temperatures, the material can be a bad choice due to the loss of strength when the temperature is raised. Also, elastomers increase in temperature when they are subjected to a cyclic deformation. This can be a problem in cyclic deformation processes as occurs in automobile tires. In this service condition, the temperature will increase considerably even though the ambient temperature might be low, causing degradation and possibly failure of the rubber.

To choose a particular elastomer, thermal aging is not the only main factor to consider. For example, it is important to know also the resistance of the product to the action of oils, organic solvents, and ozone. Ozone is a gas with high oxidizing power. Ozone will attack elastomers at the points of unsaturation, causing highly local damage in the structure. Chain scission and the appearance of deep cracks that propagate through the elastomer structure can occur, provoking failure of the material.

3.6.3 Additives

This section describes the various substances that are added to an elastomer in the manufacturing process, to improve its properties and extend its service life.

(a) Antioxidants

Antioxidants are substances that considerably reduce the oxidative aging of elastomers. To select a substance as an antioxidant, it is important to consider two factors: the volatility of the antioxidant, and its diffusion capability through the elastomer network. Protection against oxidation is needed in the outer layers of the material. Antioxidant substances should be capable of diffusing from the interior to the exterior in order to replenish the antioxidant that disappears during the protection process. However, if the elastomer is subjected to high temperatures, the antioxidant substance can evaporate. Consequently, when high service temperatures are required, substances with high molecular weight and low volatility are usually used as antioxidants.

Commercially available antioxidants include phenols and amine derivatives; the latter, though generally more effective, have the drawback of altering the coloration of dyed products. These additives are necessary to prevent, to some extent, the process of thermal oxidation of rubbers, though it has to be borne in mind that the stability of rubbers is primarily determined by the chemical nature of the chains as well as by the cross-links that define network structure.

(b) Fillers

The modulus of engineering elastomers can be modified by varying their cross-linking density. However, there are times when it is necessary to add substances in the form of particles or fibers to the elastomer to increase its rigidity and strength. These substances are called fillers, and the composite material obtained is called a reinforced elastomer. Although in some particular cases, such as when they are used in conveyor belts or tires, the elastomeric materials are reinforced with fibers such as nylon or with steel cables, the most usual method is to mix the elastomer with carbon black. This substance is produced by burning hydrocarbons in an oxygen-deficient atmosphere. Carbon black is formed by spherical particles covering a wide range of sizes. The sizes most commonly used in industry are between 20 and 30 nm in diameter. At the microscopic level, each spherical particle is formed by small laminae of graphite packed together to form a sphere.

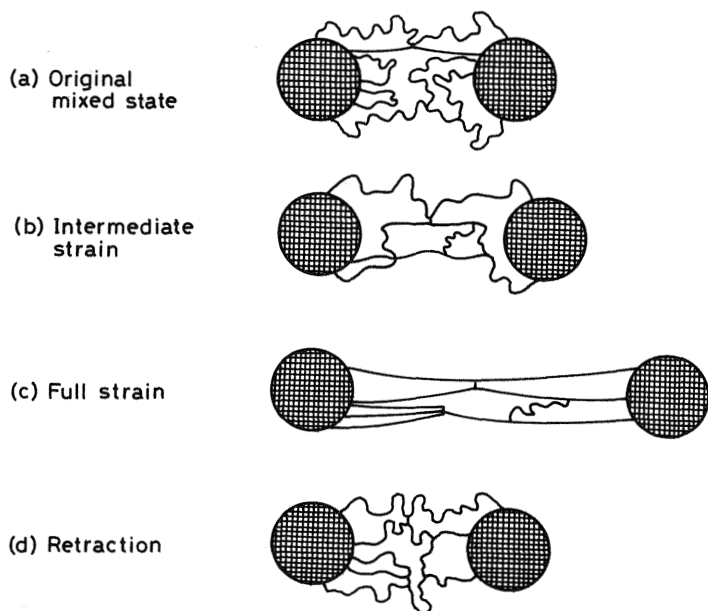


Figure 3.21 Deformation of elastomeric chains in contact with carbon black reinforcement. (From Ref. 24.)

The reinforcing action of these small spherical particles of carbon arises from reactions of unsaturations in the main chain with free radicals present on the surface of the particles. Other particles also interact weakly by means of a process in which segments of polymer are absorbed on the porous surface of the carbon black. Figure 3.21 shows how the particles of carbon black act as extra cross-links connecting chains of the elastomer. It can be seen in the scheme that the deformation results from the sliding of the chains located between two spherical particles. Once the deforming force is removed, the chains between particles more or less recover their initial length.

The effects of fillers on the behavior of elastomers are summarized in Figure 3.22. In this figure the stress-strain curves of both natural rubber reinforced with 50% carbon black and a nonreinforced natural rubber are compared. An inspection of the curves highlights three important characteristics:

1. Carbon black exerts a considerable reinforcing action on natural rubber.

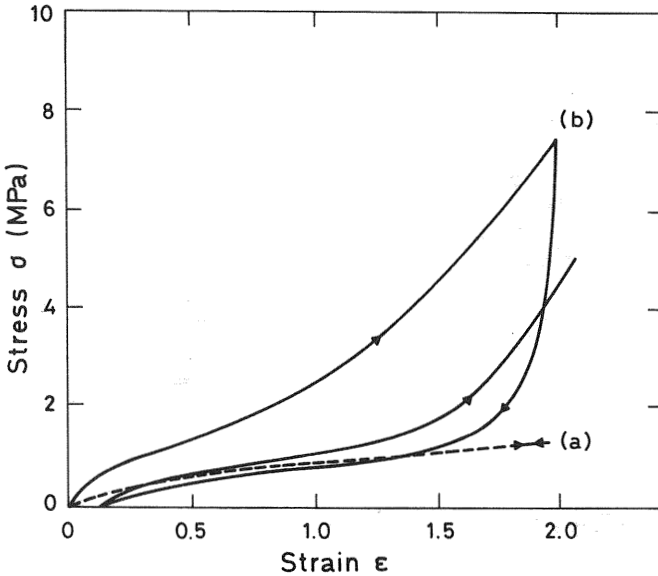


Figure 3.22 Stress–strain curves for natural rubber (a) without reinforcement and (b) with carbon black reinforcement. ($\epsilon = \lambda - 1$) (From Ref. 25.)

2. The curve corresponding to the second stress process for reinforced rubber is located below the first for any deformation value. This softening phenomenon is due to the damage caused in the structure of the rubber during the first stress process.
3. Reinforced rubber displays considerable hysteresis, which is not observed in natural rubber. In fact, the existence of pronounced mechanical hysteresis can become a serious problem due to the generation of heat involved during high speed oscillatory loading (e.g., in a rapidly revolving car tire). In practice, the content of carbon black is chosen to achieve a desirable compromise between the reinforcing effect and the mechanical hysteresis that it can provoke.

Although the last two characteristics also occur in nonreinforced rubber, they become important only when high deformations ($5 < \lambda < 7$) are achieved, situations not very usual when the elastomer is in service.

There are also other substances that can be used as fillers that behave like carbon black in terms of the reinforcing action. One example is silica, but it has the drawback of its price, and the properties of the reinforced elastomer are generally inferior to those obtained with carbon black. These

two factors restrict the use of silica to the preparation of products in which the black color must be avoided. Since silica sometimes improves the thermal resistance of elastomers, it can be used as a reinforcing agent in conjunction with carbon black when the application requires it.

(c) *Plasticizers*

Plasticizers (see Sect. 2.11.8) are also used as additives for elastomers. These substances decrease the viscosity and facilitate the flow process, improving the processing of elastomers. However, plasticizers reduce the strength of elastomers, and as a consequence these substances are used together with fillers, to control the final properties adequately. The substances commonly used as plasticizers for elastomers are aromatic oils, naphthene oils, or paraffins derived from petroleum. The plasticizer content is limited by the compatibility of the elastomer-plasticizer pair. Other factors that must be taken into consideration are the resistance to oxidation at high temperatures and the volatility of the plasticizer. The oxidative instability of an oil is due primarily to the presence of nitrogen and sulfur heterocyclics, while volatility decreases as the molecular weight and the viscosity of the oil increase. It is also possible to use low molecular weight fractions of natural rubber, which are liquids, as plasticizers. These fractions, mixed with high molecular weight natural rubber, act as nonextractable plasticizers, as they react during the vulcanization process and form part of the three-dimensional network. In the event that high thermal resistance is required, the plasticizer content of the elastomer should be significantly restricted.

3.6.4 Rigidity Under Compression

In spite of the fact that the elastic modulus of elastomers is approximately three orders of magnitude lower than that of most thermoplastic materials, elastomeric materials are widely used in engineering applications. Throughout this chapter we have been describing how an elastomer can be modified with the aim of improving its mechanical properties and making it more useful in service. Control over the cross-linking reaction and the addition of fillers are operations that have a decisive impact on the mechanical behavior of the elastomer. The addition of antioxidants increases the thermal resistance of the substance. Plasticizing substances improve the processability of these materials. It is clear that elastomers will be ideal materials when the application requires high deformability combined with the capability of recovery.

Moreover, elastomers are widely used in applications such as the manufacture of dampers, bearings, or major supporting structures such as

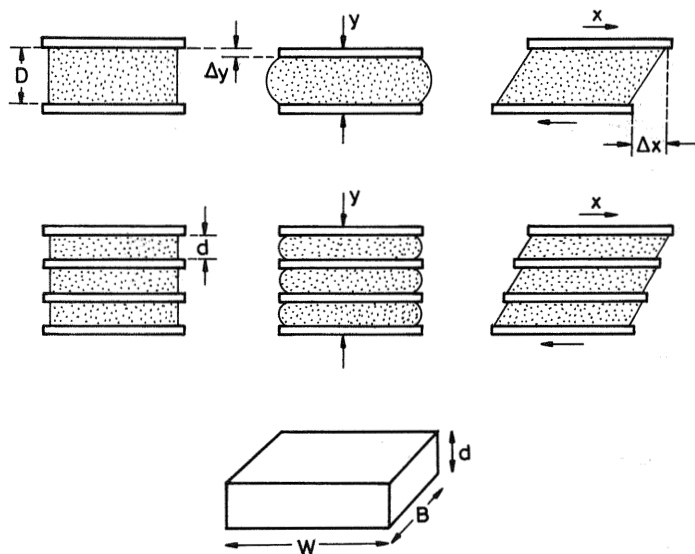


Figure 3.23 Effect of bonded steel sheets on the response of rubber blocks to compression and shear. (From Ref. 24.)

bridges or as insulators for the vibrations that a building can receive due to its proximity to a railway station, a subway station, or simply urban traffic. Elastomer materials have been used for protecting buildings from the destructive effects of the horizontal vibrations occurring during earthquakes. These applications are related with the most characteristic property of elastomers: high capability for deformation and recovery.

When an elastomer supports a major structure, it must do so without undergoing a notable compression deformation. In addition, the elastomer must be sufficiently flexible under shear to accommodate the changes that occur as a result of thermal expansions and contractions. This apparent conflict is solved if the material displays flexibility in one plane and great rigidity in another, conditions that are met by elastomers, since the typical shear modulus is around 1 MPa while the bulk modulus is approximately 2 GPa. In other words, it is much easier to change the shape of an elastomer than to change its volume. In this regard, elastomers are similar to liquids, which are capable of withstanding great hydrostatic compression. This can be proved with an experiment in which a block of elastomer of thickness D is perfectly secured to two steel sheets as shown in Figure 3.23. Under compression the structure shows great resistance, something that does not occur

under shear. Under a compressive stress the elastomer will deform and project beyond the sides that are not fixed to the steel sheets in such a way that the total volume remains constant. Under shear, the sides of the block become uniformly deformed without undergoing any kind of deformation toward the outside. If the heights of the block decreases (Fig. 3.23), the effect of the steel sheets will become clear, since the possibility of the block becoming deformed by bulging will decrease. A thin block of elastomer will therefore always be more rigid under compression than a thick block.

The influence of the geometry of the piece on the behavior of the elastomer under both compression and shear can be determined by calculating the rigidity under compression, K_c , and the rigidity under shear, K_s , defined as

$$K_c = \frac{F_y}{\Delta y} = \frac{FA}{A} \times \frac{D}{\Delta y D} = \left(\frac{F}{A} \times \frac{D}{\Delta y} \right) \times \frac{A}{D} = \frac{KA}{D} \quad (3.48)$$

and analogously,

$$K_s = \frac{F_x}{\Delta x} = \frac{GA}{D} \quad (3.49)$$

where G and K are the shear and bulk relaxation moduli, respectively, A is the area of the transverse cross section of the piece, and D is the thickness of the elastomeric block. K can be written as a function of both the tensile modulus of the elastomer, E , and the shape factor, S :

$$K = E(1 + 2kS^2) \quad (3.50)$$

where k is a numerical constant that varies between 0.93 and 0.53, depending on the hardness of the elastomer. The factor S is defined as the ratio between the surface area subjected to stress and the surface area free of stress. According to Figure 3.23,

$$S = \frac{BW}{2d(B+W)} \quad (3.51)$$

This expression indicates that a decrease in the thickness d produces an increase in S , with the consequent repercussion on the bulk relaxation modulus [Eq. (3.50)] and the rigidity under compression [Eq. (3.48)]. Figure 3.24 shows the stress-strain curves under compression for elastomer blocks of different shapes. It can be seen that as S increases the curves lose the linearity displayed in a large interval of extensions when S has a low

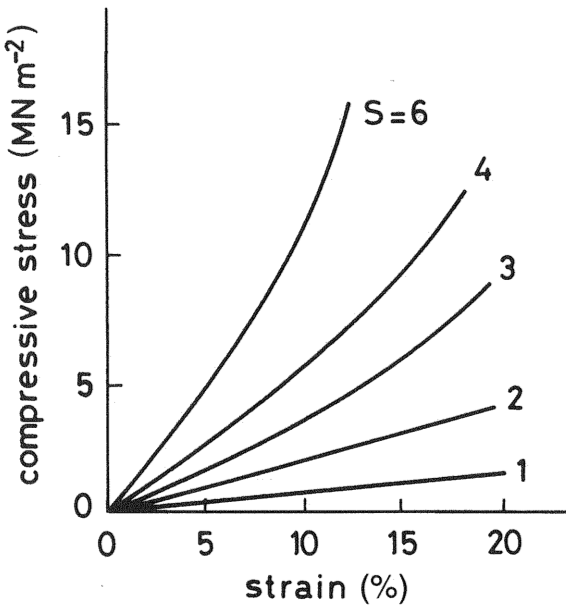


Figure 3.24 Compressive stress–strain curves for natural rubber vulcanizate showing the effect of shape factor S . (From Ref. 24.)

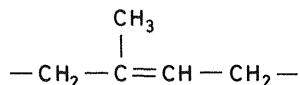
value. The way to control the rigidity under compression and shear is to construct pieces in which the elastomer is distributed in layers of thickness d supported between steel sheets. An illustrative scheme is shown in Figure 3.23. In this way, the rigidity under compression will increase as d decreases. However, the rigidity under shear, which increases when the thickness decreases [Eq. (3.49)], is not altered because it depends on the total thickness of the block D ($D = nd$, where n is the number of blocks of elastomer of thickness d).

It is very important for engineering applications to control the rigidity separately in two perpendicular directions. For example, when elastomeric materials are used in the construction of bridges, the rigidity of the materials under compression must be suitable to support the weight of the bridge and the deck and to accommodate additional loads due to traffic and ambient conditions. On the other hand, the flexibility of the elastomer admits horizontal movements of the deck caused by daily fluctuations in temperature or fluctuations between different climatic seasons. Otherwise, the horizontal movements of the deck could cause considerable bending of the pillars of the bridge, an effect that could become dangerous in the long term.

3.6.5 Most Widely Used Elastomers

(a) Natural Rubber (NR)

One of the most widely used polymers in industry is natural rubber. The industrial application of rubber is based on its exceptional elastic properties. From a chemical point of view, rubber consists exclusively of poly(*cis*-1,4-isoprene), whose repeating unit is



It is obtained from latex extracted from the *Hevea brasiliensis* tree. There exists another structural isomer called gutta-percha formed from poly(*trans*-1,4-isoprene), whose elastic properties differ from those of natural rubber.

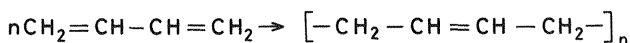
Natural rubber is composed of linear polymer chains; the glass transition temperature T_g , is -70°C , and below that temperature it is a fragile glass. The elastic properties for rubber are displayed at temperatures above T_g . Gutta-percha is a rigid crystalline solid at room temperature. The differences between natural rubber (NR) and gutta-percha derive from the capability shown by the polymer chains with the *trans* configuration to align themselves and produce a much more ordered structure than that corresponding to natural rubber. Gutta-percha displays elastic properties similar to those of rubber at temperatures above 65°C , which corresponds to the melting point of crystalline gutta-percha. The vulcanization reaction of natural rubber takes place via the double bonds of the main chain, which are highly reactive, sulfur being used as the cross-linking agent. The double bonds remaining in natural rubber chains after the vulcanization process are liable to undergo oxidation processes. For this reason the use of a powerful antioxidant agent is required.

(b) Synthetic Rubbers

A wide range of synthetic rubbers are available on the market that display elastic properties similar to those of natural rubber. Some types of rubbers of industrial interest are classified as (1) diene rubbers, (2) mono-olefinic rubbers, (3) silicones, and (4) fluoro-olefinics.

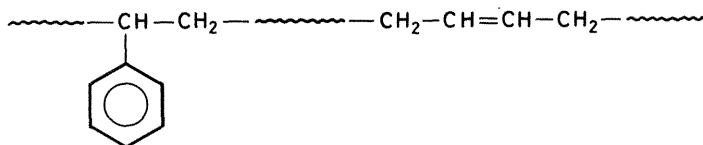
Diene Rubbers

Diene rubbers are formed from diolefins, basically butadiene, which polymerize by transposing the double bond:



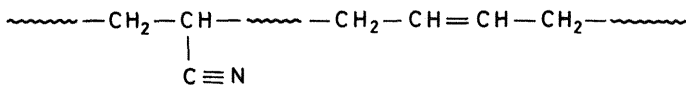
As occurs in natural rubber, only the 1,4-cis isomer exhibits elastomeric characteristics. The most important synthetic diene rubbers are polychloroprene (neoprene) and rubbers derived from butadiene such as styrene-butadiene and acrylonitrile-butadiene copolymers.

Styrene-Butadiene Rubbers. These synthetic rubbers, normally known as SBRs, are mainly used in the manufacture of tires. Their chemical structure corresponds to a random copolymer of styrene and butadiene units in a weight ratio of 23:77 and in a ratio of 1:6 in terms of structural units.



The presence of double bonds in the main chain enables the SBR chains to cross-link by a vulcanization process similar to that of natural rubber. Although the double bond is less reactive in this case, a natural tendency toward oxidation is nevertheless observed. Butadiene sequences in the chain can be obtained in the 1,4-cis isomer by using a stereospecific catalyst. Butadiene rubber (BR) is more flexible than natural rubber because the methyl group attached to the unsaturated carbon that is present in natural rubber is absent from BR. In addition, the presence of styrene units confers greater hardness and toughness on SBR. Moreover, the phenyl side group attached to the chain reduces the tendency to crystallize, in contrast with the behavior observed in natural rubber. SBR shows a high tendency toward hysteresis in load-unload cycles. Loss of strength is also observed at high temperatures, compared to natural rubber. SBR is not resistant to organic liquids, such as oil or gasoline, and it displays a tendency to absorb them, leading to swelling and the loss of mechanical properties of the rubber network.

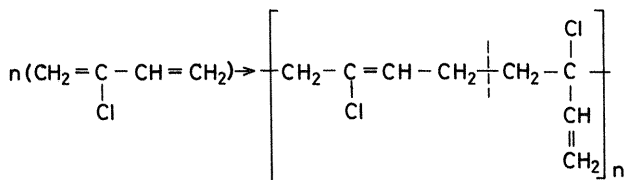
Acrylonitrile-Butadiene Rubber. This rubber, normally known as NBR, is a random copolymer of acrylonitrile and butadiene in which the acrylonitrile content lies in the range 15–50% (w/w). A diagram of the chain is shown below:



As occurs with other rubbers, the cross-linking process in NBR is carried out by means of a vulcanization process via the double bonds of the main chain. The unreacted double bonds are liable to suffer oxidation processes, particularly at high temperatures. The presence of the nitrile group as

a side substituent increases the polarity of the chains, favoring intermolecular interactions. Hydrogen bonding between adjacent chains leads to the loss of molecular flexibility. For this reason, acrylonitrile-butadiene rubbers are more resistant to the action of organic liquids. These rubbers do not display any tendency to swell in contact with petroleum. Because of this, and in spite of being more expensive than natural rubber, NBRs are used in applications requiring considerable resistance to the action of organic solvents. One of the many applications of this type of rubber in recent years has been in the automobile industry, specifically in the manufacture of engine components. In such circumstances, the rubbers have to resist high temperatures under conditions of aging by oxidation. For these applications manufacturers have resorted to using hydrogenated NBR in which the reactive double bonds of the butadiene units are saturated, in this way avoiding the oxidative process through double bonds in this elastomer. The vulcanization process is carried out using organic peroxides as cross-linking agents.

Polychloroprene (Neoprene) Rubbers. Polychloroprene or neoprene rubbers (CR) are polymers of 2-chloro-1,3-butadiene. The stereochemical structure of these rubbers is fundamentally the trans configuration (80%), with the rest being predominantly cis-1,4, though small quantities of 1,2 (1.5%) and 3,4 (1%) are also present. A scheme is given below:



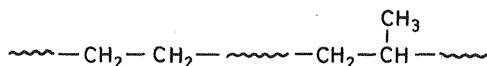
Although the polymer chains contain unsaturations, the chlorine atoms attached to the double bonds stabilize them, increasing their resistance to oxygen and ozone in such a way that the chains behave for these purposes as if they were saturated. Vulcanization is carried out using a metal Zn or Mg oxide. Owing to the presence of the chlorine atom, which confers polarity to the polymer chains, neoprenes are resistant to swelling by the action of oils and organic solvents. These rubbers show good resistance to flame and exhibit high mechanical strength. They are more expensive than other dienes, and in spite of their good properties their use is confined to special applications such as coatings for industrial cables and wires, hoses, and fastenings.

Mono-Olefinic Rubbers

Mono-olefinic rubbers are fully saturated elastomers obtained by copolymerization of linear mono-olefins. In general, the cross-linking process is

carried out by the action of organic peroxides or by introducing double bonds into the main chain that will permit vulcanization with sulfur, or organic peroxides.

Ethylene-propylene rubbers (EPR) are basically random copolymers of ethylene and propylene, with 60–70% (w/w) ethylene. Polyethylene and polypropylene are homopolymers that display too high a degree of crystallinity to be used as elastomers. Nevertheless, random copolymerization produces linear chains with sufficient structural irregularity to prevent crystallization. The copolymerization process leads to amorphous, fully saturated chains.

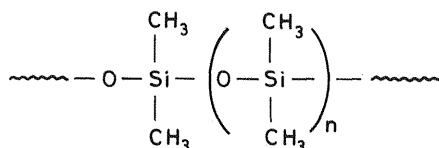


The vulcanization process is carried out by using an organic peroxide as a cross-linking agent. On some occasions, chain scission reactions take place during the cross-linking process that affect negatively the physical properties of the resulting elastomer. To avoid chemical degradation, the tendency on some occasions is to carry out the vulcanization with sulfur, and for this is it necessary to introduce a small quantity of dienes into the linear chains of the copolymers. These dienes, for example, 5-ethylidene-2-norborne, provide unsaturated sites via which the vulcanization reaction can prosper. In this way, the ter polymer-ethylene-propylene-diene monomer (EPDM) is obtained. EPDMs can also be cross-linked by using peroxides. In this case, chain scission reactions are less important than in EPRs, and consequently the physical properties of EPDMs cured with peroxides are less affected by degradative processes.

EPRs and EPDMs have excellent resistance to oxidation and ozone, compared to NR and SBR, and a relatively low cost. Their most important applications are in the manufacture of window sealing strips and in the automobile industry.

Silicones

Silicone rubbers are formed by an inorganic main chain of oxygen–silicon covalent bonds, with side substituents consisting of methyls, phenyls, vinyls, etc. The most commonly used is polydimethylsiloxane (PDMS) whose structure is given below:



As EPR and EPDM elastomers, the vulcanization process is carried out using organic peroxides because the polymer chains do not contain unsaturated bonds. If the polydimethylsiloxane chains are modified by introducing a small quantity of vinyl groups, the vulcanization is carried out using cumyl peroxide.

Silicones are rubbers possessing certain exceptional properties. For example, these rubbers display excellent resistance to oxidation processes, a wide range of accessible temperatures, -100°C to 300°C , and excellent dielectric properties, even at high temperatures, and they are also inert from the chemical and physiological points of view. Their most notable drawbacks lie in their high cost and the fact that their mechanical strength at room temperature is only moderate.

Fluoro-Olefinics

Fluoroelastomers are copolymers containing fluorine in their structure. There are different kinds of fluoroelastomers depending on the chemical composition and on the production in which the comonomers are found in the chain. As examples of comonomers, we can mention vinylidene fluoride-hexafluoropropylene and vinylidene fluoride-chlorotrifluoroethylene. The vulcanization process is performed using peroxides, diamines, and bisphenol.

The most significant properties of fluoroelastomers are: (1) excellent resistance to oxidation (they are self-extinguishing); (2) resistance to chemical attack and to organic solvents (they are among the most resistant rubbers to hydrocarbons, water, steam, and concentrated acids and alkalis; and (3) thermal resistance comparable to that of the silicones (they can support temperatures up to 250°C without undergoing degradation). However, fluoro-olefinic rubbers are very expensive materials; this disadvantage is aggravated by their high density (1.84 g/cm^3).

3.6.6 Thermoplastic Elastomers

Thermoplastic elastomers (TPEs) have been used for at least the last 25 years. These materials are also known as thermoplastic rubbers. In spite of their short life, TPE rubbers are highly regarded from the technological point of view. As their name indicates, they combine into a single material the elastic capability of an elastomer and the processability of a thermoplastic, characteristics that are explained by their structure. TPEs have managed to demonstrate that the barriers existing between the rubber industry and the plastics industry correspond more to tradition than to reality, and they are promoting the technological development of a stronger industry based on polymer materials in general.

(a) *What Is a Thermoplastic Elastomer?*

The term “thermoplastic elastomer” is normally used to describe polymeric materials that exhibit elastic properties similar to those of elastomers without containing chemical cross-links in their structure, as shown in the scheme of Figure 3.25. TPEs are biphasic materials composed of an elastomeric matrix containing a second phase of harder material dispersed within it, which acts to form physical cross-links of the TPE. While the cross-links in elastomeric networks are permanent (genuine chemical bonds), those in TPE are physical and reversible. The structure shown in Figure 3.25 can be achieved either by preparing a block copolymer or by mixing two polymers. In either event, the monomer units of one variety are not compatible with those of the second variety forming the TPE. Therefore, when the two types of monomer units come into contact, a phase separation takes place, giving rise to the biphasic structure shown in Figure 3.25. The domains acting as cross-links can display different morphologies—spherical, cylindrical, or laminar—depending on the thermal and mechanical history of the material. The hard domains, distributed through the elastomeric matrix, are made up of frozen macromolecular chains capable of restricting the gross chain motion of the chains constituting the elastomeric phase of the material.

There are certain advantages and disadvantages to this type of material compared to conventional elastomers. The advantages concern the existence of reversible physical cross-links. When a TPE is heated, the cross-links disappear if the temperature increases beyond the T_g of the hard phase or above the T_m of the hard domain if it is crystalline. In contrast, conventional elastomers display thermostable structure. The physical nature of

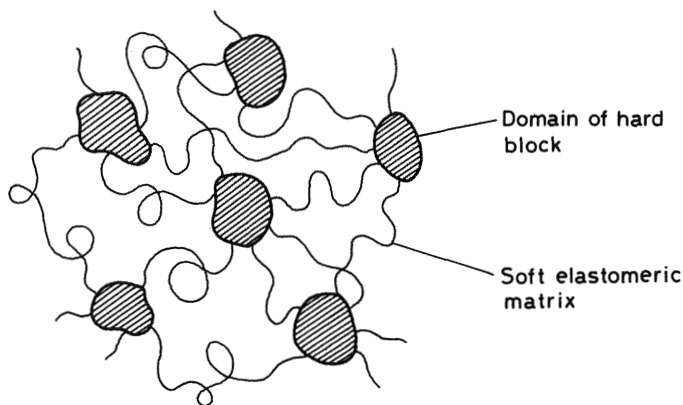


Figure 3.25 Thermoplastic elastomer phase structure (From Ref. 26).

TPE cross-links permits the processing of these materials using techniques of thermoplastics. Some disadvantages of these materials are low elastic recovery capability, limited strength at high temperatures, and low resistance against the action of acids and solvents. In general, the disadvantages are being overcome day by day with the preparation of thermoplastic elastomers with considerably improved performance for special uses in engineering.

(b) Commercial Thermoplastic Elastomers

Styrenic TPEs

Styrene-butadiene-styrene (SBS) triblock copolymers were the first thermoplastic elastomers introduced onto the market in 1965. These rubbers have been known by the generic name of styrenics. SBS are triblock (SBS) linear copolymers disposed in radial or star form. The morphology of a styrenic TPE is shown in Figure 3.26. It can be seen that the styrenic blocks are situated together, forming a domain that is separated from the elastomeric phase composed of butadiene blocks. The morphology of both phases had been extensively studied by transmission electron microscopy. The conclusion has been that commercial SBSs contain around 30% styrene and display a phase of spherical domains of polystyrene that extend in a very regular way through the elastomeric phase. On the main limitations of

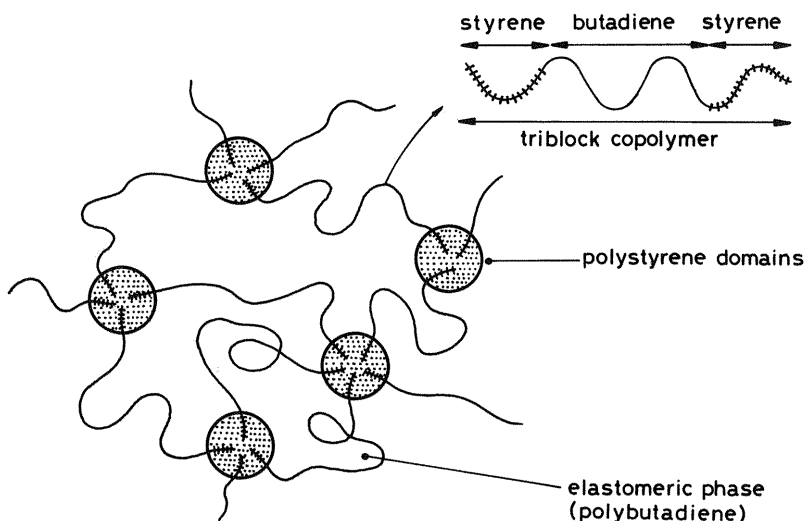


Figure 3.26 Styrenic TPE morphology.

SBSs in service is their low tolerance to moderately high temperatures. The softening temperature is determined by the T_g of the styrenic blocks. In principle, this should be around 100°C , the T_g of polystyrene. However, the blocks of polystyrene have low molecular weight, and therefore the most accepted value for the softening temperatures is 65°C . Obviously, the consequence of thermal softening is the loss of mechanical qualities of these materials, and creep and permanent elongation can be observed. In contrast, the performance is very good at low temperatures. Flexibility is maintained over a wide range of temperatures down to about -90°C with blocks of butadiene and to about -60°C if the butadiene is replaced by isoprene (SIS). The tendency to oxidation shown by this type of TPE is a drawback. This is caused by the presence of unsaturations in the elastomer phase. This problem can be partly solved if the SBS undergoes a hydrogenation process.

In spite of the disadvantages mentioned above, styrenics account for nearly 50% of the total consumption of TPEs. Their use is equally widespread in America and in Europe, a fact that could largely be due to a good quality/price ratio.

Olefinic TPEs

Olefinic TPEs are thermoplastic elastomers coming second in order of demand, making them the most important in the group after styrenics. The first ones were marketed in 1972. Unlike styrenics, they consist of a mixture of a crystalline olefin, normally polypropylene, and an elastomeric copolymer of ethylene-propylene, usually EPDM (Fig. 3.27). These materials are collectively known under the name of thermoplastic olefin (TPO) elastomers. The structure of the mixture of polypropylene (PP) and EPDM is biphasic due to the incompatibility of PP and EPDM. In principle, the crystalline phase acts in a similar way to the hard phase of styrenic TPEs. In terms of properties, TPOs are materials that cover a broad range of hardness, modulus, and tensile strength. In general, all these properties increase with the PP content of the mixture. Certain flaws in the elastic properties such as a lack of recovery capability and low resilience, particularly at high temperatures, should be mentioned as the most important drawbacks. These factors restrict their use in some applications at temperatures above 60°C . Their flexibility at low temperatures is guaranteed until nearly -50°C , the glass transition temperature of the elastomeric phase. On the other hand, since the melting temperature of PP is around 160°C , these materials are processed at temperatures between 190 and 230°C . The flaws mentioned above have been overcome to some degree by modifying the preparation of the material. The modification consists in vulcanizing EPDM, via unsaturated moieties, during the process of mixing with PP, a process known as

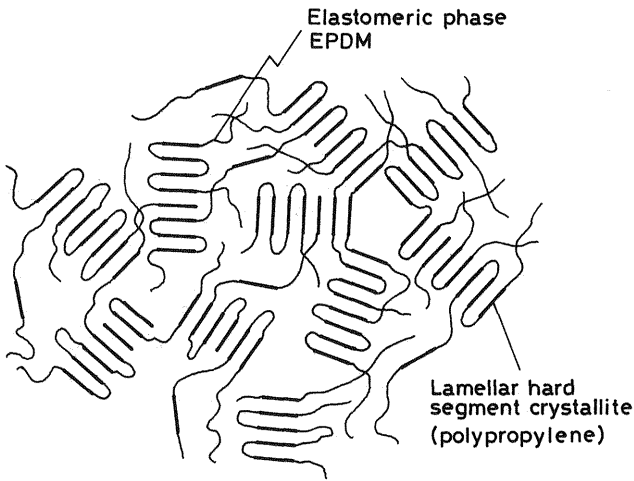


Figure 3.27 Semicrystalline TPE morphology (From Ref. 26).

dynamic vulcanization. At the structural level, the consequence of this process is the appearance of chemical cross-links in the elastomeric phase, and materials subjected to this modification are generically known by the term TPVs (vulcanized thermoplastics). TPVs obviously lack the flaws found for TPOs and display superior elastic properties and better resistance to oils and solvents.

TPEs for Engineering

A new type of materials, referred to as TPEs for engineering, have recently been developed (26). These materials show advantages over the traditional TPEs. They are all block copolymers in which the hard block is crystalline. According to certain specific groups appearing in their structure they are classified as

1. *Polyesters*. This group is formed by multiblock copolymers in which hard blocks, generally constituted by poly(butylene terephthalate) (PBT) ($T_m = 170\text{--}250^\circ\text{C}$) of approximately 10 units, alternate with soft flexible blocks consisting of poly(tetramethylene glycol terephthalate) (PTMGT) ($T_g = -50^\circ\text{C}$). This type of TPE displays a combination of interesting properties, such as flexibility at low temperatures and high softening point. These materials are also capable of covering a wide hardness range because the content of the hard phase can be modified. Nevertheless, as occurs

with all polyesters, they are liable to undergo hydrolysis at temperatures above 60°C .

2. *Polyurethanes.* Thermoplastic polyurethanes (TPUs) contain urethane groups, $-\text{O}-\text{CO}-\text{NH}-$ in their structure obtained from the reaction of a diisocyanate ($\text{OCN}-\text{R}-\text{CNO}$) with a polyol. These polyurethanes are block copolymers in which hard blocks formed by reaction of a diisocyanate with a short-chain diol alternate with soft blocks formed by reaction of a diisocyanate with a long-chain diol.
3. *Polyamides.* Polyamides are the most recently developed TPEs. Their structure does not differ from that of other TPEs for engineering. An example of a polyamide TPE is obtained from a prepolymer terminating in a hydroxyl group, which will constitute the soft blocks, capable of reacting with a polyamide terminating in carboxyl groups, which will constitute the hard blocks of the copolymer. The amide blocks could be nylon 11 or nylon 12. The flexibility of these thermoplastics is ensured at low temperatures down to -40°C . The polyamide blocks melt in the range $170-220^{\circ}\text{C}$.

The TPEs for engineering show advantages over conventional TPEs. They exhibit a good combination of properties such as resistance to abrasion and splitting, good flexibility at low temperatures, and high resistance to impact. The principal disadvantage of TPEs for engineering is their cost, which is twice to five times the cost of styrenic and olefinic TPEs.

PROBLEM SETS

Problem 3.1

Show that in Eq. (3.33), $\sigma = Nk_B T(\lambda - \lambda^{-2})$, the parameter $Nk_B T$ represents the shear modulus of the elastomer.

Solution 3.1

According to Hooke's law, the stress σ is proportional to the deformation ε of the sample, defined as the extension per unit of initial length $\varepsilon = \Delta L/L_0$ according to the equation

$$\sigma = E\varepsilon \quad (\text{P3.1.1})$$

where E is the elastic modulus of the sample.

In the case of Eq. (3.33) the deformation λ is defined as

$$\lambda = 1 + \Delta L/L_0 = 1 + \varepsilon \quad (\text{P3.1.2})$$

and therefore

$$\lambda - \lambda^{-2} = 1 + \varepsilon - (1 + \varepsilon)^{-2} \quad (\text{P3.1.3})$$

Expanding the term $(1 + \varepsilon)^{-2}$ in series, we obtain

$$\lambda - \lambda^{-2} = 1 + \varepsilon - (1 - 2\varepsilon + \dots) \quad (\text{P3.1.4})$$

For small deformations,

$$\lambda - \lambda^{-2} = 3\varepsilon \quad (\text{P3.1.5})$$

so Eq. (3.33) would be reduced to

$$\sigma = Nk_B T 3\varepsilon \quad \text{and} \quad E = 3Nk_B T \quad (\text{P3.1.6})$$

Since for an incompressible material $E = 3G$ (see Chapter 4), it can be asserted that the quantity $Nk_B T$ of Eq. (3.33) coincides with the shear modulus of the elastomer,

$$G = Nk_B T \quad (\text{P3.1.7})$$

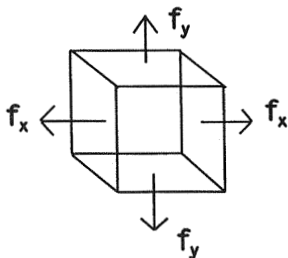
Problem 3.2

Obtain the stress–elongation relationship from Eq. (3.27) for an ideal elastomer:

- For a two-dimensional deformation $\lambda_x = \lambda_y = \lambda$ produced by the application of two forces in the x, y directions.
- For a two-dimensional deformation $\lambda_x \neq \lambda_y$ produced by the application of forces in the x, y directions.

Solution 3.2

- Figure P3.2.1 shows a representation of a sample of elastomer of initial dimensions x_0, y_0, z_0 subjected to the action of two forces

**Figure P3.2.1**

For a sample of volume $V = x_0 y_0 z_0$, the total work would be given by

$$W = \frac{1}{2} G V (\lambda_x^2 + \lambda_y^2 + \lambda_z^2 - 3) \quad (\text{P3.2.1})$$

in this particular case, $\lambda_x = \lambda_y = \lambda$ and therefore $\lambda_z = \lambda^{-2}$, which gives

$$W = \frac{G V}{2} (2\lambda^2 + \lambda^{-4} - 3) \quad (\text{P3.2.2})$$

Since $dW = f_x dx = f_y dy$,

$$f_x = f_y = \left(\frac{\partial W}{\partial \lambda_x} \right) \left(\frac{\partial \lambda_x}{\partial x} \right) = \left(\frac{\partial W}{\partial \lambda_y} \right) \left(\frac{\partial \lambda_y}{\partial y} \right) \quad (\text{P3.2.3})$$

$$f_x = \frac{G V}{2} \left(4\lambda - \frac{4}{\lambda^5} \right) \left(\frac{1}{x_0} \right) \quad (\text{P3.2.5})$$

and

$$f_y = \frac{G V}{2} \left(4\lambda - \frac{4}{\lambda^5} \right) \left(\frac{1}{y_0} \right) \quad (\text{P3.2.5})$$

Substituting $V = x_0 y_0 z_0$ into Eqs. (P3.2.4) and (P3.2.5), we obtain

$$f_x = 2G y_0 z_0 (\lambda - \lambda^{-5})$$

and

$$f_y = 2G x_0 z_0 (\lambda - \lambda^{-5}) \quad (\text{P3.2.6})$$

so the nominal stress is given by

$$\frac{f_x}{y_0 z_0} = \sigma_x = 2G(\lambda - \lambda^{-5}) = \sigma_y = \frac{f_y}{x_0 z_0} \quad (\text{P3.2.7})$$

(b)

$$\lambda_z = \frac{1}{\lambda_x \lambda_y} \quad (\text{P3.2.8})$$

Thus,

$$W = \frac{GV}{2} (\lambda_x^2 + \lambda_y^2 + \frac{1}{\lambda_x^2 \lambda_y^2} - 3) \quad (\text{P3.2.9})$$

and

$$f_x = \left(\frac{\partial W}{\partial \lambda_x} \right) \left(\frac{\partial \lambda_x}{\partial x} \right) = \frac{VG}{2} \left(2\lambda_x - \frac{2}{\lambda_x^3 \lambda_y^2} \right) \left(\frac{1}{x_0} \right) \quad (\text{P3.2.10})$$

Therefore,

$$f_x = y_0 z_0 G (\lambda_x - 1/\lambda_x^3 \lambda_y^2) \quad (\text{P3.2.11})$$

and

$$\sigma_x = G (\lambda_x - \lambda_x^{-3} \lambda_y^{-2}) \quad (\text{P3.2.12})$$

In the same way, we can derive

$$\sigma_y = G (\lambda_y - \lambda_y^{-3} \lambda_x^{-2}) \quad (\text{P3.2.13})$$

Problem 3.3

Calculate the variation in entropy corresponding to a polydimethylsiloxane network of mass 6.89 g, with an average molecular weight between cross-links $M_c = 8.3 \times 10^3$, subjected to a reversible uniaxial extension at 25°C until the length is double its initial length.

Solution 3.3

According to Eq. (3.26), the variation in entropy, ΔS , per unit volume in a deformation experiment is given by

$$\Delta S = -\frac{k_B N}{2} (\lambda_x^2 + \lambda_y^2 + \lambda_z^2 - 3) \quad (\text{P3.3.1})$$

To calculate the total variation in entropy, we replace N by ν , the total number of elastic chains of the network.

$$\Delta S_T = -\frac{k\nu}{2}(\lambda_x^2 + \lambda_y^2 + \lambda_z^2 - 3) \quad (\text{P3.3.2})$$

If the deformation occurs along the z axis, $\lambda_z = 2$, and, remembering that

$$\lambda_x \lambda_y \lambda_z = 1 \quad (\text{P3.3.3})$$

we will have

$$\lambda_x = \lambda_y = 1/\sqrt{2} \quad (\text{P3.3.4})$$

Moreover

$$\nu = \frac{m}{M_c} N_A = \frac{6.89}{8.3 \times 10^3} \times 6.023 \times 10^{23} = 5 \times 10^{20} \text{ chains} \quad (\text{P3.3.5})$$

Therefore,

$$\Delta S_T = -\frac{1.38 \times 10^{-23} \times 5 \times 10^{20}}{2} \left[\frac{1}{2} + \frac{1}{2} + 4 - 3 \right] = -6.9 \times 10^{-3} \text{ J K}^{-1} \quad (\text{P3.3.6})$$

This shows that the entropy decreases when the sample of PDMS is extended.

The heat involved in the process can also be calculated by applying the second law of thermodynamics,

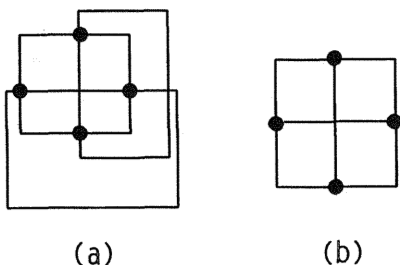
$$\Delta S = Q/T \quad (\text{P3.3.7})$$

$Q = -6.9 \times 10^{-3} \times 298 = -2.06 \text{ J}$, and since $\Delta E = 0$, the first law of thermodynamics indicates that $W = 2.06 \text{ J}$.

The results have to be interpreted as follows. The work done by the force applied to the sample of PDMS is positive, and consequently the sample of PDMS releases heat in an amount equal to the work done.

Problem 3.4

Determine the relationship existing between the structural parameters of the networks whose arrangement is shown in Figure 3.4.1.

**Figure P3.4.1****Solution 3.4**

The structural parameters of a network were stated in Section 3.3.3 as functionality ϕ , cross-link density $= \mu$ (cross-link points)/ V (nonswollen network), and ν = number of chains in the network.

For network (a),

$$\phi = 4 \text{ (four chains start from each cross-link)}$$

$$\mu = 4; \quad \nu = 8; \quad \mu/\nu = 4/8 = 1/2$$

For network (b),

$$\phi = 3 \text{ (three chains start from each cross-link)}$$

$$\mu = 4; \quad \nu = 6; \quad \mu\nu = 4/6 = 2/3$$

Moreover, in both cases the general relation $\phi\mu = 2\nu$ can be confirmed.

In addition, if the density of the sample, ρ (g/cm^3) is known, the average molecular weight between cross-links, M_c , can be obtained from the relationship

$$M_c = \frac{\rho}{\nu/V} \quad (\text{P3.4.1})$$

Problem 3.5

A 2.830 g sample of a poly(methyl methacrylate) (PMMA) network immersed in ethyl acetate (EtAc) reaches swelling equilibrium after 24 h, the final weight being 7.336 g. The cross-linking reaction was carried out with a tetrafunctional cross-linking agent in the undiluted state ($\nu_{2s} = 1$). Calculate M_c .

Data: Specific volume of the PMMA network = $0.81 \text{ cm}^3/\text{g}$; χ (polymer-solvent interaction parameter) = 0.47 ; density of EtAc = 0.900 g/cm^3 (molecular weight = 88.12).

Solution 3.5

First, the value of v_2 , the fraction by volume of PMMA at swelling equilibrium, is calculated as

$$v_2 = \frac{\text{volume of PMMA}}{\text{total volume at equilibrium (PMMA + EtAc)}} \quad (\text{P3.5.1})$$

$$\text{Volume of PMMA} = 2.830 \times 0.81 = 2.292 \text{ cm}^3$$

$$\text{Total volume} = 2.292 + (7.336 - 2.830)/0.9 = 7.299 \text{ cm}^3$$

$$v_2 = 2.292/7.299 = 0.314$$

$$\text{Degree of swelling} = v_2^{-1} = 0.314^{-1} = 3.185$$

To calculate M_c we use the classical theory, Eq. (3.46),

$$M_c = \frac{\rho A' \phi V_1 v_{2s}^{2/3} (v_2^{1/3} - v_2 \omega)}{-[\ln(1 - v_2) + v_2 + v_2^2 \chi_{12}]} \quad (\text{P3.5.2})$$

Substituting $\rho = 0.81^{-1} = 1.235 \text{ g/cm}^3$,

$$A' \phi = 1 \text{ (affine limit)}$$

$$V_1 = 88.12/0.9 = 97.91 \text{ cm}^3/\text{mol}$$

$$v_2 = 0.314; \quad v_{2s} = 1; \quad \omega = 2/4 = 0.5; \quad \chi_{12} = 0.47$$

which gives

$$M_c = 3.82 \times 10^3$$

The density of elastic chains is

$$\frac{\nu}{V} = \frac{\rho}{M_c} = \frac{1.235}{3.82 \times 10^3} = 3.2 \times 10^{-4} \text{ mol chains cm}^{-3}$$

Similarly, from the relationship between the number of chains and number of cross-links (Problem 3.4) for a tetrafunctional network, we obtain

$$\mu/V = 1.6 \times 10^{-4} \text{ mol cross-links cm}^{-3}$$

REFERENCES

1. PJ Flory. Principles of Polymer Chemistry. Ithaca NY: Cornell Univ, 1953.
2. LRG Treloar. The Physics of Rubber Elasticity. Oxford UK: Clarendon Press, 1975.
3. JE Mark. In JE Mark, J Lal, eds. Elastomers and Rubber Elasticity. Washington DC: American Chemical Society, 1982.
4. JE Mark. In: JE Mark, A Eisenberg, WW Graessly, L Mandelkern, JL Koenig, eds. Physical Properties of Polymers. Washington DC: American Chemical Society, 1984, Chap. I.
5. A Williams. Polymer Science and Engineering. Prentice-Hall Int Ser Phys Chem Eng. Englewood Cliffs NJ: Prentice Hall, 1970.
6. RL Anthony, RH Caston, E Guth. *J. Phys Chem* **46**: 826, 1942.
7. JE Mark. *J Chem Ed* **58**: 898, 1981.
8. SM Grumbell, L Mullins, RS Rivlin. *Trans Faraday Soc* **49**: 1495, 1953.
9. JE Mark, RR Rahalkar, JL Sullivan. *J Chem Phys* **70**: 1794, 1979.
10. PJ Flory. *Proc Roy Soc London* **251**: 351, 1976.
11. PJ Flory, B Erman. *Macromolecules* **15**: 800, 1982.
12. PJ Flory. *Polymer* **20**: 1317, 1979.
13. NR Langley, RA Dickie, C Wong, JD Ferry, R Chasset, P Thirion. *J Polym Sci A-2* **6**: 1371, 1968.
14. RM Johnson, JE Mark. *Macromolecules* **5**: 41, 1972.
15. JE Mark, A Eisenberg, WW Graessly, L Mandelkern, JL Koenig. *Physical Properties of Polymers*. Washington DC: American Chemical Society, 1984.
16. AL Andrad, MA Llorente, JE Mark. *J Chem Phys* **72**: 2282, 1980.
17. T-K Su, JE Mark. *Macromolecules* **10**: 120, 1977.
18. DS Chiu, T-K Su, JE Mark. *Macromolecules* **10**: 1110, 1977.
19. PJ Flory. *Macromolecules* **112**: 119, 1979.
20. MR Gómez-Antón, RM Masegosa, A Horta. *Polymer* **28**: 2116, 1987.
21. JA Brydson. *Rubber Chemistry*. New York: Elsevier Applied Science, 1978.
22. W Hofmann. *Rubber Technology Handbook*. New York: Hanser Oxford Univ Press, 1989.
23. KS Lee. In: RW Dyson ed., *Engineering Polymers*. New York: Chapman & Hall, 1990, Chap. II.
24. P Lewis. In: G Weidman, P Lewis, N Reid, eds. *Structural Materials*. London: Butterworth and Heinemann, 1996.
25. NG McCrum, CP Buckley, CB Bucknall. *Principles of Polymer Engineering*. Oxford: Oxford Science, 1994.
26. MSM Alger. In: RW Dyson, Ed., *Engineering Polymers*. New York: Chapman and Hall, 1990.

4

Stress–Strain Relations for Ideal Solids and Ideal Liquids

4.1	Ideal Solids and Liquids: Constitutive Equations	140
4.2	Stress Tensor	143
4.3	The Second Law of Dynamics	146
4.4	Strain Tensor	147
4.5	Compatibility Equations	151
4.6	Effect of Symmetry on the Relationships Between the Stress and Strain Tensors in Ideal Elastic Systems	152
4.7	Generalized Stress–Strain Hooke’s Law for Isotropic Solids	162
4.8	Navier Equations	167
4.9	Generalized Strain–Stress Relationships for Ideal Elastic Systems	170
4.10	Thermoelastic Effects	172
4.11	Viscosity of Ideal Liquids	175
	Problem Sets	177
	References	195

4.1 IDEAL SOLIDS AND LIQUIDS: CONSTITUTIVE EQUATIONS

The response of most materials to mechanical, electrical, optical and other force fields is time-dependent. The study of the responses to these force fields allows one to determine, respectively, the rheological, dielectrical and birefringence properties of materials. According to the second law of thermodynamics, part of the input energy involved in the perturbation must invariably be dissipated, and part of it is stored. It should be pointed out

that dissipation of energy does not occur instantaneously; it may take place in a time infinitely short, infinitely long, or finite, depending on the thermodynamic state and nature of the material.

In rheology, the perturbation is a mechanical force, and the response is a deformation that in certain cases becomes flow. Part of the energy involved in the deformation is stored elastically, and part is dissipated through viscous mechanisms. Because some of the energy is dissipated, the response always lags behind the perturbation. The shorter or greater the duration of the perturbation, the smaller or larger, respectively, is the amount of lag. This is a consequence of the fact that in a short perturbation the molecules comprising the material cannot rearrange sufficiently fast to accommodate to it, whereas in a perturbation of large duration there is plenty of time for molecular rearrangements. The response also depends on the intensity of the perturbation.

The establishment of relationships or constitutive equations linking the forces acting on a material and its response (deformation or flow) is one of the main objectives of rheology. However, this is not an easy task, because of the time dependence of the response. An important requirement of constitutive equations is that they must be independent of the shape and size of the material. To illustrate this, let us consider an ideal elastic material in which the lag time between the perturbation and the response is zero. Though strictly speaking this material does not exist, it could be considered as such a material in which the lag time is close to zero. Metals, for example, fulfil this requirement. To start with, let us assume a metallic rod of length L_0 and uniform cross-sectional area A_0 that is stretched by being pulled on its ends, and as a result a tensile force F is applied in the direction of the rod axis. Experience indicates that for infinitesimal deformations, $F = kA_0(L - L_0)$, where L is the length of the deformed rod. The proportionality constant k depends on the nature of the material and the initial dimensions of the rod defined by L_0 and A_0 . Moreover, for constant values of $L - L_0$ and A_0 the force is inversely proportional to the original length of the bar. Accordingly, the tensile force is given by

$$F = EA_0 \frac{L - L_0}{L_0} \quad (4.1)$$

where $E = kL_0$. The parameter E , called the modulus of elasticity, is independent of the geometry of the rod and consequently represents a characteristic material property or a material function. Rearrangement of Eq. (4.1) gives the well-known constitutive Hooke's equation (1)

$$\sigma = E\varepsilon \quad (4.2)$$

where $\sigma(= F/A_0)$ is the force per unit area or stress and $\varepsilon[(= (L - L_0)/L_0)]$ is the deformation. Both σ and E have the dimensions of newtons per square meter (N/m^2), while ε is a dimensionless quantity.

Let us now discuss the rheological behavior of ideal liquids. The storage energy of an ideal viscous liquid is zero. Though strictly speaking there is no real liquid that meets this assumption, low molecular weight liquids approach this behavior. Consider a liquid sheared between two parallel plates by a force F_A applied on the upper plate of area A that forces it to move with constant velocity v while the lower plate remains motionless. Assume that the two plates are separated by a relatively small distance h and that v is small enough that the flow is laminar. Experience indicates that the shear stress $\sigma(= F/A)$ is given by (2)

$$\sigma = \frac{F}{A} = \eta \dot{\varepsilon} \quad (4.3)$$

where $\dot{\varepsilon}(= v/h)$, the rate of shear, has the dimension of reciprocal time, s^{-1} , and the dimension of the viscosity η is kilograms per meter per second [$\text{kg}/(\text{m}\cdot\text{s})$]. The fact that the rate of shear remains constant means that the input energy is dissipated by friction of the layers that slide upon each other, their velocities decreasing from v to zero, corresponding to the liquid layers in contact with the moving plate and the motionless plate, respectively. Consequently, the viscosity is a measurement of the energy dissipated in flow, in such a way that the higher this energy is, the higher is the viscosity of the liquid.

Both E , in ideal solids, and η , in ideal liquids, are material functions independent of the size and shape of the material they describe. This holds for isotropic and homogeneous materials, that is, materials for which a property is the same at all directions at any point. Isotropic materials are so characterized because their degree of symmetry is infinite. In contrast, anisotropic materials present a limited number of elements of symmetry, and the lower the number of these elements, the higher the number of material functions necessary to describe the response of the material to a given perturbation. Even isotropic materials need two material functions to describe in a generalized way the relationship between the perturbation and the response. In order to formulate the mechanical behavior of ideal solids and ideal liquids in terms of constitutive equations, it is necessary to establish the concepts of strain and stress.

4.2 STRESS TENSOR

The introduction of the concepts of stress and deformation at a point has been a fundamental concept in the development of the mechanics of continuum media. From a physical point of view, only the displacement is a real quantity, while stress implies an idealized situation that is not directly measurable; the value of a stress can only be inferred from its effects. The effects of the force at a point P depend on the orientation of the element surface δA comprising the point, which in turn is characterized by a vector n_j ($j=1,2,3$) normal to the surface at P , as shown in Figure 4.1. The stress vector at the point P can be written as

$$t_j^{(n_i)} = \lim_{\Delta A \rightarrow 0} \frac{\Delta f_j^{(n_i)}}{\Delta A} = \frac{df_j^{(n_i)}}{dA} \quad (4.4)$$

From Newton's law of action and reaction the stress vector resulting from the force exerted by the material inside an arbitrary volume V upon the material surrounding it across the element surface δA is

$$t_j^{(n_i)} = -t_j^{(-n_i)} \quad (4.5)$$

If, as indicated in Figure 4.2, the normal to the surface δA coincides with the x_3 coordinate axis, the force acting on P can be decomposed into a component δf_{33} parallel to x_3 and a shear force located in the plane of the surface, which in turn can be decomposed into a component δf_{23} along the x_2 axis and a component δf_{13} , along x_1 . Here the second subscript indicates the axis perpendicular to the elemental surface δA and the first the axis to

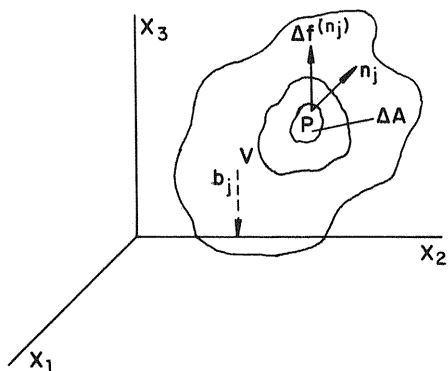


Figure 4.1 Schematic representation of the state of stress at a point of a material body.

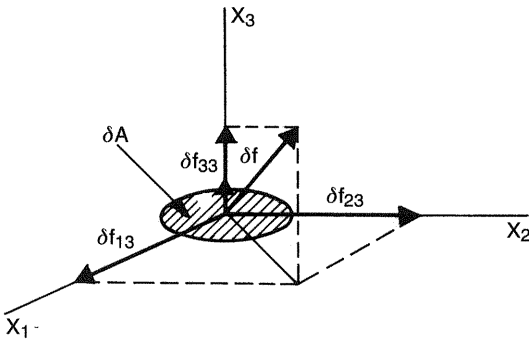


Figure 4.2 Components of force at an infinitesimal surface.

which the component of the force in the surface is parallel. The values of the limits of $\delta f_{13}/\delta A$, $\delta f_{23}/\delta A$, and $\delta f_{33}/\delta A$ when $\delta A \rightarrow 0$ are the stresses at a point that are customarily written as σ_{13} , σ_{23} , and σ_{33} , respectively. Obviously these three values do not completely define the state of the stress at the point considered because they depend on the plane of the arbitrarily chosen section. The state of the stress at a point will require specification of the components of the stress in three mutually perpendicular planes, that is, three planes perpendicular to x_1 , x_2 , and x_3 , as indicated in Figure 4.3. The vectors shown in this figure, three of stress perpendicular to the three planes

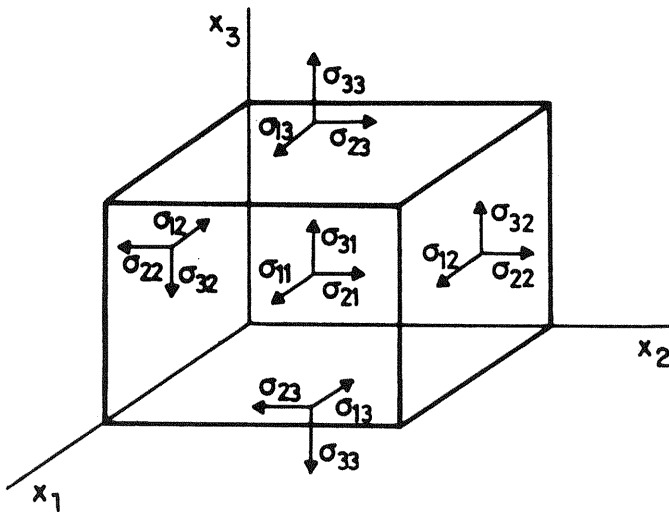


Figure 4.3 Components of the stress tensor in rectangular coordinates on an infinitesimal element.

(σ_{11} , σ_{22} , and σ_{33} , also named normal stresses) and six of shear (σ_{12} , σ_{13} , σ_{21} , σ_{23} , σ_{31} , and σ_{32}), are the components of the stress tensor represented by σ_{ij} .

Not all the components of the stress tensor are independent, as can easily be shown by taking the moments around the different coordinate axes in Figure 4.3. A balance of forces at equilibrium gives

$$(\sigma_{32} dx_1 dx_2)dx_3 - (\sigma_{23} dx_1 dx_3)dx_2 = 0 \text{ around the } x_1 \text{ axis} \quad (4.6a)$$

$$(\sigma_{21} dx_1 dx_3)dx_2 - (\sigma_{12} dx_2 dx_3)dx_1 = 0 \text{ around the } x_3 \text{ axis} \quad (4.6b)$$

$$(\sigma_{13} dx_2 dx_3)dx_1 - (\sigma_{31} dx_1 dx_2)dx_3 = 0 \text{ around the } x_2 \text{ axis} \quad (4.6c)$$

Hence, $\sigma_{ij} = \sigma_{ji}$. The stress tensor is symmetrical and consequently has only six independent components.

With the aim of relating the force per unit area at a point to the components of the stress tensor at that point, let us consider (3) the tetrahedron of Figure 4.4, in which a force per unit area, f , is applied to the oblique surface ΔS . The other surfaces of the tetrahedron, ΔS_1 , ΔS_2 , and ΔS_3 , respectively perpendicular to the x_1 , x_2 , and x_3 coordinate axes, can be obtained from ΔS from the expressions.

$$\Delta S_1 = n_1 \Delta S, \quad \Delta S_2 = n_2 \Delta S, \quad \Delta S_3 = n_3 \Delta S \quad (4.7)$$

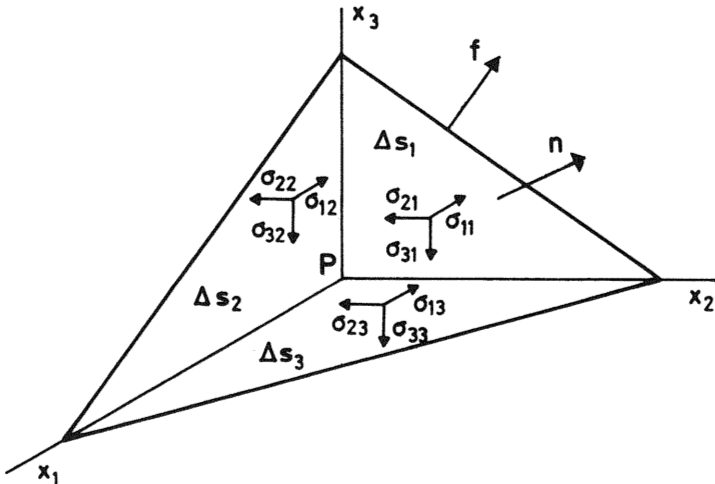


Figure 4.4 Forces and stresses on an infinitesimal tetrahedral element.

where n_1 , n_2 , and n_3 are the components of the unit vector perpendicular to ΔS in the reference frame x_1 , x_2 , and x_3 . If the tetrahedron is at equilibrium, a balance of force leads to

$$f_i \Delta S - \sigma_{1i} \Delta S_1 - \sigma_{2i} \Delta S_2 - \sigma_{3i} \Delta S_3 - \frac{1}{3} b_i \Delta S \Delta h = 0 \quad (4.8)$$

where $b = -\rho \nabla \phi$ is a conservative force emanating from a gravitational potential ϕ , ρ is the density of the body and Δh is the tetrahedron height. When $\Delta h \rightarrow 0$, Eqs (4.7) and (4.8) give

$$f_i = \sum_j n_j \sigma_{ji}, \quad j = 1, 2, 3 \quad (4.9)$$

This expression indicates that the force f is a linear combination of the components of the stress tensor. The inertial term has been neglected in this equation because the height of the tetrahedron is infinitesimal.

4.3 THE SECOND LAW OF DYNAMICS

When a body of volume V and area S is under the action of both contact and conservative forces, a balance of forces gives

$$\int_S f_j dS + \int_V b_j dV = \int_V \rho a_j dV \quad (4.10)$$

where f is the contact force per unit of surface and a is the acceleration. By substituting Eq. (4.9) into Eq. (4.10), this latter expression becomes

$$\int_S n_k \sigma_{jk} dS + \int_V b_j dV = \int_V \rho a_j dV \quad (4.11)$$

By taking into account the theorem of divergence, this equation can be written as

$$\int_V (\sigma_{jk,k} + b_j) dV = \int_V \rho a_j dV \quad (4.12)$$

where $\sigma_{jk,k} = \partial \sigma_{jk} / \partial x_k = \text{div } \sigma$. Because Eq. (4.12) holds for any volume, the following expression is obtained:

$$\text{div } \boldsymbol{\sigma} + \mathbf{b} = \rho \mathbf{a} \quad (4.13)$$

which is also called the second law of dynamics. In experiments in which the body undergoes deformation without translation, as occurs in linear elasticity, Eq. (4.13) becomes

$$\operatorname{div} \boldsymbol{\sigma} + \mathbf{b} = \mathbf{0} \quad (4.14)$$

4.4 STRAIN TENSOR

Let us consider two neighboring points in a solid body (3), indicated as A and B in Figure 4.5, whose coordinates in an orthogonal reference frame are x_i and $x_i + dx_i$, respectively, where $i = 1, 2, 3$. Let us assume further that under the action of a force field, the body is deformed and the positions of the two points are A' and B' with coordinates X_i and X_{i+1} with respect to the reference frame indicated before. According to Figure 4.5, the coordinates X_i and x_i are related by

$$X_i = x_i + u_i \quad (4.15)$$

where u_i are the components of the vector displacement \mathbf{u} . If \mathbf{u} is assumed to be a continuous function of the initial coordinates x_i , one can write

$$dX_l = dx_l + du_l = dx_l + \sum_k \frac{\partial u_l}{\partial x_k} dx_k \quad (4.16)$$

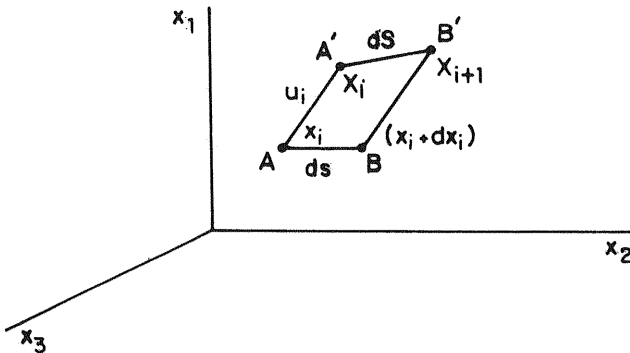


Figure 4.5 Displacements of two points A and B as a result of a force.

which leads to

$$(dX_l)^2 = (dx_l)^2 + \sum_{k,l} \frac{\partial u_l}{\partial x_k} dx_k dx_l + \sum_{ikl} \frac{\partial u_l}{\partial x_i} \frac{\partial u_l}{\partial x_k} dx_i dx_k \quad (4.17)$$

The squares of the distances between the points A and B (ds^2) and between A' and B' (dS^2) can be written as

$$ds^2 = (dx_1)^2 + (dx_2)^2 + (dx_3)^2 = \sum_l (dx_l)^2 \quad (4.18a)$$

$$dS^2 = \sum_l (dX_l)^2 = ds^2 + \sum_{ik} \frac{\partial u_i}{\partial x_k} dx_i dx_k + \sum_{ikl} \frac{\partial u_l}{\partial x_i} \frac{\partial u_l}{\partial x_k} dx_i dx_k \quad (4.18b)$$

where the mute index i , instead of l , has been used in the second term of the right-hand side of Eq. (4.18b). Consequently, the difference between dS^2 and ds^2 is given by

$$dS^2 - ds^2 = \sum_{ik} e_{ik} dx_i dx_k \quad (4.19)$$

where

$$e_{ik} = \frac{\partial u_i}{\partial x_k} + \frac{\partial u_k}{\partial u_i} + \sum_l \frac{\partial u_l}{\partial x_i} \frac{\partial u_l}{\partial x_k} \quad (4.20)$$

The assembly of values of e_{ik} forms a second-order tensor associated with the coordinates of the point A' . This tensor has the components

$$e_{11} = 2 \frac{\partial u_1}{\partial x_1} + \left(\frac{\partial u_1}{\partial x_1} \right)^2 + \left(\frac{\partial u_2}{\partial x_1} \right)^2 + \left(\frac{\partial u_3}{\partial x_1} \right)^2 \quad (4.21a)$$

$$e_{12} = \frac{\partial u_1}{\partial x_2} + \frac{\partial u_2}{\partial x_1} + \frac{\partial u_1}{\partial x_1} \frac{\partial u_1}{\partial x_2} + \frac{\partial u_2}{\partial x_1} \frac{\partial u_2}{\partial x_2} + \frac{\partial u_3}{\partial x_1} \frac{\partial u_3}{\partial x_2} \quad (4.21b)$$

⋮

It can easily be shown that e_{ij} is a symmetrical tensor, that is $e_{ij} = e_{ji}$. For very small deformations, the partial derivatives $\partial u_i / \partial x_j$ in Eq. (4.21) can be considered infinitesimal quantities of first order, so the components of the e_{ij} tensor can be approximately expressed as

$$e_{ij} = \frac{\partial u_i}{\partial x_j} + \frac{\partial u_j}{\partial x_i} \quad (4.22)$$

The displacement gradient tensor defined as

$$\varepsilon_{ij} = \frac{\partial u_i}{\partial x_j} \quad (4.23)$$

is inconvenient to measure the deformation. Let us analyze, for example, the response of a solid material to the action of a shear stress in the plane x_1x_2 . If a force \mathbf{F} is applied on a thin layer in the direction of axis x_1 , as shown in Figure 4.6a, the layer is displaced parallel to the axis in the amount $(\partial u_1/\partial x_2)dx_2$ in such a way that the deformation is given by

$$\tan \theta \simeq \frac{\partial u_1}{\partial x_2} \quad (4.24)$$

For small displacements, $\tan \theta \approx \theta$. However, if the force acts along the x_2 axis, as indicated in Figure 4.6c, the layers are displaced parallel to the x_2 axis by the amount $(\partial u_2/\partial x_1)dx_1$, and the deformation can be written as

$$\tan \theta \simeq \frac{\partial u_2}{\partial x_1} \quad (4.25)$$

where, as before, $\partial u_1/\partial x_1 = \tan \theta \approx \theta$ for a small deformation. The superposition of the two deformations indicated in Figure 4.6b and 4.6d produces a shear deformation (see Fig. 4.6e) given by

$$2\theta = \frac{\partial u_i}{\partial x_j} + \frac{\partial u_j}{\partial x_i} \quad (4.26)$$

If the force acts in the negative direction of the x_2 axis, as shown in Figure 4.6f, the layers undergo the displacements indicated in Figure 4.6g, so that superposition of the displacements of Figure 4.6b and 4.6g does not produce a deformation but the rotation presented in Figure 4.6h, whose value is

$$2\theta = \frac{\partial u_1}{\partial x_2} - \frac{\partial u_2}{\partial x_1} \quad (4.27)$$

where it has been assumed that the two shears have the same magnitude. From this one infers that the displacement gradient tensor can be separated into the so-called strain tensor, γ_{ij} , and a rotation tensor ω_{ij} , that is,

$$\frac{\partial u_i}{\partial x_j} = \frac{1}{2} \left(\frac{\partial u_i}{\partial x_j} + \frac{\partial u_j}{\partial x_i} \right) + \frac{1}{2} \left(\frac{\partial u_i}{\partial x_j} - \frac{\partial u_j}{\partial x_i} \right) = \gamma_{ij} + \omega_{ij} \quad (4.28)$$

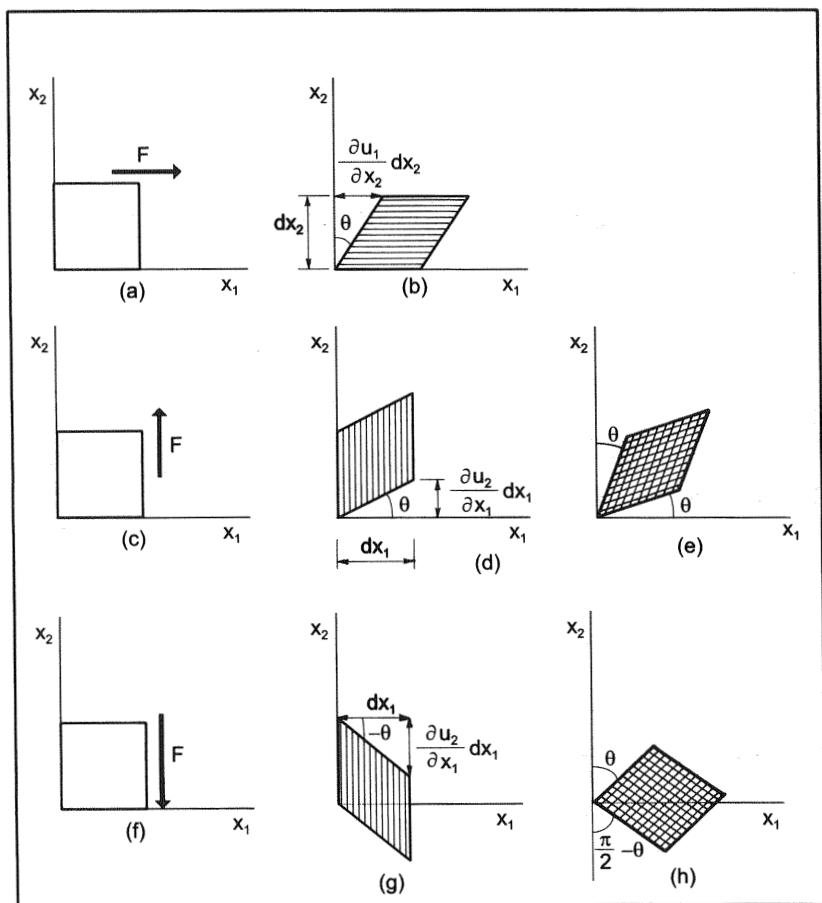


Figure 4.6 Shear forces, showing the shear responses and their superpositions. (See text for details)

where γ_{ij} and ω_{ij} are given by

$$\gamma_{ij} = \frac{1}{2} \left(\frac{\partial u_i}{\partial x_j} + \frac{\partial u_j}{\partial x_i} \right) \quad (4.29a)$$

$$\omega_{ij} = \frac{1}{2} \left(\frac{\partial u_i}{\partial x_j} - \frac{\partial u_j}{\partial x_i} \right) \quad (4.29b)$$

It is obvious that $\gamma_{ij} = \gamma_{ji}$ and $\omega_{ij} = -\omega_{ji}$. In other words, γ_{ij} and ω_{ij} are, respectively, symmetrical and antisymmetrical tensors. The strain tensor can

be written in matrix form, and the off-diagonal components are called shear strains while the components on the main diagonal are called normal strains. The shear strains represent changes in angle, whereas normal strains represents extensions or changes in length per unit length parallel to the coordinate axes.

In the case of a simple shear deformation, schematically indicated in Figure 4.6b, the only nonzero components of the displacement gradient and strain tensors are given by

$$\varepsilon_{12} = \frac{\partial u_1}{\partial x_2} \quad (4.30a)$$

and

$$\gamma_{12} = \frac{1}{2} \frac{\partial u_1}{\partial x_2} \quad (4.30b)$$

where ε_{12} and γ_{12} are the amount of shear and shear strain, respectively. It follows from Eqs. (4.30a) and (4.30b) that

$$\varepsilon_{12} = 2\gamma_{12} \quad (4.30c)$$

4.5 COMPATIBILITY EQUATIONS

Because the six components of the strain tensor are functions of three displacements u_i , they cannot all be independent, for then different portions of the material would share the same coordinate points or there would be voids (gaps), thus violating the continuity of the material. Strictly speaking, the three-dimensional problem is equivalent to determining the compatibility of six equations with three unknown variables (4).

Let us first consider the two-dimensional case. According to Eq. (4.29), the components of the strain are given by

$$\gamma_{11} = \frac{\partial u_1}{\partial x_1}; \quad \gamma_{22} = \frac{\partial u_2}{\partial x_2}; \quad \gamma_{12} = \frac{1}{2} \left(\frac{\partial u_1}{\partial x_2} + \frac{\partial u_2}{\partial x_1} \right) \quad (4.31)$$

By taking derivatives one obtains

$$\frac{\partial^2 \gamma_{11}}{\partial x_2^2} = \frac{\partial^3 u_1}{\partial x_1 \partial x_2^2}; \quad \frac{\partial^2 \gamma_{22}}{\partial x_1^2} = \frac{\partial^3 u_2}{\partial x_2 \partial x_1^2} \quad (4.32a)$$

$$\frac{\partial^2 \gamma_{12}}{\partial x_1 \partial x_2} = \frac{1}{2} \left(\frac{\partial^3 u_1}{\partial x_1 \partial x_2^2} + \frac{\partial^3 u_2}{\partial x_2 \partial x_1^2} \right) \quad (4.32b)$$

Once the derivatives of the displacements are eliminated, the following expression is obtained:

$$2 \frac{\partial^2 \gamma_{12}}{\partial x_1 \partial x_2} = \frac{\partial^2 \gamma_{11}}{\partial x_2^2} + \frac{\partial^2 \gamma_{22}}{\partial x_1^2} \quad (4.33)$$

which is the compatibility equation for the planar strain case. In the three-dimensional situation, the necessary conditions are

$$\frac{\partial^2 \gamma_{11}}{\partial x_2 \partial x_3} = \frac{\partial}{\partial x_1} \left(-\frac{\partial \gamma_{23}}{\partial x_1} + \frac{\partial \gamma_{31}}{\partial x_2} + \frac{\partial \gamma_{12}}{\partial x_3} \right) \quad (4.34a)$$

$$\frac{\partial^2 \gamma_{22}}{\partial x_3 \partial x_1} = \frac{\partial}{\partial x_2} \left(-\frac{\partial \gamma_{31}}{\partial x_2} + \frac{\partial \gamma_{12}}{\partial x_3} + \frac{\partial \gamma_{23}}{\partial x_1} \right) \quad (4.34b)$$

$$\frac{\partial^2 \gamma_{33}}{\partial x_1 \partial x_2} = \frac{\partial}{\partial x_3} \left(-\frac{\partial \gamma_{12}}{\partial x_3} + \frac{\partial \gamma_{23}}{\partial x_1} + \frac{\partial \gamma_{31}}{\partial x_2} \right) \quad (4.34c)$$

and

$$2 \frac{\partial^2 \gamma_{12}}{\partial x_1 \partial x_2} = \frac{\partial^2 \gamma_{11}}{\partial x_2^2} + \frac{\partial^2 \gamma_{22}}{\partial x_1^2} \quad (4.35a)$$

$$2 \frac{\partial^2 \gamma_{23}}{\partial x_2 \partial x_3} = \frac{\partial^2 \gamma_{22}}{\partial x_3^2} + \frac{\partial^2 \gamma_{33}}{\partial x_2^2} \quad (4.35b)$$

$$2 \frac{\partial^2 \gamma_{31}}{\partial x_3 \partial x_1} = \frac{\partial^2 \gamma_{33}}{\partial x_1^2} + \frac{\partial^2 \gamma_{11}}{\partial x_3^2} \quad (4.35c)$$

It can be demonstrated that for simply connected domains these conditions are sufficient.

4.6 EFFECT OF SYMMETRY ON THE RELATIONSHIPS BETWEEN THE STRESS AND STRAIN TENSORS IN IDEAL ELASTIC SYSTEMS

4.6.1 Introduction

A variety of experiments show that for a solid under an infinitesimal deformation, the stress tensor is a linear function of the strain tensor,

$$\sigma_{ij} = C_{ijkl}\gamma_{kl} \quad (4.36)$$

where C_{ijkl} is a modulus tensor of fourth order with 81 components that are material constants. However, not all of the components of the modulus tensor are independent. Thus $C_{ijkl} = C_{jilk}$ because the stress and strain tensors are both symmetrical ($\sigma_{ij} = \sigma_{ji}$, $\gamma_{kl} = \gamma_{kl}$), and consequently the number of independent terms reduces from 81 to 36. In order to proceed with a further reduction of independent terms, it is convenient to analyze the work W carried out in the deformation. This quantity is given by

$$W = \frac{1}{2} C_{\alpha\beta} \gamma_{\alpha} \gamma_{\beta} \quad (4.37)$$

where the reduction of indices $ij = \alpha$ and $kl = \beta$ was made. Any tensor can be written as the sum of symmetrical tensor $A_{\alpha\beta}$ and antisymmetrical tensor $B_{\alpha\beta}$. Accordingly,

$$A_{\alpha\beta} = C_{\alpha\beta} + C_{\beta\alpha}, \quad B_{\alpha\beta} = C_{\alpha\beta} - C_{\beta\alpha} \quad (4.38)$$

Hence one infers that the components of the C tensor can be written in terms of those of A and B as

$$C_{\alpha\beta} = \frac{A_{\alpha\beta} + B_{\alpha\beta}}{2} \quad (4.39)$$

From Eqs. (4.37) and (4.39), the following expression is obtained:

$$W = \frac{1}{2} C_{\alpha\beta} \gamma_{\alpha} \gamma_{\beta} = \frac{1}{4} A_{\alpha\beta} \gamma_{\alpha} \gamma_{\beta} + \frac{1}{4} B_{\alpha\beta} \gamma_{\alpha} \gamma_{\beta} \quad (4.40)$$

By taking into account that $B_{\alpha\beta} = C_{\alpha\beta} - C_{\beta\alpha}$, the second term on the right-hand side of this equation becomes

$$\frac{1}{4} B_{\alpha\beta} \gamma_{\alpha} \gamma_{\beta} = \frac{1}{4} (C_{\alpha\beta} \gamma_{\alpha} \gamma_{\beta} - C_{\beta\alpha} \gamma_{\alpha} \gamma_{\beta}) = 0 \quad (4.41)$$

This expression lets Eq. (4.37) be expressed as

$$W = \frac{1}{2} C_{\alpha\beta} \gamma_{\alpha} \gamma_{\beta} = \frac{1}{4} A_{\alpha\beta} \gamma_{\alpha} \gamma_{\beta} \quad (4.42)$$

Since $A_{\alpha\beta}$ is a symmetrical tensor, this last equation indicates that $C_{\alpha\beta}$ is also symmetrical. Hence, $C_{ijkl} = C_{klij}$, and the number of independent terms is

reduced to 21. It will be shown below that the number of independent terms of C_{ijkl} evolves with increases in the symmetry of the system.

4.6.2 Variation of the Number of Independent Components of the Modulus Tensor C_{ijkl} with the Symmetry of the System

Here only noncrystalline symmetries, which are likely to play an important role in the linear viscoelastic behavior of materials, are considered. We follow Tschoegl's approach to this subject (5). Crystalline materials and their symmetries are described in many textbooks (6,7). In order to study how the symmetry of the system affects the number of independent components of C_{ijkl} , it is convenient to reduce the number of indices of both the stress and strain tensors. Following Voigt's formulation, the reduction is made by doing $11 \rightarrow 1$, $22 \rightarrow 2$, $33 \rightarrow 3$, $12 \rightarrow 4$, $23 \rightarrow 5$, $13 \rightarrow 6$, so that the relation between the stress and the strain tensors can be written in matrix form as

$$\begin{pmatrix} \sigma_1 \\ \sigma_2 \\ \sigma_3 \\ \sigma_4 \\ \sigma_5 \\ \sigma_6 \end{pmatrix} = \begin{pmatrix} C_{11} & C_{12} & C_{13} & C_{14} & C_{15} & C_{16} \\ & C_{22} & C_{23} & C_{24} & C_{25} & C_{26} \\ & & C_{33} & C_{34} & C_{35} & C_{36} \\ & & & C_{44} & C_{45} & C_{46} \\ & & & & C_{55} & C_{56} \\ & & & & & C_{66} \end{pmatrix} \begin{pmatrix} \gamma_1 \\ \gamma_2 \\ \gamma_3 \\ \gamma_4 \\ \gamma_5 \\ \gamma_6 \end{pmatrix} \quad (4.43)$$

For reasons that will become clear later, it is convenient to write Eq. (4.43) as

$$\begin{aligned} \sigma_1 &= C_{11}\gamma_1 + C_{12}\gamma_2 + C_{13}\gamma_3 + C_{14}\gamma_4 + C_{15}\gamma_5 + C_{16}\gamma_6 \\ \sigma_2 &= \dots + C_{22}\gamma_2 + C_{23}\gamma_3 + C_{24}\gamma_4 + C_{25}\gamma_5 + C_{26}\gamma_6 \\ \sigma_3 &= \dots + C_{33}\gamma_3 + C_{34}\gamma_4 + C_{35}\gamma_5 + C_{36}\gamma_6 \\ \sigma_4 &= \dots + C_{44}\gamma_4 + C_{45}\gamma_5 + C_{46}\gamma_6 \\ \sigma_5 &= \dots + C_{55}\gamma_5 + C_{56}\gamma_6 \\ \sigma_6 &= \dots + C_{66}\gamma_6 \end{aligned} \quad (4.44)$$

Let us analyze a material having a plane of symmetry defined by the coordinates axes x_2, x_3 , as shown in Figure 4.7. The components of the stress

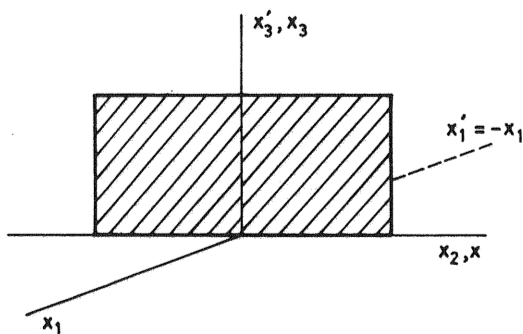


Figure 4.7 Single plane of symmetry.

tensor in a change of reference frame, for example, from $x_1x_2x_3$ to $x'_1x'_2x'_3$, are given by

$$\sigma'_{ij} = \sum_{kl} \frac{\partial x'_i}{\partial x_k} \frac{\partial x'_j}{\partial x_l} \sigma_{kl} = \sum_{kl} a_{ik} a_{jl} \sigma_{kl} \quad (4.45)$$

Taking into account the symmetry of the system, the matrix of director cosines is

$$a_{ik} = a_{jl} = \begin{pmatrix} -1 & 0 & 0 \\ 0 & 1 & 0 \\ 0 & 0 & 1 \end{pmatrix} \quad (4.46)$$

where all the elements of the matrix except those of the diagonal are zero. Accordingly,

$$\begin{aligned} \sigma'_{11} &= a_{11}a_{11}\sigma_{11} = \sigma_{11} \\ \sigma'_{22} &= a_{22}a_{22}\sigma_{22} = \sigma_{22} \\ \sigma'_{33} &= a_{33}a_{33}\sigma_{33} = \sigma_{33} \\ \sigma'_{12} &= a_{11}a_{22}\sigma_{12} = -\sigma_{12} \\ \sigma'_{23} &= a_{22}a_{33}\sigma_{23} = \sigma_{23} \\ \sigma'_{13} &= a_{11}a_{33}\sigma_{13} = -\sigma_{13} \end{aligned} \quad (4.47)$$

The same arguments as those used for the strain tensor lead to

$$\begin{aligned}
 \gamma'_{11} &= a_{11}a_{11}\gamma_{11} = \gamma_{11} \\
 \gamma'_{22} &= a_{22}a_{22}\gamma_{22} = \gamma_{22} \\
 \gamma'_{33} &= a_{33}a_{33}\gamma_{33} = \gamma_{33} \\
 \gamma'_{12} &= a_{11}a_{22}\gamma_{12} = -\gamma_{12} \\
 \gamma'_{23} &= a_{22}a_{33}\gamma_{23} = \gamma_{23} \\
 \gamma'_{13} &= a_{11}a_{33}\gamma_{13} = -\gamma_{13}
 \end{aligned} \tag{4.48}$$

Consequently, the relation between the stress tensor and the strain tensor in the reference frame $x_1x_2x_3$ is given by

$$\begin{pmatrix} \sigma_1 \\ \sigma_2 \\ \sigma_3 \\ -\sigma_4 \\ \sigma_5 \\ -\sigma_6 \end{pmatrix} = \begin{pmatrix} C_{11} & C_{12} & C_{13} & C_{14} & C_{15} & C_{16} \\ & C_{22} & C_{23} & C_{24} & C_{25} & C_{26} \\ & & C_{33} & C_{34} & C_{35} & C_{36} \\ & & & C_{44} & C_{45} & C_{46} \\ & & & & C_{55} & C_{56} \\ & & & & & C_{66} \end{pmatrix} \begin{pmatrix} \gamma_1 \\ \gamma_2 \\ \gamma_3 \\ -\gamma_4 \\ \gamma_5 \\ -\gamma_6 \end{pmatrix} \tag{4.49}$$

where the terms of the tensors σ' and γ' have been substituted by those of σ and γ , as indicated in Eqs. (4.47) and (4.48). From Eq. (4.49) one obtains

$$\begin{aligned}
 \sigma_1 &= C_{11}\gamma_1 + C_{12}\gamma_2 + C_{13}\gamma_3 + C_{14}\gamma_4 + C_{15}\gamma_5 + C_{16}\gamma_6 \\
 \sigma_2 &= \dots + C_{22}\gamma_2 + C_{23}\gamma_3 + C_{24}\gamma_4 + C_{25}\gamma_5 + C_{26}\gamma_6 \\
 \sigma_3 &= \dots + C_{33}\gamma_3 + C_{34}\gamma_4 + C_{35}\gamma_5 + C_{36}\gamma_6 \\
 \sigma_4 &= \dots + C_{44}\gamma_4 + C_{45}\gamma_5 + C_{46}\gamma_6 \\
 \sigma_5 &= \dots + C_{55}\gamma_5 + C_{56}\gamma_6 \\
 \sigma_6 &= \dots + C_{66}\gamma_6
 \end{aligned} \tag{4.50}$$

Comparison of Eqs. (4.44) and (4.50) indicates that $C_{14} = C_{16} = C_{24} = C_{26} = C_{34} = C_{36} = C_{45} = C_{56} = 0$, as a consequence of the invariance of the stress and strain tensors in the change of reference frame. Therefore the 21 independent components of the tensor C_{ijkl} are reduced to 13 when the solid has one plane of symmetry, and the relation between the stress and strain tensors can be written as

$$\begin{pmatrix} \sigma_1 \\ \sigma_2 \\ \sigma_3 \\ \sigma_4 \\ \sigma_5 \\ \sigma_6 \end{pmatrix} = \begin{pmatrix} C_{11} & C_{12} & C_{13} & 0 & C_{15} & 0 \\ & C_{22} & C_{23} & 0 & C_{25} & 0 \\ & & C_{33} & 0 & C_{35} & 0 \\ & & & C_{44} & 0 & C_{46} \\ & & & & C_{55} & 0 \\ & & & & & C_{66} \end{pmatrix} \begin{pmatrix} \gamma_1 \\ \gamma_2 \\ \gamma_3 \\ \gamma_4 \\ \gamma_5 \\ \gamma_6 \end{pmatrix} \quad (4.51)$$

If the degree of symmetry increases—for example, if the solid has an additional plane of symmetry defined by the axes x_2 and x_1 —the matrix of director cosines will be

$$a_{ik} = \begin{pmatrix} 1 & 0 & 0 \\ 0 & 1 & 0 \\ 0 & 0 & -1 \end{pmatrix} \quad (4.52)$$

Proceeding in the same way as above, the terms C_{15} , C_{25} , C_{35} , and C_{46} are found to be zero, and the number of independent components of C_{ijkl} decreases from 13 to 9. For a system with two planes of symmetry, the following relationship holds:

$$\begin{pmatrix} \sigma_1 \\ \sigma_2 \\ \sigma_3 \\ \sigma_4 \\ \sigma_5 \\ \sigma_6 \end{pmatrix} = \begin{pmatrix} C_{11} & C_{12} & C_{13} & 0 & 0 & 0 \\ & C_{22} & C_{23} & 0 & 0 & 0 \\ & & C_{33} & 0 & 0 & 0 \\ & & & C_{44} & 0 & 0 \\ & & & & C_{55} & 0 \\ & & & & & C_{66} \end{pmatrix} \begin{pmatrix} \gamma_1 \\ \gamma_2 \\ \gamma_3 \\ \gamma_4 \\ \gamma_5 \\ \gamma_6 \end{pmatrix} \quad (4.53)$$

This expression can be written in explicit form as

$$\begin{aligned} \sigma_1 &= C_{11}\gamma_1 + C_{12}\gamma_2 + C_{13}\gamma_3 \\ \sigma_2 &= \dots + C_{22}\gamma_2 + C_{23}\gamma_3 \\ \sigma_3 &= \dots + C_{33}\gamma_3 \\ \sigma_4 &= C_{44}\gamma_4 \\ \sigma_5 &= C_{55}\gamma_5 \\ \sigma_6 &= C_{66}\gamma_6 \end{aligned} \quad (4.54)$$

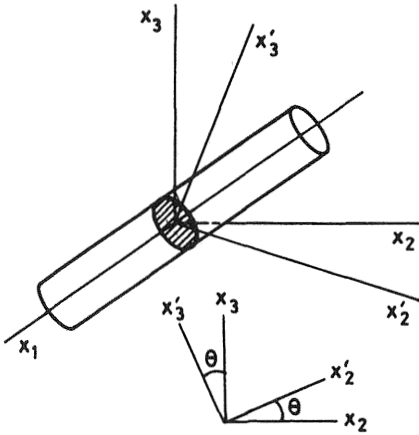


Figure 4.8 Plane and axis of symmetry.

If the system also has cylindrical symmetry as shown in Figure 4.8, where the symmetry axis is x_1 the matrix of director cosines is

$$[a_{ij}] = \begin{pmatrix} 1 & 0 & 0 \\ 0 & \cos \theta & \sin \theta \\ 0 & -\sin \theta & \cos \theta \end{pmatrix} \quad (4.55)$$

Because $\sigma'_{ij} = \sum_{kl} a_{ik} a_{jl} \sigma_{kl}$ and $\gamma'_{ij} = \sum_{kl} a_{ik} a_{jl} \gamma_{kl}$, the terms σ_{11} , σ_{12} , γ_{11} , and γ_{12} can be written as

$$\sigma'_{11} = \sum_{kl} a_{1k} a_{1l} \sigma_{kl} = a_{11} a_{11} \sigma_{11} = \sigma_{11} \quad (4.56a)$$

$$\sigma'_{12} = \sum_{kl} a_{1k} a_{2l} \sigma_{kl} = a_{11} a_{12} \sigma_{12} + a_{11} a_{23} \sigma_{13} = \sigma_{12} \cos \theta + \sigma_{13} \sin \theta \quad (4.56b)$$

$$\gamma'_{11} = \sum_{kl} a_{1k} a_{1l} \gamma_{kl} = a_{11} a_{11} \gamma_{11} = \gamma_{11} \quad (4.56c)$$

$$\gamma'_{12} = \sum_{kl} a_{1k} a_{2l} \gamma_{kl} = a_{11} a_{12} \gamma_{12} + a_{11} a_{13} \gamma_{13} = \gamma'_{12} \cos \theta + \gamma_{13} \sin \theta \quad (4.56d)$$

and so on. By using the Voigt notation, the components of the stress and strain tensors in the x'_1, x'_2, x'_3 reference frame are given by

$$[\sigma'_k] = \begin{pmatrix} \sigma_1 \\ \sigma_2 \cos^2 \theta + \sigma_3 \sin^2 \theta + 2\sigma_5 \sin \theta \cos \theta \\ \sigma_4 \cos \theta + \sigma_6 \sin \theta \\ \sigma_5(\cos^2 \theta - \sin^2 \theta) + (\sigma_3 - \sigma_2) \sin \theta \cos \theta \\ \sigma_6 \cos \theta - \sigma_4 \sin \theta \end{pmatrix} \quad (4.57)$$

and

$$[\gamma'_k] = \begin{pmatrix} \gamma_1 \\ \gamma_2 \cos^2 \theta + \gamma_3 \sin^2 \theta + 2\gamma_5 \sin \theta \cos \theta \\ \gamma_4 \cos \theta + \gamma_6 \sin \theta \\ \gamma_5(\cos^2 \theta - \sin^2 \theta) + (\gamma_3 - \sigma_2) \sin \theta \cos \theta \\ \gamma_6 \cos \theta - \gamma_4 \sin \theta \end{pmatrix} \quad (4.58)$$

Owing to the symmetry of the system, Eqs. (4.57) and (4.58) must hold for any angle of rotation about the x_1 axis, so for $\theta = 90^\circ$ these equations become

$$[\sigma'_k] = \begin{pmatrix} \sigma_1 \\ \sigma_3 \\ \sigma_2 \\ \sigma_6 \\ -\sigma_5 \\ -\sigma_4 \end{pmatrix}; \quad [\gamma'_k] = \begin{pmatrix} \gamma_1 \\ \gamma_3 \\ \gamma_2 \\ \gamma_6 \\ -\gamma_5 \\ -\gamma_4 \end{pmatrix} \quad (4.59)$$

In this case the relationship between the stress and strain tensors in the reference frame of the coordinate axes x'_1, x'_2, x'_3 is given by

$$\begin{pmatrix} \sigma_1 \\ \sigma_3 \\ \sigma_2 \\ \sigma_6 \\ -\sigma_5 \\ -\sigma_4 \end{pmatrix} = \begin{pmatrix} C_{11} & C_{12} & C_{13} & 0 & 0 & 0 \\ & C_{22} & C_{23} & 0 & 0 & 0 \\ & & C_{33} & 0 & 0 & 0 \\ & & & C_{44} & 0 & 0 \\ & & & & C_{55} & 0 \\ & & & & & C_{66} \end{pmatrix} \begin{pmatrix} \gamma_1 \\ \gamma_3 \\ \gamma_2 \\ \gamma_6 \\ -\gamma_5 \\ -\gamma_4 \end{pmatrix} \quad (4.60)$$

This relationship can be written as

$$\begin{aligned}
 \sigma_1 &= C_{11}\gamma_1 + C_{12}\gamma_3 + C_{13}\gamma_2 \\
 \sigma_3 &= \dots + C_{22}\gamma_3 + C_{23}\gamma_2 \\
 \sigma_2 &= \dots + C_{33}\gamma_2 \\
 \sigma_6 &= C_{44}\gamma_6 \\
 \sigma_5 &= C_{55}\gamma_5 \\
 \sigma_4 &= C_{66}\gamma_4
 \end{aligned} \tag{4.61}$$

By comparing Eqs. (4.54) and (4.61) and taking into account the invariance of the components of the stress and strain tensors in an operation of symmetry, one obtains

$$C_{33} = C_{22}, \quad C_{13} = C_{12}, \quad C_{66} = C_{44} \tag{4.62}$$

Consequently, the number of independent components of C_{ijkl} in a system with cylindrical symmetry is six. In this case, the relation between the stress and strain tensors can be written as

$$\begin{pmatrix} \sigma_1 \\ \sigma_2 \\ \sigma_3 \\ \sigma_4 \\ \sigma_5 \\ \sigma_6 \end{pmatrix} = \begin{pmatrix} C_{11} & C_{12} & C_{12} & 0 & 0 & 0 \\ & C_{22} & C_{23} & 0 & 0 & 0 \\ & & C_{22} & 0 & 0 & 0 \\ & & & C_{44} & 0 & 0 \\ & & & & C_{55} & 0 \\ & & & & & C_{44} \end{pmatrix} \begin{pmatrix} \gamma_1 \\ \gamma_2 \\ \gamma_3 \\ \gamma_4 \\ \gamma_5 \\ \gamma_6 \end{pmatrix} \tag{4.60}$$

A system with an additional axis of symmetry, for example x_3 , is isotropic. The components of the stress tensor in the system of coordinates x'_1, x'_2, x'_3 can be obtained from those in the reference frame of the coordinate system x_1, x_2, x_3 by means of the following cosine directors:

$$a_{ik} = \begin{pmatrix} \cos \theta & \sin \theta & 0 \\ -\sin \theta & \cos \theta & 0 \\ 0 & 0 & 1 \end{pmatrix} \tag{4.64}$$

By performing the pertinent operations, the components of σ'_{ij} and γ'_{ij} are found to be

$$[\sigma'_k] = \begin{pmatrix} \sigma_1 \cos^2 \theta + \sigma_2 \sin^2 \theta + 2\sigma_4 \sin \theta \cos \theta \\ \sigma_1 \sin^2 \theta + \sigma_2 \cos^2 \theta - 2\sigma_4 \sin \theta \cos \theta \\ \sigma_3 \\ (\sigma_2 - \sigma_1) \sin \theta \cos \theta + \sigma_4(\cos^2 \theta - \sin^2 \theta) \\ \sigma_5 \cos \theta - \sigma_6 \sin \theta \\ \sigma_5 \sin \theta + \sigma_6 \cos \theta \end{pmatrix} \quad (4.65)$$

and

$$[\gamma'_k] = \begin{pmatrix} \gamma_1 \cos^2 \theta + \gamma_2 \sin^2 \theta + 2\gamma_4 \sin \theta \cos \theta \\ \gamma_1 \sin^2 \theta + \gamma_2 \cos^2 \theta - 2\gamma_4 \sin \theta \cos \theta \\ \gamma_3 \\ (\gamma_2 - \gamma_1) \sin \theta \cos \theta + \gamma_4(\cos^2 \theta - \sin^2 \theta) \\ \gamma_5 \cos \theta - \gamma_6 \sin \theta \\ \gamma_5 \sin \theta + \gamma_6 \cos \theta \end{pmatrix} \quad (4.66)$$

For $\theta = 90^\circ$, the relation between σ'_k and γ'_k can be written as

$$\begin{pmatrix} \sigma_2 \\ \sigma_1 \\ \sigma_3 \\ -\sigma_4 \\ -\sigma_6 \\ \sigma_5 \end{pmatrix} = \begin{pmatrix} C_{11} & C_{12} & C_{12} & 0 & 0 & 0 \\ & C_{22} & C_{23} & 0 & 0 & 0 \\ & & C_{22} & 0 & 0 & 0 \\ & & & C_{44} & 0 & 0 \\ & & & & C_{55} & 0 \\ & & & & & C_{44} \end{pmatrix} \begin{pmatrix} \gamma_2 \\ \gamma_1 \\ \gamma_3 \\ -\gamma_4 \\ -\gamma_6 \\ \gamma_5 \end{pmatrix} \quad (4.67)$$

By comparing Eqs. (4.63) and (4.67) and taking into account the invariance of the components of a tensor in an operation of symmetry, one obtains

$$C_{23} = C_{12}, \quad C_{44} = C_{55}, \quad C_{22} = C_{11} \quad (4.68)$$

In this case, C_{ijkl} has three independent components, and the relation between the stress and strain tensors is given by

$$\begin{pmatrix} \sigma_1 \\ \sigma_2 \\ \sigma_3 \\ \sigma_4 \\ \sigma_5 \\ \sigma_6 \end{pmatrix} = \begin{pmatrix} C_{11} & C_{12} & C_{12} & 0 & 0 & 0 \\ & C_{11} & C_{12} & 0 & 0 & 0 \\ & & C_{11} & 0 & 0 & 0 \\ & & & C_{44} & 0 & 0 \\ & & & & C_{44} & 0 \\ & & & & & C_{44} \end{pmatrix} \begin{pmatrix} \gamma_1 \\ \gamma_2 \\ \gamma_3 \\ \gamma_4 \\ \gamma_5 \\ \gamma_6 \end{pmatrix} \quad (4.69)$$

However, an additional reduction can still be made. By substituting the values given for σ_{44} and γ_{44} in Eqs. (4.65) and (4.66) into the expression $\sigma'_4 = C_{44}\gamma'_4$, one obtains

$$(\sigma_2 - \sigma_1) \sin \theta \cos \theta \sigma_4 (\cos^2 \theta - \sin^2 \theta) = C_{44}[(\gamma_2 - \gamma_1) \sin \theta \cos \theta + \gamma_4 (\cos^2 \theta - \sin^2 \theta)] \quad (4.70)$$

On the other hand, the difference $\sigma_2 - \sigma_1$, directly obtained from Eq. (4.69), can be substituted into Eq. (4.70), giving

$$(C_{11} - C_{12})(\gamma_2 - \gamma_1) \sin \theta \cos \theta + \sigma_4 (\cos^2 \theta - \sin^2 \theta) = C_{44}[(\gamma_2 - \gamma_1) \sin \theta \cos \theta + \gamma_4 (\cos^2 \theta - \sin^2 \theta)] \quad (4.71)$$

By equating the terms containing the factors $(\gamma_2 - \gamma_1) (\sin \theta \cos \theta)$ on the left- and right-hand sides of Eq. (4.71), the following expression is obtained:

$$C_{44} = C_{11} - C_{12} \quad (4.72)$$

Therefore, for isotropic solids C_{ijkl} has only two independent components: C_{11} and C_{12} .

4.7 GENERALIZED STRESS-STRAIN HOOKE'S LAW FOR ISOTROPIC SOLIDS

4.7.1 Introduction

The components of the modulus tensor C_{ij} have traditionally been expressed in terms of the Lamé constants λ and G . Specifically,

$$C_{11} = \lambda + 2G, \quad C_{12} = \lambda, \quad C_{44} = C_{11} - C_{22} = 2G \quad (4.73)$$

Then the relation between the stress and strain tensors is given by the classical expression

$$\begin{pmatrix} \sigma_1 \\ \sigma_2 \\ \sigma_3 \\ \sigma_4 \\ \sigma_5 \\ \sigma_6 \end{pmatrix} = \begin{pmatrix} \lambda + 2G & \lambda & \lambda & 0 & 0 & 0 \\ & \lambda + 2G & \lambda & 0 & 0 & 0 \\ & & \lambda + 2G & 0 & 0 & 0 \\ & & & 2G & 0 & 0 \\ & & & & 2G & 0 \\ & & & & & 2G \end{pmatrix} \begin{pmatrix} \gamma_1 \\ \gamma_2 \\ \gamma_3 \\ \gamma_4 \\ \gamma_5 \\ \gamma_6 \end{pmatrix} \tag{4.74}$$

or in simplified form by

$$\sigma_{ij} = \lambda \Delta \delta_{ij} + 2G \gamma_{ij} \tag{4.75}$$

where

$$\Delta = \text{trace } \gamma_{ij} = \gamma_{11} + \gamma_{22} + \gamma_{33} \tag{4.76}$$

and δ_{ij} is the Kröner symbol whose value is 1 for $i = j$ and 0 otherwise. Equation (4.75) is known as the generalized constitutive equation of elasticity for isotropic solids. The physical meaning of Δ can easily be deduced by considering a prismatic solid whose edge lengths are L_{01} , L_{02} , and L_{03} . Let us assume that after application of an external force the lengths of the edges become L_1 , L_2 , L_3 . For very small deformations, the components of the strain tensor are given by

$$\gamma_{ii} = \frac{L_i - L_{0i}}{L_{0i}}, \quad i = 1, 2, 3 \tag{4.77}$$

Then the ratio between the volume of the deformed body (V) and that of the undeformed one (V_0) can be written as

$$\begin{aligned} \frac{V}{V_0} &= \left(\frac{L_1}{L_{01}}\right) \left(\frac{L_2}{L_{02}}\right) \left(\frac{L_3}{L_{03}}\right) \\ &= (1 + \gamma_{11})(1 + \gamma_{22})(1 + \gamma_{33}) \simeq 1 + \text{trace } \gamma_{ij} \end{aligned} \tag{4.78}$$

where the nonlinear terms in γ_{ij} have been neglected. Hence

$$\text{trace } \gamma_{ij} = \Delta = \frac{\Delta V}{V_0} \tag{4.79}$$

Obviously, Δ represents the dilatation (or contraction) undergone by an isotropic body because of the action of an external force. It is convenient

to express the strain tensor γ_{ij} as the sum of a dilatational tensor (γ_{ij}^{Δ}) and a deviatoric tensor (γ_{ij}^d)

$$\gamma_{ij} = \gamma_{ij}^{\Delta} + \gamma_{ij}^d \quad (4.80)$$

where

$$\gamma_{ij}^{\Delta} = \frac{1}{3} \text{diag} (\Delta, \Delta, \Delta) = \frac{\Delta \delta_{ij}}{3} \quad (4.81)$$

and

$$\gamma_{ij}^d = \gamma_{ij} - \gamma_{ij}^{\Delta} = \begin{pmatrix} \gamma_{11} - \frac{\Delta}{3} & \gamma_{12} & \gamma_{13} \\ & \gamma_{22} - \frac{\Delta}{3} & \gamma_{23} \\ & & \gamma_{33} - \frac{\Delta}{3} \end{pmatrix} \quad (4.82)$$

If the strain tensor in the generalized constitutive equation of elasticity is expressed in terms of γ_{ij}^{Δ} and γ_{ij}^d , then Eq. (4.75) becomes

$$\sigma_{ij} = \left(\lambda + \frac{2}{3} G \right) \Delta \delta_{ij} + 2G \gamma_{ij}^d = K \Delta \delta_{ij} + 2G \gamma_{ij}^d \quad (4.83)$$

where the K parameter, defined as

$$K = \lambda + \frac{2}{3} G \quad (4.84)$$

is called the bulk relaxation modulus. By substituting the value of λ given in Eq. (4.84) into Eq. (4.75), the generalized equation of elasticity as a function of the measurable quantities K and G is obtained. This expression is given by

$$\sigma_{ij} = \left(K - \frac{2}{3} G \right) \Delta \delta_{ij} + 2G \gamma_{ij} \quad (4.85)$$

In analogy with the strain, it is possible to express the stress tensor as the sum of a dilatational component, σ^{Σ} , and a deviatoric component, σ^d , that is,

$$\sigma_{ij} = \sigma_{ij}^{\Sigma} + \sigma_{ij}^d \quad (4.86)$$

Here σ_{ij}^{Σ} and σ_{ij}^d are given by

$$\sigma_{ij}^{\Sigma} = \frac{1}{3} \text{diag} (\Sigma, \Sigma, \Sigma) = \frac{\Sigma}{3} \delta_{ij} \quad (4.87)$$

where

$$\Sigma = \sigma_{11} + \sigma_{22} + \sigma_{33} = \text{trace } \sigma_{ij} \quad (4.88)$$

and

$$\sigma_{ij}^d = \sigma_{ij} - \sigma_{ij}^{\Sigma} = \begin{pmatrix} \sigma_{11} - \frac{\Sigma}{3} & \sigma_{12} & \sigma_{13} \\ & \sigma_{22} - \frac{\Sigma}{3} & \sigma_{23} \\ & & \sigma_{33} - \frac{\Sigma}{3} \end{pmatrix} \quad (4.89)$$

By combining Eqs. (4.83), (4.80), (4.81), and (4.86), the following expressions are obtained:

$$\sigma_{ij}^{\Sigma} = K \Delta \delta_{ij} = 3K \gamma_{ij}^{\Delta} \quad (4.90a)$$

$$\sigma_{ij}^d = 2G \gamma_{ij}^d \quad (4.90b)$$

which combine the dilatational and deviatoric stress tensors with the corresponding strain tensors. It is obvious that for the strain and stress deviator tensors the following relationships hold:

$$\text{trace } \gamma_{ij}^d = 0, \quad \text{trace } \sigma_{ij}^d = 0 \quad (4.91)$$

4.7.2 Relations Between Elastic Parameters

When an elastic body is under the effect of a hydrostatic pressure, both the strain and stress deviatoric tensors are zero. Owing to the fact that in this case $\gamma_{11} = \gamma_{22} = \gamma_{33}$ and $\sigma_{11} = \sigma_{22} = \sigma_{33}$, Eq. (4.85) becomes

$$\sigma_{ii} = -p = K \Delta \quad (4.92)$$

where p is an arbitrary isotropic pressure. Because $\Delta = (V - V_0)/V_0$, the measurement of the diminution of volume by action of a known hydrostatic pressure allows the experimental determination of the bulk relaxation modulus. In the same way, Eq. (4.85) indicates that the ratio between the shear stress and shear strain (for example σ_{12}/γ_{12}) gives the experimental shear relaxation modulus G . It is worth noting that when $K \gg G$, the combination

of Eqs. (4.85) and (4.92) leads to the generalized Hooke's law for an incompressible material,

$$\sigma_{ij} = -p\delta_{ij} + 2G\gamma_{ij} \quad (4.93a)$$

Equation (4.93a) indicates that the stress is defined only within an arbitrary isotropic pressure.

If an elastic body is under the effect of a force parallel to one of the coordinate axes, for example along the x_1 axis, the stress tensor has a single component. The stress and strain tensors can be written in the form

$$\sigma_{ij} = \begin{pmatrix} \sigma_{11} & 0 & 0 \\ 0 & 0 & 0 \\ 0 & 0 & 0 \end{pmatrix}; \quad \gamma_{ij} = \begin{pmatrix} \gamma_{11} & 0 & 0 \\ 0 & \gamma_{22} & 0 \\ 0 & 0 & \gamma_{33} \end{pmatrix} \quad (4.93b)$$

where for an isotropic system $\gamma_{22} = \gamma_{33}$. From Eq. (4.75) one obtains

$$\sigma_{11} = \lambda(\gamma_{11} + 2\gamma_{22}) + 2G\gamma_{11} \quad (4.94a)$$

$$\sigma_{22} = 0 = \lambda(\gamma_{11} + 2\gamma_{22}) + 2G\gamma_{22} \quad (4.94b)$$

The solution of these equations, in conjunction with the fact that $\lambda = K - (2/3)G$ [Eq. (4.84)], lead to the expression

$$E = \frac{\sigma_{11}}{\gamma_{11}} = \frac{9KG}{3K + G} \quad (4.95)$$

which relates the tensile relaxation modulus to the shear relaxation modulus, G . According to Eq. (4.95), $E \cong 3G$ if $K \gg G$.

The ratio between the components of the diagonal of the strain tensor, called Poisson's ratio, is easily obtained from Eqs. (4.84) and (4.94), giving

$$\nu = -\frac{\gamma_{22}}{\gamma_{11}} = -\frac{\gamma_{33}}{\gamma_{11}} = \frac{3K - 2G}{6K + 2G} \quad (4.96)$$

According to this equation, Poisson's ratio is $1/2$ when $K \gg G$.

Let us analyze the response of a material when it is compressed or expands in a single direction, for example along the x_1 axis, and deformations along the x_2 and x_3 axes are not permitted. This situation occurs when a material is compressed in a cylinder or when an acoustic wave propagates through the material. In these conditions, the stress and strain tensors can be written as

$$\sigma_{ij} = \begin{pmatrix} \sigma_{11} & & \\ & \sigma_{22} & \\ & & \sigma_{22} \end{pmatrix}; \quad \gamma_{ij} = \begin{pmatrix} \gamma_{11} & 0 & 0 \\ 0 & 0 & 0 \\ 0 & 0 & 0 \end{pmatrix} \quad (4.97)$$

From Eq. (4.85), one obtains

$$\sigma_{11} = \left(K - \frac{2}{3}G\right)\gamma_{11} + 2G\gamma_{11} = \left(K + \frac{4}{3}G\right)\gamma_{11} \quad (4.98)$$

Consequently, the acoustic mode is given by the expression

$$M = \frac{\sigma_{11}}{\gamma_{11}} = K + \frac{4}{3}G \quad (4.99)$$

On the other hand, Eq. (4.85) shows that $\sigma_{22} = [K - (2/3)G]\gamma_{11}$, so that the ratio σ_{22}/σ_{11} is given by

$$\frac{\sigma_{22}}{\sigma_{11}} = \frac{3K - 2G}{3K + 4G} \quad (4.100)$$

When $K \gg G$, then $\sigma_{11} = \sigma_{22} = \sigma_{33} = -p$, that is, each point of the system is under the hydrostatic pressure $-p$.

From the foregoing, one infers that the state of an ideal elastic material under small deformations is totally defined once two of the four parameters E , G , K , and ν are known. The relations between the elastic parameters can be obtained from the expressions indicated above. The pertinent relations are given in Table 4.1 (5).

4.8 NAVIER EQUATIONS

For many purposes it is convenient to express the equilibrium equations in terms of the displacements. In the absence of body forces and inertial terms, Eq. (4.14) can be written as

$$\frac{\partial \sigma_{ij}}{\partial x_j} = 0 \quad (4.101)$$

The relationship between stress and strain in terms of the tensile modulus and the Poisson ratio is given by

Table 4.1 Relationships Between Elastic Parameters^a

	G and E	G and ν	K and E	K and ν	K and G	E and ν
K	$EG/(9G - 3E)$	$2G(1 + \nu)/3(1 - 2\nu)$				$E/3(1 - 2\nu)$
G			$3KE/(9K - E)$	$3K(1 - 2\nu)/2(\nu + 1)$		$E/2(\nu + 1)$
E		$2G(1 + \nu)$		$3K(1 - 2\nu)$	$9KG/(3K + G)$	
ν	$(E/2G) - 1$		$1/2 - E/6K$		$(\frac{2}{3}K - G)/(3K + G)$	

^aIn the International System, the units of G , E , and K are N/m^2 ; ν is dimensionless.

Source: Ref. 5.

$$\sigma_{ij} = \frac{E}{1+\nu} \left(\gamma_{ij} + \frac{\nu}{1-2\nu} \gamma_{kk} \delta_{ij} \right) \quad (4.102)$$

This equation can be obtained from Eq.(4.85) and the expressions of Table 4.1 that relate K and G to E and ν . By substituting Eq.(4.102) into Eq.(4.101), one obtains

$$\frac{E}{1+\nu} \frac{\partial \gamma_{ij}}{\partial x_j} + \frac{E\nu}{(1+\nu)(1-2\nu)} \frac{\partial \gamma_{kk}}{\partial x_j} = 0 \quad (4.103)$$

Expressing the tensor strain in terms of the components of the vector displacement, Eq. (4.103) becomes

$$\frac{E\nu}{(1+\nu)(1-2\nu)} \frac{\partial^2 u_k}{\partial x_i \partial x_k} + \frac{E}{2(1+\nu)} \left[\frac{\partial^2 u_i}{\partial x_j^2} + \frac{\partial^2 u_j}{\partial x_j \partial x_i} \right] = 0 \quad (4.104)$$

which after an appropriate change of notation of some of the subscripts can be written as

$$\frac{\partial^2 u_i}{\partial x_j^2} + \frac{1}{1-2\nu} \frac{\partial^2 u_k}{\partial x_i \partial x_j} = 0 \quad (4.105)$$

Equation (4.105) can be expressed in a more compact form as

$$\Delta \mathbf{u} + \frac{1}{1-2\nu} \nabla \operatorname{div} \mathbf{u} = 0 \quad (4.106)$$

This expression is known as the Navier equation. It should be noted that since

$$\Delta \mathbf{u} = \nabla \operatorname{div} \mathbf{u} - \operatorname{rot} \operatorname{rot} \mathbf{u} \quad (4.107)$$

the Navier equation can also be written as

$$2(1-\nu) \nabla \operatorname{div} \mathbf{u} = (1-2\nu) \operatorname{rot} \operatorname{rot} \mathbf{u} \quad (4.108)$$

Finally, it is worth noting that taking the divergence and Laplacian in Eq. (4.108) one finds

$$\begin{aligned} \Delta \operatorname{div} \mathbf{u} &= 0 & (\operatorname{div} \mathbf{u} \text{ is harmonic}) \\ \Delta \Delta \mathbf{u} &= 0 & (\mathbf{u} \text{ is biharmonic}) \end{aligned} \quad (4.109)$$

It should be pointed out that the external forces should appear in the solution of these equations through the boundary conditions.

4.9 GENERALIZED STRAIN-STRESS RELATIONSHIPS FOR IDEAL ELASTIC SYSTEMS

4.9.1 Introduction

When a solid elastic body is under the action of an infinitesimal contact force, the strain tensor is related to the stress tensor by the expression

$$\gamma_{ij} = \sum_{kl} R_{ijkl} \sigma_{kl} \quad (4.110)$$

where R_{ijkl} is the compliance tensor with two independent components. By using the Voigt notation, Eq. (4.110) can be written as

$$\begin{pmatrix} \gamma_1 \\ \gamma_2 \\ \gamma_3 \\ \gamma_4 \\ \gamma_5 \\ \gamma_6 \end{pmatrix} = \begin{pmatrix} R_{11} & R_{12} & R_{12} & 0 & 0 & 0 \\ & R_{11} & R_{12} & 0 & 0 & 0 \\ & & R_{12} & 0 & 0 & 0 \\ & & & R_{44} & 0 & 0 \\ & & & & R_{44} & 0 \\ & & & & & R_{44} \end{pmatrix} \begin{pmatrix} \sigma_1 \\ \sigma_2 \\ \sigma_3 \\ \sigma_4 \\ \sigma_5 \\ \sigma_6 \end{pmatrix} \quad (4.111)$$

From the relation $\sigma_j = C_{jk} \gamma_k$, one obtains

$$\gamma_i = (C_{ij})^{-1} \sigma_j = R_{ij} \sigma_j \quad (4.112)$$

where R_{ij} is the reciprocal of the C_{ij} matrix. Because C_{ij} is a pseudodiagonal matrix, the term R_{44} is given by

$$R_{44} = C_{44}^{-1} = (2G)^{-1} = J/2 \quad (4.113)$$

where $J = \frac{1}{6}$ is the shear compliance function. The other terms of R_{ij} can be obtained from the reciprocal of the matrix

$$\begin{pmatrix} C_{11} & C_{12} & C_{12} \\ & C_{11} & C_{12} \\ & & C_{11} \end{pmatrix} \quad (4.114)$$

whose values are given by

$$\begin{aligned}
 R_{11} &= \frac{C_{11}^2 - C_{12}^2}{\Delta} \\
 R_{12} &= \frac{C_{12}(C_{12} - C_{11})}{\Delta}
 \end{aligned}
 \tag{4.115}$$

where Δ is the determinant of the matrix. From Eqs. (4.73), (4.84), and (4.115), one obtains

$$R_{11} = \frac{3K + G}{9KG} = \frac{J}{3} + \frac{B}{9}
 \tag{4.116a}$$

and

$$R_{12} = \frac{2G - 3K}{18GK} = \frac{B}{9} - \frac{J}{6}
 \tag{4.116b}$$

where $B = 1/K$ is the bulk compliance function. Using these expressions, Eq. (4.111) becomes

$$\begin{pmatrix} \gamma_1 \\ \gamma_2 \\ \gamma_3 \\ \gamma_4 \\ \gamma_5 \\ \gamma_6 \end{pmatrix} = \begin{pmatrix} \frac{J}{3} + \frac{B}{9} & \frac{B}{9} - \frac{J}{6} & \frac{B}{9} - \frac{J}{6} & 0 & 0 & 0 \\ & \frac{J}{3} + \frac{B}{9} & \frac{B}{9} - \frac{J}{6} & 0 & 0 & 0 \\ & & \frac{J}{3} + \frac{B}{9} & 0 & 0 & 0 \\ & & & \frac{J}{2} & 0 & 0 \\ & & & & \frac{J}{2} & 0 \\ & & & & & \frac{J}{2} \end{pmatrix} \begin{pmatrix} \sigma_1 \\ \sigma_2 \\ \sigma_3 \\ \sigma_4 \\ \sigma_5 \\ \sigma_6 \end{pmatrix}
 \tag{4.117}$$

which permits writing the relationship between the strain and stress tensors in the generalized form

$$\gamma_{ij} = \left(\frac{B}{9} - \frac{J}{6} \right) \Sigma \delta_{ij} + \frac{J}{2} \sigma_{ij}
 \tag{4.118}$$

where $\Sigma = \text{trace}(\sigma_{ij})$.

4.9.2 Relationships Between Compliance Functions

Let us consider that the only nonzero term of the stress tensor is σ_{11} . According to Eq. (4.118), the relationship between γ_{11} and σ_{11} is given by

$$\gamma_{11} = \left(\frac{B}{9} + \frac{J}{3} \right) \sigma_{11}
 \tag{4.119}$$

and the tensile compliance function, D , can be written as

$$D = \frac{\gamma_{11}}{\sigma_{11}} = \frac{B}{9} + \frac{J}{3} \quad (4.120)$$

This equation suggests that $D = J/3$ if $B \rightarrow 0$. In the same way, Eq. 118 indicates that the component of the strain tensor in the direction transverse to that of σ_{11} is given by

$$\gamma_{22} = \left(\frac{B}{9} - \frac{J}{6} \right) \sigma_{11} \quad (4.121)$$

This equation in conjunction with Eq. (4.119) permits us to obtain the Poisson ratio given by

$$\nu = \frac{\gamma_{22}}{\gamma_{11}} = -\frac{B/9 - J/6}{B/9 + J/3} \quad (4.122)$$

One can see that $\nu \rightarrow 1/2$ if $B \rightarrow 0$. Each of the four compliance parameters (J , D , B , and ν) can easily be obtained from the values of other two by means of the expressions developed above. The pertinent relationships are given in Table 4.2 (5).

4.10 THERMOELASTIC EFFECTS

Let us consider an isotropic material whose temperature uniformly rises owing to external causes, for example heating, or the dissipation of energy produced in the body by the deformation. The cubic dilatation taking place in the material because of the effect of the change in temperature is given by

$$\gamma_{kk} = 3\alpha \Delta T \quad (4.123)$$

where α is the linear dilatation coefficient, which can be considered approximately constant, and ΔT is the rise in temperature. To establish generalized Hookean relationships for systems in which a change of temperature ΔT occurs, consider first the dilatation of the system in isothermal conditions caused by the forces applied to the system. By taking into account that $J = 1/G$ and $B = 1/K$ and considering further that, according to Table 4.1, $K = E/3(1 - 2\nu)$ and $G = E/2(1 + \nu)$, Eq. (4.118) can be written as

$$\gamma_{ij} = \frac{\nu + 1}{E} \sigma_{ij} - \frac{\nu}{E} \sigma_{kk} \delta_{ij} \quad (4.124)$$

Table 4.2 Relationships Between Compliance Functions^a

	J and D	J and ν	D and ν	B and D	B and ν	B and J
B	$9D - 3J$	$3J(1 - 2\nu)/[2(1 + \nu)]$	$3D(1 - 2\nu)$			
J			$2D(1 + \nu)$	$3D - B/3$	$2B(1 + \nu)/[3(1 - 2\nu)]$	
D		$J/[2(1 + \nu)]$			$B/[3(1 - 2\nu)]$	$B/9 + J/3$
ν	$J/2D - 1$			$1/2 - B/6D$		$(3J - 2B)/(6J + 2B)$

^aIn the International System, the units of J , D , and B are m^2/N ; the Poisson ratio is dimensionless.

Source: Ref. 5.

The dilatation of the system in isothermal conditions obtained from Eq. (4.124) is given by

$$\gamma_{kk} = \text{trace } \gamma_{ij} = \frac{1 - 2\nu}{E} \sigma_{kk} \quad (4.125)$$

By assuming superposition of effects, the dilatation of the system caused by both the stress applied on it and a change of temperature ΔT is

$$\gamma_{kk} = \frac{1 - 2\nu}{E} \sigma_{kk} + 3\alpha \Delta T \quad (4.126)$$

and the trace of the stress tensor is given by

$$\sigma_{kk} = \frac{E}{1 - 2\nu} \gamma_{kk} - \frac{3\alpha E}{1 - 2\nu} \Delta T \quad (4.127)$$

In this case, Eq. (4.124) adopts the form

$$\gamma_{ij} = \frac{\nu + 1}{E} \sigma_{ij} - \frac{\nu}{E} \sigma_{kk} \delta_{ij} + \alpha \Delta T \delta_{ij} \quad (4.128)$$

where the contribution to the strain from the thermal dilatation is incorporated. By substitution into this equation of the value given for σ_{kk} in Eq. (4.126) and further inversion of the resulting expression, one obtains

$$\sigma_{ij} = \frac{E}{1 + \nu} \gamma_{ij} + \frac{E\nu}{(1 + \nu)(1 - 2\nu)} \gamma_{kk} \delta_{ij} - \alpha \frac{E}{1 - 2\nu} \Delta T \delta_{ij} \quad (4.129)$$

Note that by using the relationships given between E and ν and K and G indicated in Table 4.1, Eq. (4.129) also can be written as

$$\sigma_{ij} = 2G\gamma_{ij} + \left(K - \frac{2}{3}G \right) \varepsilon_{kk} \delta_{ij} - 3\alpha K \Delta T \delta_{ij} \quad (4.130)$$

At equilibrium, $\sigma_{ij,j} = 0$ [Eq. (4.14)], and as a consequence

$$\frac{\partial \sigma_{ij}}{\partial x_j} = \frac{E}{1 + \nu} \frac{\partial \gamma_{ij}}{\partial x_j} + \frac{E\nu}{(1 + \nu)(1 - 2\nu)} \frac{\partial \gamma_{kk}}{\partial x_i} - \alpha \frac{E}{1 - 2\nu} \frac{\partial T}{\partial x_j} = 0 \quad (4.131)$$

where body forces were neglected. By following the procedures outlined in Eqs. (4.104)–(4.107), the thermoelastic Navier equation is obtained:

$$\frac{1}{1+\nu} \left[(1-\nu) \nabla \operatorname{div} \mathbf{u} - \frac{1-2\nu}{2} \operatorname{rot} \operatorname{rot} \mathbf{u} \right] = \alpha \nabla T \quad (4.132)$$

where \mathbf{u} is the vector displacement

4.11 VISCOSITY OF IDEAL LIQUIDS

We have seen that the stress tensor for ideal isotropic solids is a linear function of the strain tensor, the proportional coefficient being a fourth-order modulus tensor with only two independent components. In liquids, the shear components σ_{ij} , $i \neq j$, of the stress tensor produce shear flow, while the normal components σ_{ij} , $i = j$, give rise to bulk flow. Owing to the high compressibility coefficient of liquids, bulk flow is nearly negligible in comparison with the shear flow. We can extend the generalized equation of elasticity [Eq. (4.90a)] to liquids by substituting elastic parameters for viscous ones. The analog of the relaxation modulus G is the shear viscosity η , and that of the bulk relaxation modulus K is the bulk viscosity ζ . By analogy with Eq. (4.90), the dilatant and deviator stress tensors for liquids are given by

$$\sigma_{ij}^{\Sigma} = \zeta \dot{\Delta} \delta_{ij} = 3K \dot{\gamma}_{ij}^{\Delta} \quad (4.133a)$$

and

$$\sigma_{ij}^d = 2\eta \dot{\gamma}_{ij}^d \quad (4.133b)$$

where $\dot{\gamma}_{ij}^{\Delta}$ and $\dot{\gamma}_{ij}^d$ are, respectively, the isotropic rate of strain tensor and the deviatoric rate of the strain tensor. Accordingly, the generalized equation of viscosity for liquids can be written as

$$\sigma_{ij} = \left(\zeta - \frac{2}{3} \eta \right) \dot{\Delta} \delta_{ij} + 2\eta \dot{\gamma}_{ij} \quad (4.134)$$

For simple shear flows, Eq. (4.134) becomes the familiar expression for Newtonian liquids,

$$\sigma_{ij} = 2\eta \dot{\gamma}_{ij}, \quad i \neq j \quad (4.135)$$

For a fluid flowing under a force field in which the stress tensor has only one component, σ_{11} , Eq. (4.134) can be written explicitly as

$$\sigma_{11} = \left(\zeta - \frac{2}{3} \eta \right) (\dot{\gamma}_{11} + 2\dot{\gamma}_{22}) + 2\eta \dot{\gamma}_{11} \quad (4.136a)$$

$$\sigma_{22} = 0 = \left(\zeta - \frac{2}{3} \eta \right) (\dot{\gamma}_{11} + 2\dot{\gamma}_{22}) + 2\eta \dot{\gamma}_{22} \quad (4.136b)$$

where $\dot{\gamma}_{22} = \dot{\gamma}_{33}$ because of the isotropy of fluids. Solution of these equations gives

$$\eta_L = \frac{\sigma_{11}}{\dot{\gamma}_{11}} = \frac{9\zeta\eta}{3\zeta + \eta} \quad (4.137)$$

where η_L is the elongational viscosity. In general, the bulk viscosity is much larger than the shear viscosity and consequently $\eta_L \cong 3\eta$.

Owing to the fact that a viscous material still responds elastically to an isotropic pressure, Eq. (4.133a) should be written as

$$\sigma_{ij}^{\Sigma} = 3K\gamma_{ij}^{\Delta} + 3\zeta\dot{\gamma}_{ij}^{\Delta} \quad (4.138)$$

Consequently, Eq. (4.134) can be expressed by

$$\sigma_{ij} = \left[K\Delta + \left(\zeta - \frac{2}{3} \eta \right) \dot{\Delta} \right] \delta_{ij} + 2\eta \dot{\gamma}_{ij} \quad (4.139)$$

Hence, the elongational viscosity is given by

$$\eta_L = \frac{9\zeta\eta}{3\zeta + \eta(1 - 3K\Delta/\sigma_{11})} \quad (4.140)$$

For $\zeta \gg \eta$, Eq. (4.140) again reduces to $\eta_L = 3\eta$. For incompressible liquids, Eq. (4.139) becomes

$$\sigma_{ij} = -p\delta_{ij} + 2\eta \dot{\gamma}_{ij} \quad (4.141)$$

where Eq. (4.93a) was considered. Equation (4.141) indicates that the stress is known only within an arbitrary isotropic pressure. For an isotropic material under uniaxial elongation, the stresses, strains, and rates of strain are identical in the two transverse directions. In this situation, the normal stress difference is given by

$$\sigma_{11} - \sigma_{22} = 2\eta(\dot{\gamma}_{11} - \dot{\gamma}_{22}) \quad (4.142)$$

For an incompressible fluid the rate of dilatation vanishes, and we obtain

$$\dot{\Delta} = \dot{\gamma}_{11} + 2\dot{\gamma}_{22} = 0 \quad (4.143)$$

Hence, Eq. (4.142) becomes

$$\sigma_{11} - \sigma_{22} = 3\eta\dot{\gamma}_{11} \quad (4.144)$$

By taking into account the earlier relation, $\eta_L = 3\eta$, Eq. (4.144) can be written as

$$\eta_L = \frac{\sigma_{11} - \sigma_{22}}{\dot{\gamma}_{11}} \quad (4.145)$$

which gives the elongational viscosity of an incompressible liquid in terms of the normal stress difference. Equations (4.139) and (4.141) are special forms of the generalized Newton's law.

PROBLEM SETS

Problem 4.1

Given the displacements

$$u_1 = ax_2x_3; \quad u_2 = ax_3^2; \quad u_3 = ax_1^2; \quad a \ll 1$$

where a is a positive constant, determine (a) the displacement tensor, (b) the strain tensor, and (c) the rotation tensor.

Solution 4.1

According to Eqs. (4.23), (4.29a), and (4.29b), the gradient displacement tensor, the strain tensor γ_{ij} , and the rotation tensor ω_{ij} are given by

(a)

$$\frac{\partial u_i}{\partial x_j} = \begin{pmatrix} 0 & ax_3 & ax_2 \\ 0 & 0 & 2ax_3 \\ 2ax_1 & 0 & 0 \end{pmatrix}$$

(b)

$$\gamma_{ij} = \frac{1}{2} \left(\frac{\partial u_i}{\partial x_j} + \frac{\partial u_j}{\partial x_i} \right) = \begin{pmatrix} 0 & (1/2)ax_3 & (a/2)(2x_1 + x_2) \\ (1/2)ax_3 & 0 & ax_3 \\ (a/2)(2x_1 + x_2) & ax_3 & 0 \end{pmatrix}$$

(c)

$$\omega_{ij} = \frac{1}{2} \left(\frac{\partial u_i}{\partial x_j} - \frac{\partial u_j}{\partial x_i} \right) = \begin{pmatrix} 0 & (a/2)ax_3 & -(a/2)(2x_1 - x_2) \\ -(1/2)ax_3 & 0 & ax_3 \\ (a/2)(2x_1 - x_2) & -ax_3 & 0 \end{pmatrix}$$

Problem 4.2

Write the strain tensor components in cylindrical coordinates.

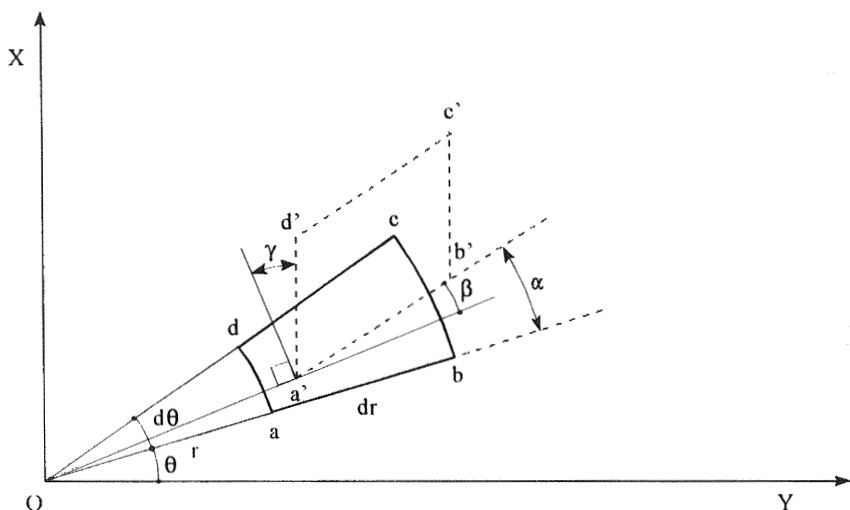
Solution 4.2

Let us represent by u_r , u_θ , and u_z the radial, angular, and axial displacements respectively, as in Figure P4.2.1.

For \overline{ab} the radial displacement is $(\partial u_r / \partial r) dr$, so

$$\gamma_{rr} = \frac{\partial u_r}{\partial r} \quad (\text{P4.2.1})$$

For \overline{ad} the total displacement is the resultant of the radial and tangential displacements according to

**Figure P4.2.1**

$$\underbrace{(r + u_r) d\theta - r d\theta}_{d, \text{ radial}} + \underbrace{u_\theta + \frac{\partial u_\theta}{\partial \theta} d\theta - u_\theta}_{d, \text{ tangential}} = u_r d\theta + \frac{\partial u_\theta}{\partial \theta} d\theta$$

Hence,

$$\gamma_{\theta\theta} = \frac{1}{r} d\theta \left(u_r + \frac{\partial u_\theta}{\partial \theta} \right) d\theta = \frac{u_r}{r} + \frac{1}{r} \frac{\partial u_\theta}{\partial \theta} \quad (\text{P4.2.2})$$

To find $\gamma_{r\theta}$ we proceed in a similar way (see Fig. P4.2.1).

$$2\gamma_{r\theta} = dab - d'a'b' = \frac{\pi}{2} - d'a'b' = \beta + \gamma$$

$$\beta = \alpha - a\theta a' = \left[\left(u_\theta + \frac{\partial u_\theta}{\partial r} dr \right) - u_\theta \right] \frac{1}{dr} - \frac{u_\theta}{r} = \frac{\partial u_\theta}{\partial r} - \frac{u_\theta}{r}$$

$$\gamma = \left(u_r + \frac{\partial u_r}{\partial \theta} d\theta - u_r \right) \left(\frac{1}{r} d\theta \right) = \frac{1}{r} \frac{\partial u_r}{\partial \theta}$$

and consequently,

$$\gamma_{r\theta} = \frac{1}{2} \left(\frac{1}{r} \frac{\partial u_r}{\partial \theta} + \frac{\partial u_\theta}{\partial r} - \frac{u_\theta}{r} \right) \quad (\text{P4.2.3})$$

Working now on the face $dr dz$, we obtain

$$\gamma_{zz} = \frac{\partial u_z}{\partial z}; \quad \gamma_{zr} = \frac{1}{2} \left(\frac{\partial u_r}{\partial z} + \frac{\partial u_z}{\partial r} \right) \quad (\text{P4.2.4})$$

and on $r d\theta dz$,

$$\gamma_{z\theta} = \frac{1}{2} \left(\frac{\partial u_\theta}{\partial z} + \frac{1}{r} \frac{\partial u_z}{\partial \theta} \right) \quad (\text{P4.2.5})$$

For an axis-symmetric problem, for example, with symmetry about the z axis, the strain tensor depends only on r , so

$$\gamma_{rr} = \frac{\partial u}{\partial r}; \quad \gamma_{\theta\theta} = \frac{u_r}{r} \quad (\text{P4.2.6})$$

If u_θ depends linearly on r , then $\gamma_{r\theta} = 0$.

For a plane strain problem (see Chap. 16), $u_z = 0$, and the only nonzero components of the strain are γ_{rr} and $\gamma_{\theta\theta}$.

Problem 4.3

Show that the volume integral of the divergence of a continuously differentiable second-order tensorial field in a finite region D is equivalent to the integral over the surface contour S enclosing that volume multiplied by the oriented normal vector \mathbf{n} at each point of the surface.

Conversely, show that the flux of a tensorial field outside a closed surface is the integral of the divergence of this field in the volume enclosed by that surface.

Solution 4.3

Obviously, it is required that the surface be piecewise continuous and the volume simply connected and convex, that is, without holes, so that its surface S can be continuously contracted through V so as to surround any point in V . The direction of the normal \mathbf{n} to S is outward from the enclosed volume.

Let σ_{jk} be a second-order tensor (e.g., the stress tensor), D the domain, and S the surface (see Fig. P4.3.1). Let us divide the volume into prisms of sides dx_2 and dx_3 . Taking the following integral over a prism of volume δD ,

$$\int_{\delta D} \frac{\partial \sigma_{jk}}{\partial x_1} dx_1 dx_2 dx_3; j, k = 1, 2, 3 \quad (\text{P4.3.1})$$

and carrying out the integration with respect to x_1 , we find

$$(\sigma_{jk} dx_2 dx_3)_{A_R} - (\sigma_{jk} dx_2 dx_3)_{A_L}$$

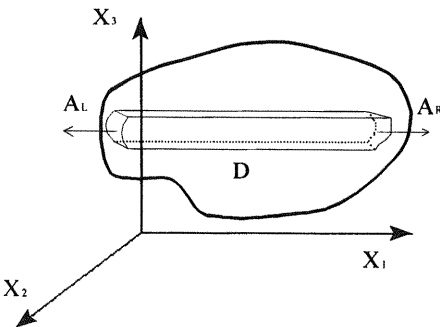


Figure P4.3.1

Here the first and second terms have been evaluated on the right- and left-hand sides of the prisms.

If \mathbf{n} is the unit vector normal to the contour S of D , and n_1 , n_2 , and n_3 are director cosines of \mathbf{n} , then the integral can be written as

$$\int_{\partial D} \frac{\partial \sigma_{jk}}{\partial x_1} dx_1 dx_2 dx_3 = \sigma_{jk} n_1 dA_R - \sigma_{jk} n_1 dA_L \tag{P4.3.2}$$

where A is the area of each side. After calculating the integral over all the prisms corresponding to the volume of D we have

$$\iiint_D \frac{\partial \sigma_{jk}}{\partial x_1} dx_1 dx_2 dx_3 = \iint_{D_R} \sigma_{jk} n_1 dA - \iint_{D_L} \sigma_{jk} n_1 dA \tag{P4.3.3}$$

The right-hand side of this equation, calculated over all the surface surrounding the volume V , can be replaced by an integral over the closed surface S , that is,

$$\iiint_D \frac{\partial \sigma_{jk}}{\partial x_i} dV = \iint_S \sigma_{jk} n_i dA \tag{P4.3.4}$$

This means that the integral of $\text{div } \sigma_{jk}$ within D is equal to the sum of the integrals within each rectangular block into which D is divided. The second member is the flux of σ_{jk} through the surfaces of each rectangular block. Note that the contributions to the surface integral along each of the integral faces will be zero, since two equal fluxes in opposite directions are added along each of these faces. Thus, the total sum equals the flux of σ_{jk} through the outer surface S .

Equation (P4.3.4), known as the Gauss–Ostrogradsky, or divergence, theorem, is usually written

$$\iiint_D \sigma_{jk,i} dV = \iint_S \sigma_{jk} n_i dA \tag{P4.3.5}$$

If σ_{jk} is a vector \mathbf{v} , we have the divergence theorem for a vector.

$$\iiint_D \text{div } \mathbf{v} dV = \iint_S \mathbf{v} \cdot d\mathbf{A} \tag{P4.3.6}$$

For a scalar field ϕ ,

$$\iiint_D \nabla \phi dV = \iint_S \phi d\mathbf{A} \tag{P4.3.7}$$

Finally, we remark that the Stokes theorem can be obtained as a two-dimensional version of the Gauss theorem.

$$\iint_S \text{rot } \mathbf{v} \, d\mathbf{A} = \int_\Gamma \mathbf{v} \, ds \quad (\text{P4.3.8})$$

where Γ is the one-dimensional contour of the surface S .

Alternatively we can say that the divergence of a vector \mathbf{v} is the number of vector lines originating in an infinitely small volume or, which is the same thing, the flux of the vector field through the surface of this volume.

$$\text{div } \mathbf{v} = \lim_{V \rightarrow 0} \frac{\iint_S \mathbf{v} \, d\mathbf{A}}{V} \quad (\text{P4.3.9})$$

We note that the divergence of a tensor is a vector, whereas the divergence of a vector is a scalar

Problem 4.4

Given the tensor field σ_{ij} ,

$$\begin{pmatrix} x & x + yz & 0 \\ x + yz & 0 & 0 \\ 0 & 0 & 0 \end{pmatrix}$$

and the domain depicted in Figure P4.4.1, (a) verify the Gauss theorem for $\sigma_{12,3}$ and (b) prove the divergence theorem over this domain for

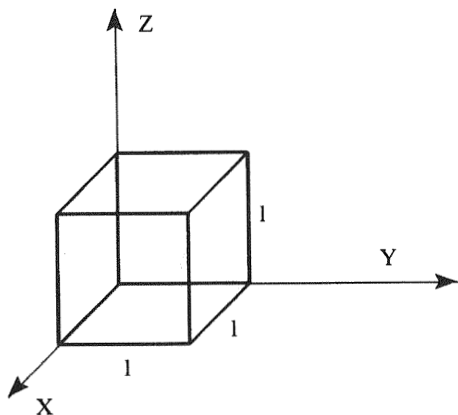
$$\mathbf{v} = x^2 y \mathbf{i} + z \mathbf{j} + y \mathbf{k}$$

Solution 4.4

(a) According to the Gauss theorem,

$$\begin{aligned} \iiint_D \sigma_{12,3} \, dV &= \iint_S \sigma_{12} n_3 \, dA, & \text{with } \sigma_{12} &= x + yz \\ \sigma_{12,3} &= \frac{\partial \sigma_{12}}{\partial z} = y \end{aligned} \quad (\text{P4.4.1})$$

Then

**Figure P4.4.1**

$$\iiint_V y \, dV = \int_0^1 \int_0^1 \int_0^1 y \, dx \, dy \, dz = \frac{1}{2} \quad (\text{P4.4.2})$$

On the other hand, in order to calculate

$$\iint_S (x + yz)n_3 \, dA$$

it is necessary to consider that

$$n_3 dA = \begin{cases} dx \, dy & \text{for } z = 1 \\ -dx \, dy & \text{for } z = 0 \\ 0 & \text{for the other sides} \end{cases}$$

Accordingly,

$$\begin{aligned} \iint_S (x + yz)n_3 dA &= \int_0^1 \int_0^1 (x + y \times 1) dx \, dy - \int_0^1 \int_0^1 (x + y \times 0) dx \, dy \\ &= \int_0^1 \int_0^1 y \, dx \, dy = \frac{1}{2} \end{aligned} \quad (\text{P4.4.3})$$

(b)

$$\begin{aligned}
 \iint\int_V v_{i,i} dv &= \iint_S v_i n_i dA, & \operatorname{div} \mathbf{v} &= 2xy \\
 \iiint_V 2xy \, dV &= \int_0^1 \int_0^1 \int_0^1 2xy \, dx \, dy \, dz = \frac{1}{2} \\
 \iint_S v_i dA &= \int_0^1 \int_0^1 y \, dy \, dz + \int_0^1 \int_0^1 z \, dx \, dz + \int_0^1 \int_0^1 z(-1) dx \, dz & \text{(P4.4.4)} \\
 &+ \int_0^1 \int_0^1 y \, dx \, dy + \int_0^1 \int_0^1 y(-1) \, dx \, dy \\
 &= \int_0^1 \int_0^1 y \, dy \, dz = \frac{1}{2}
 \end{aligned}$$

Problem 4.5

Study if the equilibrium conditions are fulfilled for the stress field

$$\begin{aligned}
 \sigma_{xx} &= -Axy; & \sigma_{xy} &= \frac{A}{2}(B^2 - y^2) + Cz; & \sigma_{xz} &= -C \\
 \sigma_{yy} &= \sigma_{zz} = \sigma_{xz} = \sigma_{yz} = 0
 \end{aligned}$$

where A , B , and C are constants.

Solution 4.5

At equilibrium and in the absence of body forces, Eq. (4.14) indicates that $\operatorname{div} \sigma = 0$. By writing $x_1 = x$, $x_2 = y$, $x_3 = z$, one obtains

$$\begin{aligned}
 \frac{\partial \sigma_{11}}{\partial x_1} + \frac{\partial \sigma_{12}}{\partial x_2} + \frac{\partial \sigma_{13}}{\partial x_3} &= -Ay - Ay = -2Ay \neq 0 \\
 \frac{\partial \sigma_{21}}{\partial x_1} + \frac{\partial \sigma_{22}}{\partial x_2} + \frac{\partial \sigma_{23}}{\partial x_3} &= 0; & \frac{\partial \sigma_{31}}{\partial x_1} + \frac{\partial \sigma_{32}}{\partial x_2} + \frac{\partial \sigma_{33}}{\partial x_3} &= 0
 \end{aligned}$$

There is no equilibrium

Problem 4.6

A differential of volume, in cylindrical coordinates, is shown in Figure P4.6.1. Obtain the equilibrium equations.

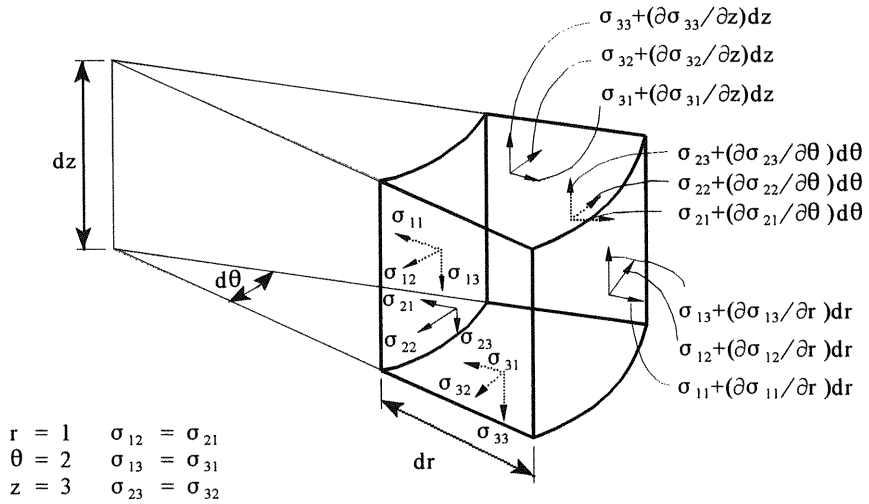


Figure P4.6.1

Solution 4.6

At equilibrium, $\Sigma \mathbf{f}_r = 0$ in the radial direction. Accordingly

$$\begin{aligned}
 & \left(\sigma_{11} + \frac{\partial \sigma_{11}}{\partial r} dr \right) (r + dr) d\theta dz - \sigma_{11} r d\theta dz + \left(\sigma_{12} + \frac{\partial \sigma_{12}}{\partial \theta} d\theta \right) \cos \frac{d\theta}{2} dr dz \\
 & \quad \left(\sigma_{12} + \frac{\partial \sigma_{12}}{\partial \theta} d\theta \right) \cos \frac{d\theta}{2} dr dz \\
 & + \left(\sigma_{22} + \frac{\partial \sigma_{22}}{\partial \theta} d\theta \right) \sin \frac{d\theta}{2} dr dz - \sigma_{22} \sin \frac{d\theta}{2} dr dz \\
 & + \left(\sigma_{12} + \frac{\partial \sigma_{13}}{\partial z} dz \right) dr \left(r + \frac{dr}{2} \right) d\theta - \sigma_{13} dr \left(r + \frac{dr}{2} \right) d\theta \\
 & + b_r r dr d\theta dz = 0
 \end{aligned}$$

(P4.6.1)

If

$$\sin \frac{d\theta}{2} \cong \frac{d\theta}{2} \quad \text{and} \quad \cos \frac{d\theta}{2} \cong 1$$

then

$$\begin{aligned} \sigma_{11} dr d\theta dz + \frac{\partial \sigma_{11}}{\partial r} r dr d\theta dz + \frac{\partial \sigma_{11}}{\partial r} (dr)^2 d\theta dz + \frac{\partial \sigma_{12}}{\partial \theta} dr d\theta dz - \sigma_{22} dr d\theta dz \\ - \frac{\partial \sigma_{22}}{\partial \theta} \frac{(d\theta)^2}{2} dr dz + \frac{\partial \sigma_{13}}{\partial z} r dr d\theta dz + \frac{\partial \sigma_{13}}{\partial z} \frac{(dr)^2}{2} d\theta dz + b_r r dr d\theta dz = 0 \end{aligned} \quad (\text{P4.6.2})$$

By neglecting high order infinitesimals and dividing by $r dr d\theta dz$, we obtain

$$\frac{\sigma_{11}}{r} + \frac{\partial \sigma_{11}}{\partial r} + \frac{1}{r} \frac{\partial \sigma_{12}}{\partial \theta} - \frac{\sigma_{22}}{r} + \frac{\partial \sigma_{13}}{\partial z} + b_r = 0 \quad (\text{P4.6.3})$$

or, equivalently,

$$\frac{\sigma_{11} - \sigma_{22}}{r} + \frac{\partial \sigma_{11}}{\partial r} + \frac{1}{r} \frac{\partial \sigma_{12}}{\partial \theta} + \frac{\partial \sigma_{13}}{\partial z} + b_r = 0$$

In an analogous way, at equilibrium,

$$\sum f_\theta = 0 \quad \text{and} \quad \sum f_z = 0 \quad (\text{P4.6.4})$$

and the corresponding equations are easily obtained:

$$\frac{2\sigma_{12}}{r} + \frac{\partial \sigma_{12}}{\partial r} + \frac{1}{r} \frac{\partial \sigma_{22}}{\partial \theta} + \frac{\partial \sigma_{23}}{\partial z} + b_\theta = 0 \quad (\text{P4.6.5a})$$

$$\frac{\sigma_{13}}{r} + \frac{\partial \sigma_{13}}{\partial r} + \frac{1}{r} \frac{\partial \sigma_{23}}{\partial \theta} + \frac{\partial \sigma_{33}}{\partial z} + b_z = 0 \quad (\text{P4.6.5b})$$

To obtain the motion equations, the inertial terms $\rho d^2 u_i / dt^2$ must be added to the right-hand side of these equations.

For a two-dimensional problem (polar plane coordinates), and in the absence of body forces, the equilibrium equations become

$$\frac{\sigma_{rr} - \sigma_{\theta\theta}}{r} + \frac{\partial \sigma_{rr}}{\partial r} + \frac{\partial \sigma_{r\theta}}{r\partial\theta} = 0 \quad (\text{P4.6.6})$$

and

$$\frac{2\sigma_{r\theta}}{r} + \frac{\partial \sigma_{r\theta}}{\partial r} + \frac{\partial \sigma_{\theta\theta}}{r\partial\theta} = 0 \quad (\text{P4.6.7})$$

Another way to obtain the equilibrium equations is to transform the Cartesian equations directly by means of the relations

$$\begin{aligned} x &= r \cos \theta; & r^2 &= x^2 + y^2 \\ y &= r \sin \theta; & \theta &= \arctan \frac{y}{x} \end{aligned} \quad (\text{P4.6.8})$$

which give

$$\begin{aligned} \frac{\partial r}{\partial x} &= \frac{x}{r} = \cos \theta; & \frac{\partial r}{\partial y} &= \frac{y}{r} = \sin \theta \\ \frac{\partial \theta}{\partial x} &= -\frac{y}{r^2} = -\frac{\sin \theta}{r}; & \frac{\partial \theta}{\partial y} &= \frac{x}{r^2} = \frac{\cos \theta}{r} \end{aligned} \quad (\text{P4.6.9})$$

The transformations of the derivatives with respect to r and θ are given by

$$\frac{\partial}{\partial x} = \cos \theta \frac{\partial}{\partial r} - \frac{\sin \theta}{r} \frac{\partial}{\partial \theta} \quad (\text{P4.6.10a})$$

$$\frac{\partial}{\partial y} = \sin \theta \frac{\partial}{\partial r} + \frac{\cos \theta}{r} \frac{\partial}{\partial \theta} \quad (\text{P4.6.10b})$$

Since the transformation of a tensor to a different reference frame is given by

$$\sigma = R \sigma' R^T$$

where R is the rotation matrix

$$\begin{pmatrix} \cos \theta & -\sin \theta & 0 \\ \sin \theta & \cos \theta & 0 \\ 0 & 0 & 1 \end{pmatrix} \quad (\text{P4.6.11})$$

the transformed stresses are

$$\sigma_{xx} = \sigma_{rr} \cos^2 \theta + \sigma_{\theta\theta} \sin^2 \theta - \sigma_{r\theta} \sin 2\theta$$

$$\sigma_{yy} = \sigma_{rr} \sin^2 \theta + \sigma_{\theta\theta} \cos^2 \theta + \sigma_{r\theta} \sin 2\theta$$

$$\sigma_{xy} = (\sigma_{rr} - \sigma_{\theta\theta}) \sin \theta \cos \theta + \sigma_{r\theta} (\cos^2 \theta - \sin^2 \theta)$$

By substituting these equations into the Cartesian equilibrium equation, we obtain

$$\left(\frac{\partial \sigma_{rr}}{\partial r} + \frac{1}{r} \frac{\partial \sigma_{r\theta}}{\partial \theta} + \frac{\sigma_{rr} - \sigma_{\theta\theta}}{r} \right) \cos \theta - \left(\frac{1}{r} \frac{\partial \sigma_{\theta\theta}}{\partial \theta} + \frac{\partial \sigma_{r\theta}}{\partial r} + 2 \frac{\sigma_{r\theta}}{r} \right) \sin \theta = 0 \quad (\text{P4.6.12})$$

Since this equation must be valid for any value of θ , Eq. (P4.6.12) becomes

$$\left(\frac{\partial\sigma_{rr}}{\partial r} + \frac{1}{r} \frac{\partial\sigma_{r\theta}}{\partial\theta} + \frac{\sigma_{rr} - \sigma_{\theta\theta}}{r}\right) = \left(\frac{1}{r} \frac{\partial\sigma_{\theta\theta}}{\partial\theta} + \frac{\partial\sigma_{r\theta}}{\partial r} + 2\frac{\sigma_{r\theta}}{r}\right) = 0 \quad (\text{P4.6.13})$$

These equations are identical to those previously obtained. The strain-displacement equations can also be transformed in a similar way.

Problem 4.7

Find the equilibrium equations for a system with radial symmetry (Fig. P4.7.1).

Solution 4.7

Owing to the symmetry of the problem, the stress, strain, and displacements are only functions of r . In this case

$$\sigma_{22} = \sigma_{33} \quad (\sigma_{\theta\theta} = \sigma_{\psi\psi}) \quad (\text{P4.7.1})$$

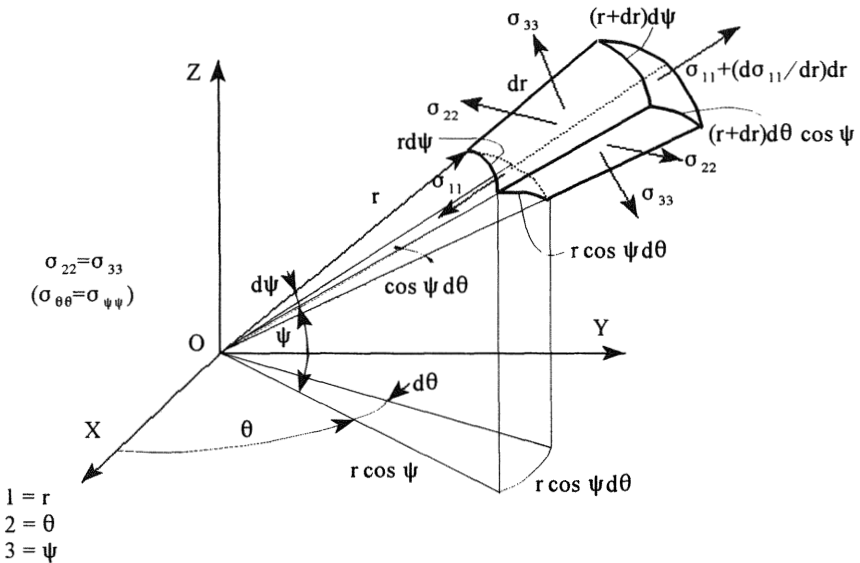


Figure P4.7.1

and

$$\sigma_{12} = \sigma_{23} = \sigma_{31} = 0 \quad (\sigma_{r\theta} = \sigma_{\theta\psi} = \sigma_{\psi r})$$

For the spherical element under consideration, the equilibrium condition in the r direction in absence of body forces will be

$$\begin{aligned} & -\sigma_{11}(r \, d\psi)(r \cos \psi \, d\theta) + \left(\sigma_{11} + \frac{d\sigma_{11}}{dr} dr \right) (r + dr) d\psi (r + dr) \cos \psi \, d\theta \\ & - \sigma_{33} \, dr (r \cos \psi \, d\theta) \left(2 \sin \frac{d\psi}{2} \right) - \sigma_{22} dr (r \, d\psi) 2 \sin \left(\cos \psi \frac{d\theta}{2} \right) = 0 \end{aligned} \quad (\text{P4.7.2})$$

By taking into account that

$$\sin \left(\cos \psi \frac{d\theta}{2} \right) \cong \cos \psi \frac{d\theta}{2} \quad \text{and} \quad \sin \frac{d\psi}{2} \cong \frac{d\psi}{2}$$

Simplifying and neglecting high order differentials, we obtain

$$\frac{d\sigma_{11}}{dr} = \frac{2}{r} (\sigma_{22} - \sigma_{11}) \quad (\text{P4.7.3})$$

Note that for the strain components

$$\gamma_{11} = \gamma_{rr} = \frac{du_1}{dr} \quad (\text{P4.7.4a})$$

and

$$\gamma_{22} = \gamma_{33} = \frac{(r + u_1)d\psi - rd\psi}{rd\psi} = \frac{u_1}{r} \quad (\gamma_{\theta\theta} = \gamma_{\psi\psi}) \quad (\text{P4.7.4b})$$

Eliminating u_1 (the remaining components of the strain tensor are null), we obtain

$$\frac{d\gamma_{\theta\theta}}{dr} = \frac{d\gamma_{\psi\psi}}{dr} = \frac{1}{r} (\gamma_{rr} - \gamma_{\theta\theta}) \Leftrightarrow \frac{d\gamma_{22}}{dr} = \frac{d\gamma_{33}}{dr} = \frac{1}{r} (\gamma_{11} - \gamma_{22}) \quad (\text{P4.7.5})$$

Problem 4.8

Given the tensor

$$\sigma_{ij} = \begin{pmatrix} 29 & 0 & 0 \\ 0 & -26 & 6 \\ 0 & 6 & 9 \end{pmatrix} \text{ MPa}$$

separate the deviatoric and dilational parts.

Solution 4.8

From Eqs. (4.80) and (4.83) one easily obtains

$$\begin{pmatrix} 25 & 0 & 0 \\ 0 & -30 & 6 \\ 0 & 6 & 5 \end{pmatrix} + \begin{pmatrix} 4 & 0 & 0 \\ 0 & 4 & 0 \\ 0 & 0 & 4 \end{pmatrix}$$

Problem 4.9

In a continuum the stress tensor in MPa is given by

$$\sigma_{ij} = \begin{pmatrix} 1 & -3 & \sqrt{2} \\ -3 & 1 & -\sqrt{2} \\ \sqrt{2} & -\sqrt{2} & 4 \end{pmatrix}$$

Determine the resulting tensor after a clockwise rotation of 45° . Determine also the eigenvalues and the invariants (that is, the coefficients of the secular equation).

Solution 4.9

As we have seen [Eq. (4.37)],

$$\sigma_{kl} = \sum_{ij} \beta_{ki} \beta_{lj} \sigma_{ij} \quad (\text{P4.9.1})$$

where σ_{ij} are the components of the tensor in a primitive reference frame and β_{ki} and β_{lj} are the matrices representing the rotations of the reference

axis with respect to the new ones, their elements being the director cosines of the angles between the new frame and the old one. In matrix notation,

$$[\sigma] = [A][\sigma][A^T] \quad (\text{P4.9.2})$$

where β_{ki} are the components of $[A]$ and β_{ij} components of its transposed A^T . Therefore,

$$\sigma'_{ij} = \begin{pmatrix} 1 & 0 & 0 \\ 0 & \cos 45^\circ & -\sin 45^\circ \\ 0 & \sin 45^\circ & \cos 45^\circ \end{pmatrix} \begin{pmatrix} 1 & -3 & \sqrt{2} \\ -3 & 1 & -\sqrt{2} \\ \sqrt{2} & -\sqrt{2} & 4 \end{pmatrix} \begin{pmatrix} 1 & 0 & 0 \\ 0 & \cos 45^\circ & \sin 45^\circ \\ 0 & -\sin 45^\circ & \cos 45^\circ \end{pmatrix} \quad (\text{P4.9.3})$$

Since

$$\cos(-45^\circ) = \cos 45^\circ = \frac{1}{\sqrt{2}}; \quad \sin(-45^\circ) = -\sin 45^\circ = -\frac{1}{\sqrt{2}}$$

this can be expressed as

$$\sigma'_{ij} = \begin{pmatrix} 1 & -\frac{3}{\sqrt{2}} - 1 & -\frac{3}{\sqrt{2}} + 1 \\ -\frac{3}{\sqrt{2}} - 1 & \frac{5}{2} + \sqrt{2} & -\frac{3}{2} \\ -\frac{3}{\sqrt{2}} + 1 & -\frac{3}{2} & \frac{5}{2} - \sqrt{2} \end{pmatrix} \quad (\text{P4.9.4})$$

Let us consider an operation that transforms the unit vector n_j in other n_i . The vector determined in this way is a scalar multiple of n_i :

$$\sigma_{ij}n_j = \lambda n_i \text{ or alternatively } [\sigma] \cdot n = \lambda n \quad (\text{P4.9.5})$$

The direction defined by n_i is a principal one, and the corresponding scalar λ is called the eigenvalue of σ .

The solution of the so-called secular equation $(\sigma_{ij} - \lambda\delta_{ij})n_j = 0$ allows the determination of the eigenvalues and consequently the diagonalization of the tensor under study.

The matrix equation is converted into a homogeneous system that has a nontrivial solution if its determinant differs from zero.

$$\begin{pmatrix} \sigma_{11} - \lambda & \sigma_{12} & \sigma_{13} \\ \sigma_{21} & \sigma_{22} - \lambda & \sigma_{23} \\ \sigma_{31} & \sigma_{32} & \sigma_{33} - \lambda \end{pmatrix} = 0 \quad (\text{P4.9.6})$$

The development of this determinant gives

$$\lambda^3 - \text{tr } \sigma_{ij} \lambda^2 + \frac{1}{2} [(\text{tr } \sigma_{ij})^2 - \text{tr}(\sigma_{ij}^2)] \lambda - \det \sigma_{ij} = \lambda^3 - \text{I} \lambda^2 + \text{II} \lambda - \text{III} = 0 \quad (\text{P4.9.7})$$

where I, II, and III are called the invariants of σ_{ij} . In this case, we have

$$(1 - \lambda)(1 - \lambda)(4 - \lambda) - 9(4 - \lambda) - 4(1 - \lambda) + 12 = 0$$

and from here,

$$\lambda^3 - 6\lambda^2 - 4\lambda + 24 = 0$$

which gives

$$\lambda_1 = 2, \quad \lambda_2 = -2, \quad \lambda_3 = 6$$

The invariants are given by

$$\text{I} = \text{tr } \sigma = \sigma_{ij} = 6 \quad (\text{P4.9.8a})$$

$$\text{II} = \frac{1}{2} [(\text{tr } \sigma)^2 - \text{tr}(\sigma^2)] = -4 \quad (\text{P4.9.8b})$$

$$\text{III} = \det \sigma = -24 \quad (\text{P4.9.8c})$$

Problem 4.10

Find the limits for the Poisson ratio.

Solution 4.10

From

$$\nu = \frac{3K - 2G}{2(3K + G)} \quad (\text{P4.10.1})$$

If

$$G \ll K, \quad \nu = 1/2 \quad (\text{P4.10.2a})$$

If

$$K \ll G, \quad \nu = -1 \quad (\text{P4.10.2b})$$

Hence,

$$-1 < \nu < 1/2$$

The upper limit corresponds to a material such that $G = E/3$, $\lambda = K = \infty$, that is, an incompressible solid. Materials with negative values of ν are still unknown, but their existence is not impossible.

Problem 4.11

Let a cubic volume element be constrained to a stress state such that

$$\sigma_{xx}, \sigma_{yy}, \sigma_{zz} \neq 0 \quad \text{and} \quad \sigma_{ij} = 0 \quad \text{for all } i, j$$

- (a) Determine the strain components as a function of σ_{ij} the tensile modulus E , and the Poisson ratio.
 (b) Determine the stress components as a function of the strain γ_{ij} , the tensile modulus E , and the Poisson ratio.

Solution 4.11

From Eq. (4.124) we obtain

$$\gamma_{xx} = \frac{1}{E} [\sigma_{xx} - \nu(\sigma_{yy} + \sigma_{zz})] \quad (\text{P4.11.1a})$$

and in an analogous way

$$\gamma_{yy} = \frac{1}{E} [\sigma_{yy} - \nu(\sigma_{xx} + \sigma_{zz})] \quad (\text{P4.11.1.b})$$

and

$$\gamma_{zz} = \frac{1}{E} (\sigma_{zz} - \nu(\sigma_{xx} + \sigma_{yy})) \quad (\text{P4.11.1.c})$$

In shear ($i \neq j$)

$$\gamma_{ij} = \frac{1}{2G} \sigma_{ij} \quad \text{with} \quad \frac{1}{2G} = \frac{1+\nu}{E} \quad (\text{P4.11.2})$$

Equation (4.83) together with the pertinent expressions of Table 4.1 lead to

$$\sigma_{xx} = \frac{E}{(1+\nu)(1-2\nu)} [(1-\nu)\gamma_{xx} + \nu(\gamma_{yy} + \gamma_{zz})] \quad (\text{P4.11.3a})$$

$$\sigma_{yy} = \frac{E}{(1+\nu)(1-2\nu)} [(1-\nu)\gamma_{yy} + \nu(\gamma_{xx} + \gamma_{zz})] \quad (\text{P4.11.3b})$$

and

$$\sigma_{zz} = \frac{E}{(1+\nu)(1-2\nu)} [(1-\nu)\gamma_{zz} + \nu(\gamma_{xx} + \gamma_{yy})] \quad (\text{P4.11.3c})$$

In shear,

$$\sigma_{ij} = 2G\gamma_{ij} \quad \text{with} \quad 2G = \frac{E}{1+\nu} \quad (\text{P4.11.4})$$

Problem 4.12

The stress tensor for an elastic material with $E = 10^{10}$ MPa and $\nu = 0.25$ is given by

$$\sigma_{ij} = \begin{pmatrix} px^3 - 2axz + bz & 0 & -\frac{3}{2}px^2z^2 + az^2 + \frac{p}{2}x^4 + c \\ 0 & 0 & 0 \\ -\frac{3}{2}px^2z^2 + az^2 + \frac{p}{2}x^4 + c & 0 & pxz^3 - 2px^3z \end{pmatrix}$$

Calculate the strain tensor in $x = z = 1$.

Solution 4.12

According to Eqs. (P4.11.1a)–(P4.11.1c) and (P4.11.2),

$$\gamma_{xx} = \frac{1}{E} [\sigma_{xx} - \nu(\sigma_{yy} + \sigma_{zz})] = \frac{1}{E} \left(\frac{3}{2} p x^3 z - \frac{1}{4} p x z^3 - 2 a x z + b z \right)$$

$$\gamma_{yy} = \frac{1}{E} [\sigma_{yy} - \nu(\sigma_{xx} + \sigma_{zz})] = -\frac{1}{4E} (-p x^3 z + p x z^3 - 2 a x z + b z)$$

$$\gamma_{zz} = \frac{1}{E} [\sigma_{zz} - \nu(\sigma_{xx} + \sigma_{yy})] = \frac{1}{E} \left(p x z^3 - \frac{9}{4} p x^3 z + \frac{a}{2} x z - \frac{b z}{4} \right)$$

$$\gamma_{xz} = \frac{1+\nu}{E} \left(-\frac{3}{2} p x^2 z^2 + a z^2 + \frac{p}{2} x^4 + c \right)$$

Therefore the strain tensor components at $x = z = 1$ will be

$$\gamma_{xx} = \left(\frac{5}{4} p - 2a + b \right) \times 10^{-10}; \quad \gamma_{yy} = \left(\frac{a}{2} - \frac{b}{4} \right) \times 10^{-10};$$

$$\gamma_{zz} = \left(-\frac{5}{4} p + \frac{a}{2} - \frac{b}{4} \right) \times 10^{-10}; \quad \gamma_{xz} = \frac{5}{4} (-p + a + c) \times 10^{-10}$$

REFERENCES

1. R Hooke. A Description of Helioscopes and Some Other Instruments. London, 1676; RT Gunther. Early Science in Oxford, Vol. 8. 1931; p. 119.
2. I Newton. Philosophiae Naturalis Principia Mathematica. London, 1687. Third edition, H Pemberton, ed., published in London in 1726; reprinted in Glasgow, 1871.
3. L Brillouin. Les Tenseurs en Mécanique et en Élasticité. Paris: Masson, 1938, Chap 10.
4. M von Laue. Sitz Ber Preuss Akad 21: 377, 1931.
5. NW Tschoegl. The Phenomenological Theory of Linear Viscoelastic Behavior. Berlin: Springer-Verlag, 1989, Chap 1.
6. IS Sokolnikoff. Mathematical Theory of Elasticity. New York: McGraw-Hill, 1956.
7. JF Nye. Physical Properties of Crystals. Oxford, Clarendon Press, 1957.

5

Linear Viscoelasticity and Viscoelastic Functions

5.1	Viscoelasticity	196
5.2	Linear Viscoelasticity—Response of Materials to Transient Experiments	198
5.3	Boltzmann Superposition Principle in Creep Experiments	207
5.4	Memory Effects in Creep Experiments	212
5.5	Boltzmann Superposition Principle in Relaxation Experiments	214
5.6	Memory Function in Relaxation Experiments	216
5.7	Ramp Experiments	217
5.8	Laplace Transform Relationships Between Transient Relaxation Moduli and Transient Compliance Functions	218
5.9	Generalization of the Superposition Principle	221
5.10	Generalized Stress–Strain Relationships in the Frequency Domain	226
5.11	Generalized Stress–Strain Relationships for Viscoelastic Systems with Any Degree of Symmetry	227
	Problem Sets	228
	References	237

5.1 VISCOELASTICITY

Perfectly elastic deformation and perfectly viscous flow are idealizations that are approximately realized in some limiting conditions. In general the condensed matter has a fading structural memory, and the velocity with which a system that has been perturbed forgets the configuration that it had in the past roughly defines its solid or liquid nature. In ordinary liquids, molecular

reorganization occurs very rapidly and structural memory at the molecular level is very short. The response is essentially viscous unless the frequency of the testing experiment is very high. Consequently the mean relaxation time, roughly defined as the time necessary for the system to forget the configuration it had previous to the perturbation, is very small. In solids, on the other hand, the relaxation of structure at the molecular level is extremely low. The response is essentially elastic. However, the distinction between solid (or elastic) and liquid (or viscous), is not an absolute distinction between different classes of materials. It should be pointed out that the distinction between solid and liquid is usually based on a subjective comparison of the relaxation time of the system and the time of observation (1). For example, water behaves as a solid at very high frequencies, and ice behaves as a fluid on a geological time scale. If we can dabble our fingers in a material we can conclude that it is a fluid, though it may return to its initial configuration after one month or one year. In the same way, if we are hit by a hard object we can think that it is a solid even though it can flow on a geological time scale. From a strict point of view, condensed matter exhibits viscoelastic behavior, though the ability to detect elastic or viscous responses depends in many cases on the time scale of the experiment. Usually, the solid or liquid character of a material is expressed by the Deborah number, N_D , defined as (2)

$$N_D = \frac{\tau}{\tau_{\text{exp}}} \quad (5.1)$$

where τ can provisionally be taken as some order-of-magnitude estimate of the time required for stress relaxation to approach completion and τ_{exp} is the time scale of the experiment. For ordinary liquids $\tau \rightarrow 0$ and $N_D \approx 0$, while for ordinary solids $\tau \rightarrow \infty$ and $N_D \rightarrow \infty$. For the so-called viscoelastic systems, τ and τ_{exp} are comparable and the Deborah number of these substances is on the order of unity.

Polymers are the most important viscoelastic systems. Above the glass transition temperature, the response of these materials to a mechanical perturbation field involves several types of molecular motion. For example, the rearrangement of flexible chains may be very fast on the length scale of a repeating unit. These motions imply some type of cooperativity in the conformational transitions that produce them. Cooperativity occurs even as the relaxation propagates along the chains, involving a growing number of segments of the backbone as time passes. At very long times, disentanglement of the chains takes place, and the longest relaxation time associated with this process shows a strong dependence on both the molecular weight and the molecular architecture (branching) of the system. The disentanglement

ment process governs the flow of the system. As a consequence of the complexity of the molecular responses, polymer chains exhibit a wide distribution of relaxation times that extend over several decades in the time or frequency domains. At short times the response is mainly elastic, whereas at long times it is mainly viscous. Obviously, the elastic component of the deformation is recoverable, but the viscous component is not. The elastic component of the deformation is of an entropic nature, and consequently it is time-dependent.

The complex relationship between the configurational distortion produced by a perturbation field in polymers and the Brownian motion that relaxes that distortion make it difficult to establish stress-strain relationships. In fact, the stress at a point in the system depends not only on the actual deformation at that point but also on the previous history of deformation of the material. As a consequence the relaxation between the stress and strain or rate of strain cannot be expressed by material constants such as G or J , as occurs in ideal elastic materials, but rather by time-dependent material functions, $G(t)$ and $J(t)$. It has been argued that the dynamics of incompressible liquids may be characterized by a function of the evolution of the strain tensor from the beginning up to the present time. According to this criterion, the stress tensor would be given by (3,4)

$$\sigma_{ij}(t) = \int_{\theta=-\infty}^t [\gamma_{ij}(t - \theta)] \quad (5.2)$$

where t is the present time and θ is the past time. It is said that the stress is a functional of the strain because it depends on the values taken by γ_{ij} in the interval $[-\infty, t]$. In a similar way, the strain may be expressed as a function of the stress

$$\gamma_{ij}(t) = \int_{\theta=-\infty}^t [\sigma_{ij}(t - \theta)] \quad (5.3)$$

If the deformations are small enough, the functional can be written in terms of linear differential equations with constant coefficients or, equivalently, in terms of convolution integrals with difference kernels.

5.2 LINEAR VISCOELASTICITY—RESPONSE OF MATERIALS TO TRANSIENT EXPERIMENTS

In the limit of infinitesimal strains, the responses of viscoelastic materials to mechanical perturbations are well described by the theory of linear visco-

elasticity. Two kinds of experiments are commonly used to study the viscoelastic behavior of materials: relaxation and creep experiments (1,4-10).

Let us consider a slab of material in a simple shearing motion. The slab is regarded as being so thin that inertial effects can be neglected. In a relaxation experiment an infinitesimal shear deformation is applied to a material, and the evolution of the stress necessary to keep this deformation constant is monitored. Let us assume that at time $t = 0$ a small shear strain $\epsilon_{12} = \delta u_1 / \delta x_2$ is imposed on the slab of Figure 5.1. This action is expressed in mathematical terms by

$$\epsilon_{12} = \epsilon = \frac{\partial u_1}{\partial x_2} H(t) \quad (5.4)$$

where $H(t)$ is the Heaviside function, or step function, whose values are 1 for $t \geq 0$ and 0 otherwise. In shear experiments we disregard the tensorial character of the stress and the strain in such a way that $\sigma_{12}(t)$ and γ_{12} (or ϵ_{12}) will simply be represented by σ and γ (or ϵ). For an ideally elastic material, the shear stress necessary to keep ϵ constant will be $\sigma = \sigma_0 H(t)$; that is, the stress remains constant for $t > 0$. For an ideal viscous liquid, the stress will be instantaneously infinite at $t = 0$ and then zero for $t > 0$, like a Dirac $\delta[= dH(t)/dt]$ function. The responses of ideal solids and liquids in relaxation experiments are schematically represented in Figure 5.2b and 5.2c, respectively.

A careful observation of the behavior of real substances reveals that neither of these idealizations is quite accurate. Thus for solids the stress decreases rather rapidly at short times and then more gradually at long times, approaching a limiting value σ_∞ . If $\sigma_\infty > 0$, the material is likely to be considered a solid, and otherwise a liquid. The evolution of the relaxation stress for real solids and liquids in relaxation experiments is schematically illustrated in Figures 5.3a and 5.3b, respectively. It should be pointed out that the determination of σ_∞ is a subjective matter that depends on the nature of the material and the nature of the observation. The relaxation time, that is, the time necessary for the stress to approach completion, may be so short that it escapes observation. In this situation the experimenter

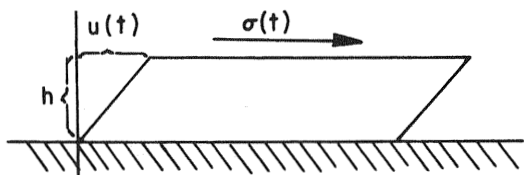


Figure 5.1 Slab of a material under simple shearing motion.

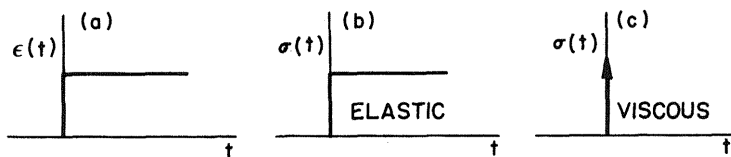


Figure 5.2 Response of ideal elastic solids (b) and ideal liquids (c) to a constant shear strain (a) in relaxation experiments.

may conclude that the material is a perfectly elastic solid or a fluid, as the case may be. If the relaxation time is so long that no relaxation is observed during the experiment, one may conclude that the material is perfectly elastic. Materials for which the relaxation time and the period of observation times are not astronomically different are called viscoelastic.

In a shear creep experiment of this type, the material undergoes a stress $\sigma = \sigma_0 H(t)$ (see Fig. 5.4a), and the evolution of the shear strain with time is registered. As shown in Figure 5.4b, the shear strain for an ideal solid is instantaneous [$\epsilon(t) = \epsilon_0 H(t)$], remaining constant with time. However, the strain for ideal liquids is a linear function of time (Fig. 5.4c). As Eq. (4.135) suggests, the shear strain for an ideal liquid is given by

$$\epsilon(t) = \frac{\sigma}{\eta} t \quad (5.5)$$

In the case of real substances, the response to the shear stress involves an instantaneous deformation of the Hookean type followed by gradual increase of the shear strain with time. If the strain at long times approaches a limiting value ϵ_∞ , the substance is considered a solid. However, if at long times the strain is a linear function of time, the substance is considered a liquid. Schematic representations of these responses are given in Figures 5.5a and 5.5b for real solids and liquids,

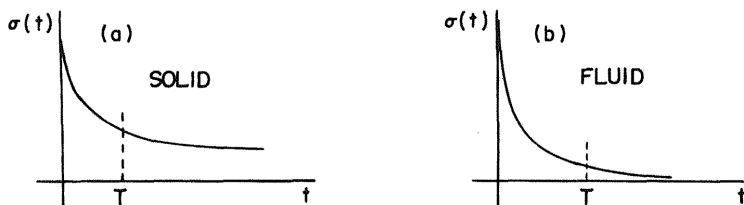


Figure 5.3 Response of real solids (a) and real liquids (b) to a constant shear strain in relaxation experiments.

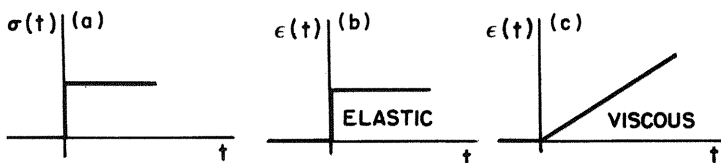


Figure 5.4 Response of ideal solids (b) and ideal liquids (c) to a constant shear stress (a) in creep experiments.

respectively. Situations may appear, for example, when $\epsilon(t) \sim t^{1/2}$ (see Fig. 5.5c), in which from a limited number of data one could think that a limiting value had been reached or that the shear strain were increasing linearly, depending on one's preconceived ideas.

5.2.1 Shear and Bulk Relaxation Moduli

If a material undergoes a sudden infinitesimal shear strain γ , the shear stress required to keep that shear strain constant is given by

$$\sigma(t) = 2G(t)\gamma = G(t)\epsilon \quad (5.6)$$

where $G(t)$ is the relaxation modulus. The substitution of $\epsilon = 2\gamma$ in this equation arises from the fact that $\epsilon_{ij} = 2\gamma_{ij}$ for $i \neq j$ and $\epsilon_{ij} = \gamma_{ij}$ for $i = j$ [see Eq. (4.30c)]. In order to get a better understanding of the concept of linearity, let us assume that in separate experiments the shear strains $\epsilon_1 H(t)$ and $\epsilon_2 H(t)$ are imposed on the slab of Figure 5.1 at $t = 0$. The time dependence of the shear stress for both cases is shown in Figure 5.6. The relaxation behavior is considered to be linear if for $t = t_a$ and $t = t_b$, the following relations hold:

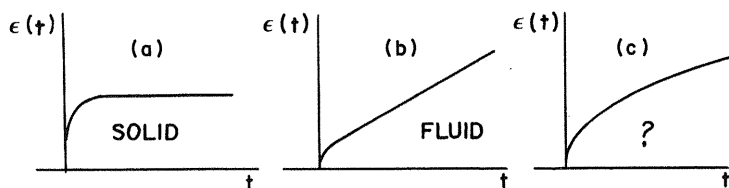


Figure 5.5 Response of real solids (a) and real liquids (b) to a constant shear stress in creep experiments.

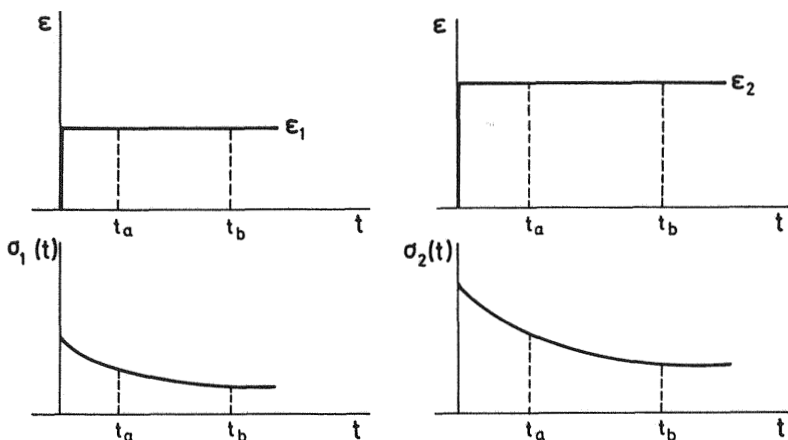


Figure 5.6 Excitations and responses in linear shear relaxation experiments.

$$\frac{\sigma_1(t_a)}{\varepsilon_1} = \frac{\sigma_2(t_a)}{\varepsilon_2} = G(t_a) \quad (5.7a)$$

$$\frac{\sigma_1(t_b)}{\varepsilon_1} = \frac{\sigma_2(t_b)}{\varepsilon_2} = G(t_b) \quad (5.7b)$$

$$G(t_a) \neq G(t_b)$$

Linearity in relaxation experiments holds only at small shear strains. A schematic diagram illustrating the linear and nonlinear behavior in relaxation experiments is shown in Figure 5.7.

In relaxation experiments carried out on solids, the shear stress continuously decreases with increasing time until a constant value G_e is obtained. Accordingly, the evolution of the relaxation modulus with time is described by the equation

$$G(t) = G_e + G_d \Phi(t) \quad (5.8)$$

where $G_e = \sigma_\infty/\varepsilon$ and G_d accounts for the maximum contribution of the entropic elasticity to $G(t)$. $\Phi(t)$ is a normalized monotonously decreasing function of time whose extreme values are 1 and 0 for $t = 0$ and $t = \infty$, respectively. Obviously, G_e is zero for liquids. The function $\Phi(t)$ is related to the entropic elastic mechanisms involved in the relaxation. The variation of $G(t)$ with time for solid and liquid polymers is shown schematically in Figure 5.8.

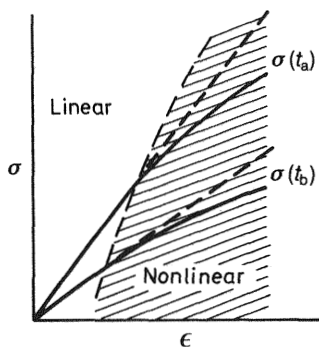


Figure 5.7 Sketch illustrating the transition from linear to nonlinear behavior in shear relaxation experiments. Note that the data must be obtained by a series of stress relaxation experiments.

If the viscoelastic material is under the effect of an isotropic deformation (dilatation or compression), the diagonal components of both the stress and strain tensors differ from zero. In analogy with Eq. (4.92), the relationship between the excitation and the response is given by

$$\sigma_{ii}(t) = -p(t) = 3K(t)\gamma_{ii} = K(t)\Delta \quad (5.9)$$

where $p(t)$ is the hydrostatic pressure and Δ is the volume compression. The bulk relaxation modulus is also a monotonous decreasing function of time given by

$$K(t) = K_e + K_d\Phi'(t) \quad (5.10)$$

where $\Phi'(t)$ is a normalized function with extreme values 1 and 0 for $t = 0$ and infinity, respectively.

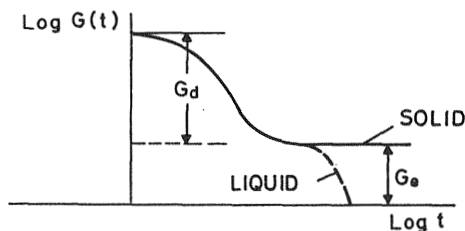


Figure 5.8 Double logarithmic plot of the shear relaxation modulus in the time domain.

The study of the response of viscoelastic systems to a tensile strength is very important on practical grounds. For a uniaxial strain $H(t)\varepsilon_{11}$, the evolution of the stress with time can be written as

$$\sigma_{11}(t) = E(t)\gamma_{11} \quad (5.11)$$

The tensile relaxation modulus, $E(t)$, is given by

$$E(t) = E_e + E_d\Phi''(t) \quad (5.12)$$

where E_e is the equilibrium elastic modulus and $\Phi''(t)$ is the decay function whose limits are 1 and 0 for $t = 0$ and infinity, respectively. For viscoelastic liquids, $E_e = 0$.

5.2.2 Shear and Bulk Compliance Functions

Let us consider the response of a system under the action of a small shear stress given by $\sigma H(t)$. In this case, the time dependence of the strain is given by

$$\gamma(t) = \frac{J(t)}{2}\sigma, \quad \varepsilon(t) = J(t)\sigma \quad (5.13)$$

where $J(t)$ is the creep compliance function. The analysis of the responses of a variety of solids and liquids demonstrates that the strain at $t = 0$ is Hookean. For $t > 0$, the strain of solids undergoes a monotonous increase with time until a constant value is reached; in the case of liquids, the strain is a linear function of t at very long times.

The term linearity in creep implies that in the perturbations and responses of Figure 5.9 the following relationships hold:

$$\frac{\varepsilon_1(t_a)}{\sigma_1} = \frac{\varepsilon_2(t_a)}{\sigma_2} = J(t_a) \quad (5.14a)$$

$$\frac{\varepsilon_1(t_b)}{\sigma_1} = \frac{\varepsilon_2(t_b)}{\sigma_2} = J(t_b) \quad (5.14b)$$

$$J(t_a) \neq J(t_b)$$

where ε_1 and ε_2 are the responses of the material to the shear stresses σ_1 and σ_2 , respectively. In other words, the shear strain must be proportional to the shear stress at a given time. However, linearity does not hold at high strains, so it is necessary to know the interval of strain in which linearity holds before performing creep experiments. From creep isochrones, curves of ε

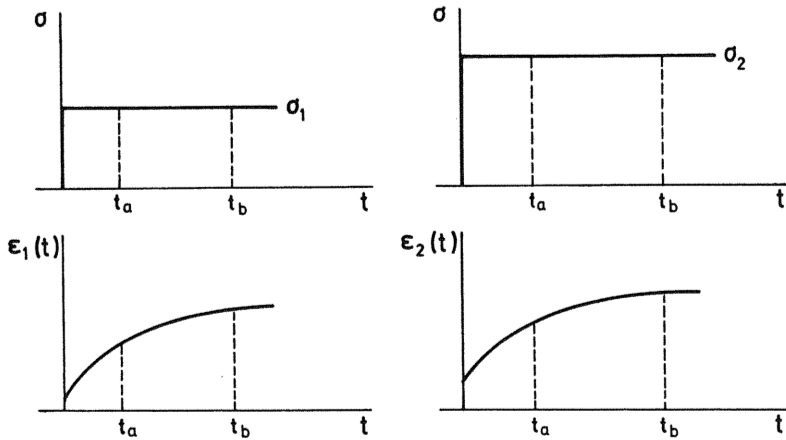


Figure 5.9 Excitations and responses in linear shear creep experiments.

against σ , similar to those presented in Figure 5.10, are obtained. It can be seen that for moderately high values of the shear stress, the shear strain is greater than one would expect from the linearity obtained in the region of small shear stresses. Unlike what occurs in the linear region, the strain for a given stress cannot be obtained from previous experiments in the nonlinear region.

The deformation is entropic for viscoelastic solids and both entropic and viscous for viscoelastic liquids. When the entropic contribution to the strain reaches its maximum value, it is said that the system has reached

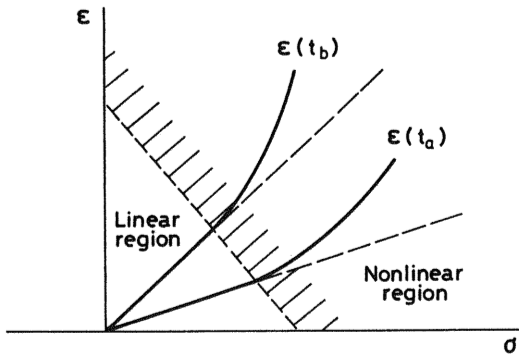


Figure 5.10 Diagrams showing the transition from linear to nonlinear behavior in shear creep experiments. Note that the data are taken from creep experiments at different deformations.

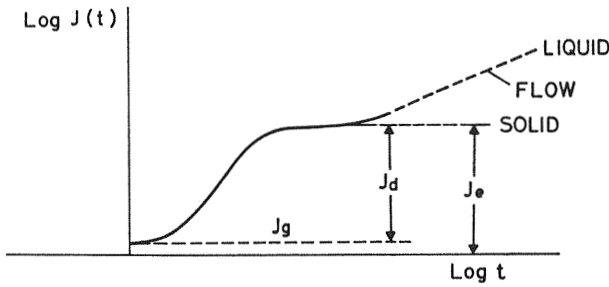


Figure 5.11 Schematic representation of the double logarithmic plot of shear creep compliance in the time domain.

steady-state conditions; in this situation, further deformation in liquids is only of the viscous type. Obviously, $J(t)$ will evolve with time like the deformation, and $J(t)$ is customarily written as

$$J(t) = J_g + J_g \Psi(t) \quad (5.15)$$

for solids and

$$J(t) = J_g + J_d \Psi(t) + \frac{t}{\eta} \quad (5.16)$$

for liquids, where η is the viscosity. An illustrative schematic curve of the creep compliance function in the time domain is presented in Figure 5.11. For solids and liquids, $\Psi(t)$ is a monotonously increasing function of time whose limiting values are 0 and 1 for $t = 0$ and $t = \infty$, respectively. J_g and J_d are, respectively, the glassy (Hookean) and maximum elastic entropic compliances. The compliance function J_e given by

$$J_e = J_g + J_d \quad (5.17)$$

is a measure of the maximum elasticity that a deformed polymeric system can store, while η is related to the maximum energy that a polymer under flow can dissipate. J_e and η are two very important viscoelastic parameters in processing. It should be pointed out that the Committee of the Society of Rheology (11) recommends using the term “equilibrium compliance”, J_e , for solids and “steady-state compliance,” J_e^o , for liquids.

For a material under a hydrostatic pressure p , Eq. (4.92) suggests that the time dependence of the trace of the strain tensor is given by

$$\Delta(t) = -pB(t) \quad (5.18)$$

where $B(t)$ is the bulk creep compliance function. While $J(t)$ may change several decades in the interval $0 < t < \infty$, the changes taking place in $B(t)$ are rather small. In analogy with the shear compliance function, $B(t)$ can be written as

$$B(t) = B_g + B_d\Psi''(t) \quad (5.19)$$

where $\Psi''(t)$ is a monotonous increasing function of time whose limiting values are 0 and 1 for $t = 0$ and $t = \infty$, respectively.

The response of a material to the tensile strength $\sigma_{11}H(t)$ is given by

$$\varepsilon_{11}(t) = D(t)\sigma_{11} \quad (5.20)$$

where $D(t)$ is the tensile compliance function, which, in analogy with the shear compliance function, can be written

$$D(t) = D_g + D_d\Psi'(t) + \frac{t}{\eta_L} \quad (5.21)$$

where D_g is the Hookean contribution, $\Psi'(t)$ is the entropic contribution whose limiting values are also 0 and 1 for $t = 0$ and $t = \infty$, respectively, and η_L is the elongational viscosity.

5.3 BOLTZMANN SUPERPOSITION PRINCIPLE IN CREEP EXPERIMENTS

5.3.1 Discrete Form

Owing to the entropic changes that take place in a viscoelastic system perturbed by a force field, the response does not vanish when the perturbation field ceases. A consequence of this fact is that the deformation depends not only on the actual stress but also on the previous stresses (mechanical history) undergone by the material in the past. Under the linear behavior regime, the responses to different perturbations superpose. Let us assume that the stresses $\Delta\sigma(\theta_1)$ and $\Delta\sigma(\theta_2)$ are applied on the material at times θ_1 and θ_2 , respectively. This stress history is shown schematically in Figure 5.12. The response is given by

$$\varepsilon(t) = J(t - \theta_1)\Delta\sigma(\theta_1) + J(t - \theta_2)\Delta\sigma(\theta_2) \quad (5.22)$$

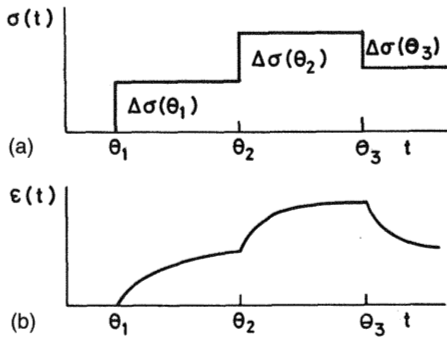


Figure 5.12 Schematic representation of the response of a viscoelastic material (b) to the shear stress history (a).

Let us assume further that the perturbation decreases $\Delta\sigma(\theta_3)$ at $t = \theta_3$. In this case, the system interprets this effect as if a stress $-\Delta\sigma(\theta_3)$ were applied to the material at time θ_3 . In that case the shear strain can be written as

$$\varepsilon(t) = J(t - \theta_1)\Delta\sigma(\theta_1) + J(t - \theta_2)\Delta\sigma(\theta_2) - J(t - \theta_3)\Delta\sigma(\theta_3) \quad (5.23)$$

The relationship between the shear strain and the shear stress can be expressed in a generalized way as

$$\varepsilon(t) = \sum_{\theta_i=-\infty}^{\theta_i=t} J(t - \theta_i)\Delta\sigma(\theta_i) \quad (5.24)$$

This equation, one of many possible forms of expressing the Boltzmann superposition principle, indicates that the effects of mechanical history are linearly additive (12,13).

For reasons that will become clear, it is important to obtain the time dependence of the shear strain under the shear stress history indicated in Figure 5.13. In this case $\sigma = \sigma H(t)$ and $H(t - \theta)\sigma = 0$. The shear strain at $t = \theta$ will be

$$\varepsilon(\theta) = J(\theta)\sigma \quad (5.25)$$

Since the shear stress is canceled at $t = \theta$, the shear strain at $t > \theta$ is expressed by (7)

$$\varepsilon(t) = J(t)\sigma - J(t - \theta)\sigma \quad (5.26)$$

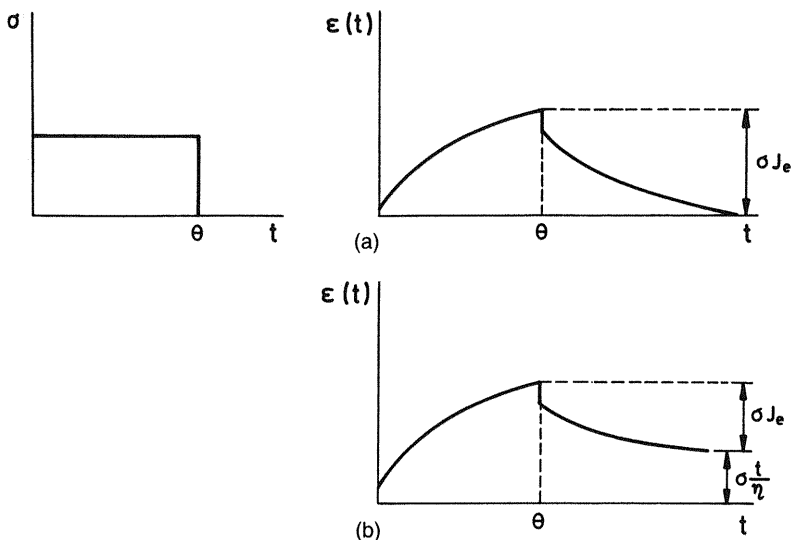


Figure 5.13 Response of a viscoelastic solid (a) and liquid (b) to a shear stress perturbation. Cancellation of the shear stress occurs at a time θ at which steady-state conditions are assumed to have been reached.

By making the change of variables $t - \theta = u$ in this equation, the elastic contribution to the strain, u units of time after the stress is canceled, can be written as

$$\epsilon(\theta) - \epsilon(\theta + u) = [J(\theta) - J(\theta + u) + J(u)]\sigma \tag{5.27}$$

Since the compliance function is a monotonous increasing function of time, $J(t + \theta) > J(t)$ if steady state is not reached. In this case one obtains

$$J_r(\theta, u) = \frac{\epsilon(\theta) - \epsilon(\theta + u)}{\sigma} < J(u) \tag{5.28}$$

If steady state is reached at the moment of canceling the shear stress, Eq. (5.27) becomes

$$\lim_{\theta \rightarrow \infty} \left[J_r(\theta, u) = \frac{\epsilon(\theta) - \epsilon(\theta + u)}{\sigma} \right] = J(\infty) - J(\infty + u) + J(u) = J(u) \tag{5.29}$$

because $J(\infty) = J(\infty + u)$. This expression shows that the recovery compliance $J_r(t)$ is an image of the compliance function $J(t)$ when the recovery

deformation is registered after the system has reached steady-state conditions.

Let us now analyze the behavior of a viscoelastic liquid whose stress history is $\sigma(t) = \sigma$ for $0 < t \leq \theta$ and $\sigma(t) = 0$ for $\theta > 0$. In this case, the strain at $t = \theta$ is given by

$$\varepsilon(\theta) = J(\theta)\sigma = \sigma \left[J_g + J_d\Psi(\theta) + \frac{\theta}{\eta} \right] \quad (5.30)$$

For $t > \theta$, the shear strain can be written as

$$\varepsilon(t) = \sigma \left[J_g + J_d\Psi(t) + \frac{t}{\eta} \right] - \sigma \left[J_g + J_d\Psi(t - \theta) + \frac{t - \theta}{\eta} \right] \quad (5.31)$$

By making $t - \theta = u$ in Eq. (5.31) and subtracting the resulting expression from Eq. (5.30), one obtains

$$\varepsilon(\theta) - \varepsilon(\theta + u) = [J_d\Psi(\theta) - J_d\Psi(\theta + u) + J_g + J_d\Psi(u)]\sigma \quad (5.32)$$

Because in non-steady-state conditions $J_d\Psi(\theta) < J_d\Psi(\theta + u)$, the recovery compliance $[\varepsilon(\theta) - \varepsilon(\theta + u)]/\sigma < J(u) - u/\eta$. For steady-state conditions ($\theta \rightarrow \infty$), Eq. (5.32) can be written as

$$\left. \frac{\varepsilon(\infty) - \varepsilon(\infty + u)}{\sigma} \right| = \frac{J_d\Psi(\infty) - J_d\Psi(\infty + u) + J_g + J_d\Psi(u)}{J_g + J_d\Psi(u)} = J_r(u) \quad (5.33)$$

where $J_r(u) = J(u) - u/\eta$. Therefore this procedure allows the experimental determination of the recoverable compliance and the viscous component of the creep compliance function.

The Boltzmann superposition principle applied to a viscoelastic material that has undergone a history of pressures or tensile stresses can be written as

$$\Delta(t) = - \sum_{\theta=-\infty}^t B(t - \theta)p(\theta) \quad (5.34a)$$

$$\varepsilon_{11}(t) = \sum_{\theta=-\infty}^t D(t - \theta)\Delta\sigma_{11}(\theta) \quad (5.34b)$$

where $\Delta(t) = \text{trace } \varepsilon_{ij}(t)$.

5.3.2 Continuous Form

If the shear stress varies with time in very small steps so that σ can be assumed to be a continuous function of time, Eq. (5.24) can be written

$$\varepsilon(t) = \int_{-\infty}^t J(t-\theta) \frac{d\sigma(\theta)}{d\theta} d\theta \quad (5.35)$$

This is the Boltzmann superposition principle for creep experiments expressed in continuous form. If the stress is a continuous function of time in the interval $-\infty < t < \theta_1$, constant in the interval $\theta_1 \leq t \leq \theta_2$, and again a continuous function for $t > \theta_2$ (see Fig. 5.14), then Eq. (5.35) cannot be used to obtain ε because the contribution of the stress to the strain in the interval $\theta_1 \leq t \leq \theta_2$ would be zero. The response for this stress history is given by

$$\begin{aligned} \varepsilon(t) = & \int_{-\infty}^{\theta_1} J(t-\theta) \frac{d\sigma(\theta)}{d\theta} d\theta + J(t-\theta_1) \Delta\sigma(\theta_1) \\ & + \int_{\theta_2}^t J(t-\theta) \frac{d\sigma(\theta)}{d\theta} d\theta \end{aligned} \quad (5.36)$$

By integrating Eq. (5.36) by parts one obtains

$$\begin{aligned} \varepsilon(t) = & J_g \sigma(t) + \int_{-\infty}^t \sigma(\theta) \frac{dJ(t-\theta)}{d(t-\theta)} d\theta \\ = & J_g \sigma(t) + \int_0^{\infty} \sigma(t-u) \frac{dJ(u)}{du} du \end{aligned} \quad (5.37)$$

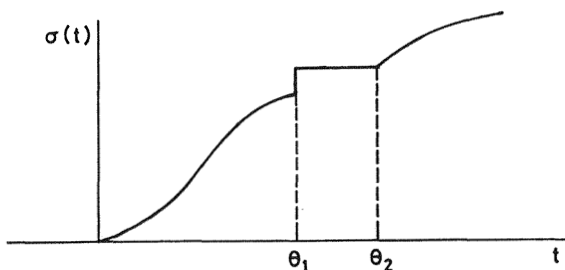


Figure 5.14 Shear stress perturbation of a viscoelastic material. Continuous and discontinuous excitations.

where the change of variables $t = \theta = u$ was made and it was considered that $\sigma(-\infty) = 0$. Equation (5.37) is an alternative way of expressing the Boltzmann superposition principle. As $J(t)$ is an increasing continuous function of time, Eq. (5.37) is more suitable than Eq. (5.35) to express the Boltzmann superposition principle.

In the same way, the dilatation for a system under a time-dependent hydrostatic pressure can be written

$$\begin{aligned}\Delta(t) &= - \int_{-\infty}^t B(t-\theta) \frac{dp(\theta)}{d\theta} d\theta \\ &= -B_g p(t) - \int_0^\infty p(t-u) \frac{dB(u)}{du} du\end{aligned}\quad (5.38)$$

where $\Delta(t) = \text{trace } \gamma_{ii}$. Finally, the Boltzmann superposition principle predicts that the tensile strain is related to the tensile stress history by equation

$$\begin{aligned}\varepsilon_{11}(t) &= \int_{-\infty}^t D(t-\theta) \frac{d\sigma_{11}(\theta)}{d\theta} d\theta \\ &= D_g \sigma_{11}(t) + \int_0^\infty \sigma_{11}(t-u) \frac{dD(u)}{du} du\end{aligned}\quad (5.39)$$

5.4 MEMORY EFFECTS IN CREEP EXPERIMENTS

To gain a better understanding of the effects of memory on the strain of viscoelastic systems, it is convenient to write Eq. (5.37) in terms of the entropic and viscous contributions to $J(t)$. The time dependence of the shear strain can be written as

$$\varepsilon(t) = J_g \sigma(t) + J_d \int_{-\infty}^t \sigma(\theta) \frac{d\Psi(t-\theta)}{d(t-\theta)} d\theta + \frac{1}{\eta} \int_{-\infty}^t \sigma(\theta) d\theta \quad (5.40)$$

This equation, formulated for liquids, also describes the behavior of solids if $\eta = \infty$ is assumed in the latter case. Experimentally it is found that $J(t) - t/\eta - J_g$ is a monotonous increasing function of time that reaches the value J_d as $t \rightarrow \infty$. The function $\Psi(t)$ modulates the entropic response to the shear stress; the time dependence of this function is indicated in Figure 5.15. Since $\Psi(t-\theta)$ is a monotonous decreasing function of time, $d\Psi(t-\theta)/d(t-\theta)$ is an increasing function of time whose slope increases considerably as θ approaches t . Consequently, $\Psi(t)$ behaves as a memory function that mod-

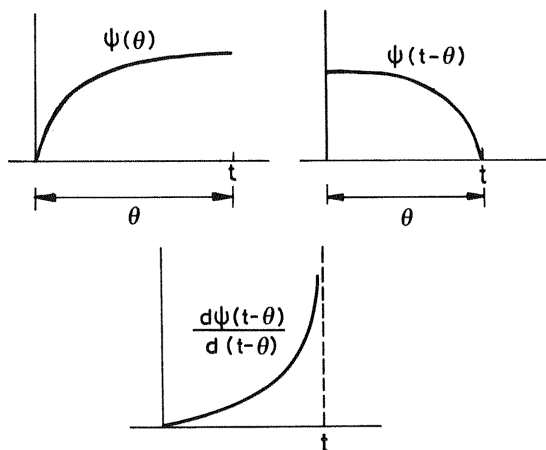


Figure 5.15 Form of the fading memory of Eq. (5.40) in a shear creep experiment.

ulates the perturbations on the material in such a way that their efforts greatly increase with the closeness of the perturbations to the time of observation. In other words, viscoelastic materials exhibit fading memory (7). This behavior is schematically represented in Figure 5.16, where the curves describing both the shear stress history and the evolution of $\psi(t)$ with time are represented.

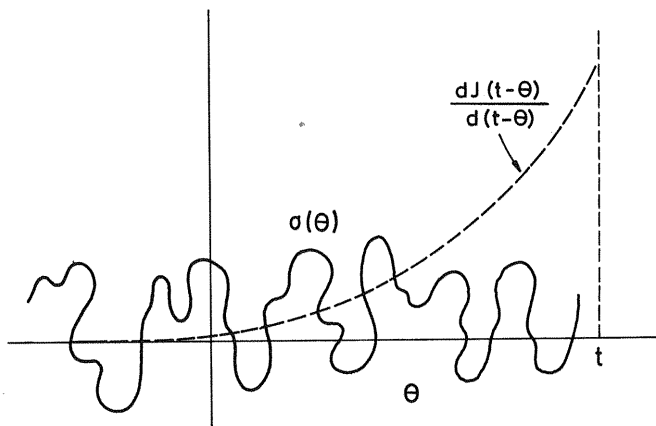


Figure 5.16 Schematic sketch showing fading memory for an arbitrary shear stress history.

5.5 BOLTZMANN SUPERPOSITION PRINCIPLE IN RELAXATION EXPERIMENTS

5.5.1 Discrete Form

Let us assume that a viscoelastic material undergoes the following shear strain history: $\Delta\varepsilon(\theta_1)H(t - \theta_1)$, and $\Delta\varepsilon(\theta_2)H(t - \theta_2)$. Let us assume further that the shear strain $\Delta\varepsilon(\theta_3)$ suddenly vanishes at $t = \theta_3$. In these circumstances the response of the material will be

$$\sigma(t) = G(t - \theta_1)\Delta\varepsilon(\theta_1) + G(t - \theta_2)\Delta\varepsilon(\theta_2) - G(t - \theta_3)\Delta\varepsilon(\theta_3) \quad (5.41)$$

As indicated above, cancellation of a given perturbation is interpreted by the material as if a perturbation of opposite sign were applied on it. The Boltzmann superposition principle can be expressed in a generalized way by

$$\sigma(t) = \sum_{\theta_i=-\infty}^{\theta_i=t} G(t - \theta_i)\Delta\varepsilon(\theta_i) \quad (5.42)$$

For a material with a history of discrete isotropic deformations, the evolution of the hydrostatic pressure with time can be written as

$$p(t) = - \sum_{\theta_i=-\infty}^{\theta_i=t} K(t - \theta_i)\Delta(\theta_i) \quad (5.43)$$

while for a viscoelastic solid with a tensile strain history the time dependence of the tensile stress is given by

$$\sigma_{11}(t) = \sum_{\theta_i=-\infty}^t E(t - \theta_i)\Delta\varepsilon_{11}(\theta_i) \quad (5.44)$$

5.5.2 Continuous Form

If the values of $\Delta\varepsilon(\theta_i)$ are very small, the time dependence of the shear stress in Eq. (5.42) can be expressed by the relationship

$$\sigma(t) = \int_{-\infty}^t G(t - \theta) \frac{d\varepsilon(\theta)}{d\theta} d\theta \quad (5.45)$$

This equation, however, does not give a good account of the histories in which the strain remains constant during a given interval of time, because in

that case the contribution of $\Delta\varepsilon$ to the relaxation would be nil. For example, if $\Delta\varepsilon(\theta_1)$ remains constant in the interval $\theta_1 < t < \theta_2$, as shown in Figure 5.17, then Eq. (5.45) should be written

$$\begin{aligned} \sigma(t) = & \int_{-\infty}^{\theta_1} G(t-\theta) \frac{d\varepsilon(\theta)}{d\theta} d\theta + G(t-\theta_1)\Delta\varepsilon(\theta_1) \\ & + \int_{\theta_2}^t G(t-\theta) \frac{d\varepsilon(\theta)}{d\theta} d\theta \end{aligned} \quad (5.46)$$

However, by integrating Eq. (5.45) by parts, one obtains the expression

$$\sigma(t) = G_g \varepsilon(t) + \int_0^\infty \varepsilon(t-u) \frac{dG(u)}{du} du \quad (5.47)$$

in which the strain history is not in the time derivative. It has been assumed in Eq. (5.47) that $\varepsilon(-\infty) = 0$ and $G_g = G(0) = G_d$ for liquids. For solids, $G_g = G_e + G_d$.

For a material undergoing a variable isotropic deformation, the time dependence of the pressure is given by

$$\begin{aligned} p(t) = & - \int_{-\infty}^t K(t-\theta) \frac{d\Delta(\theta)}{d\theta} d\theta \\ = & -K_g \Delta(t) - \int_0^\infty \Delta(t-u) \frac{dK(u)}{du} du \end{aligned} \quad (5.48)$$

In the same way, the evolution of the tensile stress with time can be expressed as

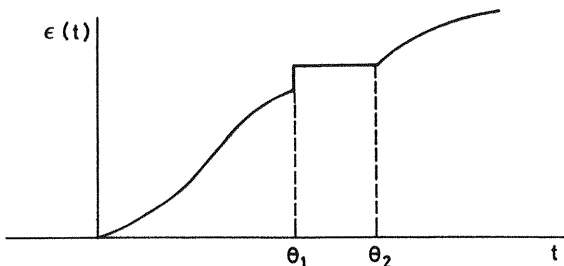


Figure 5.17 Shear strain perturbation of a viscoelastic material. Continuous and discontinuous excitations.

$$\begin{aligned}\sigma_{11}(t) &= \int_{-\infty}^t E(t-\theta) \frac{d\varepsilon_{11}(\theta)}{d\theta} d\theta \\ &= E_g \sigma_{11}(t) + \int_0^{\infty} \varepsilon_{11}(t-u) \frac{dE(u)}{du} du\end{aligned}\quad (5.49)$$

5.6 MEMORY FUNCTION IN RELAXATION EXPERIMENTS

The memory effects in relaxation processes can be observed by writing Eq. (5.47) as

$$\sigma(t) = G_g \varepsilon(t) + G_d \int_{-\infty}^t \varepsilon(\theta) \frac{d\Phi(t-\theta)}{d(t-\theta)} d\theta \quad (5.50)$$

where the change of variables $\theta = t - u$ has been made. As shown in Figure 5.18, $\Phi(t)$ is a decreasing function of time while $\Phi(t - \theta)$ is an increasing function of t . It is also an experimental fact that the value of the slope of the curve of $\Phi(t - \theta)$ versus time undergoes a sharp increase as θ approaches t . A schematic representation of $d\Phi(t - \theta)/d(t - \theta)$ together with an arbitrary history of strain is shown in Figure 5.19. It can be seen that memory effects become much more important, that is, the absolute value of $d\Phi(t - \theta)/d(t - \theta)$ becomes much larger as the time θ at which the deformation occurred is

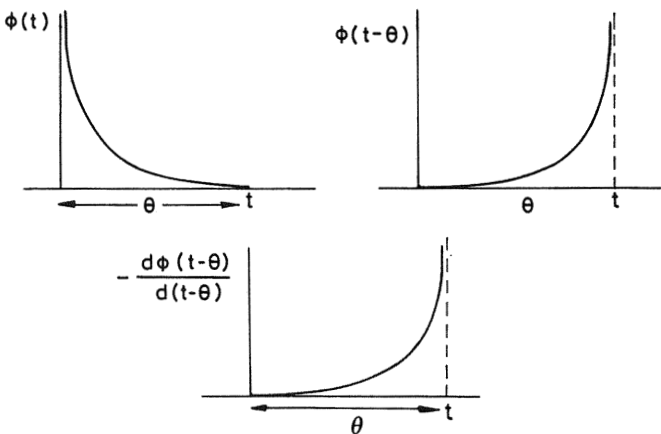


Figure 5.18 Form of the fading memory of Eq. (5.50) in a shear relaxation experiment.

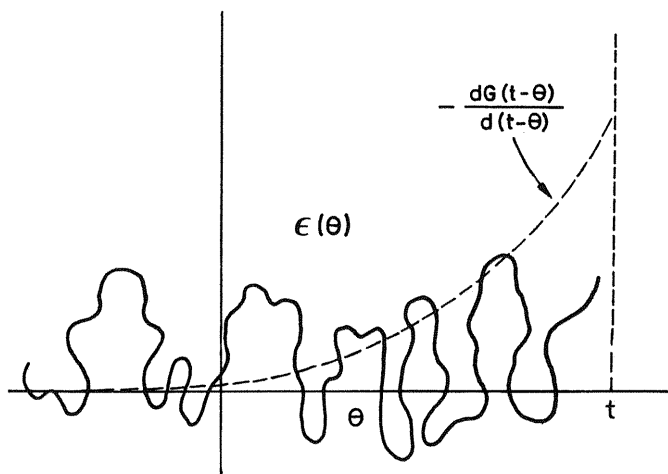


Figure 5.19 Sketch showing fading memory for an arbitrary shear strain history.

closer to the time t . Consequently the material “remembers” better the history of deformation closer to the present time; in other words, viscoelastic materials exhibit fading memory (7).

5.7 RAMP EXPERIMENTS

Let us assume that a viscoelastic material undergoes a shear strain that is a linear function of time. Let us assume further that the experiment is carried out in such conditions that the viscoelastic behavior is linear and the mechanical history is given by (7)

$$\varepsilon(t) = \begin{cases} 0 & t < 0 \\ kt, & t \geq 0 \end{cases} \quad (5.51)$$

With the change of variables $t - \theta = u$, Eq. (5.45) becomes

$$\sigma(t) = k \int_0^t G(u) du = k \int_0^t G(t) dt \quad (5.52)$$

Once steady-state conditions ($t \rightarrow \infty$) are reached, one obtains

$$\varepsilon(t) = \left(J_e + \frac{t}{\eta} \right) \sigma_\infty \quad (5.53)$$

According to this equation,

$$k = \frac{d\varepsilon}{dt} = \frac{\sigma_\infty}{\eta} \quad (5.54)$$

By substituting this value of k into Eq. (5.52), the following relationship between the viscosity and the relaxation modulus is obtained:

$$\eta = \int_0^\infty G(t) dt \quad (5.55)$$

This expression allows the determination of the viscosity at zero shear rate from the time dependence of the relaxation modulus.

On the other hand, it is possible to relate the shear compliance function to the relaxation modulus by using the ramp experiment described above. Actually, Eqs. (5.35) and (5.52) lead to the expression

$$\varepsilon(t) = \int_0^t J(t-\theta) \frac{d\sigma(t)}{dt} = k \int_0^t G(\theta) J(t-\theta) d\theta \quad (5.56)$$

By taking into account that according to the mechanical history stated in Eq. (5.51), $\varepsilon(t) = kt$, Eq. (5.56) becomes

$$\int_0^t J(t-\theta) G(\theta) d\theta = \int_0^t G(t-\theta) J(\theta) d\theta = t \quad (5.57)$$

5.8 LAPLACE TRANSFORM RELATIONSHIPS BETWEEN TRANSIENT RELAXATION MODULI AND TRANSIENT COMPLIANCE FUNCTIONS

5.8.1 Introduction

An apparently easy way to relate transient relaxation moduli and transient compliance functions is by applying Laplace transforms to Eqs. (5.35) and (5.45). By taking into account the convolution theorem, one obtains (see Appendix)

$$\bar{\epsilon}(s) = \bar{J}(s)s\bar{\sigma}(s) \quad (5.58a)$$

$$\bar{\sigma}(s) = \bar{G}(s)s\bar{\epsilon}(s) \quad (5.58b)$$

where the overbar indicates Laplace transform. These relations lead to the expression

$$\bar{J}(s)\bar{G}(s) = \frac{1}{s^2} \quad (5.59)$$

which permits the shear compliance to be obtained from the relaxation modulus and vice versa. It should be noted that Laplace transforms of the expressions of Eq. (5.57) also lead to Eq. (5.59).

Laplace transforms of Eqs. (5.38) and (5.48) give

$$\bar{\Delta}(s) = -s\bar{B}(s)\bar{p}(s) \quad (5.60a)$$

$$\bar{p}(s) = -s\bar{K}(s)\bar{\Delta}(s) \quad (5.60b)$$

These expressions lead to

$$\bar{B}(s)\bar{K}(s) = \frac{1}{s^2} \quad (5.61)$$

In the same way, from Laplace transforms of Eqs. (5.39) and (5.49) the following relationship is obtained:

$$\bar{D}(s)\bar{E}(s) = \frac{1}{s^2} \quad (5.62)$$

It should be noted that Eqs. (5.59), (5.61), and (5.62) are of limited use because of the difficulties involved in the calculations of the required transforms and their inverses.

5.8.2 Important Inequalities

The reciprocal of the Laplace transform of Eq. (5.59) gives

$$\int_0^t G(t-\theta)J(\theta)d\theta = \int_0^t J(t-\theta)G(\theta)d\theta = t \quad (5.63)$$

an expression similar to Eq. (5.57) obtained from the ramp experiment defined by Eq. (5.51). By using Leibnitz's rule, the derivative with respect to time of Eq. (5.63) can be written as

$$\int_0^t \frac{dG(u)}{du} J(t-u) du + G_g J(t) = 1 \quad (5.64a)$$

$$\int_0^t \frac{dJ(u)}{du} G(t-u) du + J_g G(t) = 1 \quad (5.64b)$$

where the change of variable $u = t - \theta$ was made. Substituting the identities

$$J(t-u) = J(t) + [J(t-u) - J(t)] \quad (5.65a)$$

and

$$G(t-u) = G(t) + [G(t-u) - G(t)] \quad (5.65b)$$

into Eqs. (5.64a) and (5.64b), respectively, one obtains

$$J(t)G(t) + \int_0^t [J(t-u) - J(t)] \frac{dG(u)}{du} du = 1 \quad (5.66a)$$

$$J(t)G(t) + \int_0^t [G(t-u) - G(t)] \frac{dJ(u)}{du} du = 1 \quad (5.66b)$$

Since $J(t)$ and $G(t)$ are, respectively, monotonously increasing and decreasing functions of time, $J(t-u) - J(t) \leq 0$ and $dG(t)/dt \leq 0$. For the same reasons, $G(t-u) - G(t) \geq 0$ and $dJ(t)/dt \geq 0$. Hence, from Eqs. (5.66), the following inequality is obtained (14);

$$J(t)G(t) \leq 1 \quad (5.67)$$

The integrals of Eqs. (5.66) vanish for $t = 0$, and consequently $J_g G_g = 1$. For viscoelastic solids, $J(t-u) - J(t)$ and $G(t-u) - G(t)$ also vanish when $t \rightarrow \infty$, and as a result, $J_e G_e = 1$. For viscoelastic liquids, $dJ(t)/dt = 1/\eta$ and $G(t) = 0$ when $t \rightarrow \infty$, so Eq. (5.66b) can be written as (7)

$$\lim_{t \rightarrow \infty} G(t)J(t) = J_e^0 G_e = 1 - \frac{1}{\eta} \int_0^\infty G(t-u) du \quad (5.68)$$

According to Eq. (5.54), the integral of Eq. (5.68) gives the viscosity. Hence, $J_e^0 G_e = 0$ for viscoelastic liquids.

The inverse of the Laplace transforms of Eqs. (5.62) and (5.61) gives

$$\int_0^t D(t-\theta)E(\theta)d\theta = \int_0^t D(\theta)E(t-\theta)d\theta = t \quad (5.69)$$

and

$$\int_0^t K(t-\theta)B(\theta)d\theta = \int_0^t B(t-\theta)K(\theta)d\theta = t \quad (5.70)$$

Obviously, the following inequalities also hold:

$$K(t)B(t) \leq 1 \quad (5.71a)$$

$$D(t)E(t) \leq 1 \quad (5.71b)$$

5.9 GENERALIZATION OF THE SUPERPOSITION PRINCIPLE

5.9.1 Introduction

The superposition principle leads to the following generalized relationship between the strain tensor and the stress tensor for viscoelastic systems:

$$\gamma_{ij}(t) = \frac{1}{2} \int_{-\infty}^t J(t-\theta) \frac{d\sigma_{ij}(\theta)}{d\theta} d\theta + \delta_{ij} \int_{-\infty}^t \left[\frac{B(t-\theta)}{9} - \frac{J(t-\theta)}{6} \right] \frac{d\Sigma(\theta)}{d\theta} d\theta \quad (5.72)$$

where $\Sigma = \text{trace } \sigma_{ij}$. The generalized relationship between the stress and strain tensors can be written as

$$\sigma_{ij}(t) = 2 \int_{-\infty}^t G(t-\theta) \frac{d\gamma_{ij}(\theta)}{d\theta} d\theta + \delta_{ij} \int_{-\infty}^t \left[K(t-\theta) - \frac{2}{3}G(t-\theta) \right] \frac{d\Delta(\theta)}{d\theta} d\theta \quad (5.73)$$

where $\Delta = \text{trace } \gamma_{ij}$. As discussed above, if the stress and strain remain constant for some time intervals in Eqs. (5.72) and (5.73), respectively, it is necessary to carry out integration by parts of the integrals of these equations in order to avoid having the derivatives $d\sigma_{ij}(\theta)/d\theta$ [$d\varepsilon_{ij}(\theta)/d\theta$] and $d\Sigma(\theta)/d\theta$ [$d\Delta(\theta)/d\theta$] appear in these integrals.

The generalized stress-strain relationships in linear viscoelasticity can be obtained directly from the generalized Hooke's law, described by Eqs. (4.85) and (4.118), by using the so-called correspondence principle. This principle establishes that if an elastic solution to a stress analysis is known, the corresponding viscoelastic (complex plane) solution can be obtained by substituting for the elastic quantities the s -multiplied Laplace transforms (8; p. 509). The application of this principle to Eq. (4.85) gives

$$\bar{\sigma}_{ij}(s) = 2s\bar{G}(s)\bar{\gamma}_{ij}(s) + \delta_{ij}(s) \left[\bar{K}(s) - \frac{2}{3}\bar{G}(s) \right] \bar{\Delta}(s) \quad (5.74)$$

It can easily be seen that the retransformation of this equation gives Eq. (5.73). In the same way, the application of the correspondence principle to Eq. (4.118) leads to the expression

$$\bar{\gamma}_{ij}(s) = \frac{1}{2} s \bar{J}(s) \bar{\sigma}_{ij}(s) + \delta_{ij} \left[\frac{\bar{B}(s)}{9} - \frac{\bar{J}(s)}{6} \right] s \bar{\Sigma}(s) \quad (5.75)$$

whose retransformation gives Eq. (5.72). This expression can be obtained directly from Eq. (5.74). In this case,

$$\begin{aligned} \bar{\gamma}_{ij}(s) &= \frac{\bar{\sigma}_{ij}(s)}{2s\bar{G}(s)} - \delta_{ij} \frac{\bar{K}(s) - (2/3)\bar{G}(s)}{\bar{G}(s)} \left(\frac{\bar{\Sigma}(s)}{2s\bar{K}(s)} \right) \\ &= \frac{1}{2} s \bar{J}(s) \bar{\sigma}_{ij}(s) + \delta_{ij} \left[\frac{\bar{B}(s)}{9} - \frac{\bar{J}(s)}{6} \right] s \bar{\Sigma}(s) \end{aligned} \quad (5.76)$$

where Eqs. (5.59) and (5.61) have been considered. Moreover, it was taken into account that

$$\bar{\Sigma}(s) = 3s\bar{K}(s)\bar{\Delta}(s) \quad (5.77)$$

and consequently

$$\bar{\Delta}(s) = \frac{\bar{\Sigma}(s)}{3s\bar{K}(s)} \quad (5.78)$$

5.9.2 Important Relationships Between Viscoelastic Functions

For a system under a tensile strength σ_{11} , Eq. (5.75) becomes

$$\bar{\gamma}_{11}(s) = \left[\frac{\bar{J}(s)}{3} + \frac{\bar{B}(s)}{9} \right] s \bar{\sigma}_{11}(s) \quad (5.79a)$$

Hence

$$\frac{\bar{\gamma}_{11}(s)}{s\bar{\sigma}_{11}(s)} = \left[\frac{\bar{J}(s)}{3} + \frac{\bar{B}(s)}{9} \right] = \bar{D}(s) \quad (5.79b)$$

The reciprocal of the Laplace transform of Eq. (5.79b) leads to the relationship

$$D(t) = \frac{J(t)}{3} + \frac{B(t)}{9} \quad (5.80)$$

In other words, independently of the viscoelastic history in the linear region, the tensile compliance function can readily be obtained from both the shear and bulk compliance functions. For viscoelastic solids and liquids above the glass transition temperature, the following relationships hold when $t \rightarrow \infty$: $J(t) \cong t/\eta$ [Eq. (5.16)], $D(t) \cong \eta_L/t$ [Eq. (5.21)], and $D(t)J(t)/3$. These relations lead to $\eta_L \cong 3\eta$; that is, the elongational viscosity is three times the shear viscosity. It is noteworthy that the relatively high value of tensile viscosity facilitates film processing.

Laplace transform of the tensile relaxation modulus can be obtained from Eqs. (5.62) and (5.80). The pertinent expression is

$$\begin{aligned} s\bar{E}(s) &= \frac{1}{s\bar{D}(s)} = \frac{1}{s[\bar{J}(s)/3 + \bar{B}(s)/9]} \\ &= \frac{1}{1/3s\bar{G}(s) + 1/9s\bar{K}(s)} \end{aligned} \quad (5.81)$$

Equation (5.81) leads to the expression

$$\bar{E}(s) = \frac{9\bar{G}(s)\bar{K}(s)}{3\bar{K}(s) + \bar{G}(s)} \quad (5.82)$$

which gives the Laplace transform of the tensile stress in terms of Laplace transforms of the shear and bulk relaxation moduli. It should be noted, once more, that Eq. (5.82) can be obtained directly from Eq. (4.95) by using the correspondence principle. Equation (5.82) in real time is given by

$$\int_0^t E(t-\theta)G(\theta)d\theta + 3 \int_0^t E(t-\theta)K(\theta)d\theta = 9 \int_0^t K(t-\theta)G(\theta)d\theta \quad (5.83)$$

This equation indicates that the tensile modulus does not show an explicit dependence on both the shear and the bulk relaxation moduli. It can easily be seen that for $K(t) \gg G(t)$, $E(t) \cong 3G(t)$.

In a tensile experiment ($\sigma_{11} \neq 0$, $\sigma_{22} = \sigma_{33} = 0$), the components of the strain tensor are γ_{11} , $\gamma_{22} = \gamma_{33}$. From Eq. (5.76) the transverse deformation is related to the tensile strain by the expression

$$\begin{aligned}\bar{\gamma}_{22}(s) = \bar{\gamma}_{33}(s) &= -\frac{\bar{J}(s)/6 - \bar{B}(s)/9}{\bar{J}(s)/3 + \bar{B}(s)/9} \bar{\gamma}_{11}(s) \\ &= -\frac{3\bar{K}(s) - 2\bar{G}(s)}{6\bar{K}(s) + 2\bar{G}(s)} \bar{\gamma}_{11}(s)\end{aligned}\quad (5.84)$$

Hence, a Laplace transform of the Poisson ratio can be written as

$$\begin{aligned}\bar{\nu}(s) &= -\frac{\bar{\gamma}_{22}(s)}{\bar{\gamma}_{11}(s)} = -\frac{\bar{\gamma}_{33}(s)}{\bar{\gamma}_{11}(s)} \\ &= \frac{\bar{J}(s)/6 - \bar{B}(s)/9}{\bar{J}(s)/3 + \bar{B}(s)/9} = \frac{3\bar{K}(s) - 2\bar{G}(s)}{6\bar{K}(s) + 2\bar{G}(s)}\end{aligned}\quad (5.85)$$

In spite of the complex dependence of $\nu(t)$ on the viscoelastic functions, the limit values of the Poisson ratio can easily be obtained. Thus the theorem of the initial and final values establishes that if a function $f(t)$ has a limit, the following relationships hold:

$$\lim_{t \rightarrow 0} f(t) = \lim_{s \rightarrow \infty} s\bar{f}(s) = f(0) \quad (5.86a)$$

$$\lim_{t \rightarrow \infty} f(t) = \lim_{s \rightarrow 0} s\bar{f}(s) = f(\infty) \quad (5.86b)$$

Accordingly, Eq. (5.85) can be written as

$$\lim_{s \rightarrow \infty} \bar{\nu}(s) = \frac{3K_g - 2G_g}{6K_g + 2G_g} = \nu_g \quad (5.87a)$$

$$\lim_{s \rightarrow 0} \bar{\nu}(s) = \frac{3K_e - 2G_e}{6K_e + 2G_e} = \nu_e \quad (5.87b)$$

where ν_g and ν_e represent, respectively, the Poisson ratio at short times ($s \rightarrow \infty$) and long times ($s \rightarrow 0$) and consequently, are called the Poisson ratio at the glass-like state and at steady-state equilibrium. Because $K_e \gg G_e$, Eq. (5.87b) predicts that $\nu_e = 0.5$. In the glassy state the values of K_g and G_g are similar ($K_g \cong 2.67G_g$) and Eq. (5.87a) suggests that $\nu_g \cong 1/3$. Like $J(t)$, $D(t)$, and $B(t)$, the Poisson ratio is a monotonously increasing function of time with the limiting values indicated

For an isotropic elastic material under a uniaxial stress along the axis x_1 , the Poisson ratio $\nu = -\gamma_{22}/\gamma_{11}$. By applying the correspondence principle, one obtains

$$\bar{\gamma}_{22}(s) = \bar{\gamma}_{33}(s) = -s\bar{\nu}(s)\bar{\gamma}_{11}(s) \quad (5.88)$$

In the time domain, Eq. (5.88) can be written as

$$\begin{aligned}\gamma_{22}(t) = \gamma_{33}(t) &= - \int_{-\infty}^t \nu(t - \theta) \frac{\partial \gamma_{11}(\theta)}{\partial \theta} d\theta \\ &= -\nu_g \sigma_{11}(t) - \int_0^{\infty} \gamma_{11}(t - u) \frac{d\nu(u)}{du} du\end{aligned}\quad (5.89)$$

Let us now find the relationship between the tensile and shear moduli in terms of the Poisson ratio. Since for ideal elastic solids $E = 2(1 + \nu)G$, the correspondence principle establishes that

$$s\bar{E}(s) = 2[1 + s\bar{\nu}(s)]s\bar{G}(s)\quad (5.90)$$

Hence, the reciprocal of the Laplace transform of Eq. (5.90) leads to the expression

$$\begin{aligned}E(t) &= 2G(t) + 2 \int_{-\infty}^t \nu(t - \theta) \frac{\partial G(\theta)}{\partial \theta} d\theta \\ &= 2G(t)[1 + \nu_g] + 2 \int_0^{\infty} G(t - u) \frac{\partial \nu(u)}{\partial u} du\end{aligned}\quad (5.91)$$

where ν_g is the glass $[\nu(0)]$ Poisson ratio. The correspondence principle also allows us to determine, at least theoretically, the bulk relaxation modulus, $K(t)$, from simultaneous measurements of the tensile relaxation modulus and the Poisson ratio. According to Table 4.1, $K = E/3(1 - 2\nu)$, and the correspondence principle yields

$$s\bar{K}(s) = \frac{s\bar{E}(s)}{3[1 - 2s\bar{\nu}(s)]}\quad (5.92)$$

Hence

$$\bar{E}(s) = 3[1 - 2s\bar{\nu}(s)]\bar{K}(s)\quad (5.93)$$

Retransforming this expression to the real t axis gives

$$E(t) = 3(1 - 2\nu_g)K(t) + 6 \int_0^t K(u) \frac{d\nu(t - \nu)}{du} du\quad (5.94)$$

This expression is a convolution integral and cannot be made explicit for $K(t)$. However, methods for its deconvolution are available (Ref. 4, p. 543).

5.10 GENERALIZED STRESS-STRAIN RELATIONSHIPS IN THE FREQUENCY DOMAIN

Exchanging in Eqs. (5.74) and (5.75) the transform $s = i\omega$ for the harmonic response forms leads to

$$\sigma_{ij}(\omega) = \left[K^*(\omega) - \frac{2}{3}G^*(\omega) \right] \Delta(\omega)\delta_{ij} + 2G^*(\omega)\gamma_{ij}(\omega) \quad (5.95)$$

$$\gamma_{ij}(\omega) = \left[\frac{1}{9}B^*(\omega) - \frac{1}{6}J^*(\omega) \right] \Sigma(\omega)\delta_{ij} + \frac{1}{2}J^*(\omega)\sigma_{ij}(\omega) \quad (5.96)$$

where the asterisk refers to the complex function. In this equation, $\Delta(\omega)$ and $\Sigma(\omega)$ are given by

$$\Delta(\omega) = \gamma_{11}(\omega) + \gamma_{22}(\omega) + \gamma_{33}(\omega) \quad (5.97a)$$

$$\Sigma(\omega) = \sigma_{11}(\omega) + \sigma_{22}(\omega) + \sigma_{33}(\omega) \quad (5.97b)$$

Relationships between different viscoelastic functions are easily obtained from these equations. Thus for a material under harmonic tensile stress,

$$\sigma_{ij}(\omega) = \begin{pmatrix} \sigma_{11}(\omega) & 0 & 0 \\ 0 & 0 & 0 \\ 0 & 0 & 0 \end{pmatrix} \quad (5.98)$$

the components of the strain tensor will be

$$\gamma_{ij} = \begin{pmatrix} \gamma_{11}(\omega) & & \\ & \gamma_{22}(\omega) & \\ & & \gamma_{22}(\omega) \end{pmatrix} \quad (5.99)$$

For Eq. (5.95) one obtains

$$\sigma_{11}(\omega) = \left[K^*(\omega) - \frac{2}{3}G^*(\omega) \right] \Delta(\omega) + 2G^*(\omega)\gamma_{11}(\omega) \quad (5.100a)$$

$$0 = \left[K^*(\omega) - \frac{2}{3}G^*(\omega) \right] \Delta(\omega) + 2G^*(\omega)\gamma_{22}(\omega) \quad (5.100b)$$

These equations lead to the expression

$$E^*(\omega) = \frac{\sigma_{11}(\omega)}{\gamma_{11}(\omega)} = \frac{9K^*(\omega)G^*(\omega)}{3K^*(\omega) + 2G^*(\omega)} \quad (5.101)$$

This equation relates the tensile complex relaxation modulus to the bulk and shear complex relaxation moduli. In the same way, Eq. (5.95) leads to the relationship

$$D^*(\omega) = \frac{1}{9}B^*(\omega) + \frac{1}{3}J^*(\omega) \quad (5.102)$$

which relates the tensile complex compliance function to the bulk and shear complex compliance functions. Because at temperatures well above the glass transition temperature of a viscoelastic material, $K^*(\omega) \gg G^*(\omega)$ and $B^*(\omega) \ll J^*(\omega)$, Eqs. (5.101) and (5.102) suggest that

$$E^*(\omega) = 3G^*(\omega) \quad \text{and} \quad D^*(\omega) \simeq \frac{1}{3}J^*(\omega) \quad (5.103)$$

Relationships between complex viscoelastic functions similar to those given in Tables 4.1 and 4.2 are obtained in the frequency domain. The difference is that the viscoelastic magnitudes in the frequency domain are of the complex type, that is, they have real and imaginary components.

5.11 GENERALIZED STRESS-STRAIN RELATIONSHIPS FOR VISCOELASTIC SYSTEMS WITH ANY DEGREE OF SYMMETRY

The analysis by Laplace transforms can be extended to any viscoelastic system with independence of its degree of symmetry. The following equations can be written.

$$\overline{\sigma_{ij}}(s) = s\overline{C_{ijkl}}(s)\overline{\gamma_{kl}}(s) \quad (5.104a)$$

$$\overline{\gamma_{ij}}(s) = s\overline{R_{ijkl}}(s)\overline{\sigma_{kl}}(s) \quad (5.104b)$$

In the axis of the real time, these equations become

$$\sigma_{ij}(t) = \int_{-\infty}^t C_{ijkl}(t-\theta) \frac{d\gamma_{kl}(\theta)}{d\theta} d\theta \quad (5.105a)$$

$$\gamma_{ij} = \int_{-\infty}^t R_{ijkl}(t-\theta) \frac{d\sigma_{kl}(\theta)}{d\theta} d\theta \quad (5.105b)$$

By using these expressions and taking into account the symmetry operations discussed in Chapter 4, one can obtain the viscoelastic responses for materials with planes of symmetry, axis of symmetry, etc.

PROBLEM SETS

Problem 5.1

Differentiate between the linear and nonlinear stress–strain relationships in the following expression.

$$(a) \varepsilon = t^2 \sigma; \quad (b) \varepsilon = t \sigma^2$$

$$(c) \varepsilon_{ij} = \int_{-\infty}^t J(t - \tau) d\sigma_{ij}(\tau)$$

Solution 5.1

(a)

$$\varepsilon_1 = t^2 \sigma_1 \text{ and } \varepsilon_2 = t^2 \sigma_2, \text{ so } \varepsilon_1 + \varepsilon_2 = t^2 (\sigma_1 + \sigma_2)$$

$$\text{Moreover } \lambda \varepsilon_1 = t^2 (\lambda \sigma_1) = \lambda t^2 \sigma \quad (\text{P5.1.1})$$

hence (a) is linear.

(b)

$$\varepsilon = t \sigma^2; \text{ if } \sigma_1 = 2\sigma \text{ then } \varepsilon_1 = 4t \sigma^2 \neq 2\varepsilon \quad (\text{P5.1.2})$$

so (b) is nonlinear.

(c)

$$\varepsilon_{ij(1)} = \int_{-\infty}^t J(t - \tau) d\sigma_{ij(1)}(\tau); \quad \varepsilon_{ij(2)} = \int_{-\infty}^t J(t - \tau) d\sigma_{ij(2)}(\tau)$$

$$\varepsilon_{ij(1)} + \varepsilon_{ij(2)} = \int_{-\infty}^t J(t - \tau) d[\sigma_{ij(1)}(\tau) + \sigma_{ij(2)}(\tau)] \quad (\text{P5.1.3})$$

$$\begin{aligned} \text{Moreover } \varepsilon'_{ij} &= \int_{-\infty}^t J(t - \tau) d[\lambda \sigma_{ij}(\tau)] \\ &= \lambda \int_{-\infty}^t J(t - \tau) d\sigma_{ij}(\tau) = \lambda \varepsilon_{ij} \end{aligned}$$

Thus (c) is also linear.

Problem 5.2

A viscoelastic material under torsion between two parallel plates separated by a distance h of 0.5 mm rotates through an angle of 1° at 10 s. Determine the compliance at $t = 10$ s if the torque is 200 Nm and the radius of the plates R , is 2 cm. See Figure P5.2.1.

Solution 5.2

If the inertial forces are neglected and the strains are infinitesimal, the stress-strain relationship can be expressed as relationships between force and displacement through the geometric characteristics of the system. For small displacements the stress will be related to the torque M by

$$\sigma = \frac{dM}{r^2 dr d\theta} \quad (\text{P5.2.1})$$

On the other hand, from the stress-strain relationship, the strain is given by

$$\sigma J(t) = \varepsilon(t) = \frac{r}{h} \varphi(t) \quad (\text{P5.2.2})$$

where $\varphi(t)$ is the angle of rotation in the mobile plate. From Eqs. (P5.2.1) and (P5.2.2),

$$J(t) \frac{dM}{r^2 dr d\theta} = \frac{r}{h} \varphi(t)$$

Hence, after integration, we obtain

$$J(t) = \frac{\pi}{2M} \left(\frac{R^4}{h} \right) \varphi(t) \quad (\text{P5.2.3})$$

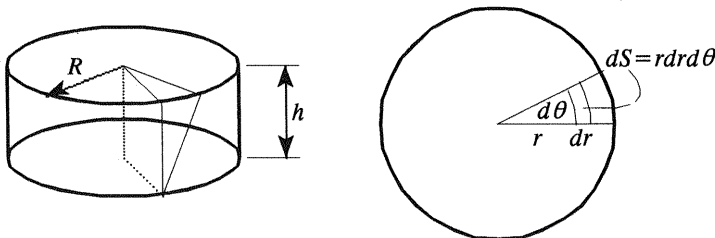


Figure P5.2.1

Therefore, for $R = 0.02$ m, $h = 0.0005$ m, and $\varphi = 2\pi/360$, $J(10 \text{ s}) \cong 4.4 \times 10^{-8} \text{ Pa}^{-1}$.

Problem 5.3

Show that for a material that fulfills Andrade's equation, $J(t) = At^{1/3}$, the torsion angle will be 2φ at $t = 8t_1$ if this angle is φ at $t = t_1$.

Solution 5.3

If Andrade's equation holds,

$$J(t_1) = At_1^{1/3} = F\varphi(t_1) = F\varphi_1 \quad (\text{P5.3.1})$$

and

$$J(t_2) = At_2^{1/3} = F\varphi(t_2) = F\varphi_2 \quad (\text{P5.3.2})$$

Hence,

$$\frac{\varphi_1}{\varphi_2} = \frac{t_1^{1/3}}{t_2^{1/3}} = \left(\frac{t_1}{8t_1}\right)^{1/3} = \frac{1}{2}$$

Therefore, $\varphi_2 = 2\varphi_1$.

Problem 5.4

Consider a viscoelastic material under torsion in a cone-plate configuration (Fig. P5.4.1). How much should we modify the base of the cone to have a rotation angle, under the same torque, twice as large at the same time and temperature?

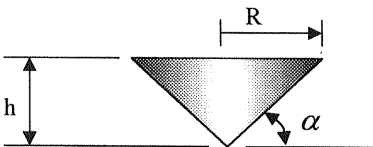


Figure P5.4.1

Solution 5.4

In this case, $\sigma = dM/(r^2 dr d\theta)$, and the stress-strain relationship takes the form

$$J(t)\sigma = \frac{r}{h}\varphi(t)$$

Since for low values of α , $h = r \tan \alpha \cong r\alpha$, we have

$$J(t) M = \frac{\varphi(t)}{\alpha} \int_0^{2\pi} \int_0^R r^2 dr d\theta = \frac{2\pi}{3} \left(\frac{R^3}{\alpha} \right) \varphi(t) \quad (\text{P5.4.1})$$

From this equation, $R_1^3 \varphi(t_1) = R_2^3 \varphi(t_2)$. Then, if $\varphi(t_2) = 2\varphi(t_1)$,

$$R_1^3 = 2R_2^3 \quad \text{and} \quad R_2 = 0.794 R_1$$

The radius should be decreased by about 21%.

Problem 5.5

The compliance of a viscoelastic material is given by $J(t) = [1.4678 - 0.8730 \exp(-0.5268t)] \times 10^{-9} \text{ MPa}^{-1}$. Determine the torsion angle, ϕ , of a cylindrical rod of this material at $t = 1 \text{ s}$, 10 min , 1001 s , 30 min , and 1 h , subjected to the following stress history:

$$\begin{aligned} t < 0, & \quad \sigma = 0 \\ 0 \leq t < 1000 \text{ s}, & \quad \sigma = 1 \text{ MPa} \\ 1000 \leq t < 2000 \text{ s}, & \quad \sigma = 2 \text{ MPa} \\ t \geq 2000 \text{ s}, & \quad \sigma = 0 \end{aligned}$$

The dimensions of the cylinder are $\ell = 10 \text{ cm}$ and $r = 2 \text{ mm}$.

Solution 5.5

Sketches of the data plots are shown in figure P5.5.1.

From Eq. (5.24),

$$\phi(t) = \frac{\ell}{r} \sum J(t - \theta) \Delta\sigma(\theta) \quad (\text{P5.5.1})$$

where it was considered that $\varepsilon = \phi r / \ell$.

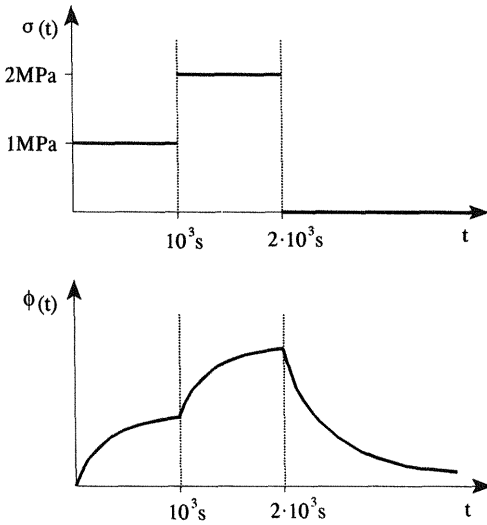


Figure P5.5.1

The torsion angles at different times are as follows.

$t = 1 \text{ s}$:

$$\phi = \frac{100}{2} \times [1.4678 - 0.8730 \exp(-0.5268 \times 1)] \times 10^{-9} \times 10^6 = 0.0476 \text{ rad}$$

$t = 600 \text{ s}$:

$$\phi = \frac{100}{2} \times [1.4678 - 0.8730 \exp(-0.5268 \times 600)] \times 10^{-9} \times 10^6 = 0.0734 \text{ rad}$$

$t = 1001 \text{ s}$:

$$\begin{aligned} \phi &= \frac{100}{2} \times [1.4678 - 0.8730 \exp(-0.5268 \times 1001)] \times 10^{-9} \times 10^6 \\ &\quad + \frac{100}{2} \times [1.4678 - 0.8730 \exp(-0.5268 \times 1)] \times 10^{-9} \times 10^6 = 0.121 \text{ rad} \end{aligned}$$

$t = 1800 \text{ s}$:

$$\begin{aligned}\phi &= \frac{100}{2} \times [1.4678 - 0.8730 \exp(-0.5268 \times 1800)] \times 10^{-9} \times 10^6 \\ &\quad + \frac{100}{2} \times [1.4678 - 0.8730 \exp(-0.5268 \times 800)] \times 10^{-9} \times 10^6 \\ &= 0.1468 \text{ rad}\end{aligned}$$

$t = 3600 \text{ s}$:

$$\begin{aligned}\phi &= \frac{100}{2} \times [1.4678 - 0.8730 \exp(-0.5268 \times 3600)] \times 10^{-9} \times 10^6 \\ &\quad + \frac{100}{2} \times [1.4678 - 0.8730 \exp(-0.5268 \times 2600)] \times 10^{-9} \times 10^6 \\ &\quad + \frac{100}{2} \times [1.4678 - 0.8730 \exp(-0.5268 \times 1600)] \times 10^{-9} \times (-2) \times 10^6 \\ &\cong 0 \text{ rad}\end{aligned}$$

Problem 5.6

Consider a cylindrical rod of 10 cm length and 2 mm radius whose shear modulus is given by

$$G(t) = 0.6812 + \exp(-1.3t) \text{ GPa} \quad (t \text{ in seconds}).$$

(a) Find the stresses at $t = 1 \text{ s}$, 10 min, 1001 s, 30 min, and 1 h for the following strain history:

$$\begin{aligned}t < 0, & \quad \theta = 0 \\ 0 \leq t < 1000 \text{ s} & \quad \theta = 0.1 \\ 1000 \text{ s} \leq t < \infty & \quad \theta = 0.04\end{aligned}$$

where θ is the torsion angle in radians.

(b) At which time will the stress be zero?

Solution 5.6

Sketches of the data plot and the response are shown in Fig. 5.6.1.

From Eq. (5.42)

$$\sigma(t) = \frac{r}{\ell} \sum G(t-t') \Delta\theta(t') \quad (\text{P5.6.1})$$

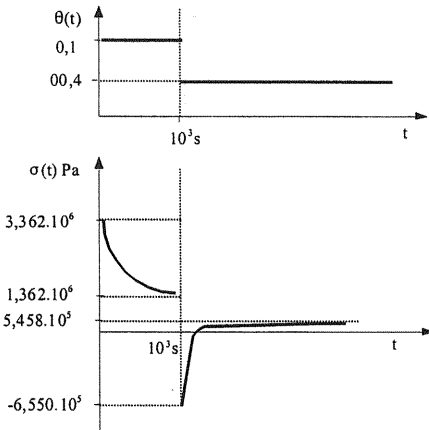


Figure P5.6.1

where it was considered that

$$\varepsilon = r\phi/l \quad (\text{P5.6.2})$$

Accordingly,

For $t = 1$ s:

$$\sigma = \frac{2 \times 10^{-3}}{10 \times 10^{-2}} [0.6812 + \exp(-1.3 \times 1)] \times 10^9 \times 0.1 = 1.907 \times 10^6 \text{ Pa}$$

For $t = 600$ s:

$$\sigma = \frac{2 \times 10^{-3}}{10 \times 10^{-2}} [0.6812 + \exp(-1.3 \times 600)] \times 10^9 \times 0.1 = 1.362 \times 10^6 \text{ Pa}$$

For $t = 1001$ s:

$$\begin{aligned} \sigma &= \frac{2 \times 10^{-3}}{10 \times 10^{-2}} \{ [0.6812 + \exp(-1.3 \times 1001)] \times 10^9 \times 0.1 \\ &\quad + [0.6812 + \exp(-1.3 \times 1)] \times 10^9 \times (0.04 - 0.1) \} \\ &= 2.18 \times 10^5 \text{ Pa} \end{aligned}$$

For $t = 1800$ s:

$$\begin{aligned}\sigma &= \frac{2 \times 10^{-3}}{10 \times 10^{-2}} \{ [0.6812 + \exp(-1.3 \times 1800)] \times 10^9 \times 0.1 \\ &\quad + [0.6812 + \exp(-1.3 \times 800)] \times 10^9 \times (0.04 - 0.1) \} \\ &= 5.458 \times 10^5 \text{ Pa}\end{aligned}$$

This increase in the stress reveals a “memory” effect produced by the strain history.

The time at which the stress is zero can be obtained from

$$\begin{aligned}\sigma &= \frac{2 \times 10^{-3}}{10 \times 10^{-2}} \{ [0.6812 + \exp(-1.3t)] \times 10^9 \times 0.1 \\ &\quad + [0.6812 + \exp(-1.3(t - 1000))] \times 10^9 \times (0.04 - 0.1) \} = 0\end{aligned}$$

which yields $t \cong 1000.6$ s.

At this time, the positive stress step is compensated for by the negative one, giving as a result zero stress.

Problem 5.7

Show that

$$\frac{d}{dt} \int_0^t G(t - \theta)J(\theta) d\theta = \int_0^t \frac{dG(u)}{du} J(t - u) du + G_g J(t) = 1 \quad (\text{P5.7.1})$$

Solution 5.7

$$\frac{d}{dt} \int_0^t G(t - \theta)J(\theta) d\theta = \lim_{\Delta t \rightarrow 0} \frac{\int_0^{t+\Delta t} G(t + \Delta t - \theta)J(\theta) d\theta - \int_0^t G(t - \theta)J(\theta) d\theta}{\Delta t} = 1 \quad (\text{P5.7.2})$$

The right-hand side of Eq. (P5.7.2) can be written as

$$\lim_{t \rightarrow 0} \frac{\int_0^t [G(t + \Delta t - \theta) - G(t - \theta)]J(\theta) d\theta + \int_t^{t+\Delta t} G(\Delta t)J(\theta) d\theta}{\Delta t} = 1 \quad (\text{P5.7.3})$$

This expression becomes

$$\int_0^t \left[-\frac{dG(t - \theta)}{d\theta} \right] J(\theta) d\theta + G_g J(t) = 1 \quad (\text{P5.7.4})$$

Where it has been taken into account that $dG(t - \theta)/dt = -dG(t - \theta)/d\theta$ and $G_g = G(0)$. Substituting $u = t - \theta$ into Eq. (P5.7.4), this expression becomes

$$\int_0^t \frac{dG(u)}{du} J(t - u) du + G_g J(t) = 1 \quad (\text{P5.7.5})$$

Problem 5.8

Deduce Eq. (5.64b) for a viscoelastic material from the following mechanical history:

$$\sigma(t) = 0 \text{ for } t < 0 \quad \text{and} \quad \sigma(t) = \varepsilon G(t) \text{ for } t > 0$$

Solution 5.8

According to Eq. (5.37), the time dependence of the deformation is given by

$$\varepsilon = J_g \sigma(t) + \int_0^t \sigma(t - u) \frac{dJ(u)}{du} du \quad (\text{P5.8.1})$$

Writing the stress as a function of the strain, Eq. (P5.8.1) becomes

$$\varepsilon = \varepsilon J_g G(t) + \varepsilon \int_0^t G(t - u) \frac{dJ(u)}{du} du \quad (\text{P5.8.2})$$

Hence,

$$J_g G(t) + \int_0^t G(t - u) \frac{dJ(u)}{du} du = 1 \quad (\text{P5.8.3})$$

Problem 5.9

Show that for $\sigma = \sigma_0 H(t)$, where $H(t)$ is the step unit function, the following relation for d viscoelastic material holds

$$H(t) = \int_0^t G(t - \theta) dJ(\theta) \quad (\text{P5.9.1})$$

Solution 5.9

From Eq. (5.45),

$$\sigma(t) = \int_0^t G(t-\theta) \frac{d\varepsilon(\theta)}{d\theta} d\theta = \sigma_0 \int_0^t G(t-\theta) dJ(\theta) \quad (\text{P5.9.2})$$

Since $\sigma(t) = \sigma_0 H(t)$, then Eq. (P5.9.1) is obtained.

REFERENCES

1. AC Pipkin. Lectures on Viscoelasticity Theory. New York: Springer-Verlag, 1972.
2. M Reiner. Phys Today, January 1964, p 62.
3. H Markovitz. Nonlinear steady flow behavior. In: Rheology, Vol. 4, Eirich ed. New York : Academic Press, pages 347–410, 1967.
4. NW Tschoegl. The Phenomenological Theory of Linear Viscoelastic Behavior. Heidelberg: Springer-Verlag, 1989, Chap 2.
5. JD Ferry. Viscoelastic Properties of Polymers. 3rd ed. New York: Wiley-Interscience, 1980.
6. J Aklonis, WJ MacKnight. Introduction to Polymer Viscoelasticity. 2nd ed. New York: Wiley, 1980.
7. H Markovitz. Lectures in Linear Viscoelasticity: An Introduction. Pittsburgh: Carnegie-Mellon University, 1978.
8. NW Tschoegl. Mech Time-Dependent Mater 1: 3, 1997.
9. NG McCrum, CP Buckley, CB Bucknall. Principles of Polymer Engineering. New York: Oxford Univ Press, 1988, Chap 4.
10. RM Christensen. Theory of Viscoelasticity, 2nd ed. New York: Academic, 1982.
11. H Leaderman. Trans Soc Rheol, 1: 213, 1957.
12. L Boltzmann. Pogg Ann Phys, 7: 624, 1876.
13. H Leaderman. Elastic and Creep Properties of Filamentous Materials and Other High Polymers. Washington DC: Textile Foundation, 1943.
14. C Zener. Elasticity and Anelasticity of Metals. Chicago: Chicago Univ Press, 1948, p. 21.

6

Dynamic Viscoelastic Functions

6.1	Introduction	238
6.2	Dynamic Relaxation Functions	239
6.3	Transformation of Relaxation Functions from the Frequency Domain to the Time Domain and Vice Versa	242
6.4	Complex Viscosity	242
6.5	Dissipated Energy in Dynamic Relaxation Experiments	243
6.6	Dynamic Creep Compliance Functions	244
6.7	Transformation of Compliance Functions from the Frequency Domain to the Time Domain and Vice Versa for Viscoelastic Solids	245
6.8	Dissipated Energy in Dynamic Creep Experiments	249
6.9	Analysis of Complex Creep Compliance Functions at Low Frequencies	250
6.10	Zero Shear Rate Viscosity and Steady-State Compliance Expressed in Terms of Viscoelastic Functions	252
6.11	Krönig–Kramers Relationships	253
6.12	Other Dynamic Viscoelastic Functions	255
	Problem Sets	257
	References	270

6.1 INTRODUCTION

The transient experiments to which we referred in the preceding chapter provide information on the linear viscoelastic behavior of materials in the

time domain for values of t larger than 0.1 s. However, it is often necessary to obtain the responses of viscoelastic materials to perturbation force fields at very short times. For example, when materials are used as acoustic isolators in buildings, or to eliminate noise in vibrating metallic sheets by depositing layers of viscoelastic materials on them, etc., it is important to know how the storage and loss viscoelastic functions change with the frequency of the perturbation. Information of this kind can be obtained by studying the responses of materials to dynamic perturbation fields (1–6). Moreover, by taking into account that an experiment carried out at a frequency ω is qualitatively equivalent to others performed in the time domain $t = \omega^{-1}$, the combination of transient and dynamic experiments provides informations on the viscoelastic behavior of materials in a wide time scale covering several decades. The information thus obtained is important not only on practical grounds but also from a basic point of view. Actually, the knowledge of viscoelastic responses over a wide time scale is important to the study of the molecular motions responsible for the viscoelastic behavior of materials.

6.2 DYNAMIC RELAXATION FUNCTIONS

Let us assume that a sinusoidal shear strain $\varepsilon(t) = \varepsilon_0 \sin \omega t$ is imposed on a viscoelastic solid, where ε_0 and ω are, respectively, the amplitude and frequency of the perturbing strain. A dynamic shear strain is illustrated in Figure 6.1. Experimentally one observes that the shear stress (response) is

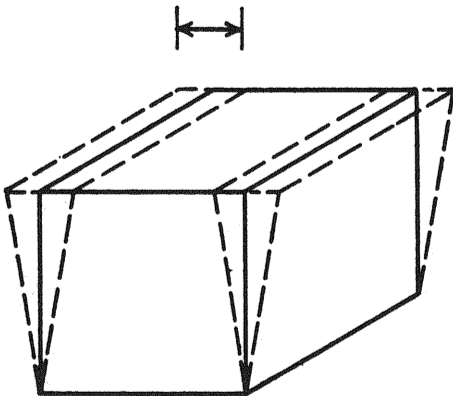


Figure 6.1 Schematic representation of the vibrating shear deformation of a material.

an angle δ out of phase with respect to the harmonic strain. A schematic representation of $\epsilon(t)$ and $\sigma(t)$ is shown in Figure 6.2. Accordingly,

$$\begin{aligned}\sigma(t) &= \sigma_0 \sin(\omega t + \delta) \\ &= \sigma_0 \cos \delta \sin \omega t + \sigma_0 \sin \delta \cos \omega t\end{aligned}\quad (6.1)$$

This equation indicates that the stress is a complex quantity with one component in phase with the perturbation ($\sigma_0 \cos \delta$) and another 90° out of phase ($\sigma_0 \sin \delta$). Because the sinusoidal shear strain is a continuous function of time, its substitution into Eq. (5.45) gives

$$\begin{aligned}\sigma(t) &= \int_{-\infty}^t [G_e + G_d \Phi(t - \theta)] \frac{\partial \epsilon(\theta)}{\partial \theta} d\theta \\ &= \epsilon_0 \left[\omega G_d \int_0^\infty \Phi(u) \cos \omega u du \right] \cos \omega t + \epsilon_0 \left[G_e + \omega G_d \int_0^\infty \Phi(u) \sin \omega u du \right] \sin \omega t \\ &= \epsilon_0 [G'(\omega) \sin \omega t + G'' \cos \omega t]\end{aligned}\quad (6.2)$$

where the change of variables $t - \theta = u$ has been performed and it has been taken into account that $G(t) = G_e + G_d \Phi(t)$ [Eq. (5.8)]. From Eq. (6.2) one obtains

$$\begin{aligned}G'(\omega) &= G_e + \omega G_d \int_0^\infty \Phi(t) \sin \omega t dt \\ &= G_e + \omega \int_0^\infty [G(t) - G_e] \sin \omega t dt\end{aligned}\quad (6.3)$$

and

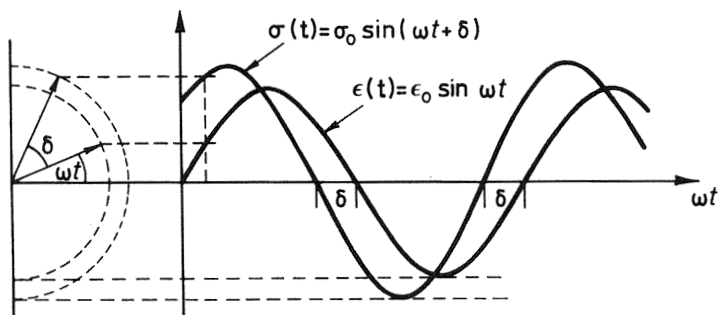


Figure 6.2 Sketch of an alternating stress leading an alternating strain by phase angle δ .

$$G''(\omega) = \omega G_d \int_0^{\infty} \Phi(t) \cos \omega t \, dt = \omega \int_0^{\infty} [G(t) - G_e] \cos \omega t \, dt \quad (6.4)$$

It is obvious that for a liquid viscoelastic material, $G_e = 0$. Comparison of Eqs. (6.1) and (6.2) leads to the expressions

$$G'(\omega) = \frac{\sigma_0}{\varepsilon_0} \cos \delta \quad (6.5a)$$

$$G''(\omega) = \frac{\sigma_0}{\varepsilon_0} \sin \delta \quad (6.5b)$$

$$\tan \delta = \frac{G''(\omega)}{G'(\omega)} \quad (6.5c)$$

where $G'(\omega)$ and $G''(\omega)$ are the components of the complex relaxation modulus $G^*(\omega)$. A vectorial scheme of the components of $G^*(\omega)$ is shown in Figure 6.3a.

By using complex notation, the perturbation and the response can be written as $\varepsilon^*(\omega) = \varepsilon_0 \text{Im}(e^{i\omega t})$ and $\sigma^*(\omega) = \sigma_0 \text{Im}(e^{i(\omega t + \delta)})$, respectively. Consequently, the relationship between the shear stress and the deformation is given by

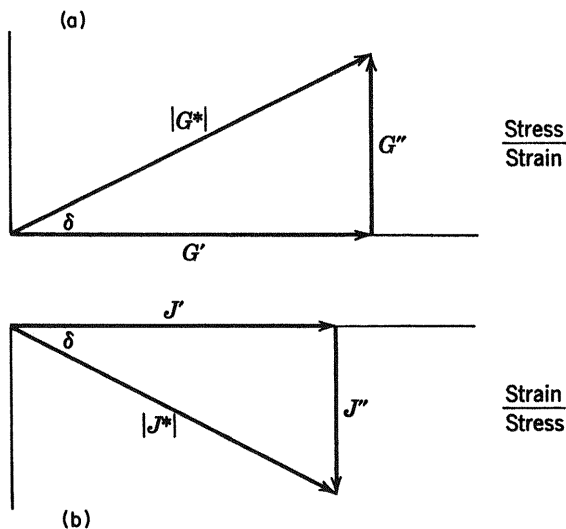


Figure 6.3 Vectorial components of (a) the complex relaxation modulus G^* and (b) the complex compliance function J^* .

$$G^*(\omega) = G'(\omega) + iG''(\omega) = \frac{\sigma_0}{\varepsilon_0} e^{i\delta} = \frac{\sigma_0}{\varepsilon_0} (\cos \delta + i \sin \delta) \quad (6.6)$$

Comparison of real and imaginary parts in this equation gives the expressions for $G'(\omega)$ and $G''(\omega)$ already indicated in Eq. (6.5).

6.3 TRANSFORMATION OF RELAXATION FUNCTIONS FROM THE FREQUENCY DOMAIN TO THE TIME DOMAIN AND VICE VERSA

Equations (6.3) and (6.4) suggest that $G'(\omega)$ and $G''(\omega)$ are the sine and cosine Fourier transforms of the relaxation modulus, respectively (see Appendix). The pertinent relations are

$$\frac{G'(\omega) - G_e}{\omega} = \mathcal{F}_s[G(t) - G_e] \quad (6.7a)$$

$$\frac{G''(\omega)}{\omega} = \mathcal{F}_c[G(t) - G_e] \quad (6.7b)$$

where \mathcal{F}_s and \mathcal{F}_c are, respectively, the symbols for the sine and cosine Fourier transforms. The relaxation modulus $G(t)$ can also be obtained from the inverse of the Fourier transform of Eqs. (6.7a) and (6.7b). The corresponding relationships are

$$G(t) = G_e + \frac{2}{\pi} \int_0^\infty \frac{G'(\omega) - G_e}{\omega} \sin \omega t \, d\omega \quad (6.8a)$$

$$G(t) = G_e + \frac{2}{\pi} \int_0^\infty \frac{G''(\omega)}{\omega} \cos \omega t \, d\omega \quad (6.8b)$$

If $G_e = 0$, Eqs. (6.7) and (6.8) are also valid for viscoelastic liquids.

6.4 COMPLEX VISCOSITY

In analogy with the definition of viscosity given in transient experiments, the complex shear stress is related to the complex shear rate deformation by the expression

$$\sigma^*(\omega) = \eta^*(\omega) \frac{d\varepsilon^*(\omega)}{dt} = i\omega\varepsilon^*(\omega)\eta^*(\omega) \quad (6.9)$$

where $\varepsilon^*(\omega) = \varepsilon_0 \text{Im} \exp(i\omega t)$ and $\eta^*(\omega)$ is the complex viscosity. From Eq. (6.9) one obtains

$$\eta^*(\omega) = \eta'(\omega) - i\eta''(\omega) = \frac{G^*(\omega)}{i\omega} = \frac{G''(\omega)}{\omega} - i\frac{G'(\omega)}{\omega} \quad (6.10)$$

where it was taken into account that $\sigma^*/\varepsilon^* = G^*$. Hence, the real and imaginary parts of $\eta^*(\omega)$ can be written as

$$\eta'(\omega) = \frac{G''(\omega)}{\omega} \quad (6.11a)$$

and

$$\eta''(\omega) = \frac{G'(\omega)}{\omega} \quad (6.11b)$$

Equation (6.11a) suggests that the viscosity of liquids at zero shear rate can be obtained from dynamic experiments by means of the expression

$$\eta_0 = \lim_{\omega \rightarrow 0} \frac{G''(\omega)}{\omega} \quad (6.12)$$

6.5 DISSIPATED ENERGY IN DYNAMIC RELAXATION EXPERIMENTS

The work performed per cycle by a material that undergoes sinusoidal shear deformation $\varepsilon^* = \varepsilon_0 \text{Im} \exp(i\omega t)$ is given by (1)

$$\begin{aligned} W &= \oint \sigma^* d\varepsilon^* = \oint [G'(\omega) + iG''(\omega)]\varepsilon^* d\varepsilon^* \\ &= \frac{1}{2} G'(\omega) \oint d\varepsilon^{*2} + \frac{G''(\omega)}{\omega} \oint \dot{\varepsilon}^* d\varepsilon^* \end{aligned} \quad (6.13)$$

where it has been considered that $i\varepsilon^* = (1/\omega)d\varepsilon^*/dt$. In the integral containing $G'(\omega)$, the work done of the material during part of the cycle is recovered during the other part of the cycle, and the integral of the cycle is zero. Consequently, $G'(\omega)$ is called the storage relaxation modulus because it is related to the stored energy. The term containing $G''(\omega)$ is related to the viscous dissipation, and hence this viscoelastic function is called the loss

relaxation modulus. The total work in a complete cycle represents the dissipated energy given by

$$W = \frac{G''(\omega)}{\omega} \oint \dot{\varepsilon}^* d\varepsilon^* = \frac{G''(\omega)}{\omega} \oint \dot{\varepsilon}^{*2} dt \quad (6.14)$$

where it has been considered that $d\varepsilon^* = (d\varepsilon^*/dt) dt$. According to this equation, the energy dissipated in a material under a sinusoidal deformation is proportional to both the loss relaxation modulus and the reciprocal of the frequency. The limits of the last integral in Eq. (6.14) are 0 and the period $T(= 2\pi/\omega)$. Accordingly, Eq. (6.14) becomes

$$W = G''(\omega)\varepsilon_0^2\omega \int_0^{2\pi/\omega} \cos^2 \omega t dt = \pi\varepsilon_0^2 G''(\omega) \quad (6.15)$$

This equation indicates that the dissipated energy is proportional to both the square of the amplitude of the deformation and the loss relaxation modulus.

6.6 DYNAMIC CREEP COMPLIANCE FUNCTIONS

The response of a material to a sinusoidal shear stress $\sigma = \sigma_0 \sin \omega t$ is delayed an angle δ with regard to the perturbation, and the relaxation between the shear deformation (response) and the shear stress is given by

$$\varepsilon(t) = \varepsilon_0 \sin(\omega t - \delta) \quad (6.16)$$

The ratio between $\varepsilon(t)$ [$= \varepsilon_0 \text{Im} \exp[i(\omega t - \delta)]$] and $\sigma(t)$ [$= \sigma_0 \text{Im} \exp[i(\omega t)]$] is the creep complex compliance function given by

$$J(\omega)^* = J'(\omega) - iJ''(\omega) = \frac{\varepsilon_0}{\sigma_0} e^{-i\delta} = \frac{\varepsilon_0}{\sigma_0} (\cos \delta - i \sin \delta) \quad (6.17)$$

From this equation one obtains

$$J'(\omega) = \frac{\varepsilon_0}{\sigma_0} \cos \delta, \quad J''(\omega) = \frac{\varepsilon_0}{\sigma_0} \sin \delta, \quad \tan \delta = \frac{J''(\omega)}{J'(\omega)} \quad (6.18)$$

These expressions relate the components of the complex compliance to the amplitudes of both the perturbation and the response as well as to the out-of-phase angle δ . The vectorial scheme of the perturbation and response is shown in Figure 6.3b.

By comparing the relations given in Eq. (6.18) with those of Eq. (6.5), one obtains

$$J^*(\omega) = \frac{1}{G^*(\omega)} \quad (6.19a)$$

$$\tan[\delta(\omega)] = \frac{G''(\omega)}{G'(\omega)} = \frac{J''(\omega)}{J'(\omega)} \quad (6.19b)$$

According to Eqs. (6.19), the relationships between the components of the complex compliance function and those of the complex relaxation modulus are given by

$$J'(\omega) = \frac{1}{G'(\omega)[1 + \tan^2 \delta(\omega)]} \quad (6.20a)$$

and

$$J''(\omega) = \frac{1}{G''(\omega)[1 + \cotan^2 \delta(\omega)]} \quad (6.20b)$$

Equations (6.20a) and (6.20b) suggest that $J'(\omega) = 1/G'(\omega)$ and $J''(\omega) = 1/G''(\omega)$ when $\delta \cong 0$ and $\delta \cong 90^\circ$, respectively. In other words, $J'(\omega)$ comes near to being the reciprocal of $G'(\omega)$ in the region of high frequencies where the dissipated energy is very small; in the zone of very low frequencies, the flow contribution is dominant and $J''(\omega)$ comes close to $1/G''(\omega)$. In the frequency interval $0 < \omega < \infty$, Eqs. (6.20a) and (6.20b) suggest the inequalities

$$J'(\omega) \leq \frac{1}{G'(\omega)} \quad \text{and} \quad J''(\omega) \leq \frac{1}{G''(\omega)} \quad (6.20c)$$

6.7 TRANSFORMATION OF COMPLIANCE FUNCTIONS FROM THE FREQUENCY DOMAIN TO THE TIME DOMAIN AND VICE VERSA FOR VISCOELASTIC SOLIDS

6.7.1 Introduction

According to the Boltzmann superposition principle, the shear strain of a solid viscoelastic material under the action of a harmonic shear stress can be written as (2)

$$\begin{aligned}
\varepsilon(t) &= \int_{-\infty}^t J(t-\theta) \frac{d\sigma(\theta)}{d\theta} d\theta \\
&= \int_{-\infty}^t \{ [J_g + J_d \Psi(\infty)] - J_d [\Psi(\infty) - \Psi(t-\theta)] \} \frac{d\sigma(\theta)}{d\theta} d\theta \quad (6.21) \\
&= \sigma(t) J_e - \int_{-\infty}^t J_d [\Psi(\infty) - \Psi(t-\theta)] \frac{d\sigma(\theta)}{d\theta} d\theta
\end{aligned}$$

where it has been considered that $J(t) = J_g + J_d \Psi(t)$, $J_g + J_d \Psi(\infty) = J_e$ [see Eqs. (5.15) and (5.17)] and $\sigma(-\infty) = 0$. If the shear stress is sinusoidal, for example $\sigma(t) = \sigma_0 \sin \omega t$, then Eq. (6.21) becomes

$$\begin{aligned}
\varepsilon(t) &= J_e \sigma_0 \sin \omega t - \sigma_0 \omega J_d \int_0^{\infty} [\Psi(\infty) - \Psi(u)] \cos \omega(t-u) du \\
&= \sigma_0 [J'(\omega) \sin \omega t - J''(\omega) \cos \omega t] \quad (6.22)
\end{aligned}$$

where the change of variables $u = t - \theta$ was made. Consequently,

$$J'(\omega) = J_e - \omega J_d \int_0^{\infty} [\Psi(\infty) - \Psi(t)] \sin \omega t dt \quad (6.23a)$$

and

$$J''(\omega) = \omega J_d \int_0^{\infty} [\Psi(\infty) - \Psi(t)] \cos \omega t dt \quad (6.23b)$$

These equations can be written as

$$J'(\omega) = J_e - \omega \int_0^{\infty} [J_e - J(t)] \sin \omega t dt \quad (6.24a)$$

and

$$J''(\omega) = \omega \int_0^{\infty} [J_e - J(t)] \cos \omega t dt \quad (6.24b)$$

Therefore these expressions permit us to transform the compliance function from the time domain to the frequency domain. The relationships of Eqs. (6.24) can also be written in terms of sine and cosine Fourier transforms:

$$\frac{J'(\omega) - J_e}{\omega} = -\mathcal{F}_s[J_e - J(t)] \quad (6.25a)$$

$$\frac{J''(\omega)}{\omega} = \mathcal{F}_c[J_e - J(t)] \quad (6.25b)$$

The inverse of the Fourier transforms of Eqs. (6.25) permits transformation of the compliance function from the frequency domain to the time domain. The pertinent equations are

$$J(t) = J_e + \frac{2}{\pi} \int_0^\infty \frac{J'(\omega) - J_e}{\omega} \sin \omega t \, d\omega \quad (6.26a)$$

and

$$J(t) = J_e - \frac{2}{\pi} \int_0^\infty \frac{J''(\omega)}{\omega} \cos \omega t \, d\omega \quad (6.26b)$$

6.7.2 Transformation of Compliance Functions from the Frequency Domain to the Time Domain and Vice Versa for Viscoelastic Liquids

In a dynamic creep experiment, the shear strain for liquids can be written as

$$\begin{aligned} \varepsilon(t) &= \int_{-\infty}^t J(t-\theta) \frac{d\sigma(\theta)}{d\theta} d\theta \\ &= \int_{-\infty}^t \left(J_g + J_d \Psi(t-\theta) + \frac{t-\theta}{\eta} \right) \frac{d\sigma(\theta)}{d\theta} d\theta \end{aligned} \quad (6.27)$$

By adding and subtracting the term $J_d \Psi(\infty)$ in the integrand of Eq. (6.27), this expression becomes (2)

$$\begin{aligned} \varepsilon(t) &= \omega \int_{-\infty}^t \left\{ [J_g + J_d \Psi(\infty)] - J_d [\Psi(\infty) - \Psi(t-\theta)] + \frac{t-\theta}{\eta} \right\} \frac{d\sigma(\theta)}{d\theta} d\theta \\ &= \sigma_0 [J'(\omega) \sin \omega t - J''(\omega) \cos \omega t] \end{aligned} \quad (6.28)$$

After some mathematical handling one obtains

$$J'(\omega) = J_e^0 - \omega \int_0^\infty \left[J_e^0 - J(t) + \frac{t}{\eta} \right] \sin \omega t \, dt \quad (6.29a)$$

and

$$J''(\omega) = \frac{1}{\omega\eta} + \omega \int_0^\infty \left[J_e^0 - J(t) + \frac{t}{\eta} \right] \cos \omega t \, dt \quad (6.29b)$$

The components of the complex compliance can be expressed in terms of the Fourier transforms by

$$\frac{J'(\omega) - J_e^0}{\omega} = \mathcal{F}_s \left[J(t) - J_e^0 - \frac{t}{\eta} \right] \quad (6.30a)$$

and

$$\frac{J''(\omega)}{\omega} - \frac{1}{\omega^2\eta} = \mathcal{F}_c \left[J_e^0 - J(t) + \frac{t}{\eta} \right] \quad (6.30b)$$

From the inverse of the Fourier transforms of these equations one obtains the relationships

$$J(t) = J_e^0 + \frac{2}{\pi} \int_0^\infty \frac{J'(\omega) - J_e^0}{\omega} \sin \omega t \, d\omega + \frac{t}{\eta} \quad (6.31a)$$

and

$$J(t) = J_e^0 - \frac{2}{\pi} \int_0^\infty \left[\frac{J''(\omega)}{\omega} - \frac{1}{\omega^2\eta} \right] \cos \omega t \, d\omega + \frac{t}{\eta} \quad (6.31b)$$

which permit transformation of the compliance functions from the frequency domain to the time domain. Equation (6.31a) can also be written

$$J(t) = J_g + J_e^0 - J_g + \frac{2}{\pi} \int_0^\infty \frac{J'(\omega) - J_g + J_g - J_e^0}{\omega} \sin \omega t \, d\omega + \frac{t}{\eta} \quad (6.32)$$

Since the complex variable theory shows that (7)

$$\int_0^\infty \frac{\sin \omega t}{\omega} \, d\omega = \frac{\pi}{2} \quad (6.33)$$

Eq. (6.32) becomes (8)

$$J(t) = J_g + \frac{2}{\pi} \int_0^\infty \frac{J'(\omega) - J_g}{\omega} \sin \omega t \, d\omega + \frac{t}{\eta} \quad (6.34)$$

This is the expression commonly found in the literature that relates the real component of the complex compliance in the frequency domain with the compliance function in the time domain.

When $t \rightarrow 0$, Eq. (6.31b) becomes

$$J_e^0 = J_g + \frac{2}{\pi} \int_{-\infty}^{\infty} \left[J''(\omega) - \frac{1}{\omega\eta} \right] d \ln \omega \quad (6.35)$$

which gives the steady-state compliance function in terms of the loss compliance function.

The value of J_e^0 obtained from this equation substituted into Eq. (6.31b) gives the relationship

$$J(t) = J_g + \frac{2}{\pi} \int_{-\infty}^{\infty} \left[J''(\omega) - \frac{1}{\omega\eta} \right] (1 - \cos \omega t) d \ln \omega + \frac{t}{\eta} \quad (6.36)$$

which is an alternative way of writing Eq. (6.31b).

6.8 DISSIPATED ENERGY IN DYNAMIC CREEP EXPERIMENTS

The energy per cycle is involved when a viscoelastic material undergoes a shear stress $\sigma(t) = \sigma_0 \sin \omega t$ can be written as

$$W = \oint \sigma^* d\varepsilon^* = \oint \sigma^* \frac{d\varepsilon^*}{dt} dt \quad (6.37)$$

This expression in conjunction with Eq. (6.22) gives

$$W = \sigma_0^2 \omega \left[\int_0^{2\pi/\omega} J'(\omega) \sin \omega t \cos \omega t dt + \int_0^{2\pi/\omega} J''(\omega) \sin^2 \omega t dt \right] \quad (6.38)$$

Since the first integral on the right-hand side of this equation is zero, the dissipated energy is obtained by solving the second integral. The expression obtained,

$$W/\text{cycle} = \pi \sigma_0^2 J''(\omega) \quad (6.39)$$

indicates that the dissipated energy is proportional to both the square of the amplitude of the shear stress and the loss shear compliance.

6.9 ANALYSIS OF COMPLEX CREEP COMPLIANCE FUNCTIONS AT LOW FREQUENCIES

6.9.1 Introduction

From Eqs. (6.24a) and (6.24b), the components of the creep compliance function for solids in the limit $\omega \rightarrow 0$ are given by

$$J'(\omega) = J_e - \omega^2 \int_0^{\infty} t[J_e - J(t)] dt \quad (6.40a)$$

and

$$J''(\omega) = \omega \int_0^{\infty} [J_e - J(t)] dt \quad (6.40b)$$

where it was assumed that $\sin(\omega)t \cong \omega t$ and $\cos(\omega t) \cong 1$ when $\omega \rightarrow 0$. Equations (6.40a) and (6.40b) indicate that $J'(0) = J_e$ and $J''(0) = 0$. In the low frequency region, the following scaling laws for solids hold:

$$J_e - J'(\omega) \sim \omega^2; \quad J''(\omega) \sim \omega \quad (6.41)$$

It can be seen that the real compliance function is a decreasing linear function of ω^2 in the low frequency region. However, the compliance loss is an increasing linear function of ω in the low frequency zone. Although the real component of the creep compliance shows the same dependence on frequency for solids and liquids, the frequency dependence of the loss compliance differs for these two states. Thus Eq. (6.29b) suggests the following scaling law for viscoelastic liquids in the low frequency region ($\omega \rightarrow 0$):

$$J''(\omega) \sim \omega^{-1} \quad (6.42)$$

Accordingly, the loss compliance increases indefinitely as the frequency decreases. A straight line of slope -1 is obtained in the double logarithmic plot of $J''(\omega)$ against ω , that is,

$$\lim_{\omega \rightarrow 0} \frac{d \log J''(\omega)}{d \log \omega} = -1 \quad (6.43)$$

6.9.2 Analysis of the Complex Relaxation Modulus at Low Frequencies

Equations (6.3) and (6.4) suggest the following expressions for the relaxation moduli of solids:

$$G'(0) = G_e; \quad G''(0) = 0 \quad (6.44)$$

Obviously, $G'(0) = G''(0) = 0$ for liquids. According to Eqs. (6.3) and (6.4), the dynamic relaxation moduli of viscoelastic liquids ($G_e = 0$) in the low frequency region are given by

$$\lim_{\omega \rightarrow 0} G'(\omega) = \lim_{\omega \rightarrow 0} \omega \int_0^{\infty} G(t) \sin \omega t \, dt \cong \omega^2 \int_0^{\infty} t G(t) \, dt \quad (6.45)$$

and

$$\lim_{\omega \rightarrow 0} G''(\omega) = \lim_{\omega \rightarrow 0} \omega \int_0^{\infty} G(t) \cos \omega t \, dt = \omega \int_0^{\infty} G(t) \, dt \quad (6.46)$$

where the approximations $\cos \omega t \cong 1$ and $\sin \omega t \cong t$ for $\omega \rightarrow 0$ were used. Since the integrals of Eqs. (6.45) and (6.46) are constant, the scaling laws $G'(\omega) \sim \omega^2$ and $G'' \sim \omega$ hold. Consequently, the double logarithmic plots of the dynamic relaxation moduli of viscoelastic liquids in the terminal region are straight lines with slopes

$$\lim_{\omega \rightarrow 0} \frac{d \log G'(\omega)}{d \log \omega} = 2 \quad (6.47a)$$

and

$$\lim_{\omega \rightarrow 0} \frac{d \log G''(\omega)}{d \log \omega} = 1 \quad (6.47b)$$

For viscoelastic solids [$G'(\omega) = G_e$ when $\omega \rightarrow 0$], and according to Eq. (6.46), $G''(\omega) \sim \omega$ in the low frequency region. Therefore,

$$\lim_{\omega \rightarrow 0} \frac{d \log G'(\omega)}{d \log \omega} = 0 \quad (6.48a)$$

and

$$\lim_{\omega \rightarrow 0} \frac{d \log G''(\omega)}{d \log \omega} = 1 \quad (6.48b)$$

Accordingly, the phenomenological theory of linear viscoelasticity predicts the same frequency dependence for the loss relaxation modulus of solids and liquids in the terminal region.

6.10 ZERO SHEAR RATE VISCOSITY AND STEADY-STATE COMPLIANCE EXPRESSED IN TERMS OF VISCOELASTIC FUNCTIONS

The combination of Eqs. (6.12) and (6.46) leads to the important relationship between the zero shear viscosity and the shear relaxation modulus (2,8,9),

$$\eta_0 = \lim_{\omega \rightarrow 0} \frac{G''(\omega)}{\omega} = \int_0^{\infty} G(t) dt \quad (6.49)$$

analogous to that obtained in Chapter 5 using a ramp deformation history. This expression relates the viscosity, usually determined from either creep measurements or the loss dynamic modulus, to the transient relaxation modulus. Another important relationship can be obtained for the steady-state compliance. Because $G^*(\omega) = 1/J^*(\omega)$, the components of the complex relaxation modulus are related to those of the complex compliance function by

$$\begin{aligned} G'(\omega) + iG''(\omega) &= \frac{1}{J'(\omega) - iJ''(\omega)} \\ &= \frac{J'(\omega)}{J'^2(\omega) + J''^2(\omega)} + i \frac{J''(\omega)}{J'^2(\omega) + J''^2(\omega)} \end{aligned} \quad (6.50)$$

At low frequencies, $G'(\omega)$ can be written as

$$\lim_{\omega \rightarrow 0} G'(\omega) = \lim_{\omega \rightarrow 0} \frac{J'(\omega)}{J'^2(\omega) + J''^2(\omega)} \cong \frac{J_e^0}{J_e^{02} + 1/(\omega\eta)^2} \quad (6.51)$$

where it has been considered that $J''(\omega) \cong 1/\omega\eta$ when $\omega \rightarrow 0$ [see Eq. (6.29b)]. In these conditions, $J_e^0 \ll 1/\omega\eta$, and Eq. (6.51) becomes

$$J_e^0 = \lim_{\omega \rightarrow 0} \left[\frac{1}{\eta^2} \left(\frac{G'(\omega)}{\omega^2} \right) \right] \quad (6.52)$$

Equation (6.52) is widely used to determine the equilibrium compliance function from the values of the components of the relaxation moduli in the terminal region. This expression in conjunction with Eqs. (6.45) and (6.49) leads to the expression

$$J_e^0 = \frac{\int_0^\infty tG(t) dt}{\eta^2} = \frac{\int_0^\infty tG(t) dt}{\left[\int_0^\infty G(t) dt\right]^2} \quad (6.53)$$

which is an alternative method of determining the steady-state compliance from transient relaxation experiments.

6.11 KRÖNIG-KRAMERS RELATIONSHIPS

Linear viscoelasticity theory predicts that one component of a complex viscoelastic function can be obtained from the other one by means of the Krönig-Kramers relations (10–12). For example, the substitution of $G(t) - G_e$ given by Eq. (6.8b) into Eq. (6.3) leads to the relationship

$$G'(\omega) - G_e = \frac{2}{\pi} \omega \lim_{R \rightarrow \infty} \int_0^\infty \frac{G''(x) dx}{x} \int_0^R \sin \omega t \cos xt dt \quad (6.54)$$

By taking into account that

$$\sin \omega t \cos xt = \frac{1}{2} [\sin(\omega - x)t + \sin(\omega + x)t] \quad (6.55)$$

Eq. (6.54) becomes

$$\begin{aligned} G'(\omega) - G_e &= \frac{2}{\pi} \omega \int_0^\infty \frac{G''(x)}{x} \left[\frac{\omega}{\omega^2 - x^2} - \frac{1}{2} \right. \\ &\quad \times \left. \lim_{R \rightarrow \infty} \left[\frac{\cos(\omega - x)R}{\omega - x} + \frac{\cos(\omega + x)R}{\omega + x} \right] \right] dx \quad (6.56) \\ &= \frac{2}{\pi} \int_{-\infty}^\infty G''(x) \frac{\omega^2}{\omega^2 - x^2} d \ln x \end{aligned}$$

It should be noted that the integrals of cosines in this equation are zero, as a simple integration by parts shows. The strength of the relaxation can be

obtained directly from Eq. (6.56) by taking the limit of $G'(\omega) - G_e$ when $\omega \rightarrow \infty$. In this case,

$$\lim_{\omega \rightarrow \infty} [G'(\omega) - G_e] = G_g - G_e = \frac{2}{\pi} \int_{-\infty}^{\infty} G''(x) d \ln x \quad (6.57)$$

Substituting the value of G_e obtained from this equation into Eq. (6.56) gives the following alternative relationship between $G'(\omega)$ and $G''(\omega)$:

$$G'(\omega) = G_g - \frac{2}{\pi} \int_{-\infty}^{\infty} G''(x) \frac{x^2}{\omega^2 - x^2} d \ln x \quad (6.58)$$

In the same way, substitution of the value of $G(t) - G_e$ given by Eq. (6.8a) into Eq. (6.4) gives

$$G''(\omega) = \frac{2}{\pi} \int_0^{\infty} \int_0^{\infty} \frac{\omega(G'(x) - G_e)}{x} \sin xt \cos \omega t dt dx \quad (6.59)$$

Following the same procedures outlined above, one obtains

$$G''(\omega) = \frac{2}{\pi} \int_{-\infty}^{\infty} \frac{\omega x [G'(x) - G_e]}{x^2 - \omega^2} d \ln x \quad (6.60)$$

Equations (6.56) and (6.60) allow the calculation of the storage relaxation modulus for a given frequency when the loss relaxation modulus is known in the whole spectrum of frequencies and vice versa. These expressions are also suitable for viscoelastic liquids, though in this case $G_e = 0$. A more rigorous deduction of the Krönig–Kramers relations can be done by using a formulation in the complex plane. With this formulation the singularities appearing in the denominators of Eqs. (6.56) and (6.60) are avoided.

From Eqs. (6.12) and (6.60) the following important relationship is obtained:

$$\eta_0 = \lim_{\omega \rightarrow 0} \frac{G''(\omega)}{\omega} = \frac{2}{\pi} \int_{-\infty}^{\infty} \frac{G'(x)}{x} d \ln x \quad (6.61)$$

which provides an alternative way of calculating the viscosity at zero shear rate for viscoelastic liquids from the storage relaxation modulus.

The relationships for the compliance functions can be obtained by using the method outlined above for the relaxation functions. The pertinent equations for viscoelastic liquids are

$$J'(\omega) = J_g + \frac{2}{\pi} \int_{-\infty}^{\infty} \frac{J''(x)x^2 - x/\eta}{x^2 - \omega^2} d \ln x \quad (6.62)$$

and

$$J''(\omega) = \frac{2}{\pi} \int_{-\infty}^{\infty} \frac{[J'(x) - J_g]\omega x}{\omega^2 - x^2} d \ln x + \frac{1}{\omega\eta} \quad (6.63)$$

For viscoelastic solids, $\eta \rightarrow \infty$, and consequently the terms x/η and $1/\omega\eta$ in Eqs. (6.62) and (6.63), respectively, vanish.

The beauty of the linear viscoelastic analysis lies in the fact that once a viscoelastic function is known, the rest of the functions can be determined. For example, if one measures the compliance function $J(t)$, the values of the components of the complex compliance function can in principle be determined from $J(t)$ by using Fourier transforms [Eqs. (6.30)]. On the other hand, the components of the complex relaxation moduli can be obtained from those of $J^*(\omega)$ by using Eq. (6.50). Even more, the real components of both the complex relaxation modulus and the complex compliance function can be determined from the respective imaginary components, and vice versa, by using the Krönig–Kramers relations. Moreover, the inverse of the Fourier transform of $G'(\omega)$ and/or $G''(\omega)$ [$J'(\omega)$ and/or $J''(\omega)$] allows the determination of the shear relaxation modulus (shear creep compliance). Finally, the convolution integrals of Eq. (5.57) allow the determination of $J(t)$ and $G(t)$ by an efficient method of numerical calculation outlined by Hopkins and Hamming (13).

6.12 OTHER DYNAMIC VISCOELASTIC FUNCTIONS

As indicated in another section, the response to an isotropic pressure as a step function of time gives the bulk creep compliance $B(t)$. However, the response to a sinusoidal pressure gives the complex bulk compliance:

$$B^*(\omega) = B'(\omega) - iB''(\omega) = \tilde{B}(\omega) \exp[-i\delta_\omega] \quad (6.64)$$

where $B'(\omega)$ and $B''(\omega)$ are, respectively, the bulk storage and the bulk loss compliance $B(t)$. The bulk phase angle is given by

$$\tan \delta_B(\omega) = \frac{B''(\omega)}{B'(\omega)} \quad (6.65)$$

The Poisson ratio, like the bulk, tensile, and shear creep compliance, is an increasing function of time because the lateral contraction cannot develop instantaneously in uniaxial tension but takes an infinite time to reach its ultimate value. In response to a sinusoidal uniaxial stretch, the complete Poisson ratio is obtained:

$$\nu(\omega) = \nu'(\omega) = i\nu''(\omega) = \tilde{\nu}(\omega) \exp[-i\delta_\nu(\omega)] \quad (6.66)$$

and the phase angle between the lateral contraction and the strain excitation is

$$\tan \delta_\nu = \frac{\nu''(\omega)}{\nu'(\omega)} \quad (6.67)$$

In the same way, the response to a sinusoidal change of volume yields the complex bulk relaxation modulus,

$$K^*(\omega) = K'(\omega) + iK''(\omega) = \tilde{K}(\omega) \exp[-i\delta_K(\omega)] \quad (6.68a)$$

and

$$\tan \delta_K = \frac{K''(\omega)}{K'(\omega)} \quad (6.68b)$$

Finally, the complex tensile compliance, $D^*(\omega)$, and the complete tensile relaxation modulus, $E^*(\omega)$, can be obtained from the responses to a sinusoidal uniaxial stress or strain, respectively. Thus,

$$D^*(\omega) = D'(\omega) - iD''(\omega) = \tilde{D}(\omega) \exp[-i\delta_D(\omega)] \quad (6.69)$$

and

$$E^*(\omega) = E'(\omega) - iE''(\omega) = \tilde{E}(\omega) \exp[-i\delta_E(\omega)] \quad (6.70)$$

with $\tan \delta_D(\omega)$ and $\tan \delta_E(\omega)$ given by

$$\tan \delta_D(\omega) = \frac{D''(\omega)}{D'(\omega)}; \quad \tan \delta_E(\omega) = \frac{E''(\omega)}{E'(\omega)} \quad (6.71)$$

It should be noted that $\tan \delta_D = \tan \delta_E$ and $\tan \delta_B = \tan \delta_K$.

PROBLEM SETS**Problem 6.1**

In many practical situations the following model for the compliance $J(t)$ is useful.

$$J(t') = J(t)x^{m(t)} \quad \text{where } t' = xt, \quad 0 < x < 1$$

Estimate $G(t)$ from $J(t)$. Apply it to

$$J(t) = 1 + t$$

and discuss the range of validity for the obtained estimation.

Solution 6.1

If $J(xt) = J(t)x^{m(t)}$, it is expected that

$$G(xt) = G(t)x^{-n(t)} \quad (\text{P6.1.1})$$

Note that $m(t)$ is the slope of a $\log J$ vs. $\log t$ plot. According to Eq. (P5.9.1), the relationship between the modulus and the compliance can be written as

$$\int_{-\infty}^t G(t-\theta) dJ(\theta) = 1 \quad (\text{P6.1.2})$$

For $\theta = xt$,

$$\int_0^1 G[t(1-x)] dJ(tx) = 1, \quad 0 < x < 1 \quad (\text{P6.1.3})$$

By substituting for $J(xt)$ and $G(xt)$ the expressions given for this quantity in (P6.1.1), we obtain

$$G(t)J(t) \int_0^1 (1-x)^{-n} m x^{m-1} dx = G(t)J(t) \frac{(-n)!(m)!}{(m-n)!} = 1 \quad (\text{P6.1.4})$$

where the Euler beta function has been used. By assuming a smooth time dependence for n and m , that is, treating the factorials as constants, we find that $G(t)$ is proportional to $J(t)^{-1}$. Then n is close to m , and the following result is obtained:

$$(m)!(-m)! = \frac{\pi m}{\sin \pi m}$$

Consequently,

$$G(t)J(t) = \frac{\sin m\pi}{m\pi} \quad (\text{P6.1.5})$$

A plot of the function represented by the right-hand side of Eq. (P6.1.5) is shown in Figure P6.1.1.

Consider now the proposed example. In this case,

$$m(t) = \frac{d \log J(t)}{d \log t} = \frac{t}{t+1} \quad (\text{P6.1.6})$$

Moreover, if $t \rightarrow 0$, then $m \rightarrow 0$ and $J \rightarrow 1$. On the other hand, if $t \rightarrow \infty$, then $m \rightarrow 1$ and $J \rightarrow \infty$. For these reasons, in the short time limit, one can assume that

$$G(t) \cong \frac{1}{1+t} \quad (\text{P6.1.7})$$

which can be expanded in series as

$$G(t) \cong 1 - t + t^2 - t^3 + \dots \quad (\text{P6.1.8})$$

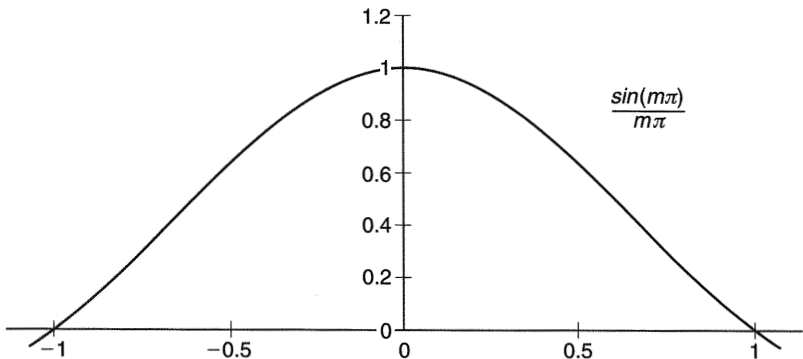


Figure P6.1.1

The exact solution can be found by using Eq. (5.59), from which we obtain

$$G(s) = \frac{1}{1+s} \quad (\text{P6.1.9})$$

By Laplace inversion we find

$$G(t) = \exp(-t) \quad (\text{P6.1.10})$$

This expression can be expanded in series as

$$G(t) = 1 - t + \frac{t^2}{2!} - \frac{t^3}{3!} \dots \quad (\text{P6.1.11})$$

Comparing Eqs. (P6.1.8) and (P6.1.11), we notice that the proposed model represents a good approximation only at short times.

We also note that

$$J(t)G(t) \cong \frac{\sin m\pi}{m\pi} \cong \frac{1}{m\pi} \left(m\pi - \frac{1}{3!} (m\pi)^3 + \dots \right) \quad (\text{P6.1.12})$$

Therefore,

$$J(t)G(t) \cong 1 - m^2 \frac{\pi^2}{6} + \dots \cong 1 - 1.6m^2 \quad (\text{P6.1.3})$$

Then, if $m = 0.1$,

$$J(t)G(t) < 0.98 \quad (\text{P6.1.14})$$

Taking $J(t) = [G(t)]^{-1}$ is less than 2% in error.

Problem 6.2

The shear modulus of a polymer at 18°C is given by

$$G(t) = [0.6812 + \exp(-1.3t)] \text{ GPa}$$

where t is given in seconds. Estimate $J(t)$.

Solution 6.2

From Eq. (5.59), we obtain

$$J(s) = \frac{1}{s^2 G(s)} \quad (\text{P6.2.1})$$

On the other hand,

$$G(s) = \mathcal{L}G(t) = \left(\frac{0.6812}{s} + \frac{1}{s+1.3} \right) \times 10^9 \quad (\text{P6.2.2})$$

Hence

$$\begin{aligned} J(s) &= \frac{s+1.3}{1.6812s^2 + 0.8856s} \times 10^{-9} \\ &= 0.5948 \times \frac{s+1.3}{s(s+0.5268)} \times 10^{-9} \text{ Pa}^{-1} \end{aligned} \quad (\text{P6.2.3})$$

Since

$$\frac{s+a}{s(s+b)} = \frac{A}{s} + \frac{B}{s+b}; \quad A = \frac{a}{b}, \quad B = 1 - \frac{a}{b} \quad (\text{P6.2.4})$$

Eq., (P6.2.3) can be written as

$$J(s) = 1.4678 \times \left(\frac{1}{s} - \frac{0.5948}{s+0.5268} \right) \times 10^{-9} \text{ Pa}^{-1} \quad (\text{P6.2.5})$$

Therefore,

$$J(t) = \mathcal{L}^{-1}J(s) = 1.4678[1 - 0.5948 \exp(-0.5268t)] \times 10^{-9} \text{ Pa}^{-1} \quad (\text{P6.2.6})$$

If we take $J(t)$ as $[G(t)]^{-1}$, the errors at $t = 10^{-2}$, 10^0 , and 10^2 s would be, respectively, 0.013%, 10.10%, and 0.014%.

Note that

$$J(t)G(t) = 1 - 0.5947 \exp(-0.5268t) + 1.4678 \exp(-1.3t) - 0.8730 \exp(-1.8268t) \neq 1$$

Obviously,

$$J_g G_g = 1 \quad \text{and} \quad J_g G_e / = 1 \quad (\text{P6.2.7})$$

Problem 6.3

Show that

$$H(t) = \int_0^t G(t - \theta) dJ(\theta) \geq G(t)J(t)$$

and

$$G(t) \int_0^t J(\theta) d\theta \leq t \leq J(t) \int_0^t G(\theta) d\theta$$

on the basis of the empirical behavior of G and J

Solution 6.3

According to Eq. (P5.9.1), and since $H(t)$ is the unity step function,

$$H(t) = \int_0^t G(t - \theta) dJ(\theta) \quad (\text{P6.3.1})$$

Because J and G are increasing and decreasing functions of time (for $t > 0$),

$$H(t) \geq G(t) \int_0^t dJ(\theta) = G(t) J(t) \quad (\text{P6.3.2})$$

By using the same arguments it is easy to see from

$$\int_0^t G(\theta) dJ(t - \theta) d\theta = \int_0^t G(t - \theta)J(\theta) d\theta = t \quad (\text{P6.3.3})$$

that

$$G(t) \int_0^t J(\theta) d\theta \leq t \leq J(t) \int_0^t G(\theta) d\theta \quad (\text{P6.3.4})$$

Problem 6.4

According to Eq. (5.55), the viscosity at zero shear rate is given by

$$\eta = \int_0^{\infty} G(t) dt$$

The divergence or nondivergence of this integral permits us to decide whether a material under study is a solid or a liquid. Check the nature (solid or liquid) of the materials whose behavior is represented by the functions (a) $G = t^{-1/2}$, (b) $J = 1 + t$, (c) $J = t^{1/2}$.

Solution 6.4

(a)

$$\eta = \int_0^{\infty} G(t) dt = \int_0^{\infty} t^{-1/2} dt \rightarrow \infty$$

The material is a solid.

(b) By taking the Laplace transform of $J(t) = 1 + t$ and using Eq. (5.59), we find that

$$G(s) = \frac{1}{s^2 J(s)} = \frac{1}{s+1}$$

Hence

$$G(t) = \mathcal{L}^{-1}[G(s)] = e^{-t}$$

Then

$$\eta = \int_0^{\infty} e^{-t} dt = 1$$

and the material is a fluid.

(c) By a procedure analogous to the one followed above; we find

$$J(s) = \frac{\sqrt{\pi}}{2} s^{-3/2}$$

and therefore

$$G(t) = \frac{2}{\pi} t^{-1/2}$$

Thus we obtain

$$\eta = \int_0^{\infty} G(t) dt = \int_0^{\infty} \frac{2}{\pi} t^{-1/2} dt \rightarrow \infty$$

Consequently the material is a solid.

Problem 6.5

Starting from $G(t') = G(t)x^{-n}$ with $t' = xt$ [Eq. (P6.1.1) of Problem 1], obtain a relationship between $G(r)$ and $G^*(\omega)$. From this relationship and for small loss angles, determine the loss modulus and the loss tangent from the storage modulus.

Solution 6.5

By taking logarithms to

$$G(t') = G(t)x^{-n} \quad (\text{P6.5.1})$$

where $x = t'/t$, we obtain

$$\log G(t') = \log G(t) - n \log t' + n \log t \quad (\text{P6.5.2})$$

This expression leads to

$$n = - \left. \frac{d \log G(t)}{d \log t} \right|_t = - \left. \frac{d \log G(t')}{d \log t'} \right|_{t'} \quad (\text{P6.5.2a})$$

Moreover, for $t = \omega^{-1}$, Eq. (P6.5.1) becomes

$$G\left(\frac{x}{\omega}\right) = G\left(\frac{1}{\omega}\right)x^{-n} = G\left(\frac{1}{\omega}\right)\omega^{-n}\left(\frac{x}{\omega}\right)^{-n} \quad (\text{P6.5.3})$$

while for $x/\omega = t'$,

$$G(t') = G\left(\frac{1}{\omega}\right)\omega^{-n}(t')^{-n} \quad (\text{P6.5.4})$$

Taking the Laplace transform of (P6.5.4) with respect to t' and considering that

$$\mathcal{L}(t^{-n}) = (-n)!s^{n-1} \quad (\text{P6.5.5})$$

we find

$$\bar{G}(s) = G\left(\frac{1}{\omega}\right)\omega^{-n}(-n)!s^{n-1} \quad (\text{P6.5.6})$$

or

$$s\bar{G}(s) = G\left(\frac{1}{\omega}\right)(-n)!\left(\frac{s}{\omega}\right)^n \quad (\text{P6.5.7})$$

For $s = i\omega$, and taking into account that $i = \exp(i\pi/2)$, Eq. (P6.5.7) can be written as

$$G^*(i\omega) = s\bar{G}(s) = G\left(\frac{1}{\omega}\right)(-n)! \exp\left(\frac{in\pi}{2}\right) \quad (\text{P6.5.8})$$

For very low values of the loss angles, Eq. (P6.5.8) becomes

$$|G^*| \cong G'(\omega) \cong G(t)(-n)! \quad (\text{P6.5.9})$$

where $t = 1/\omega$ has been assumed.

In the same way, if the loss angle is small,

$$\begin{aligned} \tan \delta &= \tan\left(\frac{n\pi}{2}\right) \cong \frac{n\pi}{2} = -\frac{\pi}{2} \frac{d \log G'}{d \log t} \Big|_{t=\omega^{-1}} \\ &= -\frac{\pi}{2} \frac{d \ln G'}{d \ln t} \Big|_{t=\omega^{-1}} = \frac{\pi}{2} \frac{d \ln G'}{d \ln \omega} \end{aligned} \quad (\text{P6.5.10})$$

Finally, from $\tan \delta = G''/G'$, we easily obtain

$$G'' \cong \frac{\pi}{2} \frac{dG'}{d \ln \omega} \quad (\text{P6.5.11})$$

A similar expression can be found for J'' .

Problem 6.6

Consider a prismatic rod of PMMA whose tensile modulus at 20°C and 1 Hz is given by $E^* = (4.62 + i0.438) \times 10^9$ Pa. The dimensions of this rod are $10 \times 3 \times 150$ mm³. In a test the rod is subjected to forced longitudinal vibrations with an amplitude of 1 kN. Determine the energy dissipated per cycle.

Solution 6.6

According to Eq. (6.39), the energy dissipated per cycle is given by

$$W = \pi \sigma_0^2 D'' \quad (\text{P6.6.1})$$

where D'' is the loss tensile compliance and σ_0 is the amplitude of the oscillating stress. Accordingly,

$$\sigma_0 = \frac{10^3}{30 \times 10^{-6}} \text{ N/m}^2; \quad D'' = \frac{E''}{E'^2 + E''^2} = \frac{E''}{|E^*|^2} = 0.02 \times 10^{-9} \text{ Pa}^{-1}$$

and $W = 7.1 \times 10^4 \text{ J/m}^3$. Since the volume of the rod is $4.5 \times 10^{-6} \text{ m}^3$, the total energy dissipated is $W = 0.3195 \text{ J}$ per cycle. If the frequency of the vibration is 1 Hz , the power dissipated as heat will be 0.3195 W .

Problem 6.7

A piece of rubber is used to damp the mechanical vibration of a structural mechanism. Determine the power dissipated by this rubber when it is subjected to shear vibrations of maximum amplitude 2×10^{-3} and frequency $\omega = 12000 \text{ rpm}$. The viscoelastic characteristics of the rubber are $G' = 2 \text{ MPa}$ and $\tan \delta = 0.5$.

Solution 6.7

In terms of the displacement and the loss modulus, the dissipated power is given by Eq. (6.15),

$$\dot{W} = \pi \gamma_0^2 G'' \omega = 3.14 \times (2 \times 10^{-3})^2 \times (2 \times 10^6 \times 0.5) \times 200 = 2.51 \text{ kW/m}^3$$

Problem 6.8

Find η_0 for a material whose loss modulus is given by

$$G''(\omega) = \text{Im} \left[G_\infty + \frac{G_0 - G_\infty}{1 + (j\omega\tau)^{1-\alpha}} \right]$$

Solution 6.8

From Eq. (6.12),

$$\eta_0 = \lim_{\omega \rightarrow 0} \frac{G''(\omega)}{\omega}$$

where

$$G''(\omega) = (G_0 - G_\infty) \frac{(\omega\tau)^{1-\alpha} \sin\left(\frac{1-\alpha}{2}\pi\right)}{1 + 2(\omega\tau)^{1-\alpha} \cos\left(\frac{1-\alpha}{2}\pi\right) + (\omega\tau)^2} \quad (\text{P6.8.1})$$

Consequently,

$$\eta_0 = \lim_{\omega \rightarrow 0} (G_0 - G_\infty) \tau^{1-\alpha} \sin \frac{1-\alpha}{2} \pi \left[\frac{\omega^{-\alpha}}{1 + 2(\omega\tau)^{1-\alpha} \cos\left(\frac{1-\alpha}{2}\pi\right) + (\omega\tau)^2} \right] \quad (\text{P6.8.2})$$

$\eta_0 = \infty$, and the material is a solid.

Problem 6.9

In the terminal region of a viscoelastic liquid $G^1 = 10^2 \text{ N/m}^2$ and $G^{11} = 10^4 \text{ N/m}^2$ at 10^{-2} rad/s and temperature T . In steady state conditions determine, at this temperature, the strain at 1 s under a shear stress of 10 kPa.

Solution 6.9

From Eqs. (6.12) and (6.52), we have

$$\eta = \lim_{\omega \rightarrow 0} \frac{G''(\omega)}{\omega} \cong \frac{10^4}{10^{-2}} = 10^6 \text{ Pa} \cdot \text{s}$$

$$J_e = \lim_{\omega \rightarrow 0} \frac{1}{\eta^2} \left(\frac{G'(\omega)}{\omega^2} \right) = \frac{10^2}{10^{12} \times 10^{-4}} = 10^{-6} \text{ Pa}^{-1}$$

The creep compliance will be

$$J(t) = J_e + \frac{t}{\eta} = 10^{-6} + 10^{-6} = 2 \times 10^{-6} \text{ Pa}^{-1}$$

Hence,

$$\varepsilon = 2 \times 10^{-6} \times 10^4 = 0.02$$

Problem 6.10

Find J_e from $G(t) = G_0 \exp(-t/\tau)$.

Solution 6.10

From Eq. (6.53), we have

$$J_e = \frac{1}{\eta^2} \int_0^{\infty} tG(t) dt = \frac{\int_0^{\infty} tG(t) dt}{\left[\int_0^{\infty} G(t) dt\right]^{1/2}} = \frac{\int_0^{\infty} tG_0 \exp(-t/\tau) dt}{\left[\int_0^{\infty} G_0 \exp(-t/\tau) dt\right]^2} = \frac{1}{G_0}$$

J_e is the reciprocal of G_0 , as expected for a solid.

Problem 6.11

Many symmetrical loss relaxation curves fit the so-called Fuoss–Kirkwood (FK) equation given by

$$G'' = G''_{\max} \operatorname{sech} m \ln \frac{f_m}{f}$$

where G''_{\max} is the loss at the peak maximum and m is an empirical parameter, $0 < m \leq 1$. Show that the relaxation strength is given by

$$\Delta G = \frac{2G''_{\max}}{m}$$

Solution 6.11

From Krönig–Kramers relationships [Eq. (6.57)],

$$\Delta G = \frac{2}{\pi} \int_0^{\infty} G''(x) \frac{dx}{x} \quad (\text{P6.11.1})$$

From the FK equation, $G''(x)$ can be written as

$$G''(x) = \frac{2G''_{\max}(x\tau)^m}{1 + (x\tau)^{2m}}, \quad \ln \frac{f_m}{f} = \ln x \quad (\text{P6.11.2})$$

By substituting Eq. (P6.11.2) into Eq. (P6.11.1), we obtain

$$\Delta G = \frac{2G''_{\max}}{m} \quad (\text{P6.11.3})$$

Problem 6.12

From

$$(a) \frac{dE'}{d\omega} = \frac{2E''}{\pi\omega} \quad \text{and} \quad (b) \frac{d \ln E'}{d\omega} = \frac{2 \tan \delta}{\pi\omega}$$

(see Problem 6.5) and assuming

$$(c) E'' = E''_{\max} \operatorname{sech} mx \quad \text{and} \quad (d) \tan \delta = \tan \delta_{\max} \operatorname{sech} m'x$$

where $x = \ln(f/f_{\max})$, find the respective expressions for E' from E'' and $\tan \delta$, specifying the assumptions made.

Solution 6.12

From (a),

$$\frac{dE'}{d \ln f} = \frac{2E''}{\pi} \quad \left(f = \frac{2\pi}{\omega} \right) \quad (\text{P6.12.1})$$

Hence,

$$\begin{aligned} dE' &= \frac{2E''}{\pi} d \ln f \\ E'(f_2) - E'(f_1) &= \frac{2}{\pi} \int_{f_1}^{f_2} E'' d \ln f \end{aligned} \quad (\text{P6.12.2})$$

By substituting (c) into Eq. (P6.12.2), we obtain

$$\begin{aligned}
 E'(f_2) - E'(f_1) &= \frac{2}{\pi} E_m'' \int_{f_1}^{f_2} \operatorname{sech} m \ln \frac{f}{f_m} d \ln f \\
 &= \frac{4}{\pi m} E_m'' \left[\arctan \left(\frac{f_2}{f_m} \right)^m - \arctan \left(\frac{f_1}{f_m} \right)^m \right]
 \end{aligned}
 \tag{P6.12.3}$$

if $f_1 = f_m$ and $f_2 = f$, then

$$E'(f) = E'(f_m) + \frac{4}{\pi m} E_{\max}'' \left[\arctan \left(\frac{f}{f_m} \right)^m - \frac{\pi}{4} \right] \tag{P6.12.4}$$

From (b) and operating as above, that is, taking

$$\tan \delta = \tan \delta_{\max} \operatorname{sech} m' x, \quad x = \ln \frac{f}{f_m} \tag{P6.12.5}$$

we obtain

$$E'(f_2) = E'(f_1) \exp \left\{ \frac{4}{\pi m'} \tan \delta_{\max} \left[\arctan \left(\frac{f_2}{f_m} \right)^{m'} - \arctan \left(\frac{f_1}{f_m} \right)^{m'} \right] \right\} \tag{P6.12.6}$$

If $f_1 = f_m$ and $f_2 = f$, then

$$E'(f) = E'(f_m) \exp \left\{ \frac{4}{\pi m'} \tan \delta_{\max} \left[\arctan \left(\frac{f}{f_m} \right)^{m'} - \frac{\pi}{4} \right] \right\} \tag{P6.12.7}$$

When $\tan \delta_{\max} \ll 1$, Eq. (P6.12.7) becomes

$$E'(f) = E'(f_m) \left\{ 1 + \frac{4}{\pi m'} \tan \delta_{\max} \left[\arctan \left(\frac{f}{f_m} \right)^{m'} - \frac{\pi}{4} \right] \right\} \tag{P6.12.8}$$

Equation (P6.11.3) indicates that

$$E(\infty) - E(0) = \frac{2}{m} E_{\max}'' \tag{P6.12.9}$$

While Eq. (P6.12.6) leads to

$$E(\infty) = E(0) \exp \left(\frac{2}{m'} \right) \tan \delta_m \tag{P6.12.10}$$

Finally, from Eqs. (P6.12.9) and (P6.12.10), we find

$$E(\infty) = \frac{(2/m)E_m'' \exp(\frac{2}{m'} \tan \delta_m)}{\exp(\frac{2}{m'} \tan \delta_m) - 1} \quad (\text{P6.12.11})$$

$$E(0) = \frac{(2/m)E_m''}{\exp(\frac{2}{m'} \tan \delta_m) - 1} \quad (\text{P6.12.2})$$

For $\frac{2}{m'} \tan \delta_m \ll 1$

$$E(\infty) \cong \frac{m'}{m} \left(\frac{E_m''}{\tan \delta_m} \right) \left(1 + \frac{2}{m'} \tan \delta_m \right) \quad (\text{P6.12.13a})$$

and

$$E(0) \cong \frac{m'}{m} \left(\frac{E_m''}{\tan \delta_m} \right) \quad (\text{P6.12.13b})$$

REFERENCES

1. AC Pipkin. Lectures on Viscoelasticity Theory. New York: Springer-Verlag, 1972, Chap. 1.
2. H Markovitz. Lectures in Linear Viscoelasticity: An Introduction. Pittsburgh: Carnegie-Mellon Univ, 1978.
3. NW Tschoegl. The Phenomenological Theory of Linear Viscoelastic Behavior. Heidelberg: Springer-Verlag, 1989.
4. JD Ferry. Viscoelastic Properties of Polymers. 3rd ed. New York: Wiley-Interscience, 1980.
5. JJ Aklonis, WJ MacKnight. Introduction to Polymer Viscoelasticity. 2nd ed. New York: Wiley, 1980.
6. NG McCrum, CP Buckley, CB Bucknall. Principles of Polymer Engineering. Oxford, UK: Oxford Univ, 1988.
7. MR Spiegel. Theory and Problems of Laplace Transforms. Schaum's Outline Ser. New York: McGraw Hill, 1965.
8. RS Marvin. Phys Rev. **86**: 644, 1952.
9. B Gross. Mathematical Structure of the Theories of Viscoelasticity. Paris: Hermann, 1953. ME Gurtin and E Sternberg. *ARMA* 11: 291, 1962.
10. RdeL Krönig. J Opt Soc Am. **12**: 547, 1926.
11. HA Kramers. Atti Cong Fisici, Como, 1927, p. 545.
12. JH van Vleck. In: DE Kerr, ed. Properties of Short Radio Waves. New York: McGraw-Hill, 1951.
13. IL Hopkins, RW Hamming. J Appl. Phys. **28**: 906, 1957.

7

Experimental Determination of Viscoelastic Properties

7.1	Introduction	272
7.2	Experimental Determination of Dynamic Viscoelastic Properties	273
7.3	Torsion Pendulum	274
7.4	Corrections in the Determination of $G^*(\omega)$ from Free Oscillations in Shear	279
7.5	Forced Oscillations	280
7.6	Secondary Effects in Torsion	280
7.7	Effective Sample Length	283
7.8	Dynamic Mechanical Analysis by Transverse Flexion	285
7.9	Response of a Viscoelastic Rod to an Instantaneous Stimulus (Free Oscillations)	290
7.10	Determination of the Corrections in the Viscoelastic Functions Due to Clamping	292
7.11	Resonance Instruments	294
7.12	Wave Propagation	294
7.13	Experimental Determination of Static Viscoelastic Properties	296
7.14	Torsional Creep	296
7.15	Tensile Creep	298
7.16	Stress Relaxation	299
	Problem Sets	300
	References	304

7.1 INTRODUCTION

There are a great number of techniques for the experimental determination of viscoelastic functions. The techniques most frequently found in the literature are devoted to measuring the relaxation modulus, the creep compliance function, and the components of the complex modulus in either shear, elongational, or flexural mode (1–4). Although the relaxation modulus and creep compliance functions are defined in the time domain, whereas the complex viscoelastic functions are given in the frequency domain, it is possible, in principle, by using Fourier transform, to pass from the time domain to the frequency domain, or vice versa, as discussed earlier.

Each of these techniques relates the response to the perturbation field with the material function under study through an auxiliary method of analysis. Under some rigorous boundary conditions, this analysis should give the exact solution to the field equations. However, to overcome in practice the inherent technical difficulties, it is necessary to introduce some approximations that can affect the equations just as the boundary conditions do. Some experimental methods are better conceived than others, and, as a general rule, a simple method is always more desirable than a more complex one because it allows these technical difficulties to be eliminated or simplified. On the other hand, most modern experimental equipment incorporates the method of analysis as part of the software, and consequently it is not possible to discern in detail the process of calculation of the physical function under study.

When the inertial forces can be neglected and the deformations are infinitesimal, the relationships between stress and strain can be assimilated into the relationships between force and displacement through a coefficient directly related to the geometry of the system, which, somewhat inadequately, is called a form factor

In the analysis of viscoelastic systems by dynamic methods, a linear one-dimensional system of second order in terms of force and displacement is customarily used. This approach also requires the introduction of the geometric form factors with the purpose of solving the real problem in a simple way (Fig. 7.1.)

As shown, a detailed study of the same problem reveals that on some occasions the factors in question depend on the physical properties of the viscoelastic system. Hence, it is important to analyze carefully the hypothesis on which such a reduction of the problem is based, in order to be able to calibrate the quality of both the approximations achieved and the results obtained. Such a critical analysis must be implemented rigorously in the experiments. The previous considerations become more important the nearer one works to the limit stipulated by the technical specifications of

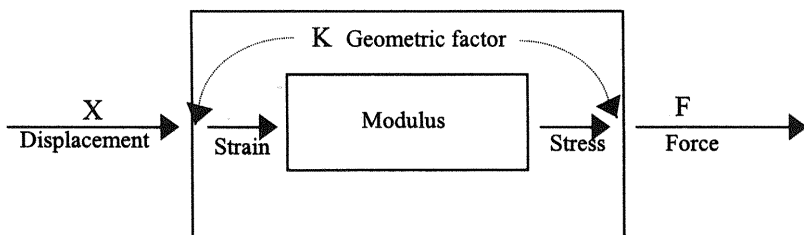


Figure 7.1 Sketch to show how the so-called “geometric factors” act as an interface between the stress–strain and force–displacement relationships.

the experimental equipment, since without this type of caution the errors made can be of the order of magnitude of the experimental measurement itself.

7.2 EXPERIMENTAL DETERMINATION OF DYNAMIC VISCOELASTIC PROPERTIES

As mentioned above, it is very difficult, for experimental reasons, to measure the relaxation modulus or the creep compliance at times below 1 s. In this time scale region, dynamic mechanical viscoelastic functions are widely employed (5,6). However, in these methods the measured forces and displacements are not simply related to the stress and strain in the samples. Moreover, in the case of dynamic experiments, inertial effects are frequently important, and this fact must be taken into account in the theoretical methods developed to calculate complex viscoelastic functions from experimental results.

Dynamic mechanical tests have been widely applied in the viscoelastic analysis of polymers and other materials. The reason for this has been the technical simplicity of the method and the low tensions and deformations used. The response of materials to dynamic perturbation fields provides information concerning the moduli and the compliances for storage and loss. Dynamic properties are of considerable interest when they are analyzed as a function of both frequency and temperature. They permit the evaluation of the energy dissipated per cycle and also provide information concerning the structure of the material, phase transitions, chemical reactions, and other technical properties, such as fatigue or the resistance to impact. Of particular relevance are the applications in the field of the isolation of vibrations in mechanical engineering. The dynamic measurements are a

complement to the transitory experiments because they provide information concerning the viscoelastic behavior of the material at short times (large frequencies). The frequencies used in dynamic measurements lie in the range 10^{-4} – 10^2 Hz. For higher frequencies (of the order of 10^3 – 10^4 Hz), echo effects in the test piece can be used, which permit determination of the dynamic modulus from the form and frequency of the resonance peaks. For still higher frequencies, ultrasonic waves are used. In this technique, the velocity of the wave and the attenuation factor permit calculation of the storage and loss moduli of the material under study at frequencies above 100 kHz.

Nevertheless, although the dynamic response of materials to oscillatory perturbations has been studied by many authors in many places, information concerning the limitations and precision of these methods is not often found in the literature. The same is true regarding the sources of error and discrepancies between different experimental methods.

7.3 TORSION PENDULUM

Simple shear experiments are inadequate to measure the rigidity of a material, owing to the magnitude of the force that is required to produce significant deformations. This problem can be avoided if the shear modulus is determined from torsion experiments carried out on large cylindrical or prismatic test samples (See Ref. 5, Chap. 3; Ref. 6, p. 27; and Ref. 7). In this type of experiment there is not a meaningful variation of volume in the test sample, such as corresponds to pure shear, and the particles of the material are moving in circular arcs around a common axis. The inertia of the system is furnished by an external device, and to avoid compression or traction in the samples the mass that produces the rotatory inertia is compensated for by another mass on the opposite arm of an appropriate balance. These considerations define the physical structure of the torsion pendulum. The experiment can be initiated by a sinusoidal type of signal in the forced vibration method or simply by producing free oscillations after separating the inertial system from its position of equilibrium. This is a very simple method because free oscillations can even be induced manually. Although the system is less versatile than the techniques used in nonresonant vibrations, it has undoubted advantages, among them great precision in the determination of viscoelastic functions in materials with small loss and the relative simplicity in the construction of the instrument. There are many automated designs of this instrument that permit the sample to be conveniently thermostated and also allow it to undergo different thermal histories.

A schematic model of a torsion pendulum is presented in Figure 7.2. The sample is clamped at the two extremes, and the upper clamp is bound to an inertial rotating counterbalanced system. Torsional oscillations can be induced by applying a torque, by using a reasonably small deformation that separates the system from its position of equilibrium in the case of free oscillations, and by applying a periodic signal in the case of forced oscillations. The temporary dependence of the angular displacement is measured through an optical or electrical system, etc. In the case of free oscillations, the decay of the amplitude of the wave permits determination of the shear modulus of the material at the frequency of the oscillation by procedures described below. It is important to avoid lateral movements of the system, and this is frequently achieved by using the same counterbalance system that is employed to avoid having the test sample undergo either traction or compression. The oscillation frequencies are ordinarily restricted to the interval 0.1–10 Hz. Furthermore, for materials with high viscous damping ($\tan \delta > 0.3$), an auxiliary elastic element is required in order to eliminate overdamping, which would impede obtaining precise measurements of the viscoelastic functions.

To find convenient expressions for the storage modulus and the loss tangent for a viscoelastic material under free oscillation in torsion, it is necessary to return to the equation of motion given by

$$I\ddot{\theta} + \left(\frac{S_D}{\omega} + K \frac{G''}{\omega} \right) \dot{\theta} + (S + KG')\theta = 0 \quad (7.1)$$

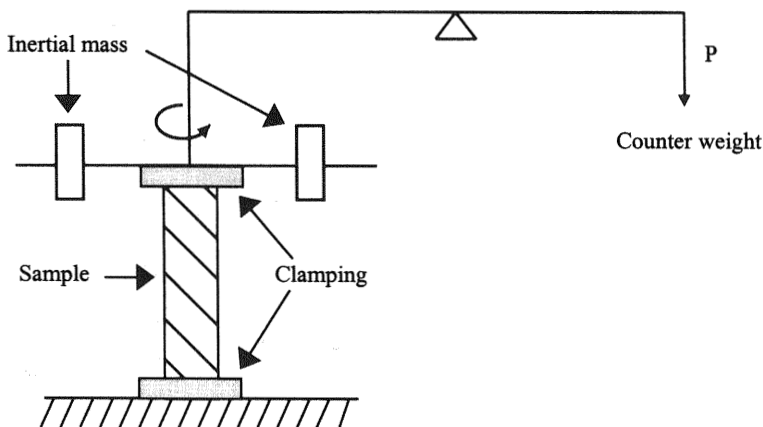


Figure 7.2 Scheme of an inverted torsion pendulum.

where G' and G'' are the storage and loss moduli of the material, S the rigidity of the auxiliary elastic element, S_D the damping of the elastic support, and I the inertial mass coupled to the system. As mentioned before, K is a "geometric" factor that depends on the form of the test sample. A simple solution of Eq. (7.1) is based on a simple model made up of an elastic element in parallel with a dashpot, that is, a Kelvin element. This procedure introduces obvious limitations to the solution of the problem.

As is well known, the solution of Eq. (7.1) is a damped sinusoidal wave that can be written as

$$\theta = \text{Re } \theta_0 \exp(-\gamma t) \exp(i\omega t) \quad (7.2)$$

where

$$\gamma = \frac{S_D + KG''}{2I\omega} \quad \text{and} \quad \omega = \left[\frac{KG' + S}{I} - \left(\frac{S_D + KG''}{2I\omega} \right)^2 \right]^{1/2} \quad (7.3)$$

The logarithmic decrement Δ , as a measure of the damping, can be defined as the logarithm of the quotient of the amplitude of two successive waves. Then

$$\begin{aligned} \Delta &= \ln \frac{\theta(t)}{\theta(t + 2\pi/\omega)} \\ &= \ln \frac{\text{Re } \theta_0 \exp(-\gamma t) \exp(i\omega t)}{\text{Re } \theta_0 \exp[-\gamma(t + 2\pi/\omega)] \exp [i\omega(t + 2\pi/\omega)]} = \frac{2\pi\gamma}{\omega} \end{aligned} \quad (7.4)$$

and

$$G'' = \frac{2I\omega\gamma - S_D}{K} = \frac{I\Delta\omega^2}{K\pi} - \frac{S_D}{K} \quad (7.5)$$

Normally the elastic support friction S_D can be disregarded, and the frequency of the wave can be written as

$$\omega = \left\{ \frac{KG' + S}{I} - \left[\frac{I\Delta\omega^2}{2\pi} \left(\frac{1}{\omega I} \right) \right]^2 \right\}^{1/2} = \left[\frac{KG' + S}{I} - \frac{\Delta^2 \omega^2}{4\pi^2} \right]^{1/2} \quad (7.6a)$$

which means that

$$G' = \frac{1}{K} \left[I\omega^2 \left(1 + \frac{\Delta^2}{4\pi^2} \right) - S \right] \quad (7.6b)$$

Furthermore, the loss tangent is given by

$$\tan \delta = K \frac{I\Delta\omega^2}{K\pi \left[I\omega^2 \left(1 + \frac{\Delta^2}{4\pi^2} \right) - S \right]} = \frac{\Delta}{\pi} \left[\frac{1}{\left(1 + \frac{\Delta^2}{4\pi^2} \right) - \frac{S}{I\omega^2}} \right] \quad (7.7)$$

The constant S can be calculated in a measurement carried out without the test sample. In fact, in many measurements the equipment is prepared in such a way that $S = 0$ that is, the purely elastic rigidity of the suspension thread, E , is negligible. Since the flexibility of suspension wires of cylindrical cross section depends on the fourth power of the diameter, this requirement is achieved by using a wire of very small diameter. In these conditions

$$G' = K^{-1} \left[I\omega^2 \left(1 + \frac{\Delta^2}{4\pi^2} \right) \right] \quad (7.8a)$$

and

$$\tan \delta = \frac{\Delta}{\pi} \left(\frac{1}{1 + \Delta^2/4\pi^2} \right) \quad (7.8b)$$

For small dampings, $\Delta/\pi < 0.1$, and consequently

$$G' = \frac{I\omega^2}{K} \quad (7.9a)$$

and

$$\tan \delta = \frac{\Delta}{\pi} \quad (7.9b)$$

If the damping is large, as occurs in amorphous polymers in the vicinity of the glass transition temperature, these simplifications are not adequate.

In order to show the drawback of the theory as a result of the inherent inaccuracies introduced in the model, it is illustrative to compare the results obtained for the viscoelastic functions with those obtained by solving the following differential equation, which is sometimes used in free oscillations (8):

$$I\ddot{\theta} + KG^*\theta = 0 \quad (7.10)$$

where G^* is the complex modulus. By substituting Eq. (7.2) into Eq. (7.10) and following the same procedure outlined above, one finds

$$G' = \frac{I\omega^2}{K} \left(1 - \frac{\Delta^2}{4\pi^2} \right); \quad G'' = \frac{I\omega^2\Delta}{K\pi} \quad (7.11)$$

and consequently

$$\tan \delta = \frac{\Delta}{\pi} \left(\frac{1}{1 - (\Delta^2/4\pi^2)} \right) \quad (7.12)$$

Because

$$\tan \delta = \frac{2 \tan \delta/2}{1 - \tan^2 \delta/2}; \quad \tan \frac{\delta}{2} = \frac{\Delta}{2\pi} \quad (7.13)$$

for small values of $\Delta/2\pi (< 0.1)$ the results obtained for the moduli and the viscoelastic damping do not greatly differ from those obtained by the method outlined above. However, the differences become important for viscous materials or in zones where viscous damping is high. The reason for the discrepancies observed is that neither the first nor the second differential equation can be used without further justification to describe the response of a viscoelastic material under free oscillation.

In reality, neither the viscosity η' ($= G''/\omega$) nor the storage modulus G' correctly defines the relationship between tensions and deformations except in the case of pure sinusoidal oscillations (9). In fact, what is measured in free oscillations is the dynamic modulus not at a real frequency but at a complex frequency.

$$\omega^* = -\gamma + i\omega \quad (7.14)$$

This problem was clarified by Struik (10), who also showed that the transient components of the solution are ruled out when the constitutive behavior of the material is artificially simplified. In fact, the two proposed differential equations permit us to find only $G^*(s)$, where $s = -\gamma + i\omega$, and not $G^*(\omega)$, which is defined only on the imaginary axis of s . For low damping materials, $G^*(s)$ can be interpreted as $G^*(\omega)$. In a similar way, to put $\eta' = G''/\omega$ is correct only for $s = i\omega$.

In this way, the formulas obtained for the two procedures discussed above can be considered, respectively, as maximum and minimum bounds for G' and $\tan \delta$, respectively, and vice versa.

7.4 CORRECTIONS IN THE DETERMINATION OF $G^*(\omega)$ FROM FREE OSCILLATIONS IN SHEAR

The problem appearing in the calculation of G' and G'' from free oscillations under torsion lies in that G^* is measured at a complex frequency and not at a real value ω as is usual in forced oscillations (11). Consequently,

$$\theta = \theta_0 \exp(i\omega^*t) \tag{7.15}$$

where $\omega^* = \omega' + i\omega''$. As a consequence, $i\omega^* = -\lambda + i\omega$ with $\omega'' = \lambda = \gamma$ and $\omega' = \omega$. It should be pointed out that the evaluation of G^* at real frequencies through an analytical continuation procedure using a Taylor series suggests that the correction for small damping is small. Actually, if $\omega' \gg \omega''$, which is equivalent to $\Delta = 2\pi\omega''/\omega' \ll 1$, expansion of the components of G^* around $\omega'' = 0$ gives

$$G'(\omega') = G'(\omega' + i\omega'') + \frac{\partial G''}{\partial \omega'} \omega'' \tag{7.16a}$$

$$G''(\omega') = G''(\omega' + i\omega'') - \frac{\partial G'}{\partial \omega'} \omega'' \tag{7.16b}$$

where the Cauchy–Riemann conditions of the complex variable theory have been considered and the evaluation of the derivatives was obtained at $\omega'' = 0$.

From the previous equations the following expressions are obtained:

$$\frac{G'(\omega') - G'(\omega' + i\omega'')}{G'(\omega')} = \frac{G''}{G'} \frac{\partial \ln G''}{\partial \ln \omega'} \frac{\omega''}{\omega'} = \tan \delta \frac{\omega''}{\omega'} \frac{\partial \ln G''}{\partial \ln \omega'} \tag{7.17}$$

$$\frac{G''(\omega') - G''(\omega' + i\omega'')}{G''(\omega')} = -\frac{1}{G''} \frac{\partial G'}{\partial \ln \omega'} \frac{\omega''}{\omega'} > 0 \tag{7.18}$$

The terms $(\partial \ln G''/\partial \ln \omega')$ and ω''/ω' in Eq. (7.17) are usually small (although the first can be positive or negative), and for this reason $G'(\omega') \cong G'(\omega' + i\omega'')$. On the other hand, since $\partial G'/\partial \ln \omega' \cong (2/\pi)G''$ (see Problem 6.5), Eq. (7.18) suggests that the corrections in G'' are also small for low values of ω''/ω' .

7.5 FORCED OSCILLATIONS

Forced oscillations in torsion are used in the most versatile and accurate technique for measuring the viscoelastic functions, in the frequency domain, of melts and concentration solutions (12). In this case, the second-order differential equation governing the motion is given by

$$I\ddot{\theta}^* + KG^*\theta^* = M^* \quad (7.19)$$

where the excitation torque appearing on the right-hand side is given by

$$M^* = M \exp(i\omega t) \quad (7.20)$$

As a result, the top of the sample undergoes the sinusoidal motion θ^* ,

$$\theta^* = \theta \exp [i(\omega t - \varphi)] \quad (7.21)$$

By substituting Eqs. (7.20) and (7.21) in Eq. (7.19) and splitting the real and imaginary parts of the resulting expression as usual, we obtain

$$G' = \frac{M \cos \varphi}{K\theta} + \frac{I\omega^2}{K}, \quad G'' = \frac{M \sin \varphi}{K\theta} \quad (7.22)$$

Therefore the phase angle is given by

$$\tan \delta = \frac{\sin \varphi}{\cos \varphi + I\omega^2\theta/M} \quad (7.23)$$

Resonance will occur near the frequency at which $\tan \varphi \rightarrow \infty$, that is,

$$f = \frac{1}{2\pi} \left(\frac{KG'}{I} \right)^{1/2} \quad (7.24)$$

7.6 SECONDARY EFFECTS IN TORSION

In a first approach it is assumed that during torsion the distance between two sections perpendicular to the torsion axis of the rod remains constant. However, in the case of torsion of rubbers or samples whose width is considerably greater than their thickness, this hypothesis is unrealistic. In fact, considering a rectangular section $b \times d$, the longitudinal fibers other than the axis experience an extension (13) when the rod is twisted. For a fiber

belonging to the edge of the bar, the strain and the stress are schematically represented in Figure 7.3. From geometric considerations, the strain is given by (see Fig. 7.4)

$$\varepsilon = \frac{\overline{ac'} - \overline{ac}}{\overline{ac}}$$

$$\varepsilon = \frac{1 - \cos \beta}{\cos \beta}, \quad \cos \beta \approx 1 - \frac{\beta^2}{2}, \quad \varepsilon \approx \frac{\beta^2}{2}$$

By writing β as a function of the torsion angle by unit length, one has $\beta = \overline{oc} \, d\alpha/dz$, and from here $\varepsilon \approx (1/8)(b^2 + d^2)(d\alpha/dz)^2$, $d\alpha/dz$ being the relative rotation of two separate sections. For a fiber at a distance r from the axis, the strain will be lower:

$$\varepsilon \cong \frac{1}{2} r^2 \left(\frac{\partial \alpha}{\partial z} \right)^2 \tag{7.25}$$

The corresponding stress will be

$$\sigma = \frac{1}{2} r^2 \left(\frac{\partial \alpha}{\partial z} \right)^2 E \tag{7.26}$$

where E is the elastic modulus.

If the stress is not fully balanced by the clamping constraints, the samples will tend to be shortened by an amount $\Delta\varepsilon$. The value of $\Delta\varepsilon$ can be obtained by assuming that the longitudinal extensional force applied to the entire surface of the section is negligible, so

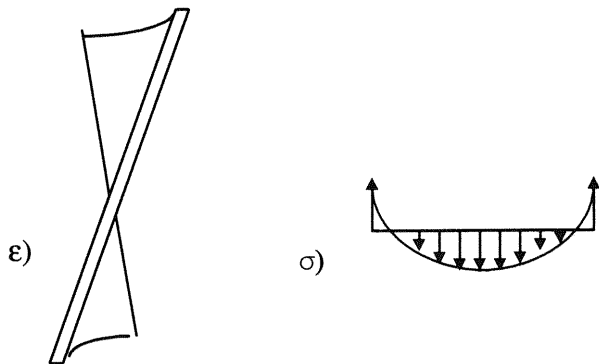


Figure 7.3 Strain and stress in the edge of a twisted thin plate.

$$\int_Q \sigma dQ = 0 \quad (7.27)$$

where Q is the area of the transverse section. In our case, and according to Eq. (7.27), one has

$$\int_{-b/2}^{b/2} \int_{-d/2}^{d/2} \left[E \left(\frac{r^2}{2} \left(\frac{\partial \alpha}{\partial z} \right)^2 - \Delta \varepsilon \right) \right] dx dy = 0, \quad r = (x^2 + y^2)^{1/2} \quad (7.28)$$

from which

$$\Delta \varepsilon = \frac{b^2 + d^2}{24} \left(\frac{\partial \alpha}{\partial z} \right)^2 \quad (7.29)$$

Consequently,

$$\sigma = \frac{E}{2} \left(\frac{\partial \alpha}{\partial z} \right)^2 \left(r^2 - \frac{b^2 + d^2}{12} \right) \quad (7.30)$$

It is clear that the maximum stress appears at the edges of the sample, as shown in Figure 7.3, and its value decreases progressively toward the axis.

The elongated fibers tend to incline because of the effect of the rotation, and taking into account that the stress acts along these fibers, it can be separated into components in two directions, parallel and perpendicular to the axis of rotation. In this way, the normal component induces a secondary torque, σ_{\perp} , that must be added to the primary one. The value of this torque is given by

$$M = \int_Q \sigma_{\perp} r dQ \quad (7.31)$$

This secondary torque depends on both the relative rotation of the two separate parallel sections $\partial \alpha / \partial z$ and the distance to the torsion axis. Consequently, for small values of β the following approximation holds:

$$\sigma_{\perp} = \sigma \sin \left(r \frac{\partial \alpha}{\partial z} \right) \cong \sigma \frac{\partial \alpha}{\partial z} r \quad (7.32)$$

Then the secondary moment can be written as

$$M_1 = \int_{-b/2}^{b/2} \int_{-d/2}^{d/2} \sigma_{\perp} r^2 dx dy = E \left(\frac{\partial \alpha}{\partial z} \right)^3 \left(\frac{bd(b^4 + d^4)}{360} \right) \quad (7.33)$$

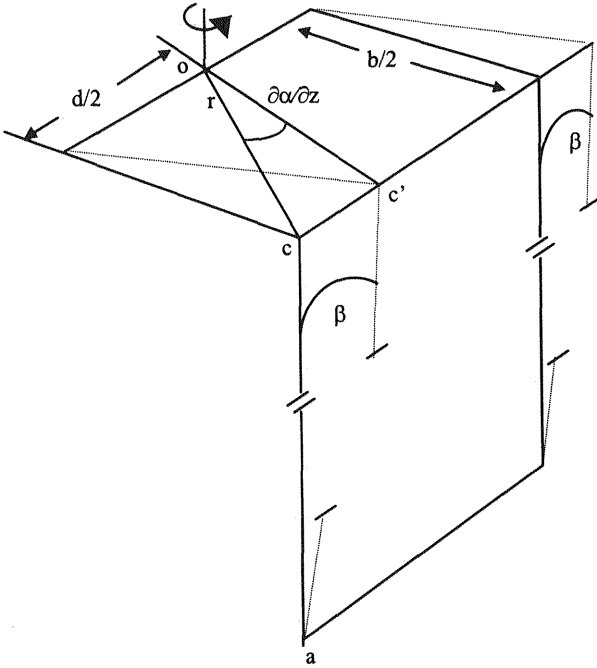


Figure 7.4 Scheme to calculate the additional strain and stress in a twisted thin plate.

Finally, the derivative of the secondary moment is given by

$$\frac{\partial M_1}{\partial z} = E \left(\frac{\partial \alpha}{\partial z} \right)^2 \frac{\partial^2 \alpha}{\partial z^2} \frac{bd(b^4 + d^4)}{120} \tag{7.34}$$

It is clear that neither the additional torque nor its derivative is a linear function of the torsion angle. Consequently the corresponding viscoelastic relationships will not be either.

7.7 EFFECTIVE SAMPLE LENGTH

The length of the sample kept between the clamps differs from the effective value, for fundamentally two reasons. On the one hand, the section in which the torsion is zero lies within the zone covered by the clamps, so that the clamp separation is smaller than the effective sample length. On the other hand, as stated earlier, the secondary effects of the torsion produce an

additional torque that tends to reduce the distance between sections, thus producing a shortening of the bar. As a consequence, these effects are of opposite sign, and their net result can be either the enlargement or shortening of the sample, depending on which of the two effects is dominant. We now discuss the method used to determine experimentally the aforementioned length correction (Ref. 5, Chap. 3). To that end, a temperature is chosen in which the viscous damping of the material is small. From Eq. (7.9a), one obtains

$$K'G'_{app} = I\omega^2L \quad (7.35)$$

where $K' = KL$, L being the length of the sample and G'_{app} the apparent value of the storage modulus. By introducing now a length change ΔL , independent of the length of the sample, the following relationship is obtained:

$$K'G' = I\omega^2(L + \Delta L) \quad (7.36)$$

If several frequencies of the vibration are computed as the clamp separation is progressively changed, then from a plot of ω^2 versus L the value of ΔL can be obtained from the intercept of the straight line obtained with the L axis. The linearity of the plot relies on the hypothesis that the modulus does not depend on the frequency as the length of the test sample is varied. In fact, the modulus is frequency-dependent, and a source of error is introduced in the estimation of the sample length by means of this method. When the measurements are carried out in glassy polymers, that error can be avoided by assuming, as a first approximation, a linear dependence of the modulus on frequency, as follows:

$$G'(\omega) = G'(\omega_0) + a(\omega - \omega_0) \quad (7.37)$$

where ω is the frequency for a separation L_n and ω_0 is a fixed value. The parameter a can easily be determined by measuring the frequency as the moment of inertia is varied at constant sample length. Thus, the slope of a plot $I\omega^2$ vs. ω will be

$$g = \frac{K'a}{L_0 + \Delta L} \quad (7.38)$$

Then, from Eqs. (7.36), (7.37), and (7.38), we obtain

$$1 + \frac{g(\omega - \omega_0)(L_0 + \Delta L)}{K'G'(\omega_0)} = \frac{I\omega^2(L_n + \Delta L)}{K'G'(\omega_0)} \quad (7.39)$$

where the quantity $g(\omega - \omega_0)/I\omega_0^2$ can be considered as the modification of the frequency due to the fact that the modulus is dependent on this same frequency. The smaller the length of the sample, the greater the correction. Because of this, it is convenient to use relatively long samples. With this modification of the frequency, the modulus at some specific length can be conveniently estimated.

In the vicinity of the glass transition, the loss factor of amorphous polymers is so high that the torsional oscillations are overdamped. As a consequence, the resulting wave is not useful for measuring the frequency. This new problem can be solved by including in the system an auxiliary elastic element. A useful method to do that is to substitute for the suspension wire a steel rod with rigidity of the order of that of the sample. The resulting equation of motion must include a term representing the restoring torque or the rigidity of this elastic element. In these conditions we return to the equations given in the first part of this chapter that include this term. However, for methodological reasons, the detailed study of this case is postponed to Chapter 17.

7.8 DYNAMIC MECHANICAL ANALYSIS BY TRANSVERSE FLEXION

One of the most important techniques used to measure dynamic viscoelastic functions is based on the application of transverse oscillations of displacement in the central part of a test piece clamped at both ends or, alternatively, at one point (which could be the extremity) of a test sample clamped at the other extreme (Ref. 5, Chap. 5). The size of the displacement is variable, and the frequencies usually cover an interval of around four decades, between 10^{-2} and 10^2 Hz. The frequencies used are limited by the resonance of the apparatus. The sample can be isothermally thermostated or can suffer a determinate thermal history. The applied forces are determined by the current, which enters the oscillatory system through a defined system of calibration. It should be noted that although the most common way of using the equipment is through flexion, small modifications in the design allow measurements to be made in elongation or in shear. The selection of the type of measurement depends on the type of material and its characteristics. Thus for threads and fibers, elongation is more convenient, whereas for gums and rubbers a shear experiment should be done. For the measurement of rubbers and gums under elongation, prestressed test samples are required. The range of measurement in terms of the storage modulus varies between 0.1 MPa and 200 GPa.

The analysis of the instrument can be carried out on the basis of Figure 7.5. In this figure m represents the mass of the leading shaft whose inertial moment is so large that the inertial momentum of the sample is negligible in comparison. The storage and loss compliance of the flexible suspension are considered in parallel with those of the measured test sample, and both are represented by using complex moduli. The remaining parts of the system are considered sufficiently rigid that their deformation can also be considered negligible. As the displacement that the test sample undergoes is the same as that of the suspension system, one can write

$$F_0 e^{i(\omega t + \delta')} = m\ddot{x} + \left(\frac{S_D}{\omega} + \frac{KE''}{\omega} \right) \dot{x} + (S + KE')x \quad (7.40)$$

For a harmonic excitation $x = x_0 e^{i\omega t}$, Eq. (7.40) becomes

$$\frac{F_0}{x_0} e^{i\delta'} = -m\omega^2 + i(S_D + KE'') + (S + KE') \quad (7.41)$$

By separating the real and imaginary parts in Eq. (7.41), we obtain

$$\frac{F_0}{x_0} \cos \delta' = KE' + S - m\omega^2 \quad \text{and} \quad \frac{F_0}{x_0} \sin \delta' = KE'' + S_D \quad (7.42a)$$

giving

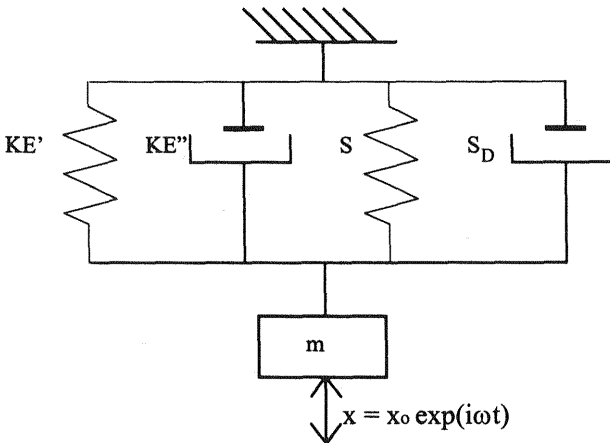


Figure 7.5 Diagram to study the flexural vibrations of a clamped bar and in general any second order system.

$$\tan \delta = \frac{E''}{E} = \frac{(F_0/x_0) \sin \delta' - S_D}{(F_0/x_0) \cos \delta' - S + m\omega^2} \quad (7.42b)$$

The process of calibrating the apparatus consists in finding the parameters m , S , and S_D that allow the solution of these equations. Without a test sample, one has

$$\frac{F_0}{x_0} \cos \delta'_1 = S - m\omega_1^2 \quad (7.43a)$$

$$\frac{F_0}{x_0} \cos \delta'_2 = S - m\omega_2^2 \quad (7.43b)$$

From these equations and taking into account that $\omega = 2\pi f$, expressions are obtained for the parameters m , and S .

$$m = \frac{F_0}{x_0} \left(\frac{\cos \delta'_1 - \cos \delta'_2}{4\pi^2(f_2^2 - f_1^2)} \right); \quad S = \frac{F_0}{x_0} \left(\cos \delta'_1 + \frac{\cos \delta'_1 - \cos \delta'_2}{f_2^2 - f_1^2} \right) f_1^2 \quad (7.44)$$

If $f_2 > 10f_1$, $f_2^2 \gg f_1^2$, and the values of m and S in Eq. (7.44) become

$$m \cong \frac{F_0}{x_0} \left(\frac{\cos \delta'_1 - \cos \delta'_2}{4\pi^2 f_2^2} \right); \quad S \cong \frac{F_0}{x_0} \cos \delta'_1 \quad (7.45)$$

In an analogous way,

$$S_D = \frac{F_0}{x_0} \sin \delta' \quad (7.46)$$

The constant K , on which the calculation of E' and E'' depends, is a function of the geometric dimensions of the sample. For a rectangular cross-sectional sample of width b and thickness d clamped at its extremities, K is given by

$$K = 2b(d/\ell)^3 \quad (7.47)$$

where ℓ is the distance between the clamping point and the force's point of application, that is, the half-length and the middle point of the bar. Hence, for a purely elastic material and a force F one obtains

$$\frac{F}{x} = 2b \left(\frac{d}{\ell} \right)^3 E \quad (7.48)$$

where x is the displacement and E is the elastic modulus. Equation (7.48) coincides formally with the equation derived from the theory of beams (14), as shown later in Chapter 17. In this respect, notice that the polar moment of inertia of a rectangular cross section, \bar{I} , with sides d and b with respect to an axis parallel to the side of length b and passing through the center of gravity (Fig. 7.6) is given by

$$\bar{I} = \int_{-d/2}^{d/2} \int_{-b/2}^{b/2} y^2 dx dy = d^3 \frac{b}{12} \quad (7.48a)$$

Substituting the value of \bar{I} given in Eq. (7.48a) into the equation for the maximum deformation, Eq. (7.48) immediately follows, and consequently Eq. (7.47) is justified.

The study of transverse vibrations of a viscoelastic beam can be carried out in a more complete way by using the elastic-viscoelastic analogy, thus following a methodology that will be outlined further in a more general context. At the present level, the usual way to solve the problem of a vibrating linear system of second order (through inertia and friction) is by applying Laplace transforms and assuming $F = F_0 \sin \omega t$ for $t \geq 0$ in the equation

$$m\ddot{x} + \left(\frac{S_D}{\omega} + K \frac{E''}{\omega} \right) \dot{x} + (S + KE')x = F \quad (7.49)$$

After assuming $x(0) = \dot{x}(0) = 0$, we obtain

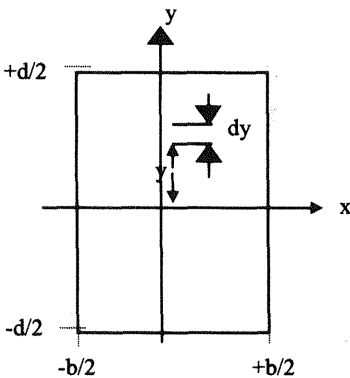


Figure 7.6 Scheme of the cross section of a rectangular rod to calculate its moment of inertia.

$$ms^2x(s) + \left(\frac{S_D}{\omega} + K\frac{E''}{\omega}\right)sx(s) + (S + KE')x(s) = F_0\frac{\omega}{\omega^2 + s^2} \quad (7.50)$$

Equation (7.50) leads to

$$(s^2 + 2\alpha s + \beta^2)x(s) = \frac{F_0}{m} \left(\frac{\omega}{\omega^2 + s^2}\right) \quad (7.51a)$$

which gives

$$x(s) = \frac{F_0}{m} \left(\frac{\omega}{(\omega^2 + s^2)(s^2 + 2\alpha s + \beta^2)}\right) \quad (7.51b)$$

where

$$\alpha = \frac{1}{2m} \left(\frac{S_D}{\omega} + \frac{KE''}{\omega}\right); \quad \beta = \left(\frac{S + KE'}{m}\right)^{1/2} \quad (7.52)$$

It should be pointed out that $\beta > \alpha$ in order to avoid exponential solutions that increase with time. The inverse Laplace transform of $x(s)$ can be achieved by decomposing $x(s)$ into simple functions

$$x(s) = \frac{As + B}{s^2 + \omega^2} + \frac{Cs + D}{s^2 + 2\alpha s + \beta^2} \quad (7.53)$$

where

$$s^2 + 2\alpha s + \beta^2 = (s + \alpha)^2 + \beta^2 - \alpha^2 \quad (7.54)$$

Hence,

$$A = -C = \frac{-2\alpha}{(\beta^2 - \omega^2)^2 + 4\alpha^2\omega^2} \quad (7.55a)$$

$$B = \frac{\beta^2 - \omega^2}{(\beta^2 - \omega^2)^2 + 4\alpha^2\omega^2} \quad (7.55b)$$

$$D = \frac{4\alpha^2 - (\beta^2 - \omega^2)}{(\beta^2 - \omega^2)^2 + 4\alpha^2\omega^2} \quad (7.55c)$$

and $x(t)$ is given by

$$\begin{aligned}
 x(t) &= \frac{F_0}{m} \left(\frac{1}{(\beta^2 - \omega^2)^2 + 4\alpha^2 \omega^2} \right)^{1/2} \\
 &\times \left\{ \sin(\omega t + \delta_1) + \frac{\omega}{(\beta^2 - \alpha^2)^{1/2}} \right. \\
 &\times \left. \exp(-\alpha t) \sin[(\beta^2 - \alpha^2)^{1/2} t + \delta_2] \right\}
 \end{aligned} \tag{7.56}$$

where

$$\delta_1 = \arctan \frac{2\alpha\omega}{\omega^2 - \beta^2}; \quad \delta_2 = \arctan \frac{2\omega}{\alpha} = \arctan \frac{2\alpha(\beta^2 - \alpha^2)^{1/2}}{2\alpha^2 - \beta^2 + \omega^2} \tag{7.57}$$

7.9 RESPONSE OF A VISCOELASTIC ROD TO AN INSTANTANEOUS STIMULUS (FREE OSCILLATIONS)

In the case of a viscoelastic rod acted on by an instantaneous stimulus,

$$F = F_0 \delta(t) \rightarrow F(s) = F_0 \tag{7.58}$$

where δ represents the Dirac delta function. The Laplace transform of Eq. (7.49) can be written as

$$ms^2 x(s) + \frac{S_D + KE''}{\omega} s x(s) + (S + KE') x(s) = F_0 \tag{7.59}$$

with the boundary conditions $x(0) = \dot{x}(0) = 0$. Hence,

$$x(s) = \frac{F_0}{m} \left(\frac{1}{s^2 + 2\alpha s + \beta^2} \right) \tag{7.60a}$$

and

$$x(t) = \mathcal{L}^{-1}[x(s)] \tag{7.60b}$$

If, as above, we assume that

$$s^2 + 2\alpha s + \beta^2 = (s + \alpha_1)^2 + \alpha_2^2 \tag{7.61}$$

where $\alpha_1 = \alpha$ and $\alpha_2 = (\beta^2 - \alpha^2)^{1/2}$ we obtain the equation

$$x(t) = \frac{F_0}{m} \left(\frac{1}{\sqrt{\beta^2 - \alpha^2}} \right) \exp(-\alpha t) \sin \left(\sqrt{\beta^2 - \alpha^2} t \right) \quad (7.62)$$

or equivalently,

$$x(t) = \frac{F_0}{m} \left(\frac{1}{\alpha_2} \right) \exp(-\alpha_1 t) \sin \alpha_2 t \quad (7.63)$$

Here

$$\alpha_2 > 0, \quad \alpha_1 > 0 \rightarrow \beta > 0$$

where

$$\alpha_1 = \frac{1}{2m} \left(\frac{S_D + KE''}{\omega} \right); \quad \beta = \left(\frac{S + KE'}{m} \right)^{1/2} \quad (7.64)$$

and

$$\alpha_2 = \sqrt{\beta^2 - \alpha^2} = \left\{ \frac{S + KE'}{m} - \left[\frac{1}{2m} \left(\frac{S_D + KE''}{\omega} \right) \right]^2 \right\}^{1/2} \quad (7.65)$$

Equations (7.64) and (7.65) allow the determination of $\tan \delta$ and E' by measuring the parameters α_1 and α_2 that are observable in the damped waves.

An alternative way to obtain the viscoelastic functions is to solve the characteristic (or frequency) equation,

$$s^2 + 2\alpha s + \beta^2 = 0, \quad s = -\lambda + i\omega \quad (7.66)$$

Splitting this into the real and imaginary parts gives

$$\omega^2 = \lambda^2 - 2\alpha\lambda + \beta^2; \quad \lambda = \alpha; \quad \omega^2 = \beta^2 - \alpha^2 = \beta^2 - \lambda^2 \quad (7.67)$$

From Eqs. (7.64) and (7.65) and assuming that $\alpha = \alpha_1$, we obtain

$$\lambda = \alpha = \frac{1}{2m} \left(\frac{S_D + KE''}{\omega} \right) \quad (7.68a)$$

$$KE'' = 2m\lambda\omega - S_D \quad (7.68b)$$

$$\omega^2 = \frac{S + KE'}{m} - \frac{1}{4m^2} \left(\frac{S_D + KE''}{\omega} \right)^2 \quad (7.69a)$$

$$4m^2\omega^2 = 4m(S + KE') - 4m^2\lambda^2 \quad (7.69b)$$

$$KE' = m(\omega^2 + \lambda^2) - S \quad (7.69c)$$

and

$$\tan \delta = \frac{E''}{E'} = \frac{2m\lambda\omega - S_D}{m(\lambda^2 + \omega^2) - S} \quad (7.70)$$

Calculations of E' , E'' , and $\tan \delta$ obviously require knowledge of the values of m , S and S_D from calibration.

7.10 DETERMINATION OF THE CORRECTIONS IN THE VISCOELASTIC FUNCTIONS DUE TO CLAMPING

The calculation from dynamic flexural experiments of elastic or viscoelastic functions is subject to errors arising from clamping (Ref. 6, p. 23). In the case of test samples whose section has dimensions of the order of magnitude of the free length, such a free length must be replaced by an effective length that represents that parameter in a more realistic way (see Fig. 7.7).

A correction of the length affects the geometric constant, which in turn influences the value of the modulus. Since the force and the displacement are the same with and without corrections, we obtain

$$KE_{\text{app}} = K'E_{\text{real}} \quad (7.71)$$

By taking into account Eqs. (7.47) and (7.48), Eq. (7.71) becomes

$$\frac{E_{\text{app}}}{L^3} = \frac{E_{\text{real}}}{(L + \Delta L)^3} \quad (7.72)$$

If we consider that the shear effects taking place in the flexural problems are small, then

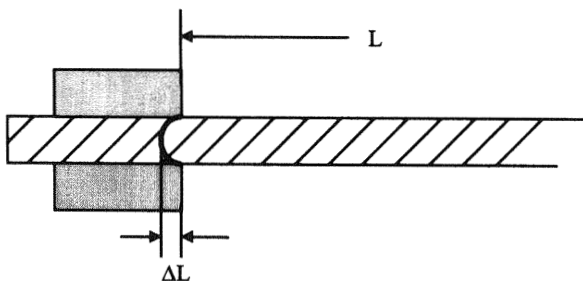


Figure 7.7 Scheme indicating the shape and size of the length correction of a clamped beam.

$$\left(\frac{E_{\text{app}}}{E_{\text{real}}}\right)^{1/3} = \frac{L}{L + \Delta L} \quad (7.73a)$$

Hence,

$$\frac{L}{E_{\text{app}}^{1/3}} = \frac{L}{E_{\text{real}}^{1/3}} + \frac{\Delta L}{E_{\text{real}}^{1/3}} \quad (7.73b)$$

The plot of $L/E_{\text{app}}^{1/3}$ versus L should give a straight line whose slope and intercept are, respectively, $E_{\text{real}}^{-1/3}$ and $\Delta L E_{\text{real}}^{-1/3}$.

The length corrections are typically 0.5–1.5 mm; usually these values increase with both the thickness of the test sample and the value of the modulus and decrease with increasing temperature. The relative uncertainties in the calculation of the free length can introduce significant errors in the absolute values of the moduli. This is an inherent limitation for all kinds of experiments in which the test sample to be analyzed is clamped. The torsion tests presented above also have similar flaws. Recent developments in classical equipment allow measurements to be made in elongation or shear. In this regard, the Rheovibron viscoelastometer should be mentioned as one of the pioneer pieces of equipment in dynamic mechanical experiments (15–18). In this equipment, a sinusoidal tensile strain is imposed on one end of the sample and a sinusoidal tensile stress is measured at the other end. The phase angle between strain and stress in the sample is measured by a direct-reading method (15). The instrument uses two transducers for detection of the complex dynamic modulus and the phase angle. The sample is driven at a certain frequency by means of a magnetic coil. The amount of strain or stress is transformed into a proportional electrical quantity by

using an unbounded type of wire strain or stress gauge. A complete description of the method is given in Refs. 17 and 18.

7.11 RESONANCE INSTRUMENTS

As mentioned above in the context of forced oscillations, resonance occurs at a frequency given by Eq. (7.24) if the phase angle is small. From the resonance frequency, ω_R , the storage modulus is readily calculated:

$$G'(\omega_R) = I\omega_R^2/K \quad (7.74)$$

In this case, measurements of the amplitudes of displacement and force, as well as the phase angle, are not required. The frequency of the force is varied while its amplitude is kept constant (ref. 6 p. 34-48). The frequency at which the amplitude of the displacement is maximum is taken as the resonance frequency. Usually several relatively decreasing maxima are obtained.

The loss tangent can be obtained from the half-width of the resonance peak according to the expression

$$\tan \delta(\omega_R) = \frac{\Delta\omega}{3\omega_R} \sqrt{3} \quad (7.75)$$

The half-width $\Delta\omega$ is the difference between two frequencies for which the amplitude of the motion is half as large as it is at resonance. See also Problem 17.3.

The resonance method is useful when the data are required at only one frequency or at a small number of frequencies. In a typical device used to measure the dynamic tensile storage modulus, the rod, which has a circular or rectangular cross section, is hung by threads at nodal points. An oscillating force is applied at one end of the rod by means of a piezoelectric transducer. The response is detected at the other end by a capacitive transducer. To achieve that, it is very convenient to paint the extremities of the rod in front of the transducers with colloidal silver or another conductive paint.

7.12 WAVE PROPAGATION

Although part of Chapter 16 is devoted to wave propagation in viscoelastic materials and some specific simple cases are studied in detail as part of the engineering applications of viscoelasticity, it is useful to mention here that there are several experimental methods to determine the dynamic response

of viscoelastic materials at high frequencies ($> 10^4$ Hz). If the wave is being propagated in a direction normal to the motion of the material, it is called a transverse wave. It should be noted that the theory is also valid for longitudinal waves, where the propagation is parallel to the motion, when G is replaced by E . The measurement of dynamic mechanical properties in the ultrasonic region requires specific techniques (4,5,19). In some specific applications, pulses of high frequency sine waves are generated by a piezoelectric crystal. Depending on the way the crystal is excited, the wave can be either transverse or longitudinal. In the case of liquids only longitudinal waves are possible. The pulses go through the specimen to a second crystal. Pulses from the latter crystal are reflected from the specimen (without transmission) and return to the first crystal, which now acts as a receiving transducer. The amplitudes of the transmitted and reflected waves are compared to measure the attenuation. The speed of propagation is obtained by measuring the time between two successive reflections.

Studies of high frequency dynamic properties in polymers are useful from the point of view of vibration and sound damping. For polymeric materials, shear waves typically travel at very low speeds and are rapidly attenuated. For this reason, the transformation of longitudinal waves into shear waves is greatly desired. The applications are centered on anechoic coatings, that is, coatings designed to reduce the reflection of sound from elastic structures, such as the walls of a tank in air or under water. The damping of flexural waves is also important for noise reduction, hearing protection, the reduction of structural fatigue. The incorporation of a viscoelastic layer in rods or beams, giving rise to composite structures, is a technical solution to achieve good damping at frequencies for which the layer is resonant. Alternatively, the effect of fillers, inclusions, or air cavities can also be studied by acoustic damping methods.

A final comment seems to be pertinent. In most cases actual measurements are not made at the frequencies of interest. However, one can estimate the corresponding property at the desired frequency by using the time (frequency)–temperature superposition techniques of extrapolation. When different apparatuses are used to measure dynamic mechanical properties, we note that the final comparison depends not only on the instrument but also on how the data are analyzed. This implies that shifting procedures must be carried out in a consistent manner to avoid inaccuracies in the master curves. In particular, the shape of the adjacent curves at different frequencies must match exactly, and the shift factor must be the same for all the viscoelastic functions. Kramers–Krönig relationships provide a useful tool for checking the consistency of the results obtained.

Indentation methods as a special type of analysis of viscoelastic stress or displacement are studied in Chapter 16. It should be noted that indentation

testing as a measure of viscoelastic modulus is not yet widely used as a laboratory test method. However, knowledge of the displacement produced by the indenter can be used to calculate the modulus by means of the formulas developed in Chapter 16. The same is valid for the calculation of the bulk modulus. Of course, the bulk modulus may be measured in the case of isotropic materials by dilatometry if the bulk modulus of the containing fluid is known. However, some special types of experiments concerning the pressurization of spheres or cylinders, as studied in Chapter 16, can give information about the bulk modulus (20).

7.13 EXPERIMENTAL DETERMINATION OF STATIC VISCOELASTIC PROPERTIES

Strictly speaking, there are no static viscoelastic properties as viscoelastic properties are always time-dependent. However, creep and stress relaxation experiments can be considered quasi-static experiments from which the creep compliance and the modulus can be obtained (4). Such tests are commonly applied in uniaxial conditions for simplicity. The usual time range of quasi-static transient measurements is limited to times not less than 10^{-1} s. The reasons for this is that in actual experiments it takes a short period of time to apply the force or the deformation to the sample, and a transitory dynamic response overlaps the idealized creep or relaxation experiment. There is no limitation on the maximum time, but usually it is restricted to a maximum of 10^4 s. In fact, this range of times is complementary, in the corresponding frequency scale, to that of dynamic experiments. Accordingly, to compare these two complementary techniques, procedures of interconversion of data (time–frequency or its inverse) are needed. Some of these procedures are discussed in Chapters 6 and 9.

7.14 TORSIONAL CREEP

Measurements of creep in torsion can be made very accurately. The reason is that deformation can be measured by measuring the large deflections of a light beam. A convenient way to simultaneously obtain shear dynamic and transient data is to combine both types of measurements in the same equipment (4). Usually this requires only small modifications of the experimental device. For example, the cross bar in a torsion pendulum can be removed and replaced by weights and pulleys to apply a constant torque to the upper clamp. In this way, a torsion creep apparatus is obtained (Fig. 7.8). The

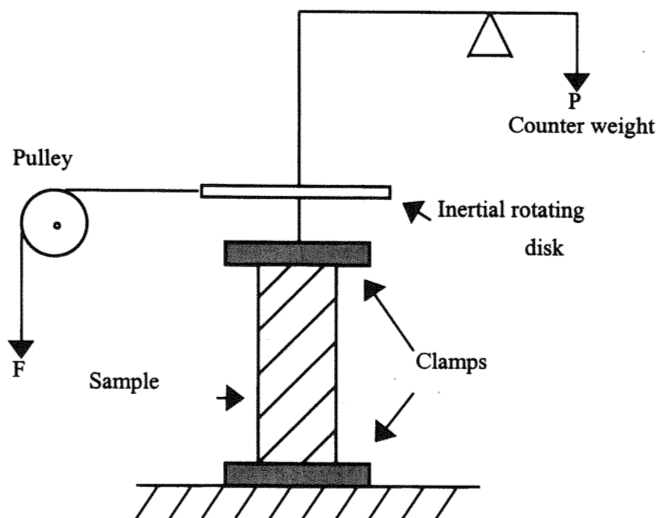


Figure 7.8 Scheme of a torsion creep apparatus.

angle of torsion is measured digitally, and from the measured values the creep compliance in shear is calculated.

According to Figure 7.9, the strain for a cylindrical geometry is given by

$$\varepsilon(t) = \frac{r\theta(t)}{L} \quad (7.76)$$

where $\theta(t)$ is the torsional angle at time t and L is the length of the specimen. For a relaxation experiment ($\theta = \text{constant}$), the evolution with time of the torque necessary to keep the twist angle constant is given by (see P5.2)

$$M(t) = \frac{\pi R^4 G(t)}{2L} \theta \quad (7.77)$$

In the same way, the time dependence of θ in a creep experiment can be written as

$$\theta(t) = \frac{MLJ(t)}{K} \quad (7.78)$$

where $J(t)$ is the creep compliance and K is a geometric factor that for cylindrical geometry is given by

$$K = \frac{\pi R^4}{2} \quad (7.79)$$

In Eq. (7.48a) it is demonstrated that this geometric factor is $bd^3/3$ for a rectangular cross section, where the thickness d is very small in comparison

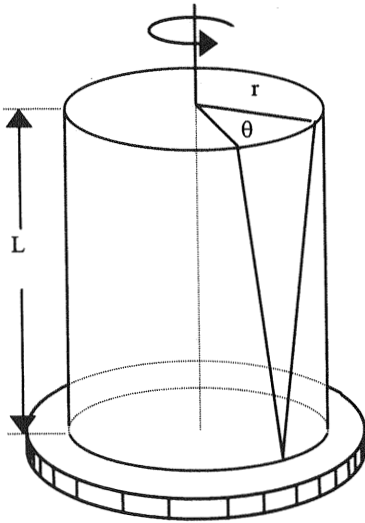


Figure 7.9 Torsion of a cylindrical bar clamped at the lower end.

with the width b . More geometric factors can be found in Ref. 4, pp. 98, 132, and 156.

Many other experimental possibilities for measuring the creep compliance are available. For example, in a torsion creep apparatus designed by Plazek (21), the rotating system is magnetically suspended and the torque is applied magnetically by means of a motor. In this way, all sources of friction are avoided, increasing the accuracy of measurements. The sample is contained between two parallel plates, and the apparatus has been designed for measurements of solid as well as liquid samples. Several geometries are allowed.

7.15 TENSILE CREEP

Creep experiments are often carried out by hanging a weight on a strip of material of rectangular or cylindrical cross section (ref. 4, page 132 and 162). In this case, the tensile creep compliance $D(t)$ is calculated as

$$D(t) = z(t) \frac{A}{mgl} \quad (7.80)$$

where $z(t)$ is the change in length, m is the mass of the applied weight, and l is the length of the sample. A linear variable differential transformer (LVDT) can be used to measure the extension. Unfortunately, it is not easy to achieve a pure and uniform extension experiment in this way, because near the clamps the deformation, and consequently the strain, differs from that close to the center of the sample. It is possible to correct the sample length, but it is more accurate to determine the fractional change in the distance between two marked points close to the center of the sample. Moreover, as the sample extends, it also becomes thinner, and this fact needs to be taken into account in calculating the stress.

7.16 STRESS RELAXATION

The measurement of the stress relaxation (21) can simply be made by connecting the sample in series with a spring of enough rigidity to undergo negligible deformation in comparison with that of the sample. For this reason any arrangement for a creep experiment can in principle be used for a stress relaxation experiment if the applied force can be accurately measured as a function of time while the deformation is constant. This can be achieved by using a dynamometer or stress gauge to play the role

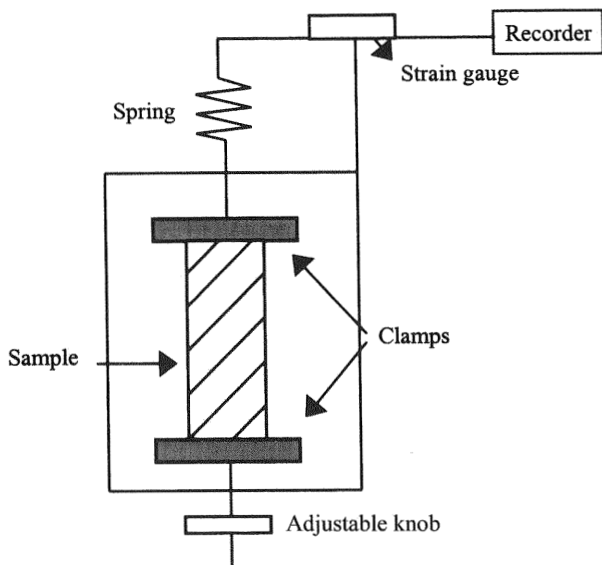


Figure 7.10 Scheme of a stress relaxation apparatus in elongation.

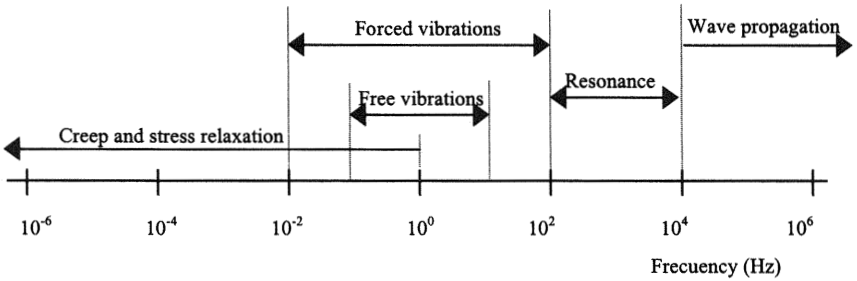


Figure 7.11 Sketch of the range of frequencies for the different apparatuses measuring viscoelastic properties.

of the stiff spring mentioned above. An LVDT or strain gauge associated with the spring element can be used to record the stress. The tensile relaxation modulus is then given by

$$E(t) = f(t)(L/Az_0) \quad (7.81)$$

where A and L are respectively the cross-sectional area and the length of the sample, f is the force to maintain the deformation constant, and z_0 is the elongation of the sample. In this test, as in creep experiments, the temperature of the sample is conveniently controlled by means of a thermostatic device (Fig. 7.10).

A sketch of the different experimental methods and the corresponding frequency ranges is given in Figure 7.11.

PROBLEM SETS

Problem 7.1

Show that during a dynamic experiment, work is done on the system only in the first quarter of the cycle.

Solution 7.1

Assume that $\varepsilon = \varepsilon_0 \sin \omega t$. In this case, the total work done on the material in the part of the cycle lying in the range $0 - \pi/n$ is given by

$$W = G'(\omega)\varepsilon_0^2\omega \int_0^{\pi/n\omega} \sin \omega t \cos \omega t \, dt \quad (\text{P7.1.1})$$

Making the substitution $\sin \omega t \cos \omega t = (\sin 2\omega t)/2$ in the integral, the value of W will be

$$W = \frac{G'(\omega)\varepsilon_0^2\omega}{2} \int_0^{\pi/n\omega} \sin 2\omega t \, dt = \frac{\varepsilon_0^2 G'(\omega)}{4} \left(1 - \cos \frac{2\pi}{n}\right) \quad (\text{P7.1.2})$$

The value of W will be maximum when $\cos(2\pi/n) = -1$, that is for $n = 2$. Therefore, work is done on the system from 0 to $\pi/2$. The work done on the system during a quarter of the cycle will be

$$W = \varepsilon_0^2 G'(\omega)/2 \quad (\text{P7.1.3})$$

During the other three-fourths of the cycle the work will be recovered. Actually,

$$W = G'(\omega)\varepsilon_0^2\omega \int_{\pi/2\omega}^{2\pi/\omega} \sin \omega t \cos \omega t \, dt = -\frac{\varepsilon_0^2 G'(\omega)}{2} \quad (\text{P7.1.4})$$

The total work done during the cycle is zero.

Problem 7.2

A circular rod of a viscoelastic material of length h and radius R located between the two clamps of a torsion pendulum is rotated slightly from its equilibrium position by a deflecting torque. The torque is released, and the system begins to oscillate. Calculate the resonance frequency of the system.

Solution 7.2

In response to the torque M , the top clamp has an angular acceleration $d^2\theta/dt^2$, where θ is the angle of deflection. Accordingly, Newton's law of motion can be written as [see Eq. (7.10)]

$$I \frac{d^2\theta}{dt^2} + k\theta = 0 \quad (\text{P7.2.1})$$

where $k = M/\theta$ is the torque applied to the specimen for unit deflection, and I is the moment of inertia of the pendulum around the central axis. The constant k is given by [see Eq. (7.78) and Problem 5.2]

$$k = \frac{\pi R^4}{2h} G' \quad (\text{P7.2.2})$$

The solution of Eq. (P7.2.1) is $\theta = \theta_0 \exp(i\omega t)$. By substituting this expression into Eq. (P7.2.1) we obtain

$$\omega = \left(\frac{\pi R^4 G'}{2Ih} \right)^{1/2} \quad (\text{P7.2.3})$$

Hence, G' can be obtained from the resonance frequency of the torsion pendulum by means of the expression

$$G'(\omega) = \frac{2Ih}{\pi R^4} \omega^2 \quad (\text{P7.2.4})$$

Problem 7.3

The amplitude θ_o of free oscillations decreases in such a way that $\theta_{oi+1} < \theta_{oi}$. Relate the loss tangent to the logarithmic decrement.

Solution 7.3

The logarithmic decrement Λ is defined as

$$\Lambda = \ln \left(\frac{\theta_{oi}}{\theta_{oi+1}} \right) \quad (\text{P7.3.1})$$

where θ_{oi+1} and θ_{oi} are the amplitudes of the cycle $i + 1$ and i , respectively. By taking into account that

$$\ln \left(\frac{\theta_{oi}}{\theta_{oi+1}} \right) = \ln \left[1 + \left(\frac{\theta_{oi}}{\theta_{oi+1}} - 1 \right) \right] \cong \left(\frac{\theta_{oi}}{\theta_{oi+1}} \right) - 1 \quad (\text{P7.3.2})$$

Eq. (P7.3.1) can be written as

$$\Lambda = \frac{\theta_{oi} - \theta_{oi+1}}{\theta_{oi+1}} \cong \frac{1}{2} \frac{\theta_{oi}^2 - \theta_{oi+1}^2}{\theta_{oi+1}^2} = \pi \tan \delta \quad (\text{P7.3.3})$$

where it has been taken into account that $\theta_{oi}^2 - \theta_{oi+1}^2$ and θ_{oi+1}^2 are, respectively, proportional to the dissipated energy [Eq. (6.15)] and the elastic energy [Eq. (P7.1.3)]. Hence,

$$G''(\omega) = G'(\omega) \tan \delta = \frac{\Lambda}{\pi} G'(\omega) \quad (\text{P7.3.4})$$

Problem 7.4

In a plate-plate geometry, the top of the sample is attached to a rigid frame of moment of inertia I , which in turn is supported by a thin wire. A torque $M^* = M_0 \exp(i\omega t)$ is applied to the rigid frame. Determine the relaxation moduli of the sample.

Solution 7.4

The net torque acting on the system is $M^* = k\theta^* + A_s G^* \theta^*$, where $k\theta^*$ and $A_s G^* \theta^*$ are respectively, the torques due to the wire and to the sample, and the response $\theta^* = \theta_0 \exp[i(\omega t - \varphi)]$ is the sinusoidal angular motion. The constant k depends on the length of the wire and its shear modulus, while $A_s = \pi R^4/2h$, where R and h are, respectively, the radius and height of the cylinder and G^* is the complex shear modulus of the sample. An angular momentum $I d^2\theta^*/dt^2$ is produced in the frame, which is related to the net torque by the equation

$$M_0 \exp[i(\omega t)] - (k + A_s G^*) \theta_0 \exp[i(\omega t - \varphi)] = -I \omega^2 \theta_0 \exp[i(\omega t - \varphi)] \quad (\text{P7.4.1})$$

By dividing the terms of this equation by $\exp(i\omega t)$ and multiplying the terms of the resulting equation by $\exp(i\varphi)$ we obtain

$$G^* = \frac{I\omega^2 - k}{A_s} + \frac{M_0}{A_s \theta_0} \exp(i\varphi) \quad (\text{P7.4.2})$$

Hence,

$$G'(\omega) = \frac{I\omega^2 - k}{A_s} + \frac{M_0}{A_s \theta_0} \cos \varphi \quad \text{and} \quad G''(\omega) = \frac{M_0}{A_s \theta_0} \sin \varphi \quad (\text{P7.4.3})$$

Note that the expression for G' is similar to that of Eq. (P7.2.4) if the torque of the wire is negligible in comparison with that of the sample and the torque is nil.

From the expressions given for G' and G'' , the following relationship is obtained for $\tan \varphi$:

$$\tan \varphi = \frac{A_s G''(\omega)}{A_s G'(\omega) - (I\omega^2 - k)} \quad (\text{P7.4.4})$$

Problem 7.5

Evaluate the frequency of resonance in Problem 7.4.

Solution 7.5

The expressions given for G' and G'' in Eqs. (P7.4.3) lead to the ratio

$$\frac{\theta_0}{M_0} = \frac{1}{\{[A_s G'(\omega) + k - I\omega^2]^2 + [A_s G''(\omega)]^2\}^{1/2}} \quad (\text{P7.5.1})$$

By substituting the value of $G''(\omega)$ given in Eq. (P7.4.4) into Eq. (P7.5.1) we obtain

$$\frac{\theta_0}{M_0} = \frac{1}{[A_s G'(\omega) + k - I\omega^2](1 + \tan^2 \varphi)^{1/2}} \quad (\text{P.7.5.2})$$

If $\varphi < 90^\circ$, resonance is achieved when $A_s G'(\omega) + k - I\omega^2 = 0$. Then the frequency of resonance will be given by

$$\omega_s = \left(\frac{A_s G'(\omega_s) + k}{I} \right)^{1/2} \quad (\text{P7.5.3})$$

If k is negligible, then Eq. (P7.5.3) is similar to Eq. (P7.2.3).

REFERENCES

1. RM Christensen. The Theory of Viscoelasticity: An Introduction. New York: Academic Press, 1971.
2. LE Nielsen. Mechanical Properties of Solid Polymers. New York: Marcel Dekker, 1974.
3. IM Ward. Mechanical Properties of Solid Polymers. 2nd. ed. Chichester: Wiley, 1983.
4. J D Ferry. Viscoelastic Properties of Polymers. 3rd. ed. New York: Wiley, 1980.
5. BE Read, GD Dean. The Determination of Dynamic Properties of Polymers and Composites. Bristol: Hilger, 1978.
6. BE Read, GD Dean, JC Duncan. Determination of dynamic moduli and loss factors. In DeBW Rossiter, RC Baetzold eds. Physical Methods of Chemistry, Vol. VII, Determination of Elastic and Mechanical Properties. New York: Wiley, 1991.
7. CJ Nederveen, CW van der Wal. Rheol Acta 6(4): 316, 1967.
8. LE Nielsen. Rev Sci Ins 22: 690, 1951.

9. H Markovitz. *J Appl Phys* 34: 21, 1963.
10. LCE Struik. *Rheol Acta* 6: 119, 1967.
11. WC Forsman. *Macromolecules* 4: 262, 1971.
12. TE Morrison, LJ Zapas, TW de Witt. *Rev Sci Inst.* 26: 357, 1955.
13. W Hoffmann. *Rheol Acta* 11: 41, 1972.
14. L Landau, E Lifschitz. *Theory of Elasticity*. 3rd ed. Oxford, UK: Pergamon, 1986, p 81.
15. M Yoshino, M Takayanagi. *J Jap Soc Test Mater* 8: 330, 1959.
16. M Takayanagi. *Mem Fac Engn Khyusu Univ* 23: 1, 1963.
17. T Murayama. *Dynamic Mechanical Analysis of Polymeric Materials*. Amsterdam: Elsevier, 1978.
18. DJ Massa. *J Appl Phys* 44: 2595, 1973.
19. H Kolsky. *Stress Waves in Solids*. New York: Dover, 1963.
20. RGC Arridge. *An Introduction to Polymer Mechanics*. London: Taylor and Francis, 1985 p 176.
21. DJ Plazek. *J Polym Sci A* 2(6): 621, 1968.

8

Viscoelastic Behavior of Polymers Above T_g

8.1	Time-Temperature Correspondence Principle	306
8.2	Prediction of the Shift Factors for Viscoelastic Liquids	321
8.3	Prediction of the Shift Factors for Viscoelastic Solids	322
8.4	Influence of Temperature on Horizontal Shift factors	323
8.5	Effect of Pressure on the Viscoelastic Response	327
8.6	Differentiation of Regions in the Master Curves of the Viscoelastic Functions	327
8.7	Influence of Diluents on the Viscoelastic Behavior of Polymers	339
8.8	Effects of Cross-Linking on the Viscoelastic Functions	343
	Problem Sets	348
	References	357

8.1 TIME-TEMPERATURE CORRESPONDENCE PRINCIPLE

The effect of temperature on the response of viscoelastic systems to perturbation fields can be qualitatively observed in Figure 8.1, where the time dependence of the deformation is schematically represented for a viscoelastic liquid. It can be seen that at the glass transition temperature the deformation remains nearly constant for comparatively long times. However, as the temperature of the system increases, the deformation undergoes a dramatic increase, which is larger the higher the temperature. If the shear stress is canceled out after steady-state conditions are reached, the time

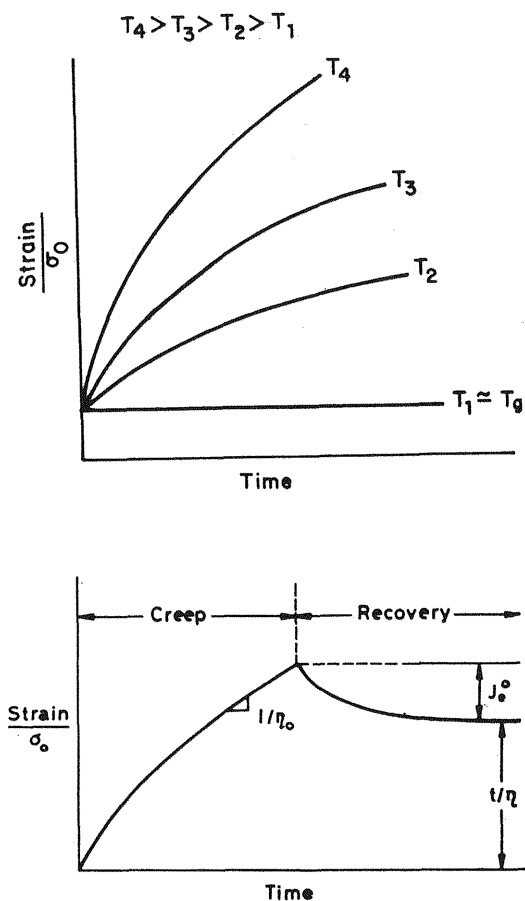


Figure 8.1 (a) Schematic representation showing the influence of temperature on the strain of a creep experiment. (b) Creep and recoverable strains.

dependence of the recoverable deformation $[\epsilon_r(t) = \epsilon(t) - \sigma t/\eta]$ is obtained. Note that the higher the temperature, the greater the unrecoverable contribution to the shear deformation, i.e., the viscous deformation

A real example of the effect of temperature on the viscoelastic functions at $T > T_g$ is shown in Figure 8.2. Here double logarithmic plots of the compliance function $J(t)$ versus time are shown at several temperatures for a solution of polystyrene ($M_v = 860,000$) in tri-*m*-tolyl phosphate (1) in which the weight fraction of polymer is 0.70. Because the glass transition temperature of the solution is 15°C , the isotherms were registered at

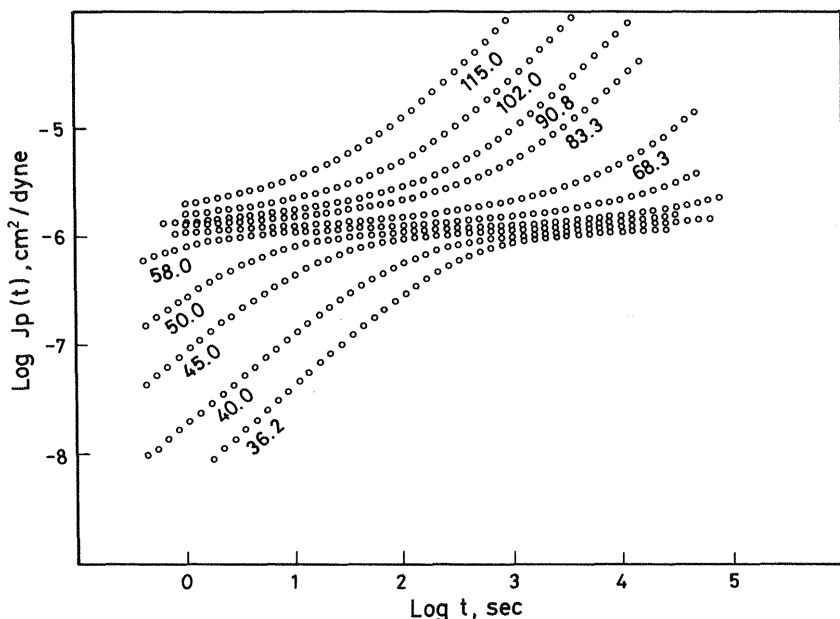


Figure 8.2 Double logarithmic plots of the creep compliance function in the time domain at various temperatures for solutions of polystyrene in tri-*m*-tolyl phosphate; the weight fraction of polymer in the solution is 0.70. The subscript *p* in $J_p(t)$ indicates that the values of this function have been reduced to a common temperature.

$T > 15^\circ\text{C}$. For $T < 36^\circ\text{C}$, the isotherms corresponding to $J_p(t)$ and the creep recovery compliance $J_{pr}(t)$ are similar. These curves are plotted in Figure 8.3. An inspection of the curves shows only a small change in the shear compliance function obtained at 16°C . However, the values of $J(t)$ at 26°C change by nearly two decades in the interval of four decades of the logarithmic time scale. The isotherm obtained at 43°C above T_g exhibits a plateau in which only a small augmentation is observed in $\log J(t)$ with increasing time. Finally, at temperatures much higher than T_g , for example 115°C , the isotherms reflect a sharp increase in the creep compliance function with increasing temperature. Obviously, the time necessary to reach steady-state conditions, i.e., $d \log J(t) / d \log t = 1$, is lower the higher is the temperature. For example, at a temperature 100°C above T_g , these conditions are reached in this system in about 10^4 s.

According to Eq. (5.16), $J(t)$ can be written as

$$J(t) = J_g + J_d \Psi(t) + \frac{t}{\eta} = J_r(t) + \frac{t}{\eta} \quad (8.1)$$

where $J_r(t)$ is the recoverable compliance function, which involves the Hookean (J_g) and the entropic [$J_d\Psi(t)$] contributions. Separation of the recoverable compliance from the compliance function can be achieved by canceling out the shear stress once steady-state conditions are reached (see Sect 5.3.1). Owing to the fact that at temperatures close to T_g a time much larger than the time scale of the experiment could be needed to reach steady-state conditions, the experimental determination of the recoverable compliance function in these cases can be performed by using the following method: A shear step stress σ is imposed on the material at temperatures well above T_g , and once steady-state conditions are reached the system is cooled to the required temperature. Then the shear stress is canceled out and $J_r(t)$ is obtained from the ratio of the recoverable deformation to the shear stress, taking as the origin of the time scale the time at which the stress was canceled out. By comparing the isotherms of $J(t)$ and $J_r(t)$ obtained for the polystyrene-tri-*m*-tolyl phosphate (70%) solution, plotted in Figures 8.2 and 8.3, respectively, one finds that the two functions nearly coincide at temperatures close to T_g . This is consequence of the fact that at these temperatures, and in the interval of time in which the measurements were performed, the viscous contribution to the deformation is nearly negligible, and consequently only the elastic contributions are important. To detect differences between $J(t)$ and $J_r(t)$ at a low temperatures would surely require unattainably large times. However, large differences between the values of $J(t)$ and $J_r(t)$ are observed at high temperatures because, in this case, the viscous contribution to the deformation is dominant. The values of $J(t)$ and $J_r(t)$ at these temperatures are similar only at short times.

8.1.1 Transient Creep Experiments

A fundamental characteristic of the so-called thermorheologically simple systems is that consecutive isotherms have similar habits, so they overlie each other when they are shifted horizontally along the $\log t$ axis. In other words, the time-temperature correspondence principle holds. This property in creep experiments can be expressed by the relation (2,3)

$$J(\log t + \log a_{0T}, T) = J(\log t, T_0) \quad (8.2)$$

where $\log a_{0T}$ is the logarithmic displacement shift factor necessary to superpose the reference isotherm at T_0 on the isotherm at T . A schematic illustration of the time-temperature shift factor is shown in Figure 8.4. If $T > T_0$, then $a_{0T} < 1$, whereas if $T < T_0$, $a_{0T} > 1$. Equation (8.2) gives the expression

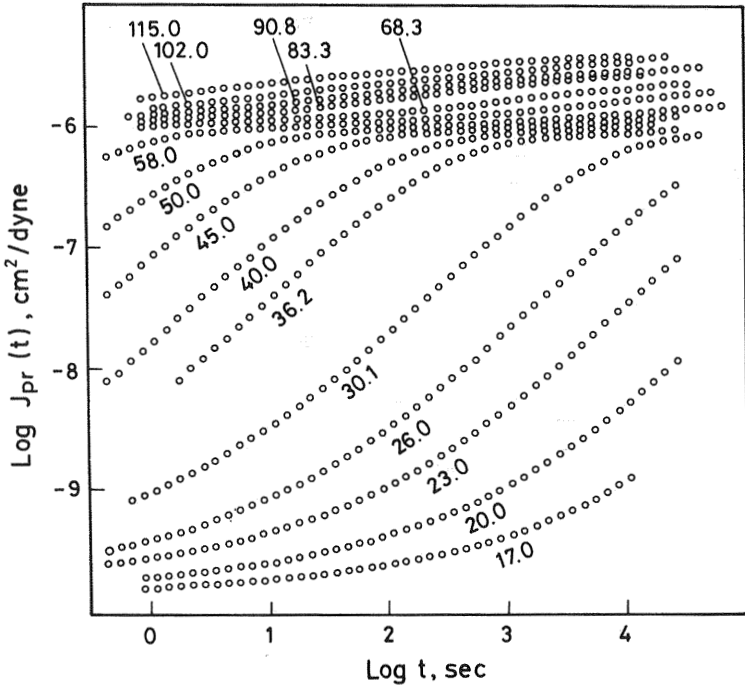


Figure 8.3 Double logarithmic plots of the recoverable creep compliance function in the time domain for the solution of Figure 8.2.

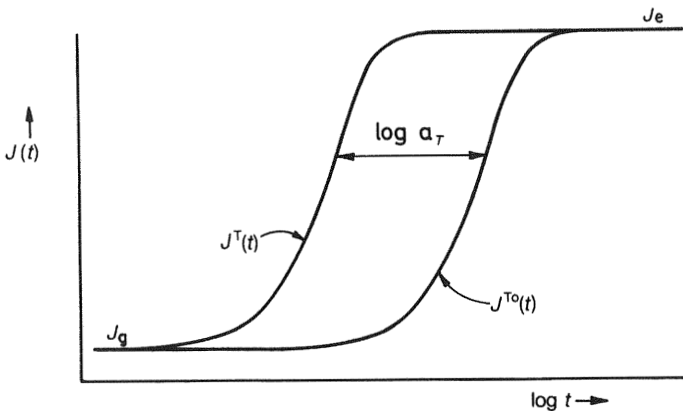


Figure 8.4 Schematic representation of the shift factor in creep experiments.

$$J(\log t, T) = J\left(\log \frac{t}{a_{0T}}, T_0\right) \quad (8.3)$$

which reduces the results at temperature T to the reference temperature T_0 . A careful observation of the experimental results suggests that in order to achieve a good superimposition the isotherms should be slightly shifted in the vertical direction. As discussed in Chapter 9, molecular theories suggest that $G(t, T) \sim \rho T$ and $J(t, T) \sim \rho^{-1} T^{-1}$, where ρ is the density. Hence (2,3),

$$\frac{J(t, T)}{b_{0T}} = J\left(\frac{t}{a_{0T}}, T_0\right) \quad (8.4)$$

where the vertical shift factor b_{0T} is given by

$$b_{0T} = \frac{\rho_0 T_0}{\rho T} \quad (8.5)$$

Equation (8.4) can alternatively be written as

$$J_p(t, T) = J(t_r, T_0) \quad (8.6)$$

where $J_p(t, T) [= J(t, T)/b_{0T}]$ is the reduced creep compliance function and $t_r = t/a_{0T}$ is the reduced time.

Horizontal shifts of double logarithmic plots of the isotherms with respect to the reference isotherm produce a master curve that extends over the whole time scale. It should be recalled that the isotherms measured at high temperatures reflect only the responses of viscoelastic mechanisms associated with the longest retardation times. The responses associated with the shortest retardation times cannot be detected in transient experiments carried out at temperatures well above T_g , dynamic experiments being necessary to achieve this purpose. Moreover, only the responses of viscoelastic mechanisms taking place at relatively short times are detected at temperatures close to T_g by means of transitory experiments. Consequently, only master curves can describe the viscoelastic behavior in the whole time scale, thus covering the responses occurring at short, medium, and long times. Thus the time-temperature correspondence principle sheds light on the viscoelastic behavior of materials within a very large time scale.

The viscosity increases as the temperature decreases, this increase being sharp in the vicinity of the glass transition temperature. According to Eq. (8.1), the value of η can be determined by means of the equation

$$\eta = \lim_{t \rightarrow \infty} \frac{1}{d J(t)/dt} \quad (8.7)$$

The viscosity of viscoelastic liquids at temperatures slightly above T_g can be determined by the procedures outlined above. Thus a step shear stress is imposed on the viscoelastic liquid at temperatures well above T_g , and once steady state is reached the sample is cooled to the temperature of interest; then the straight line of $J(t)$ vs. t is recorded, and the viscosity is determined from the reciprocal of the slope of the straight line. By assuming that the elastic and viscous mechanisms have the same temperature dependence, the shift factor can be written in terms of the viscosity as (2,5)

$$a_{0T} = \frac{\rho_0 T_0}{\rho T} \left(\frac{\eta(T)}{\eta(T_0)} \right) \quad (8.8)$$

where the longest relaxation time has been considered to be proportional to the viscosity, as the Rouse theory predicts (see Chap. 9). A superposition of the isotherms for polystyrene carried out using the shift factors determined by Eq. (8.8) is given in Figure 8.5. One can observe that the superposition is poor, suggesting that the viscous and elastic mechanisms differ in their temperature dependence. In fact, good superposition can be obtained only at long times at which the viscous contribution dominates. However, good superposition is achieved throughout the time domain if the elastic and viscous contributions to $J(t)$ are separated before the superposition is performed, as the master curve of Figure 8.6 shows.

8.1.2 Transient Relaxation Experiments

Double logarithmic plots showing the evolution of the tensile relaxation modulus of a viscoelastic liquid on a time scale of three decades are shown, for illustrative purposes, in Figure 8.7. Although the modulus decreases with increasing time, the decreasing rate of $E(t)$ depends on the temperature of the isotherms. For example, while the modulus exhibits a slight dependence on time only at -80.8°C , it undergoes a sharp decrease with increasing time at 70.6°C . At -40.1°C the variation of the modulus with time is rather small, and at 50°C $E(t)$ drops very rapidly. Thus a temperature can be reached at which the relaxation modulus can decrease to zero within the time span of the experiment. In the case of solids, $E(t)$ cannot decrease below the value of the equilibrium relaxation modulus, E_e . Similar behavior presents the shear relaxation modulus, $G(t)$.

Since the habits of neighboring relaxation curves of Figure 8.7 are similar, the isotherms can be superposed on a reference isotherm. By refer-

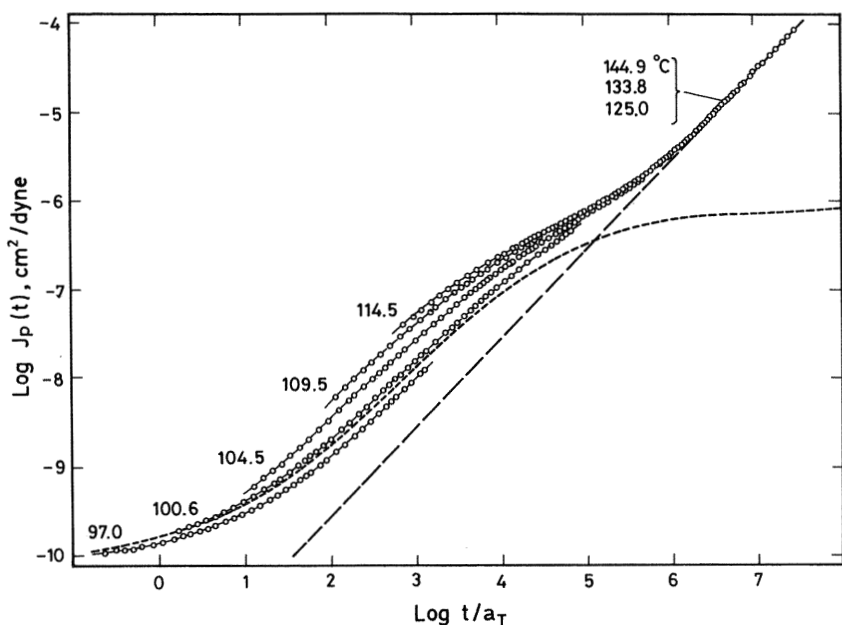


Figure 8.5 Double logarithmic plots of the creep compliance function versus t/a_T , where $a_T = (\eta/\eta_0)(\rho_0 T_0/\rho T)$ and the subindex 0 refers to 100°C. (From Ref. 5.)

ring to the shear relaxation modulus, the time-temperature correspondence principle establishes that

$$G(\log t + \log a_{0T}, T) = G(\log t, T_0) \quad (8.9)$$

where $\log a_{0T}$ is the amount by which the reference isotherm at temperature T has to be translated horizontally along the time axis to achieve coincidence with the isotherm at temperature T_0 . This equation can be written as

$$G(t, T) = G\left(\frac{t}{a_{0T}}, T_0\right) \quad (8.10)$$

On the other hand, molecular theories suggest that $G(t, T) \sim \rho T$, and as a consequence, $G(t, T)b_{0T} = G(t, T_0)$, where $b_{0T} = \rho_0 T_0/\rho T$. Hence, Eq. (8.10) can be more appropriately expressed as

$$b_{0T}G(t, T) = G\left(\frac{t}{a_{0T}}, T_0\right) \quad (8.11)$$

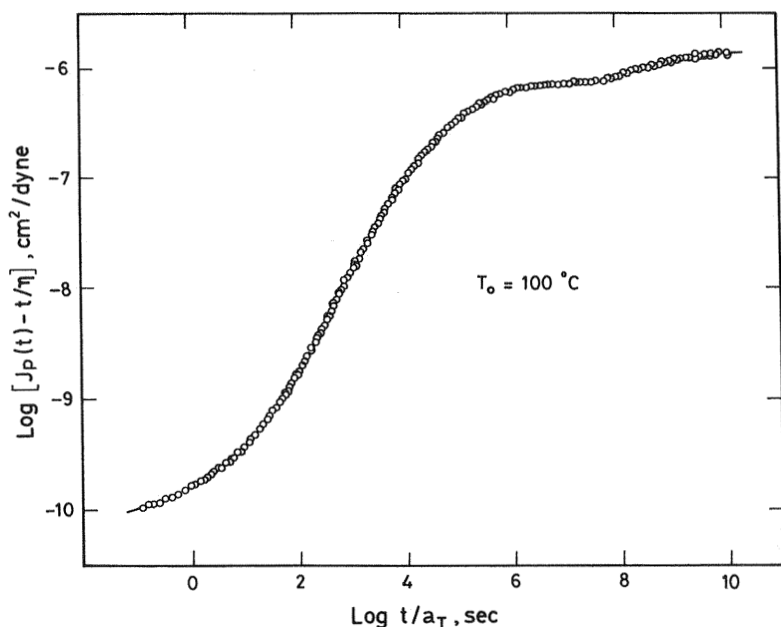


Figure 8.6 Master curve for the results of Figure 8.5 expressed in terms of the recoverable creep compliance function. (From Ref. 5.)

or

$$G_p(t, T) = G(t_r, T_0) \quad (8.12)$$

where $G_p(t, T) = b_{0T}G(t_r, T)$ is the reduced shear modulus and $t_r = t/a_{0T}$ is the reduced time. A master curve showing the time dependence of the reduced tensile relaxation modulus over a wide time scale is shown in Figure 8.8 (6). It should be pointed out that $E(t)$ [or $G(t)$] for a viscoelastic solid would not fall to zero but to the equilibrium relaxation modulus, E_e (or G_e).

8.1.3 Nontransient Creep Experiments

Isotherms at several temperatures showing the frequency dependence of the real component $J'(\omega)$ of the complex compliance $J^*(\omega)$ of a viscoelastic material are plotted on a double logarithmic scale in Figure 8.9 (7). At high temperatures and low frequencies, $J'(\omega)$ decreases slightly with increas-

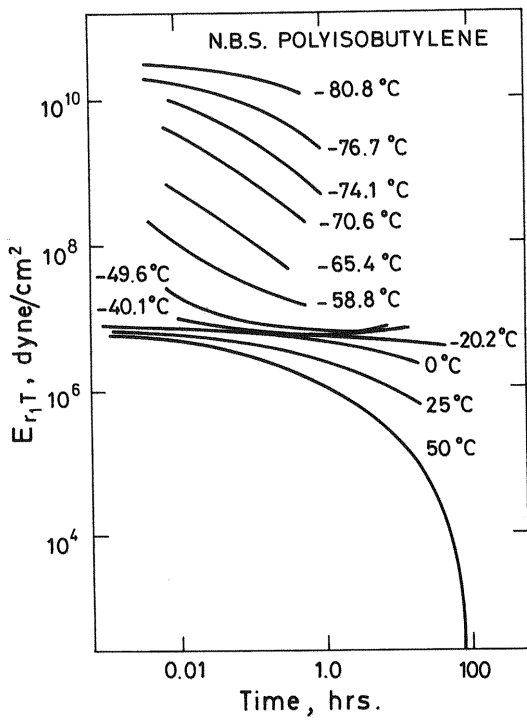


Figure 8.7 Double logarithmic plots showing the relaxation modulus of polyisobutylene in the time domain. (From Ref. 6.)

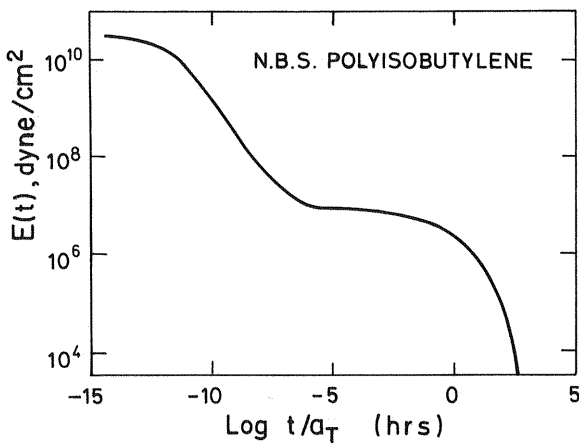


Figure 8.8 Master curve showing the tensile relaxation modulus of polyisobutylene in the time domain at 25°C. (From Ref. 6.)

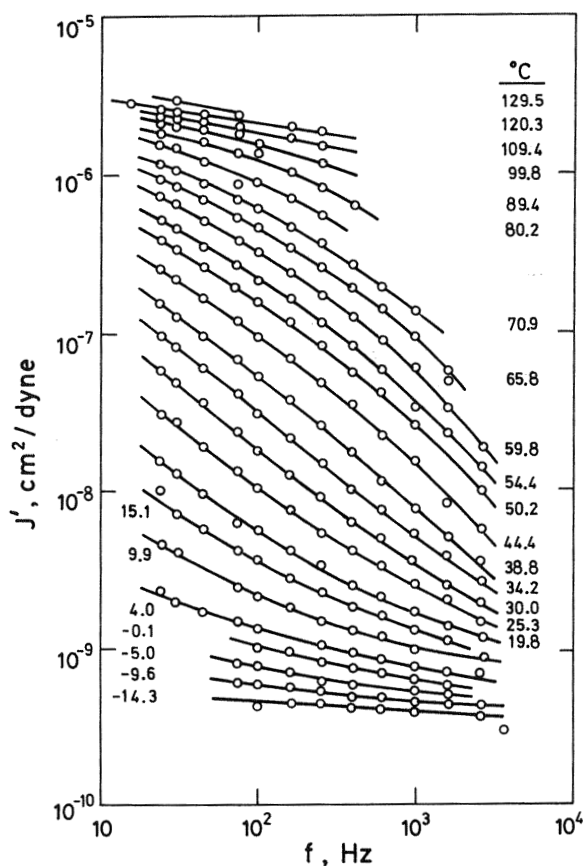


Figure 8.9 Double logarithmic plots showing isotherms reflecting the transition between the glass-like and rubber-like consistency for poly(*n*-octyl methacrylate). (From Ref. 7.)

ing frequency. The dependence of this viscoelastic function on frequency increases as the temperature of the isotherm decreases, a relatively sharp decrease with increasing frequency taking place as temperatures decrease from 70°C to 20°C. At temperatures close to T_g , $J'(\omega)$ decreases slightly as the frequency increases. As occurs with all the viscoelastic functions of thermorheological simple systems, the habits of neighboring curves are similar and the isotherms can be superposed. The master curve obtained from the isotherms of Figure 8.9 at the reference temperature of 100°C is shown in Figure 8.10.

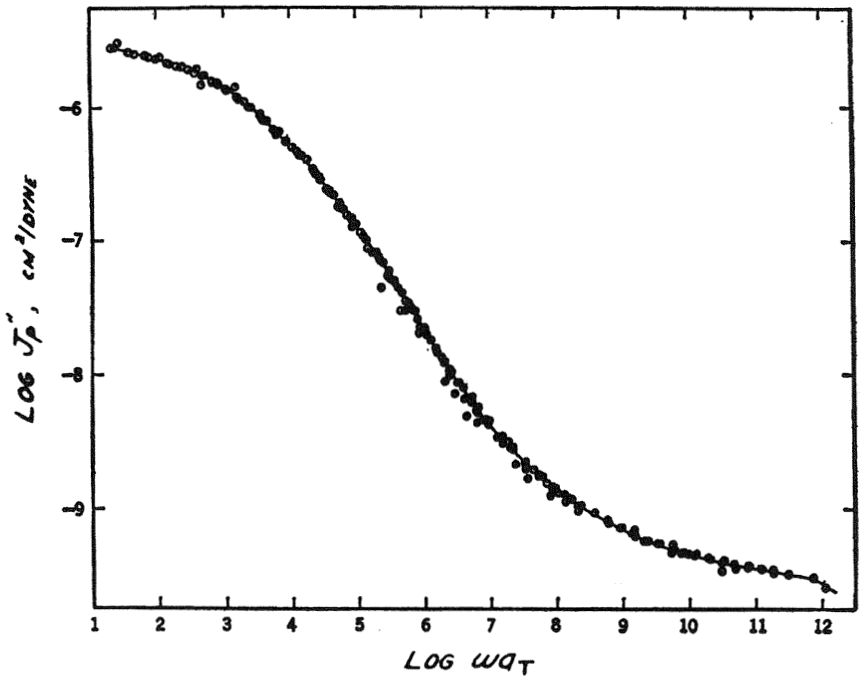


Figure 8.10 Master curve of the results of Figure 8.9 at the reference temperature $T_0 = 100^\circ\text{C}$.

By writing t/a_{0T} in terms of the reduction time, $t_r = t/a_{0T}$, Eq. (6.24) allows one to relate the values of $J'(\omega)$ at temperature T to those corresponding to the temperature of reference, T_0 . Thus (3)

$$\begin{aligned} J'(\omega, T) &= J_e^0 - \omega \int_0^\infty [J_e^0 - J(t) \sin \omega t] dt \\ &= J_e^0 - \omega a_{0T} \int_0^\infty \left[J_e^0 - J\left(\frac{t}{a_{0T}}, T_0\right) \right] \sin \omega a_{0T} t_r dt_r \end{aligned} \quad (8.13)$$

This equation leads to the relationship

$$\frac{J'(\omega, T)}{b_{0T}} = J'(\omega a_{0T}, T_0) \quad (8.14)$$

where b_{0T} is the vertical shift that must be performed on the isotherms to superpose them. Arguments similar to those used for $J'(\omega)$ lead to the following relationship for the loss compliance:

$$\frac{J''(\omega, T)}{b_{0T}} = J''(\omega a_{0T}, T_0) \quad (8.15)$$

Alternative forms of Eqs. (8.14) and (8.15) are

$$J'_p(\omega, T) = J'(\omega_r, T_0) \quad (8.16)$$

and

$$J''_p(\omega, T) = J''(\omega_r, T_0) \quad (8.17)$$

where J'_p and J''_p are, respectively, the reduced values of the real and loss components of the complex compliance function and $\omega_r = \omega a_{0T}$ is the reduced frequency.

The plots of the compliance viscoelastic functions $J_r(t)$ [$= J(t) - t/\eta$], $J'(1/t)$, and $J''(1/t)$ for a 40% solution of polystyrene in tri-*m*-tolyl phosphate are shown in Figure 8.11 (8), where the substitution $\omega = 1/t$ was made. It can be seen that $J_r(t) > J'(1/t)$, though at very high and very

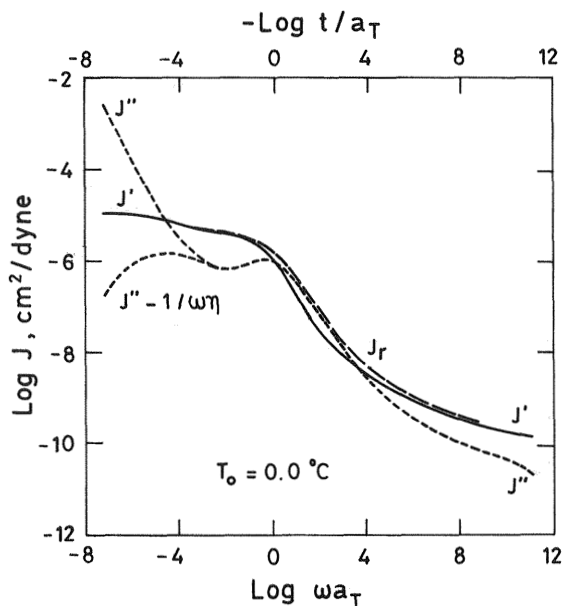


Figure 8.11 Logarithmic plots showing the recovery compliance and the complex compliance function for a 40% (w/w) solution of polystyrene ($M = 800,000$) in tri-*m*-tolyl phosphate. (From Ref. 8.)

low values of t , $J'(1/t) \approx J_r(t)$. At very low frequencies ($t \rightarrow \infty$), both $J(t) - t/\eta$ and $J'(1/t)$ approach J_e , while at very high frequencies ($t \rightarrow 0$), both $J(t) - t/\eta$ and $J'(1/t)$ approach J_g . Also, $J_r(t) > J''(1/t) - t/\eta$, but in the transition region in which $J_r(t)$ undergoes a sharp increase, $J''(1/t) - t/\eta \approx J_r(t)$. At very low frequencies, the loss $J''(1/t)$ of viscoelastic liquids continuously increases as t increases (the frequency decreases). For viscoelastic solids, $J''(1/t) \rightarrow 0$ when $t \rightarrow \infty$.

8.1.4 Nontransient Relaxation Experiments

Double logarithmic plots of the storage relaxation modulus versus frequency for a viscoelastic material are shown in Figure 8.12 (9). By taking into account Eq. (6.3), the correspondence between the results at tempera-

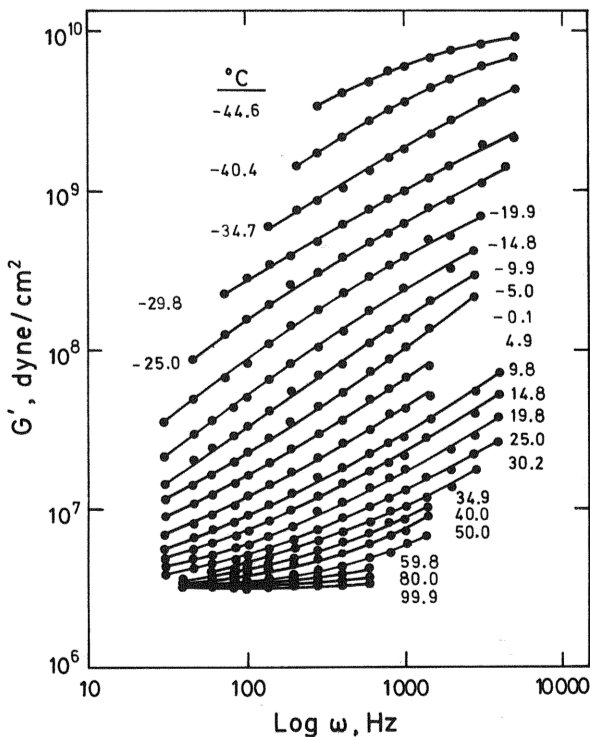


Figure 8.12 Logarithmic plots showing storage relaxation modulus of polyisobutylene in the frequency domain. The isotherms corresponding to the terminal region are not drawn. (From Ref. 9.)

ture T and those at the reference temperature T_0 for a viscoelastic solid can be written as

$$\begin{aligned} G'(\omega, T) &= \omega \int_0^{\infty} [G(t) - G_e] \sin \omega t \, dt \\ &= \omega a_{0T} \int_0^{\infty} \left[G\left(\frac{t}{a_{0T}}, T_0\right) - G_e \right] \sin \omega a_{0T} t_r \, dt_r \end{aligned} \quad (8.18)$$

where the substitution $t_r = t/a_{0T}$ has been made. Obviously, $G_e = 0$ for viscoelastic liquids. Hence, the time-temperature correspondence principle for the storage relaxation modulus can be written as

$$b_{0T} G'(\omega, T) = G'(\omega a_{0T}, T_0) \quad (8.19)$$

where b_{0T} is the vertical shift that must be performed on the isotherms before they are translated horizontally with respect to the reference isotherm to obtain the master curve. In the same way, the relationship between the relaxation loss moduli at T and T_0 is given by

$$b_{0T} G''(\omega, T) = G''(\omega a_{0T}, T_0) \quad (8.20)$$

These equations can be written in the alternative forms

$$G'_p(\omega, T) = G'(\omega_r, T_0) \quad (8.21)$$

and

$$G''_p(\omega, T) = G''(\omega_r, T_0) \quad (8.22)$$

where G'_r and G''_r are, respectively, the storage and loss relaxation moduli reduced at the reference temperature T_0 and ω_r is the reduced frequency.

Master curves showing the frequency dependence of the storage and loss relaxation moduli for 40% solution of polystyrene in tri-*m*-tolyl phosphate are shown for illustrative purposes in Figure 8.13. The curve for $G'(\omega)$ indicates that the liquid has a high rigidity at high frequencies; the rigidity of the system decreases with decreasing frequency until a plateau is reached. In the region where the flow is dominant, the storage relaxation modulus drops rather rapidly, the slope of the double logarithmic plot $G'(\omega)$ vs. ω being 2, as Eq. (6.47a) predicts. Comparison of the curves for $G''(\omega)$ and $G'(\omega)$ indicates that in the zone where the storage relaxation modulus presents a plateau, the loss presents a minimum and the slope of the double logarithmic plot of $G''(\omega)$ vs. ω in the low frequency region is 1, as Eq. (6.47b)

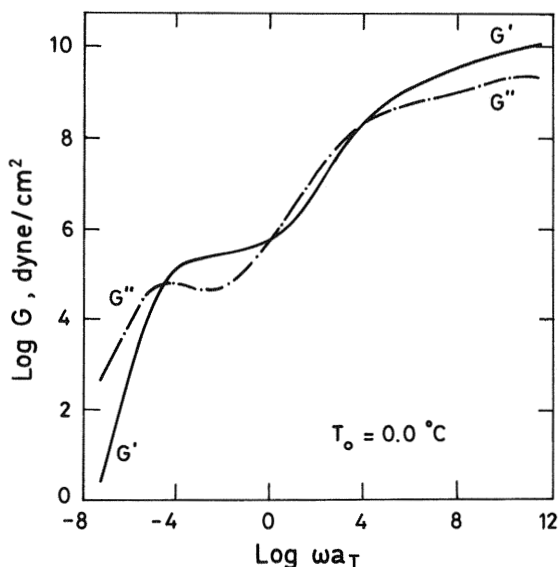


Figure 8.13 Master curves showing the storage and loss relaxation moduli of a solution of polystyrene in tri-*m*-tolyl phosphate at the reference temperature $T_0 = 0^\circ\text{C}$. (From Ref. 8.)

suggests. The differences between liquids and solids as far as the frequency dependence of the dynamic relaxation moduli is concerned appear in the terminal region. As indicated elsewhere, $G'(0) = G_e$ for solids, whereas for liquids $G'(0) = 0$. Although Eq. (6.48) suggests that the slope of the double logarithmic plot of $G''(\omega)$ vs. ω should be equal to 1 in the terminal region, this behavior was never observed in solids. The reason may be that frequencies used to observe that behavior were not low enough.

8.2 PREDICTION OF THE SHIFT FACTORS FOR VISCOELASTIC LIQUIDS

The shift factors are usually obtained by empirical methods that involve the horizontal translation of the isotherm representing the reduced viscoelastic functions in the time or frequency domains, in double logarithmic plots with respect to the reference isotherm. However, analysis of the components of the complex relaxation moduli in the terminal region ($\omega \rightarrow 0$) permits obtaining expressions that relate the shift factors to the steady-state compliance and the zero shear rate viscosity. Actually, in the region of very low

frequency, Eqs. (6.49) and (6.52) suggest that $G'(\omega)$ and $G''(\omega)$ are related to the terminal viscoelastic functions η and J_e^0 by the expressions

$$G'(\omega, T) = \omega^2 J_e^0(T) \eta^2(T); \quad G''(\omega, T) = \omega \eta(T) \quad (8.23)$$

By substituting these expressions into Eqs. (8.19) and (8.20), one obtains

$$b_{0T} \eta^2(T) J_e^0(T) = a_{0T}^2 \eta^2(T_0) J_e^0(T_0) \quad (8.24a)$$

$$b_{0T} \eta(T) = a_{0T} \eta(T_0) \quad (8.24b)$$

These equations lead to the following expression for the horizontal shift factor (2,3):

$$a_{0T} = \frac{\eta(T)}{\eta(T_0)} \left(\frac{J_e^0(T)}{J_e^0(T_0)} \right) \quad (8.25)$$

while the vertical shift factor can be written as

$$b_{0T} = \frac{J_e^0(T)}{J_e^0(T_0)} \quad (8.26)$$

Therefore, whenever the temperature dependence of the steady-state compliance and the zero shear rate are known, the shift factors for viscoelastic liquids can be obtained directly from Eqs. (8.25) and (8.26).

8.3 PREDICTION OF THE SHIFT FACTORS FOR VISCOELASTIC SOLIDS

When $\omega \rightarrow 0$, the loss compliance function for viscoelastic solids is given by

$$J''(\omega) \cong \omega \int_0^\infty [\Psi(\infty) - \Psi(t)] dt = \omega \int_0^\infty [J_e - J(t)] dt \quad (8.27)$$

where the substitution $\cos \omega t \approx 1$ has been made in Eq. (6.24). At very low frequencies, the loss relaxation modulus can be expressed in terms of the components of the complex creep compliance by the equation

$$G''(\omega) = \frac{J''(\omega)}{J'^2(\omega) + J''^2(\omega)} \cong \frac{\omega \int_0^\infty [J_e - J(t)] dt}{J_e^2} \quad (8.28)$$

where it has been considered that when $\omega \rightarrow 0$, $J'(\omega) = J_e$ and $J''(\omega) \ll J'(\omega)$. Hence,

$$\lim_{\omega \rightarrow 0} \frac{G''(\omega)}{\omega} = \eta'(0) = \frac{\int_0^{\infty} [J_e - J(t)] dt}{J_e^2} \quad (8.29)$$

This equation suggests a procedure to obtain the real component of the complex viscosity from the compliance functions at zero frequency. By taking Eq. (8.29) into account, Eq. (8.27) can be rewritten as

$$J''(\omega) = \omega J_e^2 \eta'(0) \quad (8.30)$$

By applying the time-temperature correspondence principle to $J''(\omega)$ and $J'(\omega)$ at low frequencies, one obtains

$$\frac{\eta'(0, T) J_e^2(T)}{b_{0T}} = a_{0T} \eta'(0, T_0) J_e^2(T_0), \quad \frac{J_e(T)}{b_{0T}} = J_e(T_0) \quad (8.31)$$

These equations lead to the following expression for the shift factor (3):

$$a_{0T} = \frac{\eta'(0, T)}{\eta'(0, T_0)} \left(\frac{J_e(T)}{J_e(T_0)} \right) \quad (8.32)$$

This expression is similar to the one obtained for viscoelastic liquids [Eq. (8.25)], the only difference being that η is the zero shear rate viscosity in liquids while $\eta'(0)$ for viscoelastic solids represents the real component of the complex viscosity at zero frequency.

8.4 INFLUENCE OF TEMPERATURE ON HORIZONTAL SHIFT FACTORS

The experimental evidence shows that the higher the temperature, the larger the response of a viscoelastic system to a mechanical perturbation. This behavior may be a consequence of the fact that on the one hand an increase in temperature facilitates the conformational transitions about the skeletal bonds, thus allowing the chains of the system to comply with the external perturbation, and on the other hand it increases the free volume, thus diminishing the friction coefficient between the moving segments of the molecular chains. These assumptions lead to the conclusion that the higher the free volume the lower the values of the relaxation/retardation times, τ associated with the viscoelastic mechanisms intervening in the process. Since

the free volume is governed by the temperature, the higher T is, the lower τ will be. Moreover, the time-temperature correspondence principle suggests that the retardation/relaxation times associated with the viscoelastic mechanisms in the so-called thermorheologically simple systems have the same temperature dependence. According to this, the relaxation or retardation times at temperature T associated with the viscoelastic mechanism i may be assumed to be related to the free volume by the empirical expression

$$\tau_i(T) = A \exp\left(\frac{B}{\phi(T)}\right) \quad (8.33)$$

formulated by Doolittle and Doolittle (10). Here, $\phi = (v - v_0)/v$, v and v_0 being the total and occupied specific volumes, respectively, and B is a parameter of the order of unity that is assumed to be related to the ratio between the critical volume v^* necessary for a relaxation process to take place and the volume v_m of the segments intervening in the relaxation. By assuming that the specific volume is a linear function of temperature,

$$v(T) = v_0[1 + \alpha_f(T - T_\infty)] \quad (8.34)$$

Eq. (8.33) can be written as

$$\ln \tau_i(T) = A' + \frac{m}{T - T_\infty} \quad (8.35)$$

where T_∞ may be interpreted as the temperature at which the free volume would be zero were it not for the formation of the glassy state, and $m = Bv_0/\alpha_f \cong B_v/\alpha$. Equation (8.35), known as the Vogel-Fulcher-Tammann-Hesse (VFTH) equation (11-13), was first empirically formulated to describe the variation in the viscosity of inorganic glasses at $T > T_g$. In general, this equation gives a good account of the temperature dependence of the relaxation phenomena of viscoelastic substances. The zero shear rate viscosity of substances in the vicinity of the glass transition temperature can be formulated in terms of the empirical expressions

$$\eta(T) = C \exp\left[\frac{B'}{\phi(T)}\right] \quad (8.36a)$$

and

$$\ln \eta(T) = C' + \frac{m'}{T - T_\infty} \quad (8.36b)$$

where $\phi(t)$, m' , and T_∞ have the meanings indicated above. At temperatures well above T_g , the free volume is not so critical for the flow, and the temperature dependence of the viscosity exhibits Arrhenius behavior. Typical examples of the variation of the viscosity with T are given in Figure 8.14 (14).

If the time-temperature correspondence principle holds, Eq. (8.35) suggests that the temperature dependence of the shift factor in the time (or frequency) domain can be written as

$$\begin{aligned} \ln a_{0T} &= \ln \frac{\tau_i(T)}{\tau_i(T_0)} \\ &= -\frac{Bv_0}{\alpha_f} \left[\frac{1}{T_0 - T_\infty} - \frac{1}{T - T_\infty} \right] = A' + \frac{m}{T - T_\infty} \end{aligned} \quad (8.37)$$

where T_0 is the reference temperature and the rest of the parameters have the physical meanings indicated earlier. After a simple mathematical handling, Eq. (8.37) becomes

$$\ln a_{0T} = -\frac{Bv_0}{\alpha(T_0 - T_\infty)} \left(\frac{T - T_0}{T - T_\infty} \right) = -\frac{C_1(T - T_0)}{T + C_2 - T_0} \quad (8.38)$$

where the constants C_1 and C_2 are given by

$$C_1 = \frac{Bv_0}{\alpha_f(T_0 - T_\infty)}; \quad C_2 = T_0 - T_\infty \quad (8.39)$$

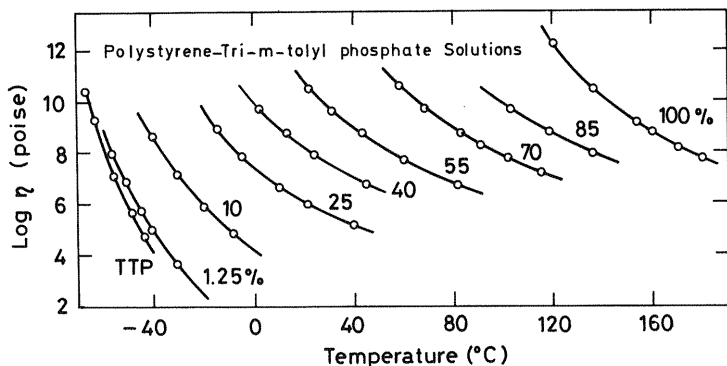


Figure 8.14 Influence of temperature on the viscosity of tri-*m*-tolyl phosphate (TTP), polystyrene, and solutions of polystyrene in tri-*m*-tolyl phosphate. (From Ref. 14.)

Equation (8.38), empirically formulated by Williams, Landel, and Ferry in the 1950s, is known as the WLF equation (15). Examples of the variation of a_{0T} with temperature are shown in Figure 8.15. The plots of $(T - T_0)/(\ln a_{0T})$ against $T - T_0$ are straight lines whose slopes and intercepts are $-1/C_1$ and $-C_2/C_1$, respectively. Though an analysis of limited data led to the postulation that C_1 and C_2 were universal constants at T_g , this assumption was not supported when the results obtained for a wide variety of viscoelastic materials were considered.

The parameters of the VFTH equation can be calculated from the values of C_1 and C_2 by using the expressions of Eq. (8.39). An alternative way of obtaining m and T_∞ is to plot $\ln a_{0T}$ versus $1/(T - T_\infty)$ and determine by trial and error the value of T_∞ that best fits the plot to a straight line. It should be pointed out that in most cases $T_\infty \approx T_g - 50$ K. By comparing Eqs. (8.33) and (8.35), the volume fraction and the coefficient of expansion at T_g are given by (16)

$$\frac{\phi_g}{B} = \frac{T_g - T_\infty}{m} \quad \text{and} \quad \alpha_f \cong \frac{1}{m} \quad (8.40)$$

It is worthwhile to indicate that for most systems the values of ϕ_g/B lie in the interval 0.025 ± 0.005 and $\alpha_f \sim 5 \times 10^{-4} \text{ K}^{-1}$. The use of the assumption that $B \approx 1$ has led to the postulation that the relative free volume for amorphous systems is 0.025 ± 0.005 at T_g .

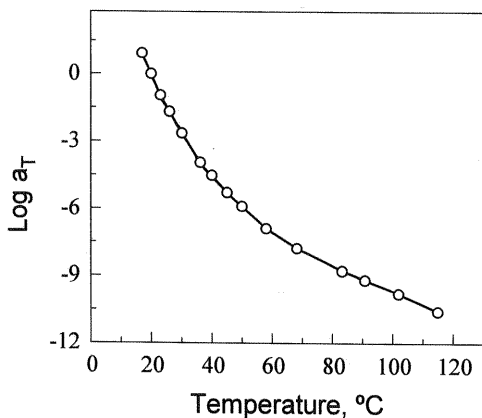


Figure 8.15 Illustrative plots showing the variation of the shift factor with temperature for the results of Figure 8.2 (Reference temperature 20°C , $T_g = 15^\circ\text{C}$.)

8.5 EFFECT OF PRESSURE ON THE VISCOELASTIC RESPONSE

While an increase in temperature speeds up the viscoelastic response, an increase in pressure slows it down. In the so-called piezorheologically simple systems, all the response times have the same dependence on pressure, and the generalized shift factor is expressed by the Fillers–Moonan–Tschoegl equation (17)

$$\log a_{T,P} = \frac{-c_1^0 [T - T_0 - \theta(P)]}{c_2^0(P) + T - T_0 - \theta(P)} \quad (8.41)$$

where

$$\theta(P) = c_3^0(P) \ln \left[\frac{1 + c_4^0(P)}{1 + c_4^0(P_0)} \right] - c_5^0(P) \ln \left[\frac{1 + c_6^0(P)}{1 + c_6^0(P_0)} \right] \quad (8.42)$$

In this latter equation, P_0 is the reference pressure and P is the experimental pressure. Obviously, Eq. (8.41) reduces to the WLF equation when $P = P_0$.

8.6 DIFFERENTIATION OF REGIONS IN THE MASTER CURVES OF THE VISCOELASTIC FUNCTIONS

Four regions can be distinguished in the master curves of the viscoelastic functions. As an example, let us take the double logarithmic plot of $J(t)$ vs. t depicted in Figure 8.6. Here, the following regions are observed: (1) the glass-like zone in which $\log J(t)$ slightly increases with time, (2) the transition region in which a dramatic change of several decades may take place in $\log J(t)$, (3) the rubbery region or plateau zone where $\log J(t)$ increases only slightly with time, and (4) the viscous or terminal zone in which the flow is dominant. The terms “glassy” and “transition” used, respectively, to designate the first and second zones are indeed unfortunate because no thermodynamic changes occur in the material at $T > T_g$. A careful inspection of the changes taking place in the recoverable compliance between the plateau and the terminal zone, which seem to be small on the logarithmic scale shows that they are even larger than those occurring in the transition zone when the results are expressed in absolute terms, as can be seen in Figure 8.16, where $J(t)$ is represented versus $\log t$.

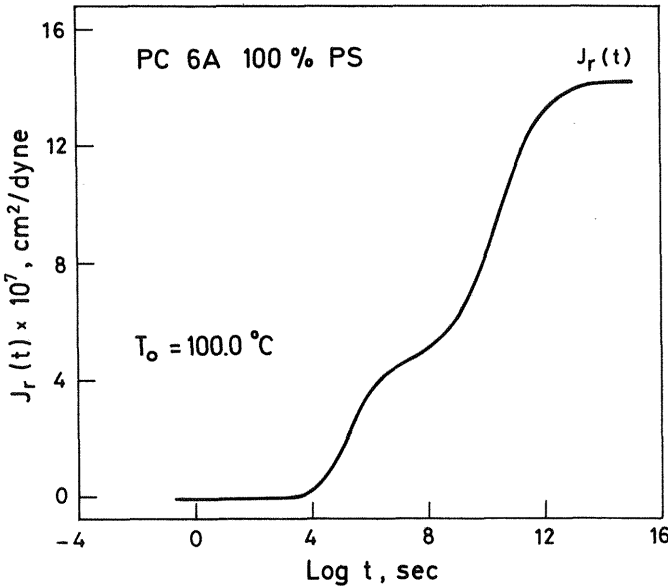


Figure 8.16 Semilogarithmic plots showing the recovery compliance of polystyrene in the time domain at $T_0 = 100^\circ\text{C}$. (From Ref. 8.)

8.6.1 Glassy-Like and Transition-Like Zones

The use of the term “glassy-like” for this zone arises from the fact that the viscoelastic mechanisms associated with the response are believed to involve local motions, such as occurs in the glassy state. The response in this region is independent of molecular weight, and the creep compliance function obeys Andrade’s equation (18,19)

$$J(t) = J_g + \beta t^{1/3} \quad (8.43)$$

By plotting $J(t)$ against $t^{1/3}$ a straight line is obtained whose intercept with the ordinates axis gives the glassy creep compliance function. Note that the value of this quantity is of the order of 10^{-9} Pa^{-1} . Equation (8.43) is often used to obtain the values of $J(t)$ at very short times. These values are particularly useful when the retardation spectrum is calculated from $J(t)$ by computing methods. Since $G_g = 1/J_g$, the glassy relaxation modulus [$G_g = G(0)$] has a value of the order of 10^9 Pa . Moreover, because $t \cong 1/\omega$, the values of $J'(\infty)$ and $G'(\infty)$ converge to those of J_g and G_g , respectively.

The transition region seems to be produced by viscoelastic mechanisms in which between 20 and 50 segments may intervene. The values of $\log J(t)$ and $\log J'(\omega)$ increase by several decades in this region at the time increases or frequency decreases, the changes being nearly independent of molecular weight for long chains. In contrast with what occurs with the compliance functions, the values of $\log G(t)$ and $\log G'(\omega)$ decrease by several decades in the transition zone (roughly from 10^9 Pa to 10^6 – 10^7 Pa for high molecular weight chains) as the time increases or the frequency decreases.

For low molecular weight fractions, the variation in the values of the compliance function increases as either the chain length or the temperature increases. The changes observed in the compliance with temperature for very low molecular weight fractions are illustrated in Figure 8.17 (16). This lack of thermorheological simplicity was also observed for other amorphous polymers, specifically poly(ethyl methacrylate) (21), poly(*n*-butyl methacrylate) (22), poly(*n*-hexyl methacrylate) (23), and low molecular weight poly(methylphenyl siloxane) (24).

The tangent of δ exhibits a prominent peak in this region, and the viscoelastic loss functions $G''(\omega)$ and $J''(\omega)$ may also exhibit an absorption in the transition zone. The relative location of the maxima of the loss functions $G''(\omega)$ and $J''(\omega)$, if they exist, can be obtained by taking into account that at the maximum of the peak of $\tan \delta$, the following relation holds:

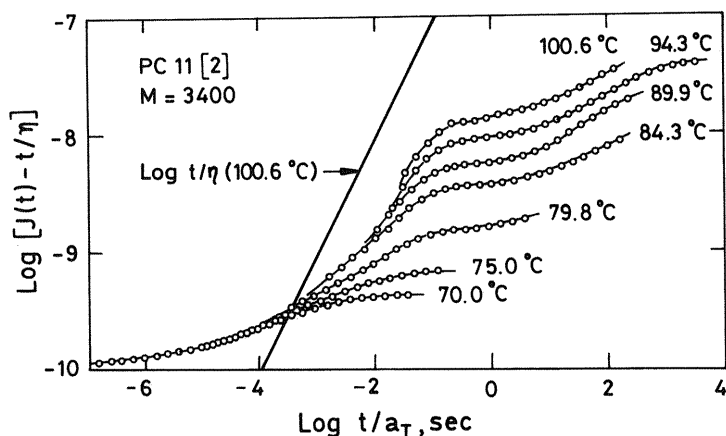


Figure 8.17 Isotherms showing the recoverable creep compliance for a narrow polystyrene distribution with molecular weight 3400. (From Ref. 16.)

$$\frac{d \log[\tan \delta(\omega)_{\max}]}{d \log \omega} = \frac{d \log G''(\omega)}{d \log \omega} - \frac{d \log G'(\omega)}{d \log \omega} = 0 \quad (8.44)$$

Because $G'(\omega)$ is a monotonous increasing function of frequency, Eq. (8.44) suggests that at the frequency at which the maximum of $\tan \delta$ is located, one obtains

$$\frac{d \log G''(\omega)}{d \log \omega} = \frac{d \log G'(\omega)}{d \log \omega} > 0 \quad (8.45)$$

Accordingly, when $\tan \delta(\omega)$ reaches its maximum, the maximum of the peak corresponding to $G''(\omega)$ has not yet been reached; consequently, $\omega(\tan \delta_{\max}) < \omega(G''_{\max})$. On the other hand, at the peak maximum of $\tan \delta$, the following relation must be fulfilled:

$$\frac{d \log(\tan \delta)_{\max}}{d \log \omega} = \frac{d \log J''(\omega)}{d \log \omega} - \frac{d \log J'(\omega)}{d \log \omega} = 0 \quad (8.46)$$

Since $J'(\omega)$ is a monotonous decreasing function of ω , Eq. (8.46) indicates that at the frequency at which the maximum of $\tan \delta$ appears, the following inequality holds:

$$\frac{d \log J''(\omega)}{d \log \omega} = \frac{d \log J'(\omega)}{d \log \omega} < 0 \quad (8.47)$$

This expression suggests that the maximum of the $J''(\omega)$ peak has already been passed when the maximum of $\tan \delta$ is reached; therefore, $\omega(\tan \delta_{\max}) > \omega(J''_{\max})$. This analysis leads to the inequalities (8)

$$\omega(J''_{\max}) < \omega(\tan \delta_{\max}) < \omega(G''_{\max}) \quad (8.48)$$

Accordingly, the loss compliance function presents a maximum in the frequency domain at lower frequency than the loss relaxation modulus. This behavior is illustrated in Figure 8.18, where the complex relaxation modulus, the complex creep compliance function, and the loss $\tan \delta$ for a viscoelastic system with a single relaxation time are plotted. Similar arguments applied to a minimum in $\tan \delta$ lead to the inequalities

$$\omega(J''_{\min}) > \omega(\tan \delta_{\min}) > \omega(G''_{\min}) \quad (8.48)$$

The relative locations of the peaks corresponding to $\tan \delta$, $G''(T)$, $G'(T)$ in the isochrones follow trends opposite to those observed in the isotherms.

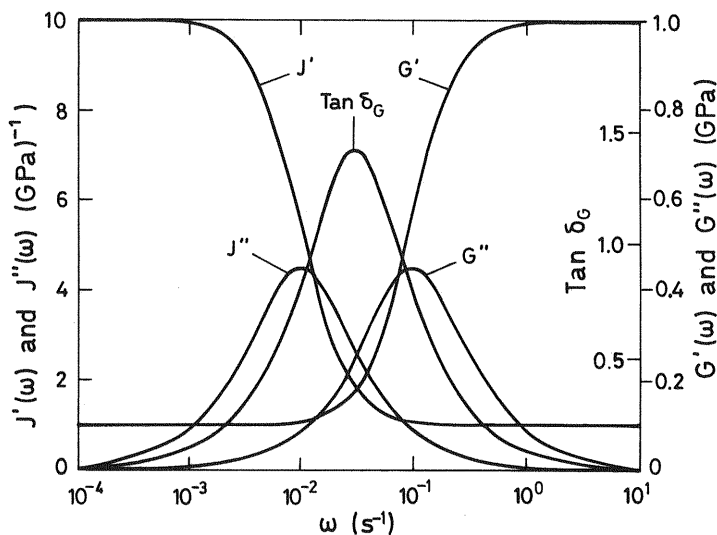


Figure 8.18 Illustrative curves describing the relative locations in the frequency domain of the complex relaxation modulus, the complex creep compliance function, and $\tan \delta$ for a viscoelastic model with a single relaxation time; $J_\infty = 1 \text{ GPa}^{-1}$; $J_d = 9 \text{ GPa}^{-1}$; $\tan \delta_G = \tan \delta_j$. (See Chap. 10 for details.)

In this case, the derivative of $\tan \delta$ with respect to temperature at the peak maximum gives

$$\frac{d \log \tan \delta_{\max}}{dT} = \frac{d \log G''(T)}{dT} - \frac{d \log G'(T)}{dT} = 0 \quad (8.49)$$

Because $G'(T)$ is a decreasing function of temperature at the glass–rubber relaxation temperature, the following relationship at the peak maximum of $\tan \delta$ holds:

$$\frac{d \log G''(T)}{dT} = \frac{d \log G'(T)}{dT} < 0 \quad (8.50)$$

Consequently, $T(G''_{\max}) < T(\tan \delta_{\max})$, that is, the maximum of $G''(T)$ is located at a lower temperature than that of $\tan \delta$ in the isochrones. Moreover, the left-hand side of Eq. (8.49) can also be written as

$$\frac{d \log \tan \delta_{\max}}{dT} = \frac{d \log J''(T)}{dT} - \frac{d \log J'(T)}{dT} \quad (8.51)$$

Owing to the fact that at the glass–rubber relaxation temperature the storage compliance function is an increasing function of temperature, the inequality

$$\frac{d \log J''(T)}{dT} = \frac{d \log J'(T)}{dT} > 0 \quad (8.52)$$

holds at the temperature at which the maximum of $\tan \delta$ occurs. Therefore, $T(J''_{\max}) > T(\tan \delta_{\max})$; in other words, if $J''(T)$ exhibits an absorption in the glass–rubber relaxation, the peak appears at a temperature higher than that of $\tan \delta$. The temperatures at which the maxima of the peaks are located in the isochrones follow the order

$$T(G''_{\max}) < T(\tan \delta_{\max}) < T(J''_{\max}) \quad (8.53)$$

8.6.2 Plateau Region

While the transition region is not very sensitive to the molecular weight, M , provided that the value of M is relatively high, the number of decades in the time or frequency domain over which the rubbery plateau extends increases as the molecular weight increases. In this region, only small changes are detected in the values of the transient functions of viscoelastic liquids, and the material behaves as if it were a solid. A plateau is also observed in the storage compliance function $J'(\omega)$ and the storage relaxation modulus $G'(\omega)$. An illustrative plot showing the length of the plateau for several fractions of different molecular weights is shown in Figure 8.19 (25). This behavior, which reminds one of that of a cross-linked rubber, has been attributed to the formation of entanglements between the chains. The entanglements act as temporal or physical cross-linking points, thus hindering the flow and impeding the total compliance of the response with the force field. Theories that can explain the rubbery plateau are discussed in Chapter 11.

The rubber elasticity theory predicts that the relaxation modulus is given by

$$G_N^0 = \frac{\rho}{M_{ec}} RT \quad (8.54)$$

where M_{ec} is the molecular weight between cross-linking points and ρ/M_{ec} is the concentration of elastically active chains. By analogy, the molecular weight between entanglements, M_e in temporal networks can be written as

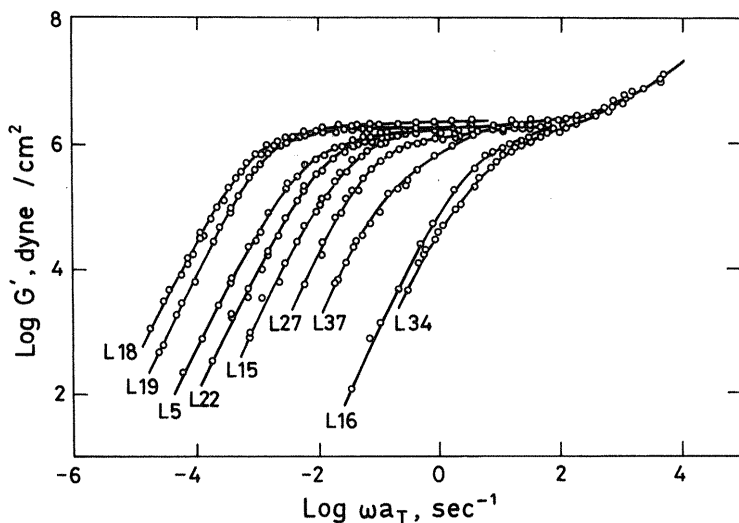


Figure 8.19 Influence of molecular weight on the plateau length of narrow distribution polystyrene. The curves represent the storage relaxation modulus in the frequency domain reduced to 160°C. Viscosity-average molecular weights from left to right, $\times 10^{-4}$: 58, 51, 35, 27.5, 21.5, 16.7, 11.3, 5.9, and 4.7. (From Ref. 25.)

$$M_e = \frac{\rho RT}{G_N^0} = \rho RT J_N^0 \quad (8.55)$$

where J_N^0 and G_N^0 are, respectively, the plateau compliance function and the plateau relaxation modulus. Moreover, it has been considered that $J_N^0 = 1/G_N^0$ for elastic systems.

The small changes taking place in the compliance function with time at the plateau also obey Andrade's equation for creep, that is (26–28),

$$J(t) = J_A + \beta t^{1/3} + \frac{t}{\eta} \quad (8.56)$$

Values of J_A have been obtained by plotting results for $J(t)$ against $t^{1/3}$ in the plateau region, where the viscous contribution is small, and further extrapolation to $t = 0$. The results thus obtained for J_A differ by less than 10% from those determined for J_N by other procedures described below.

As shown in Figure 8.20 (29), the loss functions $J''(\omega)$ and $G''(\omega)$ present absorptions at the plateau that are related to J_N^0 and G_N^0 , respectively. Since for solids $\eta \rightarrow \infty$, Eq. (6.35) leads to the expression

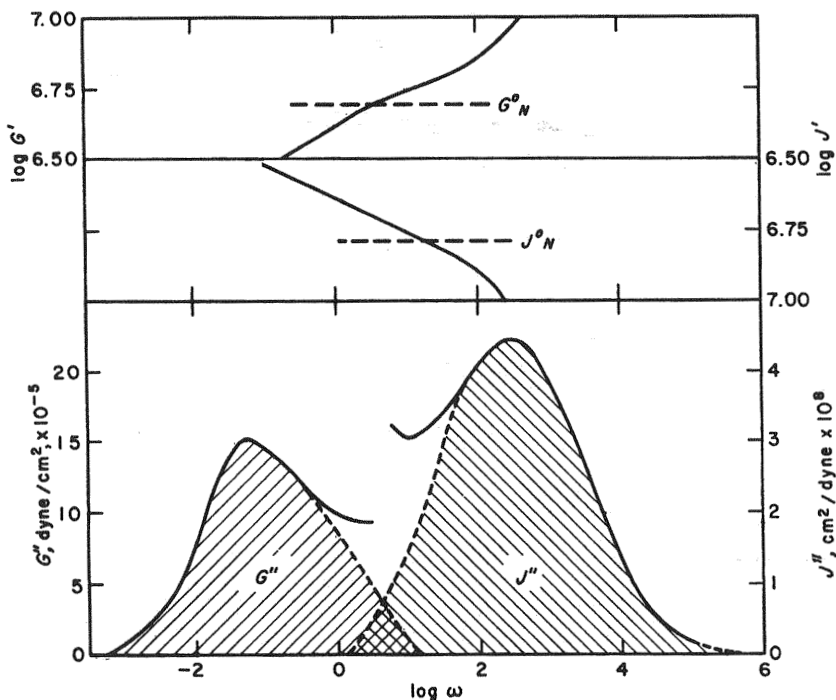


Figure 8.20 Plateau levels in G' and J' , together with the absorptions for G'' and J'' , corresponding to 1,2-polybutadiene of number-average molecular weight 99,000. Integration of these curves using Eqs (8.58) and (8.60) gives the dashed horizontal lines corresponding to the values of G_N^0 and J_N^0 . (From Ref. 29.)

$$J_e = J_g + \frac{2}{\pi} \int_{-\infty}^{\infty} J''(\omega) d \ln \omega \quad (8.57)$$

which gives the equilibrium compliance for a viscoelastic solid in terms of the loss compliance function. By analogy, the value of J_N^0 can be obtained from the peak that appears in $J''(\omega)$ by means of the equation (2)

$$J_N^0 \cong \frac{2}{\pi} \int_a^b J''(\omega) d \ln \omega \quad (8.58)$$

where the lower integration limit a is usually obtained by considering that the peak is symmetrical, and the term J_g has been neglected. Note that the contribution of the viscosity to J'' in the plateau region of uncross-linked polymers can be considered negligible. The integration limits are usually

obtained by extrapolating the curve compassing the peak until $J''(\omega) = 0$ and consequently are somewhat uncertain. It should be noted, however, that owing to the large decrease taking place in the values of $J''(\omega)$ in the extrapolated part of the absorption, the error committed is in most cases relatively small.

The relationship between the relaxation modulus and the loss relaxation modulus established by Eqs. (6.8) leads to the expression

$$\lim_{t \rightarrow 0} G(t) = \frac{2}{\pi} \int_{-\infty}^{\infty} G''(\omega) d \ln \omega = G_g \quad (8.59)$$

where it has been considered the $G_e = 0$ for liquids. The curves of $G''(\omega)$ in the frequency domain may present a peak in the high frequency region, associated with the glass-rubber transition, followed by another peak reflecting both the generalized motions of the chains between the entanglements and the disentanglement of the chains. Obviously, the mechanisms associated with generalized motions between temporally entangled points have higher rigidity than those corresponding to the terminal region. Therefore, Eq. (8.59) suggests that the relaxation modulus of a viscoelastic liquid at the plateau can be written as (2)

$$G_N^0 = \frac{2}{\pi} \int_{-\infty}^b G''(\omega) d \ln \omega \quad (8.60)$$

Usually Eq. (8.60) is evaluated by considering that in the low frequency zone the slope of the curve $G''(\omega)$ vs. ω is unity. The extrapolation of the peak in the high frequency zone is carried out by assuming that the peak is symmetrical. The values of G_N^0 should be the reciprocal of those of J_N^0 .

8.6.3 Terminal Region for Viscoelastic Liquids

The results of Figure 8.6 show that the values of the recoverable compliance function increase between the plateau and terminal regions. This increase, which seems to be small in the double logarithmic plot of $J_r(t)$ vs. t , is considerably large when the data are plotted in the normal form represented in Figure 8.16. Schematic double logarithmic representations of the compliance function $J(t)$ vs. t in the terminal region, shown in Figure 8.5, indicate that $J(t)$ undergoes a dramatic increase as time increases owing to the fact that the viscous contribution to the compliance function is dominant in the terminal region. A similar increase takes place in the value of the loss compliance function in the low frequency region.

As can be seen in Figure 8.7, the tensile relaxation modulus drops rapidly to zero in the terminal region. The fall of $E(t)$ occurs at shorter times as the molecular weight decreases. The shear relaxation moduli in the frequency domain decrease as the frequency decreases, the double logarithmic plots of $G'(\omega)$ and $G''(\omega)$ versus frequency being straight lines with slopes of 2 and 1, respectively, when $\omega \rightarrow 0$. Knowledge of the viscoelastic behavior of polymeric liquids in the terminal region is important in determining the zero shear rate viscosity η_0 and the steady-state compliance, J_e^0 , two parameters of great technological importance in the processing of viscoelastic materials. These parameters, η_0 and J_e^0 , govern, respectively, the flow and orientation of the molecular chains under the effect of a force field.

The zero shear rate viscosity is strongly dependent on molecular weight. According to the Rouse theory (see Chap. 11), the viscosity is related to M through the friction coefficient ζ_0 , so that $\eta/M \sim \zeta_0$. This parameter depends on the free volume, and as a result its value increases with molecular weight, approaching a constant limiting value ζ_{00} at high molecular weight. The friction coefficient can be expressed in terms of the Doolittle equation

$$\zeta = A \exp\left(\frac{B}{f}\right) \quad (8.60a)$$

where f , the fractional free volume, is the ratio between the free volume $v_f = (v - v_0)$ and the specific volume v and B is a parameter in the vicinity of unity. According to Eq. (8.60a), ζ_0 and ζ_{00} are related by the equation

$$\log \zeta_0 = \log \zeta_{00} + \frac{B}{2.303} \left(\frac{1}{f_M} - \frac{1}{f_0} \right) \quad (8.60b)$$

where the subscripts M and 0 to f refer to the fractional free volume at molecular weights M and infinity, respectively. It has been proposed (30) that the specific volume is a linear function of the reciprocal of the number-average molecular weight, and as a consequence the fraction free volume can be expressed as

$$f_M = f_0 + \frac{A}{M_n} \quad (8.60c)$$

Equations (8.60b) and (8.60c) suggest that $\zeta_0 \approx \zeta_{00}$ for moderately high molecular weight. To obtain a ratio η/M independent of molecular weight requires, in the low molecular weight region, expressing the viscosity in terms of $\eta\zeta_{00}/\zeta_0$ (31). It should be pointed out that the friction coefficient

can be obtained either from viscoelastic results [see Eq. (11.46) or (11.48)] or from viscosity data [see Eq. (11.34)]. Representative double logarithmic plots of η against molecular weight are shown in Figure 8.21. The experimental results can be generalized by means of the following scaling laws (2,32,33).

$$\begin{aligned} \eta &\sim M_w, & M < M_c \\ \eta &\sim M_w^{3.4}, & M > M_c \end{aligned} \quad (8.61)$$

An increase in molecular weight favors the overlapping of the domains of different chains, thus increasing the number of entanglements per molecular chain. Flow implies disentanglement of the chains, and this process involves dissipation of energy, which will be larger, the larger is the entanglement density and consequently larger the molecular weight. A comparison of the critical molecular weight obtained from the viscous data with those obtained from the viscoelastic functions G_N^0 or J_N^0 for molecular weight between entanglements permits the conclusion that

$$M_c \simeq 2M_e \quad (8.62)$$

The double logarithmic plot of J_e^0 against molecular weight, shown in Figure 8.22 (34), indicates that the steady-state compliance is a linear function of M until a critical molecular weight M_c' is reached, above which J_e^0 is nearly independent of molecular weight. Accordingly (32),

$$\begin{aligned} J_e^0 &\sim M, & M < M_c' \\ J_e^0 &\sim \text{const.}, & M > M_c' \end{aligned} \quad (8.63)$$

The analysis of the experimental data at hand suggests that $M_c' \approx 3M_c \approx 6M_e$. For nearly monodisperse flexible polymers, J_e^0 is found to be related to the plateau modulus by the approximate expression (35)

$$J_e^0 \cong \frac{2.3}{G_N^0}, \quad M \gg M_c \quad (8.64)$$

The steady-state compliance shows a strong dependence on the molecular heterodispersity. Thus the value of J_e^0 for a mixture of two fractions of the same polymer, one of low and the other of high molecular weight, may be up to 10 times as high as that of each component. This behavior can be explained by taking into account that J_e^0 is the total recoverable deformation per unit of shear stress. The chains of high molecular weight have a very

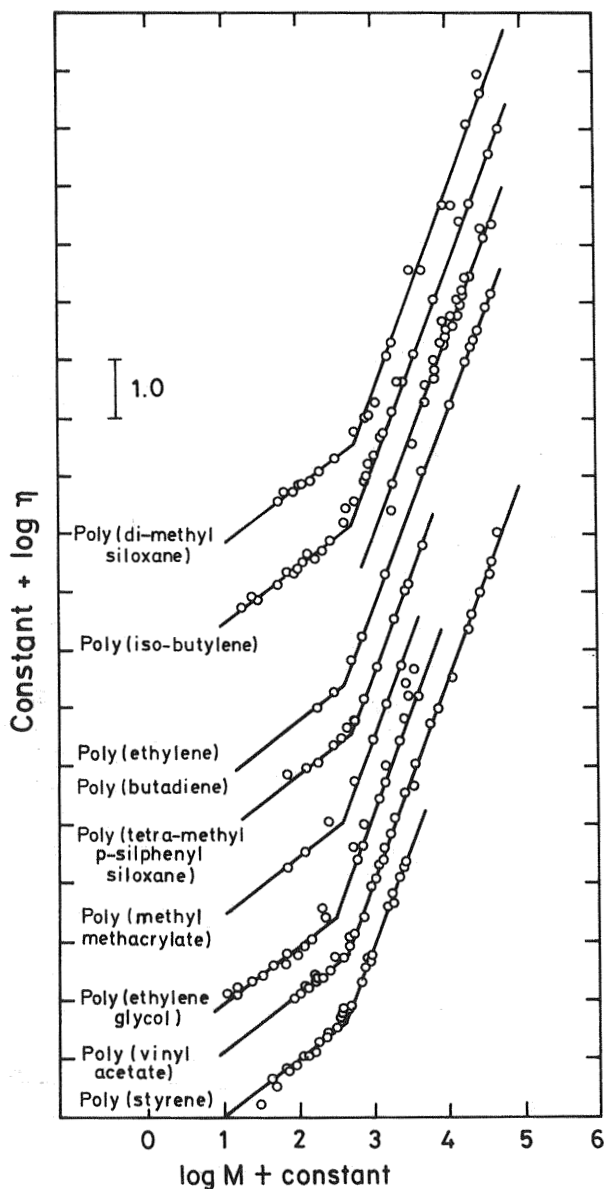


Figure 8.21 Double logarithmic plots of viscosity against molecular weight for the polymers indicated. The slopes of the lines are 1 on the left and 3.4 on the right. In the low molecular weight region the viscosity is represented in terms of $\eta_{\zeta_{00}}/\zeta_0$. (From Ref. 3.1)

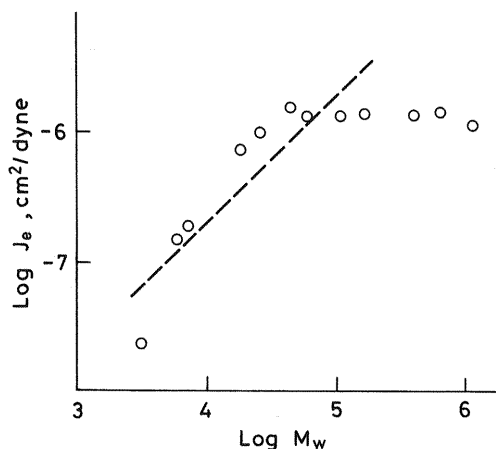


Figure 8.22 Logarithmic plot of the steady state compliance, at -30°C , versus weight-average molecular weight for poly(*cis*-isoprene). (From Ref. 34.)

large number of friction points, and therefore they share a disproportionate shear stress in the mixture with the short chains. As a consequence, the long chains are much more extended than the short ones in the force field. Since the large chains relax very slowly, they are conformationally much more distorted than the short chains in the steady state, hence the high value of J_e^0 for heterodisperse polymers.

The terminal viscoelastic functions show a strong dependence on the molecular topology (32). The exponent of the viscosity–molecular weight relationship of star molecules, comb-like polymers, etc., is larger than 3.4, the exponent corresponding to linear chains, whenever the molecular weight of the branches is larger than M_c . Moreover, the steady-state compliance of these chains is a linear function of molecular weight, in contrast with what occurs for linear flexible polymers, in which J_e^0 remains constant for $M > M'_c \approx 6M_c$.

8.7 INFLUENCE OF DILUENTS ON THE VISCOELASTIC BEHAVIOR OF POLYMERS

The intrinsic viscosity is an important physical parameter related to the volume occupied by the molecular chains in solution. This quantity, represented by $[\eta]$, is defined as

$$[\eta] = \lim_{C \rightarrow 0} \frac{\eta - \eta_0}{\eta_0 C} \quad (8.65)$$

where η and η_0 are the viscosities of the solution and the solvent, respectively, and C is the concentration of the solute. For flexible polymers, $[\eta]$ may be even larger than 1 dL/g, indicating that in very dilute solutions 1 g of polymer may occupy a volume of 100 cm³. This experimental fact suggests that molecular coils are highly expanded. In the case of very dilute solutions, the macromolecular domains are independent. However, a critical concentration can be reached above which the domains of the molecular chains overlap. Obviously, the response of the polymers to external mechanical perturbations is strongly influenced by the intermolecular interactions arising from the overlapping of the molecular domains. By assuming that the critical concentration corresponds to that at which the concentration of segments in the molecular coil is similar to the average concentration of segments in the solution (Fig. 8.23), one finds (36)

$$C^* \cong \frac{N}{b^3 N^{3\nu}} = b^{-3} N^{1-3\nu} \quad (8.66)$$

where N is the number of segments of each molecular chain and R is the radius of the coils given by

$$R \sim bN^\nu \quad (8.67)$$

Here b is the length of each segment and the exponent ν is about 0.6 in good solvents. For these solvents, Eq. (8.66) suggests that the critical volume fraction of polymer scales with molecular weight as

$$\phi^* \sim N^{1-3\nu} = N^{-4/5} \quad (8.68)$$

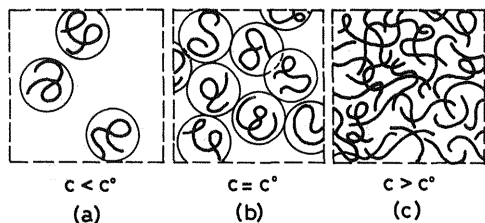


Figure 8.23 Coil domains of molecular chains at various concentrations. (From Ref. 36.)

The strong effect of molecular chains on the viscoelastic behavior of polymeric solutions, even in the most dilute ones, is shown in Figure 8.24 (37). Here the recoverable compliance of a very dilute solution of polystyrene of weight-average molecular weight 860,000 in tri-*m*-tolyl phosphate is compared with that of the solvent. It is noteworthy that the value of the steady-state compliance for the solvent is 10^{-9} cm²/dyn while that of the very dilute solution ($w_{\text{pol}} = 0.001$) is nearly 10^{-3} cm²/dyn. In other words, a very small fraction of the molecular chains are responsible for the fact that the steady-state compliance of the solution is more than 10^6 times that of the solvent.

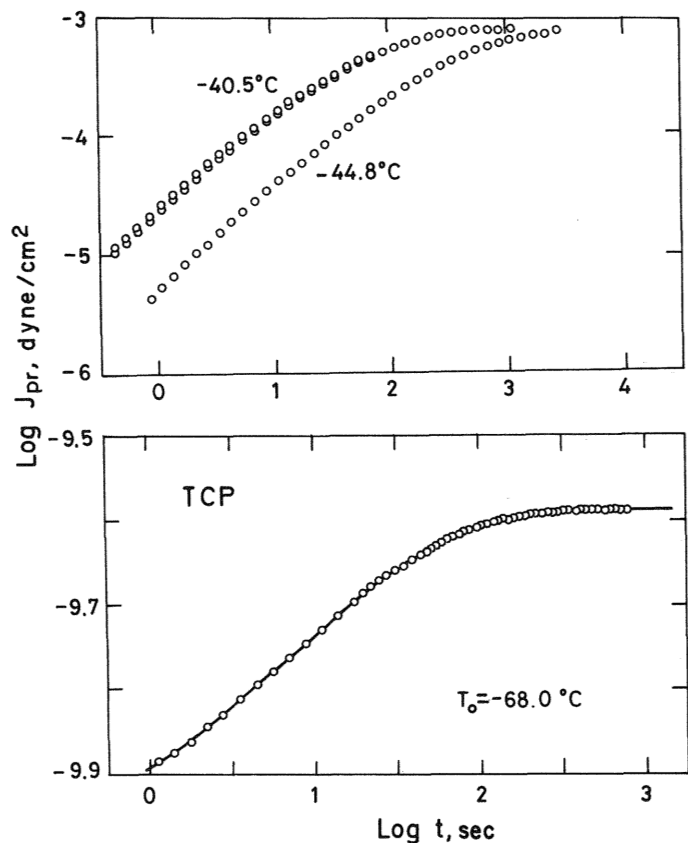


Figure 8.24 Double logarithmic plots of the recoverable compliance function in the time domain for (a) a dilute (0.1%, w/w) solution of polystyrene in tri-*m*-tolyl phosphate (b) tri-*m*-tolyl phosphate. (From Ref. 37.)

Figure 8.25 shows double logarithmic plots of both $J(t)$ and $J_r(t)$ against t for several concentrations. The plots indicate that for the solutions in which the weight fraction of polymer is larger than 0.01, the value of J_e^0 decreases, reaching a minimum value for the pure polymer. The cause of this behavior lies in the fact that an increase in concentration increases the overlapping of the molecular domains, thus favoring the formation of entangled networks. Entanglement formation prevents the chains from totally complying with the external perturbation as would be the case if the chains were unentangled, and as a consequence J_e^0 decreases with increasing concentration.

In the glass-like zone, the values of the creep compliance function seem to be independent of the concentration; however, the changes that take place in the values of $J(t)$ in the transition zone are larger the lower the concentration. The length of the plateau increases with the concentration, and the plateau and terminal zones merge into a single region at low concentrations. The location of the isotherms on the time scale is shifted to shorter chains as the concentration decreases.

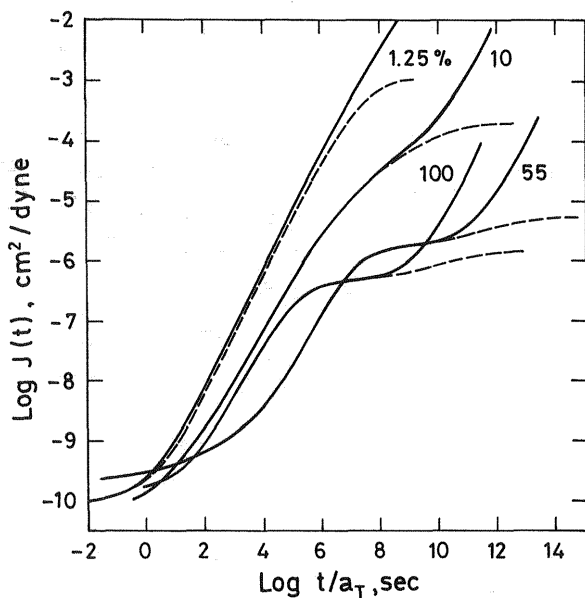


Figure 8.25 Double logarithmic plots showing the master curves of $J(t)$ (continuous line) and $J(t) - t/\eta$ (dashed line) in the time domain for polystyrene (100%) and several concentrations of polystyrene ($M_n = 860,000$) in tri-*m*-tolyl phosphate. The curves are arbitrarily located in the time domain. (From Ref. 14.)

The formation of an entangled structure depends on the interactions between segments of neighboring chains that partially or totally share the same domain. The probability of these interactions is proportional to the square of the concentrations of polymer in the solution, and therefore the molecular weight between entanglements should vary with the square of the concentration. In the same way, the steady-state compliance will be larger, the lower is the density of entanglements in the network. Based on this simple reasoning, the following scaling laws are expected for the concentration dependence of several important viscoelastic functions (2,8):

$$J_N^0 \sim C^{-2}; \quad J_e^0 \sim C^{-2}; \quad M_e \sim C^{-2}; \quad G_N^0 = \frac{1}{J_N^0} \sim C^2 \quad (8.69)$$

The plots of $\log J_N^0$ and $\log J_e^0$ against $\log C$ for semidilute and concentrated solutions of polystyrene in tri-*m*-tolyl phosphate, shown in Figure 8.26, give straight lines with a slope of -2 , in agreement with the relationships given above.

As in all amorphous systems, the viscosity of polymer solutions undergoes an anomalous increase in the vicinity of the glass transition temperature. Illustrative plots showing the temperature dependence of the viscosity of different concentrations are shown in Figure 8.14. As a consequence of the effect of the dilution on the glass transition temperature, a decrease in concentration shifts the curves to lower temperatures. Because the diluents increase the molecular weight between entanglements, the critical molecular weight at which the scaling law $\eta \sim M^{3.4}$ holds is shifted to higher values of M as the concentration decreases. Illustrative results showing the dependence of viscosity on concentration are shown in Figure 8.27 (38).

8.8 EFFECTS OF CROSS-LINKING ON THE VISCOELASTIC FUNCTIONS

The effects of cross-linking on the viscoelastic functions in the transition zone are rather small unless the cross-link density is so high that it hinders the segmental motions involved in the development of this region. In any case, cross-links shift the transition region to larger times or lower frequencies.

Cross-linking effects are more important in the plateau and terminal zones. For moderately cross-linked polymers, such as soft vulcanized rubbers, the equilibrium modulus is similar in magnitude to the entanglement network modulus before vulcanization. In some cases, however, the former modulus may be higher by as much as a factor of 2 than the latter one, thus

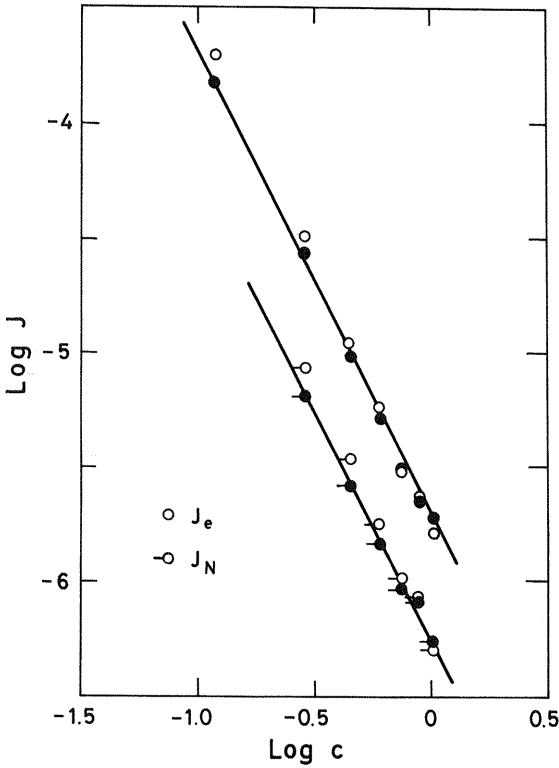


Figure 8.26 Double logarithmic plots showing the concentration dependence of both the creep compliance and the relaxation modulus at the plateau. (From Ref. 8.)

implying that the entanglements may outnumber the cross-links. In these cases cross-links do not contribute too much to the plateau, but they strongly affect the viscoelastic behavior in the terminal zone. Time-dependent processes in this region may proceed for one day or more, so the attainment of elastic equilibrium is difficult. Even when the degree of cross-linking is high, progressive changes in stress and strain are detected over relatively long periods. In some cases chemical degradation may occur, and in this situation it is necessary to distinguish between stress relaxation and loss stress due to chemical degradation.

A great number of experiments in soft cross-linked rubbers are made at substantial finite deformations. There are experimental grounds suggesting that the relaxation stress can be factored into a function of time and a function of strain (39,40),

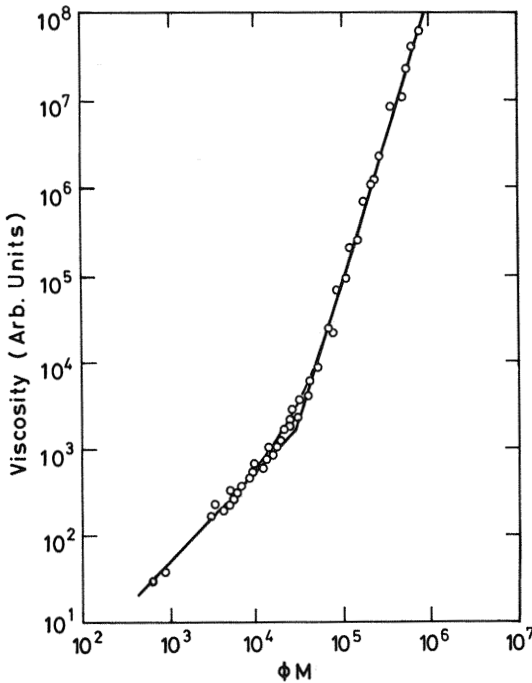


Figure 8.27 Double logarithmic plot of viscosity versus the product of polymer concentration (ϕ) and molecular weight (M) of polystyrene, in the concentration range 25–100%. The curves were adjusted to a constant friction coefficient ζ . (From Ref. 38.)

$$\sigma_{11}(t, \lambda) = \Gamma(\lambda)E(t) \quad (8.70)$$

where $\lambda (= 1 + \varepsilon)$ is the extension ratio and $\Gamma(\lambda)$ is a function of λ that approaches $\lambda - 1$ as ε approaches zero. Relaxation experiments performed at different finite deformations permit the empirical determination of the function $\Gamma(\lambda)$, and further extrapolation to $\lambda \rightarrow 1$ leads to the determination of $E(t)$. Though the equilibrium tensile relaxation modulus cannot be obtained directly from these measurements, it can be estimated from the following empirical equation, which gives a good account of many such experimental data (41):

$$E(t) = E_e[1 + (t/t_m)^{-m}] \quad (8.71)$$

The unknown values of this equation can be estimated by finding the value of E_e that best fits the double logarithmic plot of $[E(t) - E_e]/E_e$ against t to a straight line. The values of m and $m \log t_m$ can then be obtained from the slope and the intercept, respectively. By taking into account that Poisson's ratio is nearly 1/2 in this region [see Eq. (5.89)], the values of $G(t)$ are approximately equal to $E(t)/3$.

In the same way, the difficulty involved in obtaining the equilibrium shear compliance from the extrapolation of creep experiments to infinite time leads to the determination of J_e by means of an expression analogous to Eq. (8.71) (42),

$$J(t) = J_e \left[1 + \left(\frac{t}{t_m} \right)^{-m} \right]^{-1} \quad (8.72)$$

The values of J_e , m , and t_m were obtained by determining the value of J_e that best fits the double logarithmic plots of $[J_e - J(t)]/J(t)$ vs. t to a straight line. It has been found that the values of J_e , from creep and $3/E_e$ from the stress relaxation are in rather good agreement for several rubbers.

It is important to discuss, at least qualitatively, the variation of G_N and G_e for cross-linked rubbers as a function of the number of cross-linking points. According to Eq. (8.55), $G_N (= 1/J_N)$ can be written as

$$G_N = \frac{1}{J_N} = g_N \nu_N RT \quad (8.73)$$

where g_N is a factor in the vicinity of unity and ν_N is the moles of network strands per unit volume terminated by entanglements and cross-links. For uncross-linked polymers, $G_e = 0$ and $G_N = G_N^0$. However, after the gel point has been reached in the cross-linking reaction, G_N increases more rapidly than G_e as the cross-link density increases because cross-links and trapped entanglements contribute to the former modulus whereas the latter is augmented only by cross-links. A schematic representation of trapped entanglements is shown in Figure 8.28 (43). A degree of cross-linking can be reached at which all the entanglements become trapped and contribute as much to G_e as to G_N . In this situation $G_e = G_N$ and the plateau region disappears. The evolution of G_N and G_e at different stages of cross-linking is shown in Figure 8.29 (Ref. 7, p. 445).

For densely cross-linked networks, values of equilibrium modulus higher than 10^7 Pa are obtained. In this case the molecular weight between cross-linking points may become so low that Gaussian distributions of the segments between cross-links can no longer be assumed. The fact, however, that the modulus is approximately proportional to absolute temperature

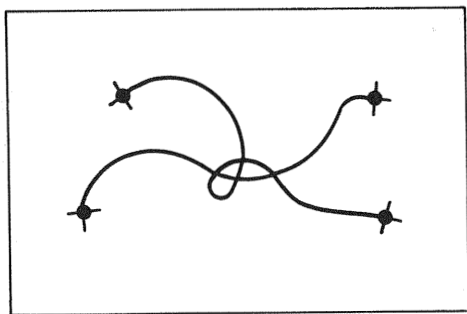


Figure 8.28 Schematic representation of trapped entanglements. (From Ref. 43.)

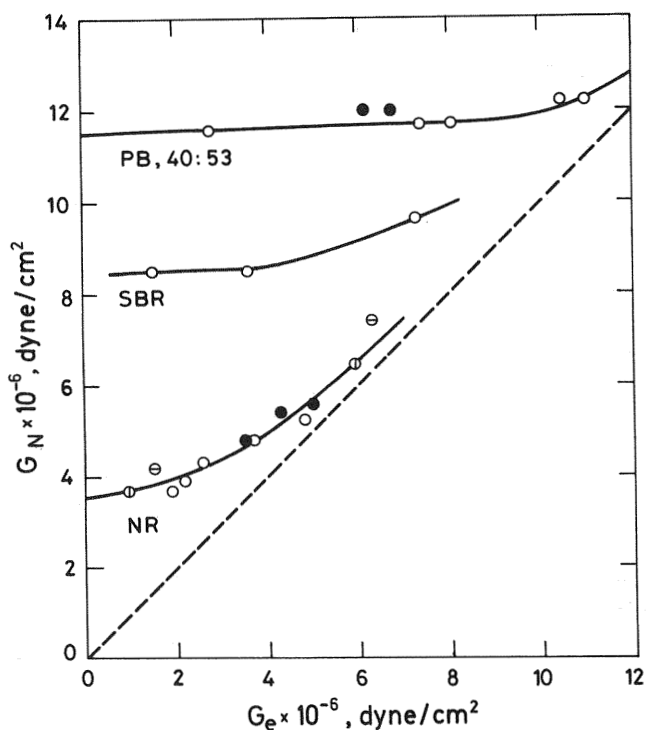


Figure 8.29 G_N plotted against G_e for three rubbers [polybutadiene (PB), styrene-butadiene copolymer (SBR), and natural rubber (NR)] at different stages of cross-linking by (O) dicumyl peroxide and (●) sulfur. (From Ref. 44.)

suggests that the storage energy in these networks is mainly based on an entropic effect.

PROBLEM SETS

Problem 8.1

The molecular weight between entanglements of a homogeneous polymer-diluent mixture in which the concentration of diluent is 0.15 g/cm^3 is $20,000 \text{ g/mol}$. Make a rough estimation of the solvent that should be added to 100 cm^3 of the mixture to give a molecular weight between entanglements of $25,000 \text{ g/mol}$.

Solution 8.1

According to Eq. (8.69), for narrow molecular weight distributions, $M_e \approx C^{-2}$, that is, $M_e = KC^{-2}$ where K is a constant. Then the polymer concentration in the mixture will be

$$C = 0.85 \times (20,000/25,000)^{1/2} \text{ g/cm}^3 = 0.76 \text{ g/cm}^3$$

And the final volume is given by

$$V = 100 \times (0.85/0.76) = 111.8 \text{ cm}^3$$

Hence, the volume of diluent that must be added is $111.8 - 100 = 11.8 \text{ cm}^3$.

Problem 8.2

A fraction of poly(methyl acrylate) presents maximum damping at 0.50 Hz at 25°C . Make a rough estimation of the diluent that must be added to shift the maximum damping to 100 Hz at the same temperature. The glass transition temperatures of the diluent and the polymer are -70°C and 10°C , respectively, and their expansion coefficients are $8.5 \times 10^{-4} \text{ K}^{-1}$ and $4.2 \times 10^{-4} \text{ K}^{-1}$, respectively.

Solution 8.2

According to Doolittle relation,

$$\ln \frac{\tau_d}{\tau_p} = \ln \frac{f_p}{f_d} = B \left(\frac{1}{\Phi_d} - \frac{1}{\Phi_p} \right) \quad (\text{P8.2.1})$$

where the symbols τ and f refer to the relaxation time and frequency (in Hz), respectively, while the subscripts p and d refer to pure and dilute polymer, respectively. Let us assume further that Φ/B at the respective T_g values for the polymer and the diluent is 0.025 and $B = 1$. Then

$$\Phi_p = 0.025 + 4.2 \times 10^{-4}(25 - 10) = 0.0313$$

$$\Phi_d = [0.025 + 8.5 \times 10^{-4}(25 + 70)]v_1 + 0.0313(1 - v_1)$$

where v_1 is the volume fraction of diluent. Hence

$$\ln 100 = \ln 0.5 - \left[\frac{1}{0.1057v_1 + 0.0313(1 - v_1)} - \frac{1}{0.0313} \right]$$

From this equation one obtains $v_1 = 0.083 \text{ cm}^3/\text{cm}^3$. Therefore the addition of diluent to a concentration of 8.3% would produce roughly the desired result.

Problem 8.3

Consider a polymer that presents a maximum in damping at 10 Hz and 50°C . If the glass transition temperature of the polymer is 20°C , the thermal expansion coefficient $\beta = (1/\nu)(\partial\nu/\partial T)_p$ is equal to $4.5 \times 10^{-4} \text{ K}^{-1}$ in the range of temperatures considered, and the compressibility coefficient, $\kappa = 1/\nu (\partial\nu/\partial p)_T$, is roughly constant and equal to $8.5 \times 10^{-11} \text{ cm}^{-2}/\text{dyn}$ in the interval 1–50 atm, calculate the frequency at which the maximum will appear at 20 atm and 50°C . Note $\Phi_g/B = 0.024$ for this polymer and ν is the specific volume.

Solution 8.3

Since the lower the free volume the larger the relaxation time, the effect of the pressure on τ can be interpreted in terms of the Doolittle equation. Accordingly,

$$\tau_0 = \exp\left(\frac{B}{\Phi_0}\right); \quad \tau_P = \exp\left(\frac{B}{\Phi_P}\right) \quad (\text{P8.3.1})$$

where the subscripts 0 and P refer, respectively, to the pressure at 1 and P atm.

Hence,

$$\ln \frac{\tau_0}{\tau_P} = \ln \frac{f_P}{f_0} = B \left(\frac{1}{\Phi_0} - \frac{1}{\Phi_P} \right) \quad (\text{P8.3.2})$$

where f is the frequency in Hz. The values of Φ_0 and Φ_P can be written as

$$\begin{aligned} \Phi_0 &= 0.024 + (4.5 \times 10^{-4})(50 - 20) = 0.0375 \\ \Phi_P &= 0.0375 - (8.5 \times 10^{-11})(20 - 1) \times 9.8 \times 10^5 = 0.0359 \end{aligned} \quad (\text{P8.3.3})$$

From Eqs. (P8.3.2) and (P8.3.3), $f_P = 3.24$ Hz; that is, the damping maximum shifts from 10 to 3.2 Hz when the pressure increases from 1 to 20 atm.

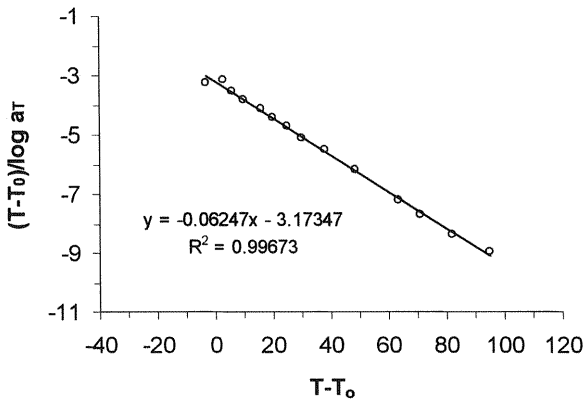
Problem 8.4

The shift factors corresponding to different isotherms representing the recovery creep compliance function of a solution of polystyrene in tri-*m*-tolyl phosphate are given in the table. Find the parameters of the WLF equation.

$T(^{\circ}\text{C})$	$(\log a_T)_{\text{exp}}$
17.0	0.93
20.0	0.00
23.0	-0.96
26.0	-1.70
30.1	-2.65
36.2	-3.94
40.0	-4.52
45.0	-5.29
50.0	-5.90
58.0	-6.90
68.3	-7.80
83.3	-8.80
90.8	-9.20
102.0	-9.80
115.0	-10.60

Solution 8.4

The reference temperature T_0 is 20°C . According to Eq. (8.38), plotting $(T - T_0)/(\log a_T)$ against $T - T_0$ gives the straight line of Figure P8.4.1. From

**Figure P8.4.1**

the slope ($m = -0.0625$) and the intercept ($I = -3.173$) and taking into account that $m = -1/C_1$ and $I = -C_2/C_1$, we find that $C_1 = 16.00$ and $C_2 = 50.80$ K.

Problem 8.5

The data in Table P8.5.1 and Figure P8.5.1 correspond to the system polystyrene (PS) + tricresyl phosphate (TCP) 70% (in PS) at 20°C . Determine the strain at 45°C at

$$t = 1, 10^2, 10^4, \text{ and } 10^6 \text{ s}$$

for a stress of $\sigma = 0.1$ MPa, knowing that the shift factor and viscosity are given by the expressions

$$\log a_T = \frac{785}{T - 239.8} - 15.64; \quad \log \eta = \frac{790}{T - 243} + 1.69$$

Solution 8.5

According to the time-temperature superposition principle,

$$J_r(t, 318 \text{ K}) = J_r(t/a_{T_0}, 290 \text{ K})$$

where for $45^\circ\text{C} = 318 \text{ K}$

Table P8.5.1

$\log t$ (s)	$\log J_r(t)$ (Pa^{-1})	$\log t$ (s)	$\log J_r(t)$ (Pa^{-1})	$\log t$ (s)	$\log J_r(t)$ (Pa^{-1})
-1	-9.81	4.0	-8.215	9.0	-5.88
-0.8	-9.80	4.2	-8.05	9.2	-5.87
-0.6	-9.785	4.4	-7.89	9.4	-5.855
-0.4	-9.770	4.6	-7.73	9.6	-5.84
-0.2	-9.745	4.8	-7.54	9.8	-5.82
0	-9.72	5.0	-7.37	10.0	-5.80
0.2	-9.69	5.2	-7.19	10.2	-5.785
0.4	-9.67	5.4	-7.01	10.4	-5.765
0.6	-9.637	5.6	-6.83	10.6	-5.74
0.8	-9.60	5.8	-6.68	10.8	-5.72
1.0	-9.57	6.0	-6.53	11.0	-5.69
1.2	-9.53	6.2	-6.41	11.2	-5.67
1.4	-9.48	6.4	-6.30	11.4	-5.645
1.6	-9.44	6.6	-6.215	11.6	-5.62
1.8	-9.38	6.8	-6.14	11.8	-5.60
2.0	-9.32	7.0	-6.085	12.0	-5.57
2.2	-9.255	7.2	-6.04	12.2	-5.54
2.4	-9.18	7.4	-6.00	12.4	-5.52
2.6	-9.10	7.6	-5.98	12.6	-5.51
2.8	-9.05	7.8	-5.96	12.8	-5.49
3.0	-8.90	8.0	-5.95	13.0	-5.485
3.2	-8.795	8.2	-5.94	13.2	-5.48
3.4	-8.67	8.4	-5.925	13.4	-5.48
3.6	-8.525	8.6	-5.915	13.6	-5.48
3.8	-8.37	8.8	-5.90		

$$\log a_T = \left(\frac{785}{T - 239.8} - 15.64 \right) = -5.602$$

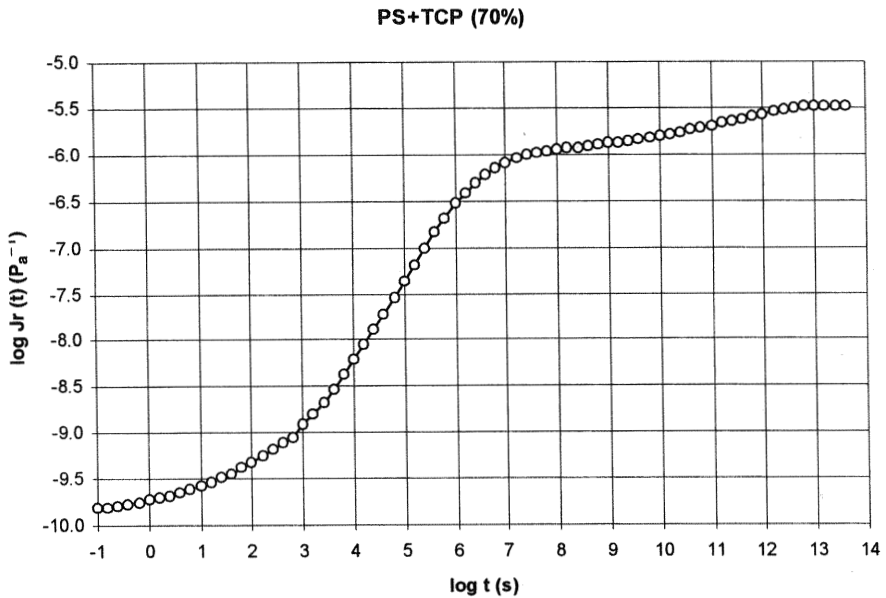
which gives

$$a_T = 10^{-5.602}$$

Hence,

$$J_r(t, 318 \text{ K}) = J_r(10^{5.602} t, 290 \text{ K})$$

On the other hand,

**Figure P8.5.1**

$$J(t) = J_r(t) + \frac{t}{\eta}$$

where

$$\log \eta = \frac{790}{T - 243} + 1.69 \quad \text{and} \quad \log \eta(290 \text{ K}) = 18.499$$

As a consequence,

$$J(t, 318 \text{ K}) = J\left(\frac{t}{a_T}, 290 \text{ K}\right) = J_r\left(\frac{t}{a_T}, 290 \text{ K}\right) + \frac{t}{a_T \eta(290 \text{ K})}$$

Note that for all the times considered in this problem, except $t = 10^6$ s, the viscosity contribution to the compliance is negligible, so that in the present case one has $J \cong J_r$ for $t < 10^4$ s.

According to the values of the compliance given in Table P8.5.1, we obtain

$$t = 1 \text{ s:}$$

$$J(1 \text{ s}, 318 \text{ K}) = J(10^{5.602} \text{ s}, 290 \text{ K}) = 10^{-6.82} \text{ Pa}^{-1}; \quad \varepsilon = J\sigma = 10^{-1.82} = 0.015$$

$$t = 10^2 \text{ s:}$$

$$J(10^2 \text{ s}, 318 \text{ K}) = J(10^{7.602} \text{ s}, 290 \text{ K}) = 10^{-5.98} \text{ Pa}^{-1}; \quad \varepsilon = J\sigma = 10^{-0.98} = 0.105$$

$$t = 10^4 \text{ s:}$$

$$J(10^4 \text{ s}, 318 \text{ K}) = J(10^{9.602} \text{ s}, 290 \text{ K}) = 10^{-5.84} \text{ Pa}^{-1}; \quad \varepsilon = J\sigma = 10^{-0.84} = 0.145$$

$$t = 10^6 \text{ s:}$$

$$\begin{aligned} J(10^6 \text{ s}, 318 \text{ K}) &= J(10^{11.602}, 290 \text{ K}) \\ &= 10^{-5.62} + \frac{10^6}{10^{-5.62} \times 10^{12.897}} = 10^{-5.60} \text{ Pa}^{-1}; \quad \varepsilon = J\sigma = 10^{-0.60} = 0.251 \end{aligned}$$

Problem 8.6

The shear modulus G' of a polymer at $T_g + 20$ is given by

$$G'(\omega, T_g + 20) = 10^8 \text{ Pa}$$

Assuming that the time-temperature superposition principle holds, estimate the frequency at which the modulus at $T_g + 50$ is equal to the modulus at $T_g + 20$. Assume that $T_g = 100^\circ\text{C}$.

Solution 8.6

From Eq. (8.40),

$$\frac{\Phi_g}{B} = \frac{T_g - T_\infty}{m} \cong 0.025 \quad (\text{P8.6.1})$$

By assuming that $T_\infty = T_g - 50$, one has $m \cong 2000$. Then

$$\ln \tau = A + \frac{m}{T - T_\infty} \quad (\text{P8.6.2})$$

and

$$\ln a_T = \ln \frac{\tau_1}{\tau_2} = m \left(\frac{1}{T_1 - T_\infty} - \frac{1}{T_2 - T_\infty} \right) \quad (\text{P8.6.3})$$

Hence,

$$\ln \frac{\omega_2}{\omega_1} = 2000 \times \left(\frac{1}{393 - 323} - \frac{1}{423 - 323} \right) \cong 6.35 \quad (\text{P8.6.4})$$

and

$$\omega_2 = 572\omega_1 \quad (\text{P8.6.5})$$

Problem 8.7

The following data were obtained from a viscoelastic experiment in the plateau of a polymer at 400 K.

$\log \omega$	G'' (Pa)
-3	1.8×10^4
-2.5	3.2×10^4
-2	7×10^4
-1.5	1.35×10^5
-1	1.4×10^5
-0.5	1.1×10^5
0	9.5×10^4

Estimate M_c if the density of the polymer is $\rho = 1.1 \times 10^3 \text{ kg/m}^3$.

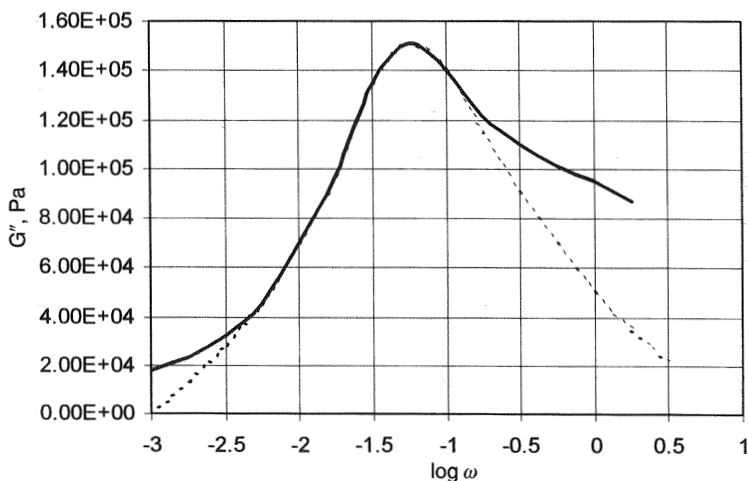


Figure P8.7.1

Solution 8.7

According to Eq. (8.60),

$$G_N^0 = \frac{2}{\pi} \int_{-\infty}^b G'' d \ln \omega \quad (\text{P8.7.1})$$

After smoothing the curve of figure P8.7.1 to avoid the contributions of the glass — rubber relaxation, one obtains by numerical integration:

$$G_N^0 \cong \frac{2 \times 2.303}{3.142} \int_{-\infty}^{0.7} G'' d \log \omega \cong 4.9 \times 10^5 \text{ Pa}$$

According to Eq. (8.54),

$$M_e = \frac{\rho RT}{G_N^0} = \frac{1.1 \times 10^3 \times 8.34 \times 400}{4.9 \times 10^5} = 7.45 \text{ kg/mol}$$

By taking into account that $M_c \cong 2M_e$, finally one has $M_c = 14,900 \text{ g/mol}$.

Problem 8.8

A sample of poly(methyl acrylate) (PMA) has a T_g of 8°C , and the constants for its WLF equation are $C_1 = 18.1$ and $C_2 = 45.0\text{K}$. Find the fractional change in its viscosity per degree at 50°C (data taken from Ref. 7).

Solution 8.8

The required percentage change can be obtained by deriving an expression that relates the viscosity to temperature, as for example the Williams-Landel-Ferry equation.

Actually,

$$\log \frac{\eta_T}{\eta_{T_g}} = -\frac{18.1(T - T_g)}{45.0 + T - T_g} \quad (\text{P8.8.1})$$

Taking natural logarithms and deriving the resulting equation with respect to temperature gives

$$\frac{d \ln \eta_T}{dT} = -\frac{1875.8}{(45.0 + T - T_g)^2} \quad (\text{P8.8.2})$$

and by substitution of the values proposed, we find

$$\frac{d \ln \eta_T}{dT} = -0.2478 \text{ K}^{-1} \quad (\text{P8.8.3})$$

That is, the percentage is -24.78% .

REFERENCES

1. E Riande, DJ Plazek, H Markovitz. Unpublished results.
2. JD Ferry. *Viscoelastic Properties of Polymers*. 3rd ed. New York: Wiley-Interscience, 1980.
3. H Markovitz. *Lectures in Linear Viscoelasticity: An Introduction*. Pittsburgh: Carnegie-Mellon University, 1978.
4. JJ. Aklonis, WJ MacKnight. *Introduction to Polymer Viscoelasticity*. 2nd ed. New York: Wiley, 1980.
5. DJ Plazek. *J. Phys Chem* 69: 3480, 1965.
6. E Catsiff, AV Tobolsky. *J Polym Sci* 19: 111, 1956.
7. JD Ferry. *Viscoelastic Properties of Polymers*. 2nd ed. New York: Wiley, 1970, Chap. 11.
8. DJ Plazek, E Riande H Markovitz, N Raghupathi. *J Polym Sci Polym Phys Ed* 17: 2189, 1979.
9. ER Fitzgerald, LD Grandine, JD Ferry. *J Appl Phys*. 24: 650, 1953.
10. AK Doolittle, BK Doolittle. *J Appl Phys* 28: 901, 1957.
11. H Vogel. *Z Phys* 22: 645, 1921.
12. GS Fulcher. *J Am Ceram Soc* 8: 339, 1925.
13. G Tammann, WZ Hesse. *Anorg Allgem Chem*. 156: 245, 1926.
14. E Riande, H Markovitz, DJ Plazek, N Raghupathi. *J Polym Sci C50*: 405, 1975.
15. ML Williams, RF Landel, JD Ferry. *J Am Chem Soc* 73: 701, 1955.
16. DJ Plazek, VM O'Rourke. *J Polym Sci A2* 9: 209, 1971.
17. WK Moonan, NW Tschoegl. *J Polym Sci Polym Phys Ed* 23: 623, 1985.
18. EN da C Andrade. *Proc Roy Soc. (Lond)* A84: 1, 1910; A90: 339, 1914.
19. DR Reid. *Br Plast* 32: 460, 1959.
20. DJ Plazek, V Tan, VM O'Rourke. *Rheol Acta* 13: 367, 1974.
21. JD Ferry, WC Child Jr, R Zand, DM Stern, ML Williams, RF Lande. *J Colloid Sci* 12: 53, 1957.
22. WC Child Jr, JD Ferry. *J Colloid Sci* 12: 327, 1957.
23. WC Child Jr, JD Ferry. *J Colloid Sci* 12: 389, 1957.
24. DJ Plazek. *J Non-Cryst Solids* 131-133: 836, 1991.
25. S Onogi, T Masuda, K Kitagawa. *Macromolecules* 3: 109, 1970.
26. DJ Plazek. *J Colloid Sci* 15: 50, 1960.
27. DJ Plazek, W Danhauser, JD Ferry. *J Colloid Sci* 16: 101, 1961.
28. DJ Plazek. *J Polym Sci A2* 4: 745, 1966.
29. JF Sanders, JD Ferry, RH Valentine. *J Polym Sci A2* 6: 967, 1968.

30. TG Fox, PJ Flory. *J Appl Phys* 21: 581, 1950.
31. GC Berry, TG Fox. *Adv Polym Sci* 5: 261, 1968.
32. W Graessley. In: JE Mark, ed. *Physical Properties of Polymers* pp (55–96). Washington DC: American Chemical Society, 1984.
33. W Graessley. *Adv Polym Sci* 16: 1, 1974.
34. N Nemoto, H Odani, M Kurata. *Macromolecules* 5: 531, 1972.
35. W Graessley. Viscoelasticity and diffusion in entangled polymer melt. In M Nagasawa, ed. *Molecular Conformation and Dynamics of Macromolecules in Condensed Systems* pp (163–184). Amsterdam: Elsevier, 1988.
36. PG de Gennes. *Scaling Concepts in Polymer Physics*. 2nd ed. Ithaca NY: Cornell Univ Press, 1985, Chap. 3.
37. DJ Plazek, E Riande, H Markovitz. Unpublished results.
38. W Graessley. In: JJ Burke, V Weiss, eds. *Characterization of Materials in Research*. Syracuse, NY: Syracuse Univ Press, 1975.
39. AV Tobolsky, RD Andrews. *J Chem Phys* 13: 3, 1945.
40. RD Andrews, AV Tobolsky. *J Polym Sci* 7: 221, 1951.
41. R Chasset, P Thirion. In: JA Prins, ed. *Proceedings of a Conference on Physics of Non-Crystalline Solids*. Amsterdam: North-Holland, 1965, p 345.
42. RA Dickie, JD Ferry. *J Phys Chem* 70: 2594, 1966.
43. RG Mancke, RA Dickie, JD Ferry. *J Polym Sci A2* 6: 1783, 1968.

9

Retardation and Relaxation Spectra

9.1	Introduction	359
9.2	Formulation of Transient and Nontransient Relaxation Moduli in Terms of Relaxation Spectra	360
9.3	Formulation of Transient and Nontransient Compliance Functions in Terms of Retardation Spectra	362
9.4	Important Inequalities Among Viscoelastic Functions	365
9.5	Determination of Viscosity and Steady-State (Equilibrium) Compliance from Relaxation and Retardation Spectra	366
9.6	Comparison of Retardation and Relaxation Times	368
9.7	Determination of Spectra from Viscoelastic Functions Using First-Order Approximations	371
9.8	Approximations of Higher Order	375
9.9	Experimental Retardation and Relaxation Spectra	378
9.10	Approximate Relationships Between Viscoelastic Functions	383
	Problem Sets	384
	References	393

9.1 INTRODUCTION

The elastic and viscous mechanisms involved in the viscoelastic responses have traditionally been modeled by combining ideal elastic elements, represented by springs, and ideal viscous elements, represented by dashpots. We shall refer to this treatment in Chapter 10; here we use another approach,

based on the analysis of the experimental curves, to express the viscoelastic functions in terms of the retardation and relaxation spectra.

9.2 FORMULATION OF TRANSIENT AND NONTRANSIENT RELAXATION MODULI IN TERMS OF RELAXATION SPECTRA

It is an experimentally demonstrated fact that when a viscoelastic material undergoes a small shear deformation, the stress necessary to maintain the deformation evolves in such a way that $d\sigma/dt$ decreases as time increases. For a simple system we could express the velocity of response by the relation $d\sigma(t)/dt = -s\sigma(t)$. By integrating this equation we obtain

$$\sigma(t) = \sigma(0) \exp(-st) \quad (9.1)$$

which expresses the evolution of σ with time in the conditions of the experiment. By dividing the two sides of this equation by the deformation, we obtain the relationship

$$G(t) = G_0 \exp(-st) \quad (9.2)$$

Because st is dimensionless, s has the units of reciprocal time and is commonly expressed as $s = 1/\tau$. The parameter τ , called relaxation time, is taken to be the time at which $t = \tau$, that is, the time at which $G(t) = G_0/e$. This approximation, however, fails even for rather simple viscoelastic systems. In fact, the curve obtained for $G(t)$ using Eq. (9.2) drops much more rapidly than that corresponding to real systems (see Fig. 9.1). A better description of these systems is achieved by using a sum of exponentials (1–5), for example, $G(t) = \sum_i G_i \exp(-s_i t)$. By assuming that the relaxation times of the viscoelastic mechanisms involved in the relaxation process vary continuously between 0 and ∞ , the sum can be replaced by an integral in such a way that $G(t)$ may be considered the Laplace transform of an unknown function $N(s)$ (2). According to this,

$$G(t) = \int_0^{\infty} N(s) \exp(-st) ds = \mathcal{L}[N(s)] \quad (9.3)$$

This expression is customarily written in terms of the relaxation times, giving

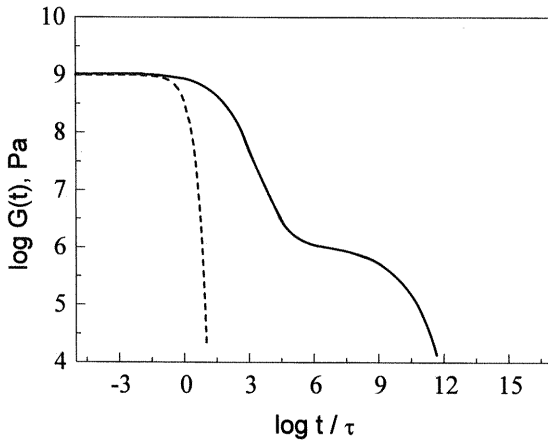


Figure 9.1 Relaxation modulus in the frequency domain for (---) a system with a single relaxation time and (—) a high molecular weight polymer.

$$G(t) = \int_0^{\infty} \frac{N(1/\tau)}{\tau} e^{-t/\tau} \frac{d\tau}{\tau} = \int_{-\infty}^{\infty} H(\tau) e^{-t/\tau} d \ln \tau \quad (9.4)$$

where $H(t) = N(1/\tau)/\tau$ is a priori an unknown function called the relaxation spectrum. $H d \ln \tau$ is defined as the contribution to rigidity of viscoelastic mechanisms associated with relaxation times whose logarithms lie in the range $\ln \tau$ to $\ln \tau + d \ln \tau$. For viscoelastic solids, Eq. (9.3) becomes

$$G(t) - G_e = \int_0^{\infty} N(s) e^{-st} ds = \mathcal{L}[N(s)] \quad (9.5)$$

which alternatively can be written as

$$G(t) = G_e + \int_{-\infty}^{\infty} H(\tau) e^{-t/\tau} d \ln \tau \quad (9.6)$$

Following the same procedure, the components of the complex relaxation modulus can be expressed in terms of the relaxation spectrum. Thus, by substituting the difference $G(t) - G_e$ given in Eq. (9.5) into Eq. (6.3), we obtain the following expression for the storage relaxation modulus:

$$\begin{aligned} G'(\omega) - G_e &= \omega \int_0^{\infty} N(s) ds \int_0^{\infty} \exp(-st) \sin(\omega t) dt \\ &= \omega \int_0^{\infty} N(s) \mathcal{L}(\sin \omega t) ds \end{aligned} \quad (9.7)$$

where \mathcal{L} represents the Laplace transform. Since $\mathcal{L}(\sin \omega t) = \omega/(\omega^2 + s^2)$, Eq. (9.7) becomes

$$\begin{aligned} G'(\omega) - G_e &= \int_0^\infty N(s) \frac{\omega^2}{\omega^2 + s^2} ds \\ &= \int_{-\infty}^\infty H(\tau) \frac{\omega^2 \tau^2}{1 + \omega^2 \tau^2} d \ln \tau \end{aligned} \quad (9.8)$$

The storage relaxation modulus for liquids is also given by Eq. (9.8) with $G_e = 0$. Proceeding in the same way for the loss modulus, one obtains

$$G''(\omega) = \omega \int_0^\infty N(s) ds \int_0^\infty \exp(-st) \cos \omega t dt = \omega \int_0^\infty N(s) \mathcal{L}(\cos \omega t) ds \quad (9.9)$$

Since $\mathcal{L}(\cos \omega t) = s/(s^2 + \omega^2)$, $G''(\omega)$ is finally given by

$$G''(\omega) = \omega \int_0^\infty N(s) \frac{s}{s^2 + \omega^2} ds = \int_{-\infty}^\infty H(\tau) \frac{\omega \tau}{1 + \omega^2 \tau^2} d \ln \tau \quad (9.10)$$

It should be noted that Eq. (9.10) is similar for solid and liquid viscoelastic systems.

9.3 FORMULATION OF TRANSIENT AND NONTRANSIENT COMPLIANCE FUNCTIONS IN TERMS OF RETARDATION SPECTRA

In the preceding section, it was assumed that a monotonously decreasing viscoelastic function, such as the relaxation modulus, can be expressed in terms of the Laplace transform of an unknown function $N'(s)$. Owing to the fact that the transient creep compliance function, $J(t)$, is a monotonous increasing function of time, the use of a strategy similar to the one used for the relaxation modulus requires that $J(t)$ be related to a decreasing function. By taking into account that for viscoelastic solids $J(t) = J_g + J_d \Psi(t)$ and $J_e = J_g + J_d \Psi(\infty)$, the difference between $\Psi(\infty)$ and $\Psi(t)$ can be written as (2)

$$\Psi(\infty) - \Psi(t) = \mathcal{L}\{N'(s)\} = \int_0^\infty N'(s) \exp(-st) ds \quad (9.11)$$

Obviously, $\Psi(0) = 0$, so according to Eq. (9.11), $\Psi(\infty)$ is given by

$$\Psi(\infty) = \int_0^{\infty} N'(s) ds \quad (9.12)$$

Therefore the memory function $\Psi(t)$ can be written as

$$\Psi(t) = \Psi(\infty) - \int_0^{\infty} N'(s)e^{-st} ds = \int_0^{\infty} N'(s)(1 - e^{-st}) dt \quad (9.13)$$

and therefore the compliance function is given by

$$J(t) = J_g + J_d\Psi(t) = J_g + J_d \int_0^{\infty} N'(s)(1 - e^{-st}) ds \quad (9.14)$$

The s parameter is the reciprocal of a time $\tau (= 1/s)$, called the retardation time, because it is associated with mechanisms of response that are delayed with respect to the perturbation. It should be pointed out that the relaxation times are somewhat lower than the retardation times. By writing Eq. (9.14) in terms of the retardation times, we obtain

$$\begin{aligned} J(t) &= J_g + J_d \int_0^{\infty} \frac{N'(1/\tau)}{\tau} \left(1 - e^{-t/\tau} \frac{d\tau}{\tau}\right) \\ &= J_g + \int_{-\infty}^{\infty} L(\tau)[1 - e^{-t/\tau}] d \ln \tau \end{aligned} \quad (9.15)$$

where $L(\tau) [= N'(1/\tau)/\tau]$ is the retardation spectrum. $L(\tau)$ represents the contribution to the compliance of the viscoelastic mechanism with retardation times whose logarithms lie in the range $\ln \tau$ to $\ln \tau + d \ln \tau$. In the case of liquids, the viscous contribution is independent of the entropic elastic contribution and $J(t)$ for viscoelastic liquids is given by

$$J(t) = J_g + \int_{-\infty}^{\infty} L(\tau)(1 - e^{-t/\tau})d \ln \tau + \frac{t}{\eta} \quad (9.16)$$

Let us now proceed with the development of the expressions for the components of the complex compliance function. According to Eqs. (6.23) and (9.11), the storage compliance function is given by

$$\begin{aligned}
J'(\omega) &= J_e^0 - \omega J_d \int_0^\infty [\Psi(\infty) - \Psi(t)] \sin \omega t \, dt \\
&= J_e^0 - \omega J_d \int_0^\infty N(s) \, ds \int_0^\infty \exp(-st) \sin \omega t \, dt \\
&= J_e^0 - \omega J_d \int_0^\infty N(s) \mathcal{L}(\sin \omega t) \, ds \\
&= J_e^0 - J_d \int_0^\infty N(s) \frac{\omega^2 s}{\omega^2 s + s^2} \, ds
\end{aligned} \tag{9.17}$$

where it has been taken into account that $\mathcal{L}(\sin \omega t) = \omega/(\omega^2 + s^2)$. Writing $s = 1/\tau$ and $L(\tau) = J_d N(1/\tau)/\tau$, Eq. (9.17) becomes

$$J'(\omega) = J_e^0 - \int_{-\infty}^\infty L(\tau) \frac{\omega^2 \tau^2}{1 + \omega^2 \tau^2} \, d \ln \tau \tag{9.18}$$

In the high frequency limit, Eq. (9.18) can be written as

$$\lim_{\omega \rightarrow \infty} J'(\omega) = J_g = J_e^0 - \int_{-\infty}^\infty L(\tau) \, d \ln \tau \tag{9.19}$$

The substitution of J_e^0 given by Eq. (9.19) into Eq. (9.18) leads to the expression

$$\begin{aligned}
J'(\omega) &= J_g + \int_{-\infty}^\infty L(\tau) \, d \ln \tau - \int_{-\infty}^\infty L(\tau) \frac{\omega^2 \tau^2}{1 + \omega^2 \tau^2} \, d \ln \tau \\
&= J_g + \int_{-\infty}^\infty L(\tau) \frac{1}{1 + \omega^2 \tau^2} \, d \ln \tau
\end{aligned} \tag{9.20}$$

which is another form of expression the real component of the complex creep compliance. This equation is also valid for solids.

To obtain the frequency dependence of the loss compliance function for liquids, use must be made of Eq. (6.29b). Accordingly

$$\begin{aligned}
J''(\omega) &= \frac{1}{\omega \eta} + \omega J_d \int_0^\infty [\Psi(\infty) - \Psi(t)] \cos \omega t \, dt \\
&= \frac{1}{\omega \eta} + \omega J_d \int_0^\infty N(s) \mathcal{L}(\cos \omega t) \, ds \\
&= \frac{1}{\omega \eta} + J_d \omega \int_0^\infty N(s) \frac{s}{s^2 + \omega^2} \, ds
\end{aligned} \tag{9.21}$$

Finally, writing s and $N(s)$ in terms of τ and $L(\tau)$, Eq. (9.21) becomes

$$J''(\omega) = \frac{1}{\omega\eta} + \int_{-\infty}^{\infty} L(\tau) \frac{\omega\tau}{1 + \omega^2\tau^2} d \ln \tau \quad (9.22)$$

The limit $n \rightarrow \infty$ leads this expression to the equation

$$J''(\omega) = \int_{-\infty}^{\infty} L(\tau) \frac{\omega\tau}{1 + \omega^2\tau^2} d \ln \tau \quad (9.23)$$

which describes the frequency dependence of the loss compliance for solids.

9.4 IMPORTANT INEQUALITIES AMONG VISCOELASTIC FUNCTIONS

Some important inequalities among viscoelastic functions can be developed by analyzing their mathematical expressions. For example, the difference between $G'(\omega)$ and $G(t = 1/\omega)$ can be written as (1,2)

$$G'(\omega) - G\left(\frac{1}{\omega}\right) = \int_{-\infty}^{\infty} H(\tau) \left[\frac{\omega^2\tau^2}{1 + \omega^2\tau^2} - e^{-1/\omega\tau} \right] d \ln \tau \quad (9.24)$$

Owing to the fact that for any value of $\omega\tau > 0$, $\omega^2\tau^2/(1 + \omega^2\tau^2) > e^{-1/\omega\tau}$, the two alternative inequalities between transient and dynamic relaxation functions are obtained:

$$G'(\omega) > G\left(\frac{1}{\omega}\right); \quad G(t) < G'\left(\frac{1}{t}\right) \quad (9.25)$$

In the same way, the fact that

$$J'(\omega) - \left[J\left(\frac{1}{\omega}\right) - \frac{1}{\omega\eta} \right] = \int_{-\infty}^{\infty} L(\tau) \left[e^{-1/\omega\tau} - \frac{\omega^2\tau^2}{1 + \omega^2\tau^2} \right] d \ln \tau < 0 \quad (9.26)$$

leads to the following inequalities between compliance functions:

$$J'(\omega) < J\left(\frac{1}{\omega}\right) - \frac{1}{\omega\eta}; \quad J(t) - \frac{t}{\eta} > J'\left(\frac{1}{t}\right) \quad (9.27)$$

Finally, from Eq. (6.21a) one obtains

$$J'(\omega) < \frac{1}{G'(\omega)}; \quad G'\left(\frac{1}{t}\right) < \frac{1}{J'(1/t)} \quad (9.28)$$

Illustrative curves showing these inequalities for liquid viscoelastic systems are represented in Figures 9.2 and 9.3.

9.5 DETERMINATION OF VISCOSITY AND STEADY-STATE (EQUILIBRIUM) COMPLIANCE FROM RELAXATION AND RETARDATION SPECTRA

Methods have been described in preceding sections to relate J_e^0 and η to viscoelastic functions in limit conditions, for example, when $\omega \rightarrow 0$. In this section, the procedures to evaluate these parameters from the relaxation and retardation spectra are analyzed.

Both the steady-state compliance function, J_e^0 , and the equilibrium compliance, J_e , can readily be obtained from the retardation spectrum. Actually, by taking the limit of Eq. (9.20) in the limit $\omega \rightarrow 0$, the following relationship for J_e^0 and J_e is obtained:

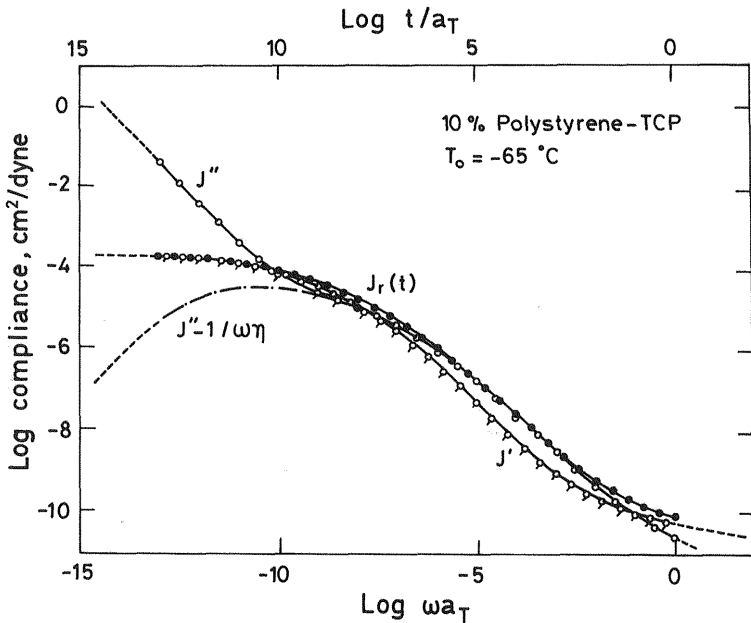


Figure 9.2 Double logarithmic plots of the creep compliance function $J(t)$ and the components J' and J'' of the complex compliance function for a 10% solution of polystyrene in tri-*m*-tolyl phosphate.

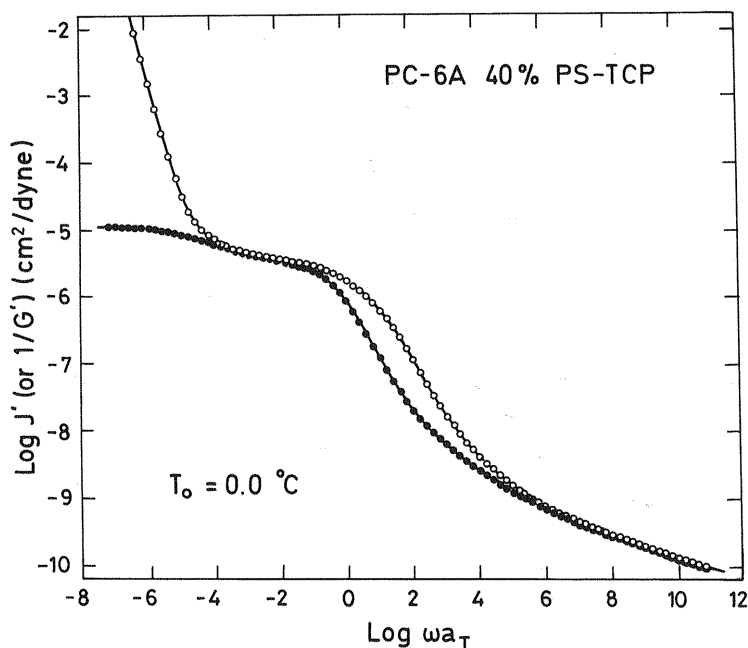


Figure 9.3 Double logarithmic plots of the storage compliance function (●) and the reciprocal of the storage modulus (○) for a 40% solution of polystyrene in tri-*m*-tolyl phosphate.

$$J_e^0 = J_e = \lim_{\omega \rightarrow 0} J'(\omega) = J_g + \int_{-\infty}^{\infty} L(\tau) d \ln \tau \cong \int_{-\infty}^{\infty} L(\tau) d \ln \tau \quad (9.29)$$

On the other hand, Eqs. (6.12) and (9.10) lead to the expression

$$\eta_0 = \lim_{\omega \rightarrow 0} \frac{G''(\omega)}{\omega} = \int_{-\infty}^{\infty} \tau H(\tau) d \ln \tau \quad (9.30)$$

which permits us to evaluate the viscosity at zero shear rate from the relaxation spectrum. The equilibrium recovery compliance function can also be readily expressed in terms of the relaxation spectrum. Thus by combining Eqs. (6.52), (9.8), and (9.30), the steady-state compliance function in terms of the relaxation spectrum is obtained:

$$J_e^0 = \frac{1}{\eta^2} \lim_{\omega \rightarrow 0} \frac{G'(\omega)}{\omega^2} = \frac{\int_{-\infty}^{\infty} H(\tau) \tau^2 d \ln \tau}{\eta^2} = \frac{\int_{-\infty}^{\infty} H(\tau) \tau^2 d \ln \tau}{\left[\int_{-\infty}^{\infty} H(\tau) \tau d \ln \tau \right]^2} \quad (9.31)$$

This equation also allows us to determine the mean relaxation time from η and J_e^0 . Actually, the mean relaxation time, $\langle\tau\rangle$, can be expressed as

$$\langle\tau\rangle = \frac{\int_0^\infty H(\tau)\tau \, d\tau}{\int_0^\infty H(\tau) \, d\tau} = \frac{\int_{-\infty}^\infty H(\tau)\tau^2 \, d \ln \tau}{\int_{-\infty}^\infty H(\tau)\tau \, d \ln \tau} \quad (9.32)$$

Combining Eqs. (9.31) and (9.32) gives

$$\langle\tau\rangle = \eta_0 J_e^0 \quad (9.33)$$

This equation indicates that the mean relaxation time is the product of two terminal viscoelastic functions, the zero shear rate viscosity and the steady-state compliance. The mean relaxation time can also be expressed in terms of the relaxation modulus by means of the expression

$$\langle\tau\rangle = \frac{\int_0^\infty tG(t) \, dt}{\int_0^\infty G(t) \, dt} = \eta_0 J_e^0 \quad (9.34)$$

where use was made of Eq. (6.53).

9.6 COMPARISON OF RETARDATION AND RELAXATION TIMES

The Laplace transform of the relaxation modulus is given by

$$\bar{G}(s) = \int_0^\infty G(t)e^{-st} \, dt \quad (9.35)$$

For small values of s , the exponential e^{-st} can be expanded in series so that Eq. (9.35) becomes

$$\bar{G}(s) = \int_0^\infty G(t)(1 - st + \dots) \, dt \quad (9.36)$$

By taking into account Eqs. (9.34) and (6.45), Eq. (9.36) can be written as

$$s\bar{G}(s) = \eta_0 s(1 - \langle\tau\rangle s + \dots) \quad (9.37)$$

where $\langle\tau\rangle$ is the mean relaxation time. This expression leads to the equation

$$G^*(\omega) = i\omega\eta_0(1 - \langle\tau\rangle i\omega + \dots) \quad (9.38)$$

which describes the behavior of the complex relaxation modulus at low frequencies. For example, $G'(\omega) \sim \omega^2$ and $G''(\omega) \sim \omega$, in agreement with Eqs. (6.45) and (6.46). Since $J^*(\omega) = 1/G^*(\omega)$, the complex creep compliance function is given by

$$J^*(\omega) = \frac{1}{i\omega\eta_0} + \frac{\langle\tau\rangle}{\eta_0} + \dots \quad (9.39)$$

The transform of J has a pole at $s = 0$,

$$\bar{J}(s) = \frac{1}{\eta_0} \left(\frac{1}{s^2} + \frac{\langle\tau\rangle}{s} + \dots \right) \quad (9.40)$$

The inverse of this transform gives the expression

$$J(t) = \frac{1}{\eta_0} (t + \langle\tau\rangle + \dots) \quad (9.41)$$

which describes the behavior of the creep compliance function at long times. Equation (9.41) suggests that the mean relaxation time and the viscosity can be obtained from the slope and the intercept with the abscissas axis, respectively, of the straight line drawn through the experimental values of $J(t)$ at long times (see Fig. 9.4).

In order to compare the relaxation and retardation times, let us consider first the Laplace transform of the relaxation modulus of a solid. According to Eq. (6.4),

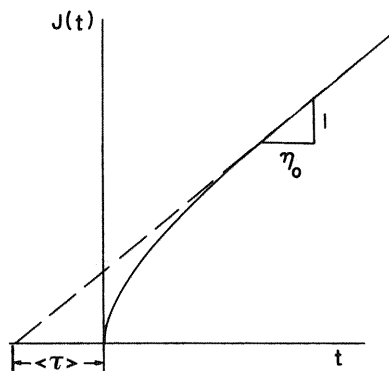


Figure 9.4 Schematic representation of the compliance function versus time. The values of η and $\langle\tau\rangle$ are indicated.

$$s\bar{G}(s) = G_e + s \int_0^{\infty} [G(t) - G_e] e^{-st} dt \quad (9.42)$$

By following the same procedure as before, for small values of s , Eq. (9.42) becomes

$$s\bar{G}(s) = G_e + \eta'(0)(s - \langle\tau\rangle s^2 + \dots) \quad (9.43)$$

where $\eta'(0)$ is the real component of the complex viscosity at frequency zero, which, according to Eqs. (6.4) and (6.11), is given by

$$\eta'(0) = \int_0^{\infty} [G(t) - G_e] dt \quad (9.44)$$

while the product $\eta'(0)\langle\tau\rangle$, in analogy with Eq. (9.34), can be written as

$$\eta'(0)\langle\tau\rangle = \int_0^{\infty} t[G(t) - G_e] dt \quad (9.45)$$

From Eq. (9.43), the complex relaxation modulus is given at low frequencies by

$$G^*(\omega) = G_e + \eta'(0)[i\omega - \langle\tau\rangle(i\omega)^2 + \dots] \quad (9.46)$$

From the reciprocal of $G^*(\omega)$, the expression for $J^*(\omega)$ is

$$J^*(\omega) = J_e \{1 - J_e \eta'(0) i\omega + J_e \eta_0 [\langle\tau\rangle + J_e \eta'(0)] (i\omega)^2 - \dots\} \quad (9.47)$$

where it was taken into account that for solids $J_e = 1/G_e$. The transform of Eq. (9.47) gives

$$s\bar{J}(s) = J_e \{1 - J_e \eta'(0) s + J_e \eta'(0) [\langle\tau\rangle + J_e \eta'(0)] s^2 - \dots\} \quad (9.48)$$

In order to determine the terms of Eq. (9.48), let us express the creep compliance function as the identity $J(t) \equiv J_e - [J_e - J(t)]$. The Laplace transform of this equation is given by

$$s\bar{J}(s) = J_e - s \int_0^{\infty} [J_e - J(t)] e^{-st} dt \quad (9.49)$$

For low values of s , Eq. (9.49) can be written as

$$s\bar{J}(s) = J_e - s \int_0^{\infty} [J_e - J(t)] dt + s^2 \int_0^{\infty} t[J_e - J(t)] dt - \dots \quad (9.50)$$

By comparing Eqs. (9.48) and (9.50) we obtain

$$J_e^2 \eta'(0) = \int_0^{\infty} [J_e - J(t)] dt \quad (9.51a)$$

$$J_e^3 (\eta'(0))^2 + J_e \eta'(0) \langle \tau \rangle = \int_0^{\infty} t [J_e - J(t)] dt \quad (9.51b)$$

Hence,

$$\eta'(0) = \frac{1}{J_e^2} \int_0^{\infty} [J_e - J(t)] dt = \int_0^{\infty} [G(t) - G_e] dt \quad (9.52)$$

On the other hand, the mean retardation time $\langle \tau' \rangle$ is defined as

$$\langle \tau' \rangle = \frac{\int_0^{\infty} t [J_e - J(t)] dt}{\int_0^{\infty} [J_e - J(t)] dt} \quad (9.53)$$

This equation in conjunction with Eqs. (9.51a) and (9.51b) gives

$$\langle \tau' \rangle = \langle \tau \rangle + \frac{\eta'(0)}{G_e} \quad (9.54)$$

Accordingly, the mean retardation time is always greater than the mean relaxation time.

9.7 DETERMINATION OF SPECTRA FROM VISCOELASTIC FUNCTIONS USING FIRST-ORDER APPROXIMATIONS

In the previous sections we have seen that the compliance and relaxation viscoelastic functions can be expressed in terms of the retardation and relaxation spectra, respectively. However, the spectra cannot be determined beforehand; they can only be calculated from viscoelastic functions. For example, $N(s)$ and $N'(s)$ in Eqs. (9.5) and (9.11) can be obtained by using the expressions

$$N(s) = \mathcal{L}^{-1}[G(t) - G_e] \quad (9.55a)$$

and

$$N'(s) = \mathcal{L}^{-1}[J_e - J(t)] \quad (9.55b)$$

where the symbol \mathcal{L}^{-1} represents the inverse of the Laplace transform. In principle, once $N(s)$ and $N'(s)$ are known, $H(\tau)$ and $L(\tau)$ can be obtained immediately. However, in most cases it is not an easy task to get the analytical functions of $G(t)$ and $J(t)$. Even if these functions are known, the determination of $N(s)$ and $N'(s)$ by analytical means from Eq. (9.55) may not be possible. In spite of these difficulties, approximate methods have been devised to determine the spectra from viscoelastic functions; these are briefly described below.

9.6.1 Relaxation Spectra

The function $\exp(-t/\tau)$ in the integrand of Eq. (9.6) converges to 0, 1 when $\tau \rightarrow 0, \infty$. By plotting $\exp(-t/\tau)$ against $-\ln(t/\tau)$, a sigmoidal curve is obtained that intercepts the ordinate axis at e^{-1} ($= 0.34$). The area beneath the curve of Figure 9.5 is considered to be equal to the area of the rectangle of height unity. Actually the area in excess between the asymptote $e^{-t/\tau} = 1$ and the curve in the first quadrant is roughly compensated by the area limited by the curve and the abscissa axis in the second quadrant (2). It should be pointed out that in the first quadrant the relaxation times are larger than the time of observation, while the opposite is true in the second quadrant. As a result $e^{-t/\tau}$ can be approximated by:

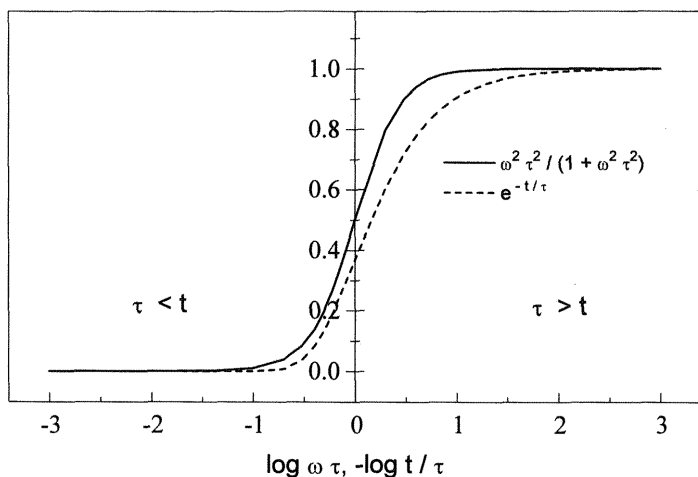


Figure 9.5 Plots of the kernels of the relaxation modulus and the storage relaxation modulus versus $-\log t/\tau$ and $\log \omega\tau$, respectively.

$$\begin{aligned} H(t/\tau) &= 0, & \ln(t/\tau) > 0 \\ H(t/\tau) &= 1, & \ln(t/\tau) \leq 0 \end{aligned} \quad (9.55c)$$

Consequently the relaxation modulus is given approximately by (1,2)

$$G(t) - G_e \approx \int_{\ln t}^{\infty} H(\tau) d \ln \tau \quad (9.56)$$

where it has been taken into account that the lower limit of the integral in this approximation is $\tau = t$. Hence Eq. (9.56) suggests that a first-order approximation for the relaxation spectrum can be obtained by means of the relationship

$$H(\tau) \cong - \left. \frac{d[G(t) - G_e]}{d \ln t} \right|_{t=\tau} = -G(t) \left. \frac{d \log G(t)}{d \log t} \right|_{t=\tau} \quad (9.57)$$

Because the relaxation spectra are similar for transient and dynamic relaxation viscoelastic functions, $H(t)$ can also be obtained from the storage relaxation modulus. The plot of the kernel of the integral of Eq. (9.8), $\omega^2 \tau^2 / (1 + \omega^2 \tau^2)$, versus $\log \omega \tau$ is a sigmoidal curve that intercepts the ordinate axis at 0.5 and reaches the value of 1 in the limit $\omega \tau \rightarrow \infty$ (see Fig. 9.5). The kernel can be approximated by the step function

$$\begin{aligned} H(\omega t) &= 0, & \ln(\omega t) < 0 \\ H(\omega t) &= 1, & \ln(\omega t) \geq 0 \end{aligned} \quad (9.57a)$$

Therefore the storage relaxation modulus can be written approximately as

$$G'(\omega) - G_e \cong \int_{-\ln \omega}^{\infty} H(\tau) d \ln \tau \quad (9.58)$$

The value of $-\ln \omega$ in the lower limit of the integration arises from the fact that here $\tau = 1/\omega$. Then the relaxation spectrum is approximately given by

$$H(\tau) = \left. \frac{d[G'(\omega) - G_e]}{d \ln \omega} \right|_{\tau=1/\omega} = G'(\omega) \left. \frac{d \log G'(\omega)}{d \log \omega} \right|_{\tau=1/\omega} \quad (9.59)$$

In order to obtain the relaxation spectrum for $G''(\omega)$, it is convenient to write Eq. (9.10) as

$$\omega G''(\omega) = \int_{-\infty}^{\infty} \frac{H(\tau)}{\tau} \left(\frac{\omega^2 \tau^2}{1 + \omega^2 \tau^2} \right) d \ln \tau \cong \int_{-\ln \omega}^{\infty} H(\tau) \omega d \ln \tau \quad (9.60)$$

From this equation the relaxation spectrum is approximately obtained in terms of the loss relaxation modulus,

$$H(\tau) \cong \frac{1}{\omega} \frac{d}{d \ln \omega} [\omega G''(\omega)]_{\omega=1/\tau} = G''(\omega) \left[1 + \frac{d \log G''(\omega)}{d \log \omega} \right]_{\tau=1/\omega} \quad (9.61)$$

9.6.2 Retardation Spectra

In the transient compliance function, $J(t)$, the retardation spectrum $L(\tau)$ is modulated by the function $1 - \exp(-t/\tau)$ [see Eq. (9.15)]. Plotting this function against $\ln t/\tau$ gives the sigmoidal curve shown in Figure 9.6. We should note that the time of observation (t) in the first quadrant is greater than the retardation times, and as a result τ varies between zero and t . Then the creep compliance function for viscoelastic liquids is approximately given by (1,2)

$$J(t) \cong J_g + \int_{-\infty}^{\ln t} L(\tau) d \ln \tau + \frac{t}{\eta} \quad (9.62)$$

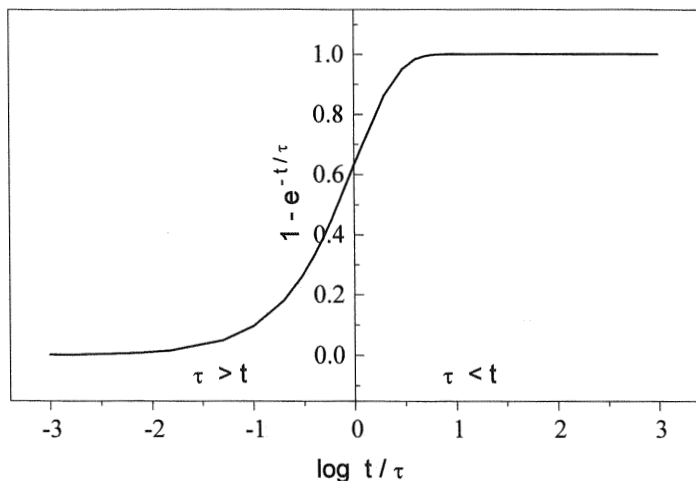


Figure 9.6 Plot of the kernel of the creep compliance function versus $\log t/\tau$.

The approximate value of the retardation spectrum is obtained from this equation by means of the relationship

$$L(\tau) \cong \frac{d}{d \ln t} \left[J(t) - J_g - \frac{t}{\eta} \right]_{t=\tau} = \left[J(t) - \frac{t}{\eta} \right] \frac{d \log [J(t) - t/\eta]}{d \log t} \Big|_{t=\tau} \quad (9.63)$$

For viscoelastic solids ($\eta = \infty$), Eq. (9.63) becomes

$$L(\tau) \cong J(t) \frac{d \log J(t)}{d \log t} \Big|_{t=\tau} \quad (9.64)$$

The approximate value of $L(\tau)$ can be derived from the storage compliance function $J'(\omega)$ following the method outlined to calculate $H(\tau)$ from $G'(\omega)$. Thus by taking into account Eq. (9.18), $J'(\omega)$ can be written as

$$J'(\omega) = J_e - \int_{-\infty}^{\infty} L(\tau) \frac{\omega^2 \tau^2}{1 + \omega^2 \tau^2} d \ln \tau \cong J_e - \int_{-\ln \omega}^{\infty} L(\tau) d \ln \tau \quad (9.65)$$

where $\omega = 1/\tau$. Hence,

$$L(\tau) \cong -J'(\omega) \frac{d \log J'(\omega)}{d \log \omega} \Big|_{\tau=1/\omega} \quad (9.66)$$

Finally, by following a method analogous to that used to determine the relaxation spectrum from $G''(\omega)$, Eq. (9.22) can be written as (2)

$$\omega J''(\omega) = \int_{-\infty}^{\infty} \frac{L(\tau)}{\tau} \left(\frac{\omega^2 \tau^2}{1 + \omega^2 \tau^2} \right) d \ln \tau + \frac{1}{\eta} \cong \int_{-\ln \omega}^{\infty} \omega L(\tau) d \ln \tau + \frac{1}{\eta} \quad (9.67)$$

Therefore, a first-order approximation for the retardation spectrum can be derived from the loss compliance function by means of the expression

$$L(\tau) = \left[J''(\omega) - \frac{1}{\omega \eta} \right] \left[1 + \frac{d \log [J''(\omega) - 1/\omega \eta]}{d \log \omega} \right]_{\tau=1/\omega} \quad (9.68)$$

9.8 APPROXIMATIONS OF HIGHER ORDER

The calculation of viscoelastic functions by means of spectra calculated by first-order approximations may lead to values of these functions that are in error with respect to the true values. These errors are lower if correction

factors obtained from the assumption of a certain function for the spectra are used. For example, the fact that $G(t) - G_e$ is a monotonous decreasing function of time suggests, as first approximation, that $H(\tau)$ could be expressed by (1,6)

$$H(\tau) = A\tau^{-m} \quad (9.69)$$

It should be noted that the equation assumed for the spectrum should be valid over at least two decades in the time scale. Substituting Eq. (9.69) into Eq. (9.6) and making $t/\tau = u$, gives the relationship

$$G(t) - G_e = A \int_0^{\infty} t^{-m} e^{-u} u^{m-1} du = \Gamma(m) A t^{-m} \quad (9.70)$$

where Γ is the gamma function. By taking into account the first-order approximation [Eq. (9.57)], we find

$$H_1(\tau) = - \left. \frac{d[\Gamma(m)A\tau^{-m}]}{d \ln \tau} \right|_{t=\tau} = \Gamma(m+1) A \tau^{-m} \quad (9.71)$$

Accordingly, $H_1(\tau)$ is in error with respect to the assumed function, $A\tau^{-m}$, by the factor $\Gamma(m+1)$, and consequently,

$$H(\tau) = - \left. \frac{G(t) - G_e}{\Gamma(m+1)} \frac{d \log[G(t) - G_e]}{d \log t} \right|_{t=\tau} \quad (9.72)$$

Equation (9.72) provides a more precise method for determining the relaxation spectrum. The strategy to follow in the calculation of the relaxation spectrum involves the determination of provisional values of $H(\tau)$, at $t = \tau$, at a series of points equally spaced on the logarithmic scale using $m = 0$ in Eq. (9.72). Then from a double logarithmic plot of $H(\tau)$ against τ , the slope $-m$ is determined at each point. The reciprocal of $\Gamma(m+1)$ multiplied by the provisional value of H gives the value of the relaxation spectra.

This method can be used to obtain the retardation spectrum from the compliance function $J(t)$. Equation (9.15) can be written as

$$J(t) = J_e - \int_{-\infty}^{\infty} L(\tau) e^{-t/\tau} d \ln \tau + \frac{t}{\eta} \quad (9.73)$$

Since $J(t)$ is a monotonous increasing function of time, the relation $L(\tau) = A\tau^m$ can be assumed to be a good approximation for the retardation spectrum. Then the integral of Eq. (9.73) is give by

$$\tilde{\phi}(t) = \int_{-\infty}^{\infty} A\tau^m e^{-t/\tau} d \ln \tau = \int_0^{\infty} At^m u^{-m-1} e^{-u} du = At^m \Gamma(-m) \quad (9.74)$$

where the substitution $t/\tau = u$ was made. According to Eq. (9.57), $L_1(\tau) = [-d\tilde{\phi}(\tau)/d \ln \tau]|_{t=\tau} = -A\tau^m m \Gamma(-m)|_{t=\tau}$, the value of the spectrum at $t = \tau$ is in error by the factor $\Gamma(1 - m)$ with respect to the assumed value. Since $\tilde{\phi}(\tau) = J_e - [J(t) - t/\eta]$, $L(\tau)$ is finally given by

$$L(\tau) = \frac{1}{\Gamma(1 - m)} \left[J(t) - \frac{t}{\eta} \right] \left[\frac{d \log [J(t) - t/\eta]}{d \log t} \right]_{t=\tau} \quad (9.75)$$

It should be pointed out that m is positive, and its value lies in the range $0 < m \leq 1$. Following analogous procedures, the retardation and relaxation spectra can be obtained from dynamic relaxation and dynamic compliance functions, respectively. The pertinent equations can be found in Ref. 1.

Other approximations of higher order can be used in the evaluation of the relaxation and retardation spectra. Let us define the function

$$\bar{\phi}(t) = \int_0^{\infty} \phi(\lambda) \exp(-\lambda t) d\lambda = \mathcal{L}[\phi(\lambda)] \quad (9.76)$$

where $\bar{\phi}(t) = G(t) - G_e$ in relaxation experiments and $\bar{\phi}(t) = J(t) - J_e - t/\eta$ in creep experiments. Moreover, Eqs. (9.4) and (9.15) indicate that $\phi(\lambda) = \tau H(\tau)|_{\tau=\lambda-1}$ and $\phi(\lambda) = \tau L(\tau)|_{\tau=\lambda-1}$ in the respective experiments. According to this,

$$\phi(\lambda) = \mathcal{L}^{-1}[\bar{\phi}(t)] \quad (9.77)$$

Owing to the fact that t is restricted to real values, the evaluation of the reciprocal of the Laplace transform in the real axis of the complex plane can be performed by using the Post-Widder equation (7)

$$\phi(\lambda) = \lim_{k \rightarrow \infty} \frac{(-1)^k}{k!} t^{k+1} \frac{d^k}{dt^k} \bar{\phi}(t) \Big|_{t=k/\lambda} \quad (9.78)$$

Since

$$D_t^k = t^k \frac{d^k}{dt^k} = \frac{d^k}{d \ln^k t} \quad (9.79)$$

Eq. (9.78) can be written

$$\phi(\lambda) = \lim_{k \rightarrow \infty} \frac{(-1)^k t}{k!} D_t^k \bar{\phi}(t) \Big|_{\lambda=k/t} \quad (9.80)$$

This expression indicates that the inversion of $\bar{\phi}(t)$ can be carried out by a differentiation process of infinite order, an approach that is not feasible. However, an approximation of order k can be obtained. The first-, second- and third-order approximations are given by (5)

$$H_1(\tau) = - \frac{dG(t)}{d \ln t} \Big|_{t=\tau} \quad (9.81a)$$

$$H_2(\tau) = - \frac{dG(t)}{d \ln t} + \frac{d^2 G(t)}{d \ln^2 t} \Big|_{t=2\tau} \quad (9.81b)$$

$$H_3(\tau) = - \frac{dG(t)}{d \ln t} + \frac{3 d^2 G(t)}{2 d \ln^2 t} - \frac{1 d^3 G(t)}{2 d \ln^3 t} \Big|_{t=3\tau} \quad (9.81c)$$

On the other hand, the approximations of first, second, and third order for the retardation spectrum are

$$L_1(\tau) = \frac{dJ(t)}{d \ln t} - \frac{t}{\eta} \Big|_{t=\tau} \quad (9.82a)$$

$$L_2(\tau) = \frac{dJ(t)}{d \ln t} - \frac{d^2 J(t)}{d \ln^2 t} \Big|_{t=2\tau} \quad (9.82b)$$

$$L_3(\tau) = \frac{dJ(t)}{d \ln t} - \frac{3 d^2 J(t)}{2 d \ln^2 t} + \frac{1 d^3 J(t)}{2 d \ln^3 t} \Big|_{t=3\tau} \quad (9.82c)$$

An alternative procedure for calculating the spectra involves fitting the experimental results for the viscoelastic functions by means of spline functions. The derivatives of Eqs. (9.81) and (9.82) are determined by means of these functions, and thus the spectra can be obtained. A summary of these and other approximations used to calculate retardation and relaxation spectra from the measured compliance and relaxation functions, respectively, can be found in Refs. 1 and 5.

9.9 EXPERIMENTAL RETARDATION AND RELAXATION SPECTRA

Double logarithmic plots of the retardation spectra versus the retardation times are represented in Figure 9.7. For high molecular weights the spectra

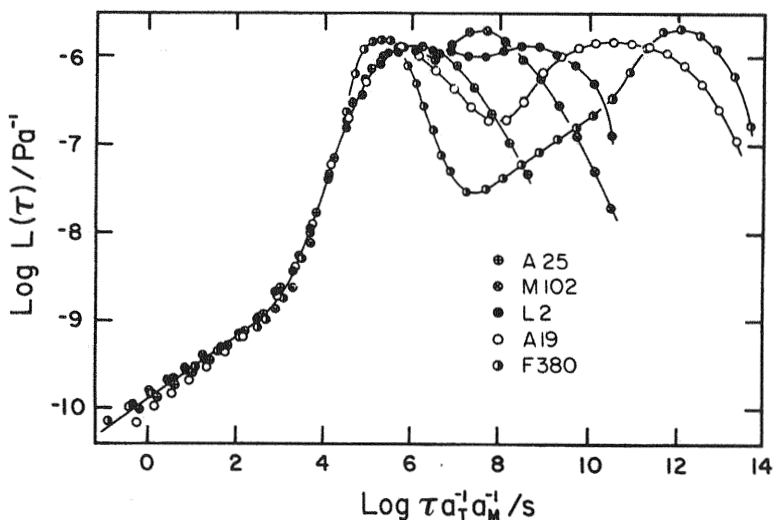


Figure 9.7 Double logarithmic plots of the retardation spectra as a function of the retardation time for different fractions of polystyrene of narrow molecular weight distributions: (\oplus) 4.7×10^4 , (\otimes) 9.4×10^4 , (\bullet) 1.9×10^5 , (\circ) 6.0×10^5 , and (\ominus) 3.8×10^6 . The spectra were shifted to superpose them in the glassy-like region. (Reference temperature 100°C ; molecular weight, 1.9×10^5). (From Ref. 8.)

present a softening peak associated with the transition from the glassy-like region to the rubbery region, followed by a minimum corresponding to the plateau region and finally another peak associated with the terminal region. The distance between the two retardation peaks decreases as the molecular weight decreases (Ref. 1, Chap. 3). The two peaks tend to overlap as the molecular weight approaches the critical molecular weight, forming a single peak for molecular weights below M_c (see Fig. 9.8). Consequently, the two peaks exhibited by the retardation spectra of high molecular weight polymers reflect their entangled nature.

The influence of the concentration on the formation of entangled networks in polymer-diluent mixtures is shown in Figures 9.9 and 9.10, where the retardation spectra for several concentrations of a high molecular weight polymer in solution are shown. For concentrated solutions the spectra present the rubber and terminal peaks, as occurs with undiluted polymers, and the two peaks merge into a single peak for semidilute and dilute solutions. It is not possible to superpose the retardation spectra by any horizontal translation of the logarithmic plots. This behavior suggests that the two peaks differ in their dependence on concentration. However, the softening peak L_s ,

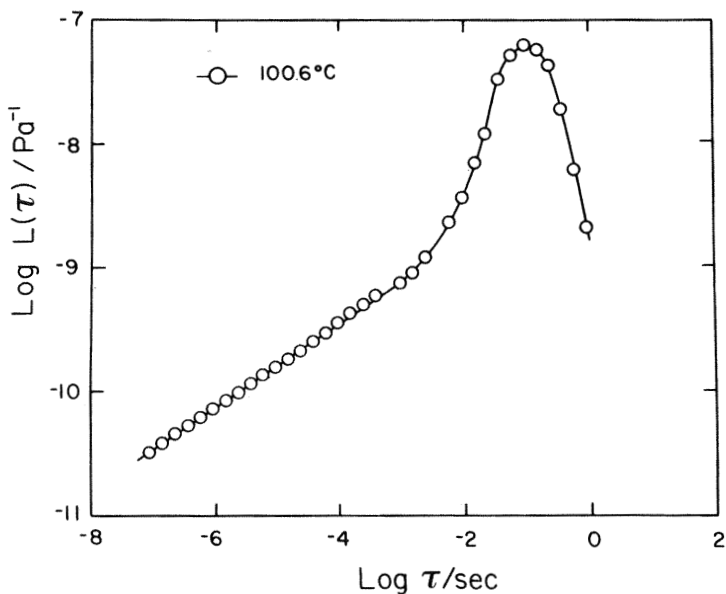


Figure 9.8 Double logarithmic plot of the retardation spectrum versus the retardation time for a polystyrene fraction of molecular weight 3400 with a narrow molecular weight distribution. (From Ref. 8.)

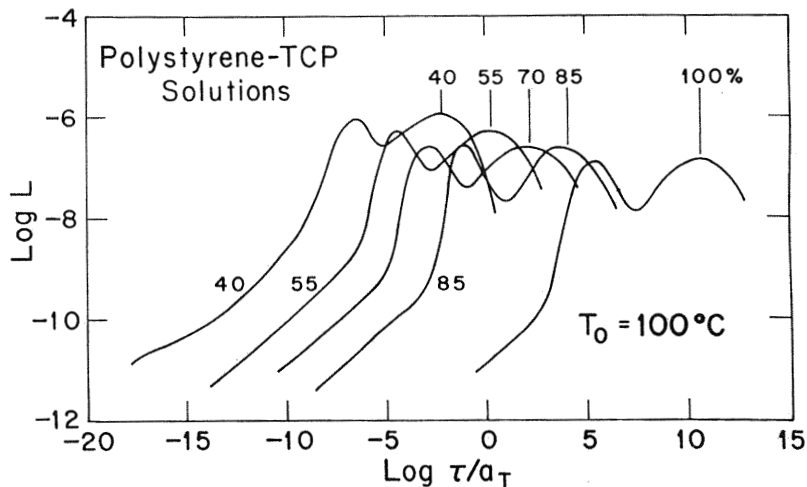


Figure 9.9 Double logarithmic plots of retardation spectra against reduced time for several high concentrated solutions of polystyrene in tri-*m*-tolyl phosphate. (From Ref. 9.)

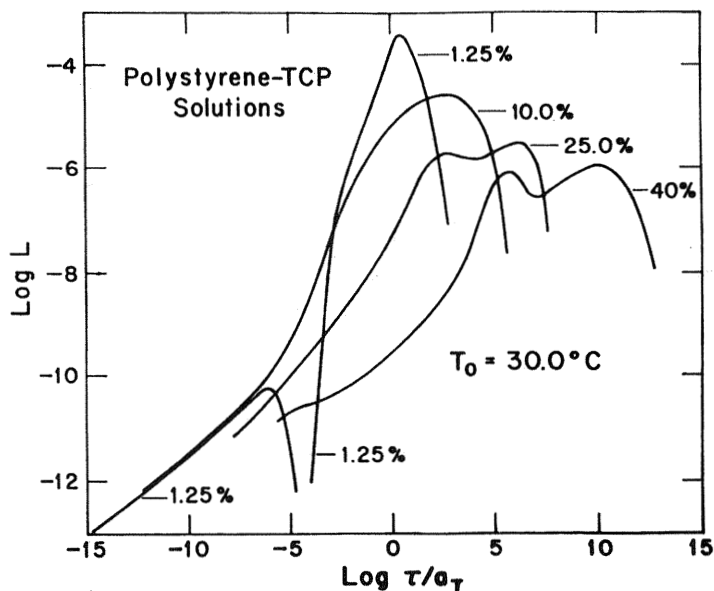


Figure 9.10 Retardation spectra versus reduced time for concentrated, semi-dilute, and dilute solutions of polystyrene in tri-*m*-tolyl phosphate. (From Ref. 9.)

and the terminal peak L_w can be independently superposed as Figures 9.11 and 9.12 suggest. Figure 9.11 shows the results of superposing the spectra of Figures 9.9 and 9.10 for the more concentrated solution in the vicinity of the short-time L_s peak. The peaks were shifted by an amount $\log a_{c,s}$ along the $\log \tau$ axis and by $\Delta \log L_s$ along the vertical axis, so that they are superimposed on the spectrum of the pure polymer at the reference temperature T_0 . Again, the terminal peaks of the retardation spectra of different concentrations were shifted both horizontally and vertically by the amounts $\log a_{c,w}$ and $\Delta \log L_w$, respectively, with respect to the terminal peak of the undiluted polymer.

The distance between the L_s and L_w peaks, $\Delta \log \tau_m$, decreases as the concentration decreases (Ref. 1, Chap. 4) (see Fig. 9.13). This distance is important because it provides an objective measure of the length of the rubbery plateau. The results at hand seem to suggest that the plot of $\Delta \log \tau_m$ against $\log \phi M$, where ϕ is the volume fraction of polymer, gives a line of slope 3.4. The line intercepts the abscissa at a value of $\log(\phi M)$ that is identical with that found from the break in the $\log \eta_0$ vs $\log(\phi M)$ plot, where η_0 is the zero shear rate viscosity.

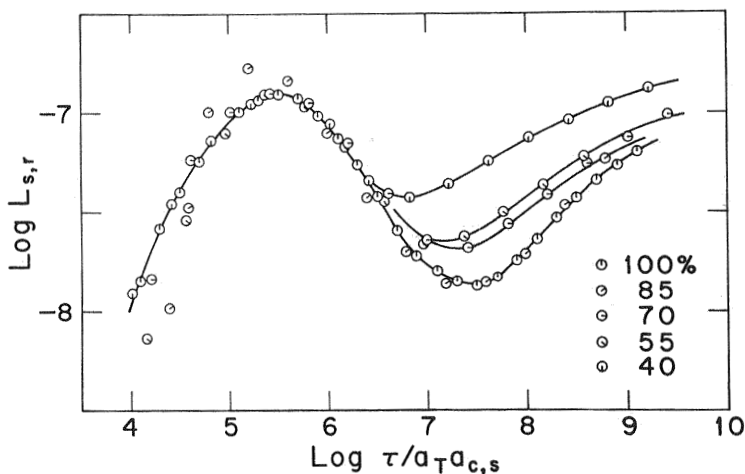


Figure 9.11 Reduced plots of the retardation spectra of the more concentrated solutions of polystyrene in tri-*m*-tolyl phosphate represented in Figure 9.9. The superposition was carried out in the neighborhood of the L_s (short time) maximum. The reference curve corresponds to polystyrene at 100°C. (From Ref. 9.)

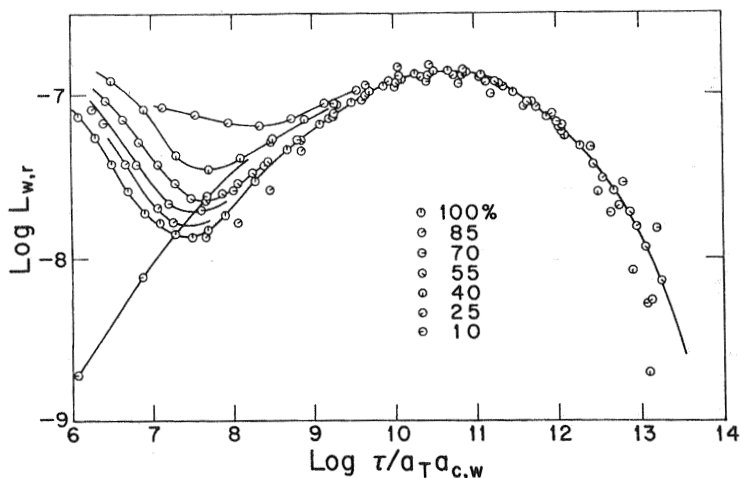


Figure 9.12 Reduced plots of the retardation spectra of solutions (10% and above) of polystyrene in tri-*m*-tolyl phosphate represented in Figure 9.9 and 9.10. The superposition was carried out in the neighborhood of the L_w (long time) maximum. The reference curve corresponds to polystyrene at 100°C. (From Ref. 9.)

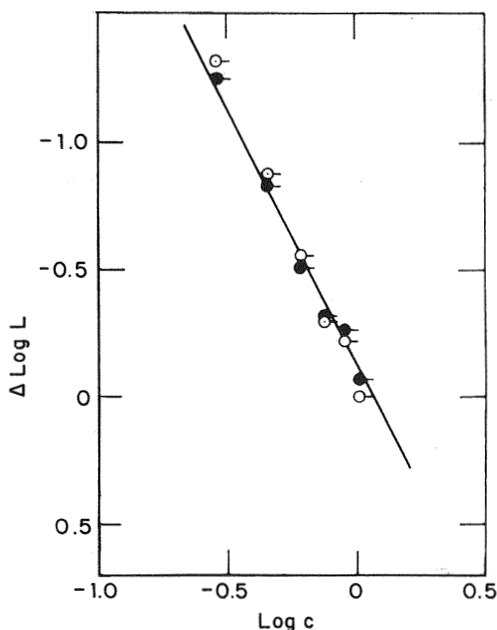


Figure 9.13 Double logarithmic plot showing the concentration dependence of $\Delta \log \tau_m$ for concentrated solutions of polystyrene in tri-*m*-tolyl phosphate. (From Ref. 9.)

Illustrative curves showing the double logarithmic plot of the relaxation spectra of polymers against the relaxation time are shown in Figure 9.14. In the transition from the glassy-like to the rubbery region, or softening region, $H(\tau)$ decreases as τ increases. It remains nearly constant in the rubbery region and finally drops to zero in the terminal region. As occurs with the retardation spectra, the region of the relaxation spectra corresponding to the plateau region disappears for unentangled chains, that is, for chains with $M < M_c$ (Ref. 1, Chap. 3).

9.10 APPROXIMATE RELATIONSHIPS BETWEEN VISCOELASTIC FUNCTIONS

Once a relaxation (retardation) spectrum is obtained from a relaxation (creep compliance) viscoelastic function, any other function can be obtained. Alternatively, approximate methods have been developed to calculate viscoelastic functions from one another (10). By taking into account

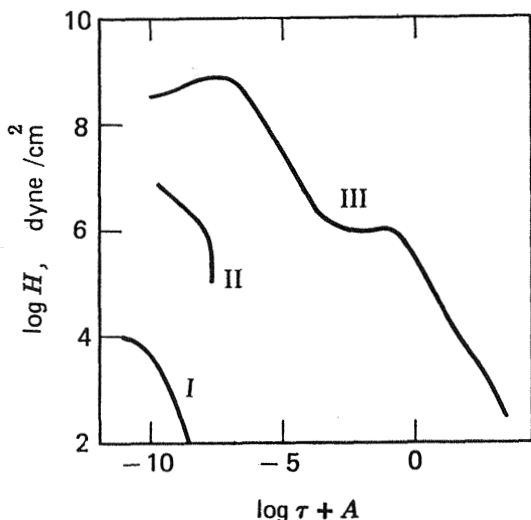


Figure 9.14 Relaxation spectra for high (III) and low (II) molecular weight fractions of polymers: (I) represents the relaxation spectrum of a dilute polymer solution. (From Ref. 1.)

that the relaxation spectrum is the same for transient and nontransient viscoelastic functions, it is possible to obtain the complex relaxation modulus from the relaxation modulus and vice versa. The method entails expressing the kernel of a viscoelastic function in terms of the kernels of other viscoelastic functions with the same relaxation (or retardation) spectrum. For example, the function used to evaluate the storage relaxation modulus from the relaxation modulus has the form

$$\begin{aligned} G'(\omega) &= G'(1/t) \\ &= A_1 G(t) + A_2 G(2t) + B_2 G(t/2) + A_4 G(4t) + B_4(t/4) + \dots \end{aligned} \quad (9.83)$$

where A_j and B_j are specified constants. A detailed study of these methods with analysis of errors can be found in Ref. 10.

PROBLEM SETS

Problem 9.1

Calculate the relaxation time spectrum from the equation

$$E''(\omega) = \int_0^{\infty} \phi(\tau) \frac{\omega\tau}{1 + \omega^2\tau^2} d\tau, \quad 0 < \omega < \infty$$

Solution 9.1

Assume that $E''(\omega)$ is continuous, non-negative, and such that

$$\lim_{\omega \rightarrow \infty} E''(\omega) = 0 \quad (\text{P9.1.1})$$

Let us assume further that the function to be found (continuous, non-negative, and of bounded variation in the neighbourhood of each point) is in $L^1(0, \infty)$, i.e., it is modulus-integrable, and

$$\int_0^{\infty} \phi(\tau) d\tau = 1 \quad (\text{P9.1.2})$$

After making the changes

$$\tau = \tau_0 \exp t, \quad \omega = \tau_0^{-1} \exp(-\Omega)$$

the integral equation becomes

$$E''(\tau_0^{-1} e^{-\Omega}) = \int_{-\infty}^{\infty} \phi(\tau_0 e^t) \tau_0 e^t 2^{-1} \operatorname{sech}(\Omega - t) dt \quad (\text{P9.1.3})$$

or, alternatively,

$$G(\Omega) = E''(\tau_0^{-1} e^{-\Omega}) \quad \text{and} \quad g(t) = \phi(\tau_0 e^t) \tau_0 e^t \quad (\text{P9.1.4})$$

$$G(\Omega) = \int_{-\infty}^{\infty} g(t) 2^{-1} \operatorname{sech}(\Omega - t) dt, \quad -\infty < \Omega < \infty \quad (\text{P9.1.5})$$

In Eq. (P9.1.5) the function g is continuous, non-negative, and of bounded variation in the neighbourhood of each point; moreover, the following condition holds:

$$g \in L^1(\mathbb{R}) \quad \text{and} \quad \int_{-\infty}^{\infty} g(t) dt = 1 \quad (\text{P9.1.6})$$

On the other hand, G is continuous, non-negative, and satisfies the expressions

$$G \in L^1(\mathbb{R}), \quad G \in L^2(\mathbb{R}), \quad \lim_{|\Omega| \rightarrow \infty} G(\Omega) = 0 \quad (\text{P9.1.7})$$

To apply Fourier transforms, Eq. (P9.1.5) can be written as

$$G = \sqrt{2\pi}(2^{-1}\text{sech}) * g \quad (\text{P9.1.8})$$

Note that if $u, v \in L^1(\mathbb{R})$, the convolution is given by

$$(u * v)(x) = (2\pi)^{-1/2} \int_{-\infty}^{\infty} u(x-y)v(y) dy \quad (\text{P9.1.9})$$

except for a null measure set. Denoting the Fourier transform by a caret ($\hat{\cdot}$), we obtain

$$\begin{aligned} \hat{G}(s) &= \sqrt{2\pi}(2^{-1}\text{sech})\hat{(s)}\hat{g}(s) \\ &= 2^{-1}\pi\text{sech}(\pi s/2)\hat{g}(s) \end{aligned}$$

where we have used the equation

$$(\text{sech})\hat{(s)} = \sqrt{\pi/2} \text{sech}(\pi s/2)$$

so that

$$\hat{g}(s) = \frac{2}{\pi} \cosh\left(\frac{\pi s}{2}\right) \hat{G}(s), \quad -\infty < s < \infty \quad (\text{P9.1.11})$$

Now, g being integrable, continuous, and locally of the bounded variation, we can use the Fourier inversion formula to find

$$\begin{aligned} g(t) &= \frac{1}{\sqrt{2\pi}} PV \int_{-\infty}^{\infty} \hat{g}(s) e^{ist} ds \\ &= \frac{2}{\pi} \left(\frac{1}{\sqrt{2\pi}} \right) PV \int_{-\infty}^{\infty} \cosh\left(\frac{\pi}{2}s\right) \hat{G}(s) e^{ist} ds \end{aligned} \quad (\text{P9.1.12})$$

(where PV means principal value). Taking into account that

$$\tau = \tau_0 e^t$$

Eq. (P9.1.12) can be written as

$$\tau\phi(\tau) = \frac{2}{\pi} \left(\frac{1}{\sqrt{2\pi}} \right) PV \int_{-\infty}^{\infty} \cosh\left(\frac{\pi}{2}s\right) \hat{G}(s) \left(\frac{\tau^{is}}{\tau_0^{is}} \right) ds \quad (\text{P9.1.13})$$

and for the solution of the integral equation we find

$$\begin{aligned}\phi(\tau) &= \frac{2}{\pi\sqrt{2\pi}} PV \int_{-\infty}^{\infty} \cosh\left(\frac{\pi}{2}s\right) \left(\frac{1}{\sqrt{2\pi}} \int_{-\infty}^{\infty} G(\Omega) e^{-i\Omega s} d\Omega \right) \left(\frac{\tau^{is-1}}{\tau_0^{is}} \right) ds \\ &= \frac{1}{\pi^2} PV \int_{-\infty}^{\infty} \cosh\left(\frac{\pi}{2}s\right) \left(\int_{-0}^{\infty} E''(\omega) \omega^{is-1} d\omega \right) \tau^{is-1} ds, \quad 0 < \tau < \infty\end{aligned}\tag{P9.1.14}$$

If G has an analytical prolongation to the horizontal band,

$$-\frac{\pi}{2} < \text{Im } z < \frac{\pi}{2}$$

and

$$\sup_{|\eta| < \pi/2} \int_{-\infty}^{\infty} |G(\Omega + i\eta)|^2 d\Omega < \infty$$

it is possible to show¹ that there exist limiting functions such that

$$G\left(\Omega \pm i\frac{\pi}{2}\right) \in L^2(R)\tag{P9.1.15}$$

and

$$\hat{G}(s) \cosh\left(\frac{\pi}{2}s\right) \in L^2(R)\tag{P9.1.16}$$

On this basis, the function

$$g(t) = \frac{1}{\pi} \left[G\left(t - i\frac{\pi}{2}\right) + G\left(t + i\frac{\pi}{2}\right) \right], \quad -\infty < t < \infty\tag{P9.1.17}$$

is in $L^2(R)$ and is a solution of the integral equation. By considering Eq. (P9.1.4) and taking into account that

$$t = \ln \frac{\tau}{\tau_0}$$

we obtain

$$\phi(\tau) = \frac{1}{2\pi} \left[E''\left(\frac{i}{\tau}\right) + E''\left(-\frac{i}{\tau}\right) \right]\tag{P9.1.18}$$

¹EC Titchmarsh. Introduction to Theory of Fourier Integrals. 2nd ed. Oxford UK: Clarendon Press 1937, Sect. 118.

Problem 9.2

The following semiempirical model has been proposed to represent the complex modulus E^* at $T = \text{constant}$.

$$E^* = E_0 + \frac{E_\infty - E_0}{1 + \delta(i\omega\tau_0)^{-k} + (i\omega\tau_0)^{-h}}$$

where E_0 and E_∞ are, respectively, the relaxed and unrelaxed moduli and τ_0 , k , h , and δ are adjustable parameters. Find the corresponding relaxation time spectrum.

Solution 9.2

Let

$$H(\tau) = \tau g(\tau) \quad (\text{P9.2.1a})$$

where

$$E^* = E_0 + (E_\infty - E_0) \int_{-\infty}^{\infty} \frac{\tau g(\tau) d \ln \tau}{1 + i\omega\tau} \quad (\text{P9.2.1b})$$

and

$$\int_{-\infty}^{\infty} \tau g(\tau) d \ln \tau = 1 \quad (\text{P9.2.2})$$

The relaxation time spectrum is calculated through Eq. (P9.1.18) as

$$H(\tau) = \tau g(\tau) = \frac{1}{2\pi} \left[E'' \left(\frac{i}{\tau} \right) + E'' \left(-\frac{i}{\tau} \right) \right] \quad (\text{P9.2.3})$$

After long algebraic calculations, the following result is obtained:

$$\tau g(\tau) = \frac{1}{\pi} \left(\frac{\tau}{\tau_0'} \right)^k \left[\frac{\sin h\pi(\tau/\tau_0)^{h-k} + \delta \sin k\pi}{\left(\frac{\tau}{\tau_0} \right)^{2h} + \delta^2 \left(\frac{\tau}{\tau_0} \right)^{2k} + 2\delta \cos(h-k)\pi \left(\frac{\tau}{\tau_0} \right)^{h+k} + 2 \cos h\pi \left(\frac{\tau}{\tau_0} \right)^h + 2\delta \cos k\pi \left(\frac{\tau}{\tau_0} \right)^k + 1} \right] \quad (\text{P9.2.4})$$

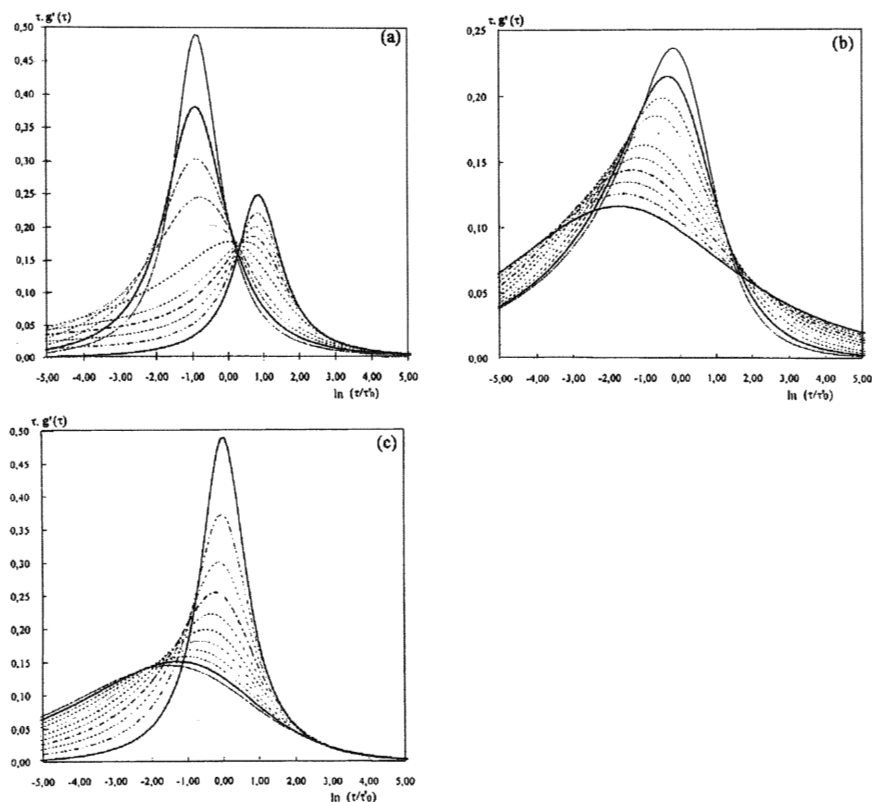
**Figure P9.2.1**

Fig. a

$$k = 0.00, 0.05, 0.10, 0.15, 0.20, 0.30, \dots, 0.80$$

$$h = 0.8; \delta = 1; \tau_0 = 10^{-5} \text{ s}$$

Fig. b

$$h = 0.40, 0.45, 0.50, \dots, 0.90$$

$$k = 0.4; \delta = 1; \tau_0 = 10^{-5} \text{ s}$$

Fig. c

$$\delta = 0, 0.2, 0.4, \dots, 2.0$$

$$h = 0.8; k = 0.4; \tau_0 = 10^{-5} \text{ s}$$

Diagrams showing the change in the distribution of the relaxation times for different parameters of the proposed model.

which is the expression for the relaxation time spectrum.

The variation of the relaxation spectrum with the parameters k , h , and δ is shown in Figures P9.2.1a, b, and c, respectively.

Problem 9.3

For a polymer melt,

$$J_e = 10^{-6} \text{ Pa}^{-1} \quad \text{and} \quad \eta_0 = 10^9 \text{ Pa/s}$$

Find the mean relaxation time $\langle \tau \rangle$.

Solution 9.3

Equations (9.30), (9.31), and (9.32) lead to

$$\langle \tau \rangle = \frac{\int_0^{\infty} H(\tau) \tau \, d\tau}{\int_0^{\infty} H(\tau) \, d\tau} = \frac{\int_0^{\infty} H(\tau) \tau \, d\tau \int_0^{\infty} H(\tau) \, d\tau}{\left[\int_0^{\infty} H(\tau) d\tau \right]^2} = J_e \eta_0 \quad (\text{P9.3.1})$$

and

$$\langle \tau \rangle = 10^{-6} \times 10^9 \text{ s} = 10^3 \text{ s}$$

Problem 9.4

Derive an expression for the first-, second-, and third-order approximation of the relaxation spectrum for a Maxwell element in shear.

Solution 9.4

As is well known, a Maxwell element in shear is defined by

$$G(t) = G_0 \exp(-t/\tau_0) \quad (\text{P9.4.1})$$

According to Eq. (9.81) and taking into account that

$$\frac{dG(t)}{d \ln t} = -G_0 \frac{t}{\tau_0} \exp\left(-\frac{t}{\tau_0}\right) \quad (\text{P9.4.2})$$

$$\frac{d^2 G(t)}{d \ln t^2} = -G_0 \frac{t}{\tau_0} \exp\left(-\frac{t}{\tau_0}\right) + G_0 \left(\frac{t}{\tau_0}\right)^2 \exp\left(-\frac{t}{\tau_0}\right) \quad (\text{P9.4.3})$$

$$\frac{d^3 G(t)}{d \ln t^3} = -G_0 \frac{t}{\tau_0} \exp\left(-\frac{t}{\tau_0}\right) + 3G_0 \left(\frac{t}{\tau_0}\right)^2 \exp\left(-\frac{t}{\tau_0}\right) - G_0 \left(\frac{t}{\tau_0}\right)^3 \exp\left(-\frac{t}{\tau_0}\right) \quad (\text{P9.4.4})$$

we obtain the expression

$$H_1(\tau) = G_0 \frac{\tau}{\tau_0} \exp\left(-\frac{\tau}{\tau_0}\right) \quad (\text{P9.4.5})$$

$$H_2(\tau) = 4G_0 \left(\frac{\tau}{\tau_0}\right)^2 \exp\left(-2\frac{\tau}{\tau_0}\right) \quad (\text{P9.4.6})$$

$$H_3(\tau) = \frac{27}{2} G_0 \left(\frac{\tau}{\tau_0}\right)^3 \exp\left(-3\frac{\tau}{\tau_0}\right) \quad (\text{P9.4.7})$$

Problem 9.5

Show that as a consequence of the retardation spectrum being positive,

$$0 \leq \frac{d \ln J(t)}{d \ln t} \leq 1$$

Solution 9.5

We consider the function $J(t)$ as the sum of positive functions Ψ such that

$$\Psi(t) = 1 - \exp\left(-\frac{t}{\tau}\right) \quad (\text{P9.5.1})$$

Now, we have

$$\frac{d \ln \Psi(t)}{d \ln t} = t \frac{\dot{\Psi}(t)}{\Psi(t)} = \frac{t}{\tau} \left(\frac{e^{-t/\tau}}{1 - e^{-t/\tau}} \right) \leq 1 \quad (\text{P9.5.2})$$

as can easily be shown. As a consequence,

$$0 \leq \frac{d\Psi}{d \ln t} \leq \Psi(t) \quad (\text{P9.5.3})$$

or

$$0 \leq \frac{d \ln \Psi}{d \ln t} \leq 1 \quad (\text{P9.5.4})$$

This equation holds for the sum of such functions Ψ , that is, for J .

Problem 9.6

Give an approximate expression for the retardation spectrum of a visco-elastic solid whose creep compliance is given by

$$J(t) = J_e \left[1 + \left(\frac{t}{t_m} \right)^{-m} \right]^{-1}$$

Solution 9.6

According to Eq. (9.64),

$$L(\tau) = J(t) \frac{d \ln J(t)}{d \ln t} \Big|_{t=\tau} \quad (\text{P9.6.1})$$

Substituting the equation proposed for the creep compliance into Eq. (P9.6.1), we obtain

$$L(\tau) = \frac{m t_m J(\tau)}{1 + (\tau/t_m)^m} \quad (\text{P9.6.2})$$

or, alternatively,

$$L(\tau) = \frac{m t_m J_e}{2[1 + \cosh][\ln(\tau/t_m)^m]} \quad (\text{P9.6.3})$$

Problem 9.7

Find the complex dynamic moduli corresponding to a “box” distribution of relaxation times spectrum, i.e., that

$$\begin{aligned} F(\tau) &= F_0 & \tau_{\min} < \tau < \tau_{\max} \\ F(\tau) &= 0 & \tau < \tau_{\min}, \tau > \tau_{\max} \end{aligned}$$

Solution 9.7

The normalization condition requires

$$\int_{-\infty}^{+\infty} H(\tau) d \ln \tau = H_0 \int_{\tau_{\min}}^{\tau_{\max}} d \ln \tau = G_g - G_e \quad (\text{P9.7.1})$$

so that

$$H_0 = \frac{G_g - G_e}{\ln \frac{\tau_{\max}}{\tau_{\min}}} \quad (\text{P.9.7.2})$$

Hence,

$$\begin{aligned} H(\tau) &= \frac{G_g - G_e}{\ln \frac{\tau_{\max}}{\tau_{\min}}}; \tau_{\min} \leq \tau < \tau_{\max} \\ &= 0 & \tau < \tau_{\min}; \tau \geq \tau_{\max} \end{aligned} \quad (\text{P9.7.3})$$

According to Eqs (9.8) and (9.10), one obtains

$$G'(\omega) = G_e + \frac{G_g - G_e}{\ln \frac{\tau_{\max}}{\tau_{\min}}} \int_{\tau_{\min}}^{\tau_{\max}} \frac{\omega^2 \tau^2}{1 + \omega^2 \tau^2} d \ln \tau = G_e + \frac{G_g - G_e}{\ln \frac{\tau_{\max}}{\tau_{\min}}} \ln \frac{1 + \omega^2 \tau_{\max}^2}{1 + \omega^2 \tau_{\min}^2} \quad (\text{P9.7.4a})$$

$$G''(\omega) = \frac{G_g - G_e}{\ln \frac{\tau_{\max}}{\tau_{\min}}} (\text{arc tan } \omega \tau_{\max} - \text{arc tan } \omega \tau_{\min}) \quad (\text{P9.7.4b})$$

The loss modulus has a maximum at

$$\omega = (\tau_{\max} \tau_{\min})^{-1/2}$$

for which

$$G''_{\max} = \frac{G_g - G_e}{\ln \frac{\tau_{\max}}{\tau_{\min}}} \text{arc tan } \frac{\tau_{\max} - \tau_{\min}}{2\sqrt{\tau_{\max} \tau_{\min}}} \quad (\text{P9.7.5})$$

REFERENCES

1. JD Ferry. *Viscoelastic Properties of Polymers*. 3rd ed. New York: Wiley-Interscience, 1980.
2. H Markovitz. *Lectures in Linear Viscoelasticity: An Introduction*. Carnegie-Mellon University, 1978.
3. AC Pipkin. *Lectures on Viscoelasticity Theory*. New York: Springer-Verlag, 1972.
4. JJ Aklonis, WJ MacKnight. *Introduction to Polymer Viscoelasticity*. 2nd. ed. New York: Wiley, 1980.
5. NW Tschoegl. *The Phenomenological Theory of Linear Viscoelastic Behavior*. Heidelberg: Springer Verlag, 1989.
6. JD Ferry, ML Williams. *J Colloid Sci* 7: 347, 1952.
7. DV Widder. *The Laplace Transform*. Princeton, NJ: Princeton Univ Press, 1946.
8. DJ Plazek. *J Non-Cryst Solids* 131-133: 836, 1991.
9. DJ Plazek, E Riande, H Markovitz, N Raghupathi. *J Polym Sci Polym Phys Ed* 17: 2189, 1979.
10. FR Schwarzl. *Rheol Acta* 10: 166, 1971. CE Struik, FR Schwarzl. *Adv. Mol. Relax. proc.* 201, 1, 1968.

10

Viscoelastic Models

10.1	Introduction	394
10.2	Maxwell's Model	395
10.3	The Kelvin–Voigt Model	398
10.4	Three-Element Standard Solid	400
10.5	Burgers Model	404
10.6	Maxwell and Kelvin–Voigt Generalized Models	406
10.7	Ladder Models	408
10.8	Distributed Constants Models	409
	Problem Sets	413
	References	422

10.1 INTRODUCTION

The mechanical response of viscoelastic materials to mechanical excitation has traditionally been modeled in terms of elastic and viscous components such as springs and dashpots (1–3). The corresponding theory is analogous to the electric circuit theory, which is extensively described in engineering textbooks. In many respects the use of mechanical models plays a didactic role in interpreting the viscoelasticity of materials in the simplest cases. However, it must be emphasized that the representation of the viscoelastic behavior in terms of springs and dashpots does not imply that these elements reflect the molecular mechanisms causing the actual relaxation

behavior of complex materials. Moreover, there are a multiplicity of models, nearly all equivalent, to represent the same viscoelastic behavior.

10.2 MAXWELL'S MODEL

As is well known, springs and dashpots represent, respectively, ideal elastic and viscous responses to step stress perturbations. In a similar way, a combination of the two can be used to describe the viscoelastic behavior of materials. The Maxwell model, a spring in series with a dashpot, is the more immediate idealization of this behavior (Fig. 10.1).

Let us consider first the response of the Maxwell model to a step stress $\sigma = \sigma_0 H(t)$, where $H(t)$ is the step unit. The strain ε is given by

$$\varepsilon = \varepsilon_1 + \varepsilon_2 \quad (10.1)$$

where ε_1 and ε_2 are the strains of the spring and dashpot, respectively. Since the stresses in the spring and in the dashpot are the same, we have

$$\varepsilon_1 = \frac{\sigma}{G} \quad (10.2)$$

$$\dot{\varepsilon}_2 = \frac{\sigma}{\eta} \quad (10.3)$$

Equations (10.1), (10.2), and (10.3) lead to the equation

$$\dot{\varepsilon} = \frac{\dot{\sigma}}{G} + \frac{\sigma}{\eta} \quad (10.4)$$

This expression allows the evaluation of the response to a step stress or step strain. A convenient way of solving this differential equation is to take the Laplace transform,

$$s\bar{\varepsilon}(s) - \varepsilon(0^+) = \frac{1}{G}[s\bar{\sigma}(s) - \sigma(0^+)] + \frac{1}{\eta}\bar{\sigma}(s) \quad (10.5)$$

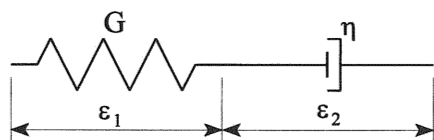


Figure 10.1 Schematic representation of the Maxwell model.

According to Eq. (10.5), the response of the model is to a step stress input $\sigma(t) = \sigma_0 H(t)$ is given by

$$\bar{\varepsilon}(s) = \frac{\varepsilon(0)}{s} + \frac{\sigma_0}{\eta s^2} \quad (10.6)$$

where the boundary conditions $\varepsilon(0^+) = \varepsilon_0$ and $\sigma(0^+) = \sigma_0$ were used. The inverse of the Laplace transform of Eq. (10.6) gives

$$\varepsilon(t) = \sigma_0 \left(\frac{1}{G} + \frac{t}{\eta} \right) \quad (10.7)$$

where $G = \sigma_0/\varepsilon_0$ (see Fig. 10.2). Consequently, the creep compliance function is expressed by

$$J(t) = \frac{\varepsilon(t)}{\sigma_0} = \frac{1}{G} + \frac{t}{\eta} \quad (10.8)$$

The Laplace transform of this equation leads to the complex compliance function

$$s \frac{\bar{\varepsilon}(s)}{\sigma_0} = s \bar{J}(s) = J^*(s) = \frac{1}{G} \left(1 + \frac{1}{\tau s} \right) \quad (10.9)$$

where it has been taken into account that $sJ(s) = J^*(s)$ and $\tau = \eta/G$ is the relaxation time. The complex function in this equation and other equations

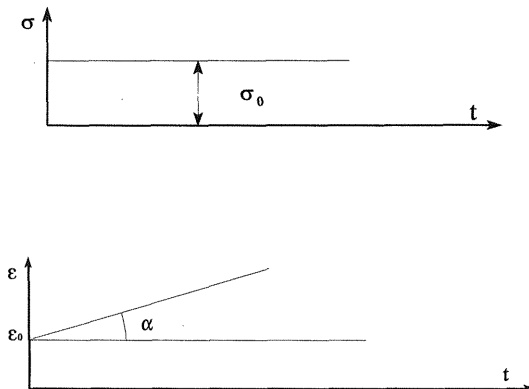


Figure 10.2 Response of an ideal liquid to a shear step stress input.

given below can be expressed in a more common form by carrying out the substitution $s = i\omega$. In this way, Eq. (10.9) can be written as

$$J^*(i\omega) = \frac{1}{G} \left(1 + \frac{1}{i\omega\tau} \right) \quad (10.10)$$

For a stress relaxation experiment, the response to the input strain $\varepsilon(t) = \varepsilon_0 H(t)$ can be obtained by considering that according to Figure 10.1,

$$\varepsilon_0 = \varepsilon_1 + \varepsilon_2 \quad (10.11)$$

Hence,

$$\dot{\varepsilon}_1 + \dot{\varepsilon}_2 = 0 \quad (10.12)$$

By combining Eqs. (10.11), (10.12), (10.2), and (10.3), we obtain

$$\frac{\dot{\sigma}}{G} + \frac{\sigma}{\eta} = 0 \quad (10.13)$$

whose Laplace transform adopts the form

$$\frac{1}{G} [s\bar{\sigma}(s) - \sigma(0^+)] + \frac{\bar{\sigma}(s)}{\eta} = 0 \quad (10.14)$$

From this expression, we find

$$\bar{\sigma}(s) = \frac{\eta}{G + \eta s} \sigma(0^+) \quad (10.15)$$

whose inverse gives

$$\sigma(t) = \sigma(0^+) \exp\left(-\frac{t}{\tau}\right) \quad (10.16)$$

where $\tau = \eta/G$. The input and output of the system are schematically represented in Figures 10.3a and 10.3b. The relaxation modulus is given by

$$G(t) = \frac{\sigma(t)}{\varepsilon_0} = \frac{\sigma(0^+)}{\varepsilon_0} \exp\left(-\frac{t}{\tau}\right) \quad (10.17)$$

and the complex relaxation modulus by

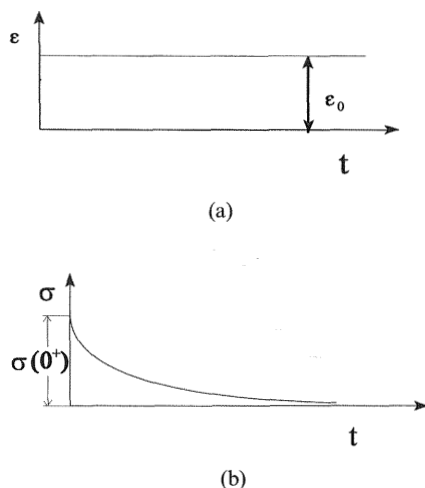


Figure 10.3 Response of a Maxwell liquid to a shear step strain input.

$$\frac{s\bar{\sigma}(s)}{\varepsilon_0} = s\bar{G}(s) = G^*(s) = G_0 \frac{s}{s + \tau^{-1}} \quad (10.18)$$

10.3 THE KELVIN-VOIGT MODEL

An alternative model with a degree of complexity similar to that of the Maxwell model is the Kelvin–Voigt element. This model, consisting of a spring in parallel with a dashpot (see Fig. 10.4), is adequate to describe creep behavior. The total stress in the model is the sum of the stress in the spring and that in the dashpot,

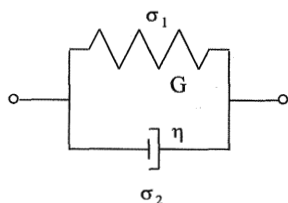


Figure 10.4 Schematic representation of the Kelvin–Voigt model.

$$\sigma = \sigma_1 + \sigma_2, \quad \text{or} \quad \sigma = G\varepsilon + \eta\dot{\varepsilon} \quad (10.19)$$

The Laplace transform of this equation for a step input gives

$$\frac{\sigma_0}{s} = G\bar{\varepsilon}(s) + \eta[s\bar{\varepsilon}(s) - \varepsilon(0^+)] \quad (10.20)$$

Since $\varepsilon(0^+) = 0$, Eq. (10.20) can be written as

$$\bar{\varepsilon}(s) = \frac{\sigma_0}{s(G + \eta s)} \quad (10.21)$$

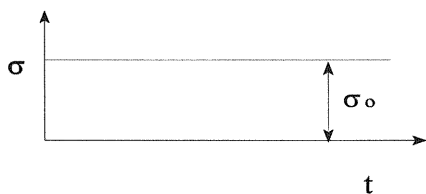
The inverse of $\bar{\varepsilon}(s)$ gives

$$\varepsilon(t) = \frac{\sigma_0}{G} \left[1 - \exp\left(-\frac{t}{\tau}\right) \right] \quad (10.22)$$

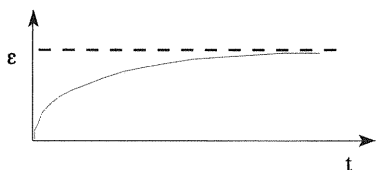
The response to the stress input of the Kelvin–Voigt element is schematically represented in Figure 10.5. From Eq. (10.22), the creep compliance function is easily obtained as

$$J(t) = J \left[1 - \exp\left(-\frac{t}{\tau}\right) \right] \quad (10.23)$$

where $J = 1/G$ for an elastic spring. The corresponding complex compliance function is



(a)



(b)

Figure 10.5 Response of a Kelvin–Voigt solid to a shear step stress input.

$$J^*(s) = \frac{s\bar{\varepsilon}(s)}{\sigma_0} = \frac{1}{G(1+s\tau)} = \frac{J}{(1+s\tau)} \quad (10.24)$$

The Maxwell and Kelvin–Voigt models are unable to represent conveniently the material response of a viscoelastic system. A better approach to the actual behavior is achieved by using more complex models.

10.4 THREE-ELEMENT STANDARD SOLID

What is commonly called the three-element standard, or simply the standard solid (or Zener's solid), is a combination of either a Kelvin–Voigt element in series with a spring or, alternatively, a Maxwell element in parallel with a spring (see Fig. 10.6). The strain response of the first model to the stress input $\sigma = \sigma_0 H(t)$ can be written as

$$\varepsilon = \varepsilon_1 + \varepsilon_2 \quad (10.25)$$

From this equation and taking into account that

$$\sigma = G_0 \varepsilon_1; \quad \sigma = G_1 \varepsilon_2 + \eta \dot{\varepsilon}_2 \quad (10.26)$$

we find

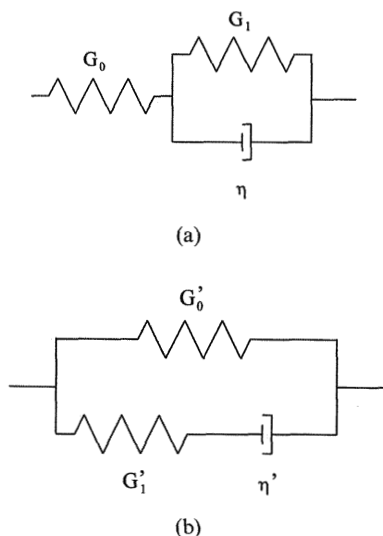


Figure 10.6 Two equivalent schemes of the Zener's solid.

$$\frac{G_1}{\eta} \varepsilon + \dot{\varepsilon} = \frac{1}{\eta} \left(1 + \frac{G_1}{G_0} \right) \sigma + \frac{\dot{\sigma}}{G_0} \quad (10.27)$$

For a stress history $\sigma = \sigma_0 H(t)$, the Laplace transform of Eq. (10.27) gives

$$\bar{\varepsilon}(s) = \frac{\varepsilon(0)}{s + \tau^{-1}} + \frac{\sigma_0}{\eta} \left(1 + \frac{G_1}{G_0} \right) \left(\frac{1}{s(s + \tau^{-1})} \right) \quad (10.28)$$

where $\tau = \eta/G_1$. The inverse of $\bar{\varepsilon}(s)$ is the strain response given by

$$\varepsilon(t) = \frac{\sigma_0}{G_0} + \frac{\sigma_0}{G_1} \left[1 - \exp\left(-\frac{t}{\tau}\right) \right] \quad (10.29)$$

Then the creep compliance function can be written as

$$J(t) = \frac{1}{G_0} + \frac{1}{G_1} \left[1 - \exp\left(-\frac{t}{\tau}\right) \right] = J_g + J_1 \left[1 - \exp\left(-\frac{t}{\tau}\right) \right] \quad (10.30)$$

where $J_g = G_0^{-1}$ and $J_1 = G_1^{-1}$. From the Laplace transform of Eq. (10.30), the complex compliance function is obtained as

$$J^*(s) = J_g + \frac{J_1}{1 + s\tau} \quad (10.31)$$

For a step strain input $\varepsilon = \varepsilon_0 H(t)$, the Laplace transform of Eq. (10.27) is

$$\frac{G_1}{\eta} \bar{\varepsilon}(s) = \frac{1}{\eta} \left(1 + \frac{G_1}{G_0} \right) \bar{\sigma}(s) + \frac{1}{G_0} \left[s \bar{\sigma}(s) - \sigma(0^+) \right] \quad (10.32)$$

The Laplace inverse of Eq. (10.32) gives the response of the model to the step strain input:

$$\sigma(t) = \sigma_0 \left\{ \left(G_1 \frac{\varepsilon_0/\sigma_0}{1 + G_1/G_0} \right) + \frac{1}{1 + G_1/G_0} \exp\left[-\frac{G_0}{\eta} \left(1 + \frac{G_1}{G_0} \right) t \right] \right\} \quad (10.33)$$

where $\sigma_0 = \sigma(0^+) = \varepsilon_0 G_0$. Then the relaxation modulus can be written as

$$G(t) = \frac{\sigma(t)}{\varepsilon_0} = \frac{G_1}{1 + G_1/G_0} + \frac{G_0}{1 + G_1/G_0} \exp\left[-\frac{G_0}{\eta} \left(1 + \frac{G_1}{G_0} \right) t \right] \quad (10.34)$$

while the complex relaxation modulus obtained from the Laplace transform of Eq. (10.34) is given by

$$G^*(s) = [J^*(s)]^{-1} = \left(\frac{1 + s\tau}{1 + s\tau + G_0/G_1} \right) G_0 \quad (10.35)$$

Let us consider now the response of the solid standard model located on the right-hand side of Figure 10.6 to a step strain function (Fig. 10.7). In this case,

$$\sigma = \sigma_1 + \sigma_2 \quad (10.36)$$

where $\sigma_1 = G_0 \varepsilon$ and

$$\dot{\varepsilon} = \frac{\dot{\sigma}_1}{G_1} + \frac{\sigma_2}{\eta'} \quad (10.37)$$

Equations (10.36) and (10.37) lead to the generalized differential equation

$$\tau' \dot{\sigma} + \sigma = \tau(G_0' + G_1') \dot{\varepsilon} + G_0' \varepsilon \quad (10.38)$$

where $\tau' = \eta'/G_1'$ and $\tau = \eta/G_1$. The response of the model to the input strain $\varepsilon(t) = \varepsilon_0 H(t)$ is easily obtained from the inverse of the Laplace transform of Eq. (10.38). The pertinent equation is

$$\sigma(t) = \varepsilon_0 [G_0' + G_1' \exp(-t/\tau')] \quad (10.39)$$

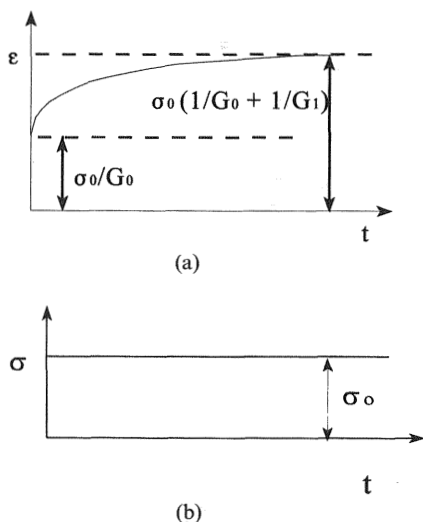


Figure 10.7 Response of the Zener model (Fig. 10.6a) to a shear step stress input.

The relaxation moduli in the time and frequency domains are given by

$$G(t) = G'_0 + G'_1 \exp(-t/\tau') \tag{10.40}$$

and

$$s\bar{G}(s) = G^*(s) = G'_0 + \frac{G'_1 s \tau'}{1 + s \tau'} \tag{10.41}$$

The schemes of the strain input and the stress response are given in Figures 10.8a and 10.8b. In the same way, the response of the model to the shear stress input $\sigma = \sigma_0 H(t)$ can be obtained from the Laplace transform of Eq. (10.38). The corresponding equation is

$$\varepsilon(t) = \sigma_0 \left\{ \frac{1}{G'_0 + G'_1} + \frac{G'_1}{G'_0(G'_0 + G'_1)} \left[1 - \exp\left(-\frac{t}{\tau'}\right) \right] \right\} \tag{10.42}$$

where $\tau' = (\tau/G_0)(G_0 + G_1)$.

By comparing Eqs. (10.29) and (10.42) on the one side and Eqs. (10.33) and (10.39) on the other, it is easy to obtain the equivalence between the two models of three elements. The pertinent relationships are

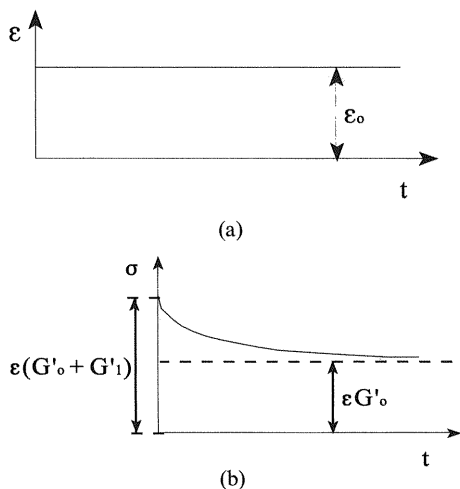


Figure 10.8 Response of the Zener model (Figure 10.6b) to a shear step strain input.

$$G_0 = G'_0 + G'_1 \quad (10.43a)$$

$$G_1 = \frac{G'_0}{G'_1} (G'_0 + G'_1) \quad (10.43b)$$

and

$$\tau = \tau' \frac{G'_0 + G'_1}{G'_0} \quad (10.43c)$$

and conversely

$$G'_0 = \frac{G_0 G_1}{G_0 + G_1} \quad (10.44a)$$

$$G'_1 = \frac{G_0^2}{G_0 + G_1} \quad (10.44b)$$

and

$$\tau' = \tau \frac{G_1}{G_0 + G_1} \quad (10.44c)$$

10.5 BURGERS MODEL

The Burgers model, also called a linear liquid of four elements, is a combination of the Maxwell model with a Kelvin–Voigt element (see Fig. 10.9). For a stress input, the strains are additive,

$$\varepsilon = \varepsilon_1 + \varepsilon_2 + \varepsilon_3 \quad (10.45)$$

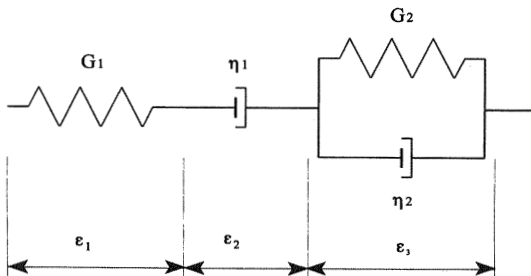


Figure 10.9 Schematic representation of the Burgers model.

Moreover,

$$\varepsilon_1 = \frac{\sigma_0}{G_1}; \quad \dot{\varepsilon}_2 = \frac{\sigma_0}{\eta_1}; \quad \dot{\varepsilon}_3 + \frac{G_2}{\eta_2} \varepsilon_3 = \frac{\sigma_0}{\eta_2} \quad (10.46)$$

After eliminating ε_1 , ε_2 , and ε_3 between these equations, one obtains

$$\sigma + \left[\frac{\eta_2}{G_2} + \eta_1 \left(\frac{1}{G_1} + \frac{1}{G_2} \right) \right] \dot{\sigma} + \frac{\eta_1 \eta_2}{G_1 G_2} \ddot{\sigma} = \eta_1 \dot{\varepsilon} + \frac{\eta_1 \eta_2}{G_2} \ddot{\varepsilon} \quad (10.47)$$

The response to a step stress input $\sigma = \sigma_0 H(t)$ is given by

$$\varepsilon(t) = \sigma_0 \left\{ \frac{1}{G_1} + \frac{t}{\eta_1} + \frac{1}{G_2} \left[1 - \exp\left(-\frac{t}{\tau_2}\right) \right] \right\} \quad (10.48)$$

where $\tau_2 = \eta_2/G_2$. The complex compliance function obtained from the Laplace transform of Eq. (10.48) is

$$J^*(s) = \frac{1}{G_1} + \frac{1}{\eta_1 s} + \frac{1}{G_2(s\tau_2 + 1)} \quad (10.49)$$

For a strain step input $\varepsilon(t) = \varepsilon_0 H(t)$, Eq. (10.47) becomes

$$\sigma + r_1 \dot{\sigma} + r_2 \ddot{\sigma} = q_1 \varepsilon_0 \delta(t) + q_2 \varepsilon_0 \frac{d}{dt} \delta(t) \quad (10.50)$$

where $\delta(t)$ is the Dirac delta function and the parameters r_1 , r_2 , q_1 , and q_2 , are

$$\begin{aligned} r_1 &= \eta_1 \left(\frac{1}{G_1} + \frac{1}{G_2} \right) + \frac{\eta_2}{G_2}; & r_2 &= \frac{\eta_1 \eta_2}{G_1 G_2} \\ q_1 &= \eta_1; & q_2 &= \frac{\eta_1 \eta_2}{G_2} \end{aligned} \quad (10.51)$$

Solution of Eq. (10.5) gives

$$\sigma(t) = \frac{\varepsilon_0}{A} [(q_1 - q_2 r_1) \exp(-r_1 t) - (q_1 - q_2 r_2) \exp(-r_2 t)] \quad (10.52)$$

r_1 , r_2 and A being

$$r_1 = \frac{z_1 - A}{2z_2}; \quad r_2 = \frac{z_1 + A}{2z_2}; \quad A = [z_1^2 - z_2^2]^{1/2} \quad (10.53)$$

where z_1 and z_2 are the roots of the equation $r_2 z^2 + r_1 z + 1 = 0$. The linear liquid standard model of four elements is adequate to study the response of a liquid system under a creep recovery test.

10.6 MAXWELL AND KELVIN-VOIGT GENERALIZED MODELS

The elementary models studied above describe the rheological behavior of only very simple systems. The models assume that a single relaxation time governs the response of the material to a mechanical perturbation. However, there exists experimental evidence of a distribution of relaxation or retardation times. Such a distribution may be considered either discrete or continuous. On this experimental basis it is possible to generalize the models so that they more closely represent the actual behavior of materials. These generalizations can easily be carried out by assuming an arrangement of Maxwell elements in parallel or, alternatively, an arrangement of Kelvin-Voigt elements in series. The corresponding schemes are displayed in Figure 10.10. In Figure 10.10a an elastic element has been added to account for the instantaneous response. In Figure 10.10b a Maxwell element has been added in series to reflect the liquid behavior.

The relaxation and retardation functions for these models in the case of a discrete distribution of relaxation or retardation times are obviously given by

$$G(t) = G_e + \sum_{i=1}^n G_i \exp \frac{-t}{\tau_i} \quad (10.54a)$$

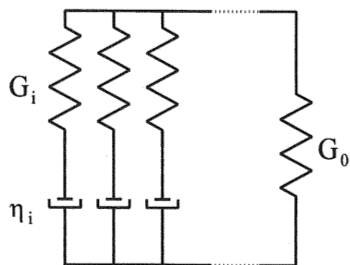
and

$$J(t) = J_g + \sum_{i=1}^n J_i \left(1 - \exp \frac{-t}{\tau_i} \right) + \frac{t}{\eta_0} \quad (10.54b)$$

where $J_g = G_g^{-1}$ and $J_i = G_i^{-1}$. In the case of a continuous distribution of retardation or relaxation times the retardation $J(t)$ and relaxation $G(t)$ functions can be written as

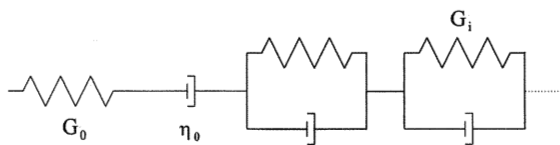
$$G(t) = G_e + \int_0^{\infty} G(\tau) \exp \frac{-t}{\tau} d\tau \quad (10.55a)$$

and



$$\tau_i = \eta_i / G_i$$

(a)



$$\tau_i = \eta_i / G_i$$

(b)

Figure 10.10 (a) Maxwell's elements in parallel (b) Kelvin-Voigt elements in series.

$$J(t) = J_g + \int_0^\infty J(\tau) \left(1 - \exp\left(-\frac{t}{\tau}\right)\right) d\tau + \frac{t}{\eta_0} \tag{10.55b}$$

where

$$\int_0^\infty G(\tau) d\tau = 1; \quad \int_0^\infty J(\tau) d\tau = 1 \tag{10.56}$$

Equations (10.55a) and (10.55b) can alternatively be written as

$$G(t) = G_e + \int_{-\infty}^\infty H(\tau) \exp\left(-\frac{t}{\tau}\right) d \ln \tau \tag{10.57a}$$

and

$$J(t) = J_g + \int_{-\infty}^\infty L(\tau) \left(1 - \exp\left(-\frac{t}{\tau}\right)\right) d \ln \tau + \frac{t}{\eta_0} \tag{10.57b}$$

where $H(\tau) = \tau G(\tau)$ and $L(\tau) = \tau J(\tau)$ are, respectively, the relaxation and retardation times to which we have already referred in Chapter 9. Obviously, Maxwell elements in parallel can describe the liquid viscoelastic behavior of materials if the spring G_e is eliminated from Figure 10.10a. In the same way, the Kelvin-Voigt elements in series of Figure 10.10b also describe the viscoelastic behavior of solids if the dashpot η_0 in the Maxwell element is eliminated.

10.7 LADDER MODELS

As we have seen in Eq. (10.18), the complex relaxation modulus obtained from the Maxwell model is given by

$$G^*(s) = \frac{G_0 s}{s + \tau^{-1}} \quad (10.58)$$

When we deal with n terms of the same type, their sum can be represented by means of a rational fraction

$$G^*(s) = \frac{sP_{n-1}(s)}{Q_n(s)} \quad (10.59)$$

where $n - 1$ and n are the degrees of the polynomials $P(s)$ and $Q(s)$ appearing in the numerator and denominator, respectively, of the fraction. By taking into account that $J^*(s) = [G^*(s)]^{-1}$, the complex compliance function can be written as

$$J^*(s) = \frac{Q_n(s)}{sP_{n-1}(s)} \quad (10.60)$$

By developing Eq. (10.60) according to the continuous fraction formalism, the following ladder function is found:

$$J^*(s) = [G^*(s)]^{-1} = a_1 + \frac{1}{b_1 s + \frac{1}{a_2 + \frac{1}{\ddots + \frac{1}{b_n s}}}} \quad (10.61)$$

This expression corresponds to the mechanical model shown in Figure 10.11, called the discrete ladder model, where a_i and b_i are the coefficients of the elastic and viscous components respectively. This model was initially proposed by Marvin and Gross.

10.8 DISTRIBUTED CONSTANTS MODELS

It is well known that the behavior of electrical transmission lines can be represented in terms of distributed passive elements. As we mentioned at the beginning of this chapter, there exists an analogy between the electrical and mechanical behavior of the systems. Returning to the Maxwell model, one has

$$\bar{\sigma}(s) = s\bar{\epsilon}(s)\frac{G}{s + \tau^{-1}} \quad (10.62)$$

On the other hand, according to Ohm's law, the electrical admittance is given by

$$Y(s) = \frac{I(s)}{V(s)} \quad (10.63)$$

The electromechanical analogy indicates that $\dot{\epsilon}(t)$ can be identified with $I(t)$ (electrical intensity of current) and $\sigma(t)$ with $V(t)$ (electrical voltage). Therefore, $s\bar{\epsilon}(s)$ and $\bar{\sigma}(s)$ correspond, respectively, to $I(s)$ and $V(s)$ so that the mechanical admittance can be written as

$$Y(s) = \frac{s}{G} + \frac{1}{\eta} \quad (10.64)$$

where use was made of Eq. (10.62). Accordingly, the dashpot viscosity corresponds to the electrical resistor, and the inverse of the spring elasticity

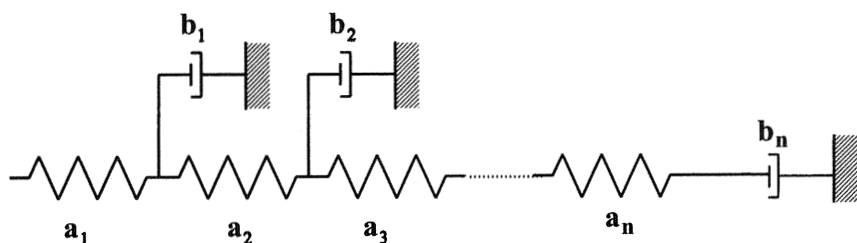


Figure 10.11 Ladder model.

modulus corresponds to the capacitance. The analogous electrical scheme of the Maxwell model is given in Figure 10.12. The equivalences between elastic and electrical parameters are

$$\begin{aligned} R &= \eta; & G^{-1} &= C; & \tau &= RC \\ Y(s) &= Cs + G; & G &= R^{-1} = \eta^{-1} \end{aligned} \quad (10.65)$$

We notice that the elements in series in the mechanical model are transformed in parallel in the electrical analogy. The converse is true for the Kelvin–Voigt model. The electrical analog of a ladder model is thus an electrical filter.

We can generalize the analogy by considering the viscoelastic materials as a continuum where the theory of transmission lines can be applied. In this way, a continuous distribution of passive elements such as springs and dash-pots can be used to model the viscoelastic behavior of materials. Thus the relevant equations for a mechanical transmission line can be written following the same patterns as those in electrical transmission lines. By representing the impedance and admittance per unit of length by g and j respectively, one has

$$\frac{dV}{dx} = gI; \quad \frac{dI}{dx} = jV \quad (10.66)$$

while the mechanical analog can be written as

$$\frac{d\sigma}{dx} = \sigma' = g\dot{\epsilon}; \quad \frac{d\dot{\epsilon}}{dx} = \dot{\epsilon}' = j\sigma \quad (10.67)$$

From Eq. (10.67) one has

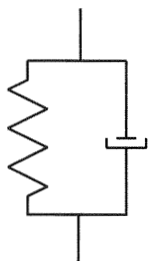


Figure 10.12 Electrical scheme analogous to the Maxwell model.

$$\sigma'' = gj\sigma; \quad \varepsilon'' = jg\varepsilon \quad (10.68)$$

The solutions of these second-order differential equations are

$$\begin{aligned} \sigma_x &= A \cosh \beta x + B \sinh \beta x \\ \dot{\varepsilon}_x &= A' \cosh \beta x + B' \sinh \beta x \end{aligned} \quad (10.69)$$

where x is the distance from the terminus of the line to a characteristic point of the same line, and $\beta = (gj)^{1/2}$ is called the propagation constant. From the boundary conditions one finds

$$\text{For } x = 0, \quad \sigma(0) = A \text{ and } \dot{\varepsilon} = A' \quad (10.70a)$$

$$\text{For } x = L, \quad B = A' \frac{\beta}{j} = A' \frac{g}{\beta} = \dot{\varepsilon} G \quad (10.70b)$$

$$B' = A \frac{j}{\beta} = \frac{\sigma(0)}{G} \quad (10.70c)$$

where the characteristic mechanical impedance G is given by

$$G = \left(\frac{g}{j} \right)^{1/2} = \frac{\beta}{j} = \frac{g}{\beta} \quad (10.71)$$

Accordingly, Eqs. (10.69) can be written as

$$\sigma_x = \sigma(0) \cosh \beta x + \dot{\varepsilon}(0) G \sinh \beta x \quad (10.72a)$$

$$\dot{\varepsilon}_x = \dot{\varepsilon}(0) \cosh \beta x + \frac{\sigma(0)}{G} \sinh \beta x \quad (10.72b)$$

Several specific situations can be considered:

1. For a short-circuit regime, the stress at the end of the line is null, $\sigma(0) = 0$, and Eqs. (10.72) become

$$\sigma_x = \dot{\varepsilon}(0) G \sinh \beta x \quad (10.73a)$$

and

$$\dot{\varepsilon}_x = \dot{\varepsilon}(0) \cosh \beta \quad (10.73b)$$

Hence,

$$\frac{\sigma_x}{\dot{\epsilon}_x} = G \tanh \beta x \quad (10.74)$$

The Laplace transform of Eq. (10.74) gives the complex relaxation modulus of the viscoelastic material in terms of its characteristic impedance,

$$G^*(s) = sG(s) \tanh \beta(s)x \quad (10.75)$$

2. For $x = L$, Eqs. (10.72) become

$$\sigma_L = \sigma(0) \cosh \beta L + \epsilon(0)G \sinh \beta L \quad (10.76a)$$

and

$$\dot{\epsilon}_L = \dot{\epsilon}(0) \cosh \beta L + \frac{\sigma(0)}{G} \sinh \beta L \quad (10.76b)$$

σ_L and $\dot{\epsilon}_L$ being the values of the shear stress and the strain rate at the beginning of the transmission line where the mechanical excitation line is applied. From these equations one easily finds

$$\sigma(0) = \sigma_L \cosh \beta L - \dot{\epsilon}_L G \sinh \beta L \quad (10.77a)$$

$$\dot{\epsilon}(0) = \dot{\epsilon}_L \cosh \beta L - \frac{\sigma_L}{G} \sinh \beta L \quad (10.77b)$$

3. For an infinitely long chain, $x \rightarrow \infty$, $\lim \tanh \beta x \rightarrow 1$, and from Eq. (10.74) one finds

$$\frac{\sigma(\infty)}{\dot{\epsilon}(\infty)} = G \quad (10.78)$$

That is, the characteristic impedance G is the impedance at any point of the transmission line.

4. Equations (10.72) can be written in terms of the distance to the origin, adopting, in this case, the forms

$$\sigma_r = \sigma(0) \cosh \beta(L - r) + \dot{\epsilon}(0)G \sinh \beta(L - r) \quad (10.79a)$$

and

$$\dot{\epsilon}_r = \dot{\epsilon}(0) \cosh \beta(L - r) + \frac{\sigma(0)}{G} \sinh \beta(L - r) \quad (10.79b)$$

where $r = L - x$. Alternatively, the substitution of the values given for $\sigma(0)$ and $\dot{\epsilon}(0)$ in Eqs. (10.72) into Eqs. (10.79) gives

$$\sigma_r = \sigma_L \cosh \beta r - \dot{\epsilon}_L G \sinh \beta r \quad (10.80a)$$

$$\dot{\epsilon}_r = \dot{\epsilon}_L \cosh \beta r - \frac{\sigma_L}{G} \sinh \beta r \quad (10.80b)$$

For an infinite transmission line ($r \rightarrow \infty$, $L \rightarrow \infty$), Eqs. (10.80) become

$$\sigma_r = \sigma_L \exp(-\beta r) \quad \text{and} \quad \dot{\epsilon}_r = \dot{\epsilon}_L \exp(-\beta r) \quad (10.81)$$

These expressions indicate that the input impedance is the same at any point of the line. Alternatively, if the final impedance of a transmission line is the characteristic impedance, such a line behaves as an infinite line.

PROBLEM SETS

Problem 10.1

Determine the harmonic response for an input given by

$$\epsilon(t) = 0, \quad t < 0$$

$$\epsilon(t) = \epsilon_0 e^{i\omega t}, \quad t \geq 0$$

of a material whose viscoelastic behavior is given by a standard solid formed by a spring in parallel with a Maxwell element.

Solution 10.1

From Eq. (5.50)

$$\sigma(t) = G_0 \epsilon(t) + \int_{-\infty}^t \epsilon(\tau) \dot{G}(t - \tau) d\tau \quad (\text{P10.1.1})$$

If $\epsilon(t) = \epsilon_0 \exp(i\omega t)$, one obtains

$$\begin{aligned}\sigma(t) &= \varepsilon_0 \exp(i\omega t) \left[G_0 + \int_0^\infty e^{-i\omega s} \dot{G}(s) ds \right] \\ &= \varepsilon_0 \exp(i\omega t) \left[G_0 + \int_0^\infty \dot{G}(s) \cos \omega s ds + i \int_0^\infty \dot{G}(s) \sin \omega s ds \right] \quad (\text{P10.1.2})\end{aligned}$$

$$G^*(i\omega) = G'(\omega) + iG''(\omega) = G_0 + \int_0^\infty \dot{G}(s) \cos \omega s ds + i \int_0^\infty \dot{G}(s) \sin \omega s ds \quad (\text{P10.1.3})$$

For a standard solid such as that shown in Figure P10.1.1, the relaxation modulus is given by

$$G(t) = G_0 + G \exp\left(\frac{-t}{\tau_0}\right), \quad \frac{\eta}{G} = \tau_0 \quad (\text{P10.1.4})$$

Then

$$\dot{G}(s) = -\frac{G}{\tau_0} \exp\left(-\frac{s}{\tau_0}\right) \quad (\text{P10.1.5})$$

and Eq. (P10.1.3) becomes

$$G^*(i\omega) = G_0 + \int_0^\infty e^{-i\omega s} \dot{G}(s) ds \quad (\text{P10.1.6})$$

From Eqs. (P10.1.5) and (P10.1.6) one obtains

$$G^*(i\omega_0) = G_0 + G \frac{\omega^2 \tau_0^2}{1 + \omega^2 \tau_0^2} + i \frac{G\omega\tau_0}{1 + \omega^2 \tau_0^2} \quad (\text{P10.1.7})$$

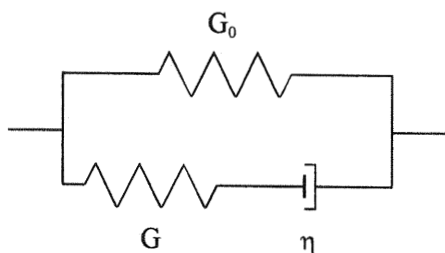


Figure P10.1.1

By applying a Laplace transform to a three-element standard solid, the transitory response can also be obtained. In this case, Eq. (P10.1.7) can be written as

$$G_0 + \frac{G\tau s}{1 + \tau s} = G^*(s) \quad (\text{P10.1.8})$$

where $s = i\omega$. By assuming a sinusoidal excitation $\varepsilon(t) = \varepsilon_0 \sin \omega t$, one obtains

$$\bar{\sigma}(s) = \bar{\varepsilon}(s)G^*(s) = \varepsilon_0 \left(G_0 + \frac{G\tau s}{1 + \tau s} \right) \left(\frac{\omega}{\omega^2 + s^2} \right) \quad (\text{P10.1.9})$$

where it was considered that

$$\varepsilon(s) = \frac{\varepsilon_0 \omega}{\omega^2 + s^2} \quad (\text{P10.1.10})$$

As usual, in order to calculate the inverse transform of (P10.1.9) the following decomposition can be used:

$$\bar{F}(s) = \frac{\tau s}{1 + \tau s} \left(\frac{\omega}{\omega^2 + s^2} \right) = \frac{A}{1 + \tau s} + \frac{Bs + C\omega^2}{\omega^2 + s^2} \quad (\text{P10.1.11})$$

where

$$A = -\frac{\omega\tau^2}{1 + \omega^2\tau^2}; \quad B = \frac{\omega\tau}{1 + \omega^2\tau^2}; \quad C = \frac{\omega\tau^2}{1 + \omega^2\tau^2} \quad (\text{P10.1.12})$$

Therefore

$$\bar{F}(s) = \frac{\omega^2\tau^2}{1 + \omega^2\tau^2} \left(\frac{\omega}{\omega^2 + s^2} \right) + \frac{\omega\tau}{1 + \omega^2\tau^2} \left(\frac{s}{\omega^2 + s^2} \right) - \frac{\omega\tau}{1 + \omega^2\tau^2} \left(\frac{1}{s + 1/\tau} \right) \quad (\text{P10.1.13})$$

whose Laplace inverse can be written as

$$F(t) = \frac{\omega^2\tau^2}{1 + \omega^2\tau^2} \sin \omega t + \frac{\omega\tau}{1 + \omega^2\tau^2} \cos \omega t - \frac{\omega\tau}{1 + \omega^2\tau^2} e^{-t/\tau} \quad (\text{P10.1.14})$$

The final result for $\sigma(t)$ is given by

$$\sigma(t) = \epsilon_0 \left[\left(G_0 + \frac{G\omega^2\tau^2}{1 + \omega^2\tau^2} \right) \sin \omega t + \frac{G\omega\tau}{1 + \omega^2\tau^2} \cos \omega t - \frac{G\omega\tau}{1 + \omega^2\tau^2} \exp\left(-\frac{t}{\tau}\right) \right] \tag{P10.1.15}$$

The last term on the right-hand side of this equation is the transitory response that decays rapidly with time.

Thus at long time, Eq. (P10.1.15) leads to Eq. (P10.1.7).

Problem 10.2

A standard solid (Kelvin–Voigt element in series with a spring) (Figure 10.2.1) is under a stress σ for a long time. Calculate the response of the solid after the load is eliminated (creep recovery experiment).

Solution 10.2

Method 1

The strain response to a load $\sigma(t) = \sigma_0 H(t)$ has two components. The first corresponds to an elastic element given by

$$\epsilon_1 = \frac{\sigma_0 H(t)}{G_1} \tag{P10.2.1}$$

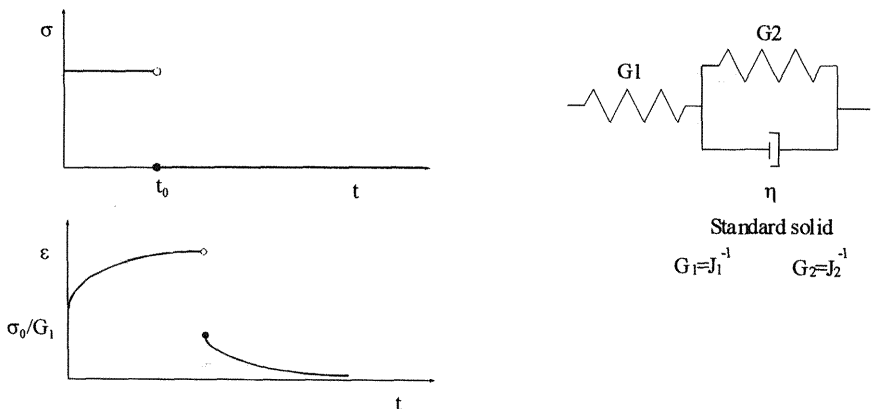


Figure P10.2.1

where $H(t)$ is the step unit. The second is a creep function governed by the equation

$$\sigma_0 H(t) = \varepsilon G_2 + \dot{\varepsilon} \eta_2 \quad (\text{P10.2.2})$$

The solution of this differential equation is given by

$$\varepsilon(t) = \frac{\sigma_0}{G_2} \left[1 - \exp\left(\frac{-t}{\tau_2}\right) \right] H(t), \quad \tau_2 = \frac{\eta_2}{G_2} \quad (\text{P10.2.3})$$

The total strain response can be written as

$$\begin{aligned} \varepsilon &= \left\{ \frac{\sigma_0}{G_1} + \frac{\sigma_0}{G_2} \left[1 - \exp\left(\frac{-t}{\tau}\right) \right] \right\} H(t) \\ &= \sigma_0 \left\{ \frac{1}{G_1} + \frac{1}{G_2} \left[1 - \exp\left(\frac{-t}{\tau}\right) \right] \right\} H(t), \quad 0 < t \leq t_0 \end{aligned} \quad (\text{P10.2.4})$$

When the load is eliminated at $t = t_0$, Eq. (P10.2.2) gives

$$\dot{\varepsilon} \eta_2 + \varepsilon G_2 = 0$$

from which

$$\varepsilon = C \exp\left(-\frac{t - t_0}{\tau_2}\right) \quad (\text{P10.2.5})$$

The constant C is given by $\varepsilon = \varepsilon(t_{0+})$, and consequently for $t > t_0$,

$$\varepsilon(t_{0+}) = \frac{\sigma_0}{G_2} \left[1 - \exp\left(\frac{-t_0}{\tau}\right) \right] \quad (\text{P10.2.6})$$

By combining Eqs. (P10.2.5) and (P10.2.6), the recoverable compliance is obtained as

$$\begin{aligned} \varepsilon(t) &= \frac{\sigma_0}{G_2} \left[1 - \exp\left(\frac{-t_0}{\tau}\right) \right] \exp\left(\frac{-(t - t_0)}{\tau_2}\right) \\ &= \frac{\sigma_0}{G_2} \left[\exp\left(\frac{t_0}{\tau}\right) - 1 \right] \exp\left(\frac{-t}{\tau}\right), \quad t \geq t_0 \end{aligned} \quad (\text{P10.2.7})$$

Method 2

From Eq. (5.35),

$$\varepsilon(t) = \int_0^{\infty} J(t - \tau) \frac{d\bar{\sigma}(\tau)}{d\tau} d\tau \quad (\text{P10.2.8})$$

Taking the Laplace transform, we have

$$\bar{\varepsilon}(s) = s\bar{\sigma}(s)\bar{J}(s) \quad (\text{P10.2.9})$$

Let us calculate $sJ(s)$ for Kelvin–Voigt element. The constitutive equation is

$$\sigma = G\varepsilon + \eta\dot{\varepsilon} \quad (\text{P10.2.10})$$

The Laplace transform of this equation is given by

$$\bar{\sigma}(s) = (G + \eta s)\bar{\varepsilon}(s) \quad (\text{P10.2.11})$$

Hence,

$$\bar{\varepsilon}(s) = \frac{\bar{\sigma}(s)}{G + \eta s} = \bar{\sigma}(s) \frac{J}{1 + s\tau} \quad (\text{P10.2.12a})$$

with

$$\tau = \frac{\eta}{G} \quad \text{and} \quad J = G^{-1} \quad (\text{P10.2.12b})$$

After adding an elastic element, we obtain

$$s\bar{J}(s) = J_1 + \frac{J_2}{1 + s\tau_2} = \frac{\bar{\varepsilon}(s)}{\bar{\sigma}(s)} \quad (\text{P10.2.13})$$

By taking into account that for a stress step input

$$\bar{\sigma}(s) = \frac{1}{s}\sigma_0 \quad (\text{P10.2.14})$$

the inverse Laplace transform of Eq. (P10.2.13) is given by

$$\varepsilon(t) = \sigma_0 \{J_1 + J_2[1 - \exp(-t/\tau_2)]\} H(t) \quad (\text{P10.2.15})$$

where $J_1 = G_1^{-1}$ and $J_2 = G_2^{-1}$, the same result as that obtained by the first method.

For a creep recovery test, we obtain

$$\varepsilon(t) = \sigma_0 J(t), \quad 0 \leq t < t_0 \quad (\text{P10.2.16})$$

or

$$\varepsilon(t) = \sigma_0 [J(t) - J(t - t_0)], \quad t \geq t_0 \quad (\text{P10.2.17})$$

From Eqs. (P10.2.15) and (P10.2.17) we finally find

$$\begin{aligned} \frac{\varepsilon(t)}{\sigma_0} &= J_1 + J_2 \left[1 - \exp\left(-\frac{t}{\tau}\right) \right] - \left\{ J_1 + J_2 \left[1 - \exp\left(-\frac{t-t_0}{\tau}\right) \right] \right\} \\ &= J_2 \left[\exp\left(\frac{t_0}{\tau} - 1\right) \right] \exp\left(-\frac{t}{\tau}\right), \quad t \geq t_0 \end{aligned} \quad (\text{P10.2.18})$$

which is the same result as that obtained by the first method.

Problem 10.3

In a dynamic viscoelastic test the following results are obtained:

f (Hz)	J' (Pa^{-1})	$\tan \delta$
0.1	10^{-9}	0.1
10	0.8×10^{-9}	0.08

Fit this behavior to that of a standard solid (spring in series with Kelvin-Voigt element).

Solution 10.3

For the standard solid model, the real and imaginary parts of the complex compliance function are

$$J' = J_0 \left(1 + \frac{J_1/J_0}{1 + \omega^2 \tau^2} \right) \quad (\text{P10.3.1})$$

and

$$J'' = J_1 \left(\frac{\omega \tau}{1 + \omega^2 \tau^2} \right) \quad (\text{P10.3.2})$$

According to the data of the problem,

$$J''(0.1 \text{ Hz}) = 10^{-1} \times 10^{-9} \text{ Pa}^{-1}$$

$$J''(10 \text{ Hz}) = 0.08 \times 8 \times 10^{-10} \text{ Pa}^{-1}$$

From Eqs. (P10.3.1) and (P10.3.2) we obtain

$$10^{-9} = J_0 \left(1 + \frac{J_1/J_0}{1 + (0.2\pi\tau)^2} \right) \quad (\text{P10.3.3})$$

$$0.8 \times 10^{-9} = J_0 \left(1 + \frac{J_1/J_0}{1 + (20\pi\tau)^2} \right) \quad (\text{P10.3.4})$$

$$10^{-10} = J_1 \left(\frac{0.2\pi\tau}{1 + (0.2\pi\tau)^2} \right) \quad (\text{P10.3.5})$$

$$0.64 \times 10^{-10} = J_1 \left(\frac{20\pi\tau}{1 + (20\pi\tau)^2} \right) \quad (\text{P10.3.6})$$

From these equations the following parameters are obtained:

$$\tau = 0.205 \text{ s}; \quad J_1 = 8.08 \times 10^{-10} \text{ Pa}^{-1}; \quad J_0 = 3.16 \times 10^{-9} \text{ Pa}^{-1}$$

Problem 10.4

Find the response of a Burgers element to a creep recovery experiment. With the help of a sketch of the strain response, find the parameters of the model.

Solution 10.4

The mechanical history for a creep recovery experiment is given in Figure P10.4.1.

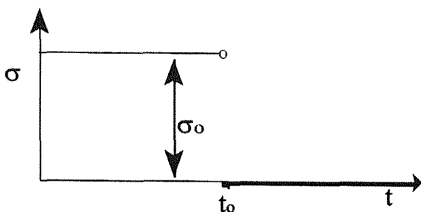


Figure P10.4.1

According to Eq. (10.48), the strain for the Burgers model at $t < t_0$ is given by

$$\varepsilon(t) = \sigma_0 \left\{ \frac{1}{G_1} + \frac{t}{\eta_1} + \frac{1}{G_2} \left[1 - \exp\left(-\frac{t}{\tau_2}\right) \right] \right\} \tag{P10.4.1}$$

Hence,

$$\varepsilon(t_0^-) = \sigma_0 \left\{ \frac{1}{G_1} + \frac{t_0}{\eta_1} + \frac{1}{G_2} \left[1 - \exp\left(-\frac{t_0}{\tau_2}\right) \right] \right\} \tag{P10.4.2}$$

For $t > t_0$, we obtain

$$\begin{aligned} \varepsilon(t) = \sigma_0 \left[\left\{ \frac{1}{G_1} + \frac{t}{\eta_1} + \frac{1}{G_2} \left(1 - \exp\left(-\frac{t}{\tau_2}\right) \right) \right\} \right. \\ \left. - \left\{ \frac{1}{G_1} + \frac{t-t_0}{\eta_1} + \frac{1}{G_2} \left[1 - \exp\left(-\frac{t-t_0}{\tau_2}\right) \right] \right\} \right] \end{aligned} \tag{P10.4.3}$$

or, equivalently,

$$\varepsilon(t) = \sigma_0 \left\{ \frac{t_0}{\eta_1} + \frac{1}{G_2} \exp\left(-\frac{t}{\tau_2}\right) \left[\exp\left(\frac{t_0}{\tau_2}\right) - 1 \right] \right\} \tag{P10.4.4}$$

Hence,

$$\varepsilon(t_0^+) = \sigma_0 \left\{ \frac{t_0}{\eta_1} + \frac{1}{G_2} \left[1 - \exp\left(-\frac{t_0}{\tau_2}\right) \right] \right\} \tag{P10.4.5}$$

The parameters of the Burgers model are shown in Figure P10.4.2.

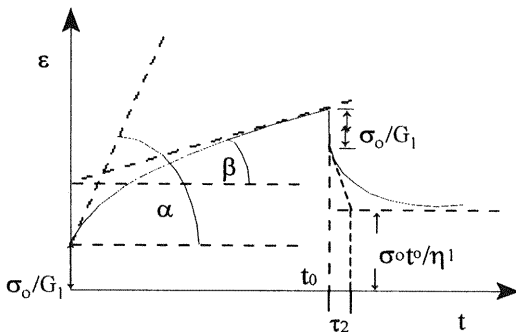


Figure P10.4.2

$$\varepsilon(0) = \frac{\sigma_0}{G_1}; \quad \varepsilon(\infty) = \frac{\sigma_0 t_0}{\eta_1}$$

$$\varepsilon(0) = \sigma_0 \left(\frac{1}{\eta_1} + \frac{1}{\eta_2} \right) = \tan \alpha$$

$$\lim_{t \rightarrow \infty} \varepsilon(t < t_0) = \frac{\sigma_0}{\eta_1} = \tan \beta$$

$$\tau_2 = \frac{\varepsilon(t > t_0) - \varepsilon_{\infty}|_{t=t_0}}{\dot{\varepsilon}(t > t_0)|_{t=t_0}}$$

Although in principle it would be possible to find the parameters η_1 , η_2 , G_1 , and G_2 of the model from a creep recovery experiment, in practice technical difficulties prevent finding them with acceptable accuracy.

REFERENCES

1. N Tscoegl. The Phenomenological Theory of Linear Viscoelasticity. Berlin: Springer, Chaps 3 and 5.
2. B Gross. J Polym Sci 20: 123, 1956.
3. RS Marvin, H Oser. Natl Bur Stand 66B: 171, 1962.

11

Molecular Models of Viscoelastic Polymers

11.1	Concentration Regimes	423
11.2	Isolated Chains as Hookean Elements	425
11.3	Spring–Bead Model: Rouse Theory	425
11.4	Spring–Bead Model: Zimm Theory	428
11.5	Tube Model	430
11.6	Polydispersity and the Tube Model	434
11.7	Rouse Dynamics: Viscosity and Steady-State Compliance for Low Molecular Weight Chains in the Melt	434
11.8	Reptation Dynamics: Viscosity and Steady-State Compliance for High Molecular Weight Chains in the Melt	436
11.9	Comparison of Theoretical and Experimental Viscoelastic Results	439
11.10	Friction Coefficient	440
11.11	Concentration Dependence of Viscoelastic Functions in the Semidilute and Concentrated Regimes	443
11.12	Branched Polymers	446
	Problem Sets	447
	References	452

11.1 CONCENTRATION REGIMES

In theta solvents, excluded volume effects vanish and flexible molecular chains behave as phantom chains (1). The characteristic ratio $C_n = \langle r^2 \rangle_0 / Nl^2$, where $\langle r^2 \rangle_0$ is the mean square end-to-end distance of a

chain with N bonds each of average length l , depends on short-range interactions and consequently is conditioned by the chemical structure. Each molecular chain on average occupies in these conditions a spherical region of radius $R = [\langle r^2 \rangle_0]^{1/2}$. In good solvents the net interaction between the polymer segments is repulsive and the excluded volume parameter v is positive and large. In these conditions, the radius of the coil (or the spherical domain of the chains) increases. In general, $R \sim N^v$, the value of v being 0.6 in good solvents (1,2).

In dilute solutions, interactions between neighboring domains are negligible. Any physical property such as the osmotic pressure or the intrinsic viscosity can be expressed in terms of power series of the concentration of the polymer. However, as the concentration increases, the polymer domains come closer together. A critical concentration C^* can be reached at which molecular domains start to overlap, and the average concentration of polymer segments in the solution is similar to that inside the coil. This concentration is estimated as

$$C^* = \frac{M/N_A}{(4/3)\pi R^3} \quad (11.1)$$

where R is the radius of the coil, M the molecular weight of the chain, and N_A Avogadro's number. Since $R \sim M^v$, the molecular weight dependence of C^* can be written as (2)

$$C^* \propto M^{1-3v} \quad (11.2)$$

The higher the molecular weight, the lower the value of C^* . For polystyrene of $M = 10^6$ in a good solvent ($v = 0.6$), $C^* \simeq 0.005$ g/mL. Solutions in which $C < C^*$ are called dilute solutions.

For solutions in which $C > C^*$, overlapping of domains occurs. Solutions whose concentration lies in the range $C^* < C < C^{**}$ are said to be semidilute, while concentrated solutions are those for which $C > C^{**}$. The crossover concentration from semidilute to concentrated is estimated as (3)

$$C^{**} = \frac{v(M_0 N_A)}{b^6} \quad (11.3)$$

where M_0 and b are, respectively, the molecular weight and length of the statistical chain segments, and v is the excluded volume parameter. For concentrated solutions, $C > C^{**}$. Obviously, the high concentration limit

is the melt. It should be pointed out that the crossover point between different regimes is not sharp and is consequently difficult to determine.

While both dilute and semidilute solutions are characterized by the large and correlated fluctuations in segment density, the fluctuations become small in concentrated solutions and can be treated by a simple mean-field theory.

11.2 ISOLATED CHAINS AS HOOKEAN ELEMENTS

As has been shown elsewhere in this book (Chapter 1), a flexible high molecular weight chain can be represented by a large number N of freely jointed segments of length b . According to Eqs. (1.13) and (1.14), the free energy associated with a freely jointed chain whose end-to-end distance is r can be written as (4)

$$F(r) = F(0) + \frac{3k_B T}{2b^2} r^2 \quad (11.4)$$

where it has been considered that

$$F(r) = -k_B T \ln P(r)$$

Hence, the force necessary to keep the two ends of the chain at the distance r is given by

$$\mathbf{f} = \frac{\partial F(r)}{\partial r} = \frac{3k_B T}{b^2} r \quad (11.5)$$

This equation indicates that an isolated molecular chain behaves like a Hookean elastic element.

11.3 SPRING-BEAD MODEL: ROUSE THEORY

In a real situation, the motion of the segments of a chain relative to the molecules of the solvent environment will exert a force in the liquid, and as a consequence the velocity distribution of the liquid medium in the vicinity of the moving segments will be altered. This effect, in turn, will affect the motion of the segments of the chain. To simplify the problem, the so-called free-draining approximation is often used. This approximation assumes that hydrodynamic interactions are negligible so that the velocity of the liquid medium is unaffected by the moving polymer molecules. This assumption was used in the model developed by Rouse (5) to describe the dynamics of polymers in dilute solutions.

In the Rouse model, each molecular chain is subdivided into several submolecules that are each large enough that they obey Gaussian statistics. Each submolecule is represented by a spring, which accounts for its elasticity, while its mass, which is responsible for the energy dissipated by the moving submolecule in the viscous medium, is represented by a bead. Therefore a molecular chain is considered to be a succession of beads whose spatial location is defined by the vectors \mathbf{r} in Figure 11.1, separated by springs along the vectors $\mathbf{b}_i, \dots, \mathbf{b}_n$. According to Eq. (11.4), the Helmholtz free energy of the n th subchain depends on the energies corresponding to the neighboring $(n-1)$ th and $(n+1)$ th subchains:

$$F_{n,n-1} = \frac{3k_B T}{2b^2} (\mathbf{r}_{n-1} - \mathbf{r}_n)^2 \quad (11.6a)$$

$$F_{n+1,n} = \frac{3k_B T}{2b^2} (\mathbf{r}_{n+1} - \mathbf{r}_n)^2 \quad (11.6b)$$

Therefore the force exerted on the n th submolecule from the two neighbors is given by

$$f_n = \frac{\partial(F_{n,n-1} + F_{n,n+1})}{\partial \mathbf{r}_n} = -\frac{3k_B T}{b^2} [(\mathbf{r}_{n+1} - \mathbf{r}_n) - (\mathbf{r}_n - \mathbf{r}_{n-1})] \quad (11.7)$$

The work done by the driving force is dissipated by the friction energy of the moving submolecule, represented by a bead, in the viscous medium, so that

$$\zeta_0 \frac{d\mathbf{r}_n}{dt} + f_n = 0 \quad (11.8)$$

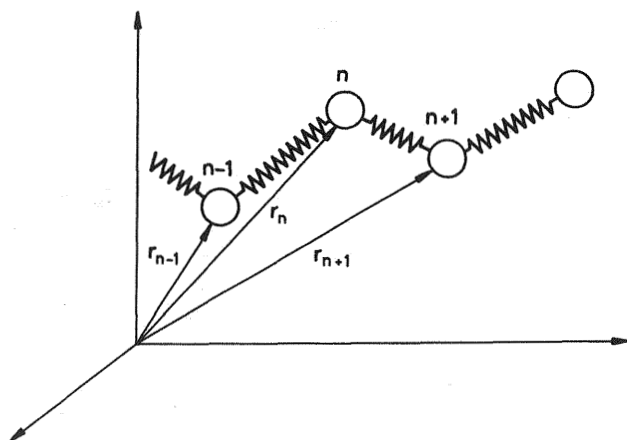


Figure 11.1 Sketch of the spring-bead model.

where ζ_0 is the friction coefficients per submolecule. Because $\mathbf{r}_{n+1} - \mathbf{r}_n$ and $\mathbf{r}_n - \mathbf{r}_{n-1}$ are infinitesimal increments, the combination of Eqs. (11.7) and (11.8) leads to the second-order differential equation

$$\frac{\partial \mathbf{r}_n}{\partial t} = \frac{3k_b T}{b^2 \zeta_0} \frac{\partial^2 \mathbf{r}_n}{\partial n^2} \quad (11.9)$$

By using the boundary conditions

$$\left. \frac{\partial \mathbf{r}_n}{\partial n} \right|_{n=0} = \left. \frac{\partial \mathbf{r}_n}{\partial n} \right|_{n=N} = 0 \quad (11.10)$$

the solution of Eq. (11.9) is the wave function (6)

$$\mathbf{r}_n = \mathbf{r}_n^0 \cos\left(\frac{p\pi n}{N}\right) e^{-t/\tau_p} \quad (11.11)$$

where τ_p and r_n^0 are, respectively, the relaxation time and amplitude of the wave associated with the p mode ($p = 1, 2, 3, \dots$) and N is the number of submolecules in the chain. By substituting Eq. (11.11) into Eq. (11.9), we obtain

$$\tau_p = \frac{b^2 \zeta_0}{3k_B T p^2 \pi^2} N^2 \quad (11.12)$$

The largest relaxation time ($p = 1$) is the characteristic time of the rotation of the whole chain. The value of this quantity is given by

$$\tau_1 = \tau_r = \frac{b^2 \zeta_0}{3k_B T \pi^2} N^2 \quad (11.13)$$

The relaxation time associated with the p mode ($p > 1$) is related to the largest relaxation time by the expression $\tau_p = \tau_r/p^2$. Thus the second mode, $\tau_2 = \tau_r/4$, describes changes over distances of one-half the molecule, and so forth. Equation (11.13) suggests that τ_r is strongly dependent on molecular weight and temperature. The dependence of this latter parameter on temperature arises from the factor $1/T$ and, especially, the enhancement caused in the molecular mobility ($1/\zeta_0$) by an increase in temperature. Accordingly, the Rouse theory is in qualitative agreement with the experimental results.

The Rouse theory predicts that the diffusion coefficient of the chains in very dilute solutions can be written as

$$D = \frac{k_B T}{N \zeta_0} \quad (11.14)$$

By taking into account that $N \sim M$, the scaling relations for D and τ_r are found to be

$$D \sim M^{-1}; \quad \tau_r \sim M^2 \quad (11.15)$$

These results are in disagreement with the scaling laws obtained from experimental results in theta conditions, which can be summarized as (Ref. 3, p. 96)

$$D \sim M^{-1/2}; \quad \tau_r \sim M^{3/2} \quad (11.16)$$

This failure has been attributed to the fact that hydrodynamic interactions are neglected in the Rouse model.

11.4 SPRING-BEAD MODEL: ZIMM THEORY

The theory of Zimm (7) uses the assumptions of the Rouse theory and in addition considers hydrodynamic interactions between the moving submolecules and the solvent. The theory also makes use of the method formulated by Kirkwood and Riseman for the evaluation of the viscosity of dilute polymer solutions. A parameter $h = v^{1/2} \zeta_0 / (12\pi)^{1/2} b^2 \eta_s$, where η_s is the viscosity of the solvent, is defined to account for the hydrodynamic interaction whose value is close to zero ($h \ll 1$) for vanishing interactions (free-draining) and much larger than 1 ($h \gg 1$) when these interactions are dominant (non-free-draining). The mathematical details, which are beyond the scope of this book, are given elsewhere (7). It is convenient to point out, however, that scaling arguments can be used to obtain in any easy way expressions for both D and τ , that are in agreement with those obtained in Zimm's theory. Actually, the diffusion coefficient of molecular chains in very dilute solutions depends on b , N , η_s , and the thermal energy $k_B T$. The use of dimensional analysis gives

$$D = \frac{k_B T}{\eta_s b} f(N) \quad (11.17)$$

Since the statistical property of a Gaussian chain does not depend on the local structure, the original Gaussian chain consisting of N segments of bond length b can be substituted for a new Gaussian chain consisting of N'

= N/λ segments with bond length $b\lambda^v$, where $v = 1/2$ and 0.6 in theta and good solvents, respectively. The transformation from the old to the new chain involves the transformation (Ref. 3, p. 104)

$$N \rightarrow N/\lambda \quad \text{and} \quad b \rightarrow b\lambda^v \quad (11.18)$$

By applying this transformation to Eq. (11.17), we obtain

$$\frac{k_B T}{\eta_s b} f(N) = \frac{k_B T}{\eta_s b \lambda^v} f\left(\frac{N}{\lambda}\right) \quad (11.19)$$

For this equation to hold for any arbitrary value of λ , $f(N)$ should have the form

$$f(N) = \text{constant} \times N^{-v} \quad (11.20)$$

so that $f(N/\lambda) = \text{constant} \times (N/\lambda)^{-v}$. Hence,

$$D = \text{constant} \times \frac{k_B T}{\eta_s b} N^{-v} \simeq \frac{k_B T}{\eta_s R} \quad (11.21)$$

where $R = bN^v$ is the radius of the coil.

In the same way, the rotational relaxation time can be assumed to depend on b , $k_B T$, η_s , and N . In this case, the two-dimensional analysis suggests that

$$\tau_r = \frac{b^3 \eta_s}{k_B T} f(N) \quad (11.22)$$

Applying the transformation of Eq. (11.18) to Eq. (11.22) gives

$$\frac{b^3 \eta_s}{k_B T} f(N) = \frac{b^3 \lambda^{3v} \eta_s}{k_B T} f\left(\frac{N}{\lambda}\right) \quad (11.23)$$

Fulfillment of Eq. (11.23) for any arbitrary value of λ requires that

$$f(N) = \text{constant} \times N^{3v} \quad (11.24)$$

Hence, τ_r can be written as

$$\tau_r = \text{constant} \times \frac{\eta_s (bN^v)^3}{k_B T} \simeq \frac{\eta_s R^3}{k_B T} \quad (11.25)$$

In theta solvents $\nu \cong 1/2$, and consequently $R \sim N^{1/2}$. Therefore, Eqs. (11.21) and (11.25) suggest that the scaling laws for the diffusion coefficient and the rotational relaxation time are

$$D \sim M^{-1/2} \quad \text{and} \quad \tau_r \sim M^{3/2} \quad (11.26)$$

in agreement with the experimental results.

11.5 TUBE MODEL

Overlapping of molecular domains imposes serious constraints on the motions of polymers that strongly affect their dynamical properties. A wealth of information suggests that as long as the polymer is linear and flexible and its molecular weight is above a critical value M_c , the viscosity of polymer melts and concentrated solutions scales with the 3.2–3.4 power of molecular weight (8). Moreover, these systems exhibit an ostensible elasticity. If a specimen of a melt is stretched and the resulting deformation is maintained, the restoring force decreases with time. One can observe that the specimen shrinks like rubber if stretching is released before the restoring force vanishes completely. The longest relaxation time of the restoring force obeys the scaling law $\tau_{\max} \sim M^x$, with $x = 3.4$. Both the viscosity and the elasticity of melts and concentrated solutions suggest that relaxation of the molecular conformation is strongly retarded by the entangled structure of molecular chains.

These observations are accounted for by the tube model developed in the decade of the 1970s (9–11). According to this model, topological constraints in melts and concentrated solutions confine molecular chains in a tube-like region made of the surrounding chains. Obviously, the tube of each chain is continuously renewing itself, the time of renewal being strongly affected by temperature, concentration, and molecular weight. The chain reptates inside the dynamic tube, different relaxation times defining the motions of the chains inside the tube. The primitive path for a given conformation of the polymer is the shortest path connecting the two ends of the chain with the same topology as the chain itself relative to the constraints (Fig. 11.2). At very short times, the polymer is regarded as wriggling around the primitive path. On the long-time scale, the conformation of the primitive path changes as the polymer reptates, creating and destroying the ends of the primitive path.

The main assumptions made in the theory of the reptation theory are as follows (3).

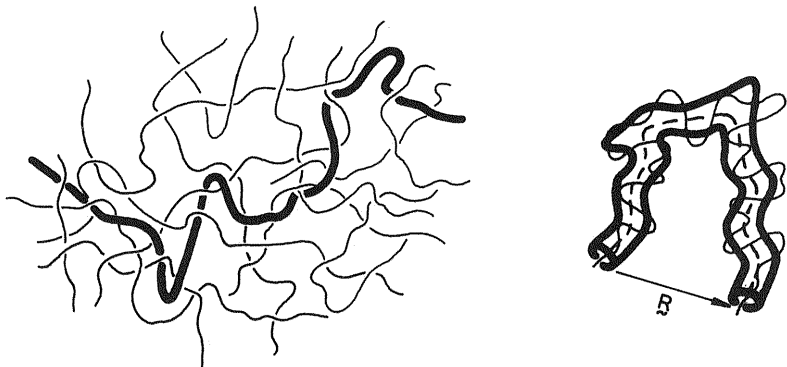


Figure 11.2 (a) Overlapping of molecular domains in melts and concentrated solutions. (b) Schematic representation of the tube model; the dashed line represents the primitive chain.

1. The primitive chain has a constant contour length L , so fluctuations of the contour length are neglected.
2. The primitive chain reptates along itself with a diffusion constant that can be identified as the diffusion coefficient of the Rouse model. Under the action of a force f , the velocity of the polymer in the tube is $v = f/\zeta$, where ζ is the overall friction coefficient of the chain. It is expected that ζ is related to the friction coefficient of the individual segments, ζ_0 , by the expression

$$\zeta = \zeta_0 N \quad (11.27)$$

where N is the number of segments of the polymer. Hence, the overall diffusion coefficient of the chain in the tube can be written as

$$D_t = \frac{k_B T}{\zeta} = \frac{k_B T}{\zeta_0 N} = \frac{D_1}{N} \quad (11.28)$$

where $D_1 = k_B T/\zeta_0$ is the diffusion coefficient of the individual monomer or segment of the chain.

3. The conformation of the primitive chain becomes Gaussian on a large length scale. This means that if the position of two points on the primitive chain are $\mathbf{r}(s, t)$ and $\mathbf{r}(s', t)$, where s and s' are the contour lengths measured from the chain end, then

$$\langle [\mathbf{r}(s, t) - \mathbf{r}(s', t)]^2 \rangle = a|s - s'| \quad (11.29)$$

for $|s - s'| \gg a$. Hence, the mean square end-to-end vector of the primitive chain is La . The parameter a is identified as the step length of the primitive chain.

The three parameters necessary for the characterization of the primitive chain, L , D , and a can be expressed in terms of the Rouse model parameters N , b , and ζ . Thus D is given by Eq. (11.14), while La is equal to Nb^2 , the mean square end-to-end distance of the Rouse chain. As a result, the length of the primitive chain can be written as

$$L = \frac{Nb^2}{a} \quad (11.30)$$

The parameter a has been identified as the radius of the tube, and its value is close to the root mean square of the end-to-end distance of the chain with molecular weight M_e , that is, the molecular weight between entanglements.

At very short times, the moving segments are not constrained by the tube formed by neighboring chains, and the dynamics are described by the Rouse theory. A time τ_e can be defined such that for $t < \tau_e$ the chain behaves like a Rouse chain in free space. For $t \geq \tau_e$, tube constraints become important and the dynamics of the chains involve two processes, the relaxation of the contour length and the disengagement from the deformed tube, that are characterized by the Rouse relaxation time τ_r , given by Eq. (11.10) and the disengagement time τ_d , respectively. This latter parameter is taken as the time necessary for the chain to move the distance L defined in Eq. (11.30). At time $t = \tau_e$, the chain is confined in a deformed tube. However, for $t > \tau_e$, the polymer reptates, and as time passes, the ends of the chains become disengaged from the deformed tube while the remaining parts in the middle are still confined in the tube. Consequently, at $t = \tau_e$, the Rouse-like behavior smoothly crosses over the reptation behavior. Complete disengagement of the polymer from the tube occurs at $t = \tau_d$.

To emphasize the central role played in chain dynamics by both τ_r and τ_d , let us assume that the system is deformed instantaneously and then allowed to relax. Just upon deformation, the tube and the chain are stretched and oriented so that the curvilinear length of the tube becomes greater than the length L of the undeformed tube given by Eq. (11.30). As time passes, the deformed tube will shrink back to the equilibrium curvilinear length L as a consequence of the fact that the chain inside the tube regains the looseness that had been reduced by the deformation. Such a process is not hindered by entanglements, and it takes a length of time of the order of τ_r .

At the end of the first relaxation process, the chain is still inside the old tube that existed right after the deformation, in the sense that the orientations of its parts are those produced by the deformation. The chain renews the tube by reptation, thus relaxing those orientations. This process requires a time τ_d that is much greater than the Rouse relaxation time τ_R . The two processes merge into a single one for unentangled chains. In this case the chains relax according to the Rouse time τ_R .

The relationship between τ_d and molecular weight can easily be obtained by using scaling arguments. Thus τ_d can be viewed as the time necessary for the chain to diffuse along the primitive path. Hence (Ref. 2, Chap. 8),

$$\tau_d \cong \frac{L^2}{D_t} \propto \frac{N^3}{D_1} \sim M^3 \quad (11.31)$$

where Eqs. (11.28) and (11.30) have been considered. This expression indicates that the disengagement or maximum relaxation time scales with the third power of molecular weight.

In the same way, the scaling laws for the diffusion coefficient of the chains in the melt or in concentrated solutions can be obtained by taking into account that during the time τ_d the reptating chain moves along its tube a length $L \sim Na$. However, because the tubes are contorted, the real displacement of the chain is $R \approx N^{1/2}b$. Moreover, after such a time τ_d the memory of the original conformation is lost, and as a consequence successive time intervals of length τ_d are statistically independent. Therefore the molecular weight dependence of the diffusion coefficient of the reptating chain in the melt is given by

$$D \cong \frac{R^2}{\tau_d} = D_1 N^{-2} \quad (11.32)$$

where it has been taken into account that for melts and concentrated solutions of flexible molecules the relationship $R^2 \sim N$ holds. It is noteworthy that whereas the scaling law obtained from the reptation model for the diffusion coefficient of the chains is in agreement with the experiment results, the theoretical molecular weight dependence $\tau_d \sim M^3$ is weaker than the experimental one; the experimental exponent ranges from 3.2 to 3.4.

The theory predicts (Ref. 3, p. 214) that $\tau_e \cong Z^{-2}\tau_R$ and $\tau_d \cong Z\tau_r$, where $Z = L/a = Nb^2/a^2$ is the number of steps of the primitive chain, often referred to as the number of entanglements per chain. These relationships have been confirmed by computer simulations (12).

11.6 POLYDISPERSITY AND THE TUBE MODEL

Most polymers exhibit a wide distribution of molecular weights. The molecular weight of polymers is given as an average value, the averages most often used being the number average M_n and the weight average M_w . The breadth of the distribution is usually characterized by the ratio M_w/M_n in such a way that the larger the ratio, the wider the distribution.

As an effect of the polydispersity, the distribution of relaxation times of melts and concentrated solutions becomes broader. The stress carried by the shorter chains relaxes sooner than that associated with the larger chains. However, the relaxations of short and long chains are not independent of each other, and as a consequence the effects are not simply additive.

In interpreting the relaxation behavior of polydisperse systems by means of the tube model, one must consider that renewal of the tube occurs because the chain inside it moves thermally, either by reptation mode, by fluctuation of the tube length in time (breathing motion), or in both ways (13,14). Moreover, the tube wall can be renewed independently of the motion of the chain inside the tube because the segments of the chains of the wall are themselves moving. The relaxation mechanism associated with the renewal of the tube is called constraint release.

For nearly monodisperse systems, many chains reptate away before the tube wall changes significantly. Consequently, the contribution of constraint release to relaxation is nearly negligible. However, for polydisperse systems the situation is quite different. Let us consider a system made up of short and long chains with molecular weights M_s and M_l , respectively. Let us assume further that the disengagement times are τ_s and τ_l . It is expected that the shorter chains relax as in a monodisperse melt. However, the tubes of long chains in the mixture are partly made up by the short chains that move faster, and consequently the contribution of the constraint release to the relaxation may become significant. Limiting situations can be reached in which short chains merely act as diluents of the relaxation behavior of long chains.

The interpretation of the relaxation behavior of polymers with an arbitrary distribution of molecular weights is complex. This problem has not yet been resolved and so far remains an empirical matter.

11.7 ROUSE DYNAMICS: VISCOSITY AND STEADY-STATE COMPLIANCE FOR LOW MOLECULAR WEIGHT CHAINS IN THE MELT

As indicated above, low molecular weight polymers are unentangled in the melt, and according to the reptation theory these systems should obey

Rouse dynamics. After some lengthy mathematical handling, beyond the scope of this book,* the Rouse theory predicts that the relaxation modulus is given by

$$G(t) = \frac{c}{N} k_B T \sum_p e^{-2tp^2/\tau_r} \quad (11.33)$$

where c is the concentration of segments in the melt, N is the number of segments per molecular chain, and τ_r is given by Eq. (11.13). Consequently, the term c/N is the concentration of molecular chains in the melt. An alternative way to obtain Eq. (11.33) qualitatively is to use the theory of rubber elasticity in conjunction with the phenomenological theory of viscoelasticity. Actually, the rubber elasticity theory indicates that the relaxation modulus is expressed by $G = (c/N)k_B T$. Moreover, dissipation of energy occurs by friction of the moving beads with the viscous medium, and in this situation the phenomenological theory of viscoelasticity predicts that $G(t)$ decays with time according to the equation

$$G(t) = \frac{c}{N} k_B T \sum_p \exp\left(-\frac{t}{\tau_p}\right)$$

We should note that $\tau_1 = \tau_r/2$, which accounts for the factor 2 appearing in Eq. (11.33). This equation in combination with Eq. (6.49) leads to the expression

$$\begin{aligned} \eta &= \int_0^\infty G(t) dt = \frac{c}{N} k_B T \int_0^\infty \sum_p \exp\left[-\frac{2p^2 t}{\tau_r}\right] dt = -\frac{c}{N} k_B T \sum_p \frac{\tau_r}{2} \exp\left[-\frac{2p^2 t}{\tau_r}\right] \Bigg|_0^\infty \\ &= \frac{cb^2 \zeta_0 N}{6\pi^2} \left[1 + \frac{1}{2^2} + \frac{1}{3^2} + \dots\right] = \frac{c\zeta_0}{36} Nb^2 \end{aligned} \quad (11.34)$$

which relates the viscosity to the number of segments of the molecular chains. In the same way, the steady-state compliance J_e^0 can be obtained from Eqs. (6.52) and (11.33), giving

*For details, see Ref. 3, Chap. 7.

$$\begin{aligned}
 J_e^0 &= \frac{\int_0^\infty tG(t) dt}{\eta^2} = \frac{ck_B T \int_0^\infty \sum_p \exp\left[-\frac{2p^2 t}{\tau_r}\right] dt}{\eta^2 N} = \frac{ck_B T}{\eta^2 N} \left(\frac{\tau_r^2}{2^2}\right) \sum_p p^{-4} \\
 &= \frac{ck_B T}{\eta^2 N} \left(\frac{\tau_r^2}{2^2}\right) \left[1 + \frac{1}{2^4} + \frac{1}{3^4} + \dots\right] = \frac{2N}{5ck_B T}
 \end{aligned}
 \tag{11.35}$$

By taking into account that $c = (\rho/M)NN_A$, where ρ is the density of the polymer in grams per cubic centimeter in the melt, M is the molecular weight of the chains, N_A is Avogadro's number, and N is the number of segments per chain, we obtain

$$\eta_0 = \frac{\pi^2}{12} \left(\frac{\rho N_A k_B T}{M}\right) \tau_r \propto \rho M
 \tag{11.36a}$$

and

$$J_e^0 = \frac{2M}{5\rho N_A k_B T}
 \tag{11.36b}$$

where it was considered that $\tau_r \sim M^2$ [see Eq. (11.13)]. The experimental results obtained for the viscosity and steady-state compliance of polymer melts of low molecular weight fit rather well to the theoretical predictions (8.15).

11.8 REPTATION DYNAMICS: VISCOSITY AND STEADY-STATE COMPLIANCE FOR HIGH MOLECULAR WEIGHT CHAINS IN THE MELT

For $t > \tau_e$, the number of part of the polymer disengaged from the deformed tube, beginning from the ends, increases with time. Since only the segments remaining in the tube are oriented and contribute to the stress, the relaxation modulus for $t \gg \tau_e$ can be written as

$$G(t) = G_N^0 \phi(t)
 \tag{11.37}$$

where G_N^0 is a certain constant (in fact, it is the relaxation modulus at the plateau indicated in the Fig. 11.3) independent of molecular weight and $\phi(t)$ is the fraction of the segments confined in the tube given by (3)

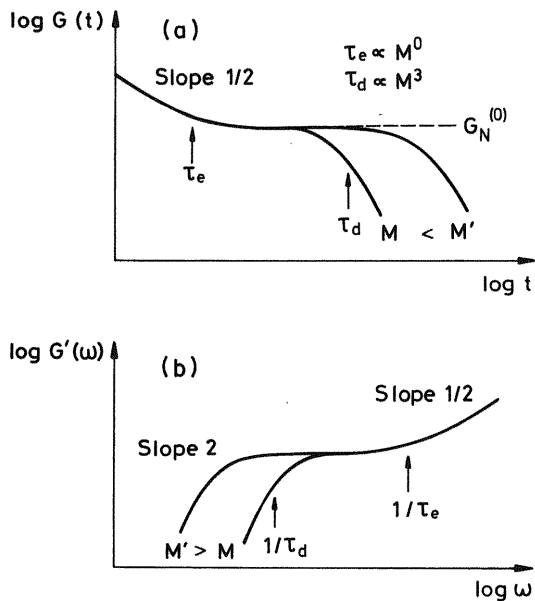


Figure 11.3 Schematic curves showing the times at which Rouse-like behavior smoothly crosses over reptation behavior ($t = \tau_e$) and the region ($t > \tau_d$) in which disentanglement of the chains from the tube occurs (from Ref. 3).

$$\phi(t) = \sum_{p \text{ odd}} \frac{8}{p^2 \pi^2} \exp\left(-\frac{p^2 t}{\tau_d}\right) \quad (11.37a)$$

with

$$\tau_d = \frac{\zeta N^3}{k_B T} \left(\frac{b^2}{a\pi}\right)^2 \quad (11.37b)$$

From Eqs. (6.49), (11.37a), and (11.37b), the following expression is obtained for η_0

$$\eta_0 = G_n^0 \int_0^\infty \phi(t) dt = \frac{\pi^2}{12} G_n^0 \tau_d \sim M^3 \quad (11.38)$$

whereas the steady-state compliance is given by

$$J_e^0 = \frac{\int_0^\infty t G(t) dt}{\eta_0^2} = \frac{6}{5 G_N^0} \sim M^0 \quad (11.39)$$

where scaling of both τ_d and η_0 with the third power of molecular weight was considered. The scaling relationships suggested by the theory for the representative viscoelastic functions of highly entangled systems can be summarized as

$$\eta \sim M^3; \quad J_e^0 \sim M^0; \quad D \sim M^{-2} \quad (11.40)$$

The Doi–Edwards theory provides expressions for G_N^0 , η , J_e'' , and D that contain two adjustable parameters: the friction coefficient and the primitive path step length L . The friction coefficient can be obtained from the relationship between the viscosity and molecular weight in the Rouse theory [Eq. (11.36)] or from the relaxation spectrum discussed below. Moreover, the step length a can be determined from the plateau modulus G_N^0 . Actually, according to the Doi–Edwards theory

$$G_n^0 = \frac{4}{5} \left(\frac{\rho N_A k_B T}{a^2} \right) \left(\frac{R^2}{M} \right) \quad (11.41)$$

where R^2 is the mean square end-to-end distance. Equation (11.41), in conjunction with Eq. (8.54), allows us to express the parameter a as a function of the molecular weight between entanglements, M_e

$$a^2 = \frac{4}{5} \left(\frac{R^2}{M} \right) M_e = 0.80 R_{M_e}^2 \quad (11.42)$$

where $R_{M_e}^2$ is the mean square end-to-end distance of the chain between entanglements. It is then possible to express the values of the viscosity, steady-state compliance, and diffusion coefficients in terms of measurable magnitudes. Thus (13),

$$\eta = \frac{15}{4} \left(\frac{M}{M_e} \right)^2 \eta_R \quad (11.43a)$$

$$J_e^0 = \frac{6}{5G_N^0} \quad (11.43b)$$

and

$$D = \frac{4}{15} \left(\frac{M}{M_e} \right)^{-1} D_R \quad (11.43c)$$

where D_R and η_R are, respectively, the diffusion coefficient and the viscosity predicted by the Rouse theory.

11.9 COMPARISON OF THEORETICAL AND EXPERIMENTAL VISCOELASTIC RESULTS

The overall shape of the theoretical double logarithmic plot of $G(t)$ versus t is shown in Figure 11.3 (see Ref. 3, p. 229). For $t < \tau_e$, $\log G(t)$ is a linear function of $\log t$ with slope $-1/2$. The relaxation modulus is nearly flat in the range of time $\tau_e < t < \tau_d$; since $\tau_d \sim M^3$, the width of the plateau increases with molecular weight. Finally, $G(t)$ drops for $t > \tau_d$ because the fraction of segments still confined in the deformed tube and consequently contributing to the stress decreases rapidly. The main features of the plot are in rather good agreement with the experimental results.

By comparing theory and experiment we find that the reptation model gives a good account of the molecular weight dependence of the diffusion coefficient and the steady-state compliance in highly entangled polymer systems. However, the exponent 3 predicted by the theory for the molecular weight dependence of both η_0 and τ_d differs from the values 3.4–3.7 found for this quantity in experiments. There are strong arguments supporting the exponent 3 that the theory predicts. Actually, according to the linear theory of viscoelasticity, the mean relaxation time is given by $\langle \tau \rangle = \eta_0 J_e^0$ [see Eq. (9.33)]. After Eq. (11.32), the ratio between $\langle \tau \rangle$ and τ_d can be written as

$$\Gamma = \frac{\langle \tau \rangle}{\tau_d} = \frac{D \eta_0 J_e^0}{R^2} \quad (11.44)$$

It is expected that $\langle \tau \rangle$ and τ_d are the same order of magnitude so that Γ should be independent of molecular weight. However, since $D \sim M^{-2}$, $R^2 \sim M$, and $J_e^0 \sim M^0$, one finds that $\Gamma \sim M^{0.4}$ if the exponent 3.4 is used for the molecular weight dependence of the viscosity. In this case, Γ would continuously increase with molecular weight, a result that seems to be unlikely. However, the ratio becomes independent of molecular weight if the exponent 3 is used, in consonance with what one would expect. The power law $\eta/M^3 \propto M^{0.4}$ describes reasonably well the experimental results (16) for values of M up to $200M_c$, but, as Figure 11.4 shows, a pattern of negative departure develops beyond this range. Graessley conjectured that pure reptation behavior will be observed only for molecular weights higher than $800M_c$. Thus an exponent larger than 3 would be the result of a crossover region in the viscosity from Rouse-like behavior to pure reptation behavior.

Though theory predicts the molecular weight independence of J_e^0 for $M \gg M_c' (\approx 6M_e)$, the theoretical values of J_e^0 are somewhat lower than the experimental ones. It should be pointed out that a certain degree of polydispersity may enhance the experimental values of the steady-state compliance of even so-called monodisperse systems. Finally, the theoretical

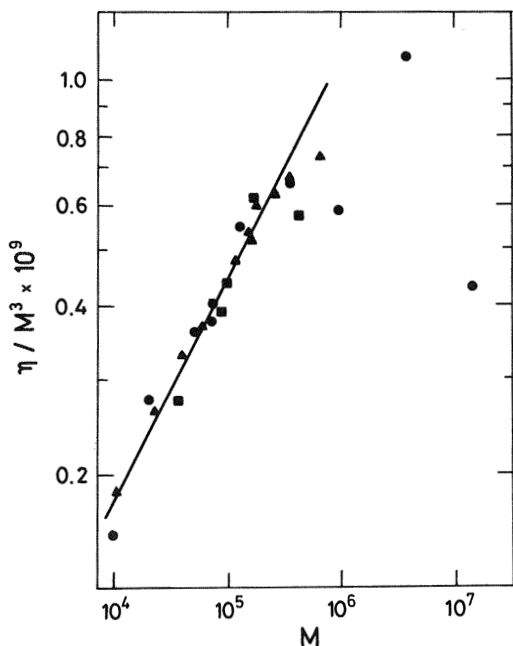


Figure 11.4 Molecular weight dependence of the ratio η/M^3 for different narrow molecular weight distribution fractions of polystyrene. (From Ref. 16.)

prediction for chain mobility expressed by the diffusion coefficient is in rather good agreement with the limited experimental results available (17), as the plots of Figure 11.5 indicate. Actually, the results of this figure show that $D \sim M^{-1}$ for low molecular weight fractions ($M < M_c$), as the Rouse theory predicts, while for long chains ($M > M_c$) $D \sim M^{-2}$, in agreement with the tube theory prediction.

11.10 FRICTION COEFFICIENT

For $t \ll \tau_e$, the dynamics of entangled polymer melts are described by the Rouse model. Owing to the fact that $\tau_e \ll \tau_r$, Eq. (11.33) can be written as

$$G(t) = \frac{c}{N} k_B T \int_0^\infty \exp\left(-\frac{2tp^2}{\tau_r}\right) dp = \frac{c}{2\sqrt{2}N} k_B T \left(\frac{\tau_r}{t}\right)^{1/2} \quad (11.45)$$

Hence, $d \log G(t)/d \log t = -1/2$ at short times; moreover, since $\tau_r \sim N^2$, Eq. (11.45) suggests that $G(t)$ and G_n^0 are independent of molecular weight.

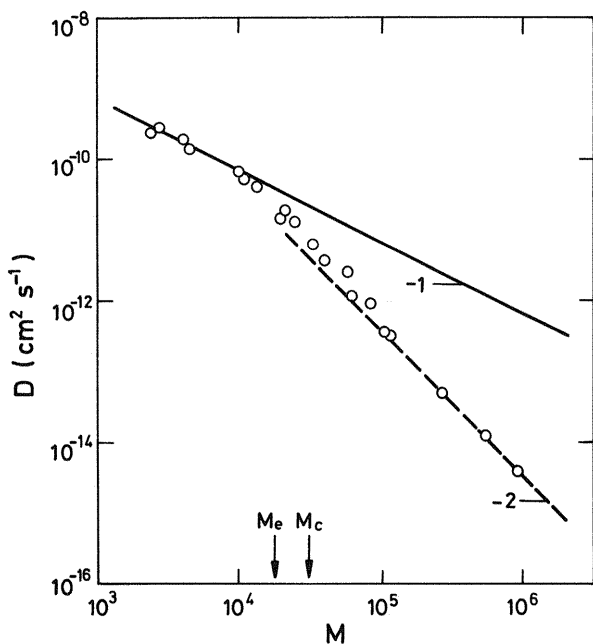


Figure 11.5 Double logarithmic plots showing the diffusion coefficient versus molecular weight for linear polystyrene. (From Ref. 17.)

The friction coefficient is customarily obtained from either the relaxation or retardation spectrum, $H(\tau)$ or $L(\tau)$, respectively. At short times, i.e., on the transition from the glassy-like to the rubbery plateau, the viscoelastic processes obey Rouse dynamics, and the relaxation modulus is given by Eq. (11.45). Since $H(\tau) = -dG/d \ln \tau|_{t=\tau}$, one obtains

$$H(\tau) = \frac{1}{2} \left(\frac{\rho b N_A}{M_0} \right) \left(\frac{\zeta_0 k_B T}{6} \right)^{1/2} \tau^{-1/2} \quad (11.46)$$

where use was made of Eq. (9.37). In Eq. (11.46), ρ is the concentration of polymer (g/cm^3 or kg/m^3), M_0 the molecular weight of the statistical link, and b its length. A double logarithmic plot of $H(\tau)$ against τ should give a straight line with slope $-1/2$ in the region of long times of the glass-rubber relaxation of amorphous polymers (18). Typical spectra for this relaxation process are shown in Figure 11.6. An inspection of these spectra suggests that the molecular theory is valid in a region covering only about two to three decades of τ . By writing Eq. (11.46) as

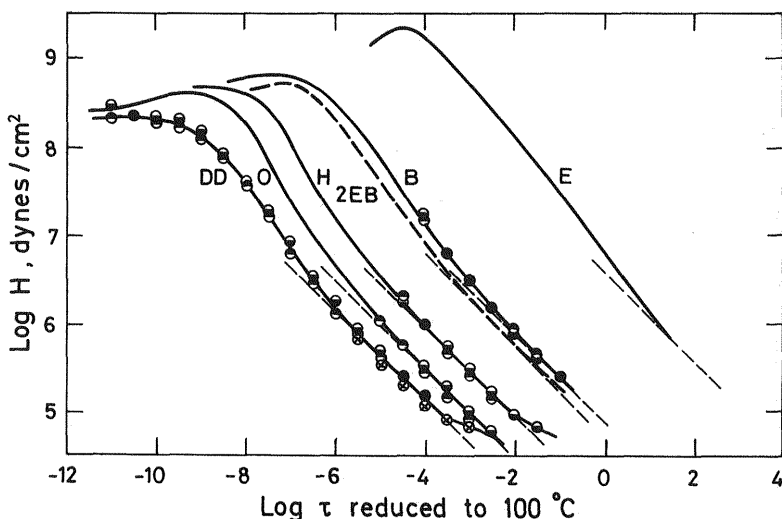


Figure 11.6 Double logarithmic plot showing the relaxation spectrum in the transition zone for six methacrylate polymers reduced to 100°C. E, B, H, O, DD, and 2-EB refer to ethyl, *n*-butyl, *n*-hexyl, *n*-octyl, *n*-dodecyl and 2-ethyl butyl, respectively. Dash lines represent the portions of the spectra where the slope is $-1/2$ (From Ref. 18.)

$$\log \zeta_0 = 2 \log H + \log \tau + \log \left(\frac{6}{k_B T} \right) + 2 \log \left(\frac{2\pi M_0}{\rho N_A b} \right) \quad (11.47)$$

the coefficient of friction can be determined by taking the corresponding values of H and τ in the region of the spectrum where the molecular theory holds, that is, where the slope of the double logarithmic plot of $\log H(\tau)$ versus τ is $-1/2$.

The coefficient of friction can alternatively be obtained from the retardation spectrum. In this case,

$$L(\tau) = \frac{2M_0}{\rho b N_A} \left(\frac{6}{\zeta_0 k_B T} \right)^{1/2} \tau^{1/2} \quad (11.48)$$

A double logarithmic plot of $L(\tau)$ versus τ gives a straight line with slope $1/2$ at short times. Values of ζ_0 can be obtained from Eq. (11.48) by using the procedures described above to evaluate this parameter from the relaxation spectrum.

In general, the coefficient of friction is not sensitive to molecular weight provided that the chains are not very short. This coefficient decreases for

polymers containing side chains that act as internal plasticizers. The friction coefficient is governed by the free volume, and its temperature dependence is described by the VFTH equation.

11.11 CONCENTRATION DEPENDENCE OF VISCOELASTIC FUNCTIONS IN THE SEMIDILUTE AND CONCENTRATED REGIMES

It is expected that the same picture that gives a good account of the linear viscoelastic behavior of polymer melts should also hold for semidilute and concentrated solutions. In the case of semidilute solutions some conclusions can be drawn from scaling arguments (19,3, p. 235). In this way, concentration dependence of the maximum relaxation time τ_{\max} , the zero shear rate viscosity η_0 , and the plateau modulus G_N^0 can be obtained, where η_s is the viscosity of the solvent. The relevant parameters needed to obtain τ_{\max} as a function of concentration are b , c , N , $k_B T$, and η_s . Dimensional analysis shows that

$$\tau_{\max} = \frac{\eta_s b^3}{k_B T} f_1(cb^3, N) \quad (11.49)$$

where λ segments are grouped,

$$N \rightarrow N/\lambda; \quad b \rightarrow b\lambda^v; \quad c \rightarrow c/\lambda \quad (11.50)$$

Equation (11.49) must be invariant under this transformation, whence

$$b^3 f_1(cb^3, N) \rightarrow b^3 \lambda^{3v} f_1\left(\frac{c}{\lambda} b^3 \lambda^{3v}, \frac{N}{\lambda}\right) = b^3 \lambda^{3v} f_1\left(cb^3 \lambda^{3v-1}, \frac{N}{\lambda}\right) \quad (11.51)$$

This requires that

$$b^3 f_1(cb^3, N) = N^{3v} b^3 f_1(cb^3 N^{3v-1}) \quad (11.52)$$

By taking into account that the critical concentration c^* at which overlapping of molecular domains occurs is

$$c^* \simeq \frac{N}{R^3} = \frac{N}{b^3 N^{3v}} = \frac{N^{1-3v}}{b^3} \quad (11.53)$$

Eq. (11.49) becomes

$$\tau_{\max} = \frac{\eta_s N^{3\nu} b^3}{k_B T} f_1\left(\frac{c}{c^*}\right) \quad (11.54)$$

The concentration dependence of τ_{\max} can be obtained by imposing the condition that $\tau_{\max} \sim N^3$. In this case, $N^{3\nu} b^3 f_1(cb^3 N^{3\nu-1}) \simeq N^{3\nu} b^3 (cb^3 N^{3\nu-1})^x \sim N^3$. Accordingly, $(3\nu - 1)x + 3\nu = 3$, and $x = (3 - 3\nu)/(3\nu - 1)$. For good solvents ($\nu = 0.6$), so that Eq. (11.54) becomes

$$\tau_{\max} \simeq \frac{\eta_s N^{3\nu} b^3}{k_B T} \left(\frac{c}{c^*}\right)^{(3-3\nu)/(3\nu-1)} \propto C^{3/2} M^3 \quad (11.55)$$

where it has been considered that C (g/mL) $\sim c$ and $M \sim N$.

The parameters governing the zero shear rate viscosity η_0 are the same as those indicated above for the longest relaxation time. Dimensional analysis shows that

$$\eta_0 = \eta_s f_2(cb^3, N) \quad (11.56)$$

Invariance under the transformation of Eq. (11.50) leads to

$$f_2(cb^3, N) \rightarrow f_2\left(cb^3 \lambda^{3\nu-1}, \frac{N}{\lambda}\right) \quad (11.57)$$

For this to be satisfied, $f_2(cb^3, N) = f_2(cb^3 N^{3\nu-1})$. Hence, Eq. (11.56) can be written as

$$\eta_0 = \eta_s f_2(c/c^*) \quad (11.58)$$

The condition $\eta_0 \sim N^3$ consistent with the reptation prediction

$$\eta_0 \simeq \eta_s (cb^3 N^{3\nu-1})^x \sim N^3 \quad (11.59)$$

requires that $(3\nu - 1)x = 3$. Therefore, $x = 3/(3\nu - 1)$, and Eq. (11.59) is given by

$$\eta_0 \simeq \eta_s \left(\frac{c}{c^*}\right)^{3/(3\nu-1)} \propto C^{15/4} M^3 \quad (11.60)$$

Let us now analyze the concentration dependence of the diffusion coefficient of polymer solutions. By using the methods outlined above, we find that

$$D = \frac{k_B T}{b \eta_s} f_3(cb^3, N) \quad (11.61)$$

The invariance of this equation under the transformation of Eq. (11.50),

$$\frac{1}{b}f_3(cb^3, N) = \frac{1}{b\lambda^v}f_3\left(cb^3\lambda^{3v-1}, \frac{N}{\lambda}\right) \quad (11.62)$$

requires that

$$\frac{1}{b}f_3(cb^3, N) = \frac{1}{bN^v}f_3(cb^3N^{3v-1}) \quad (11.63)$$

Consequently, Eq. (11.63) can be written as

$$D = \frac{k_B T}{\eta_s N^v b} f_3(cb^3 N^{3v-1}) = \frac{k_B T}{\eta_s N^v b} f_3\left(\frac{c}{c^*}\right) \quad (11.64)$$

If the restriction $D \sim N^{-2}$ is imposed, then $(3v - 1)x - v = -2$, and $x = (v - 2)/(3v - 1)$. In this case Eq. (11.64) becomes

$$D \simeq \frac{k_B T}{\eta_s b} \left(\frac{c}{c^*}\right)^{(v-2)/(3v-1)} \propto M^{-2} c^{-7/4} \quad (11.65)$$

Finally, by taking into account that $G_N^0 \sim N^0$, the plateau modulus dependence of the concentration is expressed by

$$G_N^0 = \frac{c}{N} k_B T \left(\frac{c}{c^*}\right)^{1/(3v-1)} \propto C^{9/4} M^0 \quad (11.66)$$

The exponents of C in Eqs. (11.55), (11.60), (11.65), and (11.66) were obtained assuming $v \approx 0.6$. These equations approximately agree with the experimental results in the semidilute regime in good solvents. The validity of the scaling arguments in theta solvents has not yet been established. It should be pointed out that the exponents in the molecular weight dependence of η_0 and τ_{\max} are somewhat higher than 3.

For high concentrations the dynamics of the chains are the same as in melts. Excluded volume effects and the hydrodynamic interaction are not important. However, both the radius of the tube and the friction coefficient strongly depend on the concentration. Because the dependence of ζ_0 on C is nontrivial, there are no scaling laws relating τ_{\max} and η_0 to the concentration. For the plateau modulus, it was found experimentally that (8)

$$G_N^0 \propto C^2 \quad (11.67)$$

11.12 BRANCHED POLYMERS

As indicated in Chapter 8, the viscoelastic properties of high molecular weight branched polymers differ from those of linear polymers. Most of the experimental work related to the viscoelastic behavior of branched polymers was carried out on star-shaped polymers in which three or more arms are connected to a center. The diffusion coefficient of a polymer of this kind is significantly lower than that of a linear polymer of similar molecular weight (20). The steady-state compliance is proportional to the molecular weight, even if M is high, thus showing Rouse-like behavior in this regard (21). The zero shear rate viscosity of the melts of star-like polymers increases more rapidly with molecular weight than that of linear polymers (22,23).

Let us analyze the tube model for star-like molecules in concentrated systems. Each arm of the star is surrounded by its tube of topological constraints such as occurs for linear chains (see Fig. 11.7). However, the star-like molecule cannot reptate in the tubes because the branch point shared by all the arms opposes the reptation. The motion of the arms in the tubes is promoted by the fluctuation of the tube length over time. This motion, called chain breathing, superimposes upon reptation, thus contributing to a faster relaxation. Actually, when the length of the tube becomes shorter than average in its breathing motion, the end parts of the tube vanish. Though breathing motion also occurs in linear chains, its contribution to relaxation is a marginal one. However, breathing is the only mechanism by which star-like polymers can relax.

Owing to the strong dependence of the motion of star-like molecules on fluctuations, the relaxation time must be inversely proportional to the probability that the fluctuation of an arm brings the corresponding tube to an essentially zero length. Obviously, the relaxation time should be a rapidly increasing function of the arm length. According to the tube model, the relationship between the relaxation time and the molecular weight is given by (14)

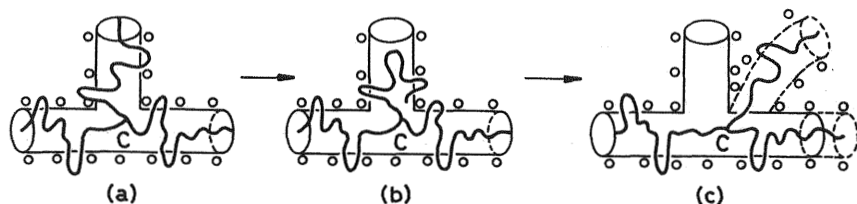


Figure 11.7 Reptation of star chains in the tube model. (From Ref. 3.)

$$\tau = \tau_0 \exp\left(\frac{M}{fM_e}\right) \quad (11.68)$$

The model also predicts for η_0 and J_e^0 the following expressions (Ref. 3, p. 281):

$$\eta_0 \propto \left(\frac{M}{fM_e}\right)^2 \exp\left(\frac{15M}{8fM_e}\right) \quad (11.69a)$$

and

$$J_e^0 = \frac{15M}{8fRT} \quad (11.69b)$$

where f is the number of arms of the star and M_e is the molecular weight between entanglements. These equations are in qualitative agreement with the experimental results. However, there is a strong discrepancy between theory and experiment. For example, the viscosity is smaller than the calculated values and the best agreement with experiments is obtained by replacing the numerical factor 15/8 by a smaller one, 1/2. It should be pointed out, however, that the viscosity of a branched polymer of not too large molecular weight may be lower than that of its linear counterparts. Actually, the comparison is made at equal values of the overall molecular weight, and for stars with relatively short arms the exponential factor of Eq. (11.70) may be lower than the third power of Eq. (11.40).

PROBLEM SETS

Problem 11.1

Calculate the number of macromolecules sharing the same domain in a polyethylene melt with a molecular weight of 140,000 g/mol.

Data: Density = 0.9 g/cm³; characteristic ratio $\langle r^2 \rangle / n\ell^2 = 7.6$, where n is the number of segments per macromolecule and $\ell_{\text{bond}} = 1.53 \text{ \AA}$ ($1 \text{ \AA} = 10^{-10} \text{ m}$).

Solution 11.1

The macromolecular radius is given by

$$R = \langle r^2 \rangle^{1/2} = \left(7.6 \times \frac{140,000}{14} \times 1.53^2\right)^{1/2} = 421.8 \text{ \AA}$$

Volume of an isolated macromolecule = $(4\pi/3) \times 421.8^3 = 3.14 \times 10^8 \text{ \AA}^3$.

Number of macromolecules per volume unit:

$$\frac{0.9 \text{ g/cm}^3}{140,000 \text{ g/mol}} \times 6.023 \times 10^{23} \text{ molecules/mol} = 3.87 \times 10^{18} \text{ molecules/cm}^3$$

Number of molecules sharing the same domain ($1 \text{ cm}^3 = 10^{24} \text{ \AA}^3$)

$$3.14 \times 10^8 \times 3.87 \times 10^{18} / 10^{24} = 1216 \text{ macromolecules/domain}$$

Problem 11.2

Using scaling arguments, show that the square root of the mean square end-to-end distance of a flexible chain is given by

$$\langle r^2 \rangle^{1/2} = R \approx bN^{\nu}$$

where angled brackets denote average and ν is the scaling exponent.

Solution 11.2

It is expected that R will not only be a function of the number of segments of the chain, N , but will also depend on the segment length, b . Therefore,

$$R = bf(N) \tag{P11.2.1}$$

Let us group λ segments of the chain in such a way that

$$N \rightarrow \frac{N}{\lambda}; \quad b \rightarrow b\lambda^{\nu} \tag{P11.2.2}$$

Since R must be invariant under this transformation, we obtain

$$R = bf(N) = b\lambda^{\nu} f\left(\frac{N}{\lambda}\right) \tag{P11.2.3}$$

The only way that Eq. (P11.2.3) holds is that

$$f(N) = \text{constant} \times N^{\nu} \tag{P11.2.4}$$

Consequently, Eq. (P11.2.1) becomes

$$R = \text{constant} \times bN^v \approx bN^v \quad (\text{P11.2.5})$$

The value of v in ideal (theta) and good solvents is, respectively, 0.5 and 0.6.

Problem 11.3

By using scaling arguments, show that $D \sim N^{-1}$ and $\tau_r \sim N^2$ in the Rouse theory.

Solution 11.3

Dimensional analysis suggests that D is the product of two factors: one containing the thermal energy ($k_B T$), the friction coefficient (ζ), and the bond length (b), and the other containing the number of segments N . Accordingly,

$$D = (k_B T)^a \zeta_0^d b^c f(N)$$

Hence

$$\begin{aligned} L^2 T^{-1} &= (M L^2 T^{-2})^a (M T^{-1})^d L^c \\ -2a - d &= -1 \\ a + d &= 0 \\ 2a + c &= 2 \end{aligned}$$

Solution of these equations gives $a = 1$; $d = -1$; $c = 0$. Consequently,

$$D = (k_B T / \zeta_0) f(N)$$

By performing the transformation $N \rightarrow N/\lambda$; $\zeta \rightarrow \lambda\zeta$; $b \rightarrow b\lambda^v$, we obtain

$$(k_B T / \zeta_0) f(N) = (k_B T / \lambda \zeta_0) f(N/\lambda)$$

This equation requires that

$$f(N) = \text{constant} \times N^{-1} \quad \text{and} \quad D = \frac{k_B T}{\zeta_0} f(N) \simeq \frac{k_B T}{\zeta_0 N} \sim N^{-1}$$

In the same way,

$$\begin{aligned} \tau_r &= (k_B T)^a \zeta_0^d b^c f(N); & T &= (ML^2 T^{-2})^a (MT^{-1})^d L^c f(N) \\ -2a - d &= 1 \\ 2a + c &= 0 \\ a + d &= 0 \\ a &= -1; & c &= 2; & d &= 1 \\ \tau_r &= (b^2 \zeta_0 / k_B T) f(N) \\ (b^2 \zeta_0 / k_B T) f(N) &= (b^2 \lambda^{2\nu} \zeta_0 / k_B T) f(N/\lambda) = (b \zeta_0 \lambda^{1+2\nu} / k_B T) f(N/\lambda) \end{aligned}$$

The last equation requires that $f(N) = \text{constant} \times N^{1+2\nu}$. Hence,

$$\tau_r \cong (b^2 \zeta_0 / k_B T) N^{1+2\nu} \sim N^{1+2\nu}$$

Taking into account that $\nu = 1/2$ in the Rouse model, we obtain $\tau_r \sim N^2$.

Problem 11.4

Discuss the determination of the statistical segment for polyethylene whose structural unit is $(-\text{CH}_2-\text{CH}_2-)_x$ knowing that $C_n = \langle r^2 \rangle_0 / nl^2 = 7.6$, where $\langle r^2 \rangle_0$ is the mean square end-to-end distance of a chain of n skeletal bonds each of length $l (= 1.53 \text{ \AA})$, and nl^2 is the mean square end-to-end distance of the chain in the idealization that the skeletal bonds are freely jointed.

Solution 11.4

We can replace the n skeletal bonds of length l each by n' freely jointed skeletal bonds of length l' . Then $7.6nl^2 = n'l'^2$; hence $l' = 7.6^{1/2} l = 2.76l = 4.2 \text{ \AA}$; l' is often represented in the literature by b .

An alternative way of expressing the statistical weight segments is to assume that the chains are formed by n' segments, each of length l' that obey the relationships

$$r_{\max} = n'l' \quad (\text{P11.4.1})$$

and

$$n'l'^2 = 7.6nl^2 \quad (\text{P11.4.2})$$

where r_{\max} is the maximum length of the chain. Since the C—C—C bond angle is 110° , $r_{\max} = nl \cos 35^\circ = 0.82nl$. Hence, $n/n' \cong 9.2$ and $l' = 0.82 \times 1.53 \times 9.2 = 11.5 \text{ \AA}$

Problem 11.5

The double logarithmic plots of η_0 versus M for low molecular weight fractions ($M < M_0$) may not obey the Rouse scaling law ($\eta \sim M$) unless corrections for the dependence of the coefficient of friction ζ on molecular weight is made (see Chap. 8, Sect. 8.6.3). If the viscosity of a polymer chain of average molecular weight 5000 is 2×10^3 poise and $T_g = -55^\circ\text{C}$, estimate the viscosity corrected for the chain length effect at -30°C , knowing the following data for chains of high molecular weight: $\langle r^2 \rangle_0/nl^2 = 6.2$; number of skeletal bonds, 2; molecular weight per monomer, 71. Moreover, in the transition region in which $d \log H(\tau)/d \log \tau = -1/2$, $H(\tau)$ is $2 \times 10^6 \text{ dyn/cm}^2$ for $\tau = 10^{-2} \text{ s}$ at -30°C ; $\rho = 0.97 \text{ g/cm}^3$; $\Phi_g/B = 0.031$; and $\alpha_f = 4.5 \times 10^{-4} \text{ K}^{-1}$.

Solution 11.5

As shown in Eq. (11.14),

$$\eta = k\zeta_0 M \quad (\text{P11.5.1})$$

where ζ_0 is the coefficient of friction, which depends on molecular weight. By multiplying the two sides of this equation by the ratio ζ_{00}/ζ_0 , where ζ_{00} and ζ_0 represent the friction coefficient for chains of molecular weight infinity and M , respectively, Eq. (P11.5.1) becomes

$$\eta\zeta_{00}/\zeta_0 = k\zeta_{00} = k' \quad (\text{P11.5.2})$$

The mean square end-to-end length per monomer unit is given by

$$b = \left[\frac{\langle r^2 \rangle_0}{(n/2)l^2} \right]^{1/2} \quad l = (6.6 \times 2)^{1/2} \times 1.53 \text{ \AA} = 5.56 \text{ \AA/monomer} \quad (\text{P11.5.3})$$

According to Eq. (11.47), the friction coefficient for a fraction of high molecular weight is $\zeta_{00} = 1.364 \times 10^{-3} \text{ dyn.s/cm}$.

By assuming that the coefficient of friction is governed by the free volume, the values of ζ_{00} (high molecular weight fraction) and ζ_0 (low molecular weight fraction) can be written as

$$\zeta_{00} = \exp\left(\frac{B}{\Phi_{00}}\right); \quad \zeta_0 = \exp\left(\frac{B}{\Phi_0}\right) \quad (\text{P11.5.4})$$

where Φ_{00} and Φ_0 represent, respectively, the free volumes of the fractions of high and low molecular weight.

Hence,

$$\log \zeta_0 = \log \zeta_{00} + \frac{B}{2.303} \left(\frac{1}{\Phi_0} - \frac{1}{\Phi_{00}} \right) \quad (\text{P11.5.5})$$

The values of Φ_{00} and Φ_0 at -30°C are 0.040 and $0.0423 \text{ cm}^3/\text{cm}^3$, respectively. Therefore, $\zeta_0 = 3.5 \times 10^{-4} \text{ dyn.s.cm}^{-1}$. Hence

$$k' = 2000 \times \frac{1.364 \times 10^{-3}}{3.5 \times 10^{-4}} = 7800 \text{ poise}$$

REFERENCES

1. PJ Flory. Principles of Polymer Chemistry. Ithaca NY: Cornell Univ Press, 1953.
2. PG de Gennes. Scaling Concepts in Polymer Physics. 2nd ed. Ithaca NY: Cornell Univ. Press, 1985.
3. M Doi, SF Edwards. Theory of Polymer Dynamics. Oxford UK: Clarendon Press, 1986.
4. A Ciferri. J Polym Sci 54: 149, 1961.
5. PE Rouse. J Chem Phys 21: 1272, 1953.
6. PG de Gennes. Scaling Concepts in Polymer Physics. 2nd ed. Ithaca NY: Cornell Univ Press, 1985, Chap 6.
7. BH Zimm. J Chem Phys 24: 269, 1956.
8. W Graessley. Adv Polym Sci 16: 1, 1974.
9. SF Edwards, JW Grant. J Phys A6: 1169, 1186, 1973.
10. PG de Gennes. J Chem Phys 55: 572, 1971.
11. M Doi, SF Edwards. J Chem Soc Faraday Trans II 74: 1789, 1802, 1818, 1978.
12. K Kremer. Macromolecules 16: 1632, 1983.
13. WW Graessley. Viscoelasticity and diffusion in entangled polymers. In: M Nagasawa, ed. Molecular Conformation and Dynamics of Macromolecules in Condensed Systems. Amsterdam: Elsevier, 1987, p 163.
14. G Marrucci. Microrheological modelling. In: JA Covas, JF Agassant, AC Diogo, J Vlachopoulos, K Walters, eds. Rheological Fundamentals of Polymer Processing'. NATO ASI Ser. London: Kluwer Academic Publishers, 1994, p 37

15. JD Ferry. *Viscoelastic Properties of Polymers*. 3rd ed. New York: Wiley-Interscience, 1980.
16. RH Colby, LJ Fetters, WW Graessley. *Macromolecules* 20: 2226, 1987.
17. H Watanabe, T Kotaka. *Macromolecules* 20: 530, 1987.
18. JD Ferry. *Viscoelastic Properties of Polymers*. 2nd ed. New York: Wiley-Interscience, 1970, p 360.
19. PG de Gennes. *Macromolecules* 9: 587, 594, 1976.
20. J Klein, D Fletcher, JL Fetters. *Faraday Symp Chem Soc* 18: 159, 1983.
21. VR Raju, EV Menezes, G Marin, WW Graessley, JL Fetters. *Macromolecules* 14: 1668, 1981.
22. CR Bartels, B Crist, LJ Fetters, WW Graessley. *Macromolecules* 19: 785, 1986.
23. WW Graessley, J Roovers. *Macromolecules* 12: 959, 1979.

12

Viscoelasticity of Glassy and Semicrystalline Polymers

12.1	General Considerations	454
12.2	Relaxations in the Frequency Domain at Temperatures Slightly Higher Than T_g	457
12.3	Topology of the Dynamics in the Vicinity of the Glass Transition Temperature	460
12.4	Viscoelastic Functions for Glassy Systems in the Frequency Domain	463
12.5	Dispersions in the Glassy State and the Glass Transition	464
12.6	Molecular Cooperativity in the Glass Transition	468
12.7	Structural Recovery in the Glassy State: Aging	473
12.8	Memory Effects and Physical Aging	474
12.9	Influence of Physical Aging on the Viscoelastic Functions: Time-Aging Time Correspondence Principle	478
12.10	Nonlinear Behavior in Aging	482
12.11	Final Remarks on Aging Processes	483
12.12	Relaxation Behavior of Semicrystalline Polymers: General Considerations	485
12.13	General Features of Crystalline Polymers	494
12.14	Time-Temperature Correspondence Principle	496
12.15	Modeling the Viscoelastic Behavior of Crystalline Polymers	496
	Problem sets	498
	References	507

12.1 GENERAL CONSIDERATIONS

When an amorphous material in the liquid state is cooled, a temperature is reached in the vicinity of which a transition from the liquid state to the

glassy state occurs. The glassy state may also be formed if a molten crystalline material is cooled at a heating rate high enough that the development of crystalline order is prevented. Low molecular weight organic substances, inorganic salts and oxides, polymers, etc. can develop the glassy state. As Eq. (6.33) indicates, the mean relaxation time of a liquid is given by $\langle \tau \rangle = \eta_0 J_e^0$, where η_0 and J_e^0 are, respectively, the viscosity and the steady-state compliance. The viscosity undergoes an anomalous increase with decreasing temperature as the temperature of the liquid comes closer to T_g , so the value of $\langle \tau \rangle$ becomes larger than the time scale of any available experiment. In this situation, the system falls out of equilibrium and the glassy state is formed.

The temperature dependence of the viscosity of liquids led to their classification as fragile and strong liquids (1). For fragile liquids the variation of the viscosity with temperature is described by the Vogel–Fulcher–Tammann–Hesse (VFTH) equation, while for strong liquids the viscosity follows Arrhenius behavior. As shown in Figure 12.1, the jumps in the specific heat at T_g are much larger for fragile liquids than for strong ones. Examples of fragile liquids are organic liquids, polymers, and inorganic salts; liquids like SiO_2 and GeO_2 are examples of strong liquids. It should be pointed out that polymeric materials are the most fragile liquids

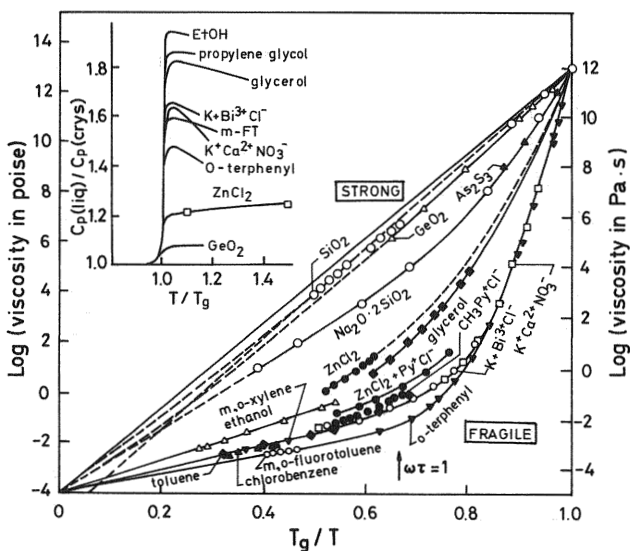


Figure 12.1 Variation of the viscosity and the specific heat (inset) with temperature for various glasses. (From Ref. 1.)

identified to date. However, they cannot be accommodated in Figure 12.1 without modification, because the viscosity of a polymer liquid is largely controlled by its molecular weight.

Let us analyze now the variation of the heat capacity of a molten crystalline substance with temperature. If the melt is slowly cooled, a temperature is reached at which a sharp decrease in the heat capacity C_p , caused by the liquid \rightarrow crystal transition, occurs. The variation of C_p with temperature is shown in Figure 12.2. The heat capacity decrease with decreasing temperature at $T < T_m$, becoming zero at $T = 0$ K. However, the heat capacity of a supercooled melt slowly decreases as the temperature declines, the difference C_p (liquid) $- C_p$ (crystal) increasing as the temperature decreases. At the temperature at which the liquid \rightarrow glass transition occurs, a sharp fall in C_p takes place, and the value of C_p at T_g becomes only slightly higher than that of the crystal at the same temperature. The curves showing the variation of both the heat capacity and the entropy for the crystal and the supercooled liquid at $T < T_g$ indicate that a temperature T_K is reached, called the Kauzmann temperature, at which the crystal and the glassy liquid exhibit the same entropy (2). Because the structural entropy of the crystal is zero, one would expect that the value of this quantity also would be nil for a completely relaxed glass at the Kauzmann temperature. This reasoning

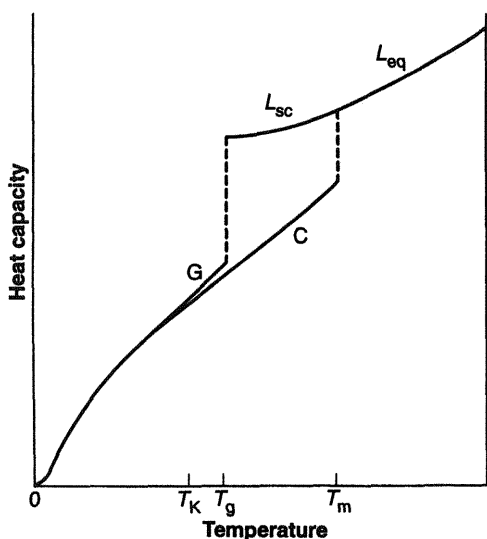


Figure 12.2 Variation of the heat capacity for fragile glass formers in crystal (C), supercooled liquid (L_{sc}), equilibrium liquid (L_{eq}) and glass (G) phases. T_K is the Kauzmann temperature.

suggests the possibility of reaching an ideal glassy state if the cooling rate is slow enough. It should be pointed out, however, that local motions of particles would hinder the possibility of reaching ideal glassy structures.

A dramatic change in the viscoelastic functions is the most important characteristic of the glass-rubber transition. An abrupt decrease is observed in the values of the compliance functions $J(t)$ and $J'(\omega)$ in the liquid \rightarrow glass transition, in contrast with what occurs with the values of the moduli $G(t)$ and $G'(\omega)$, which undergo a sharp increase. The opposite occurs in the variation of these viscoelastic functions in the glass \rightarrow liquid transition. The loss functions $J''(\omega)$, $G''(\omega)$, and $\tan \delta$ exhibit a maximum in the transition (3). In contrast with the sharp changes undergone by the viscoelastic functions in the glass \rightarrow liquid transition, the temperature dependence of these functions in the glassy state is comparatively small. However, the isochrones corresponding to $\tan \delta$ or any other viscoelastic loss function exhibit noticeable absorptions in the glassy region (4), suggesting that important mechanical activity may take place in the glassy state, even at temperatures well below T_g . Illustrative plots showing the temperature dependence of the storage relaxation modulus and the logarithmic decrement in the glassy state and the glass-rubber transition are shown in Figure 12.3.

12.2 RELAXATIONS IN THE FREQUENCY DOMAIN AT TEMPERATURES SLIGHTLY HIGHER THAN T_g

The curves showing the frequency dependence of loss functions [$\tan \delta$, $G''(\omega)$, or $J''(\omega)$] permit the detection in the frequency domain, at temperatures just slightly above the glass transition temperature, of a prominent absorption or α process. The unavailability of experimental devices to measure mechanical viscoelastic functions at high frequencies impedes the detection of a fast process or β relaxation in the high frequency region. This latter process is usually detected in the glassy state at low frequencies.

The presence of the α and β processes in the frequency domain is observed, for example, in the curves of the dielectric loss obtained at temperatures slightly above T_g . It should be noted that in this case experimental devices are available that permit measurement of the complex dielectric permittivity from 10^{-3} to 10^9 Hz. As the temperature increases, both the α and β processes are shifted to higher frequencies. Owing to the fact that the activation energy of the α process is much greater than that of β relaxation, an increase in temperature decreases the distance between the α (low frequency) and β (high frequency) processes. The two relaxations eventually overlap, forming the $\alpha\beta$ relaxation (5). This behavior is observed in Figure 12.4, where the dielectric loss in the frequency domain for poly(methyl

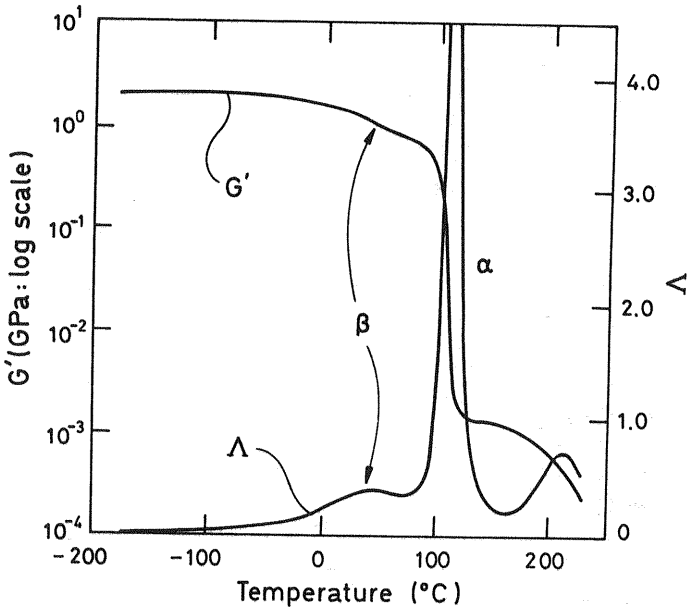


Figure 12.3 Illustrative curves showing the temperature dependence of both the storage relaxation modulus G' and the logarithmic decrement Δ in the glassy state and glass-rubber transition. (From Ref. 47.)

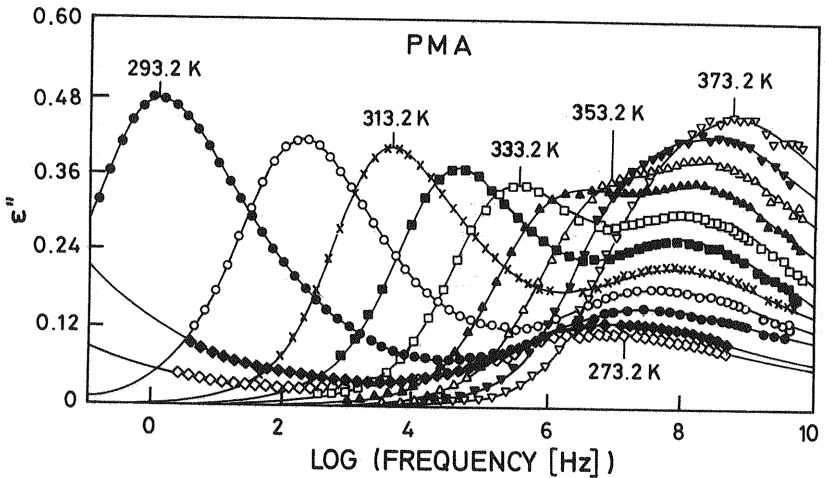


Figure 12.4 The dielectric loss in the frequency domain, at different temperatures, for poly(methyl acrylate). (From Ref. 6.)

acrylate) is shown (6). It is noteworthy that no thermodynamic change occurs above T_g for amorphous substances, and consequently the α relaxation in the frequency domain is not associated with a thermodynamic change in the material. The average relaxation time of the α process also obeys the VFTH equation.

The α relaxation in the frequency domain can be interpreted in terms of a stretch mean relaxation time, as discussed below. According to Eq. (5.37), the response of a viscoelastic material to a shear stress $\sigma(t)$ is given by

$$\varepsilon(t) = J_{u\alpha}\sigma(t) + J_{d\alpha} \int_0^\infty \sigma(t-u) \frac{d\Psi(u)}{du} du \quad (12.1)$$

Here $J_{d\alpha} = J_{r\alpha} - J_{u\alpha}$, where $J_{r\alpha}$ and $J_{u\alpha}$ are, respectively, the unrelaxed and relaxed compliance functions in the α relaxation process. The values of these quantities could in principle be obtained by extrapolation methods from complex plane plots of $J''(\omega)$ versus $J'(\omega)$. If $\sigma(t) = \sigma_0 \text{Im exp}(i\omega t)$, then Eq. (12.1) can be written as

$$\varepsilon(t) = J_{u\alpha}\sigma_0 \text{Im exp}(i\omega t) + J_{d\alpha} \int_0^\infty \{\sigma_0 \text{Im exp}[i\omega(t-u)]\} \frac{d\Psi(u)}{du} du \quad (12.2)$$

Since $J^*(\omega) = \varepsilon(t)/[\sigma_0 \text{Im exp}(i\omega t)]$, Eq. (12.2) leads to the expression

$$\frac{J^*(\omega) - J_{u\alpha}}{J_{r\alpha} - J_{u\alpha}} = \int_0^\infty -\frac{d\Phi(t)}{dt} \exp(-i\omega t) dt = \mathcal{L}\left(-\frac{d\Phi}{dt}\right) \quad (12.3)$$

where \mathcal{L} signifies the Laplace transform. Here the buildup function $\Psi(t)$ has been replaced by the decay function $\Phi(t) = 1 - \Psi(t)$. For relaxation experiments we obtain

$$\frac{G_{u\alpha} - G^*(\omega)}{G_{u\alpha} - G_{r\alpha}} = - \int_0^\infty \frac{d\Phi(t)}{dt} \exp(-i\omega t) dt = -\mathcal{L}\left(\frac{d\Phi(t)}{dt}\right) \quad (12.4)$$

$G_{u\alpha}$ and $G_{r\alpha}$ being the unrelaxed and relaxed relaxation moduli at infinite and zero frequencies, respectively.

It is an experimentally demonstrated fact that the α relaxation in the time domain fits the stretch exponential decay function $\Phi(t)$ or the Kohlrausch-Williams-Watts (KWW) equation (7,8)

$$\Phi(t) = \exp\left[-\left(\frac{t}{\tau_0}\right)^{\bar{\gamma}}\right] \quad (12.5)$$

where $0 < \bar{\gamma} \leq 1$. The parameter τ_0 is a mean relaxation time whose temperature dependence in the vicinity of the glass transition temperature is governed by the VFTH equation. The value of $\bar{\gamma}$ depends on the breadth of the α relaxation in the frequency domain. In the case of a process described by a single relaxation time or Debye-type relaxation, the value of the exponent $\bar{\gamma}$ is unity. As the complexity of the α relaxation process increases, the value of $\bar{\gamma}$ decreases. In other words, the wider the distribution of relaxation times, the smaller the exponent of the KWW equation. Substitution of the KWW equation into Eq. (12.3) or (12.4) allows the determination of the compliance and relaxation functions, respectively, in the frequency domain at temperatures slightly higher than T_g .

12.3 TOPOLOGY OF THE DYNAMICS IN THE VICINITY OF THE GLASS TRANSITION TEMPERATURE

The experimental evidence indicates that when a non crystallizable liquid is cooled, a temperature is reached at which the $\alpha\beta$ absorption splits into two relaxations: the slow α relaxation, which obeys the VFTH equation and remains kinetically frozen at temperatures below T_g , and the faster β relaxation, which follows Arrhenius behavior and remains operative below T_g . This behavior, illustrated (9) in Figure 12.5, is exhibited by low and high molecular weight liquids. To interpret this bifurcation it is convenient to consider that condensed phases owe their existence to interactions between the constituent particles: atoms, ions, or molecules. These interactions are embodied in a potential energy function $\Phi(\mathbf{r}_1, \mathbf{r}_2, \dots, \mathbf{r}_N)$ that depends on the local position of those particles, a schematic representation of which is given in Figure 12.6(2).

The evolution of the system is conditioned by the interparticle interactions, and the classical Newtonian equations give a good account of the dynamics of the system. Minima, maxima, and saddle points are detected in the topographic representation of the potential energy function. The minima correspond to mechanically stable arrangements of the particles of the system in space, with vanishing force and torque in each particle. Any small displacement from such an arrangement produces a restoring force that returns the particles to their undisplaced arrangement. The lower minimum would be occupied by the system if it were cooled to absolute zero slowly enough to maintain thermal equilibrium. This situation corresponds to a perfect crystal. Above the melting temperature, higher minima appear that correspond to particles packing in the equilibrium liquid phase. As the temperature of the liquid decreases, the configuration point of the system, $\mathbf{r}(t)$, is forced into regions of increasingly rugged and

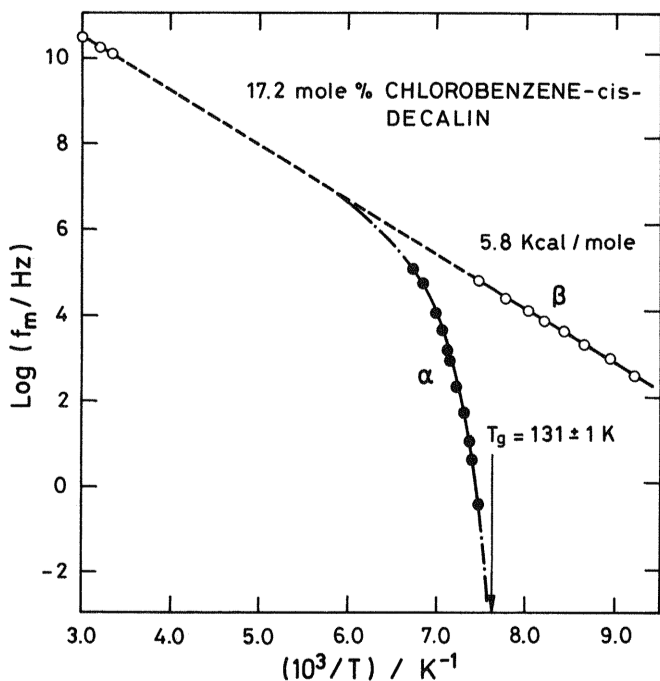


Figure 12.5 Illustrative curve showing the temperature dependence of peak relaxation frequencies for a glass-forming liquid. (From Ref. 9.)

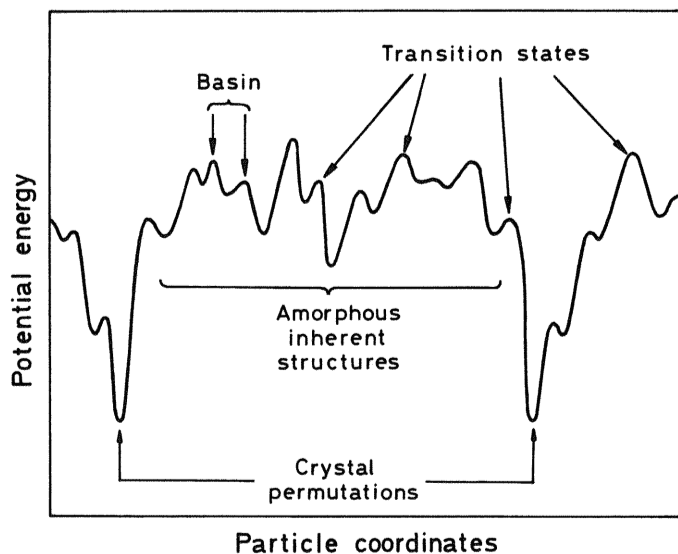


Figure 12.6 Schematic diagram of the potential energy hypersurface in the multi-dimensional configurational space for a many-particle system. (From Ref. 2.)

heterogeneous topography, seeking out ever deeper basins or craters. The craters are in turn connected by elementary basins that account for reorganization of the particles at the local level.

The β relaxation will arise from transitions between elementary basins, while the α relaxation will be produced by large-distance intercrater transitions. This behavior is illustrated in Figure 12.7. This latter transition involves a large sequence of elementary transitions, and consequently the activation energy associated with the α relaxation is much larger than that of the β process. At the glass transition temperature, the intercrater distance will be too great, and only elementary transitions within each crater will occur. Owing to the wide variety of elementary basins within each crater, β processes exhibit a wide distribution of relaxation times.

The differences between strong and fragile liquids to which we referred earlier can be explained in terms of the topographic view of the potential energy function $\Phi(\mathbf{r}_1, \dots, \mathbf{r}_N)$. Surfaces with few minima (craters) and high energy barriers between minima generate strong liquids (2). Owing to the low density of craters in the potential energy surface of strong liquids, large-distance intercrater transitions that produce α relaxation rarely occur; in this case, only elementary interbasin transitions associated with the β relaxation are important. Consequently, the α relaxation has very low intensity, and the bifurcation shown in Figure 12.5 is not clearly detected. In contrast, the rather high configurational jumps in C_p at T_g suggest that fragile liquids should have a high density of minima per unit energy increase. The high density of craters facilitates long-distance intercrater transitions in fragile liquids. Here the α relaxation has high intensity, and the bifurcation appearing in the temperature dependence of the peak relaxation of glass-forming liquids is clearly observable.

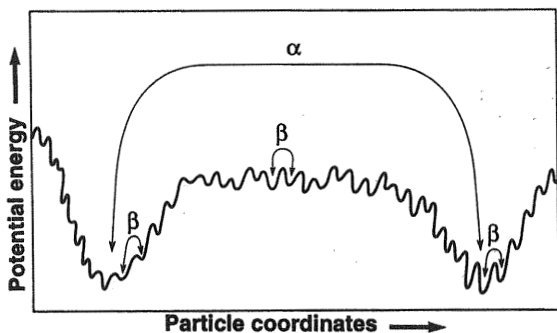


Figure 12.7 Configurational space explored by a fragile liquid in the vicinity of the glass transition temperature (From Ref. 2).

12.4 VISCOELASTIC FUNCTIONS FOR GLASSY SYSTEMS IN THE FREQUENCY DOMAIN

In general, the components of both the complex relaxation modulus and the complex compliance function of glassy systems exhibit a small dependence on frequency. This behavior is mainly responsible for the small magnitude of the loss $\tan \delta$, so high precision is necessary to determine it. Quenching a system from the liquid state to the glassy state produces a large portion of excess volume that shifts the dispersions to shorter times. As will be discussed later, the dependence of the free volume on the thermal history may be responsible for the lack of agreement among results reported by different authors.

The information obtained for glassy polymers from shear experiments is not equivalent to that obtained from elongation experiments owing to the perceptible change in volume produced by elongation (10). As can be seen in Figure 12.8, both G' and E' may undergo a gradual increase of nearly 50% with increasing frequency. However, the inflection occurring in G' lies at about a tenfold lower frequency. It is noteworthy that the values of $\tan \delta_E (= E''/E')$ and $\tan \delta_G (= G''/G')$ are similar within experimental error.

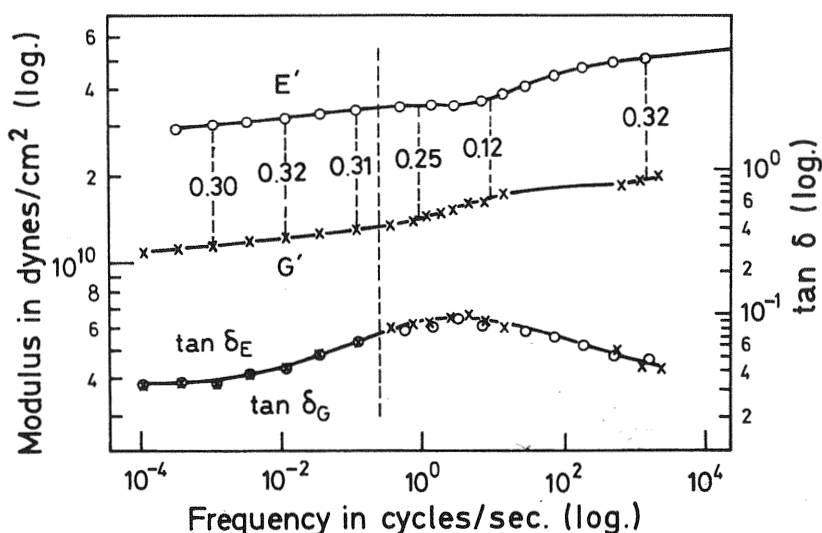


Figure 12.8 Values of G' , E' , $\tan \delta_G$, and $\tan \delta_E$ for poly(methyl methacrylate) in the vicinity of 25°C. The numbers between G' and E' denote values of Poisson's ratio. (From Ref. 10.)

12.5 DISPERSIONS IN THE GLASSY STATE AND THE GLASS TRANSITION

The mechanical activity detected in the glassy state can be determined from isochrones showing the temperature dependence of a loss function. The curves present an ostensible glass-rubber absorption (glass-liquid absorption for low molecular weight amorphous substances), called α relaxation, followed at decreasing temperatures by one or more absorptions called β , γ , etc., relaxations. Illustrative curves showing these relaxations are plotted in Figure 12.9. The temperature dependence of the relaxation times associated with the glass-rubber relaxations of high molecular weight materials and glass-liquid relaxations of low molecular weight materials is described by the VFTH equation [Eq. (8.35)]. As occurs with the glass-rubber relaxation, secondary relaxations shift to higher temperatures with increasing frequencies. The kernel of Eq. (9.10) presents a maximum for $\omega\tau = 1$, indicating that for a sub-glass absorption with a single relaxation time τ , the value of τ is given by the reciprocal of the frequency at which the maximum of the peak is observed. Consequently, the average relaxation time, $\tau (= 1/\omega = 1/2\pi f$, where f is the frequency in hertz), of a given absorption in the glassy state corresponds to the temperature of the isochrone

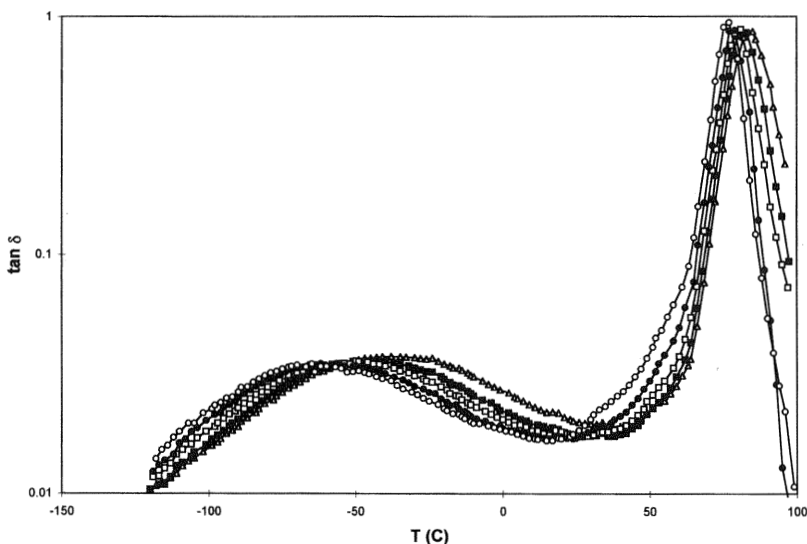


Figure 12.9 Temperature dependence of $\tan \delta$ for poly(vinyl chloride) at frequencies of (○) 0.1 Hz, (●) 0.3 Hz, (□) 3 Hz, and (△) 10 Hz.

(see Fig. 12.9) at which the maximum of the peak is located. The curves representing the variation of the storage relaxation modulus with temperature exhibit an inflection point in the vicinity of the temperatures at which the loss plots present a maximum. Illustrative plots are shown in Figure 12.10.

Sub-glass (β) relaxations can be obtained in the frequency domain at $T < T_g$. In principle, α and β dispersions can be obtained in the frequency domain at temperatures slightly higher than the glass transition temperature. However, the low range of frequencies available renders it difficult to detect them by mechanical experiments.

12.5.1 Activation Energies of Sub-Glass Relaxation Processes

Sub-glass relaxation phenomena are thermally activated processes that exhibit Arrhenius behavior,

$$\tau = \tau_0 \exp\left(\frac{E_a}{RT}\right) \quad (12.6)$$

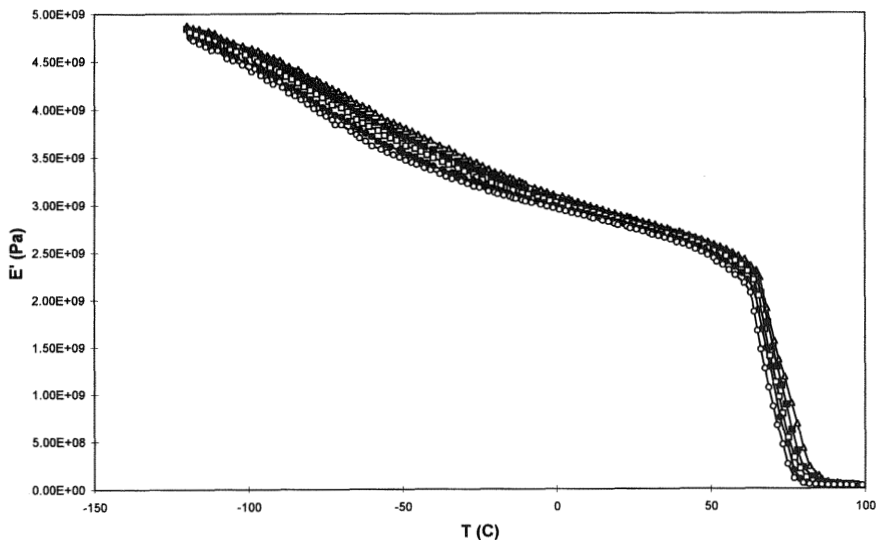


Figure 12.10 Temperature dependence of the tensile storage relaxation modulus for poly(vinyl chloride) at frequencies of (\circ) 0.1 Hz, (\bullet) 0.3 Hz, (\square) 1 Hz, (\blacksquare) 3 Hz, and (\triangle) 10 Hz.

where E_a , the activation energy associated with the process, depends on the viscoelastic mechanisms involved in the relaxation. By taking into account that $f = (2\pi\tau)^{-1}$, where f is the frequency in hertz, Eq. (12.6) can be written as

$$\ln f = \ln f_0 - \frac{E_a}{RT_{\max}} \quad (12.7)$$

where T_{\max} is the temperature corresponding to the maximum of the peak. Arrhenius plots give intercepts, $\log f_0$, lying in the range 13–15; for most polymeric systems the value of this quantity is 13.5 ± 1 . Assuming that $\log f_0 = 13$, Eq. (12.7) leads to the expression (11)

$$E_a = [0.060 - 0.0046 \log f] T_m(f) \quad (12.8)$$

where E_a is given in kilocalories per mole. For $f = 1$ Hz, Eq. (12.8) predicts that $E_a = 0.060 T_m$ (1 Hz). In Figure 12.11, the values of the activation energy for the sub-glass relaxation of a series of polymers are plotted against the temperature associated with the maximum of the peak at 1 Hz. It can be seen that the predictions of Eq. (12.8) hold satisfactorily for polymers with flexible side groups. However, the predictions are not so satisfactory for other types of molecular chains.

12.5.2 Molecular Origin of Sub-Glass Relaxations

Sub-glass relaxations in polymers with flexible side groups are believed to arise from motions taking place in these groups either alone or coupled with local motions of the backbone. The curves showing the temperature dependence of the loss functions of acrylate and methacrylate polymers containing cyclohexyl rings in the alcohol residue (12,13), shown in Figure 12.12, present a strong secondary absorption in the glassy state located at -80°C at 1 Hz. The fact that the activation energy of this process (≈ 11 kcal/mol) is of the same order of magnitude as that determined by NMR for the chair-to-chair inverse conformational transition of the cyclohexane ring led to the conclusion that flipping motions of the ring are responsible for the secondary relaxation process. In general, polymers with flexible side groups present specific secondary relaxations, and consequently dynamic experiments carried out on the glassy state are useful for the characterization of polymeric systems (4,14,15).

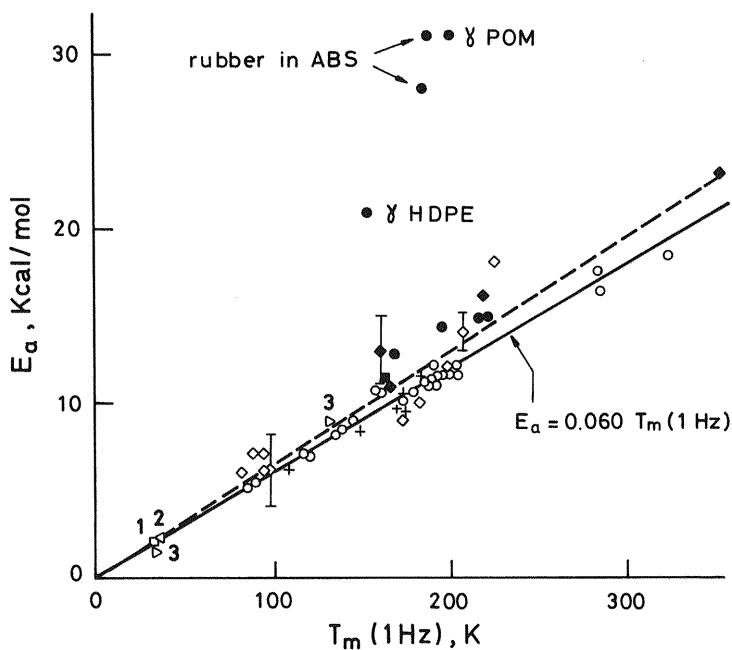


Figure 12.11 Activation energy E_a as a function of the temperature associated with the peak maximum of the β relaxation at 1 Hz. Filled symbols, main-chain motions; open symbols, side group motions; crosses, motions within molecules dissolved in the polymer matrix. (From Ref. 11.)

Secondary (sub-glass) relaxations appear not only in the relaxation spectra of polymers containing flexible side groups but also in symmetrical molecular chains [poly(ethylene glycol terephthalate), polyethylene, etc.] or in asymmetrical chains without flexible side groups [poly(vinyl chloride), polypropylene, etc.]. Illustrative curves showing the sub-glass relaxations of polymers without flexible side groups are shown in Figure 12.13. In this case, secondary processes are believed to be produced by local motions, that is, by local conformational changes occurring in the main chain. The lack of dependence of the relaxation times associated with these processes on the chain length suggests that there must be cooperativity in the conformational transitions taking place in the intervening segments in order to ensure that the volume swept by the adjacent tails of the chains is negligible; otherwise the friction energy, and hence the relaxation times, would increase with molecular weight. Simulations carried out in simple polymers such as polyethylene show that the conformational transitions are mostly of the following type (16):

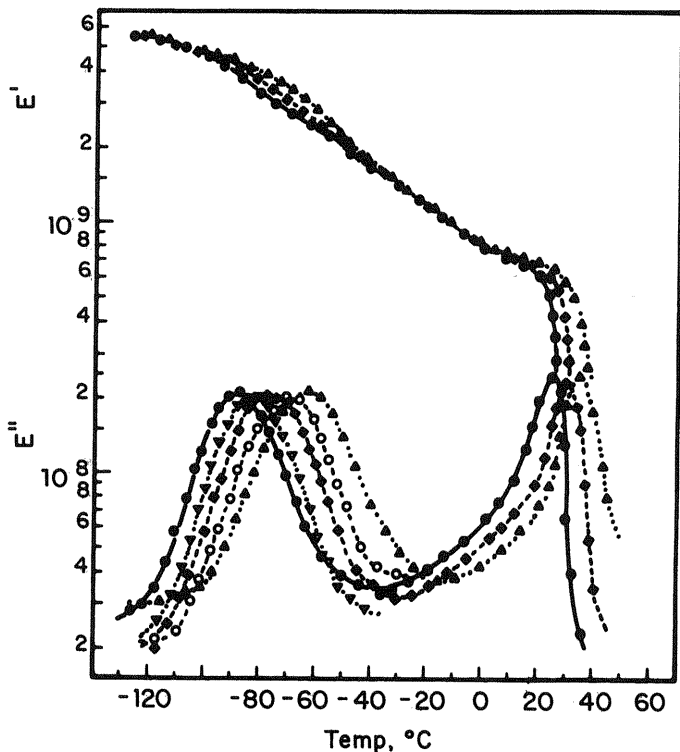
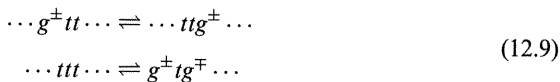


Figure 12.12 Variation of both the storage and loss relaxation moduli with temperature for poly(cyclohexyl acrylate) at several frequencies. Results obtained at (●) 0.1, (▽) 0.3, (◆) 1, (○) 3, and (▲) 10 Hz.



As shown in Figure 12.14, these transitions produce changes only in the central segment, the extreme segments remaining in positions parallel to the initial ones.

12.6 MOLECULAR COOPERATIVITY IN THE GLASS TRANSITION

The fact that the relaxation times associated with the glass–rubber transition and the secondary relaxations are independent of molecular weight suggests

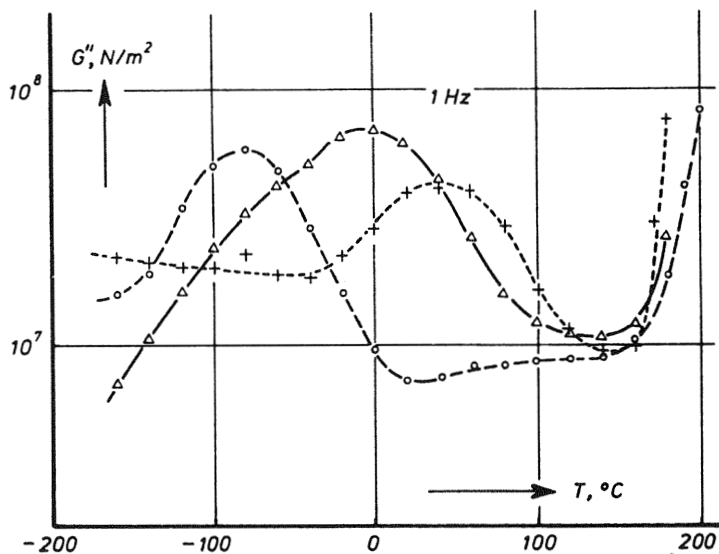
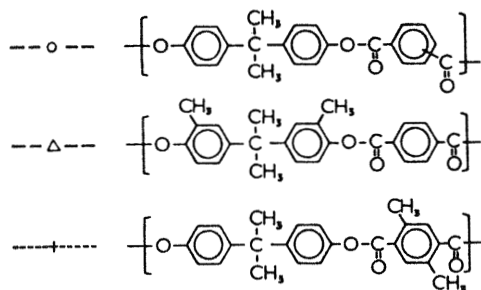


Figure 12.13 Shear loss relaxation modulus G'' as a function of temperature for three amorphous polyesters in the glassy state. (From Ref. 11.)

some sort of cooperativity among the molecular segments taking part in the response. The relaxation time associated with the rotation about a C—C bond placed between two methylenic units may be about 10^{-10} s at room temperature (17). In isolated chains the intramolecular response implies more complex motions involving even triads. Obviously, the activation energy should slightly increase with the segment length.

The dynamics of polymers may be interpreted by assuming the existence of domains. At high temperature ($T \gg T_g$), each domain is occupied by a single conformer and the interactions between neighboring segments or conformers are considered to be negligible. Once the potential barrier is crossed, conformers relax independently of their neighbors. Each domain

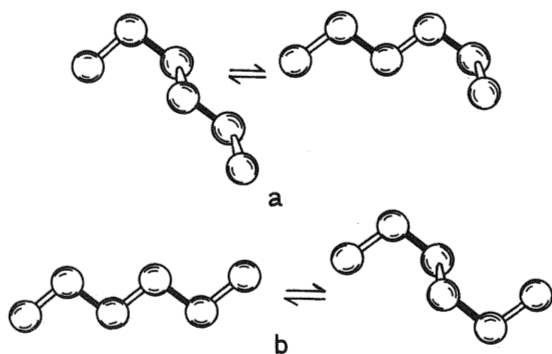


Figure 12.14 Molecular models illustrating secondary conformational transitions for symmetrical chains. (From Ref. 16.)

contains the rotational states associated with each conformer; in most cases, there are three such states (trans, t ; gauche positive, g^+ ; and gauche negative, g^-). The number of conformers occupying a domain increases as the temperature decreases, that is, as the densification of the system increases. A temperature T_∞ can be defined at which different domains merge, forming a macrodomain of infinite conformers. Between the two extremes are the domains associated with the condensed matter. In what follows we study cooperativity processes in systems in thermodynamic equilibrium. Matsuoka (17) developed a theoretical approach to describe the glass transition of polymer chains that is briefly described below.

Statistical mechanical principles suggest that the conformational entropy S_c of 1 mol of conformers occupying N_z domains is given by

$$S_c = N_z k_B \ln c_1 \quad (12.10)$$

where c_1 is the number of rotational states of each conformer and k_B is the Boltzmann constant. If each molecular chain behaves as if it were isolated, that is, a single conformer occupying one domain, the conformational entropy of 1 mol of conformers, s^* , can be written as

$$s^* = N_A k_B \ln c_1 \quad (12.11)$$

where N_A is Avogadro's number. Because $z = N_A/N_z$ from Eqs. (12.10) and (12.11), the number of conformers per domain is expressed by

$$z = \frac{s^*}{S_c} \quad (12.12)$$

This expression indicates that the size z is proportional to the reciprocal of the conformational entropy.

Therefore, when $T^* \gg T_g$, $N_z \approx N_A$, and consequently $S_c \sim s^*$. For $T < T^*$, S_c will diminish with decreasing temperature more rapidly when s^* , reaching the value of zero at T_∞ . On the other hand, the conformational population will be in the lowest energy state at $T = 0$ K; in this case, $c_1 = 1$ and $s^* = 0$. Curves showing the temperature dependence of the enthalpies H_c and h^* are plotted in Figure 12.15. At high temperature ($T = T^*$), the molecular chains behave as if they were isolated, and $H_c(T^*) = h^*(T^*)$. Here the enthalpy is approximately proportional to the concentration of higher energy conformations calculated from rotational isomeric statistics. Curve B in Figure 12.15 includes the intermolecular interactions between neighboring bonds, which begin to be larger than zero at $T > T_\infty$. Taking into account that $\Delta C_p = (\delta H/\delta T)_p$ yields the expression

$$\frac{H_c(T)/H_c(T^*)}{h^*(T)/h^*(T^*)} \simeq \frac{(T - T_\infty)/(T^* - T_\infty)}{T/T^*} \quad (12.13)$$

where it has been considered that

$$H(T^*) = h(T^*) \simeq \Delta C_p(T^* - T_\infty) \simeq \Delta c_p^* T^* \quad (12.14a)$$

$$H_c(T) = \Delta C_p(T - T_\infty) \quad (12.14b)$$

$$h^*(T) = \Delta c_p^* T \quad (12.14c)$$

On the other hand, near equilibrium, $H \approx TS$, so

$$\frac{H_c(T)}{h^*(T)} \simeq \frac{S_c}{s^*} \quad (12.15)$$

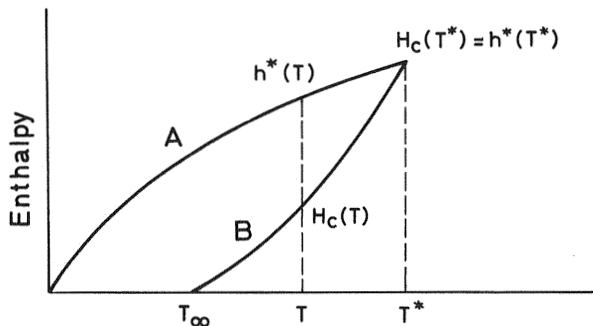


Figure 12.15 Variation of the enthalpy of a glass-forming liquid with temperature. For $T > T^*$ each conformer occupies on domain. (From Ref. 17.)

Combining Eqs. (12.14) and (12.15), the ratio of entropies can be written as

$$\frac{S_c}{s^*} = \frac{\Delta C_p}{\Delta c_p^*} \left(\frac{T - T_\infty}{T} \right) \quad (12.16)$$

The probability for a conformer to relax is $p = \exp(-\Delta g/RT)$, where Δg is the free energy barrier, while the probability that the z conformers of the same domain relax simultaneously is given by

$$p' = \exp\left(-\frac{z\Delta g}{k_B T}\right) \quad (12.17)$$

Consequently, the ratio between the relaxation time (τ) associated with the domains occupied by z conformers and that (τ^*) corresponding to those occupied by a single conformer can be written as

$$\ln \frac{\tau}{\tau^*} = \frac{\Delta g}{k_B} \left(\frac{z}{T} - \frac{1}{T^*} \right) = \frac{\Delta g}{k_B} \left(\frac{s^*}{TS_c} - \frac{1}{T^*} \right) \quad (12.18)$$

where use has been made of Eqs. (12.12) and (12.17). It should be pointed out that Eq. (12.18) is similar to that proposed by Adam and Gibbs, with the difference that in Matsuoka's approach inter- and intramolecular interactions are considered. From Eqs. (12.14), (12.16), and (12.18), the Vogel-Fulcher-Tammann-Hesse (VFTH) equation is obtained:

$$\ln \frac{\tau}{\tau^*} = \frac{\Delta g^*}{k_B} \left(\frac{1}{T - T_\infty} \right) - \frac{\Delta g^*}{k_B} \left(\frac{1}{T^* - T_\infty} \right) \quad (12.19)$$

where the expression

$$\Delta g^* = \Delta g \frac{T^* - T_\infty}{T^*} \quad (12.20)$$

was used. Traditionally, the VFTH equation has been written

$$\ln \frac{\tau}{\tau^*} = \frac{1}{\alpha_f(T - T_\infty)} - \frac{1}{\alpha_f(T^* - T_\infty)} \quad (12.21)$$

where T^* is the reference temperature and $\alpha_f [= (1/V)(\delta V/\delta T)_p]$ is the expansion coefficient. By comparing Eqs. (12.19) and (12.21) we obtain the relationship

$$\Delta g^* \simeq \frac{N_A k_B}{\alpha_f} = \frac{R}{\alpha_f} \quad (12.22)$$

where R is the gas constant. Because for most polymer systems $\alpha_f \approx 6 \times 10^{-4} \text{ K}^{-1}$, Eq. (12.22) suggests that Δg^* exhibits a nearly universal value of 3.3 kcal per mole of conformer. By considering, however, that $\Delta g = \Delta g^* T^* / (T^* - T_\infty)$, it is possible to conclude that the intramolecular relaxation of one skeletal bond is greater with polymers that have higher T_∞ and hence higher T_g . Comparison of Eqs. (8.40) and (12.22) allows us to relate the free volume fraction at T_g with the potential barrier Δg^* . The expression obtained is

$$\Phi_g = \frac{R(T_g - T_\infty)}{\Delta g^*} \quad (12.23)$$

Experimentally it is found that $T_g - T_\infty \approx 50 \text{ K}$ for most polymers; hence polymers having the same value of Δg^* will have the same value of Φ_g .

12.7 STRUCTURAL RECOVERY IN THE GLASSY STATE: AGING

Owing to the fact that the glassy state is a nonequilibrium or metastable state, the thermodynamic properties of a glassy system (volume, enthalpy, etc.) in isothermal conditions will evolve toward thermodynamic equilibrium. The evolution of the volume is usually expressed in terms of $\delta = (v - v_e)/v_e$, where v and v_e are, respectively, the specific volume at time t and at equilibrium. After a T-jump cooling experiment, the variation of δ with time, in isothermal conditions, follows trends similar to those shown (18) in Figure 12.16. This process is known as structural recovery.

The nonequilibrium state of a glassy system is often identified by its fictive temperature T_f (19). This parameter can be determined by drawing a line through the specific volume value on a volume-temperature plot with a slope equal to that of a glass line. The value of T_f is that at which the glass line intersects the equilibrium liquid line (see Fig. 12.17). In other words, T_f can be defined as the temperature at which the excess in a thermodynamic property (volume, enthalpy, etc.) would be zero. Because of the structural recovery of glassy systems, the fictive temperature decreases as the aging time, t_{age} , increases (20). This behavior is shown in Figure 12.18, where the fictive temperature of polycarbonate is plotted against $\log t_{\text{age}}$ at three temperatures. Here T_f is roughly a linear decreasing function of $\log t_{\text{age}}$. In general, the value of a given thermodynamic property of the glassy system

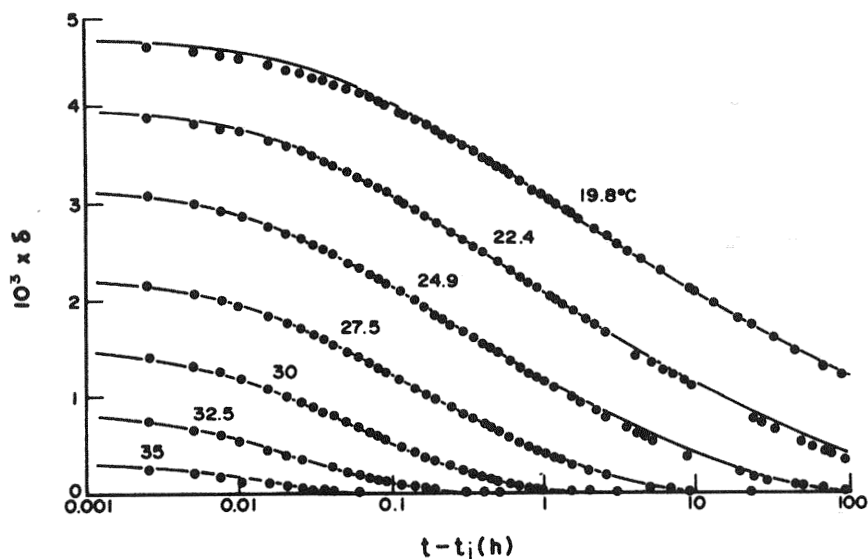


Figure 12.16 Isotherms showing the contraction of glucose glass at selected temperatures. (From Ref. 18.)

is above the corresponding value at equilibrium, except in the case in which the glassy system is rapidly heated. This situation is reflected in Figure 12.19, where it can be seen that the expansion volume or enthalpy undergoes a delay with respect to the heating rate so that the values of these thermodynamic parameters lie below those corresponding to equilibrium. Therefore, the glass transition temperature determined by this method will be higher than the fictive temperature, and as a consequence the difference between T_g and T_f will increase as both the heating rate and the time of aging increase. However, if a glass is heated more slowly than it was cooled, an exothermic peak is observed as result of the contraction toward the equilibrium curve during the slow heating. This behavior is schematically reflected in Figure 12.20. The intensity of the exothermic peak increases as the ratio of the heating rate to the cooling rate decreases.

12.8 MEMORY EFFECTS AND PHYSICAL AGING

Memory effects play an important role in structural recovery (18), as can be seen in Figure 12.21, where illustrative plots of the evolution of volume with time for different thermal histories are shown. Curve 1 presents the

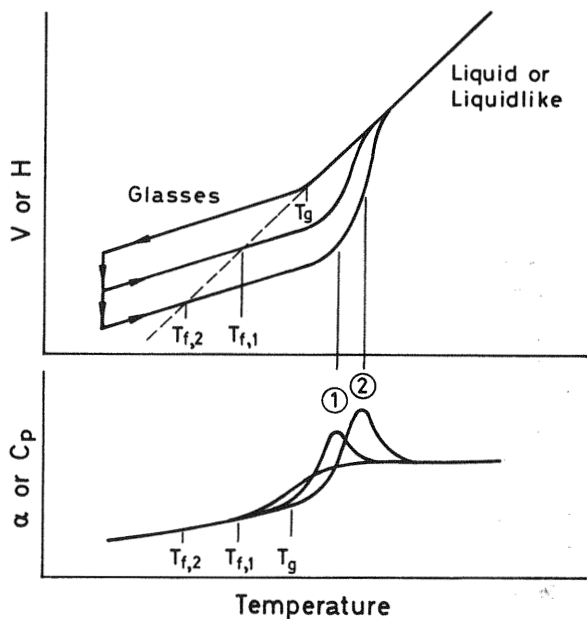


Figure 12.17 Volume or enthalpy cooling curves followed by annealing at constant temperature $T < T_g$. Curves corresponding to subsequent heating at a rate equal to that of the cooling process are also represented. Endotherm peaks for the expansion coefficient (α) and the specific heat are also shown. The fictive temperatures T_f are indicated.

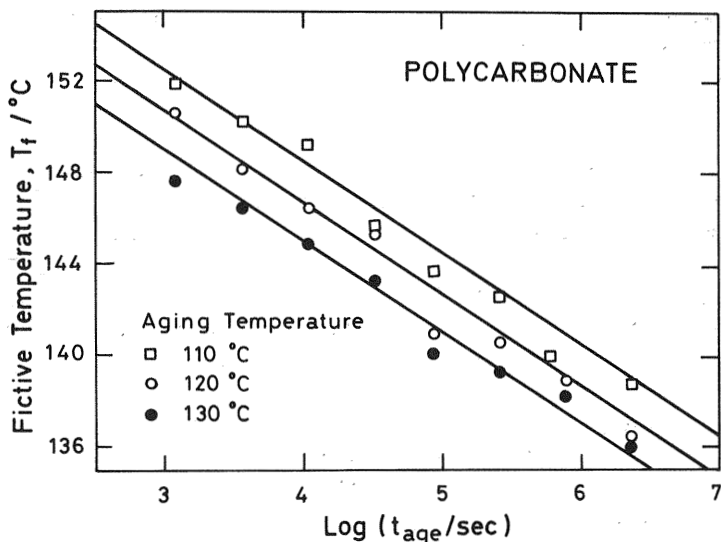


Figure 12.18 Fictive temperatures of polycarbonate following aging for different lengths of time at the temperatures indicated. (From Ref. 20.)

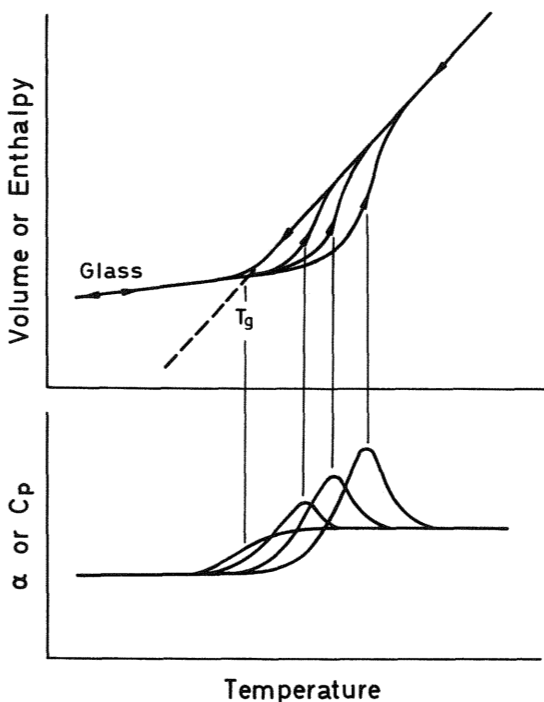


Figure 12.19 Endotherm peaks for the expansion coefficient α or the specific heat C_p generation without annealing below T_g by heating at a rate greater than that of the preceding cooling. The corresponding curves for the volume V and enthalpy are shown in the upper curves.

variation of δ with time at 30°C for a sample of poly(vinyl acetate) quenched from 40°C (liquid state) to 30°C . Equilibrium ($\delta = 0$) is reached in about 1000 h in this case. Curves 2, 3, and 4 correspond to glasses prepared by quenching the same polymer from 40°C , to respectively, 10°C (for 160 h), 15°C (for 140 h), and 25°C (for 90 h), followed in all cases by upward jumps to 30°C . It can be seen in these curves that δ is nearly zero at short times. However, the glass does not remain at equilibrium, but “remembers” its previous history, and as time passes δ goes through a maximum before it approaches the response of a downward jump directly to 30°C at long times. Such behavior can be described by means of sums of exponential functions (distributions of retardation times) or stretched exponential functions.

The evolution of the thermodynamic properties with time governs the viscoelastic response of materials in the glassy state. The volume relaxation

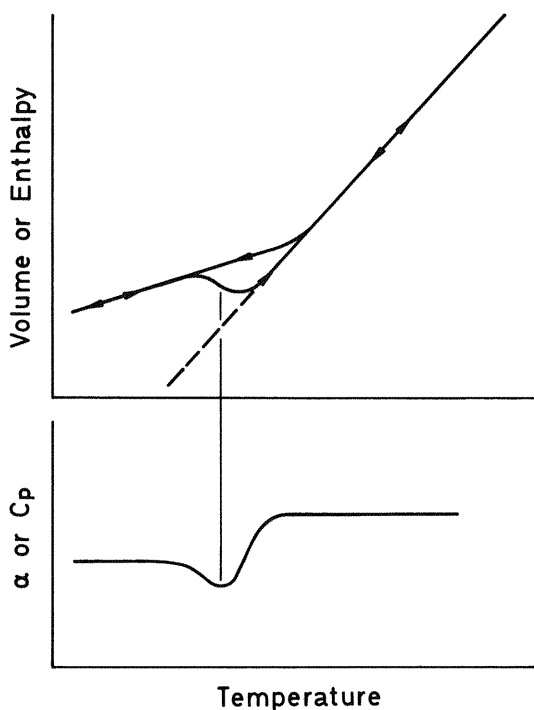


Figure 12.20 Negative expansion coefficient obtained by heating more slowly than the previous rate of cooling. (From Ref. 20.)

that takes place in the glassy system is called physical aging in polymers and structural relaxation, annealing, or stabilization in inorganic glasses. The term "physical aging" was coined by Struik (21) to refer to the variation of the physical properties of materials with time when they are kept at temperatures below the glass transition temperature. In general, the importance of aging increases as the temperature of the glass comes closer to T_g . Obviously, aging effects are much more important in organic glasses than in inorganic glasses as a consequence of the fact that the temperature of use is closer to the glass transition temperature in organic systems than in inorganic systems. Among the properties and applications affected by physical aging are the design and manufacture of composite materials (e.g., parts for automobiles), permeability of materials for packaging, adhesives, materials for use in nonlinear optics, curing of epoxy resins, mechanical properties of materials used in reprography, and glass-metal joint seals.

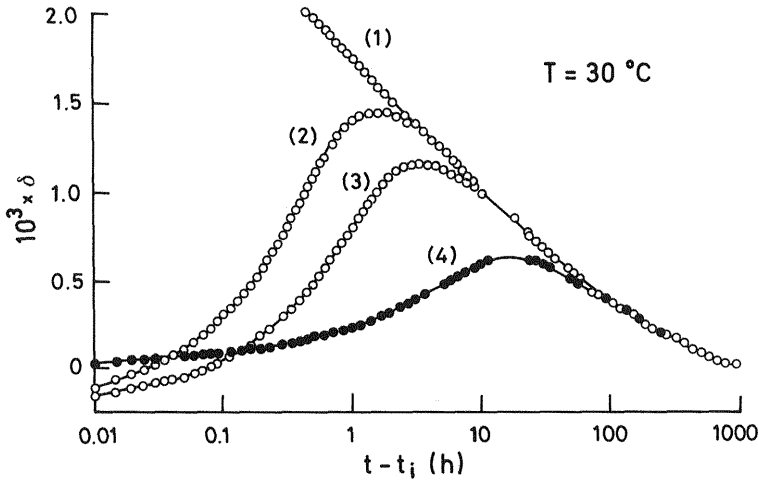


Figure 12.21 Structural recovery of poly(vinyl acetate) at 30°C after several thermal histories. See text for details. (From Ref. 18.)

12.9 INFLUENCE OF PHYSICAL AGING ON THE VISCOELASTIC FUNCTIONS: TIME-AGING TIME CORRESPONDENCE PRINCIPLE

Physical aging affects in an important manner the time scale of the mechanical relaxation properties of glassy systems. Rate processes such as those of viscoelastic and dielectric dispersions, slow down with increasing aging time. Thus, transient viscoelastic functions such as the creep compliance function and stress relaxation modulus shift to longer times when plotted as functions of the logarithm of time, while dynamic properties such as the complex compliance function and the complex shear modulus shift to lower frequencies in the frequency domain. The conjunction of aging effects with the thermodynamic properties leads to nonlinear processes in glasses that may complicate the analysis and interpretation of the mechanical properties of polymers. Consequently, the behavior of a glassy material depends not only on the actual state of the system but also on its previous history. Phenomenological equations have been developed that describe reasonably well the structural recovery of glasses (22–24).

The evolution of the tensile creep compliance of a glassy epoxy resin at different aging times is shown, as an example, in Figure 12.22. The glasses were obtained by quenching the resin from $T_g + 22^\circ\text{C}$ to $T_g - 9^\circ\text{C}$ and were kept at this temperature for different intervals of time. The results obtained show that as the aging time increases, the values of $J(t)$ for comparable

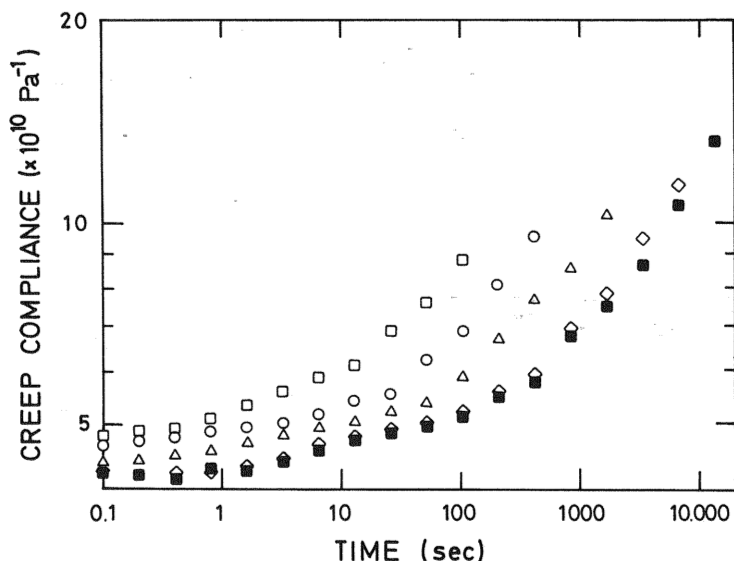


Figure 12.22 Evolution of the creep compliance with time for an epoxy glass quenched from $T_g + 22^\circ\text{C}$ to T_g and kept at this temperature for (\square) 28 min, (\circ) 126 min, (\triangle) 503 min, (\diamond) 2013 min, and (\blacksquare) 4026 min. (From Ref. 25.)

times decrease (25). Actually, an increase in the aging of the glass also increases its densification; that is, both the fractional free volume and the excess of entropy decrease, and consequently the molecular mobility diminishes. The results at hand suggest that when a system undergoes a temperature jump from above T_g to below T_g , the volume recovery is accompanied by a mechanical response of the glass. The creep curves obtained at different aging times after the temperature jump can be superimposed by a shift factor along the time axis.

Horizontal shifts of the isotherms obtained in aging processes combined with suitable vertical shifts give master curves that permit prediction of the viscoelastic behavior of aged systems over a wide interval of time. The time-aging time correspondence principle for poly(vinyl chloride) (26) is shown in Figure 12.23. The retardation times in these creep experiments are related to the aging time, t_a , by means of the expression

$$\tau_\delta = \tau_0 t_a^\mu \quad (12.24)$$

where τ_δ and τ_0 are, respectively, the retardation times of volume for the aged and non-aged glass and μ is the Struik shift factor (21). This equation

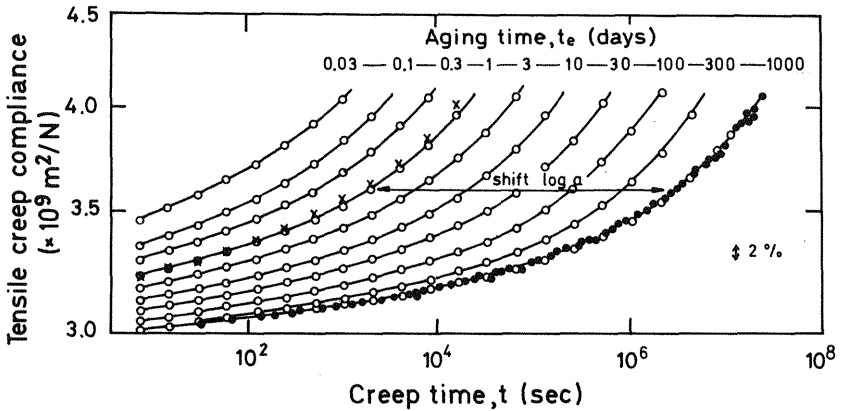


Figure 12.23 Small strain tensile creep curves for poly(vinyl chloride) quenched from 90°C (i.e., above T_g) to 20°C and further aged for different lengths of time. The master curve (●) was obtained by horizontal displacement of the curves with only slight vertical shifts. (From Ref. 26.)

indicates that the retardation time increases with increasing aging time. The viscoelastic creep observed in Figures 12.22 and 12.23 suggests that molecular chains have significant mobility in the glassy state. Chain mobility is determined by the free volume, v_f , and configurational entropy, S_c , both parameters being functions of temperature. The decrease that aging produces in v_f and S_c results in the lengthening of τ_8 with aging. In the linear viscoelastic regime, the experiments at hand indicate that the slope of the double logarithmic plot of the shift factors versus aging time is equal to or less than unity. Though the aging regime exists mainly above the β relaxation, there is little doubt that aging also occurs during this process. However, the structural recovery is different in β and α relaxations, and the time-aging time superposition will break down in this regime. It is noteworthy that data from stress relaxation experiments carried out on poly(methyl methacrylate) ($T_g = 104^\circ\text{C}$) at different aging times could not be superimposed below 80°C, and this was attributed to the influence of the strong and broad β relaxation in this polymer.

The temperature dependence of τ_0 in physical aging may be expressed in terms of the Adam-Gibbs equation (27,28)

$$\tau_0 = A \exp\left(\frac{B}{T(1 - T_K/T_f)}\right) \quad (12.25)$$

where T_K is the thermodynamic Kauzmann temperature (the temperature at which the configurational entropy vanishes), T_f is the fictive temperature,

and A and B are constants. Above the glass transition temperature, $T_f = T$, and Eq. (12.25) simplifies to the VFTH equation. The Kauzmann temperature and the parameters A and B can be obtained by fitting equilibrium data to the VFTH equation and used further to predict the glassy state effective activation energy $BR/(1 - T_\kappa/T_f)$. It should be pointed out that the predictions thus obtained are often accurate for both polymeric and nonpolymeric materials although the relationship between equilibrium (linear) and non-equilibrium (nonlinear) relaxations is not well understood (28).

When the temperature of the aged glass is increased above the glass transition temperature, the aging effects are erased. Therefore, the same aging curves are produced if the system undergoes the primitive thermal history. In ideal conditions, a change in temperature or δ (volume) causes each retardation time to be shifted by the same amount, and the amount of shift due to changes in temperature is independent of that due to the departure from equilibrium, i.e. structure (22).

The shift factors are also dependent on the aging temperature (31), as shown in Figure 12.24, where double logarithmic plots of the aging time shift factor versus aging time are shown for an epoxy aged at different temperatures. It is noteworthy that upon aging two types of behavior are detected in the glassy state. On the one hand, at aging temperatures far below T_g , the aging continues for the duration of the experiment. On the

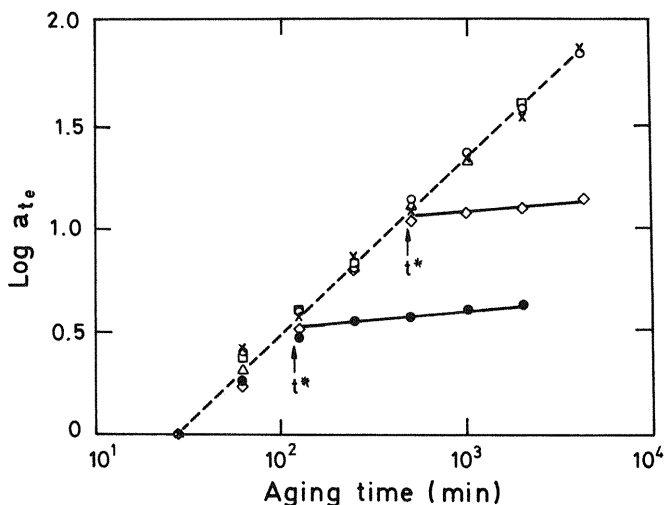


Figure 12.24 Double logarithmic plot of the aging time shift factors versus aging time, t_e , for an epoxy glass aged at different temperatures below its T_g . $T - T_g$: (○) 30°C, (X) 24°C, (□) 20.8°C; (◇) 10.3°C; (●) 6.3°C. (From Ref. 30.)

other hand, at aging temperatures close to T_g , the aging seems to nearly cease at some time t^* that might be expected to be an equilibration time for the glass.

12.10 NONLINEAR BEHAVIOR IN AGING

The time-aging time correspondence principle does not hold for all glasses. The diminution of both the entropy S_c and the fractional free volume v_f by the effect of aging increases the retardation and relaxation times, but the stress may also affect both S_c and v_f , and as a result the mechanical behavior is nonlinear. The application of a stress to a glassy material gives rise to an increase in free volume. This produces a decrease in the values of the relaxation times, so situations may arise in which the values of these parameters are lower than those corresponding to temperatures slightly higher than T_g . In other words, at a given time the creep compliance at large stresses is shifted to shorter times relative to the small stress response. Accordingly, with an increase in aging time, the slope of the double logarithmic plot of the time-aging time shift factor versus aging time decreases with increasing stress of the creep experiments. An illustrative plot reflecting this behavior is shown in Figure 12.25. This behavior has been interpreted as indicative that the large stress erases the prior aging. For this reason this process is called rejuvenation.

Many authors have attributed the yield point and the fragile \rightarrow ductile transition occurring in many glasses to the decrease in the values of the retardation times resulting from the increase in volume produced by stress in the glassy system.

The nonlinearity exhibited by the aging process suggests that the characteristic relaxation time τ_0 of the KWW equation is not a constant but a variable. A nonlinear function can be obtained for the KWW equation by defining a reduced time given by (28,29)

$$\theta(t) = \int_0^t \frac{dt'}{\tau_0(t')} \quad (12.26)$$

so that Eq. (12.5) can be written as

$$\Phi(t) = \exp[-(\theta)^{\bar{\gamma}}] = \exp \left[- \left(\int_0^t \frac{dt'}{\tau_0(t')} \right)^{\bar{\gamma}} \right] \quad (12.27)$$

where the integration begins at the time at which the system was last at equilibrium.

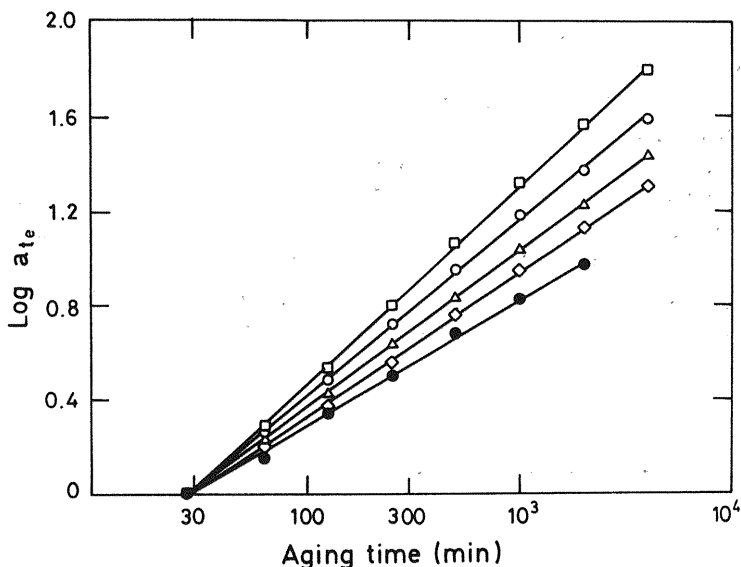


Figure 12.25 Double logarithmic plot of the aging time shift factors versus aging time, t_e , for an epoxy glass aged at $T_g - 13.2^\circ\text{C}$. Symbols represent different levels of applied stress: (□) 1 MPa, (○) 5 MPa, (△) 10 MPa, (◇) 15 MPa, (●) 20 MPa. (From Ref. 25.)

12.11 FINAL REMARKS ON AGING PROCESSES

Aging may be affected by external factors such as the absorption and desorption of gases in glassy systems. Thus, the free volume decreases with aging, and consequently this process affects adversely the solubility of gases in the glass. In the same way, occupation of the free volume by gases increases the values of the retardation or relaxation times, thus delaying the aging processes. Conversely, the rapid desorption of absorbed gases speeds up aging processes. Aging decreases the free volume, thus increasing the diffusive path, and as a result the diffusion coefficient of gases decreases.

Aging or structural recovery has a strong influence on engineering properties such as yield, creep rupture, and dimensional stability. There is a wealth of experimental work showing that the yield stress of a glass-forming polymer increases with increasing aging time after quenching. Though the failure of materials is influenced by aging, relatively little work has been done on the failure of materials in creep rupture conditions. Double logarithmic plots of creep rupture time versus applied stress for poly(methyl

methacrylate) are shown in Figure 12.26. The plots indicate that the time to failure, for a given stress, increase with aging time (30). However, this behavior is not general; for example, it is not observed in polystyrene.

The nonexponential and nonlinear character of aging processes makes it difficult to analyze the influence of mechanical and thermal histories on the viscoelastic behavior of glassy systems. Phenomenological theories have been developed that describe aging processes of strong glasses that undergo purely thermal histories (22–24). However, these theories are not appropriate for fragile glasses such as polymers. Theories are also lacking that describe the effect of nonthermal perturbations on the aging behavior of polymers.

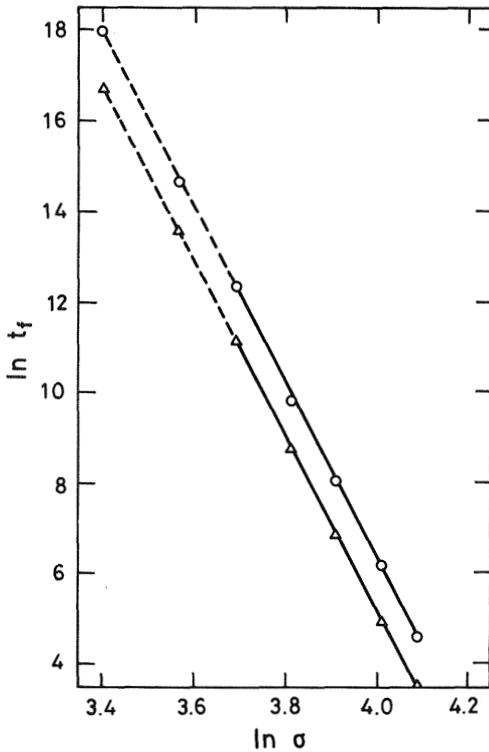


Figure 12.26 Double logarithmic plot showing the creep rupture time, t_f , as a function of the applied stress, σ , for poly(methyl methacrylate) at 24°C. Data obtained for (Δ) freshly quenched samples and (\circ) samples aged at 24°C for 5 years. (From Ref. 30.)

12.12 RELAXATION BEHAVIOR OF SEMICRYSTALLINE POLYMERS: GENERAL CONSIDERATIONS

The viscoelastic behavior of crystalline polymers is strongly affected by their morphology. Amorphous and crystalline phases separated by immobilized interfacial layers coexist in semicrystalline polymers. There are two temperatures at which the viscoelastic response of semicrystalline materials changes dramatically: the melting temperature, T_m , and the glass transition temperature, T_g . At T_g the relaxation modulus experiences a relatively sharp drop, depending on the degree of crystallinity. Above T_m , semicrystalline polymers are viscoelastic liquids for which the power law that relates the viscosity at shear zero rate for amorphous polymers to their molecular weight holds. Thus, above a critical molecular weight, M_c , the viscosity of melts scales with the 3.4 power of the molecular weight, while below M_c the viscosity is proportional to the molecular weight. In addition to the sub-glass absorption and glass-rubber absorption, crystalline polymers may, at temperatures close to the melting temperature, present an additional absorption called α relaxation. When semicrystalline polymers present this relaxation, the glass-rubber relaxation (α absorption for amorphous polymers) is called β relaxation and the sub-glass absorption (β absorption for amorphous polymers) is denoted γ relaxation (3,4,14,15). The α relaxation presumably is produced by motions in which the crystalline entities play an important role. It is believed that the perturbing effect of the crystals in response to the force field is confined to the immobilized interfacial phases, and therefore the remaining amorphous phase is not perturbed.

The crystalline phase affects the viscoelastic dynamic functions describing the glass-rubber relaxation. For example, the location of this absorption in the relaxation spectrum is displaced with respect to that of the amorphous polymer and greatly broadened. Consequently, the perturbing effects of crystal entities in dynamic experiments propagate throughout the amorphous fraction. The empirical Boyer-Beaman law (32)

$$\frac{1}{2} < \frac{T_g}{T_m} < \frac{2}{3} \quad (12.28)$$

is useful to predict the interval of temperature at which the glass-rubber relaxation appears (17). As for the sub-glass relaxation, it is believed to arise, at least in part, from local motions taking place in the amorphous phase, though some researchers have considered it to have an important component from the crystalline phase also.

By considering their crystallization behavior, crystalline polymers can be classified into three overlapping categories: low, medium, and high

crystallinity polymers. The principal characteristic of the first kind of polymers is that their crystallization rate is rather small, so their degree of crystallinity can vary from zero to 50% at most. These polymers can be obtained in completely amorphous form by quenching them from the melt. Actually, as the undercooling (difference between the melting temperature and the crystallization temperature) increases, the crystallization rate increases until a maximum is reached, after which it decreases, its value being nearly zero at relatively high undercoolings (see Chapter 2, sect 2.5.2). Examples of low crystallinity polymers are poly(ethylene terephthalate) and aromatic polycarbonates. The degree of crystallinity of medium crystallinity polymers lies in the range 30–60%. Unlike low crystallinity polymers, medium crystallinity polymers do not become amorphous when they are quenched from the melt. Examples of these polymers are polyamides and aliphatic polyesters. Finally, high crystallinity polymers exhibit degrees of crystallinity lying in the range of 60–80%. The degree of crystallinity of these polymers, quenched from the melt, is about 50%. Polyethylene, polypropylene, polyoxymethylene, and polyoxyethylene are examples of this kind of polymers.

12.12.1 Relaxation Behavior of Low Crystallinity Polymers

Illustrative curves showing the temperature dependence of the storage and loss relaxation moduli of samples of poly(ethylene terephthalate) with degree of crystallinity varying from zero to 40% are plotted in Figure 12.27. The relaxation corresponding to the glass–rubber transition of the amorphous polymer is reflected by a sharp drop of several decades in the storage relaxation modulus. As the crystallinity content of the sample increases, the fall in G' associated with the glass transition decreases; a plateau appears whose length increases as the degree of crystallinity increases (33). The isochrones representing the temperature dependence of G'' present an absorption associated with the glass–rubber transition. In these latter samples another sharp drop occurs in G' when the melting temperature is reached. The intensity of the glass–rubber relaxation decreases with increasing crystallinity, and the location of the relaxation is shifted in most cases to higher temperatures as the crystallinity increases. Moreover, the width of the glass–rubber relaxation becomes broader as the crystallinity of the samples increases. It should be pointed out that a relaxation at high temperatures is not observed in the relaxation spectrum of these polymers and as a result the notation α and β is used for the glass–rubber and sub-glass relaxations, respectively, of these polymers (33).

The isochrones showing the temperature dependence of the components of the complex relaxation modulus are rather insensitive to the crystallinity

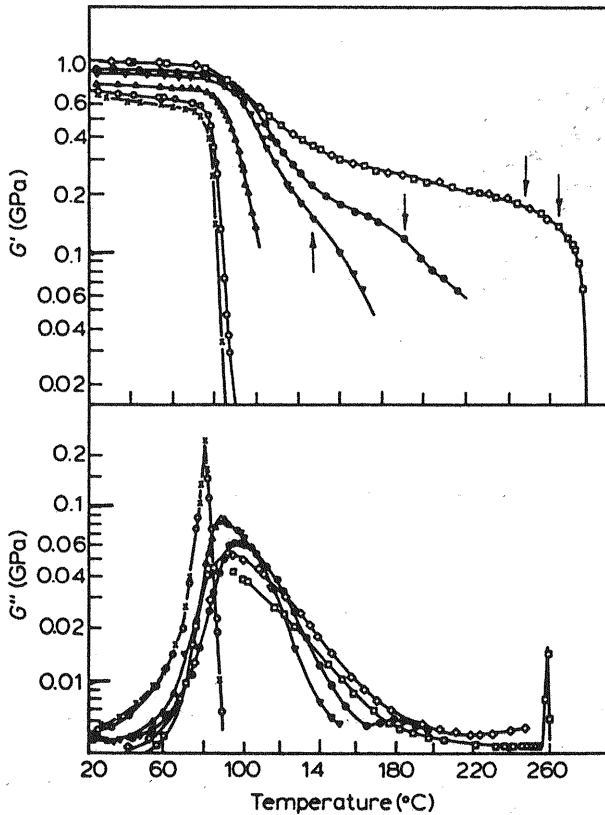


Figure 12.27 Variation of the complex relaxation modulus of poly(ethylene terephthalate) with temperature, in the vicinity of the glass-rubber relaxation, for samples of various crystallinities obtained in isothermal crystallizations: (\square) 46%, (\diamond) 40%, (\bullet), (∇) 26%, (\square) 2–3%, and (\circ) 0%. (From Ref. 33.)

of the samples. This behavior can be observed in Figure 12.28, where the variation of the complex relaxation modulus with temperature, in the glassy region, is shown. The curves corresponding to the storage relaxation modulus present an inflection in the vicinity of -80°C , the temperature at which the loss presents a maximum. The intensity of this absorption, called β relaxation, shows only a slight dependence on the crystallinity of the samples.

Like other retardation processes, the strength of the mechanical glass-rubber relaxation can, in principle, be determined by means of the empirical Havriliak–Negami equation (34)

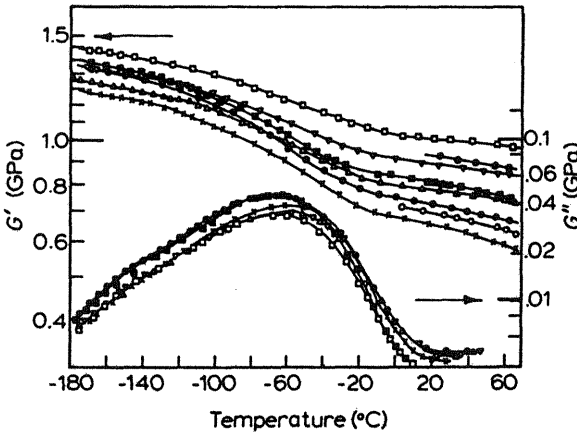


Figure 12.28 Temperature dependence of the complex relaxation modulus of poly(ethylene terephthalate), in the glassy region, for the same samples of Figure 12.27.

$$J^* = J_\infty + \frac{J_r - J_\infty}{[1 + (i\omega\tau_0)^{\bar{\alpha}}]^{-\bar{\beta}}} \quad (12.29)$$

where J_r and J_∞ represent the relaxed and unrelaxed compliance functions corresponding to zero and infinite frequencies, respectively, τ_0 is the mean relaxation time of the process, and $\bar{\alpha}$ and $\bar{\beta}$ are empirical parameters lying in the range 0–1. Taking the mirror image of the J'' versus J' plot for Eq. (12.29), the complex relaxation modulus can be written as

$$G^* = G_r + (G_\infty - G_r)[1 + (i\omega\tau_0)^{-\bar{\alpha}}]^{-\bar{\beta}} \quad (12.30)$$

where G_r and G_∞ are the relaxed and unrelaxed storage relaxation moduli at 0 and ∞ frequencies, respectively. In general, the relaxation strength of the glass–rubber relaxation, expressed as $G_\infty - G_r$, decreases as the degree of crystallinity increases, whereas the relaxation strength of the sub-glass relaxation is quite insensitive to the crystallinity of the material.

Sub-glass relaxations for crystalline and amorphous polymers in the frequency domain are described by the empirical Fuoss–Kirkwood equation (35)

$$G''(\omega) = G''(\omega_{\max}) \operatorname{sech} \left[m \ln \frac{\omega}{\omega_{\max}} \right] \quad (12.31)$$

where m , an empirical parameter related to the width of the relaxation, lies in the interval $0 < m \leq 1$. The larger m is, the narrower is the relaxation, so that $m = 1$ for a Debye peak. With the assumption that the relaxation obeys Arrhenius behavior, that is, $\omega = A \exp(E_a/RT)$, Eq. (12.31) becomes

$$G''(T) = G''(T_{\max}) \operatorname{sech} \left[m \frac{E_a}{R} \left(\frac{1}{T} - \frac{1}{T_{\max}} \right) \right] \quad (12.32)$$

Sub-glass relaxations fit this equation. Plotting $\cosh^{-1}[G''(T_{\max})/G(T)]$ versus T^{-1} gives straight lines from whose slopes ($= mE_a/R$) the evolution of the parameter m with the frequency of the isochrones can be evaluated. The Fuoss-Kirkwood equation also allows determination of the relaxation strength of sub-glass absorptions.

12.12.2 Relaxation Behavior of Medium Crystallinity Polymers

The isochrones showing the temperature dependence of the storage relaxation modulus exhibit a small drop in the glassy region followed by a strong decrease in the value of this parameter at higher temperatures. The curves corresponding to the loss relaxation modulus exhibit relaxation peaks in the regions in which the storage relaxation modulus drops. Though strong relaxation is believed to be associated with the glass-rubber relaxation, it is not possible to know at first sight whether this assignment is correct, because these polymers cannot be obtained in the amorphous state by quenching. This difficulty can be circumvented by investigating whether the same relaxation process observed in the solid can be detected in the melt. However, the relaxation appearing at moderate frequencies in the solid shifts to frequencies so high in the melt that it is unattainable by mechanical experiments. In this case it is necessary to combine mechanical and dielectric experiments. For example, the strong glass-rubber relaxation process of nylon 6,10 moves to higher frequencies with increasing temperature, and it is possible to follow it in the melt by performing dielectric measurements at frequencies close to 10 GHz (36).

Aliphatic polyesters may present a crystalline α process, and as a consequence the notations β and γ are adopted for the glass-rubber and sub-glass relaxations, respectively. Although fully amorphous polymers cannot be achieved by quenching, it is possible to obtain polyesters with different degrees of crystallinity by copolymerization with a noncrystallizable diol. For example, the polyester of 1,6-hexanediol condensed with adipic acid is about 60% crystalline, while the polyester of this diacid with 2,5-hexanediol is completely amorphous. By varying the 1,6-hexanediol/2,5-hexanediol

ratio, copolyesters with different degrees of crystallinity can be obtained. The complex relaxation modulus of copolyesters with different degrees of crystallinity is shown (37) in Figure 12.29. The isochrones present a β absorption whose intensity decreases with increasing degree of crystallinity. The crystalline entities severely restrict the micro-Brownian motions of the chains in

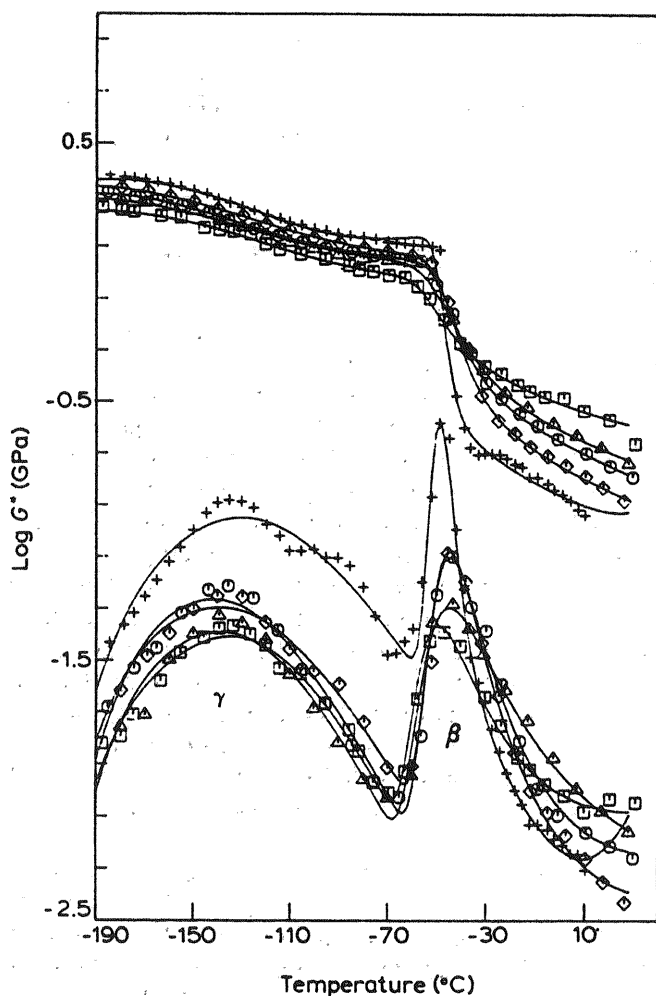


Figure 12.29 Curves showing the variation of the complex relaxation modulus with temperature, at 1 Hz, for aliphatic polyesters of different degrees of crystallinity: (□) 60%, (△) 44%, (○) 36%, (◇) 30%, and (+) 20%. (From Ref. 37.)

the amorphous phase, thus producing a dramatic decrease in the intensity of the β relaxations.

Aliphatic polyesters also present a prominent γ absorption caused by motions taking place in the amorphous phase. Neither the location nor the intensity of this process is sensitive to the degree of crystallinity. The variations observed in the intensity of the γ relaxations in Figure 12.29 are due to changes in the chemical composition rather than to changes in the crystallinity.

12.12.3 Relaxation in Highly Crystalline Polymers

The most distinguishing feature of highly crystalline polymers is that they present an α relaxation in whose development crystalline entities play an important role. The shape of the curves of $\tan \delta$ versus temperature for semicrystalline polymers depends on both the degree of crystallinity and the chemical flaws (imperfections) produced during the synthesis of the molecular chains. These effects are observed in the relaxation spectrum of polyethylene. The synthesis of polyethylene via radical polymerization at high pressure gives rise to molecular chains with branches of 2 to 4 methylenic groups every 1000 carbon atoms of the backbone. Branching hinders molecular packing in the crystalline entities, and the degree of crystallinity of the polymer decreases. By using organic oxides, at low pressure polyethylene can be obtained in which branching is nearly nonexistent. Finally, the so-called linear low density polyethylene (LLDPE) is obtained by copolymerization of ethylene and a small fraction of 1-butene, 1-hexene, or 1-octene as a comonomer. Branched polyethylene can develop a crystallinity of the order of 50%; it is then called low density polyethylene (LDPE). The degree of crystallinity of polyethylene in which branching is negligible can be as high as 80%, that is why it is called high density polyethylene (HDPE). The degree of crystallinity of LLDPE may be lower than 30%.

Curves showing the variation in the storage and loss tensile relaxation moduli with temperature for HDPE, LDPE, and LLDPE are shown in Figures 12.30 and 12.31, respectively (38). A common characteristic of the curves is that they all present the γ and α relaxations. However, only branched polyethylene exhibits a well-developed β absorption, suggesting that the development of this process requires the presence of branches in the chains. On the other hand, the fact that the intensity of the β relaxation increases with the degree of branching indicates that this process is mainly caused by motions taking place in the amorphous phase of the polymer. Consequently, this relaxation has been associated with the glass transition of polyethylene. Since the β relaxation is centered in the interval -10°C to $+27^{\circ}\text{C}$, depending on the crystallinity of the polymer, the glass transition

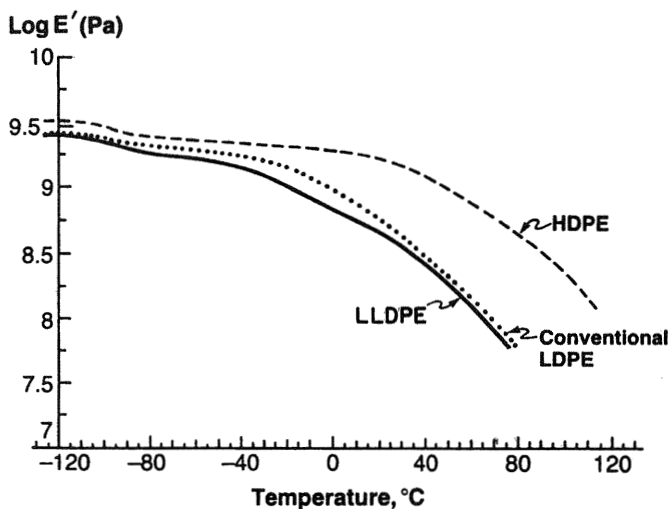


Figure 12.30 Storage tensile relaxation modulus plotted versus temperature for several polyethylenes.

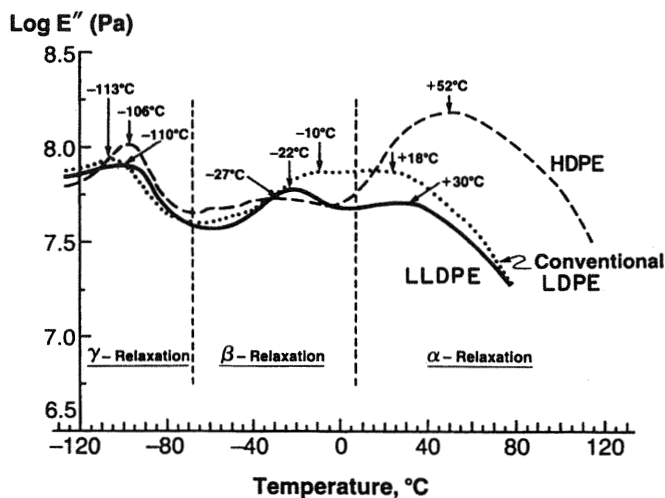


Figure 12.31 Loss tensile relaxation modulus plotted versus temperature for various polyethylenes (From Ref. 38).

temperature would be located in the vicinity of these temperatures. It should be noted that the relatively low relaxation strength of the β process of HDPE is not due to a lesser degree of softening through the process but rather to a stronger γ process that results in a lower unrelaxed modulus for the β relaxation.

The γ relaxation of polyethylene, expressed in terms of $\tan \delta$, is centered in the vicinity of -120°C at 1 Hz. This relaxation is believed to be caused by molecular motions occurring in the amorphous phase as indicated by the fact that the relaxation is very weak in highly crystalline polyethylene crystallized from dilute solutions (39,40). The relatively high intensity and universality of the γ relaxation in polyethylenes, independent of whether they do or do not have branches in their structure, seems to suggest that the γ relaxation may be associated with the glass transition. According to this interpretation, the glass transition temperature of polyethylene would be located in the vicinity of -120°C .

It is convenient to point out that the elucidation of the glass transition temperature of polyethylene is still an unresolved issue. In fact, values covering the range of -120°C to $+30^\circ\text{C}$ have been reported for T_g in the literature. In favor of associating the γ relaxation with T_g is the fact that it is displayed by both high density and low density polyethylenes. Opposing this interpretation is the fact that the γ relaxation exhibits an activation energy much lower than that reported for the glass-rubber relaxation of most polymers.

As indicated above, α relaxation is associated with molecular motions in which crystalline entities take part. However, the development of this process apparently requires the presence of an amorphous phase. Actually, as shown in Figure 12.32, the relaxation curves of polymethylenic waxes in which the crystallites are formed by totally extended chains (degree of crystallinity 100%) do not present α relaxation (41,42). Since neither totally crystalline nor totally amorphous polymers display α relaxation, one must conclude that this absorption is caused by molecular motions occurring in the crystalline-amorphous interphase.

Other highly crystallinity polymers such as polyisopropylene and polyoxymethylene also exhibit in order of increasing temperature the γ , β , and α relaxation processes. It is worth noting that while polyisopropylene exhibits a well-developed β absorption, polyoxymethylene, like HDPE, exhibits two prominent α and γ relaxations and a small β relaxation whose intensity seems to increase as the degree of crystallinity decreases (43). This behavior is illustrated in Figure 12.33, where both the shear relaxation modulus and the logarithmic decrement of polyoxymethylene are plotted against temperature.

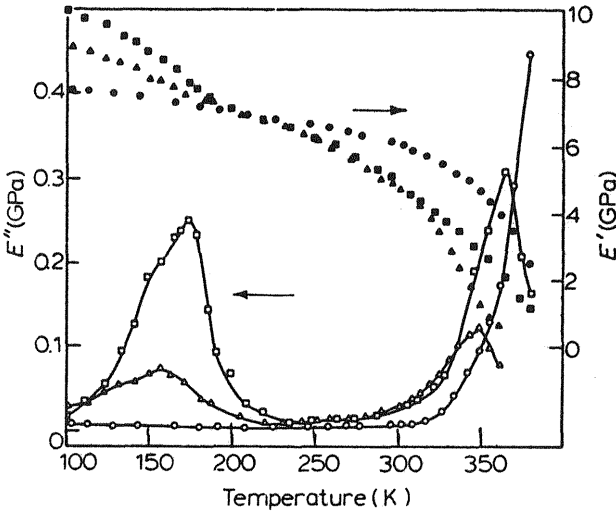


Figure 12.32 Comparison of storage and loss tensile relaxation moduli of a paraffin [$C_{94}H_{190}$, (●) and (○) respectively] and two low molecular weight HDPE fractions [(△) and (▲) \approx 1860 MW; (□) and (■) 3800 MW]. (From Ref. 42.)

12.13 GENERAL FEATURES OF CRYSTALLINE POLYMERS

Most crystalline polymers with methylenic groups in their structure and with a degree of crystallinity below 50% present a sub-glass relaxation whose intensity and location scarcely differ from those observed for the amorphous polymer in the glassy state. The temperature dependence of this relaxation follows Arrhenius behavior, and its activation energy is of the same order as that found for secondary processes in amorphous polymers.

Crystallinity strongly affects the relaxation associated with the glass transition. The intensity and breadth of the relaxation are, respectively, smaller and higher than those reported for the same systems in the amorphous state. Therefore, the stretch exponent in the KWW equation is lower than that reported for the amorphous state. The storage relaxation modulus of glassy semicrystalline polymers reaches a value similar to that exhibited by amorphous polymers in this state. As the temperature increases, the modulus slightly decreases, a small inflection appearing in the vicinity of the temperature at which the maximum of G'' is located (see Fig. 12.28). A sharp decrease in the value of the storage relaxation modulus occurs in the vicinity of the glass transition, the diminution of the modulus being lower the higher the degree of crystallinity of the polymer

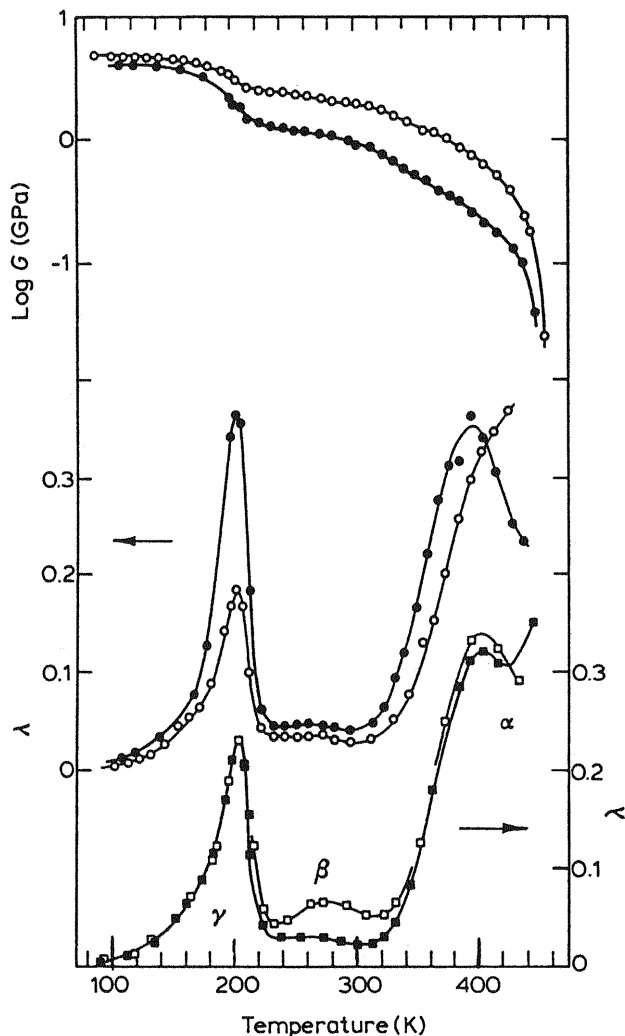


Figure 12.33 Storage relaxation modulus and logarithmic decrement for polyoxymethylene specimens of two crystallinities: (○) 76% and (●) 54%. Squares refer to the values of G' and Λ of a specimen measured immediately after storage at room temperature (■). (From Ref. 43.)

(see Fig. 12.27). Another abrupt decrease takes place as a result of the melting of the crystalline entities.

Annealing promotes crystallite thickening at the expense of the crystalline–amorphous interphase and the amorphous phase. This process decreases the intensity of the glass–rubber relaxation and enhances that of the α relaxation if the crystalline polymer develops this absorption.

12.14 TIME-TEMPERATURE CORRESPONDENCE PRINCIPLE

Semicrystalline polymers are heterodisperse systems in which the free volume of the coexistent phases is different. As a result, the time–temperature correspondence principle does not hold unless methods are developed to separate the contributions of the different phases to the viscoelastic functions (44). This behavior becomes evident in the inspection of the results of Figure 12.34, where the loss compliance function in the frequency domain for polyethylene is shown. One can observe that if the isotherms superpose in the high frequency region, the superposition fails in the low frequency region and vice versa. The master curve obtained by empirical superposition of the results in the high frequency region, shown in Figure 12.35, suggests the presence of a relaxation in the vicinity of 30°C. It is advisable to stress, however, that semicrystalline polymers are not thermorheologically simple systems, and consequently conclusions cannot be drawn about the nature of the relaxations observed in master curves obtained from partial superpositions.

12.15 MODELING THE VISCOELASTIC BEHAVIOR OF CRYSTALLINE POLYMERS

The viscoelastic properties of the crystalline zones are significantly different from those of the amorphous phase, and consequently semicrystalline polymers may be considered to be made up of two phases each with its own viscoelastic properties. The best known model to study the viscoelastic behavior of polymers was developed for copolymers as ABS (acrylonitrile-butadiene-styrene triblock copolymer). In this system, spheres of rubber are immersed in a glassy matrix. Two cases can be considered. If the stress is uniform in a polyphase, the contribution of the phases to the complex tensile compliance should be additive. However, if the strain is uniform, then the contribution of the polyphases to the complex modulus is additive. The

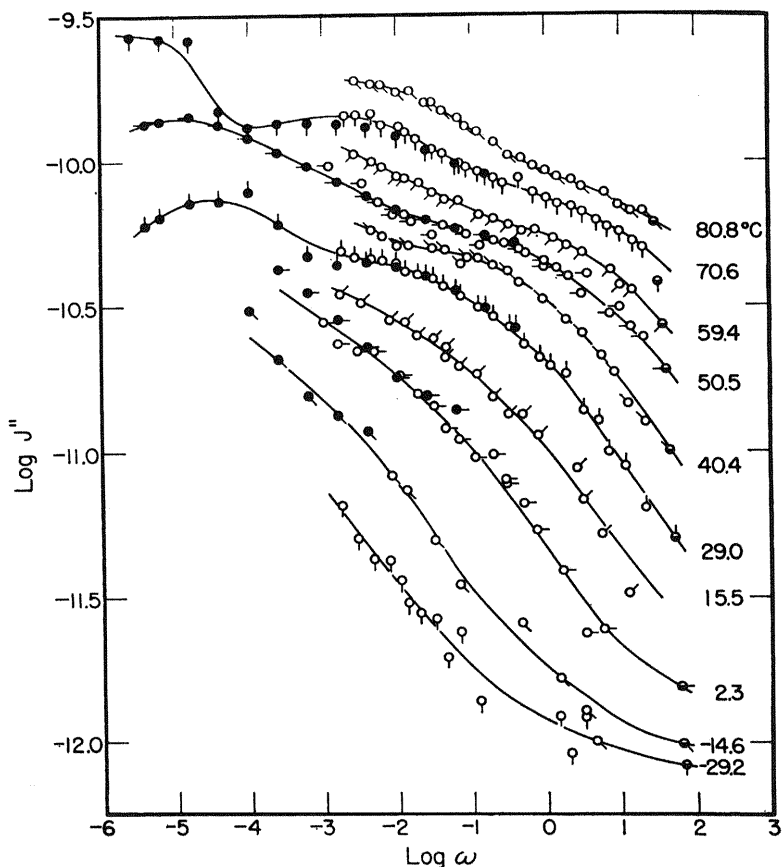


Figure 12.34 Loss compliance isotherms in the frequency domain of linear polyethylene crystallized from the melt. (From Ref. 44.)

application of this model to semicrystalline polymers gives the following equation for the tensile relaxation modulus (45):

$$E = \frac{\phi}{\lambda E_A + (1 - \lambda) E_c} + \frac{1 - \phi}{E_c} \quad (12.33)$$

where ϕ is the effective fraction of amorphous mass in the direction parallel to the force, λ is the value of this quantity in the transverse direction, and E_A and E_c are, respectively, the tensile relaxation moduli for the amorphous and crystalline phases. The parameters ϕ and λ can be calculated by means of the relationships

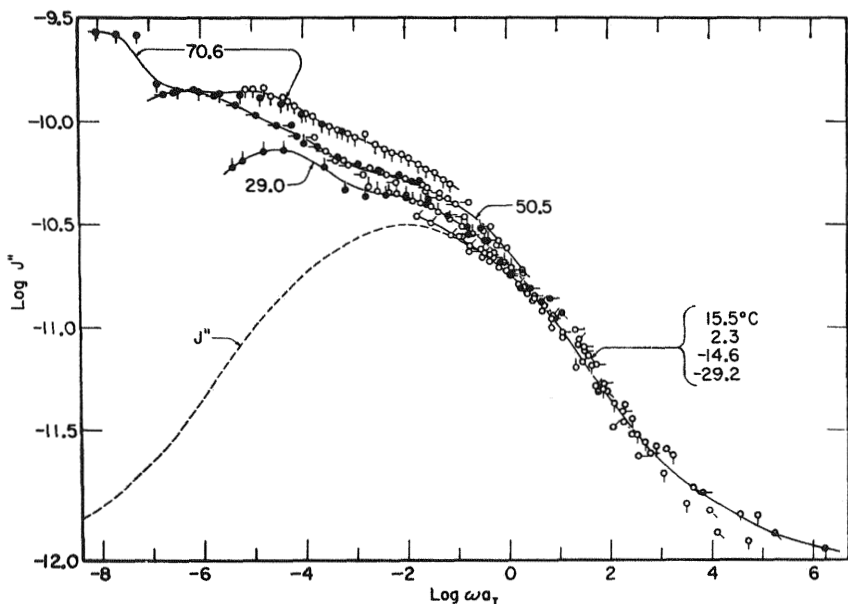


Figure 12.35 Data of Figure 12.33 reduced to 29°C with shift factors applicable to the results of higher frequencies.

$$\lambda = \frac{2 + 3(1 - x_c)}{5} \quad \text{and} \quad \phi = \frac{5(1 - x_c)}{2 + 3(1 - x_c)} \quad (12.34)$$

where x_c is the degree of crystallinity. These last expressions, formulated by Kerner (46), have been successfully applied by Takayanagi and coworkers to many crystalline systems. It should be noted that since $E_A \ll E_c$ the evaluation of E_A from Eq. (12.33) requires only knowledge of the degree of crystallinity and the tensile relaxation modulus of the crystalline phase.

PROBLEM SETS

Problem 12.1

The theory of two potential wells of nearly equal depth has been used to explain secondary relaxations in amorphous polymers. Recent results by L. C. E. Struik led to the result

$$G_{\infty} - G_r = \frac{G_r}{G_{\infty}} \left(\frac{c}{T} \right)$$

where G_r and G_{∞} are, respectively, the relaxed and unrelaxed moduli, c is a constant, and T is the absolute temperature. Assuming that the temperature decrement of the modulus in the glassy zone caused by the thermal expansion coefficient is nearly 10^{-3} K^{-1} , estimate the temperature dependence of the relaxation strength of secondary relaxations.

Solution 12.1

The proposed equation can be written as

$$\frac{1}{\Delta G} = \frac{T}{c} + \frac{1}{G_{\infty}} \quad (\text{P12.1.1})$$

where $\Delta G = G_g - G_e$ is the relaxation strength.

After derivation with respect to the temperature and subsequent rearrangements, we obtain

$$-\frac{d \ln \Delta G}{d \ln T} = \frac{G_r}{G_{\infty}} - \left(1 - \frac{G_r}{G_{\infty}} \right) \frac{d \ln G_{\infty}}{d \ln T} \quad (\text{P12.1.2})$$

Since $G_r/G_{\infty} \leq 1$ and $d \ln G_{\infty}/d \ln T < 0$, then

$$-\frac{d \ln \Delta G}{d \ln T} < 1 \quad (\text{P12.1.3})$$

Note that for weak relaxation, where G_r/G_{∞} is close to unity,

$$-\frac{d \ln \Delta G}{d \ln T} \cong 1 \quad (\text{P12.1.4})$$

These results indicate that the relaxation strength decreases with increasing temperature.

Problem 12.2

Find the temperature at which the storage shear relaxation modulus of PMMA at 10 Hz will be the same as at 1 Hz and 18°C. Activation energy for the β relaxation in this region is 75 kJ/mol.

Solution 12.2

By assuming that the time–temperature superposition principle holds in this zone, we obtain

$$G'(\omega_1, T_1) = G'(\omega_2, T_2) \quad (\text{P12.2.1})$$

According to the Arrhenius equation, the relationship between the two frequencies is

$$\ln \frac{\omega_2}{\omega_1} = \ln a_T = \frac{E_a}{R} \left(\frac{1}{T_1} - \frac{1}{T_2} \right) = \frac{75 \times 10^3}{8.314} \left(\frac{1}{273 + 18} - \frac{1}{273 + x} \right)$$

from which $x = 41.4^\circ\text{C}$.

Problem 12.3

The shear modulus of a PMMA sample at 18°C can be written as

$$G(t) = 2.6 \times 10^9 [0.262 + 0.3843 \exp(-1.309t) + 0.3535 \exp(-105.97t)] \text{ Pa}$$

Find the modulus at $t = 1$ s, and estimate the modulus at 30°C , assuming that the activation energy is 75 kJ/mol.

Solution 12.3

From the given equation, we immediately find

$$G(1) = 0.951 \times 10^9 \text{ Pa}$$

To estimate the modulus at any temperature we can assume the validity of the time–temperature superposition principle in this region, that is,

$$G(t, T) = G(a_T t, T') \quad (\text{P12.3.1})$$

The shift factor can be written approximately as

$$\ln a_T = \frac{75 \times 10^3}{8.314} \left(\frac{1}{273 + 18} - \frac{1}{273 + 30} \right); \text{ hence } a_T = 3.413$$

Then

$$G(t)_{30^\circ\text{C}} = 2.6 \times 10^9 [0.262 + 0.3843 \exp(-4.4676t) + 0.3535 \exp(-361.676t)] \text{ Pa}$$

and

$$G(1)_{30^\circ\text{C}} = 0.693 \times 10^9 \text{ Pa}$$

Problem 12.4

Show that for an exponential decay function the complex compliance follows the Debye equation.

Solution 12.4

From Eq. (12.3),

$$\frac{J^* - J_\infty}{J_0 - J_\infty} = \mathcal{L}(-\dot{\phi}(t)) \quad (\text{P12.4.1})$$

If

$$\phi(t) = \exp\left(-\frac{t}{\tau}\right), \text{ then } \dot{\phi}(t) = -\frac{1}{\tau} \exp\left(-\frac{t}{\tau}\right) \quad (\text{P12.4.2})$$

$$\mathcal{L}(-\dot{\phi}(t)) = \int_0^\infty e^{s t} \frac{1}{\tau} e^{-t/\tau} dt = \frac{1}{\tau} \left(\frac{1}{s + 1/\tau} \right) = \frac{1}{s\tau + 1} \quad (\text{P12.4.3})$$

If $s = i\omega$

$$\frac{J^* - J_\infty}{J_0 - J_\infty} = \frac{1}{1 + i\omega\tau} \quad (\text{P12.4.4})$$

and splitting this into its real and imaginary parts, the well-known Debye equations are obtained:

$$J' = J_\infty + \frac{J_0 - J_\infty}{1 + \omega^2\tau^2} \quad (\text{P12.4.5a})$$

$$J'' = \frac{J_0 - J_\infty}{1 + \omega^2\tau^2} \omega\tau \quad (\text{P12.4.5b})$$

Problem 12.5

A convenient way to analyze physical aging processes (structural recovery) is to use a relaxation function $\phi(t)$ defined as

$$\phi(t) = \frac{M(t) - M_\infty}{M_0 - M_\infty}$$

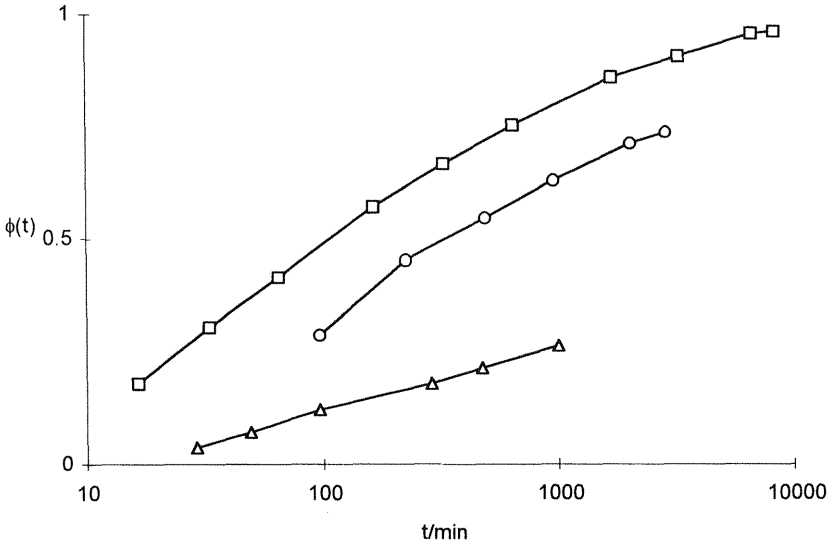
where $M(t)$ is the magnitude under analysis at a time t after starting the aging process, M_0 is the unrelaxed (time zero) magnitude, and M_∞ is the

fully relaxed magnitude in analogy with the viscoelastic properties. The curves of Figure P12.5.1 present the evolution with time (in minutes) of the recovery function for the storage modulus (\square), specific volume (\circ), and enthalpy (\triangle) of a sample of PMMA after a sudden cooling process from $T_g + 20^\circ\text{C}$ ($T_g = 104^\circ\text{C}$) to 103°C .

Compare the kinetics of these three relaxation processes.

Solution 12.5

According to the time scale of the experiment, and for values between 100 and 1000 min, the following results are obtained:



1. The kinetics of relaxation in volume is about 14 times as fast as that of the enthalpy.
2. The kinetics of the storage modulus is 43 times as fast as that of the enthalpy.
3. The kinetics of the storage modulus is about 3 times as fast as that of the volume.

Problem 12.6

It is well known that the molecular origin of the γ relaxation in polyethylene (PE) (-120°C , 1 Hz) is the motion of linear sequences of $-\text{CH}_2-$ group in the amorphous phase, whereas the α relaxation (50°C , 1 Hz) can be

attributed to the crystalline phase. From a dynamic mechanical test at constant frequency, the following data were obtained for two samples of linear PE:

X (% crystallinity)	G''_{\max} (Pa), γ	G''_{\max} (Pa), α
84	8.7×10^7	12.7×10^7
55	11.7×10^7	3.4×10^7

Estimate the maximum shear loss modulus for a sample with 70% crystallinity.

Solution 12.6

By assuming a linear variation of the crystallinity with the maximum of the shear loss modulus for the γ and α mechanical relaxations, a simple linear interpolation leads to

$$G''_{\max}(X = 70\%) = 10.05 \times 10^7 \text{ Pa, for the } \gamma \text{ relaxation}$$

$$G''_{\max}(X = 70\%) = 8.2 \times 10^7 \text{ Pa, for the } \alpha \text{ relaxation}$$

Problem 12.7

Show that when the loss modulus attains the maximum in a double logarithmic plot, the slopes of the storage modulus and $\tan \delta$ are the same but of opposite signs. Estimate the value of this slope in terms of $\tan \delta$.

Solution 12.7

Starting from the equation

$$\tan \delta = \frac{E''}{E'} \quad (\text{P12.7.1})$$

taking logarithms, and deriving with respect to $\log \omega$ we have

$$\frac{d \log \tan \delta}{d \log \omega} = \frac{d \log E''}{d \log \omega} - \frac{d \log E'}{d \log \omega} \quad (\text{P12.7.2})$$

At the maximum of the loss modulus,

$$\left. \frac{d \log \tan \delta}{d \log \omega} \right|_{E''_{\max}} = - \left. \frac{d \log E'}{d \log \omega} \right|_{E''_{\max}} \quad (\text{P12.7.3})$$

as required by the problem.

Moreover, according to Problem 6.5 of Chapter 6,

$$\frac{dE'}{d \ln \omega} = \frac{2}{\pi} E'' \quad (\text{P12.7.4})$$

and after substitution of Eq. (P12.7.4) into Eq. (P12.7.3), we easily obtain

$$\left. \frac{d \tan \delta}{d \log \omega} \right|_{E''_{\max}} = - \frac{4.606}{\pi} \left(\frac{E''}{E'} \right) \cong -1.47 \tan \delta \quad (\text{P12.7.5})$$

Problem 12.8

A function extensively used to represent empirical dynamic data in the glass transition zone is the Havriliak–Negami (HN) function given by

$$G^* = G_r + \frac{\Delta G}{[1 + (j\omega\tau_0)^{-\alpha}]^\beta}$$

where G_r is the relaxed modulus, ΔG is the strength of the relaxation, and τ_0 , α , and β are adjustable parameters. Calculate the frequency and intensity of the loss maximum, knowing that α and $\alpha\beta \leq 1$.

Solution 12.8

Splitting the HN equation into its real and imaginary parts, we obtain

$$G' = G_r + \Delta G r^{\beta/2} \cos \beta\theta \quad (\text{P12.8.1a})$$

$$\text{mod } G'' = \Delta G r^{\beta/2} \sin \beta\theta \quad (\text{P12.8.1b})$$

where

$$r = \left[1 + (\omega\tau_0)^{-\alpha} \cos \frac{\pi}{2} \alpha \right]^2 + \left[(\omega\tau_0)^{-\alpha} \sin \frac{\pi}{2} \alpha \right]^2 \quad (\text{P12.8.2})$$

and

$$\theta = \arctan \frac{(\omega\tau_0)^{-\alpha} \sin(\pi/2\alpha)}{1 + (\omega\tau_0)^{-\alpha} \cos(\pi/2\alpha)} \quad (\text{P12.8.3})$$

From the condition of maximum,

$$\left| \frac{dG''}{d(\omega\tau_0)} \right|_{\omega=\omega_{\max}} = 0 \quad (\text{P12.8.4})$$

and after some calculations we obtain

$$(\omega\tau_0)^{-\alpha} = \frac{\sin(\frac{\pi}{2}\alpha - \beta\theta)}{\sin \beta\theta} \quad (\text{P12.8.5})$$

Equation (P12.8.3) leads to

$$(\omega\tau_0)^{-\alpha} = \frac{\sin \theta}{\sin(\frac{\pi}{2}\alpha - \theta)} \quad (\text{P12.8.6})$$

From Eqs. (P12.8.5) and (P12.8.6) and taking into account the trigonometric relation

$$\tan((1 + \beta)\theta) = \frac{\tan \beta\theta + \tan \theta}{1 - \tan \beta\theta \tan \theta} \quad (\text{P12.8.7})$$

we find

$$\frac{\pi}{2}\alpha = (1 + \beta)\theta \quad (\text{P12.8.8})$$

Hence

$$(\omega\tau_0)^{-\alpha} = \frac{\sin \frac{\pi}{2} \left(\frac{\alpha}{1+\beta} \right)}{\sin \frac{\pi}{2} \left(\frac{\alpha\beta}{1+\beta} \right)} \quad (\text{P12.8.9})$$

Therefore, the value of the loss maximum can be obtained by substituting Eq. (P12.8.9) into Eq. (P12.8.1b) and taking into account Eqs. (P12.8.2) and (P12.8.3). The final result is given by the expression

$$G''_{\max} = \Delta G \frac{\left(\sin \frac{\pi}{2} \left(\frac{\alpha\beta}{1+\beta} \right) \right)^{1+\beta}}{\left(\sin \frac{\pi}{2} \alpha \right)^\beta} \quad (\text{P12.8.10})$$

An important conclusion of these results is that for $\beta > 1$ the maximum loss appears at higher frequency than that corresponding to the characteristic relaxation time.

Problem 12.9

The semiempirical function

$$\frac{G''}{\Delta G} = \frac{\omega^m}{(\omega_p^{2s} + \omega^{2s})^{(1-n+m)/2s}}$$

was proposed by Hill (Nature 275: 96, 1978) to represent both dynamic mechanical and dielectric relaxation losses. In this function, ΔG is the strength of the relaxation and ω_p , s , n , and m are adjustable parameters. Describe a simple way to estimate these parameters

Solution 12.9

After derivation of the equation with respect to the frequency ω , the condition of maximum gives

$$\omega_{\max} = \omega_p \left(\frac{m}{1-n} \right)^{1/s} \quad (\text{P12.9.1})$$

from which

$$\frac{G''_{\max}}{\Delta G} = \frac{\omega_{\max}^{n-1}}{[(1-n+m/m)]^{(1-n+m/2s)}} \quad (\text{P12.9.2})$$

On the other hand, the asymptotic behavior is given by

$$\lim_{\omega \rightarrow 0} \frac{G''}{\Delta G} \approx \omega^m; \quad \lim_{\omega \rightarrow \infty} \frac{G''}{\Delta G} \approx \omega^{n-1} \quad (\text{P12.9.3})$$

Assuming that the strength of the relaxation is known (by means of a Cole-Cole plot or other procedure), the preceding four equations allow us to estimate the parameters appearing in Hill's equation. Notice that ω_p does not correspond to the maximum frequency, that is, the frequency at the top of the peak (except in the case where $m = 1 - n$), although it is of the same order of magnitude as that frequency.

REFERENCES

1. CA Angell. *Science* 267: 1924, 1995.
2. FH Stillinger. *Science* 267: 1935, 1995.
3. JD Ferry. *Viscoelastic Properties of Polymers*. New York: John Wiley & Sons, Inc. 1980.
4. NG McCrum, BE Read, G Williams. *Anelastic and Dielectric Effects in Polymeric Solids*. New York: John Wiley & Sons, Inc. 1967 and Dover, 1991.
5. G Williams. Dielectric relaxation spectroscopy of amorphous polymer systems: The modern approaches. In: E Riande, ed. *Keynote Lectures in Selected Topics of Polymer Science*. Madrid: CSIC, 1995 page 1.
6. F Kremer, A Hofman, EW Fischer. *Am Chem Soc Polym Preprn* 33: 96, 1992.
7. R Kohlrausch. *Ann Phys Chem* 91: 179, 1854.
8. G Williams, DC Watts. *Trans Faraday Soc* 66: 80, 1970.
9. GP Johari. *Ann NY Acad Sci* 279: 117, 1976.
10. J Kopplemann. *Rheol Acta* 1: 20, 1958.
11. J Heijboer. *Ann NY Acad Sci* 279: 104, 1976.
12. J Heijboer. *Doctoral Thesis, University of Leiden, The Netherlands*, 1972.
13. R Diaz-Calleja, E Riande, J San Román. *Macromolecules* 25: 2875, 1992.
14. RH Boyd. *Polymer* 26: 323, 1984.
15. RH Boyd. *Polymer* 26: 1123, 1984.
16. H Helfand. *Science* 226: 647, 1984.
17. S Matsuoka. *Relaxation Phenomena in Polymers*. Munich: Carl Hanser Verlag, 1992.
18. AJ Kovacs. *Fortschr Hochpolym-Forsch* 3: 394, 1964.
19. AQ Tool. *J Res Natl Bur Stand* 37: 73, 1946.
20. DJ Plazek, RA Andrekanik. The physical aging of amorphous polymers. In: E Riande, ed. *Keynote Lectures in Selected Topics of Polymer Science*. Madrid: CSIC, 1995 page 117.
21. LCE Struik. *Physical Aging in Amorphous Polymers and Other Materials*. Amsterdam: Elsevier, 1978.
22. AJ Kovacs, JJ Aklonis, JM Hutchinson, AR Ramos. *J Polym Sci Polym Phys Ed.* 17: 1097, 1979.
23. OS Narayanaswamy. *J Am Ceram Soc* 54: 491, 1971.
24. CT Moynihan, PB Macedo, CJ Montrose, PK Gupta, MA DeBolt, JF Dill, BE Dom, PW Drake, AJ Easteal, PB Elterman, RP Moeller, H Sasabe, JA Wilder. *Ann NY Acad Sci* 279: 15, 1976.
25. A Lee, GB McKenna. *Polymer* 31: 423, 1990.
26. LC Struik. *Ann NY Acad Sci* 279: 78, 1976.
27. GW Scherer. *Relaxation in Glass and Composites*. New York: John Wiley & Sons, Inc. 1986.
28. IM Hodge. *Science* 267: 1945, 1995.
29. GB McKenna. On the physics required for prediction of long term performance of polymers and their composites. In: E Riande, ed. *Keynote Lectures in Selected Topics of Polymer Science*. Madrid: CSIC, 1995 page 139.

30. GM Crissman, GB McKenna. *J Polym Sci Polym Phys Ed* 25: 1667, 1987.
31. A Lee, GB McKenna. *Polymer* 29: 1812, 1988.
32. RF Boyer. *Rubber Chem Technol* 36: 1303, 1963.
33. KH Illers, H Breuer. *J Colloid Sci* 18: 1 1963.
34. S Havriliak Jr, S Negami. *Polymer* 8: 161, 1967.
35. R Fuoss, JG Kirkwood. *J Am Chem Soc* 63: 385, 1941.
36. RH Boyd, CH Porter. *J Polym Sci A-2* 10: 647, 1972.
37. RH Boyd, PA Aylwin. *Polymer* 25: 340, 1984.
38. YP Khanna, EA Turi, TJ Taylor, VV Vickroy, RF Abbot. *Macromolecules* 18: 1302, 1985.
39. CF Stehling, L Mandelkern. *Macromolecules* 3: 242, 1979.
40. RH Boyd. *Polym Eng Sci* 14: 1010, 1979.
41. JM Crissman, E Passaglia. *J Appl Phys* 42: 4636, 1971.
42. JM Crissman. *J Polym Sci Polym Phys Ed* 13: 1407, 1975.
43. NG McCrum. *J Polym Sci* 54: 561, 1961.
44. H Nakayasu, H Markovitz, DJ Plazek. *Trans Soc Rheol* 5: 261, 1961.
45. M Takayanagi. *Mem Fac Eng Kyushu Univ* 13: 41, 1963.
46. DH Kerner. *Proc Phys Soc B* 69: 808, 1956.
47. K Schmieder, K Wolf. *Kolloid-Z* 134: 149, 1953.

13

Flow Behavior of Polymer Melts and Solutions

13.1	Introduction	510
13.2	Constitutive Equations	510
13.3	Second-Order Fluids in Simple Shearing Flow	515
13.4	Normal Stresses	517
13.5	Rheometry	518
13.6	Intrinsic Viscosity of Polymers	524
13.7	Flow Through a Slit	529
13.8	Sources of Error in Capillary and Slit Flows	531
13.9	Coaxial Cylinder: Couette Flow	536
13.10	Cone-Plate Viscometers	539
13.11	Plate-Plate Viscometers	541
13.12	Experimental Determination of Normal Stresses. Coaxial Cylinders	542
13.13	Factors Governing the Non-Newtonian Behavior of Polymers	546
13.14	Non-Newtonian Viscosity Models	550
13.15	Cox-Merz Rule	552
13.16	Influence of Diluents and Plasticizers, Blends, and Fillers on Flow	553
13.17	Parameters Influencing the First Normal Stress Difference	557
13.18	Die Swelling	558
13.19	Melt Index	560
13.20	Thixotropy and Rheopexy	562
13.21	Stretching Flow	563
	Problem Sets	568
	References	579

13.1 INTRODUCTION

The flow of polymer melts and concentrated solutions is a complex process in which degradation of energy and memory effects embodied in the viscosity and the equilibrium recovery compliance function, respectively, play a determinant role. While the viscosity of monomers is perfectly defined at a given temperature, the answer to the question "What is the value of the viscosity of a polymer?" is not a simple one, because the value may vary within several orders of magnitude. Actually, the viscosity of polymers depends on molecular weight, molecular weight distribution, topology of the chains (linear, comb-like, and star structures; irregular branching; etc.), and temperature. In addition, the viscosity of molecular chains, unlike that of monomers or low molecular weight compounds, shows a strong dependence on the shear rate. In most cases the viscosity decreases with increasing shear rate. Normal stress effects are also detected in these fluids. For example, in steady Couette flow, high molecular weight polymers exert a greater normal thrust on the rotating inner cylinder than on the steady outer cylinder, in opposition to what one would expect on the basis of considering only inertial forces. In cone-plate flow, a greater normal thrust is exerted on the plate near the center than at the edge. In general, normal stress effects increase with shear rate.

A mathematical expression relating forces and deformation motions in a material is known as a constitutive equation. However, the establishment of constitutive equations can be a rather difficult task in most cases. For example, the dependence of both the viscosity and the memory effects of polymer melts and concentrated solutions on the shear rate renders it difficult to establish constitutive equations, even in the cases of simple geometries. A rigorous treatment of the flow of these materials requires the use of fluid mechanics theories related to the nonlinear behavior of complex materials. However, in this chapter we aim only to emphasize important qualitative aspects of the flow of polymer melts and solutions that, conventionally interpreted, may explain the nonlinear behavior of polymers for some types of flows. Numerous books are available in which the reader will find rigorous approaches, and the corresponding references, to the subject matter discussed here (1-16).

13.2 CONSTITUTIVE EQUATIONS

The laws of mechanics alone are not sufficient to determine the relationships between forces and motions in a body. It is necessary to know the evolution with time of functions that depend on the nature of the material, that are in

turn specified by means of constitutive equations that must satisfy certain basic physical principles in order to be valid models of the physical behavior of materials. These principles are the causality indifference principle, the local action principle, the frame indifference principle, and the material indifference principle (2,4,6,17–22).

The *causality indifference principle* states that the physical behavior of a material at a time t is independent of all future events. Thus, the stress of material at a point P at time t depends only on motions at times $\theta \leq t$.

The *local action principle* establishes that the behavior of a particular element of a material is determined by the motion properties of that element and is independent of the behavior of any other element. The causality indifference principle together with the local action principle lead to the *principle of determinism*, which states that the stress of a given element of a material at time t depends only on the deformation of that element at times $\theta \leq t$.

The *frame indifference principle* states that constitutive equations must exhibit coordinate indifference, that is, the properties of a material must be independent of the reference frame.

Finally, the *material indifference principle* establishes that the physical behavior of a material is independent of the motion of an observer (21).

Most constitutive equations have been developed for incompressible fluids owing to the fact that the treatment of these substances is easier than that of compressible fluids. In what follows, the constitutive equations of different kinds of fluids are briefly summarized (22):

1. The inviscid perfect fluid is a fluid under only hydrostatic pressure. It has constitutive equations

$$\sigma_{ij} = -p\delta_{ij}; \quad \pi_{ij} = \sigma_{ij} + p\delta_{ij} = 0 \quad (13.1)$$

where p is the hydrostatic pressure and δ_{ij} is the Kronecker delta.

2. The constitutive equation of the so-called Newtonian liquids reflects the behavior of fluids in which the stress is a linear function of the shear rate; specifically,

$$\sigma_{ij} = -\delta_{ij} + 2\eta\dot{\gamma}_{ij} \quad (13.2)$$

where $\dot{\gamma}_{ij} [= (1/2)(\partial\dot{x}_i/\partial x_j + \partial\dot{x}_j/\partial x_i)]$ is the shear deformation rate and η , the viscosity, is independent of the shear rate. The substitution of this equation into the first law of Cauchy [$\text{div } \sigma_{ij} + \rho b_i = \ddot{x}_i$; Eq. (4.13)] leads to the Navier–Stokes equation. Except in extreme conditions, for example in tur-

bulent flow, the behavior of fluids of low molecular weight obey Eq. (13.2), and therefore this expression is one of the most used in hydrodynamics.

3. The Reiner–Rivlin equation is based on the assumption that the relationship between the stress and the shear rate does not necessarily have to be linear. The constitutive equation can be written as

$$\sigma_{ij} = -p\delta_{ij} + \mathcal{P}_1 \dot{\gamma}_{ij} + \mathcal{P}_2 \sum_k \dot{\gamma}_{ik} \dot{\gamma}_{kj} \quad (13.3)$$

where \mathcal{P}_1 and \mathcal{P}_2 are functions of two of the principal invariants of $\dot{\gamma}_{ij}$, II and III, defined by the expressions

$$\text{II} = \text{trace } \dot{\gamma}_{ij}^2 = \sum_i \sum_j \dot{\gamma}_{ij} \dot{\gamma}_{ji} \quad (13.4)$$

$$\text{III} = \det \dot{\gamma}_{ij}$$

Because the coefficients of the invariants are not specified, the use of the Reiner–Rivlin equation is rather arbitrary. On the other hand, the time-dependent characteristics of viscoelastic fluids are not described by this equation. Neither are normal stresses in Couette flow correctly described by Eq. (13.3).

4. The Rivlin–Ericksen constitutive equation gives a good account of some characteristics of both the time dependence of the viscoelastic behavior and the normal stress effects. This relationship is based on the assumption that the stress depends not only on the velocity (\dot{x}_k) and the shear rate gradient ($\partial \dot{x}_l / \partial x_m$) but also on derivatives of higher order (\ddot{x}_k , $\partial \ddot{x}_p / \partial x_q \dots x_r^{(N)}$, $\delta x_s^{(N)} / \delta x_1$). As a consequence of the principle of material indifference, all the terms depending on the velocity \dot{x}_j and its higher time derivatives vanish, so the Rivlin–Ericksen constitutive equation can be written as (19)

$$\sigma_{ij} = -p\delta_{ij} + f_{ij}(A_{ik}^{(1)}, A_{nm}^{(2)}, \dots, A_{rs}^{(N)}) \quad (13.5)$$

where f_{ij} is an isotropic function and $A_{ij}^{(n)}$ are symmetrical tensors defined as

$$A_{ij}^{(1)} = 2\dot{\gamma}_{ij} \quad (13.6a)$$

and

$$A_{ij}^{(n+1)} = \dot{A}_{ij}^{(n)} + \sum_k \left(\frac{\partial \dot{x}_k}{\partial x_j} A_{ik}^{(n)} + \frac{\partial \dot{x}_k}{\partial x_i} A_{kj}^{(n)} \right) \quad (13.6b)$$

The two latter constitutive equations indicate that the stress vanishes if the fluid is steady. Consequently, these equations cannot reproduce the relaxation phenomena in which, though the fluid is motionless, relaxation stress is occurring in response to a previous deformation.

5. The models to which we have referred above are special cases of the so-called memory fluid or simple fluid. In this fluid it is assumed that the stress at a given particle, and at a given time, is appropriately determined by the relative deformation gradient $F_{ik}(\theta)$. To define $F_{ik}(\theta)$, let us take the configuration of the body at time t as the reference configuration. Let us assume further that x_k are the coordinates of a given material point in the reference configuration with respect to a specified coordinate system. As the fluid deforms, the position of the material point changes, and its coordinates at time θ , $\zeta_i(\theta)$, will depend on the coordinates at the previous time t , so that $\zeta_i(\theta) = \zeta_i(x_k, \theta; t)$. Therefore, F_{ij} is defined by

$$F_{ij}(\theta) = F_{ij}(x_k, \theta; t) = \frac{\partial \zeta_i}{\partial x_k} \quad (13.7)$$

Obviously, when $\theta = t$, no deformation with respect to the reference configurations has taken place, and $F_i(x_k, t; t) = \delta_{ik}$, where δ_{ik} is the Kronecker delta. The actual strain of the relative deformation tensor is better expressed by the symmetrical tensor

$$J_{ij} = \sum_k F_{ki} F_{kj} - \delta_{ij} = \sum_k \frac{\partial \zeta_k}{\partial x_i} \frac{\partial \zeta_k}{\partial x_j} - \delta_{ij} \quad (13.8)$$

According to Eq. (13.8), $J_{ij} = 0$ for a rigid body, while $J_{ij} \neq 0$ for a strained material. The constitutive equation for a memory fluid can be written as (2)

$$\sigma_{ij}(t) = -p\delta_{ij} + \mathfrak{C}_{ij} \int_0^\infty [J_{kl}(t - \theta)] \quad (13.9)$$

where \mathfrak{C}_i is a functional whose value is determined when its argument $J_{kl}(t - \theta)$ is known for all times θ previous to the current time t . In the evaluation of $J_{kl}(t - \theta)$, the reference configuration is taken as the one corresponding to time t .

Though the stress at time t in memory fluids is expected to depend on the history of the deformation, the dependence is stronger for recent deformations than for ancient ones. In other words, these fluids exhibit fading memory (23). The *slow flow* and *small deformation* approximations have been used to establish constitutive equations for memory fluids. In the *slow flow* approximation (23), a sequence of deformation histories is assumed in which each history differs from a reference history in that the time scale is slowed by a

factor α , where $0 < \alpha < 1$. This means that the deformation occurring at time t is the same as occurred in the reference history at time αt . The stress in this approximation can be expressed in terms of power series of α . If the series is truncated at the n th term, the equation for the stress is called the constitutive equation for the n th-order fluid. Thus, the inviscid fluid is the zero-order fluid; the first-order fluid is the Newtonian fluid. The constitutive equation for the second-order fluid is given by

$$\sigma_{ij} = -p\delta_{ij} + \eta_0 A_{ij}^1 + \beta \sum_k A_{ik}^{(1)} A_{kj}^{(1)} + \gamma A_{ij}^{(2)} \quad (13.10)$$

where $A_{ij}^{(n)}$ are the Rivlin–Ericksen tensors defined by Eq. (13.6); η_0 is the viscosity; and β and γ are given by the expressions (24)

$$\eta_0 = \int_0^\infty G(\theta) d\theta \quad (13.11a)$$

$$-\gamma = \int_0^\infty \theta G(\theta) d\theta = \eta_0^2 J_e^0 \quad (13.11b)$$

$$\beta = \int_0^\infty \int_0^\infty \theta r a(\theta, r) d\theta dr \quad (13.11c)$$

where the relationships between the viscosity η_0 and the relaxation modulus $G(t)$ and between the integral of γ and the steady-state compliance J_e^0 are given in Eqs. (6.49) and (6.53), respectively.

In the *small deformation* approximation, it is assumed that the deformations undergone by the material are small, at least in the recent past. Approximations of different orders can be developed. The approximation of first order for an incompressible fluid is given by Boltzmann's equation of linear viscoelasticity,

$$\sigma_{ij}(t) = -p\delta_{ij} + 2G(0)\gamma_{ij}(t) + 2 \int_0^\infty \frac{dG(\theta)}{d\theta} \gamma_{ij}(t - \theta) d\theta \quad (13.12)$$

where $G(t)$ is the relaxation modulus and γ_{ij} is the infinitesimal strain tensor. For a fluid of second order with no limitation to infinitesimal deformation, the constitutive equation can be written as (22)

$$\begin{aligned} \sigma_{ij} = & -p\delta_{ij} + \int_0^\infty \frac{dG(\theta)}{d\theta} J_{ij}(\theta) d\theta + \sum_k \int_0^\infty \int_0^\infty [a(\theta, \theta') J_{ik}(\theta) J_{kj}(\theta') \\ & + b(\theta, \theta') J_{kk}(\theta) J_{ij}(\theta')] d\theta d\theta' \end{aligned} \quad (13.13)$$

where G , a , and b are material functions.

Many constitutive equations have been proposed in addition to those indicated above, which are special cases of fluids with memory. Most of these expressions arise from the generalization of linear viscoelasticity equations to nonlinear processes whenever they obey the material indifference principle. However, these generalizations are not unique, because there are many equations that reduce to the same linear equation. It should be noted that a determined choice among the possible generalizations may be suitable for certain types of fluids or special kinds of deformations. In any case, the use of relatively simple expressions is justified by the fact that they can predict, at least qualitatively, the behavior of complex fluids.

13.3 SECOND-ORDER FLUIDS IN SIMPLE SHEARING FLOW

Three functions (η , β , and γ) are necessary to characterize the flow of a second-order fluid. Let us determine these functions for a memory fluid under simple shearing flow (25, 26), as shown in Figure 13.1. In this case, the coordinates of a given point at time t will be $x_1 = x_1$, $x_2(t) = [x_2(t)/x_1]x_1 = x_1 \tan \delta(t)$, and $x_3 = x_3$. The velocity field is given by

$$\dot{x}_1 = 0; \quad \dot{x}_2 = \kappa x_1; \quad \dot{x}_3 = 0 \quad (13.14)$$

where $\kappa = [\dot{x}_2(t)/x_1]$ is a constant called the rate of shear. The position of the point at time θ can be obtained by solving the differential equations

$$\dot{\zeta}_1 = 0; \quad \dot{\zeta}_2 = \kappa \zeta_1; \quad \dot{\zeta}_3 = 0 \quad (13.15)$$

Let us take the configuration at time t as the configuration of reference. If the coordinates of the point at time t are x_1 , x_2 , and x_3 , the coordinates at time θ will be

$$\zeta_1 = x_1; \quad \zeta_2 = x_2 + \kappa x_1(\theta - t); \quad \zeta_3 = x_3 \quad (13.16)$$

The components of the relative deformation gradient F_{ij} and the symmetrical tensor J_{ij} can be calculated, respectively, from Eqs. (13.7) and (13.8), giving

$$\|F_{ij}(\theta)\| = \begin{pmatrix} 1 & 0 & 0 \\ \kappa(\theta - t) & 1 & 0 \\ 0 & 0 & 1 \end{pmatrix}; \quad \|J_{ij}(t - u)\| = \begin{pmatrix} \kappa^2 u^2 & -\kappa u & 0 \\ -\kappa u & 1 & 0 \\ 0 & 0 & 0 \end{pmatrix} \quad (13.17)$$

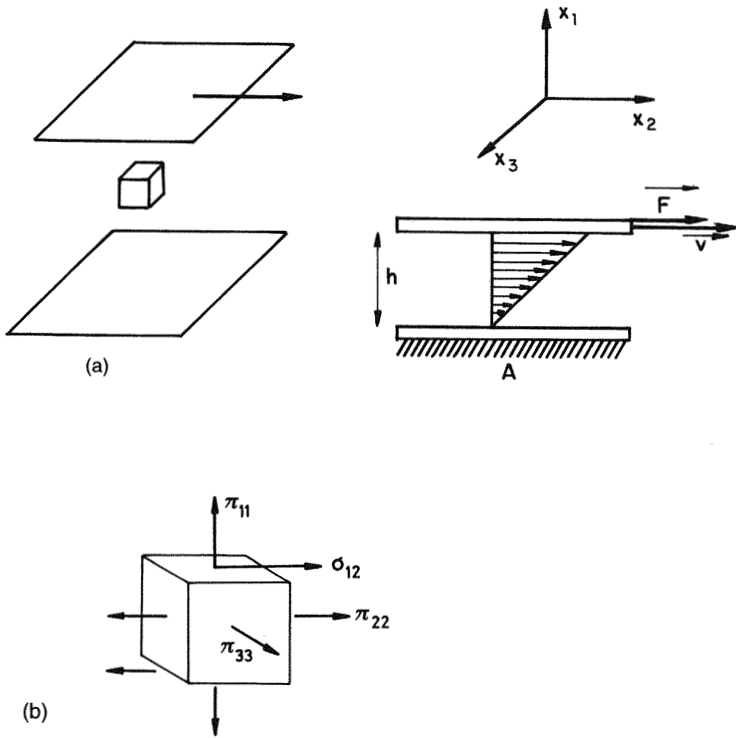


Figure 13.1 (a) Simple shear. (b) Shear stress and normal stresses for a fluid under a shear force.

where in the last matrix the substitution $t - \theta = u$ was made. Hence, by taking into account the Rivlin–Ericksen tensors defined in Eq. (13.6), $J_{ij}(t - u)$ can be written as

$$J_{ij}(t - u) = -uA_{ij}^{(1)} + \frac{1}{2}u^2A_{ij}^{(2)} \quad (13.18)$$

where $A_{ij}^{(1)}$ and $A_{ij}^{(2)}$ are independent of t and are given by

$$\|A_{ij}^{(1)}\| = \kappa \begin{pmatrix} 0 & 1 & 0 \\ 1 & 0 & 0 \\ 0 & 0 & 0 \end{pmatrix}; \quad \|A_{ij}^{(2)}\| = 2\kappa^2 \begin{pmatrix} 1 & 0 & 0 \\ 0 & 0 & 0 \\ 0 & 0 & 0 \end{pmatrix} \quad (13.19)$$

The constitutive equation of second-order fluids indicates that the stress tensor is determined by $J_{ij}(t-u)$, and consequently $\sigma_{ij}(t)$ is independent of t and depends only on $A_{ij}^{(1)}$ and $A_{ij}^{(2)}$. Thus the function \mathfrak{C}_{ij} reduces to a function β_{ij} , and the constitutive equation for second-order fluids [Eq. (13.9)] can be expressed as

$$\sigma_{ij}(t) = -p\delta_{ij} + \overset{\infty}{\mathfrak{C}}_{ij} J(t-\theta) = -p\delta_{ij} + \beta_{ij}(A_{kl}^{(1)}, A_{mn}^{(2)}) \quad (13.20)$$

where the principle of material indifference requires that β_{ij} be an isotropic function.

13.4 NORMAL STRESSES

For simple shear experiments, somewhat lengthy mathematical arguments indicate that the stress tensor for second-order fluids is given by (2)

$$\|\pi_{ij}\| = \begin{pmatrix} \sigma_{11} + p & \sigma_{12} & 0 \\ \sigma_{21} & \sigma_{22} + p & 0 \\ 0 & 0 & \sigma_{33} + p \end{pmatrix} = \begin{pmatrix} \pi_{11} & \sigma_{12} & 0 \\ \sigma_{21} & \pi_{22} & 0 \\ 0 & 0 & \pi_{33} \end{pmatrix} \quad (13.21)$$

This expression in combination with Eqs. (13.10) and (13.18) leads to the relationship

$$\|\pi_{ij}\| = \eta_0 \begin{pmatrix} 0 & 1 & 0 \\ 1 & 0 & 0 \\ 0 & 0 & 0 \end{pmatrix} + \beta\kappa^2 \begin{pmatrix} 1 & 0 & 0 \\ 0 & 1 & 0 \\ 0 & 0 & 0 \end{pmatrix} + 2\gamma\kappa^2 \begin{pmatrix} 1 & 0 & 0 \\ 0 & 0 & 0 \\ 0 & 0 & 0 \end{pmatrix} \quad (13.22)$$

Hence,

$$\sigma(\kappa) = \sigma_{12} = \sigma_{21} = \eta_0\kappa \quad (13.23a)$$

$$\pi_1(\kappa) = \pi_{11} - \pi_{33} = \sigma_{11} - \sigma_{33} = (\beta + 2\gamma)\kappa^2 \quad (13.23b)$$

$$\pi_2(\kappa) = \pi_{22} - \pi_{33} = \sigma_{22} - \sigma_{33} = \beta\kappa^2 \quad (13.23c)$$

where $\sigma(\kappa)$ is the shear stress and $\pi_1(\kappa)$ and $\pi_2(\kappa)$ are called the normal stress functions. A schematic representation of the shear and normal stresses for a liquid under a shear force is given in Figure 13.1. According to Eq. (13.23), the viscosity is a constant for second-order fluids as it is for Newtonian fluids. However, the normal stresses are nonzero, and consequently

second-order fluids exhibit normal stress effects. On the other hand, while the shear stress is an odd function of the shear rate, the normal stress functions are even functions of κ , that is,

$$\sigma(\kappa) = -\sigma(-\kappa); \quad \pi_1(\kappa) = \pi_1(-\kappa); \quad \pi_2(\kappa) = \pi_2(-\kappa) \quad (13.24)$$

From Eqs. (13.23) and (13.11), the primary normal stress difference can be expressed in terms of viscoelastic parameters as

$$N_1 = \pi_{22} - \pi_{11} = \sigma_{22} - \sigma_{11} = 2\eta_0^2 J_e^0 \kappa^2 \quad (13.25)$$

In the region in which the fluid is Newtonian, $\sigma = \eta_0 \kappa$, Eq. (13.25) becomes

$$N_1 = 2J_e^0 \sigma^2 \quad (13.26)$$

which suggests that the N_1/σ^2 ratio remains practically constant in the Newtonian regime for second-order fluids. In other words, the normal stress N_1 is a linear function of the square of either the shear rate or the shear stress for second-order fluids.

Finally, it should be stressed that second-order fluids present normal stresses and, as a consequence, nonlinear effects at shear rates corresponding to the Newtonian regime. It is noteworthy that the first normal stress coefficient starts at $2J_e \eta_0^2$, and, like the viscosity, it decreases with increasing shear rate for complex fluids.

The parameter N_1 is also related to the storage relaxation modulus. Actually, from Eqs. (6.52) and (13.25),

$$\frac{1}{2} \lim_{\kappa \rightarrow 0} \left(\frac{\pi_{22} - \pi_{11}}{\kappa^2} \right) = \lim_{\omega \rightarrow 0} \left(\frac{G'(\omega)}{\omega^2} \right) \quad (13.27)$$

Accordingly, the value of N_1 at very low shear rates is twice that of the storage relaxation modulus at very low frequencies. The second normal stress difference, $N_2 = \pi_{11} - \pi_{33}$, is negative and smaller in magnitude than the first normal stress difference. The ratio $-N_2/N_1$ lies in the interval 0.1–0.3.

13.5 RHEOMETRY

Whenever the flow is laminar, the shear stress is a linear function of the shear rate for liquids of low molecular weight. The viscosity of fluids of this type is independent of the shear rate, and for this reason they are known as

Newtonian fluids. Complex fluids, such as polymers, exhibit Newtonian behavior for low values of the shear rate until a value of κ is reached above which the shear stress falls below the linear relationship of σ_{12} versus κ . Hence the apparent viscosity decreases as κ increases, and these fluids exhibit non-Newtonian behavior. For a comparatively small number of fluids, the viscosity increases as the shear rate increases. Typical curves showing the dependence of the shear stress on the shear rate are shown in Figure 13.2. For some fluids, known as Bingham fluids, a critical stress is necessary for flow to occur. The flow behavior for different Bingham fluids is also shown in Figure 13.2.

In measurements of viscosities, several flow geometries can be used (27,28), the most important being capillary, concentric cylinders (Couette), cone-plate, and concentric disk geometries (Fig. 13.3). The type of geometry used depends on the shear rate at which one needs to measure the viscosity. Oscillatory measurements are used at very low shear rates. For low and moderate shear rates, the viscosities can be measured using cone-plate, plate-plate, concentric cylinders and capillary geometries. The latter two geometries are commonly used to measure viscosities at moderate shear rates and, finally, capillary geometry is used to measure viscosities at moderately high shear rates.

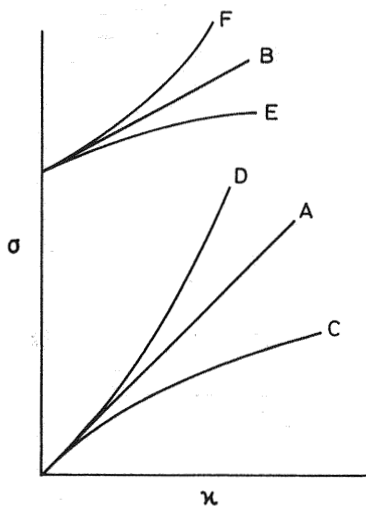


Figure 13.2 Schematic representation of different kinds of flows. A, Newtonian; B, Bingham Newtonian; C, shear thinning (pseudoplastic); D, shear thickening (dilatant); E, Bingham shear thinning; F, Bingham shear thickening.

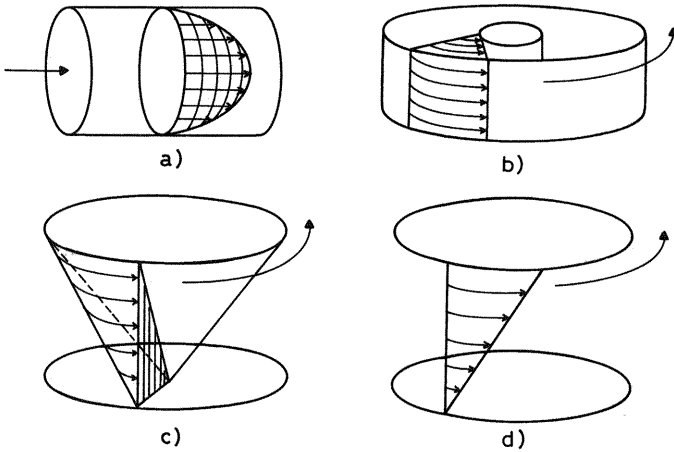


Figure 13.3 Geometries used in rheometry. a, capillary; b, cylindrical; c, cone-plate; d, plate-plate.

A schematic representation showing the intervals of shear rates at which different geometries are used is given in Figure 13.4. In this figure, the interval of shear rates at which polymeric materials are processed is also included. It should be noted that injection molding tends to the upper shear rate values while compression molding tends to the lower shear rates.

Rheometry is an important subject from a practical point of view. Though the properties of a material depend on molecular weight and molec-

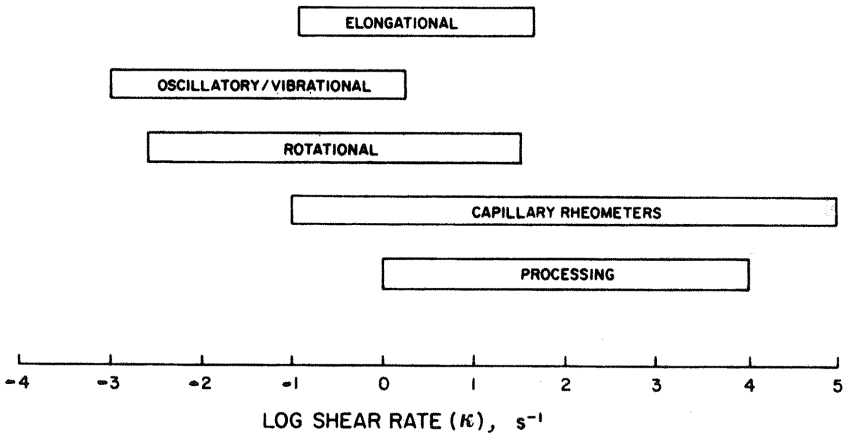


Figure 13.4 Approximate shear rate ranges for different geometries.

ular weight distribution, the way that molecules are packed together, which controls the final properties of the material, is controlled by the processing conditions. These conditions are often dictated by the rheological behavior induced through the fabrication method—melt drawing, film blowing, spinning, etc.

13.5.1 Capillary Rheometry

Capillary viscometry was the first method used to measure the viscosity of fluids. This procedure, based on the relationship between pressure drop and flow rate, was independently developed by Hagen and Poiseuille (see Ref. 29). It is one of the most widely used techniques for studying the flow behavior of fluids.

When there is a difference of pressure between two points of a capillary tube, the fluid flows from the high pressure side to the low pressure side of the tube. Let us assume that a Newtonian liquid flows through a capillary tube of radius r and length ΔL (Fig. 13.5). Once steady-state conditions are reached, that is, the applied energy is totally dissipated into friction energy, a simple balance of energy gives

$$2\pi r dz \sigma(r) + \pi r^2 dP = 0 \quad (13.28)$$

Hence,

$$\sigma(r) = -\frac{r}{2} \frac{dP}{dz} = -\frac{r}{2} \frac{\Delta P}{\Delta L} \quad (13.29)$$

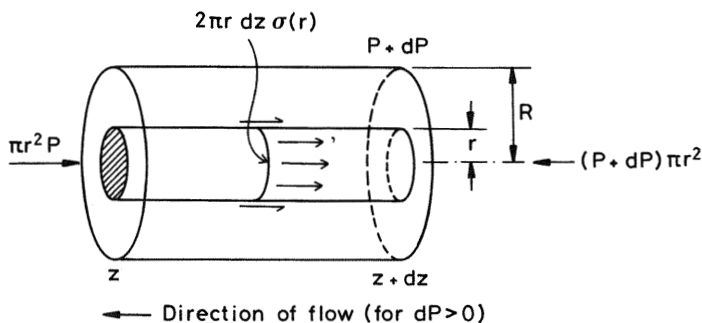


Figure 13.5 Force balance in capillary flow.

Since $\Delta P < 0$, $\sigma(r) > 0$. The shear stress increases as r increases, reaching a maximum value at the wall of the capillary tube. The value of the shear stress at the wall is given by

$$\sigma_w = -\frac{R}{2} \frac{\Delta P}{\Delta L} \quad (13.30)$$

From Eq. (13.29) and Newton's law,

$$\sigma(r) = \eta \kappa = -\eta \frac{dv}{dr} \quad (13.31)$$

which yields

$$v(r) = \left(-\frac{\Delta P}{4\eta \Delta L} \right) (R^2 - r^2) \quad (13.32)$$

This expression indicates that the fluid presents a distribution of velocities whose profile corresponds to a paraboloid of revolution; the velocity of the fluid reaches its maximum value [$v_{\max} = (\Delta P/4\eta \Delta L)R^2$] at the center of the capillary and 0 at the capillary wall. The flow of the fluid through an infinitesimal cylinder defined by r and $r + dr$ is $dQ = 2\pi r dr v(r)$. Then the volumetric flow rate can be written as

$$Q = 2\pi \int_0^R r dr v(r) = \frac{\pi R^4}{8\eta} \left(-\frac{\Delta P}{\Delta L} \right) \quad (13.33)$$

Equation (13.32) leads to the following expression for the shear rate:

$$\kappa(r) = -\frac{dv(r)}{dr} = \frac{r}{2\eta} \left(-\frac{\Delta P}{\Delta L} \right) \quad (13.34)$$

In this equation, $\kappa(r) > 0$, because $\Delta P < 0$. By combining Eqs. (13.33) and (13.34), the shear rate at the wall is obtained:

$$\kappa_w = \frac{4Q}{\pi R^3} \quad (13.35)$$

Determination of the viscosity involves the measurement of the pressure gradient and Q , from whose values the results for σ_w and κ_w can be obtained. The viscosity is then determined by means of the relationship

$$\eta = \sigma_w / \kappa_w \quad (13.36)$$

13.5.2 Flow Through a Capillary: Non-Newtonian Behavior

An analysis similar to that described for Newtonian flow shows that the shear stress at the radius r , $\sigma(r)$, and at the wall, σ_w , is given by Eqs. (13.29) and (13.30), respectively. However, the shear stress and the shear rate are related in these liquids by the power law

$$\sigma = \eta \kappa^n = \eta \left(-\frac{dv}{dr} \right)^n \quad (13.37)$$

where η is the apparent viscosity. From Eqs. (13.29) and (13.37), we obtain

$$\kappa = -\frac{dv}{dr} = \left(-\frac{\Delta P}{2\eta \Delta L} \right)^{1/n} r^{1/n} \quad (13.38)$$

Integration of this equation gives the following expression for the profile of the velocity along the radius:

$$v(r) = \frac{n}{1+n} \left(-\frac{\Delta P}{2\eta \Delta L} \right)^{1/n} \left(R^{(n+1)/n} - r^{(n+1)/n} \right) \quad (13.39)$$

where it has been considered that the velocity vanishes at the capillary wall. Then the volumetric flow rate, Q is given by

$$\begin{aligned} Q &= 2\pi \int_0^R v(r)r \, dr = \frac{n\pi}{3n+1} R^3 \left(-\frac{\Delta P}{2\eta \Delta L} \right)^{1/n} R^{1/n} \\ &= \frac{n\pi}{3n+1} R^3 \kappa_{wNN} \end{aligned} \quad (13.40)$$

where κ_{wNN} , the shear rate for non-Newtonian flows, was obtained by making $r = R$ in Eq. (13.38). This latter magnitude is related to Q by the expression

$$\kappa_{wNN} = \frac{3n+1}{n\pi R^3} Q = \frac{3n+1}{4n} \left(\frac{4Q}{\pi R^3} \right) = \frac{3n+1}{4n} \kappa_w \quad (13.41)$$

where κ_w for the Newtonian flow is given by Eq. (13.35). Equation (13.41) is written in a more convenient way as

$$\kappa_{wNN} = \frac{1}{\pi R^3} \left(3Q + \Delta P \frac{dQ}{d\Delta P} \right) \quad (13.42)$$

where it has been taken into account that $Q/n = \Delta P(dQ/d\Delta P)$. Equation (13.42), known as the Rabinowitsch expression (30), allows the determination of the shear rate for non-Newtonian flows. The strategy to follow in the calculation of the apparent viscosity as a function of the shear rate involves the measurement of Q for different values of increments of pressure. Then the values of $dQ/d\Delta P$ for different values of ΔP are obtained from the slopes of the plots of Q versus ΔP . The values of σ_w calculated by Eq. (13.30) are plotted against those of κ_{wNN} [Eq. (13.41)] for each value of ΔP , and the results for the apparent viscosity are obtained from the slopes of the resulting curves.

The Rabinowitsch correction and the velocity profile are simple analytical functions of the power law exponent n . A schematic diagram of velocity profiles for power law fluids is shown in Figure 13.6.

13.6 INTRINSIC VISCOSITY OF POLYMERS

Owing to the coiled configurations of molecular chains, the viscosity η of dilute polymer solutions increases with respect to that of the solvent, η_s . The difference $\eta - \eta_s$ is proportional to the radius of the coil and the number of coils per unit of volume is $(C/M)N_A$, where C is the concentration of polymer in the solution, M is the molecular weight of the polymer, and N_A is Avogadro's number. Since the radius of the coil can be expressed in terms of the mean square end-to-end distance, $\langle r^2 \rangle$, the specific increment of the viscosity of the solution due to the polymer can be written as

$$\frac{\eta - \eta_s}{\eta_s} \sim CN_A \frac{\langle r^2 \rangle^{3/2}}{M} \quad (13.43)$$

When $C \rightarrow 0$, Eq. (13.43) becomes (31)

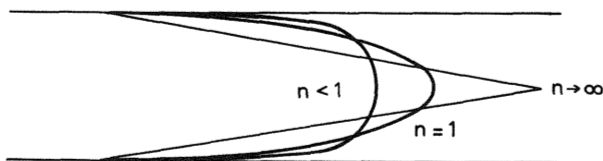


Figure 13.6 Velocity profiles for different power-law fluids.

$$[\eta] = \lim_{C \rightarrow 0} \frac{\eta - \eta_s}{\eta_s C} = \Phi \left(\frac{\langle r^2 \rangle}{M} \right)^{3/2} M^{1/2} \quad (13.44)$$

where $[\eta]$ is the intrinsic viscosity and Φ is a universal constant whose value is 2.5×10^{21} when the intrinsic viscosity is given in deciliters per gram and r in centimeters. In theta solvents, the segment–segment and segment–solvent interaction energies are similar, and consequently excluded volume effects vanish. The coils are unperturbed by the solvent, and their dimensions correspond to those of the isolated chains. For long chains, $\langle r^2 \rangle_0/M = \text{constant}$, and Eq. (13.44) becomes (32)

$$[\eta] = \Phi \left(\frac{\langle r^2 \rangle_0}{M} \right)^{3/2} M^{1/2} = K_\theta M^{1/2} \quad (13.45)$$

where $\langle r^2 \rangle_0$ is the mean square end-to-end distance of the unperturbed chains. Accordingly, the intrinsic viscosity of polymer solutions in theta solvents scales with the $1/2$ power of molecular weight. In good solvents, $\langle r^2 \rangle / \langle r^2 \rangle_0 = \alpha^2$, where α is the expansion coefficient, which scales with the exponent ν of molecular weight ($\alpha \sim M^\nu$). Then Eq. (13.44) can be written as (32)

$$[\eta] = \Phi \left(\frac{\langle r^2 \rangle_0}{M} \right)^{3/2} \alpha^3 M^{1/2} = KM^a \quad (13.46)$$

where $a = 0.5 + 3\nu$. The value of the exponent ν for flexible chains in good solvents is 0.1, so the exponent a in Eq. (13.46) lies in the range $0.5 \leq a \leq 0.8$.

The intrinsic viscosity is usually measured in a Ubbelohde-type viscometer, a scheme of which is given in Figure 13.7. If the volume V of liquid between the marks a and b flows in a time t , then $Q = V/t$. The liquid flows under the increment of pressure given by

$$\Delta P = \rho g \frac{h_a - h_b}{\ln h_a/h_b} \quad (13.47)$$

where h_a and h_b are, respectively, the length of the capillary tube from the marks a and b in Figure 13.7 and ρ is the density of the solution. According to Eq. (13.33), the viscosity of the liquid flowing through the capillary tube can be written as

$$\eta = \Delta P t \quad (13.48)$$

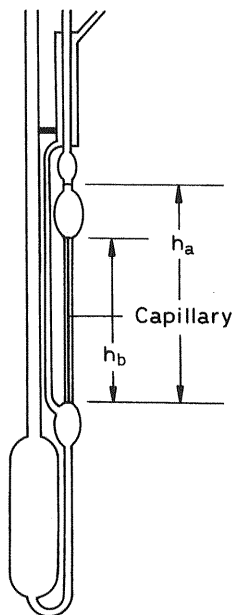


Figure 13.7 Ubbelohde viscometer.

where A is a constant depending on the geometry of the viscometer. The specific viscosity is defined as

$$\eta_{\text{sp}} = \frac{\eta - \eta_s}{\eta_s} \cong \frac{t}{t_s} - 1 \quad (13.49)$$

where t and t_s are, respectively, the times required for the solution and solvent to flow. The ratio between the specific viscosity and the concentration, called the reduced viscosity, is given by (33)

$$\frac{\eta_{\text{sp}}}{C} = [\eta] + k'[\eta]^2 C \quad (13.50)$$

where k' is the Huggins constant. The intrinsic viscosity can then be obtained by extrapolating η_{sp}/C to zero concentration. An alternative way of obtaining $[\eta]$ is the extrapolation of $(\ln \eta_r)/C$ at zero concentration, where $\eta_r = t/t_s$ is the relative viscosity. The corresponding relation involving η_r is given by

$$\frac{\ln \eta_r}{C} = [\eta] + k''[\eta]^2 C \quad (13.51)$$

where k'' is the Kraemer constant. When $C \rightarrow 0$, $k' - k'' = 0.5$.

Interest in the intrinsic viscosity lies in the fact that this magnitude permits one to obtain the hydrodynamic volume of the molecular coils [see Eq. (13.45)], on the one hand, and the molecular weight [see Eq. (13.46)], on the other hand. However, the intrinsic viscosity depends on the shear rate, and care should be taken that the measurements are carried out under laminar regime. Actually, the coils of very flexible chains are nearly spherical, and consequently the viscosity of the solutions show only a weak dependence on the shear rate. However, as the rigidity of the chains increases, the symmetry of the coils decreases, the chains adopting an ellipsoidal shape. In this case the energy dissipated during flow depends on the direction of the larger semiaxis with respect to the flow, reaching a minimum value when this semiaxis is parallel to the direction of flow. As a result, the orientation of the coils depends on the rate of shear, and the intrinsic viscosity is strongly dependent on shear rate.

Illustrative curves representing the variation in the reduced viscosity with the shear stress for solutions of semirigid chains (34) are shown in Figure 13.8. The reduced viscosity remains nearly constant at low values of σ until a critical value σ_c is reached at which there is a relatively sharp drop in the values of η_{sp} with increasing shear stress. It can be seen that the critical shear stress is independent of the concentration of the solutions. The intrinsic viscosity was obtained as a function of the shear stress from the results of Figure 13.8, and the ratio of the value of this magnitude at κ to that at $\kappa = 0$ is plotted as a function of κ in Figure 13.9. It is interesting to note that the intrinsic viscosity at high shear rate can reach a value that is only 50% of that corresponding to zero shear rate.

In poly(benzyl glutamate), helix conformations are stabilized by intramolecular hydrogen bonding between hydrogens of the amide groups and the carbonyl groups. Conformations of this kind are maintained in solvents such as cresol, and the corresponding configuration of the chains is an ellipsoid. However, the helix conformations are destroyed by solvents such as chloroacetic acid, the chain passing from an ellipsoidal to a coiled configuration. The transition from helix to coil gives rise to a big decrease in the intrinsic viscosity. Values of the intrinsic viscosity ratio are plotted as a function of the shear rate in Figure 13.10. The intrinsic viscosity of the solution in which the configuration of the chains is an ellipsoid experiences a sharp drop after a critical shear stress is reached (35). However, the decrease observed for the intrinsic viscosity ratio of the coiled configuration is, in comparison, rather small.

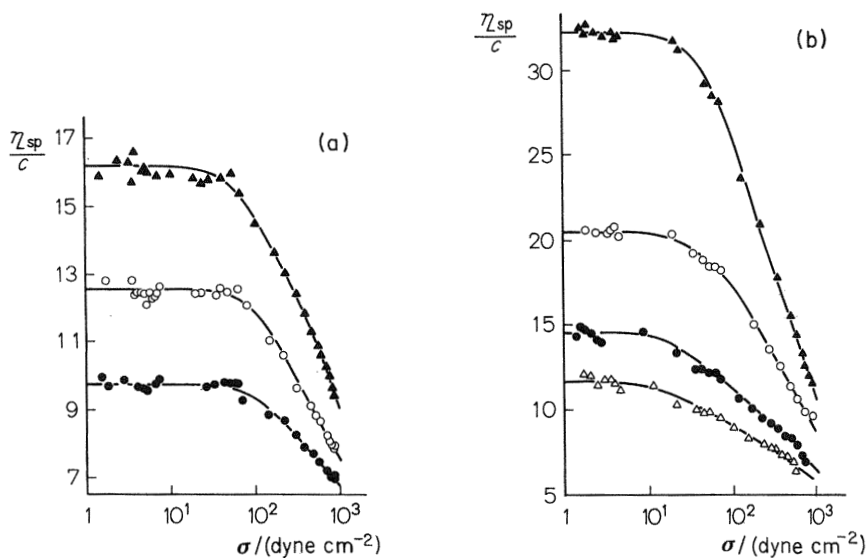


Figure 13.8 (a) Reduced viscosity in dL/g as a function of the shear stress for different concentrations of cellulose ($M_n = 3.30 \times 10^5$) in cadoxene: (\blacktriangle) 0.40 g/dL; (\circ) 0.30 g/dL; (\bullet) 0.18 g/dL. (b) Reduced viscosity as a function of the shear stress for different concentrations of cellulose ($M_n = 4.29 \times 10^5$) in cadoxene/water (1:1): (\blacktriangle) 0.45 g/dL; (\circ) 0.32 g/dL; (\bullet) 0.18 g/dL; (\triangle) 0.11 g/dL. (From Ref. 34.)

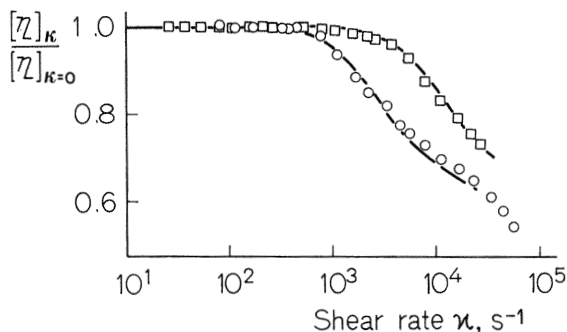


Figure 13.9 Relative intrinsic viscosity as a function of the shear rate κ . (\circ) Cellulose ($M_n = 4.29 \times 10^5$) in cadoxene/water (1:1); (\square) cellulose ($M_n = 3.30 \times 10^5$) in cadoxene. Lines are theoretical curves. (From Ref. 34.)

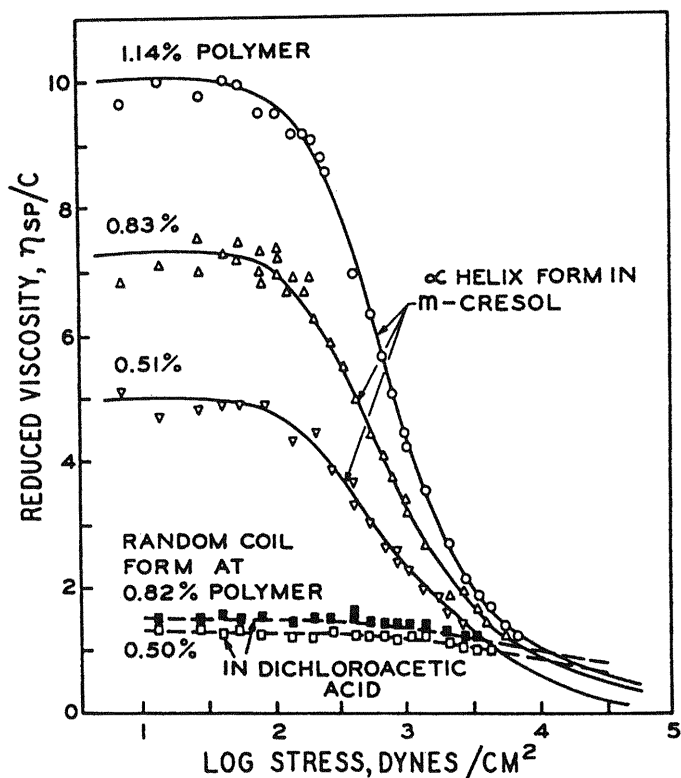


Figure 13.10 Reduced viscosity in dL/g as a function of the shear rate for solutions of poly(benzyl glutamate) in *m*-cresol and dichloroacetic acid. (From Ref. 35).

13.7 FLOW THROUGH A SLIT

Assume a slit rheometer made up by a reservoir and a rectangular channel having a width, w , much greater than its thickness, h , as shown in Figure 13.11. Assume further that the edge effects are negligible in the flow geometry, so the steady flow may be considered two-dimensional. If the reference frame is located in such a way that the y ordinate is measured from the center of the plane defined by wh , a force balance on a rectangular element of the fluid gives

$$\sigma_{yz}Lw + wy \Delta P = 0 \quad (13.52)$$

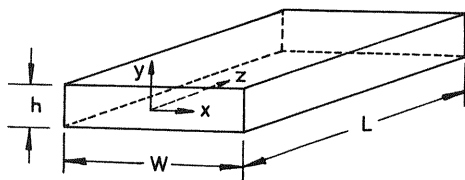


Figure 13.11 Flow through a slit rheometer.

where ΔP is the driving force. Hence the shear stress is given by

$$\sigma(y) = \sigma_{yz}(y) = \left(-\frac{\Delta P}{L}\right)y \quad (13.53)$$

Therefore, shear stress at the wall is

$$\sigma_w = \left(-\frac{\Delta P}{L}\right)\left(\frac{h}{2}\right) \quad (13.54)$$

Since $\Delta P < 0$, $\sigma_w > 0$. The shear stress is related to the shear rate by the power law

$$\sigma = \eta\kappa^n = \eta\left(-\frac{dv}{dy}\right)^n \quad (13.55)$$

Considering the boundary condition $v = 0$ for $y = h/2$, the integration of Eq. (13.55) gives the velocity profile along the y axis:

$$v(y) = \frac{2nw}{2n+1} \left(-\frac{\Delta P}{\eta L}\right)^{1/n} \left[\left(\frac{h}{2}\right)^{(n+1)/n} - y^{(n+1)/n} \right] \quad (13.56)$$

The volumetric flow rate can be written as

$$Q = 2 \int_0^{h/2} v(y)w \, dy = \frac{2nw}{2n+1} \left(-\frac{\Delta P}{\eta L}\right)^{1/n} \left(\frac{h}{2}\right)^{1/n+2} \quad (13.57)$$

From Eq. (13.56), the shear rate at the wall is given by

$$\kappa_w = -\frac{dv(y)}{dy} = \left(-\frac{\Delta P}{\eta L}\right)^{1/n} \left(\frac{h}{2}\right)^{1/n} \quad (13.58)$$

For Newtonian and non-Newtonian liquids, the shear stress at the wall is given by Eq. (13.54). The shear rate at the wall for Newtonian liquids can be expressed in terms of the volumetric flow, making $n = 1$ in Eqs. (13.57) and (13.58). In this case, this quantity can be written as

$$\kappa_w = \frac{6Q}{h^2 w} \quad (13.59)$$

In the case of a non-Newtonian fluid, the true wall shear rate $\dot{\gamma}_{wNN}$ can be calculated by using a procedure similar to the Rabinowitsch equation for capillary flow, obtaining

$$\kappa_{wNN} = \kappa_w \left[\frac{2 + (d \ln \kappa_w)/(d \ln \sigma_w)}{3} \right] \quad (13.60)$$

where κ_w and σ_w are given by Eqs. (13.59) and (13.54), respectively.

Capillary rheometers allow observation of flow by optical techniques and also permit the installation of pressure transducers along the slit, thus eliminating the need for end corrections.

13.8 SOURCES OF ERROR IN CAPILLARY AND SLIT FLOWS

In the study of flow through capillary and slit rheometers, the temperature and the specific volume are assumed to be constant. However, owing to the high viscosity of polymer melts, heat is generated during flow that gives rise to an increase in temperature and hence to a decrease in viscosity (36). Considering that the work done during flow degrades to heat, the volume average temperature rise is given by

$$\Delta T = \frac{\Delta P}{\rho c_p} \quad (13.61)$$

where ρ is the density and c_p is the specific heat. For example, if it is assumed that $\Delta P = 10^8 \text{ N/m}^2$, $\rho = 1000 \text{ kg/m}^3$, and $c_p = 2.2 \text{ KJ/kg} \cdot \text{K}$, the value of ΔT is about 45°C . However, the distribution of temperature is not uniform along the radius, since T is larger in the high shear region near the wall. On the other hand, the consideration of incompressibility in liquids, an assumption often made in the study of the flow of these substances, must be removed. Actually, polymer liquids are highly compressible. For example, a pressure of 10^8 N/m^2 will cause approximately a 10% increase in density, which in turn will give rise to a viscosity two to five times larger than that

corresponding to 1 atm. Although temperature and pressure effects may individually be large, they are to a large extent mutually canceling. Obviously, minimization of these effects would require minimizing the pressure effects by using capillary tubes in which the length-to-radius ratio is small.

Another source of error in the determination of the apparent viscosity in capillary flow lies in the fact that as the polymer liquid converges from the barrel to the capillary, the convergence of the flow requires a sharp pressure drop due to the elongational viscosity flow. This effect is illustrated in Figure 13.12. The drop in pressure is not $(P_2 - P_1)/L$ but rather $(P_2 - P_1)/L^*$, in which L^* is related to L by

$$L^* = L + mR \quad (13.62)$$

where m lies in the range $1 < m < 15$. Bagley (37) realized that a plot of the driving pressure versus the capillary length-to-radius ratio (L/R) at a fixed wall shear rate gives a straight line with an intercept a (see Fig. 13.13) at $\Delta P = 0$. The value of a , which is dependent on the wall shear rate, should be used to correct the wall shear stress. Accordingly,

$$\sigma_w = \frac{R \Delta P}{2(L + aR)} \quad (13.63)$$

This method needs extensive experimentation, and in practice the choice of two capillary tubes may be adequate. The best results with this approach are

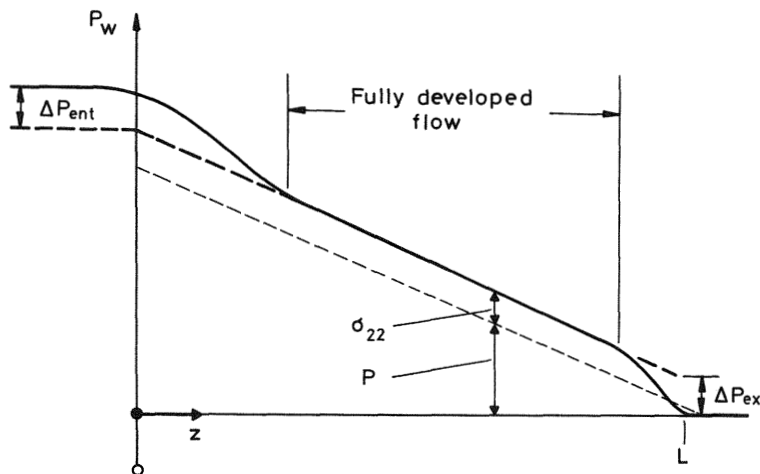


Figure 13.12 Variation of pressure along a capillary tube.

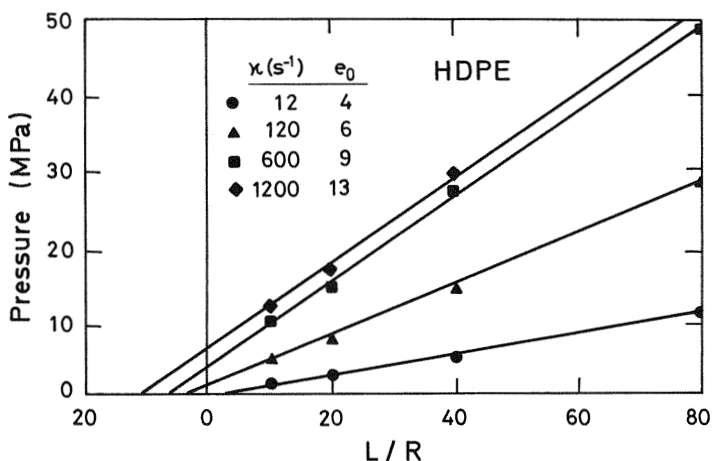


Figure 13.13 Bagley plots to determine the effective length of a capillary tube.

obtained by combining a relatively long capillary ($L/R = 32$) with an orifice ($L/R = 0$).

In the evaluation of the rheological equations for the shear rate, it is assumed that there is no polymer slippage at the capillary wall. However, it is an experimentally demonstrated fact that viscous low molecular weight liquids display brittleness at very high deformation rates, behaving like glassy solids. From a qualitative point of view, loss of fluidity occurs in these cases when the reciprocal of the deformation rate is much lower than the mean relaxation time of the system. There are some grounds for believing that polymer melts lose fluidity at deformation rates at which transition from the fluid to the highly elastic state occurs, without displaying the brittleness typical of the glassy state.

The streamlines for Newtonian fluids at low Reynolds numbers stretch in a regular manner from the reservoir down to the capillary or the slit. However, the streamlines of viscoelastic fluids present vortices in the corner regions, as shown in Figure 13.14. These vortices may become pulsating, leading to flow instabilities and distortions of the melt extrudate. There is also a high degree of tensile extension at the entrance of the slit or capillary, and it is possible to obtain an apparent extensional viscosity using entrance drop measurements. As a consequence, some linear polymers display a jumpwise increase in the flow. This phenomenon is very important in polyethylene, spurting being both more pronounced and occurring at a low deformation rate in PE samples with narrow molecular weight distributions (38). Figure 13.15 shows the volumetric

flow rate of nearly monodisperse polybutadiene of molecular weight 2.4×10^4 through a capillary 1 mm diameter and 25 mm in length. Photographs accompanying the graph, which show the appearance of the polymer extrudate at the capillary outlet, indicate that development of shape disturbances or elastic turbulence occurs at flow regimes close to Newtonian. When the critical stress and the shear rate corresponding to spurling are reached, the polymer discharge increases jumpwise. The extrudate in this regime begins to exhibit a screw form, then follows a cylindrical section whose diameter and length are close to those of the capillary. In this regime a shear stress σ_s can be reached at which the extrusion rate may increase by a decimal order or more. The curves of Q vs. σ show a small dependence on the L/D ratio of the capillary for this system in the sense that the anomalous jump in Q takes place at lower values of σ as L/D increases. However, as shown in Figure 13.16 the stress at which the anomalous jump occurs seems to be rather insensitive to molecular weight and temperature.

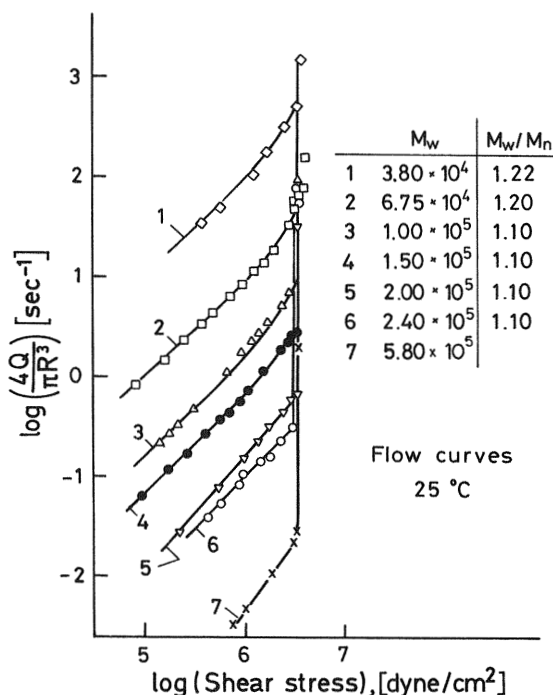


Figure 13.16 Flow as a function of the shear stress for different monodisperse fractions of polybutadiene (From Ref. 38.).

13.9 COAXIAL CYLINDER: COUETTE FLOW

In the last decade of the nineteenth century, Maurice Couette invented the concentric cylinder viscometer. This instrument was probably the first rotating device used to measure viscosities. Besides the coaxial cylinders (Couette geometry), other rotating viscometers with cone-plate and plate-plate geometries are used. Most of the viscometers used nowadays to determine apparent viscosities and other important rheological functions as a function of the shear rate are rotating devices.

An earlier scheme of coaxial cylinder, shown in Figure 13.17 illustrates how a coaxial cylinder works. The rotation is produced by a weight that transmits a torque to an inner cylinder via a string and a pulley. In this design the inner cylinder rotates and the outer one is fixed. Coaxial cylinders are also available in which the torque is transmitted to the outer cylinder. In this case the outer cylinder rotates and the inner cylinder is steady. Commercially sophisticated instruments are now available with computer control and software for data analysis that allows the measurement of apparent viscosity as a function of the shear rate in an easy way.

The fluid fills the gap between the two cylinders, and the outer cylinder acts as a reservoir for the fluid. The layer in contact with the rotating cylinder rotates with the angular velocity of the cylinder. Drag reduction

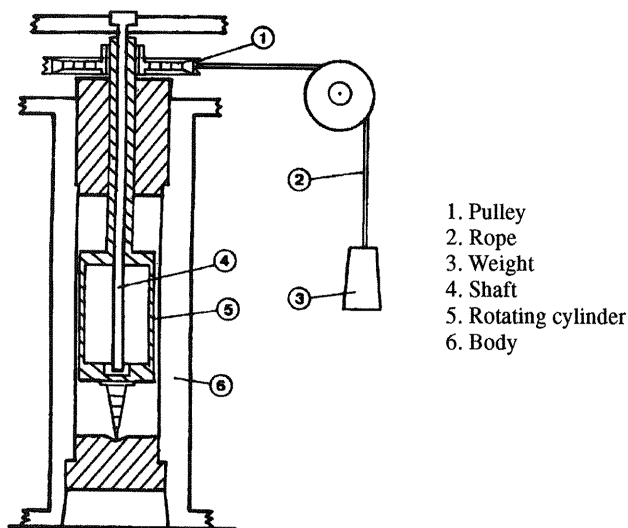


Figure 13.17 Old version of a coaxial viscometer

in the angular velocity of concentric cylindrical layers occurs as the distance from the layers to the rotating cylinder increases. The angular velocity of the layer in contact with the steady cylinder is zero.

Couette flow has a velocity field whose contravariant components are (2,22,29)

$$\dot{x}_1 = 0; \quad \dot{x}_2 = \omega(r); \quad \dot{x}_3 = 0 \quad (13.64)$$

in a cylindrical coordinate axis with $x_1 = r$, $x_2 = \theta$, and $x_3 = z$.

Let us assume that the coaxial cylinder has a length L and that the radii of the inner and outer cylinders are R_1 and R_2 , respectively. The shear stress acting on a cylindrical layer of fluid of radius r is related to the torque M applied to the inner cylinder by the expression

$$M = 2\pi r^2 L \sigma_{r,\theta} \quad (13.65)$$

On the other hand, the angular velocity ω of the concentric layers of fluid decreases from the inner to the outer cylinder, and the shear rate can be written as

$$\kappa = -r \frac{d\omega}{dr} \quad (13.66)$$

From Eqs. (13.65) and (13.66) and Newton's law ($\sigma_{r,\theta} = \eta\kappa$) we obtain

$$\frac{M}{2\pi r^2 L} = -\eta r \frac{d\omega}{dr} \quad (13.67)$$

The negative sign in this expression arises from the fact that for a device with the inner cylinder rotating and the outer one steady, the angular velocity decreases as r increases. However, the sign of $d\omega/dr$ is positive when the outer cylinder rotates and the inner one is stationary. Integrating Eq. (13.67) yields

$$\omega(r) = \frac{M}{4\pi\eta L} \left(\frac{1}{r^2} \right) + C \quad (13.68)$$

The constant C can be obtained from the second boundary condition given below:

$$\omega(R_1) = \Omega; \quad \omega(R_2) = 0 \quad (13.69)$$

The angular velocity profile is given by the expression

$$\omega(r) = \frac{M}{4\pi\eta L} \left(\frac{1}{r^2} - \frac{1}{R_2^2} \right) \quad (13.70)$$

By taking into account that $v = \omega r$, the velocity profile of the fluid layers in the Couette viscometer with rotating inner cylinder is given in Figure 13.18. Equation (13.70) in combination with the first boundary condition in Eq. (13.69) gives

$$\Omega = \frac{M}{4\pi\eta L} \left(\frac{1}{R_1^2} - \frac{1}{R_2^2} \right) \quad (13.71)$$

where Ω is the angular velocity of the rotating inner cylinder. Accordingly, once the torque and the angular velocity are known, the viscosity can be determined. A similar expression is obtained from an experimental device in which the inner cylinder is steady and the outer one rotates.

For non-Newtonian fluids a power law can be used to determine the viscosity. In this case.

$$\frac{M}{2\pi r^2 L} = \eta \left[r \left(-\frac{d\omega}{dr} \right) \right]^n \quad (13.72)$$

Solving this equation using the boundary conditions indicated in Eq. (13.69), we obtain the expression (29)

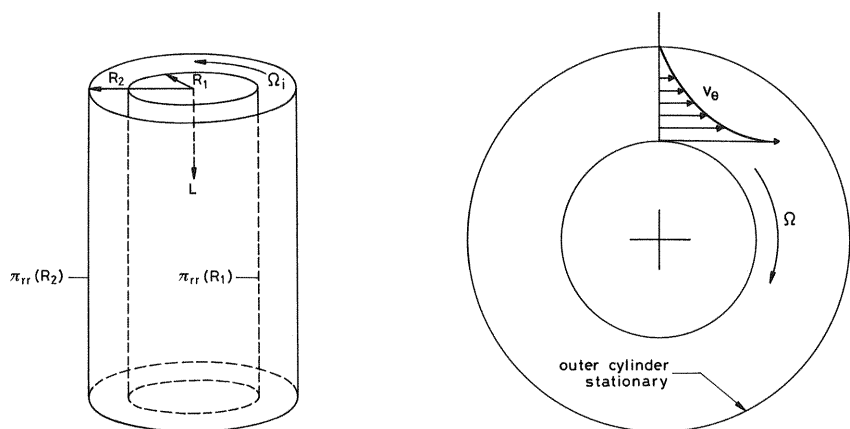


Figure 13.18 Schematic representations of a coaxial cylinder (left) and velocity profiles (right). The inner cylinder rotates and the outer one is steady.

$$M = 2\pi R_2^2 L \eta \left[\frac{2\Omega}{n \left[\left(\frac{R_2}{R_1} \right)^{2/n} - 1 \right]} \right]^n \quad (13.73)$$

The exponent n can be obtained from the slope of the double logarithmic plot of M versus Ω and the apparent viscosity from the intercept.

End effects, mostly due to additional resistance of the outer cylinder bottom, may alter the viscometric measurements performed with coaxial cylinders. These effects may be greatly reduced by using a small-gap geometry. End effects can be evaluated by measuring the viscosities of standard Newtonian fluids with a series of constant-diameter cylinders of different lengths and the same gap. The plot of torque versus length for various values of the angular velocity gives a straight line, the intercept of which with the abscissa is a correction term L_c . This term is equivalent to the additional length due to the end effects. Therefore, $L + L_c$ should be used instead of L in Eqs. (13.70) and (13.73).

13.10 CONE-PLATE VISCOMETERS

The cone-plate geometry is widely used in rheological measurements of viscoelastic fluids. The fluid is placed between a plate of radius R and a cone of the same radius. The angle, α , between the cone and the plate is usually smaller than 3° (see Fig. 13.19).

In cone-plate geometry, the velocity field of a simple shearing flow has the following components in a spherical coordinate system (2,23,29):

$$\dot{x}_1 = 0; \quad \dot{x}_2 = \omega(\theta); \quad \dot{x}_3 = 0 \quad (13.74)$$

in a spherical coordinates reference frame with $x_1 = \theta$, $x_2 = \phi$, and $x_3 = r$.

The shear stress can be obtained by taking into account that the torque applied on an infinitesimal surface of the fluid in contact with the rotating plate is $dM = 2\pi\sigma_{\theta\alpha}r^2 dr$. Hence, the shear stress and the shear rate can be written as

$$\sigma_{\theta\alpha} = \frac{dM}{2\pi r^2 dr}; \quad \kappa = \frac{r\Omega}{h} = \frac{\Omega}{\alpha} \quad (13.75)$$

where α is the angle between the cone and the plate. In Eq. (13.75) the relation $h = r \tan \alpha \cong \alpha$ was used. Accordingly,

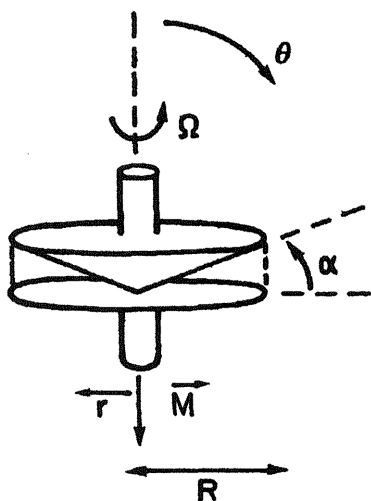


Figure 13.19 Schematic representation of a cone-plate rheometer.

$$\frac{dM}{2\pi r^2 dr} = \eta \frac{\Omega}{\alpha} \quad (13.76)$$

Integrating this equation gives the following expression for the torque:

$$M = \frac{2\pi R^3 \Omega \eta}{3\alpha} \quad (13.77)$$

The cone-plate geometry has several advantages over other geometries, one of the most important being that the shear rate is constant along the radius. This does not occur with alternative geometries. On the other hand, a very small amount of sample is required, an aspect of great importance in the determination of viscosities of polymers obtained in small amounts in research laboratories. The system allows good temperature control, and, finally, end effects are negligible for low rotational speeds.

Important disadvantages of this geometry are evaporation and free boundary effects for polymer solutions prepared with volatile solvents. Moreover, measurements are restricted to relatively low shear rates because polymer melts and other fluids will not stay in the gap at high rotational speeds. The cone-plate geometry is not recommended for measuring the viscosity of multiphase systems because in some cases domain sizes may be of the same order of magnitude as the gap size.

13.11 PLATE-PLATE VISCOMETERS

In plate-plate viscometers (Fig. 13.3), the shear stress and the shear rate are related to the torque M and angular velocity Ω respectively, by the expressions

$$\sigma_{z\theta} = \frac{dM}{2\pi r^2 dr} \quad \text{and} \quad \kappa = \frac{r\Omega}{h} \quad (13.78)$$

where h is the gap separation. For Newtonian fluids the relation between the shear stress and the shear rate is given by

$$\frac{dM}{2\pi r^2 dr} = \eta \frac{r\Omega}{h} \quad (13.79)$$

From this expression we obtain

$$M = \eta \frac{\pi R^4 \Omega}{2h} \quad (13.80)$$

The shear rate in this geometry depends on the radius, and since the viscosity of non-Newtonian fluids depends on the shear rate and thus changes with the radius, integration of Eq. (13.79) gives

$$M = 2\pi \left(\frac{\Omega}{h} \right) \int_0^R \eta(r) r^3 dr \quad (13.81)$$

This equation is more conveniently written in terms of the shear rate by means of the expression

$$M = 2\pi \left(\frac{h}{\Omega} \right)^3 \int_0^{\kappa} \eta(\kappa) \kappa^3 d\kappa = 2\pi \left(\frac{R}{\kappa_R} \right)^3 \int_0^{\kappa} \eta(\kappa) \kappa^3 d\kappa \quad (13.82)$$

where use was made of the expression given for the shear rate in Eq. (13.78). In Eq. (13.82), $\kappa_R (= \Omega R/h)$ is the shear rate at $r = R$. By taking the derivative of Eq. (13.82) with respect to the maximum shear rate, we obtain

$$\frac{d(M/2\pi R^3)}{d\kappa_R} = \eta(\kappa_R) - 3\kappa_R^{-4} \int_0^{\kappa_R} \eta(\kappa) \kappa^3 d\kappa \quad (13.83)$$

where Leibnitz's rule was used. This expression can alternatively be expressed in a more convenient way as (14)

$$\eta(\kappa_R) = \frac{M}{2\pi R^3 \kappa_R} \left[3 + \frac{d \ln(M/2\pi R^3)}{d \ln \kappa_R} \right] \quad (13.84)$$

This equation suggests that the determination of the viscosity of non-Newtonian fluids with plate-plate geometry requires that $\ln M$ first be plotted against $\ln \kappa_R$. Consequently, the determination of the shear-dependent viscosity requires that the torque be measured at different shear rates. The value of the viscosity is then determined with the value of the local slope in conjunction with Eq. (13.84). If the fluid obeys a power law, then

$$\ln M \sim n \ln \kappa_R \quad (13.85)$$

so that Eq. (13.84) becomes

$$\eta(\kappa_R) = \frac{M}{2\pi R^3 \kappa_R} (3 + n) \quad (13.86)$$

Plate-plate geometry has all the disadvantages of the cone-plate geometry and none of its advantages. However, this technique is better than the cone-plate geometry for measuring the viscosity of polymer melts, pastes, and suspensions containing large particles.

13.12 EXPERIMENTAL DETERMINATION OF NORMAL STRESSES. COAXIAL CYLINDERS

Normal stress effects are observed in many experiments. For example, concentrated polymeric solutions climb up the stirrer by effect of the normal stresses, in contrast with what occurs with low molecular weight liquids, in which inertial effects are dominant. Schematic representations of this behavior are shown in Figure 13.20. The streamlines of flow in polymer melts and concentrated solutions are arcs that pull out or partially stretch the

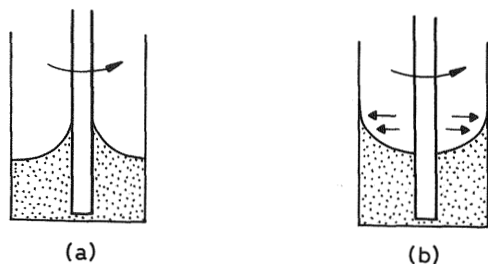


Figure 13.20 (a) Rod-climbing effect of a viscoelastic fluid caused by rotation of the rod in the fluid. (b) The same situation for a Newtonian fluid.

polymer chain. The chain tends to coil back up due to entropic driving forces and displays a retractive force, a component of which is given in Figure 13.21. This force squeezes the inner fluid of the vessel, forcing it to climb the stirring rod.

Normal stress differences can be observed in Couette flow, cone-plate and plate-plate geometries, and capillary flow. The only nonzero components of the stress tensor in coaxial cylinders are $\sigma_{r\theta}(r)$, $\sigma_{rr}(r)$, $\sigma_{\theta\theta}(r)$, and σ_{zz} . The r component of the equation of motion [Eq. (4.13)] is given by (14,22) [see Eq. (P4.6.6)]

$$\frac{\partial p}{\partial r} + \left(\frac{1}{r} \frac{d}{dr} (r\sigma_{rr}) - \frac{\sigma_{\theta\theta}}{r} \right) = \rho\omega^2 r \quad (13.87)$$

For any z position, Eq. (13.87) can be written as

$$\frac{d}{dr} (p + \sigma_{rr}) = \frac{d\pi_{rr}}{dr} = \rho\omega^2 r + \frac{\sigma_{\theta\theta} - \sigma_{rr}}{r} \quad (13.88)$$

After integrating this equation, the difference of total pressures measured at the outer and inner cylinders is given by

$$\pi_{rr}(R_2) - \pi_{rr}(R_1) = \int_{R_1}^{R_2} \left(\rho\omega^2 r + \frac{\sigma_{\theta\theta} - \sigma_{rr}}{r} \right) dr = \int_{R_1}^{R_2} \left(\rho\omega^2 r - \frac{N_1(r)}{r} \right) dr \quad (13.89)$$

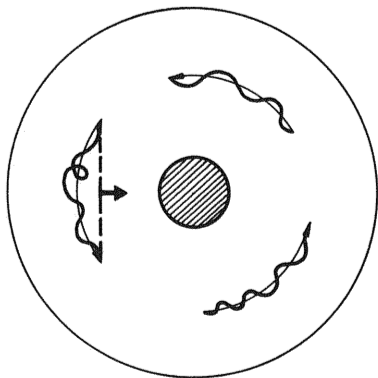


Figure 13.21 Schematic representation of a rod-climbing experiment, for a polymer solution viewed from the top. The dashed line represents a force component resulting from the retraction force of the chain.

where $N_1 (= \sigma_{rr} - \sigma_{\theta\theta})$ is the primary normal stress difference. Since the radius dependence of N_1 is not known, Eq. (13.89) cannot be integrated. However, for a small gap some mathematical handling of Eq. (13.89) leads to the approximate relationship (14)

$$\pi_{rr}(R_2) - \pi_{rr}(R_1) \approx -\frac{R_2 - R_1}{R_1} N_1 \quad (13.90)$$

For low molecular weight liquids, $N_1 = 0$ and, according to Eq. (13.89), $\pi_{rr}(R_2) > \pi_{rr}(R_1)$. This means that the inertial component forces the liquid to climb the outer steady cylinder. For polymeric melts and concentrated solutions, $N_1 > 0$ and $\pi_{rr}(R_2) < \pi_{rr}(R_1)$, so the pressure at the wall of the inner rotating cylinder is greater than the pressure at the outer wall of the steady cylinder. As a result the fluid will climb the inner cylinder wall. The act of the solution climbing the rotating cylinder is called the Weissenberg effect.

13.12.1 Cone-Plate Geometry

By effect of the normal stresses, a thrust among the plates occurs in non-Newtonian fluids that tends to separate them. This behavior is a consequence of the fact that tension along the lines of force causes the outer layers of liquid to squeeze inward upon the inner layers. Thus a pressure is built up between the cone and the plate from near zero in the edge to a maximum in the center.

Since there is no shear force in the r direction, the $r\phi$ and $r\theta$ components of the stress tensor are zero and the flow is symmetrical with respect to ϕ . By neglecting the inertial forces ($\rho r \omega^2 \rightarrow 0$), the r component of the equation of motion [Eq. (4.13)] for this system can be written as (14,22) [see Eq. (P4.7.3)]

$$\frac{\partial p}{\partial r} + \frac{1}{r^2} \frac{\partial}{\partial r} (r^2 \sigma_{rr}) - \frac{\sigma_{\theta\theta} + \sigma_{\phi\phi}}{r} = 0 \quad (13.91)$$

By taking into account that the total components are $\pi_{ii} = p + \sigma_{ii}$, Eq. (13.91) is expressed by

$$-\frac{1}{r^2} \frac{\partial}{\partial r} (r^2 \pi_{rr}) + \frac{\pi_{\theta\theta} + \pi_{\phi\phi}}{r} = 0 \quad (13.92)$$

or in the alternative form,

$$\frac{\partial \pi_{rr}}{\partial \ln r} = \pi_{\theta\theta} + \pi_{\phi\phi} - 2\pi_{rr} \quad (13.93)$$

However,

$$\pi_{rr} - \pi_{\theta\theta} = \sigma_{rr} - \sigma_{\theta\theta} \quad (13.94)$$

and since the normal stress difference, which is a unique function of the shear rate, has a constant value, one obtains

$$\frac{\partial \pi_{rr}}{\partial \ln r} = \frac{\partial \pi_{\theta\theta}}{\partial \ln r} = \frac{\partial \sigma_{\theta\theta} + p}{\partial \ln r} \quad (13.95)$$

By taking this expression into account, Eq. (13.93) can be written as

$$\frac{\partial}{\partial \ln r} (p + \sigma_{\theta\theta}) = (\sigma_{\phi\phi} - \sigma_{\theta\theta}) + 2(\sigma_{\theta\theta} - \sigma_{rr}) = \text{constant} \quad (13.96)$$

Integration of this equation from $r = r$ to $r = R$ gives

$$\pi_{\theta\theta}(r) = \pi_{\theta\theta}(R) + [(\sigma_{\phi\phi} - \sigma_{\theta\theta}) + 2(\sigma_{\theta\theta} - \sigma_{rr})] \ln \frac{r}{R} \quad (13.97)$$

According to this equation, the thrust profile can, in principle, be measured on the upper cone or lower plate. Note that the normal stress differences are assumed to be independent of position. By plotting $\pi_{\theta\theta}(r)$ against $-\ln(r/R)$, a straight line is obtained from whose slope a combination of the primary $(\sigma_{\phi\phi} - \sigma_{\theta\theta})$ and secondary $(\sigma_{\theta\theta} - \sigma_{rr})$ normal stress differences is obtained. Though the pressure profile is difficult to measure, the primary stress difference can be readily determined from the force F exerted on the cone or plate. The value of F is given by

$$F = -2\pi \int_0^R \pi_{\theta\theta} \Big|_{\theta=\pi/2} r dr \quad (13.98)$$

By substituting Eq. (13.97) into Eq. (13.98) and integrating by parts, we obtain

$$F = -\pi R^2 \pi_{\theta\theta}(R) + \frac{1}{2} \pi R^2 (\pi_{\phi\phi} + \pi_{\theta\theta} - 2\pi_{rr}) \quad (13.99)$$

By using the boundary condition that at the free surface ($r = R$) the sample presents a spherical shape with no effect of surface tension, we have $\pi_{rr}(R) = -p_a$ where p_a is the atmospheric pressure. Then rearrangement of Eq. (13.99) gives

$$F = \pi R^2 p_a - \pi R^2 [\pi_{\theta\theta}(R) - \pi_{rr}(R)] + \frac{1}{2} \pi R^2 [(\pi_{\theta\theta} - \pi_{rr}) + (\pi_{\phi\phi} - \pi_{rr})] \quad (13.100)$$

If we consider that

$$\pi_{\theta\theta}(R) - \pi_{rr}(R) = \pi_{\theta\theta} - \pi_{rr} = \sigma_{\theta\theta} - \sigma_{rr} \quad (13.101)$$

and

$$\pi_{\phi\phi} - \pi_{rr} = (\sigma_{\phi\phi} - \sigma_{\theta\theta}) + (\sigma_{\theta\theta} - \sigma_{rr}) \quad (13.102)$$

Eq. (13.100) becomes

$$F - p_a = \frac{1}{2}\pi R^2(\sigma_{\phi\phi} - \sigma_{\theta\theta}) = \frac{1}{2}\pi R^2(\sigma_{22} - \sigma_{11}) \quad (13.103)$$

Hence the primary normal stress difference N_1 is given by (14,39)

$$N_1 = \sigma_{22} - \sigma_{11} = \frac{2F^*}{\pi R^2} \quad (13.104)$$

where $F^* = F - p_a$ is the normal force in excess of that due to the atmospheric pressure.

In the development of Eq. (13.104), inertial forces have been neglected, and consequently this expression can be used only for low shear rates. It should be pointed out that in the shear rate region in which the flow behavior is Newtonian, the scaling law $N_1 \sim \kappa^2$ predicted for second-order fluids is fulfilled. Centrifugal forces give rise to circulation of fluid toward the center at the fixed plate and toward the edges at the rotating cone. This produces higher torques and negative normal forces for Newtonian fluids. Therefore, to minimize centrifugal force effects in the measurements of the primary normal stress difference of polymer melts and solutions, it is convenient to use high viscosity solvents. Methods have been developed for torque and normal force corrections that the reader will find elsewhere (14). In spite of the shortcomings involved in the cone-plate geometry, this is at present the best method for measuring N_1 for polymer melts and solutions.

13.13 FACTORS GOVERNING THE NON-NEWTONIAN BEHAVIOR OF POLYMERS

13.13.1 Shear Rate

The main factors governing the non-Newtonian behavior of polymer melts and concentrated solutions are the weight-average molecular weight, molecular weight distribution, and molecular topology (branching), and concentration. As can be seen in Figure 13.22, the curves showing the evolution of viscosity with shear rate for several fractions of the same polymer of differ-

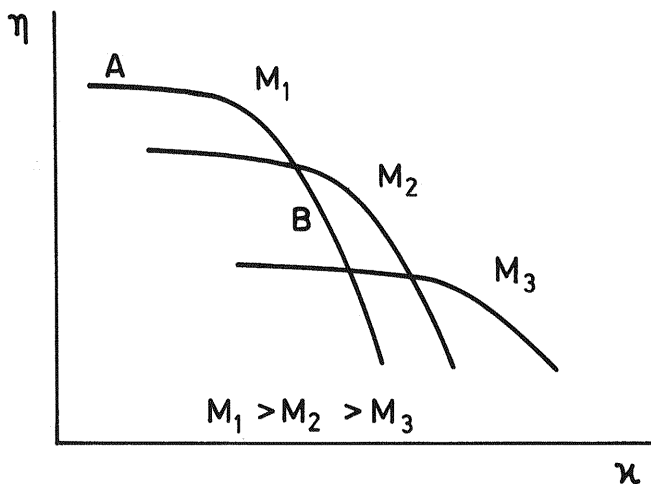


Figure 13.22 Schematic plot showing the influence of molecular weight on the variation of the viscosity with the shear rate.

ent molecular weights exhibit the same shape. In the curves, one region, *A*, can be distinguished at low values of κ where the viscosity remains nearly independent of the shear rate, followed by another, *B*, in which a relatively sharp fall in the value of the viscosity with increasing shear rate occurs. Moreover, the region in which the behavior is nearly Newtonian becomes shorter as the molecular weight increases.

To explain the non-Newtonian behavior of polymer melts it is convenient to remember that the domains of different molecular chains overlap and the chains become entangled. Entanglements confer a physical network structure to polymer melts and concentrated solutions. Though the entanglements, unlike chemical cross-linking, are not permanent, the response of entangled networks to an external shear stress is similar to that of a cross-linked rubber at short times (40). Hence the entangled structure of polymer melts and concentrated solutions governs the flow properties of these materials. As was shown elsewhere [Eq. (9.33)], the average relaxation time of an entangled network can be expressed as

$$\langle \tau \rangle = \eta_0 J_e^0 \quad (13.105)$$

where η_0 and J_e^0 are, respectively, the viscosity at zero shear rate and the steady-state compliance. The value of $\langle \tau \rangle$ can be viewed as the average time necessary for the renewal of the entangled network. For flows in which the reciprocal of the shear rate is larger than $\langle \tau \rangle$, that is, for low values of κ , the

process occurs in a network whose entanglement density is not affected by the flow process. In these conditions, the viscosity does not depend on the shear rate and the flow is Newtonian. For shear rates at which $\kappa^{-1} < \eta_0 J_e^0 (= \langle \tau \rangle)$, the flow will be compatible only with an entangled network with a lower relaxation time, that is with a network of lower entanglement density. Since the energy is dissipated in the entanglement points during flow, a decrease in the density of these points with increasing shear rate should decrease the viscosity. As a consequent, the higher the shear rate, the lower the viscosity must be. According to this approach, a critical shear rate κ_c will be found above which the viscosity decreases with increasing values of κ , that is, the system exhibits non-Newtonian behavior. The value of κ_c can be obtained by means of the equation (39)

$$\kappa_c J_e^0 \eta_0 \approx 1 \quad (13.106)$$

The viscosity at zero shear rate is strongly dependent on molecular weight for long chains ($\eta = KM^{3.4}$, $M > 2M_e$), while J_e^0 remains nearly constant for nearly monodisperse fractions ($J_e = \text{constant}$, $M > 6M_e$). As a consequence, Eq. (13.106) suggests that the critical shear rate above which the flow exhibits non-Newtonian behavior strongly decreases with increasing molecular weight.

In addition to regions *A* and *B* in the curves showing the shear rate dependence of the viscosity, a third region, *C*, could be postulated. This latter region would occur at shear rates high enough that the fluid structure in terms of molecular entanglements is lost. In this case only segmental frictional forces would resist the flow, just as occurs in low molecular weight compounds, thereby giving rise to a Newtonian response (40). the reason the onset of this Newtonian region is not experimentally observed is that the molecular chains cannot move fast enough to rearrange and relieve the incurred shear stress. As result, chain scission occurs, mostly in the longest chains that have the longest relaxation times. Moreover, lowering the temperature causes a decrease in molecular mobility, and consequently the response time will increase. Hence, for a given molecular weight, a decrease in temperature will cause more chain scission at a given shear rate.

13.13.2 Molecular Weight, Molecular Heterodispersity, and Molecular Topology

The influence of molecular heterodispersity (or molecular weight distribution) on the evolution of viscosity with shear rate is shown (41) in Figure 13.23. As the width of the distribution increases, the flow departs from Newtonian behavior at lower values of κ_c than would occur in a nearly

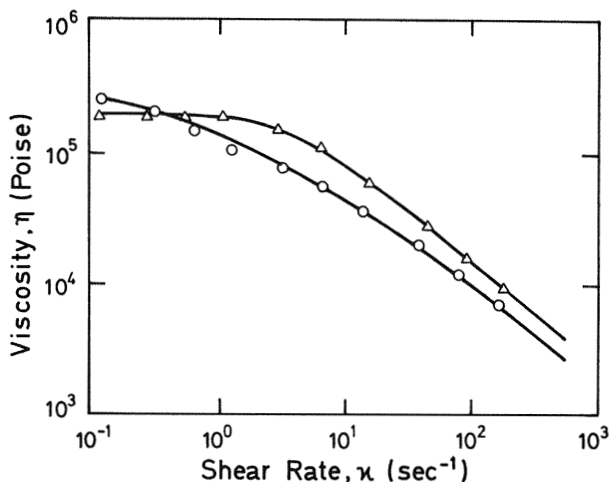


Figure 13.23 Influence of the width of the molecular weight distribution on the shear rate dependence of the viscosity. (Δ), Narrow distribution; (\circ), wide distribution. (From Ref. 41.)

monodisperse polymer with a molecular weight similar to the average molecular weight of the heterodisperse polymer. Moreover, the drop in viscosity with increasing values of shear rate is lower in wide distributions than in narrow ones with the same molecular weight average. This behavior can be explained by taking into account that wide distributions embody extremely high and low molecular weight tails. Long chains in the heterodisperse distribution enhance the steady-state compliance (J_e^0) and η_0 , thus shifting the critical shear rate to lower values (39,40). In contrast, the low molecular weight tails exhibit non-Newtonian behavior at relatively large values of κ . The combined effects give a smaller drop in viscosity than that occurring in a narrow distribution with comparable average molecular weight. Moreover, the fall of η with κ extends over a rather wide range of values of shear rate.

Molecular topology has a decisive influence in the non-Newtonian behavior of polymers. Branches of high molecular weight produce an anomalous dependence of η on M in the sense that the value of the viscosity is greater than that corresponding to linear chains of similar molecular weight (42,43). In contrast with what occurs in linear chains, the steady state compliance for branched chains increases with increasing molecular weight. Consequently, ηJ_e^0 is larger for branched polymers than for linear ones, and hence branches of high molecular weight decrease the shear rate at which the flow departs from Newtonian behavior (see Fig. 13.24).

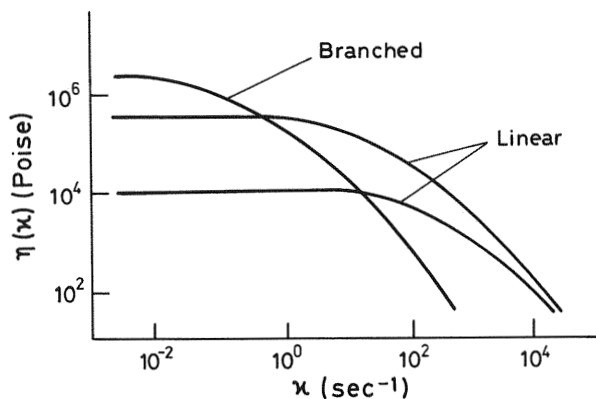


Figure 13.24 Schematic representation showing the influence of branching on the variation of viscosity with shear rate.

13.13.3 Temperature

The viscosity of polymers is strongly dependent on temperature. The viscosity at zero shear rate obeys the VFTH equation at temperatures above T_g , while at temperatures much higher than T_g it is described by the Arrhenius equation. Curves showing the dependence of viscosity on shear rate, at different temperatures, are plotted in Figure 13.25 (44). Owing to the fact that η_0 decreases dramatically with increasing temperature while J_e^0 undergoes only a relatively small increase, the shear rate at which the flow departs from Newtonian behavior increases as the temperature increases. As shown in Figure 13.26, horizontal shifts of the normalized isotherms with respect to reference isotherm produce a master curve that permits us to predict the dependence of η on the shear rate in a wide interval of values of κ .

13.14 NON-NEWTONIAN VISCOSITY MODELS

Several models have been proposed to describe the dependence of viscosity on shear rate. One of the most used in engineering applications is the two-parameter Ostwald–De Waele model given by (45)

$$\eta = m|\kappa|^{n-1} \quad (13.107)$$

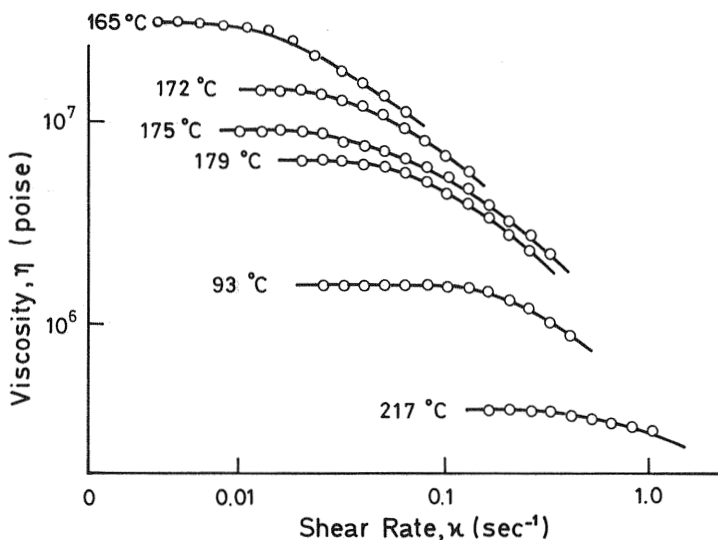


Figure 13.25 Variation of viscosity with shear rate at indicated temperatures for linear polystyrene (From Ref. 44.)

where $n < 1$ for shear thinning fluids and $n > 1$ for shear thickening fluids. A serious drawback of this model is that the viscosity of shear thinning fluids goes to infinity as the shear rate approaches zero. In general, the model gives anomalously high values for the viscosity of shear thinning fluids in the region where the shear rate is very small.

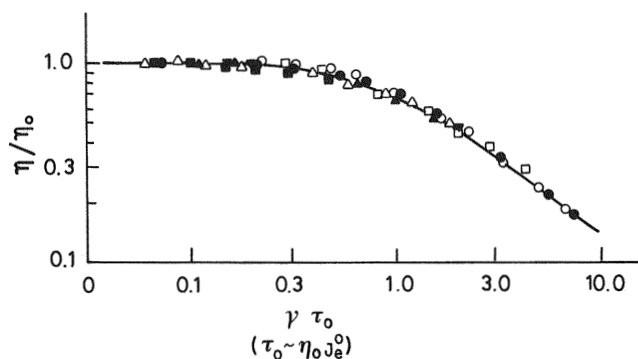


Figure 13.26 Time-temperature superposition for the results of Figure 13.25

The Ellis (46), Carreau (47), and Cross–Williamson (48) models are three-parameter models. The Ellis model gives the viscosity as a function of η_0 , the shear rate σ , the parameter $\sigma_{1/2}$, which is the shear rate for which the viscosity is $\eta_0/2$, and a dimensionless parameter α . The equation is

$$\eta = \frac{\eta_0}{1 + |\sigma/\sigma_{1/2}|^{\alpha-1}} \quad (13.108)$$

The model predicts a zero shear rate viscosity at low values of the shear rate; at higher values of κ , the model predicts shear-thinning behavior, while η is underpredicted at very high shear rates.

The Carreau model is a function of η_0 , a characteristic time t_1 , and a dimensionless parameter n . It can be written as

$$\eta = \frac{\eta_0}{[1 + (t_1\kappa)^2]^{(1-n)/2}} \quad (13.109)$$

Though the model predicts very well the variation of viscosity with shear rate for polymer solutions, it slightly underestimates the zero shear rate viscosity.

The Cross–Williamson model is expressed by

$$\eta = \frac{\eta_0}{[1 + (t_1\kappa)]^{1-n}} \quad (13.110)$$

This model also gives a good account of the shear rate dependence of the viscosity for shear thinning polymers. It slightly overpredicts the value of η_0 and it also predicts longer transitions from the zero shear rate to the shear thinning behavior.

Four- and five-parameter models have also been proposed. An example of the four-parameter model is the Cross–Williamson model given by (14)

$$\frac{\eta - \eta_\infty}{\eta_0 - \eta_\infty} = \frac{1}{1 + |t_1\kappa|^{1-n}} \quad (13.111)$$

where η_∞ is the viscosity when $\kappa \rightarrow \infty$. The corresponding extension to the four-parameter Carreau model can be readily made (49).

13.15 COX–MERZ RULE

By comparing the viscosity of polystyrene samples obtained by oscillatory measurements and in steady-state conditions, Cox and Merz (50) found that

the modulus of the complex viscosity at the angular frequency ω was roughly equal to the viscosity obtained at a shear rate $\dot{\gamma} = \omega$. That is,

$$\eta(\dot{\gamma}) = |\eta^*(\omega)|_{\dot{\gamma}=\omega} \quad (13.112)$$

where $|\eta^*(\omega)| = [\eta'{}^2(\omega) + \eta''{}^2(\omega)]^{1/2}$. This relationship holds for homogeneous polymer solutions and melts, as shown in Figure 13.27 for poly(oxethylene) solutions (51). The empirical Cox–Merz relation is important because it allows us to determine the shear rate dependence of the viscosity at shear rates significantly higher than those permitted for cone–plate and plate–plate geometries.

13.16 INFLUENCE OF DILUENTS AND PLASTICIZERS, BLENDS, AND FILLERS ON FLOW

Diluents and plasticizers in polymeric systems increase the steady-state compliance and decrease the zero shear rate viscosity. These two combined opposing effects give rise to a diminution in the value of $\eta_0 J_e^0$. Hence the critical value of the shear rate in dilute systems is shifted to higher values as the dilution increases (see Fig. 13.28).

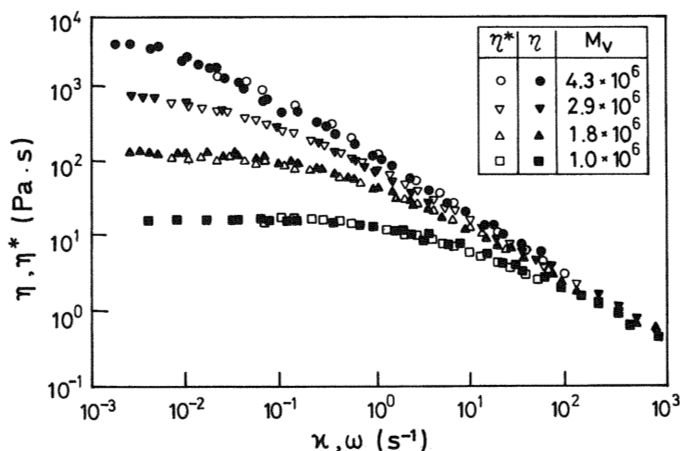


Figure 13.27 Comparative plots showing the variation of the viscosity η and the modulus of the complex viscosity, $|\eta^*|$, as functions of the shear rate, κ , and the frequency, ω , respectively. (From Ref. 51.)

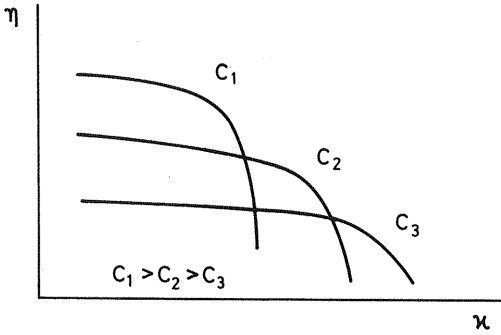


Figure 13.28 Schematic plot showing the influence of concentration on the shear rate dependence of the viscosity of polymer solutions.

The flow behavior of blends depends on the compatibility of their components. The viscosity of a compatible blend, for example polystyrene and polyoxyethylene, is the average of the viscosity of the components (52). Blends made up of high viscosity incompatible polymers may have lower viscosity than either component (53) (see Fig. 13.29). This effect may be the

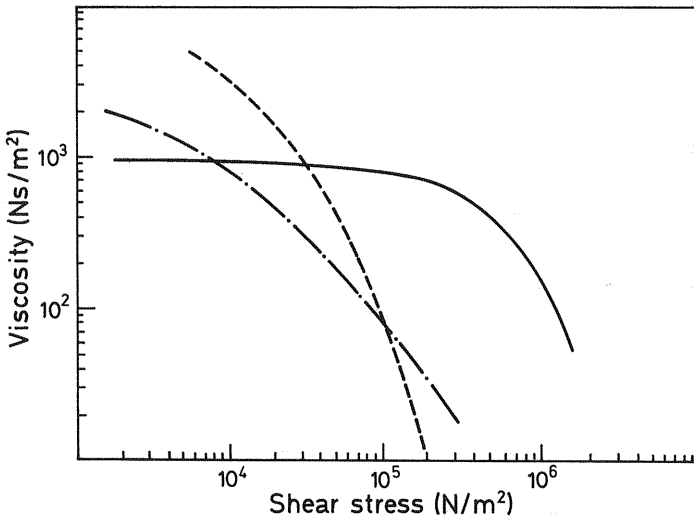


Figure 13.29 High viscosity blends prepared from incompatible polymers at 275°C. (—), polycarbonate (PC); (---), 4-methyl pentene-1 (M); (- · -), 50/50 PC/MP blend. (From Ref. 36.)

result of the weakness at the planes between the interfaces. Finally, low viscosity melts may form blends that have higher viscosity than either polymer component alone (36) (see Fig. 13.30). These latter blends are highly elastic, presumably as a consequence of the large internal surface that is produced at a $1\ \mu\text{m}$ level. During flow, the spherical shape of the droplet is deformed to an ellipsoidal form, thus greatly increasing the surface area. The high elasticity exhibited by these blends is the result of the fact that the work done during the flow process is recovered as the stress is removed and the droplet reverts to its spherical shape. An interesting review of the rheology of polymer blends is given in Ref. 54.

Fillers usually enhance the viscosity of the polymer melts. The viscosity of these systems depends not only on the characteristics of the melt but also to a great extent on the nature and volume of the filler. Several empirical relationships have been proposed between the viscosity of the melt and that of the melt filled with noninteractive particles for Newtonian flow. Among them, the empirical equation of Maron and Pierce (55) stands out:

$$\frac{\eta_c}{\eta} = \left(1 - \frac{c}{c_0}\right)^{-2} \quad (13.113)$$

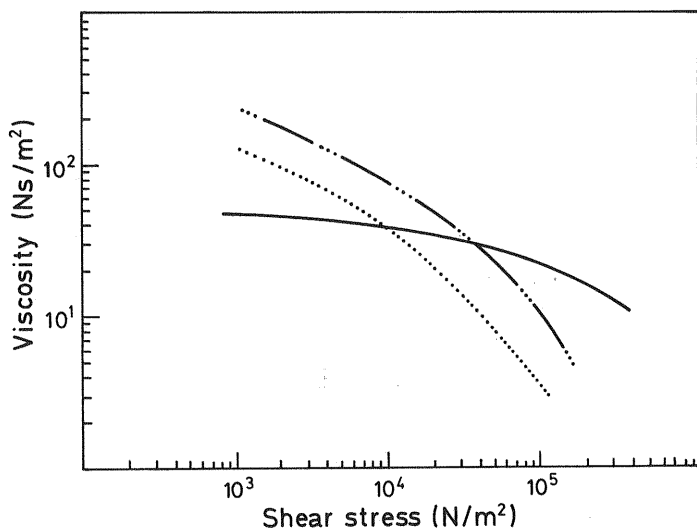


Figure 13.30 Blends of low viscosity polymers: (—), nylon 66; (···), polypropylene; (- · · -), 70/30 nylon-polypropylene blend.

where η is the viscosity of the polymer, η_c is the viscosity of the filled melt at a volume concentration c of filler, and c_0 is the volume concentration for close packing. The value of c_0 for highly filled polymers may range from 0.61 for glass beads to 0.34 for mica.

As shown in Figure 13.31, the curves describing the variation in the viscosity of polymers filled with homodisperse noninteractive spheres are reminiscent of those of the unfilled polymers, at least up to a solid fraction close to maximum packing (56). The data fit to the Carreau equation (47)

$$\eta_s = \eta_{s0} [1 + (t_s \kappa)^2]^{(n-1)/2} \quad (13.114)$$

where the subscript s refers to the suspension, η_{s0} is the zero shear viscosity, and t_s is a characteristic time. The results at hand suggest that the non-Newtonian viscosity of a filled polymer at a certain shear stress can be obtained from that of the polymer at the same shear stress by means of Eq. (13.113). Finally, polymers filled with polydisperse spheres exhibit lower viscosity than their counterparts containing the same volume fraction of homodisperse fillers.

In most cases the elastic response of filled polymers is severely reduced with respect to that of the polymer, though occasionally fillers may form an entangled structure with the melt exhibiting an anomalous elastic response. The study of the flow behavior of polymers filled with interacting particles presents serious complications. A major one is the agglomeration of

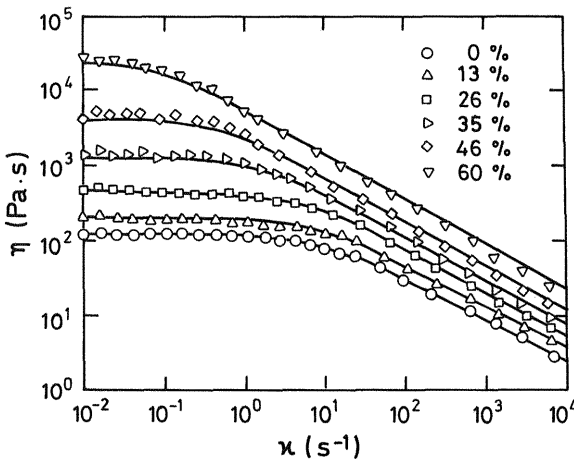


Figure 13.31 Influence of the volume fraction of glass spheres dispersed in a thermoplastic polymer at 150°C on the viscosity. (From Ref. 56.)

particles when interparticle interactions compared to viscous forces are important.

13.17 PARAMETERS INFLUENCING THE FIRST NORMAL STRESS DIFFERENCE

Because the value of N_1 depends on the square of the viscosity, all the parameters enhancing the viscosity will affect the primary normal stress difference. Thus N_1 increases with molecular weight and concentration (51) (see Fig. 13.32). The typical behavior of the shear rate dependence of both the shear stress and the normal stress difference N_1 for a fluid is shown in Figure 13.33. At very low shear rates, N_1 is lower than the shear stress. However, by taking into account that $N_1 \sim \kappa^2$ and $\sigma_{12} \sim \kappa$, a shear rate κ_c may be reached above which $N_1 > \sigma_{12}$, the difference $N_1 - \sigma_{12}$ being larger the larger the shear rate. The fluid is Newtonian (viscosity is constant) for values of κ in which $N_1 < \sigma_{12}$; however, for $\kappa > \kappa_c$ the curves show that $\sigma_{12} < \eta_0 \kappa$, and consequently the behavior is non-Newtonian.

The time-temperature correspondence principle holds not only for the viscosity but also for the normal stresses. In the latter case, however, the

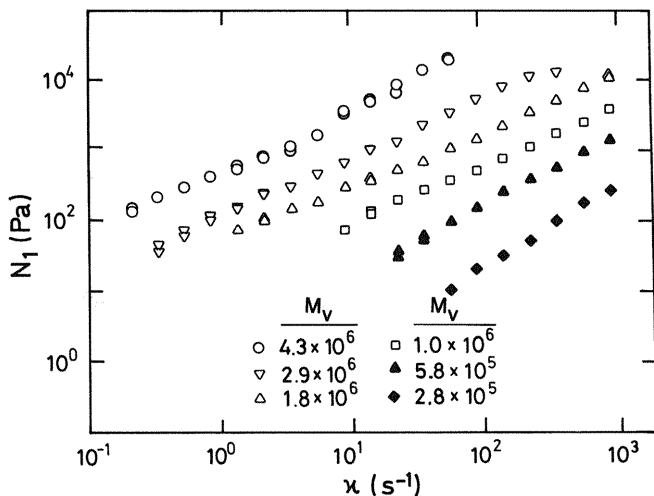


Figure 13.32 Primary normal stress difference as a function of the shear rate and molecular weight for 3% (mass) poly(oxyethylene) solutions in water and glycerine. (From Ref. 51.)

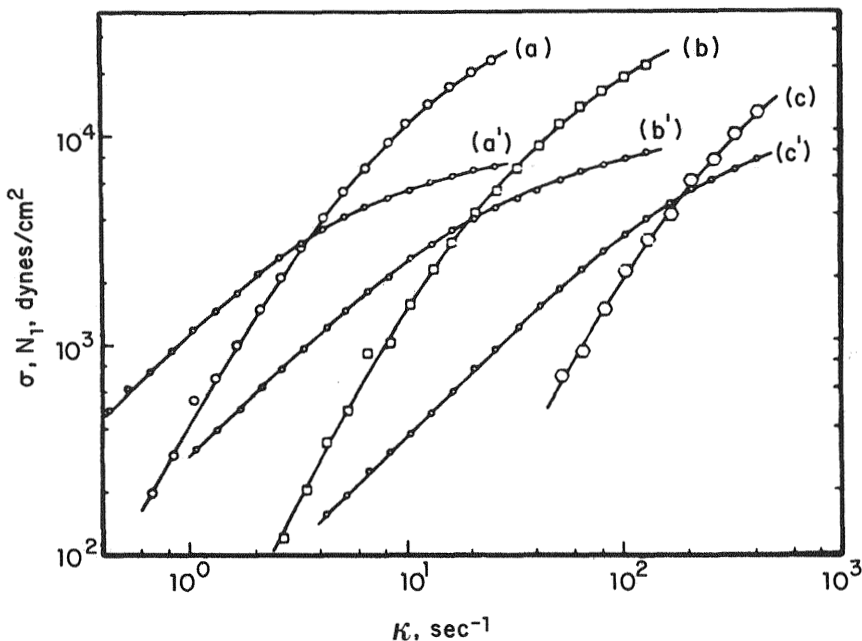


Figure 13.33 Variation of shear stress (a' , b' , c') and primary normal stress (a , b , c) with the shear rate for three fractions of a viscosity-thinning polymer.

temperature dependence of the results expressed in terms of N_1/σ^2 [Eq. (13.26)] is nearly negligible. Actually, the decrease that takes place in N_1 as an effect of the increase in temperature is balanced by the relative decrease that occurs in σ^2 , and hence the ratio N_1/σ^2 remains nearly constant.

The shear rate dependence of the viscosity and that of the normal stress difference N_1 for a viscoelastic fluid follow opposite trends. Thus the first parameter decreases with increasing values of κ , while the second increases. It is noteworthy to remark once more that viscoelastic fluids may present nonlinear effects, expressed by the normal stresses, in regions in which the shear stress is a linear function of the shear rate. However, these viscoelastic systems are still called Newtonian fluids due to the fact that the viscosity is independent of the shear rate.

13.18 DIE SWELLING

The non-Newtonian behavior of polymers has important technological implications. Thus the decrease in viscosity with increasing shear rate

makes it possible in many cases to carry out the processing of polymeric materials at temperatures low enough to avoid degradative effects in the molecular chains. The molecular chains flowing in a capillary are partially uncoiled and oriented in the direction of flow. Once the oriented chains leave the capillary, they re-coil, and the diameter of the extrudate becomes higher than that of the capillary. When the length of the capillary increases, the residence time of the macromolecules in the capillary increases and the molecules have more time to adopt the conformations of lower energy compatible with the force field. As a consequence, re-coiling of the oriented molecules after they leave the capillary decreases as the length of the capillary L increases. Consequently, the die swelling ratio D/D_0 , where D and D_0 are the diameters of the extrudate and capillary, respectively, decreases as L increases. This behavior is schematically represented in Figure 13.34.

From a phenomenological point of view, the swelling of the extrudate can be explained in terms of the normal stresses. As the melt leaves the die, the confinement by the capillary wall is no longer acting and the tension along the lines of flow draws the extrudate back so that it rearranges in a larger diameter. Since the first normal stress N_1 is dependent on the square of the shear rate, the D/D_0 ratio will increase with increasing values of κ . Equation (13.25) also predicts, at least at the qualitative level, the effect of temperature on the D/D_0 ratio. Actually, the first normal stress experiences

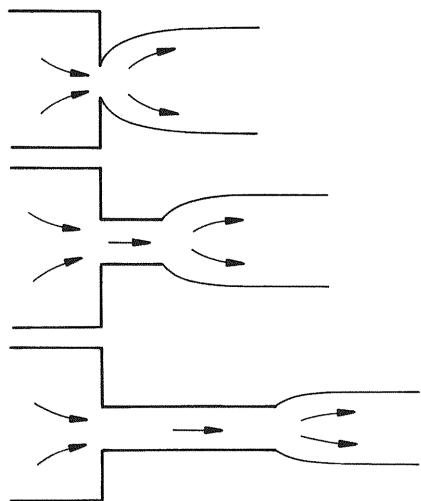


Figure 13.34 Schematic representation of swell ratio with shear rate at various temperatures for commercial polystyrene. (From Ref. 41.)

a sharp decrease with increasing temperature because $N_1 \sim \eta_0^2$. Hence, for a given shear rate, the D/D_0 ratio will decrease as temperature increases (41). This behavior is clearly shown in Figure 13.35, where values of D/D_0 for polystyrene are plotted as a function of the shear rate at selected temperatures.

Molecular heterodispersity has a strong influence on the swelling ratio. According to Eq. (13.25), N_1 depends on the steady-state compliance, J_e^0 . Since J_e^0 undergoes a high increase with molecular heterodispersity, D/D_0 is expected to increase with distribution breadth at constant shear rate (41). The dependence of D/D_0 for narrow and wide distributions, shown in Figure 13.36, is in agreement with this prediction. In general, the viscosity and the swell ratio show opposite dependence on the shear rate. Thus while the viscosity decreases with increasing shear rate, the swell ratio increases. This behavior is illustrated in Figure 13.37.

13.19 MELT INDEX

The melt index test, widely used for technological purposes, measures the rate of extrusion of a polymer melt through a given capillary (57). This is a

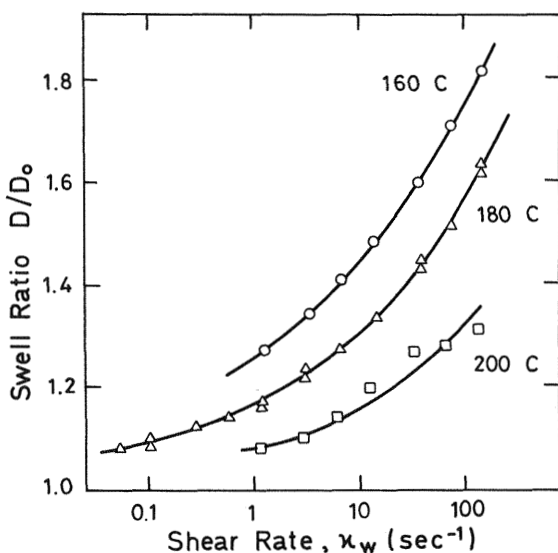


Figure 13.35 Variation of swell ratio with shear rate at various temperatures for commercial polystyrene. (From Ref.41.)

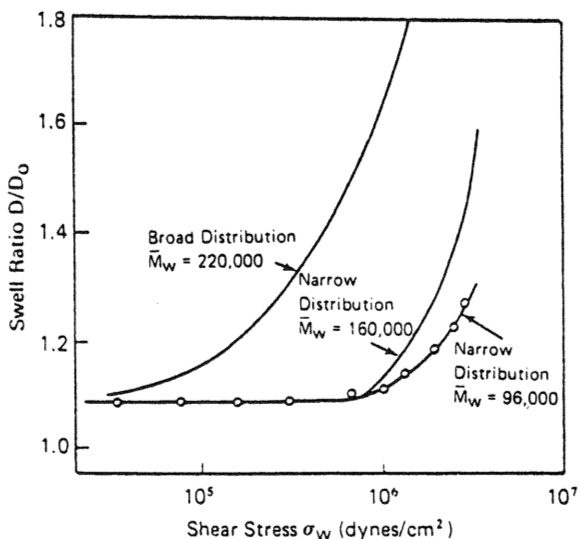


Figure 13.36 Curves showing the variation of the swell ratio for narrow and broad molecular weight distributions. (From Ref. 39.)

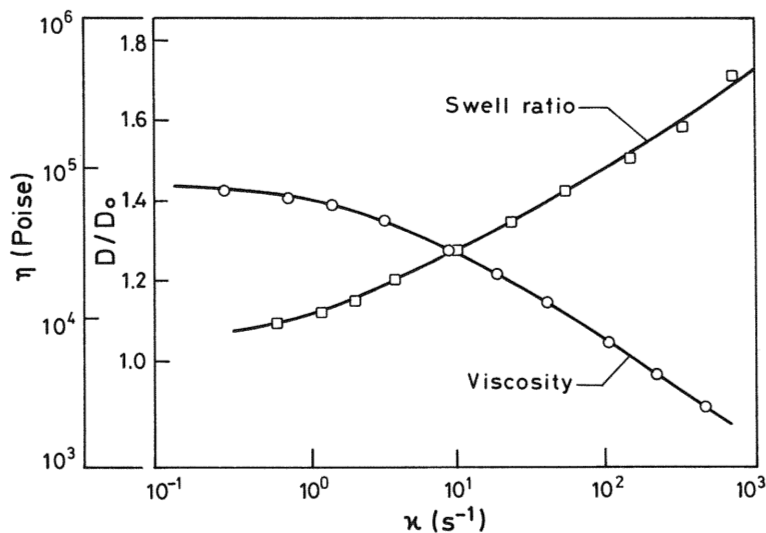


Figure 13.37 Dependence of both viscosity and swell ratio on the shear rate. (From Ref. 39.)

simplified variant of the capillary flow experiment. A sketch of the melt index apparatus together with the pertinent dimensions and specifications is given in Figure 13.38. Polymer in granular form is fed into the apparatus and is melted by heating at a temperature $T > T_m$, where T_m is the melting temperature of the polymer. Then the viscoelastic liquid at temperature T is forced through the capillary by a pressure induced by a piston of mass M . The flow is determined by weighing the extrudate that has flowed through the orifice in a given time. This test is especially useful in quality control and product specification of polyethylene. In this case, the flow rate at 190°C under a mass of 2.160 kg (≈ 0.30 MPa), measured in grams per 10 minutes, is the melt flow index (MFI). In order for resins with different apparent viscosities and melting points to be indexed, another 12 tests have been specified with T in the range of 125 – 275°C and pressure in the interval 0.045 – 3.0 MPa.

13.20 THIXOTROPY AND RHEOPEXY

For Newtonian fluids the viscosity is independent of time. However, for most non-Newtonian fluids the viscosity at a shear rate high enough to place the fluid in the non-Newtonian region evolves with time as schematically indicated by the lower curve of Figure 13.39. The viscosity decreases with time until steady-state conditions are reached. This phenomenon is called thixotropy. The cause of this behavior lies in the fact

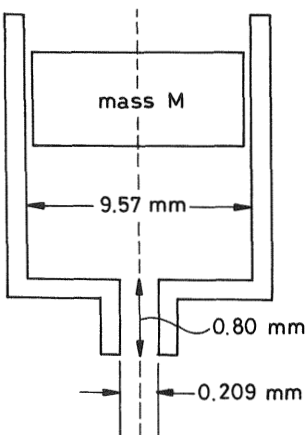


Figure 13.38 Melt index apparatus.

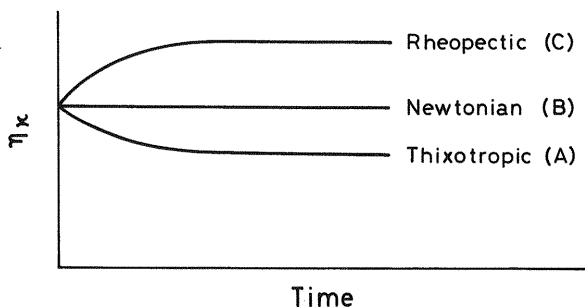


Figure 13.39 Time dependence of viscosity for different types of fluids: A, thixotropic; B, Newtonian; C, rheopectic.

that at the beginning of the experiment the entanglement density is compatible with that of the Newtonian region. It takes time to reach a structure compatible with that of the specific shear rate in the non-Newtonian region. A certain amount of time is needed to reach the steady state. Obviously, the transition time will be dependent on external variables such as temperature and pressure that affect the liquid structure as well as internal variables such as molecular weight, molecular weight distribution, and degree of branching.

The viscosity of some fluids (particle solutions or suspensions) measured at a fixed shear rate that places the fluid in the non-Newtonian regime increases with time as schematically shown by curve *C* of Figure 13.39. This behavior can be explained by assuming that in the Newtonian region the particles pack in an orderly manner, so flow can proceed with minimum interference between particles. However, high shear rates facilitate a more random arrangement for the particles, which leads to interparticle interference and thus to an increase in viscosity. Models that illustrate the thixotropic and rheopectic behavior of structural liquids can be found elsewhere (58,59).

13.21 STRETCHING FLOW

During stretching flow, material is drawn from one cross-sectional area to another. This type of flow dominates fibre, film, blow molding, and vacuum forming processes (57). Let us assume that a filament of a molten polymer is hauled off under a force F (see Fig. 13.40). Taking the die of the extruder as the origin of the reference frame, the cross-sectional area A of the filament

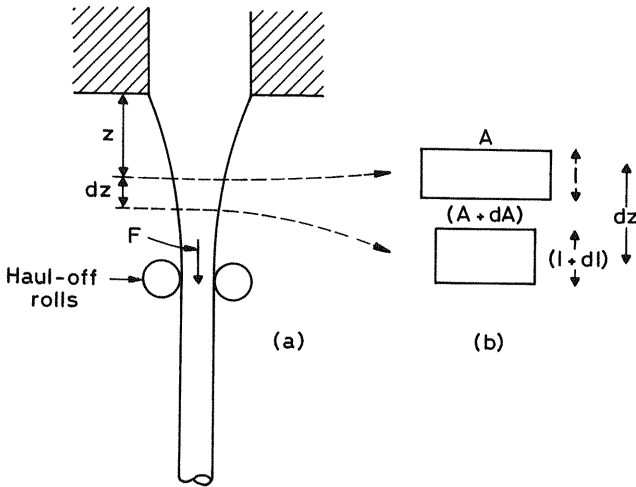


Figure 13.40 Filament of liquid polymer continuously pulled from a reservoir by a force F .

decreases as z increases. Both the stress $\sigma [= F/A(z)]$ and the velocity of the extrudate increase as z increases. If at time t the velocity of a point at distance z is v , the motion of the point after a time dt is $dz = v dt$. In moving the point from z to $z + dz$, the cross-sectional area changes from A to $A + dA$. By considering that $Az = (A + dA)(z + dz)$, we obtain

$$\frac{dA}{A} = -\frac{dz}{z} \quad (13.115)$$

where the second order $dA dz$ was considered negligible. On the other hand, the volume flow $Q (= Av)$ is constant and consequently independent of z . Then $dQ = A dv + v dA = 0$, leading to the relationship

$$\frac{dA}{A} = -\frac{dv}{v} \quad (13.116)$$

From Eqs. (13.115) and (13.116) we obtain

$$d\varepsilon_t = \frac{dz}{z} = \frac{dv}{v} \quad (13.117)$$

where ε_t is the change in strain as the element moves for z to $z + dz$. Let us assume that the extrusion process is carried out at temperature high enough

that the response can be considered to be mainly viscous. In that case the strain rate can be written as

$$\frac{d\varepsilon_t}{dt} = \frac{dv}{dz} \quad (13.118)$$

where Eq. (13.117) together with the expression $dz = v dt$ have been considered. If it is assumed further that the flow is Newtonian, that is, $\sigma_t = \eta_L d\varepsilon_t/dt$, then the apparent value of the elongational viscosity is given by (57)

$$\eta_L = \frac{F}{A dv/dz} = \frac{Fv}{Q dv/dz} \quad (13.119)$$

Accordingly, the measurements of both F and Q and the experimental determination of the values of v versus z permit us to determine the apparent extensional viscosity. This parameter can alternatively be obtained from the total strain, which, according to Eq. (13.117), is given by

$$\varepsilon_t = \int_{v_0}^{v_1} \frac{dv}{v} = \ln \frac{v_1}{v_0} \quad (13.120)$$

where v_1 and v_0 are the velocities at the haul-off and the die exit, respectively. Then η_L can be written as

$$\eta_L = \frac{\sigma_{\varepsilon_t} t}{\varepsilon_t} = \frac{Fd}{Q \ln(v_1/v_0)} \quad (13.121)$$

where $d = vt$ is the draw distance between the die exit and the haul-off. Equation (13.121) suggests an easy way of determining the elongational viscosity.

Chain branching has a strong effect on stretching flows. For example, high density polyethylene (linear chains) (HDPE) and low density polyethylene (branched chains) (LDPE) have similar shear flow behavior and similar elastic response, but their stretching flows exhibit dramatic differences (36). Curves showing the dependence of the elongational viscosity, η_L , on the tensile stress, σ_t , for HDPE and LDPE are plotted in Figure 13.41. At low stresses, the curves present a region in which η_L is independent of the stress. However, at high stresses, η_L decreases with σ_t for HDPE and increases with σ_t for LDPE. This behavior suggests that when molecular chains become highly ordered by stretching flow, branching points act as hooks, thus increasing the resistance to flow. In contrast, highly ordered linear chains easily slide by each other as the liquid elongates, and the stretching flow increases at high elongational stresses. LDPE may show a resistance to

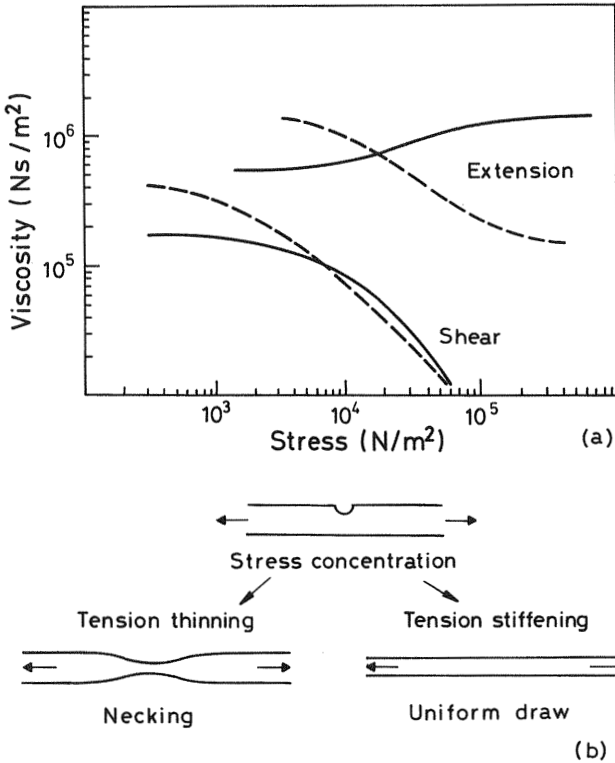


Figure 13.41 (a) Shear flow and stretching flow behavior of (---) linear and (—) branched polyethylene. MFI (melt flow index) = 0.3 at 150°C. (b) Effects of stress concentrations on stretching films. (From Ref. 36.)

high stress extensional flow two orders of magnitude larger than that of HDPE. This result is remarkable indeed if it is considered that this behavior occurs even in the cases in which high and low density polyethylene exhibit similar shear viscosity. The tendency of LDPE to stiffen at high shear stresses means that local stress concentrations have less of a destabilizing effect in stretching flows for this polymer than for HDPE. An incipient neck in HDPE will remain localized in the stretching flow, and failure will occur at relatively low extension. Local stresses in the incipient neck of LDPE will be counteracted totally or in part by the increased viscosity. The tension-stiffening response of branched polyethylene confers stability to the bubble in polyethylene film blowing, and this is one of the major reasons that low

density polyethylene and linear low density polyethylene are widely used in the film market.

Though the results at hand seem to indicate that branching strongly influences elongational flow, it is far from clear what the optimum branch length is, how branches are distributed along the chains, and how the branches operate. Tension-stiffening melts can also be prepared from polyesters, polyacrylates, etc, by incorporating specific functional groups in the polymerization. However, there have been few studies of stretching flows for polymers other than branching polyethylene.

Elongational flow experiments were carried out on poly(methyl methacrylate) at temperatures well above its glass transition temperature by using an extensometer in which the sample is clamped at both ends, with controlled elongational velocity. Illustrative results are shown in Figure 13.42. For short times the elongational viscosity obeys a unique and increasing function of time (60). A plateau is detected for the results obtained at the lowest elongational rates, i.e., $\dot{\epsilon} = 0.002 \text{ s}^{-1}$, while for higher rates the elongational growth function increases with time at large times. In this case, the plateau is not attained, mostly because of experimental limitations. The results of Figure 13.42 also show that Trouton's law,

$$\eta_L = 3\eta_0 \quad (13.122)$$

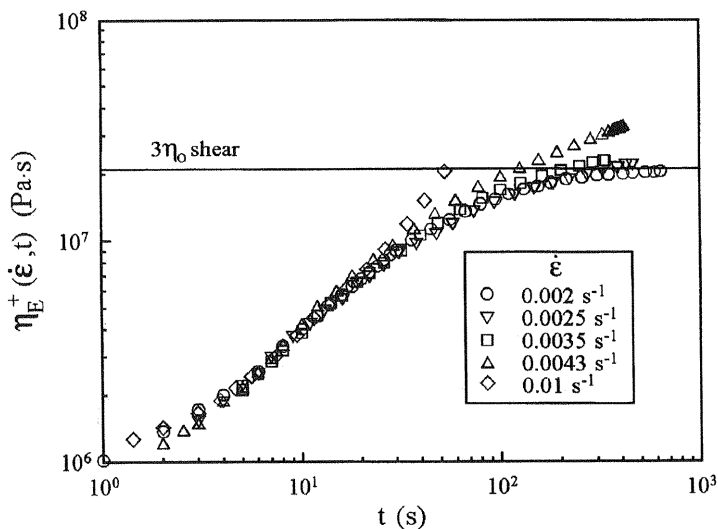


Figure 13.42 Dependence of the elongational viscosity on time for poly(methylmethacrylate) at 170°C ; $M_w = 130,000$, $M_w/M_n = 1.9$. (From Ref. 60.)

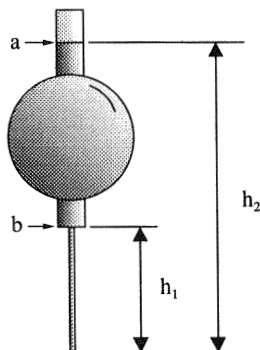
is verified at low elongational rates under steady-state conditions. The measurement of elongational flow of low viscosity fluids involves severe difficulties. Although many experimental techniques have been developed, the results obtained with them can differ by several orders of magnitude (61).

PROBLEM SETS

Problem 13.1

A capillary tube of radius 0.25 mm and length 15 cm is connected to the bulb indicated in Figure P13.1. 0.9 cm^3 of a liquid contained between the two marks *a* and *b* flows through the capillary, placed in vertical position, in 4 min. If the density of the liquid is $\rho = 1.2 \text{ g/cm}^3$ and $h_2 = 16.5 \text{ cm}$, estimate (a) the shear stress at the wall of the capillary; (b) the viscosity of the liquid; and (c) the velocity of the liquid at the center of the capillary.

Solution 13.1



(a) The liquid flows under the driving pressure, ΔP , given by

$$\Delta P = \rho g h_m = \rho g \frac{h_2 - h_1}{\ln(h_2/h_1)} = 1.2 \times 980 \frac{16.5 - 15}{\ln(16.5/15)} = 1.8 \times 10^4 \text{ dyn/cm}^2$$

According to Eq. (13.30),

$$\sigma_w = \frac{2.5 \times 10^{-2} \times 1.85 \times 10^4}{2 \times 15} = 15.41 \text{ dyn/cm}^2$$

(b) From Eqs. (13.30), (13.35), and (13.36), the viscosity of the liquid is obtained as

$$\eta = \frac{\pi R^4 \Delta P t}{8 V L} = \frac{3.14 \times (2.5 \times 10^{-2})^4 \times 1.85 \times 10^4 \times 240}{8 \times 0.93 \times 15} = 4.87 \times 10^{-2} \frac{\text{g}}{\text{cm} \cdot \text{s}}$$

(c) According to Eq. (13.32),

$$v_m = \frac{1.89 \times 10^4 \times (2.5 \times 10^{-2})^2}{4 \times 4.98 \times 10^{-2} 15} = 3.95 \text{ cm/s} \quad (\text{P13.1.1})$$

Problem 13.2

The zero shear rate viscosity of a narrow molecular weight distribution fraction of polystyrene is 6.5×10^6 poise at 160°C . If the molecular weight between entanglements in this polymer is about 18,000 g/mol, make a rough estimate of the shear rate κ_c , above which this fraction will display non-Newtonian behavior.

Solution 13.2

According to Eq. (8.55), the value of the plateau relaxation modulus G_N^0 is

$$G_N^0 = \frac{\rho}{M_e} RT \cong 2 \times 10^6 \text{ dyn/cm}^2 \quad (\text{P13.2.1})$$

The steady-state compliance can be obtained by means of the approximation [see Eq. (8.64)]

$$J_e^0 = \frac{2.3}{G_N^0} \cong 1.2 \times 10^{-6} \text{ cm}^2/\text{dyn} \quad (\text{P13.2.2})$$

According to Eq. (9.33), the mean relaxation time of the entangled network is

$$\langle \tau \rangle = \eta_0 J_e^0 \cong 7.8 \text{ s} \quad (\text{P13.2.3})$$

Hence, the approximate shear rate at which non-Newtonian behavior appears is

$$\kappa_c = 1/\langle \tau \rangle = 0.13 \text{ s}^{-1} \quad (\text{P13.2.4})$$

Problem 13.3

A fluid obeying a power law given by $\sigma = \eta\kappa^{0.5}$ [see Eq. (13.37)] with viscosity $250 \text{ N} \cdot \text{s}/\text{m}^2$, flows through a slit channel of narrow rectangular section, driven by a pressure drop per unit length of $\Delta P/\Delta L = 2.5 \times 10^6 \text{ Pa}/\text{m}$. The channel has $h = 2 \text{ mm}$ thickness, and its width is $w = 20 \text{ cm}$. Find an equation giving the velocity profile into the channel and the velocity gradient at the wall as a function of the flow rate Q .

Solution 13.3

According to Eq. (13.56), with $n = 0.5$,

$$v = \frac{1}{3} \left(\frac{P}{\eta L} \right)^2 \left[\left(\frac{h}{2} \right)^3 - y^3 \right] \quad (\text{P13.3.1})$$

Substituting the corresponding values the velocity profile is found to be

$$v = \frac{1}{30} [1 - (10^3 y)^3] \text{ m/s} \quad (\text{P13.3.2})$$

The flow rate from Eq. (13.57) is given by

$$Q = \frac{w}{32} \left(\frac{\Delta P}{\eta L} \right)^2 h^4 \quad (\text{P13.3.3})$$

By substituting the numerical values we find

$$Q = 10 \text{ cm}^3/\text{s} \quad (\text{P13.3.4})$$

The velocity gradient at the wall is

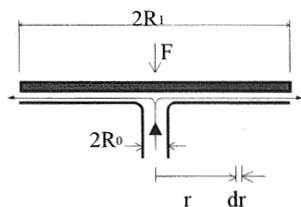
$$\kappa_w = \left(\frac{\Delta P}{\eta L} \right)^2 \left(\frac{h}{2} \right)^2 = \frac{8Q}{wh^2} = 100 \text{ s}^{-1} \quad (\text{P13.3.5})$$

Problem 13.4

A viscoelastic lubricant enters vertically with pressure p_0 into the center of the lower of two circular horizontal plates (Fig. P13.4.1), filling the recess of radius R_0 before being discharged radially into a thin chamber containing bearing elements.

- Determine the velocity distribution in this squeeze-film of external radius R_1 .
- Calculate the mean velocity of flow and the outflow rate of the lubricant.
- Calculate the pressure as a function of the radius and the flow rate required to maintain a hydrostatic film of thickness h .

Solution 13.4

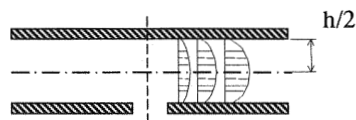


Let us assume Newtonian behavior. By considering the equilibrium of an element of volume at radius r and height y above the central line, and assuming by considerations of symmetry that there are no forces on the face determined by the coordinates r, y , we obtain the equilibrium condition

$$\frac{dP}{dr} = \frac{\partial \sigma}{\partial y} = \eta \frac{\partial^2 v}{\partial y^2} \quad (\text{P13.4.1})$$

where the Newtonian viscosity law has been used.

After integrating twice with the boundary condition given by $v = 0$ at $y = h/2$, we obtain



$$v = -\frac{h^2}{8\eta} \left(\frac{dP}{dr} \right) \left(1 - \frac{y^2}{(h/2)^2} \right) \quad (\text{P.13.4.2})$$

which gives a parabolic velocity profile.

The mean velocity can be found by averaging v along the thickness of the film, that is,

$$\bar{v} = \frac{\int_{-h/2}^{h/2} \frac{h^2}{8\eta} \frac{dP}{dr} \left(1 - \frac{4y'^2}{h^2}\right) dy'}{h} \quad (\text{P13.4.3})$$

From Eq. (P13.4.3) we find that the mean velocity is two-thirds of the maximum velocity (at $y = 0$), that is,

$$\bar{v} = (2/3)v_m \quad (\text{P13.4.4})$$

where

$$v_m = -\frac{h^2}{8\eta} \frac{dP}{dr} \quad (\text{P13.4.5})$$

On the other hand, dP/dr can be evaluated on continuity grounds, equalizing the volume of liquid swept in a time dt to the volume of liquid crossing the periphery of the circular plate in the same instant, that is,

$$\pi r^2 dh = 2\pi r h \bar{v} dt \quad (\text{P13.4.6})$$

according to which

$$\bar{v} = \frac{r}{2h} \frac{dh}{dt} \quad (\text{P13.4.7})$$

From Eqs. (P13.4.5) and (P13.4.7), we find

$$\frac{dP}{dr} = \frac{6\eta r}{h^3} \frac{dh}{dt} \quad (\text{P13.4.8})$$

from which an alternative expression for the velocity profile can be obtained as

$$v = -\frac{3r}{4h} \frac{dh}{dt} \left(1 - \frac{4y^2}{h^2}\right) \quad (\text{P13.4.9})$$

The outflow rate of the lubricant, at a radial distance r , can be found by using the value of the mean velocity. The pertinent value is given by

$$Q = 2\pi r h \bar{v} = -\frac{\pi r h^3}{6\eta} \frac{dP}{dr} \quad (\text{P13.4.10})$$

By integration with respect to r with the boundary conditions $P = 0$ at $r = R$, the external radius, we have

$$P = \frac{6\eta Q}{\pi h^3} \ln \frac{R}{r} \quad (\text{P13.4.11})$$

and by integration between the internal and the external radius we obtain for the flow

$$Q = \frac{\pi h^3 P_0}{6\eta \ln(R/R_0)} \quad (\text{P13.4.12})$$

where P_0 is the supply pressure at radius R_0 .

Note that the thrust load F to be applied to the upper part of the bearing is supported by the pressure P_0 acting over the area of radius R_0 and by the variable pressure P acting over the remaining area of the bearing. Accordingly,

$$F = \pi R_0^2 P_0 + \int_{R_0}^R 2\pi r P \, dr \quad (\text{P13.4.13})$$

Substituting the expression for P given in Eq. (P13.4.11) into (P13.4.13), after some calculations we obtain

$$F = \frac{\pi P_0}{2} \left(\frac{R^2 - R_0^2}{\ln R/R_0} \right) \quad (\text{P13.4.14})$$

The last two equations are useful in bearing design.

Problem 13.5

(a) Show that $\lim \eta_{\text{sp}}/c = \lim(\ln \eta_r)/c$, when $c \rightarrow 0$. (b) Show that $k' - k'' = 0.5$.

Solution 13.5

(a) For low concentration solutions

$$\ln \eta_r = \ln[1 + (\eta_r - 1)] \cong (\eta_r - 1) - \frac{1}{2}(\eta_r - 1)^2 + O^3 \quad (\text{P13.5.1})$$

When $c \rightarrow 0$, $(\eta_r - 1)^2$ is a second-order infinitesimal and

$$\lim_{c \rightarrow 0} \frac{\ln \eta_r}{c} = \lim_{c \rightarrow 0} \frac{\eta_r - 1}{c} = \lim_{c \rightarrow 0} \frac{\eta_{\text{sp}}}{c} = [\eta] \quad (\text{P13.5.2})$$

(b) From Eq. (P13.5.1), we obtain

$$\frac{\ln \eta_r}{c} = \frac{\eta_{sp}}{c} - \frac{c}{2} \left(\frac{\eta_{sp}}{c} \right)^2 \quad (\text{P13.5.3})$$

Substitution of Eq. (13.50) into Eq. (P13.5.3) gives

$$\frac{\ln \eta_r}{c} = [\eta] + k'[\eta]^3 c - \frac{c}{2} ([\eta]^2 + k^2[\eta]^4 c^2 + 2k'[\eta]^3 c) \quad (\text{P13.5.4})$$

For low concentrations, the contribution of the terms for which the exponent of c is larger than 1 is negligible, so that by comparing Eqs. (13.51) and (P13.5.4), we obtain

$$[\eta]^2 c \left(k' - \frac{1}{2} \right) = [\eta]^2 c k'' \quad (\text{P13.5.5})$$

Hence

$$k' - k'' = 1/2 \quad (\text{P13.5.6})$$

Problem 13.6

A paint described by the Bingham model, with a yield stress of 12 Pa, is applied to a vertical wall. Calculate the maximum film thickness of the paint that can be applied without dropping.

Solution 13.6

From the equation of motion, we obtain

$$-\frac{d\sigma_{zx}}{dx} + \rho g = 0 \quad (\text{P13.6.1})$$

where ρ is the density of the paint. Integrating this equation, assuming no air resistance in the liquid film, that is, $\sigma_{zx} = 0$ for $z = 0$, gives

$$\sigma_{zx} = \rho g \delta_{\max} \quad (\text{P13.6.2})$$

where δ_{\max} is the maximum thickness of the paint. By assuming that $\rho = 1000 \text{ kg/m}^3$, we obtain $\delta_{\max} = 12/(1000 \times 9.8) = 1.17 \times 10^{-3} \text{ m}$.

Problem 13.7

A thin layer of a molten polymer of 2 mm thickness is sandwiched between two plates. If a shear stress of 120 kPa is applied to the melt, and the apparent viscosity of the melt is $4 \times 10^4 \text{ kg}(\text{m} \cdot \text{s})^{-1}$, calculate the relative sliding velocity of the two plates.

Solution 13.7

The uniform shear stress through the layer will also cause a uniform strain rate given by

$$\frac{dv}{dr} = \frac{\sigma}{\eta} = \frac{120 \times 10^3}{4 \times 10^4} = 3 \text{ s}^{-1} \quad (\text{P13.7.1})$$

Hence, $\Delta v = 3 \times 2 = 6 \text{ mm/s}$.

Problem 13.8

The velocity and radius of a filament leaving a die exit are $v_0 = 1 \text{ ms}^{-1}$ and $r_0 = 1 \text{ mm}$, respectively, while the radius of the filament and the force at the haul are, respectively, $r_1 = 0.8 \text{ mm}$ and $F = 100 \text{ N}$. Assuming Newtonian behavior, calculate the tensile viscosity if the distance between the die and the haul is 0.5 m.

Solution 13.8

According to Eq. (13.117), the total strain is given by

$$\varepsilon = \int_{v_0}^{v_1} \frac{dv}{v} = \ln \frac{v_1}{v_0} \quad (\text{P13.8.1})$$

where v_1 and v_0 are, respectively, the velocities at the haul-off and die exit. Assuming Newtonian behavior, the elongational viscosity can be written as

$$\eta_L = \frac{\sigma_{e,t}}{\varepsilon_t} = \frac{Fd}{Q \ln(v_1/v_0)} \quad (\text{P13.8.2})$$

where $d = vt$ is the draw distance between the die exit and the haul-off. Equation (13.121) suggests an easy way of determining the elongational viscosity. Because $\pi r_0^2 v_0 = \pi r_1^2 v_1$, $v_1 = 1.56 \text{ m/s}$. From Eq. (P13.8.2) we obtain

$$\eta_L = 100 \times 0.5 / [3.14 \times 10^{-6} \ln(1.56)] = 3.6 \times 10^7 \text{ Pa} \cdot \text{s}$$

Problem 13.9

Oscillation experiments are performed in a polymer melt with cone-plate geometry, obtaining G' and $G'' = 10^1$ and 10^3 N/m^2 , respectively, at $\omega = 10^{-3} \text{ rad/s}$. If in this region G' and G'' are linear functions of frequency, estimate the force per unit area tending to separate the cone and the upper plate when the lower plate rotates at an angular velocity $\Omega = 10^{-4} \text{ rad/s}$. The cone-plate angle is $\alpha = 2^\circ$.

Solution 13.9

From Eq. (13.98), the force tending to separate the cone and the upper plate is given by

$$F/\pi R^2 = (\sigma_{22} - \sigma_{11})/2 \quad (\text{P13.9.1})$$

On the other hand, according to Eq. (13.105), for small shear rates the following expression holds:

$$\sigma_{22} - \sigma_{11} = 2\eta_0^2 J_e^0 \kappa^2 \quad (\text{P13.9.2})$$

The shear rate is $\kappa = 90 \times 10^{-4} / \pi = 2.86 \times 10^{-3} \text{ s}^{-1}$.

From Eqs. (6.11b) and (6.52), we obtain

$$\eta_0 = 10^3 / 10^{-3} = 10^6 \text{ Pa} \cdot \text{s} \quad \text{and} \quad J_e^0 = 10^1 (10^{-6} \times 10^{12}) = 10^{-5} \text{ m}^2/\text{N}$$

Then

$$\frac{F}{\pi R^2} = 10^{12} \times 10^{-5} \times 2.86^2 \times 10^{-6} \text{ N/m}^2 = 0.82 \times 10^2 \text{ N/m}^2$$

Problem 13.10

Polymer melts flowing through a capillary are subjected to high pressures. Estimate the increase in the density of a polyethylene melt at 140°C and 160°C when the pressure increases from 1 atm to 100 atm. It is assumed that the compressibility coefficient is nearly constant in this interval of pressure

and its values at 140°C and 160°C are 0.102×10^{-3} and $0.103 \times 10^{-3} \text{ atm}^{-1}$, respectively.

Solution 13.10

The compressibility coefficient is given by

$$\beta = -\frac{1}{v} \left(\frac{\partial v}{\partial P} \right)_T = \frac{1}{\rho} \left(\frac{\partial \rho}{\partial P} \right)_T \quad (\text{P13.10.1})$$

where v and ρ are, respectively, the specific volume and the density of the melt. This equation leads to

$$\int_{P_1}^{P_2} \beta \, dP = \int_{\rho_1}^{\rho_2} \frac{d\rho}{\rho} \quad (\text{P13.10.2})$$

Since β is assumed to be constant, Eq. (P13.10.2) becomes

$$\frac{\rho_2}{\rho_1} = \exp(\beta \Delta P) \quad (\text{P13.10.3})$$

Hence, $\rho_2/\rho_1 = \exp(0.0101) = 1.010$ at 140°C, while at $\rho_2/\rho_1 = \exp(0.0102) = 1.010$ at 160°C. Therefore the density increases by 1% when the pressure increases from 1 to 100 atm.

Problem 13.11

During processing, polymer melts are subjected to high pressures. Determine the work carried out to compress 1 kg of polyethylene melt from 1 atm pressure to 1000 atm at 140°C, assuming that the process is carried out under isothermal and reversible conditions.

Solution 13.11

The work involved in a reversible process can be written as

$$W = \int P \, dv \quad (\text{P13.11.1})$$

where v is the specific volume. Assuming that the compressibility coefficient β is constant, then, according to Eq. (P13.10.1), the pressure dependence of v on P is given by

$$v = v_0 \exp(-\beta P) \quad (\text{P13.11.2})$$

Hence, the work per gram is

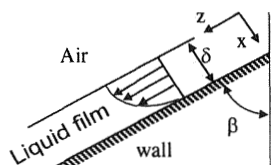
$$W = -v_0 \beta \int_0^{P_2} P \exp(\beta P) dP = v_0 \left[\frac{1}{\beta} [\exp(-\beta P_2) - 1] + P_2 \exp(-\beta P_2) \right] \quad (\text{P13.11.3})$$

It should be pointed out that in order to simplify Eq. (P13.11.3), the initial pressure was assumed to be 0 instead of 1 atm. Note that the error is negligible. Taking for β and v_0 the values of 10^{-4} atm and $1.29 \text{ cm}^3/\text{g}$, $W = -5914 \text{ J/kg}$. It should be stressed that this quantity is the lower bound of W because the compression in real situations is not performed in a reversible manner and the actual value of W may be significantly larger.

Problem 13.12

Determine an expression for the isothermal flow of an incompressible fluid on an inclined plane, assuming that the film thickness is δ and the angle formed by the plane with the vertical is β (see Fig. P13.12.1). Assume that the flow behavior of the fluid is described by a power law equation.

Solution 13.12



In this case, the components of the velocity are

$$v_x = 0, \quad v_y = 0, \quad v_z = v_z(x) \quad (\text{P13.12.1})$$

The shear stress is related to the shear rate by

$$\sigma_{xz} = \eta \left(\frac{dv_z}{dx} \right)^n \quad (\text{P13.12.2})$$

Neglecting the inertial term, the motion equation of the film can be written as

$$\frac{d\sigma_{xz}}{dx} - \rho g \cos \beta = 0 \quad (\text{P13.12.3})$$

where ρ is the density of the fluid and g the acceleration of gravity. Integration of Eq. (P13.12.3) leads to

$$\sigma_{xz} = \rho g x \cos \beta = \sigma_{\delta} \left(\frac{x}{\delta} \right) \quad (\text{P13.12.4})$$

where it was taken into account that at $z = 0$, $\sigma_{xz} = 0$ and $\sigma_0 = \rho g \delta \cos \beta$. By considering the boundary condition $v_z = 0$ at $x = \delta$, the integral of the equation resulting from the substitution of Eq. (P13.12.4) into Eq. (P13.12.2) yields the velocity profile of v_z along the x axis as

$$v_z = \frac{n\delta}{n+1} \left(\frac{\sigma}{\eta} \right)^{1/n} \left[\left(\frac{x}{\delta} \right)^{1+1/n} - 1 \right] \quad (\text{P13.12.5})$$

The flow will be given by

$$Q = \int_0^W \int_0^{\delta} v_z dx dy = \frac{W\delta^2}{2+1/n} \left(\frac{\sigma\delta}{\eta} \right)^{1/n} \quad (\text{P13.12.6})$$

REFERENCES

1. C Truesdell, W Noll. The Non-Linear Field Theories of Mechanics. In S Flüge Ed. Handbuchder Physik Berlin/Heidelberg/New York: Springer III/3, 1965. New York: Springer-Verlag.
2. B Coleman, H Markovitz, W Noll. Viscometric Flows. New York: Springer-Verlag, 1966.
3. JG Oldroyd. J Non-Newtonian Fluid Mech 14: 9-46 1984.
4. AS Lodge. Elastic Liquids. New York: Academic, 1964.
5. BD Coleman, W. Noll. Simple Fluids with Fading Memory. Second Order Effects in Elasticity, Plasticity, and Fluid Dynamics. Intl. Symp. Haifa. New York: Macmillan Corp. 530-552, 1964.
6. AS Lodge. Body-Tensor fields in Continuum Mechanics. New York: Pergamon, 1974.
7. W Schowalter. Mechanics of Non-Newtonian Fluids. New York: Pergamon, 1978.
8. RB Bird, RA Armstrong, O Hassager. Dynamics of Fluid Polymeric Liquids, Vol I, Fluid Mechanics. 2nd ed. New York: Wiley, 1987.
9. RB Bird, RA Armstrong, O Hassager. Dynamics of Fluid Polymeric Liquids, Vol II, Kinetic Theory. 2nd ed. New York: Wiley, 1987.

10. HA Barnes, JF Hutton, K Walter. *An Introduction to Rheology*. New York: Elsevier, 1989.
11. RG Larson. *Constitutive Equations for Polymer Melts and Solutions*. Boston: Butterworth, 1988.
12. JA Covas, JF Agassant, AC Diogo, J Vlachopoulos, K Walters, eds. *Rheological Fundamentals of Polymer Processing*. NATO ASI Series. London: Kluwer, 1994.
13. JM Dealy, KF Wissbrun. *Melt Rheology and Its Role in Plastics Processing: Theory and Applications*. New York: Van Nostrand Reinhold, 1990.
14. PJ Carreau, DCR de Kee, RP Chhabra. *Rheology of Polymeric Systems*. New York: Hanser, 1997.
15. K Walters. *Rheometry*. London: Chapman and Hall, 1975.
16. K Walters, ed. *Rheometry: Industrial Applications*. New York: Wiley, 1980.
17. C Truesdell, R Toupin. *The Classical Field Theories* In: S Flüge, ed. *Handbuch der Physik*, Berlin/Göttingen/Heidelberg: Springer III/1. Vol. 3, Pt. 1. p 226 1960.
18. JG Oldroyd. *Proc Roy Soc (Lond) A200*: 345, 523, 1950.
19. JG Oldroyd. *Proc Roy Soc (Lond) A245*: 278, 1958.
20. JG Oldroyd. *Proc Roy Soc (Lond) A283*: 115, 1965.
21. W Noll. *Arch Rational Mech Anal* 2: 197, 1958.
22. H Markovitz. *Nonlinear steady-flow behavior*. In: FR Eirich, ed. *Rheology*, Vol 4. New York: Academic, 1967, p 354.
23. BD Coleman, W Noll. *Arch Rational Mech Anal* 6: 355, 1960.
24. BD Coleman, H Markovitz. *J Appl Phys* 39: 1, 1964.
25. BD Coleman, W Noll. *Arch Rational Mech Anal* 3: 289, 1959.
26. BD Coleman, W Noll. *Ann NY Acad Sci* 89: 672, 1961.
27. HA Barnes, JJ Hutton, K Walters. *An Introduction to Rheology*. New York: Elsevier, 1988.
28. AA Collyer, DW Clegg. *Rheological Measurements*. London: Elsevier, 1988.
29. RB Bird, WE Stewart, EN Lightfoot. *Transport Phenomena*. New York: Wiley, 1960.
30. B Rabinowitsch. *Z Phys Chem A145*: 1, 1929.
31. PJ Flory, TG Fox. *J Am Chem Soc* 73: 1904, 1951.
32. PJ Flory. *Principles of Polymer Chemistry*. Ithaca NY: Cornell Univ Press, 1953.
33. MJ Huggins. *J Am Chem Soc* 64: 2716, 1942.
34. E Riande, JM Pereña. *Makromol Chem* 175: 2923, 1974.
35. JY Yang. *J Am Chem Soc* 80: 1783, 1958.
36. FN Cogswell. *Polymer Melt Rheology*. New York: John Wiley & Sons, Inc. 1981.
37. EB Bagley. *J Appl Phys* 28: 264, 1957.
38. GV Vinogradov. *Pure Appl Chem* 26: 423, 1971.
39. WW Graessley. *Viscoelasticity and flow in polymer melts and concentrated solutions*. In JE Mark, ed. *Physical Properties of Polymers*. Washington DC: American Chemical Society, 1984, p 97.

40. JL Wilkes. *J Chem Educ* 58: 880, 1981.
41. WW Graessley. *Acc Chem Res* 10: 332, 1977.
42. M Doi, SF Edwards. *Theory of Liquids*. New York: Oxford Univ Press, 1986.
43. PG de Gennes. *Scaling Concepts in Polymer Physics*. 2nd ed. Ithaca NY: Cornell Univ Press, 1985.
44. WW Graessley. In: JJ Burke, V Weiss, eds. *Characterization of Materials in Research*. Syracuse NY: Syracuse Univ Press, 1975, Chap 15.
45. W Ostwald. *Kolloid Z* 36: 99, 1925.
46. RB Bird, RA Armstrong, O Hassager. *Dynamics of Fluid Polymeric Liquids, Vol I, Fluid Mechanics*. New York: Wiley, 1977.
47. PJ Carreau. *Trans Soc Rheol* 16: 99, 1972.
48. MM Cross. *J Colloid Sci* 20: 417, 1965.
49. PJ Carreau, D De Kee, M Daroux. *Can J Chem Eng* 57: 135, 1979.
50. W Cox, E Merz. *J Polym Sci* 28: 619, 1958.
51. ME Ortiz. *Comportement rhéologique du poly(oxyéthylène) en solution*. PhD Thesis. Ecole Polytechnique of Montreal, Montréal, Québec, Canada.
52. WN Prest, RS Porter. *Polym J* 4: 163, 1973.
53. CD Han. *Rheology in Polymer Processing*. New York: Academic, 1976.
54. H van Oenen. In: DR Paul, S Newman, eds. *Polymer Blends, Vol 1*. New York: Academic, 1978, pp 295–352.
55. SH Maron, PE Pierce. *J Colloid Sci* 11: 80, 1956.
56. AJ Polinski, ME Ryan, RK Gupta, SG Seshadri, FJ Frechette. *J Rheol* 32: 703, 751, 1988.
57. NG McCrum, CP Buckley, CB Bucknall. *Principles of Polymer Engineering*. New York: Oxford Univ Press, 1988.
58. D De Kee, CF Chan Man Fong. *Polym Eng Sci* 34: 438, 1994.
59. D Quemada. In: J Casas-Vazquez, D Jou, eds. *Rheological Modelling: Thermodynamical and Statistical Approaches*. New York: Springer-Verlag, 1991, p 158.
60. M Bousmina. *Etude des corrélations entre la morphologie et les propriétés rhéologiques linéaires et non-linéaires de mélanges de polymères incompatibles à l'état fondu*. PhD Thesis, Université Louis-Pasteur de Strasbourg, France.
61. NE Hudson, TER Jones. *J Non-Newtonian Fluid Mech* 46: 69, 1993.

14

Yield Crazing and Fracture

14.1	Introduction: Ductile and Brittle Behavior	582
14.2	Shear Yield	584
14.3	Crazing	602
14.4	Fracture in Polymers	613
	Problem Sets	642
	References	651

14.1 INTRODUCTION: DUCTILE AND BRITTLE BEHAVIOR

The most common type of stress–strain tests is that in which the response (strain) of a sample subjected to a force that increases with time, at constant rate, is measured. The shape of the stress–strain curves is used to define ductile and brittle behavior. Since the mechanical properties of polymers depend on both temperature and observation time, the shape of the stress–strain curves changes with the strain rate and temperature. Figure 14.1 illustrates different types of stress–strain curves. The curves for hard and brittle polymers (Fig. 14.1a) show that the stress increases more or less linearly with the strain. This behavior is characteristic of amorphous poly-

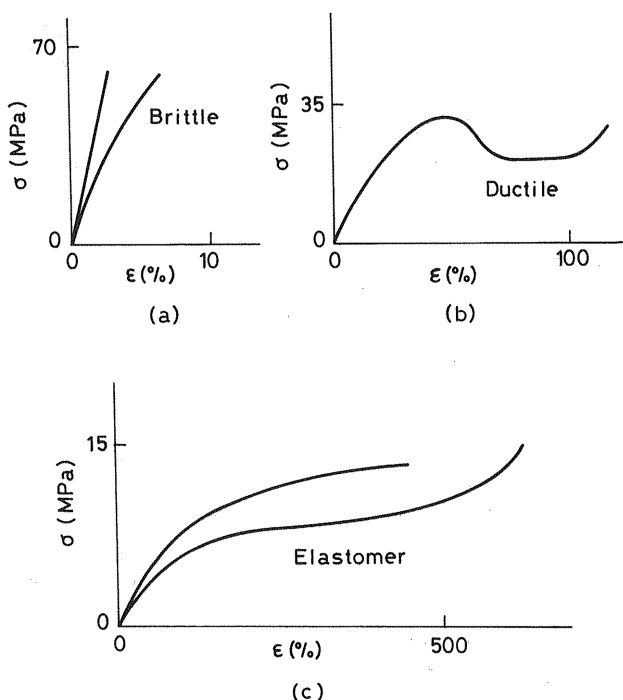


Figure 14.1 Typical stress-strain curves for polymers. (The scales reflect the order of magnitude commonly found.)

mers at temperatures well below the glass transition temperature ($T \ll T_g$); these materials (e.g., polystyrene, $T_g \approx 100^\circ\text{C}$) fail at low strains, leading to brittle fracture at room temperature. Semicrystalline polymers and thermoset resins at $T \ll T_g$ also exhibit the pattern shown in Figure 14.1a. The curve in Figure 14.1b represents polymers showing a ductile behavior that yields before failure. The most ductile polymers undergo necking and cold drawing. Semicrystalline polymers are typical examples that display this behavior at temperatures intermediate between melting and glass transition ($T_g < T < T_m$) (e.g., polyethylene at room temperature). The curves in Figure 14.1c are characteristic of elastomers ($T > T_g$) (see Chapter 3). An inspection of the curves of Figure 14.1 shows that the brittle behavior is that displayed by a sample that fails due to fracture at the maximum stress with relatively small strains ($< 10\%$), while ductile samples display a maximum in the stress, failing at higher strains. Although very ductile plastics, like polyethylene, can reach strains of up to 250% prior to final failure, some polymers fail immediately after yielding.

In polymer materials it is difficult to distinguish between elastic deformation (recoverable) and plastic deformation (nonrecoverable), since the degree to which a sample recovers its original dimensions depends on temperature and time. High molecular mass thermoplastics can return to their original dimensions from high strains if they are heated after the load is removed. As in elastomers (see Chap. 3) the recovering force giving rise to this process has an entropic character. Entanglements among chains in thermoplastics play a role similar to that of chemical cross-links in elastomers, and as a result the strain can be recovered as long as the entanglements are not destroyed. The most important mechanisms that can lead to plastic deformation in polymers are shear yielding and crazing. Shear yielding takes place at constant volume and leads to a large change in specimen shape. Crazes are the result of localized yield and are formed by microcavities bridged by fibrils; crazing leads to an increase in volume and is precursor to brittle fracture. Yielding is involved in ductile failure of polymers and also in local crazing, which precedes brittle fracture. The understanding of yield in crystalline polymers is not as advanced as in other polycrystalline materials such as metals and ceramics. The reason is that the physical microstructure of a polymer is much more irregular and heterogeneous, making it more difficult to establish a correlation between yield and structure. Moreover, the mechanical behavior of polymers is viscoelastic. Therefore, yield in polymers depends on temperature and strain rate and is also affected by pressure, and the stress-strain curves are dependent on the type of test: tension, bending, or compression.

14.2 SHEAR YIELD

14.2.1 Basic Concepts

Figure 14.2 shows a stress-strain curve corresponding to a tensile test for ductile polymers. Nominal stress, σ_n , is plotted against nominal strain, ϵ_n . The lower diagram shows a side view of the change in the cross section of the specimen used in the test in the different strain regions. In region OA the dependence of σ on ϵ is linear. In this region Hooke's law is obeyed and the polymer recovers the original shape when the stress is removed (linear elastic or viscoelastic behavior). Starting at point A the curve changes slope until it reaches a maximum point, called the yield point, defined by its coordinates, i.e., the yield stress σ_y and the corresponding strain, ϵ_y . In general, the yield point marks the beginning of the plastic deformation of the material. However, when we are referring to polymer materials such a statement has to be considered with care. In polymers it is possible to detect plastic deformation before the yield point, and for strains greater than ϵ_y , polymers

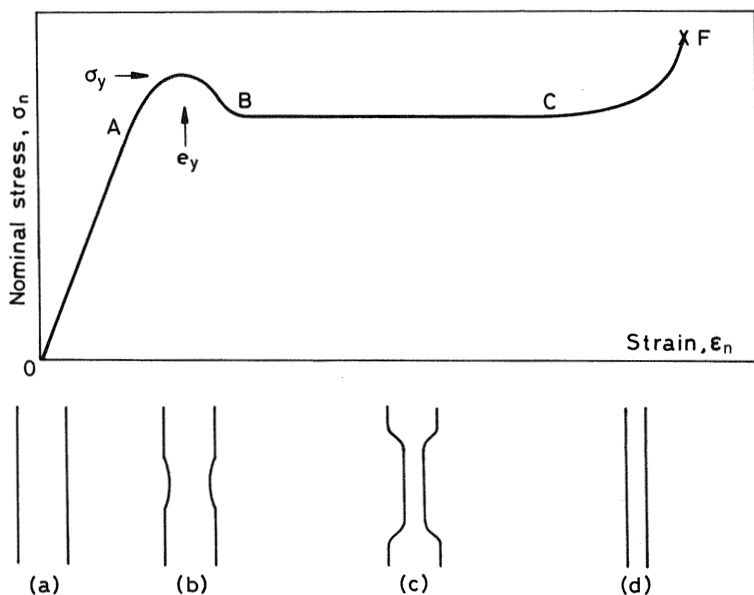


Figure 14.2 Nominal stress, σ_n , versus strain, ϵ_n , for a ductile polymer and consequent change in the dimensions of the specimen. (X indicates final fracture.)

can recover the undeformed macroscopic shape if the temperature is suitably increased. For example, in glassy and semicrystalline polymers the plastic deformation is recoverable if the polymer is heated above its glass transition temperature, T_g or melting temperature, T_m , respectively. In general, it can be stated that for polymer materials the value of ϵ_y stands at around 5%, which is notably higher than for metal (ϵ_y around 0.1%). For strains higher than ϵ_y , the nominal stress decreases until the value corresponding to point B. In the region BC the material is strained without any apparent change of the nominal stress, giving rise to the phenomenon called cold drawing. Starting from point C the material becomes rigid, and the slope of the stress-strain curve again changes, increasing considerably. After that, fracture of the material occurs at point F.

The changes observed in the stress-strain curve of Figure 14.2 are related to the change of shape undergone by the polymer shape, as is shown in the bottom diagrams. In the first region, or linear zone, the deformation occurs uniformly, and the cross section decreases as length increases [scheme (a)]. When the yield point σ_y is reached, the cross section of the sample decreases appreciably in a defined region and the neck is formed [scheme (b)]. The formation of a neck always involves the concen-

tration of permanent deformation in a small region of the specimen. This can occur in two different ways. First, if the cross section of the sample is not uniform, the volume element of smaller cross section will be subjected to higher stresses and therefore will reach yield faster than any other volume element. Second, a fluctuation in the properties of the material could cause a localized reduction in the yield stress in a volume element in which case yield occurs at a lower load value. When an element of the sample has undergone yield, it is easier to continue the deformation from this element. Once the neck forms, it extends along the gage section (region of the specimen with reduced area) at a fairly constant flow or propagating stress. The process by which the neck is extended along the sample is called the cold drawing process [scheme (c)]. Hardening of the sample starts from a certain value of strain, region *CF* in Figure 14.2. This behavior, observed in many polymers, always occurs at high strains when the polymer chains are oriented in long extensions. Under these conditions, the neck propagates through the length of the specimen until it reaches the fracture point *F* [scheme (d)].

14.2.2 Yield at the Microscopic Level

When a solid undergoes shear yielding, the local packing of its constituent units—atoms, molecules, or ions—changes to a new configuration that is stable in the absence of stresses. In glassy and semicrystalline polymers the plastic deformation takes place by means of local shear strains, without any appreciable changes in volume or density.

In glassy polymers, the local shear strains provoke the displacement of the polymer chains to new equilibrium positions, probably metastable positions. Local shear is accomplished by the disruption and reestablishment of weak intermolecular forces. The covalent bonds along the chains are not affected, and consequently the deformation process in glassy polymers occurs through changes in the conformation of the polymer chains. The scheme of the deformation process of a polymer chain, shown in Figure 14.3, explains the essentially recoverable nature of plastic deformation when a glassy polymer is heated above its glass transition temperature T_g . Above T_g , polymer chains tend to recover the original conformations corresponding to maximum entropy (see Chap. 3, Sect. 3.3.1).

Semicrystalline polymers must be considered two-phase mixtures of amorphous regions between lamellar crystals. It has been demonstrated that the yield stress increases with increasing crystallinity when the deformation process occurs at temperatures above the glass transition temperature of the amorphous phase and below, but close to, the melting

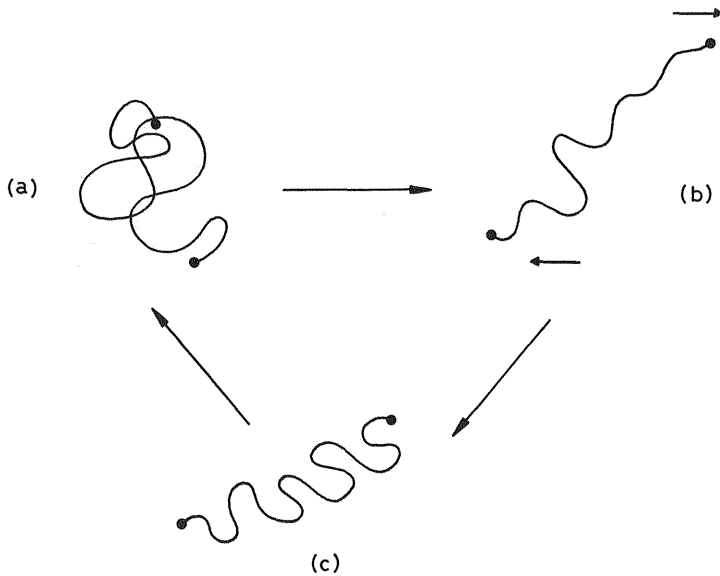


Figure 14.3 (a) Isotropic polymer chain. (b) Chain extended and partially oriented by the action of local shear. (c) The conformation corresponding to (b) is maintained in glass (or crystal) due to the fact that new intermolecular forces have been established. Forces of an entropic nature cause the chain to adopt its original conformation when the sample is heated.

temperature of the crystalline phase (1–3). Above T_g , amorphous materials behave approximately as rubbers, without undergoing shear yielding, while below T_g they deform as glassy polymers. There are several interpretations of yielding in semicrystalline polymers. One of them (2–4) considers that the dominant mechanism in yielding involves partial or local melting due to heating produced by local stress concentration. The melted chains stretch in response to the applied stress and recrystallize in oriented fibrillar morphology. This process causes the original spherulitic microstructure to be converted to a fibrillar one. Another alternative to the melting transformation model is based on more conventional approaches to crystal plasticity according to which the crystalline regions deform by a combination of slip and twinning (5–7). Figure 14.4 shows a scheme of the change in spherulitic morphology during the deformation process. The Peterlin model (8) represented in Figure 2.11 (see Chap. 2) assume that polymer chains constituting the crystalline structure slip along the deformation direction, giving rise to large macroscopic strains that produce a fibrillar morphology.

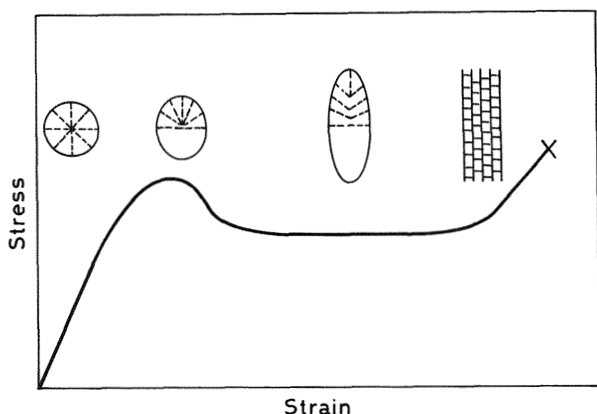


Figure 14.4 Diagram of the change of a spherulite during the cold drawing of a semicrystalline polymer. (From Ref. 25.)

14.2.3 Mechanical Tests

A brief description of mechanical tests that can be performed to obtain information on yielding in polymer materials is given below. Figure 14.5 shows some diagrams that reproduce the conditions of each type of experiment.

Figure 14.5a refers to the most common procedure corresponding to uniaxial tension deformation. The material is tested in the gage section of reduced area A_0 , which has a length l_0 . The larger section zones are used as attaching points for the clamps. The clamps are separated at a constant rate, and the force F is measured as a function of this separation. The stress can be obtained as the true stress $\sigma_t = F/A$, where A is the area of the section tested at each instant, or as the nominal stress $\sigma_n = F/A_0$, A_0 being the area of the original section of the tested piece. The strain is calculated as the displacement of the clamps per unit length and is commonly written as

$$\varepsilon_n = (l - l_0)/l_0 = \Delta l/l_0 \quad (14.1)$$

where l is the instantaneous gage length of the zone tested. The true uniaxial strain is the integral of the infinitesimal nominal strains:

$$\varepsilon_t = \int_{l_0}^l \frac{dl}{l} = \ln\left(\frac{l}{l_0}\right) \quad (14.2)$$

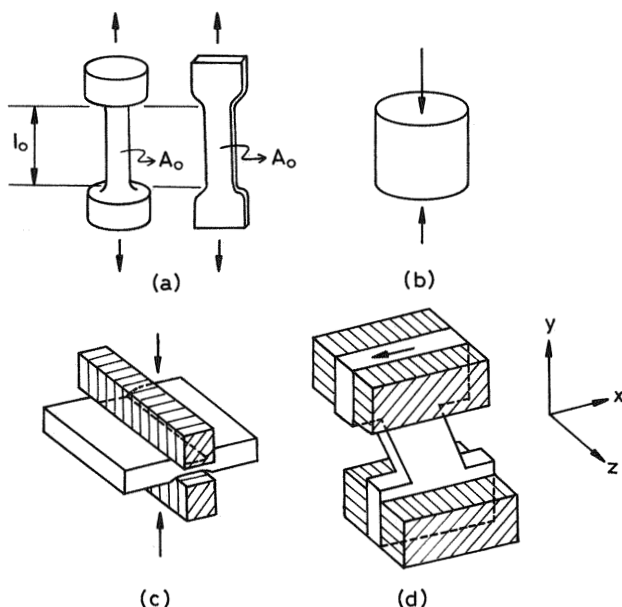


Figure 14.5 Scheme of tests used for determining yield in polymers: (a) Tension; (b) uniaxial compression; (c) plane strain compression; (d) simple shear.

Although the uniaxial tension test is the one most widely used, it has two drawbacks when it is used to provide information on the yielding of polymers. First, the tensile stress applied can lead to brittle fracture before yield takes place, and second, yield occurs in an inhomogeneous way due to the formation of a neck accompanying the tensile test. In any case, given that the section of sample decreases as the stress increases, $\sigma_t \sigma_n$.

Figure 14.5b represents the uniaxial compression test, which uses samples with cylindrical or rectangular cross section. The stress and strain are defined in an analogous way to that of the tensile test. This test overcomes the disadvantages mentioned in relation to a tensile test. The stress is compressive, and consequently there is no possibility of the brittle fracture observed in tensile deformation. Plastic yield can even be seen in thermo-stable materials, which, under other conditions, can be brittle. In addition, the determination of the yield stress is made under conditions of stable deformation since there is no geometrical reason for the formation of a neck such as occurs in tension. A problem that can arise in this test concerns the diameter/height ratio of the sample. If this ratio is too large friction between plates and sample will introduce a constraint, and if it is very small

the sample could buckle. In practice, a ratio of 0.5 is a good compromise. Finally, since the cross-sectional area of the specimen increases when the test is conducted, $\sigma_t < \sigma_n$, in contrast to what occurs in a tensile test.

Another alternative is the plane strain compression test, shown in Figure 14.5c. The advantage displayed by this experiment is that the area of the specimen remains constant over the test and therefore $\sigma_t = \sigma_n$. This test can be classified as a pure shear test as only two of the three sample dimensions are changed.

Finally, Figure 14.5d shows a schematic of simple shear deformation. The specimen is clamped between steel blocks. The blocks must move parallel to each other in order to get a shear strain that is uniform along the waisted region. The shear stress is calculated as $\tau = F/A$, where F is the force applied to the plane of area A . In this test it is not necessary to distinguish between nominal and true stress because the shear strain does not affect A . The shear strain is defined as $\gamma = \Delta x/y$, where Δx is the displacement of planes separated by a distance y , Δx being measured in the direction of the force applied, which is perpendicular to y . As in the case of the compression plane strain test, there is no change in the dimension of the sample along the z axis.

14.2.4 Stress-Strain Curves. Considère Construction

The curves shown in Figure 14.6 represent the mechanical behavior of polymers in tensile deformation. Some polymers deform by forming a stable neck during the deformation process and undergoing cold drawing, as shown by curve B. In other polymers necking starts at the maximum value of σ , but the neck rapidly becomes thinner, causing failure of the specimen immediately after yielding begins (curve A, Fig. 14.6). In other words, the volume element that experiences yielding undergoes a reduction in area ($A < A_0$) in such a way that the true stress, σ_t , is sufficiently high to produce fracture. The Considère construction, which is discussed below, considers the possibility of the formation of a stable neck as response of polymer materials to the action of a uniaxial tensile stress.

If the strain takes place at constant volume, then

$$Al = A_0l_0 \quad (14.3)$$

where A and l represent the area of the cross section and the length of the sample, respectively, at each instant, and the subscript 0 refers to the original values of the two magnitudes.

According to Eq. (14.1),

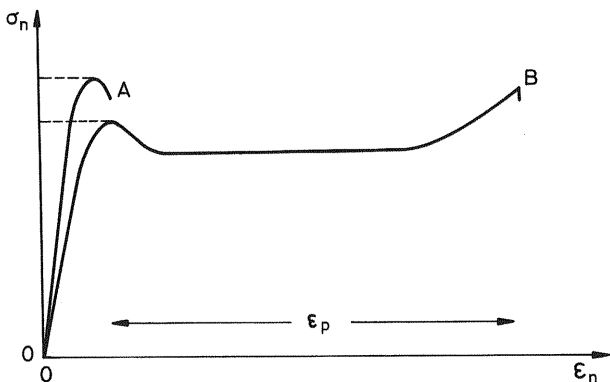


Figure 14.6 Curve of nominal stress versus nominal strain, curve A with necking and fracture, curve B with formation and propagation of a stable neck. The broken lines represent the magnitude of the yield stress σ_y , and ϵ_p is the nonrecoverable plastic strain.

$$\frac{l}{l_0} = 1 + \epsilon_n = \lambda \quad (14.4)$$

Bearing in mind the definitions of true stress, σ_t , and nominal stress, σ_n , given in the previous section and Eqs. (14.3) and (14.4), the following relation is easily deduced:

$$\sigma_n = \frac{\sigma_t}{1 + \epsilon_n} = \frac{\sigma_t}{\lambda} \quad (14.5)$$

For a uniaxial tensile test, $\lambda > 1$, and consequently $\sigma_n < \sigma_t$.

When the development of the neck starts, the applied load on the specimen ceases to increase as the strain increases, reaching a maximum in the curve of σ_n vs. ϵ_n . Mathematically the condition for obtaining a maximum is met when $dF/d\epsilon_n = 0$ or $d\sigma_n/d\epsilon_n = 0$. If this condition is applied to Eq. (14.5), one obtains

$$\frac{d\sigma_n}{d\epsilon_n} = 0 = \frac{1}{1 + \epsilon_n} \frac{d\sigma_t}{d\epsilon_n} - \frac{\sigma_t}{(1 + \epsilon_n)^2} \quad (14.6)$$

Hence,

$$\frac{d\sigma_t}{d\epsilon_n} = \frac{\sigma_t}{1 + \epsilon_n} = \frac{\sigma_t}{\lambda} \quad (14.7)$$

Equation (14.7) corresponds to the slope of the tangent to the curve σ_t vs. ϵ_n drawn from the point $\epsilon_n = -1$ or $\lambda = 0$. Figure 14.7 shows the true stress versus nominal strain curves for polymer samples A and B. Curves B_1 and B_2 are compatible with curve B of Figure 14.6. The so-called Considère construction, Eq. (14.7), is satisfied with the tangent to the curves drawn from $\epsilon_n = -1$. The tangential point corresponds to the maximum observed in the curve σ_n vs. ϵ_n and therefore with the maximum load that the specimen can support. In practice, the Considère construction is used as a criterion to decide when a polymer will form an unstable neck or form a neck accompanied by cold drawing.

For curve A it is possible to draw only one tangent from $\epsilon_n = -1$. This implies that once the neck has started in the sample it will continue becoming thinner and thinner until fracture is reached. In the case of curves B_1 and B_2 there is the possibility of drawing two tangents that fit Eq. (14.7). The second tangent in each case corresponds to the appearance of a minimum in the curve of nominal stress versus nominal strain, which is necessary for the neck to be stable. Therefore it can be stated that the formation of a stable neck, and thus the existence of cold drawing, will take place when the condition established by Eq. (14.7) is met at two points of the curve of σ_t vs. ϵ_n .

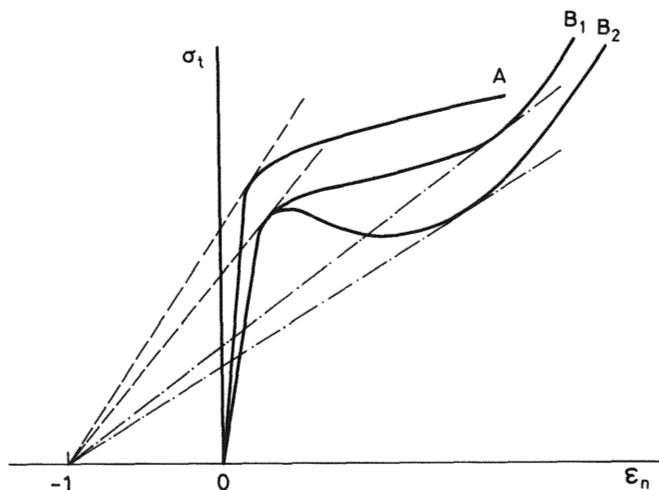


Figure 14.7 Considère construction for tensile strain. The maximum and minimum values of σ_n in Figure 14.6 are given by the tangents to the curve of true stress σ_t from $\epsilon_n = -1$. Polymer A forms an unstable neck; polymers B_1 and B_2 form stable necks.

Two phenomena can be observed once yielding starts. These are strain softening and strain hardening. Strain softening can be defined as a drop in the true stress with increasing strain (9). This behavior is observed in curve B_2 of Figure 14.7. Strain softening is an intrinsic property of polymers and can be detected fundamentally in compression and shear tests. All amorphous glassy polymers show strain softening, though some materials become oriented and quickly harden. The behavior in which no strain softening is observed, represented by curve B_1 , is typical of some crystalline or fiber-forming glassy polymers that crystallize on drawing. The orientation, or strain hardening, can also be observed in many polymers and corresponds to the region where the true stress increases after yield. It occurs in the zone of high strains in which orientation of the polymer chains in the direction of the applied force has already largely taken place. Curves B_1 and B_2 of Figure 14.7 show strain hardening. This phenomenon is important to stabilize regions of unstable plastic deformation, particularly when the material is being strained under tension. If the material does not harden, the regions affected by yield will continue to be strained until failure takes place due to one of various possible mechanisms. Most commercial polymers show strain hardening; those that do not display this characteristic are difficult to process and are not very reliable in service.

14.2.5 Yield Criteria

One criterion of yield is the critical condition that has to be met by the applied stress tensor for yield to take place. In order to represent the state of stress of a body it is convenient to choose a suitable set of orthogonal coordinates such that the shear stresses are zero. In this case the stress state is described by three normal stresses σ_1 , σ_2 , and σ_3 .

(a) *The Tresca Yield Criterion*

The yield criterion first suggested for metals was Tresca's criterion, which proposes that in isotropic materials yield occurs when the maximum shear stress τ reaches a critical value (10)*.

If σ_1 , σ_2 , and σ_3 are the principal stresses and $\sigma_1 > \sigma_2 > \sigma_3$, then

$$\sigma_1 - \sigma_3 = 2\tau_y \quad (14.8)$$

where τ_y is the stress required for yield in pure shear and depends on temperature, strain rate, and pressure. In a simple tensile test, σ_1 is equal to the applied stress and $\sigma_2 = \sigma_3 = 0$, so that at yield

*Normal stresses in other chapters are represented by σ_{ii} and shear stresses by σ_{ij} .

$$\sigma_1 = 2\tau_y = \sigma_y \quad (14.9)$$

where σ_y is the yield stress in tension. Although the Tresca yield criterion was developed for metals, most metals obey the von Mises criterion better.

(b) The von Mises Criterion

In spite of the relative simplicity of the Tresca criterion, conditions for shear yielding in isotropic polymers are best summarized by the von Mises criterion (11),

$$(\sigma_1 - \sigma_2)^2 + (\sigma_2 - \sigma_3)^2 + (\sigma_3 - \sigma_1)^2 = 6\tau_y^2 \quad (14.10)$$

Equation (14.10) corresponds to the condition that yield occurs when the elastic shear strain energy density in the stressed material reaches a critical value.

In the case of simple tension, $\sigma_2 = \sigma_3 = 0$, and Eq. (14.10) becomes

$$\sigma_y = \sqrt{3}\tau_y \quad (14.11)$$

Equation (14.11) can be compared with Eq. (14.9), which corresponds to the Tresca criterion. According to Eq. (14.9) the shear yield stress is one-half the tensile yield stress, whereas Eq. (14.11) predicts that the shear yield stress is $1/\sqrt{3}$ times the tensile yield stress.

Experimental data show that neither the Tresca nor the von Mises criterion adequately describes the shear yielding behavior in polymers.

(c) Pressure-Dependent Yield Behavior

Figure 14.8 shows stress-strain curves for polycarbonate at 77 K obtained in tension and in uniaxial compression (12), where it can be seen that the yield stress differs in these two tests. In general, for polymers the compressive yield stress is higher than the tensile yield stress, as Figure 14.8 shows for polycarbonate. Also, yield stress increases significantly with hydrostatic pressure on polymers, though the Tresca and von Mises criteria predict that the yield stress measured in uniaxial tension is the same as that measured in compression. The differences observed between the behavior of polymers in uniaxial compression and in uniaxial tension are due to the fact that these materials are mostly van der Waals solids. Therefore it is not surprising that their mechanical properties are subject to hydrostatic pressure effects. It is possible to modify the yield criteria described in the previous section to take into account the pressure dependence. Thus, τ_y in Eq. (14.10) can be expressed as a function of hydrostatic pressure P as

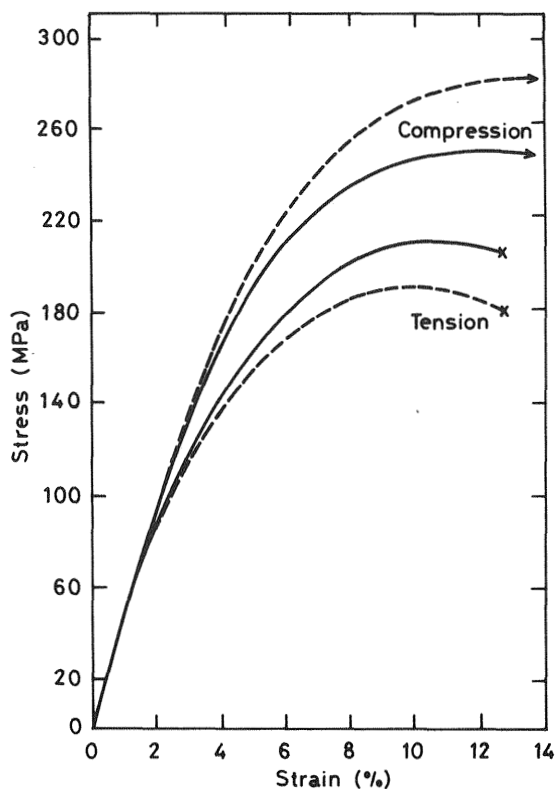


Figure 14.8 Stress-strain curves for polycarbonate at $T = 77$ K determined under tension and uniaxial compression. The nominal stress curves, σ_n , correspond to the dashed lines, and those for the true stress, σ_t , correspond to solid lines. The material tested under tension fractures immediately after reaching yield, unlike the situation that occurs under compression. (From Ref. 12.)

$$\tau_y = \tau_y^0 - \mu P \quad (14.12)$$

where τ_y^0 is the strain rate dependent yield stress at zero pressure, μ is a material constant that describes the effect of pressure, and P is given by

$$P = \frac{1}{3}(\sigma_1 + \sigma_2 + \sigma_3) \quad (14.13)$$

The hydrostatic pressure P is taken to be positive for uniaxial tensile loading and negative in uniaxial compression. In a compressive stress field (hydro-

static pressure $P < 0$) the strain energy terms on the left-hand side of Eq. (14.10) must increase; yield is more difficult at higher pressures.

(d) *Geometric Representation of the Modified von Mises and Tresca Criteria*

For macroscopically isotropic polymers, the Tresca and von Mises yield criteria take very simple analytical forms when expressed in terms of the principal stresses σ_1 , σ_2 , and σ_3 . Thus the yield criteria form surfaces in the principal stress space. The shear yield surface for the pressure-dependent von Mises criterion [Eqs (14.10) and (14.12)] is a tapering cylinder centered on the $\sigma_1 = \sigma_2 = \sigma_3$ axis ([1,1,1] crystallography direction), which broadens as the applied pressure increases. The shear yield surface of the pressure-dependent Tresca criterion [Eqs (14.8) and (14.12)] is a hexagonal pyramid. To determine which of the two criteria is the most appropriate for a particular polymer it is necessary to determine the yield behavior of the polymer under different states of stress. This is done by working in plane stress ($\sigma_3 = 0$) and obtaining yield stresses for simple uniaxial tension and compression, pure shear ($\sigma_1 = -\sigma_2$), and biaxial tension ($\sigma_1, \sigma_2 > 0$). Figure 14.9 shows the experimental results for glassy polystyrene (13), where the

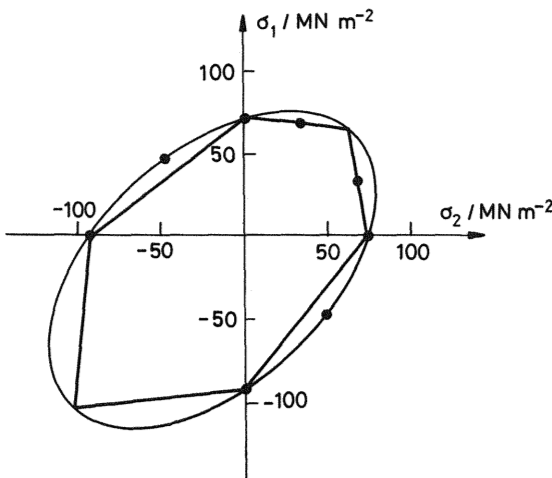


Figure 14.9 Section of the yield surface in the plane $\sigma_3 = 0$ choosing the Tresca criterion (hexagonal envelope) and von Mises criterion (elliptical envelope) for polystyrene. The points correspond to experiments performed under pure shear ($\sigma_1 = -\sigma_2$), biaxial tension ($\sigma_1, \sigma_2 > 0$), and uniaxial tension and compression. (From Ref. 13.)

cross sections correspond to the modified von Mises criterion and the Tresca criterion that fit the experimental data. Points lying closer to the origin than to the yield surface represent a recombination of stresses where yield does not occur; points on or outside the surface represent a combination of stresses where yield occurs.

14.2.6 Viscoelastic Nature of Yield Behavior: The Eyring Model

The yield behavior in polymers is strongly dependent on the temperature and rate of testing. In general, glassy and semicrystalline polymers tested at $T \ll T_g$ show negative temperature dependence of the yield strength σ_y (14) and positive strain rate dependence of σ_y (14). These behaviors are depicted in Figures 14.10 and 14.11, respectively. When the temperature chosen for mechanical testing approaches the glass transition temperature, the visco-

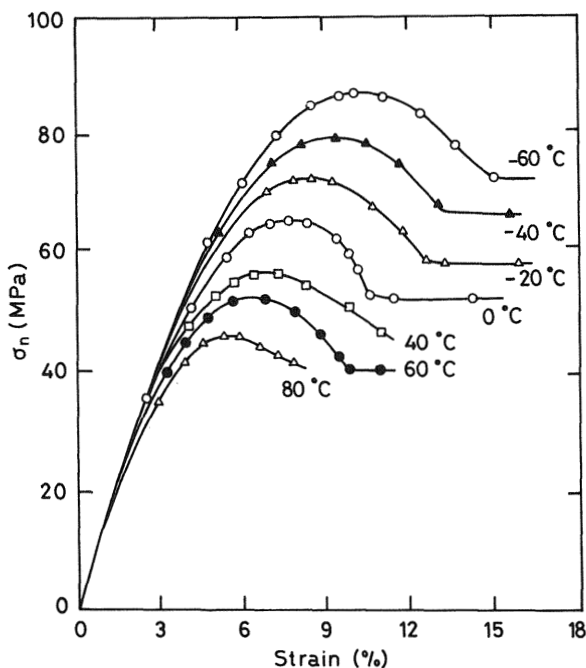


Figure 14.10 Tensile stress–strain curves for polycarbonate as a function of temperature at $\dot{\epsilon}_n = 0.083 \text{ s}^{-1}$. The yield stress σ_y (maximum in the curve) decreases with increasing temperature. (From Ref. 14.)

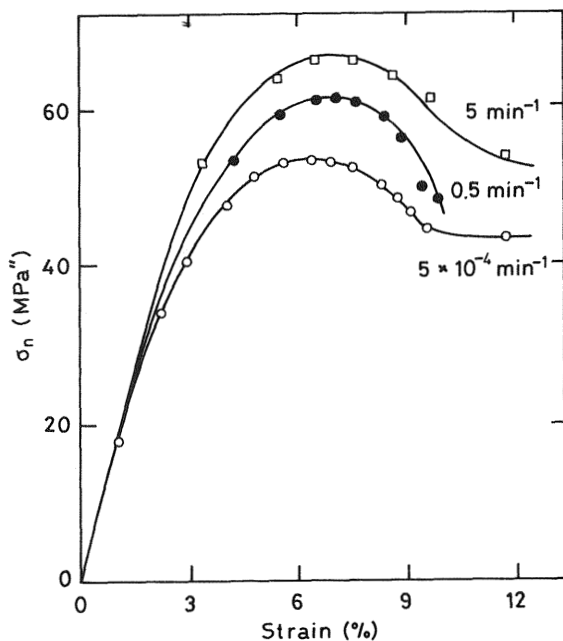


Figure 14.11 Tensile stress–strain curves for polycarbonate as a function of strain at 25°C. The yield stress, σ_y (maximum in the curve σ_n vs. ϵ_n), increases with increasing strain rate. (From Ref. 14.)

elastic behavior of glassy polymers becomes more evident. Figure 14.12 shows the temperature and strain rate dependence of the elastic modulus of polystyrene ($T_g = 100^\circ\text{C}$) tested at 75°C and 80°C (15). Semicrystalline polymers are usually treated as two-phase mixtures of amorphous regions coexisting with crystalline zones. There are two important temperatures for semicrystalline polymers, T_g for the amorphous regions and T_m for crystals. The viscoelastic behavior described for glassy polymers close to T_g is the same as that exhibited by semicrystalline polymers at $T_g < T < T_m$.

The Eyring model (16) was developed to describe the viscous flow in liquids. The fundamental ideas of this model can be applied to clarify some aspects of yield behavior of glassy polymers.

The model assumes that when a segment of a macromolecule has to move to an adjacent site it must pass over an energy barrier represented as ΔE^* (see Fig. 14.13a). In the absence of stress, the segments of the polymer jump over the barrier infrequently, and they do so in random directions. The frequency with which the segments jump the barrier is represented by the Arrhenius equation,

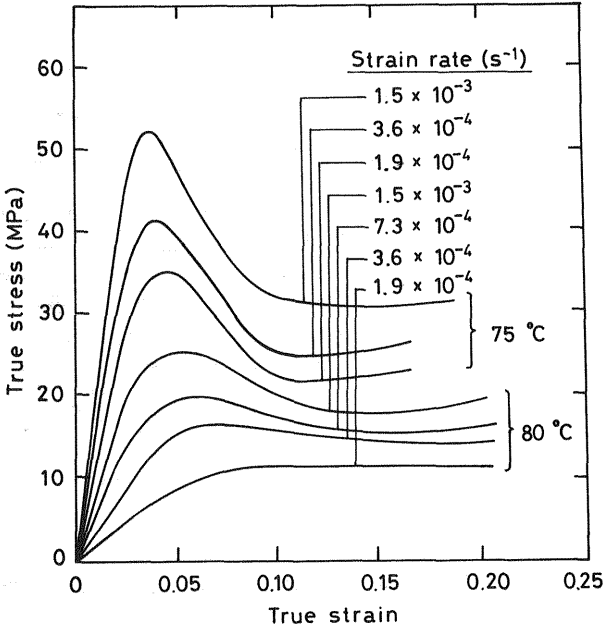


Figure 14.12 True stress–true strain curves for polystyrene determined in plane strain compression at 75°C and 80°C as a function of strain rate. (From Ref. 15.)

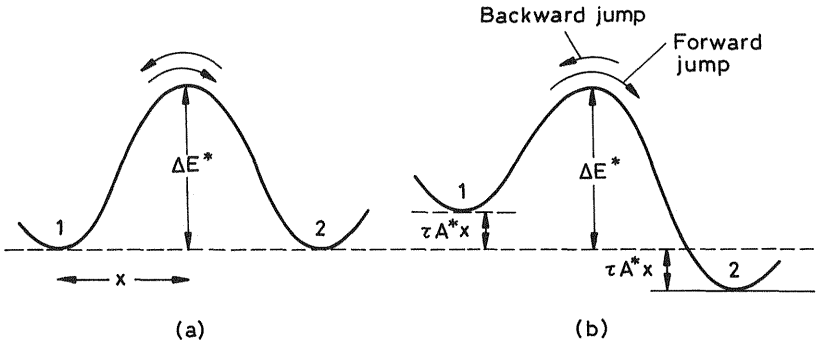


Figure 14.13 Eyring’s model. (a) Before applying the stress, the positions of the segments identified as 1 and 2 are separated by an energy barrier ΔE^* . The jump between the two is equally probable in both directions, $1 \rightleftharpoons 2$. (b) After application of the stress the energy barrier drops by $\Delta E^* - \tau A^* x$ in such a way that the jump from position 1 to 2 is favored, therefore causing jumping over the barrier to occur preferentially in the direction of the stress. (From Ref. 36.)

$$v_0 = A' \exp\left[-\frac{\Delta E^*}{KT}\right] \quad (14.14)$$

where A' is a constant and ΔE^* is the energy required to take a segment from the potential well to the top of the barrier (see Fig. 14.13a).

According to the Eyring model, the application of a shear stress modifies the barrier height. In the direction of stress, the rate at which segments jump forward over the barrier will be increased, and consequently the height of the barrier will be reduced. If τ is the shear stress applied and A^* is the effective area of the polymer segment, the height of the barrier is reduced by an amount $\tau A^* x$ that corresponds to the work done in moving a segment a distance x . The new situation is illustrated in Figure 14.13b. The frequency with which the segments jump the new barrier in the forward direction is

$$v_1 = A' \exp\left[-\frac{\Delta E^* - \tau A^* x}{KT}\right] \quad (14.15)$$

Equation (14.15) implies that the jump rate along the direction of shear stress is increased. Consequently, the energy barrier for polymer segments jumping in the backward direction (opposed to the shear stress) is raised. The frequency in the backward direction is given by

$$v_{-1} = A' \exp\left[-\frac{\Delta E^* + \tau A^* x}{KT}\right] \quad (14.16)$$

The net rate of flow in the stress direction is the difference between Eqs. (14.15) and (14.16):

$$v_1 - v_{-1} = A' \left[\exp\left(-\frac{\Delta E^* - \tau A^* x}{KT}\right) - \exp\left(-\frac{\Delta E^* + \tau A^* x}{KT}\right) \right] \quad (14.17)$$

Since the frequency with which the polymer segments jump in the backward direction [Eq. (14.16)] is very low, the reverse jump rate can be neglected in comparison with the forward jump rate, and Eq. (14.17) becomes

$$\text{Net rate of flow} = A' \exp\left(-\frac{\Delta E^*}{KT}\right) \exp\left(\frac{\tau A^* x}{KT}\right) \quad (14.18)$$

The product $A^* x = V^*$ has the dimensions of volume and is called the activation volume. Equation (14.18) corresponds to the final form of the Eyring equation. According to Eq. (14.18), yielding is described as viscous flow in which the activation energy barrier ΔE^* for load shear displacements

of polymer segments is decreased by the applied stress τ . The imposed strain rate, $\dot{\epsilon}_y$ can be considered proportional to the net rate flow, and τ can be considered the maximum shear stress; then $\tau = \sigma_y/2$, σ_y being the tensile yield stress. Consequently, Eq. (14.18) becomes

$$\dot{\epsilon}_y = \dot{\epsilon}_0 \exp\left(\frac{\Delta E^*}{KT}\right) \exp\left(\frac{\sigma_y V^*}{2KT}\right) \quad (14.19)$$

where $\dot{\epsilon}_0$ is a constant.

Equation (14.19) can be arranged as

$$\sigma_y = \left[K \times 2.303 \log\left(\frac{\dot{\epsilon}_y}{\dot{\epsilon}_0}\right) + \frac{\Delta E^*}{T} \right] \left(\frac{2T}{V^*} \right) \quad (14.20)$$

Equation (14.20) describes the temperature and strain rate dependence of the yield stress, σ_y .

Figure 14.14 shows the plots of σ_y vs. $\log \dot{\epsilon}_y$ for polycarbonate ($T_g = 140^\circ\text{C}$) in the range of temperature $21.5^\circ\text{C} < T < 140^\circ\text{C}$ (17). The data of this figure indicate that the Eyring model accounts for many features of yielding in glassy polymers. On the one hand, the negative temperature

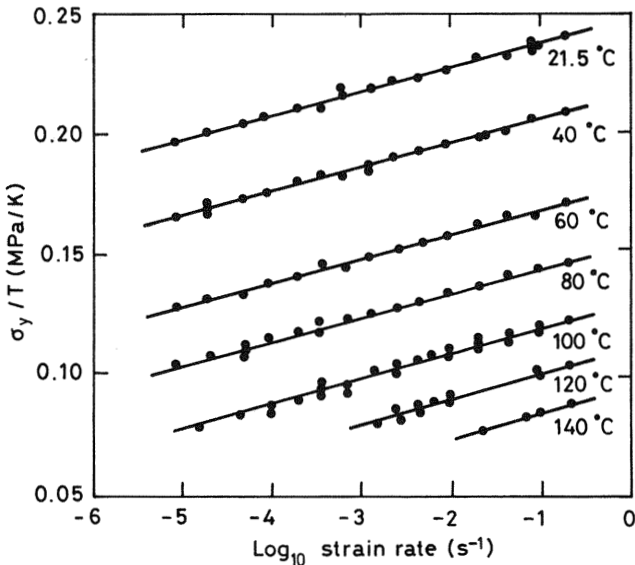


Figure 14.14 Eyring plot of σ_y/T versus $\log \dot{\epsilon}$ for polycarbonate at different temperatures. (From Ref. 17.)

dependence of the yield stress σ_y is revealed, since at strain rate constant σ_y/T decreases with increasing temperature. On the other hand, the plots show the positive strain rate dependence of σ_y , since at any temperature, σ_y/T increases linearly with $\log \dot{\epsilon}_y$. Also, the Eyring model has been successfully employed to describe the time-dependent yielding of polymers subjected to a constant applied stress (18,19). This model can predict the delay time, i.e., the time between application of the load and the onset of yielding.

However, Eq. (14.20) fails when it tries to describe the yield behavior of polymers over a wide range of temperatures. This has led to a modification of the model (20,21) that assumes that the deformation process involves two different flow processes that have different values of ΔE^* and V^* . Finally, another simple modification of Eyring's equation [Eq. (14.20)] (22) is to include the effect of hydrostatic pressure. This modification reflects the different yield behavior of polymers observed in tension and those in compression.

14.3 CRAZING

Crazing is a characteristic of thermoplastic polymers and plays a major role in their fracture, particularly in cases of brittle fracture and ambient degradation. It can even be stated that fracture in polymers cannot be explained without mentioning crazing. Crazes are usually observed on the surface of glassy polymers such as PS and PMMA (23,24) when they are subjected to a tensile stress; their appearance is like that shown in Figure 14.15. It was initially thought that crazes were microcracks that occurred on the surface of the samples, but it has been demonstrated that they are not simply microcracks. The basic difference between crazes and cracks is that crazes contain polymer, about 50% by volume, whereas cracks do not. If a craze at the tip crack extends through the cross section of a sample, the sample will still exhibit some capacity to resist loads.

Crazes are observed in high molecular weight glassy polymers other than thermosets. They can also occur in crystalline polymers such as polypropylene and polyamides. Crazes are found in the interior of the material and on its surface as well as at the tips of cracks. In glassy polymers the microstructure of crazes is generally independent of where they are located. The formation of crazes is affected by the distribution of microscopic defects on the surface and inside the samples. Crazes that occur on the surface, in particular, are considerably affected by the environment. In general, crazing is significantly accelerated by the presence of organic liquids and grease. In practice, the use of many glassy polymers is limited by their tendency to undergo crazing at low stresses in the presence of crazing agents.

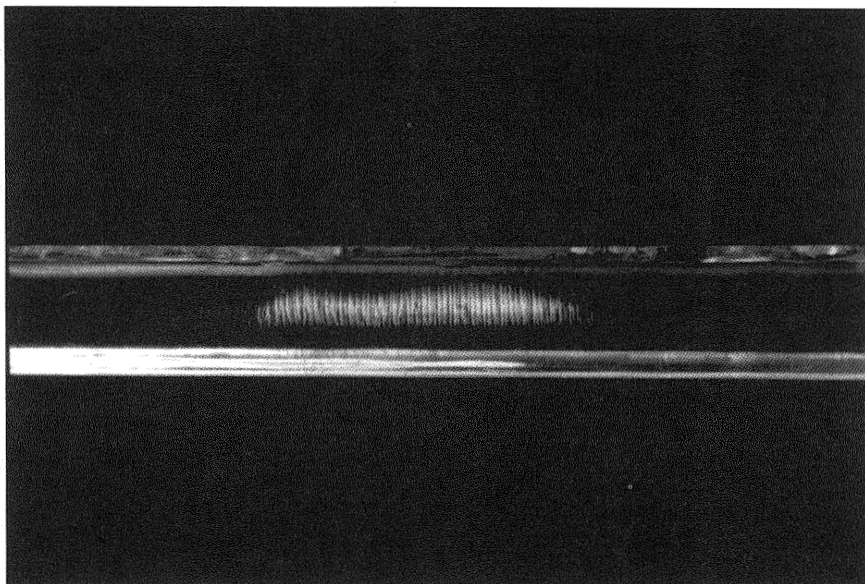


Figure 14.15 Crazes in a sample of polystyrene.

In most cases, the propagation of the crack is preceded by crazing at the crack tip. Crazing at the crack tip requires a large amount of energy and can therefore cause a relaxation of the concentration of stresses in that area. In general a craze commences when a tensile stress causes microcavities at points of high stress concentration in the polymer due to scratches, defects, cracks, dust particles, molecular heterogeneities, etc. These microcavities develop in a plane perpendicular to the principal tensile stress, but they do not join up to form a real crack because they become stabilized by fibrils of oriented polymer material that are plastically strained. As a result, an interpenetrating system of cavities and polymer fibrils is obtained, known as a craze. Crazing occurs before the yield point is reached. The breakage of the fibrillar structure of a craze generates a crack.

Crazing stress depends on both temperature and strain rate (25). This is shown in Figure 14.16, where the stress necessary to provoke crazing in samples of polystyrene (a uniaxial tensile stress is applied) are plotted against temperature. The crazing-initiating stress drops as the temperature increases and as the rate of loading decreases. Crazing may initiate at stresses below those that can cause shear yielding (26). As can be seen in Figure 14.17, the yield stress for polystyrene rises when temperature decreases, but more quickly than the crazing stress. So for this polymer, crazing will be the

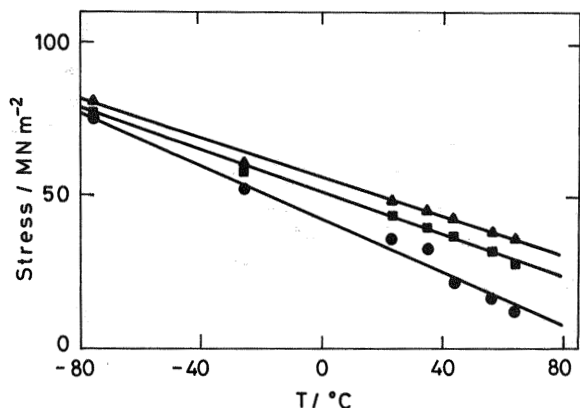


Figure 14.16 Dependence of crazing stress on temperature at different strain rates for polystyrene. Strain rates: (●) 0.00067 s^{-1} , (■) 0.0267 s^{-1} , (▲) 0.267 s^{-1} . (From Ref. 25.)

dominant micromechanism of failure of the material except at high temperatures close to the glass transition temperature ($\sim 100^\circ\text{C}$).

Unfortunately, the initiation and evolution of crazes do not concern only the majority of thermoplastic glassy polymers, which exhibit brittle behavior. Crazes usually also constitute the dominant micromechanism for failure when many polymers generally considered tough are subjected

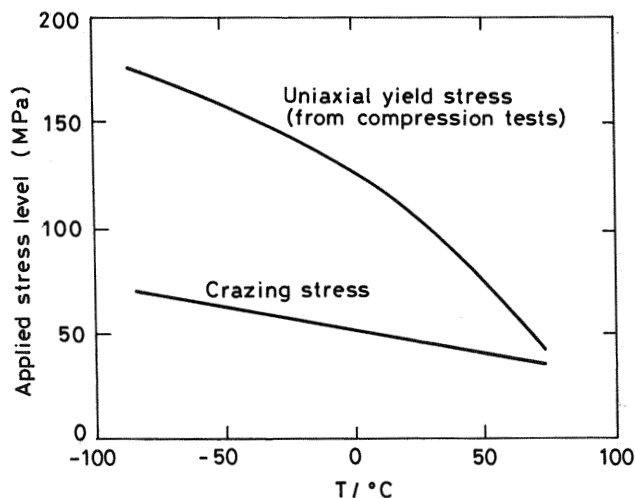


Figure 14.17 Relationship between yield stress and crazing stress with temperature, for polystyrene. (From Ref. 26.)

to a high degree of strain, aggressive ambient, liquids, etc. Therefore, a ductile–brittle transition will have an influence on these polymers in service and has to be taken into account in design.

14.3.1 Morphology and Type of Crazes

Crazes, in all cases, consist of elongated cavities and fibrils oriented in the main direction of the stress. (This means that the structure is not significantly dependent on the environment.) The structure is like that of a sponge. It is accepted that the fibrils within the craze are formed by local yielding and cold drawing processes, the fibrils remaining intact because they contain oriented molecules and are stronger than the uncrazed polymer. The crazes form thin lamellae in a plane perpendicular to the tensile axis because the tensile stress is highest across this plane. The surrounding uncrazed material constrains the craze, and consequently it grows only laterally and thickens.

Crazes in amorphous polymers can be classified into three types depending on where crazing occurs: (1) surface crazes, (2) crazes at a crack tip, and (3) internal crazes. Surface crazes occur on the surface of a sample. An example is shown in Figure 14.15. The length of crazes can reach values around 10 mm, while their thickness is very small, between 0.1 μm and several micrometers. Environmental factors have an important influence on this type of craze.

Crazes can also be initiated at the tips of cracks and be propagated in the direction normal to the maximum stress. Depending on the load conditions, these crazes can grow and cross the entire sample. Crazes of the third type occur in the interior of a polymer and are caused by mechanical conditions. The environment has a minor influence on the initiation and growth of internal crazes. Figure 14.18 illustrates an internal craze in a notched sample of polycarbonate. Internal crazes can occur in isolation or in large numbers. In the latter case, internal crazes constitute an important mechanism to improve toughening in polymers such as high impact polystyrene and other styrenic polymers.

Crazes can also be observed in semicrystalline polymers such as nylon 6. In general, the morphology and structure of crazes in semicrystalline polymers are affected by the crystalline structure. Crazes that form in crystalline polymers above their T_g (i.e., PE at room temperature) are short and irregular because their growth is affected by local stress directions and the spherulitic structure. The crazes formed at temperatures below the T_g of semicrystalline polymers are in general very few in number and are long compared with those formed above the T_g . They grow normal to the principal stress direction as in an amorphous polymers. Although the appear-

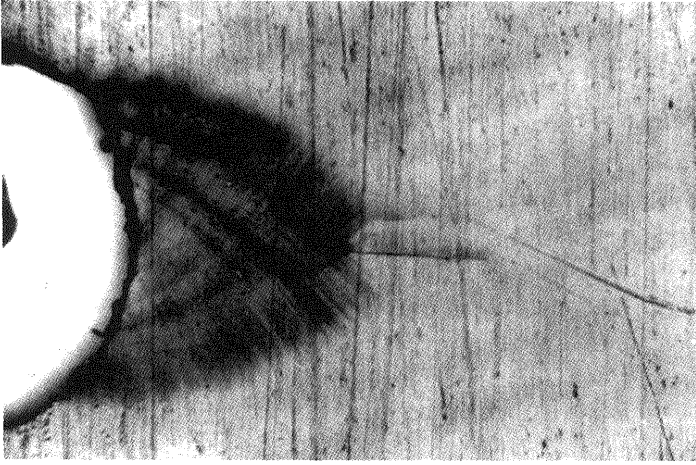


Figure 14.18 Internal craze in a notched sample of polycarbonate. (From Ref. 24.)

ance of the internal structure of crazes in crystalline polymers is similar to that found in amorphous polymers, the craze fibrils are much thinner.

14.3.2 Crazing Criteria

(a) Introduction

Crazing involves a localized or inhomogeneous plastic strain of the material as in the formation of shear bands. Nevertheless, while yield essentially occurs at constant volume, crazing is a cavitation process and takes place with an increase in volume. The initiation of crazing normally requires the presence of a dilative component of the stress tensor and can be inhibited by applying a hydrostatic pressure, though it is favored by the presence of triaxial tensile stresses. This latter state of stress exists in defects of bulky samples subjected to plane strains. Moreover, under such conditions crazing is favored, because the application of a tensile stress necessary for yield is high owing to the restriction displayed by the chains. The cavitation involved in the crazing permits the material to achieve plastic strain faster. So the presence of marked cracks or defects in bulky samples will favor the initiation of crazing. These defects are points of high concentration of stresses and can cause the formation of initial microvoids.

Some criteria have been proposed for craze initiation. The earliest criterion states that crazing occurs when the uniaxial tensile stress reaches a critical value (27). Since the crazing stress depends on the strain rate and

temperature and can also be affected by molecular orientation and environment, this simple criterion is inadequate to describe the behavior in multi-axial stress systems. Since crazing formation is a dilatational process, a criterion has been suggested that includes a dilatational stress component.

(b) Sternstein–Ongchin Criterion

Sternstein and Ongchin (28) considered that if cavitation occurs in crazes the criterion for crazing initiation should include the dilative stress component. They proposed the criterion to fit the experimental data for surface craze initiation in PMMA when the polymer is subjected to biaxial tension. The segmental mobility of the polymer will increase due to dilative stresses, thus provoking cavitation and the orientation of molecular segments along the maximum stress direction.

The Sternstein–Ongchin criterion is expressed in terms of the stress such that

$$\sigma_b = A + \frac{B}{I_1} \quad (14.21)$$

where σ_b is the stress required to orient the fibrils, and A and B are time- and temperature-dependent parameters. I_1 is the first stress invariant of the stress tensor and represents the dilatational component:

$$I_1 = \sigma_1 + \sigma_2 + \sigma_3 = 3p > 0 \quad (14.22)$$

where σ_1 , σ_2 , and σ_3 are the principal stresses and p is the hydrostatic pressure or mean stress [see Eq. (14.13)]. It is difficult to evaluate σ_b for a general triaxial state of stress. As with the yield criteria, the easiest way to test craze criteria is to make measurements in plane stress. In plane stress conditions $\sigma_1 > \sigma_2$ and $\sigma_3 = 0$, so $\sigma_b = \sigma_1 - \sigma_2$, and Eq. (14.21) becomes

$$\sigma_1 - \sigma_2 = A + \frac{B}{\sigma_1 + \sigma_2} \quad (14.23)$$

This equation is plotted in Figure 14.19, where A and B were chosen by fitting the curve to experimental data of crazing in PMMA under biaxial stress. Crazing cannot occur unless there is sufficient overall hydrostatic pressure [i.e., $(\sigma_1 + \sigma_2 + \sigma_3) > 0$] to allow cavitation to take place. The curves obtained from Eq. (14.23) will be asymptotic to the line where $\sigma_1 = -\sigma_2$. Figure 14.19 also shows the pressure-dependent von Mises curve corresponding to criteria for shear yield (see Sect. 14.2.5). Having both the yield and craze envelopes on the same figure permits prediction of the type

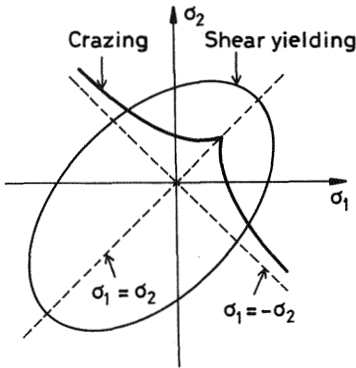


Figure 14.19 Envelopes for the initiation of crazing and shear yielding in PMMA. (From Ref. 28.)

of yielding that may occur under any general state of stress. In the first quadrant of stress space, the crazing envelope is inside the shear yielding envelope. This means that for PMMA all combinations of tensile biaxial stress produce crazing instead of shear yielding. However, in the second and fourth quadrants the behavior is different. The pure shear line, defined by $\sigma_1 = -\sigma_2$, establishes the boundary between hydrostatic compression and hydrostatic tension. Below this line, crazing does not occur because the pressure component of the stress matrix tends to reduce volume instead of increasing it. Above the line, crazing is the main mechanism of failure. For a particular combination of stresses the shear yielding envelope and the crazing envelope intersect. For stresses having I_1 less than the value of I_1 at which this intersection takes place, the preferred mode of plastic deformation is shear yielding rather than crazing.

Although crazing is a response to stress, an externally applied stress is not always required to cause it. Internal stresses can be generated from differential contraction during cooling in injection molding or by relaxation or oriented molecules. On the other hand, craze initiation in the presence of an aggressive liquid differs from craze initiation in air. The surface becomes very susceptible to crazing under an applied tensile stress, and the stress required to initiate crazing does not depend on the value of I_1 .

14.3.3 Crazing and Polymer Structure

The effect of polymer structure on crazing has been explained in terms of molecular entanglements. It has been suggested that molecular entangle-

ments not only determine whether a polymer will undergo crazing, as opposed to shear yielding, but also influence the micromechanical behavior of crazes. For a craze to be stable, there must be molecular entanglements (29). The deformation of a craze can be related to the deformation of the molecular segments between entanglements. For polymer chains of molecular weight high enough that they can be considered Gaussian coils, the maximum extent that the chain between entanglements can be stretched, λ_{\max} , is

$$\lambda_{\max} = l_e/d \quad (14.24)$$

where l_e is the chain contour length between entanglements and d is the average distance between entanglements, which can be considered as the root mean square end-to-end distance of a chain of molar mass M_e (the entanglement molar mass):

$$d = \langle r^2 \rangle_e^{1/2} \quad (14.25)$$

In Figure 14.20, values of the experimental extension ratios (average extension ratios), λ , of crazes for various homo- and copolymers are plotted against the theoretical maximum extension ratios, λ_{\max} . The results indicate that the experimental values agree quite well with the λ_{\max} values calculated. For some polymers such as poly(*tert*-butylstyrene) (PTBS), the experimental λ is much greater than λ_{\max} . This occurs at high values of λ_{\max} at which high stresses in the crazes cause scission or disentanglements that lead to values of λ greater than λ_{\max} . For small values of λ_{\max} (greater entanglement density), the polymers tend to deform by shear yielding (at temperatures below T_g). The crazing to shear yielding transition can be explained by considering that the increase in entanglement density facilitates shear yielding versus crazing. However, thermoset polymers (with a very low l_e value) exhibit a high degree of strain localization at a crack tip, and when chain scission occurs in these materials the localized zone is formed via shear deformation. The explanation for these results is not obvious from the above arguments.

Since entanglements are so important in the deformation of crazes, the molecular weight will influence the number and configuration of crazes. The higher the molecular weight, the higher the entanglement density, and as a consequence fibrils will have more difficulty forming a craze. Therefore crazing stress should increase with increasing molecular weight. However, experimental results on the molecular weight dependence of crazing stress for surface crazes of PS (Fig. 14.21) reveal that for $M_n > 2M_e$ that dependence does not exist (30). For $M_n < 2M_e$, the process leads only to fracture.

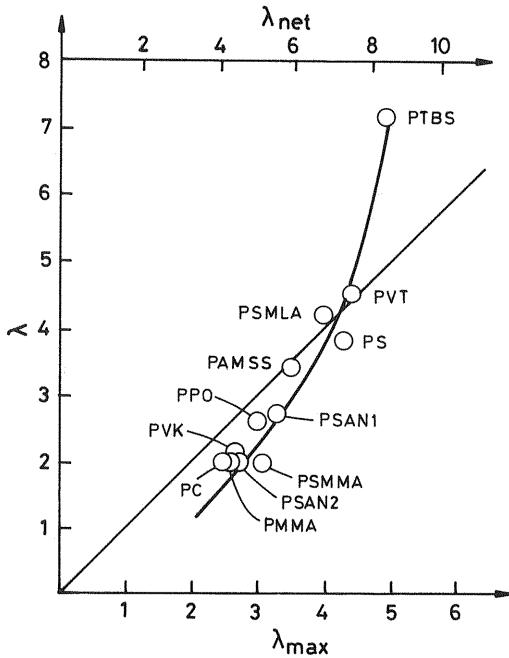


Figure 14.20 Experimental extension ratios of crazes, λ , in homo- and copolymers versus the theoretical maximum extension ratio λ_m . (From Ref. 29.)

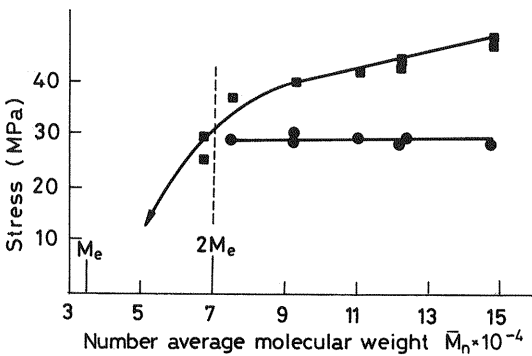


Figure 14.21 Molecular weight dependence of (■) fracture stress and (●) crazing stress for polystyrene. (From Ref. 30.)

For $M_n \geq 2M_e$, crazing occurs and the failure starts from crazes, the fracture stress increasing as the molecular weight increases.

14.3.4 Crazing and Environmental Agents

In general, environmental agents reduce the stress or strain required to initiate crazing. Environmental liquids decrease the surface energy during cavitation and accelerate the fibril orientation in crazes. They act as plasticizers of the polymers due to absorption. This absorption depends on the solubility parameters of the polymer and solvent. The glass transition temperature T_g of polymers will decrease, and as a consequence molecular segments will move at lower stresses. Figure 14.22 reveals the decreases in T_g of PS versus the critical stress of crazing (31). The data correspond to two sets of samples treated differently; in one set, samples of PS were plasticized with dichlorobenzene in advance; in the second set, samples of PS were swollen to equilibrium in various solvents. All the results indicate that a decrease in T_g causes accelerated crazing independently of the method of swelling used.

Analogous results have been found for other polymers. Crazing at crack tips exhibits exactly the same behavior. In order to evaluate the acceleration of crazing by action of a solvent, the interaction between the polymer and the solvent can be quantified by means of the solubility parameter, δ , defined as the cohesive energy density $(\Delta H_v/V)^{1/2}$, where ΔH_v is the vaporization enthalpy and V is the molar volume. Figure 14.23 shows the relationship between the critical crazing of a polymer and the solubility parameter of solvents. When the solubility parameter of the polymer, δ_p is similar to that of the solvent, δ_s , the polymer will dissolve in the liquid or will be cracked.

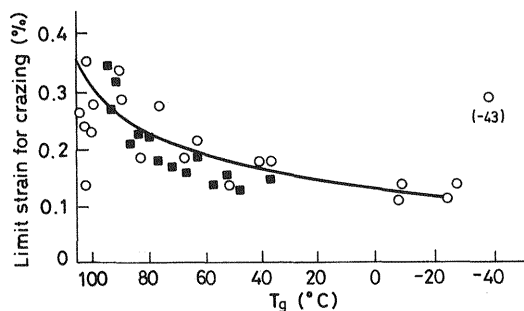


Figure 14.22 Effect of a decrease in T_g on the critical strain for crazing, for polystyrene. (○) Swollen samples in various solvents, (■) samples plasticized with dichlorobenzene. (From Ref. 31.)

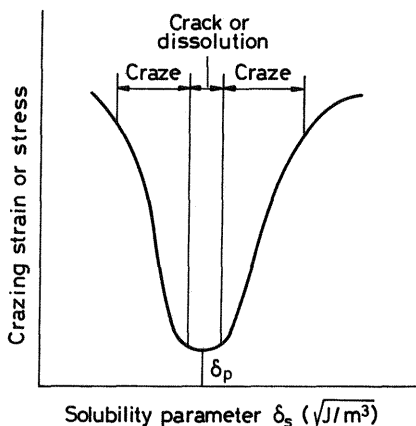


Figure 14.23 Relationship between the critical strain of a polymer and the solvent solubility parameter. (From Ref. 24.)

Crazing will occur if δ_p and δ_s are different. This figure reveals the situation for a nonpolar polymer and a nonpolar liquid. However, when polarity or hydrogen bonding are involved, a different relationship might be expected. Crazing can also be accelerated by agents such as nitrogen, oxygen and carbon dioxide at cryogenic temperatures.

14.3.5 Stress–Strain Behavior of Crazes

As could be expected, the mechanical properties of a crazed polymer differ from those of the bulk polymer. A craze containing even 50% microcavities can still withstand loads because fibrils, which are oriented in the direction of the load, can bear stress. Some experiments with crazed polymers such as polycarbonate were carried out to get the stress–strain curves of the craze matter. To achieve this aim, the polymer samples were previously exposed to ethanol. The results are shown in Figure 14.24 where the cyclic stress–strain behavior of bulk polycarbonate is also illustrated (32). It can be seen that the modulus of the crazed polymer is similar to that of the bulk polymer, but yielding of the craze occurs at a relatively low stress and is followed by strain hardening. From the loading and unloading curves, larger hysteresis loops are obtained for the crazed polymer than for the bulk polymer.

Similar stress–strain curves have been obtained for polystyrene crazes. However, these results do not necessarily reveal the real mechanical behavior of the craze. The removal of the solvent from samples will cause shrinkage and have a significant plasticizing effect on the craze fibrils. This has to

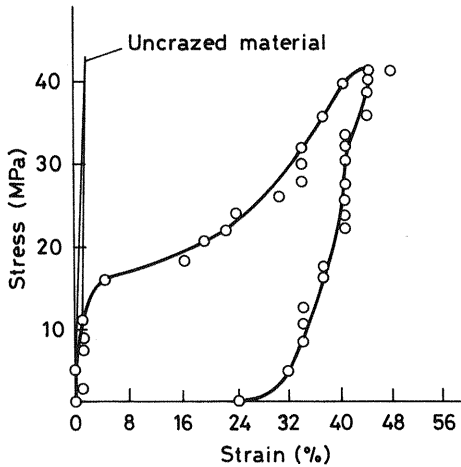


Figure 14.24 Stress-strain behavior of crazes in polycarbonate. (From Ref. 32.)

be taken into account if the real mechanical behavior of crazes (in the absence of an environmental liquid) needs to be predicted.

14.4 FRACTURE IN POLYMERS

Fracture is the creation of two new surfaces in a material by the application of external forces. Fracture failure of engineering components has catastrophic consequences, and one of the main objectives of the materials engineers and researchers is to develop materials and designs that are resistant to fracture failure. Fracture can be studied by regarding the material as a continuum, ignoring its molecular structure. Nevertheless, a complete idea cannot be gained of how fracture occurs in polymers without taking into account their molecular structure and morphology. Therefore, we begin this section with a description of the phenomenology, then study the molecular processes that take place and the theories and models applicable to the fracture of polymers, and finally we describe the behavior of polymers under particular load conditions such as impact and fatigue.

14.4.1 Brittle-Ductile Transition

Figure 14.25 shows how a typical amorphous thermoplastic, poly(methyl methacrylate) ($T_g = 105^\circ\text{C}$), changes in behavior from brittle to ductile with

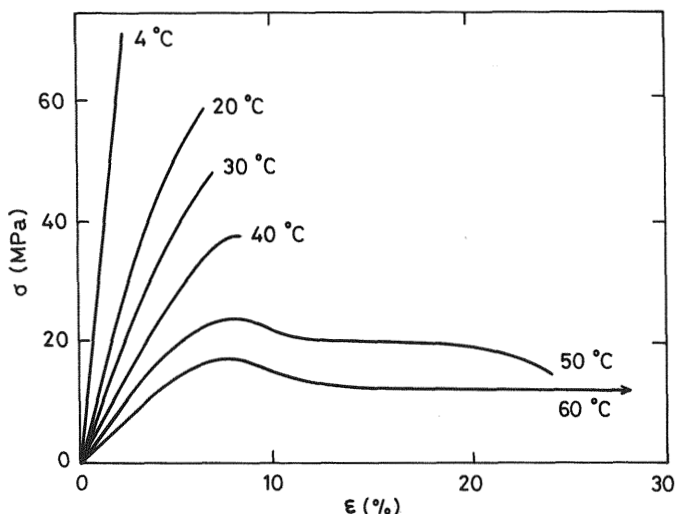


Figure 14.25 Stress–strain curves for poly(methyl methacrylate) (PMMA) in uniaxial tension at constant strain rate at several temperatures. (From Ref. 33.)

a simple increase in temperature (33). At low temperatures the fracture is brittle, whereas at high temperatures the polymer shows yield and ductile failure. The deformation of a thermoplastic is considered to be a competition between crazing and shear yielding. If crazing dominates, the behavior of the polymer is brittle, but if shear yielding occurs, the polymer is ductile. Hence the brittle–ductile transition can be explained by considering that brittle fracture and yield are independent processes that differ in their dependence on temperature (34), as is illustrated schematically in Figure 14.26. Both the fracture strength (stress required to cause brittle fracture), σ_B , and the yield stress, σ_Y , decrease with increasing temperature, but the variation of σ_Y is more marked. There will be a critical value of temperature, T_B , at which $\sigma_B = \sigma_Y$. At temperatures below T_B , the yield stress exceeds the brittle fracture strength and the process that takes place is the one requiring the lowest stress, i.e., brittle fracture. At $T > T_B$, the situation is reversed and $\sigma_Y < \sigma_B$, leading to yield and ductile failure. The temperature T_B is called the brittle–ductile transition temperature.

On the other hand, it is expected that the strain rate also influences T_B . It has been found that while brittle fracture is hardly affected, the yield stress changes significantly with the strain rate. As shown in Figure 14.26, when the strain rate increases, σ_Y increases. Therefore the brittle–ductile transition temperature increases, as does the strain rate. This is easily illu-

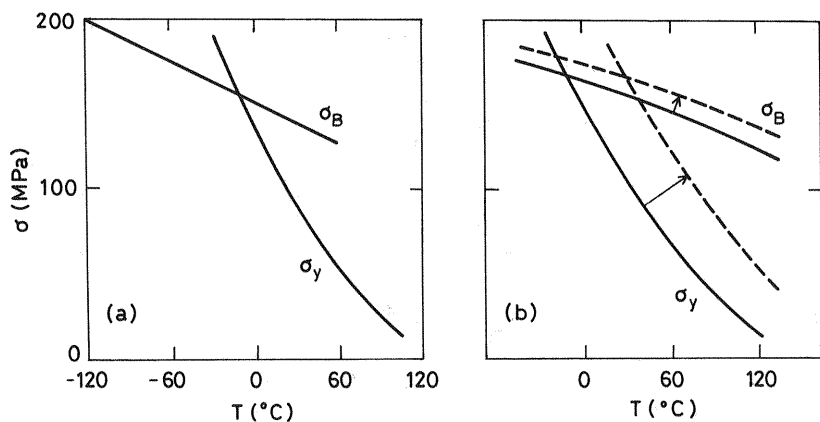


Figure 14.26 Ductile–brittle transition. (a) Variation with temperature of the brittle strength, σ_B (measured in flexion), and of the yield stress, σ_Y (measured in tension), for PMMA. (From Ref. 34.) (b) Effect of the strain rate on T_B . (—) Low rate of strain; (---) high rate of strain.

strated by changing the strain rate in a sample of nylon subjected to uniaxial tension: At low strain rates the sample is ductile and displays cold drawing, but at high strain rates fracture occurs in a brittle manner.

The brittle–ductile transition temperature depends on the characteristics of the sample such as thickness, surface defects, and the presence of flaws or notches. Increasing the thickness of the sample favors brittle fracture; a typical example is polycarbonate at room temperature. The presence of surface defects (scratches) or the introduction of flaws and notches in the sample increases T_B . A polymer that displays ductile behavior at a particular temperature can break in the brittle mode if a notch is made in it; examples are PVC and nylon. This type of behavior is explained by analyzing the distribution of stresses in the zone of the notch. When a sample is subjected to a uniaxial tension, a complex state of stresses is created at the tip of the notch and the yield stress σ_Y increases, thus increasing T_B . If T_B increases above the temperature at which the test is conducted, the sample will display brittle behavior known as “notch brittleness.” Brittle behavior is favored by sharp notches and thick samples where plane strain deformation prevails over plane stress deformation.

Moreover, the brittle–ductile transition temperature depends on the molecular structure and morphology of the polymer sample. The correlation between chemical structure and fracture behavior is not yet well understood. It is recognized that entanglements control the fracture behavior of glassy

thermoplastics, through their effect on crazing and shear yielding. Entanglements are essential for stable craze formation (see Sect. 14.3). They determine whether a polymer undergoes crazing or shear yielding and, as a result, its brittle or ductile behavior. The dependence of the fracture strength on the molecular weight is also controlled by entanglements. Low molecular weight polymers have very low tensile strengths; the strength increases as the molecular weight increases. Although attempts have been made to relate T_B to molecular relaxation processes, in particular to the glass transition, T_g , no general relationship has been established yet. Molecular relaxations are detected in the linear viscoelastic zone, at low strains, while T_B is detected at high strains and depends on factors such as the presence of notches and cracks, which do not affect the molecular relaxation processes. In some polymers, such as natural rubber and polystyrene, T_B virtually coincides with T_g , but other polymers display ductile behavior at $T < T_g$. Moreover, T_B is not clearly related to other viscoelastic relaxations taking place at $T < T_g$, although some energy absorption can take place through low-strain deformation of the sample due to viscoelastic relaxations. The addition of plasticizers reduces σ_Y and therefore also decreases T_B . Plasticizers are used to increase the toughness of polymers; a typical example is poly(vinyl chloride) (PVC), which, when not plasticized, displays brittle behavior at room temperature. T_B increases as the cross-linking and crystallinity of the polymer increase (both factors tend to increase σ_Y without significantly affecting σ_F). Thermosets (highly cross-linked polymers, with high T_g values) are brittle polymers (see Fig. 14.1a). In contrast with glassy thermoplastics, there is not conclusive evidence for crazing occurring in cross-linked polymers, which leads to brittle fracture with localized plastic deformation at the crack tip. The fracture behavior of semicrystalline polymers presents some differences with respect to that of amorphous polymers. Semicrystalline polymers can exhibit different morphologies (see Chap. 2), going from oriented fibers to the spherulites produced in isotropically crystallized polymers. Figure 14.27 shows the stress-strain curves for crystalline polymers with different morphologies. Oriented polymer fibers have high stiffness and strength, while isotropic crystallized polymers are tough and flexible, especially at $T > T_g$.

14.4.2 Fracture at the Molecular Level

(a) Theoretical Strength of a Solid

When a sample of polymer is fractured, the creation of the new surfaces must necessarily involve the breakage of primary (covalent) bonds or secondary bonds (van de Waals interactions and hydrogen bonds), or both

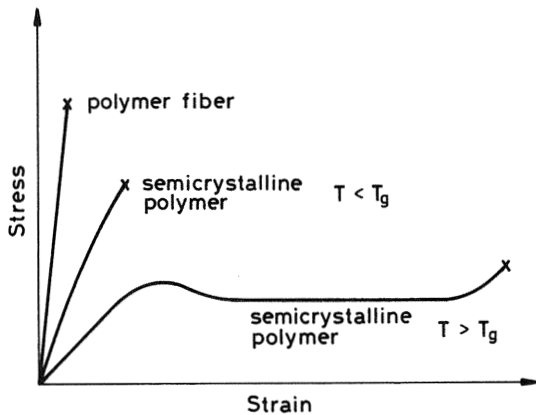


Figure 14.27 Schematic stress–strain curves for crystalline polymers.

simultaneously. From the potential energy describing the interactions among the atoms or molecules, it is possible to estimate the energy needed for breaking the bonds and to calculate a theoretical value for the strength of a solid. To do this, it is necessary to assume an isotropic solid with perfectly elastic behavior. As shown in Figure 14.28, the application of a tensile stress σ_0 causes an increase in the interatomic distances with respect to the equilibrium position h_e and therefore an increase in the potential energy. The force involved in the interatomic separation, x , will increase until it reaches the value corresponding to the point of inflection of the potential, in which that force (first derivative of the potential) achieves its maximum value. The dependence of the stress on x can be expressed in an approximate way by a sinusoidal function:

$$\sigma_0 = \sigma_T \sin(2\pi x/\lambda) \quad (14.26)$$

where σ_T is the maximum value of the tensile stress and λ is the wavelength of the sine function. For low strains ($x \rightarrow 0$),

$$\sigma_0 = \sigma_T 2\pi x/\lambda \quad (14.27)$$

Since the material is assumed to be perfectly elastic, having a modulus E ,

$$\sigma_0 = Ex/h_e \quad (14.28)$$

The work done in stressing the sample to fracture will be equal to the surface energy of the new surfaces created, G_0 :

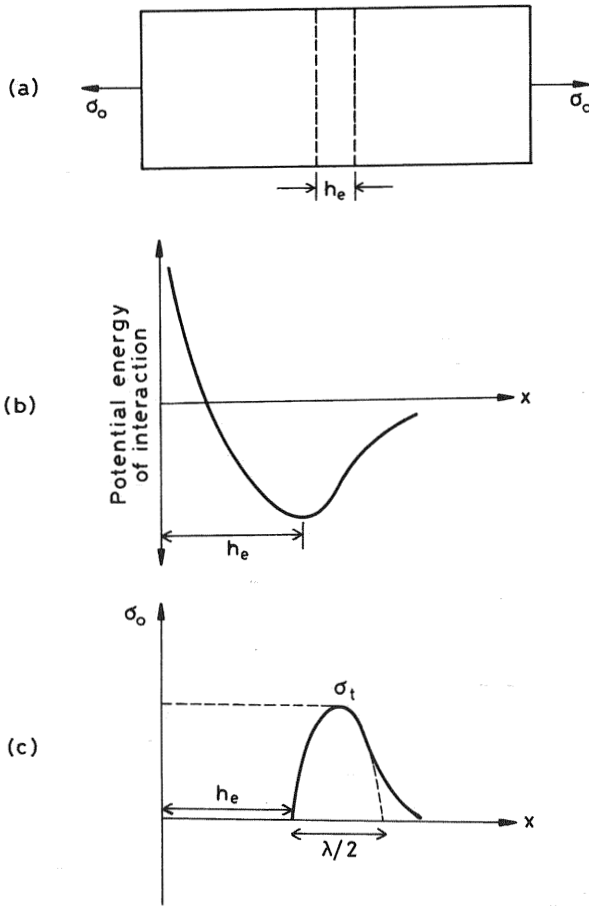


Figure 14.28 Strain of an isotropic elastic solid. (a) Application of a stress σ_0 to a sample having an equilibrium separation of atomic planes, h_e . (b) Potential energy as a function of the separation x . (c) Dependence of σ_0 on x . (From Ref. 35.)

$$\int_0^{\lambda/2} \sigma_T \sin\left(\frac{2\pi x}{\lambda}\right) dx = G_0 \quad (14.29)$$

Integrating gives

$$G_0 = \lambda \sigma_T / \pi \quad (14.30)$$

G_0 , called the intrinsic fracture energy, is the energy per unit area necessary to create the new surfaces, i.e., required to break bonds (secondary or

primary). Combining Eqs. (14.27) (14.28), and (14.30), the theoretical strength of a perfectly elastic solid to tension is given by

$$\sigma_T = \left(\frac{EG_0}{2h_e} \right)^{1/2} \quad (14.31)$$

From the usual values of $G_0 = 2\gamma$ (γ being the surface energy), E , and h_e , Eq. (14.31) can be approximated to

$$\sigma_T \approx E/10 \quad (14.32)$$

For most materials the values of the tensile strengths (fracture stress) are significantly lower than the values obtained from Eq. (14.32). This is attributed to the presence of defects or flaws. For polymers, the strength values are of the order of $E/50$ – $E/100$ (see Table 14.1). Only for some single-crystal fibers containing few defects, which are not capable of undergoing plastic strain, does the strength approach the theoretical value. On the other hand, the fracture energy in polymers is much higher than the surface energy. The strength is reduced by the presence of defects or flaws, while the fracture energy increases due to the appearance in the fracture of localized viscoelastic and/or plastic strain processes, such as microyield and microcrazing at the crack tip, that absorb energy.

Table 14.1 Elastic Modulus E , Experimental Tensile Strength^a, σ_F , and Theoretical Strength σ_T of Selected Polymers

Material	E (MPa)	σ_F (MPa)	σ_T (MPa)
Glassy polymer (PMMA)	3,000	50	300
Semicrystalline polymer (HDPE)	2,000	20	200
Thermoset polymer (epoxy resin)	3,500	70	350
Polymer fiber (nylon 6)	6,000	500	600
Single-crystal fiber (polydiacetylene)	60,000	2,000	6,000

^aMeasured at room temperature and moderate rate of strain.

Source: Ref. 35.

(b) *Molecular Sliding and Bond Breakage*

The fracture of polymers can take place via the breakage of covalent bonds and/or intermolecular interactions. Both mechanisms appear, but the extent to which each occurs depends on the type of polymer and on the test conditions. In thermoset resins the failure is produced by the breakage of primary bonds; in thermoplastics the failure can occur by sliding some chains over others, without any molecular breakage. When an amorphous thermoplastic in which the chains are oriented at random is subjected to tension, the chains tend to orient themselves in the direction of the strain. This process of sliding and separation of chains can occur in preference to molecular breakage, because the covalent bonds are stronger than the intermolecular interactions. In semicrystalline samples or in cross-linked polymers, the crystalline zones and the cross-links prevent the chains from sliding. In highly entangled thermoplastics, entanglements act as cross-links, making it difficult for the chains to be pulled out at $T < T_g$. When the fraction of crystals or entanglements is very high, chain sliding is prevented, so the chains are subjected to tension from the start of the strain, and they can therefore break. This happens in oriented polymers when they are subjected to tension in the direction of the orientation. Only molecular chains that have been oriented will withstand the external stress. Therefore, a nonuniform distribution of stresses will appear at the molecular level. These polymers usually display brittle fracture, the breakage of the primary bonds being the dominating factor. Similarly, the chains in the amorphous and crystalline zones of semicrystalline polymers withstand different loads. When the tensile stress increases, the extended chains start to break; when the number of broken chains is high, microvoids start to form that will become crazes and microcracks. A single crack is enough to initiate macroscopic fracture. The cracks will propagate by breaking chains (primary bonds) or destroying intermolecular interactions at their tips, and if microvoids have been formed in the sample they will facilitate the propagation of the crack.

Nowadays, techniques exist that permit calculation of the number of primary bonds broken during the fracture process. The most widely used is electron spin resonance (ESR) spectroscopy, which detects the free radicals produced in the breakage of the covalent bonds of the polymer chains and can quantify the number and nature of the radicals originated. Polymers in which the sliding of chains dominates over the breakage of the primary bonds display crazing (localized plastic strain) and yielding (plastic strain that is extended over large zones of the sample).

14.4.3 Fracture Mechanics

(a) Origin of the Fracture: Microcracks

The theoretical strength of a solid to fracture is of the order of a tenth of its Young's modulus [see Eq. (14.32)]. Although the elastic moduli of brittle polymers ($T < T_g$) are of the order of 3 GPa, with which one could expect a resistance of 300 GPa, the experimental strengths are very much lower (10–100 MPa), as occurs in many other materials. The most useful theory to explain fracture in brittle polymers is that of Griffith, which was initially developed to explain the brittle behavior of glass. In this theory, the low toughness of brittle solids is attributed to the presence of defects. These defects could be internal flaws or microcracks (of the order of $1\ \mu\text{m}$) or surface scratches that appear naturally in materials during their manufacture or are caused by external damage. The stresses applied to the material are amplified in the defects; i.e., the local stresses in the proximity of vertices or the tips of the microcracks are significantly greater than those applied to the material as a whole.

Let us consider a thin sheet of width W and thickness B containing an internal elliptical crack, as shown in Figure 14.29. The axes of the ellipse are $2a$ and $2b$, and the laminar sample is assumed to have infinite width, i.e., $W \gg 2a$. If a force F is applied at the end surfaces, the sample will be supporting a stress, σ ;

$$\sigma = F/WB \quad (14.33)$$

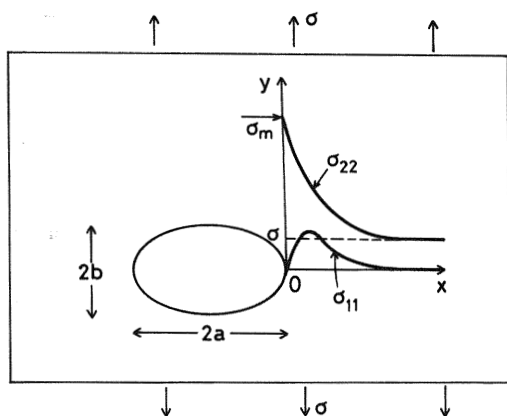


Figure 14.29 Internal elliptical crack in an elastic lamina subjected to a stress σ . Distribution of local stresses in the positive x direction.

The presence of the crack originates a local distribution of stresses in its environment (36–38). Figure 14.29 shows the variation of stresses along the line OX . The stress in the direction Y , σ_{22} , reaches a maximum value, σ_m , at the surface of the ellipse ($X = 0$) and decreases as X increases, taking the value σ at distances away from the crack. The stress in the direction X , σ_{11} , is zero on the surface of the ellipse and increases with X , reaching a maximum value close to σ , becoming zero at large distances from the crack. The amplification of the stress is maximum at the end of the major axis and is described by (37)

$$\frac{\sigma_m}{\sigma} = 1 + \frac{2a}{b} \quad (14.34)$$

Therefore, the stresses are amplified in the tips of internal cracks. The ratio σ_m/σ for circular cracks ($a = b$) takes the value 3, but for thin holes ($a > b$) it will be much greater. Equation (14.34) can be written as a function of the radius of curvature, $\rho = b^2/a$:

$$\frac{\sigma_m}{\sigma} = 1 + 2\left(\frac{a}{\rho}\right)^{1/2} \quad (14.35)$$

which for sharp cracks ($a \gg \rho$) can be approximated to

$$\frac{\sigma_m}{\sigma} = 2\left(\frac{a}{\rho}\right)^{1/2} \quad (14.36)$$

Therefore, sharp cracks cause a concentration of stresses with a maximum amplification at their tips, which can reach the value of the material's strength, even for low applied stresses, thus giving rise to interatomic separation, propagation of the crack via its tip, and fracture of the lamina later. The cracks are not necessarily perfect ellipses; even so, their effect would be similar, and when $\rho \rightarrow 0$ the amplification would be infinite and the failure imminent. For this reason, local stresses alone cannot be taken as a criterion for fracture. The solution to this problem is given by Griffith's theory of fracture (39), which defines the critical energy of fracture, and the alternative proposed by Irwin (40), which defines the critical stress intensity factor; the two are related. Moreover, as has already been mentioned, plastic strain processes (localized crazing and localized yield) occur in polymers at the crack tips. These processes absorb energy and delay failure, so the crack will propagate only if the total energy of the system decreases. Although Griffith's theory is formulated for perfectly elastic solids (linear elastic behavior, low strains), it is also applicable to real situations in which plastic

strain occurs at the crack tips provided that there is no bulk yielding in the sample.

(b) *Griffith's Theory of Fracture*

Griffith's theory (39) is based on the energy changes produced when a crack propagates in a material, setting the condition that the crack will propagate only if the total energy of the system decreases. The total energy of the system is divided into two terms: the stored elastic energy and the work done in the crack propagation. The fracture occurs if the energy required to produce the new surfaces is balanced by a decrease in the elastically stored energy. Let us consider a thin lamina (such as that shown in Fig. 14.30) of thickness B , with a sharp internal crack of length $2a$ perpendicular to the direction of the applied stress σ . The stress is applied as the ends of the lamina are kept fixed. The elastic strain energy per unit volume at distances far from the crack will be $\sigma^2/2E$. If the sample has a volume V , the total elastic strain energy without the presence of cracks will be $V\sigma^2/2E$. The introduction of the crack modifies the local distribution of stresses in its environment (see preceding subsection). When the stresses are calculated at all points around the crack, and from them the elastic energy is evaluated, it is found that the introduction of a crack decreases the stored elastic energy

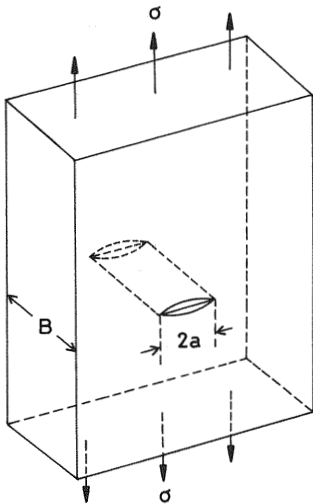


Figure 14.30 Sharp crack of length $2a$ inside a thin lamina of thickness B subjected to a tensile stress.

by a factor $\sigma^2 \pi a^2 B/E$. A simple approximation suggests that the crack suppresses the stored elastic energy in a cylindrical volume of radius a centered on the crack. The decrease in elastic energy would be

$$\text{Volume of cylinder} \times \frac{\sigma^2}{2E} = \frac{\sigma^2 \pi a^2 B}{2E}$$

which differs from the correct result by a factor of 2.

The work done to propagate a unit area of crack is G_c . Griffith's theory assumes that no heat is dissipated and that the work is done to form the two new surfaces without plastic deformation taking place. The work needed to form a crack of length $2a$ is

$$\text{Surface area of crack} \times G_c = 2aBG_c$$

and the total energy change is

$$\Delta U = -\frac{\sigma^2 \pi a^2 B}{E} + 2aBG_c \quad (14.37)$$

The dependence of ΔU on the length a is shown in Figure 14.31. For small values of a , the second term on the right in Eq. (14.37) (the term linear in a), which represents the work done when the crack propagates, is dominant. For large values of a , the first term on the right in Eq. (14.37) (a^2 term), which represents the decrease in elastic energy in the propagation of the crack, becomes dominant. When the crack is at the initial point of growth

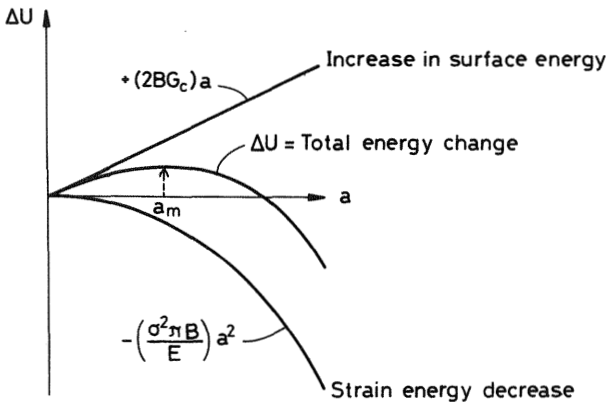


Figure 14.31 Dependence of the total energy change, ΔU , on a at constant σ . ($2a$ = crack length; a_m = critical size.)

under the stress σ , the decrease in elastic energy just balances the work of crack propagation:

$$\frac{d}{da} \left(\frac{\sigma^2 \pi a^2 B}{E} \right) = \frac{d}{da} (2aBG_c) \quad (14.38)$$

Therefore

$$\sigma^2 \pi a = EG_c \quad (14.39)$$

This point represents a maximum in the curve ΔU vs. a , with σ being kept constant. The value of a at the maximum, a_m , represents the limit from which the crack ceases to be stable:

$$a_m = \frac{EG_c}{\pi \sigma^2} \quad (14.40)$$

For values of $a > a_m$, $d \Delta U / da$ is negative and the energy of the system decreases as a increases; in this case the crack will propagate up to the fracture of the lamina. For values of $a < a_m$, the crack will not propagate, since this implies an increase in total energy, i.e., fracture is prevented for the stress σ . Therefore, from Eq. (14.39), the stress required to propagate a crack of length $2a$ up to fracture, σ_F (fracture strength), is

$$\sigma_F = \left(\frac{EG_c}{\pi a} \right)^{1/2} \quad (\text{plane stress}) \quad (14.41)$$

Equation (14.41) is obeyed under the condition of plane stresses at the tip of the crack ($\sigma_{33} = 0$), which occurs in laminae of narrow thickness (thin laminae). For thick laminae, the condition that occurs is that of plane strain ($\epsilon_{33} = 0$), and this leads to (38) (see also Chapter 16)

$$\sigma_F = \left(\frac{EG_c}{\pi(1 - \nu^2)a} \right)^{1/2} \quad (\text{plane strain}) \quad (14.42)$$

where ν is Poisson's ratio. In thin laminae, the thickness of the lamina at the tip of the crack decreases due to the Poisson contraction, leading to the condition of plane stress ($\sigma_{11} \neq 0$, $\sigma_{22} \neq 0$, $\sigma_{33} = 0$). In thick laminae, the thickness of the sample at the tip of the crack does not decrease due to Poisson's contraction, since stresses are generated [$\sigma_{33} = \nu(\sigma_{11} + \sigma_{22}) \neq 0$] that balance the contraction, leading to the condition of plane strain

($\varepsilon_{33} = 0$). Equations (14.41) and (14.42) are equivalent and can be written in a generalized way as

$$\sigma_F = \left(\frac{E^* G_c}{\pi a} \right)^{1/2} \quad (14.43)$$

where E^* is the reduced modulus, equal to Young's modulus for thin laminae and to $E/(1 - \nu^2)$ for thick laminae. The fracture energy, G_c , is considered a material parameter that depends on the test conditions. The fracture strength is controlled mainly by the size of the largest cracks in the sample. This theory gives good predictions for the fracture of brittle polymers such as polystyrene and poly(methyl methacrylate) at room temperature. Figure 14.32 shows the variation in the fracture strength under uniaxial tension for samples of these polymers in which notches of length a have been made. We

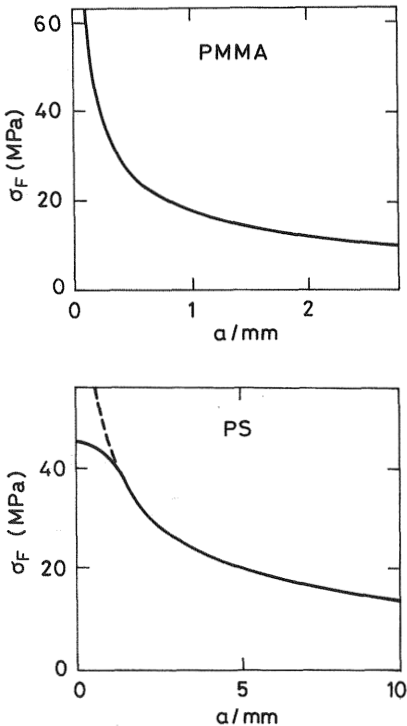


Figure 14.32 Variation of strength (fracture stress at uniaxial tension) with the length of the crack, a for polystyrene and poly(methyl methacrylate). (From Ref. 41.)

can see that, as predicted by Griffith's theory, there is a clear correlation between σ_F and a . Nevertheless, a discrepancy exists with respect to G_c . When G_c is calculated on the basis of those curves through Eq. (14.43), using the Young's modulus of these polymers, the values obtained are $G_c \approx 210 \text{ J/m}^2$ for PMMA and $G_c = 1700 \text{ J/m}^2$ for PS. These values are very much higher than the surface energy of these polymers, which are estimated to be of the order of $\gamma \approx 1 \text{ J/m}^2$. (The surface energies of solids are calculated from the measurement of the surface contact angles of liquids, using the Young-Laplace equation). The discrepancy $G_c \gg 2\gamma$ is explained by considering that Griffith's theory assumes linear elastic behavior, without taking into account that polymers display plastic deformation. As has already been remarked, even polymers that show brittle fracture without any generalized yield display plastic strain at the local level at the tip of the cracks. The energy absorbed in the plastic strain is much greater than the surface energy—hence the high values obtained for G_c in comparison with γ . Thus G_c is interpreted as the energy required to increase the crack per unit area, which includes all the energy losses. $G_c = G_0 + \Psi$, where Ψ is the energy dissipated in plastic and viscoelastic deformations at the tips of the crack and G_0 is the intrinsic fracture energy. If only secondary bonds are broken in the fracture, then $G_0 = 2\gamma$, but if fracture involves the breakage of covalent bonds, then $G_0 > 2\gamma$. Since Ψ is frequently the biggest contribution to G_c , this latter parameter is sharply dependent on the rate and temperature at which the test is conducted.

Griffith's theory establishes that the fracture of a material is determined by the size of the cracks present in it. Consequently, the strength of a sample can be increased by reducing the size of the cracks. For example, glass fibers become superficially damaged by rubbing against others, which reduces their resistance. To avoid this damage, glass fibers are subjected to a surface treatment of coating with a protective layer of polydimethylsiloxane (silanizing). Another treatment that increases the resistance of the glass to fracture consists of washing the fibers with hydrofluoric acid, which reduces the surface cracks. In brittle polymers, such as PS and PMMA (Fig. 14.32), the reduction in the size of the cracks also leads to an increase in the strength (41). Nevertheless, this increase is not unlimited, and below a determined crack size of approximately 1 mm for PS and 0.07 mm for PMMA at room temperature, σ_F becomes independent of the crack size. Brittle polymers, therefore, behave as if they had inherent cracks on the limit size, which do not modify their strength to fracture. However, although PS behaves as if it had natural or inherent cracks of size 1 mm, these cracks have never been detected in nonstrained samples. The inherent cracks are formed during the strain processes; in particular, crazes of approximately 1 mm can be seen in PS when the material is subjected to tension at room temperature, while for

PMMA the crazes are much smaller. Therefore, it is deduced that fracture takes place via crazes that are transformed into cracks. When the samples display artificial cracks bigger than inherent ones, fracture takes place by propagation of the artificial cracks.

(c) *Irwin's Model*

Irwin (40) gave an alternative formulation to fracture by considering the distribution or field of stresses around a crack in an elastic material. He proposed that such a distribution could be expressed as a function of a parameter K , known as the stress intensity factor, and he established that the fracture would occur when K exceeds a critical value K_c characteristic of each material. Figure 14.33 shows a sharp crack of length $2a$ in an infinite lamina subjected to a tensile stress σ . The equations defining the local stresses σ_{11} , σ_{22} , σ_{12} are (42)

$$\sigma_{11} = \sigma \left(\frac{a}{2r}\right)^{1/2} \cos\left(\frac{\theta}{2}\right) \left[1 - \sin\left(\frac{\theta}{2}\right) \sin\left(\frac{3\theta}{2}\right)\right] \quad (14.44a)$$

$$\sigma_{22} = \sigma \left(\frac{a}{2r}\right)^{1/2} \cos\left(\frac{\theta}{2}\right) \left[1 + \sin\left(\frac{\theta}{2}\right) \sin\left(\frac{3\theta}{2}\right)\right] \quad (14.44b)$$

$$\sigma_{12} = \sigma \left(\frac{a}{2r}\right)^{1/2} \cos\left(\frac{\theta}{2}\right) \sin\left(\frac{\theta}{2}\right) \cos\left(\frac{3\theta}{2}\right) \quad (14.44c)$$

with $\sigma_{23} = \sigma_{13} = 0$ and $\sigma_{33} = 0$ (plane stress) or $\sigma_{33} = \nu(\sigma_{11} + \sigma_{22})$ (plane strain). As should be expected, the local stresses are proportional to the external stress, σ . In these equations, when $r \rightarrow 0$ the local stresses approach

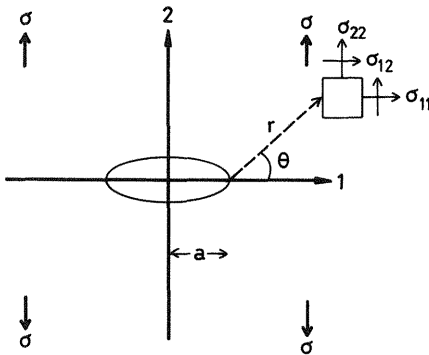


Figure 14.33 Sharp crack of length $2a$, in an infinite lamina, subjected to a tensile stress σ .

infinity. As mentioned earlier, this means that the distribution of stresses cannot be taken as a criterion of fracture, since the value of the strength of a material, which is always finite, would be exceeded at the tip of sharp cracks. Equations (14.44) can be rewritten in the generalized form

$$\sigma_{ij} = \frac{K_I}{(2\pi r)^{1/2}} f_{ij}(\theta) \quad \text{with} \quad K_I = \sigma(\pi a)^{1/2} \quad (14.45)$$

where K_I is the stress intensity factor, the subscript I indicating the mode of the load normal to the crack (other modes are not going to be considered here). In general, K_I can be expressed as

$$K_I = Q\sigma a^{1/2} \quad (14.46)$$

where Q is a dimensionless geometrical factor, so that for an infinite lamina with an internal crack of length $2a$ K takes the value $\pi^{1/2}$. The whole stress field at the crack tip is known when K_I is known. Cracks of different sizes, e.g. a and $4a$ have similar stress fields if they are loaded to σ and 2σ , respectively. K_I determines the intensity of the local stresses around the crack, due to which Irwin postulated as the criterion for fracture the condition

$$K_I = K_{Ic} \quad (14.47)$$

where K_{Ic} is known as the fracture toughness. K_{Ic} is a measure of the crack resistance of a material. For infinite laminae

$$K_{Ic} = \sigma_F(\pi a)^{1/2} \quad (14.48)$$

where σ_F is the stress at fracture. The determination of K_{Ic} by means of Eq. (14.48) requires measurement of the strength σ_F at which an internal crack of length $2a$ will start to propagate. The use of K_{Ic} to determine whether a material will support a particular stress σ implies knowledge of the size a of the cracks present in the sample. If $K_I = \sigma(\pi a)^{1/2} \geq K_{Ic}$, the material will fail due to brittle fracture.

On the basis of Eqs. (14.41), (14.42), and (14.48), the relationship between K_{Ic} and G_c is obtained. In the case of thin laminae,

$$K_{Ic} = (EG_c)^{1/2} \quad (\text{plane stress}) \quad (14.49)$$

and for thick laminae,

$$K_{Ic} = [EG_c/(1 - \nu^2)]^{1/2} \quad (\text{plane strain}) \quad (14.50)$$

as can be seen in Chapter 16.

The criterion for fracture based on reaching a critical value K_{Ic} is identical to considering a critical value for the fracture energy, G_c . The relationships given above for G and K correspond to solids that behave like perfectly elastic materials. The experimental values of K_c and G_c vary with the sample thickness. This is because there is always some local plastic deformation at the crack tips in polymers and the state of stress near the crack tip is plane stress in thin laminae and plane strain in thick ones. Yielding cannot occur in pure triaxial tension. The yield stress is greater in a triaxial stress field (plane strain) than in a biaxial one (plane stress). Therefore, in thick laminae (plane strain), yielding at the crack tip is reduced and so too are G_c and K_c . In practical cases, it is worth considering states of plane strain since the materials display the lowest values of toughness for $K_{Ic} (\text{plane stress}) > K_{Ic} (\text{plane strain})$ and $G_c (\text{plane stress}) > G_c (\text{plane strain})$.

Owing to the amplification of stresses at the crack tip, the value of the yield stress can be exceeded in that zone, leading to localized plastic strain. Nevertheless, the size of the plastic zone at the crack tip can be assumed to be sufficiently small that the sample obeys Hooke's law as far as linear elastic fracture mechanics (LEFM) is concerned. The size of that zone (see Fig. 14.34) can be estimated by determining the distance from the crack tip, r^* , at which the local stress σ_{11} exceeds the yield stress σ_y . Substituting $\sigma_y = \sigma_{11}$ into Eq. (14.44), with $\theta = 0$, gives

$$r^* = \frac{K_I^2}{2\pi\sigma_y^2} \quad (\text{plane stress}) \quad (14.51)$$

In the case of plane strain, the zone with plastic strain is smaller than the one with plane stress (38):

$$r^* = \frac{K_I^2}{6\pi\sigma_y^2} \quad (\text{plane strain}) \quad (14.52)$$

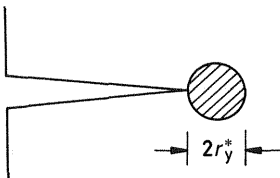


Figure 14.34 Zone of plastic strain at the tip of a crack.

(d) Measurement of K_{Ic}

In the definition of K_{Ic} [Eq. (14.48)] we assumed a lamina of infinite width with an internal crack of length $2a$. In practice, the determination of σ_F in extremely wide laminae ($W \gg a$) is not satisfactory, and therefore we resort to other geometries. The dimensions of K_{Ic} and K_I are always going to be those of the product of a stress and the square root of a length, so the change in geometry implies just the introduction of a dimensionless geometrical factor, Q , as in Eq. (14.46):

$$K_{Ic} = \sigma_F(a)^{1/2}Q \quad (14.53)$$

The simplest case would be a finite lamina of width W and thickness B with an internal crack of size $2a$, as shown in Figure 14.35, subjected to a stress $\sigma = F/(BW)$, where F is the value of the applied force at which the crack starts to grow. The expressions for K_I and K_{Ic} are (43)

$$K_I = \sigma(\pi a)^{1/2} \left[\frac{W}{\pi a} \tan\left(\frac{\pi a}{W}\right) \right]^{1/2} \quad (14.54)$$

and

$$K_{Ic} = \sigma_F(\pi a)^{1/2} \left[\frac{W}{\pi a} \tan\left(\frac{\pi a}{W}\right) \right]^{1/2} \quad (14.55)$$

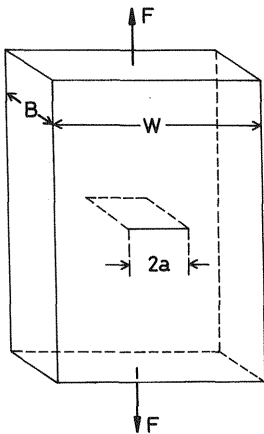


Figure 14.35 Crack of length $2a$ in a finite lamina of width W and thickness B . ($2a$ and W are of the same order of magnitude.)

Clearly, for $W/a \rightarrow \infty$, Eq. (14.55) becomes Eq. (14.48). A case that derives from the above is that of a lamina with a side crack (see Fig. 14.36). The equations in this case for K_I and K_{Ic} are identical to Eqs. (14.54) and (14.55), except that they are simply multiplied by a geometrical correction factor to account for the additional strain in the free surface. The configurations or geometries most often used in studying the fracture of rigid plastics are compact tension and three-point bend, also illustrated in Figure 14.36. The most usual techniques to evaluate the geometrical factor Q involve numerical methods the expressions of K_I for the three configurations are summarized in Table 14.2. In all cases the value of B has to be sufficiently large that at the tip of the crack the state of plane strain occurs. It has been found that this condition is met if B , $W - a$, and a are greater than $2.5 (K_{Ic}/\sigma_Y)^2$. Under these conditions, the zone of plastic strain at the tip of the crack is less than 2% and the K_{Ic} that is determined is a genuine property of the material. The measured values of K_{Ic} are dependent on the sharpness of the crack in such a way that when blunt cracks are used, unrealistically high values of K_{Ic} are obtained. The crack must be sharp because Eq. (14.44), which is the origin of the definition of K_I , is limited to sharp cracks. Despite this, linear elastic fracture mechanics is always used in engineering to obtain the failure conditions in the worst case for greater security. If an element is

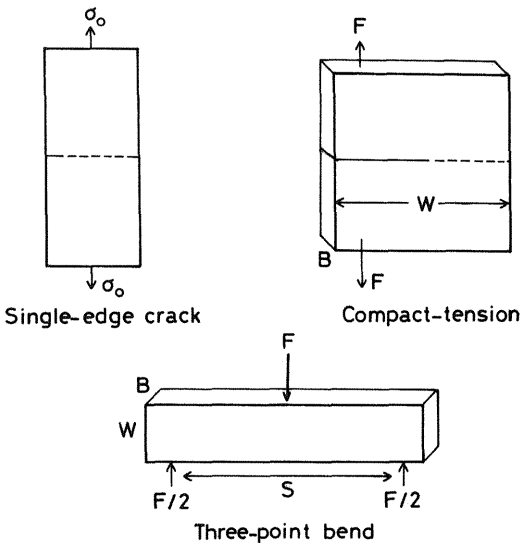


Figure 14.36 Scheme of the most typical specimen geometries used in studying the fracture of brittle polymers.

Table 14.2 Expressions of K_I for Specimens of Different Geometries Commonly Used in the Fracture of Polymers

Geometry	Expression for K_I
Single-edge crack	$K_I = \sigma(\pi a)^{1/2} \left[1.12 - 0.23 \left(\frac{a}{W} \right) + 10.55 \left(\frac{a}{W} \right)^2 - 21.71 \left(\frac{a}{W} \right)^3 + 30.38 \left(\frac{a}{W} \right)^4 \right]$ $\sigma = F/WB$
	or
	$K_I = 1.12\sigma(\pi a)^{1/2} a/W \rightarrow 0$
Three-point bend	$\sigma = 3SF/2BW^2$ $S = 8W$ $K_I = \sigma(\pi a)^{1/2} [1.11 - 1.55(a/W) + 7.71(a/W)^2 - 13.5(a/W)^3 + 14.2(a/W)^4]$ $S = 4W$ $K_I = \sigma(\pi a)^{1/2} [1.09 - 1.73(a/W) + 8.20(a/W)^2 - 14.17(a/W)^3 + 14.55(a/W)^4]$
Compact tension	$K_I = \sigma(\pi a)^{1/2} [16.7 - 104.7(a/W) + 369.9(a/W)^2 - 573.8(a/W)^3 + 360.5(a/W)^4]$ $\sigma = F/WB$

^a F = applied force; B = thickness; W = width; S = span between supports.

Source: Refs. 44 and 45.

designed so that it will not fail when it develops sharp cracks, then it will become safer if the cracks are blunt, since in that case the amplification of stresses at the crack tip is less.

The values of the fracture toughness K_{Ic} depend on the structural and morphological characteristics of the polymer sample such as molecular mass, degree of cross-linking, and degree of crystallinity, but they also

depend on the conditions under which the test is conducted, such as temperature and strain, and even on the thickness of the specimen being tested (as was already discussed). Table 14.3 gives the values of K_{Ic} for some typical polymers. The comparison of the toughness values has to be made with care considering their dependence on the factors mentioned above. In general, it can be stated that thermoset (highly cross-linked) resins have low values of K_{Ic} and therefore are brittle materials. Traditional thermoplastics, such as PS and PMMA, present low values of toughness, in contrast to engineering plastics, such as polyamides (nylon), poly(ethylene terephthalate) (PET), poly(methylene oxide) (PPO), or poly(ether etherketones) (PEEK), which are tougher.

14.4.4 Impact Strength

Impact strength tests determine the capability of a material to maintain its structural integrity and to absorb energy in a sudden impact. Many practical applications require materials to be resistant to impact loads, and impact toughness is the deciding factor in the selection of these materials. Many polymers that are ductile in normal conditions, with high values of fracture toughness when they are tested under tension with moderate strain rates, display brittle fracture under impact loads (very high strain rate). Moreover, the brittle behavior is more likely to occur if the impact on the sample takes place at low temperatures and if the sample contains stress concentration centres such as cracks and notches. The resistance to impact depends on the geometry of the sample and on the type of test, and therefore it is not a

Table 14.3 Values of K_{Ic} for Some Polymers at 20°C

Polymer	K_{Ic} (MPa m ^{1/2})
Epoxies	0.6
Polystyrene (PS)	0.7–1.1
Poly(methyl methacrylate) (PMMA)	0.7–1.6
Poly(vinyl chloride) (PVC)	2.0–4.0
Polypropylene (PP)	3.0–4.4
Poly(methylene oxide) (PMO)	~ 4
Nylon 6.6	2.5–3.0
Poly(ethylene terephthalate) (PET)	~ 5
Poly(ether ketone) (PEEK)	7

Source: Ref. 37.

defined property of the material. The most commonly used tests are those of Izod and Charpy. In these tests, a bar of material is struck by a pendulum, as shown in Figure 14.37, and the energy required to fracture the sample is determined by the loss of energy of the weight or hammer. The impact energy is calculated as the energy per unit surface area of fracture, though it is sometimes tabulated as energy per unit length of the notch. Table 14.4 gives some values of the impact energy determined for rigid polymers by the Izod test. Obviously, there has to exist a proportional relationship between the impact energy and the fracture toughness K_{Ic} or fracture energy G_c , but as a consequence of their dependence on the factors mentioned above (geometry of the sample) as well as the actual sample characteristics (capacity to display yield at the tip of the notch), there is no universal formula to correlate the values of the impact energy with those of G_c .

14.4.5 Impact-Resistant Polymers: Polymers Modified with Rubbers

Glassy polymers, PMMA and PS, are suitable for many applications, but they are brittle when subjected to impact loads. The same thing happens with thermoset polymers such as epoxy or phenolic resins. To solve this problem, impact-resistant polymers have been developed that basically consist of a matrix of the brittle polymer in which a second elastomeric

Table 14.4 Izod Impact Test for Rigid Polymers at 24°C

Polymer	Impact energy (kJ/m ²)
Polystyrene	1.3–2.1
High-impact PS (polystyrene + polybutadiene)	3–42
ABS poly(acrylonitril- <i>co</i> -butadiene- <i>co</i> -styrene)	5–53
Rigid PVC	2–16
PMMA	2.1–2.6
Nylon	5.3–16
PMO	10–16
Low density PE	> 84
High density PE	2.6–105
PP	2.6–11
Polycarbonate (bisphenol A)	63–95
Epoxy resin	1–26

Source: Ref. 46.

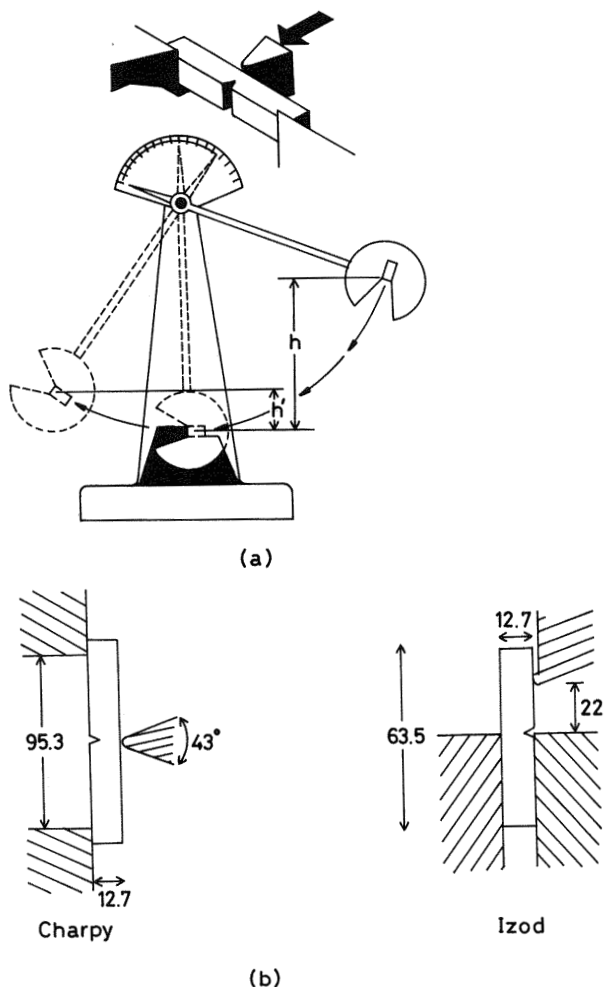


Figure 14.37 (a) Schematic diagram of an impact test machine. (b) Geometry of the specimen in the Izod and Charpy tests.

phase has been dispersed (25,47). There are two mechanisms to obtain this morphology; the first is by blending an immiscible elastomer with the polymer; the second process is via the synthesis of block copolymers in which one part of the molecule consists of the glassy polymer while the other gives rise to the elastomeric phase, both phases being immiscible. In this latter case the chemical bonding between the glassy blocks and the

elastomer blocks ensures a good interfacial join between the phases. A typical example is the ABS block copolymer acrylonitril-*co*-butadiene-*co*-styrene. In the preparation of high impact epoxies, the resins before cross-linking are mixed with the elastomer, for example a nonvulcanized rubber, which usually contains nitril groups. The polarity of this rubber causes it to be miscible with the resin prior to cross-linking, and when the cross-linking of the epoxy resin is carried out the elastomer phase becomes dispersed in the form of small aggregates. The molecules of rubber usually contain terminal carboxyl groups [poly(butadiene-*co*-acrylonitril) terminating in carboxyl groups; CTBN] that react with the epoxy matrix in order to ensure good anchorage of the two phases: elastomer and brittle epoxy matrix. In general, for the resistance to impact to be enhanced by dispersion of an elastomer phase in the vitreous matrix, (1) the T_g of the rubber must be much lower than the working temperature; (2) the rubber must be immiscible with the glassy matrix; and (3) there must be a good adhesion between the elastomer and the glassy phases. The introduction of the elastomeric phase into the glassy matrix converts the brittle polymer into a tough material. Figure 14.38 shows the stress-strain curves for PS and high-impact PS; untreated polystyrene displays brittle behavior, while polystyrene modified with butadiene displays ductile behavior, yielding

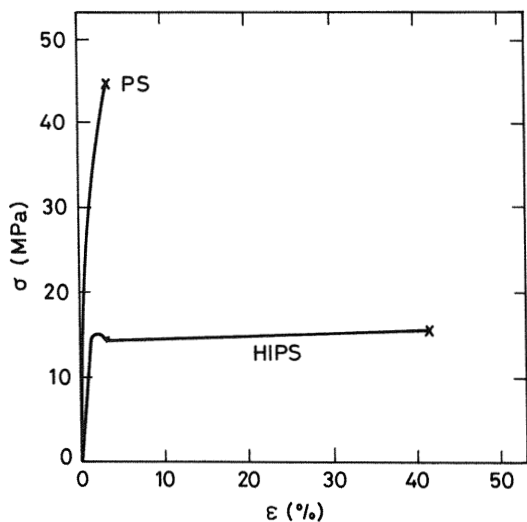


Figure 14.38 Stress-strain curves for polystyrene and high impact polystyrene. (From Ref. 48.)

and failing with a strain of 40%. Table 14.5 gives the values of the elastic modulus and the fracture toughness of various polymers modified with rubber.

Yield and crazing are plastic strain mechanisms that absorb energy and increase G_c . It can therefore be expected that the procedures for increasing the toughness of polymers, such as modification with elastomers, will be effective because they favor the plastic strain in a way that can be controlled at the local level. Indeed, the elastomeric phase dispersed in the glassy matrix possesses an elastic modulus that is several orders of magnitude lower than that of the matrix itself, giving rise to a concentration of stresses at the surfaces of the particles when the material is strained that is similar to the concentration produced at the tips of cracks. This concentration of stresses produces microcrazing or yield at the local level around each elastomer particle, and because of that the material will absorb a great amount of energy during strain, thereby increasing its toughness and resistance to impact. In the case of high impact polystyrene, large microcrazes starting from the particles or aggregates of butadiene can be seen when the material is observed with a transmission electron microscope. In the modification of PMMA, a dispersion is achieved of very small particles of poly(*n*-butyl acrylate-*co*-styrene) that have a refractive index similar to that of the PMMA matrix and are smaller than the wavelength of visible light. This dispersion increases the toughness of the material without altering the transparency of PMMA. In this case, the mechanism that confers toughness is assumed to be the shear bands around the particles, which, because they do not give rise to changes in density, cannot be detected by an electron microscope in the way that microcrazing can.

Table 14.5 Young's Modulus, E , and Fracture Toughness, K_{Ic} , for Some Polymers

Polymer	E (GPa)	K_{Ic} (MPa m ^{1/2})
PS	3.0	1.1
High impact PS	2.1	5.8
PMMA	3.0	1.2
PMMA modified with rubber	2.1	2.4
Epoxy resin	2.8	0.5
Epoxy resin modified with rubber	2.4	2.2

Source: Ref. 25.

14.4.6 Fatigue

The term “fatigue” refers to the fracture undergone by a material when it is subjected over a long period of time to stresses that are lower than its strength. Under certain conditions, the microcracks existing in a material grow slowly, and, with this, K_I increases until it reaches the critical value K_{Ic} . At that moment, a sudden brittle fracture occurs in the part that had been supporting constant or alternating loads over a long period of time. Two types of fatigue can be distinguished: static and dynamic. What is called static fatigue occurs under conditions of constant load in which the stress applied is less than that needed to produce a fracture, σ_F , under conditions of monotonically growing load (stress-strain tests). Static fatigue is represented by curves of the applied stress versus the time required for failure. Illustrated in Figure 14.39 is an example of polyethylene at various temperatures. Clearly, the greater the stress applied, the less the time taken for the sample to fail. In static fatigue, both failure mechanisms, ductile and brittle, can occur. In general, at high stresses and short times, ductile fracture occurs, while at low stresses and long times, the failure is brittle. The ductile–brittle transition is shifted to longer times as the temperature decreases (see Fig. 14.39). This transition does not depend only on the actual

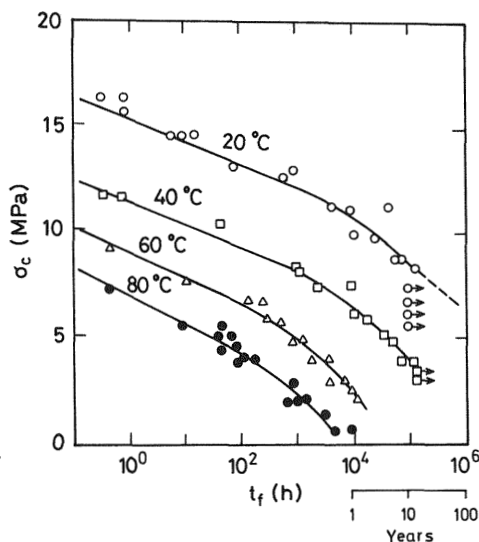


Figure 14.39 Applied stress versus failure time (static fatigue) for a sample of high density polyethylene at various temperatures. The inflection shows the point of change from brittle failure to ductile failure. (From Ref. 49.)

characteristics of the material (molecular mass, microstructure, crystallinity, etc.) and temperature; it is also affected by external agents in such a way that chemically aggressive environments favor brittle fracture (50).

Dynamic fatigue is the failure or fracture of a material under oscillatory loads ($\sigma \ll \sigma_F$). Dynamic failure is a very serious problem because materials fail at stress levels much lower than under monotonic loading. Moreover, for a given stress amplitude, the time to failure is shorter than in static fatigue. Most common dynamic tests employ sinusoidal loading, controlling the stress amplitude [$\sigma_a = (1/2)(\sigma_{\max} - \sigma_{\min})$] over unnotched specimens, with different loading methods, e.g., bending or torsion. The classical fatigue curves represent the stress amplitude versus the logarithm of the number of cycles to failure, such as those shown in Figure 14.40. The time to failure increases with decreasing stress amplitude. The curves have a sigmoidal shape, but at intermediate stress a linear relation is obtained. For large numbers of cycles (10^7) the curves become horizontal. Thus there is a limit stress amplitude value under which the material can be cycled without causing failure; it is called the endurance limit. The fatigue of polymers is strongly dependent on the load frequency. Figure 14.41 illustrates the typical fatigue behavior of a thermoplastic at several frequencies. The viscoelastic behavior of polymers provokes some heat dissipation in each loading cycle, which, together with the lower thermal conductivity of polymers, causes large increases in the temperature of the material at high

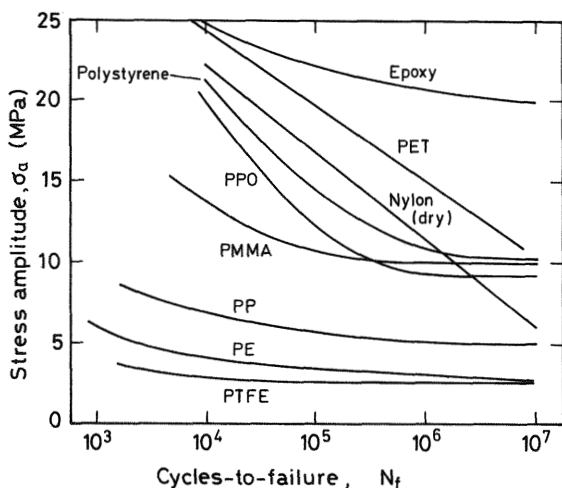


Figure 14.40 Stress amplitude versus $\log N_f$ for several polymers. N_f = cycles to failure. (From Ref. 51.)

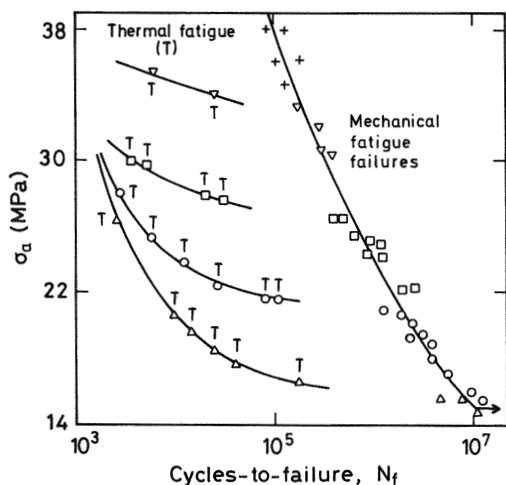


Figure 14.41 Stress amplitude versus $\log N_f$ for a polyacetal copolymer at (+) 0.167, (∇) 0.5, (\square) 1.67, (\circ) 5.0, and (\triangle) 10.0 Hz. N_f = cycles to failure. (From Ref. 52.)

stresses and high test frequencies. Under these conditions, the failure takes place by way of thermal softening; this type of failure is called thermal fatigue failure. The curves of fatigue in Figure 14.41 show two different regimes, one for conventional mechanical fatigue and the other for softening thermal fatigue. Mechanical fatigue involves the initiation and posterior propagation of a crack. Fatigue cracks are developed from surface or internal defects or flaws. In the propagation stage, the fatigue crack grows by a small amount in each cycle; this stage seems to control the fatigue life. Thus the usual studies of fatigue involve monitoring the growth of a crack that has macroscopic dimensions over the number of cycles applied. For brittle polymers the propagation rate is proportional to the stress intensity factor range, $\Delta K_I = K_{I\max} - K_{I\min}$ (53,54):

$$\frac{da}{dN} = A \Delta K_I^m \quad (14.56)$$

where m and A are constants for each polymer sample that depend on temperature, frequency, stress ratio, and the characteristics of the polymer such as molecular weight and crystallinity. In Figure 14.42, double logarithmic plots of da/dN versus ΔK_I are presented for several polymers. It can be seen that the behavior is linear. However, in some cases the pattern may be sigmoidal because A and m are not truly constants.

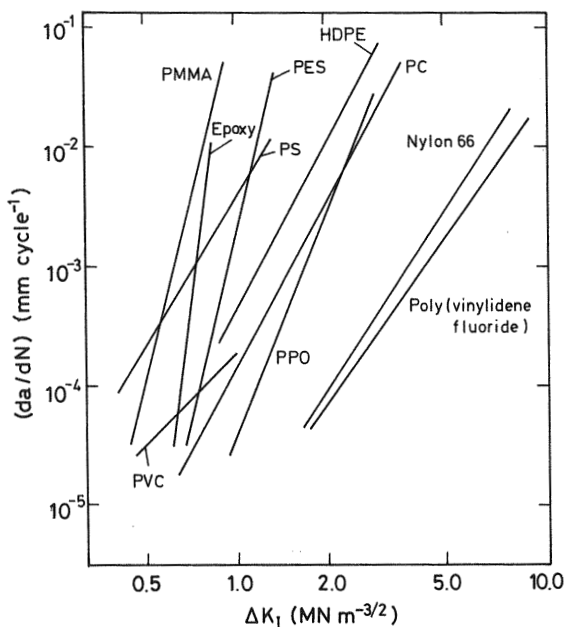


Figure 14.42 Fatigue crack growth rate da/dN versus ΔK_I for several polymers. (From Refs. 55 and 56.)

PROBLEM SETS

Problem 14.1

The stress-strain curve for a material can be represented by means of the function $\sigma_t = 12 \varepsilon^{0.85}$, where σ_t represents the true tension stress in MPa and ε is strain. Calculate the value of the strain at the necking point and the value of the yield stress, σ_y .

Solution 14.1

According to Eq. (14.5), the nominal stress and the true stress are related by

$$\sigma_n = \sigma_t / (1 + \varepsilon) \quad (\text{P14.1.1})$$

Also, necking takes place when

$$\frac{d\sigma_n}{d\varepsilon} = 0 \quad (\text{P14.1.2})$$

According to Eq. (P14.1.1),

$$\sigma_n = 12\varepsilon^{0.85}/(1 + \varepsilon) \quad (\text{P14.1.3})$$

By substituting Eq. (P14.1.3) into Eq. (P14.1.2), we obtain

$$\frac{12 \times 0.85\varepsilon^{-0.15}}{1 + \varepsilon} - \frac{12\varepsilon^{0.85}}{(1 + \varepsilon)^2} = 0 \quad (\text{P14.1.4})$$

This expression leads to

$$\varepsilon = \frac{10.20}{12 - 10.20} = 5.67 \quad (\text{P14.1.5})$$

Then the value of σ_y is given by

$$\sigma_y = 12 \times 5.67^{0.85} = 52.44 \text{ MPa} \quad (\text{P14.1.6})$$

Problem 14.2

A sample of polypropylene tested at 30°C and 10^{-2} s^{-1} shows a yield stress of 35 MPa in uniaxial tension and 38 MPa under uniaxial compression. Calculate the hydrostatic pressure that must be superimposed in order to reach yield stress of 80 MPa. Assume that the material obeys the pressure-dependent von Mises criterion.

Solution 14.2

Equations (14.10) and (14.12) give the pressure-dependent von Mises criterion. Also, for any state of stresses, P is an invariant given by the expression $P = (1/3)(\sigma_1 + \sigma_2 + \sigma_3)$. On the basis of this expression, in a uniaxial tension test ($\sigma_2 = \sigma_3 = 0$)

$$P = (1/3)\sigma_1 \quad (\text{P14.2.1})$$

According to (P14.2.1), in tension,

$$P = (1/3)\sigma_1 = (1/3)(35) = 11.67 \text{ MPa} \quad (\text{P14.2.2})$$

and in compression,

$$P = (1/3)\sigma_1 = (1/3)(-38) = -12.67 \text{ MPa} \quad (\text{P14.2.3})$$

From Eqs. (14.11) and (14.12),

$$\sigma_y = \sqrt{3}(\tau_y^0 - \mu P) \quad (\text{P14.2.4})$$

Therefore, in tension,

$$35 = \sqrt{3}(\tau_y^0 - \mu 11.67) \quad (\text{P14.2.5})$$

and in compression,

$$38 = \sqrt{3}(\tau_y^0 + \mu 12.67) \quad (\text{P14.2.6})$$

From Eqs. (P14.2.5) and (P14.2.6) we obtain $\tau_y^0 = 21.04$ MPa and $\mu = 0.071$ (for P in MPa). When the mechanical test is made in a pressure chamber, the hydrostatic stress term is expressed as the sum of the hydrostatic component of the stress applied in the mechanical experiment and the pressure superimposed. Then

$$P = \frac{1}{3}\sigma_y + P_{\text{imposed}} \quad (\text{P14.2.7})$$

By substituting Eq. (P14.2.7) into Eq. (P14.2.4) we obtain

$$\sigma_y = \sqrt{3}\left(\tau_y^0 - \mu\frac{1}{3}\sigma_y - \mu P_{\text{imposed}}\right) \quad (\text{P14.2.8})$$

Since $\sigma_y = 80$ MPa, $\tau_y^0 = 21.04$ MPa, and $\mu = 0.071$ (for P in MPa), $P_{\text{imposed}} = -381$ MPa. The negative value expresses the fact that the pressure is compressive.

Problem 14.3

For a sample of polyethylene, the values of the yield stress σ_y for different strain rates at $T = 25^\circ\text{C}$ and $T = 18^\circ\text{C}$ are given in the following table:

	$T = 25^\circ\text{C}$			$T = 15^\circ\text{C}$		
$\dot{\epsilon} \times 10^2 \text{ (s}^{-1}\text{)}$	0.833	8.33	83.3	0.833	8.33	83.3
$\sigma_y \text{ (MPa)}$	22.6	26.9	31.9	25.6	30.52	34.56

Determine ΔE and V^* for the yielding of polyethylene.

Solution 14.3

According to Eq. (14.20), a plot of σ_y/T vs. $\log \dot{\epsilon}_y$ (Fig. P14.3.1) gives a straight line from whose slope,

$$\frac{d(\sigma_y/T)}{d(\log \dot{\epsilon}_y)} = \frac{2 \times 2.303R}{V^*} \quad (\text{P14.3.1})$$

the value of V^* can be obtained. Thus,

$$V^* = \frac{2 \times 2.303 \times 8.3143}{15.6 \times 10^3} = 2.45 \times 10^{-3} \text{ m}^3/\text{mol} \quad (\text{P14.3.2})$$

For a constant value of σ_y/T at two different temperatures, one obtains:

$$\frac{\Delta E^*}{T_1} + 2.303 \times R \times \log[\dot{\epsilon}_y(T_1)] = \frac{\Delta E^*}{T_2} + 2.303R \log[\dot{\epsilon}_y(T_2)] \quad (\text{P14.3.3})$$

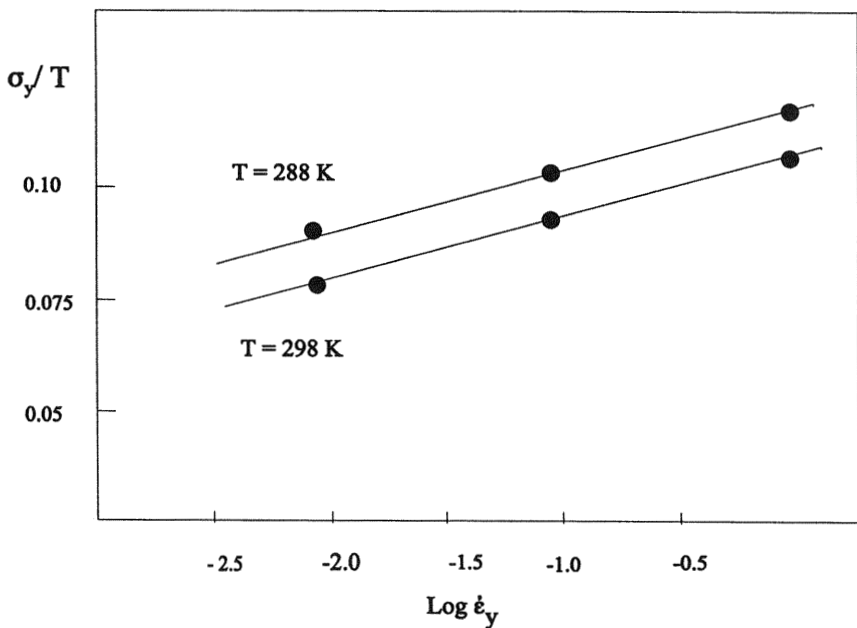


Figure P14.3.1.

Therefore,

$$\Delta E^* = \frac{2.303R\{\log[\dot{\epsilon}_y(T_2)] - \log[\dot{\epsilon}(T_1)]\}}{1/T_1 - 1/T_2} = 151.2 \text{ kJ/mol} \quad (\text{P14.3.4})$$

The physical meaning of V^* and ΔE^* , if any, is obscure. The size of V^* per jumping segment is

$$\frac{V^*}{\text{Avogadro's number}} = \frac{2.45 \times 10^{-3}}{6.02 \times 10^{23}} = 4.1 \text{ nm}^3 \quad (\text{P14.3.5})$$

Taking into account that the volume of a unit cell of polyethylene, with four units of CH_2 inside, is $0.254 \times 0.736 \times 0.492 = 0.1 \text{ nm}^3$, V^* is a volume containing nearly 160 polymer carbon atoms. The value of ΔE^* is typical of a deformation process associated with polymers. Although it cannot usually be related to any molecular relaxation process, ΔE^* near T_g may approach the activation barrier energy of the α molecular relaxation.

Problem 14.4

A wide sheet of polycarbonate that contains a central sharp crack of length $2a = 20 \text{ mm}$ fractures at a stress of 13.5 MPa .

- Calculate K_{Ic} for polycarbonate.
- Calculate the fracture stress of a wide sheet containing a crack of length 40 mm .
- Will a crack of 10 mm in a similar sheet fracture under a stress of 10 MPa ?

Solution 14.4

(a) According to Eq. (14.48),

$$K_{Ic} = \sigma_F(\pi a)^{1/2} = 13.5 \left(\pi \frac{0.020}{2} \right)^{1/2} = 2.4 \text{ (MPa m}^{1/2}\text{)} \quad (\text{P14.4.1})$$

(b) The fracture stress [Eq. (14.48)] is given by

$$\sigma_F = K_{Ic}(\pi a)^{-1/2} = 2.4 \left(\pi \frac{0.040}{2} \right)^{-1/2} = 9.57 \text{ MPa} \quad (\text{P14.4.2})$$

(c)

$$K_I = \sigma(\pi a)^{1/2} = 10 \left(\pi \frac{0.010}{2} \right)^{1/2} = 1.25 \text{ MPam}^{1/2} \quad (\text{IP14.4.3})$$

Since $K_I < K_{Ic}$, the sheet will not fracture.

Problem 14.5

A rectangular bar of polymer of thickness $B = 8$ mm and width $W = 20$ mm has a central notch of length $a = 10$ mm. The bar is loaded in a three-point bending test with an 80 mm span, S , at room temperature. The bar fractures when the force applied is 300 N. Calculate (a) K_{Ic} for the polymer and (b) the force needed to fracture in a compact tension test a specimen of dimensions $W = 50$ mm, $B = 10$ mm, having a single-edge sharp crack of $a = 25$ mm.

Solution 14.5

(a) According to the expression given in Table 14.2 for the three-point bending test with the geometry $S = 4W$,

$$K_{Ic} = \sigma_F(\pi a)^{1/2} Y \quad (\text{P14.5.1})$$

where Y is a geometric factor [see Eq. (14.53)] ($Q = \pi^{1/2} Y$),

$$Y = 1.09 - 1.73(a/W) + 8.20(a/W)^2 - 14.17(a/W)^3 + 14.55(a/W)^4$$

Since $a/W = 0.5$,

$$Y = 1.09 - 1.73 \times 0.5 + 8.20 \times (0.5)^2 - 14.17 \times (0.5)^3 + 14.55 \times (0.5)^4$$

$$Y = 1.413 \quad (\text{P14.5.2})$$

For this kind of test the elasticity theory gives (see Table 14.2)

$$\sigma_F = \frac{3SF}{2BW^2} = \frac{3 \times 0.080 \times 300}{2 \times 0.008 \times (0.020)^2} = 11.25 \text{ MPa} \quad (\text{P14.5.3})$$

Therefore,

$$K_{Ic} = 11.25 \times (0.01\pi)^{1/2} \times 1.413 = 2.82 \text{ (MPa m}^{1/2}\text{)} \quad (\text{P14.5.4})$$

(b) On the other hand, for compact tension tests (see Table 14.2),

$$\sigma_F = \frac{K_{Ic}}{Y(\pi a)^{1/2}} \quad (\text{P14.5.5})$$

where

$$Y = 16.7 - 104.7(a/W) + 369.9(a/W)^2 - 573.8(a/W)^3 + 360.5(a/W)^4 \quad (\text{P14.5.6})$$

Since $a/W = 0.5$ and $Y = 7.63$,

$$\sigma_F = \frac{2.82}{7.63 \times (\pi \times 0.025)^{1/2}} = 1.3 \text{ MPa} \quad (\text{14.5.7})$$

Therefore,

$$F = \sigma_B W = 1.3 \times 10^6 \times 0.010 \times 0.05 = 650 \text{ N} \quad (\text{P14.5.8})$$

Problem 14.6

A rectangular bar of polycarbonate of thickness $B = 20$ mm and width $W = 20$ mm is loaded in a three-point bending test with an 160 mm span. Calculate (a) the force needed to fracture the bar if it has a notch of length $a = 10$ mm and (b) the minimum notch length, a , needed to initiate brittle fracture before yield occurs.

Data for PC: $E = 3.2$ GPa, $\nu = 0.40$, $\sigma_Y = 64$ MPa, and $G_c = 1.5$ kJ (plane strain).

Solution 14.6

According to Eq. (14.50),

$$K_{Ic} = \left(\frac{3.2 \times 10^9 \times 1.5 \times 10^3}{1 - 0.4^2} \right)^{1/2} = 2.39 \times 10^6 \text{ Pam}^{1/2} = 2.39 \text{ MPam}^{1/2} \quad (\text{P14.6.1})$$

For three-point bending with $S/W = 8$ (see Table 14.2),

$$K_{Ic} = \sigma_F (\pi a)^{1/2} Y \quad (\text{P14.6.2})$$

$$Y = 1.11 - 1.55(a/W) + 7.71(a/W)^2 - 13.5(a/W)^3 + 14.2(a/W)^4$$

where Y is a geometric factor.

For $a/W = 0.5$,

$$Y = 1.11 - 1.55 \times 0.5 + 7.71 \times (0.5)^2 - 13.5 \times (0.5)^3 + 14.2 \times (0.5)^4 = 1.46 \quad (\text{P14.6.3})$$

Then the fracture stress [Eq. (14.53) with $Q = \pi^{1/2} Y$] is obtained as

$$\sigma_F = \frac{K_{Ic}}{Y(\pi a)^{1/2}} = \frac{2.39}{1.46 \times 0.010 \times \pi^{1/2}} = 9.24 \text{ MPa} \quad (\text{P14.6.4})$$

Since (see Table 14.2)

$$\sigma_F = 3SF/2BW^2 \quad (\text{P14.6.5})$$

the force necessary to fracture the bar is

$$F = \frac{9.2413 \times 33210^6 \times 2 \times (0.020)^2 \times 0.020}{3 \times 0.160} = 77 \text{ N} \quad (\text{P14.6.6})$$

(b) Brittle fracture occurs when $K_I \geq K_{Ic}$, so

$$K_{Ic} \leq K_I = \sigma_Y(\pi a)^{1/2} Y$$

$$Y = 1.11 - 1.55(a/W) + 7.71(a/W)^2 - 13.5(a/W)^3 + 14.2(a/W)^4 \quad (\text{P14.6.7})$$

Hence,

$$\begin{aligned} 2.39 \times 10^6 &\leq 64 \times 10^6 (\pi a)^{1/2} \\ &\times [1.11 - 1.55 \times (a/0.02) + 7.71 \times (a/0.02)^2 - 13.5 \times (a/0.02)^3 + 14.2 \\ &\times (1/0.02)^4] \end{aligned} \quad (\text{P14.6.8})$$

Therefore, $a \geq 0.4 \text{ mm}$.

Problem 14.7

The table shows the force needed to fracture single-edge bars of several polymers at room temperature in a three-point bending test. Bar dimensions are $W = 10 \text{ mm}$, $B = 6 \text{ mm}$, $a = 5 \text{ mm}$; the test span S is 80 mm . The second column in the table gives the corresponding yield stress. Calculate K_{Ic} for each polymer, and indicate in which cases valid plane strain conditions exist.

Polymer	Data		Results	
	F (N)	σ_Y (MPa)	K_{Ic} (MPam ^{1/2})	$2.5(K_{Ic}/\sigma_Y)^2$ (mm)
Epoxy resin	16.4	100	0.60	0.09
Epoxy (toughened (CTBN)	63	65	2.3	3.1
Nylon 66	85	75	3.1	4.3
Polycarbonate	60	63	2.2	3.0
Poly(oxymethylene)	156	62	5.7	21.1
Polystyrene	30	50	1.1	1.2

Solution 14.7

For three-point bending tests (see Table 14.2),

$$\sigma_F = 3SF/2BW^2 \quad (\text{P14.7.1})$$

When $S = 8W$,

$$K_{Ic} = \sigma_F(\pi a)^{1/2} Y \quad (\text{P14.7.2})$$

where

$$Y = 11 - 1.55(a/W) + 7.71(a/W)^2 - 13.5(a/W)^3 + 14.2(a/W)^4$$

By substituting the values of the bar dimensions into Eq. (P14.7.1), we find

$$\sigma_F = 2 \times 10^5 F \quad (\text{P14.7.3})$$

and

$$K_{Ic} = 2 \times 10^5 \times F \times (0.005 \times \pi)^{1/2} \times 1.46 \quad (\text{P14.7.4})$$

where the force in newtons is given in the second column of Table P14.7. The results for K_{Ic} calculated from Eq. (P14.7.4) for each polymer are given in the third column of the table. The dimensions B , $W - a$, and a should be greater than $2.5(K_{Ic}/\sigma_Y)^2$ for plane strain fracture (plane strain conditions at the crack tip) so the plastic deformation at the crack tip will be negligible and the K_{Ic} calculated a true material property. The fourth column in the table shows the values obtained for $2.5(K_{Ic}/\sigma_Y)^2$ in each case.

As can be seen, the value of $2.5 (K_{IC}/Jy)^2$ for poly(oxymethylene) is larger than the dimensions of B , $W - a$, and a ; therefore, this sample undergoes plastic deformation at the crack tip and the K_{IC} value is not reliable.

REFERENCES

1. FHJ Baltá-Calleja. *Adv Polym Sci* 66: 117, 1985.
2. R Popli, L Mandelkern. *J Polym Sci B Polym Phys* 24: 441, 1987.
3. B Crist, CJ Fisher, PR Howard. *Macromolecules* 22: 1709, 1989.
4. T Juska, IR Harrison. *Polym Eng Sci* 22: 766, 1982.
5. PB Bowden, RJ Young. *J Mater Sci* 9: 2034, 1974.
6. RJ Young. In: EH Andrews, ed. *Developments in Polymer Fracture*, Vol 1. London: Applied Science, 1979, pp. 223–261.
7. RF Saraf, RS Porter. *J Polym Sci B Polym Phys* 26: 1049, 1988.
8. A Peterlin. *J Polym Sci C9*: 61, 1965.
9. RN Haward. *The Physics of Glassy Polymers*. London: Applied Science, 1973.
10. AH Cottrell. *Dislocations and Plastic Flow in Crystals*. Oxford UK: Clarendon Press, 1953.
11. R von Mises. *Gottingen Nach Math-Phys K1* 1913, p 582.
12. Y Imai, N Brown. *J Polym Sci Polym Phys Ed* 14: 273, 1976.
13. W Whitney, RD Andrews. *J Polym Sci C-14*: 2981, 1967.
14. S Matsuoka. In: W Brostow, R Corneliussen, eds. *Failure of Plastics*. Munich: Carl Hanser, Chap 3, 1986.
15. PB Bowden, S Raha. *Phil Mag* 22: 463, 1970.
16. G Halsey, HJ White, H Eyring. *Text Res J* 15: 295, 1945.
17. CF Bauwens-Crowet, JA Bauwens, G Homes. *J Polym Sci A2* 7: 735, 1969.
18. RE Robettson. *J Appl Polym Sci* 7: 443, 1963.
19. J Narisawa, M Ishikawa, H Ogawa. *J Polym Sci Polym Phys Ed* 14: 1459, 1978.
20. RD Gales, NJ Mills. *Eng Fract Mech* 6: 93, 1974.
21. GP Marshall, LH Coutts, JG Williams. *J Mater Sci* 9: 1409, 1974.
22. RP Kambour. *J Polym Sci A-2* 4: 349, 1966.
23. AJ Kinloch, RJ Young. *Fracture Behavior of Polymers*. London: Applied Science, 1983. Chap 5.
24. A Narisawa, F Yee. *Crazing and fracture in polymers*. In RW Cahn, P Haasen, EJ Kramer eds. *Material Science and Technology*, Vol 12. New York: WCH 1993, p. 699.
25. RJ Young, PA Lovell. *Introduction to Polymers*. New York: Chapman & Hall, 1991.
26. RN Haward. *Amorphous Materials*. RW Douglas, B Ellis, eds. London: Wiley-Interscience, 1972.
27. RP Kambour. *Macromol Rev* 7: 1, 1973.
28. SS Sternstein, L Ongchin. *Polym Prepr Am Chem Soc* 19: 1117, 1969.
29. EJ Kramer. *Adv Polym Sci* 52/53: 1, 1983.
30. JF Fellers, BF Kee. *J Appl Polym Sci* 18: 2355, 1974.

31. RP Kambour, CL Gruner, EE Romagosa. *J Polym Sci Phys* 11: 1879, 1973.
32. RP Kambour, RW Kopp. *J Polym Sci A-2* 7: 183, 1969.
33. EH Andrews. *Fracture in Polymers*. London: Oliver & Boyd, 1968.
34. IM Ward, DW Hadley. *Mechanical Properties of Solid Polymers*. New York: Wiley & Sons, Inc, 1993.
35. AJ Kinloch, RJ Young. *Fracture Behaviour of Polymers*. London: Applied Science, 1983, Chap 2.
36. CB McCrum, CP Buckley, CB Bucknall. *Principles of Polymer Engineering*. London: Oxford Science, 1997, Chap 5.
37. JW Williams. *Fracture Mechanics of Polymers*. Chichester: Ellis Horwood, 1984, Chaps 4 and 6.
38. AJ Kinloch, RJ Young. *Fracture Behaviour of Polymers*. London: Applied Science, 1983, Chap 3.
39. AA Griffith. *Phil Trans Roy Soc A*221: 163, 1920.
40. GR Irwin. *Appl Mater Res* 3: 1964; *J Appl Mech* 24: 361, 1957.
41. JP Berry. In: H Liebowitz, ed. *Fracture VII*. New York: Academic, 1972, Chap 2.
42. JR Rice. In: H Liebowitz ed. *Fracture: An Advanced Treatise*, Vol 2. New York: Academic, 1968, p. 192.
43. D Broek. *Elementary Engineering Fracture Mechanics*. Alphen aan den Rijn, The Netherlands: Sijthof & Noordhoff, 1978, Chap 3.
44. ASTM-E399-78. *Plane-Strain Fracture Toughness of Metallic Materials*. Philadelphia: ASTM, 1978.
45. WF Brown, JE Srawley. *Plane-strain crack toughness testing of high strength metallic materials*. ASTM, STP 410, 1966, p 12.
46. LE Nielsen, PF Landel. *Mechanical Properties and Composites*. New York: Marcel Dekker, 1994.
47. AJ Kinloch, RJ Young. *Fracture Behaviour of Polymers*. London: Applied Science, 1983, Chap 11.
48. CB Bucknall. *Toughened Plastics*. London: Applied Science, 1977.
49. E Gaube, HH Kausch. *Kunststoffe* 63: 391, 1973.
50. AJ Kinloch, RJ Young. *Fracture Behaviour of Polymers*. London: Applied Science, 1983, Chap 6.
51. MN Riddell. *Plast Eng* 30(4): 71, 1974.
52. RJ Crawford, RP Benham. *Polymer* 16: 908, 1975.
53. PC Paris, MP Gomez, WE Anderson. *Trends Eng* 13: 9, 1961.
54. PC Paris, F Erdogan. *J Basic Eng* 85: 528, 1963.
55. RW Hertzberg, JA Manson. *Fatigue of Engineering Plastics*. New York: Academic, 1980.
56. RW Hertzberg, JA Manson, MD Skibo. *Polym Eng Sci* 15: 252, 1964.

15

Reinforced Polymers

15.1	Introduction	653
15.2	Polymer Matrices	655
15.3	Reinforcements: Fibers	664
15.4	Properties of Reinforced Polymers	670
15.5	Mechanical Properties of Unidirectional Composites	672
15.6	Laminates	681
15.7	Short Fiber Composites	684
	Problem Sets	690
	References	695

15.1 INTRODUCTION

In general, polymers have low stiffness and strength in comparison with other materials, e.g., metals and ceramics, and consequently these materials present serious difficulties in structural applications. To improve their mechanical properties, polymers are reinforced by the addition of rigid particles or fibers to form composite materials (1). Thus, polymer matrix composite materials are made up of a low modulus phase, the polymer matrix, and a high modulus phase, the reinforcement, which is usually carbon or glass. The modulus of the composite is higher than that of the polymer matrix, and the increment is proportional to the volume fraction of the reinforcement. In general, the properties of the composite depend not

only on the properties of the components and their relative proportions, but also on the shape, size, and distribution of the reinforcement and the degree of adhesion between the phases.

Composites can be classified into three groups according to the forms of reinforcement: particulate-reinforced, fiber-reinforced, and laminate composites (see Fig. 15.1). A reinforcement is considered to be a "particle" if all of its dimensions are similar; particles can have spherical, platelet, or any regular or irregular geometric form. Particles, usually referred to as fillers, are in some cases added to polymers to reduce costs rather than to reinforce them. Fiber-reinforced composites contain fibers whose lengths are much greater than their cross-sectional dimensions. When the properties vary with

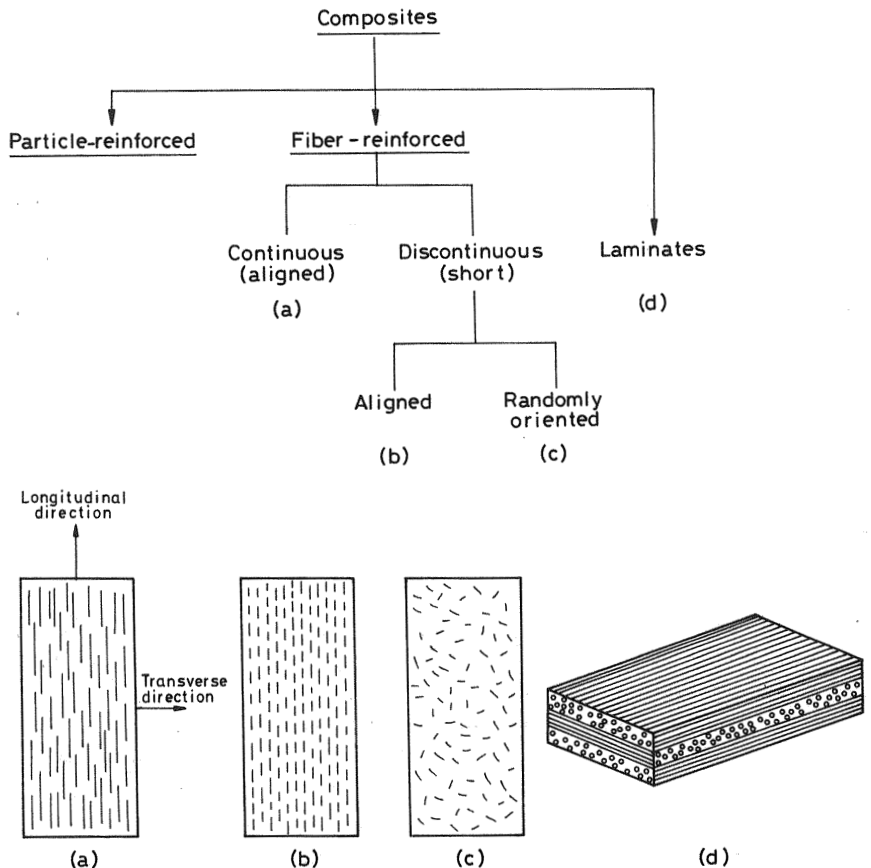


Figure 15.1 Classification of composites according to the reinforcement forms.

fiber length, the materials are called discontinuous fiber composites. On the other hand, when the properties do not change when the length of the fibers is increased, the material is considered a continuous fiber-reinforced composite. Laminar composites are formed by combination of layers of materials. This structure confers an anisotropic character to the composite. Particulate-reinforced polymers exhibit isotropic properties when particles are uniformly distributed. Fiber composites may be either isotropic or anisotropic. Fiber-reinforced composites are more prominent than other types of composites because most materials are stronger and stiffer in the fibrous form than in any other form, so we will refer preferentially to them throughout this chapter.

Fiber polymer matrix composites can offer mechanical properties that make them competitive with common metals such as aluminum and steel. Structural weight reduction is one of the major advantages in using polymer matrix composite materials instead of metals. The remarkable specific properties of polymer matrix composites can be seen in Table 15.1, where a comparison of the properties of polymer matrix composites and metals is given (2). In addition, fiber-reinforced composites can be tailored to present high strength and modulus in the directions in which the high loads will be applied. Fiber-reinforced polymers can be designed with excellent structural damping features, and consequently they are less noisy and transmit vibrations less than metals, making them useful for automotive and marine construction. Polymer composite materials are widely applied, their uses ranging from consumer products to aerospace components. A great variety of consumer products are manufactured with inexpensive glass fiber composites (e.g., panels and small boats). Advanced fiber composites formed by small diameter high strength, high modulus fibers give rise to anisotropic materials; owing to their high cost, these composites are used mainly in aerospace applications, where their expense is offset by their high specific strength (strength/density) and high specific modulus (modulus/density).

15.2 POLYMER MATRICES

The main functions of the matrix in a fiber-reinforced composite are to bind the fibers and to transfer loads to and between them; only a small amount of the applied load is supported by the matrix. Let us consider a bunch of unidirectionally aligned continuous fibers subjected to a tensile stress. If a fiber breaks down, it becomes useless; but if the fibers are embedded in a polymer matrix (see Fig. 15.1a), the load distributes around the break point and the fiber remains useful. Furthermore, the matrix protects the fibers from self-abrasion and scratches on handling, keeps the reinforcement in

Table 15.1 Typical Values of the Properties of Polymer Matrix Composites and Metals at 20°C

Material ^a	Density (g/cm ³)	Young's modulus (GN/m ²)	Tensile strength (MN/m ²)	Elongation to fracture (%)	Coefficient of thermal expansion (10 ⁻⁶ °C ⁻¹)	Specific Young's modulus (10 ⁶ m ² s ⁻²)	Specific tensile strength (10 ³ m ² s ⁻²)	Heat resistance (°C)
High strength Al-Zn-Mg alloy	2.80	72	503	11	24	25.7	180	350
Quenched and tempered low alloy steel	7.85	207	2050–600	12–28	11	26.4	261–76	800
Carbon fiber–epoxy resin unidirectional laminae ($V_f = 0.60$)								
Parallel to fibers	1.62	220	1400	0.8	-0.2	135	865	260
Perpendicular to fibers	1.62	7	38	0.6	30			
Glass fiber–polyester resin unidirectional laminae ($V_f = 0.50$)								
Parallel to fibers	1.93	38	750	1.8	11	19.7	390	250
Perpendicular to fibers	1.93	10	22	0.2				

^a V_f is the volume fraction of fibers.

Source: Ref. 6.

the original orientation, and provides resistance to crack propagation; it also contributes to fracture toughness. On the other hand, the matrix is the “weak” part of the composite. The modulus of the matrix is significantly lower than that corresponding to the fiber. The matrix determines the compressive strength and interlaminar shear of the composite. It is desirable to prepare matrices with high modulus, strength, and toughness. High modulus and high toughness favor compressive strength and avoid delamination, respectively, but a good combination of these properties is not entirely achieved. Also, for practical reasons, the matrix selected should be easy to process. The matrix generally limits the service temperature of the composite and its environmental resistance, i.e., chemical corrosion or oxidation and moisture absorption.

One of the most important characteristics to consider in choosing a matrix is its adhesion with the fiber. The fiber/matrix interfacial adhesion plays a critical role in the mechanical properties of the composite. The loads are transferred from the matrix to the fiber through the interface, and the strength of the composite depends on the bond between fiber reinforcement and matrix.

Organic matrices are divided into thermosets and thermoplastics. The main thermoset matrices are polyesters, epoxies, phenolics, and polyimides, polyesters being the most widely used in commercial applications (3,4). Epoxy and polyimide resins are applied in advanced composites for structural aerospace applications (1,5). Thermoplastics like polyolefins, nylons, and polyesters are reinforced with short fibers (3). They are known as traditional polymeric matrices. Advanced thermoplastic polymeric matrices like poly(ether ketones) and polysulfones have a higher service temperature than the traditional ones (1,6). They have service properties similar to those of thermoset matrices and are reinforced with continuous fibers. Of course, composites reinforced with discontinuous fibers have weaker mechanical properties than those with continuous fibers. Elastomers are generally reinforced by the addition of carbon black or silica. Although they are reinforced polymers, traditionally they are studied separately due to their singular properties (see Chap. 3).

15.2.1 Thermoplastic Matrices

In thermoplastic matrices, the intrinsic characteristics derived from the linear chain structure have to be considered, mainly the capability of flow under stress at high temperatures. Thus, in amorphous and semicrystalline matrices, the service temperatures will be determined by T_g or T_g and T_m , respectively. Without reinforcement, creep is a major problem at temperatures lying in the interval $T_g < T < T_m$, but when the matrices are

reinforced with fibers, the increase in stiffness enables them to be used at temperatures approaching the T_g of amorphous polymers or the melting temperature of crystalline polymers. On the other hand, the degree of crystallinity increases the modulus of the polymer, so reproducible control of crystallinity is very important in processing these matrices. In many cases the composite materials have to be resistant to solvents, e.g., when they are used as pipes and tanks for hydraulic fluids and fuels. Semicrystalline thermoplastic matrices also ensure solvent resistance.

Polyolefins such as polyethylene and polypropylene are semicrystalline polymers. These polymers have very low glass transition temperatures, so they tend to creep under stress. Linear polyethylene presents a high degree of crystallinity, but side-chain branching reduces it. Increasing crystallinity augments density, stiffness, hardness, tensile strength and thermal and chemical stability, and decreases creep and stress-crack resistance. Polypropylene (PP) is similar to high density polyethylene (HDPE) but has lower density. To improve their stiffness and to reduce deformation and deflection under load, glass fibers are incorporated into these polyolefins. Table 15.2 presents some data for these polymers (7).

Aliphatic polyamides (nylons) and thermoplastic polyesters are linear polar polymers containing polar —CONH— and —COO— groups, respectively, in the repeating unit. Therefore, they have some common characteristics (3). For example, polyamides and polyesters are semicrystalline polymers whose glass transition temperatures are above room temperature. As a consequence of intermolecular interactions, these polymers have high melting points, usually higher than 200°C , and due to their high crystallinity they are resistant to most organic solvents. Nylons and thermoplastic polyesters have similar mechanical properties such as high toughness, high impact strength and flexibility, and good fatigue and abrasion resistance. The mechanical properties of nylons are significantly affected by humidity,

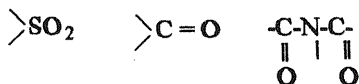
Table 15.2 Properties of High Density Polyethylene (HDPE) and Polypropylene (PP)

	HDPE	PP	Modified PP (30% glass fiber)
Density (g/cm^3)	0.96	0.90	1.12
Young's modulus (GPa)	0.8	1.5	6.5
Elongation to fracture (%)	30	50	4
Heat distortion temp. ($^\circ\text{C}$)	~ 20	~ 20	148

Source: Ref. 7.

while those of polyesters are little affected. Glass fiber reinforcement of these polymers leads to a substantial increase in tensile strength, hardness, creep resistance, and heat distortion temperature, so they can operate up to relatively high temperatures. These glass fiber-reinforced thermoplastics are used in many engineering applications. Glass-reinforced nylons are the most important group of glass-reinforced thermoplastics. Carbon fiber-reinforced nylons have an important use in the airframe industry.

In recent years new thermoplastic matrices have been developed to improve the stiffness/toughness balance and the service temperature, in comparison to the epoxy thermoset matrices used in high performance composites. These materials, usually referred to as advanced thermoplastic matrices (8), include polymers that have great structural similarities, with aromatic moieties in the main chain spaced by groups of the type diagrammed below.



In Table 15.3 are shown the chemical structures and T_g and T_m of some representative thermoplastic polymers for use at high temperature (3,9). These matrices have high continuous service temperatures (120–200°C) even under wet environmental conditions. Advantages of thermoplastic over thermoset matrices are their shorter fabrication cycle (generally controlled environment storage is not required) and the possibility to be reprocessed and reconsolidated after manufacture. Poly(ether ether ketone) is a strong contender with epoxy resins for use as a matrix in composite prepregs with carbon fibers to be utilized in structural aircraft components.

15.2.2 Thermoset Matrices

Thermoset matrices have dominated the composites industry for a number of years; epoxies, polyesters, phenolics, and bismaleimides are the most widely used (1,3). In all cases the precursor is a thermosetting resin formed by relatively small molecules (monomers or oligomers). Thermosetting resins become set, i.e., infusible and insoluble, as a consequence of chemical cross-linking reaction referred to as curing; after curing the thermoset is a network molecular structure of primary covalent bonds (see Chap. 1). Most thermosets are cross-linked by heat or a combination of heat and pressure. The curing of a thermoset is a complex process that begins by formation of linear chains that soon become branched and then cross-linked (10). In this process the original viscous liquid is transformed into an elastic gel formed

Table 15.3 Chemical Structures, T_g , and T_m of Representative Advanced Thermoplastics

Thermoplastic	T_g ($^{\circ}\text{C}$)	T_m ($^{\circ}\text{C}$)	Monomer structure
Poly(ether ether ketone)	143	334	
Poly(phenylene sulfide)	85	285	
Poly(ether sulfone)	225	— ^a	
Poly(ether-imide)	215	— ^a	
Polysulfone	193	— ^a	

^a Generally 95% or more noncrystalline.

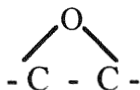
Source: Ref. 9.

by a network of infinite molecular weight. This irreversible transformation is called gelation. Gelation is characteristic of thermosets and it is critical for processing; beyond gelation the polymer is unable to flow, and it cannot be recycled and reused. However, gelation does not inhibit the curing process. The reaction will proceed increasing the cross-link density to that of the fully cured thermoset. Another transformation occurring during the curing process is vitrification of the growing chains or network. As the curing reaction proceeds, the glass transition temperature of the polymer increases, and when it reaches the curing temperature, the system vitrifies (the viscous liquid or elastic gel turns into a glass). After vitrification, curing is practically halted. Vitrification is a reversible transition. The most convenient curing temperature is one that leads to vitrification after gelation, when the full cure is reached.

Thermosets with high cross-link density possess high thermal stability, high rigidity, and dimensional stability as well as resistance to creep. Compared with thermoplastics, thermosets have some advantages, the most important being low melt viscosities in the prepolymer stage, which favor good fiber wetting and require lower processing temperatures. But the processing time is longer, and they need controlled storage as they have a finite shelf life.

(a) Epoxies

Epoxy resins are the major matrices for low temperature applications (from -50°C to $+120^{\circ}\text{C}$) and have gained wide acceptance in composites for aerospace applications (5). Epoxy resins contain the epoxide group:



The prepolymer stage in most cases is DGEBA (diglycidyl ether bisphenol A) (see Fig. 15.2a).

DGEBA is a living commercial liquid having a number-average molecular weight of 340–400 ($n \approx 0$). Larger molecular weights around 3000 ($n = 13$) correspond to the solid resin. A curing agent (hardener) is used for the cross-linking process (3). For room temperature curing the hardener is usually a polyfunctional amine such as triethylenetetramine. For higher curing temperatures, curing agents such as aromatic amines or acid anhydrides are used. In Figure 15.2b the reaction scheme for DGEBA with a diamine is shown. In epoxy polymerization no volatiles are evolved, so epoxies are free of void-forming volatiles. Epoxies provide low shrinkage

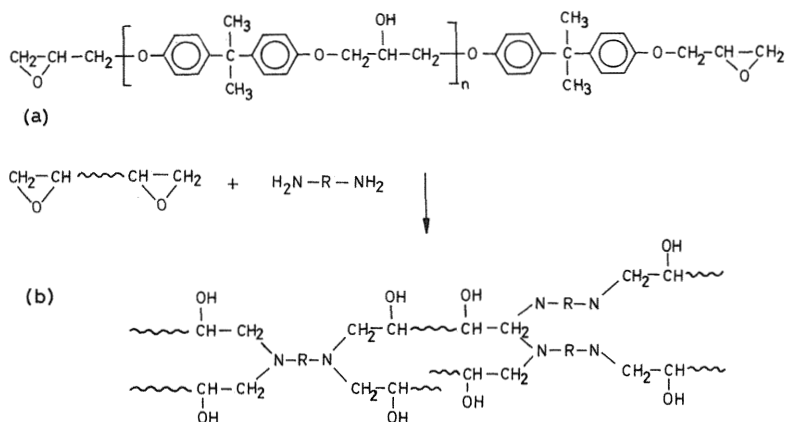


Figure 15.2 (a) Bisphenol A diglycidyl ether. (b) Curing reaction on an epoxy resin with a diamine.

on curing. For room temperature curing, the epoxy resin and the hardener are supplied separately in a two-parts formulation. When the hardening reaction proceeds at high temperature, the supplier often adds the hardener to the epoxy resin in a single-part formulation. In this case, the material is usually supplied in the form of a prepreg, i.e., in sheet form, constituted by fiber cloth impregnated with resin and hardener, ready for curing. Epoxy matrices are suitable for use with glass, carbon/graphite, aramid, boron, and other reinforcements and hybrids. These matrices have to be modified to improve their impact resistance. The toughness of epoxies is improved by adding a rubber (see Sect. 14.4.5), usually a carboxyl-terminated copolymer of butadiene and acrylonitrile designed to react with the epoxy group of the resin through the —COOH group before the hardening reaction has proceeded very far. As a result, a microstructure of small rubber particles bonded to the epoxy matrix is originated. This confers toughness to the composite without major losses in other mechanical properties. Moisture absorption decreases the glass transition temperature of epoxy resins. The absorbed moisture worsens the mechanical properties, especially at high temperatures, and this effect has to be considered in design.

(b) Polyesters

Unsaturated polyesters have reactive double carbon-carbon covalent bonds that can be cross-linked to form thermosetting materials. The polymers are usually cross-linked with vinyl-type molecules such as styrene, using a peroxide to generate free radicals (see Fig. 15.3). Commercial resins are viscous

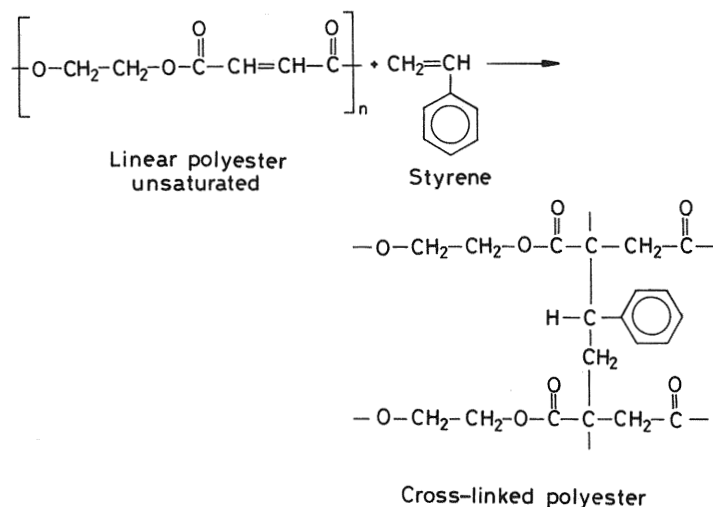


Figure 15.3 Cross-linking of an unsaturated polyester with styrene.

liquids with molecular weights lying in the range 1500–3000, which are supplied dissolved in styrene monomer (30–50% composition). In practice, the peroxide cure agent is blended into the resin before the resin is applied to the reinforcement, which is usually glass fiber. Glass-reinforced polyester resins are low cost composites widely used in commercial, industrial, and transportation applications. They offer good mechanical properties such as stiffness, strength, toughness, and good chemical resistance (3). The maximum service temperature of these composites is about 100°C. Polyester resins present problems of adhesion to carbon and aramid fibers, which, together with the large shrinkage during curing (in comparison with epoxies) (2), limit the application of polyester matrices in high performance composites.

(c) Phenolics

Phenolics are the oldest of the thermoset polymers. They are obtained by reaction of phenol with formaldehyde through a condensation reaction leading to a cross-linked polymer (see Chap. 1). These resins have good dimensional and thermal stability (3). Most phenolics have different fillers incorporated in them to reduce cost and shrinkage on curing and also to improve some properties such as electrical insulation and heat resistance. Unfortunately, during the curing process water evolves as a by-product, producing voids. The presence of voids introduces local stress concentrations that, if high, can result in initial localized failure. However, these resins

produce low smoke and less toxic by-products during combustion, so they are used in aircraft interior panels.

(d) Polyimides

Polyimides, are among the most recently developed matrices; they are obtained by the reactions of dianhydrides with diamines in a two-stage process (3). In the first stage a soluble and fusible polymer is formed, and processing is carried out at that moment. Then the second stage begins; the resin is heated until an insoluble and infusible polymer (thermoset) is formed, whose structure is shown in Figure 15.4. Polyimide glass fiber composites are applied in electronics and aerospace. The limitations in the processing of these substances have led to the development of modified polyimides such as polybismaleinimides. These polymers are obtained from bismaleimides by reaction with bifunctional compounds like diamines, as shown in Figure 15.5. If the reaction is carried out with a deficiency of diamine, the polymer will have terminal double bonds capable of being cross-linked. The linear polymer is easily processed like a thermoplastic and then cross-linked to form a thermoset. Polybismaleinimides are used as matrices with glass and carbon fibers in advanced composites. In general, polyimides do not possess the easy processibility and toughness of epoxy resins, but they have superior heat resistance.

15.3 REINFORCEMENTS: FIBERS

The reinforcement is mainly responsible for the structural properties of a composite such as strength and stiffness. Fibers are the most effective rein-

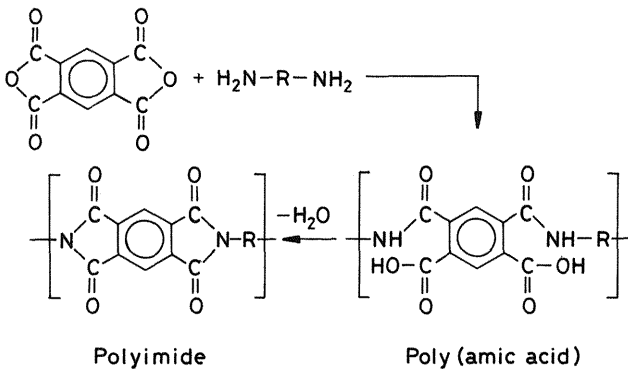


Figure 15.4 Reaction to obtain a polyimide.

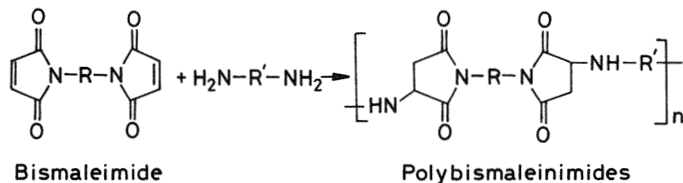


Figure 15.5 Reaction to obtain a polybismaleinimide.

forcements because of their geometry. Almost all fibers in use today have cylindrical geometry, the aspect ratio, α (length/diameter), being much higher than unity. The ratio of surface area to volume of fibers increases with α , so to maximize the reinforcement–matrix interaction interface, fibers with large α values are the most convenient. On the other hand, a fiber is inherently stronger than the bulk material, because the size of the flaws is limited by the smaller diameter of the fiber. The smaller the diameter, the greater the strength of the fiber. As has already been mentioned, matrices can be reinforced with short (discontinuous) or long fibers. In either case, fibers are manufactured as bundles of continuous filaments. A filament is the basic structural element, with a diameter in the range of 5–10 μm . A bundle of a large number of filaments (3000–12,000) is known as tow or yarn. Usually the bundles of filaments are characterized by the linear density expressed as the weight in grams of fiber tow per 9000 m (denier). The unit proposed by ASTM is the tex (weight in grams per 1000 m). The planar textile structures produced by interlacing yarns are called fabrics. The principal types of fibers used as reinforcements of polymer matrices are glass, carbon, aramide, and polyethylene fibers.

15.3.1 Glass Fibers

Glass fibers are the most widely used reinforcements in composites owing to their low cost and ease of processing. Glass fibers are produced by drawing monofilaments of glass from a furnace containing molten glass (6). Their composition is based on silica (SiO_2). The fiber structure is a noncrystalline network of silicon tetrahedra linked together by oxygen atoms. Other oxides such as B_2O_3 and Al_2O_3 can form part of the network; the groups BO_4^{4-} and AlO_4^{4-} can replace some of the SiO_4^{4-} tetrahedra. Other oxides such as MgO and CaO , known as modifiers, are added and in this case metallic ions are interspersed throughout the network. The oxygen atoms enter the silica network at points joining the tetrahedra. A consequence of this structure is the isotropy of glass fibers;

i.e., the modulus, thermal expansion, and other properties have the same value in the axial and radial directions. The most common glass used is known as E-glass, a calcium aluminoborosilicate glass having good mechanical, chemical, and electrical properties. Certain special glasses, such as S-glass, of higher strength and stiffness have been developed to replace E-glass for specific applications. S-glass is a magnesium aluminosilicate with a higher alumina content than E-glass. In Table 15.4 typical values of the density, strength, and modulus are given for individual filaments of reinforcing fibers (7). The fiber strength is strongly dependent on the processing and environmental conditions. Moisture and rubbing provoke surface damage, and consequently the strength of the fibers in use is roughly half that of the freshly drawn ones. To protect glass fibers they are coated with silane coupling agents, which are compatible with polyesters and epoxy matrices. Coupling agents are very efficient in ensuring good matrix–fiber interaction. An additional advantage of glass is its transparency to visible light. Glass fiber composites take the color of the matrix.

15.3.2 Carbon Fibers

Carbon fibers are obtained from several precursor fibers such as polyacrylonitrile (PAN), cellulose (rayon), and pitch fibers. PAN-based fibers offer the highest strength and the best balance of mechanical properties. The preparation of these fibers involves the transformation of PAN into graphite through controlled steps of heat treatment and tension to form the appropriately ordered graphite structure (6). Graphite has a layered structure in which the carbon atoms in the layers are covalently bonded in hexagonal arrays, with weak secondary bonds between layers. In carbon fibers, layers are parallel to the fiber axis, and as a consequence these fibers are highly anisotropic. Regular structure and the absence of voids are conditions required to get fibers of high modulus and high strength. Depending on the heat treatment used during processing, carbon fibers are available in three forms: high tensile strength (HTS) fiber, high modulus (HM) fiber, and ultrahigh modulus (UHM) fiber.

Typical values of density, modulus, and strength of these fibers are given in Table 15.4. It must be noted that as a consequence of the anisotropic structure of fibers the modulus in the transverse fiber direction is much lower than the modulus in the axial direction. Carbon fibers are among the stiffest and strongest fibers. Furthermore, taking into account that carbon fibers have lower density than glass fibers, their outstanding specific properties (modulus and strength) make them ideal for reinforcing composites in spite of their much higher cost. With proper selection and

Table 15.4 Typical Properties of Some Reinforcing Fibers

Property	E-glass	S-glass	Carbon HTS	Carbon HM	Carbon UHM	Aramid (Kevlar-49)
Density (g/cm^3)	2.54	2.49	1.79	1.86	1.95	1.45
Axial tensile modulus (GPa)	72	86	230	340	480	124
Axial tensile strength (GPa)	1.5–3.5 ^a	1.9–4.6	3.2	2.5	1.8	2.8

^a Freshly drawn fibers.

Source: Ref. 7.

placement of carbon fibers, composite structural elements that are stronger, stiffer, and much lighter than steel can be prepared. In Figure 15.6, tensile stress–strain and specific stress–strain curves for various types of reinforcing fibers are presented. It can be seen that the fibers are linearly elastic up to fracture. The high modulus fibers (carbon) are limited to 1% strain or less, while glass and aramid fibers can accommodate strains of 3–4%. However, the same linear range may not be achieved in composites because of the nonlinear response of the matrix. Carbon fiber composites have much better response to fatigue than glass or aramide composites. Furthermore, the thermal expansion coefficient in the axial direction is negative, thus allowing the design of composite structures with almost no thermal volume change. Carbon fibers impart black color to the composites.

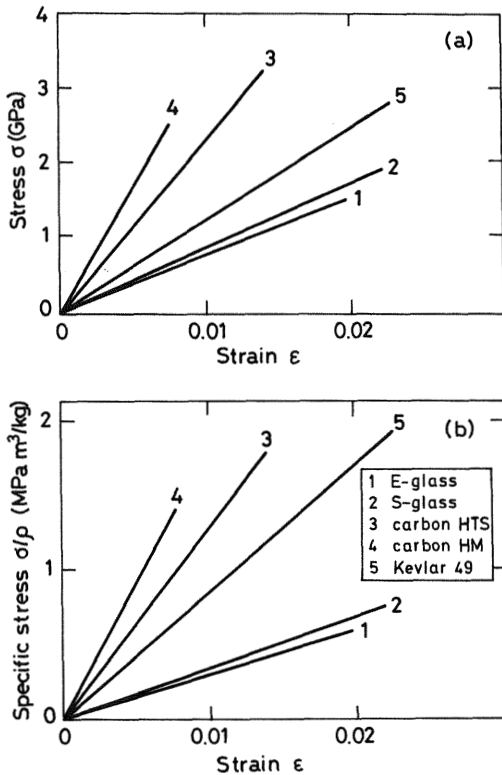
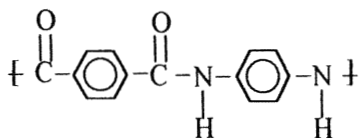


Figure 15.6 Tensile stress versus tensile strain (a) and specific stress versus strain curves (b) for some reinforcing fibers. (From Ref. 7.)

15.3.3 High Performance Polymer Fibers

High performance polymer fibers (HPPF) have excellent mechanical properties compared to traditional textile fibers such as nylon. The typical HPPFs are aramid and polyethylene fibers (6). Aramid is a generic name for a class of aromatic polyamide fibers, most of which are varieties of poly(*p*-phenylene terephthalamide). Kevlar is the trade name of the varieties of aramid polymers introduced commercially by Dupont. The molecules in the fibers of these materials are oriented in the axial direction. Poly(*p*-phenylene terephthalamide) is a rigid molecule with the following structure:



As was mentioned in Chapter 2, these rod-like molecules pack together, establishing hydrogen bonds between them. In fibers of these materials, molecules are oriented in the axial direction, thus presenting anisotropic properties. Consequently, Kevlar fibers have high strength and high modulus in the longitudinal direction and weak strength and comparatively low modulus in the transverse direction. Polyaramids have low density, so their specific tensile strength and axial specific modulus are higher than those of other types of fibers (see Table 15.4 and Fig. 15.6). Aramid fibers have good high temperature properties, and their glass transition temperatures lie in the vicinity of 360°C. However, Kevlar fibers have poor compressive strength compared to carbon fibers, so when higher compressive strength is required, hybrid composite materials of Kevlar and carbon fibers are used. Kevlar has extreme toughness and thus a high capacity to absorb energy upon impact; for this reason Kevlar composite fibers are applied in items such as bulletproof vests. A drawback of Kevlar is its hygroscopic character, which has to be taken into account in design.

Ultrahigh molecular weight polyethylene fibers (e.g., Spectra) have been recently developed. Their structure corresponds to that of extended chain crystallites. Polyethylene fibers resist impact better than glass or carbon and, like aramids, are used in antiballistic protective gear. Polyethylene has the lowest density of any fiber so its specific properties are superior to those of Kevlar. The major drawback of PE fibers is PE's service temperature, limited by its relatively low melting temperature (130°C). An additional difficulty in using HPPFs is its poor wettability by liquid organic resins, which leads to weak adhesion with the matrices. The fibers can be surface treated to improve their wettability.

15.4 PROPERTIES OF REINFORCED POLYMERS

It is important to predict the properties of a composite from its components. Some properties, like density, can be estimated by using the simple rule of mixtures, knowing only the relative proportions of the components. The theoretical prediction of mechanical properties is not easy because of the complexity of the stress and strain distribution in the composite under load. However, reasonably accurate predictions can be made for simple fiber arrangements using some assumptions about the stress and strain distributions.

Let us consider a composite of mass m , volume V , and density ρ that contains a mass of fibers, m_f , and a mass of polymeric matrix, m_m , occupying a volume V_m . Then

$$m = m_f + m_m \quad (15.1)$$

Assuming that there are no voids,

$$V = V_f + V_m \quad (15.2)$$

The relative proportion of the components is expressed as the volume fraction, given by

$$\phi_f = V_f/V; \quad \phi_m = V_m/V \quad (15.3)$$

Dividing Eq. (15.1) by V and substituting $m_f = V_f\rho_f$ and $m_m = V_m\rho_m$, where ρ_f and ρ_m are the densities of the fiber and matrix, respectively, the following rule of mixtures is obtained

$$\rho = \phi_f\rho_f + \phi_m\rho_m \quad (15.4)$$

In practical cases, composite materials contain voids formed by air or vapors trapped in the resin and in the resin/fiber interface. These voids are a source of weakness, points of stress concentration that favor crack propagation. In advanced composite materials the proportion of voids is limited to about 0.5% (2,5,7).

The voids fraction, evaluated from the density of the composite and the components, is taken as a quality control. If the mass of voids is considered negligible and the volume they occupy is V_v , then

$$V = V_f + V_m + V_v \quad (15.5)$$

As in the previous case, from Eq. (15.1) we obtain

$$\rho = \phi_f \rho_f + \phi_m \rho_m$$

Since the volume fraction of voids is defined as

$$\phi_v = V_v/V \quad (15.6)$$

Eq. (15.5) can be written as

$$1 = \phi_f + \phi_m + \phi_v \quad (15.7)$$

and

$$\frac{1}{\rho} = \frac{\phi_f}{\rho} + \frac{\phi_m}{\rho} + \frac{\phi_v}{\rho} \quad (15.8)$$

where

$$\frac{\phi_f}{\rho} = \frac{V_f/V}{\rho} = \frac{m_f}{\rho_f m} = \frac{w_f}{\rho_f} \quad (15.9)$$

Similarly,

$$\frac{\phi_m}{\rho} = \frac{w_m}{\rho_m} \quad (15.10)$$

where w_f and w_m are, respectively, the weight fractions of fiber and matrix in the composite. By substituting Eqs. (15.9) and (15.10) into Eq. (15.8), we obtain

$$\frac{1}{\rho} = \frac{w_f}{\rho_f} + \frac{w_m}{\rho_m} + \frac{\phi_v}{\rho} \quad (15.11)$$

Appropriate rearrangement of Eq. (15.11) leads to

$$\phi_v = 1 - \left(\frac{w_f}{\rho_f} + \frac{w_m}{\rho_m} \right) \rho \quad (15.12)$$

an expression that allows us to evaluate ϕ_v from the weight fractions and densities of the matrix and fibers and the density of the composite.

The weight fractions w_m and w_f are determined from a weighed piece of composite, eliminating the polymer matrix and weighing the remaining

fibers (2). If the fibers are glass fibers, the polymer matrix is eliminated by oxidation at 600°C in air atmosphere, but in the case of carbon fibers the polymer has to be degraded by chemical reaction, e.g., concentrated HNO_3 for epoxy.

15.5 MECHANICAL PROPERTIES OF UNIDIRECTIONAL COMPOSITES

15.5.1 Elastic Constants

Consider a unidirectional composite with fibers so long that end effects can be ignored, as shown in Figure 15.7. Assume further an ideal composite in which matrix and fibers are linearly elastic, the two are perfectly adhered, and the fibers are uniformly distributed. When a load is applied parallel to the fibers (axis 1), the strain in the fibers and in the matrix are the same (2,6,7,11):

$$\varepsilon_{f_1} = \varepsilon_{m_1} = \varepsilon_1 \quad (15.13)$$

and the total load is shared by the two components:

$$P_{c_1} = P_{m_1} + P_{f_1} \quad (15.14)$$

where P is the load and the subscripts c , m , and f refer to composite, matrix, and fiber, respectively. Since $P = \sigma A$ (σ being the stress and A the cross-sectional area), Eq. (15.14) can be written as

$$\sigma_{c_1} A_c = \sigma_{m_1} A_m + \sigma_{f_1} A_f \quad (15.15)$$

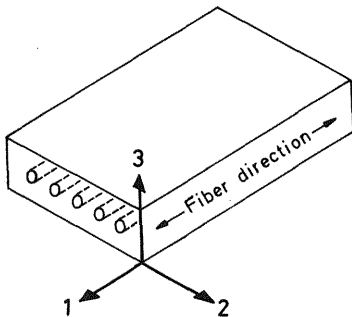


Figure 15.7 Unidirectional composite.

where A_c , A_f , and A_m are the cross-sectional areas. Since the fibers extend over the entire length of the composite, the ratio A_m/A_c can be replaced by the volume fraction $\phi_m = V_m/V_c$ and, similarly, $\phi_f = A_f/A_c$. Then Eq. (15.15) is given by

$$\sigma_{c_1} = \sigma_{m_1} \phi_m + \sigma_{f_1} \phi_f \quad (15.16)$$

an expression that represents the rule of mixture for stresses. Considering that fibers and matrix are linearly elastic gives

$$\sigma_{f_1} = E_f \varepsilon_1; \quad \sigma_{m_1} = E_m \varepsilon_1$$

and

$$\sigma_{c_1} = E_c \varepsilon_1 \quad (15.17)$$

where E_f , E_m , and E_c are the respective tensile moduli of fibers, matrix and composite. Equation (15.16) can be rewritten to give the following rule of mixtures for moduli:

$$E_{c_1} = E_{m_1} \phi_m + E_{f_1} \phi_f \quad (15.18)$$

The analysis is based on the assumption that fibers and matrix carry pure axial tension with no stress in the transverse directions. This is not strictly true, since the difference between the Poisson's ratios of matrix and fibers ($\nu_m \neq \nu_f$) will give additional transverse stresses. However, the experimental values of E_{c_1} obtained for many fiber composites differ by less than 2% from the corresponding ones calculated from Eq. (15.18). An example of the application of Eq. (15.18) is given in Figure 15.8 for a glass fiber polyester composite ($E_m = 3.8 \text{ GN/m}^2$, $E_f = 86 \text{ GN/m}^2$). It can be seen that for the typical volume fiber fraction of 0.5, the modulus of the composite is 10 times that of the matrix. Most polymer matrices have a similarly low modulus, about 2–6 GN/m^2 , while fiber reinforcement is available in a wide high modulus range, 80–350 GN/m^2 (see Table 15.4). Therefore, without serious error, the matrix contribution to the modulus of the composite can be neglected and Eq. (15.18) can be written as

$$E_{c_1} \simeq E_{f_1} \phi_f \quad (15.19)$$

It is worth noting that ideal arrangements of fibers of circular cross section with the highest packing, hexagonal arrays with the fibers touching, would lead to a theoretical volume fiber fraction of $\simeq 0.9$. This value is never

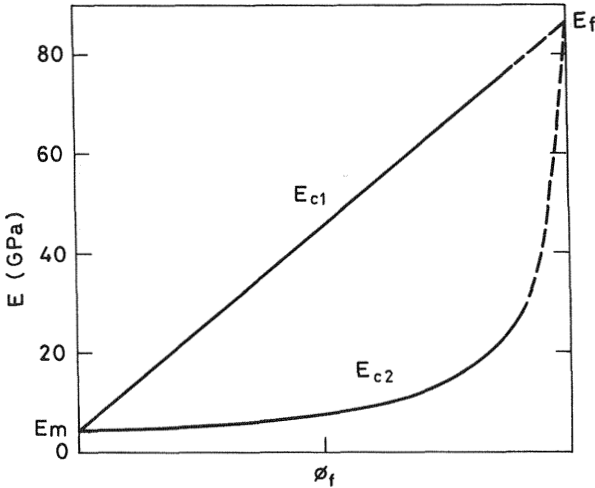


Figure 15.8 Predicted tensile moduli for aligned glass fiber reinforced polyester in parallel direction to the fibers (E_{c1}) and in transverse direction (E_{c2}). (From Ref. 7.)

achieved in practice, the maximum volume fiber content in high performance composites being around 0.7. This fiber content prevents contacts between fibers, which cause fiber damage. Since the strains on the components are equal [Eq. (15.13)], the ratio between the loads carried by the fiber and the matrix is given by

$$\frac{P_f}{P_m} = \frac{E_f}{E_m} \left(\frac{A_f}{A_m} \right) = \frac{E_f}{E_m} \left(\frac{\phi_f}{\phi_m} \right) \quad (15.20)$$

As a consequence of the fiber's high modulus, the load on a composite will be carried mostly by the fibers, thus ensuring that ϕ_f is higher than a critical value, $\phi_f' = E_m / (E_f + E_m)$.

For the study of the properties in the transverse direction, let us consider a unidirectional composite with a load applied at right angles to the fiber direction. The real composite could be replaced by the simple model shown in Figure 15.9, where the fibers are grouped together as a continuous phase. In these conditions, the thicknesses t_f and t_m are proportional to the volume fractions of the fiber and matrix, respectively. The applied load transverse to the fiber acts equally on the fiber and the matrix, so that

$$\sigma_{f2} = \sigma_{m2} = \sigma_{c2} \quad (15.21)$$

where the strains are

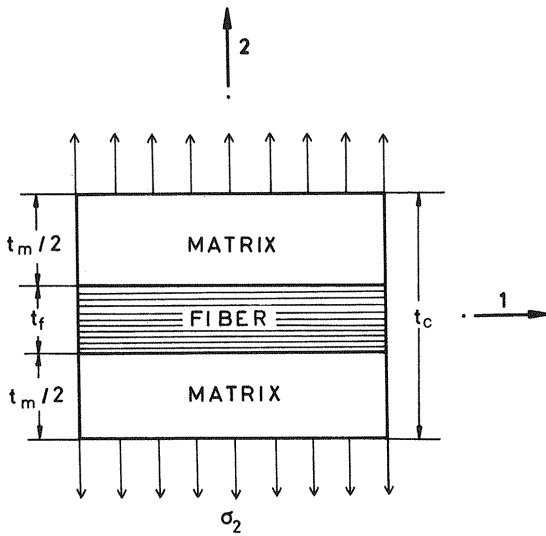


Figure 15.9 Simple composite model, with fibers grouped together.

$$\varepsilon_{f_2} = \frac{\sigma_{f_2}}{E_{f_2}}; \quad \varepsilon_{m_2} = \frac{\sigma_{m_2}}{E_m}; \quad \varepsilon_{c_2} = \frac{\sigma_{c_2}}{E_{c_2}} \quad (15.22)$$

The total extension, δ , caused by the load is the sum of the extensions of the two components:

$$\delta_{c_2} = \delta_{f_2} + \delta_{m_2} \quad (15.23)$$

where $\delta_{i2} = \varepsilon_{i2}t_i$, $i = c, f$ or m .

Therefore Eq. (15.23) can be written as

$$\varepsilon_{c_2}t_c = \varepsilon_{f_2}t_f + \varepsilon_{m_2}t_m \quad (15.24)$$

That is,

$$\varepsilon_{c_2} = \varepsilon_{f_2} \frac{t_f}{t_c} + \varepsilon_{m_2} \frac{t_m}{t_c} \quad (15.25)$$

Since the volume fractions of fiber and matrix can be expressed as

$$\phi_m = \frac{t_m}{t_c}; \quad \phi_f = \frac{t_f}{t_c} \quad (15.26)$$

Eq. (15.25) can be written as

$$\varepsilon_{c2} = \varepsilon_{f2}\phi_f + \varepsilon_{m2}\phi_m \quad (15.27)$$

This equation indicates that the total strain is the weighted sum of strains in fibers and matrix. As we are assuming elastic behavior, Eq. (15.5) becomes

$$\frac{\sigma_{c2}}{E_{c2}} = \frac{\sigma_{f2}}{E_{f2}}\phi_f + \frac{\sigma_{m2}}{E_m}\phi_m \quad (15.28)$$

the transverse modulus of the composite is given by

$$\frac{1}{E_{c2}} = \frac{\phi_f}{E_{f2}} + \frac{\phi_m}{E_m} \quad (15.29)$$

where use was made of Eq. (15.21).

Figure 15.8 shows the variation of E_{c2} calculated from Eq. (15.29) with ϕ_f for a glass fiber polyester composite. As can be seen, the modulus of the fiber composite is lower in the transverse direction than in the longitudinal direction. In this example, matrix and fibers are isotropic and E does not depend on the direction. All matrices are isotropic, but some fibers, such as carbon and aramid, are anisotropic, and as a consequence their longitudinal modulus E_{f1} is higher than transverse one, E_{f2} . The simplifications made using the above model are unrealistic, because the fibers are not grouped together and the load distributes differently between fibers and matrix. Therefore the values calculated for E_{c2} from Eq. (15.29) are less accurate than those obtained for E_{c1} through Eq. (15.18).

Since the elastic modulus of fibers is higher than that of polymer matrices, Eq. (15.29) can be simplified as

$$E_{c2} \simeq \frac{E_m}{1 - \phi_f} \quad (15.30)$$

This equation suggests that E_{c2} , unlike E_{c1} , is strongly influenced by the matrix modulus. Therefore, if the modulus of the matrix in practical cases decreases due to water absorption or creep relaxation, the transverse modulus will be seriously affected, in contrast to E_{c1} .

When a shear stress is applied parallel to the fibers of a unidirectional composite (Fig. 15.7), the prediction of the shear modulus $G_{c12} = G_{c13}$ can be deduced with a model similar to the one used above to obtain E_{c2} . The pertinent expression, similar to Eq. (15.29), is

$$\frac{1}{G_{c12}} = \frac{\phi_f}{G_{f12}} + \frac{\phi_m}{G_m} \quad (15.31)$$

It is difficult to determine the shear modulus of fibers, though sometimes it is estimated from E_f and Poisson's ratio, ν_f , using the relationship for an isotropic material, $G = E/2(1 + \nu)$ (see Table 4.1). It should be pointed out that it is necessary to assume a value for ν owing to the difficulty involved in determining this coefficient. As expected, the values of G_f are much higher than those of G_m and as a consequence G_{c12} will also be determined mainly by the shear modulus of the matrix. The same model can be used to predict Poisson's ratio for the composite. Thus, the expression for $\nu_{c12} = \nu_{c13}$ [the contraction in axis 2 when a load is applied parallel to the fibers (along axis 1)] is

$$\nu_{12} = \nu_{f12}\phi_f + \nu_m\phi_m \quad (15.32)$$

15.5.2 Strength

The strength of composites is more difficult to predict than their stiffness because the strength is an extremely microstructure-sensitive property, and a composite can fail in different ways involving fiber, matrix, or interface failures, depending on the external loading conditions. The objective is to know the behavior of the composite under load in order to predict its strength in terms of the strength of both fibers and matrix. To achieve this, simple models are also used. As for the stiffness (E modulus), the prediction of the strength in the longitudinal direction is more suitable than in the transverse direction. Let us consider a unidirectional lamina in which a tensile load is applied in the direction of the fibers. Assume further that the fibers are perfectly bonded to the matrix ($\epsilon_c = \epsilon_m = \epsilon_f$) and that all fibers have the same strength. In this case, the stress of the unidirectional composite will be given by

$$\sigma_c = \phi_f\sigma_f + (1 - \phi_f)\sigma_m \quad (15.33)$$

Notice that subscripts 1 and 2 in this section are omitted because only one direction is considered.

Fibers are linearly elastic up to fracture ($\sigma = E\epsilon$), but the stress-strain relations of typical polymer matrices are nonlinear, as a consequence of their viscoelastic behavior (see Fig. 15.10); therefore, σ_m cannot be replaced by $E_m\epsilon_m$. Furthermore, the fibers and the matrix in the laminae are assumed to fail independently, as if they were each tested alone. The behavior of the

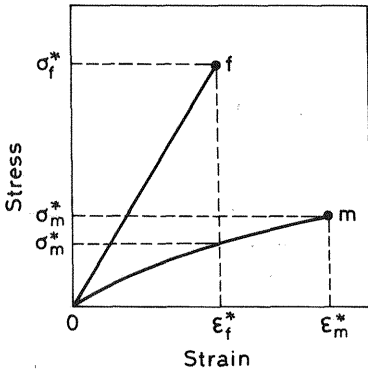


Figure 15.10 Tensile stress versus tensile strain curves for brittle fibers in a ductile matrix.

composite depends on both ϕ_f and the strain to failure of the components. Two cases must be considered: $\epsilon_f^* < \epsilon_m^*$ and $\epsilon_m^* < \epsilon_f^*$, where the asterisk denotes the corresponding fracture value. These cases represent a composite where the brittle component is the fiber or the matrix, respectively.

The first case, $\epsilon_f^* < \epsilon_m^*$, is typical of polymer matrix composites; schematic stress–strain curves are given in Figure 15.10. When $\epsilon_f^* < \epsilon_m^*$, two different modes of failure can take place depending on ϕ_f . Figure 15.11 gives a schematic representation on the stress–strain curves of the components multiplied by their respective volume fractions as well as the stress–

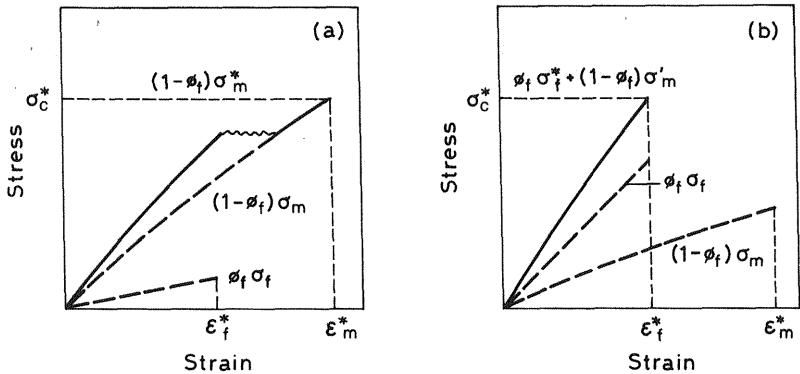


Figure 15.11 Tensile stress versus tensile strain curves for aligned fiber composite containing brittle fibers and ductile matrix. (a) Low fiber volume fraction ϕ_f ; (b) high ϕ_f . (From Ref. 7.)

strain curve of the composite calculated by Eq. (15.33) for low and high values of ϕ_f (7). As the strain increases, the fibers begin to break at ϵ_f^* . For composites with low ϕ_f , the matrix will carry the extra load at rupture, so the fibers can be ignored. In this case the strength of the composite is given by

$$\sigma_c^* = (1 - \phi_f)\sigma_m^* \quad (15.34)$$

and the strain at failure is $\epsilon_c^* = \epsilon_m^*$.

When ϕ_f is large, the load is very high once the fibers break at ϵ_f^* . The matrix cannot support the load, so the composite fails at $\epsilon_c^* = \epsilon_f^*$, and the composite strength is given by

$$\sigma_c^* = \phi_f \sigma_f^* + (1 - \phi_f)\sigma_m' \quad (15.35)$$

where $\sigma_m' = \sigma_m(\epsilon_f^*)$ is the stress of the matrix at the failure strain of the fibers.

The dependence of σ_c^* on ϕ_f is illustrated in Figure 15.12. The crossover point obtained from Eqs. (15.34) and (15.35) is

$$\bar{\phi}_f = \frac{\sigma_m^* - \sigma_m'}{\sigma_f^* + \sigma_m^* - \sigma_m'} \quad (15.36)$$

$\bar{\phi}_f$ gives the minimum fiber volume for which $\sigma_c^* \geq (1 - \phi_f)\sigma_m^*$. In reality a real fiber strengthening would require σ_c^* to be higher than

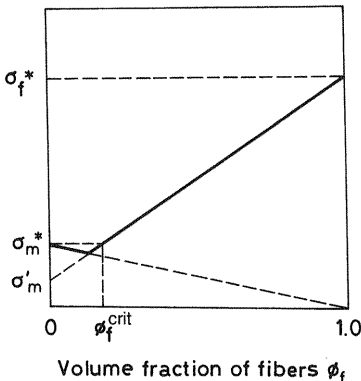


Figure 15.12 Dependence of tensile strength σ_c^* on fiber volume fraction ϕ_f for aligned fiber composite containing brittle fibers and ductile matrix.

σ_m^* , i.e., $[\sigma_f^* \phi_f + \sigma_m'(1 - \phi_f) \geq \sigma_m^*]$. Thus a critical fiber volume fraction is needed to achieve a strengthening effect:

$$\phi_f^{\text{crit}} = \frac{\sigma_m^* - \sigma_m'}{\sigma_f^* - \sigma_m'} \quad (15.37)$$

As Figure 15.12 suggests, the composite tensile strength is mainly provided by the fibers, so, except for very low values of ϕ_f , the critical stress at rupture can be approximated as

$$\sigma_c^* \simeq \phi_f \sigma_f^* \quad (15.38)$$

For most polymer matrix fiber composites, Eq. (15.38) gives a reasonable description of the tensile strength.

When $\epsilon_m^* < \epsilon_f^*$, two different modes of failure can occur depending on ϕ_f (see Fig. 15.13). As noted, the strength of the composite σ_c^* for small fiber volume fractions depends essentially on the matrix. When the matrix fails, all the load is transferred to the fibers, but, as there are not enough fibers to take the load, the composite will fail. The strength of the lamina can be written as

$$\sigma_c^* = \phi_f \sigma_f' + (1 - \phi_f) \sigma_m^* \quad (15.39)$$

where $\sigma_f' = \sigma_f(\epsilon_m^*)$ is the stress of the fibers at the failure strain of the matrix. For high values of ϕ_f , the fibers will take most of the load after

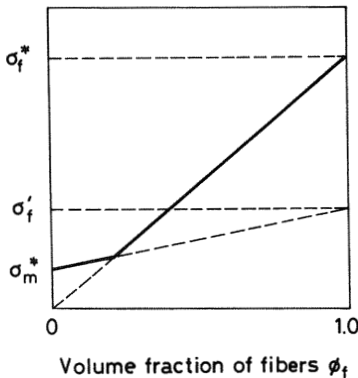


Figure 15.13 Dependence of tensile strength σ_c^* on fiber volume fraction ϕ_f for aligned fiber composite containing ductile fibers and brittle matrix.

the matrix fails, and the failure strength of the composite, σ_c^* , will be determined by the failure strength of the fibers, σ_f^* given by

$$\sigma_c^* = \phi_f \sigma_f^* \quad (15.40)$$

Figure 15.13 reflects the variation of σ_c^* with ϕ_f . The crossover point obtained from Eqs. (15.39) and (14.40) is expressed by

$$\bar{\phi}_f = \sigma_m^* / (\sigma_f^* - \sigma_f' + \sigma_m^*) \quad (15.41)$$

It can be concluded that the changes in failure behavior depend not only on the fiber volume fraction but also on whether the failure strain of the fibers, ϵ_f^* , is higher or lower than that of the matrix, ϵ_m^* . When the component having the smaller fracture strain (the brittle one) breaks, the load carried by this component is transferred to the other one. If the component with a higher fracture strain can bear this additional load, the brittle component will show multiple fracture before the composite breaks. Figure 15.14 illustrates schematically the details of failure for a unidirectional lamina under a longitudinal tensile stress. In all the cases, high strengths are obtained for high fiber fractions, in good agreement with experimental measurements. When the unidirectional lamina is under a tensile stress applied in any direction other than parallel to the fibers, its response will be much weaker. This can be understood by considering that $\sigma_m^* < \sigma_f^*$ for all matrices, so a crack can easily propagate through the matrix and the fiber matrix interface, avoiding the fibers. As a result, the strength of the matrix in the direction normal to the fibers determines the strength of the composite. The transverse tensile strength of the lamina is reduced with respect to that of the matrix by a factor of about 2. In contrast to the effect of fiber on the longitudinal tensile strength, the fibers now have a negative reinforcing effect. This is attributed to stress and strain concentrations in the matrix, which reach maximum values between the fibers. The prediction of the strength in the transverse direction is not so simple as in the longitudinal direction because many factors influence this property, among them the matrix strength, interface bond strength, presence and distribution of voids, and internal stress and strain distributions.

15.6 LAMINATES

As we have seen above, unidirectional laminae present maximum strength and modulus along the direction of the fibers. However, the laminae are too weak in the transverse direction, tensile failure occurs at very low stresses,

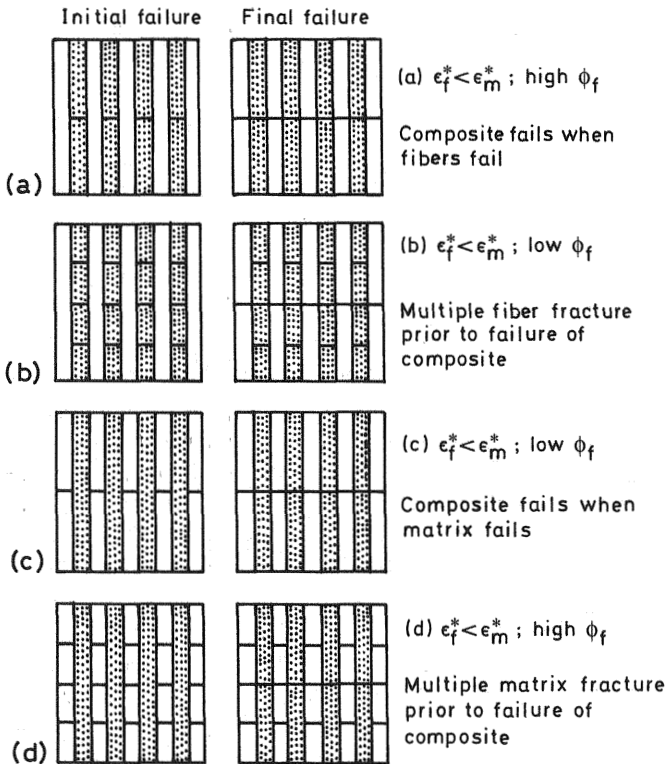
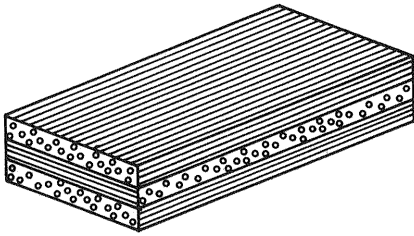


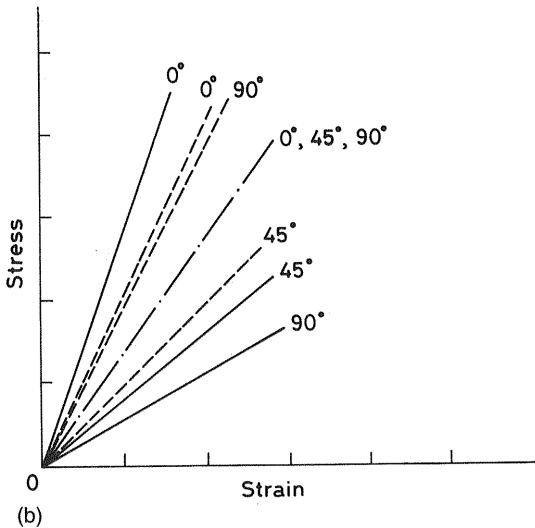
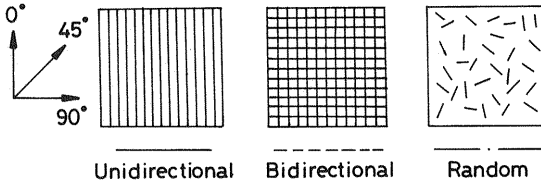
Figure 15.14 Different failure behaviors depending on relative values of fiber and matrix failure strains and fiber volume fraction.

and the transverse strength does not differ by much from the matrix strength. To overcome this problem, laminates consisting of stacks of laminae (also called plies) bonded together are prepared. The elastic properties of the laminate depend on the elastic properties of the individual laminae (2,12). A simple flat laminate with unidirectional laminae oriented at 90° to each other is shown in Figure 15.15a. In general, the arrangements of the laminae are more complicated.

The influence of the orientation of the laminae on the stiffness of the composite is illustrated in Figure 15.15b, where generic stress-strain curves for unidirectional cross-ply random laminates are shown. In the design of laminates it is necessary to define not only the orientation of the plies but also the stacking sequence, i.e., the order in which the plies are placed through the thickness. Figure 15.16 shows examples of symmetrical and non-symmetrical laminates. The most standard ply orientations are 0° ,



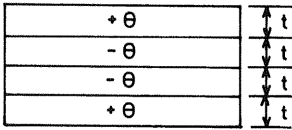
(a)



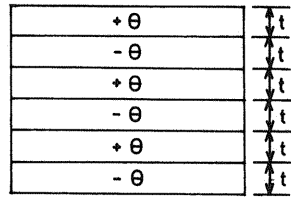
(b)

Figure 15.15 (a) Simple laminate with unidirectional laminae oriented at 90° to each other. (b) Stress-strain curves for unidirectional (—), cross-ply (---) and random (-·-) laminates. The tensile load is applied in the direction indicated by the angles shown in the figure.

Symmetrical laminates



Non-symmetrical laminates



Angle-ply

Figure 15.16 Symmetrical and nonsymmetrical laminates. The angle θ indicates the orientation of each lamina.

45° , -45° , and 90° . There are laminate sign conventions and symbol rotations. Thus $(0, 45, -45, 90)_s$ is a symmetrical and equilibrated laminate [there are the same number of laminae at θ (45°) and $-\theta$ (-45°)]; this configuration confers nearly isotropic properties to the laminates (quasi-isotropic laminate). The properties of a laminate consisting of various combinations of laminae placed at different angles are calculated from the properties, orientation, and distribution of the individual laminae (laminate theory). To produce the best design, it is important to predict the response of the laminate to external loads.

15.7 SHORT FIBER COMPOSITES

Although the best mechanical properties of polymer composites are reached with continuous fiber reinforcement, many composites, especially those with thermoplastic matrices, are reinforced with short fibers. In general, continuous fibers are more expensive than short ones, and, on the other hand, short fiber composites offer the possibility of using processing techniques such as extrusion or injection molding, which are faster and cheaper than lay-up processes. There is no specific length that distinguishes short and long fibers. Instead, a critical fiber length, l_c , is defined for each matrix–reinforce couple in order to assess the effectiveness of the fiber reinforcement. This parameter l_c is often used as a reference to discriminate short and long fibers in such a way that fibers with length $l > 15l_c$ are usually considered long or continuous fibers. Figure 15.17 shows a schematic representation of the deformation in the vicinity of a short fiber embedded in a matrix of lower modulus ($E_m < E_f$) subjected to a tensile load parallel to the fiber. As a consequence of their different moduli, matrix and fiber exhibit different

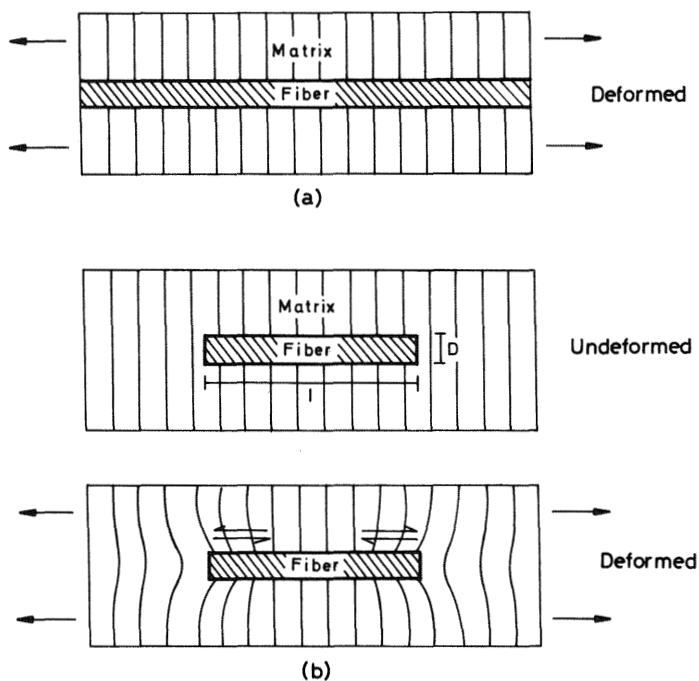


Figure 15.17 Representation of deformation in the vicinity of a long fiber (a) and (b) a short fiber embedded in a matrix.

strains. It can be seen that the strain in the fiber end regions is lower than that in the matrix. This strain difference causes important shear stresses at the fiber/matrix interface that transmit tensile stress to the fiber. The shear stress at the interface, τ , and the tensile stress in the fiber, σ_f , have been theoretically calculated assuming that both fiber and matrix behave elastically and are perfectly bonded. The tensile stress distribution along the fiber length, represented in Figure 15.18, reveals that the tensile stress is zero at the fiber ends and reaches its maximum value at the center. In contrast, the shear stress around the fiber attains maximum values at the end of the fibers and the lowest at the center. As the fiber stress falls to zero at the ends, the average stress in a short fiber embedded in a matrix is lower than that in a continuous fiber subjected to the same external load. Consequently, the axial tensile modulus of unidirectional short fiber composites (see Fig. 15.19) becomes lower than that of continuous fiber composites, and its value is given by (2,4,7)

$$E_1 = \eta_L \phi_f E_f + (1 - \phi_f) E_m \quad (15.42)$$

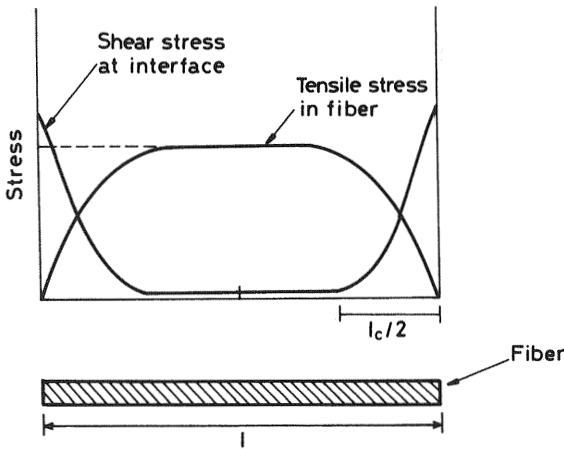


Figure 15.18 Tensile stress distribution in a fiber and shear stress distribution at the interface.

where $\eta_L < 1$ is a correction factor that, according to Eq. (15.18), approaches unity for continuous fibers. Thus the stiffening and reinforcing effects of short fibers will be lower than those obtained with continuous fibers.

The reinforcing efficiency of fibers also depends on the interface strength, since the load transfer needs a strong interfacial bond. As the interfacial stresses are concentrated at the fiber ends, these are the weak points in the composite, where the interface first fails and interfacial shear debonding begins. This effect occurs when τ reaches the interfacial shear strength, τ^* . It is clear that as the strain augments, the tensile stress in the fiber increases until the maximum stress that can be supported by the fiber, σ_f^* , is reached, after which the fiber eventually breaks (see Fig. 15.20a). However, rupture of fibers will occur only if the fibers are longer than a

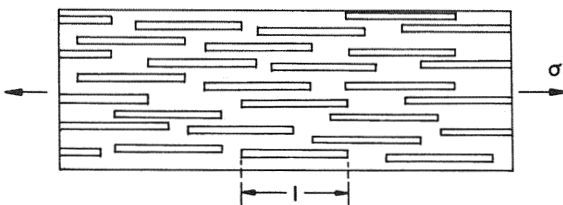


Figure 15.19 Unidirectional short fiber composite.

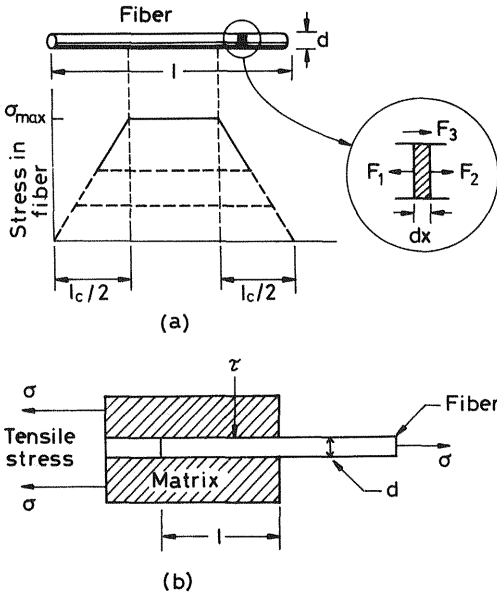


Figure 15.20 (a) Variation of the stress in a short fiber along its length. A total l_c at the two ends carries less than maximum stress $\sigma_{\max} = \sigma_f^*$. (b) Interfacial strength of the matrix fiber.

critical length, l_c ; if $l < l_c$, the debonding process will extend along the full length of the fiber and the fibers will not break. The critical fiber length, l_c , is the minimum fiber length that will allow tensile failure of the fiber rather than shear failure of the interface.

In order to determine l_c , we now consider a simple model of a fiber of length l embedded in a polymer matrix (see Fig. 15.20b). The tensile stress on the fiber required to produce fiber debonding and pullout is determined in a first approximation by balancing the tensile and shear forces,

$$\sigma \pi r^2 = 2 \pi r l \tau^* \tag{15.43}$$

where σ is the applied tensile stress. Thus the fiber length debonded will be

$$l = \sigma r / 2 \tau^* \tag{15.44}$$

The plot of σ vs. l given in Figure 15.20a shows that σ increases with l . However, a sharp cutoff occurs when $\sigma = \sigma_f^*$, corresponding to the fracture of the fiber, and consequently the critical length l_c is given by

$$l_c = \sigma_f^* r / 2\tau^* \quad (15.45)$$

A similar balance can be made for fibers embedded in a matrix of a composite under tensile stress, but in this case we have to take into account that both ends on the fiber carry interfacial shear stress, so the critical fiber length will be

$$l_c = \sigma_f^* d / 2\tau^* \quad (15.46)$$

where d is the fiber diameter.

Figure 15.21 shows the stress versus fiber length diagrams corresponding to the three possibilities $l < l_c$, $l = l_c$, and $l > l_c$. If the fiber has a length $l < l_c$, the stress variation along the fiber indicates that the stress never reaches the value necessary to break and the debonding regions extend along the full length of the fiber. When the matrix finally fails, the fiber

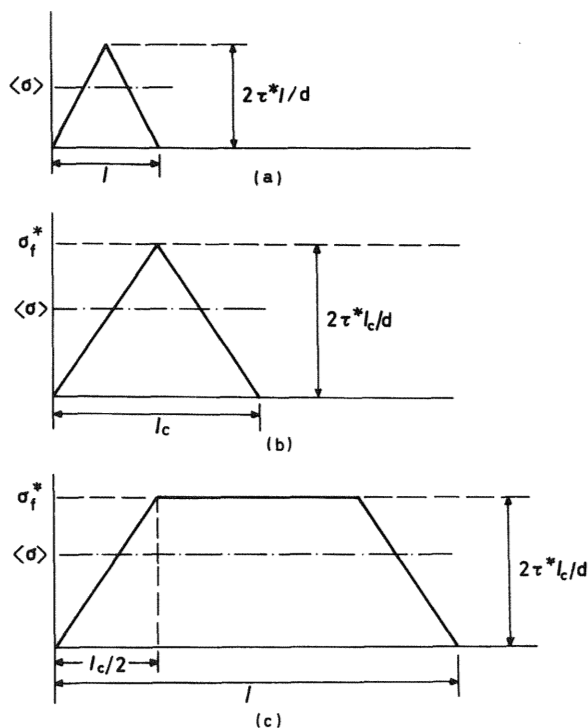


Figure 15.21 Tensile stress distribution in short fibers: (a) $l < l_c$; (b) $l = l_c$; (c) $l > l_c$.

simply slides out of the matrix. If $l = l_c$, the stress reaches the maximum value σ_f^* just at the midpoint of the fiber; but for $l > l_c$, the fiber length that supports the maximum stress σ_f^* is longer and the fiber becomes more effective. In these cases the composite will fail through tensile fracture of the fiber rather than shear failure at the interface.

Typical values of l_c for carbon fibers in an epoxy matrix and for glass fiber in epoxy and polyester matrices are 0.2, 0.8, and 0.5mm, respectively. The average fiber stress $\langle \sigma_f \rangle$ can be determined by calculating the area under the stress versus fiber length curve and dividing it by the fiber length. For $l < l_c$

$$\langle \sigma \rangle = \tau^* l / d \quad (15.47)$$

For $l = l_c$,

$$\langle \sigma \rangle = \tau^* l_c / d \quad (15.48)$$

and for $l > l_c$,

$$\langle \sigma \rangle = \left(1 - \frac{l_c}{2l} \right) \sigma_f^* \quad (15.49)$$

It is evident that getting the average fiber stress as close as possible to σ_f^* will require fibers considerably longer than the critical length.

Depending on τ_i^* , σ_f^* , and σ_m^* , two failure modes are possible for aligned short brittle fiber composites: fiber pullout and fiber fracture. Let us consider a composite in which $\epsilon_m^* > \epsilon_f^*$. If $l < l_c$, the average stress in the fiber will be given by Eq. (15.47), so the strength in the composite can be written as

$$\sigma_c^* = \frac{\tau^* l}{d} \phi_f + (1 - \phi_f) \sigma_m^* \quad (15.50)$$

In this case, fracture occurs when the matrix stress is reached; stress in the fibers is insufficient to cause fiber fracture, and the fibers pull out of the matrix. For low values of ϕ_f , Eq. (15.50) can be compared with the corresponding one for a long-fiber composite [Eq. (15.34)]. It can be seen that the strength of short-fiber composite exceeds that obtained for continuous fibers at low ϕ_f . The second failure mode will occur in the most practical case in which $l > l_c$ at high ϕ_f . As in long fibers, the strength of the composite is limited by the fracture strength of the fibers [Eq. (15.35)]. However, when σ_f^* is reached the average stress on the fibers is given by Eq. (15.49), and this expression combined with Eqs. (15.35) yields

$$\sigma_c^* = \left(1 - \frac{l_c}{2l}\right)\sigma_f^*\phi_f + \sigma'_m(1 - \phi_f) \quad (15.51)$$

where σ'_m is the stress of the matrix at the failure strain of the fibers. This strength is significantly lower than that obtained for continuous fibers.

Discontinuous fibers are normally supplied with standard lengths between 3 and 50 mm. These values are higher than the l_c values. In practice, the strength and modulus of short fiber composites are significantly lower than those theoretically predicted. Equations (15.50) and (15.51) apply to ideal composites having uniaxial arrangements of fibers. In real cases, however, fibers are not totally aligned parallel to each other. This reduces the efficiency of the reinforcement, and as a result the fiber orientation is strongly dependent on the processing techniques. Finally, it is worthwhile noting that a direct consequence of the more random distribution of fibers is less efficient packing, so lower ϕ_f values can be reached than when long fibers are used.

PROBLEM SETS

Problem 15.1

Calculate (a) the modulus of elasticity, (b) the tensile strength, and (c) the fraction of the load carried by the fibers for a continuous glass fiber-reinforced epoxy resin, with 60% by volume E-glass fiber, stressed under iso-strain conditions. The tensile strength and modulus of the fibers are 1800 MPa and 76 GPa, respectively, and the values of these quantities for the matrix are 60 MPa and 2.4 GPa, respectively.

Solution 15.1

(a) The modulus of elasticity of the composite, calculated by applying the rule of mixtures for binary composites [Eq. (15.18)], is

$$E_c = 2.4 \times 0.4 + 76 \times 0.6 = 46.6 \text{ GPa} \quad (\text{P15.1.1})$$

(b) According to Eq. (15.16), the tensile strength of the composite is

$$\sigma_c = 60 \times 0.4 + 1800 \times 0.6 = 1104 \text{ MPa} \quad (\text{P15.1.2})$$

(c) The fraction of load carried by the fibers is

$$\frac{P_f}{P_c} = \frac{E_f \phi_f}{E_f \phi_f + E_m \phi_m} \quad (\text{P15.1.3})$$

Consequently,

$$P_f/P_c = (76 \times 0.6)/(76 \times 0.6 + 2.4 \times 0.4) = 0.98$$

Problem 15.2

A composite sample of carbon fiber and epoxy weighs 2 g. When the sample is submerged in water (density = 1 g/cm³), its weight is 0.633 g. The weight of the fibers is 0.966 g after the epoxy is degraded with concentrated nitric acid. Calculate (a) the volume fraction of fibers, (b) the density of the composite, and (c) the volume fraction of voids.

Data: Densities (g/cm³): carbon fiber, 1.85; epoxy resin, 1.3.

Solution 15.2

(a) Volume of the initial sample: $2 - 0.633 = 1.337 \text{ cm}^3$.

Volume fraction of fibers, ϕ_f :

$$0.966 \text{ g} \times \frac{1}{1.85 \text{ g/cm}^3} = 0.52 \text{ cm}^3, \quad \text{so} \quad \phi_f = \frac{0.52 \text{ cm}^3}{1.337 \text{ cm}^3} = 0.389$$

(b) Volume fraction of the matrix, ϕ_m :

Mass of the matrix: $2 - 0.966 = 1.034 \text{ g}$

$$1.034 \text{ g} \times \frac{1}{1.3 \text{ g/cm}^3} = 0.795 \text{ cm}^3, \quad \text{hence, } \phi_m = \frac{0.795 \text{ cm}^3}{1.337 \text{ cm}^3} = 0.595$$

According to Eq. (15.4); the density of the composite is

$$\rho_c = 0.389 \times 1.85 + 0.594 \times 1.3 = 1.492 \text{ g/cm}^3$$

(c) As the sample has voids, the total volume of the composite is $V_c = V_f + V_m + V_v$, where V_v is the volume of the voids. Thus, $1.337 = 0.52 + 0.795 + V_v = 1.315 + V_v$. Therefore,

$$V_v = 0.022 \quad \text{and} \quad \phi_v = 0.017$$

The same result for the volume fraction of voids will be obtained by applying Eq. (15.12), which allows the determination of ϕ_v from the weight fraction and densities of the matrix and fibers and the density of the composite.

Problem 15.3

For a short-fiber Nylon 6.6–E glass aligned composite material, tested in tension in the fiber direction, predict the mean fiber stress at failure and the axial tensile strength of the composite made up of 40% fiber volume (interface shear strength $\tau_i^* = 20$ MPa, fiber diameter $d = 12$ μm , and length $l = 1$ mm). The tensile strengths of the E-glass fibers and the nylon matrix are 1800 MPa and 70 MPa, respectively. The tensile moduli are 76 GPa for E-glass fibers and 2.7 GPa for nylon 6.6.

Solution 15.3

The critical fiber length, l_c , is the minimum fiber length that will allow tensile failure of the fiber rather than shear failure of the interface. It can be calculated from Eq. (15.46):

$$l_c = \frac{1800 \times 12}{2 \times 20} = 540 \mu\text{m} \quad (15.3.1)$$

The strain of the matrix is

$$\varepsilon_m^* = \frac{\sigma_m^*}{E_m} = 70/2700 = 2.59 \times 10^{-2} \quad (\text{P15.3.2})$$

while the strain of the fiber is

$$\varepsilon_f^* = \frac{\sigma_f^*}{E_f} = 1800/76,000 = 2.37 \times 10^{-2} \quad (\text{P15.3.3})$$

As a consequence, failure occurs in the fiber first, and the strain in the composite is

$$\varepsilon = 2.37 \times 10^{-2}$$

The stress carried by the matrix is

$$\sigma_m' = E_m \varepsilon_f^* = 2700 \times 2.37 \times 10^{-2} = 64 \text{ MPa} \quad (\text{P15.3.4})$$

The mean stress carried by the fibers can be calculated by using Eq. (15.49):

$$\langle \sigma_f \rangle = \left(1 - \frac{1_c}{2l}\right) \sigma_f^* = \left(1 - \frac{0.540}{2 \times 1}\right) \times 1800 = 1314 \text{ MPa} \quad (\text{P15.3.5})$$

and the stress in the composite is given by

$$\sigma_c = 0.4 \times 1314 + 0.6 \times 64 = 564 \text{ MPa} \quad (\text{P15.3.6})$$

Problem 15.4

A unidirectional laminate consists of continuous glass fibers in an epoxy matrix and has a 60% fiber volume fraction. Calculate the strains (a) when a tensile stress of 100 MPa is applied in the fiber direction and (b) when a stress of 20 MPa is applied in the direction transverse to the fibers. The tensile moduli and Poisson's ratios for the glass and epoxy are $E_f = 80 \text{ GPa}$, $E_m = 2.5 \text{ GPa}$, $\nu_f = 0.2$ and $\nu_m = 0.35$, respectively.

Solution 15.4

(a) The axial strain, ε_1 (see Fig. 15.7) is calculated by using Eq. (15.17), where the axial tensile modulus of the laminate, E_{c1} , can be evaluated by using the rule of mixtures [Eq. (15.18)]:

$$E_{c1} = 0.4 \times 2.5 + 0.6 \times 80 = 49 \text{ GPa} \quad (\text{P15.4.1})$$

$$\varepsilon_1 = (100 \times 10^6) / (49 \times 10^9) = 2.04 \times 10^{-3} \quad (\text{P15.4.2})$$

The tensile stress provokes a contraction in directions transverse to the fibers. The corresponding strain, ε_2 , is calculated from the Poisson's ratio of the laminate, ν_{c12} , obtained through Eq. (15.32):

$$\nu_{c12} = 0.4 \times 0.35 + 0.6 \times 0.2 = 0.26 \quad (\text{P15.4.3})$$

$$\varepsilon_2 = -\nu_{c12} \varepsilon_1 = -0.26 \times 2.04 \times 10^{-3} = -5.3 \times 10^{-4} \quad (\text{P15.4.4})$$

(b) When the load is applied in the direction transverse to the fibers (see Fig. 15.7), the strain transverse to the fibers is obtained from Eq. (15.22) by using Eq. (15.29) to calculate the transverse tensile modulus, E_{c2} :

$$E_{c2} = \frac{80 \times 2.5}{0.6 \times 2.5 + 0.4 \times 80} = 5.97 \text{ GPa} \quad (\text{P15.4.5})$$

$$\varepsilon_2 = (20 \times 10^6)/(5.97 \times 10^9) = 3.35 \times 10^{-3} \quad (\text{P15.4.6})$$

In order to calculate the contraction in the axial direction, the Poisson's ratio, ν_{c21} , must be estimated. According to linear elasticity theory,

$$\nu_{c21} = \nu_{c12}E_{c2}/E_{c1} = 0.26(5.97/49) = 0.032 \quad (\text{P15.4.7})$$

Hence,

$$\varepsilon_1 = -\nu_{c21}\varepsilon_2 = 0.032(3.35 \times 10^{-3}) = 1.07 \times 10^{-4} \quad (\text{P15.4.8})$$

Problem 15.5

Consider a unidirectional glass fiber–epoxy matrix laminate.

(a) Calculate the fiber volume fraction needed to reach an axial modulus 10 times as high as that of the matrix.

(b) If some of the glass fibers are replaced by carbon fibers, with the total fiber volume fraction remaining unchanged, determine the fraction of carbon fibers needed to double the original axial modulus.

Data: Moduli of the glass fibers, carbon fibers, and epoxy matrix: $E_{fg} = 76 \text{ GPa}$; $E_{fc} = 300 \text{ GPa}$; $E_m = 2.5 \text{ GPa}$.

Solution 15.5

By substituting the condition given, $E_{c1} = 10E_m$, into Eq. (15.18), we obtain

$$10E_m = E_f\phi_f + E_m(1 - \phi_f) \quad (\text{P15.5.1})$$

Rearranging and substituting in the pertinent data give

$$\phi_f = \frac{9E_m}{E_f - E_m} = \frac{9 \times 2.5}{76 - 2.5} = 0.31 \quad (\text{P15.5.2})$$

(b) With a fraction of the glass fibers replaced with carbon fibers, the modulus of the laminate according to the rule of mixtures [Eq. (15.18)] will be given by

$$E_{c1} = E_{fc}\phi_{fc} + E_{fg}\phi_{fg} + E_m\phi_m \quad (\text{P15.5.3})$$

On the other hand,

$$\phi_{fc} + \phi_{fg} = 0.31 \quad \text{and} \quad \phi_m = 0.69 \quad (\text{P15.5.4})$$

and the modulus of the composite is

$$E_{c1} = 2 \times 10 \times E_m = 50 \text{ GPa} \quad (\text{P15.5.5})$$

Consequently Eq. (P15.5.3) becomes

$$50 = 300\phi_{fc} + 76(0.31 - \phi_{fc}) + 2.5 \times 0.69 \quad (\text{P15.5.6})$$

Hence, $\phi_{fc} = 0.11$.

REFERENCES

1. TJ Reinhart. Introduction to composites. In: TJ Reinhart et al. Eds. *Engineered Materials Handbook, Vol. 1. Metals Park OH: ASM International, 1987. p. 27.*
2. D Hull. *An Introduction to Composite Materials.* Cambridge, UK: Cambridge University Press, 1981.
3. M Chanda, SK Roy. *Plastics Technology Handbook.* New York: Marcel Dekker, 1993.
4. FL Matthews, RD Rawlings. *Composite Materials: Engineering and Science.* New York: Chapman & Hall, 1995.
5. MCY Niu. *Composite Airframe Structures.* Hong Kong: Conmilit Press, 1992.
6. KK Chawla. *Composite Materials.* New York: Springer-Verlag, 1987.
7. NG McCrum, CP Buckley, CB Bucknall. *Principles of Polymer Engineering.* New York: Oxford Univ Press, 1988.
8. RB Gosnell. Thermoplastic resins. In: TJ Reinhart et al. Eds. *Engineered Materials Handbook, Vol. 1. Metals Park OH: ASM International, 1987. p. 97.*
9. LL Clements. Polymer science for engineers. In: JN Epel et al. Eds. *Engineered Materials Handbook, Vol. 2. Metals Park OH: ASM International, 1995. p. 48.*
10. A Turi. *Thermal Characterization of Polymeric Materials.* London: Academic Press, 1981.
11. LE Nielsen. *Mechanical Properties of Polymers and Composites.* New York: Marcel Dekker, 1974.
12. EA Humphreys, BW Rosen. Properties analysis of laminates. In: TJ Reinhart et al. Eds. *Engineered Materials Handbook, Vol. 1. Metals Park OH: ASM International, 1987. p. 218.*

16

Multiaxial Analysis of Linear Viscoelastic Stress

16.1	Introduction	697
16.2	Integral Formulation of Viscoelastic Problems	697
16.3	Differential Form for the Constitutive Stress–Strain Relationship	701
16.4	Constitutive Equations in Differential Form for Multiaxial Tension States	703
16.5	Thermoviscoelasticity	706
16.6	Special Problems in Structural Linear Viscoelasticity	708
16.7	Formulation and Classification of the Boundary Problems in Viscoelasticity	708
16.8	Applicability of the Correspondence Principle. Quasi-static and Dynamic Problems	709
16.9	Superposition and Saint Venant Principles	710
16.10	Problems with Special Symmetries	710
16.11	The Dynamic Problem	716
16.12	Plane Strain Problems	721
16.13	Plane Stress Problems	727
16.14	Indentation and Impact Problems	735
16.15	Roller Ball Indentation	740
16.16	Wave Propagation in Viscoelastic Materials	748
	Problem Sets	754
	References	767

16.1 INTRODUCTION

The design of pieces that form part of either a structure or a machine often requires an analysis of the distribution of stresses and strains in these pieces. Without taking into account, for the moment, the thermal and calorific effects, the tensions and deformations at each point of the sample should simultaneously satisfy the balance and constitutive equations.

One must note that the balance equations are not dependent on either the type of material or the type of action the material undergoes. In fact, the balance equations are consequences of the laws of conservation of both linear and angular momenta and, eventually, of the first law of thermodynamics. In contrast, the constitutive equations are intrinsic to the material. As will be shown later, the incorporation of memory effects into constitutive equations either through the superposition principle of Boltzmann, in differential form, or by means of viscoelastic models based on the Kelvin-Voigt or Maxwell models, causes solution of viscoelastic problems to be more complex than the solution of problems in the purely elastic case. Nevertheless, in many situations it is possible to convert the viscoelastic problem into an elastic one through the employment of Laplace transforms. This type of strategy is accomplished by means of the *correspondence principle*.

Owing to the multiaxial character of the problems addressed in this chapter, the field equations depend not only on time but also on the position defined by their coordinates. Finally, it is necessary to stress that the solution of viscoelastic problems requires, as in the elastic case, specification of adequate boundary conditions. In this chapter, in addition to considering both integral and differential multiaxial stress-strain relationships, some viscoelastic problems of interest in technical applications are solved.

16.2 INTEGRAL FORMULATION OF VISCOELASTIC PROBLEMS

Among the equations that govern a viscoelastic problem, only the constitutive equations differ formally from those corresponding to elastic relationships. In the context of an infinitesimal theory, we are interested in the formulation of adequate stress-strain relationships from some conveniently formalized experimental facts. These relationships are assumed to be linear, and field equations must be equally linear. The most convenient way to formulate the viscoelastic constitutive equations is to follow the lines of Coleman and Noll (1), who introduced the term "memory" by stating that the current value of the stress tensor depends upon the past history

of the strain tensor. The main hypothesis, formulated in the context of the theory for simple materials with fading memory, can be formally expressed as in Eq. (5.2) by means of the functional relationship

$$\sigma_{ij}(t) = \underset{\theta=-\infty}{\overset{t}{\mathfrak{C}}} (\gamma_{kl}(t-\tau), \gamma_{kl}(t)) \quad (16.1)$$

where \mathfrak{C} is a tensor-valued functional that transforms the strain history into stress history. As a rule, all the field variables should be considered functions of position. If it is assumed that the history of the deformations is continuous and the functional is linear, then a theorem of Riesz permits us to write such a functional as a Stieltjes integral (2–4),

$$\sigma_{ij}(t) = G_{ijkl}(0)\gamma_{kl}(t) + \int_0^\infty \gamma_{kl}(t-\tau) dG_{ijkl}(\tau) \quad (16.2)$$

where $G_{ijkl}(t)$ is a fourth-order tensor. The nonconvolutive term was introduced through the integration of Dirac delta functions in order to account for discontinuous strain histories. An expression identical to Eq. (16.2) was formulated in Chapter 5 on semiempirical arguments. In fact, Eq. (16.2) is formally equivalent to the continuous form of the superposition principle of Boltzmann, which represents the linear stress–strain relationship for viscoelastic materials. The convolutive form of Eq. (16.2) ensures the property of translational invariance, thus implying that a shift of the mechanical input along the time scale results in a corresponding shift of the response without another change (2–4). On the other hand, the symmetry of the stress and strain tensors implies that

$$G_{ijkl}(t) = G_{jikl}(t) = G_{ijlk}(t) = G_{lkij} = G_{kaji} \quad (16.3)$$

If $G_{ijkl}(t)$ and its first derivative are continuous in $0 \leq t < \infty$, then Eq. (16.2) can be written as

$$\sigma_{ij}(t) = G_{ijkl}(0)\gamma_{kl}(t) + \int_0^\infty \gamma_{kl}(t-\tau)\dot{G}_{ijkl}(\tau) d\tau \quad (16.4)$$

Another approach to formulating the constitutive stress–strain relationship is through a simple variables change, $\theta = t - \tau$. After integration by parts, we obtain

$$\sigma_{ij}(t) = \int_{-\infty}^t G_{ijkl}(t-\theta)d\gamma_{kl}(\theta) \quad (16.5)$$

If $\gamma_{kl}(t)$ is continuous, and if it is null for $t < 0$, then

$$\sigma_{ij}(t) = \int_0^t G_{ijkl}(t - \theta) \dot{\gamma}_{kl}(\theta) d\theta \tag{16.6a}$$

Since $G(t)$ is zero for negative values of t , we can set the upper limit of integration equal to infinity, that is,

$$\sigma_{ij}(t) = \int_0^\infty G_{ijkl}(t - \theta) \dot{\gamma}_{kl}(\theta) d\theta \tag{16.6b}$$

This integral representation has the advantage that its formulation does not require an appeal to models based on dashpots and springs, and it is purely formal. Alternatively, the roles of stress and strain could be reversed, giving

$$\gamma_{ij}(t) = \int_{-\infty}^t J_{ijkl}(t - \theta) d\sigma_{kl}(\theta) \tag{16.7}$$

where the following symmetry conditions also hold:

$$J_{ijkl}(t) = J_{ijlk}(t) = J_{jikl}(t) = J_{klij} = J_{lkji} \tag{16.8}$$

The requirement of isotropy permits the representation of the fourth-order tensor in terms of two material functions in such a way that the stress-strain relationship becomes

$$\begin{aligned} \sigma_{ij} &= 2 \int_{-\infty}^t G(t - \theta) d\gamma_{ij}(\theta) + \delta_{ij} \int_{-\infty}^t \left(K(t - \theta) - \frac{2}{3} G(t - \theta) \right) d\Delta\theta \\ &= \int_{-\infty}^t G(t - \theta) d\varepsilon_{ij}(\theta) + \delta_{ij} \int_{-\infty}^t \left(K(t - \theta) - \frac{2}{3} G(t - \theta) \right) d\Delta\theta \end{aligned} \tag{16.9}$$

where Δ is the trace of γ_{ij} and $K - (2/3)G = \lambda$, the first coefficient of Lamé (see Chap. 4). Note that $\varepsilon_{ij} = 2\gamma_{ij}$ for $i \neq j$ and $\varepsilon_{ij} = \gamma_{ij}$ for $i = j$ [see Eq. (4.18)]. The Laplace transform of Eq. (16.9) is given by

$$\bar{\sigma}_{ij}(s) = 2s\bar{G}(s)\bar{\gamma}_{ij}(s) + \delta_{ij}s\left(\bar{K}(s) - \frac{2}{3}\bar{G}(s)\right)\bar{\Delta}(s) \tag{16.10}$$

which is formally equivalent to Eq. (5.75).

In order to describe the viscoelastic behavior of a system subjected to multiaxial tensions, it is convenient to separate the shear (deviatoric) effects from the purely dilatational components. This is due to the fact that in

viscoelastic materials the response to shear can be different from that in dilatation or bulk. In other words, different types of stress can produce different responses. In these conditions, Eq. (16.9) can be written as

$$\sigma_{ij} = \delta_{ij} \int_{-\infty}^t K(t-\theta) \dot{\Delta}_{kk}(\theta) d\theta + 2 \int_{-\infty}^t G(t-\theta) \left(\dot{\gamma}_{ij}(\theta) - \frac{1}{3} \delta_{ij} \dot{\Delta}(\theta) \right) d\theta \quad (16.11)$$

whose Laplace transform is

$$\sigma_{ij}(s) = \delta_{ij} s K(s) \Delta(s) + 2s G(s) \left(\gamma_{ij}(s) - \frac{1}{3} \delta_{ij} \Delta(s) \right) \quad (16.12)$$

As a consequence

$$\sigma_{ij}^d(t) = \int_{-\infty}^t 2G(t-\theta) d\gamma_{ij}^d(\theta) \quad (16.13a)$$

and

$$\sigma_{kk}(t) = \int_{-\infty}^t 3K(t-\theta) d\gamma_{kk}(\theta) \quad (16.13b)$$

where

$$\sigma_{ij}^d = \sigma_{ij} - \frac{1}{3} \delta_{ij} \sigma_{kk}; \quad \sigma_{ii}^d = 0 \quad (16.14a)$$

and

$$\gamma_{ij}^d = \gamma_{ij} - \frac{1}{3} \delta_{ij} \gamma_{kk}; \quad \gamma_{ii}^d = 0 \quad (16.14b)$$

and the superscript d indicates deviatoric components.

Laplace transforms and the properties of the integral of convolution permit us to establish simple relationships between distinct functions defined in the present context such as those outlined in Chapter 5. Thus,

$$\bar{\sigma}_{ij}^d(s) = 2s\bar{G}(s)\bar{\gamma}_{ij}^d(s) = s\bar{G}(s)\bar{\varepsilon}_{ij}^d(s) \quad (16.15a)$$

and

$$\bar{\sigma}_{kk}(s) = 3s\bar{K}(s)\bar{\gamma}_{kk}(s) \quad (16.15b)$$

In the same way, the following inverse relationships hold:

$$\bar{\gamma}_{ij}^d(s) = \frac{1}{2} s \bar{J}(s) \bar{\sigma}_{ij}^d(s) \quad (16.16a)$$

and

$$\bar{\gamma}_{ii}(s) = s \left(\frac{\bar{B}(s)}{9} + \frac{\bar{J}(s)}{3} \right) \bar{\sigma}_{ii}(s) \quad (16.16b)$$

where B and J are, respectively, the bulk and shear compliances [see Eq. (5.79a) of Chap. 5].

16.3 DIFFERENTIAL FORM FOR THE CONSTITUTIVE STRESS-STRAIN RELATIONSHIP

The integral form is not the only possible form in which stress-strain relationships can be written. The constitutive equation for an isotropic material whose response is sensitive to the derivatives of stress and strain can be written as (5)

$$f(\sigma, \dot{\sigma}, \ddot{\sigma}, \dots; \gamma, \dot{\gamma}, \ddot{\gamma}, \dots) = 0 \quad (16.17)$$

where both the stress and strain depend on time and the dots over the letters indicate time derivatives. In this case, the memory is represented by these derivatives. In a more compact form, one can write

$$P\sigma = Q\gamma \leftrightarrow P(D)\sigma_{ij}(t) = Q(D)\gamma_{ij}(t) \quad (16.18)$$

where the derivative temporal operators are given by

$$P(D) = \sum_{r=0}^N p_r \frac{\partial^r}{\partial t^r} \quad \text{and} \quad Q(D) = \sum_{r=0}^N q_r \frac{\partial^r}{\partial t^r} \quad (16.19)$$

where D is the operator d/dt .

Though the preceding equations represent a convenient way to express the relationship between stress and strain, it is necessary that they be consistent with the integral formulation of Section 16.2 (6). Consequently, taking the Laplace transform of both formulations and identifying them, we obtain

$$\sum_{r=k}^N p_r \sigma_{ij}^{(r-k)}(0) = \sum_{r=k}^N q_r \gamma_{ij}^{(r-k)}(0) \quad (16.20)$$

where $\sigma_{ij}^{(r-k)}(0)$ designates the $(k-r)$ th order derivative of the stress and strain at $t=0$. The conditions of linearity imposed require that p_r and q_r be independent of the stress and strain, though obviously they can be functions of time.

Appropriate combinations of the coefficients of Eq. (16.20) can reproduce determined idealized behavior of viscoelastic materials such as those corresponding to the Maxwell and Kelvin-Voigt models. Thus, for the Maxwell model in shear,

$$p_0 = 1, \quad p_1 = \eta/G; \quad q_0 = 0; \quad q_1 = 2\eta \quad (16.21)$$

while for the Kelvin-Voigt model,

$$p_0 = 1, \quad p_1 = 0; \quad q_0 = 2G, \quad q_1 = 2\eta \quad (16.22)$$

Additional terms in the general equation, Eq. (16.18), give a better account of the actual behavior of the material. However, the resulting equations are not easily solved unless Laplace transforms are used. In this way, the expression obtained is

$$\bar{\sigma}_{ij}(s) \left(\sum_{i=0}^n p_i s^i \right) = \bar{\gamma}_{ij}(s) \left(\sum_{i=0}^n q_i s^i \right) \quad (16.23)$$

For a viscoelastic solid this equation can be written in an alternative form as (7)

$$\bar{\sigma}(s) = \frac{q_0 + q_1 s + q_2 s^2 + \cdots}{p_0 + p_1 s + p_2 s^2 + \cdots} \bar{\gamma}(s) \quad (16.24)$$

In some cases rational polynomial fractions such as those appearing in Eq. (16.24) can be decomposed into a constant plus a sum of elementary fractions,

$$\frac{c_i}{s + p_i} \quad (16.25)$$

where c_i and p_i are, respectively, the real zeros and poles of these fractions. Moreover, they should be alternated on the negative real axis according to

$$p_1 < c_1 < p_2 < c_2 < \cdots < c_{n-1} < p_n < c_n \quad (16.26a)$$

for the creep function and

$$c_1 < p_1 < c_2 < p_2 < \cdots < p_{n-1} < c_n < p_n \quad (16.26b)$$

for the relaxation function. As Bland (7) has proved, this is a consequence of the properties of linear dissipative systems.

The Laplace inverse of simple fractions such as

$$c_i/(s + p_j) \quad (16.27)$$

is a decreasing exponential characterized by a relaxation time $(p_j)^{-1}$. The sum of such exponentials would correspond to a discrete collection of viscoelastic elements, each governed by a relaxation time, that is, a collection of Maxwell elements in parallel or a collection of Kelvin–Voigt elements in series. Following the continuum fraction methodology, ladder models can also be obtained (see Chap. 10).

Alternatively, if we dispose of dynamic data in a sufficient wide range of frequencies, for example, the master curves for $E'(\omega)$ and $E''(\omega)$ (or for the corresponding compliances), it is possible to represent $E^*(\omega)$ as a quotient of two polynomials of equal degree. This is achieved (8) by approximating the curve representing the double logarithmic plot of the modulus $E^*(\omega)$ versus frequency to an alternative succession of horizontal and straight lines with slope +1. In this way, the experimental curve is replaced by an approximate contour (called the approximate Bode's contour) whose representative equation has the form

$$E^*(\omega) = A \prod_{i=1}^n \left(\frac{j\omega + c_i}{j\omega + p_i} \right) \quad (16.28)$$

where $j\omega = s$ and c_i and p_i indicate zeros and poles of the function $E^*(\omega)$, which can be considered as a transfer function that fulfills the conditions of the Bland theorem (Eqs. [16.26a] and [16.26b]).

The loss angle, or equivalently the phase angle, can be obtained by simple addition of the contributions from each factor that appears in Eq. (16.28), that is,

$$\varphi = \sum_{i=1}^n \arctan\left(\frac{\omega}{c_i}\right) - \sum_{i=1}^n \arctan\left(\frac{\omega}{p_i}\right) \quad (16.29)$$

Evidently, this procedure is valid only when the slope of the double logarithmic plot is less than one.

16.4 CONSTITUTIVE EQUATIONS IN DIFFERENTIAL FORM FOR MULTIAXIAL TENSION STATES

If the dilational and deviatoric components are separated, reasoning similar to that used in the case of integral representation leads to the equations (5, p. 78)

$$P_1 \sigma_{ij}(t) = Q_1 \gamma_{ij}(t) \quad \text{and} \quad P_2 \sigma_{ii}^d(t) = Q_2 \gamma_{ii}^d(t) \quad (16.30)$$

where now P_1 , P_2 , Q_1 , and Q_2 are operators of the type

$$P_1 = p_0 + p_1 \frac{\partial}{\partial t} + p_2 \frac{\partial^2}{\partial t^2} + \cdots + p_n \frac{\partial^n}{\partial t^n} \quad (16.31)$$

Comparison of Eqs. (16.15) and (16.30) gives

$$G = \frac{1}{2} \left(\frac{Q_1}{P_1} \right); \quad K = \frac{1}{3} \left(\frac{Q_2}{P_2} \right) \quad (16.32)$$

As Eqs. (5.84) and (5.87) indicate, the tensile modulus and the Poisson ratio are related to the shear and bulk relaxation moduli by the formulae

$$E = \frac{9KG}{3K + G} \quad \text{and} \quad \nu = \frac{3K - 2G}{6K + 2G} \quad (16.33)$$

Equations (16.32) suggest that these relationships for a viscoelastic material under multiaxial stresses can be written as

$$E = \frac{3Q_1 Q_2}{P_2 Q_1 + 2P_1 Q_2} = \frac{Q^E}{P^E} \quad (16.34a)$$

and

$$\nu = \frac{P_1 Q_2 - P_2 Q_1}{P_2 Q_1 + 2P_1 Q_2} = \frac{Q^\nu}{P^\nu} \quad (16.34b)$$

Note that equations similar to Eq. (16.33) hold for the dynamic functions, that is,

$$E^* = \frac{9K^* G^*}{3K^* + G^*} \quad \text{and} \quad \nu^* = \frac{3K^* - 2G^*}{6K^* + 2G^*} \quad (16.35)$$

In the same way, the relationships between the different elastic functions can be generalized for the viscoelastic case.

As mentioned above, the shear response of some viscoelastic materials can differ from the dilatational response. Thus, while the response in shear is viscoelastic, the dilatational response is elastic. It is clear that in these conditions, the analysis of the multiaxial problems differs from that of the uniaxial and simple shear cases.

For a material that behaves as a Hookean solid in hydrostatic compression but as a Maxwell element in shear, the corresponding values of the operators are

$$P_2 = 1; \quad Q_2 = 3K \tag{16.36a}$$

and

$$P_1 = 1 + \frac{\eta}{G}s; \quad Q_1 = 2\eta s \tag{16.36b}$$

The results of the previous example as well other more complex models that are analyzed in the problems section at the end of the chapter show that the relationships between the different components of the stress and strain tensors for viscoelastic materials can be established in terms of the operators P and Q . For example (9), for an elongational test

$$P^E \sigma_{xx} = Q^E \gamma_{xx}; \quad P^v \gamma_{yy} = -Q^v \gamma_{xx} \tag{16.37}$$

where now the superscripts E and v refer to the tensile modulus and the Poisson ratio, respectively. When all these relationships are transformed through the Laplace transform into functions of the operational variable, they express the already cited elastic–viscoelastic correspondence principle.

Consequently, the direct and inverse stress–strain relationships present in terms of the P and Q operators the form

$$\sigma_{ij} = \frac{Q^E/P^E}{1 + Q^v/P^v} \gamma_{ij} - \frac{Q^E Q^v/P^E P^v}{(1 + Q^v/P^v)(1 - 2Q^v/P^v)} \gamma_{kk} \delta_{ij} \tag{16.38a}$$

and

$$\gamma_{ij} = \frac{1 + Q^v/P^v}{Q^E/P^E} \sigma_{ij} - \frac{Q^v/P^v}{Q^E/P^E} \sigma_{kk} \delta_{ij} \tag{16.38b}$$

As for the relationships of G and K with E and ν , we obtain

$$\frac{Q_1}{P_1} = \frac{Q^E/P^E}{1 + Q^v/P^v}; \quad \frac{Q_2}{P_2} = \frac{Q^E/P^E}{1 - 2Q^v/P^v} \tag{16.39}$$

The balance equations can also be transformed in terms of the operational variable, thus completing the preliminary step in the solutions of a viscoelastic problem.

16.5 THERMOVISCOELASTICITY

A theory of thermoviscoelasticity that includes the temperature dependence of the relaxation or retardation functions is necessarily nonlinear, and consequently the elastic–viscoelastic correspondence principle is not applicable. Nevertheless, a linear theory of thermoviscoelasticity can be developed in the framework of rational thermodynamics with further constitutive assumptions (Ref. 5, Chap. 3; see also Ref. 10).

However, for thermorheologically simple materials, that is, for those materials for which the time–temperature superposition principle holds, the mechanical properties data can be shifted parallel to the time or frequency axis. This fact suggests an additional hypothesis that can be very useful in solving some specific thermoviscoelastic problems. According to this hypothesis, the net effect of temperature in the response must be equivalent to a variation in the rates of creep or relaxation of the material. Thus for $T > T_0$ the process occurs at a higher rate than at T_0 .

In general, the effective time ξ will be related to t according to the expression

$$d\xi = a(T(t), T_0)dt \quad (16.40)$$

where the function a can be considered to be associated with some activation energy of the material in the range of temperatures considered. Moreover, Eq. (16.40) leads to

$$\xi = \int_0^t a(T(\tau), T_0)d\tau \quad (16.41)$$

When a is dependent on $T - T_0$ [that is, a Williams–Landel–Ferry (WLF) dependence] or on T (Arrhenius dependence), then ξ is a linear function of time.

To formalize the main hypothesis, the nonisothermal functional given by Eq. (16.1) is modified by a new isothermic functional with a modified time scale to account for the temperature history. Now, according to the basic hypothesis of linear theory, the specific form of the stress–strain relationship can be written as

$$\sigma_{ij}(x, t) = \int_{-\infty}^t G_{ijkl}(\xi - \xi') \frac{\partial}{\partial \theta} (\gamma_{kl}(x_i, \theta) - \alpha_{kl}(\theta)) d\theta \quad (16.42)$$

where α is the strain caused in the stress-free state by changes in temperature, being a function of the current temperature, and ξ is given by Eq. (16.41). The form of Eq. (16.42) for the isotropic case is given by

$$\sigma_{ij}^d(x, t) = 2 \int_{-\infty}^t G(\xi - \xi') \frac{\partial \gamma_{ij}^d(x_i, \theta)}{\partial \theta} d\theta \tag{16.43a}$$

and

$$\sigma_{kk}(x_i, t) = 3 \int_{-\infty}^t K(\xi - \xi') \frac{\partial}{\partial \theta} (\gamma_{kk}(x_i, \theta) - \alpha(\theta)) d\theta \tag{16.43b}$$

Equations (16.43a) and (16.43b) are the relevant constitutive equations to be solved. However, they are not of the convolution type, and for this reason we cannot apply the Laplace transform to them. Nevertheless, note that ξ is a monotonically increasing function of t , and by inverting the functional relationship given by Eq. (16.41) the convolution integrals in terms of the new time scale ξ are obtained. The pertinent equations are

$$\sigma_{ij}^d(x_i, \xi) = 2 \int_{-\infty}^{\xi} G(\xi - \xi') \frac{\partial}{\partial \xi'} \gamma_{ij}^d(x_i, \xi') d\xi' \tag{16.44a}$$

and

$$\sigma_{kk}(x_i, \xi) = 3 \int_{-\infty}^{\xi} K(\xi - \xi') \frac{\partial}{\partial \xi'} (\gamma_{kk}(x_i, \xi') - \alpha(\xi')) d\xi' \tag{16.44b}$$

Notice that the same symbol is used for the dependence of the strains on ξ and t in Eqs. (16.43) and (16.44).

Note also that infinitesimal temperature changes are not required in this approach. An interesting particular case is that one which external forces are absent. In this situation, the deformation (expansion or contraction) of the viscoelastic system can be due only to temperature effects. In the case of a temperature jump ΔT , Eq. (16.44b) leads to the relation

$$3 \int_{-\infty}^{\xi} K(\xi - \xi') d\gamma_{kk}(\xi') = \beta \Delta T K(\xi) \tag{16.45}$$

where β is identified with the thermal expansion coefficient and $\beta \Delta T$ is the relative change in volume caused by the deformation.

16.6 SPECIAL PROBLEMS IN STRUCTURAL LINEAR VISCOELASTICITY

The solution of a problem in linear viscoelasticity requires the determination of the stress, strain, and displacement histories as a function of the space coordinates. The uniqueness of the solution was proved originally by Volterra (11). The analysis carried out in this chapter refers exclusively to isotropic materials under isothermal conditions. As a rule, it is not possible to give a closed solution to a viscoelastic problem without previous knowledge of the material functions. The experimental determination of such functions and the relationships among them have been studied in a specific way in separate chapters, and therefore the reader's knowledge of them is assumed. At the same time, the methods of analysis carried out in this chapter and in Chapter 17 will allow us to optimize the calculation of the material functions.

The necessary conditions to be fulfilled are the equilibrium conditions, the strain-displacement relationships (kinematic equations), and the stress-strain relationships (constitutive equations). As in linear elasticity theory (12), these conditions form a system of 15 equations that permit us to obtain 15 unknowns: three displacements, six strain components, and six stress components.

16.7 FORMULATION AND CLASSIFICATION OF THE BOUNDARY PROBLEMS IN VISCOELASTICITY

Boundary conditions allow us to obtain specific results for each three-dimensional viscoelastic problem. If the stresses on the surface of the body are stated (first boundary problem), then the system of 15 basic equations is reduced to one of only six independent differential equations containing the six independent stress components. The strategy to follow implies the formulation of the compatibility equations in terms of the stress (Beltrami-Michell compatibility equations).

If the displacements on the surface of the body are given (second boundary problem), the stress-displacement relationships are obtained first, and their substitution into the equilibrium equations permits us to eliminate the stress variables and thus to obtain the three equilibrium equations in terms of the displacements (see Navier equations in

Chapter 4). Mixed boundary conditions are possible, of course, where tractions are prescribed for part of the surface whereas displacements are given for the rest of the surface.

16.8 APPLICABILITY OF THE CORRESPONDENCE PRINCIPLE. QUASI-STATIC AND DYNAMIC PROBLEMS

In general, it is not possible to solve any viscoelastic problem in a unified way. On the contrary, special techniques are required for each particular situation (13,14). In the present chapter some specific problems, interesting from a practical point of view, are studied. In particular, problems with special symmetries, plane strain or plane stress as well as dynamic problems are considered. These problems are also interesting from the academic point of view because their solutions illustrate the strategies to be followed in solving typical structural problems in viscoelasticity. Most of the problems studied here are simply the viscoelastic counterparts of classical elasticity problems. For this reason, the elastic problem will be solved prior to solving the viscoelastic one. As mentioned in the preceding section, the usual tool for solving a problem of this type is the elastic-viscoelastic correspondence principle, which requires Laplace transforms. In Chapter II of Ref. 6, a complete account is given of the elastic-viscoelastic constitutive and field equations to be solved via Laplace transforms. The main limitation to this approach lies in the character of the boundary conditions. In fact, the applicability of the correspondence principle is restricted to situations where the prescribed boundary conditions are independent of time. A representative situation of the time-dependent boundary conditions that is related to a curved indentation, is considered here.

The inertial terms present in the equilibrium equations convert the problems into dynamic ones. The most studied dynamic viscoelastic boundary problems have been those referring to the unidirectional propagation of waves. In particular, forced oscillations have been widely used in the determination of dynamic moduli.

The technique of separation of variables, that is, the possibility of separating the spatial and temporal variables in the stress and strain fields, is particularly useful in the solution of dynamic viscoelastic problems. As a rule, this requires us to assume that the Poisson ratio is constant, a reasonable assumption in many cases. Alternatively, the divergence of the displacement vector must be constant. A particularly important case of application of the variables separation method, where the assumption concerning the constancy of the Poisson ratio is relaxed, occurs in those problems in which the boundary conditions or the forces of volume are

harmonic functions of time in a stationary regime. Furthermore, the incorporation of inertial terms in these cases does not pose an additional complication.

16.9 SUPERPOSITION AND SAINT VENANT PRINCIPLES

In linear elasticity or viscoelasticity, the superposition principle states that the resulting effects of the different causes (stress or displacements), acting separately, can be superposed to give the total values due to these combined causes. This principle is a consequence of the linearity of the equations governing the stress, strain, and displacements.

According to the Saint Venant principle, the stresses of two statically equivalent applied loads are closely similar except near the point of application of the load. This principle, which can be empirically tested, allows the boundary conditions to be expressed in terms of a resultant force rather than an exact distribution of stresses. Obviously, this principle is of great significance in many practical problems.

16.10 PROBLEMS WITH SPECIAL SYMMETRIES

The geometric characteristics of some interesting viscoelastic problems have special symmetries. For example, spherical shells have wide applications in pressure vessels, heat exchangers, and nuclear reactors. Loading of these structures can occur not only in accidental conditions but also in normal situations, e.g., during overpressurization. These spherical shells are radially symmetrical.

To start with, let us determine the stress and the deformation of a hollow sphere (outer radius R_2 , inner radius R_1) under a sudden increase in internal pressure if the material is elastic in compression but a standard solid (spring in series with a Kelvin–Voigt element) in shear (Fig. 16.1). As a consequence of the radial symmetry of the problem, spherical coordinates with the origin in the center of the sphere will be used. The displacement, obviously radial, is a function of r alone as a consequence of the fact that the components of the strain and stress tensors are also dependent only on r . As a consequence, the Navier equations, Eq. (4.108), predict that $\text{rot } \mathbf{u} = 0$. Hence, $\text{grad div } \mathbf{u} = 0$. This implies that

$$\text{div } \mathbf{u} = \text{tr } \gamma_{ij} = 3m \quad (16.46)$$

From the result of Problem 4.7 in Chapter 4, the following differential equation for the displacement u (assuming $u_r = u$) is obtained:

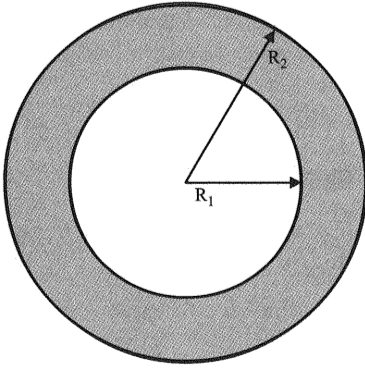


Figure 16.1. Hollow sphere with inner and external radii R_1 and R_2 .

$$\operatorname{div} \mathbf{u} = \frac{du}{dr} + 2\frac{u}{r} = \frac{1}{r^2} \frac{d}{dr}(r^2 u) = 3m \quad (16.47)$$

where m is a constant

The solution of Eq. (16.47) is given by

$$u = mr + \frac{n}{r^2} \quad (16.48)$$

where n is an integration constant to be determined from the boundary conditions.

The nonzero strain tensor components are easily obtained as

$$\gamma_{rr} = m - \frac{2n}{r^3} \quad \text{and} \quad \gamma_{\theta\theta} = \gamma_{\varphi\varphi} = m + \frac{n}{r^3} \quad (16.49)$$

The radial and transverse stresses can be determined from the stress-strain relationships. Owing to the orthogonality of the spherical coordinates, the formal structure of the generalized Hooke's law, given by Eq. (P4.11), is preserved, so that the nonzero components of the stress tensor are expressed in terms of the strain tensors as

$$\sigma_{rr} = \frac{E}{(1+\nu)(1-2\nu)} [(1-\nu)\gamma_{rr} + 2\nu\gamma_{\theta\theta}] \quad (16.50)$$

and

$$\sigma_{\theta\theta} = \sigma_{\varphi\varphi} = \frac{E}{(1+\nu)(1-2\nu)} [(1-\nu)\gamma_{\theta\theta} + (\gamma_{rr} + \gamma_{\theta\theta})] \quad (16.51)$$

It should be noted that these equations were obtained from Eq. (4.76) by substituting the Lamé moduli in terms of the tensile modulus E and the Poisson ratio ν , by means of the relations of Table 4.1, as is usual in elasticity theory (see also Problem 4.12).

By substituting the values of the strain given in Eqs. (16.49) in Eqs. (16.50) and (16.51), the following expressions for the components of the stress tensor are obtained:

$$\sigma_{rr} = \frac{mE}{1-2\nu} - \frac{2nE}{1+\nu} \left(\frac{1}{r^3} \right) \quad (16.52a)$$

$$\sigma_{\theta\theta} = \sigma_{\varphi\varphi} = \frac{mE}{1-2\nu} + \frac{nE}{1+\nu} \left(\frac{1}{r^3} \right) \quad (16.52b)$$

The values of m and n in Eqs. (16.52) can be found by solving these two equations for the two boundary conditions

$$\sigma_{rr} = -p_1 \quad \text{for } r = R_1 \quad (16.53a)$$

and

$$\sigma_{rr} = -p_2 \quad \text{for } r = R_2 \quad (16.53b)$$

where p_1, p_2 are the internal and external pressures, respectively. The values of m and n thus obtained in combination with Eq. (16.48) give the displacement as

$$u = \frac{p_1 R_1^3 - p_2 R_2^3}{R_2^3 - R_1^3} \left(\frac{1-2\nu}{E} \right) r + \frac{R_1^3 R_2^3 (p_1 - p_2)}{R_2^3 - R_1^3} \left(\frac{1+\nu}{2E} \right) \left(\frac{1}{r^2} \right) \quad (16.54)$$

Before proceeding with the calculations of the stresses and displacement for any specific input, we consider several special cases.

Case 1. Consider a hollow sphere under an internal pressure. Here the boundary conditions are

$$p_1 = p \quad (16.55a)$$

and

$$p_2 = 0 \quad (16.55b)$$

Then the displacement given by Eq. (16.54) becomes

$$u = \frac{pR_1^3}{R_2^3 - R_1^3} \left[\frac{1 - 2\nu}{E} r + \frac{R_2^3}{r^2} \left(\frac{1 + \nu}{2E} \right) \right] \quad (16.56)$$

whereas the components of the stress tensor can be written as

$$\sigma_{rr} = \frac{pR_1^3}{R_2^3 - R_1^3} \left(1 - \frac{R_2^3}{r^3} \right) \quad (16.57a)$$

and

$$\sigma_{\theta\theta} = \sigma_{\varphi\varphi} = \frac{pR_1^3}{R_2^3 - R_1^3} \left(1 + \frac{R_2^3}{2r^3} \right) \quad (16.57b)$$

Case 2. Consider an infinite medium with a spherical cavity of radius R subjected to hydrostatic compression. In this case the boundary conditions are $p_1 = 0$, $p_2 = p$. After making R_2 approach infinity and putting $R_1 = R$, Eqs. (16.52a) and (16.52b) become

$$\sigma_{rr} = -p \left(1 - \frac{R^3}{r^3} \right) \quad (16.58a)$$

and

$$\sigma_{\theta\theta} = \sigma_{\varphi\varphi} = -p \left(1 + \frac{R^3}{2r^3} \right) \quad (16.58b)$$

and the tangential stress in the surface of the cavity is given by

$$\sigma_{\theta\theta}|_{r=R} = \sigma_{\varphi\varphi}|_{r=R} = -\frac{3}{2}p \quad (16.59)$$

Moreover, the displacement can be written as

$$u = -\frac{p}{E} \left((1 - 2\nu)r + \frac{R^3}{2r^2} (1 + \nu) \right) \quad (16.60)$$

where the displacement at R is given by

$$u(R) = -\frac{3}{2}pR \frac{1 - \nu}{E} \quad (16.61)$$

Case 3. Consider an infinite medium with a spherical cavity of radius R subjected to internal pressurization. If the boundary conditions $p_1 = p$ and $p_2 = 0$ are assumed, then the components of the stress tensor are

$$\sigma_{rr} = -\frac{R_1^3}{r^3}p \quad (16.62a)$$

$$\sigma_{\theta\theta} = \sigma_{\varphi\varphi} = \frac{R_1^3}{2r^3}p \quad (16.62b)$$

and

$$\sigma_{rr}(R) = -p \quad (16.63a)$$

$$\sigma_{\theta\theta}(R) = \sigma_{\varphi\varphi}(R) = \frac{p}{2} \quad (16.63b)$$

Case 4. For a spherical ball subjected to an external pressure p , $R_1 = 0$ and $R_2 = R$. The corresponding stresses and displacement are

$$\sigma_{rr} = \sigma_{\theta\theta} = \sigma_{\varphi\varphi} = -p \quad (16.64a)$$

and

$$u = -pr \frac{1-2\nu}{E} \quad (16.64b)$$

Case 5. For a thin spherical shell, $R_2 - R_1 = h \ll R_1, R_2$, and the following approximation holds:

$$R_2^3 - R_1^3 = (R_2 - R_1)(R_2^2 + R_1R_2 + R_1^2) \cong 3R^2h \quad (16.65)$$

From Eqs. (16.54) and (16.65) we obtain

$$u = \frac{1-\nu}{E} \left(\frac{R^2 p}{2h} \right) \quad (16.66a)$$

$$\bar{\sigma}_{rr} = \frac{p}{2} \quad (16.66b)$$

$$\sigma_{\theta\theta} = \sigma_{\varphi\varphi} = \frac{pR}{2h} \quad (16.66c)$$

where the average value of σ_{rr} is given by

$$\bar{\sigma}_{rr} = \frac{\int_{R_1}^{R_2} \sigma_{rr} ds}{S} = \frac{2 \int_{R_1}^{R_2} \sigma_{rr} r dr}{R_2^2 - R_1^2} \quad (16.67)$$

Let us return to the proposed problem of calculating the displacement of a viscoelastic thin hollow sphere after a sudden internal pressurization. According to Eq. (16.66a), the determination of the displacement u requires to obtain an expression for $(1 - \nu)/E$ in the viscoelastic system. From the differential operators of a standard solid and the equations for the tensile modulus and the Poisson ratio developed, respectively, in Problems 16.2 and 16.4 at the end of this chapter, the following expression for $(1 - \nu)/E$ is obtained:

$$\begin{aligned} \frac{1 - \nu}{E} &= \frac{1}{18K} \left(\frac{4 + 3K \left(\frac{1}{G_1} + \frac{1}{G_2} \right) + \left(4 + \frac{3K}{G_1} \right) \left(\frac{\eta}{G_2} \right) s}{1 + (\eta/G_2)s} \right) \\ &= \frac{1}{6G_1} + \frac{1}{9K} \left(2 + \frac{3/2K/G_2}{1 + (\eta/G_2)s} \right) \end{aligned} \quad (16.68)$$

On the other hand, for a step input pressure $p(t) = p_0 H(t)$, where $H(t)$ is the Heaviside step function, the Laplace transform of Eq. (16.66a), in combination with Eq. (16.68), gives the displacement in terms of the operational variable s as

$$\bar{u}(s) = \frac{R^2 p_0}{2h} \left(\frac{1}{s} \right) \left[\frac{1}{6G_1} + \frac{1}{9K} \left(2 + \frac{\frac{3}{2}K/G_2}{1 + (\eta/G_2)s} \right) \right] \quad (16.69)$$

where it was taken into account that the Laplace transform of $p(t) = p_0 H(t)$ is p_0/s . The inverse of Eq. (16.69) is

$$u(t) = \frac{R^2 p_0}{2h} \left\{ \frac{3K + 4G_1}{18KG_1} + \frac{1}{6G_2} \left[1 - \exp\left(-\frac{t}{\tau}\right) \right] \right\}; \quad \tau = \frac{\eta}{G_2} \quad (16.70)$$

The values of u for two extreme situations are given below. Thus, for $t = 0$,

$$u(0) = \frac{R^2 p_0}{2h} \left(\frac{3K + 4G_1}{18KG_1} \right) \quad (16.71)$$

and for $t \rightarrow \infty$,

$$u(\infty) = \frac{R^2 p_0}{2h} \left[\frac{2}{9K} + \frac{1}{6} \left(\frac{1}{G_1} + \frac{1}{G_2} \right) \right] \quad (16.72)$$

It is also interesting to consider now a sinusoidal input of frequency ω . Taking into account that the Laplace transform of the sine function is given by

$$\mathcal{L}(\sin \omega t) = \frac{\omega}{\omega^2 + s^2} \quad (16.73)$$

we obtain for the displacement in terms of the variable s the expression

$$\bar{u}(s) = \frac{R^2 p_0}{2h} \left(\frac{\omega}{\omega^2 + s^2} \right) \left[\frac{1}{6G_1} + \frac{1}{9K} \left(2 + \frac{\frac{3}{2}K/G_2}{1 + (\eta/G_2)s} \right) \right] \quad (16.74)$$

The inverse of Eq. (16.74) can easily be obtained by considering that

$$\frac{1}{s + \tau^{-1}} \left(\frac{\omega}{s^2 + \omega^2} \right) = \frac{A}{s + \tau^{-1}} + \frac{Bs + C\omega}{s^2 + \omega^2}; \quad \tau = \frac{\eta}{G_2} \quad (16.75)$$

from which

$$A = \frac{\omega\tau^2}{1 + \omega^2\tau^2}; \quad B = -A; \quad C = \frac{A}{\omega\tau} \quad (16.76)$$

The final result for the displacement in the time domain is

$$u(t) = \frac{R^2 p_0}{2h} \left\{ \frac{3K + 4G_1}{18KG_1} \sin \omega t + \frac{1}{6G_2} \left(\frac{1}{(1 + \omega^2\tau^2)^{1/2}} \right) \right. \\ \left. \left[\frac{\omega\tau}{(1 + \omega^2\tau^2)^{1/2}} \exp\left(-\frac{t}{\tau}\right) + \sin(\omega t - \delta) \right] \right\} \quad (16.77)$$

where

$$\delta = \arctan(\omega\tau) \quad (16.78)$$

16.11 THE DYNAMIC PROBLEM

Although in viscoelasticity pure static problems do not exist, the example discussed above can be considered quasi-static, because inertial terms are neglected. Let us consider the dynamic problem concerning the radial vibra-

tions of the same viscoelastic sphere to which we referred in the preceding section. We follow the main line of Bland (7, Chap. 3).

In the present case the equation of motion is obtained by adding the inertial term to the right-hand side of the equilibrium equation as follows [see Eq. (P4.7.3)]:

$$\frac{\partial \sigma_{rr}}{\partial r} + \frac{2}{r}(\sigma_{rr} - \sigma_{\theta\theta}) = \rho \frac{\partial^2 u}{\partial t^2} \quad (16.79)$$

The stress–displacement equations can be more conveniently expressed in terms of the Lamé coefficients (see Table 4.1 of Chap. 4), giving

$$\sigma_{rr} = \lambda \left(\frac{\partial u}{\partial r} + \frac{u}{r} \right) + 2G \frac{\partial u}{\partial r} \quad (16.80a)$$

$$\sigma_{\theta\theta} = \sigma_{\varphi\varphi} = \lambda \left(\frac{\partial u}{\partial r} + \frac{2u}{r} \right) + 2G \frac{u}{r} \quad (16.80b)$$

where according to Eqs. (16.48) and (16.49)

$$\frac{\partial u}{\partial r} + 2 \frac{u}{r} = \text{tr } \gamma_{ij} = \gamma_{rr} + \gamma_{\theta\theta} + \gamma_{\varphi\varphi} \quad (16.81)$$

The substitution of Eqs. (16.80a) and (16.80b) in Eq. (16.79) gives

$$(\lambda + 2G) \left(\frac{\partial^2 u}{\partial r^2} + \frac{2}{r} \frac{\partial u}{\partial r} - \frac{2}{r^2} u \right) = \rho \frac{\partial^2 u}{\partial t^2} \quad (16.82)$$

or, equivalently,

$$\frac{\partial}{\partial r} \left(\frac{\partial u}{\partial r} + \frac{2u}{r} \right) = \frac{1}{c^2} \frac{\partial^2 u}{\partial t^2} \quad (16.83)$$

where c^2 , the square of the speed of the radial wave propagation, can be written as

$$c^2 = \frac{\lambda + 2G}{\rho} = \frac{E(1 - \nu)}{\rho(1 + \nu)(1 - 2\nu)} \quad (16.84)$$

It should be noted that the quasi-static case is a limiting situation of the corresponding dynamic problem when the value of c is large.

Owing to the radial symmetry of the problem, and taking into account that the excitation is harmonic, the solution for the differential equation can be assumed to be

$$u(t) = u(r)e^{j\omega t} \quad (16.85)$$

Substituting Eq. (16.85) into Eq. (16.83), we find

$$\frac{\partial^2 u}{\partial r^2} + \frac{2}{r} \frac{\partial u}{\partial r} - \frac{2}{r^2} u = -\frac{\omega^2 u}{c^2} \quad (16.86)$$

with

$$u(0, r) = \dot{u}(0, r) = 0 \quad (16.87)$$

as initial boundary conditions for the displacement.

Equation (16.86) can be considered the Fourier transform of the motion equation.

As in Section 16.10, several specific cases will be discussed.

Case 1. Let us consider first the free vibrations of a hollow sphere with outer and inner radii R_2 and R_1 , respectively, as in the quasi-static example described above. A solution of Eq. (16.86) is

$$u = \frac{(Ax - B) \cos x - (A + Bx) \sin x}{x^2} \quad (16.88)$$

where $x = \omega r/c$ and A and B are constants. The boundary conditions at $r = R_1, R_2$ for the free vibrations case are given by

$$(\lambda + 2G) \frac{\partial u}{\partial r} + 2\lambda \frac{u}{r} = 0 \quad (16.89)$$

Substituting Eq. (16.88) in Eq. (16.89) gives

$$\begin{aligned} & \{(\lambda + 2G)[(2 - x_i^2) \sin x_i - 2x_i \cos x_i] + 2\lambda(x_i \cos x_i - \sin x_i)\} A \\ & + \{(\lambda + 2G)[(2 - x_i^2) \cos x_i + 2x_i \sin x_i] - 2\lambda(x_i \sin x_i + \cos x_i)\} B = 0 \end{aligned} \quad (16.90)$$

where the subscript $i = 1, 2$, $x_1 = \omega R_1/c$, and $x_2 = \omega R_2/c$. Eliminating A and B from Eq. (16.90), we obtain for the eigenvalue equation the expression

$$\frac{kx_1 + (x_1^2 - k) \tan x_1}{(x_1^2 - k) - kx_1 \tan x_1} = \frac{kx_2 + (x_2^2 - k) \tan x_2}{(x_2^2 - k) - kx_2 \tan x_2} \quad (16.91)$$

where

$$k = \frac{4G}{\lambda + 2G} = \frac{2(1 - 2\nu)}{1 - \nu} \tag{16.92}$$

Equation (16.91) gives the free vibration modes of the sphere. From the trigonometric relationship

$$\tan(x_2 - x_1) = \frac{\tan x_2 - \tan x_1}{1 + \tan x_2 \tan x_1} \tag{16.93}$$

and using the series expansion

$$\tan x = x + \frac{x^3}{3} + \dots \tag{16.94}$$

the simplified frequency equation

$$x^2 - xk + k^2 = 0 \tag{16.95}$$

for a thin spherical shell is obtained. The value of x in Eq. (16.95) is given by

$$x^2 = \frac{2(1 + \nu)(1 - 2\nu)}{(1 - \nu)^2} \tag{16.96}$$

where $x = \omega R/c$, R being the mean radius of the spherical shell. Since

$$\omega = \frac{2\pi}{T} \quad \text{and} \quad c^2 = \frac{2G(1 - \nu)}{\rho(1 - 2\nu)} \tag{16.97}$$

the period of oscillations of the elastic hollow sphere is given by

$$T = \pi R \left[\left(\frac{\rho}{G} \right) \left(\frac{1 - \nu}{1 + \nu} \right) \right]^{1/2} \tag{16.98}$$

It should be pointed out, however, that the frequency of vibrations for a viscoelastic material is a complex quantity. Let us assume a Maxwell material with a constant Poisson ratio $\nu = \frac{1}{4}$. According to Eq. (10.18), the complex shear modulus can be written as

$$s\bar{G}(s) = \frac{G_s}{s + \tau^{-1}} \tag{16.99}$$

It follows from this equation that the following approximation for a low loss material can be made:

$$[\bar{G}(s)]^{1/2} = G^{1/2} \frac{1}{(1 + 1/\tau s)^{1/2}} \cong G^{1/2} \left[1 + \frac{i}{2} \left(\frac{1}{\omega\tau} \right) \right] \tag{16.100}$$

where $s = i\omega$ and $\tau = \eta/G$. From Eqs. (16.97), (16.98), and (16.100), we obtain the following approximate relationship for the complex frequency:

$$\omega^* \cong \frac{x}{R} \left(\frac{3G}{\rho} \right)^{1/2} + \frac{i}{2} \left(\frac{G}{\eta} \right) \quad (16.101)$$

or, more conveniently,

$$\omega^* \cong \frac{2\sqrt{15}}{3R} \left(\frac{G}{\rho} \right)^{1/2} + \frac{i}{2} \left(\frac{G}{\eta} \right) \quad (16.102)$$

Accordingly, the temporal component of the wave is given by

$$e^{i\omega^* t} \simeq \exp\left[-\frac{t}{2\tau}\right] \exp\left[i \frac{2\sqrt{15}}{3R} \left(\frac{G}{\rho} \right)^{1/2} t\right] \quad (16.103)$$

The mechanical loss, represented by the imaginary part of Eq. (16.102) or by the decaying exponential in Eq. (16.103), is obviously caused by the internal friction due to the viscoelastic character of the material.

Case 2. Let us consider now a solid sphere. The following equation represents a solution of the problem that is finite in the center of the sphere:

$$u = A \frac{\cos x - \sin x}{r^2} = A \frac{\partial}{\partial r} \left(\frac{\sin x}{r} \right), \quad x = \frac{\omega r}{c} \quad (16.104)$$

According to Eq. (16.89), on the surface of a freely vibrating sphere,

$$(\lambda + 2G) \frac{\partial u}{\partial r} \Big|_{r=R} + 2\lambda \frac{u}{r} \Big|_{r=R} = 0 \quad (16.105)$$

This equation leads to

$$u = -R \frac{\lambda + 2G}{2\lambda} \frac{\partial u}{\partial r} \Big|_{r=R} \quad (16.106)$$

After some calculations similar to those of case 1, the following equation is obtained for the frequency:

$$1 - x \cot x = \frac{\lambda + 2G}{4G} x^2 = \frac{1 - \nu}{2(1 - 2\nu)} x^2 \quad (16.107)$$

where $x = \omega R/c$. If, as before, ν is taken to be $1/4$, the resulting equation for the eigenvalues is

$$\tan x = \frac{x}{1 - (3/4)x^2} \quad (16.108)$$

whose first real solution is $x_1 = 2.5635$. Consequently, the frequency of a Maxwell material under the same conditions as in case 1 can be written as

$$\omega^* \cong \frac{4.44}{R} \left(\frac{G}{\rho} \right)^{1/2} + i \frac{G}{2\eta} \quad (16.109)$$

Here only free vibrations have been considered. For forced vibrations, it is difficult to obtain a closed analytical solution by Laplace inversion (6).

16.12 PLANE STRAIN PROBLEMS

A plane strain state is defined as a state of strain where the components of the vector displacement take the form

$$u_x = u_x(x, y) \quad (16.110a)$$

$$u_y = u_y(x, y) \quad (16.110b)$$

$$u_z = 0 \quad (16.110c)$$

These equations imply that the strains γ_{zz} , γ_{xz} , and γ_{yz} are zero. From the stress-strain relationships, Eq. (4.75),

$$\sigma_{xz} = \sigma_{yz} = 0 \quad (16.111)$$

The equilibrium equations are reduced by two, since σ_{zz} is a function of only x and y , as Eq. (4.75) immediately shows. Consequently, no body force exists in the z direction in a plane strain state. Problems of this type are two-dimensional and therefore are governed by only eight equations, which let us find eight unknowns: σ_{xx} , σ_{yy} , σ_{xy} , γ_{xx} , γ_{yy} , γ_{xy} , u_x , and u_y . As will be shown below, σ_{zz} depends on σ_{xx} , and σ_{yy} .

In practice, the body must be cylindrical or prismatic with uniform cross section and fixed ends. An alternative condition to the last one is that the tractions on the lateral surface are normal to the axis of the system and are functions of only x and y . Obviously, these conditions are only approximately fulfilled in actual situations.

The use of cylindrical coordinates is particularly suitable in the solution of axisymmetrical problems. It is worth noting that for a non-simply connected cross section, as occurs in the case of a hollow cylinder, the compatibility equations are not sufficient to guarantee single-valued displacements. In this situation, the displacements themselves must be considered.

Let us consider now the deformation and stresses of a cylindrical pipe under two different boundary conditions (Fig. 16.2). In both cases the length of the pipe is considered constant according to the requirements for a plane strain problem. The external and internal radii are R_2 and R_1 , respectively. If the applied forces and the displacements are also uniform, the deformation is purely radial, and in cylindrical coordinates $u_r = u(r)$. According to the Navier equations, $\text{rot } \mathbf{u} = 0$. Hence, $\nabla \text{div } \mathbf{u} = 0$, which implies

$$\text{div } \mathbf{u} = \text{constant} \quad (16.112)$$

By using cylindrical coordinates [see Eq. (16.81)], Eq. (16.112) can be written as

$$\text{div } \mathbf{u} = tr \gamma_{ij} = \frac{du}{dr} + \frac{u}{r} = \frac{1}{r} \frac{d(ru)}{dr} = 2m \quad (16.113)$$

where m is a constant. Equation (16.113) immediately leads to

$$u = mr + \frac{n}{r} \quad (16.114)$$

The only nonzero components of the strain tensor are

$$\gamma_{rr} = m - \frac{n}{r^2} \quad (16.115a)$$

and

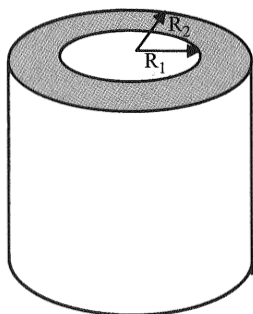


Figure 16.2. Cylindrical pipe with internal and external radii R_1 and R_2 .

$$\gamma_{\theta\theta} = m + \frac{n}{r^2} \quad (16.115b)$$

That is, the only non-null components of the stress tensor are those corresponding to the diagonal. The constants m and n can be obtained from the boundary conditions. Let us consider two cases.

Case 1. Let us assume first a uniform internal displacement in which the external radius is rigidly constrained, that is,

$$u(R_1) = u_0; \quad u(R_2) = 0 \quad (16.116)$$

Then

$$u_0 = mR_1 + \frac{n}{R_1} \quad (16.117a)$$

and

$$0 = mR_2 + \frac{n}{R_2} \quad (16.117b)$$

From these equations we obtain

$$m = -u_0 \frac{R_1}{R_2^2 - R_1^2} \quad (16.118a)$$

and

$$n = u_0 \frac{R_1 R_2^2}{R_2^2 - R_1^2} \quad (16.118b)$$

The values of m and n indicated above, substituted in Eqs. (16.115a) and (16.115b), give the strain tensor components as

$$\gamma_{rr} = -\frac{u_0 R_1}{R_2^2 - R_1^2} \left(1 + \frac{R_2^2}{r^2} \right) \quad (16.119a)$$

$$\gamma_{\theta\theta} = -\frac{u_0 R_1}{R_2^2 - R_1^2} \left(1 - \frac{R_2^2}{r^2} \right) \quad (16.119b)$$

The stress-strain relationship [Eq. (P4.11)] together with Eqs. (16.119a) and (16.119b) give the stress tensor components as follows

$$\sigma_{rr} = \frac{E}{1+\nu} \left(\frac{u_0 R_1}{R_2^2 - R_1^2} \right) \left(\frac{1}{1-2\nu} + \frac{R_2^2}{r^2} \right) \quad (16.120a)$$

$$\sigma_{\theta\theta} = \frac{E}{1+\nu} \left(\frac{u_0 R_1}{R_2^2 - R_1^2} \right) \left(\frac{1}{1-2\nu} - \frac{R_2^2}{r^2} \right) \quad (16.120b)$$

$$\sigma_{zz} = \frac{E\nu}{(1+\nu)(1-2\nu)} \left(\frac{2R_1 u_0}{R_2^2 - R_1^2} \right) \quad (16.120c)$$

Case 2. If the pipe is internally pressurized, then the boundary conditions are

$$\sigma_{rr} = 0, \quad r = R_2 \quad (16.121a)$$

$$\sigma_{rr} = -p, \quad r = R_1 \quad (16.121b)$$

In this case, the system of equations to be solved to find m and n is

$$0 = \frac{E}{(1+\nu)(1-2\nu)} \left[(1-\nu) \left(m - \frac{n}{R_2^2} \right) + \nu \left(m + \frac{n}{R_2^2} \right) \right] \quad (16.122a)$$

$$-p = \frac{E}{(1+\nu)(1-2\nu)} \left[(1-\nu) \left(m - \frac{n}{R_1^2} \right) + \nu \left(m + \frac{n}{R_1^2} \right) \right] \quad (16.122b)$$

The values of m and n obtained from these equations are

$$m = \frac{pR_1^2}{(R_2^2 - R_1^2)} \left(\frac{(1+\nu)(1-2\nu)}{E} \right) \quad (16.123a)$$

$$n = \frac{pR_1^2 R_2^2}{R_2^2 - R_1^2} \left(\frac{1+\nu}{E} \right) \quad (16.123b)$$

Substituting Eqs. (16.123a) and (16.123b) into Eqs. (16.115a) and (16.115b), we obtain the components of the strain tensor,

$$\gamma_{rr} = \frac{pR_1^2(1+\nu)}{(R_2^2 - R_1^2)E} \left((1-2\nu) - \frac{R_2^2}{r^2} \right) \quad (16.124a)$$

$$\gamma_{\theta\theta} = \frac{pR_1^2(1+\nu)}{(R_2^2 - R_1^2)E} \left((1-2\nu) + \frac{R_2^2}{r^2} \right) \quad (16.124b)$$

and from Eqs. (16.114), (16.123a), and (16.123b), the displacement is obtained as

$$u = \frac{pR_1^2}{R_2^2 - R_1^2} \left(\frac{1 + \nu}{E} \right) \left((1 - 2\nu)r + \frac{R_2^2}{r} \right) \quad (16.125)$$

Combining Eqs. (4.75), (16.124a), and (16.124b), gives the components of the stress tensor as

$$\sigma_{rr} = \frac{pR_1^2}{R_2^2 - R_1^2} \left(1 - \frac{R_2^2}{r^2} \right) \quad (16.126a)$$

$$\sigma_{\theta\theta} = \frac{pR_1^2}{R_2^2 - R_1^2} \left(1 + \frac{R_2^2}{r^2} \right) \quad (16.126b)$$

$$\sigma_{zz} = \frac{2\nu p R_1^2}{R_2^2 - R_1^2} \quad (16.126c)$$

To complete the problem for a viscoelastic material, it is necessary to assume a constitutive equation that, in the present case, is the one corresponding to a standard solid defined as in case 2 of Problem 16.2. That is,

$$P_1 = \frac{1}{\eta} + \frac{s}{G_2}; \quad Q_1 = 2 \left[\frac{G_1}{\eta} + \left(1 + \frac{G_1}{G_2} \right) s \right]; \quad P_2 = 1; \quad Q_2 = 3K \quad (16.127)$$

Laplace transforms of Eqs. (16.120), (16.124), (16.125), and (16.126c) require the calculation of $\bar{\nu}$, $(1 + \nu)/E$, and $(1 + \nu)(1 - 2\nu)/E$ in terms of Eqs. (16.127). From Eqs. (16.34), the pertinent expressions are

$$\bar{\nu}(s) = \frac{P_1 Q_2 - P_2 Q_1}{P_2 Q_1 + 2P_1 Q_2} = \frac{3K - 2G_1 + (3K - 2G_1 - 2G_2)\tau s}{6K + 2G_1 + (6K + 2G_1 + 2G_2)\tau s} \quad (16.128a)$$

$$\frac{1 + \bar{\nu}(s)}{\bar{E}(s)} = \frac{P_1}{Q_1} = \frac{1}{2} \left[\frac{1 + \tau s}{G_1 + (G_1 + G_2)\tau s} \right] \quad (16.128b)$$

$$\frac{[1 + \bar{\nu}(s)][1 - 2\bar{\nu}(s)]}{\bar{E}(s)} = \frac{3P_1 P_2}{P_2 Q_1 + 2P_1 Q_2} = \frac{3(1 + \tau s)}{6K + 2G_1 + (6K + 2G_1 + 2G_2)\tau s} \quad (16.128c)$$

From these expressions, the inverse Laplace transforms of the two cases considered above are given by

$$\sigma_{rr}(t) = \frac{u_0 R_1}{R_2^2 - R_1^2} \left\{ \left(2K + \frac{2G_1}{3} \right) + \frac{2G_2}{3} \exp\left(-\frac{t}{\tau}\right) + 2\frac{R_2^2}{r^2} \left[G_1 + G_2 \exp\left(-\frac{t}{\tau}\right) \right] \right\} \quad (16.129a)$$

$$\sigma_{\theta\theta}(t) = \frac{u_0 R_1}{R_2^2 - R_1^2} \left\{ \left(2K + \frac{2G_1}{3} \right) + \frac{2G_2}{3} \exp\left(-\frac{t}{\tau}\right) - 2\frac{R_2^2}{r^2} \left[G_1 + G_2 \exp\left(-\frac{t}{\tau}\right) \right] \right\} \quad (16.129b)$$

$$\sigma_{zz}(t) = \frac{2u_0 R_1}{R_2^2 - R_1^2} \left\{ K - \frac{2}{3} \left[G_1 + G_2 \exp\left(-\frac{t}{\tau}\right) \right] \right\} \quad (16.129c)$$

where $\tau = \eta/G_2$, and

$$u(t) = \frac{pR_1^2}{R_2^2 - R_1^2} \left(\left\{ \frac{3}{6K + 2G_1} - \frac{3G_2}{2(3K + G_1)(3K + G_1 + G_2)} \exp\left[-\frac{3K + G_1}{3K + G_1 + G_2} \left(\frac{t}{\tau}\right)\right] \right\} + \frac{R_2^2}{2r} \left\{ \frac{1}{G_1} - \frac{G_2}{G_1(G_1 + G_2)} \exp\left[-\frac{G_1}{G_1 + G_2} \left(\frac{t}{\tau}\right)\right] \right\} \right) \quad (16.130a)$$

$$\gamma_{rr}(t) = \frac{pR_1^2}{R_2^2 - R_1^2} \left(\left\{ \frac{3}{6K + 2G_1} - \frac{3G_2}{2(3K + G_1)(3K + G_1 + G_2)} \exp\left[-\frac{3K + G_1}{3K + G_1 + G_2} \left(\frac{t}{\tau}\right)\right] \right\} - \frac{R_2^2}{2r^2} \left\{ \frac{1}{G_1} - \frac{G_2}{G_1(G_1 + G_2)} \exp\left[-\frac{G_1}{G_1 + G_2} \left(\frac{t}{\tau}\right)\right] \right\} \right) \quad (16.130b)$$

$$\gamma_{\theta\theta}(t) = \frac{pR_1^2}{R_2^2 - R_1^2} \left(\left\{ \frac{3}{6K + 2G_1} - \frac{3G_2}{2(3K + G_1)(3K + G_1 + G_2)} \exp\left[-\frac{3K + G_1}{3K + G_1 + G_2} \left(\frac{t}{\tau}\right)\right] \right\} + \frac{R_2^2}{2r^2} \left\{ \frac{1}{G_1} - \frac{G_2}{G_1(G_1 + G_2)} \exp\left[-\frac{G_1}{G_1 + G_2} \left(\frac{t}{\tau}\right)\right] \right\} \right) \quad (16.130c)$$

$$\sigma_{zz}(t) = \frac{pR_1^2}{R_2^2 - R_1^2} \left\{ \frac{3K - 2G_1}{6K + 2G_1} - \frac{9KG_2}{2(3K + G_1)(3K + G_1 + G_2)} \exp\left[-\frac{3K + G_1}{3K + G_1 + G_2} \left(\frac{t}{\tau}\right)\right] \right\} r \quad (16.130d)$$

where $\tau = \frac{\eta}{G_2}$.

The results for a thin-walled pipe can be easily found by using in Eqs. (16.129) and (16.130) the approximations

$$\frac{R^2}{R_2^2 - R_1^2} \cong \frac{R}{2h}; \quad R_1 + R_2 \cong 2R \quad (16.131)$$

where $h = R_2 - R_1$ and

$$\frac{R_2^2}{r} \cong R; \quad \frac{R_2^2}{r^2} \cong 1 \quad (16.132)$$

16.13 PLANE STRESS PROBLEMS

It is said that a state of plane stress exists when the stress components fulfill the conditions

$$\sigma_{zz} = \sigma_{xz} = \sigma_{yz} = 0 \quad (16.133)$$

According to these equations and using, as above, cylindrical coordinates in the stress-strain relationships, the zz component of the stress tensor can be written as

$$\sigma_{zz} = 0 = \frac{E\nu}{(1+\nu)(1-2\nu)}(\gamma_{rr} + \gamma_{\theta\theta} + \gamma_{zz}) + \frac{E}{1+\nu}\gamma_{zz} \quad (16.134)$$

For this equation one immediately obtains

$$\gamma_{zz} = -\frac{\nu}{1-\nu}(\gamma_{rr} + \gamma_{\theta\theta}) \quad (16.135)$$

After substituting Eq. (16.135) into Eq. (4.76), the remaining stresses are given by

$$\sigma_{rr} = \frac{E}{1-\nu^2}(\gamma_{rr} + \nu\gamma_{\theta\theta}) \quad (16.136a)$$

and

$$\sigma_{\theta\theta} = \frac{E}{1-\nu^2}(\gamma_{\theta\theta} + \nu\gamma_{rr}) \quad (16.136b)$$

An inspection of these results permits us to conclude that all the plane stress equations may be converted to the corresponding equations for the state of plane strain if E and ν are replaced by E' and ν' , respectively, where

$$E' = \frac{E}{1-\nu^2} \quad (16.137a)$$

and

$$v' = \frac{v}{1 - v} \quad (16.137b)$$

Conversely, all the plane strain equations may be converted to those of plane stress if E and v are replaced by E'' and v'' , respectively, where

$$E'' = \frac{E(1 + 2v)}{(1 - v)^2} \quad (16.138a)$$

and

$$v'' = \frac{v}{1 + v} \quad (16.138b)$$

In fact, the solution for a plane stress problem can be determined from the solution of the corresponding plane strain problem and vice versa. Note that in contrast to the plane strain case, the remaining stresses in the plane stress are not required to be independent of z . In fact, the three-dimensionality of plane stress is closely linked to the fact that the conditions fulfilled by the stresses no longer lead to a single nontrivial compatibility equation. In other words, if the remaining stresses σ_{xx} , σ_{yy} , and σ_{xy} are functions of only x and y , the strain–displacement equations cannot in general be satisfied.

We shall see that for a prismatic or cylindrical body with the same symmetry as in the case of plane strain and loaded normal to the z axis but now with its ends load-free, a plane stress problem is obtained in which the nonzero stresses vary with z . Strictly speaking, a true plane stress state is present only in thin plates with the main surfaces load-free and with external forces z -independent but symmetrically distributed through its thickness.

To illustrate the plane stress situation let us consider the problem of a viscoelastic cylinder rotating uniformly around its axis, with special application to flat geometries (discs) (Fig. 16.3).

The starting point is once more the Navier equations. At equilibrium, the gravitational force corresponding to the inertial term is included in the linear momentum equation [Eq. (4.35), where $b_i = \rho g_i$], so that

$$\frac{\partial \sigma_{ij}}{\partial x_j} + \rho g_i = 0 \quad (16.139)$$

where g is the gravity and ρ the mass density. Then the Navier equations become

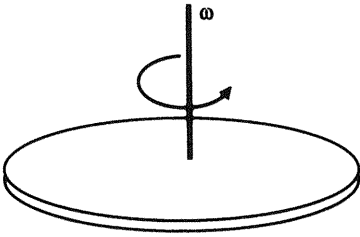


Figure 16.3. Rotating disc with angular speed ω .

$$\Delta \mathbf{u} + \frac{1}{1 - 2\nu} \text{grad div } \mathbf{u} = -\rho \mathbf{g} \frac{2(1 + \nu)}{E} \tag{16.140}$$

or alternatively

$$\text{grad div } \mathbf{u} - \frac{1 - 2\nu}{2(1 - 2\nu)} \text{rot rot } \mathbf{u} = -\rho \mathbf{g} \frac{(1 + \nu)(1 - 2\nu)}{E(1 - \nu)} \tag{16.141}$$

If the gravitational force is replaced by centrifugal force and Eq. (16.113) is considered, then Eq. (16.141) becomes

$$\nabla \text{div } \mathbf{u} = \frac{d}{dr} \left(\frac{du}{dr} + \frac{u}{r} \right) = -\rho \omega^2 r \frac{(1 + \nu)(1 - 2\nu)}{(1 - \nu)E} \tag{16.142}$$

where ω is the angular velocity.

The solution of Eq. (16.142) given in Ref. 15, p. 19 is

$$u = \frac{\rho \omega^2 (1 + \nu)(1 - 2\nu)}{8(1 - \nu)E} r[(3 - 2\nu)R^2 - r^2] \tag{16.143}$$

and the maximum displacement obtained from

$$\frac{\partial u}{\partial r} = 0 \tag{16.144}$$

is given by

$$u_{\max} = \frac{\rho \omega^2}{4E} R^3 \frac{(1 + \nu)(1 - 2\nu)}{(1 - \nu)} \left(1 - \frac{2\nu}{3}\right)^{3/2} \quad \text{at} \quad r = R \left(1 - \frac{2\nu}{3}\right)^{1/2} \tag{16.145}$$

From the stress–displacement relationships, the following values for the stresses are obtained:

$$\sigma_{rr} = \frac{\rho\omega^2}{8}(R^2 - r^2)\left(\frac{3 - 2\nu}{1 - \nu}\right) \quad (16.146a)$$

$$\begin{aligned} \sigma_{\theta\theta} &= \frac{\rho\omega^2}{8}\left(\frac{1}{1 - \nu}\right)[(3 - 2\nu)R^2 - (1 + 2\nu)r^2] \\ &= \frac{\rho\omega^2}{8}\left(\frac{1}{1 - \nu}\right)[(3R^2 - r^2) - 2\nu(R^2 + r^2)] \end{aligned} \quad (16.146b)$$

These expressions are valid for plane strain. However, we are dealing with a plane stress problem, and consequently the ends of the cylinder are not restricted. For this reason, close to such parts,

$$\int_0^R \sigma_{zz}(2\pi r) dr = 0 \quad (16.147)$$

where, according to the equilibrium equations in cylindrical coordinates,

$$\sigma_{zz} = \left(\frac{\partial u}{\partial r} + \frac{u}{r} + B\right)\lambda + 2G\frac{u_z}{\partial z} \quad (16.148)$$

It should be noted that $u_z = B$ close to the ends of the cylinder. From Eqs. (16.147) and (16.148), and after some calculations, we obtain

$$u = -\frac{\rho\omega^2 R^2 \nu(1 + \nu)(1 - 2\nu)}{2(1 - \nu)E} z \quad (16.149)$$

$$\sigma_{zz} = \frac{\rho\omega^2 \nu}{4} [(1 - 2\nu)R^2 - 2r^2] \quad (16.150)$$

The inclusion of a new term in Eq. (16.142) does not modify the main result.

Note that the condition expressed by Eq. (16.147) is an integral instead of $\sigma_{zz} = 0$; this fact represents the application of the Saint Venant principle to the z face of the cylinder. For this reason the stress state in the cylinder is only precise enough for points far from the ends of the cylinder.

According to Eq. (16.138), it is possible to convert the equations for plane strain to those corresponding to plane stress, thus finding (15, p. 17)

$$u = \frac{\rho\omega^2(1 - \nu^2)}{8E} r \left(\frac{3 + \nu}{1 + \nu} R^2 - r^2\right) \quad (16.151)$$

From Eqs. (16.144) and (16.151), the maximum displacement is found to be

$$u_{\max} = \frac{\rho\omega^2}{4E} R^3 \left(\frac{3 + \nu}{3(1 + \nu)} \right)^{3/2} \quad (16.152)$$

at

$$r = R \left(\frac{3 + \nu}{3(1 + \nu)} \right)^{1/2} \quad (16.153)$$

Moreover, the stresses obtained in the usual way are

$$\sigma_{rr} = \frac{\rho\omega^2}{8} (R^2 - r^2)(\nu + 3) \quad (16.154)$$

and

$$\sigma_{\theta\theta} = \frac{\rho\omega^2}{8} [(3R^2 - r^2) + \nu(R^2 - 3r^2)] = \frac{\rho\omega^2}{8} [R^2(\nu + 3) - r^2(1 + 3\nu)] \quad (16.155)$$

These results are adequate for plane discs.

Let us consider now another important problem consisting of an annular disc with internal and external radii represented, respectively, by R_1 and R_2 . The equation to be solved, according to the plane stress conditions, is

$$\frac{d}{dr} \left(\frac{du}{dr} + \frac{u}{r} \right) = \rho\omega^2 r \frac{1 - \nu^2}{E} \quad (16.156)$$

A convenient solution is given by

$$u = C_1 r + \frac{C_2}{r} - \frac{\rho\omega^2 r^3 (1 - \nu^2)}{E} \quad (16.157)$$

From the stress-strain relationships [Eq. (P4.11)], we obtain

$$\sigma_{rr} = \frac{E}{1 - \nu^2} (\gamma_{rr} + \nu\gamma_{\theta\theta}); \quad \sigma_{\theta\theta} = \frac{E}{1 - \nu^2} (\gamma_{\theta\theta} + \nu\gamma_{rr}) \quad (16.158)$$

where

$$\gamma_{rr} = \frac{\partial u}{\partial r} \quad (16.159)$$

and

$$\gamma_{\theta\theta} = \frac{u}{r} \quad (16.160)$$

The boundary conditions indicate that for $r = R_1, R_2$

$$\sigma_{rr} = 0 \quad (16.161)$$

Hence the constants appearing in Eq. (16.157) are

$$C_1 = \frac{\rho\omega^2(1-\nu^2)}{8E} \left(\frac{3+\nu}{1+\nu} \right) (R_1^2 + R_2^2) \quad (16.162)$$

$$C_2 = \frac{\rho\omega^2(1-\nu^2)}{8E} \left(\frac{3+\nu}{1-\nu} \right) R_1^2 R_2^2 \quad (16.163)$$

By combining Eqs. (16.157)–(16.163) we obtain

$$\sigma_{rr} = \frac{\rho\omega^2}{8} (R_2^2 - r^2) \left(1 - \frac{R_1^2}{r^2} \right) \quad (16.164a)$$

$$\sigma_{\theta\theta} = \frac{\rho\omega^2}{8} (\nu + 3) \left[R_2^2 - \frac{1+3\nu}{3+\nu} r^2 - R_1^2 \left(1 - \frac{R_2^2}{r^2} \right) \right] \quad (16.164b)$$

$$u = \frac{\rho\omega^2(1-\nu^2)}{E} \left[\frac{1}{8} \left(\frac{3+\nu}{1+\nu} \right) \left((R_1^2 + R_2^2)r + \frac{R_1^2 R_2^2}{r} \right) - r^3 \right] \quad (16.164c)$$

Now we are ready to solve the corresponding viscoelastic problem. As usual, a step input angular velocity $\omega = \omega_0 H(t)$ is assumed. According to that, $\omega^2 = \omega_0^2 H(t)$, implying that

$$\omega^2(s) = \omega_0^2/s \quad (16.165)$$

Moreover, the material is considered elastic in compression but viscoelastic (standard solid) in shear. Accordingly,

$$P_1 = \frac{1}{\eta} + \frac{s}{G_2}; \quad Q_1 = 2 \left[\frac{G_1}{\eta} + \left(1 + \frac{G_1}{G_2} \right) s \right] \quad P_2 = 1; \quad Q_2 = 3K \quad (16.166)$$

Since

$$v = \frac{P_1 Q_2 - P_2 Q_1}{2P_1 Q_2 + P_2 Q_1} \quad (16.167)$$

$$v + 3 = \frac{7P_1 Q_2 + 2P_2 Q_1}{2P_1 Q_2 + P_2 Q_1} \quad (16.168)$$

$$1 + 3v = \frac{5P_1 Q_2 - 2P_2 Q_1}{2P_1 Q_2 + P_2 Q_1} \quad (16.169)$$

the calculation of the corresponding Laplace inverses for the solid disc and the annular disc leads to the following expressions.

For a solid disc,

$$\begin{aligned} \sigma_{rr} = & \left\{ \frac{21K + 4G_1}{6K + 2G_1} - \frac{9KG_2}{2(3K + G_1)(3K + G_1 + G_2)} \exp \left[-\frac{3K + G_1}{3K + G_1 + G_2} \left(\frac{t}{\tau} \right) \right] \right\} \\ & \times \frac{\rho \omega_0^2}{8} (R^2 - r^2) \end{aligned} \quad (16.170a)$$

$$\begin{aligned} \sigma_{\theta\theta} = & \left\{ \frac{3K - 2G_1}{6K + 2G_1} - \frac{9KG}{2(3K + G_1)(3K + G_1 + G_2)} \exp \left[-\frac{3K + G_1}{3K + G_1 + G_2} \left(\frac{t}{\tau} \right) \right] \right\} \\ & \times \frac{\rho \omega_0^2}{8} (R^2 - 3r^2) + \frac{\rho \omega_0^2}{8} (3R^2 - r^2) \end{aligned} \quad (16.170b)$$

or equivalently

$$\begin{aligned} \sigma_{\theta\theta} = & \frac{\rho \omega_0^2}{8} \left(R^2 \left\{ \frac{21K + 4G_1}{6K + 2G_1} - \frac{9KG_2}{2(3K + G_1)(3K + G_1 + G_2)} \right. \right. \\ & \left. \left. \exp \left[-\frac{3K + G_1}{3K + G_1 + G_2} \left(\frac{t}{\tau} \right) \right] \right\} \right. \\ & \left. - r^2 \left\{ \frac{15K - 4G_1}{6K + 2G_1} - \frac{27KG_2}{2(3K + G_1)(3K + G_1 + G_2)} \exp \left[-\frac{3K + G_1}{3K + G_1 + G_2} \left(\frac{t}{\tau} \right) \right] \right\} \right) \end{aligned} \quad (16.170c)$$

For an annular disc,

$$\sigma_{rr} = \left\{ \frac{21K + 4G_1}{6K + 2G_1} - \frac{9KG_2}{2(3K + G_1)(3K + G_1 + G_2)} \exp \left[-\frac{3K + G_1}{3K + G_1 + G_2} \left(\frac{t}{\tau} \right) \right] \right\} \\ \times \frac{\rho\omega_0^2}{8} (R_2^2 - r^2) \left(1 - \frac{R_1^2}{r^2} \right) \quad (16.171a)$$

$$\sigma_{\theta\theta} = \frac{\rho\omega_0^2}{8} \left(\left[R_2^2 - R_1^2 \left(1 - \frac{R_2^2}{r^2} \right) \right] \left\{ \frac{21K + 4G_1}{3K + 2G_1} - \frac{9KG_2}{2(3K + G_1)(3K + G_1 + G_2)} \right. \right. \\ \left. \left. \exp \left[-\frac{3K + G_1}{3K + G_1 + G_2} \left(\frac{t}{\tau} \right) \right] \right\} \right. \\ \left. - r^2 \left\{ \frac{15K - 4G_1}{6K + 2G_1} - \frac{27KG_2}{2(3K + G_1)(3K + G_1 + G_2)} \exp \left[-\frac{3K + G_1}{3K + G_1 + G_2} \left(\frac{t}{\tau} \right) \right] \right\} \right) \quad (16.171b)$$

with $\tau = \eta/G_2$.

Note that if we take the limit $r \rightarrow 0$ in Eq. (16.170c), we obtain

$$\sigma_{\theta\theta}(t) = \frac{\rho\omega_0^2 R^2}{8} \left\{ \frac{21K + 4G_1}{6K + 2G_1} - \frac{9KG_2}{2(3K + G_1)(3K + G_1 + G_2)} \right. \\ \left. \exp \left[-\frac{3K + G_1}{3K + G_1 + G_2} \left(\frac{t}{\tau} \right) \right] \right\} \quad (16.172)$$

In a similar way, if we take the limits $r \rightarrow 0$ and $R_1 \rightarrow 0$ in Eq. (16.171b), we obtain

$$\sigma_{\theta\theta}(t) = \frac{\rho\omega_0^2 R^2}{4} \left\{ \frac{21K + 4G_1}{6K + 2G_1} - \frac{9KG_2}{2(3K + G_1)(3K + G_1 + G_2)} \right. \\ \left. \exp \left[-\frac{3K + G_1}{3K + G_1 + G_2} \left(\frac{t}{\tau} \right) \right] \right\} \quad (16.173)$$

These results suggest that the value of the tangential stress close to the central hole of the annular disc is double that corresponding to the solid disc. This fact indicates that a little hole close to $r = 0$ is under a stress concentration factor of 2.

Finally, the maximum values of the radial and angular stresses for the annular disc are easily obtained from the stress equations as

$$\sigma_{rr, \max} = \frac{\rho\omega_0^2}{8} (\nu + 3)(R_2 - R_1)^2 \quad \text{for} \quad r = (R_1 R_2)^{1/2} \quad (16.174)$$

and

$$\sigma_{\theta\theta \max} = \frac{\rho\omega^2}{4}(\nu + 3)\left(R_2^2 - \frac{2(1 + \nu)}{3 + \nu}R_1^2\right)^2 \quad \text{for} \quad r = R_1 \quad (16.175)$$

The calculation of the maximum displacements is left to the reader as an exercise (Ref. 16, p. 611).

16.14 INDENTATION AND IMPACT PROBLEMS

Contact problems have their origins in the works of Hertz (1881) and Boussinesq (1885) on elastic materials. Indentation problems are an important subset of contact problems (17,18). The assessment of mechanical properties of materials by means of indentation experiments is an important issue in polymer physics. One of the simplest pieces of equipment used in the experiments is the scleroscope, in which a rigid metallic ball indents the surface of the material. To gain some insight into this problem, we consider the simple case of a flat circular cylindrical indenter, which presents a relatively simple solution. This problem is also interesting from the point of view of soil mechanics, particularly in the theory of the safety of foundations. In fact, the impacting cylinder can be considered to represent a circular pillar and the viscoelastic medium the solid upon which it rests.

The problem is specified as the determination of the state of stress and the deformation produced in viscoelastic half-space ($z \leq 0$) by a circular punch of radius a whose force is P (Fig. 16.4). As is well known (Ref. 15, p. 25), the displacement of a half-space caused by forces applied to its free surface with the condition of null deformation at infinite distance is given by

$$u_z = \frac{P}{4\pi rG} \left[2(1 - \nu) + \frac{z^2}{r^2} \right] \quad r = (x^2 + y^2 + z^2)^{1/2} \quad (16.176)$$

where G and (x, y, z) are, respectively, the shear modulus and the coordinates of a characteristic point. The displacement of the surface can be written as

$$u_z|_{z=0} = \frac{(1 - \nu)P}{2\pi rG}, \quad r = (x^2 + y^2)^{1/2} \quad (16.177)$$

Since the deflection of all the points of the punch are the same, it follows from Eq. (16.177) that

$$u' = \frac{1 - \nu}{2\pi G} \iint_s \frac{p(x', y') dx' dy'}{(x'^2 + y'^2)} = \text{constant} \quad (16.178)$$

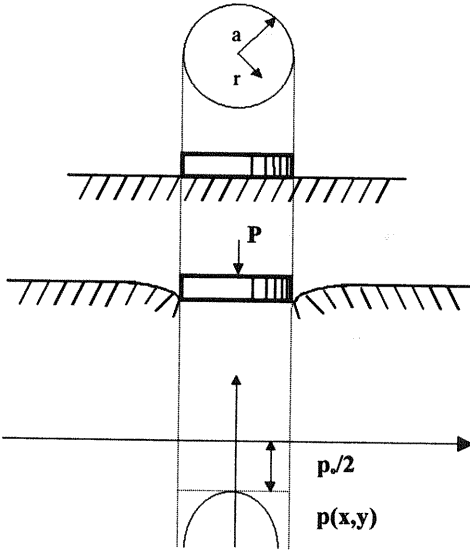


Figure 16.4. Plane indentation caused by a flat cylindrical indenter of radius r under a total force P .

where the integral is taken on the surface S to which the force is applied and $x'^2 + y'^2 \leq a^2$.

In Eq. (16.178) $p(x', y')$ indicates the distribution of forces on the surface due to the load P given by

$$P = \iint_S p(x', y') dx' dy', \quad x'^2 + y'^2 = r^2 \quad (16.179)$$

Changing Eqs. (16.178) and (16.179) to polar coordinates and solving the resulting expression, we obtain

$$p(r) = \frac{P}{2\pi a^2(1 - r^2/a^2)^{1/2}} \quad (16.180)$$

If the mean pressure $P/\pi a^2$ is denoted by p_0 , then the distribution $p(r)$ can be expressed as

$$p(r) = \frac{p_0}{2(1 - r^2/a^2)^{1/2}} \quad (16.181)$$

As can be seen in Figure 16.4, the pressure increases from $p_0/2$ at the center of the indentation to infinity at the edge. For this reason the solution is hardly realistic in the vicinity of $r = a$.

To study the viscoelastic case it is convenient to assume a constant Poisson ratio. This hypothesis is essentially correct in most cases. In fact, if the material is incompressible, one has $\nu = 1/2$. Taking the input as the applied force instead of the distribution $p(r)$, Eq. (16.177) suggests that the time dependence of the displacement for a viscoelastic materials is given by

$$u(t) = \frac{1-\nu}{2\pi r} \int_0^\infty J(t-\theta) dP(\theta) \quad (16.182)$$

where $J(t)$ is the compliance function in shear and $P(t) = 0$ for $t < 0$. Moreover, the upper limit of the integral is set to infinity for convenience. For a step function $P(t) = P_0 H(t)$, the Laplace transform of Eq. (16.182) gives

$$\bar{u}(s) = \frac{1-\nu}{2\pi r} s\bar{J}(s)\bar{P}(s) = \frac{1-\nu}{2\pi r} \left(\frac{\bar{P}(s)}{s\bar{G}(s)} \right) \quad (16.183)$$

where $\bar{P}(s) = P_0/s$. This equation will be applied to three different situations.

Case 1. For a standard solid in shear, the complex relaxation modulus (see Chap. 10 for details) is given by

$$\frac{\bar{\sigma}(s)}{\bar{\epsilon}(s)} = s\bar{G}(s) = \frac{Q_1}{2P_1} = \frac{(1 + G_1/G_2)s + G_1/\eta}{1/\eta + s/G_2} \quad (16.184)$$

The Laplace inverse of the equation resulting from substituting Eq. (16.184) into Eq. (16.183) gives

$$u(t) = \frac{(1-\nu)P_0}{2\pi r G_1} \left\{ 1 - \frac{G_2}{G_1 + G_2} \exp\left[-\frac{G_1}{G_1 + G_2} \left(\frac{t}{\tau}\right)\right] \right\}, \quad \tau = \eta/G_2 \quad (16.185)$$

where the initial and final values of the displacement can be written as

$$u(0) = \frac{(1-\nu)P_0}{2\pi r(G_1 + G_2)} \quad (16.186a)$$

and

$$u(\infty) = \frac{(1-\nu)P_0}{2\pi r G_1} \quad (16.186b)$$

Case 2. Let us consider now a viscoelastic material for which

$$J(t) = J_0 \sinh at \quad (16.187)$$

Then the Laplace transform of the shear compliance function is given by

$$\frac{J_0 a}{s^2 - a^2} \quad (16.188)$$

Under an input $P_0 \sin \omega t$, Eq. (16.183) becomes

$$u(s) = \frac{1 - \nu}{2\pi r} \left(\frac{J_0 P_0 a \omega s}{(s^2 - a^2)(s^2 + \omega^2)} \right) \quad (16.189)$$

The evaluation of the inverse of this equation requires us to decompose it into rational fractions, as follows:

$$\frac{s}{(s^2 - a^2)(s^2 + \omega^2)} = \frac{A}{s + a} + \frac{B}{s - a} + \frac{Cs + D}{s^2 + \omega^2} \quad (16.190)$$

where

$$A = B = \frac{1}{2(\omega^2 + a^2)} \quad (16.191a)$$

$$C = -\frac{1}{\omega^2 + a^2} \quad (16.191b)$$

$$D = 0 \quad (16.191c)$$

Then the inverse of Eq. (16.189) gives the displacement in the time domain as

$$u(t) = \frac{1 - \nu}{2\pi r} \left(\frac{J_0 P_0 a \omega}{\omega^2 + a^2} \right) [\cosh at - \cos at] \quad (16.192)$$

Case 3. Let us consider now the case of a depression in the surface produced by impact. According to Newton's second law,

$$P(t) = -m\ddot{u} \quad (16.193)$$

The Laplace transform of Eq. (16.193) gives

$$P(s) = -m(s^2 u - V_0) \quad (16.194)$$

where V_0 is the initial impact velocity at $t = 0$, obtained from the height from which the ball impacts. On the other hand, Eq. (16.183) leads to

$$\bar{P}(s) = \frac{2\pi r}{1-\nu} s\bar{u}(s)\bar{G}(s) \tag{16.195}$$

Finally, Eqs. (16.194) and (16.195) give

$$\bar{u}(s) = \frac{V_0}{s^2 + [2\pi r/m(1-\nu)]s\bar{G}(s)} \tag{16.196}$$

A simple way to solve this equation for low damping materials ($\tan \delta \leq 0.1$) is to make

$$s\bar{G}(s) = G^*(s) \cong G^*(\omega) \tag{16.197}$$

where $G^*(\omega) = G'(\omega) + iG''(\omega)$. In this case, the following approximation holds for the displacement u in the s space:

$$\bar{u}(s) \cong \frac{V_0}{s^2 + \omega^2 + (\alpha s/\omega)G''} \tag{16.198}$$

where

$$\omega^2 = \frac{2\pi r}{m(1-\nu)} G'(\omega) \tag{16.199a}$$

$$\alpha = \frac{2\pi r}{m(1-\nu)} \tag{16.199b}$$

$$s = i\omega \tag{16.199c}$$

Equation (16.198) can alternatively be written as

$$\bar{u}(s) \cong \frac{V_0}{[s + \frac{1}{2}(\frac{\alpha}{\omega})G'']^2 + \omega^2 - \frac{1}{4}\alpha^2 \frac{G''^2}{\omega^2}} \tag{16.200}$$

whose inverse gives

$$u(t) = \frac{V_0}{\omega[1 - (\tan^2 \delta)/4]^{1/2}} \exp\left(-\frac{\omega t}{2} \tan \delta\right) \sin \left[\omega t \left(1 - \frac{\tan^2 \delta}{4}\right)^{1/2} \right] \tag{16.201}$$

where

$$\tan \delta = \frac{\alpha G''}{\omega^2} \quad (16.202)$$

The expansion of the term $[1 - (\tan^2 \delta)/4]^{1/2}$ in series permits us to write Eq. (16.201) in a more convenient way as

$$u(t) \cong \frac{V_0}{\omega[1 - (\tan^2 \delta)/8]} \exp\left(-\frac{\omega t}{2} \tan \delta\right) \sin\left[\omega t \left(1 - \frac{\tan^2 \delta}{8}\right)\right] \quad (16.203)$$

16.15 ROLLER BALL INDENTATION

Now we consider roller ball indentations. Let us consider first a rigid ball that does not roll but indents a viscoelastic half-space; this analysis will be extended to a rolling ball. This is a typical situation in which the elastic-viscoelastic analogy is, in general, no longer applicable.

According to Figure 16.5, immediate geometric considerations indicate that for $z = 0$ (the plane in which the indentation takes place) and $r \leq a(t)$,

$$x^2 + y^2 = \{2R - [\alpha(t) - u(t)]\}[\alpha(t) - u(t)] \cong 2R[\alpha(t) - u(t)] \quad (16.204)$$

where r is the radial coordinate, R the radius of the indenter, $\alpha(t)$ the displacement, and $a(t)$ the radius of the contact area. This expression leads to

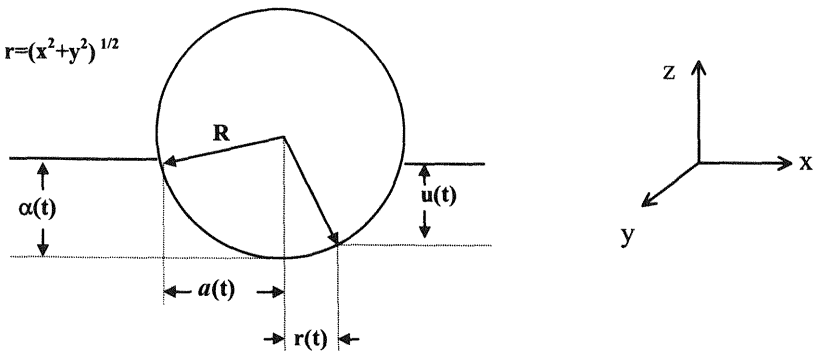


Figure 16.5. Spherical indenter of radius R . Boundary conditions are time-dependent, and the correspondence principle is not applicable.

$$u(x, y, z) \cong \alpha(t) - \frac{x^2 + y^2}{2R} H(t) \tag{16.205}$$

where $H(t)$ is the unit step function.

It should be pointed out that for $z = 0$ and $r \geq a(t)$,

$$\sigma_{zz} = 0 \quad \text{and} \quad \sigma_{yz} = \sigma_{xz} = 0 \tag{16.206}$$

To solve this problem, we shall refer to the elastic solution given in Ref. 15 (p. 25). According to this approach, the displacement of a point (x, y) of the half-plane caused by the load applied at (x', y') is given by

$$u_z(x, y, 0) = \frac{(1 - \nu)P}{2\pi G} \left(\frac{1}{[(x - x')^2 + (y - y')^2]^{1/2}} \right) \tag{16.207}$$

where P is the applied force and G the shear modulus. The radial stress at $z = 0$ is expressed (15) by

$$\sigma_{rr} = \frac{(1 - \nu)P}{2\pi[(x - x')^2 + (y - y')^2]} \tag{16.208}$$

Using the same approach as in the plane indentation of elastic materials, the displacement of a viscoelastic system by the action of a concentrated load is given by

$$u_z(x, y, 0, t) = \frac{1 - \nu}{2\pi} \int_0^\infty \rho^{-1} J(t - \theta) P(\theta) d\theta = \alpha(t) - \frac{x^2 + y^2}{2R} H(t) \tag{16.209}$$

where

$$\rho = [(x - x')^2 + (y - y')^2]^{1/2} \tag{16.210}$$

and ν is assumed to be constant. In the case of distributed forces, Eq. (16.209) becomes

$$\begin{aligned} u_z(x, y, 0, t) &= \frac{(1 - \nu)}{2\pi} \int_0^\infty J(t - \theta) d\theta \iint_{\Omega_m} \rho^{-1} p_z(x', y', \theta) dx' dy' \\ &= \alpha(t) - \frac{x^2 + y^2}{2R} H(t) \end{aligned} \tag{16.211}$$

where $p(x', y', \theta)$ represents such a distribution and Ω_m is the maximum contact area.

For a given p_z this problem can be solved by using the correspondence principle. Thus, for a monotonically increasing $a(t)$, Ω_m can be replaced by the current contact area $\Omega(t)$. In these conditions, Eq. (16.211) can be written as

$$u_z(x, y, 0, t) = \frac{1-\nu}{2\pi} \iint_{\Omega(t)} \rho^{-1} q(x', y', a(t)) dx' dy' = \alpha(t) - \frac{x^2 + y^2}{2R} H(t) \quad (16.212)$$

where

$$q(t) = \int_0^\infty J(t - \theta) dp_z(\theta) \quad (16.213)$$

The value of q for the corresponding elastic problem is given by

$$q = \frac{4}{\pi(1-\nu)R} [a^2(t) - (x^2 + y^2)]^{1/2} \quad (16.214)$$

On substituting Eq. (16.214) into Eq. (16.212), we find

$$\alpha(t) = \frac{a^2(t)}{R} \quad (16.215)$$

as in the elastic case.

By inverting Eq. (16.213) and noting that $s\bar{J}(s) = [s\bar{G}(s)]^{-1}$, we obtain

$$\begin{aligned} p_z(t) &= \int_0^\infty G(t - \theta) dq(\theta) \\ &= \frac{4}{\pi(1-\nu)R} \int_0^\infty G(t - \theta) \frac{d}{d\theta} [a^2(\theta) - (x^2 + y^2)]^{1/2} d\theta \end{aligned} \quad (16.216)$$

so the total force is given by

$$P = 2\pi \int_0^a r p_z dr \quad (16.217)$$

Substituting Eq. (16.216) into Eq. (16.217), the evolution of P with time can be written as

$$P(t) = \frac{8}{3(1-\nu)R} \int_0^\infty G(t - \theta) \frac{d}{d\theta} a^3(\theta) d\theta \quad (16.218)$$

The response to a total applied force given by $P(t)$ can be easily found by inversion of Eq. (16.218). The pertinent result is

$$a^3(t) = \frac{3(1-\nu)R}{8} \int_0^\infty J(t-\theta) dP(\theta) \tag{16.219}$$

These results indicate that the area of contact $\pi a^2(t)$ is proportional to the two-thirds power of the applied force, whereas the depth of indentation is proportional to the first power of that force.

The integral in Eq. (16.211) can be solved analogously to similar problems in the theory of the potential in electrostatics. In fact, the integral is close to that of a uniformly charged ellipsoid or sphere. Omitting the technical details, which can be found in Ref. 15, the function $p_z(x', y', t)$ has the form

$$p_z = \frac{3P}{2\pi a^2} \left(1 - \frac{x^2 + y^2}{a^2}\right)^{1/2} = \frac{3P}{2\pi a^2} \left(1 - \frac{r^2}{a^2}\right)^{1/2} \tag{16.220}$$

where the total force over the contact area is given by

$$P = \iint p_z dx dy \tag{16.221}$$

The mean pressure is

$$p_m = \frac{P}{\pi a^2} \tag{16.222}$$

so that for $r = 0$ Eqs. (16.220) and (16.222) indicate that

$$p(0, 0) = 3/2 p_m \tag{16.223}$$

Accordingly, the pressure in the center of the region is 1.5 times the mean pressure. Substituting the value given for p_z in Eq. (16.220) into Eq. (16.211), we obtain

$$u(x, y, t) = \frac{3(1-\nu)P}{4\pi^2} \int_0^\infty J(t-\theta) d\theta \iint_{\Omega(t)} \rho^{-1} \frac{[1 - (x'^2 + y'^2)/a^2(\theta)]^{1/2} dx' dy'}{a^2(\theta)} \tag{16.224}$$

where now a depends on time. According to Ref. 15 (p. 29), the integral of the right-hand side of Eq. (16.224) for a spherical indenter is given by

$$\frac{\pi a^2}{2} \int_0^\infty \left(1 - \frac{x^2 + y^2}{a^2 + u}\right) \frac{du}{u^{1/2}(a^2 + u)} \quad (16.225)$$

from which Eq. (16.224) becomes

$$u(x, y, t) = \frac{3(1 - \nu)P}{8\pi} \int_0^\infty J(t - \theta) d\theta \int_0^\infty \frac{1 - [(x^2 + y^2)/(a^2 + u)] du}{(a^2 + u)u^{1/2}} \quad (16.226)$$

This expression must be fulfilled by any values of x and y , so, on account of the right-hand side of Eq. (16.211), we obtain

$$\frac{3(1 - \nu)P}{8\pi} \int_0^\infty J(t - \theta) d\theta \int_0^\infty \frac{du}{(a^2 + u)u^{1/2}} = \alpha(t) \quad (16.227)$$

and

$$\frac{3(1 - \nu)P}{8\pi} \int_0^\infty J(t - \theta) d\theta \int_0^\infty \frac{du}{(a^2 + u)^2 u^{1/2}} = \frac{1}{2R} \quad (16.228)$$

Since the values of the second integrals in these equations are, respectively, π/a and $\pi/2a^3$, Eqs. (16.227) and (16.228) can be written as

$$\frac{1}{R} = \frac{3(1 - \nu)P}{8} \int_0^\infty J(t - \theta) \frac{1}{a^3(\theta)} d\theta \quad (16.229)$$

and

$$\alpha(t) = \frac{3(1 - \nu)P}{8} \int_0^\infty J(t - \theta) \frac{1}{a(\theta)} d\theta \quad (16.230)$$

The response of a standard solid (a spring with shear rigidity given by G_1 in parallel with a Maxwell element with shear rigidity G_2 and viscosity η) to a sudden force P_0 can be found from Eq. (16.219) by taking, as usual, Laplace transforms. After the pertinent calculations [see Eqs. (16.127) and (16.184)] we obtain

$$a^3(t) = \frac{3(1 - \nu)RP_0}{8G_1} \left\{ 1 - \frac{G_2}{G_1 + G_2} \exp\left[-\frac{G_1}{G_1 + G_2} \left(\frac{t}{\tau}\right)\right] \right\}, \quad \tau = \frac{\eta}{G_2} \quad (16.231)$$

Conversely, if $a(t)$ or $\alpha(t)$ is given, then $P(t)$ can be found from the viscoelastic properties of the material in terms of $J(t)$ or $G(t)$.

Now let us deal with the rolling contact problem (19). The analysis of rolling contact for spherical or cylindrical machine elements is an important

issue in precision assemblies and machinery. In fact, a good design of these elements usually implies the need to ensure precise spacing between moving surfaces. In rolling contact bearings, the preservation of the sliding is ensured by introducing compression between the elements. A transition to sliding would cause overheating in high speed applications such as aircraft engines. In general, as the rolling speed increases, two effects occur:

1. A size effect that produces an overall reduction in the area of contact caused by the stiffening of the viscoelastic material, which increases with the speed (or frequency) of indentation. Speed v and angular velocity ω are related to some length a that depends on the specific configuration involved in the rolling problem. This length is interpreted as the diameter of the contact surface.
2. A shape effect due to the asymmetry of the contact caused by damping or delayed recovery of the viscoelastic material. Usually this asymmetry is restored at high sliding speeds but the contact area is reduced. The asymmetry arises from the inability of the viscoelastic material to slide, owing to asperities on the surface. These asperities, equivalent to periodic indentations, generate heat by hysteresis and in turn induce a softening effect. Thus, an increase in frequency causes stiffening, but the accompanying temperature rise creates a compensating softening effect.

Geometric considerations indicate that the circle of contact in rolling spheres has the equation (Fig. 16.6)

$$x^2 + y^2 = a^2 = R^2 - [R - \alpha(t)]^2 \quad (16.232)$$

where a , α , and $u(t)$ are defined in the figure and the equation of the sphere is

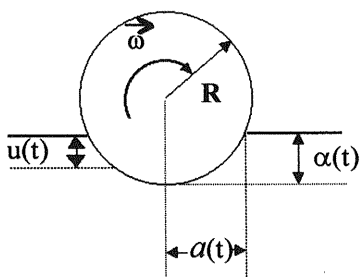


Figure 16.6. Roller ball indentation.

$$x^2 + y^2 + [u(t) + R - \alpha(t)]^2 = R^2 \quad (16.233)$$

where $u(t)$ is the depth of the indentation.

From Eqs. (16.232) and (16.233), we obtain

$$u(t) = (R^2 - x^2 - y^2)^{1/2} - [R - \alpha(t)] = (R^2 - x^2 - y^2)^{1/2} - \{R^2 - [a(t)]^2\}^{1/2} \quad (16.234)$$

To simplify the problem, let us assume that the circle of contact is constant. The modulus of the penetration velocity will be given by

$$\dot{u}(t) = \frac{du}{dx} \frac{dx}{dt} = \nu x (R^2 - x^2 - y^2)^{-1/2} \quad (16.235)$$

where the linear speed of the rolling sphere is $\nu = dx/dt$. If the assumption is made that the elastomer follows Kelvin–Voigt behavior, then

$$\sigma = G\varepsilon + \eta\dot{\varepsilon} \quad (16.236)$$

Note that, assuming the Poisson ratio to be constant, the tensile modulus E is proportional to the shear modulus G , and for this reason the conclusions concerning the behavior of G are the same as for E . Moreover, the strain and the rate of strain are given by

$$\frac{\varepsilon}{2} = \gamma = \frac{u}{a} \quad \text{and} \quad \frac{\dot{\varepsilon}}{2} = \dot{\gamma} = \frac{\dot{u}}{a} \quad (16.237)$$

Substituting Eqs. (16.234), (16.235), and (16.237) into Eq. (16.236) gives

$$\frac{\sigma a}{2GR} = \left\{ \left(1 - \frac{x^2 + y^2}{R^2} \right)^{1/2} - \left[1 - \left(\frac{a}{R} \right)^2 \right]^{1/2} \right\} + \frac{\eta x \nu}{GR^2} \left(1 - \frac{x^2 + y^2}{R^2} \right)^{-1/2} \quad (16.238)$$

an expression that can be approximated to

$$\frac{\sigma a}{2GR} \cong \frac{1}{2} \left(\frac{a}{R} \right)^2 - \frac{1}{2} \left(\frac{x^2 + y^2}{R^2} \right) + \frac{\beta x}{R} \left(1 + \frac{x^2 + y^2}{2R^2} \right) \quad (16.239)$$

where the dimensionless quantity $\beta = \eta\nu/GR$ has been used. Neglecting third-order terms, we obtain

$$\frac{\sigma a}{2GR} \cong \frac{1}{2} \left(\frac{a}{R} \right)^2 - \frac{1}{2} \left(\frac{x^2 + y^2}{R^2} \right) + \frac{\beta x}{R} \quad (16.240)$$

Equation (16.240) suggests that the values of $x = -x_0$ and $y = -y_0$ obtained from $\sigma = 0$ are given by

$$1 - \frac{x_0^2 + y_0^2}{a^2} - 2\zeta \frac{x_0}{a} = 0 \tag{16.241}$$

where

$$\zeta = \frac{\beta R}{a} = \frac{\eta \nu}{Ga} \tag{16.242}$$

Equation (16.241) can be solved in terms of x_0/a , giving

$$\frac{x_0}{a} = \left[1 + \zeta^2 - \left(\frac{y_0}{a} \right)^2 \right]^{1/2} - \zeta \tag{16.243}$$

This expression can be written approximately as

$$\frac{x_0}{a[1 - (y_0/a)^2]^{1/2}} \cong (1 + \zeta^2)^{1/2} - \zeta \tag{16.244}$$

where the left-hand side represents a dimensionless asymmetrical contact. One should note that

$$\zeta = \frac{\eta \nu}{Ga} \cong \frac{\omega \eta}{G} = \frac{G''}{G'} = \tan \delta \tag{16.245}$$

where $\omega = \nu/a$ is a pseudofrequency of deformation experienced by the viscoelastic material. Consequently, from Eqs. (16.244) and (16.245), we obtain

$$\frac{x_0}{a[1 - (y_0/a)^2]^{1/2}} = (1 + \tan^2 \delta)^{1/2} - \tan \delta \tag{16.246}$$

This expression leads to the conclusion that the asymmetry contact factor decreases as the viscous damping, $\tan \delta$, increases.

The evolution of the semi-contact length a for a standard solid with speed ν and consequently with angular velocity frequency ν/a can be obtained from Eq. (16.231) by noting that at low frequency (low speed ν), that is, long times, the following limit holds:

$$a \propto G_1^{-1/3} \tag{16.247}$$

In contrast, for very high frequency (very high speed v), that is, short times,

$$a \propto (G_1 + G_2)^{-1/3} \quad (16.248)$$

Summing up, the overall decrease in the contact area with increasing speed can be predicted by assuming that at zero speed the elastic contact condition prevails. However, at high speed the material is viscoelastic, giving rise to the aforementioned stiffening, and it is assumed that the new (and smaller) area of contact is related to the viscoelastic moduli in a similar way. Finally, at very high speed, the contact tends to also be constant.

16.16 WAVE PROPAGATION IN VISCOELASTIC MATERIALS

Wave propagation is the result of an applied disturbance in a medium. When the applied disturbance is of mechanical origin, stress waves are produced. If the material upon which the stress wave propagates is viscoelastic, there is not only attenuation in the propagation of the viscoelastic waves but also a dispersion effect due to the fact that the phase velocity is frequency-dependent. In other words, the shape of the wave is changing as it propagates across the viscoelastic material. The propagation of mechanical disturbances is one of the most thoroughly studied problems in dynamic viscoelasticity (6, Chap. IV; 20–24). The interest in wave propagation was primarily motivated by the advances in testing techniques and the facility with which stress waves of relatively high frequency are produced and detected.

The mechanical properties of materials can be determined from wave propagation techniques. Thus the responses of composite polymers to mechanical perturbations as well as information on specific problems related to microstructural inhomogeneities can be obtained by using these techniques.

Although most of the important features associated with wave propagation occur in a single dimension, one must not forget that the material may also undergo shear stresses, and in this case the motion of the particles would occur not only in the direction of the wave motion but also, in some cases, in the transverse direction.

Strictly speaking, a wave in a continuous medium is a propagating surface of discontinuity. The propagation involves the motion of such a surface. In the present context, we are concerned with the propagation of discontinuous stress and strain waves. That implies the propagation of discontinuities in the first derivative of the displacement. Waves of this type are

commonly called shock waves. In general, the surface of discontinuity is said to be singular surface of n th order if it is singular with respect to the n th derivative of the displacement. Accordingly, a second-order wave is a discontinuity in the acceleration.

Laplace of Fourier transforms can be used to solve wave propagation problems. In certain special cases, for example, for harmonic excitations, the inversion integral can be evaluated directly or through the use of residues theory. However, in the general case an analytical evaluation is impracticable.

In the first part of this chapter we studied the radial vibrations of a solid or hollow sphere. This problem was considered an extension to the dynamic situation of the quasi-static problem of the response of a viscoelastic sphere under a step input in pressure. Let us consider now the simple case of a transverse harmonic excitation in which separation of variables can be used to solve the motion equation. Let us assume a slab of a viscoelastic material between two parallel rigid plates separated by a distance h , in which a sinusoidal motion is imposed on the lower plate. In this case we deal with a transverse wave, and the viscoelastic modulus to be used is, of course, the shear modulus. As shown in Figure 16.7, let us consider a Cartesian coordinate system associated with the material, with its x_2 axis perpendicular to the shearing plane, its x_1 axis parallel to the direction of the shearing displacement, and its origin in the center of the lower plate. Under steady-state conditions, each part of the viscoelastic slab will undergo an oscillatory motion with a displacement $u_1(x_2, t)$ in the direction of the x_1 axis whose amplitude depends on the distance from the origin x_2 .

The stress-strain relationship in dynamic shearing can be written as

$$\sigma_{12}^*(x_2, t) = G^* \frac{d}{dx_2} [u_1^*(x_2, t)] \quad (16.249)$$

On the other hand, the equation of motion for the uniaxial case is given by

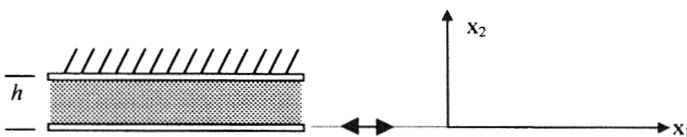


Figure 16.7. Slab of viscoelastic material between two rigid plates.

$$\frac{d}{dx_2} \left(\frac{\sigma_{12}^*}{dx_2} \right) = \rho \ddot{u}_1^* \quad (16.250)$$

where Eq. (4.34) was considered. Combining Eqs. (16.249) and (16.250), we obtain

$$\frac{d^2 u_1^*(x_2, t)}{dx_2^2} = \frac{\rho}{G^*} \frac{d^2 u_1^*(x_2, t)}{dt^2} \quad (16.251)$$

This is the equation for the displacement propagation wave. It should be noted that a similar equation could be obtained for the stress propagation wave.

For a prescribed harmonic excitation $u_1^*(x_2, t) = u(x_2) \exp(i\omega t)$, the solution of Eq. (16.251) can be conveniently written as

$$u(x_2, t) = A \exp(ax_2) \exp[i(bx_2 + \omega t)] + B \exp(-ax_2) \exp[-i(bx_2 - \omega t)] \quad (16.252)$$

The values of a and b can be determined from the boundary conditions given by

$$u(0, t) = u_0 \exp(i\omega t) \quad (16.253a)$$

and

$$u(h, t) = 0 \quad (16.253b)$$

The results obtained indicate that a and b are the real and imaginary components of a complex quantity m^* according to

$$m^* = a + bi = \left(\frac{\rho \omega^2}{2|G^*|^2} \right)^{1/2} \left[(|G^*| - G')^{1/2} + i(|G^*| + G')^{1/2} \right] \quad (16.254)$$

where $|G^*|$ means the modulus of G^* . This expression suggests that $b > a$. From the results obtained, the motion of the wave along the x_2 axis is described by

$$\begin{aligned} u(x_2, t) &= u_0 \exp(i\omega t) \frac{\exp[(a + ib)(h - x_2)] - \exp[-(a + ib)(h - x_2)]}{\exp[(a + ib)h] - \exp[-(a + ib)h]} \\ &= u_0 \exp(i\omega t) \left(\frac{\sinh m(h - x_2)}{\sinh mh} \right) \end{aligned} \quad (16.255)$$

By writing Eq. (16.255) in terms of trigonometric and hyperbolic functions, we obtain

$$u(x_2, t) = u_0 \exp(i\omega t) \frac{\sin[b(h-x)] \cosh[a(h-x)] - i \cos[b(h-x)] \sinh[a(h-x)]}{\sin(bh) \cosh(ah) - i \cos(bh) \sinh(ah)} \tag{16.256}$$

and the wave propagation equation can be written as

$$u(x_2, t) = [u_r(x_2) + iu_i(x_2)] \exp(i\omega t) \tag{16.257}$$

where the subscripts *r* and *i*, respectively, refer to real and imaginary parts. The equation representing the spatial propagation of the wave is complex, which means that different points are not in phase, the out-of-phase angle being

$$\tan \delta = \frac{u_i(x_2)}{u_r(x_2)} \tag{16.258}$$

Several cases can be analyzed. For example, if $bh = \pi/2$, then Eq. (16.258) becomes

$$\tan \delta = \frac{\tanh[a(h-x_2)]}{\tanh[b(h-x_2)]} \tag{16.259}$$

However, if $x_2 \rightarrow h$, the phase angle is given by

$$\tan \delta = \frac{a}{b} \tag{16.260}$$

where the limits $\tan x/x \rightarrow 1$ and $\tanh x/x \rightarrow 0$ for $x \rightarrow 0$ are used. Equation (16.259) suggests that $\tan \delta$ increases as x_2 increases, reaching the limiting value of a/b when $x_2 = h$. The limiting value of the phase angle of the traveling waves will be 45° . For a pure viscous material, $G' = 0$, and from Eqs. (16.253) and (16.260), $\tan \delta = 1$.

If $bh = \pi$, the phase angle becomes

$$u(x_2) = \frac{\sin[b(h-x)] \cosh[a(h-x)] - i \cos[b(h-x)] \sinh[a(h-x)]}{\sin h(ah)} \tag{16.261}$$

By plotting the modulus of the amplitude against x_2 , a curve with a maximum value of $h = \pi$ is obtained. The phase angle increases with x_2 until a limiting value is obtained.

The general solution [Eq. (16.248)] suggests that the characteristics of the motion are very sensitive to the distance h . For this reason two limiting cases will be considered.

Case 1. h is very large ($h \rightarrow \infty$). This case is equivalent to considering a semi-infinite rod. In this situation, Eq. (16.255) the wave propagation equation has the form

$$u(x_2, t) = u_0 \exp(i\omega t) \exp[-(a + ib)x_2] \quad (16.262)$$

This equation represents the motion of a harmonic plane wave that depends on space and time, with amplitude oscillating between $\pm u_0 \exp(-ax_2)$. The amplitude attenuates with the distance from the perturbative shearing plate, approaching zero as $x_2 \rightarrow \infty$. As a consequence, the exponent a in Eq. (16.262) is called the attenuating factor per unit length. The zeros of u in Eq. (16.262) occur when $bx_2 = n\pi$, $n = 1, 2, 3, \dots$, at distances $x_2 = \lambda/2, \lambda, 3\lambda/2, \dots$. This requires that $b = 2\pi/\lambda$, where λ is the wavelength. The velocity of the propagating wave is $v = \lambda\nu$, where ν is the linear frequency. Since $\nu = 1/T$, where $T (= 2\pi/\omega)$ is the period, $v = \omega/b$. Equation (16.254) indicate that the higher the loss modulus and the lower the storage modulus, the higher is the attenuation factor. This is the origin of the use of high damping viscoelastic materials for vibration damping and isolators (25).

The wavelength of the transverse wave propagating along the x_2 axis is given by

$$\lambda = \frac{2\pi}{b} = \frac{2\pi}{\omega} \left(\frac{2}{\rho}\right)^{1/2} |G^*|(|G^*| + G')^{-1/2} \quad (16.263)$$

while the speed of the wave propagation can be written as

$$v = \frac{\omega}{b} = \left(\frac{2}{\rho}\right)^{1/2} |G^*|(|G^*| + G')^{-1/2} \quad (16.264)$$

In the development of these two latter expressions Eq. (16.254) was used. For an elastic material ($G'' \rightarrow 0$), $v = (G'/\rho)^{1/2}$.

Case 2. If the distance between the two plates is very small ($h \rightarrow 0$), the exponentials in Eq. (16.256) can be approximated to the first two terms of the series expansion

$$e^x = 1 + \frac{x}{1!} + \frac{x^2}{2!} + \dots \quad (16.265)$$

which gives

$$u(x_2, t) = u_0 \frac{h - x_2}{h} \exp(i\omega t) \quad (16.266)$$

This result indicates that in this case the amplitude of the wave oscillates between two straight lines and all the points of the material in motion are in phase. The expression obtained for the shear deformation demonstrates that this quantity does not depend on the position but only on time.

Let us consider now the more complicated case of an arbitrary excitation. The approach to be followed in this case uses the Laplace transform. From Eqs. (16.249) through (16.251), the transformed equations for the displacement and stress can be written as

$$\frac{\partial^2 \bar{u}(x, s)}{\partial x^2} = \frac{\rho s^2}{G^*(s)} \bar{u}(x, s) \quad (16.267a)$$

and

$$\frac{\partial^2 \bar{\sigma}(x, s)}{\partial x^2} = \frac{\rho s^2}{G^*(s)} \bar{\sigma}(x, s) \quad (16.267b)$$

The general solution of these equations is given by

$$\bar{\sigma}(s) \text{ or } \bar{u}(s) = \bar{A}(s) \exp[\bar{m}(s)x] + \bar{B}(s) \exp[-\bar{m}(s)x] \quad (16.268)$$

where

$$\bar{m}(s) = \left(\frac{\rho}{G^*(s)} \right)^{1/2} s \quad (16.269)$$

where $G^*(s)/\rho$ is the square of the velocity of propagation of the transverse wave when the loss is very small [see Eq. (16.264)] and $A(s)$ and $B(s)$ are functions to be calculated from the boundary conditions

$$\sigma(0, t) = \sigma_0 H(t) \quad \text{and} \quad \sigma(h, t) = 0 \quad (16.270)$$

whose Laplace transforms are

$$\bar{\sigma}(0, s) = \sigma_0/s \quad \text{and} \quad \bar{\sigma}(h, s) = 0 \quad (16.271)$$

After the corresponding calculations, Eq. (16.268) becomes

$$\bar{\sigma}(s) = \frac{\sigma_0}{s} \left(\frac{\sinh(h-x)\bar{m}(s)}{\sinh(h\bar{m}(s))} \right) \quad (16.272)$$

It is important to note that when the slab is very thin ($h \rightarrow 0$) the hyperbolic functions can be replaced by their arguments, and Eq. (16.272) adopts the form

$$\bar{\sigma}(s) = \frac{\sigma_0}{s} \left(1 - \frac{x}{h} \right) \quad (16.273)$$

This indicates a linear dependence of the shear wave on the distance x_2 and consequently a time dependence of the strain in phase with the displacement and the stress. In other words, a thin slab is nearly consistent with a linear response.

Another interesting case to be considered is when $h \rightarrow \infty$. The constant A must be taken equal to zero. The solution of the differential equation for the stresses will be

$$\bar{\sigma}(x, s) = \bar{B}(s) \exp[-\bar{m}(s)x] \quad (16.274)$$

The Laplace inverse presents difficulties except in some special cases. For example, Christensen (6, p. 113) has given a closed solution for a Maxwell material under velocity step input. Alternatively, an asymptotic solution can be obtained to overcome these difficulties.

PROBLEM SETS

Problem 16.1

In the table the values of the dynamic modulus $|E^*(\omega)|$ are given as a function of the frequency for poly(2-chlorophenyl acrylate) at 75°C. The data were obtained by superimposing the experimental results for the real and imaginary parts of the complex modulus obtained at different frequency with a DMTA apparatus (26, 27).

$\log f$	$ E^* (\text{Pa})$
-0.5	1.46×10^7
0	2.42×10^7
0.5	5.2×10^7
1	1.12×10^8
1.5	1.99×10^8
2	3.25×10^8
2.5	4.54×10^8
3	6.22×10^8
3.5	6.81×10^8
4	9.41×10^8
4.5	1.09×10^9
5	1.20×10^9
5.5	1.28×10^9
6	1.32×10^9

Find a Bode three-section contour for the data. That is, approach the experimental data by a contour formed by three horizontal segments alternating with three segments of slope +1. Find also, by Laplace inversion, the tensile relaxation modulus in the time domain.

Solution 16.1

It is clear that the choice of the number as well as the place of the different sections necessary to obtain an approximate fit of the experimental curve is arbitrary. Obviously, accuracy increases with the number of sections. Once the number of sections is chosen, their locations can be optimized to obtain the minimal mean square deviation from the experimental results. However, as a general rule, the middle point of each section on the experimental curve is taken. The choice of the point where the first slope section starts determines the rest of the sections. The middle point of the last section can be determined once the values of the relaxed moduli are known and a careful choice has been made. In the regions of high and low frequencies, the horizontal sections will be longer than in the central zone of the relaxation, where the representative curve of the modulus has a greater slope.

In Figure P16.1.1 the data are represented together with an approximate boundary contour made by three horizontal sections and three sloping sections.

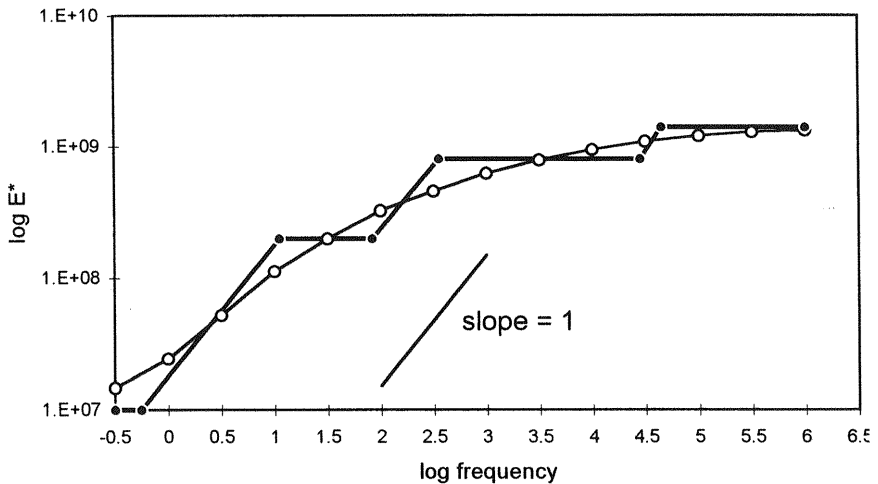


Figure P16.1.1.

According to Eqs (16.24) and (16.26b), the complex relaxation modulus can be written as

$$E^*(\omega) = s' \bar{E}(s') = \frac{A \bar{P}_n(s')}{Q_n(s')} = A \frac{\prod_{i=0}^n (s' + c_i)}{\prod_{i=0}^n (s' + p_i)} \quad (\text{P16.1.1})$$

where $s' = s/2\pi$. The transfer function that results from this approximation is

$$s' \bar{E}(s') = 1.40 \times 10^9 \frac{(s' + 0.55)(s' + 86)(s' + 27,000)}{(s' + 11)(s' + 363)(s' + 45,000)} \quad (\text{P16.1.2})$$

Hence,

$$E(t) = A_0 \left(a_0 + \sum_{i=0}^n a_i \exp(-p_i t) \right) \quad (\text{P16.1.3})$$

with

$$a_0 = \left| \frac{\prod_{i=0}^n c_i}{\prod_{i=0}^n p_i} \right|; \quad a_i = \frac{P_n(-p_i)}{p_i Q_{n,i}(-p_i)}; \quad Q_{n,i} = \frac{\bar{Q}_n(s')}{s + p_i} \quad (\text{P16.1.4})$$

Therefore the tensile relaxation modulus is given by

$$E(t) = 1.40 \times 10^9 [7.11 \times 10^{-3} + 0.1214 \exp(-69.11t) + 0.4694 \exp(-2281t) + 0.402 \exp(-282,745t)] \quad (\text{P16.1.5})$$

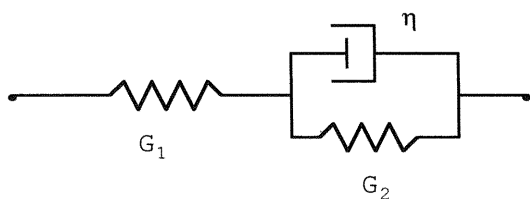
Problem 16.2

Write the equations corresponding to E and ν for a material that behaves as an elastic in bulk compression but reacts as a standard solid model in shear. Analyze the sign of the viscoelastic Poisson ratio.

Solution 16.2

Let us analyze the two cases of standard solids (see Chap. 10).

Case 1. For a stress input in shear it is more convenient to use the three-element model of Figure P16.2.1, whose differential equation is given by


Figure P16.2.1.

$$\left(\frac{1}{G_1} + \frac{1}{G_2}\right)\sigma + \frac{\eta}{G_1 G_2} \dot{\sigma} = \varepsilon + \frac{\eta}{G_2} \dot{\varepsilon} \quad (\text{P16.2.1})$$

where

$$P_1(s) = \left(\frac{1}{G_1} + \frac{1}{G_2}\right) + \frac{\eta}{G_1 G_2} s, \quad Q_1(s) = 2\left(1 + \frac{\eta}{G_2} s\right) \quad (\text{P16.2.2})$$

In bulk the behavior is purely elastic, so

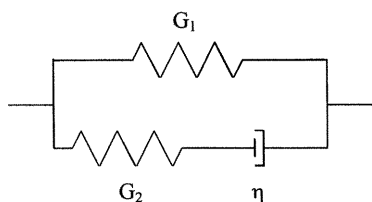
$$P_2(s) = 1, \quad Q_2(s) = 3K \quad (\text{P16.2.3})$$

According to Eq. (16.34),

$$\bar{E}(s) = \frac{9K[1 + (\eta/G_2)s]}{1 + 3K(1/G_1 + 1/G_2) + (1 + 3K/G_1)(\eta/G_2)s} = \frac{Q^E}{P^E} \quad (\text{P16.2.4})$$

$$\bar{v}(s) = \frac{3K(1/G_1 + 1/G_2) - 2 + (3K/G_1 - 2)(\eta/G_2)s}{2 + 6K(1/G_1 + 1/G_2) + (2 + 6K/G_1)(\eta/G_2)s} = \frac{Q^V}{P^V} \quad (\text{P16.2.5})$$

Case 2. A convenient model for a strain input is shown in Figure P16.2.2. The general constitutive equation for this model is


Figure P16.2.2.

$$\frac{\sigma}{\eta} + \frac{\dot{\sigma}}{G_2} = \varepsilon \frac{G_1}{\eta} + \dot{\varepsilon} \left(1 + \frac{G_1}{G_2} \right) \quad (\text{P16.2.6})$$

Consequently,

$$P_1(s) = \frac{1}{\eta} + \frac{s}{G_2}, \quad Q_1(s) = 2 \left[\frac{G_1}{\eta} + \left(1 + \frac{G_1}{G_2} \right) s \right] \quad (\text{P16.2.7})$$

In bulk one obtains

$$P_2(s) = 1, \quad Q_2(s) = 3K \quad (\text{P16.2.8})$$

According to Eq. (16.34), E and ν are given by

$$\bar{E}(s) = \frac{9K[G_1/\eta + (1 + G_1/G_2)s]}{(G_1 + 3K)/\eta + [1 + (1/G_2)(G_1 + 3K)]s} = \frac{Q^E}{P^E} \quad (\text{P16.2.9})$$

$$\bar{\nu}(s) = \frac{(3K - 2G_1)/\eta + [(3K - 2G_1)/G_2] - 2s}{(2G_1 + 6K)/\eta + [2 + (1/G_2)(2G_1 + 6K)]s} = \frac{Q^\nu}{P^\nu} \quad (\text{P16.2.10})$$

We note that in this second case the complex shear modulus can be written as

$$G^*(s) = s\bar{G}(s) = G_1 + \frac{G_2\tau_G s}{1 + \tau_G s}, \quad \tau_G = \frac{\eta}{G_2} \quad (\text{P16.2.11})$$

E^* can be reformulated as

$$E^*(s) = \frac{E_1 + (E_1 + E_2)\tau_E s}{1 + \tau_E s} \quad (\text{P16.2.12})$$

This equation has a structure similar to that of Eq. (P16.2.11), the relationship between the corresponding parameters being given by

$$E_1 = \frac{9KG_1}{G_1 + 3K}; \quad E_2 = \frac{27K^2G_2}{(G_1 + 3K)(G_1 + G_2 + 3K)} \quad (\text{P16.2.13})$$

$$\tau_E = \tau_G \frac{G_1 + G_2 + 3K}{G_1 + 3K} = \tau_G \left(1 + \frac{G_2}{G_1 + 3K} \right) \quad (\text{P16.2.14})$$

Moreover

$$\nu^*(s) = \frac{\nu_1 + (\nu_1 + \nu_2)\tau_\nu s}{1 + \tau_\nu s} \quad (\text{P16.2.15})$$

with

$$\nu_1 = \frac{3K - 2G_1}{6K + 2G_1} \quad \text{and} \quad \nu_2 = \frac{-G_2}{(3K + G_1)} \quad (\text{P16.2.16})$$

$$\tau_E = \tau_\nu = \tau_G \left(1 + \frac{G_2}{G_1 + 3K} \right) \quad (\text{P16.2.17})$$

Thus, if a material is elastic under hydrostatic compression but viscoelastic in shear, according to a solid standard model, then it is viscoelastic in elongation and in the transverse deformation produced by such elongation, according to a similar model but with different parameters.

The expression obtained for the complex viscoelastic Poisson ratio, Eq. (P16.2.10), is given by

$$\nu^* = \frac{a + bs}{c + ds} = s\bar{\nu}(s) \quad (\text{P16.2.18})$$

with

$$a = \frac{3K - 2G_1}{\eta}; \quad b = \frac{3K - 2G_1 - 2G_2}{G_2}; \quad c = \frac{2G_1 + 6K}{\eta}; \quad d = 21 \left(+ \frac{G_1 + 3K}{G_2} \right) \quad (\text{P16.2.19})$$

The inverse Laplace of $\nu(s)$ has the form

$$\nu(t) = \frac{a}{c} + \frac{bc - ad}{cd} \exp\left(-\frac{c}{d}t\right) \quad (\text{P16.2.20})$$

Two limiting values for ν are obtained:

$$\text{If } t \rightarrow 0, \nu \rightarrow \frac{b}{d}; \quad \text{if } t \rightarrow \infty, \nu \rightarrow \frac{a}{c} \quad (\text{P16.2.21})$$

As a rule, $3K > 2G_1$, but $3K$ is comparable to $2(G_1 + G_2)$.

In this case b can be negative, so for very short times the material can exhibit a negative Poisson ratio. Thus we find

$$\nu = 0 \quad \text{for } t = -\frac{d}{c} \ln\left(\frac{ad}{ad - bc}\right) \quad (\text{P16.2.22})$$

For times below that given by Eq. (P16.2.22), the Poisson ratio becomes negative. This means that in this case the cross-sectional area of the longitudinally strained material will increase, a result that, even though it has not been experimentally observed, is not mathematically impossible.

Problem 16.3

Express the equations of motion in terms of displacements for a linear viscoelastic system.

Solution 16.3

By combining the equations that define the strain tensor in terms of displacements (see Chap. 4) with Eq. (16.9), and substituting the remaining equation into the equilibrium equation (see Chap. 4), we immediately obtain the equation

$$\int_{-\infty}^t G(t-\theta) \dot{u}_{i,jj}(\theta) d\theta + \int_{-\infty}^t \left[K(t-\theta) + \frac{1}{3} G(t-\theta) \right] \dot{u}_{k,ki} d\theta + b_i = p \ddot{u}_i \quad (\text{P16.3.1})$$

Problem 16.4

Calculate the longitudinal strain of a viscoelastic rod of a material that behaves like (a) a Maxwell model, (b) a Maxwell solid in shear but an elastic solid in bulk and (c) a viscoelastic solid standard in shear but an elastic solid in bulk. The material is constrained in such a way that the lateral dimensions cannot vary when it is under uniform forces of compression at both ends of the rod.

Solution 16.4

Let us assume that the z axis corresponds to the principal axis of the rod. In this case, the only non-null component of the strain tensor is γ_{zz} . When Lamé coefficients are expressed in terms of the tensile modulus and Poisson ratio [see Eq. (4.102)], the relationship between the stress and strain tensors is given by

$$\sigma_{ij} = \frac{E}{1+\nu} \left(\gamma_{ij} + \frac{\nu}{1-\nu} \gamma_{ll} \delta_{ij} \right) \quad (\text{P16.4.1})$$

Conversely, the relationship between the strain and the stress can be written as

$$\gamma_{ij} = \frac{1}{E} [(1+\nu)\sigma_{ij} - \nu\sigma_{ll}\delta_{ij}] \quad (\text{P16.4.2})$$

[see Eq. (4.124)]. As a consequence, the only non-null components of the stress tensor for the present case will be

$$\sigma_{zz} = \frac{E(1-\nu)}{(1+\nu)(1-2\nu)} \gamma_{zz} \quad \text{and} \quad \sigma_{xx} = \sigma_{yy} = \frac{E\nu}{(1+\nu)(1-2\nu)} \gamma_{zz} \quad (\text{P16.4.3})$$

Let us assume that a uniform compression force is applied to the material on the lateral side in such a way that

$$\sigma_{zz} = PH(t) \quad (\text{P16.4.4})$$

where $H(t)$ is the unit step function. In this case,

$$\gamma_{zz} = \frac{(1-\nu)(1-2\nu)}{E(1-\nu)} PH(t) \quad (\text{P16.4.5})$$

where E and ν are given by Eq. (16.34), as was seen in Problem 16.2. Consequently, from Eq. (P16.4.5),

$$\bar{\gamma}_{zz}(s) = \frac{3P_1P_2}{2P_2Q_1 + P_1Q_2} \left(\frac{P}{s} \right) \quad (\text{P16.4.6})$$

Case a. For a material that behaves as a Maxwell element (in compression and shear), we have

$$\begin{aligned} P_1(s) &= 1 + \tau's; & P_s(s) &= 1 + \tau''s \\ Q_1(s) &= 2\eta's; & Q_2(s) &= 3\eta''s \end{aligned} \quad (\text{P16.4.7})$$

where $\tau' = \frac{\eta'}{G}$ and $\tau'' = \frac{\eta''}{K}$.

Accordingly, Eq. (P16.4.6) becomes

$$\bar{\gamma}_{zz}(s) = \frac{3 + 3(\tau' + \tau'')s + 3\tau'\tau''s^2}{[(4\eta' + 3'') + (4\tau''\eta' + 3\tau'\eta'')s]^2 s^2} \quad (\text{P16.4.8})$$

where E and ν have been replaced by their respective values.

Taking the Laplace inverse of Eq. (P16.4.8), we obtain

$$\begin{aligned} \gamma_{zz}(t) &= 3P \left[\frac{1}{4\eta' + 3\eta''} t + \frac{4\eta'\tau' + 3''\tau''}{(4\eta' + 3'')^2} \right. \\ &\quad \left. - \frac{12\eta'\eta''(\tau' - \tau'')^2}{(4\tau''\eta' + 3\tau'\eta'')(4\eta' + 3\eta'')^2} \exp\left(-\frac{4\eta' + 3\eta''}{4\tau''\eta' + 3\tau'\eta''} t\right) \right] \end{aligned} \quad (\text{P16.4.9})$$

By using an analogous procedure, the following equations for the transverse stresses are obtained:

$$\begin{aligned}\sigma_{xx}(t) &= \sigma_{yy}(t) \\ &= P \left[\frac{3\eta'' - 2\eta'}{3\eta'' + 4\eta'} + \frac{18\eta'\eta''(\tau' - \tau'')}{(3\tau'\eta'' + 4\tau''\eta')(3\eta'' + 4\eta')} \exp\left(-\frac{3\eta'' + 4\eta'}{3\tau'\eta'' + 4\tau''\eta'} t\right) \right]\end{aligned}\quad (\text{P16.4.10})$$

It is noteworthy that if the relaxation times in compression and shear are equal, that is, if

$$\tau' = \tau'' = \tau \quad (\text{P16.4.11})$$

the previous expressions for the strain and the transverse stresses will remain

$$\gamma_{zz}(t) = \frac{3P}{3K + 4G} \left(1 + \frac{t}{\tau}\right) \quad \text{and} \quad \sigma_{xx} = \sigma_{yy} = P \frac{3K - 2G}{3K + 4G} \quad (\text{P16.4.12})$$

Case b. If the material is viscoelastic in shear but elastic in compression, then

$$P_2(s) = 1 \quad \text{and} \quad Q_2(s) = 3K \quad (\text{P16.4.13})$$

and the following expressions are obtained:

$$\gamma_{zz}(t) = \frac{P}{K} \left[1 - \frac{4G}{4G + 3K} \exp\left(-\frac{3K}{3K + 4G} t\right) \right] \quad (\text{P16.4.14})$$

$$\sigma_{xx}(t) = \sigma_{yy}(t) = P \left[1 - \frac{6G}{4G + 3K} \exp\left(-\frac{3K}{3K + 4G} t\right) \right] \quad (\text{P16.4.15})$$

If the material behaves as an elastic solid in bulk but as a viscoelastic standard solid in shear, as in many cases occurs, from the results of Problem 16.2 (case 1) and after some algebra, we obtain

$$\bar{\gamma}_{zz}(s) = \frac{3P(G_1 G_2 + \eta s)}{s[4G_1 G_2 + 3K(G_1 + G_2) + (4G_1 + 3K)\eta s]} \quad (\text{P16.4.16})$$

and

$$\bar{\sigma}_{xx}(s) = \bar{\sigma}_{yy}(s) = \frac{\bar{v}}{1 - \bar{v}} \left(\frac{P}{s} \right) \quad (\text{P16.4.17})$$

or, equivalently,

$$\bar{\sigma}_{xx}(s) = \bar{\sigma}_{yy}(s) = \frac{[3K(G_1 + G_2) - 2G_1 G_2] + (3K - 2G_1)\eta s}{[3K(G_1 + G_2) + 4G_1 G_2] + (3K + 4G_1)\eta s} \left(\frac{P}{s} \right) \quad (\text{P16.4.18})$$

The Laplace inverse of these expressions leads to

$$\gamma_{zz}(t) = \frac{3P}{(4G_1 + 3K)(4G_1G_2 + 3K(G_1 + G_2))} \left\{ (G_1 + G_2)(4G_1 + 3K) - 4G_1^2 \exp \left[-\frac{3K(G_1 + G_2) + 4G_1G_2}{3K + 4G_1} \left(\frac{t}{\eta} \right) \right] \right\} \quad (\text{P16.4.19})$$

and

$$\begin{aligned} \sigma_{xx}(t) &= \sigma_{yy}(t) \\ &= \frac{P}{(3K + 4G_1)[3K(G_1 + G_2) + 4G_1G_2]} \left[(3K + 4G_1)[3K(G_1 + G_2) - 2G_1G_2] \right. \\ &\quad \left. - 18KG_1^2 \exp -\frac{3K(G_1 + G_2) + 4G_1G_2}{3K + 4G_1} \cdot \frac{t}{\eta} \right] \end{aligned} \quad (\text{P16.4.20})$$

where $\eta = \tau G_2$.

Problem 16.5

A thin rod of PMMA rigidly clamped at its ends is initially at 18°C. Suddenly it is heated to 60°C. Determine the stress 1 h after starting the experiment, knowing that at 18°C the tensile relaxation modulus is given by

$$E(t) = 7.25 \times 10^9 \left(\frac{1 + 1.778 \times 10^{-2}t}{1 + 1.778 \times 10^2t} \right)^{0.143} \text{ Pa}$$

The dilatation coefficient is $\beta = 4 \times 10^{-4} \text{ K}^{-1}$, and the activation energy at the temperature range under study is 75 kJ/mol.

Solution 16.5

We assume constant length, and the possibility of flexion is ruled out. According to the boundary conditions for a doubly clamped rod in the x direction,

$$\gamma_{xx} = 0 \quad \text{and} \quad \sigma_{yy} = \sigma_{zz} = 0 \quad (\text{P16.5.1})$$

The nondiagonal components of the stress and strain tensors are also null. For the thermoelastic case, the stress–strain relationship is

$$0 = \frac{1}{E} [\sigma_{xx} - \nu(\sigma_{yy} + \sigma_{zz})] + \alpha \Delta T = \frac{\sigma_{xx}}{E} + \alpha \Delta T \quad (\text{P16.5.2})$$

from which

$$\sigma_{xx} = -\beta \Delta T E \quad (\text{P16.5.3})$$

If $\Delta T > 0$ the sample is compressed, and if $\Delta T < 0$ the sample is stretched. The remaining components of the strain are

$$\gamma_{yy} = \gamma_{zz} = -\frac{\nu \sigma_{xx}}{E} + \beta \Delta T \quad (\text{P16.5.4})$$

The decomposition in deviatoric and dilatational components of both the stress and strain tensors are

$$\begin{pmatrix} \sigma_{xx} & 0 & 0 \\ 0 & 0 & 0 \\ 0 & 0 & 0 \end{pmatrix} = \begin{pmatrix} \frac{2\sigma_{xx}}{3} & 0 & 0 \\ 0 & -\frac{\sigma_{xx}}{3} & 0 \\ 0 & 0 & \frac{\sigma_{xx}}{3} \end{pmatrix} + \begin{pmatrix} \frac{\sigma_{xx}}{3} & 0 & 0 \\ 0 & \frac{\sigma_{xx}}{3} & 0 \\ 0 & 0 & \frac{\sigma_{xx}}{3} \end{pmatrix} \quad (\text{P16.5.5})$$

and

$$\begin{pmatrix} 0 & 0 & 0 \\ 0 & \gamma_{yy} & 0 \\ 0 & 0 & \gamma_{yy} \end{pmatrix} = \begin{pmatrix} \frac{-2\gamma_{yy}}{3} & 0 & 0 \\ 0 & \frac{\gamma_{yy}}{3} & 0 \\ 0 & 0 & \frac{\gamma_{yy}}{3} \end{pmatrix} + \begin{pmatrix} \frac{2\gamma_{yy}}{3} & 0 & 0 \\ 0 & \frac{2\gamma_{yy}}{3} & 0 \\ 0 & 0 & \frac{2\gamma_{yy}}{3} \end{pmatrix} \quad (\text{P16.5.6})$$

We make use of the auxiliary variable $\xi = a_T t$, which in fact is an effective time related to the real time through a time-dependent function a_T , that is also dependent on an activation energy. Taking into account Eqs. (P16.5.5) and (P16.5.6), the corresponding stress-strain relationship for the viscoelastic case are found to be

$$\sigma_{xx}(\xi) = -2 \int_{-\infty}^{\xi} G(\xi - \xi') \frac{\partial}{\partial \xi'} \gamma_{yy} d\xi' \quad (\text{P16.5.7})$$

and

$$\sigma_{xx}(\xi) = 3 \int_{-\infty}^{\xi} K(\xi - \xi') \frac{\partial}{\partial \xi'} (2\gamma_{yy} - 3\beta \Delta T) d\xi' \quad (\text{P16.5.8})$$

where G and K are, respectively, the shear and bulk relaxation moduli. Taking Laplace transforms, we find

$$\bar{\sigma}_{xx}(s) = -2s\bar{G}(s)\bar{\gamma}_{yy}(s) \quad (\text{P16.5.9})$$

and

$$\bar{\sigma}_{xx}(s) = 3s\bar{K}(s)[2\bar{\gamma}_{yy}(s) - 3\bar{\gamma}(s)], \quad \text{where } \gamma = \beta\Delta T \quad (\text{P16.5.10})$$

These equations lead to

$$\bar{\gamma}_{yy}(s) = \bar{\gamma}_{zz}(s) = \frac{9\bar{K}(s)\bar{\gamma}(s)}{2(\bar{\mu}(s) + 3\bar{K}(s))} = [1 + \bar{\nu}(s)]\bar{\gamma}(s) \quad (\text{P16.5.11})$$

and

$$\bar{\sigma}_{xx}(s) = -s\bar{E}(s)\bar{\gamma}(s) \quad (\text{P16.5.12})$$

where, as indicated in Chapter 5,

$$\bar{E}(s) = \frac{9\bar{G}(s)\bar{K}(s)}{\bar{G}(s) + 3\bar{K}(s)} \quad (\text{P16.5.13})$$

and

$$\bar{\nu}(s) = \frac{3\bar{K}(s) - 2\bar{G}(s)}{2[\bar{G}(s) + 3\bar{K}(s)]} \quad (\text{P16.5.14})$$

We note that elastic and viscoelastic solutions have the same formal structure. For a step temperature input, the inverse Laplace of Eq. (P16.5.12) is given by

$$\sigma_{xx}(t) = -\beta\Delta T E(a_T t) \quad (\text{P16.5.15})$$

where

$$a_T = \exp\left[\frac{E_a}{R}\left(\frac{1}{T} - \frac{1}{T_0}\right)\right] \quad (\text{P16.5.16})$$

Here it has been assumed that the Arrhenius equation is valid for the glassy zone of this polymer.

Since $E_a = 75 \text{ kJ/mol}$, $T_0 = 291\text{K}$, and $T = 333$ from Eq. (P16.5.16), we obtain $a_T = 0.0200$.

The stress will be given by

$$\sigma_{xx} = -(4 \times 10^{-4})(333 - 291)(7.25 \times 10^9) \left(\frac{1 + (1.778 \times 10^{-2})(t/0.02)}{1 + (1.778 \times 10^{-2})(t/0.02)} \right)^{0.143} \quad (\text{P16.5.17})$$

Therefore, for $t = 3600 \text{ s}$, $\sigma_{xx} = 3.26 \times 10^7 \text{ Pa}$.

Problem 16.6

Let us assume a viscoelastic material that exhibits instantaneous elasticity [see Eq. (16.24)]

$$s\bar{G}(s) = \frac{q_n s^n + q_{n-1} s^{n-1} + \cdots + q_0}{r_n s^n + r_{n-1} s^{n-1} + \cdots + r_0}$$

Estimate the long-time behavior after a discontinuous change in the stress at $x = 0$ produced by a shear wave in a slab of infinite thickness.

Solution 16.6

The Laplace transform of the stress input $\sigma(0, t) = \sigma_0 H(t)$ is given by,

$$\bar{\sigma}(0, s) = \frac{\sigma_0}{s} \quad (\text{P16.6.1})$$

Consequently, from Eq. (16.274) we have:

$$\bar{\sigma}(x, s) = \frac{\sigma_0}{s} \exp[-m(s)x] \quad (\text{P16.6.2})$$

where m is given by Eq. (16.269). For short frequencies ($s = i\omega$), that is, large times,

$$s\bar{G}(s) = \frac{q_0}{r_0} + \frac{r_1}{r_0} \left(\frac{q_1}{r_1} - \frac{q_0}{r_0} \right) s + O'(s^2) = \frac{q_0}{r_0} \left[1 + s \left(\frac{q_1}{q_0} - \frac{r_1}{r_0} \right) + O(s^2) \right] \quad (\text{P16.6.3})$$

From Eq. (16.269):,

$$\bar{m}(s) = \left(\frac{\rho r_0}{q_0} \right)^{1/2} \left(\frac{s}{1 + s\alpha + \cdots} \right)^{1/2} \quad (\text{P16.6.4})$$

where

$$\alpha = \frac{q_1}{q_0} - \frac{r_1}{r_0} \quad (\text{P16.6.5})$$

Therefore, Eq. (P16.6.2) can be written as

$$\bar{\sigma}(s) = \frac{\sigma_0}{s} \left\{ \exp \left[-x \left(\frac{\rho r_0}{q_0} \right)^{1/2} \left(\frac{s}{(1 + s\alpha + \dots)^{1/2}} \right) \right] \right\} \quad (\text{P16.6.6})$$

By expanding Eq. (P16.6.6) in series, and after some approximations, we obtain

$$\bar{\sigma}(s) \approx \frac{\sigma_0}{s} \left[1 - x \left(\frac{\rho r_0}{q_0} \right)^{1/2} \left(\frac{s}{(1 + s\alpha + \dots)^{1/2}} \right) \right] \cong \sigma_0 \left[\frac{1}{s} - x \left(\frac{\rho r_0}{q_0} \right)^{1/2} \left(\frac{1}{(1 + s\alpha)^{1/2}} \right) \right] \quad (\text{P16.6.7})$$

whose Laplace inverse is given by

$$\sigma(t) = \sigma_0 \left[1 - x \left(\frac{\rho r_0}{q_0} \right)^{1/2} \left(\frac{\exp(-t/\alpha)}{(\pi\alpha t)^{1/2}} \right) \right] \quad (\text{P16.6.8})$$

where we have used the following formula for the Laplace transform of a fractional power of $(s + \alpha)$:

$$\mathcal{L}^{-1} \frac{1}{(s + \alpha)^v} = \frac{t^{v-1} \exp(-\alpha t)}{\Gamma(v)}, \quad \text{Re } v > 0 \quad (\text{P16.6.9})$$

where the symbol Γ represents the gamma function. Equation (P16.6.8) indicates that for long times the velocity of the disturbance is damped, with the time due to the dissipative character of the material.

REFERENCES

1. BD Coleman, W Noll. Foundation of linear viscoelasticity. *Rev Mod Phys* 33: 239, 1961.
2. ME Gurtin, E Sternberg. On the linear theory of viscoelasticity. *ARMA* 11: 291, 1962.
3. MJ Leitman, GMC Fisher. The linear theory of viscoelasticity. In: C Truesdell, ed. *Handbuch der Physik*, Vol 3. Berlin: Springer-Verlag, 1973, p.1.
4. AC Pipkin. Berlin: Springer-Verlag, 1972.
5. WN Findlay, JS Lai, K Onaran. *Creep and Relaxation of Non-Linear Viscoelastic Materials*. Amsterdam, North-Holland, 1976, 71.

6. RW Christensen. *Theory of Viscoelasticity: An Introduction*. New York: Academic Press, 1971, p.15.
7. DR Bland. *The Theory of Linear Viscoelasticity*. Oxford, UK: Pergamon, 1960, Chap 2.
8. NP Vinh Tuong. Sur le passage du regime harmonique au regime transitoire. Extrait des Cahiers du Groupe Francais de Rheologie No 1, Tome II, 1969.
9. IH Shames, FA Cozzarelli. *Elastic and Inelastic Stress Analysis*. Englewood Cliffs, NJ: Prentice-Hall, 1992.
10. YM Haddad. *Viscoelasticity of Engineering Materials*. London: Chapman & Hall, 1995.
11. V Volterra. *Atti Reale Lincei* 18(2): 295, 1909.
12. PC Chou, NJ Pagano. *Elasticity: Tensor, Dyadic, and Engineering Approaches*. New York: Dover, 1992, Chap 4.
13. EH Lee. Stress analysis in viscoelastic bodies. *Quart Appl Math* 13: 183, 1955.
14. C Hunter. The solution of boundary problems in linear viscoelasticity. *Proc 4th Naval Structural Mechanics*. Oxford: Pergamon, 1965, p. 257.
15. LD Landau, EM Lifshitz. *Theory of Elasticity*. 3rd ed. Oxford: Pergamon, 1986.
16. IH Shames, FA Cozzarelli. *Elastic and Inelastic Stress Analysis*. Englewood Cliffs, NJ: Prentice-Hall, 1992, Chap 13.
17. SC Hunter. The Hertz problem for a rigid spherical indenter and a viscoelastic half-space. *J Mech Phys Solids* 8: 219, 1960.
18. GAC Graham. The contact problem in the linear theory of viscoelasticity. *Int J Eng Sci* 3: 27, 165.
19. DF Moore. *Viscoelastic Machine Elements*. Oxford; Butterworths-Heinemann, 1993.
20. H Kolsky. *Stress Waves in Solids*. New York: Dover, 1963.
21. RN Thurston. *Waves in solids*. In: C Truesdell, ed. *Handbuch der Physik*. Vol Vla, No. 4. Berlin: Springer-Verlag, 1974.
22. EH Lee, JA Morrison. *J. Polym Sci* 19: 93, 1956.
23. JD Achenbach, DP Reddy. *Z Angew Math Phys* 18: 141, 1967.
24. KC Valanis, S Chang. Stress wave propagation in a finite viscoelastic thin rod with a constitutive law of the hereditary type. In: TC Huang, MW Johnson, eds. *Developments in Theoretical and Applied Mechanics*. New York: Wiley, 1965.
25. RD Corsaro, LH Sperling. *Sound and Vibration Damping with Polymers*. ACS Symp Ser 424. Washington DC: Am Chem Soc, 1990.
26. R Díaz-Calleja, E Riande, J San Roman. *Macromolecules* 24: 1854, 1991.
27. R Díaz-Calleja, E Riande, J San Roman. *Polymer* 22: 2995, 1991.

17

Flexion and Torsion of Viscoelastic Beams and Rods

17.1	Introduction	770
17.2	Beam Bending: Preliminary Hypotheses and Stress Tensor	770
17.3	Bending Moment	772
17.4	Radius of Curvature	772
17.5	Momentum and Force Balances in Beams	775
17.6	Indentation of a Clamped Beam	776
17.7	Shear Stress Analysis in Elastic Beams	779
17.8	Shear Strain Analysis	783
17.9	Viscoelastic Beams	788
17.10	Transverse Vibrations in Viscoelastic Beams	789
17.11	Thermal Effects on Transverse Vibrations	808
17.12	Torsion of Viscoelastic Rods	816
17.13	Displacement and Strain Tensor in Torsion	816
17.14	Stress Tensor in Torsion	818
17.15	Equilibrium Equations for Torsion	819
17.16	Boundary Conditions	820
17.17	Torsion Function Found by Separation of Variables	821
17.18	Moment of Torque	822
17.19	Motion and Boundary Condition Equations	824
17.20	Analysis of Torsional Oscillations Using an Elastic Auxiliary Element	832
	Problem Sets	836
	References	864

17.1 INTRODUCTION

The analysis of the stresses and strains in beams and thin rods is a subject of great interest with many practical applications in the study of the strength of materials. The geometry associated with problems of this type determines the specific type of solution. There are cases where small strains are accompanied by large displacements, flexion and torsion in relatively simple structures being the most relevant examples. Problems of this type were solved for the elastic case by Saint Venant in the nineteenth century. The flexion of viscoelastic beams and the torsion of viscoelastic rods are studied in this chapter.

17.2 BEAM BENDING: PRELIMINARY HYPOTHESES AND STRESS TENSOR

In a first approach to the study of beam bending, it is convenient to make some hypotheses (1). The first of these hypotheses is that the sections that are flat before flexion remain flat after flexion. For slender beams—that is, for beams whose transverse dimensions are small in comparison with their length—this hypothesis is substantially correct. In this case, the shear effects in the cross sections are relatively negligible. It will be further assumed that the inertial forces arising from the rotation of each element around its center of mass can be ignored. This is, in fact, the second hypothesis.

In a beam under flexion, some parts are stretched and others are compressed. A “neutral” surface exists inside the beam in which the components of the stress vanish. Let us take the origin of the coordinate reference frame on this surface, and let us assume that the free length of the beam is located along the X axis. Let us assume further that the length of the undistorted bar is L and the deformations in flexion are produced in the XY plane. It is clear that for homogeneous beams of uniform cross section, either rectangular or circular, the axis will pass through the center of gravity (see Fig. 17.1). In this case the neutral surface is a line that can coincide with the X axis.

The analysis of the balance of forces on the lateral surface of the beam carried out on the basis of the preliminary hypothesis indicates that the only nonzero component of the stress tensor is σ_{xx} . A deformation of this type is a compression or a simple extension. In fact, some parts of the transverse section are under tension, and others are under compression, and the two effects combined produce the flexion. According to Figure 17.1, the component γ_{xx} of the strain is given by

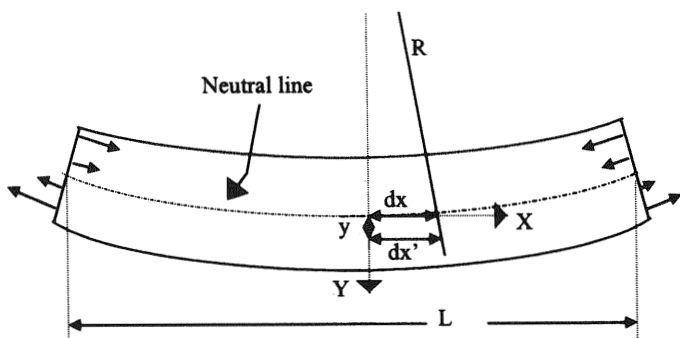


Figure 17.1 Element of a beam showing the stresses and the neutral line.

$$\gamma_{xx} = \frac{dx' - dx}{dx} = \frac{dx'}{dx} - 1 \quad (17.1)$$

Since

$$\frac{dx'}{dx} = \frac{R + y}{R} = \frac{y}{R} + 1$$

we obtain

$$\gamma_{xx} = y/R \quad (17.2)$$

where R is the local radius of curvature of the neutral line. Of course, $\gamma_{xx} = 0$ on this neutral line.

According to the differential operators for the tensile modulus $E(Q^E, P^E)$ and the Poisson ratio $\nu(Q^V, P^V)$ in Eqs. (16.34) and (16.37), the remaining components of the viscoelastic strain and stress, respectively, are given by

$$\gamma_{yy} = \gamma_{zz} = -\frac{Q^V}{P^V} \gamma_{xx} = -\frac{Q^V}{P^V} \left(\frac{y}{R} \right) \quad (17.3a)$$

and

$$\sigma_{xx} = \frac{y}{R} \left(\frac{Q^E}{P^E} \right) \quad (17.3b)$$

17.3 BENDING MOMENT

The force acting on the transverse section S of the beam[†] is given in the viscoelastic case by

$$\int_S \sigma_{xx} dS = \int_S \frac{y}{R} \left(\frac{Q^E}{P^E} \right) dS \quad (17.4)$$

On the other hand, the bending moment M on a cross section of the beam can be written as

$$M = \int_S y \sigma_{xx} dS \quad (17.5)$$

By applying the differential operator P^E to both sides of Eq. (17.5) and using (17.3b), we obtain

$$\begin{aligned} P^E(M) &= \int_S y P^E(\sigma_{xx}) dS = \int_S y Q^E(\gamma_{xx}) dS = \int_S y^2 Q^E \left(\frac{1}{R} \right) dS \\ &= Q^E \left(\frac{1}{R} \right) I = \frac{1}{y} Q^E(\gamma_{xx}) I = \frac{1}{y} P^E(\sigma_{xx}) I \end{aligned} \quad (17.6)$$

where I is the polar moment of inertia of the transverse section*. The brackets of type $P^E(\cdot)$ can be interpreted either as a commutative differential operator (2) or as a Boltzmann convolution integral. These two different possibilities arise from the two different forms that can be used to represent the viscoelastic stress-strain relationship as defined in the preceding chapters. The inverse of the Laplace transform of Eq. (17.6) leads to the following expression for the flexural moment:

$$M(x, t) = I \sigma_{xx}(x, y, t) / y \quad (17.7)$$

17.4 RADIUS OF CURVATURE

In the preceding calculations, a radius of curvature of the neutral line appears, which in the case of thin beams can be identified with the radius of curvature of the beam. According to Figure 17.2,

[†]In this Chapter the polar moment of inertia of a cross-section area (dimensions L^4) and the mass moment of inertia (dimensions ML^4) are represented by I and J , respectively.

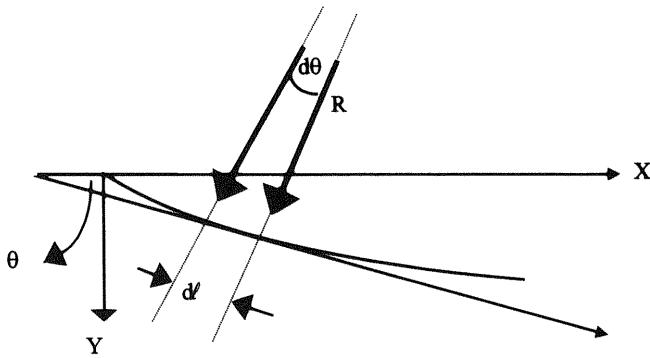


Figure 17.2 Sketch of a slender beam to calculate the radius of curvature.

$$\tan \theta = \frac{du_y}{dx}; \quad \theta = \arctan \frac{du_y}{dx} \quad (17.8a)$$

$$\frac{1}{R} = -\frac{d\theta}{dl} = -\frac{d\theta}{dx} \frac{dx}{dl} = -\frac{d^2u_y/dx^2}{[1 + (du_y/dx)^2]^{3/2}} \quad (17.8b)$$

where u_y is the displacement, and it is considered that

$$dl = R d\theta \quad \text{and} \quad (dl)^2 = (dx)^2 + (du_y)^2 \quad (17.9)$$

For small curvatures, Eq. (17.8b) becomes

$$\frac{1}{R} \cong -\frac{d^2u_y}{dx^2} \quad (17.10)$$

and by combining this equation with that of the flexural moment [Eq. (17.6)] we obtain

$$P^E(M) = -IQ^E(u_y'') \quad (17.11)$$

This expression is similar to

$$P^E(\sigma_{xx}) = Q^E(\epsilon_{xx}) \quad (17.12)$$

and on the same grounds as Eqs. (16.6a), (16.6b), and (17.11) can be written in integral form as

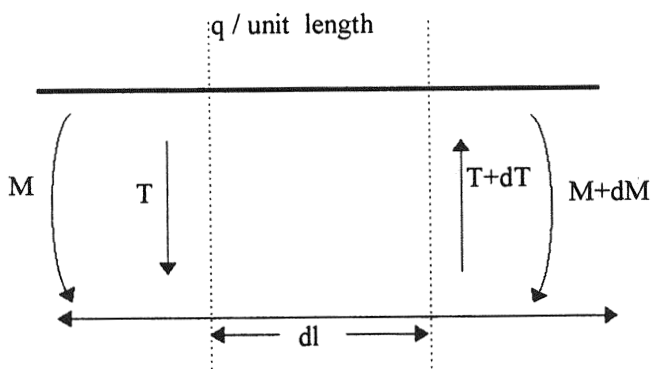


Figure 17.3 Section of a beam showing the flexural moment, shear force, and external applied force and the way of calculating the relations among them.

$$-\frac{1}{R} = u_y'' = -\frac{1}{I} \int_0^\infty D(t - \theta) dM(\theta) \quad (17.13a)$$

where D is the tensile compliance, or, alternatively, as

$$I \int_0^\infty E(t - \theta) \frac{\partial^3 u_y}{\partial x^2 \partial \theta} d\theta = -M \quad (17.13b)$$

where E is the tensile modulus. Taking the Laplace transform of Eq. (17.13a) leads to the expression

$$-\frac{I}{\bar{R}(s)} = I \bar{u}_y''(s) = -s \bar{M}(s) \bar{D}(s) \quad (17.14)$$

which is equivalent to the Laplace transform of Eq. (17.13b),

$$Is \bar{E}(s) \bar{u}_y''(s) = -\bar{M}(s) \quad (17.15)$$

as a consequence of the fact that the complex compliance function is the reciprocal of the complex tensile modulus. The corresponding equation for an elastic material is given by

$$u_y'' = -M/EI \quad (17.15b)$$

This expression, known as the Euler–Bernoulli equation, is standard in texts on strength of materials.

17.5 MOMENTUM AND FORCE BALANCES IN BEAMS

Let us consider (Fig. 17.3) a beam element under a small deflection in which two close sections are separated by an infinitesimal distance $dx = dl$. M and T in the figure are, respectively, the flexural momentum and the shear force, while q is the external applied force (including the weight of the beam) per unit length. From the momentum balance, and momentarily disregarding the vectorial character of the magnitudes, we obtain

$$M - (M + dM) + (T + dT)dl - qdl \frac{dl}{2} = 0 \quad (17.16)$$

Neglecting the second-order infinitesimals, Eq. (17.16) becomes

$$\frac{dM}{dx} = T \quad (17.17)$$

This equation represents, in fact, the momentum balance condition for a beam element located between two sections separated by a very small distance. However, this is not the only balance condition. The resulting force acting on a bar element is $dT + qdx$, where dT is the difference between the forces acting on two limiting sections of the beam element. If

$$q = -\frac{dT}{dx} \quad (17.18)$$

then the resultant force in the balance equation vanishes. This is the force balance equation for the bent beam.

In cases in which the external forces applied to the beam are concentrated in a specific section, then in the regions of the beam where the forces do not act, the balance equation is greatly simplified. Actually, if $q = 0$, then T is constant. Integration of Eq. (17.17) gives

$$M = Tx + \text{constant} \quad (17.19)$$

Moreover, if the flexion of the beam is produced by concentrated forces, T experiences a jump in the points at which the forces are applied.

Finally, if the flexion of the beam is produced by concentrated torques, then T is constant throughout the beam and the momentum M experiences jumps at the points at which the torques are applied.

By combining Eqs. (17.16), (17.17), and (17.18), the following equations for viscoelastic materials in terms of the operational variable s are obtained:

$$I s \bar{E}(s) \bar{u}_y''(s) = -\bar{M}(s) \quad (17.20a)$$

$$I s \bar{E}(s) \bar{u}_y'''(s) = -\bar{T}(s) \quad (17.20b)$$

$$I s \bar{E}(s) \bar{u}_y^{IV}(s) = \bar{q}(s) \quad (17.20c)$$

Equations (17.20) are Laplace transforms of the equations of viscoelastic beams and can be considered a direct consequence of the elastic-viscoelastic correspondence principle. The second, third, and fourth derivatives of the deflection, respectively, determine the forces moment, the shear stresses, and the external forces per unit length. The sign on the right-hand side of Eqs. (17.20) depends on the sense in which the direction of the strain is taken.

It should be noted that the solution of any viscoelastic beam problem requires knowledge of the boundary conditions at the ends of the rod. These conditions depend on whether the bar is supported, articulated, clamped, free, etc., and for this reason the boundary conditions play a crucial role in the solution of the problem.

17.6 INDENTATION OF A CLAMPED BEAM

Let us consider now a double-sided plane indentation for a clamped beam (Fig. 17.4). To simplify the problem, we will study a slender beam, neglecting shear and rotatory inertial terms. Let $d(t)$ and $P(t)$ express the time dependence of both the displacement of the indenter and the applied load. Furthermore $2a$ is the length of contact, and l is the half-length of the beam. The origin of coordinates will be taken at the center of the beam. Owing to the symmetry of the problem, only the solution for $x \geq 0$ will be considered.

From the conditions of the problem, and taking the deflection as positive

$$\begin{aligned} u_y(t) &= d(t) && \text{for } x < a \\ u_y(t) &= C_1 + C_2x + C_3x^2 + C_4x^3 && \text{for } l > x > a \end{aligned} \quad (17.21)$$

where C_1 , C_2 , C_3 , and C_4 are functions of time. The condition that the shear at the ends of the beam balance the applied load $P(t)$, in conjunction with Eq. (17.21), allows us to write Eq. (17.20b) as

$$12I \int_0^\infty E(t-\theta) \frac{d}{d\theta} C_4(\theta) d\theta = P(t) \quad (17.22)$$

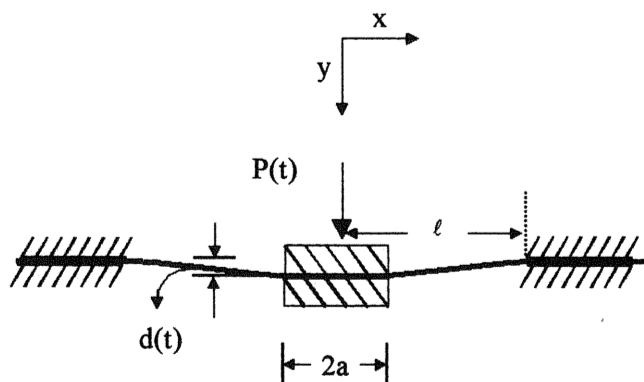


Figure 17.4 Plane indentation of a double-clamped beam.

From the boundary conditions,

$$u_y = \frac{du_y}{dx} = 0 \quad \text{at } x = l \quad (17.23)$$

Eq. (17.21b) can be written as

$$C_1 + C_2l + C_3l^2 + C_4l^3 = 0 \quad (17.24a)$$

$$C_2 + 2C_3l + 3C_4l^2 = 0 \quad (17.24b)$$

On the other hand, the boundary conditions at the edge of the contact region ($x = a$),

$$u_y|_{x=a} = d(t), \quad \left. \frac{du_y}{dx} \right|_{x=a} = 0 \quad (17.25)$$

lead Eq. (17.21b) to

$$C_1 + C_2a + C_3a^2 + C_4a^3 = d(t) \quad (17.26a)$$

$$C_2 + 2C_3a + 3C_4a^2 = 0 \quad (17.26b)$$

It is clear that the system formed by Eqs. (17.22), (17.24), and (17.26) is nonlinear. Two cases will be considered: (1) when the applied load is known and (2) when the displacement is known.

Case 1. If $P(t)$ is known, the Laplace transform of Eq. (17.22) gives

$$12Is\bar{E}(s)\bar{C}_4(s) = \bar{P}(s) \quad (17.27)$$

from which $C_4(t)$ can be obtained. The remaining unknown C_i parameters can easily be found by solving Eqs. (17.24) and (17.26b). The results are

$$C_1 = C_4 \frac{l^2}{2}(l - 3a); \quad C_2 = 3C_4al; \quad C_3 = -\frac{3}{2}C_4(l + a) \quad (17.28)$$

while from Eq. (17.26a) we find

$$d(t) = \frac{C_4}{2}(l - a)^3 \quad (17.29)$$

Accordingly, from Eqs. (17.21) and (17.28) the deflection in case 1 is found to be

$$u_y(x, t) = C_4(t) \left(x^3 - \frac{3}{2}x^2(l + a) + 3xal + \frac{l^2}{2}(l - 3a) \right) \quad (17.30)$$

Case 2. Let us consider now the case in which $d(t)$ is known. Solution of the system formed by Eqs. (17.24) and (17.26) gives

$$C_1 = \frac{l^2(l - 3a)d(t)}{(l - a)^3}; \quad C_3 = \frac{-3(l + a)d(t)}{(l - a)^3} \quad (17.31a)$$

$$C_2 = \frac{6lad(t)}{(l - a)^3}; \quad C_4 = \frac{2d(t)}{(l - a)^3} \quad (17.31b)$$

Taking the inverse Laplace of Eq. (17.27), we obtain

$$P(t) = \frac{24I}{(l - a)^3} L^{-1}[s\bar{E}(s)\bar{d}(s)] \quad (17.32)$$

By substituting the value of C_4 given in Eq. (17.31) into Eq. (17.21b), we obtain the deflection for this case:

$$u_y(x, t) = \frac{d(t)}{(l - a)^3} [2x^3 - 3x^2(l + a) + 6xal + l^2(l - 3a)] \quad (17.33)$$

In the first case [$P(t)$ is known], let us consider a standard solid that is viscoelastic in shear (spring in parallel with a Maxwell element) but elastic in compression. By assuming a step input, we obtain in the usual way

$$C_4(t) = \frac{P_0}{36IK} \left\{ \frac{3K + G_1}{3G_1} - \frac{KG_2}{G_1(G_1 + G_2)} \exp\left[\frac{-G_2}{G_1 + G_2} \left(\frac{t}{\tau} \right) \right] \right\}; \quad \tau = \frac{\eta}{G_2} \quad (17.34)$$

where K is the bulk relaxation modulus; G_1 , G_2 , and η are the characteristic parameters of the standard solid material; and P_0 is the intensity of the step input in the load.

In the same conditions as above, the solution for the load in the second case [$d(t)$ is given] can be written as

$$P(t) = \frac{24Id_0}{(l-a)^3} \left[\frac{9KG_1}{3K + G_1} + \frac{27K^2G_2}{(3K + G_1)(3K + G_1 + G_2)} \exp\left(-\frac{3K + G_1}{3K + G_1 + G_2} \cdot \left(\frac{t}{\tau} \right) \right) \right]; \quad \tau = \frac{\eta}{G_2} \quad (17.35)$$

where d_0 is the step input of displacement of the indenter.

17.7 SHEAR STRESS ANALYSIS IN ELASTIC BEAMS

It is well known that the elementary theory of beams described above becomes inadequate for beams with transverse dimensions of the same order of magnitude as their length. This section deals with the theory to be applied to thick non-slender beams. This theory appears to be relevant in the context of dynamic mechanical analysis. The first fact to be considered is that when the beam is flexed it experiences a shear stress that provokes a relative sliding of the adjacent transverse sections. As a consequence, the larger the transverse section, the higher is this shear strain. The final effect is an increase in the total deflection of the beam (Fig. 17.5).

The starting approach will be the elasticity theory (3). In the elementary theory of beams, the only component of the stress tensor differing from zero is $\sigma_{xx} = Ey/R$, which, according to the theory developed for the elastic case, can be written as

$$\sigma_{xx} = \frac{M}{I} y \quad (17.36)$$

By considering a plane stress, that is, $\sigma_{zz} = \sigma_{xz} = \sigma_{yz} = 0$, at equilibrium, Eq. (4.14) can be written as

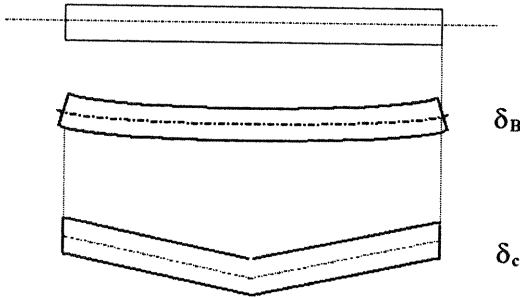


Figure 17.5 Bending and shear deflections of a non-slender beam.

$$\frac{\partial \sigma_{xx}}{\partial x} + \frac{\partial \sigma_{xy}}{\partial y} = 0 \quad (17.37)$$

where the body forces are neglected. By combining Eqs. (17.36) and (17.37), we obtain

$$\frac{\partial \sigma_{xy}}{\partial y} = -\frac{\partial \sigma_{xx}}{\partial x} = -\frac{y}{I} \frac{dM}{dx} = -\frac{y}{I} T \quad (17.38)$$

where it is assumed that the shear stress T is independent of y . Integration of Eq. (17.38) leads to the expression

$$\sigma_{xy} = -\frac{T}{I} \left(\frac{y^2}{2} + c \right) \quad (17.39)$$

For a rectangular beam, such as that shown in Figure 17.6, $\sigma_{xy} = 0$ for $y = \pm d/2$, so $c = -d^2/8$. As a consequence, Eq. (17.39) becomes

$$\sigma_{xy} = \frac{T}{2I} \left(\frac{d^2}{4} - y^2 \right) \quad (17.40)$$

This expression reflects a parabolic distribution of the stresses whose maximum value $\sigma_{xy,\max} = Td^2/8I$ is reached at $y = 0$. For a rectangular section, $I = bd^3/12$ and the maximum shear stress is given by

$$\sigma_{xy} = \frac{3T}{2bd} \quad (17.41)$$

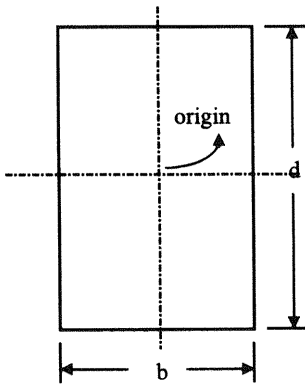


Figure 17.6 Transverse section of a rectangular beam.

On the other hand, Eq. (17.36) indicates that the maximum for the longitudinal stress is:

$$\sigma_{xx,\max} = \frac{Ed}{2R} = \frac{Md}{2I} \quad (17.42)$$

so that, for a rectangular beam,

$$\sigma_{xx,\max} = \frac{6M}{bd^2} \quad (17.43)$$

Note that

$$\frac{\sigma_{xy}}{\sigma_{xx}} = \frac{T}{2M} \left(\frac{d^2/4 - y^2}{y} \right) \quad (17.44)$$

Since T/M and $(d^2/4 - y^2)/y$ are of the order of L^{-1} and d , respectively, and for slender beams $d/L \ll 1$, Eq. (17.44) suggests that the shear stresses are negligible along the beam.

Another component of the stress, σ_{yy} , can be obtained from the remaining equilibrium condition,

$$\frac{\partial \sigma_{xy}}{\partial x} + \frac{\partial \sigma_{yy}}{\partial y} = 0 \quad (17.45)$$

From Eqs. (17.40) and (17.45), the following expression is obtained:

$$\frac{\partial \sigma_{yy}}{\partial y} = \frac{1}{2I} \left(y^2 - \frac{d^2}{4} \right) \frac{\partial T}{\partial x} \quad (17.46)$$

integration of which gives

$$\sigma_{yy} = \frac{1}{2I} \frac{dT}{dx} \left(\frac{y^3}{3} - \frac{d^2 y}{4} + C \right) \quad (17.47)$$

For $y = -d/2$, $\sigma_{yy} = 0$, and C is given by

$$C = -d^3/12 \quad (17.48)$$

Consequently, Eq. (17.47) can be written as

$$\sigma_{yy} = \frac{1}{2I} \frac{dT}{dx} \left(\frac{y^3}{3} - \frac{d^2 y}{4} - \frac{d^3}{12} \right) \quad (17.49)$$

and

$$\sigma_{yy} \left(\frac{d}{2} \right) = -\frac{1}{12I} \frac{dT}{dx} d^3 - \frac{1}{b} \frac{dT}{dx} \quad (17.50)$$

Note that

$$\frac{\sigma_{yy}}{\sigma_{xx}} = \frac{dT/dx}{Md} \left(\frac{y^3}{3} - \frac{d^2 y}{4} - \frac{d^3}{12} \right) \quad (17.51)$$

so that the values of σ_{yy} are of the order of $(d/L)^2$, L being the total length of the beam. The results expressed by Eqs. (17.44) and (17.51) justify the assumptions made in the elementary theory of beams. On the other hand, if the cross-sectional dimensions of the beams are of the order of their lengths, the shear effects can become important.

The viscoelastic counterpart of these equations can easily be obtained by using the differential operators as in the previous section. However, we postpone the viscoelastic analysis for a forthcoming paragraph.

17.8 SHEAR STRAIN ANALYSIS

After the study of the stresses produced by shear, to obtain the additional deflection we analyze the corresponding strains. The relevant components of the strain are

$$\gamma_{xx} = \frac{\partial u_x}{\partial x} \quad (17.52)$$

and

$$\gamma_{xy} = \frac{1}{2} \left(\frac{\partial u_x}{\partial y} + \frac{\partial u_y}{\partial x} \right) \quad (17.53)$$

On the other hand, the absolute value of the radius of curvature is given by Eq. (17.10),

$$\frac{\partial^2 u_y}{\partial x^2} = \frac{1}{R} \quad (17.54)$$

where u_y is the vertical displacement or deflection. From Eqs. (17.52), (17.53), and (17.54), we obtain

$$\frac{1}{R} = \frac{\partial^2 u_y}{\partial x^2} = 2 \frac{\partial \gamma_{xy}}{\partial x} - \frac{\partial^2 u_x}{\partial x \partial y} = 2 \frac{\partial \gamma_{xy}}{\partial x} - \frac{\partial \gamma_{xx}}{\partial y} \quad (17.55)$$

The strain–stress relationships in the present case are

$$\gamma_{xx} = \frac{\sigma_{xx}}{E} - \frac{\nu}{E} \sigma_{yy} = \frac{M}{EI} y - \frac{\nu}{E} \sigma_{yy}; \quad \gamma_{xy} = \frac{\sigma_{xy}}{2G} \quad (17.56)$$

and taking derivatives of Eq. (17.56), we find

$$\frac{\partial \gamma_{xx}}{\partial y} = \frac{M}{EI} - \frac{\nu}{E} \frac{\partial \sigma_{yy}}{\partial y} = \frac{M}{EI} + \frac{\nu}{E} \frac{\partial \sigma_{xy}}{\partial x}; \quad \frac{\partial \gamma_{xy}}{\partial x} = \frac{1}{2G} \frac{\partial \sigma_{xy}}{\partial y} \quad (17.57)$$

The substitution of Eq. (17.57) into the derivative of Eq. (17.53) leads to the following expression

$$\frac{\partial^2 u_y}{\partial x^2} = -\frac{M}{EI} - \frac{\nu}{E} \frac{\partial \sigma_{xy}}{\partial x} + \frac{1}{G} \frac{\partial \sigma_{xy}}{\partial x} \quad (17.58)$$

Finally, from Eqs. (17.40) and (17.48), we obtain the second-order differential equation

$$\frac{\partial^2 u_y}{\partial x^2} = -\frac{M}{EI} + \left(\frac{1}{G} - \frac{\nu}{E}\right) \left(\frac{1}{2I}\right) \left(\frac{d^2}{4} - y^2\right) \frac{\partial T}{\partial x} \quad (17.59)$$

which can be written as

$$\frac{\partial^2 u_y}{\partial x^2} = -\frac{M}{EI} - \left(\frac{2+\nu}{E}\right) \left(\frac{1}{2I}\right) \left(y^2 - \frac{d^2}{4}\right) \frac{\partial T}{\partial x} \quad (17.60)$$

Where G in Eq. (17.59) has been written in terms of the tensile modulus [$E = 2G(1 + \nu)$; Table 4.1]. Equation (17.60) expresses the additivity of the deformations as the superposition principle indicates. In fact, the second term on the right-hand side represents the additional deflection due to shear

It is worth noting the explicit dependence of both the radius of curvature and the deflection on y [see Eq. (17.60)]. For the neutral line, and assuming a rectangular cross section for which $I = bd^3/12$, we obtain

$$\frac{\partial^2 u_y}{\partial x^2} = -\frac{M}{EI} - \left(\frac{2+\nu}{E}\right) \left(\frac{3}{2bd}\right) \frac{\partial T}{\partial x} \quad (17.61)$$

The double integration of the second term on the right-hand side of this equation gives the deflection due to shear effects u_{ys} as

$$u_{ys} = -\frac{3T\ell}{2bd} \left(\frac{2+\nu}{E}\right) \quad (17.62)$$

The corresponding viscoelastic equations can easily be found by using differential operators for the viscoelastic modulus or alternatively the integral representation. For this purpose the following main conclusions of the preceding analysis should be considered:

1. The cross sections have a parabolic shape after deformation.
2. Owing to the nonuniformity of the shear stress in the section, an effective value A^* for the area of this section, instead of the geometric value $A = bd$, should be used. This is a consequence of considering only the deformation of the neutral fiber of the beam. In this way, A^*/A would be the relationship between the “mean” shear effects and the shear effects in the neutral fiber. Its value is always less than 1. The controversial question is now to decide the real meaning of the word “mean” in the present context. If the “mean” value corresponding to the neutral fiber is taken, then according to Eqs. (17.61) and (17.62), $A^* = 2A/3$. However, this is a naive assumption. A much more convenient approach to

finding the relationship A^*/A is the energetic one. Let us consider the free energy of the deformation per unit of volume, f , which at constant temperature is given by (1, p.8)

$$df = \sigma_{ij} d\gamma_{ij} \quad (17.63)$$

According to Euler's theorem of thermodynamics,

$$\gamma_{ij} \frac{\partial f}{\partial \gamma_{ij}} = 2f \quad (17.64)$$

where the partial derivatives are taken at constant temperature.

This equation in combination with that obtained from Eq. (17.63),

$$\frac{\partial f}{\partial \gamma_{ij}} = \sigma_{ij} \quad (17.65)$$

gives the free energy as

$$f = \frac{1}{2} \sigma_{ij} \gamma_{ij} \quad (17.66)$$

Alternatively, by substituting the strain in Eq. (17.66) as a linear function of the stress, the free energy can be represented as a quadratic function of σ_{ij} . Applying once more the Euler theorem, the corresponding counterpart of Eq. (17.64) in terms of the stress is obtained as

$$\sigma_{ij} \frac{\partial f}{\partial \sigma_{ij}} = 2f \quad (17.67)$$

Comparison of Eqs. (17.66) and (17.67) gives

$$\frac{\partial f}{\partial \sigma_{ij}} = \gamma_{ij} \quad (17.68)$$

Accordingly, the total free energy of the deformed body due to shear effects will be given by

$$F = \int_V f dV \quad (17.69)$$

where dV is the element of volume. By writing the strain tensor in Eq. (17.66) in terms of the stress tensor following procedures described in Chapter 4, the deformation energy can be written as

$$f = \frac{1}{2} \left(\frac{\sigma_{xy}^2}{2G} + \frac{\sigma_{yy}}{E} (\sigma_{yy} - \nu \sigma_{xx}) \right) \quad (17.70)$$

In order to calculate the integral in Eq. (17.69) the values of the stress tensor components in Eq. (17.70) must be substituted for those given in Eqs. (17.40) and (17.49). The limits of the double integral in Eq. (17.69) are 0, L for the variable x and $-d/2$, $d/2$ for the variable y . The terms $\int_0^L \left(\frac{dT}{dx}\right)^2 dx$ and $\int_0^L M \frac{dT}{dx} dx$ appearing in the double integral can be interpreted and calculated as Stieltjes integrals. The values of the first and second integrals are zero and $T^2 L/2$, respectively.

The final result for Eq. (17.69) contains two separate terms: the free energy of the flexion in the absence of shear effects, and the free energy due to the shear effects. The latter is given by the expression

$$F = \frac{3T^2 L}{10bd} \left(\frac{1}{G} - \frac{\nu}{E} \right) \quad (17.71)$$

This equation also reflects the fact that F is a quadratic function of T (the shear force). According to Eq. (17.68), and considering the beam as a whole, the additional deflection due to the shear effects is given by the derivative of Eq. (17.71) expressed by

$$u_y = \frac{\partial F}{\partial T} = \frac{3}{5} \left(\frac{TL}{bd} \right) \left(\frac{1}{G} - \frac{\nu}{E} \right) = \frac{6}{5} \left(\frac{T\ell}{bd} \right) \left(\frac{2+\nu}{E} \right) \quad (17.72)$$

where $\ell (= L/2)$ is the half-length of the beam.

A comparison with Eq. (17.62) indicates that the “effective” section in this case is given by $A^* = 5A/6$. This value seems to be much more convenient than that corresponding to the neutral line.

In a 1975 review (4), Kaneko concluded what the best value for A^*/A is $(5 + 5\nu)/(6 + 5\nu)$. This value is only slightly higher than that obtained from energetic considerations. For this reason we adopt for the additional deflection a corrected version of Eq. (17.61), given by

$$\frac{\partial^2 u_y}{\partial x^2} = -\frac{M}{EI} - \left(\frac{2+\nu}{E} \right) \left(\frac{1}{\kappa bd} \right) \frac{dT}{dx} \quad (17.73)$$

where κ is A^*/A . Then the total deflection is obtained by addition of the bending and shear contributions. For a rectangular cross section double-clamped beam loaded at its midpoint by a force P , $T = P/2$. By integrating Eq. (17.73), taking into account the boundary conditions $u_y = \dot{u}_y = 0$ at $x = \pm d/2$ for a double-clamped beam, the total deflection is found to be

$$u_y = u_{yb} + u_{ys} = \frac{P\ell^3}{24EI} + \frac{2+\nu}{E} \left(\frac{1}{\kappa bd} \right) \left(\frac{P\ell}{4} \right) = \frac{P\ell^3}{24EI} \left[1 + \frac{1}{\kappa} (\nu + 2) \left(\frac{d}{\ell} \right)^2 \right] \quad (17.74)$$

where u_{yb} and u_{ys} are, respectively, the values of the bending and shear deflections. For $\kappa = 5/6$,

$$u_y = \frac{P\ell^3}{24IE} \left[1 + \frac{6}{5} (2 + \nu) \left(\frac{d}{\ell} \right)^2 \right] \quad (17.75)$$

Alternatively, by assuming $\kappa = A^*/A = (5 + 5\nu)/(6 + 5\nu)$, we obtain

$$u_y = \frac{P\ell^3}{24IE} \left[1 + \frac{(6 + 5\nu)(2 + \nu)}{5(1 + \nu)} \left(\frac{d}{\ell} \right)^2 \right] \quad (17.76)$$

For Poisson ratio values of 0.3, 0.4, and 0.5, the following shear corrections are obtained from these formulas:

	$\nu = 0.3$	$\nu = 0.4$	$\nu = 0.5$
$\frac{6}{5}(2 + \nu)$	2.76	2.88	3
$\frac{(6 + 5\nu)(2 + \nu)}{5(1 + \nu)}$	2.65	2.74	2.83

As we can see, the differences between the values calculated for the two proposed expressions for A^*/A are not significant. On the other hand, uncertainties in the Poisson ratio are not critical for the calculations.

Equation (17.76) can be written as

$$\frac{P}{u_y} = KE \quad (17.77)$$

where

$$K = 2b \left(\frac{d}{\ell} \right)^3 \left[1 + \frac{6}{5} (2 + \nu) \left(\frac{d}{\ell} \right)^2 \right]^{-1} \quad (17.78)$$

or

$$K = 2b \left(\frac{d}{\ell} \right)^3 \left[1 + \frac{(6 + 5\nu)(2 + \nu)}{5(1 + \nu)} \left(\frac{d}{\ell} \right)^2 \right]^{-1} \quad (17.79)$$

depending on the value assumed for A^*/A .

It is worth noting that the so-called geometrical factor that affects the determination of the modulus E does not have a pure geometric character since it depends through ν on the material properties.

17.9 VISCOELASTIC BEAMS

Until now, we have considered only elastic beams. To generalize the elastic results to the viscoelastic case is relatively easy. Actually, the correspondence principle (5) indicates that if E tends to E^* then G approaches G^* , where the asterisk indicates a complex magnitude. Then, according to Eqs. (17.75) and (17.78), we can write

$$E_r^* = E_a^* \left[1 + \frac{6}{5}(2 + \nu^*) \left(\frac{d}{\ell} \right)^2 \right] \quad (17.80)$$

where $\nu^* = (E_a^*/2G_a^*) - 1$, and the subscripts r and a refer to the real (corrected for shear) and apparent (uncorrected) values of the complex tensile modulus. By separating real and imaginary parts, after some mathematical handling, we find

$$E_r' = E_a' \left[1 + \frac{6}{5} \left(\frac{d}{\ell} \right)^2 \right] + \frac{3}{5} \left(\frac{d}{\ell} \right)^2 \left(\frac{(E_a'^2 - E_a''^2)G_a' + 2E_a'E_a''G_a''}{E_a'(G_a'^2 + G_a''^2)} \right) \quad (17.81a)$$

$$E_r'' = E_a'' \left[1 + \frac{6}{5} \left(\frac{d}{\ell} \right)^2 \right] + \frac{3}{5} \left(\frac{d}{\ell} \right)^2 \left(\frac{2E_a'E_a''G_a' - (E_a'^2 - E_a''^2)G_a''}{E_a''(G_a'^2 + G_a''^2)} \right) \quad (17.81b)$$

In the glassy zone, where the loss is small, Eq. (17.81a) can be simplified to

$$E_r' \cong E_a' \left[1 + \frac{6}{5} \left(\frac{d}{\ell} \right)^2 \left(1 + \frac{E_a'}{2G_a'} \right) \right] \quad (17.82)$$

The same expression is obtained for the relationship between E_r'' and E_a'' . These results lead to $\tan \delta_E \cong \tan \delta_{Ea}$; in other words, $\tan \delta$ is much less sensitive than the moduli to the corrections for shear stresses. The corrections in the moduli depend on the d/ℓ ratio. For $d/\ell = 0.1$, the correction is about 3%, of the order of the experimental error, whereas for $d/l = 0.2$, the

correction is about 12%, which cannot be neglected. Note that in the evaluation of the errors it is assumed that $E'_a \cong 3G'_a$.

When a beam is loaded at its midpoint, the sections tend to bend. Symmetry considerations indicate that the central section must remain plane. However, since a discontinuous change in the sections adjacent to the central one is not possible, a progressive bending of the cross sections starting from the central one is produced, so that only at a certain distance from the center are the values predicted by theory expected. In other words, in the central section where the load is applied, the shear forces are smaller than those predicted by theory. Consequently, the deflection will also be smaller. The distribution of stresses in a beam under the action of a concentrated load is an important problem addressed by several authors (see Ref. 6), who concluded that the modulus calculated by means of Eq. (17.82) is overestimated by about 25–30%.

17.10 TRANSVERSE VIBRATIONS IN VISCOELASTIC BEAMS

Vibrations of beams frequently occur in engineering applications (7). In this context, the use of polymers in the design of better damping structures has become an important topic of structural mechanics (8). On the other hand, vibrations can be artificially produced in order to study the viscoelastic properties of polymers and other materials. Transverse vibrations in viscoelastic beams are, in this respect, a particular case of wave propagation, and the inherent study of this type of waves is closely related to the physical situation existing in several experimental devices used in the measurement of the viscoelastic properties of polymeric materials. This section is mainly focused on the study of the vibrations of clamped rods, though this study can easily be generalized to other cases. We shall proceed by steps, considering first slender beams, in which shear and inertial effects are negligible. Afterwards, a more general theory, including rotary inertia and shear deformations, is considered for both free vibrations and sinusoidal excitations.

17.10.1 Elementary Theory of Free Vibrations

As has been shown in preceding paragraphs, the classical theory of Euler and Bernoulli describing transverse vibrations in elastic beams can be generalized for the viscoelastic case. According to Eq. (17.13b), and based on the same grounds as Eq. (16.6b), we can write

$$I \int_0^{\infty} E(t - \theta) \frac{\partial^3 u_y}{\partial x^2 \partial \theta} d\theta = -M \quad (17.83)$$

where M is the flexural moment, E the viscoelastic modulus, and I the polar moment of inertia of the transverse section. The corresponding equation of motion is obtained by equalizing the second derivative of the moment, that is, the force, with the inertial term:

$$\frac{\partial^2 M}{\partial x^2} = \rho A \frac{\partial^2 u_y}{\partial t^2} \quad (17.84)$$

where the transverse section A and the mass density ρ are assumed to be constant. By combining Eqs. (17.83) and (17.84) we obtain

$$I \int_0^{\infty} E(t - \theta) \frac{\partial^5 u_y}{\partial x^4 \partial \theta} d\theta + \rho A \frac{\partial^2 u_y}{\partial t^2} = 0 \quad (17.85)$$

Free vibration, the motion that persists after the excitation is removed, is governed by Eq. (17.85), in which the applied transverse force has been made zero. Let us assume a solution of the form $u_y(x, t) = f(x) \exp(i\omega t)$, where $f(x)$ specifies the lateral displacement and ω is the angular frequency of the motion. For low loss viscoelastic materials, the free vibrations can be assumed to be quasi-harmonic, and therefore the complex modulus in the equation of motion can be used. The Laplace transform of Eq. (17.85) gives

$$Is\bar{E}(s)f^{\text{IV}}(x, s) = -\rho As^2 f(x) \quad (17.86)$$

or alternatively,

$$\mathbf{f}^{\text{IV}}(x) = \lambda^4 \mathbf{f}(x) \quad (17.87)$$

where

$$\lambda^4 = -\frac{\rho As}{I\bar{E}(s)} \quad (17.88)$$

The most general solution of Eq. (17.87) is given by

$$\mathbf{f}(x) = C_1 \sin \lambda x + C_2 \cos \lambda x + C_3 \sinh \lambda x + C_4 \cosh \lambda x \quad (17.89)$$

where C_i are constants to be determined according to the boundary conditions. For a double-clamped beam, these conditions are

$$u_y = u'_y = 0 \quad \text{for } x = 0, 2\ell \quad (17.90)$$

Equation (17.89) has the trivial solution $C_1 = C_2 = C_3 = C_4 = 0$, except for the values of λ satisfying the secular equation

$$\cos 2\lambda\ell \cosh 2\lambda\ell = 1 \quad (17.91)$$

This equation is obtained by equalizing to zero the determinant formed by the coefficients $C_1, C_2, C_3,$ and C_4 in Eq. (17.89) under the four boundary conditions given by Eq. (17.90). This eigenvalue equation has infinite solutions for $\lambda\ell$. The six first values are given in the following table.

n	0	1	2	3	4	5
$\lambda_n\ell$	0	2.365	3.9265	5.498	7.0685	8.6395

In general,

$$\lambda_n\ell \cong (2n+1)\frac{\pi}{4} \quad \text{for } n > 5 \quad (17.92)$$

Each eigenvalue determines, through Eq. (17.91), a natural frequency of free vibration of the beam, while Eq. (17.89) gives the mode shape function $\mathbf{f}_n(x)$.

From an experimental point of view, knowledge of the modes is important because it makes it possible to optimize the location of the detector and supports in the experimental devices in order to minimize effects due to spurious stiffness, inertia, or damping (5, p. 90) (see also Chap. 7). By making $s = -\lambda + i\omega$, as corresponds to a free vibration experiment, expressions for the real and imaginary parts of the dynamic modulus and for the loss tangent at the resonance frequency $\omega = \omega_r$ can be obtained. The resulting equations are

$$E' = \frac{\rho AL^4}{I(\lambda_n\ell)^4} (\omega_r^2 - \lambda^2) \quad (17.93)$$

$$E'' = \frac{2\rho AL^4 \omega_r \lambda}{I(\lambda_n\ell)^4} \quad (17.94)$$

and

$$\tan \delta = \frac{2\omega_r \lambda}{\omega_r^2 - \lambda^2} \quad (17.95)$$

and for low damping,

$$E' = \frac{\rho A \omega_r^2}{I \lambda_n^4} \quad (17.96)$$

and

$$\tan \delta = \frac{2\lambda}{\omega_r} \quad (17.97)$$

For a beam of circular cross sections $I = \pi r^4/12$, where r is the radius of the cross section. According to Eq. (17.96), the storage modulus can be written as

$$E' = \frac{8\pi}{(\lambda_n \ell)^4} \left(\frac{L}{r}\right)^3 \left(\frac{m}{r}\right) f_r^2 \quad (17.98)$$

where $f_r = \omega_r/2\pi$ and $m = \rho AL$ is the mass of the beam.

17.10.2 Elementary Theory of Forced Vibrations

In the case of forced vibrations, a term corresponding to the external forces must be added to the motion equation, giving

$$I \int_0^\infty E(t - \theta) \frac{\partial^5 u_y}{\partial x^4 \partial \theta} d\theta + \rho A \frac{\partial^2 u_y}{\partial t^2} = f(x)g(t) \quad (17.99)$$

where the separation of variables method has been used as it corresponds to a harmonic excitation. A convenient method to solve this equation (9) is based on the double application of the Laplace transform, first with respect to time and then with respect to the x variable, that is,

$$t \xrightarrow{\mathcal{L}} s; \quad x \xrightarrow{\mathcal{L}} q$$

Thus, the following equation is obtained:

$$Is\bar{E}(s) \frac{\partial^4 \bar{u}_y(s, x)}{\partial x^4} + s^2 \rho A \bar{u}_y(s, x) = f(x)\bar{g}(s) \quad (17.100)$$

where

$$u_y(0, x) = \dot{u}_y(0, x) = 0 \quad (17.101)$$

Taking the Laplace transform with respect to x , Eq. (17.100) becomes

$$Is\bar{E}(s)[q^4\bar{u}_y(s, q) - q^3\bar{u}_y(s, 0) - q^2\bar{u}'_y(s, 0) - q\bar{u}''_y(s, 0) - \bar{u}'''_y(s, 0)] + \rho As^2\bar{u}_y(s, q) = \bar{f}(q)\bar{g}(s) \quad (17.102)$$

from which

$$\bar{u}_y(q, s) = \frac{\bar{f}(q)\bar{g}(s) + Is\bar{E}(s)[q\bar{u}''_y(0, s) - \bar{u}'''_y(0, s)]}{Is\bar{E}(s)q^4 + \rho As^2} \quad (17.103)$$

Let us consider a sinusoidal excitation at $x = \ell'$:

$$F\delta(x - \ell') \sin \omega t \quad (17.104)$$

where δ is the impulse function. Consequently, $\delta = 0$ for all $x \neq \ell'$ and

$$\bar{f}(q) = Fe^{-q\ell'}; \quad \bar{g}(s) = \frac{\omega}{s^2 + \omega^2} \quad (17.105)$$

After some rearrangements, Eq. (17.103) becomes

$$\bar{u}_y(q, s) = \frac{Fe^{-q\ell'} \frac{\omega}{s^2 + \omega^2} \left(\frac{1}{Is\bar{E}(s)} \right) + [q\bar{u}''_y(0, s) + \bar{u}'''_y(0, s)]}{q^4 - \lambda^4} \quad (17.106)$$

where

$$\lambda^4 = -\frac{\rho As}{I\bar{E}(s)} \quad (17.107)$$

The inverse Laplace of Eq. (17.106) with respect to x is obtained by making $q^4 - \lambda^4 = (q^2 - \lambda^2)(q^2 + \lambda^2)$. The pertinent result is

$$\bar{u}_y(x, s) = \frac{1}{2\lambda^2} \left[\frac{F\omega}{s^2 + \omega^2} \left(\frac{1}{s\bar{E}(s)I\lambda} \right) [\sinh \lambda(x - \ell') - \sin \lambda(x - \ell')] + \bar{u}''_y(0, s)(\cosh \lambda x - \cos \lambda x) + \frac{1}{\lambda} \bar{u}'''_y(0, s)(\sinh \lambda x - \sin \lambda x) \right] \quad (17.108)$$

which is valid for $\ell \leq x \leq 2\ell$. For $0 \leq x \leq \ell$, the solution is found from the symmetry of the boundary conditions. To evaluate $\bar{u}''_y(0, s)$ and $\bar{u}'''_y(0, s)$ we

make $\bar{u}_y(2\ell, s) = \dot{\bar{u}}_y(2\ell, s) = 0$, and the following system of equations is obtained:

$$\lambda \bar{u}_y''(0, s)(\cosh 2\lambda\ell - \cos 2\lambda\ell) + \bar{u}'''_y(0, s)(\sinh 2\lambda\ell - \sin 2\lambda\ell) = \bar{\alpha}[\sin \lambda(2\ell - \ell') - \sinh \lambda(2\ell - \ell')] \quad (17.109a)$$

$$\lambda \bar{u}_y''(0, s)(\sinh 2\lambda\ell + \sin 2\lambda\ell) + \bar{u}'''_y(0, s)(\cosh 2\lambda\ell - \cos 2\lambda\ell) = \bar{\alpha}[\cos \lambda(2\ell - \ell') - \cosh \lambda(2\ell - \ell')] \quad (17.109b)$$

where

$$\bar{\alpha} = F \frac{\omega}{(\omega^2 + s^2)Is\bar{E}(s)} \quad (17.110)$$

Substituting the expressions obtained for $\bar{u}''(0, s)$ and $\bar{u}'''_y(0, s)$ from Eqs. (17.109) into Eq. (17.108) gives

$$\begin{aligned} \bar{u}_y(x, s) = & \frac{1}{4\lambda^3} \left(\frac{F\omega}{s^2 + \omega^2} \right) \left(\frac{1}{s\bar{E}(s)I} \right) \{ 2[\sinh \lambda(x - \ell') - \sin \lambda(x - \ell')] \\ & + \frac{\cosh \lambda x - \cos \lambda x}{1 - \cosh 2\lambda\ell \cos 2\lambda\ell} [\sinh \lambda\ell' + \sin \lambda\ell' + \sin \lambda(2\ell - \ell') \cosh 2\lambda\ell \\ & - \cos \lambda(2\ell - \ell') \sinh 2\lambda\ell + \sinh \lambda(2\ell - \ell') \cos 2\lambda\ell - \cosh \lambda(2\ell - \ell') \sin 2\lambda\ell] \\ & + \frac{\sinh \lambda x - \sin \lambda x}{1 - \cosh 2\lambda\ell \cos 2\lambda\ell} [-\cosh \lambda\ell' - \cos \lambda\ell' - \sin \lambda(2\ell - \ell') \sinh 2\lambda\ell \\ & + \cos \lambda(2\ell - \ell') \cosh 2\lambda\ell + \sinh \lambda(2\ell - \ell') \sin 2\lambda\ell \\ & + \cosh \lambda(2\ell - \ell') \cos 2\lambda\ell] \} \end{aligned} \quad (17.111)$$

In order to handle Eq. (17.111), the trigonometric and hyperbolic functions can be expanded in series by assuming that the arguments of these functions are smaller than unity. According to that,

$$\begin{aligned} \sinh x &= x + \frac{x^3}{3!} + \frac{x^5}{5!} + \dots; & \cosh x &= 1 + \frac{x^2}{2!} + \frac{x^4}{4!} + \dots \\ \sin x &= x - \frac{x^3}{3!} + \frac{x^5}{5!} - \dots; & \cos x &= 1 - \frac{x^2}{2!} + \frac{x^4}{4!} - \dots \end{aligned} \quad (17.112)$$

It is further assumed that the excitation is applied at the center of the beam, that is, $\ell' = \ell$. In this way, after long but not difficult calculations, the following expression for the deflection is obtained:

$$\bar{u}_y(x, s) = \frac{F\omega}{24Is\bar{E}(s)(\omega^2 + s^2)} [4(x - \ell)^3 + 3x^2\ell - 2x^3] \quad (17.113)$$

In the center of the beam $x = \ell$, and Eq. (17.113) can be written as

$$\bar{u}_y(\ell, s) = \frac{1}{24} \left(\frac{F\omega}{s^2 + \omega^2} \right) \left(\frac{\ell^3}{s\bar{E}(s)I} \right) = \frac{1}{192} \left(\frac{F\omega}{s^2 + \omega^2} \right) \left(\frac{(2\ell)^3}{s\bar{E}(s)I} \right) \quad (17.114)$$

To obtain a closed solution it is necessary to assume a viscoelastic model. For example, if a standard solid model is adopted, the following value for the dynamic modulus is found:

$$s\bar{E}(s) = E_1 + (E_0 - E_1) \left(\frac{s\tau}{1 + s\tau} \right) = \frac{E_1 + E_0s\tau}{1 + s\tau} \quad (17.115)$$

By making use of the decomposition

$$\frac{1 + \tau s}{(s^2 + \omega^2)(1 + \tau' s)} = \frac{As + B}{s^2 + \omega^2} + \frac{C}{1 + \tau' s} \quad (17.116)$$

where

$$A = \frac{\tau - \tau'}{1 + \omega^2\tau'^2}; \quad B = \frac{1 + \omega^2\tau'\tau}{1 + \omega^2\tau'^2}; \quad C = -\frac{\tau'(\tau - \tau')}{1 + \omega^2\tau'^2} \quad (17.117)$$

and after Laplace inversion of Eq. (17.113), we find

$$u_y(x, t) = \frac{F\omega[4(x - \ell)^3 + 3x^2\ell - 2x^3]}{24I(E_1^2 + E_0^2\omega^2\tau^2)} (E_0 - E_1) \\ \times \tau \left[\exp \left[-\frac{E_1}{E_0} \left(\frac{t}{\tau} \right) \right] - \left[1 + \left(\frac{1 + \omega^2\tau^2(E_0/E_1)}{\omega\tau[1 - (E_0/E_1)]} \right)^2 \right]^{1/2} \sin(\omega t + \phi) \right] \quad (17.118)$$

where

$$\phi = \arctan \frac{\omega\tau(1 - E_0/E_1)}{1 + \omega^2\tau^2(E_0/E_1)} \quad (17.119)$$

Equation (17.118) suggests that the viscoelastic response of the material is the sum of a sinusoidal wave delayed with respect to the input wave and a damped exponential. This last component corresponds to the simple three-element standard model governed by a single relaxation time. For a distribution of relaxation times, the response obtained would include a sum of such exponentials.

17.10.3 Free Vibrations with Rotary Inertia and Shear Stress

As mentioned above, when the transverse dimensions of the beam are of the same order of magnitude as the length, the simple beam theory must be corrected to introduce the effects of the shear stresses, deformations, and rotary inertia. The theory becomes inadequate for the high frequency modes and for highly anisotropic materials, where large errors can be produced by neglecting shear deformations. This problem was addressed by Timoshenko et al. (7) for the elastic case starting from the balance equations of the respective moments and transverse forces on a beam element. Here the main lines of Timoshenko et al.'s approach are followed to solve the viscoelastic counterpart problem.

From Figure 17.7, the moment with respect to an axis normal to the xy plane that passes through the center of gravity of the element of beam under consideration is given by

$$-\rho I \frac{\partial^3 u_{yb}}{\partial x \partial t^2} dx = \frac{\partial M}{\partial x} dx \quad (17.120)$$

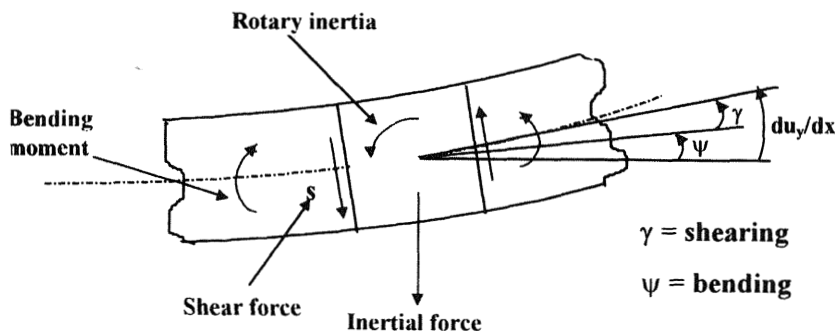


Figure 17.7 Sketch of a section of a beam showing the bending moment, the shear force, the rotary inertia, the inertial force, and the curvature due to bending and shearing.

where $\partial^2 u_{yb}/\partial t^2$ is the acceleration and the subscript b denotes bending. In the absence of external forces, this effect must be added to that due to pure flexion, so Eq. (17.85) becomes

$$I \int_0^\infty E(t-\theta) \frac{\partial^5 u_y}{\partial x^4 \partial \theta} d\theta + \rho A \frac{\partial^2 u_y}{\partial t^2} - \rho I \frac{\partial^4 u_y}{\partial x^2 \partial t^2} = 0 \quad (17.121)$$

Moreover, owing to the shear forces, the slope of the neutral fiber of the beam will be greater than that predicted by the Euler–Bernoulli theory (see Fig. 17.7). For the elastic case, these shear forces are given by

$$\frac{du_{ys}}{\partial x} = \frac{T}{A^*G} \quad (17.122)$$

where the subscript s denotes shear. By taking into account that the total deflection y is the sum of the bending y_B , and shear, y_s , deflections, Eq. (17.122) can be written as

$$T = \left(\frac{du_y}{dx} - \frac{du_{yb}}{dx} \right) GA^* \quad (17.123)$$

For the viscoelastic case, Eq. (17.123) becomes

$$T = A^* \int_0^\infty G(t-\theta) \left(\frac{\partial^2 u_y}{\partial x \partial \theta} - \frac{\partial \psi}{\partial \theta} \right) d\theta \quad (17.124)$$

where

$$\frac{du_{yb}}{dx} = \psi \quad (17.125)$$

The equation for the bending moment is

$$M = -I \int_0^\infty E(t-\theta) \frac{\partial^2 \psi}{\partial x \partial \theta} d\theta \quad (17.126a)$$

or alternatively,

$$M = -I \int_0^\infty E(t-\theta) \frac{\partial^3 u_{yb}}{\partial^2 x \partial \theta} d\theta \quad (17.126b)$$

On the other hand, the differential equations for the translation and rotation of the beam are

$$-\frac{\partial M}{\partial x} + T = \rho I \frac{\partial^2 \psi}{\partial t^2} \quad (17.127)$$

and

$$-\frac{\partial T}{\partial x} = \rho A \frac{\partial^2 u_y}{\partial t^2} \quad (17.128)$$

Then, after replacing M and T by their respective values given by Eqs. (17.124) and (17.126b) and some mathematical handling, we obtain the following equations for the deflections u_{yb} and u_y :

$$I \int_0^\infty E(t-\theta) \frac{\partial^4 u_{yb}}{\partial x^3 \partial t} d\theta + A^* \int_0^\infty G(t-\theta) \left(\frac{\partial^2 u_y}{\partial x \partial \theta} - \frac{\partial^2 u_{yb}}{\partial x \partial \theta} \right) d\theta = \rho I \frac{\partial^3 u_{yb}}{\partial x \partial t^2} \quad (17.129)$$

$$\rho A \frac{\partial^2 u_y}{\partial t^2} = A^* \int_0^\infty G(t-\theta) \left(\frac{\partial^3 u_y}{\partial x^2 \partial \theta} - \frac{\partial^3 u_{yb}}{\partial x^2 \partial \theta} \right) d\theta \quad (17.130)$$

The total deflection, u_y , can be obtained by eliminating u_{yb} between these two equations after taking Laplace transforms with the boundary conditions given by

$$u_y(x, 0) = \dot{u}_y(x, 0) = 0; \quad u_{yb}(x, 0) = \dot{u}_{yb}(x, 0) = 0 \quad (17.131)$$

In this way, we find

$$I \bar{E}(s) \bar{u}_y^{IV}(s, x) - \bar{u}_y''(s, x) \left(1 + \frac{A \bar{E}(s)}{A^* \bar{G}(s)} \right) \rho I s + \bar{u}_y(s, x) \left(1 + \frac{\rho s I}{A^* \bar{G}(s)} \right) A \rho s = 0 \quad (17.132)$$

A similar equation can be written for u_{yb} . These are the viscoelastic equations corresponding to the elastic ones in the elastic beam theory (7).

The classical solution of these equations (10) requires obtaining the secular equation for the eigenvalues by means of suitable boundary conditions. For that purpose, it is convenient to use the reduced variable $\xi = x/L$, where L is the total length of the beam. Accordingly,

$$Y^{IV} + Y'' b^2 (r^2 + t^2) - b^2 (1 - b^2 r^2 t^2) Y = 0 \quad (17.133)$$

where Y is a function of s and ξ , while the parameters b , r , and t are given by

$$b^2 = -\frac{\rho A s L^4}{\bar{E}(s) I}; \quad r^2 = \frac{I}{A L^2}; \quad t^2 = \frac{\bar{E}(s) I}{A^* \bar{G}(s) L^2} \quad (17.134)$$

An expression similar to Eq. (17.133) is obtained for Y_B , where Y_B is the new variable corresponding to u_{yb} after the aforementioned change of variable $x \rightarrow \xi$ has been made. For double-clamped bars the following boundary conditions hold:

$$\left. \begin{array}{l} Y = 0, \quad Y_B = 0 \\ \dot{Y} = 0, \quad \dot{Y}_B = 0 \end{array} \right\} \text{for } \xi = 0 \text{ and } 1 \quad (17.135)$$

The roots of the characteristic equation corresponding to Eq. (17.133) are given by

$$\pm \frac{b}{\sqrt{2}} \left[-(r^2 + t^2) + \left((r^2 - t^2)^2 + \frac{4}{b^2} \right)^{1/2} \right]^{1/2} = \pm b\alpha \quad (17.136a)$$

$$\pm \frac{b}{\sqrt{2}} i \left[(r^2 + t^2) + \left((r^2 - t^2)^2 + \frac{4}{b^2} \right)^{1/2} \right]^{1/2} = \pm b\beta i \quad (17.136b)$$

where

$$\left((r^2 - t^2)^2 + \frac{4}{b^2} \right)^{1/2} > r^2 + t^2 \quad (17.137)$$

The general solution of the fourth-order differential equations (17.133) will be given, respectively, by

$$Y = C_1 \cosh \alpha b \xi + C_2 \sinh \alpha b \xi + C_3 \cos \beta b \xi + C_4 \sin \beta b \xi \quad (17.138a)$$

$$Y_B = C'_1 \sinh \alpha b \xi + C'_2 \cosh \alpha b \xi + C'_3 \sin \beta b \xi + C'_4 \cos \beta b \xi \quad (17.138b)$$

According to the boundary conditions, the constants appearing in these equations are not independent. In fact, they must fulfill the following conditions:

$$Y(0) = C_1 + C_3 = 0 \quad (17.139a)$$

$$Y(1) = C_1 \cosh b\alpha + C_2 \sinh b\alpha + C_3 \cos b\beta + C_4 \sin b\beta = 0 \quad (17.139b)$$

$$Y_B(0) = C'_2 + C'_4 = 0 \quad (17.139c)$$

$$Y_B(1) = C'_1 \sinh b\alpha + C'_2 \cosh b\alpha + C'_3 \sin b\beta + C'_4 \cos b\beta = 0 \quad (17.139d)$$

where

$$C_1 = \frac{L}{b\alpha} [1 - b^2 t^2 (\alpha^2 + r^2)] C'_1; \quad C'_1 = \frac{b}{L} \left(\frac{\alpha^2 + t^2}{\alpha} \right) C_1 \quad (17.140a)$$

$$C_2 = \frac{L}{b\alpha} [1 - b^2 t^2 (\alpha^2 + r^2)] C'_2; \quad C'_2 = \frac{b}{L} \left(\frac{\alpha^2 + t^2}{\alpha} \right) C_2 \quad (17.140b)$$

$$C_3 = \frac{L}{b\beta} [1 + b^2 t^2 (\beta^2 - r^2)] C'_3; \quad C'_3 = -\frac{b}{L} \left(\frac{\beta^2 - t^2}{\beta} \right) C_3 \quad (17.140c)$$

$$C_4 = \frac{L}{b\beta} [1 + b^2 t^2 (\beta^2 + r^2)] C'_4; \quad C'_4 = \frac{b}{L} \left(\frac{\beta^2 + t^2}{\beta} \right) C_4 \quad (17.140d)$$

To obtain solutions different from the trivial ones for Eq. (17.139), the following characteristic equation must be fulfilled:

$$1 - \cosh b\alpha \cos b\beta + \frac{b}{2(1 - b^2 r^2 t^2)^{1/2}} [b^2 t^2 (r^2 - t^2)^2 + (3t^2 - r^2)] \sinh b\alpha \sin b\beta = 0 \quad (17.141)$$

A procedure similar to that outlined in the elementary theory of flexion allows the determination of the normal modes. However, this method is not only tedious but also has the inconvenience that some terms in the secular equation depend explicitly on the material properties, that is, on the modulus. Instead of developing a solution of Eq. (17.132) in the classical way, it is more convenient to establish a method based on comparison of the apparent and real viscoelastic moduli (11,12). The basic idea is to compare Eq. (17.132) with the Laplace transform of Eq. (17.85), which is

$$I\bar{E}_A(s)\bar{u}^{IV}_y(s, x) = -\rho A s \bar{u}_y(s, x) \quad (17.142)$$

where \bar{E}_A is the apparent modulus, that is, the modulus without taking into account the shear and rotatory inertial effects. By using the reduced length $\xi = x/L$ as a variable, Eq. (17.142) can be written as

$$Y^{IV} - a^2 Y = 0 \quad (17.143)$$

where

$$a^2 = -\rho A s L^4 / I\bar{E}_A(s) \quad (17.144)$$

The expression $\cos a^{1/2} \cosh a^{1/2} = 1$ is the characteristic equation whose eigenvalues have previously been obtained.

By assuming that the mode shapes are approximately sinusoidal, as occurs in the absence of shear and rotary inertia, the new solution proposed for Eq. (17.143) is

$$Y = C \cos \omega t \sin a^{1/2} \xi \quad (17.145)$$

where a is given by Eq. (17.144). Substituting Eq. (17.145) in Eq. (17.133), we obtain

$$a^2 - ab^2(r^2 + t^2) - b^2(1 - b^2r^2t^2) = 0 \quad (17.146)$$

By replacing b^2 by $-\rho AsL^4/\bar{E}(s)I$ in such a way that $\bar{E}(s)/\bar{E}_A(s) = a^2/b^2$ and replacing r^2 and t^2 by their respective expressions given in Eqs. (17.134), we obtain the equation

$$\bar{E}(s) = \bar{E}_A(s) \left[1 + \frac{aI}{AL^2} \left(1 + \frac{\bar{E}(s)}{\kappa\bar{G}(s)} \right) - \left(\frac{aI}{AL^2} \right)^2 \left(\frac{\bar{E}(s)}{\kappa\bar{G}(s)} \right) \right] \quad (17.147)$$

where $\kappa = A^*/A$, as defined before. From this equation, the actual value of the dynamic modulus is obtained as

$$\bar{E}(s) = \bar{E}_A(s) \frac{1 + \frac{aI}{AL^2} - \left(\frac{aI}{AL^2} \right)^2 \left(\frac{\bar{E}_A(s)}{\kappa\bar{G}(s)} \right)}{1 - \frac{aI}{AL^2} \left(\frac{\bar{E}_A(s)}{\kappa\bar{G}(s)} \right)} \quad (17.148)$$

For a rectangular beam of thickness d , the polar moment of inertia is given by

$$\frac{I}{AL^2} = \frac{1}{12} \left(\frac{d}{L} \right)^2 \quad (17.149)$$

This equation in combination with Eq. (17.148) finally gives

$$\bar{E}(s) = \bar{E}_A(s) \frac{1 + \frac{a}{12} \left(\frac{d}{L} \right)^2 - \left[\frac{a}{12} \left(\frac{d}{L} \right)^2 \right]^2 \left(\frac{\bar{E}_A(s)}{\kappa\bar{G}(s)} \right)}{1 - \frac{a}{12} \left(\frac{d}{L} \right)^2 \left(\frac{\bar{E}_A(s)}{\kappa\bar{G}(s)} \right)} \quad (17.150)$$

or, equivalently,

$$\bar{E}(s) = \bar{E}_A(s) \left(1 + \frac{a}{12} \left(\frac{d}{L} \right)^2 + \frac{\frac{a}{12} \left(\frac{d}{L} \right)^2 \left(\frac{\bar{E}_A(s)}{\kappa \bar{G}(s)} \right)}{1 - \frac{a}{12} \left(\frac{d}{L} \right)^2 \left(\frac{\bar{E}_A(s)}{\kappa \bar{G}(s)} \right)} \right) \quad (17.151)$$

This expression can be written approximately as

$$\bar{E}(s) \cong \bar{E}_A(s) \left[1 + \frac{a}{12} \left(\frac{d}{L} \right)^2 \left(1 + \frac{\bar{E}_A(s)}{\kappa \bar{G}(s)} \right) \right] \quad (17.152)$$

From these results it is clear that the calculated modulus without inertial and shear corrections is smaller than the actual one. These corrections, as mentioned above, depend not only on the geometrical dimensions of the sample but also on its material properties.

17.10.4 Forced Vibrations with Inertial and Shear Effects

Let us consider now the more general case involving forced vibrations together with rotatory inertia and shear stresses. Under harmonic excitation, Eqs. (17.129) and (17.130) must be modified to introduce the external excitation as follows.

$$I \int_0^\infty E(t-\theta) \frac{\partial^4 u_{yb}}{\partial x^3 \partial \theta} d\theta + A^* \int_0^\infty G(t-\theta) \left(\frac{\partial^2 u_y}{\partial x \partial \theta} - \frac{\partial^2 u_{yb}}{\partial x \partial \theta} \right) d\theta = \rho I \frac{\partial^3 u_{yb}}{\partial x \partial t^2} \quad (17.153)$$

$$\rho A \frac{\partial^2 u_y}{\partial t^2} - A^* \int_0^\infty G(t-\theta) \left(\frac{\partial^3 u_y}{\partial x^2 \partial \theta} - \frac{\partial^3 u_{yb}}{\partial x^2 \partial \theta} \right) d\theta = F(x, t) \quad (17.154)$$

where $F(x, t) = f(x)g(t) = F_0 \delta(x - x_0) \sin \omega t$ is the applied external force and x_0 is the coordinate of the point where the force is applied. Following the main lines of the method developed for free vibrations, after taking the Laplace transform and using the reduced length variable ξ , one obtains

$$\begin{aligned} Y^{IV} + b^2(r^2 + t^2)Y'' - b^2Y(1 - b^2r^2t^2)Y \\ = [F(\xi)g(s)(1 - b^2r^2t^2) - F''(\xi)g(s)t^2] \frac{L^4}{IE^*} \end{aligned} \quad (17.155)$$

where $g(s)$ is the Laplace transform of the sine function. Laplace transforms of the delta function and its second derivative;

$$\bar{F}(\xi) = F\mathcal{L}_\xi\delta(x - x_0) = \frac{F_0}{L}\exp(-q\xi_0) \quad (17.156a)$$

$$\bar{F}''(\xi) = F_0\mathcal{L}_\xi\delta''(x - x_0) = \frac{F_0}{L}q^2\exp(-q\xi_0) \quad (17.156b)$$

where $\xi_0 = x_0/L$, together with the boundary conditions given by

$$\bar{Y}(s, 0) = \bar{Y}'(s, 0) = 0 \quad (17.157)$$

lead Eq. (17.155) to

$$\bar{Y}(s, q) = \frac{L^3}{Is\bar{E}(s)} \left(\frac{\frac{F_0\omega}{s^2+\omega^2}\exp(-q\xi_0)[(1-b^2r^2t^2)-q^2t^2] + [qY''(s, 0) + Y'''(s, 0)]}{q^4 + b^2(r^2 + t^2)q^2 - b^2(1-b^2r^2t^2)} \right) \quad (17.158)$$

The solutions of the characteristic equation are

$$q_{\pm 1} = \pm b\alpha = \pm \frac{b}{\sqrt{2}} \left\{ -(r^2 + t^2) + \left[(r^2 - t^2)^2 + \frac{4}{b^2} \right]^{1/2} \right\}^{1/2}; \quad q_{\pm 1}^2 = q_1 \quad (17.159a)$$

$$q_{\pm 2} = \pm ib\beta = \pm \frac{b}{\sqrt{2}} \left\{ (r^2 + t^2) + \left[(r^2 - t^2)^2 + \frac{4}{b^2} \right]^{1/2} \right\}^{1/2}; \quad q_{\pm 2}^2 = q_2 \quad (17.159b)$$

Then the characteristic equation can be written as

$$\begin{aligned} q^4 + q^2b^2(r^2 + t^2) - b^2(1 - b^2r^2t^2) &= (q^2 - b^2\alpha^2)(q^2 + b^2\beta^2) \\ &= (q^2 - q_1^2)(q^2 - q_2^2) \end{aligned} \quad (17.160)$$

where

$$q_1^2 + q_2^2 = b^2(\alpha^2 + \beta^2) = b^2 \left((r^2 - t^2)^2 + \frac{4}{b^2} \right)^{1/2} \quad (17.161)$$

By taking into account the equality

$$\frac{1}{(q^2 - q_1^2)(q^2 + q_2^2)} = \frac{A}{q^2 - q_1^2} + \frac{B}{q^2 + q_2^2} \quad (17.162)$$

where

$$A = (q_1^2 + q_2^2)^{-1} \quad B = -(q_1^2 + q_2^2)^{-1} \quad (17.163)$$

we find

$$\begin{aligned} \bar{Y}(s, q) &= \frac{L^3}{Is\bar{E}(s)} \left(\frac{1}{q_1^2 + q_2^2} \right) \left(\frac{F_0\omega}{s^2 + \omega^2} \right) \\ &\times \left\{ e^{-q\xi_0} [(1 - b^2 r^2 t^2) - q^2 t^2] + qY''(s, 0) + Y'''(s, 0) \right\} \left(\frac{1}{q^2 - q_1^2} - \frac{1}{q^2 + q_2^2} \right) \end{aligned} \quad (17.164)$$

The inverse Laplace of this equation leads to

$$\begin{aligned} \bar{Y}(s, \xi) &= A \left(\frac{1}{q_1} \sinh q_1(\xi - \xi_0) - \frac{1}{q_2} \sin q_2(\xi - \xi_0) \right) \\ &- B [q_1 \sinh q_1(\xi - \xi_0) + q_2 \sin q_2(\xi - \xi_0)] \\ &+ CY''(s, 0)(\cosh q_1\xi - \cos q_2\xi) + DY'''(s, 0) \left(\frac{1}{q_1} \sinh q_1\xi - \frac{1}{q_2} \sin q_2\xi \right) \end{aligned} \quad (17.165)$$

where

$$A = \frac{L}{Is\bar{E}(s)} \left(\frac{1}{q_1^2 + q_2^2} \right) \left(\frac{F_0\omega}{\omega^2 + s^2} \right) (1 - b^2 r^2 t^2) \quad (17.166a)$$

$$B = \frac{At^2}{1 - b^2 r^2 t^2}; \quad C = \frac{A}{1 - b^2 r^2 t^2} \quad (17.166b)$$

By considering further the boundary conditions

$$\bar{Y}(s, \xi) = \bar{Y}'(s, \xi) = 0 \quad \text{for } \xi = 1 \quad (17.167)$$

a system of equations for $\bar{Y}''(s, 0)$ and $\bar{Y}'''(s, 0)$ is obtained. With the values determined for $\bar{Y}''(s, 0)$ and $\bar{Y}'''(s, 0)$ and after the corresponding substitutions, Eq. (17.165) finally becomes

$$\begin{aligned}
\bar{Y}(s, \xi) = & \frac{F_0 \omega L^3}{Is \bar{E}(s)(s^2 + \omega^2)(q_1^2 + q_2^2)} \left(\left[\left(\frac{1 - b^2 r^2 t^2}{q_1} - t^2 q_1 \right) \sinh q_1 (\xi - \xi_0) \right. \right. \\
& \left. \left. - \left(\frac{1 - b^2 r^2 t^2}{q_2} + t^2 q_2 \right) \sin q_2 (\xi - \xi_0) \right] \right. \\
& + \frac{q_1 q_2}{2q_1 q_2 - 2q_1 q_2 \cosh q_1 \cos q_2 - (q_2^2 - q_1^2) \sinh q_1 \sin q_2} \\
& \times \left\{ (\cosh q_1 \xi - \cos q_2 \xi) \left[\left(\frac{1 - b^2 r^2 t^2}{q_1} - t^2 q_1 \right) \sinh q_1 \xi_0 \right. \right. \\
& \left. \left. + \left(\frac{1 - b^2 r^2 t^2}{q_2} + t^2 q_2 \right) \sin q_2 \xi_0 \right] \right. \\
& + \left(t^2 q_2 + \frac{1 - b^2 r^2 t^2}{q_2} \right) [\cosh q_1 \sin q_2 (1 - \xi_0)] - \left(\frac{t^2 q_2^2}{q_1} + \frac{1 - b^2 r^2 t^2}{q_1} \right) \\
& \times [\sinh q_1 \cos q_2 (1 - \xi_0)] + \left(\frac{1 - b^2 r^2 t^2}{q_1} - t^2 q_1 \right) [\cos q_1 \sinh q_1 (1 - \xi_0)] \\
& \left. + \left(\frac{t^2 q_1^2}{q_2} - \frac{1 - b^2 r^2 t^2}{q_2} \right) [\sin q_2 \cosh q_1 (1 - \xi_0)] \right\} \\
& + \left(\frac{1}{q_1} \sinh q_1 \xi - \frac{1}{q_2} \sin q_2 \xi \right) \{ [t^2 q_1^2 - (1 - b^2 r^2 t^2)] \cosh q_1 \xi_0 \\
& - [t^2 q_2^2 (1 - b^2 r^2 t^2)] \cos q_2 \xi_0 + [(1 - b^2 r^2 t^2) - t^2 q_1^2] \cos q_2 \cosh q_1 (1 - \xi_0) \\
& + [t^2 q_2^2 + (1 - b^2 r^2 t^2)] \cosh q_1 \cos q_2 (1 - \xi_0) \\
& + \left[\frac{q_2}{q_1} (1 - b^2 r^2 t^2) - t^2 q_1 q_2 \right] \sin q_2 \sinh q_1 (1 - \xi_0) \\
& \left. - \left[t^2 q_1 q_2 + (1 - b^2 r^2 t^2) \frac{q_2}{q_1} \right] \sinh q_1 \sin q_2 (1 - \xi_0) \right\} \Big) \Big)
\end{aligned}$$

(17.168)

To handle this equation, it is necessary, as above, to introduce the customary approximations into the hyperbolic and trigonometric functions appearing in it. Then, after long calculations, Eq. (17.168) can be written as

$$\begin{aligned} \bar{Y}(s, \xi) = & \frac{F_0 \omega L^3}{Is \bar{E}(s)(s^2 + \omega^2)} \left\{ \left(-t^2(\xi - \xi_0) + \frac{1}{6}(1 - b^2 r^2 t^2)(\xi - \xi_0)^3 \right. \right. \\ & + \frac{t^2 b^2}{6}(\xi - \xi_0)^3(r^2 + t^2) \left. \right) + 2\xi^2 \left[\left(\frac{1 - b^2 r^2 t^2}{4} \xi_0(\xi_0 - 1)^2 - \frac{t^2}{2}(3\xi_0 - 2) \right) \right. \\ & \left. \left. - \xi \left[\frac{1 - b^2 r^2 t^2}{12}(\xi_0 - 1)^2(2\xi_0 + 1) - t^2 \left(\xi_0 - \frac{1}{2} \right) \right] \right] \right\} \end{aligned} \quad (17.169)$$

It should be noted that the rotary inertia is relevant only at high frequencies ($f > 10^4$ Hz). In most cases,

$$1 \gg b^2 t^2 (r^2 + t^2) \quad \text{and} \quad 1 - b^2 r^2 t^2 \cong 1 \quad (17.170)$$

so Eq. (17.169) can be simplified to

$$\begin{aligned} \bar{Y}(s, \xi) = & \frac{F_0 \omega L^3}{Is \bar{E}(s)(s^2 + \omega^2)} \\ & \left\{ \frac{1}{6}(\xi - \xi_0)^3 - t^2(\xi - \xi_0) + 2\xi^2 \left[\left(\frac{\xi_0}{4}(\xi_0 - 1)^2 - \frac{t^2}{2}(3\xi_0 - 2) \right) \right. \right. \\ & \left. \left. - \xi \left(\frac{(\xi_0 - 1)^2(2\xi_0 + 1)}{12} - t^2 \left(\xi_0 - \frac{1}{2} \right) \right) \right] \right\} \end{aligned} \quad (17.171)$$

Therefore the deflection at $x = x_0 = \xi_0 L$ is given by

$$\bar{Y}(s, x) = \frac{F_0 \omega L^3}{192Is \bar{E}(s)(s^2 + \omega^2)} \left[\left(\frac{x_0}{\ell} \right)^3 \left(\frac{2\ell - x_0}{\ell} \right)^3 + \frac{1 + \nu}{\kappa} \left(\frac{d}{\ell} \right)^2 \left(\frac{x_0}{\ell} \right)^2 \left(\frac{2\ell - x_0}{\ell} \right)^2 \right] \quad (17.172)$$

where $\ell = L/2$, $\kappa = A^*/A$, and d is the thickness of the beam.

When the load is applied in the middle of the beam, $x_0 = \ell$, the deflection is

$$\bar{Y}(s, x) = \frac{F_0 \omega L^3}{192Is \bar{E}(s)(s^2 + \omega^2)} \left[1 + \frac{1 + \nu}{\kappa} \left(\frac{d}{\ell} \right)^2 \right] \quad (17.173)$$

Errors can appear in experimental devices when the force is not applied at the center of the beam. In this case ($x_0 \neq \ell$), the error committed is a factor given by

$$\left(\frac{x_0}{\ell}\right)^2 \left(\frac{2\ell - x_0}{\ell}\right)^2 \frac{\frac{x_0}{\ell} \left(\frac{2\ell - x_0}{\ell}\right) + \frac{1+\nu}{\kappa} \left(\frac{d}{\ell}\right)^2}{1 + [(1+\nu)/\kappa](d/\ell)^2} \quad (17.174)$$

If the out-of-center distance is $\delta = x_0 - \ell$, the error factor can be written as

$$\left[1 - \left(\frac{\delta}{\ell}\right)^2\right]^3 + \frac{[1 - (\delta/\ell)^2]^2 (\delta d/\ell^2)^2 [(1+\nu)/\kappa]}{1 + [(1+\nu)/\kappa](d/\ell)^2} \quad (17.175)$$

This means that the value of the modulus is smaller than the actual value by a factor given by Eq. (17.175). It should be pointed out that when the inertial and shear effects are not considered, then Eq. (17.172) can be written as

$$\bar{Y}(s, x) = \frac{F_0 \omega L^3}{192 I s \bar{E}(s)(s^2 + \omega^2)} \left(\frac{x}{\ell}\right)^3 \left(\frac{2\ell - x_0}{\ell}\right)^3 \quad (17.176)$$

For a load applied at the center of the beam, Eq. (17.114) is recovered:

$$\bar{Y}(s, L/2) = \frac{F_0 \omega L^3}{192 I s \bar{E}(s)(s^2 + \omega^2)} \quad (17.177)$$

and consequently the error involved in the application of the load out-of-center is given by

$$\left[1 - \left(\frac{\delta}{\ell}\right)^2\right]^3 \cong 1 - 3\left(\frac{\delta}{\ell}\right)^2 \quad (17.178)$$

It can be seen that the error for $\delta/\ell = 0.1$ is about 3%. However, as the displacement is, in general, independent of the free length, the errors will be larger for shorter samples.

It is interesting to compare the shear corrections obtained by the three different methods analyzed here. Let us assume, for instance, that $A^*/A = 5/6$ and $\nu = 0.5$. The pertinent corrections are

- | | |
|---|----------------|
| 1. From elasticity theory [Eq. (17.75)] | $3(d/l)^2$ |
| 2. From the free vibration modes theory
(first normal mode) [Eq. (17.152)] | $2.144(d/l)^2$ |
| 3. From the forced vibrations theory [Eq. (17.173)] | $1.8(d/l)^2$ |

As mentioned above, the first correction must be reduced by a factor of about 0.7, and as a consequence, the resulting value, $2.1(d/l)^2$, for the correction derived from the elasticity theory agrees with the value obtained

from the free vibration theory when the first normal mode is considered. On the other hand, the correction derived through the forced vibrations theory is the lower one.

17.11 THERMAL EFFECTS ON TRANSVERSE VIBRATIONS

In Chapter 7, the effects of clamping on the free length and the effective modulus of viscoelastic samples were discussed. Owing to the fact that the samples are simultaneously subjected to both mechanical and thermal fields, it is important to consider now the influence of thermal history on the measured properties. Moreover, in dynamic mechanical tests, measurements are usually carried out in two ways: (1) nonisothermal constant-rate frequency multiplexing or (2) multiplexing at isothermal steps. The first type of measurements are usually conducted well below the glass transition temperature. The second type is a good prescription for measurements around the glass transition in order to improve equilibrium conditions. On the other hand, samples are usually clamped at room temperature. As some instruction manuals for equipment state, clamping force affects the measured modulus, and the best value of this viscoelastic function is attained at a certain level of the clamping force. Although it is possible to reclamp the sample at low temperatures to ensure good clamping conditions, this practice should be avoided to prevent condensation or freezing of water on or close to the sample. Moreover, brittle materials must be clamped close to their T_g to avoid rupture of the sample. In this case it is convenient to reclamp at temperatures progressively lower than T_g . In any case, it is clear that the sample undergoes a complex thermal history prior to the measurements. This thermal history is superimposed on the mechanical force field, and this fact obviously influences the material response. In these conditions, the beam may be subjected to axial tension or compression in addition to the transverse load. Axial tension tends to straighten the beam and, as a result, to reduce the bending moment produced by the transverse load. In contrast, axial compression, having the opposite effect, increases the moment and consequently the deflection.

Let us start by outlining the thermoviscoelastic problem associated with the thermal cooling or heating of double-clamped beams where these effects are more critical than in single-clamped beams. The analysis will follow the main lines developed in Chapter 16 (Section 5) though conveniently simplified, due to the complexity of the phenomena involved. However, some insights can be gained into the spurious effects appearing in clamped samples that undergo heating or cooling histories.

It will be assumed that the temperature field is uniform, that is, the sample is homogeneously cooled or heated, and for this reason there is no spatial temperature dependence. Also a constant dilatation coefficient and a sudden jump in the temperature will be assumed. This thermal history, though not very realistic, refers to the most unfavorable situation.

To complete the solution of the problem, it is necessary to specify the viscoelastic properties of the sample. For simplification reason, the Poisson ratio will be assumed to be constant. According to the results of Problem 16.5, which presents a similar situation, the Laplace transform of the stress is given by

$$\bar{\sigma}_{xx}(s) = -\beta\Delta T\bar{E}(s) \quad (17.179)$$

whose inverse Laplace gives

$$\sigma_{xx}(\xi) = -\alpha\Delta tE(\xi) \quad (17.180)$$

This expression indicates that the viscoelastic response for this special case has the same formal structure as the elastic one, except for the shifting variable, $\xi = a_T t$. Therefore the longitudinal tension Q in the beam will be given by

$$Q = -\beta\Delta TAE(a_T t) \quad (17.181)$$

where A is the area of the transverse section of the beam. According to the time-temperature correspondence principle, the modulus appearing in Eq. (17.181) is equivalent to the modulus at some temperature above or below the clamping temperature, depending on the sign of ΔT . However, in the glassy zone the tensile modulus varies smoothly with temperature, and in order to avoid unnecessary complications, E will be assumed to be constant. This means that the viscoelastic problem can be handled in a first approximation as an elastic one.

Obviously, the sign of the longitudinal force will depend on the sign of the temperature jump. If the sample is clamped at room temperature or higher, then under cooling ($\Delta T < 0$), the sample will be stretched. On the other hand, if the sample is clamped at low temperature, a compression will appear in the sample after heating ($\Delta T > 0$).

It should be pointed out that the analysis of the complete problem requires us to take into account the longitudinal stretching of the sample when it is transversely loaded by an alternating force. In this case, even in the absence of an external longitudinal stress, a temperature jump gives rise to a force along the rigidly clamped bar. This force is a consequence of the

longitudinal displacement caused by the transverse loading. Accordingly, the total strain, which in this case will be obviously different from zero, will be the sum of the strain due to this force and the strain due to the thermal effects:

$$\gamma'_{xx} = \frac{\sigma_{xx}}{E} + \beta \Delta T \quad (17.182)$$

where the two terms on the right-hand side correspond to the stress and thermal contributions, respectively. Strictly speaking, β should be interpreted as the difference between the thermal expansion coefficient of the material under study, usually a polymer, and the corresponding thermal expansion coefficient of the metallic clamps due to the fact that the clamps also undergo dilatation or compression under thermal histories.

For a slender beam,

$$\gamma'_{xx} = \frac{\Delta \ell}{\ell} \quad (17.183)$$

where ℓ represents the half-length of the beam. On the other hand, it is easy to show that the total half-length of the deformed beam, considered as a curved line, is given by

$$\ell + \Delta \ell = \int_0^\ell [(dx)^2 + (du_y)^2]^{1/2} = \int_0^\ell \left[1 + \left(\frac{du_y}{dx} \right)^2 \right]^{1/2} dx \quad (17.184)$$

For relatively small flexural forces, and after expanding the integrand of Eq. (17.184) in series, we can write

$$\Delta \ell \cong \frac{1}{2} \int_0^\ell \left(\frac{du_y}{dx} \right)^2 dx \quad (17.185)$$

or, equivalently,

$$\Delta L \cong \frac{1}{2} \int_0^L \left(\frac{du_y}{dx} \right)^2 dx \quad (17.186)$$

The total stress,

$$\sigma_{xx} = \frac{Q}{A} = E \left(\frac{\Delta L}{L} - \beta \Delta T \right) \quad (17.187)$$

together with Eq. (17.186), gives the longitudinal tension as

$$Q = EA \left[\frac{1}{2L} \int_0^L \left(\frac{du_y}{dx} \right)^2 dx - \beta \Delta T \right] \quad (17.188)$$

From this result, it is clear that the axial tension depends on the deflection. Moreover, if $\Delta T < 0$ (cooling), $Q > 0$ and the sample is strengthened; if $\Delta T > 0$ (heating), the sign of Q will depend on the relative values of each term on the right-hand side of Eq. (17.188).

Once the longitudinal tension has been calculated the deflection of the beam under simultaneous axial and transverse loading will be addressed. Let us return first to the equilibrium equation for the beam [Eq. (17.17)]. In the simplified analysis of the equilibrium conditions described above, the vectorial character of the moments and forces in the balance equations has not been considered. Strictly speaking, if the vectorial character of the magnitudes is taken into account, the equilibrium for the momentum, \mathbf{M} , and forces \mathbf{T} , should be written as (1, p. 76)

$$d\mathbf{M} = \mathbf{T} \times d\boldsymbol{\ell} \quad (17.189)$$

where the symbol \times indicates a vector product. Dividing this equation by $d\boldsymbol{\ell}$, and defining $\mathbf{t} = d\boldsymbol{\ell}/d\ell$ as the unit vector tangential to the deformed beam with a component $\partial u_y/\partial x \simeq \partial u_y/\partial \ell$ along the Y axis, we obtain

$$\frac{d\mathbf{M}}{d\ell} = \mathbf{T} \times \mathbf{t} \quad (17.190)$$

The derivative of Eq. (17.190) with respect to ℓ gives

$$\frac{d^2\mathbf{M}}{d\ell^2} = \mathbf{t} \times \mathbf{q} + \mathbf{T} \times \frac{d\mathbf{t}}{d\ell} \quad (17.191)$$

The second term on the right-hand side of Eq. (17.191) is usually neglected, because for small deflections $d\mathbf{t}/d\ell$ is negligible. However, when the tension \mathbf{T} has a component along the beam, Q is large in comparison with the other two components, and this second term must be retained. By developing the vector products in Eq. (17.191) and using Eq. (17.20a), we find

$$IEu_y^{IV} = q \pm Qu_y'' \quad (17.192)$$

where the positive and negative signs are valid, respectively, for strength and compression. In the present context, Eq. (17.192) corresponds to the case for which the bending and axial tension are of the same order of magnitude. The retention of only the first term of the right-hand side of Eq. (17.192)

corresponds, as usual, to the limiting case of negligible longitudinal stress. The opposite limiting situation corresponds to the case in which the resistance to bending is small in comparison with the resistance to stretching. In this situation, the first term on the right in Eq. (17.192) can be neglected in comparison with the components of the second term on the right. Viscoelastic beams and rods under tensions much stronger than the bending forces are called viscoelastic strings.

According to the correspondence principle, the equation describing a viscoelastic beam under transversal and longitudinal effects is given by

$$I \int_0^\infty E(t - \theta) \frac{\partial^5 u_y}{\partial x^4 \partial \theta} d\theta = q \pm \int_0^\infty Q(t - \theta) \frac{\partial^3 u_y}{\partial x^2 \partial \theta} d\theta \quad (17.193)$$

For a sinusoidal steady excitation and small deflections, the elastic and viscoelastic solutions are formally similar, as the separation of variables methodology outlined above suggests. Thus, in this case, the viscoelastic response is dependent on only the specific material properties of the sample under study. Moreover, on the basis of one of the hypotheses mentioned above, the thermoviscoelastic problem can be reduced to a thermoelastic one. Therefore, in the present context only the elastic solution of the problem will be discussed.

For a double-clamped beam of length L , transversely loaded at its midpoint with a weight P , the deflection will be given by the equations (13)

$$u_y = \frac{P}{kQ} \left[(\cosh kx - 1) \frac{2 \sinh(kL/2) - kL \cosh(kL/2) + (kL/2) \cosh kL - \sinh kL + (kL/2)}{2 - 2 \cosh kL + kL \sinh kL} - \frac{1}{2} (\sinh kx - kx) \right] \quad (17.194a)$$

for a strengthened beam, and

$$u_y = \frac{P}{kQ} \left[(\cos kx - 1) \frac{2 \sin \frac{kL}{2} - kL \cos \frac{kL}{2} + \frac{kL}{2} \cos kL - \sin kL + \frac{kL}{2}}{2 - 2 \cos kL + kL \sin kL} - \frac{1}{2} (\sin kx - kx) \right] \quad (17.194b)$$

for a compressed beam. In these expressions,

$$k = (Q/EI)^{1/2} \quad (17.195)$$

The deflection at the midpoint, which in this case is the maximum deflection, is obtained by making $x = L/2$ in Eqs. (17.194a) and (17.194b). The results are

$$u_{ym} = \frac{P}{kQ} \left(\tanh \frac{kL}{4} - \frac{kL}{4} \right) \quad (17.196a)$$

when the beam is stretched and

$$u_{ym} = \frac{P}{kQ} \left(\tan \frac{kL}{4} - \frac{kL}{4} \right) \quad (17.196b)$$

when the beam is compressed.

For relatively small values of k , the approximations

$$\tan x \cong x + \frac{x^3}{3} + \frac{2x^5}{15} + \dots \quad (17.197a)$$

and

$$\tanh x \cong x - \frac{x^3}{3} + \frac{2x^5}{15} + \dots \quad (17.197b)$$

in conjunction with Eq. (17.195) give the following result for the maximum deflection:

$$u_{ym} = \frac{PL^3}{192IE} \left(1 \mp \frac{QL^2}{40IE} + \dots \right) \quad (17.198)$$

where the negative and positive signs hold, respectively, for stretching and compression.

The next step is to express Q as a function of the maximum deflection and the temperature jump. The peak-to-peak deflection corresponding to the sinusoidal displacement is usually specified in the experimental measurements. For this reason, the stress produced in the beam due to the deflection will be calculated in the absence of thermal effects, and, according to the superposition principle, it will superimpose later with the temperature contribution to the longitudinal stress. Thus the nonthermal contribution to Q , given by

$$Q' = EA \left[\frac{1}{2L} \int_0^L \left(\frac{du_y}{dx} \right)^2 dx \right] \quad (17.199)$$

must be determined by combining the corresponding derivative,

$$\frac{dQ'}{dx} = \frac{EA}{2L} \left(\frac{du_y}{dx} \right)^2 \quad (17.200)$$

with Eqs. (17.194a) and (17.194b), the expressions corresponding to the deflection of the beam. By using the approximation $du_y/dx \cong P/Q'$, and the series expansions for $\sin x$, $\cos x$, $\sinh x$, and $\cosh x$, after long algebraic calculations, we obtain

$$Q' \cong \frac{P^2 L^4 A}{15,360 EI^2} \quad (17.201)$$

The maximum deflection without longitudinal tension or compression is given by

$$u_{ym} = \frac{PL^3}{192IE_p} \quad (17.202)$$

where the subscript p is used to denote the modulus calculated without considering thermal or other effects. According to Eq. (17.202), Q' can be expressed in terms of this maximum deflection by

$$Q' = \frac{12}{5} \left(\frac{E_p^2 A}{EL^2} \right) u_{ym}^2 \quad (17.203)$$

As a consequence, the total longitudinal tension for a specified u_{ym} can be written as

$$Q = EA \left[\frac{12}{5} \left(\frac{u_{ym}}{L} \right)^2 \left(\frac{E_p}{E} \right)^2 - \beta \Delta T \right] \quad (17.204)$$

Substituting this equation into the expression for the deflection [Eq. (17.198)] gives

$$u_{ym} = \frac{PL^3}{192IE} \left\{ 1 - \frac{AL^2}{40I} \left[\frac{12}{5} \left(\frac{u_{ym}}{L} \right)^2 \left(\frac{E_p}{E} \right)^2 - \beta \Delta T \right] + \dots \right\} \quad (17.205)$$

where the sign for the correction, combining longitudinal and thermal stresses in the beam, has been taken into account. For rectangular cross section beams with thickness d ,

$$\frac{AL^2}{40I} = \frac{3}{10} \left(\frac{L}{d} \right)^2 \quad (17.206)$$

Eq. (17.205) adopts the form

$$u_{ym} = \frac{PL^3}{192IE} \left\{ 1 - \frac{3}{10} \left(\frac{L}{d} \right)^2 \left[\frac{12}{5} \left(\frac{u_{ym}}{L} \right)^2 \left(\frac{E_p}{E} \right)^2 - \beta \Delta T \right] + \dots \right\} \quad (17.207)$$

It is convenient to compare the actual modulus E with that calculated in the absence of thermal and longitudinal stresses, that is, from Eq. (17.202). From Eqs. (17.202) and (17.207), we find

$$E = E_p \left\{ 1 - \frac{3}{10} \left(\frac{L}{d} \right)^2 \left[\frac{12}{5} \left(\frac{u_{ym}}{L} \right)^2 \left(\frac{E_p}{E} \right)^2 - \beta \Delta T \right] \dots \right\} \quad (17.208)$$

from which, after some rearrangements, we obtain

$$\left(\frac{E}{E_p} \right)^3 - \left[1 + \frac{3}{10} \left(\frac{L}{d} \right)^2 \beta \Delta T \right] \left(\frac{E}{E_p} \right)^2 + \frac{18}{25} \left(\frac{u_{ym}}{d} \right)^2 = 0 \quad (17.209)$$

Let us assume, for instance, the following values for the parameters appearing in Eq. (17.209):

$$\begin{aligned} A &= 10^{-5} m^2; & d &= 10^{-3} m; & L &= 2 \times 10^{-2} m \\ u_{ym} &= \frac{10^{-3}}{16} m; & \beta &= 4 \times 10^{-5} K^{-1} \end{aligned}$$

Then the corrections for different temperature jumps are

$\Delta T(^{\circ}C)$	+1	-1	+10	-10	+100	-100
E/E_p	1.00	0.99	1.05	0.95	1.48	0.52

The preceding analysis suggests that the thermal effects are clearly dominant over those due to the longitudinal tension for relatively high values of $|\Delta T|$. That is, for a thermal jump of several tens of degrees,

$$E \cong E_p \left[1 + \frac{3}{10} \left(\frac{L}{d} \right)^2 \beta \Delta T \right] \quad (17.210)$$

It is worth noting that the thermal stress effect can also be diminished to some degree by the slipping process existing between the bar and the clamps. For this reason, the values of the preceding table are surely overestimated.

Thermal effects can explain some phenomena observed in the experimental results. Thus when the sample is clamped at room temperature, it stretches during cooling ($\Delta T < 0$), and the measured modulus tends to be lower than the actual one (Fig. 17.8). However, when the stretched sample is heated from low to high temperature during the measurements, and, more specifically, when a polymer passes through the glass transition, the thermal stresses disappear, and the experimental curves may exhibit an increase in the modulus as shown in Figure 17.9.

17.12 TORSION OF VISCOELASTIC RODS

A new example of deformation of a rod, in which small strains are compatible with large displacements of parts of the rod, is torsion (1, p. 59). In a rod under torsion whose axis is kept straight, without flexion or bulge, each transverse section rotates relative to those located close to it. Consequently, if the rod is long, two sufficiently distant sections can rotate through a large angle relatively to each other.

17.13 DISPLACEMENT AND STRAIN TENSOR IN TORSION

Let us consider a straight rod with an arbitrary cross section, as shown in Figure 17.10. If the axis of torsion coincides with the vertical axis, which

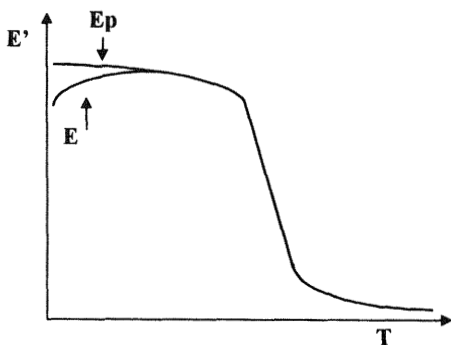


Figure 17.8 Variation of the storage relaxation modulus, E , with temperature measured during a cooling experiment. E_p represents the actual value of the storage relaxation modulus in absence of contraction forces which increase the longitudinal tension.

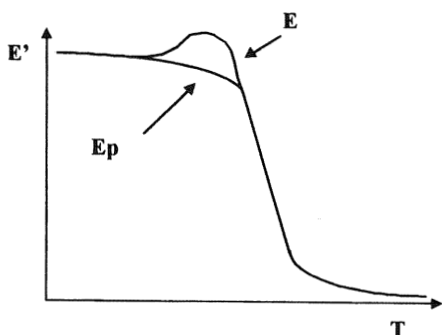


Figure 17.9 Variation of the storage relaxation modulus E , with temperature measured during a heating experiment. E_p represents the actual value of the storage relaxation modulus in absence of dilatational forces which reduce the longitudinal tension.

passes through the center of gravity of the bar, the following vector product holds.

$$\delta \mathbf{r} = \boldsymbol{\alpha} \times \mathbf{r} \quad (17.211)$$

where $\boldsymbol{\alpha}$ is the vector whose absolute value is the torsion angle, directed along the torsion axis that will be considered the Z axis. Consequently,

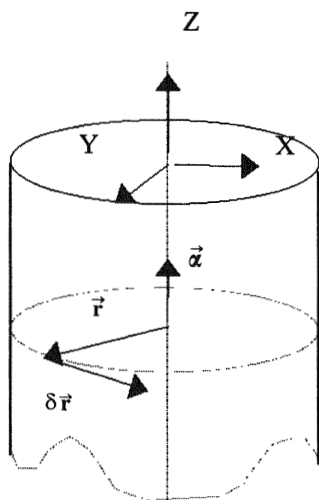


Figure 17.10 Torsion of a cylindrical rod, showing the torsion vector $\boldsymbol{\alpha}$ and the displacement vector $\delta \mathbf{r}$.

the rotation takes place in the XY plane. The vector α in Eq. (17.211) will depend on both z and time.

It should be pointed out that during torsion the initially planar sections lose their planarity because each of their points experiences a displacement parallel to the z axis. This displacement is proportional (1) to a function ψ , called the torsion function, which depends on the position of the point on the section before the deformation is produced, and (2) to the magnitude of the relative rotation between two very close sections, that is, the derivative of α with respect to the z direction. Consequently, the vector displacement has the components

$$\mathbf{u} = \delta \mathbf{r} = \left(-y\alpha, x\alpha, \psi \frac{\partial \alpha}{\partial z} \right) \quad (17.212)$$

where $\psi = \psi(x, y)$. The components of the strain tensor according to Eq. (4.29a) are

$$\begin{aligned} \gamma_{xx} = \gamma_{yy} = 0; \quad \gamma_{zz} = \psi \frac{\partial^2 \alpha}{\partial z^2}; \quad \gamma_{xy} = \gamma_{yx} = 0 \\ \gamma_{xz} = \gamma_{zx} = \frac{1}{2} \left(-y + \frac{\partial \psi}{\partial x} \right) \frac{\partial \alpha}{\partial z}; \quad \gamma_{yz} = \gamma_{zy} = \frac{1}{2} \left(x + \frac{\partial \psi}{\partial y} \right) \frac{\partial \alpha}{\partial z} \end{aligned} \quad (17.213)$$

17.14 STRESS TENSOR IN TORSION

Substituting Eqs. (17.213) into the stress-strain relationship for viscoelastic materials, we obtain the following expressions for the components of the stress tensor:

$$\sigma_{xx} = \sigma_{yy} = \int_0^\infty \left[K(t-\theta) - \frac{2}{3} G(t-\theta) \right] \frac{\partial^3 \alpha}{\partial z^2 \partial \theta} \psi d\theta, \quad (17.214a)$$

$$\sigma_{zz} = 2 \int_0^\infty G(t-\theta) \frac{\partial^3 \alpha}{\partial z^2 \partial \theta} \psi d\theta + \int_0^\infty \left[K(t-\theta) - \frac{2}{3} G(t-\theta) \right] \frac{\partial^3 \alpha}{\partial z^2 \partial \theta} \psi d\theta \quad (17.214b)$$

$$\sigma_{xy} = \sigma_{yx} = 0; \quad \sigma_{xz} = \sigma_{zx} = \int_0^\infty G(t-\theta) \left(-y + \frac{\partial \psi}{\partial x} \right) \frac{\partial^2 \alpha}{\partial z \partial \theta} d\theta \quad (17.214c)$$

$$\sigma_{yz} = \sigma_{zy} = \int_0^\infty G(t-\theta) \left(x + \frac{\partial \psi}{\partial y} \right) \frac{\partial^2 \alpha}{\partial z \partial \theta} d\theta \quad (17.214d)$$

17.15 EQUILIBRIUM EQUATIONS FOR TORSION

The substitution of the components of the stress tensor, given in the preceding section, into the equilibrium equations [Eq. (4.14) with $b = 0$] leads to

$$\int_0^\infty \left[K(t - \theta) - \frac{2}{3} G(t - \theta) \right] \frac{\partial \psi}{\partial x} \frac{\partial^3 \alpha}{\partial z^2 \partial \theta} d\theta + \int_0^\infty G(t - \theta) \frac{\partial^3 \alpha}{\partial z^2 \partial \theta} \left(-y + \frac{\partial \psi}{\partial x} \right) d\theta = 0 \quad (17.215a)$$

$$\int_0^\infty \left[K(t - \theta) - \frac{2}{3} G(t - \theta) \right] \frac{\partial \psi}{\partial y} \frac{\partial^3 \alpha}{\partial z^2 \partial \theta} d\theta + \int_0^\infty G(t - \theta) \frac{\partial^3 \alpha}{\partial z^2 \partial \theta} \left(x + \frac{\partial \psi}{\partial y} \right) d\theta = 0 \quad (17.215b)$$

$$\int_0^\infty \left[K(t - \theta) - \frac{2}{3} G(t - \theta) \right] \psi \frac{\partial^4 \alpha}{\partial z^3 \partial \theta} d\theta + \int_0^\infty G(t - \theta) \frac{\partial \alpha}{\partial \theta} \left(\frac{\partial^2 \psi}{\partial x^2} + \frac{\partial \psi^2}{\partial y^2} \right) d\theta + 2 \int_0^\infty G(t - \theta) \psi \frac{\partial^4 \alpha}{\partial z^3 \partial \theta} d\theta = 0 \quad (17.215c)$$

Taking derivatives in the first two equations with respect to x and y , respectively, and adding the resulting expressions, we obtain

$$\frac{\partial^2 \alpha}{\partial z^2} \Delta \psi = 0 \quad (17.216a)$$

where

$$\Delta \psi = \frac{\partial^2 \psi}{\partial x^2} + \frac{\partial^2 \psi}{\partial y^2} \quad (17.216b)$$

Disregarding the trivial case, $\psi = 0$, Eqs. (17.216a) and (17.215c) imply that

$$\Delta \psi = 0 \quad (17.217)$$

that is, ψ is a harmonic quantity. At the same time, α can be linear as well as quadratic in z . This implies that the fibers initially parallel to the torsion axis are inclined straight lines or, alternatively, have parabolic form after deformation.

As in the elastic case, it can be demonstrated (1, p. 63) that if the torsion is produced by the application of a torque at one end of the rod, whereas the other end is fixed, then on the basis of the minimum for the total energy of the distorted bar, the fibers parallel to the torsion axis will be distorted along

a straight line. In fact, the rotation angle is a linear function of z , that is, $\alpha = Cz$, and as a result the two factors appearing in Eq. (17.216a) are null.

17.16 BOUNDARY CONDITIONS

To determine the boundary conditions on the surface of the rod, it should be noted that for thin rods the external forces acting on the lateral surface are considered negligible in comparison with the internal tensions, and the following equation holds for the sides of the rod:

$$\sum \sigma_{ij} n_j = 0 \quad (17.218)$$

As the axis of the bar is directed along the z axis, this is equivalent to

$$\sigma_{zx} n_x + \sigma_{zy} n_y = 0 \quad (17.219)$$

Substituting the stress tensor components [Eqs. (17.214c) and (17.214d) into Eq. (17.219), we obtain

$$y \, dy + x \, dx - \frac{\partial \psi}{\partial x} dy + \frac{\partial \psi}{\partial y} dx = 0 \quad (17.220)$$

In the development of this expression it was taken into account that the components of the vector normal to a plane contour are $n_x = -dy/dl$ and $n_y = dx/dl$, where x and y are the coordinates of the points on the contour, l being an element of arc. However, for the present purposes, it is more convenient to use a function F related to ψ by

$$\frac{\partial \psi}{\partial x} = y + 2 \frac{\partial F}{\partial y}; \quad \frac{\partial \psi}{\partial y} = -x - 2 \frac{\partial F}{\partial x} \quad (17.221)$$

The substitution of Eq. (17.221) into Eq. (17.220) leads to $dF = 0$, whence

$$F = \text{constant} \quad (17.222a)$$

Accordingly, the stress function F is required to be constant along the section boundary. This constant may be chosen arbitrarily for a simply connected boundary because it has no effect on the stress tensor components. For the forthcoming discussion we assume, without loss of generality, the boundary condition

$$F = 0 \quad (17.222b)$$

On the other hand, taking the derivative of Eq. (17.221a) with respect to y and that of Eq. (17.221b) with respect to x , and subtracting the resulting expressions, we obtain

$$\Delta F = -1 \quad (17.223)$$

This new function is obviously not harmonic.

17.17 TORSION FUNCTION FOUND BY SEPARATION OF VARIABLES

For certain cross sections of simple geometry, for example the circular one, closed solutions for the modified torsion function F may be obtained (14). On the other hand, for arbitrary cross sections, such as a rectangular one, it is not possible to find a solution from the boundary equation. In this case, the method of separation of variables is used, and the following solution is proposed.

$$F = \sum_{\substack{2n+1 \\ n \geq 0}}^{\infty} Y_n \cos \frac{n\pi x}{d} \quad (17.224)$$

where Y_n is a function of y . In order to fix ideas, let us consider a prismatic bar of thickness d and width b . In view of the symmetry of the problem, the solution is taken in the form of even functions. Substituting Eq. (17.224) into Eq. (17.223), we obtain

$$-\sum_{\substack{2n+1 \\ n \geq 0}}^{\infty} Y_n \frac{n^2 \pi^2}{d^2} \cos \frac{n\pi x}{d} + \sum_{\substack{2n+1 \\ n \geq 0}}^{\infty} \frac{\partial^2 Y}{\partial y^2} \cos \frac{n\pi x}{d} = -1 \quad (17.225)$$

The identity

$$-1 = \sum_{\substack{2n+1 \\ n \geq 0}}^{\infty} (-1)^{(n-1)/2} \left(\frac{-4}{n\pi} \right) \cos \frac{n\pi x}{d} \quad (17.226)$$

leads Eq. (17.225) to the differential equation

$$\frac{\partial^2 Y_n}{\partial y^2} - \frac{n^2 \pi^2}{d^2} Y_n = -(-1)^{(n-1)/2} \left(\frac{4}{n\pi} \right) \quad (17.227)$$

whose solution is given by

$$Y_n = a_n \sinh \frac{n\pi y}{d} + b_n \cosh \frac{n\pi y}{d} + (-1)^{(n+1)/2} \left(\frac{-4d^2}{n^3 \pi^3} \right) \quad (17.228)$$

On account of the symmetry of the Y_n with respect to the axis OX , for all $a_n = 0$ and for $y = \pm b$, the following equality must be fulfilled:

$$Y_n \left(\pm \frac{b}{2} \right) = 0 \quad (17.229)$$

Consequently,

$$b_n = -(-1)^{(n+1)/2} \left(\frac{4d^2}{n^3 \pi^3} \right) \left(\frac{1}{\cosh(n\pi b/2d)} \right) \quad (17.230)$$

and Eq. (17.224) becomes

$$F = \sum_{\substack{n \\ 2n+1 \\ n \geq 0}} -(-1)^{(n+1)/2} \left(\frac{4d^2}{n^3 \pi^3} \right) \left(1 - \frac{\cosh(n\pi y/d)}{\cosh(n\pi b/2d)} \right) \cos \frac{n\pi x}{d} \quad (17.231)$$

Taking derivatives with respect to x and y , we obtain

$$\frac{\partial F}{\partial x} = \sum_{\substack{2n+1 \\ n \geq 0}} (-1)^{(n+1)/2} \left(\frac{4d}{n^2 \pi^2} \right) \left(1 - \frac{\cosh(n\pi y/d)}{\cosh(n\pi b/2d)} \right) \sin \frac{n\pi x}{d} \quad (17.232a)$$

$$\frac{\partial F}{\partial y} = \sum_{\substack{2n+1 \\ n \geq 0}} (-1)^{(n+1)/2} \left(\frac{4d}{n^2 \pi^2} \right) \left(\frac{\sinh(n\pi y/d)}{\cosh(n\pi b/2d)} \right) \cos \frac{n\pi x}{d} \quad (17.232b)$$

These derivatives in combination with Eqs. (17.214c) and (17.214d) permit us to express the components σ_{yz} and σ_{xz} of the stress tensor as

$$\sigma_{\ell z} = 2 \frac{\partial F}{\partial \ell} \int_0^\infty G(t - \theta) \frac{\partial^2 \alpha}{\partial z \partial \theta} \partial \theta; \quad \ell = x, y \quad (17.233)$$

17.18 MOMENT OF TORQUE

The moment of torque is given by

$$M(z, t) = \int_Q (x\sigma_{yz} - y\sigma_{xz}) dQ \quad (17.234)$$

where dQ is an element of the cross-sectional area. Equations (17.233) and (17.234) lead to

$$M(z, t) = -2 \int_Q \int_0^\infty G(t - \theta) \frac{\partial^2 \alpha}{\partial \tau \partial \theta} \left(x \frac{\partial F}{\partial x} + y \frac{\partial F}{\partial y} \right) d\theta dQ \quad (17.235)$$

The integral with respect to the cross-sectional area in the moment of torque can alternatively be expressed in vector notation as

$$-2 \int_Q \mathbf{r} \nabla F dQ \quad (17.236)$$

and according to the well-known formula of vector calculus,

$$\nabla(\mathbf{r}F) = \mathbf{r} \cdot \nabla F + F \cdot \nabla \mathbf{r} \quad (17.237)$$

we find

$$2 \int_Q \mathbf{r} \nabla F dQ = -2 \left[\int_Q \nabla(\mathbf{r}F) dQ - \int_Q F \nabla \mathbf{r} dQ \right] = -2 \oint \mathbf{r} F dQ + 2 \int_Q F \nabla \mathbf{r} dQ \quad (17.238)$$

If the cross section is singly connected, the first integral taken along the boundary surface where the condition given by Eq. (17.222b) holds, becomes null. Moreover, the first integral is taken along the boundary where $F = 0$, so that

$$\nabla \mathbf{r} = 2 \quad (17.239)$$

Accordingly, Eq. (17.238) can be written as

$$-2 \iint \left(x \frac{\partial F}{\partial x} + y \frac{\partial F}{\partial y} \right) dx dy = 4 \iint F dx dy \quad (17.240)$$

with the boundary conditions given by (see Fig. 17.6)

$$x \rightarrow -\frac{d}{2}, +\frac{d}{2}; \quad y \rightarrow -\frac{b}{2}, +\frac{b}{2} \quad (17.241)$$

The value of the resulting integral on the right-hand side of Eq. (17.240) can be found from Eq. (17.231) taking into account that $\sum_{\substack{\infty \\ 2n+1 \\ n \geq 0}} (1/n)^4 = \frac{\pi^4}{96}$. The pertinent result is given by the series

$$\frac{bd^3}{3} \left[1 - \frac{192}{\pi^5} \left(\frac{d}{b} \right) \sum_{\substack{2n+1 \\ n \geq 0}}^{\infty} \frac{1}{n^5} \tanh \frac{n\pi b}{2d} \right] = \frac{bd^3}{3} f\left(\frac{d}{b}\right) \quad (17.242)$$

The function f could be tabulated for different values of d/b . Thus for $d = b$ (square section), we obtain

$$f(1) = 1 - 0.63 \left[\tanh \frac{\pi}{2} + \frac{1}{3^5} \tanh \frac{3}{2} \pi + \frac{1}{5^5} \tanh \frac{5}{2} \pi + \dots \right] \cong 0.423 \quad (17.243)$$

If $d/b \leq 1/3$, then

$$f(d/b) = 1 - 0.63d/b \geq 0.79 \quad (17.244)$$

Finally, Eqs. (17.235) and (17.242) lead to the following expression for the moment of torque of a viscoelastic rod:

$$M(z, t) = \frac{bd^3}{3} f\left(\frac{d}{b}\right) \int_0^{\infty} G(t - \theta) \frac{\partial^2 \alpha}{\partial z \partial \theta} d\theta \quad (17.245)$$

17.19 MOTION AND BOUNDARY CONDITION EQUATIONS

The torsional motion of the rod will be studied following the method outlined by Elder (15) [see also the paper by Glauz (16)]. Let us consider again the rectangular sample. The relative change in the moment of a section placed at a distance z from the origin with respect to another located at $z + dz$ is given by $\partial M / \partial z$. This derivative is given by

$$\frac{\partial M}{\partial z} = \rho I \ddot{\alpha} \quad (17.246)$$

where ρ is the mass density and I is the polar moment of inertia of the cross section. In the present case, the derivative appearing on the left hand side of Eq. (17.246) can be calculated from Eq. (17.245), thus obtaining the motion equation

$$\frac{\partial M}{\partial z} = \frac{bd^3}{3} f\left(\frac{d}{b}\right) \int_0^{\infty} G(t - \theta) \frac{\partial^3 \alpha}{\partial z^2 \partial \theta} d\theta = \rho I \ddot{\alpha} \quad (17.247)$$

On the other hand, the value of I for a rectangular cross section with dimensions comparable to those of the lateral faces is given by

$$\frac{bd}{12}(b^2 + d^2) \quad (17.248)$$

where b and d are the lateral dimensions. Moreover, in the case of free vibrations, the boundary conditions are

$$\begin{aligned} J\ddot{\alpha} + M &= 0, & z &= \ell \\ \alpha &= 0, & z &= 0 \end{aligned} \quad (17.249)$$

where J is the mass moment of inertia of the disk located at the end of the rod.

Substituting the equation for the moment M [Eq. (17.245)] into Eq. (17.249), we obtain

$$J\ddot{\alpha} + \frac{bd^3}{3}f\left(\frac{d}{b}\right) \int_0^\infty G(t-\theta) \frac{\partial^2 \alpha}{\partial z \partial \theta} d\theta = 0; \quad z = \ell \quad (17.250a)$$

$$\alpha = 0; \quad z = 0 \quad (17.250b)$$

By integrating by parts and taking into account the boundary conditions [Eq. (17.250)], the motion equation [Eq. (17.247)] can alternatively be written as

$$\int_0^\infty \alpha'' \dot{G}(t-\theta) d\theta = \rho I_0 \ddot{\alpha} \quad (17.251)$$

$$\begin{aligned} J_0 \ddot{\alpha} + \int_0^\infty \alpha' \dot{G}(t-\theta) d\theta &= 0, & z &= \ell \\ \alpha &= 0, & z &= 0 \end{aligned} \quad (17.252)$$

where I_0 and J_0 are given by

$$I_0 = \frac{1}{(bd^3/3)f(d/b)}; \quad J_0 = \frac{J}{(bd^3/3)f(d/b)} \quad (17.253)$$

For the solution of this system of integrodifferential equations, we can adopt a method of separation of variables and develop the solution in terms of a series that depends on the eigenvalues and the corresponding eigenfunctions of the characteristic equation. By assuming

$$\alpha(z, t) = \phi(t) \sin \lambda z \quad (17.254)$$

and carrying this expression to Eqs. (17.251) and (17.252), we obtain

$$\int_0^{\infty} \varphi(\theta) \dot{G}(t - \theta) d\theta = -\frac{\rho I_0}{\lambda^2} \ddot{\varphi}(t) \quad (17.255a)$$

$$\int_0^{\infty} \varphi(\theta) \dot{G}(t - \theta) d\theta = -\frac{J_0 \tan \lambda z}{\lambda} \ddot{\varphi}(t); \quad z = \ell \quad (17.255b)$$

Comparison of the right-hand sides of Eqs. (17.255a) and (17.255b) for $z = \ell$ together with further rearrangements, give

$$\lambda \ell \tan \lambda \ell = \frac{\rho \ell I_0}{J_0} \quad (17.256)$$

This is the secular or frequency equation, which, for convenience, can be expressed as

$$\beta_n \tan \beta_n = \mu \quad (17.257)$$

where $\mu = \rho \ell I_0 / J_0$ and $\beta_n = \lambda_n \ell$. It should be pointed out that the roots of Eq. (17.257) are real positive numbers depending on the geometry of the test sample but not on the viscoelastic properties of the material. Separation of the real and imaginary parts leads to

$$(\beta'_n + i\beta''_n) \frac{\tan \beta'_n + i \tanh \beta''_n}{1 - i \tan \beta'_n \tanh \beta''_n} = \mu \quad (17.258)$$

The imaginary part must be zero, implying that $\beta''_n = 0$ for all β'_n . Therefore, Eq. (17.258) becomes

$$\beta'_n \sinh 2\beta''_n + \beta''_n \sin 2\beta'_n = 0 \quad (17.259)$$

An approximate solution to the frequency equation is found for small values of α , making $\tan \beta \cong \beta + (1/3)\beta^3$. Then from Eq. (17.257) we easily obtain

$$\beta = \left(\frac{-3 + \sqrt{12\mu + 9}}{2} \right)^{1/2} \quad (17.260)$$

The solutions of the free vibrations problem will be the eigenvalues $\sin \lambda_n z$ corresponding to the eigenvalues λ_n . Such functions form an orthogonal set in $(0, \ell)$ with the orthogonality condition

$$\mu \int_0^{\ell} \sin \lambda_n \sin \lambda_m z \, dz + \ell \sin \lambda_n \ell \sin \lambda_m \ell = 0 \quad (17.261)$$

provided $m \neq n$. This completes the free vibrations problem.

On the other hand, a suitably restricted function can be developed in a series, in terms of the former sine eigenfunctions, in such a way that

$$\phi(z) = \sum_{n=1}^{\infty} a_n \sin \lambda_n z \quad (17.262)$$

where

$$a_n = \frac{\mu \int_0^{\ell} \phi(z) \sin \lambda_n z \, dz + \ell \phi(z) \sin \lambda_n \ell}{\mu \int_0^{\ell} \sin^2 \lambda_n z \, dz + \ell \sin^2 \lambda_n \ell} \quad (17.263)$$

is the orthonormalization condition.

To study the problem of forced vibrations, the series expansion of $\phi(z) = z/\ell$ is required. In this case,

$$\sum_{n=1}^{\infty} a_n \sin \lambda_n z = \frac{z}{\ell}; \quad 0 \leq z \leq \ell \quad (17.264)$$

so that the orthonormalization condition for the coefficients is given by

$$a_n = \frac{\mu \int_0^{\ell} (z/\ell) \sin \lambda_n z \, dz + \ell \sin \lambda_n \ell}{\mu \int_0^{\ell} \sin^2 \lambda_n z \, dz + \ell \sin^2 \lambda_n \ell} \quad (17.265)$$

On calculating the required integrals, we obtain

$$a_n = \frac{2 \sin \beta_n}{\beta_n (\beta_n + \sin \beta_n \cos \beta_n)} \quad (17.266)$$

In this case, by assuming a torque $M(t) = M_0$, we can proceed in the following way.

Starting from Eq. (17.252), we have

$$J_0 \ddot{\alpha} + \int_0^{\infty} \alpha'(\theta) \dot{G}(t - \theta) d\theta = M_0; \quad z = \ell \quad (17.267)$$

with the boundary conditions

$$\begin{aligned} \alpha(z, t) = 0; & \quad \dot{\alpha}(z, t) = 0; & \quad t = 0^+; & \quad 0 \leq z \leq \ell \\ \alpha(z, t) = 0; & \quad z = 0 & & \end{aligned} \quad (17.268)$$

We consider a solution of the type

$$\alpha(z, t) = \sum_{n=1}^{\infty} d_n Q_n(t) \sin \lambda_n z \quad (17.269)$$

where $Q_n(t)$ denotes a normal coordinate.

Substituting Eq. (17.269) into Eq. (17.267) and considering Eqs. (17.256) and (17.257), it follows that

$$\frac{\mu J_0}{\ell} \sum_{n=1}^{\infty} \frac{d_n}{\lambda_n} \ddot{Q}_n(t) \cos \lambda_n \ell + \sum_{n=1}^{\infty} d_n \lambda_n \cos \lambda_n \ell \int_0^{\infty} Q_n(\theta) \dot{G}(t - \theta) d\theta = M_0 \quad (17.270)$$

where it was taken into account that $z = \ell$. To obtain the corresponding equations for the normal coordinates, it is convenient to express the applied torque as a series. For this purpose, by taking the derivative of Eq. (17.264) with respect to z , we can write

$$M_0 = M_0 \sum_{n=1}^{\infty} a_n \lambda_n \ell \cos \lambda_n \ell \quad (17.271)$$

where

$$\sum_{n=1}^{\infty} a_n \lambda_n \ell \cos \lambda_n \ell = 1 \quad (17.272)$$

By substituting Eq. (17.271) into the right-hand side of Eq. (17.270), the following condition is found:

$$d_n = a_n \frac{\ell^2 \lambda_n^2}{\rho \ell I_0} \quad (17.273)$$

Equation (17.266), together with the identity $\beta_n = \lambda_n \ell$, gives the following alternative expression for d_n :

$$d_n = \frac{1}{\rho \ell I_0} \left(\frac{2\beta_n \sin \beta_n}{\beta_n + \sin \beta_n \cos \beta_n} \right) \quad (17.274)$$

By defining the variable

$$\Omega_n^2 = \lambda_n^2 / \rho I_0 \quad (17.275)$$

the motion equation for an arbitrary torque can be written in terms of the normal modes as

$$\ddot{Q}_n(t) + \Omega_n^2 \int_0^\infty Q_n(\theta) \dot{G}(t - \theta) d\theta = M(t) \quad (17.276)$$

The Laplace transform of Eq. (17.276) together with the boundary conditions

$$Q(0) = \dot{Q}(0) = 0 \quad \forall n \quad (17.277)$$

gives

$$s^2 \bar{Q}_n(s) + \Omega_n^2 s \bar{G}(s) \bar{Q}_n(s) = \bar{M}(s) \quad (17.278)$$

This equation leads to

$$\bar{Q}_n(s) = \frac{\bar{M}(s)}{s^2 + s\Omega_n^2 \bar{G}(s)} \quad (17.279)$$

This type of equation appears in many vibrating systems. The solution of the outlined problem requires knowledge of the viscoelastic properties of the material. In any case, on account of Eq. (5.58), we can write

$$\bar{Q}_n(s) = \frac{\bar{M}(s)\bar{\epsilon}(s)}{s^2\bar{\epsilon}(s) + \Omega_n^2\bar{\sigma}(s)} \quad (17.280)$$

where $\bar{\epsilon}(s)$ and $\bar{\sigma}(s)$ are, for a viscoelastic solid, polynomials of degree m , and the equation $s^2\bar{\epsilon}(s) + \Omega_n^2\bar{\sigma}(s) = 0$, which gives the poles of the function $Q_n(s)$, has $m + 2$ roots. In the simplest case—for example, a solid standard governed by only a single relaxation time—the complex relaxation modulus is given by [Eq. (10.41)]

$$G^*(s) = s\bar{G}(s) = \frac{G_1 + G_0\tau s}{1 + \tau s} \quad (17.281)$$

Accordingly, the poles of Eq. (17.280) can be obtained by solving the third-degree equation

$$s^3 + \frac{1}{\tau}s^2 + \Omega_n^2 G_0 s + \frac{\Omega_n^2}{\tau} G_1 = 0 \quad (17.282)$$

which has a real negative root together with two conjugate imaginary roots, with negative real part, as can be seen in Figure 17.11.

In Figure 17.11 the values of $sG(s) = G^*(s)$ and $-s^2/\Omega_n^2$ are generically represented as functions of s . If the degree of the polynomials $\bar{\sigma}(s)$ and $\bar{\varepsilon}(s)$ is m , as mentioned above, then the number of real negative roots also is m . Let us consider several physical situations. If the input is given by a Dirac delta function, as occurs in free oscillations, the solution of the problem contains a transient response through an exponential or a sum of exponentials [according to the degree of the polynomials representing $\bar{\sigma}(s)$ and $\bar{\varepsilon}(s)$] that decreases quickly together with a damped sine wave.

If the input is a step, then $\bar{M}(s) = M_0/s$ and $\bar{Q}_n(s)$ possess a pole at $s = 0$. The solution would contain, in addition to the already mentioned terms, an additive constant.

If the input is a stationary sinusoidal wave, then the Laplace transform of the sine function,

$$\bar{M}(s) = M_0 \frac{\omega}{s^2 + \omega^2} \quad (17.283)$$

introduces into the denominator of Eq. (17.279) or Eq. (17.280) two pure conjugated roots that cause a non-damped sinusoidal response out of phase with the input. In this case, the eigenfunction $\bar{Q}_n(s)$ is given by

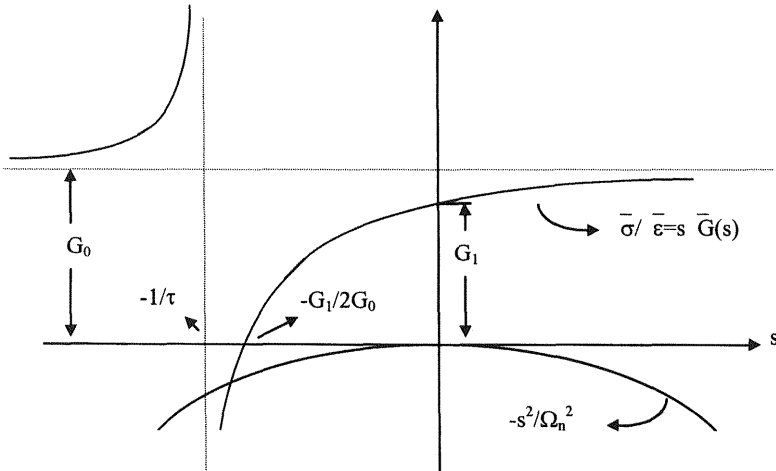


Figure 17.11 Schematic location of the real root of Eq. (17.282).

$$\bar{Q}_n(s) = M_0 \frac{\omega}{s^2 + \omega^2} \left(\frac{1 + \tau s}{\tau s^3 + s^2 + \tau \Omega_n^2 G_0 s + \Omega_n^2 G_1} \right) \quad (17.284)$$

The decomposition of Eq. (17.284) into rational fractions can be written as

$$\frac{A}{s + \lambda} + \frac{Bs + C}{(s + \beta)^2 + \xi^2} + \frac{Ds + E}{s^2 + \omega^2} \quad (17.285)$$

where λ and $\pm i\xi - \beta$ are, respectively, the real and imaginary conjugate roots of Eq. (17.282), while the unknown quantities A , B , C , D , and E are given by

$$A = -\frac{1}{\omega^2 + \lambda^2} \left(\frac{(\lambda + \tau^{-1}) \{ [\omega^2 - (\beta^2 + \xi^2)]^2 + 4\beta^2 \omega^2 \}}{[(\omega + \xi)^2 + \beta^2][(\omega - \xi)^2 + \beta^2][(-\beta + \lambda)^2 + \xi^2]} \right) \quad (17.286a)$$

$$B = \frac{\{ \lambda[\omega^2 - (\beta^2 + \xi^2)] + 2\beta(\beta^2 + \xi^2) \} - \tau^{-1}[\omega^2 - (\beta^2 + \xi^2) - 2\beta(\lambda - 2\beta)]}{[(\omega + \xi)^2 + \beta^2][(\omega - \xi)^2 + \beta^2][\xi^2 + (-\beta + \lambda)^2]} \quad (17.286b)$$

$$C = \frac{\{ \beta^2 + \xi^2 \} [\omega^2 - (\beta^2 + \xi^2) - 2\beta(\lambda - 2\beta)] + \tau^{-1} \{ \lambda[\omega^2 - (\beta^2 + \xi^2)] - 4\beta(\beta^2 - \lambda\beta - \xi^2) \}}{[(\omega + \xi)^2 + \beta^2][(\omega - \xi)^2 + \beta^2][\xi^2 + (-\beta + \lambda)^2]} \quad (17.286c)$$

$$D = \frac{1}{\omega^2 + \lambda^2} \left(\frac{\{ -2\beta\omega^2 - \lambda[\omega^2 - (\beta^2 + \xi^2)] \} + \tau^{-1}[\omega^2 - (\beta^2 + \xi^2) - 2\beta\lambda]}{[(\omega + \xi)^2 + \beta^2][(\omega - \xi)^2 + \beta^2]} \right) \quad (17.286d)$$

$$E = \frac{1}{\omega^2 + \lambda^2} \left(\frac{-\omega^4 [(-\beta + \lambda)^2 + \xi^2] + \omega^2 \{ (\beta^2 + \xi^2)^2 + \lambda^2 [\beta^2 + \xi^2 + 2\beta(\lambda - 2\beta)] \}}{+ \tau^{-1} \{ \omega^2 \{ (-2\beta - \lambda)[(-\beta + \lambda)^2 + \xi^2] \} + \lambda(\beta^2 + \xi^2)[(\beta + \lambda)^2 + \xi^2] \}}{[(\omega + \xi)^2 + \beta^2][(\omega - \xi)^2 + \beta^2][\xi^2 + (-\beta + \lambda)^2]} \right) \quad (17.286e)$$

After taking the inverse Laplace of Eq. (17.284), we obtain

$$Q_n(t) = M_0\omega \left\{ A \exp(-\lambda t) + B \left[1 + \left(\frac{C - \beta B}{B\xi} \right)^2 \right]^{1/2} \exp(-\beta t) \sin(\xi t + \phi_1) + D \left[1 + \left(\frac{E}{D\omega} \right)^2 \right]^{1/2} \sin(\omega t + \phi_2) \right\} \quad (17.287)$$

where

$$\phi_1 = \arctan \frac{\xi B}{C - \beta B}; \quad \phi_2 = \arctan \frac{D\omega}{E} \quad (17.288)$$

17.20 ANALYSIS OF TORSIONAL OSCILLATIONS USING AN ELASTIC AUXILIARY ELEMENT

As mentioned in the chapter devoted to experimental measurements, viscous damping becomes important in rubbers and, in general, in amorphous polymers above the glass transition temperature. In the case of free vibrations, and for values of $\tan \delta > 0.3$, the torsional oscillations appear overdamped, and in these conditions it is impossible to measure the frequency and the viscous damping. To overcome this difficulty, it is common practice to use as a torsion suspension wire an elastic element with a rigidity of the order of that of the material instead of a metallic thread of negligible rigidity. This was the methodology outlined in the chapter 7 [see Eq. (7.1)]. Since the constant of torsional rigidity depends on the moment of inertia of the section, and this in turn depends on the fourth power of the radius of the section in the case of circular cross sections, in practice a stainless steel rod with transverse dimensions of a few millimeters is used. In this case, the equation that governs the movement of the free end of the viscoelastic rod under torsional oscillations will be

$$J_0 \ddot{\alpha} + K\alpha + \int_0^\infty \alpha'(\theta) \dot{G}(t - \theta) d\theta = M(t); \quad z = \ell \quad (17.289)$$

where K represents the elastic constant of the new element introduced. Therefore, Eq. (17.289) represents a modified version of Eq. (17.267). If, as above, a solution in terms of separate variables is adopted, that is, $\alpha(z, t) = \phi(t) \sin \lambda z$ [see Eq. (17.254)], it is easy to obtain from Eq. (17.289), and for $z = \ell$, the expression

$$(J_0 s^2 + K) \bar{\varphi}(s) \sin \lambda \ell - \frac{\rho I_0}{\lambda} \bar{\varphi}(s) s^2 \cos \lambda \ell = \bar{M}(s) \quad (17.290)$$

where

$$\lambda^2 = -\frac{\rho I_0 s}{\bar{G}(s)} = -\frac{\mu J_0 s}{\ell \bar{G}(s)} \quad (17.291)$$

as obtained from Eq. (17.255a) after taking the Laplace transform and using Eq. (17.256).

Equation (17.290) leads to

$$\bar{\varphi}(s) = \frac{\lambda \bar{M}(s)}{\lambda(J_0 s^2 + K) \sin \lambda \ell - \rho I_0 s^2 \cos \lambda \ell} \quad (17.292)$$

and consequently the function $\bar{\alpha}(z, s)$ can be written as

$$\bar{\alpha}(z, s) = \frac{\lambda \ell \sin \lambda z \bar{M}(s)}{\lambda \ell (J_0 s^2 + K) \sin \lambda \ell - \rho \ell I_0 s^2 \cos \lambda \ell} \quad (17.293)$$

The poles of $\bar{\alpha}(z, s)$ are the zeros of the equation

$$\lambda \ell (J_0 s^2 + K) \sin \lambda \ell - \rho \ell I_0 s^2 \cos \lambda \ell = 0 \quad (17.294)$$

and from here we obtain

$$s^2 = \frac{K \lambda \ell}{\rho \ell I_0 \cot \lambda \ell - J_0 \lambda \ell} = \frac{K \lambda \ell / J_0}{\mu \cot \lambda \ell - \lambda \ell} \quad (17.295)$$

where, as usual,

$$\mu = \rho \ell I_0 / J_0 \quad (17.296)$$

Equation (17.295) together with Eq. (17.291) determine the real zeros. For small values of the argument $\lambda \ell$, we can write

$$\cot \lambda \ell \cong \frac{1}{\lambda \ell} \left(1 - \frac{1}{3} (\lambda \ell)^2 \right) \quad (17.297)$$

With this approximation, Eq. (17.295) becomes

$$s^2 \cong \frac{K}{J_0} \left(\frac{(\lambda \ell)^2}{\mu [1 - (\lambda \ell)^2 / 3] - (\lambda \ell)^2} \right) \quad (17.298)$$

which also can be written in the forms

$$s^2 \cong -\frac{K}{J_0} \left(\frac{1}{\frac{\bar{G}(s)}{J_0 \ell s} \left(1 + \frac{\mu J_0 \ell s}{3 \bar{G}(s)} \right) + 1} \right) = -\frac{K}{J_0} \left(\frac{1}{\frac{\bar{G}(s)}{J_0 \ell s} + \frac{\mu}{3} + 1} \right) \quad (17.299)$$

If the viscoelastic material under consideration is a standard solid governed by a single relaxation time, then by combining Eqs. (17.281) and (17.299), we obtain

$$\frac{G_1 + G_0 \tau s}{J_0 \ell s^2 (1 + \tau s)} = -\left(\frac{K}{J_0 s^2} + 1 + \frac{\mu}{3} \right) \quad (17.300)$$

or, alternatively,

$$s^3 + s^2 \frac{1}{\tau} + \frac{3}{J_0 \ell} \left(\frac{G_0 + K \ell}{\mu + 3} \right) s + \frac{3}{J_0 \ell \tau} (G_1 + 3K \ell) = 0 \quad (17.301)$$

As indicated in Figure 17.12, the real solution of Eq. (17.301) is negative. The other two solutions are imaginary conjugated with negative real parts. It is important to point out that in this case, and in contrast with the situation in which the auxiliary elastic element is missing, the values of λ depend not only on the geometry but also on the viscoelastic properties of the material Eq. (17.291).

On the other hand, the comments made for the case of nonutilization of an auxiliary elastic element in relation to the different types of response are also pertinent in the present context. In fact, if the trigonometric functions appearing in Eq. (17.293) are approximated by

$$\sin \lambda \ell \cong \lambda \ell - \frac{1}{6} (\lambda \ell)^3 \quad \text{and} \quad \cos \lambda \ell \cong 1 - \frac{1}{2} (\lambda \ell)^2 \quad (17.302)$$

then the following equation for $\bar{\alpha}(z, s)$ is obtained:

$$\bar{\alpha}(z, s) \cong \frac{-\lambda \ell \sin \lambda z \bar{M}(s)}{(J_0 s^2 + K) \left[\frac{\mu \ell J_0 s^2}{s \bar{G}(s)} + \frac{1}{6} \left(\frac{\mu \ell J_0 s^2}{s \bar{G}(s)} \right)^2 \right] + \rho \ell I_0 s^2 \left[1 + \frac{1}{2} \left(\frac{\mu \ell J_0 s^2}{s \bar{G}(s)} \right) \right]} \quad (17.303)$$

or, alternatively,

$$\bar{\alpha}(z, s) = \frac{-\lambda \ell \sin \lambda z \bar{M}(s)}{\rho \ell I_0 s^2 + \frac{\mu \ell J_0 s^2}{s \bar{G}(s)} \left(\frac{1}{2} \rho \ell I_0 s^2 + J_0 s^2 + K \right)} \quad (17.304)$$

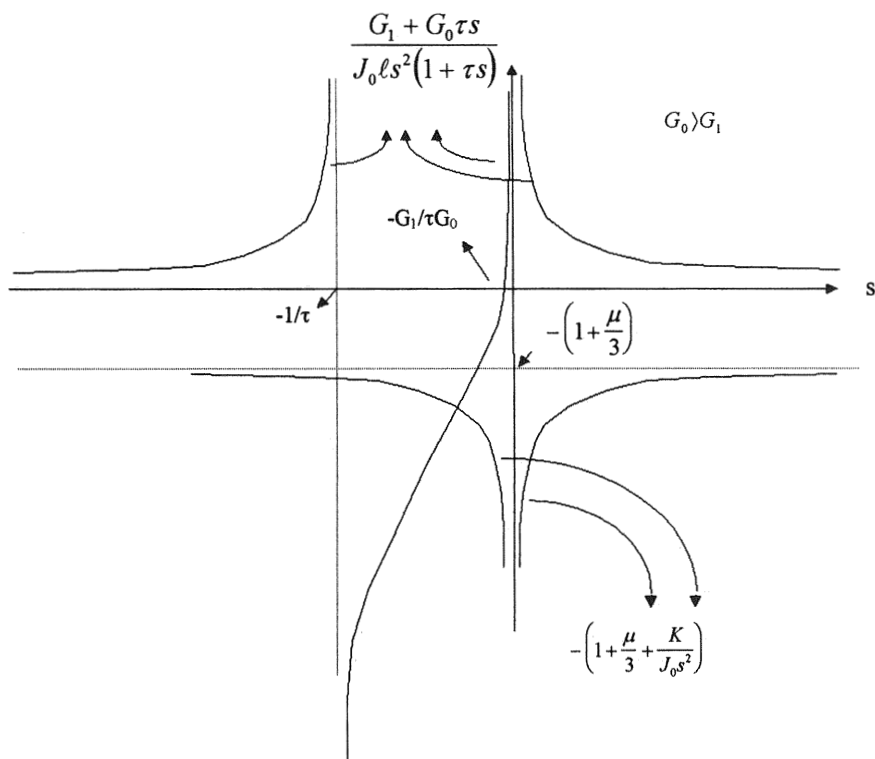


Figure 17.12 Schematic location of the real root of Eq. (17.301).

The appearance of a double pole is not a serious problem, because we can make the approximations

$$\sin \lambda z \cong \lambda z; \quad \lambda \ell \sin \lambda z \cong \lambda^2 \ell z = -\frac{z \mu J_0 s}{\bar{G}(s)} \quad (17.305)$$

Considering once again a solid standard governed by a single relaxation time,

$$\lambda \ell \sin \lambda \ell \cong -\frac{\mu z J_0 s^2 (1 + \tau s)}{G_1 + G_0 \tau s} \quad (17.306)$$

In this way, the singularity in the origin is eliminated and Eq. (17.304) becomes

$$\bar{\alpha}(z, s) = \frac{(z/\ell)(s + \tau^{-1})\eta\bar{M}(s)}{s^3 + \tau^{-1}\eta^{-1}s^2 + Ks + K\tau^{-1}} \quad (17.307)$$

where

$$\eta^{-1} = \frac{\rho I_0}{\mu J_0} G_0 + \frac{1}{2} \rho \ell I_0 + J_0 = \frac{G_0}{\ell} + \frac{1}{2} \rho \ell I_0 + J_0 \quad (17.312)$$

It can be observed that the solution of this problem is similar to that of the case already studied with $K = 0$.

PROBLEM SETS

Problem 17.1

Calculate the displacement of a beam that behaves as an elastic solid under compression but as a viscoelastic standard solid in shear. The flexural moment as a function of time is $M(t) = MH(t)$, where $H(t)$ is the step function.

Solution 17.1

Let us take as the origin of coordinates the middle point of the bar, which will be assumed fixed. It is more convenient to start by solving the elastic case and then consider the viscoelastic one by making use of the correspondence principle.

From Eqs. (17.1), (17.2), and (17.3), the components of the stress and strain tensors are

$$\sigma_{xx} = \frac{My}{I} = \frac{yE}{R}; \quad \gamma_{xx} = \frac{y}{R}; \quad \gamma_{yy} = \gamma_{zz} = -\nu \frac{y}{R} \quad (\text{P17.1.1})$$

where M is the flexural moment, E is the tensile modulus, and ν is the Poisson ratio. The strain tensor components as

$$\gamma_{xx} = \frac{\partial u}{\partial x} = \frac{y}{R}; \quad \gamma_{yy} = \frac{\partial u_y}{\partial y} = -\frac{\nu y}{R} \quad \gamma_{zz} = \frac{\partial u_z}{\partial z} = -\frac{\nu y}{R} \quad (\text{P17.1.2})$$

and

$$\gamma_{xz} = \gamma_{zx} = \gamma_{yz} = 0 \quad (\text{P17.1.3})$$

By integrating Eq. (P.17.1.2) the following expressions for the displacements are obtained:

$$u_x = \frac{xy}{R} + C_1(y, z); \quad u_y = -\frac{vy^2}{2R} + C_2(x, z); \quad u_z = -\frac{vyz}{R} + C_3(x, y) \quad (\text{P17.1.4})$$

Furthermore, the displacements at the origin $(0, 0, 0)$ are zero, that is

$$u_x = u_y = u_z = 0 \quad (\text{P17.1.5})$$

Moreover, in order to eliminate rotations of the body as a whole, the following equations at $(0, 0, 0)$ should be fulfilled:

$$\omega_x = \frac{1}{2} \left(\frac{\partial u_z}{\partial y} - \frac{\partial u_y}{\partial z} \right) = 0 \quad (\text{P17.1.6a})$$

$$\omega_y = \frac{1}{2} \left(\frac{\partial u_x}{\partial z} - \frac{\partial u_z}{\partial x} \right) = 0 \quad (\text{P17.1.6b})$$

$$\omega_z = \frac{1}{2} \left(\frac{\partial y_x}{\partial y} - \frac{\partial u_y}{\partial x} \right) = 0 \quad (\text{P17.1.6c})$$

Equations (P17.1.4) and (P17.1.6) imply that

$$\frac{x}{R} + \frac{\partial C_1(y, z)}{\partial y} = -\frac{\partial C_2(x, z)}{\partial x} \quad (\text{P17.1.7a})$$

$$\frac{\partial C_1(y, z)}{\partial z} = -\frac{\partial C_3(x, y)}{\partial x} \quad (\text{P17.1.7b})$$

and

$$\frac{\partial C_2(x, z)}{\partial z} = \frac{vz}{R} - \frac{\partial C_3(x, y)}{\partial y} \quad (\text{P17.1.7c})$$

The derivative of Eq. (P17.1.7a) with respect to y gives

$$\frac{\partial^2 C_1(y, z)}{\partial y^2} = 0 \quad \text{This implies that } C_1 = f(z) + ay + b \quad (\text{P17.1.8})$$

where, on the basis of the conditions (P17.1.5), $b = 0$. Then

$$\frac{\partial C_1}{\partial y} = a = -\frac{x}{R} - \frac{\partial C_2(x, z)}{\partial x} \quad (\text{P17.1.9})$$

Integrating with respect to x , the second equality in Eq. (P17.1.9) gives

$$C_2(x, z) = -x^2/2R - ax + g(z) + d \quad (\text{P17.1.10})$$

From Eq. (P17.1.5), $d = 0$. By taking the derivative of Eq. (P17.1.10) with respect to z and taking into account Eq. (P17.1.7c), we obtain

$$\frac{\partial C_2(x, z)}{\partial z} = \frac{dg(z)}{dz} = \frac{vz}{R} - \frac{\partial C_3(x, y)}{\partial y} \quad (\text{P17.1.11})$$

Moreover, Eqs. (P17.1.7) and (P17.1.8) indicate that

$$\frac{\partial C_1(y, z)}{\partial z} = -\frac{\partial C_3(x, y)}{\partial x} = \frac{df(z)}{dz} = f'(z) \quad (\text{P17.1.12})$$

Since C_3 is independent of z , $f'(z) = m(\text{constant})$, and

$$C_3 = mx + n \quad (\text{P17.1.13})$$

Therefore, $\partial C_3/\partial y = 0$. From Eq. (P17.1.4c) and the conditions given by Eq. (P17.1.5), $n = 0$. Integrating (P17.1.11), we obtain

$$g(z) = \frac{vz^2}{2R} + h \quad (\text{P17.1.14})$$

where, according to Eq. (P17.1.5), $h = 0$. Therefore,

$$C_1 = f(z) = mz; \quad C_2 = -\frac{x^2}{2R} + \frac{vz^2}{2R} - ax; \quad C_3 = mx \quad (\text{P17.1.15})$$

Moreover, Eqs. (P17.15a) and (P17.1.9) imply that

$$a = 0 \quad (\text{P17.1.16})$$

while Eq. (P17.1.7b) shows that

$$\frac{\partial C_1(y, z)}{\partial z} = -\frac{\partial C_3(x, y)}{\partial x} \text{ implying that } m = -m \text{ and, consequently, } m = 0 \quad (\text{P17.1.17})$$

This result suggests that $C_1 = C_3 = 0$. Hence Eq. (P17.1.4) can be written as

$$u_x = \frac{xy}{R} \quad (\text{P17.1.18a})$$

$$u_y = -\frac{vy^2}{2R} - \frac{x^2}{2R} + \frac{vz^2}{2R} = -\frac{1}{2R}[x^2 + v(y^2 - z^2)] \quad (\text{P17.1.18b})$$

$$u_z = -vyz/R \quad (\text{P17.1.18c})$$

For the plane section containing the origin of coordinates, $x = 0$. Then

$$u_x = 0; \quad u_y = -\frac{v}{2R}(y^2 - z^2); \quad u_z = -\frac{vyz}{R} \quad (\text{P17.1.19})$$

Assuming that the dimensions of the transverse cross section are a and b , the values of u_y and u_z for $z = \pm b/2$ are

$$u_y = -\frac{v}{2R}\left(y^2 - \frac{b^2}{4}\right); \quad u_z = \pm \frac{vyb}{2R} \quad (\text{P17.1.20})$$

while for $y = \pm a/2$,

$$u_y = -\frac{v}{2R}\left(\frac{a^2}{4} - z^2\right); \quad u_z = \pm \frac{vaz}{2R} \quad (\text{P17.1.21})$$

These equations suggest that the superior and inferior faces of the cross section are distorted, forming parabolas. For a section in which $x \neq 0$, for example $x = x_0$, the x component of the displacement, given by

$$u_x = \frac{x_0 y}{R} \quad (\text{P17.1.22})$$

indicates that the elementary flexion preserves the flatness of the cross sections.

If $y = z = 0$, then

$$u_y = -x^2/2R \quad (\text{parabola}) \quad (\text{P17.1.23})$$

along the x axis. According to this equation, $d^2 u_y / dx^2 = -1/R$, thus justifying considering R constant along the beam. This fact implies that the beam is deformed as a circumferential arc.

The viscoelastic solution of the Euler–Bernoulli equation, Eq. (17.15b).

$$1/R = M/EI \quad (\text{P17.1.24})$$

can be obtained by means of the elastic–viscoelastic correspondence principle

$$\bar{\sigma}_{xx}^E(s) = \bar{M}/(s\bar{E}(s)I) \quad (\text{P17.1.25})$$

$$\bar{u}_x(s) = \frac{xy}{s\bar{E}(s)} \left(\frac{\bar{M}(s)}{I} \right) \quad (\text{P17.1.26})$$

$$\bar{u}_y(s) = \frac{-1}{s\bar{E}(s)} [x^2 + s\bar{v}(s)(y^2 - z^2)] \frac{\bar{M}(s)}{2I} \quad (\text{P17.1.27})$$

$$\bar{u}_z(s) = -\frac{\bar{v}(s)yz}{\bar{E}(s)} \left(\frac{\bar{M}(s)}{I} \right) \quad (\text{P17.1.28})$$

In the preceding expressions $E(s)$ and $v(s)$ should be written in terms of the operators P_α , Q_α ; $\alpha = 1, 2$. The corresponding expressions are

$$\frac{1}{s\bar{E}(s)} = \frac{1 + \tau_E s}{E_1 + (E_1 + E_2)\tau_E s} = \frac{1 + \tau s}{E_1 + (E_1 + E_2)\tau s} \quad (\text{P17.1.29})$$

$$\frac{\bar{v}(s)}{\bar{E}(s)} = \frac{1 + \tau_E s}{1 + \tau_v s} \left(\frac{v_1 + (v_1 + v_2)\tau_v s}{E_1 + (E_1 + E_2)\tau_E s} \right) = \frac{v_1 + (v_1 + v_2)\tau s}{E_1 + (E_1 + E_2)\tau s} \quad (\text{P17.1.30})$$

$$\tau_v = \tau_E = \tau = \tau_G \left(1 + \frac{G_2}{G_1 + 3K} \right) \quad (\text{P17.1.31})$$

where use has been made of the equations developed in Problem 16.2 (Chap. 16). On the other hand, taking the Laplace transform of the applied moment, that is, $\bar{M}(s) = M_0/s$, we obtain

$$\bar{u}_x(s) = \frac{xy}{I} \left(\frac{M_0}{s} \right) \left(\frac{1 + \tau s}{E_1 + (E_1 + E_2)\tau s} \right) \quad (\text{P17.1.32})$$

$$\bar{u}_y(s) = -\frac{M_0}{2I} \left(\frac{1}{s} \right) \left[x^2 \left(\frac{1 + \tau s}{E_1 + (E_1 + E_2)\tau s} \right) + (y^2 - z^2) \left(\frac{v_1 + (v_1 + v_2)\tau s}{E_1 + (E_1 + E_2)\tau s} \right) \right] \quad (\text{P17.1.33})$$

$$\bar{u}_z(s) = -\frac{yz}{I} M_0 \left(\frac{1}{s} \right) \left[\frac{v_1 + (v_1 + v_2)\tau s}{E_1 + (E_1 + E_2)\tau s} \right] \quad (\text{P17.1.34})$$

whose Laplace inverses are

$$u_x(x, y, t) = \frac{xy}{I} M_0 \left[\frac{1}{E_1} - \frac{E_2}{E_1(E_1 + E_2)} \exp\left(-\frac{E_1 t}{(E_1 + E_2)\tau}\right) \right] \quad (\text{P17.1.35})$$

$$u_y(x, y, z, t) = -\frac{M_0}{2I} \left\{ x^2 \left[\frac{1}{E_1} - \frac{E_2}{E_1(E_1 + E_2)} \exp\left(-\frac{E_1 t}{(E_1 + E_2)\tau}\right) \right] \right. \\ \left. + (y^2 - z^2) \left[\frac{v_1}{E_1} + \frac{(E_1 v_2 - E_2 v_1)}{E_1(E_1 + E_2)} \exp\left(-\frac{E_1 t}{(E_1 + E_2)\tau}\right) \right] \right\} \quad (\text{P17.1.36})$$

$$u_z(y, z, t) = -\frac{yzM_0}{I} \left[\frac{v_1}{E_1} + \frac{(E_1 v_2 - E_2 v_1)}{E_1(E_1 + E_2)} \exp\left(-\frac{E_1 t}{(E_1 + E_2)\tau}\right) \right] \quad (\text{P17.1.37})$$

The initial values are obtained by making $t = 0$ in these equations. Accordingly,

$$u_x(x, y, 0) = \frac{xy}{I} M_0 \left(\frac{1}{E_1} + \frac{1}{E_2} \right) \quad (\text{P17.1.38})$$

$$u_y(x, y, z, 0) = -\frac{M_0}{2I} \left[x^2 \left(\frac{1}{E_1} + \frac{1}{E_2} \right) + (y^2 - z^2) \left(\frac{v_1 + v_2}{E_1 + E_2} \right) \right] \quad (\text{P17.1.39})$$

$$u_z(y, z, 0) = -\frac{yz}{I} M_0 \left(\frac{v_1 + v_2}{E_1 + E_2} \right) \quad (\text{P17.1.40})$$

The long-time behavior is found by taking the limit of Eqs. (P17.1.38)–(P17.1.40) as $t \rightarrow \infty$, that is

$$u_x(x, y, \infty) = \frac{xy}{I} M_0 \frac{1}{E_1} \quad (\text{P17.1.41})$$

$$u_y(x, y, z, \infty) = -\frac{M_0}{2I} \left(\frac{x^2}{E_1} + (y^2 - z^2) \frac{v_1}{E_1} \right) \quad (\text{P17.1.42})$$

$$u_z(y, z, \infty) = -\frac{yzM_0}{I} \left(\frac{v_1}{E_1} \right) \quad (\text{P17.1.43})$$

Problem 17.2

Determine the shape of a single cantilevered beam, whose material behavior in tension is that of a viscoelastic standard solid, under a load P applied at its free end and a uniform load P_1 per unit length of the beam (see Fig. P17.2.1).

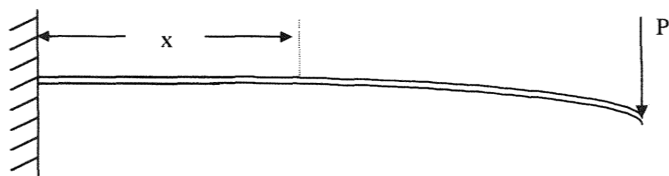


Figure P17.2.1

Solution 17.2

The differential equation for the deflection y of a slender elastic beam under the hypothesis of linearity is given by Eq. (17.19a),

$$\frac{d^2 u_y}{dx^2} = \frac{1}{EI} M(x) \quad (\text{P17.2.1})$$

where the minus sign in the deflection has been disregarded. In this equation $M(x, t)$ is the flexural moment, I the polar moment of inertia of the transverse section, and E the elastic modulus. For a viscoelastic material, Eq. (P17.2.1) can be written as

$$I \frac{d^2 u_y(x, t)}{dx^2} = \int_0^t D(t - \theta) \dot{M}(x, \theta) d\theta \quad (\text{P17.2.2})$$

where D is the tensile compliance [see Eq. (17.13a)]. According to the principle of superposition of loads and deflections, and assuming that the load P is applied at a time t_0 after P_1 is applied, the momentum at $t > t_0$ is

$$M(x, t) = -P(l - x)H(t - t_0) - \frac{P_1}{2}(l - x)^2 H(t) \quad (\text{P17.2.3})$$

where l is the length of the bar, x the distance from the clamping to a generic point, and $H(t)$ the unit step function.

The Laplace transform of Eq. (P17.2.2) is given by

$$I \frac{d^2 \bar{u}_y(x, s)}{dx^2} = s \bar{D}(s) \bar{M}(s, x) \quad (\text{P17.2.4})$$

where

$$M(x, t)|_{t=0} = 0 \quad (\text{P17.2.5})$$

while the Laplace transform of the momentum equation, (P17.2.3), is given by

$$\bar{M}(s, x) = -P(l-x)\left(\frac{1}{s}\right) \exp(-st_0) - \frac{P_1}{2}(l-x)^2\left(\frac{1}{s}\right) \quad (\text{P17.2.6})$$

Moreover, according to Eq. (10.31), the following expression for a viscoelastic standard solid holds:

$$s\bar{D}(s) = D_1 + D_2/(1 + \tau s) \quad (\text{P17.2.7})$$

Integration of Eq. (P17.2.2) using the boundary conditions

$$u_y = 0, \quad \frac{du_y}{dx} = 0 \quad \text{for } x = 0 \quad (\text{P17.2.8})$$

gives

$$I\bar{u}_y(x, s) = \left(D_1 + \frac{D_2}{1 + \tau s}\right)\left(\frac{1}{s}\right) \left[-P\left(lx - \frac{x^2}{2}\right)e^{-st_0} - \frac{P_1}{2}\left(\frac{l^2x^2}{2} - \frac{lx^3}{3} + \frac{x^4}{12}\right) \right] \quad (\text{P17.2.9})$$

whose is given by

$$Iu_y(x, t) = -\left\{D_1H(t) + D_2H(t)\left[1 - \exp\left(-\frac{t}{\tau}\right)\right]\right\}\left(\frac{P_1}{2}\right)\left(\frac{l^2x^2}{2} - \frac{lx^3}{3} + \frac{x^4}{12}\right) \\ + P\left(\frac{lx^2}{2} - \frac{x^3}{6}\right)\left\{D_1H(t-t_0) + D_2H(t-t_0)\left[1 - \exp\left(-\frac{t-t_0}{\tau}\right)\right]\right\} \quad (\text{P17.2.10})$$

Problem 17.3

Study the free and forced transverse vibrations of a beam clamped at one end and free at the other when the force is applied at the free end.

Solution 17.3

This is a modified version of the problem solved in section 17.10, though the boundary conditions are different. However, new aspects of the general problem of a transverse vibrating beam are considered here.

The expressions for free and forced vibrations are given, respectively, by Eqs. (17.85) and (17.99). If the origin of coordinates is taken at the clamped end of the beam, the assumed boundary conditions are

$$u_y(0, t) = u'_y(0, t) = u''_y(\ell, t) = u'''_y(\ell, t) = 0 \quad (\text{P17.3.1})$$

where in this case ℓ is the length of the beam. We consider the two cases separately.

Case 1. In the free vibrations case the secular or frequency equation is easily obtained as

$$\cosh \lambda \ell \cos \lambda \ell = -1 \quad (\text{P17.3.2})$$

whose lower mode is given by $\lambda \ell = 1.875$ and

$$\lambda \ell = \frac{2n-1}{2} \pi \quad (\text{P17.3.3})$$

for $n \geq 5$.

According to Eq. (17.88), a resonance frequency is obtained as

$$\omega^2 = \beta^4 s \bar{E}(s) I / \rho A \ell^4 \quad (\text{P17.3.4})$$

for each value of β , where $\beta = \lambda \ell$, and the remaining symbols have been defined in the main text.

Case 2. In the case of forced vibrations, and following the double Laplace transform method, we obtain

$$\begin{aligned} \bar{u}_y(x, s) = \frac{1}{2\lambda^2} \left[\frac{F\omega}{s^2 + \omega^2} \left(\frac{1}{s\bar{E}(s)I\lambda} \right) [\sinh \lambda(x - \ell') - \sin \lambda(x - \ell')] \right. \\ \left. + \bar{u}''_y(0, s)(\cosh \lambda x - \cos \lambda x) + \frac{1}{\lambda} \bar{u}'''_y(0, s)(\sinh \lambda x - \sin \lambda x) \right] \end{aligned} \quad (\text{P17.3.5})$$

In order to find $\bar{u}''_y(0, s)$ and $\bar{u}'''_y(0, s)$, we must calculate $\bar{u}''_y(x, s)$ and $\bar{u}'''_y(x, s)$ at $x = \ell$, where, according to the boundary conditions, these derivatives are zero.

Moreover, if $\ell' = \ell$ after the pertinent derivations in Eq. (P17.3.5), the following system of equations is obtained:

$$\lambda \bar{u}_y''(0, s) [\cosh \lambda \ell - \cos \lambda \ell] + \bar{u}_y'''(0, s) [\sinh \lambda \ell - \sin \lambda \ell] = 0 \quad (\text{P17.3.6a})$$

$$\lambda \bar{u}_y''(0, s) [\sinh 2\lambda \ell + \sin 2\lambda \ell] + \bar{u}_y'''(0, s) [\cosh 2\lambda \ell - \cos 2\lambda \ell] = -\frac{2F\omega}{s^2 + \omega^2} \left(\frac{1}{s\bar{E}(s)I} \right) \quad (\text{P17.3.6b})$$

These equations lead to

$$\bar{u}_y''(0, s) = \alpha \frac{\sinh \lambda \ell + \sin \lambda \ell}{1 + \cosh \lambda \ell \cos \lambda \ell} \quad (\text{P17.3.7})$$

and

$$\bar{u}_y'''(0, s) = -\lambda \alpha \frac{\cos \lambda \ell + \cosh \lambda \ell}{1 + \cosh \lambda \ell \cos \lambda \ell} \quad (\text{P17.3.8})$$

where

$$\bar{\alpha}(s) = \frac{F\omega}{(s^2 + \omega^2)s\bar{E}(s)I\lambda} \quad (\text{P17.3.9})$$

After substituting these equations into Eq. (P17.3.6), the maximum deflection at the end of the beam is given by

$$\bar{u}_y(\ell, s) = \frac{F\omega}{(s^2 + \omega^2)s\bar{E}(s)I\lambda^3} \left(\frac{\sin \lambda \ell \cosh \lambda \ell - \sinh \lambda \ell \cos \lambda \ell}{1 + \cosh \lambda \ell \cos \lambda \ell} \right) \quad (\text{P17.3.10})$$

when the load is applied at the end of the beam. By expanding in series the trigonometric and hyperbolic functions appearing in Eq. (P17.3.10) and taking the first terms in the corresponding expansions, we obtain

$$\bar{u}_y(\ell, s) = \frac{F\omega \ell^3}{3(s^2 + \omega^2)s\bar{E}(s)I} \quad (\text{P17.3.11})$$

When the driving frequency is close to the natural, or in this case, the resonance frequency, the amplitude of the vibration for low-loss materials is dominated by the contribution of this mode. Writing $s = -\lambda + i\omega$, where $2\lambda \cong \omega \tan \delta$, u_y we have

$$u_y \simeq [(\omega_r^2 - \omega^2)^2 + 4\lambda^2 \omega^2]^{-1/2} \quad (\text{P17.3.12})$$

The deflection has a maximum at $\omega = \omega_r$, given by

$$u_{y,\max} = \frac{1}{2\lambda\omega_r} \cong \frac{1}{\omega_r^2 \tan \delta} \quad (\text{P17.3.13})$$

Note that if ω_1 and ω_2 are two frequencies at each side of ω_r , the following relationship holds

$$Cu_y^2 = u_{y,\max}^2 \quad (\text{P17.3.14})$$

where C is a constant. Then, according to Eqs. (P17.3.13) and (P17.3.14), C can be written as

$$C = 1 + \frac{(\omega_r^2 - \omega_i^2)^2}{\omega_r^4 \tan^2 \delta} \quad (\text{P17.3.15})$$

where $i = 1, 2$ and $\omega \cong \omega_1 \cong \omega_2 \cong \omega_r$. From this equation and assuming that $C = 2$, we obtain

$$\tan \delta \cong \frac{\Delta\omega}{\omega} \quad (\text{P17.3.16})$$

where $\Delta\omega = \omega_2 - \omega_1$. This equation is frequently used in resonance experiments to determine $\tan \delta$.

Finally, to obtain a closed solution, we assume a viscoelastic material [Eq. (10.41) for which

$$s\bar{E}(s) = (E_1 + E_0\tau s)/(1 + \tau s) \quad (\text{P17.3.17})$$

The corresponding inverse Laplace for the equation of the deflection is obtained from Eqs. (P17.3.11) and (P17.3.17). The final result is

$$u_y(x, t) = \frac{F\omega}{6I(E_1^2 + E_0^2\omega^2\tau^2)}(E_0 - E_1)\tau \left\{ \exp\left[-\frac{E_1}{E_0}\left(\frac{t}{\tau}\right)\right] - \left[1 + \left(\frac{1 + \omega^2\tau^2(E_0/E_1)}{\omega\tau(1 - E_0/E_1)}\right)^2\right]^{1/2} \sin(\omega t + \phi) \right\} \quad (\text{P17.3.18})$$

where

$$\phi = \arctan \frac{\omega\tau(1 - E_0/E_1)}{1 + \omega^2\tau^2(E_0/E_1)} \quad (\text{P17.3.19})$$

The response consists of a decreasing exponential and an out-of-phase sinusoidal wave. As we can see, this result is formally similar to those

obtained in the main text, the differences arising, of course, from the boundary conditions.

Problem 17.4

According to each one of the three formulas for shear correction in a beam (see Sect. 17.10), estimate the values of d/l for which the corrections due to shear effects are less than 5%.

Solution 17.4

Let

$$1 + C(d/l)^2 \leq 1.05 \quad (\text{P17.4.1})$$

C being a factor that depends on the approach followed to obtain the shear correction. The values of d/l are 0.129, 0.153, 0.167, respectively. These results suggest that if the accuracy of the experiment device to calculate the tensile modulus is better than 5%, corrections due to shear effects are unnecessary for values of d/l lower than 0.1.

Problem 17.5

As a first approach, let us assume a sinusoidal shape for the deformed beam considered in Section 17.11, given by

$$u_y = u_{ym} \sin \frac{\pi}{L} x$$

From this expression, calculate the value of Q' given in Eq. (17.199) and discuss its accuracy in comparison with the more sophisticated calculation outlined in the main text.

Solution 17.5

By substituting the proposed expression for u_y into Eq. (17.185) and subsequent integration, we obtain

$$\frac{1}{2l} \int_0^l \left(\frac{du_y}{dx} \right)^2 dx = \frac{\pi^2 u_{ym}^2}{4L^2} \quad (\text{P17.5.1})$$

where $L = 2l$.

Then the non thermal total longitudinal tension Q' can be written as

$$Q' = EA \left[\frac{\pi^2}{4} \left(\frac{u_{ym}^2}{L^2} \right) \right] \quad (\text{P17.5.2})$$

It can be seen that if $E \cong Ep$, the discrepancy with the more correct result given by Eq. (17.203) is less than 3%.

Problem 17.6

Find the torsion function and the torque for a viscoelastic hollow rod of elliptical cross section.

Solution 17.6

We have shown in section 17.16 that the function F must be constant on the boundary of a simply connected section. Actually, since the applied forces on the lateral surfaces are zero, the function F for a multiply connected cross section must be constant along each boundary. However, the constants are not the same, and only one of these constants can be arbitrarily chosen.

Let us consider the doubly connected cross section of the elliptical rod. Without losing generality we shall consider F to be zero on the outer boundary. The value of F on the inner boundary is determined by the condition that the warping u_z must be single-valued. The line integral along the contour line corresponding to the inner boundary is given by

$$\oint_C du_z = \oint_C \left(\frac{\partial u_z}{\partial x} dx + \frac{\partial u_z}{\partial y} dy \right) = \oint_C \left(\frac{\partial \psi}{\partial x} \frac{\partial \alpha}{\partial z} dx + \frac{\partial \psi}{\partial y} \frac{\partial \alpha}{\partial z} dy \right) \quad (\text{P17.6.1})$$

where the displacement u_z is expressed in terms of the torsion function ψ and the relative torsion angle $\partial\alpha/\partial z$. Taking the Laplace transform of the stress-strain relationships [Eqs. (17.214)], we obtain

$$\bar{\sigma}_{zx}(s) = s\bar{G}(s) \left(-y + \frac{\partial \psi}{\partial x} \right) \frac{\partial \bar{\alpha}(s)}{\partial z} \quad (\text{P17.6.2})$$

$$\bar{\sigma}_{zy}(s) = s\bar{G}(s) \left(x + \frac{\partial \psi}{\partial y} \right) \frac{\partial \bar{\alpha}(s)}{\partial z} \quad (\text{P17.6.3})$$

By substituting these equations into the Laplace transform of Eq. (P17.6.1), after some rearrangements, we obtain

$$\oint_C d\bar{u}_z = \frac{1}{s\bar{G}(s)} \oint_C [\bar{\sigma}_{zx}(s) dx + \bar{\sigma}_{zy}(s) dy] - \frac{\partial \bar{\alpha}(s)}{\partial z} \oint_C (x dy - y dx) \quad (\text{P17.6.4})$$

Since u_z is a single-valued function and the integration is taken over a closed path, the left hand side of Eq. (P17.6.4) is zero. Accordingly,

$$\oint_C [\bar{\sigma}_{zx}(s)dx + \bar{\sigma}_{zy}(s)dy] = 2s\bar{G}(s) \frac{\partial \bar{\alpha}(s)}{\partial z} A \quad (\text{P17.6.5})$$

where A is the area enclosed by the inner boundary. This equation must also be fulfilled by the torsion function F . In general it is difficult to find such a function that satisfies these conditions. However, if the solution for a solid rod is known, a solution for the hollow rod can be easily found.

The equation of the outer boundary for a solid elliptical cylinder having as axes $2a$ and $2b$ is

$$\frac{x^2}{a^2} + \frac{y^2}{b^2} = 1 \quad (\text{P17.6.6})$$

Let us assume a stress function

$$F = k \left(\frac{x^2}{a^2} + \frac{y^2}{b^2} - 1 \right) \quad (\text{P17.6.7})$$

where k is a constant. Then F vanishes on the boundary, and from $\Delta F = -1$ [Eq. (17.223)], we obtain

$$k = -a^2 b^2 / 2(a^2 + b^2) \quad (\text{P17.6.8})$$

From knowledge of the function F it is easy to obtain $\partial\psi/\partial x$ and $\partial\psi/\partial y$, and according to Eqs. (P17.6.2) and (P17.6.3) the shear stresses are given by

$$\bar{\sigma}_{zx}(s) = -\frac{2ya^2}{a^2 + b^2} \left(\frac{\partial \bar{\alpha}(s)}{\partial z} \right) s\bar{G}(s) \quad (\text{P17.6.9})$$

and

$$\bar{\sigma}_{zy}(s) = \frac{2xb^2}{a^2 + b^2} \left(\frac{\partial \bar{\alpha}(s)}{\partial z} \right) s\bar{G}(s) \quad (\text{P17.6.10})$$

from which we obtain

$$\sigma_{zy}/\sigma_{zx} = -xb^2/ya^2 \quad (\text{P17.6.11})$$

On the other hand, from the equation of the ellipse we easily find

$$y' = -xb^2/ya^2 \quad (\text{P17.6.12})$$

Equations (P17.6.11) and (P17.6.12) indicate that the shear stress at any point within the cross section of an elliptical cylinder under torsion is tangent to an ellipse passing through this point with the same axis ratio, a/b , as that of the boundary ellipse. In other words, the lines of shear stress are concentric ellipses. Consequently, the inner boundary also coincides with a line of shear stress. Therefore the shear stress acting normally on the internal surface parallel to the z axis is null. Moreover, if a concentric cylinder is removed from the rod, the stress distribution in the remaining portion will be the same as in the solid cylinder. For this reason, the stress function will be given by

$$F = -\frac{a^2b^2}{2(a^2 + b^2)} \left(\frac{x^2}{a^2} + \frac{y^2}{b^2} - 1 \right) \quad (\text{P17.6.13})$$

Now we consider the hollow elliptical cross section obtained from the solid cylinder where a concentric elliptical area has been removed. The axes of the area eliminated are respectively $2ka$ and $2kb$, where, obviously, $k < 1$.

The moment of torque can be calculated in the usual way as the difference between the torque acting on the solid cylinder and the torque corresponding to the part removed to produce the hollow cylinder. For the solid cylinder, and according to the prescriptions made in the main text [Eqs. (17.235) and (17.245),

$$M(z, t) = 4 \iint_Q F \, dx \, dy \int_0^\infty G(t - \theta) \frac{\partial^2 \alpha}{\partial \tau \partial \theta} d\theta \quad (\text{P17.6.14})$$

where Q is the area of the cross section. The double integral can be calculated as follows:

$$4 \iint_Q F \, dx \, dy = 4k \left(\frac{1}{a^2} \iint_Q x^2 \, dx \, dy + \frac{1}{b^2} \iint_Q y^2 \, dx \, dy - \iint_Q dx \, dy \right) \quad (\text{P17.6.15})$$

where the first two integrals on the right represent the moment of inertia of the cross section about the y and x axes, respectively, whereas the third integral is the area of that cross section. The values of these three integrals are respectively given by $(\pi/4)a^3b$, $(\pi/4)ab^3$, and πab . If the value of k given by Eq. (P17.6.8) is taken into account, the moment of torque given by Eq. (P17.6.14) can be written as

$$M = \frac{\pi a^3 b^3}{a^2 + b^2} \int_0^\infty G(t - \theta) \frac{\partial^2 \alpha}{\partial \tau \partial \theta} d\theta \quad (\text{P17.6.16})$$

Then, the total torque will be given by

$$\begin{aligned} M &= \left(\frac{\pi a^3 b^3}{a^2 + b^2} - \frac{\pi k^6 a^3 b^3}{(ka)^2 + (kb)^2} \right) \int_0^\infty G(t - \theta) \frac{\partial^2 \alpha}{\partial \theta \partial z} d\theta \\ &= \frac{\pi a^3 b^3}{a^2 + b^2} (1 - k^4) \int_0^\infty G(t - \theta) \frac{\partial^2 \alpha}{\partial \theta \partial z} d\theta \end{aligned} \quad (\text{P17.6.17})$$

By making $a = b$ in Eq. (P17.6.17), the torque for a cylinder of circular cross section is obtained as

$$M = \frac{\pi}{2} (r_o^4 - r_i^4) \int_0^\infty G(t - \theta) \frac{\partial^2 \alpha}{\partial \theta \partial z} d\theta \quad (\text{P17.6.18})$$

where r_o and r_i , respectively, are the outer and inner radii of the hollow circular cylinder.

Problem 17.7

Study the forced oscillations in a straight circular viscoelastic cylinder (see Fig. P17.7.1).

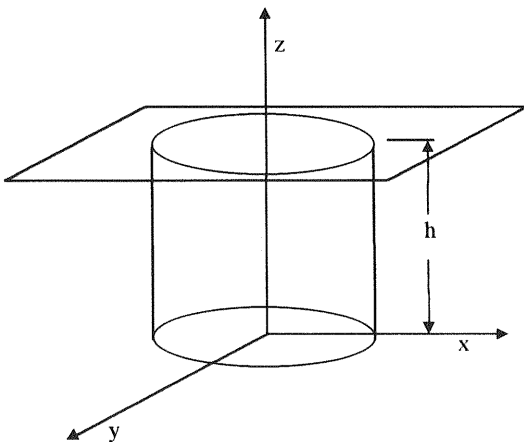


Figure P17.7.1

Solution 17.7

To solve this problem we shall start, as usual, with the elastic case, using cylindrical coordinates. According to Problem 4.6 (Chap. 4), the equation of motion is

$$\frac{2\sigma_{r\theta}}{r} + \frac{\partial\sigma_{r\theta}}{\partial r} + \frac{1}{\theta} \frac{\partial\sigma_{\theta\theta}}{\partial\theta} + \frac{\partial\sigma_{\theta z}}{\partial z} + b_\theta = \rho \frac{\partial^2 u_\theta}{\partial t^2} \quad (\text{P17.7.1})$$

where it has been taken into account that $u_r = u_z = 0$ and $u_\theta = \hat{u}_\theta(r, z, t)$. Here volume forces are not considered, and consequently $b_\theta = 0$. From the stress-strain relationship we find

$$\sigma_{r\theta} = 2G\gamma_{r\theta}; \quad \sigma_{\theta z} = 2G\gamma_{\theta z}; \quad \sigma_{\theta\theta} = \frac{G}{2(1-2\nu)} [(1-\nu)\gamma_{\theta\theta} + \nu(\gamma_{rr} + \gamma_{zz})] \quad (\text{P17.7.2})$$

where the strain tensor components, according to Problem 4.2 are given by

$$\gamma_{r\theta} = \frac{1}{2} \left(\frac{\partial u_\theta}{\partial r} - \frac{u_\theta}{r} \right); \quad \gamma_{\theta z} = \frac{1}{2} \frac{\partial u_\theta}{\partial z}; \quad \gamma_{\theta\theta} = \frac{1}{r} \frac{\partial u_\theta}{\partial\theta} \quad (\text{P17.7.3a})$$

$$\gamma_{rr} = 0; \quad \gamma_{zz} = 0 \quad (\text{P17.7.3b})$$

After accomplishing the appropriate substitutions in the equilibrium equation, we obtain

$$\frac{\partial^2 u_\theta}{\partial r^2} + \frac{1}{r} \frac{\partial u_\theta}{\partial r} - \frac{u_\theta}{r^2} + \frac{\partial^2 u_\theta}{\partial z^2} = \frac{\rho}{G} \frac{\partial^2 u_\theta}{\partial t^2} \quad (\text{P17.7.4})$$

Assuming a linear dependence of u_θ upon r ,

$$\gamma_{r\theta} = \gamma_{\theta z} = \sigma_{\theta\theta} = \sigma_{r\theta} = 0 \quad (\text{P17.7.5})$$

Thus the only nonzero component of the stress tensor is $\sigma_{\theta z}$. Therefore the equation of motion will be

$$\frac{\partial^2 u_\theta}{\partial z^2} = \frac{\rho}{G} \frac{\partial^2 u_\theta}{\partial t^2} \quad (\text{P17.7.6})$$

After separation of variables, we can write

$$u_\theta = r f(z) \exp(i\omega t) \quad (\text{P17.7.7})$$

whose substitution into Eq. (P17.7.6) leads to

$$f''(z) + \frac{\rho\omega^2}{G}f(z) = 0 \quad (\text{P17.7.8})$$

The solution of the viscoelastic problem is found by assuming $G = G^*(\omega)$. By assuming furthermore that the sample is fixed at $z = h$ and that the torque is applied at $z = 0$, the solution of the previous differential equation is given by

$$f(z) = A \sin\left(\frac{\rho}{G^*}\right)^{1/2} \omega z + B \cos\left(\frac{\rho}{G^*}\right)^{1/2} \omega z \quad (\text{P17.7.9})$$

From Eq. (17.246)

$$\frac{\partial M(z, t)}{\partial z} = \rho I \frac{\partial^2 \alpha}{\partial t^2} \quad (\text{P17.7.10a})$$

where

$$\alpha = u_\theta / r = f(z)e^{i\omega t} \quad (\text{P17.7.10b})$$

Moreover, $M(t) = M_0 \exp(i\omega t)$, with $I = (\pi/2)R^4$, where R is the radius of the circular cylinder.

Integrating Eq. (P17.7.10), we obtain

$$M = \frac{\pi}{2} R^4 \frac{\rho\omega^2 h}{\Omega^*} \left(A \cos \frac{\Omega^*}{h} - B \sin \frac{\Omega^*}{h} \right) e^{i\omega t} \quad (\text{P17.7.11a})$$

where

$$\Omega^* = \omega h \left(\frac{\rho}{G^*} \right)^{1/2} \quad (\text{P17.7.11b})$$

By taking into account the boundary conditions mentioned earlier we have.

$$z = 0, \quad \alpha(0, t) = B e^{i\omega t}; \quad M(0, t) = \frac{\pi}{2} R^4 \frac{\rho\omega^2 h}{\Omega^*} A e^{i\omega t} \quad (\text{P17.7.12})$$

$$\alpha(h, t) = 0 = e^{i\omega t} (A \sin \Omega^* + B \cos \Omega^*) \quad (\text{P17.7.13})$$

These conditions imply that $A = -B \cot \Omega^*$. Therefore,

$$\frac{M(0, t)}{\alpha(0, t)} = \frac{\pi R^4}{2} \rho \omega^2 h \frac{\cot \Omega^*}{\Omega^*} \quad (\text{P17.7.14})$$

If G^* is known, the torsion angle $\alpha(0, t)$ at $z = 0$ is given by

$$\alpha(0, t) = \frac{2M(0, t)\Omega^*}{\pi R^4 \rho \omega^2 h} \tan \Omega^* \quad (\text{P17.7.15})$$

where $\alpha(0, t)$ is a complex value.

Conversely, if the torsion angle is known, then the modulus, G^* , for a given torque can be calculated. If the inertial terms can be neglected,

$$\cot \Omega^* \cong \frac{1}{\Omega^*} \quad \text{and} \quad \frac{M(0, t)}{\alpha(0, t)} = \frac{\pi R^4}{2h} G^* \quad (\text{P17.7.16})$$

Note that neglecting the inertial terms, we linearize the problem in terms of Ω^* . If the applied torque at $z = 0$ is known, then $\alpha(0, t)$ is a complex quantity, its modulus being $f(0)$ and its argument the phase angle between the modulus and the applied torque.

Problem 17.8

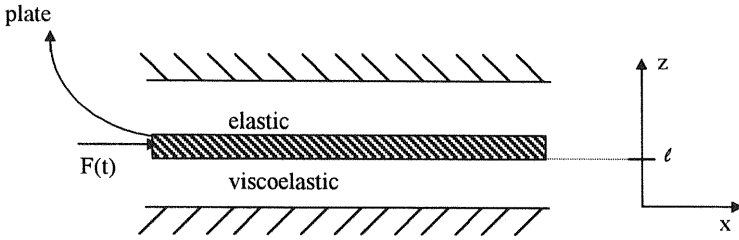
In order to explain and solve the problems inherent to the calculation of the complex modulus from free vibration experiments, Markovitz (17) proposed the resolution of the following problem.

An infinite slab of viscoelastic material is located between a fixed infinite plane at $x = 0$ and a perfectly rigid, infinite, flat moving plate having a mass per unit area M at $x_1 = l$. The motion of the plate in the X direction is restrained by a purely elastic slab and by the viscoelastic sample (see Fig. P17.8.1). When the plate undergoes a displacement in the transverse direction, it will experience a force per unit area $ku_x(t)$ due to the elastic element and a stress σ_{xz} due to the viscoelastic one, σ_{xz} being dependent on the deformation as well as on the properties of the sample. Study the inertial and noninertial responses.

Solution 17.8

If an external force per unit area, $F(t)$, is applied to the rigid plate in the x direction, a displacement u is produced, and the motion will be governed by

$$M\ddot{u}_x + \sigma_{xz}(\ell, t) + ku_x(t) = F(t) \quad (\text{P17.8.1})$$

**Figure P17.8.1**

First we study the problem for $F(t) = F_0\delta(t)$, where $\delta(t)$ is the Dirac function, as is usual in the study of free vibrations. According to the conditions of the problem, the displacements will be

$$u_x = u(z, t); \quad u_y = 0; \quad u_z = 0 \quad (\text{P17.8.2})$$

Since in this case the only component of the tensor of deformation is $\gamma_{xz} = \gamma_{zx}$, the general stress-strain relationship is given by Eqs. (5.73) as

$$\sigma_{ij}(t) = 2 \int_{-\infty}^t G(t-\theta) \frac{\partial \gamma_{ij}}{\partial \theta} d\theta + \delta_{ij} \int_{-\infty}^t \left[K(t-\theta) - \frac{2}{3} G(t-\theta) \right] \frac{\partial \gamma_{kk}}{\partial \theta} d\theta \quad (\text{P17.8.3})$$

where K and G are, respectively, the bulk and shear relaxation moduli. According to the conditions of the present problem, the only nonzero components of the stress tensor are

$$\sigma_{xz} = \sigma_{zx} = 2 \int_{-\infty}^t G(t-\theta) \frac{\partial \gamma_{xz}}{\partial \theta} d\theta \quad (\text{P17.8.4})$$

and the equation of motion expressed in terms of the displacements is reduced to

$$\int_{-\infty}^t G(t-\theta) \frac{\partial u_{x,zz}}{\partial \theta} d\theta = \rho i i_x, \quad \frac{\partial u_{x,zz}}{\partial \theta} = 2 \frac{\partial^2 \gamma_{xz}}{\partial \theta \partial z} \quad (\text{P17.8.5})$$

since in this case $\gamma_{xz} = (1/2) \partial u_x / \partial z$ and the comma in the subscript x, zz means differentiation with respect to z .

The boundary conditions are

$$u(0, t) = 0; \quad u(\ell, t) = u_m \quad (\text{P17.8.6})$$

The Laplace transform of Eq. (P17.8.5) can be written as

$$\bar{G}(s) \frac{\partial^2 \bar{u}_x(s)}{\partial z^2} = \rho s \bar{u}_x(s) \quad (\text{P17.8.7})$$

whose solution is given by

$$\bar{u}_x(z, s) = A \exp(qz) + B \exp(-qz), \quad q = [\rho s / \bar{G}(s)]^{1/2} \quad (\text{P17.8.8})$$

The coefficients A and B , calculated from the boundary conditions, are

$$A = -B = \frac{\bar{u}_m(s)}{2 \sinh ql} \quad (\text{P17.8.9})$$

Consequently,

$$\bar{u}_x(z, s) = \bar{u}_m(s) \frac{\sinh qz}{\sinh ql} \quad (\text{P17.8.10})$$

and

$$\bar{\sigma}_{xz}(z, s) = 2s\bar{G}(s)\bar{\gamma}_{xz}(z, s) = qs\bar{G}(s)\bar{u}_m(s) \frac{\cosh qz}{\sinh ql} \quad (\text{P17.8.11})$$

The Laplace transform of Eq. (P17.8.1) together with Eq. (P17.8.11) lead to

$$\bar{u}_m(s) = \frac{\bar{F}(s)}{Ms^2 + k + q\rho\bar{G}(s) \coth ql}, \quad u(0) = 0; \quad \dot{u}(0) = 0 \quad (\text{P17.8.12})$$

From Eqs. (P17.8.10) and (P17.8.12) we have

$$\bar{u}_x(z, s) = \frac{\bar{F}(s) \sinh qz}{(Ms^2 + k) \sinh ql + qs\bar{G}(s) \cosh ql} \quad (\text{P17.8.13})$$

which is the sought solution.

In order to complete the problem it is necessary to specify $F(t)$ and $G(t)$. It should be noted that Eq. (P17.8.13) represents the solution of many other problems, depending on the form proposed for $\bar{F}(s)$. Each case requires a specific treatment. Let us consider first the noninertial solution.

As we have seen in the previous section, the density of the sample included on the right-hand side of the equation of motion gives, as a solution of the problem, the propagation of the stress wave through the sample. In the present context, this part of the phenomenon is of limited

interest and in a first approach can be ignored. In these conditions, the noninertial equation of motion becomes

$$\frac{d^2 \bar{u}_x(z, s)}{dz^2} = 0 \quad (\text{P17.8.14})$$

whose solution is given by

$$\bar{u}_x = az + b \quad (\text{P17.8.15})$$

By taking into account the boundary condition given in Eq. (P17.8.6), we obtain

$$u_x = \bar{u}_m(s)(z/\ell) \quad (\text{P17.8.16})$$

Hence,

$$\sigma_{xz} = s\bar{G}(s)\bar{u}_m(s)/\ell \quad (\text{P17.8.17})$$

$$\bar{u}_m(s) = \bar{F}(s)/[Ms^2 + k + s\bar{G}(s)/\ell] \quad (\text{P17.8.18})$$

$$\bar{u}_x = \bar{F}(s)z/[(Ms^2 + k)\ell + s\bar{G}(s)] \quad (\text{P17.8.19})$$

Note once more that the suppression of the inertial terms is equivalent to linearizing the hyperbolic and trigonometric functions appearing in the problem.

Let us consider once more the input $F(t) = F_0\delta(t)$; then $\bar{F}(s) = F_0$. For a standard solid (see Chap. 10), we have

$$\left(\frac{1}{G_1} + \frac{1}{G_2}\right)\sigma + \frac{\eta}{G_1G_2}\dot{\sigma} = \varepsilon + \frac{\eta}{G_2}\dot{\varepsilon} \quad (\text{P17.8.20})$$

Since

$$\bar{\sigma}(s)/\bar{\varepsilon}(s) = s\bar{G}(s) \quad (\text{P17.8.21})$$

the Laplace transform of Eq. (P17.8.20) can be written as

$$\frac{\bar{\sigma}(s)}{\bar{\varepsilon}(s)} = s\bar{G}(s) = \frac{G_1G_2(1 + \tau s)}{G_1 + G_2 + \tau G_2s}, \quad \tau = \frac{\eta}{G_2} \quad (\text{P17.8.22})$$

By combining Eqs. (P17.8.19) and (P17.8.22) we obtain

$$\bar{u}_x(s) = \frac{F_0 z(G_1 + G_2 + \tau G_2 s)}{M\ell\tau G_2 s^3 + M\ell(G_1 + G_2)s^2 + \tau s G_2(G_1 + k\ell) + G_1 G_2 + k\ell(G_1 + G_2)} \quad (\text{P17.8.23})$$

For convenience, this result can be expressed in terms of the nondimensional quantities

$$F_0 \left(\frac{G_1 + G_2}{G_1 G_2} \right) = f; \quad \frac{G_2}{G_1 + G_2} = g \quad (\text{P17.8.24a})$$

$$\tau s = \phi; \quad k\ell \left(\frac{G_1 + G_2}{G_1 G_2} \right) = \psi; \quad \frac{M\ell}{\tau^2} \left(\frac{G_1 + G_2}{G_1 G_2} \right) \quad (\text{P17.8.24b})$$

Then

$$\frac{\bar{\mu}_x}{z} = \frac{f}{\mu} \left(\frac{\phi + g^{-1}}{\phi^3 + (1/g)\phi^2 + [(1 + g\psi)/\mu g]\phi + (1 + \psi)/\mu g} \right) \quad (\text{P17.8.25})$$

If it is supposed that the denominator has a negative real root ($-\lambda$) and two imaginary conjugated roots ($-\beta \pm i\xi$), we obtain

$$\frac{\phi + g^{-1}}{\phi^3 + \frac{1}{g}\phi^2 + \left(\frac{1+g\psi}{\mu g}\right)\phi + \frac{1+\psi}{\mu g}} = \frac{A}{\phi + \lambda} + \frac{B\phi + C}{\phi^2 + 2\phi\beta + \beta^2 + \xi^2} \quad (\text{P17.8.26})$$

with

$$\lambda + 2\beta = 1/g \quad (\text{P17.8.27a})$$

$$\beta^2 + 2\beta\lambda + \xi^2 = (1 + g\psi)/\mu g \quad (\text{P17.8.27b})$$

$$\lambda(\beta^2 + \xi^2) = (1 + \psi)/\mu g \quad (\text{P17.8.27c})$$

A , B , and C in Eq. (P17.8.26) being

$$A = \frac{g^{-1} - \lambda}{(\beta - \lambda)^2 + \xi^2}; \quad B = -A = -\frac{g^{-1} - \lambda}{(\beta - \lambda)^2 + \xi^2}; \quad C = \frac{\beta^2 + \xi^2 - g^{-1}(2\beta - \lambda)}{(\beta - \lambda)^2 + \xi^2} \quad (\text{P17.8.28})$$

Therefore Eq. (P17.8.25) becomes

$$\frac{\bar{\mu}_x}{z} = \frac{f}{\mu} \left[\frac{A/\tau}{s + \lambda/\tau} + \frac{1}{\tau^2} \left(\frac{B\tau s + C}{s^2 + (2\beta/\tau)s + (\beta^2 + \xi^2/\tau^2)} \right) \right] \quad (\text{P17.8.29})$$

Taking the Laplace inverse of Eq. (P17.8.29), we finally obtain

$$\frac{\bar{\mu}(t)}{z} = \frac{f}{\mu} \left\{ \frac{A}{\tau} \exp\left(-\frac{\lambda t}{\tau}\right) + \frac{B}{\tau} \left[1 + \frac{1}{\xi^2} \left(\frac{\beta^2 + \xi^2 - \beta\lambda - g^{-1}(\beta - \lambda)}{\lambda - g^{-1}} \right)^2 \right]^{1/2} \exp\left(-\frac{\beta t}{\tau}\right) \sin\left(\frac{\xi}{\tau} t + \delta\right) \right\} \quad (\text{P17.8.30})$$

or, alternatively,

$$\frac{\bar{\mu}_z(z, t)}{z} = \frac{f}{\mu\tau} \left(\frac{g^{-1} - \lambda}{(\beta - \lambda)^2 + \xi^2} \right) \left\{ \exp\left(-\frac{\lambda t}{\tau}\right) - \left[1 + \frac{1}{\xi^2} \left(\frac{\beta^2 + \xi^2 - \beta\lambda - g^{-1}(\beta - \lambda)}{\lambda - g^{-1}} \right)^2 \right]^{1/2} \exp\left(-\frac{\beta t}{\tau}\right) \sin\left(\frac{\xi}{\tau} t + \delta\right) \right\} \quad (\text{P17.8.31})$$

where

$$\delta = \arctan\left(\frac{\xi(\lambda - g^{-1})}{\xi^2 + \beta^2 - \beta\lambda - g^{-1}(\beta - \lambda)}\right) \quad (\text{P17.8.32})$$

In this equation, the logarithmic decrement (assuming that $|\lambda| \gg |\beta|$) will be

$$\Delta = 2\pi\beta/\xi \quad \text{and} \quad \omega = \xi/\tau \quad (\text{P17.8.33})$$

It should be stressed that the form of the response is not altered if $k = 0$, that is, if the material that surrounds the vibrating slab is viscoelastic. The obtained solution consists of a decreasing exponential and a damped out-of-phase sinusoidal wave.

Let us now assume an input of the rectangular type, according to

$$\begin{aligned} f(t) &= H(t), & 0 \leq t \leq a \\ f(t) &= 0, & t > a \end{aligned} \quad (\text{P17.8.34})$$

whose Laplace transform is

$$[1 - \exp(-as)]/s \quad (\text{P17.8.35})$$

In this case, the displacement will be expressed as

$$\bar{u}_x = \frac{1 - e^{-as}}{s} \left(\frac{z(G_1 + G_2 + \tau G_2 s)}{M\ell\tau G_2 s^3 + M\ell(G_1 + G_2)s^2 + \tau s G_2(G_1 + k\ell) + G_1 G_2 + k\ell(G_1 + G_2)} \right) \quad (\text{P17.8.36})$$

By employing the nondimensional quantities given by Eqs. (P17.8.24), Eq. (P17.8.36) becomes

$$\frac{\bar{\mu}_x}{z} = \frac{f}{\mu} \left(\frac{(\phi + g^{-1})(1 - e^{-as})}{s \left[\phi^3 + \frac{1}{g}\phi^2 + \left(\frac{1+g\psi}{\mu g} \right) \phi + \frac{1+\psi}{\mu g} \right]} \right) \quad (\text{P17.8.37})$$

Let us calculate first the Laplace inverse of the function

$$\frac{\phi + g^{-1}}{s \left[\phi^3 + \frac{1}{g}\phi^2 + \left(\frac{1+g\psi}{\mu g} \right) \phi + \frac{1+\psi}{\mu g} \right]} \quad (\text{P17.8.38})$$

It can be written as

$$\frac{1}{s} \left(\frac{A}{\phi + \lambda} \right) + \frac{B\phi + C}{s(\phi^2 + 2\beta\phi + \beta^2 + \xi^2)} \quad (\text{P17.8.39})$$

where A , B , and C are given as functions of β , ξ , g , and λ in Eq. (P17.8.28). Then, by using Eq. (P17.8.24c), the first term of Eq. (P17.8.39) becomes

$$\frac{1}{s} \left(\frac{A/\tau}{s + \lambda/\tau} \right) = \frac{A}{\lambda} \left(\frac{1}{s} - \frac{1}{s + \lambda/\tau} \right) \quad (\text{P17.8.40})$$

whose inverse is

$$\frac{A}{\lambda} \left[u(t) - \exp\left(-\frac{\lambda}{\tau}t\right) \right] \quad (\text{P17.8.41})$$

On the other hand, the second term of Eq. (P17.8.39) can be written as

$$\begin{aligned} \frac{B\phi + C}{s(\phi^2 + 2\beta\phi + \beta^2 + \xi^2)} &= \frac{B}{\tau} \left(\frac{s + C/B\tau}{s(s^2 + (2\beta/\tau)s + (\xi^2 + \beta^2)/\tau^2)} \right) \\ &= \frac{C}{\xi^2 + \beta^2} \left(\frac{1}{s} - \frac{s - (1/C\tau)[B(\xi^2 + \beta^2) - 2\beta C]}{s^2 + (2\beta/\tau)s + (\xi^2 + \beta^2)/\tau^2} \right) \end{aligned} \quad (\text{P17.8.42})$$

whose Laplace inverse is given by

$$\frac{C}{\xi^2 + \beta^2} \left[H(t) - \frac{((\beta[\beta^2 + \xi^2 - g^{-1}(2\beta - \lambda)] + (g^{-1} - \lambda)(\beta^2 + \xi^2))^2 + \xi^2[\beta^2 + \xi^2 - g^{-1}(2\beta - \lambda)]^2)^{1/2}}{\xi[\beta^2 + \xi^2 - g^{-1}(2\beta - \lambda)]} \right. \\ \left. \exp\left(-\frac{\beta}{\tau}t\right) \sin\left(\frac{\xi}{\tau}t + \delta\right) \right] \quad (\text{P17.8.43})$$

or, alternatively,

$$\frac{C}{\xi^2 + \beta^2} \left\{ H(t) - \left[1 + \left(\frac{\beta}{\xi} + \frac{(g^{-1} - \lambda)(\xi^2 + \beta^2)}{\xi[\beta^2 + \xi^2 - g^{-1}(2\beta - \lambda)]} \right)^2 \right]^{1/2} \exp\left(-\frac{\beta}{\tau}t\right) \sin\left(\frac{\xi}{\tau}t + \delta\right) \right\} \quad (\text{P17.8.44})$$

where

$$\delta = \arctan \frac{\xi[\beta^2 + \xi^2 - g^{-1}(2\beta - \lambda)]}{\beta[\beta^2 + \xi^2 - g^{-1}(2\beta - \lambda)] + (g^{-1} - \lambda)(\xi^2 + \beta^2)} \quad (\text{P17.8.45})$$

Hence, the inverse of (P17.8.37) is given by

$$\frac{u_x}{z} = \frac{f}{\mu} \left\{ \frac{A}{\lambda} [H(t) - H(t-a)] - \left[\exp\left(-\frac{\lambda}{\tau}t\right) - \exp\left(-\frac{\lambda}{\tau}(t-a)\right) \right] \right. \\ \left. + \frac{C}{\xi^2 + \beta^2} [H(t) - H(t-a)] - \left[1 + \left(\frac{\beta}{\xi} + \frac{(g^{-1} - \lambda)(\xi^2 + \beta^2)}{\xi[\beta^2 + \xi^2 - g^{-1}(2\beta - \lambda)]} \right)^2 \right]^{1/2} \right. \\ \left. \times \left[\exp\left(-\frac{\beta}{\tau}t\right) \sin\left(\frac{\xi}{\tau}t + \delta\right) - \exp\left(-\frac{\beta}{\tau}(t-a)\right) \sin\left(\frac{\xi}{\tau}(t-a) + \delta\right) \right] \right\} \quad (\text{P17.8.46})$$

where A and C are given by Eq. (P17.8.28).

Let us consider now a more realistic input, defined as

$$f(t) = \sin(\pi t/a), \quad 0 \leq t \leq a \\ f(t) = 0, \quad t > a \quad (\text{P17.8.47})$$

whose Laplace transform is

$$\frac{\pi}{a} \left(\frac{1 + \exp(-as)}{s^2 + \pi^2/a^2} \right) \quad (\text{P17.8.48})$$

In this case, the following expression for the deformation is obtained:

$$\begin{aligned} \bar{u}_x &= \frac{\pi}{a} \left(\frac{1 + \exp(-as)}{s^2 + \pi^2/a^2} \right) \\ &\times \left(\frac{z(G_1 + G_2 + \tau G_2 s)}{M\ell\tau G_2 s^3 + M\ell(G_1 + G_2)s^2 + \tau s G_2(G_1 + k\ell) + G_1 G_2 + k\ell(G_1 + G_2)} \right) \end{aligned} \quad (\text{P17.8.49})$$

By using the methodology described above, u_x can be expressed in terms of the dimensionless variables f , g , ϕ , ψ , and μ as

$$\frac{\bar{u}_x}{z} = \frac{\pi}{a} \left(\frac{1 + \exp(-as)}{s^2 + \frac{\pi^2}{a^2}} \right) \left(\frac{f}{\mu} \right) \left(\frac{\phi + g^{-1}}{\phi^3 + \frac{1}{g}\phi^2 + \left(\frac{1+g\psi}{\mu g}\right)\phi + \frac{1+\psi}{\mu g}} \right) \quad (\text{P17.8.50})$$

or

$$\frac{\bar{u}_x}{z} = \frac{\pi f}{a\mu} \left(\frac{1 + \exp(-as)}{s^2 + \frac{\pi^2}{a^2}} \right) \left[\frac{A/\tau}{s + \frac{\lambda}{\tau}} + \frac{1}{\tau^2} \left(\frac{B\tau s + C}{s^2 + \frac{2\beta}{\tau}s + \frac{\beta^2 + \xi^2}{\tau^2}} \right) \right] \quad (\text{P17.8.51})$$

where A , B , and C are functions of g , λ , β , and ξ as usual.

The Laplace inverse of the previous expression can be expressed as

$$\begin{aligned} \frac{1}{z} u_x(t) &= \frac{\pi f}{a\mu} \left\{ \frac{A}{\tau} \left[\frac{a\tau^2}{\pi(\lambda^2 a^2 + \pi^2 \tau^2)^{1/2}} \sin\left(\frac{\pi}{a}t - \delta\right) + \frac{a\tau^2}{a^2 \lambda^2 + \pi^2 \tau^2} \exp\left(-\frac{\lambda}{\tau}t\right) \right] \right. \\ &+ \frac{a\tau^2}{\pi(\lambda^2 a^2 + \pi^2 \tau^2)^{1/2}} \sin\left(\frac{\pi}{a}(t-a) - \delta\right) + \frac{a\tau^2}{a^2 \lambda^2 + \pi^2 \tau^2} \exp\left(-\frac{\lambda}{\tau}(t-a)\right) \left. \right\} \\ &+ \frac{1}{\tau^2} \left[\frac{[B^2 \tau^2 (\pi^2/a^2) + C^2]^{1/2}}{\left[\frac{\pi}{a} \left[\frac{\pi^2}{a^2} \mu^2 + \left(v - \frac{\pi^2}{a^2}\right)^2 \right] \right]^{1/2}} \left[\sin\left(\frac{\pi}{a}t - \delta'\right) + \sin\left(\frac{\pi}{a}(t-a) - \delta'\right) \right] \right] \\ &+ \frac{1}{\xi \tau^2} \left(\frac{1}{(v - \alpha^2)^2 + \alpha^2 \mu^2} \right) \\ &\times \left\{ [(C\mu - B\tau v)\mu\tau - C\tau(v - \alpha^2) - 2\beta(B\tau\alpha^2 + C\mu - B\tau v)]^2 \right. \\ &+ \xi^2 (B\tau\alpha^2 + C\mu - B\tau v)^2 \left. \right\}^{1/2} \\ &\times \left[\exp\left(-\frac{2\beta}{\tau}t\right) \sin\left(\frac{\xi}{\tau}t + \delta''\right) + \exp\left(-\frac{2\beta}{\tau}(t-a)\right) \sin\left(\frac{\xi}{\tau}(t-a) + \delta''\right) \right] \end{aligned} \quad (\text{P17.8.52})$$

where

$$\alpha = \pi/a \quad (\text{P17.8.53})$$

and

$$\delta = \arctan\left(-\frac{\pi\tau}{a\lambda}\right) \quad (\text{P17.8.54})$$

$$\delta' = \arctan\left(-\frac{\pi}{a}\right) \left(\frac{B\tau(\pi^2/a^2) + C\mu - B\tau\nu}{B\tau\mu(\pi^2/a^2) + C(\nu - \pi^2/a^2)}\right) \quad (\text{P17.8.55})$$

$$\delta'' = \arctan\left(\frac{\xi(B\tau\alpha^2 + C\mu - B\tau\nu)}{\tau\mu(C\mu - B\tau\nu) - C\tau(\nu - \alpha^2) - 2\beta(B\tau\alpha^2 + C\mu - B\tau\nu)}\right) \quad (\text{P17.8.56})$$

In the preceding calculations we made use of the following identities:

$$\frac{1}{s^2 + \alpha^2} \left(\frac{1}{s + \lambda}\right) = \frac{M}{s + \lambda} + \frac{Ns + \tilde{N}}{s^2 + \alpha^2} \quad (\text{P17.8.57})$$

where

$$M = \frac{1}{\lambda^2 + \alpha^2}; \quad N = -\frac{1}{\lambda^2 + \alpha^2}; \quad \tilde{N} = \frac{\lambda}{\lambda^2 + \alpha^2} \quad (\text{P17.8.58})$$

and

$$\frac{B\tau s + C}{(s^2 + \alpha^2)(s^2 + \mu s + \nu)} = \frac{M's + N'}{s^2 + \alpha^2} + \frac{R's + S'}{s^2 + \mu s + \nu} \quad (\text{P17.8.59})$$

with

$$\mu = 2\beta/\tau; \quad \nu = (\beta^2 + \xi^2)/\tau^2 \quad (\text{P17.8.60})$$

$$M' = -\frac{1}{\mu} \left(\frac{B\tau\alpha^2 + C\mu - B\tau\nu}{(\nu - \alpha^2)^2 + \alpha^2\mu^2}\right) \quad (\text{P17.8.61})$$

$$N' = \frac{C(\nu - \alpha^2) + B\tau\alpha^2\mu}{(\nu - \alpha^2)^2 + \alpha^2\mu^2} \quad (\text{P17.8.62})$$

$$R' = -M' = \frac{1}{\mu} \left(\frac{B\tau\alpha^2 + C\mu - B\tau\nu}{(\nu - \alpha^2)^2 + \alpha^2\mu^2}\right) \quad (\text{P17.8.63})$$

$$S' = \frac{(C\mu - B\tau\nu)\mu - C(\nu - \alpha^2)}{(\nu - \alpha^2)^2 + \alpha^2\mu^2} \quad (\text{P17.8.64})$$

We note that when the losses are too large, free oscillations cannot be excited. For this reason it is compulsory to use the elastic auxiliary element in order to get information on the viscoelastic functions. A stiff elastic element, with constant k , can be added to reduce the loss. When the loss of the system is sufficiently small, the discrepancies between the results obtained from the former theory and the solution based on the classical second-order differential equation [see Eq. (7.49), for example]

$$M\ddot{x} + K\eta\dot{x} + (KG' + k)x = 0 \quad (\text{P17.8.65})$$

are experimentally indistinguishable. Here K is a geometric factor, η is the viscosity, and G' is the real part of the dynamic shear modulus.

As a general rule, the larger the losses, the larger are the discrepancies between these two solutions to the free vibration problem. However, it is possible to have greater discrepancies even for a low loss material due to changes in the damped sinusoidal term. For a more complex linear viscoelastic material consisting of a finite number of elementary viscoelastic elements, the solution would include a sum of decreasing exponential terms and damped sinusoidal waves.

REFERENCES

1. LD Landau, EM Lifshitz. Theory of Elasticity, 3rd ed. Oxford UK: Pergamon, 1986, p 64.
2. IH Shames, FA Cozzarelli. Elastic and Anelastic Stress Analysis. Englewood Cliffs NJ: Prentice-Hall, 1992, Chap 10.
3. JG Williams. Stress Analysis of Polymers. Norfolk, UK: Longman, 1973, Chap 4.
4. T Kaneko. On Timoshenko correction for shear in vibrating beams. J Phys D Appl Phys 8: 1927, 1975.
5. B Read, GD Dean. The Determination of Dynamic Properties of Composites. Bristol UK: Adam Hilger, 1978, p 11.
6. S Timoshenko, JN Goodier. Theory of Elasticity. New York: McGraw-Hill, 1951.
7. SP Timoshenko, DH Young, W Weaver Jr. Vibration Problems in Engineering, 4th ed. New York: Wiley, 1974.
8. RD Corsaro, LH Sperling. Sound and Vibration Damping with Polymers. ACS Symp Ser 424. Washington DC: Am Chem Soc, 1990.
9. NW McLachlan. Theory of Vibrations. New York: Dover, 1957.
10. TC Huang. The effect of rotatory inertia and of shear deformation on the frequency and normal mode equations of uniform beams with simple end conditions. J Appl Mech 28: 579, 1961.

11. E Goens. Uber di Bestimmung des Elastizitatsmoduls von Staben mit Hilfe von Biegungsschwingungen. *Ann Phys Leipzig* 5(11): 649, 1931.
12. CJ Nederveen, FR Schwarzl. Corrections for shear and rotatory inertia on flexural vibrations of beams. *Br J Appl Phys* 15: 323, 1964.
13. WC Young. *Roark's Formulas for Stress and Strain*. 6th ed. New York 1989, McGraw-Hill, pp 162, 177.
14. PC Chou, NJ Pagano. *Elasticity: Tensor, Dyadic and Engineering Approaches*. New York: Dover, 1992.
15. AS Elder. The transient response of a viscoelastic torsional pendulum. *Trans Soc Rheol* 9(2): 187, 1965.
16. RD Glauz. *J Polym Sci A-1* 8: 329, 1970.
17. H Markovitz. *J Appl Phys* 34: 21, 1963.

Appendix

A.1	Laplace Transformation	866
A.2	Properties of the Laplace Transformation	867
A.3	Inverse of the Laplace Transformation	867
A.4	Carson Transformation	868
A.5	Fourier Transformation	868
A.6	Stieltjes Transformation	869
A.7	Table of Laplace Transformations	869
A.8	Reference	869

A.1 LAPLACE TRANSFORMATION

Let $f(t)$ be a function of t , for $t > 0$. Its Laplace transform, denoted by $L(f(t))$ is defined by

$$L(f(t)) = \bar{f}(s) = \int_0^{\infty} f(t)e^{-st} dt \quad (\text{A.1})$$

Thus, Eq. (A.1) transforms the function $f(t)$ into a new function $\bar{f}(s)$.

The sufficient conditions for the existence of $\bar{f}(s)$ are:

- 1) $f(t)$ is piecewise continuous in a certain interval.
- 2) $|f(t)| \leq Me^{at}$ for some values of M and a .

A.2 PROPERTIES OF THE LAPLACE TRANSFORMATION

1) Linearity

$$L(\alpha_1 f_1(t) + \alpha_2 f_2(t) + \dots) = \alpha_1 \bar{f}_1(s) + \alpha_2 \bar{f}_2(s) + \dots \quad (\text{A.2})$$

2) Shift function transform

$$L(f(t - a)) = e^{-as} \bar{f}(s) \quad (\text{A.3})$$

3) Transform of the derivatives

$$L(f^{(n)}(t)) = s^n \bar{f}(s) - s^{n-1} f(0) - \dots - s f^{(n-2)}(0) - f^{(n-1)}(0) \quad (\text{A.4})$$

4) Transform of integrals

$$L\left(\int_0^t \dots \int_0^t f(\zeta) d\zeta\right) = \frac{\bar{f}(s)}{s^n} \quad (\text{A.5})$$

5) Convolution theorem

$$L\left(\int_0^t f(t - \tau)g(\tau) d\tau\right) = L\left(\int_0^t g(t - \tau)f(\tau) d\tau\right) = \bar{f}(s)\bar{g}(s) \quad (\text{A.6})$$

6) Initial value theorem

$$\lim_{t \rightarrow 0} f(t) = \lim_{s \rightarrow \infty} s \bar{f}(s) \quad (\text{A.7})$$

7) Final value theorem

$$\lim_{t \rightarrow 0} f(t) = \lim_{s \rightarrow 0} s \bar{f}(s) \quad (\text{A.8})$$

A.3 INVERSE OF THE LAPLACE TRANSFORMATION

If the Laplace transform of a function $f(t)$ is $\bar{f}(s)$, then $f(t)$ is the inverse Laplace transform of $\bar{f}(s)$. Although an integral inversion formula can be used to obtain the inverse Laplace transform, in most cases it proves to be too complicated. Instead, a transform table (1), is used to find the image function $f(t)$. For more complicated functions, approximate methods are available. In many cases the inverse of a ratio of two polynomials must be

calculated. A partial fraction expansion can then be done. Notice that the transformed variable s can be real or complex. In the context of the theory of the viscoelasticity, the variable s will be taken as $i\omega$ in the case of forced oscillations, whereas will be assumed as $-2 + i\omega$ in the case of free oscillations.

A.4 CARSON TRANSFORMATION

Let $f(t)$ be a function of t , with the same properties than before, the Carson transform is then defined as

$$\bar{f}^*(s) = s\bar{f}(s) \quad (\text{A.9})$$

where $\bar{f}(s)$ is the Laplace transform of $f(t)$. Thus, the Carson transform gives us the complex dynamic modulus or compliances.

A.5 FOURIER TRANSFORMATION

Fourier analysis makes it possible to analyse a sectionally continuous periodic function into an infinite series of harmonics. For a non-periodic absolutely integrable function, the summation over discrete frequencies becomes an integral

$$\bar{f}(\omega) = \frac{1}{\sqrt{2\pi}} \int_{-\infty}^{\infty} f(t)e^{-i\omega t} dt \quad (\text{A.10})$$

The corresponding inverse is given by

$$\bar{f}(t) = \frac{1}{\sqrt{2\pi}} \int_{-\infty}^{\infty} \bar{f}(\omega)e^{-i\omega t} d\omega \quad (\text{A.11})$$

The sine and cosine Fourier transforms are defined, respectively, as

$$\bar{f}_s(\omega) = \int_0^{\infty} f(t) \sin \omega t dt \quad (\text{A.12a})$$

$$\bar{f}_c(\omega) = \int_0^{\infty} f(t) \cos \omega t dt \quad (\text{A.12b})$$

and the corresponding inverses are given by

$$f(t) = \frac{2}{\pi} \int_{-\infty}^{\infty} \bar{f}_s(\omega) \sin \omega t \, d\omega = \frac{2}{\pi} \int_{-\infty}^{\infty} \bar{f}_c(\omega) \cos \omega t \, d\omega \quad (\text{A.13})$$

For even and odd functions we, respectively, have

$$\bar{f}(\omega) = \sqrt{\frac{2}{\pi}} \bar{f}_c(\omega) \quad (\text{A.14a})$$

$$\bar{f}(\omega) = -i \sqrt{\frac{2}{\pi}} \bar{f}_s(\omega) \quad (\text{A.14b})$$

A.6 STIELTJES TRANSFORMATION

A Stieltjes transform is a double Laplace transform. It can be calculated as follows:

$$L_z(L_s(f(t))) = \int_0^{\infty} e^{-sz} ds \int_0^{\infty} e^{-st} f(t) dt = \int_0^{\infty} f(t) dt \int_0^{\infty} e^{-s(z+t)} ds = \int_0^{\infty} \frac{f(t) dt}{z+t} \quad (\text{A.15})$$

A.7 TABLE OF LAPLACE TRANSFORMS

Function of the time	Laplace Transform
$h(t)$ (step function)	$1/s$
$\delta(t)$ (Dirac function)	1
$\delta^{(n)}(t)$	s^n
t	$1/s^2$
t^k ($k > -1$)	$\Gamma(k+1)/s^{k+1}$
e^{-at}	$1/(s+a)$
$t^n e^{-at}$	$\Gamma(n+1)/(s+a)^{n+1}$
$\sin at$	$a/(s^2+a^2)$
$\cos at$	$s/(s^2+a^2)$
$e^{-bt} \sin at$	$a/((s^2+b^2)+a^2)$
$e^{-bt} \cos at$	$(s+b)/((s^2+b^2)+a^2)$
$\text{sh } at$	$a/(s^2-a^2)$
$\text{ch } at$	$s/(s^2-a^2)$

A.8 REFERENCE

1. A Erdelyi, Tables of Integral Transforms. Vol 1. McGraw Hill, New York. 1954.

Index

- α -relaxation 459
- $\alpha\beta$ -relaxation 457
- Acrylic polymers 8
- Acrylonitrile-butadiene rubber (NBR)
 - 124
- Adamm-Gibbs equation 480
- Addition polymerization 7
- Addition polymers 4
- Affine deformation model 96, 101
- Aging 60, 475
- Alternating copolymers 5
- Amorphous polymers 29, 58, 63
- Amorphous regions 29
- Amorphous state 30
- Andrade equation 328, 333
- Annealing temperature 39, 477
- Arrhenius behavior 465
- Aramid 667-669
- Atactic configuration 14
- Average relaxation time 464
- Avrami equation 46
- Bagley corrections 532
- Beams 769, 770
 - bending moment 772
 - balance equations 775
 - forced vibrations 792, 802
 - free vibrations 789, 796
 - shear stresses 779
 - transverse vibrations 789
 - transverse vibrations, thermal effects 808
 - viscoelastic 788
- Bending 770
- Benzoyl peroxide 7
- Bingham fluids 519
- Block copolymers 5
- Boltzman equation 93
- Boltzmann superposition principle
 - 207, 208, 214, 245
- Branched polymers 2
- Brittle behavior 583
- Brittle-ductile transition 613-616
- Brittle fracture 613

- Bulk compliance functions 171, 204, 223, 227
- Bulk creep compliance 207, 255
- Bulk flow 175
- Bulk loss compliance 255
- Bulk relaxation modulus/ i 164, 165, 201, 225
- Bulk storage compliance 255
- Bulk viscosity 175
- Burgers model 404

- Capillary rheometers 521
- Carbon black fibers 656, 659, 666
- Carbon black fillers 116, 666
- Carreau model 552
- Cauchy law 511
- Chain polymerization 7
- Charpy test 636
- Cholesteric 54
- Cis-conformation 16, 17
- Clamping
 - effects in the viscoelastic measurements 292
 - length corrections 293
- Cold drawing 585
- Compatibility equations 151
- Complex viscoelastic functions
 - bulk compliance 255
 - bulk relaxation modulus 256
 - creep compliance functions 250, 318
 - relaxation modulus 241, 251, 369
 - shear stress 242
 - shear rate deformation 242
 - tensile compliance 256
 - tensile relaxation modulus 256
 - viscosity 242
- Compliance functions
 - 171,173,206,247,307,318,363
- Compliance loss 250
- Compliance parameters 172
- Composites 654
- Compressibility coefficient 175
- Condensation polymerization 8
- Cone-plate viscometer 539
- Configuration 13
- Conformation 13,16,18,19
- Conformational isomers 13
- Conformational states 16
- Conformational transitions 197
- Considère construction 590
- Constitutive equations 140, 141, 510, 703
- Contact (or indentation) curved 740
- Contact (or indentation) plane 736
- Contact (rolling) 744
- Convolution integrals 198, 225
- Cooperativity 197
- Copolymers 3, 72
 - alternating 5
 - block 5
 - graft 5
 - random 3
 - statistical 3
- Correspondence principle 221, 709
- Couette flow 536
- Couette rheometers 536
- Cox–Merz relation 553
- Cracks 620
- Crazes 602
- Crazing 602
 - crazing criteria 606
 - crazing stress 607
 - crazing agents 611
- Creep compliance function 308, 313, 370
- Creep experiments 199-200, 205, 207, 212
- Creep in torsion 296
- Critical concentration 424
- Cross-link:
 - density 104
 - effect on modulus 105
 - effect on T_g 71
 - elastomer networks 105
 - molecular weight between 105
- Cross-linking reactions 10
- Cross-links 86, 104
- Cross-Williamsom model 552
- Crystal structure 31, 33
- Crystals growth rate 45

- Crystalline lamella 37, 38
- Crystalline morphology 31, 37
- Crystalline polymers 29
- Crystalline regions 29
- Crystallization 32, 44
- Crystallization temperature 38
- Crystallinity of polymers 32, 75
- Cure shrinkage 663
- Curing temperatures 661

- Debonding of fibers 687
- Deborah's number 197
- Degree of crystallinity 33, 43
- Degree of polymerization 10
- Denier 665
- DGEBA 661
- Deviatoric component of stress tensor 164, 165, 704
- Die swelling 558
- Diffusion coefficient 428
- Dilatational component of the stress tensor 164, 704
- Discotic mesophases 54
- Disengagement time 432
- Disentanglement 197, 337
- Displacement gradient tensor 149
- Distributed constants models 409
- Doi-Edwards theory 438
- Doolittle equation 64
- Di Marzio and Gibbs equation 73
- Ductile and brittle behavior 582
- Ductile failure 64
- Ductile polymers 582
- Dynamic
 - creep compliance functions 244
 - creep experiment 249
 - mechanical test 273
 - relaxation experiments 243
 - relaxation functions 239
 - viscoelastic properties 273

- Effective sample length 283
- Eigenfunctions 827
- Eigenvalues 791, 800, 826
- End to end distance 19, 20

- Elastic:
 - deformation 584
 - deformation (changes in internal energy and entropy) 87, 98
 - entropic compliance 206
 - force of a network 100
 - force of a polymer chain 95
 - parameters 165, 168
- Elastic and viscous mechanism modeled 359
- Elasticity (molecular mechanisms) 87
- Elastomers 6, 9, 85
 - additives 116
 - degradation 114
 - effects of fillers 117
 - in service 111
 - rigidity under compression 119, 121
 - rigidity under shear 121
 - shear and bulk relaxation moduli 121
 - thermal aging 114
- Ellis model 552
- Elongational viscosity 176, 177, 207, 223
- End corrections 283, 292
- Energy dissipation in shear dynamic experiments
 - creep 249
 - relaxation 244
- Entanglements 337
- Epoxy resins 661
- Ethylene-propylene rubber 126
- Entropic elasticity 202
- Entropy of a chain 97
- Equilibrium compliance 206, 253, 366
- Equilibrium elastic modulus 204
- Eyring's model 598

- Fading memory 216, 217
- Fading structural memory 196, 213
- Fatigue 639
- Fibers 41, 42
- Fiber reinforcement 654, 664
- Fibrils 42
- Fictive temperature 473

- Fillers 117, 654
 Fillers- Moonan-Tschoegl equation 327
 First-order approximation. relaxation spectra 372
 First-order approximation. retardation spectra 374
 First-order approximations 371
 Fringed-micelle 31
 Flaws 615
 Fluoroolefines rubbers 127
 Folded chain 38
 Forced oscillation in torsion 280
 Fourier transforms 247, 248, 868-869
 Fox equation 73
 Fracture energy 624-627
 Fracture toughness 613
 Fracture strength 621
 Fragile liquids 455
 Free oscillation in torsion 279, 290
 Free volume 62-65, 70
 Freely jointed chain 23, 24
 Frequency domain 226, 242, 246, 247
 Friction coefficient 438, 440
 Fringed-micelle model 31
 Functionality 7-9, 104

 Gauche conformation 17
 Gaussian function 21, 22, 24
 Gel point 346
 Gelation 659
 Generalized Newton's law 177
 Generalized stress-strain Hooke's law 162
 Generalized stress-strain relations 221, 226, 227
 Glass-fiber 665
 Glass transition 57-75, 464
 Glass transition (molecular cooperativity) 468
 Glass transition temperature 57, 223
 Glassy compliance 206
 Glassy-like zone 328
 Glassy Poisson's ratio 225
 Glassy polymer 30

 Glassy state 57, 58, 328, 464
 Glassy systems (viscoelastic functions) 463
 Graft- copolymer 5
 Graphite 666
 Griffith theory 623

 Hardener 662
 Hardening reactions 662
 Hardening strain 592
 Heaviside function 199
 Helical conformation 29,35
 Higher order approximation 375
 High-impact polystyrene 637
 Homopolymer 2
 Hooke's equation 141
 Hydrogen bonding 35
 Hydrostatic pressure 165, 212

 Ideal elastic solids 200
 Ideal elastic systems 152
 Ideal elastomers 92
 Ideal liquids 200, 396
 Impact 735
 Impact energy 635
 Impact-resistant polymers 635
 Impact strength 635
 Impact tests 636
 Imperfections in polymer networks 87
 Indentation methods 295, 735, 777
 Indifference principle 511
 Intrinsic viscosity 525
 Irwin's model 628
 Isotactic configuration 14
 Isotropic liquid 55
 Isotropic solids 162
 Isotropy 699
 Izod impact test 636

 Kauzman temperature 456, 480
 Kelvin-Voigt generalized model 406
 Kelvin-Voigt model 398
 Kelvin-Voigt solid 399
 Kevlar 31,52
 Kinetic of crystallization 44

- Kohlrausch-Williams-Watts (KWW) equation 459
- Kronig-Kramers relations 253
- Ladder models 408
- Lamé constants 162
- Lamella 57
- Laminate 681
- Laplace transform 218, 866
- LC polymers
 lyotropics 52, 55
 main-chain LC 52, 55
 side-chain LC 52, 56
 thermotropic 52, 56
- Linear dilatation coefficient 172
- Linear viscoelasticity 147, 198, 221, 252
- Liquid-crystal state 51
- Loss compliance functions 364
- Loss modulus 362
- Loss relaxation modulus 243, 252
- Loss viscoelastic functions 239
- Main-chain LC polymers 52, 55
- Master curves 314, 315, 317, 321, 327
- Matrices 655
- Maxwell generalized model 406
- Maxwell liquid 398
- Maxwell model 395
- Mean-relaxation time 197, 368, 460
- Melt index 560, 562
- Melting 46
- Melting enthalpy 48, 50
- Melting entropy 48, 50
- Melting point depression
- Melting temperature 39, 47, 50, 69
 of equilibrium 48, 49
- Memory effects 212
- Memory functions 216
- Mesophases 53, 54
- Meso configuration 15
- Mesogen groups 52, 53
- Microcracks 620
- Microvoids 620
- Model networks 105
- Modulus of elasticity 141
- Modulus tensor 154
- Molecular cooperativity (glass transition) 468
- Molecular weight 10
- Molecular weight between crosslinks 105
- Molecular weight distribution 10, 11
- Monomer 1
- Monomeric unit 1,2
- Mono-olefinic rubber 125
- Mooney-Rivlin equation 103
- Multiaxial tension 703
- Natural rubber (NR) [see also poly(cis-1,4-isoprene)] 123
- Navier equations 167
- Neck formation 585
- Nematic mesophases 54, 55
- Neoprene see also polychloroprene 125
- Newtonian behavior 519
- Newtonian liquids 175
- Nomenclature of polymers 3
- Nominal stress of a rubber 100
- Non-Gaussian networks 107
- Non-Gaussian statistics of rubber elasticity 106
- Non-Newtonian behavior 519
- Nonrecoverable deformation 584
- Nontransient creep experiments 314
- Nontransient relaxation experiments 319
- Normal strains 151
- Notch 635
- Nucleation 44
- Number average molecular weight 11
- Nylon 5, 42, 36
- Olefinic TPES 130
- Overlapping 337
- Particulate reinforcement 654
- Phantom chains 423
- Phantom network model 100

- Phenolics resin 9, 10
- Physical aging 474, 477
 nonlinear behavior 482
 viscoelastic functions 478
- Piezorheologically simple systems 327
- Planar zig-zag conformation 29, 34
- Plane strain 721
- Plane stress 727
- Plasticizers 73-75
- Plastic deformation 584
- Plate-plate viscometer 541
- Plateau region 332
- Poisson's ratio 166, 225, 256, 346
- Polyacrylonitrile 4, 33
- Polyamides 8, 31, 36
- Polybutadiene 4, 338
- Polycarbonate 8, 475, 597, 598, 601
- Polychloroprene (neoprene) (CR) 4, 125
- Poly(cyclohexyl acrylate) 468
- Poly (cis-1,4-butadiene) 33
- Poly(cis-1,4-isoprene) (natural rubber) 9, 10, 50, 113, 339
- Poly(decamethylen sebacamide) 50
- Poly(decamethylene terephthalate) 50
- Poly(dimethylsiloxane) 105, 338
- Poly(ϵ -caprolactone) 49
- Poly(ethylene oxide) 66
- Poly(ethylene terephthalate) 5, 8, 42
- Poly(ethyleneglycol) 338
- Poly(ethyleneglycol terephthalate) 467
- Poly(ethylmethacrylate) 329
- Poly(m-hexylmethacrylate) 329
- Poly(methyl acrylate) 4, 32
- Poly(methyl methacrylate) 4, 338, 458, 463, 480, 484
- Poly(methylphenylsiloxane) 329
- Poly(p-xylene) 66
- Poly(tetrafluorethylene) 4, 34, 35
- Poly(tetra-methyl p-silphenylsiloxane) 338
- Poly(tetramethylene glycol terphthalate) 39, 41
- Poly(tetramethylene terphthalate) 50
- Poly(trans-1,4-isoprene) (gutapercha) 50
- Poly(vinyl acetate) 32, 61, 338
- Poly(vinyl alcohol) 33
- Poly(vinyl chloride) 4, 13, 68, 75, 464, 467, 479, 480
- Poly(vinyl fluoride) 33
- Poly(vinyl terbutyl ether) 67
- Polydispersity 12, 434
- Polyester resins 662
- Polyesters 8
- Polyether ether ketone 660
- Polyethers 8,67
- Polyethylene 4, 31, 34, 37, 41, 47, 50, 66, 338, 467, 599
- Polyimides 664
- Polyisobutylene 67, 315, 319, 338
- Polyisoprene 4
- Polymer mixtures 73
- Polymer network 86
- Polymer-polymer interaction parameter 51
- Polymer-solvent interaction parameter 51
- Polymerization processes 7
- Polymorphism 34
- Polypropylene 4, 36, 50, 62, 67
- Polystyrene 4, 7, 36, 50, 70, 318, 321, 325, 328, 329, 338
- Polysulfide cross-linking 113
- Polyurethanes 5, 8
- Potential energy functions (interactions) 460
- Primitive chain 431
- Rabinowitsch expression 524
- Racemic configuration 15
- Ramp experiments 217
- Random copolymer 3
- Rate of shear 142
- Rate of strain tensor 175
- Real compliance function 250
- Real liquids 201
- Real solids 201
- Recoverable compliance 210, 328, 341

- Recoverable compliance function 309
Recoverable creep compliance 310, 329
Recoverable deformation 584
Recovery compliance 209, 318
Reduced stress affine model
Reiner- Rivlin equation 512
Relative viscosity 526
Relaxation experiments 199-202, 214
Relaxations in the frequency domain 457
Relaxation modulus 202, 204, 273, 315
Relaxation spectrum 361, 372
Relaxation time 197, 199, 360, 369
Reptation 436
Repeating unit 2, 3
Resonance 294, 791
Retardation spectra 362, 363
Retardation time 369
Rheology 141
Rheometry 519
Rheopexy 562
Rheovibron viscoelastometer 293
Rivling-Ericksen equation 512
Rivling-Ericksen tensors 514
Rotary inertia 796
Rotation tensor 149
Rouse theory 312, 326
- Saint-Venant principle 710
Scaling laws 250
Scaling laws applied to the determination of
diffusion coefficient 428
plateau modulus 337
relaxation times 428
viscosity 337
Second law of dynamics 146
Second order fluid 515
Secondary normal stress difference 518
Semicrystalline polymer 43, 60
Semicrystalline state 30
Shear compliance functions 170, 171, 204, 223, 227, 308
creep compliance 206
deformation 149
experiments 205
flow 175
forces 150
forces in beams 779, 796
modulus of the elastomer 100
relaxation modulus/i 165, 201, 203
strain 151
stress 142, 149
thickening 519
thinning 519
viscosity 223
yield 584
Shift factors 311, 321-323, 326,
Short fiber composite 684
Side chain LC polymers 52, 56
Silica as filler of elastomers 119
Silicones 126
Single crystal 37, 38
period 38
Slit rheometer 529
Slow flow approximation 513
Small deformation approximation 513
Smectic mesophases 53, 55
Softening strain 592
Spectra 31
Spherulite 39, 40, 41
Standar deviation of a molecular weight distribution 12
Static viscoelastic properties 296
Statistical coil 18
Statistical copolymers 3
Statistical treatment of rubber elasticity 93
Steady-state compliance 206, 252, 321, 337, 339, 341, 366, 367
Sten Stein and Ongchin (crazing criterion) 607
Stereoregular polymers 16
Step function 199
Step polymers 5
Storage compliance function 363

- Storage relaxation modulus 243, 254, 332, 362
- Storage viscoelastic functions 239
- Strain deviator tensor 165
- Strain induced crystallization in elastomers 87, 108
- Strain stress relations 170
- Strain tensor 147, 149, 152, 158, 166, 221, 816
- Stretching flow 563
- Stress deviator tensor 165
- Stress intensity factor 629
- Stress-strain curves:
behavior of crazes 613
of brittle polymers 614
Considère construction 590
of ductile polymers 614
- Stress relaxation 299
- Stress-strain relations 696, 701
- Stress-strain relationship in terms of the P and Q operators 705
- Stress-strain relationship including thermal effects 706
- Stress tensor 142, 146, 152, 158, 221, 698, 818
- Strong liquids 455
- Structural memory 197
- Structural recovery 474
- Structural relaxation 475
- Styrene-butadiene rubbers (SBR) 124
- Styrenic TPEs 129
- Sub-glass relaxations 465-467
- Superposition principle 221
- Suspensions
Maron Pierce equation 555
- Swelling of polymer networks 109, 111
- Swelling theory of polymer networks (Flory and Rehner) 110
- Symmetry 152, 154, 227
- Syndiotactic configuration 14
- Tensile compliance function 172, 207, 223, 227
- Tensile creep 298
- Tensile force 141
- Tensile relaxation modulus 225
- Terminal regions 335
- Thermoelastic effects 172
- Thermoelastic Navier equation
- Thermoplastics 6
- Thermoplastic elastomers 127-131
- Thermorheological simple systems 309
- Thermosets 6,9
- Thermoviscoelasticity 706, 808
- Thixotropy 562
- Three-element standard solid 400
- Time domain 242, 246, 247
- Time temperature superposition principle 306, 496
- Torsion
creep apparatus 296
function 818, 821, 848
pendulum 274
secondary effects 280
theory 818
- Torsional creep 296
- Toughness 638, 657
- TPEs for engineering 131, 132
- Trans conformation 17
- Transition-like zone 328
- Transverse flexion 285, 789
- Transverse oscillation 285
- Tresca (yield criterium) 596
- Trouton relation 567
- Tschoegls approach 154
- Tube model 430
- Ubbelohde viscometer 526
- Undercooling 39, 45, 48
- Unidirectional composite 672, 677
- Vectra 52
- Vinyl polymers 8, 32, 67
- Viscoelastic
beams 769, 788
behavior 238, 306
cylinder pipe 722
functions 222, 252, 327
functions and physical aging 478

[Viscoelastic]

- functions for glassy systems 463
 - hollow sphere 710
 - liquid 209, 247, 319, 321
 - loss functions 329
 - material 200, 208, 245, 327, 394
 - models 394
 - problems 708
 - rod (free oscillations) 290
 - rotating disc 728
 - solid 209, 314, 319, 322
 - systems 227
- Viscoelasticity 197
- Viscometer 536, 539, 541
- Viscosity 52, 142, 175, 206, 338
- effect of molecular weight 524, 548
 - effect of temperature 531, 550
 - intrinsic viscosity 525
- Viscosity determination from
- capillary 521
 - Couette 538
 - cone-plate geometry 539
 - plate-plate geometry 541
- Viscosity models
- Carreau model 552
 - Cross-Williamson model 552
 - Ellis model 551
- Viscous flow:
- effect of pressure 532
- Vitrification 661
- Vogel-Fulcher-Tammann-Hesse equation 324, 455
- Voigt formulation 154, 170
- von Mises (yield criterion) 594
- Vulcanization 9, 10, 112
- Wave propagation in viscoelastic material 294, 748
- Waves in viscoelastic materials 748
- Weight average molecular weight 12
- Weissenberg effect 544
- Williams-Landel-Ferry equation 65, 325
- X-ray diffraction 33, 42
- Xydar 52
- Yield
- criteria 593
 - mechanical test 588
 - strain 584
 - stress 584
 - viscoelastic behavior 597
- Zener model 403
- Zener solid 400
- Zero-shear rate viscosity from
- creep compliance 312
 - loss relaxation modulus 243, 252
 - relaxation modulus 218, 252
- Zimm theory 428